Durham E-Theses

System modelling and control

Gill, Kenneth Fred

How to cite:

Gill, Kenneth Fred (1990) *System modelling and control*, Durham theses, Durham University. Available at Durham E-Theses Online: http://etheses.dur.ac.uk/6193/

Use policy

UNIVERSITY OF DURHAM

APPLICATION FOR THE DEGREE OF D.Sc.

1990

KENNETH FRED GILL

**B.Sc. (Dunelm) M.Sc., Ph.D. (Birmingham)
C.Eng., M.I.Mech.E., M.I.E.E.**

Part 1.

CONTENTS

Part 1.

Part 2.

1. CURRICULUM VITAE

1. CURRICULUM VITAE

Name:	Kenneth Fred Gill
Address:	Heortnesse,
	Miles Garth
	Rigton Hill
	Bardsey
	LEEDS
Date of birth:	20.7.31
Marital Status:	Married, with two children.

1.1 General Statement of Career

I obtained my engineering training with a company manufacturing
large steam turbine and alternating equipment for the
electrical power supply industry. My higher education was
gained at Durham and Birmingham Universities. I was awarded the
degree of B.Sc. from the former in 1955. From the latter, I
received the degrees of M.Sc. in 1958 and Ph.D. in 1961. I am
a corporate member of both the Institution of Mechanical
Engineers and the Instititution of Electrical Engineers.

I spent two further periods working in industry, one of 3 years
as a control engineer with Bristol Siddeley Engines, Coventry,
and the other for a period of 2 years as a Senior Scientific
Officer at the Admiralty Underwater Weapons Establishment,
Portland.

For the last 27 years, I have been a Lecturer, then Senior
Lecturer at Leeds University, teaching control engineering and
engineering dynamics to final year honours students reading for
undergraduate degrees in Mechanical Engineering, and Control
Engineering.

Chief among my terms of reference, on being appointed to the
department, was to create an undergraduate course in Control
Engineering. This course ran successfully for some 10 years.
In consequence control engineering is now an established
component in the honours degree courses given in both
Departments of Mechanical Engineering and Electronic and
Electrical Engineering.

I organized and made a major contribution to 24 short courses
in control engineering. Each course was of five days duration
and most of the participants, totalling over 500, came from
industry or the armed forces. The course material varied from
year to year, ranging from elementary to advanced levels.

My research interest, until recently, has been in the fields of modelling and control. In this period I have supervised 25 postgraduate students, 21 were awarded Ph.D. degrees, 2 M.Phil degrees and 2 M.Sc. degrees.

In the same period, I was active in a number of industrial and research projects. The principal of these were:-

1.   Head Wrightson Ltd (1973-1976)

      I acted as a consultant to this firm advising on sinter plant control. The design problem was large inherent transportation delays in moving the raw feed stock to the mixing drum and from the drum to the strand for sintering.

2.   S.E.R.C. Grant B/RG/44672 (1973-78)

      The attitude control problem of a three axis flexible satellite was identified. A control design procedure was proposed to improve satellite pointing accuracy.

3.   S.E.R.C. Grant GR/A/51204 (1978-80)
      An optical attitude measurement system was proposed for incorporation into a satellite control system. This measurement scheme was designed to minimize the effects of gyroscope drift and random torque variations caused by environment noise.

4.   S.E.R.C. Grant GR/B/41049 (1980-84)
      A Teaching Company, of which I was leader, was formed between a local company and the University, to improve the company's manufacturing efficiency, product quality and to provide an industrial environment for a training in research.

5.   S.E.R.C. Grant 88501763 (1988-1991)

      To develop a machine vision system for robotic assembly, a linked project (CASE) was undertaken with the Ford Motor Company, Dagenham.

The published results from these projects are included in the publications listed.

I was external examiner for the Bachelor of Science course in Mechanical Engineering, at Sheffield City Polytechnic from 1979 to 1984. From 1985, I have been external examiner of the Open University course (T394) in Control Engineering. I have been external examiner for a number of Ph.D. candidates from other Universities and internal examiner for a number within my own department. I have also acted as an examiner for mature applicants for membership of the Institution of Mechanical Engineers.

My contribution to University administration has been a period on the Board of the Faculty of Engineering (6 years), a member of Senate (3 years) and the Academic Staff Committee (2 years). I have also been a member of a number of appointing committees for academic staff.

1.2   Current Commitments

My principal commitments are:-

a)   Teaching

I lecture to first year students in Pascal programming and to third year students in Control and Machine Vision. The latter two courses, which I created and developed are popular with students. I supervise laboratory periods in computing, measurement and engineering applications.

b)   Research

Together with a colleague, Dr R.M. Baul, I currently supervise 10 postgraduate students, 9 registered for the degree Ph.D. and 1 for an M.Sc. All the projects are in the area of manufacturing.

c)   Administration

I was appointed Admissions Tutor for the Department of Mechanical Engineering in September, 1989, and elected to the University Committee on Promotion and Progression in May, 1988.

1.3   Prizes of the Institution of Mechanical Engineers.

1.   William Sweet Smith Prize, 1988, for the paper:-

Knowledge representation database for the development of a fixture design expert system [60].

2.   Joseph Whitworth Prize, 1989, for the paper:-

Experimental evaluation of 'shape from shading' for engineering component profile measurement [65].

1.4   List of Publications

1.   The Application of Analogue Computer Techniques to the Design
      of Aero-Engine Control Systems. Saville, H. and Gill, K.F.
      Brit. I.R.E. Convention on Electronics in Automation 1957,
      p. 1-15.

2.   Influence of Exhaust Induction Systems on Air Consumption of a
      Two-Stroke Oil Engine. Wright, E.H. and Gill, K.F. The
      Engineer, Vol. 216, No. 5618, 1963, p. 501-506.

3.   Theoretical Analysis of the Exhaust System of an Oil Engine.
      Wright, E.H. and Gill, K.F. The Engineer, Vol. 218,
      No. 5666, 1964, p. 311-319.

4.   Analysis of a Gas Turbine Fuel System. Schwarzenbach, J.
      and Gill, K.F. The Engineer, Vol. 219, No. 5688, 1965,
      p. 209-218.

5.   Heat Transfer through a Piston by Electrical Analogy.
      Coney, J.E.R. and Gill, K.F. The Engineer, Vol. 221,
      No. 5753, 1966, p. 643-646.

6.   Theoretical Analysis of the unsteady gas flow in the exhaust
      system of an engine. Wright, E.H. and Gill, K.F. J. Mech.
      Eng. Sci., Vol. 8, No. 1, 1966, p.70-90.

7.   Dynamic Characteristics of a Hydrostatic Thrust Bearing.
      Schwarzenbach, J. and Gill, K.F. The Engineer, Vol. 222,
      No. 5770, 1966, p. 309-312.

8.   Determination of Root Loci. Gill, K.F. and Walker, P.H. The
      Engineer, Vol. 223, No. 5801, 1967, p. 479-481.

9.   Stability Analysis for the Practical Engineer. Gill, K.F.,
      Schwarzenbach, J. and *Harland, G.E. The Engineer,
      Vol. 224, No. 5822, 1967, P. 247-254.

10.   Design of an optimum relay - type governor for a gas-turbine
      engine. Gill, K.F. and Schwarzenbach, J. Control, Vol. 12,
      No. 118, 1968, p. 322-327.

11.   A theoretical look at the use of functional non-linearities in
      a gas turbine control system. Part 1. Gill, K.F. and
      Schwarzenbach, J. Control, Vol. 10, No. 99, 1966,
      p. 465-468.

12. A theoretical look at the use of functional non-linearities in a gas turbine control system. Part 1. Gill, K.F. and Schwarzenbach, J. Control, Vol. 10, No. 100, 1966, p. 531-535.

13. Design Analysis of Model Reference Adaptive Control Systems Applied to a Gas-turbine Aircraft Engine. Gill, K.F., Schwarzenbach, J. and *Harland, G.E. Proc. I.E.E., Vol. 115, No. 3, March 1968, p. 460-466.

14. Pseudo-random signal testing applied to a Diesel engine. *Harland, G., *Panko, M., Gill, K.F. and Schwarzenbach, J. Control, February 1969, p. 137-140.

15. Automatic Control of Pulsating Air Flow. Gill, K.F., Imrie, B.W., and *Harland, G.E. A Symposium on the Measurement of Pulsating flow, April 1970, University of Surrey. Organised by the Institute of Measurement and Control, p.77-85.

16. A Study into the use of p.r.b.s. pressure disturbances to measure sonic velocity in a two phase flow system. Gill, K.F. and *Reed, E.W. Proceedings I.M.E. 1972. Vol. 186, 39/72, p. 449-455.

17. Theoretical design of an adaptive controller for an internal combustion engine. Gill, K.F., *Harland, G.E., and Schwarzenbach, J. Control and Instrumentation. October 1972, p.50-53.

18. A practical investigation into the validity of the electrical analogy used to represent the dynamic characteristics of a pipe restriction. *Ali, M.A., *Reed, E.W., Gill, K.F. and Imrie, B.W. International Symposium on Measurement and Process Identification by Correlation and Spectral Techniques, Bradford Univ., Jan. 1973. Published by Institution of Measurement and Control.

19. Measurement by correlation of small amplitude pressure wave propagation velocity in a gas-solids flow. *Reed, E.W., Mobbs, F.R. and Gill, K.F. International Symposium on Measurement and Process Identification by Correlation and Spectral Techniques, Bradford Univ., Jan. 1973. Published by Institution of Measurement and Control.

20. Design of model reference adaptive control for an I.C. engine. *Harland, G.E., and Gill, K.F. Measurement and Control. Vol. 6, April 1973, p. 167-173.

21. A Guide for the practising engineer into the use of correlation techniques. *Reed, E.W. and Gill, K.F. Journal of Royal Electrical and Mechanical Engineers. No. 23, April 1973, p. 11-13.

22. An experimental technique for minimizing resonance within a
    ducted fluid.. *Reed, E.W. and Gill, K.F. J.M.E.S.
    Vol. 15, No. 2, April 1973, p. 95-101.

23. A correlation method for measuring reflection coefficients of
    sharp edged orifices for small amplitude pressure waves.
    *Ali, M.A., *Reed, E.W., and Gill, K.F. J.M.E.S. Vol. 15,
    No. 5, October 1973, p. 321-325.

24. An investigation of non-reflecting end conditions within a duct
    using pseudo random pressure pulses. *Reed, E.W., *Ali,
    M.A. and Gill, K.F. Journal of Sound and Vibration (1974)
    33(4), p. 391-397.

25. Effects of flexibility on a momentum stabilized communication
    satellite attitude control system. *Gething, J.M.
    ᵞHolt, J.A. *Smart, D.R., and Gill, K.F. Proc. I.E.E. Vol
    120, No. 5, May 1973, p. 613-619.

26. Pseudo random pressure pulses used to determine the shape of
    reflected waves from an opening. *Reed, E.W., *Ali, M.A.,
    and Gill, K.F. Measurement and Control. Vol. 7, No. 1,
    January 1974, p. 31-34.

27. Pseudo-random binary-sequence pressure-pulse testing in the
    study of flow behaviour. *Reed, E.W., *Ali, M.A., and
    Gill, K.F. I. Chen. E. Symposium Series. No. 38,
    Strathclyde University, April 1974.

28. Relay Control of undamped linear systems using Lyapunov's
    Second Method. *Gething, J.M., and Gill, K.F. Proc. I.E.E.
    Vol. 121, No. 4, April 1974, p. 301-306.

29. The measurement of pulsating gas flow velocities using P.R.B.S.
    pressure pulses. *Reed, E.W., *Ali, M.A. and Gill, K.F.
    Measurement and Control. Vol 7, No. 9, September 1974,
    p. 346-348.

30. Dynamic analysis of flexible space vehicles having uncoupled
    control axes. *Smart, D. R., Gill K.F., *Gething, J.M., and
    ᵞHolt, J.A. The Aeronautical Journal. December 1974,
    No. 768, Vol. 78, p. 560-569.

31. Attitude control of a flexible space vehicle by means of a
    linear state observer. *Smart, D.R., and Gill, K.F.. The
    Aeronautical Journal. Vol. 79, No. 770, February 1975,
    p. 86-95.

32 A digital state observer for the attitude control of a flexible
    space vehicle. ᵞSmith, E.H. and Gill, K.F. The
    Aeronautical Journal. Vol. 79, No. 779, November 1975,
    p. 506-509.

33. An attitude control system for a flexible satellite providing active damping of flexural motion. *Gething, J.M., and Gill, K.F. The Aeronautical Journal, March 1976, Vol. 80, No. 783, p. 134-139.

34. Flexible Space vehicle control based on state observation and Lyapunov's Method. ᵞSmith, E.H., and Gill, K.F. E.S.A. Symposium on the dynamics and control of non-rigid space-vehicles. ESRIN-Frascati - Italy, May 1976.

35. Data collection for plant control studies. *Fenna, D.S., Gill, K.F., and Jowett, A. Institution of Mining & Metallurgy Transactions/Section C, Vol. 85, March 1976, p. 7 - 14.

36. The estimation of natural frequencies by use of sturm sequences. *Longbottom, G., and Gill, K.F. The International Journal of Mechanical Engineering Education. Vol. 4, No. 4, October 1976, p. 319-328.

37. Controlling the attitude and two flexure-modes of a flexible satellite. ᵞSmith, E.H. and Gill, K.F. The Journal of the Royal Aeronautical Society. January 1977, No. 442, p. 41-44.

38. On the design of optimal discrete observers with particular reference to a flexible communication satellite. ᵞSmith, E.H., and Gill, K.F. The Journal of the Royal Aeronautical Society. April 1978, No. 534, p. 174-178.

39. Dynamic modelling and multi-axis attitude control of a highly flexible satellite. *Longbottom, G., ᵞTate, D., and Gill, K.F. A link between science and application of automatic control. Proc. of the 7th Triennial World Congress of the IFAC. 1978, Vol. 3, p. 2435-2441. Pergamon Press, Oxford.

40. Textbook: System modelling and control. Schwarzenbach, J. and Gill, K.F., 1978, Edward Arnold Ltd.

41. The effect of mass flow rate on the reflection behaviour of small-amplitude pressure waves from duct terminations. *Ali, M.A., Gill K.F., and Imrie, B.W. The Journal of Mechnanical Engineering Sciences. Vol. 20, No 4, August. 1978, p. 229-235.

42. Attitude control of a flexible satellite in a noisy environment. *Fenton, J. ᵞHorton, D. and Gill, K.F. Proc. IEE, Vol 126, No. 12, December 1979, p. 1307-1310.

43. Flexible spacecraft attitude control using a simple PD algorithm. *Fenton, J., and Gill, K.F. Journal of the Royal Aeronautical Society. May 1981, No. 890, p. 185-189.

44. Attitude estimation and control of a flexible spacecraft using inertial and optical measurements. [Y]Horton, D., *Fenton, J. and Gill, K.F. Journal of the Royal Aeronautical Society. June 1981, p. 240-243.

45. Controlling systems with long time delays using pole-positioning technique and optimal-linear-regulator theory. *Badrah, S.M.M. and Gill, K.F. Trans. Inst. M.C., Vol. 3, No. 3, July. 1981, p. 115-120.

46. Flexible spacecraft attitude measurement and control scheme incorporating static estimation. *Fenton, J., [Y]Horton, D., and Gill, K.F. Optimal Control Application and Methods. Vol. 3, 1982, p. 23-40 (1982) John Wiley & Sons Ltd.

47. System modelling and control (Second Edition). Schwarzenbach, J., and Gill, K.F. 1984, Edward Arnold Ltd.

48. A justification for the wider use of fuzzy logic control algorithms. *Daly, S., and Gill, K.F. Proc. Inst. Mech. Engrs. Vol. 199, No. C1, 1985, p. 43-49.

49. The fuzzy logic controller: An alternative design scheme. *Daly, S., and Gill, K.F. Computers in Industry. Vol. 6, No. 1, February 1985, p. 3-14.

50. Identification of surface roughness. *Mulvaney, D.S., Newland, D.E. and Gill, K.F. Proc. Inst. Mech. Engrs. Vol. 199, C4, 1985, pp. 281-286.

51. A design study of self-organising fuzzy logic controller. *Daley, S. and Gill, K.F. Proc. Inst. Mech. Engrs. Vol. 200, No. C1, 1986, p. 59-69.

52. Performance of a telescopic dual-tube automotive damper and the implications for vehicle ride prediction. *Hall, B.B. and Gill, K.F. Proc. Inst. Mech. Engrs. Vol. 200, No. D2, 1986, p. 115-123.

53. A characterization of surface texture profiles. *Mulvaney, D.J., Newland, D.E. and Gill, K.F. Proc. Inst. Mech. Engrs. Vol. 200, No. C3, 1986, p. 167-178.

54. Identification of surface texture signals. *Mulvaney, D.J., Newland, D.E., and Gill, K.F. 8th IASTED INTERNATIONAL SYMPOSIUM on measurement, signal processing and control. TAORMINA - ITALY, September 1986.

55. A study of fuzzy logic controller robustness using the parameter plane. *Daley, S., and Gill, K.F. Computers in Industry. Vol. 7, No. 6, December 1986, p. 511-521.

56. A comparison of orthogonal transforms in their application to surface texture analysis. *Mulvaney, D.J., Newland, D.E. and Gill, K.F. Proc. Inst. Mech. Engrs. Vol. 200, No. C6, 1986, P. 407-414.

57. Attitude control of a spacecraft using an extended self-organising fuzzy logic controller. *Daley, S. and Gill, K.F. Proc. Inst. Mech. Engrs. Vol. 201, No. C2, 1987, p. 97-106.

58. Performance evaluation of motor vehicle active suspension systems. *Hall, B.B., and Gill, K.F. Proc. Inst. Mech. Engrs. Vol 201, No. D2, 1987, p. 135-148.

59. The drying and curing of latex-backed carpets. Baul, R.M., Gill, K.F., and Holme, I. Conference of the Textile Institute Floorcoverings Group, Blackpool, September 1987. Textile Progress, 19, No. 3 (1988) p. 50-59.

60. Knowledge representation database for the development of a fixture design expert system. *Darvishi, A.R., and Gill, K.F. Proc. Inst. Mech. Engrs. Vol. 202, No. B1, 1988, p. 37-49.
(Awarded William Sweet Smith Prize)

61. Use of fuzzy logic in robotics. *Wakileh, B.A.M., and Gill, K.F. Computers in Industry. 10 (1988) p. 35-46.

62. A complete description of surface texture profiles. *Mulvaney, D.J., Newland, D.E., and Gill, K.F. Wear, 132 (1989) p. 173-182.

63. Comparison of a fuzzy logic controller with a P+D control law. *Daly, S. and Gill, K.F. Transactions of the ASME. Vol. 111, June 1989, p. 128-137.

64. An experimental evaluation of normalised Fourier descriptors in the identification of simple engineering objects. *Nikravan, B., Baul, R.M., and Gill, K.F. Computers in Industry. 13 (1989) p. 37-47.

65. Experimental evaluation of "shape from shading" for engineering component profile measurement. *Al-Kindi, G.A.H., Baul, R.M. and Gill, K.F. Proc. Inst. Mech. Engrs. Vol. 203, 1989, p. 211-216.
(Awarded Joseph Whitworth Prize)

1.5 Papers Under Review

66. Robot control using self-organising fuzzy logic.
    Accepted by the journal Computers in Industry.

67. A contribution to fixture design rules: An expert system.
    Accepted by the International Journal of Production Research.

68. A comparison of orthogonal transforms in engineering computer vision.
    Accepted by Proc.Inst.Mech.Engrs.

69. Monitoring and assessment of engineering surface texture using computer vision.

2. STATEMENT OF CONTRIBUTION AND ORIGINALITY

2. STATEMENT OF CONTRIBUTION AND ORIGINALITY

As an engineer, my research and scholarship has been in response to identified industrial requirements as shown by my publications in the learned society literature. This work has been concerned with the modelling, measurement and control of engineering processes. For ease of presentation, the material is grouped under the following headings:

1. Gas turbine modelling and control.

2. Satellite modelling and control.

3. Non-steady gas flow in ducts.

4. Gas flow measurement.

5. Publications of a general nature.

6. Textbook on Modelling and Control.

7. Measurement and control in manufacture.

I acknowledge the enjoyable collaboration I have had with colleagues and postgraduate students over the years, which has resulted in publications under joint authorship and are a reflection of an equal partnership. Almost all of the work presented was conceived and initiated by me. The progress of all work undertaken by students was supervised by me at all times. Over ninety per cent of the papers published were actually written by me. Where a research student's work has been used, I list his name first.

2.1 Gas turbine modelling and control
(Papers 1, 4, 10, 11, 12, 13)

The aim of a control system is twofold. Firstly, it is to relieve the

operator of the arduous and sometimes impractical task of controlling a system and secondly, it is to enable the system to function more efficiently. Early control systems, starting with the Watt governor of 1788 were developed by trial-and-error design and adjustment; only limited, if any, consideration was given to theoretical analysis. The variations possible in the lines of approach when seeking satisfactory systems resulted in many failures, and intuitive knowledge gained by people with years of practical experience was an important factor in the development of a successful system. With the entry of the gas turbine engine into military service and the demand for improvements in its dynamic performance, the trial and observation approach to system design became unacceptable.

In the late 1940's and early 1950's, attempts were made to achieve the required aircraft engine dynamic performance by the utilization of fuel scheduling speed control. For example, · ·imple pump, throttle valve and a means of altitude compensation were fitted to the Meteor and Vampire aircraft.

To employ fuel scheduling, a thorough knowledge of the full operational requirements of the aircraft is necessary. For aircraft of the early 1950's, this information was available and the systems proved acceptable when temperature variation about standard atmospheric conditions was negligible. Readjustment was required, however, for tropical operation. As flight specification became more demanding, fuel scheduling inaccuracies widened and it was impractical to continue employing open loop controllers for more advanced military aircraft engine control. The 3-term controller was introduced into the system [1] and papers [4, 10, 11, 12] represent an extension to the work.

As more severe performance requirements for military aircraft developed, attendant difficulties of design, production and maintenance of the controller for scheduling loop adjustment would result and the need for adaptive control became apparent [13].

The six pieces of work cited above made a useful contribution to the knowledge available to practitioners working on engine systems.

2.2 Satellite modelling and control

(Papers 25, 28, 30, 31, 32, 33, 34, 37, 38, 39, 42, 43, 44, 46, 48, 49, 51, 55, 57, 63)

In January 1958, Explorer I became the first United States satellite to achieve orbit. The vehicle was designed to be spin stabilised about its principal axis of minimum moment of inertia, which is stable only if the structure of the vehicle is totally rigid. The gyroscopic precession of the spin axis, however, excited vibrations of four relatively small whip antennae. The energy dissipated, due to structural damping within these antennae, caused the unstable motion to increase to such an extent that the minimum energy dynamic state was reached, when the vehicle was spinning about its axis of maximum moment of inertia.

Similar problems occurred in Alouette I, launched in September 1962, the Orbiting Geophysical Observatory satellite, OGO III, launched June 1966, and

Mariner 10, launched October 1973. The effects of interaction between control systems and structural dynamic responses had been appreciated for some time in the fields of aircraft and missile attitude control; it was now observed in space satellites.

Although the possible effects of interaction between control systems and vehicle structure was more generally appreciated, the control system design technique employed assumed a rigid vehicle, on which to design a system for attitude stabilisation. Simulation of the control system and the flexible dynamics of the controlled vehicle was used to ensure that attitude stabilisation specifications were not exceeded due to interactive effects.

The author considered that, with increasingly stringent attitude stabilisation and power requirements, problems of structural interaction would become much more important in the future. In particular, the high power requirements would lead to the adoption of large area solar arrays. These are lightly constructed so as not to impose too severe a weight penalty at launch, their construction inevitably implying extreme flexibility. In consequence high pointing accuracy has to be achieved in the presence of a high degree of structural flexibility. Technological ingenuity was able to provide the necessary modifications to ensure that, in any particular system design, the required specifications were met. The cost of space technology, however, requires that the most efficient solution be achieved. Hence, the question arose as to whether detailed consideration of structural flexibility, at the outset of a control system design study, should be made to produce a more efficient solution.

The outcome of such studies are reported in [25, 28, 30, 31, 32, 33, 34, 37,

38, 39, 43] and represents a general appraisal of the effects of flexibility on attitude control system design, especially for highly flexible satellite configurations.

The stringent pointing requirements of a highly flexible craft places a severe demand upon attitude measurement systems making it necessary that problems of sensor anomalies such as noise, non-linearities and gyroscope drift be minimized. The work presented [42, 44, 46], investigates the problem and gives an analysis of an inertial optical measurement system and studies a control scheme for improving vehicle pointing accuracy in the presence of flexibility and attitude sensor noise.

Turning to more recent work [48, 49, 51, 55, 57, 63], this has been principally concerned with the application of fuzzy logic to industrial processes. The shortcomings of previously proposed analysis and design methods are discussed and a novel approach to the selection of controller parameters is presented [48, 49]. The method is based upon a stability constraint formulated from Lyapunov's second method as applied to discrete systems.

It is argued in the literature that a fuzzy logic controller should only be adopted when conventional control cannot be utilized successfully; its range of application will be extremely limited. The fuzzy logic controller displays insensitivity to process change; its robustness is studied [55] to strengthen the justification for its wider use. Models of an idealized

flexible satellite and a more complex earth resources satellite are used to investigate robustness. The attempt to obtain a quantitative measure of the fuzzy logic controller robustness is based on the use of the parameter plane technique; its limitation was recognised.

Qualitative studies [51, 57] reveal that areas exist where the fuzzy logic scheme is superior to more conventional controllers. These studies emphasize the benefits that might be gained from the more general adoption of the approach [63].

2.3 Non-steady gas flow in ducts
(Papers 2, 3 6)

My choice of research topic for my PhD studies at Birmingham University was largely influenced by earlier work which I carried out in industry on the design of a variable geometry intake for a gas turbine. The work was a preliminary control study into likely problems, which could occur in supersonic flight.

The project involved the analysis of wave action in a plain duct-conical diffuser by the theory of characteristics, a topic which I believed relevant to the earlier work on gas turbine intakes.

2.4 Gas flow measurement
(Papers 15, 16, 18, 19, 22, 23, 24, 26, 27, 29, 41)

In most industrial situations, pulsating flow invariably occurs and the need

for developing an appropriate means of metering is highly desirable. The square root law devices for measuring steady flow are well established and widely accepted because of their accuracy and simplicity. Experimental work [15] revealed the presence of flow pulsations, caused in metering errors when a square root law device and a manometer combination are used.

The published work suggested that one possible source of error, encountered when metering pulsating flow using a constriction manometer arrangement, could be attributed to the dynamic characteristic of the constriction with special reference to the relative phase shift between the pressure signal measured upstream and the corresponding pressure signal measured downstream of the constriction. Of course before the measurement of such dynamic characteristics can be made (reported in [18]), all reflected wave action must be suppressed.

An investigation of reflections of pressure waves within a duct was carried out to find experimental means of minimising end reflections [22, 23, 24, 26, 27, 41] in an attempt to produce a non-reflecting duct end condition, i.e. the theoretically infinitely long pipe configuration.

The application of small pseudo random binary sequence pressure pulses was used to demonstrate an experimental means of measuring the mean flow velocity of a pulsating gas flow without the use of pipe constrictions [29]. From this work, a novel method was developed to measure sonic velocity [16] in gas solids flow which was later shown to be valuable in the modelling of two phase flow systems [19].

2.5 Publications of a general nature

(Papers 5, 7, 8, 9, 14, 17, 20, 21, 35, 36, 45, 52, 58, 59)

The projects of this section are largely the outcome of industrial enquiries. Although it does not form part of my main research thrust, the combination of modelling and controller design is very closely related.

Described in [5, 7, 8, 9, 21, 36] is the application of classical theoretical techniques written in a manner more suitable for the industrial engineer. Problems associated with process identification is reported in [14, 35] and the application of adaptive control to an operating engine in [17, 20].

Reported in [45] is a solution to a problem largely created by a manufacturer, because insufficient thought had been given to process control. A sinter plant had been designed and its layout agreed before serious attention was given to control. It was later realised that the lengths of conveyor employed on the plant for movement of feedstock would introduce long time delays and these delays would cause difficulty when tuning the proposed 3-term controller. Process disturbance, largely caused by variations in raw feedstock composition, is compensated for by changes in strand speed, which in turn affects the rate of sintering.

Similarly, in another investigation, a telescopic dual-tube automotive damper [52] was manufactured for sale before an analytical dynamic study was undertaken. The subsequent predicted performance was largely supported by experiment. The work continued into the performance evalutions described in [58] on active suspension, a subject now receiving much attention.

In the carpet industry, one operation in the continuous production of broadloom carpet is drying and curing of the latex backing. In the past manufacturers have made only a minimal attempt to optimize energy usage; the work reported in [59] is one of the few on-line studies on this matter. The results attracted much interest from both inside and outside the industry.

2.6 Textbook

A major effort of scholarship in the mid-1970's was the preparation of a textbook on control theory [40] which was published in 1978, reprinted twice, and selected by the British Council for publication in an ELBS edition. An updated and expanded second edition [47] was published late 1984, and reprinted in 1986. An expanded third edition is in preparation.

The book, intended for both students and practising engineers, has been widely adopted. It is standing the test of time in a field, which has seen a proliferation of books on this topic.

2.7 Measurement and control in manufacture
(Papers 50, 53, 54, 56, 60, 61, 62, 64, 65)

The current area of research is manufacturing, a most rewarding area to have entered. The Institution of Mechanical Engineers awarded the William Sweet Smith Prize for paper [60] and the Joseph Whitworth Prize for paper [65].

My introduction to this research area was the identification of surface texture signals. The analysis of surfaces is common to us all. Running a finger over a material yields knowledge, which is not available from a simple visual inspection; for example, its smoothness gives information as to how firmly it has to be gripped in order to pick it up. Information relating to shape is also important, but this is normally investigated as part of the visual identification process rather than being a tactile examination.

In the field of engineering, an assessment of the surface finish produced by a manufacturing process is often required in order to predict the performance of the component. Until recently, the sole design criterion for surface texture was that the mean amplitude of the measured surface undulations should be within specified tolerance limits. Consequently, it was only necessary to obtain a single roughness parameter to indicate the 'average height' of the surface undulations; this is still the only parameter normally quoted.

The continually increasing demands being placed on the components of mechanical systems has led to the necessity for a more precise description of the form of surface texture data. The work carried out [50, 53, 54, 62] was aimed at meeting this need by considering methods of improving the characterization of surface texture data by the application of orthogonal transforms [56]. Except for limited use of the Fourier transform for this purpose, no reference could be found to any previous work on the subject. It was considered that the ability to carry out on-line measurement and real time assessment of a component surface would enhance the control of a wide

range of manufacturing processes and allow current performance to be estimated. One physically realizable approach to the continuous monitoring of surface finish would be to use computer vision. In [69] the capability of a machine vision system to monitor texture is explored experimentally and confirms the importance of surface colour, lighting conditions, surface geometry and tarnishing when interpreting the measurement data.

Symbolic models of image features can also be employed; shape from shading is one such analytical approach. Application of this allows a representation of shape suitable for surface contour measurement and object recognition [65].

Developments in robotics, machine vision and expert systems are disciplines being combined to create the integrated manufacturing system. Part of my work has been to study control algorithms [61, 66] that might ᵥ suitable for use with a robot utilizing vision [64, 68] for component recognition and handling. A robot that can 'see' and 'feel' will be able to perform a greater variety of more complex tasks with the minimum of human intervention.

Jigs and fixtures are links in the production chain. They ensure that manufacturing tolerances are maintained and precise duplication is possible. Developed in the work presented [60, 67] is a prototype fixture design expert system to meet the demands of the Flexible Manufacturing system. No major published work employing the expert system is available and the author believes the work must be among some of the earliest attempted. The system proposed provides a database to encompass most of the facilities required in the manufacturing environment. The individual data structure employed for

object class representation includes a sufficient number of attributes to ensure unique representation to permit efficient information retrieval.

3. GAS TURBINE MODELLING AND CONTROL

PAPER 1

THE APPLICATION OF ANALOGUE COMPUTER TECHNIQUES TO THE DESIGN OF AERO ENGINE CONTROL SYSTEMS*

by

H. Saville, B.Sc.(Eng.)‡ and K. Gill, B.Sc. (Eng.)‡

A paper to be presented at the Convention on "Electronics in Automation" in Cambridge on 29th June 1957

SUMMARY

The problem of aero engine control systems is shown to have reached the degree of complexity at the present time that makes it necessary to embark on analogue methods of simulation in order to predict the behaviour of the system. The parameters to be controlled are discussed and the way in which interaction may affect the individual loops is explained together with a review of the requirements of a control system from the pilot's handling, and the performance view points. As illustrations, examples of control system functional components are used to illustrate the methods of adaptation of a practical hydraulic system to analogue methods. The use of the computer results is discussed in formulating an optimum system design.

1. Introduction

When the gas turbine engine was introduced into Service use in the Meteor and Vampire aircraft about 12 or 13 years ago the control systems used largely fulfilled the promise of early writers that the complication of the highly developed piston engine carburettor or fuel injection system could be left behind. In their place we were to be blessed with simple systems involving only a pump, throttle valve and means of altitude compensation. No longer would it be necessary to worry about such things as mixture strength, boost controls, fuel enrichment over-rides, etc. This was, of course, true in those days when piston engines were stretched to the limits to produce the performance demanded and when the thrusts of early jet engines gave such big improvements in aircraft performance that the engine performance was no longer a limiting factor and the engine control requirements could easily be · met by the simpler system.

The first systems used, known as the Barometric Pressure Control or B.P.C. system

were only suitable for very limited applications and were soon replaced by "flow scheduling" systems. The B.P.C. system delivered fuel to the engine at a controlled pressure. Since the flow was a function of this pressure, the flow requirements could be matched to this controlled pressure to schedule the flow under any flight conditions. Inaccuracies at altitude with this system have made it only suitable for very limited uses. Hence the flow scheduling system was introduced.

In the flow scheduling system, the fuel required for any flight condition is metered to a value which is calculated from the known engine performance data as for the B.P.C. system, but the fuel is measured by means of a pressure drop across a metering orifice of known area.

The parameters used for metering the fuel flow in both systems were the throttle position and the atmospheric ram pressure. This ram pressure is the total head pressure due to aircraft altitude and forward speed and therefore is sensitive to these two main operating variables of the aircraft in flight. Only the variation of atmospheric temperature is then not accounted for in the schedule system.

It can be seen in Fig. 1 that a scheduling system based on the ram pressure can only give

an approximately correct fuel flow over the complete flight speed range of the aircraft. For aircraft of several years ago this variation only amounted to an error of about ± 1 per cent. on engine speed when temperature variations about standard atmospheric conditions were neglected.
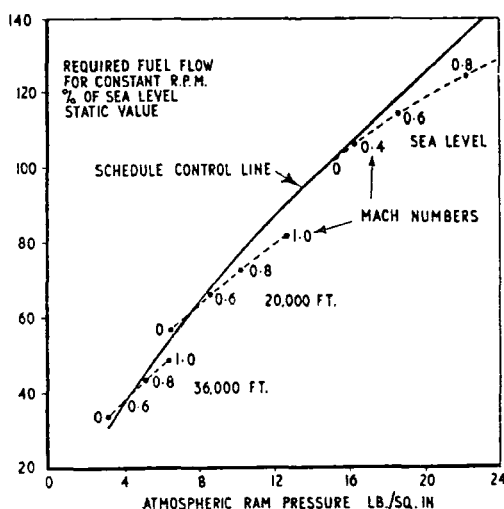

Fig. 1. Fuel flow as a function of ram pressure for a schedule system.

However as speed ranges have increased in recent years this scheduling inaccuracy has widened until it is now completely impracticable to use a single pressure parameter to schedule the fuel. For instance, the total variation of engine speed for an aircraft capable of sonic speeds at sea-level, when temperature variations from arctic to tropical have to be considered as well, may amount to ±400 rev/min. on an engine datum speed of 8000 rev/min.

Those who would prolong the use of scheduling systems have devised methods of correction to maintain a certain amount of compensation and so the fuel system has grown like a Christmas tree with possible additions such as air temperature corrections, augmentor valves, pressure potentiometer devices etc., until we are now in danger of arriving at systems which are equal in complexity to the piston-engine carburettor system.

The advent of high supersonic speeds has now made accurate scheduling extremely difficult and it has therefore become clear that

a new approach based on closed loop, or governing systems instead of the open loop or scheduling system has become necessary.

Speed governors have been used on aero engines in the past but they have taken the form of top speed limiting devices and have not been the primary functional element of the control system. As a result the governor has taken the second place in design and its development has not kept pace with the requirements.

These comments relate to pure jet engines. In the case of propeller turbine engines, development has followed slightly different lines, since a further variable is available, namely propeller pitch. Thus the fuel flow can control engine power supply while the propeller pitch can be used to control the power loading. Hence the engine speed can be chosen to give optimum efficiency conditions. The development of propeller control systems for piston engines was readily adapted to turbine engines and used for governing the speed while the fuel flow remained basically a scheduling system.

Such governing systems which have been attempted for pure jet engines have been developed by trial and error design and adjustment with only limited consideration given to the theory of stability. The variations possible in arriving at a satisfactory system resulted in many wrong lines of approach being tried without success.

This trial and error method would eventually provide satisfactory test-bed running, but then in flight testing much the same procedure had to be adopted. The possibilities of this method together with the use of intuitive knowledge gained by people with years of practical experience, however, should not be relied upon completely in the unknown realms of supersonic flight, where the slightest suggestion of instability in some control loop may prove disastrous.

It is therefore clear that only a full theoretical approach with practical design considerations linked at the outset will now suffice for future aero engine control systems.

If we now accept that this approach is necessary the methods of carrying this out must be considered. Full mathematical methods are

ANALOGUE COMPUTER FOR AERO ENGINE CONTROL PROBLEMS

available and are well known so far as analysis of linear systems are concerned. In addition, methods have been developed by which non-linearities may be introduced.

The calculation, however, is an extremely long and tedious process particularly when building up a control system where many possibilities may require separate investigation. The arithmetical work may, of course, be considerably eased by application of digital computer techniques. This method however can carry out no further work than could in principle be done by manual methods, the only saving is in time.

In a digital machine, the numerical value of a quantity is directly represented by a train of electrical pulses following each other in time sequence. Each pulse represents a digit (generally in the binary scale for ease of manipulation) and each train of pulses, known as a "word," represents a number on which arithmetic operations are to be performed. Since a word generally consists of a large number of digits a very high degree of accuracy may be obtained: for example, if a change is made in the least significant digit of a binary number of, say, fourteen digits, the change produced is one part in 2^{14}, i.e. one part in 16,384. The arithmetic operations performed on the numbers within a digital computer take place at very high speed, of the order of milliseconds, so that where many calculations have to be carried out on large quantities of similar data, a digital computer has obvious advantages.

Information is generally fed into a digital computer by means of punched tape and the output is produced in the form of typewritten sheets of numbers or as a punched tape. If the results of a computation are required in the form of graphs, for instance, these would have to be plotted manually or additional equipment would be required involving the expenditure of larger sums of money than the £20,000 to £50,000 required for a basic digital installation.

Fortunately the results required by a control engineer are not wanted in highly accurate mathematical form but more in a qualitative pictorial form. This being so, a method of solution where the results are presented on an oscilloscope in the form of a continuous

function of time provides the ideal form of solution. In this way the results appear directly in the form that would be seen by an observer watching the actual machinery being controlled.

The apparatus to produce results in this form is the analogue computer. It will be seen later that this machine may be used to incorporate the non-linear effects met in practical systems; that it may simulate completely in an electrical form the exact behaviour of a mechanical system; or when the system becomes more complex and when individual components have been investigated separately it may be used to solve the combined simultaneous differential equations representing the transient behaviour of the complete system.
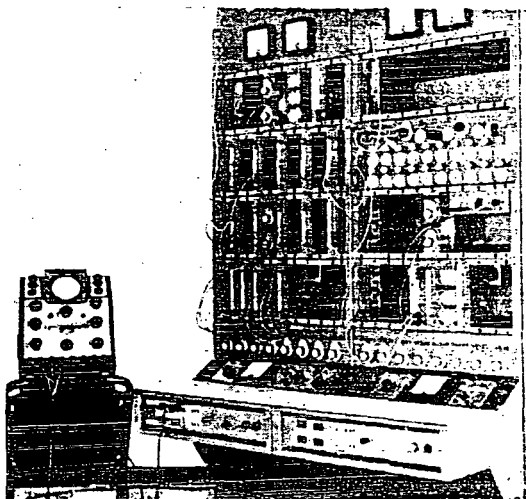
Fig. 2. Analogue computer for aero engine control problems.

In an analogue machine, a quantity is represented by a voltage on some suitable scale. The voltages are therefore true analogues of the variables under consideration and not a numerical representation digit by digit. The basic computing element is the d.c. amplifier which can be set up to perform summation, integration, differentiation etc. By the inclusion of further units, non-linear relationships can also be studied. An analogue computer result is obtained in the form of a voltage varying with time. This can be measured on a cathode-ray oscilloscope or plotted in graphical form using a pen recorder. Consequently, the

accuracy of the results is generally not greater than 0·5 to 1·0 per cent. of the full-scale value unless special precautions are taken, which may require more expensive equipment than the £3,000 to £15,000 needed for a general purpose machine.

Figure 2 shows a typical analogue computer set up to investigate the problem given later in this paper.

One of the advantages of an analogue computer lies in its ability to be a small machine for small problems and to be easily extended to deal with more complex problems. As the results are produced instantaneously on switching on, the machine enables the engineer to set up a model of his system and to study the effects of including or excluding certain portions and, after observing the results, to make changes in the most suitable parameters and to see immediately their effects.

A further advantage of an analogue computer is that it can be operated in real time, that is, the variables in the machine change at the same rate as the variable in the problem. As a result the machine can be used to simulate part of a system under design and can be operated with existing machinery to determine their combined performance.

There is a danger when considering the applications of analogue computers in attempting to simulate too big a problem at once. One should not depart too radically from a parallel theoretical consideration of the problem and the methods described in this paper provide a means of making a step-by-step attack on complicated control problems without losing an understanding of the order of the results to be expected and at the same time making the most economical use of computing equipment.

It is difficult to generalize on the amount of equipment necessary for any type of problem, but from experience gained on the problems of aero engine control, it does appear that complicated computer "set-ups" become unwieldy. It is thought that the simplifying techniques explained later will enable most problems to be reduced to a practical size. Additional space, however, must be available on the computer for the non-linear elements, multipliers, etc., when required.

In conclusion, a digital machine provides very accurate results at high speed but is generally only economic if used for large numbers of calculations and where numerical answers are required. An analogue machine is more suitable for less accurate work where immediate flexibility in operation and real-time working are useful and where graphical results are required.

2. Requirements of Aero Engine Control Systems

It is proposed now to discuss the many requirements that have to be satisfied by an aero engine control system.

These differ to some extent according to the application of the engine. For instance, an engine in a fighter aircraft will be handled much more roughly than in a bomber or passenger transport aircraft. On the other hand, the accuracy of control of an engine in a transport aircraft will require to be higher, in order that the engine may be left to continue to run at its most economical condition for long periods without attention by the flight engineer.

These differences are mainly in degree and in any case it is necessary to have a control system which will allow the engine to respond rapidly to throttle movements, be able to limit over-shoots and oscillation, have a high degree of accuracy over a wide range of operating conditions, and prevent engine damage due to stalling, combustion blow-out, exceeding the limiting engine speed, or exceeding limiting engine temperatures. In addition the system requires to be compact, designed to very strict weight requirements, and have safety features to prevent engine damage in the event of any failure of the control.

Considering these points we find that the first four relating to response, overshoot, damping, and accuracy are all concerned with the dynamic characteristics of the system and the engine, and it is these that have to be determined by an analysis of the system.

So far as speed control is concerned, the target should be to produce stable governing systems with an accuracy of not less than ±20 rev/min. in 8000 rev/min. and with overshoots on acceleration of not more than 100 rev/min. Damping should be such that the oscillation virtually disappears within 2 cycles.

Additional controlling requirements which will produce closed loops interacting on the

main speed governing loop are required for jet pipe temperature control, variable nozzle controls, reheat controls, and variable intake controls. Any of these may be required on a given engine installation depending on the aircraft application, and in a full study the interaction of the closed loop would require investigation.

However, the principal loop and the one requiring highest performance on an engine installation is the speed governor and this will be considered further in the following sections.

3. Control System Development Using Computer Techniques

The system to be analysed here by way of example is one which does not exist in its entirely on any present engine but it is hoped by means of the example to show how the control system design can be developed along lines which will provide the optimum operation for a given application.

We shall assume that initial discussion between the engine and accessory manufacturers have suggested a system based on a variable displacement piston type pump and an altitude corrected flow control. The pump is engine driven and its displacement is varied by means of a servo-operated piston controlled by the flow control signal. The flow control measures the fuel flow as a pressure drop across a restrictor and this pressure drop is compared with a selected pressure drop and the error signal used to control the pump servo piston. It can be seen now that if we control the restrictor size by means of an altitude control, and the selected pressure drop by means of the pilot's throttle, we have a simple "schedule system" described earlier. This principle uses the well-known hydraulic equation for turbulent flow through a restrictor where flow is proportional to the restrictor size and the square root of the pressure drop across it.

In our example we propose to retain the altitude control but to vary the selected pressure drop, and therefore the fuel flow by means of an engine speed error sensing device. This then controls the fuel flow to maintain a governed rate of revolutions and we have replaced the scheduling system by a speed-controlled closed loop system.

This system can then be represented in block diagram form as shown in Fig. 3, where it can be seen that the main loop (shown in double lines), has two subsidiary loops.

It should be noted that the retaining of the altitude corrected flow control when "closing the loop" has two advantages. In the first place, as the aircraft is flown to high altitude, the range of fuel flow allowed by the fuel system from idling to full throttle is considerably reduced. Secondly as the "gain" of the engine (rev/min. change for fuel flow change) increases with altitude, the gain of the fuel system (fuel flow change for rev/min. change on governor) is reduced by the altitude control, so maintaining approximately constant "loop gain."
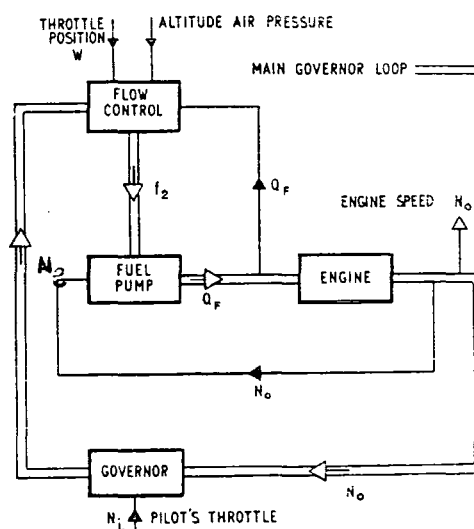
Fig. 3. Block diagram of engine control problem.

In our example, with the altitude control retained we would expect that on open loop, or scheduling control, we would have a possible engine speed variation of, say, ± 400 rev/min. about a datum and our aim is to reduce this wander to less than ± 20 rev/min. It is necessary to restrict overshoots and to achieve change in selected datum in the minimum possible time. For the purpose of illustration of the techniques to be adopted, we shall neglect the special requirements of acceleration control, idling datum shift, jet pipe temperature control etc. and investigate solely the behaviour of the loop shown in Fig. 3.

3.1. *Linearized Analysis of Proposed System Components*

3.1.1. Flow control and pump

In order to establish the complete transfer function for the flow control and pump system it is necessary to have a preliminary idea of the type of system envisaged. In our example this is taken to be of the form shown in Fig. 4 which shows how the pump displacement lever is moved by the control valve f_2 through a hydraulic amplifier. This valve f_2 is moved by the flow control to establish a balance between the pressure drop across the restrictor f_E and the load applied by the throttle lever W. Restrictors f_3 and f_4 represent the fluid friction in the pipe lines to the diaphragm chamber when movement is taking place following a disturbance.

It should be noted that this is the basic concept of the devised system; deviations in performance and their effects will be considered later when the initial design analysis of the whole loop has been carried out.

We shall now establish the individual transfer functions for the pump and flow control showing the response of the fuel flow change to a change in throttle position W. Modifications will be made later to show how the speed signal is to be introduced to the flow control.

To simplify the mechanism of analysis we will assume that Δ implies the total small variation of any parameter about a datum value. At this stage it is implied that the analysis to follow is linearized and Nyquist criterion for stability would be used to estimate the system performance if analogue techniques were not used.

The pump and flow control are considered separately as follows:

(a) Pump: Fixed Speed.

The flow equation for an incompressible fluid flowing through a restriction is

$Q = f\sqrt{(\Delta P)}$ (gallons per hour say)

The linearization of this type of equation can be achieved in many ways, but for simplicity we shall take logarithms and differentiate. The quantities and suffices are as defined in Fig. 4 and it is noted that

Q = fuel flow
P = fuel pressure

f = flow number, which is a function of restriction over coefficient of discharge and fluid density
A = area
R = spring rate

The suffix "0" implies initial or datum conditions.

$$Q_{s1} = f_2 \sqrt{(P_2 - P_a)}$$
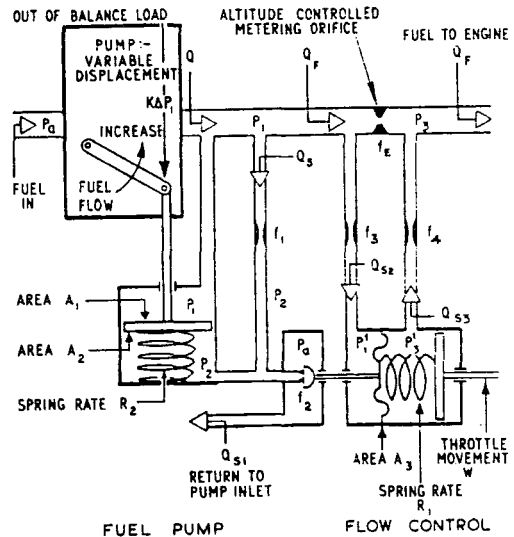
Fig. 4. Schematic diagram of the pump and flow control system.

$$\frac{\Delta Q_{s1}}{Q_{s10}} = \frac{\Delta f_2}{f_{20}} - \frac{\Delta(P_2 - P_a)}{2(P_2 - P_a)_0}$$

i.e. $\Delta Q_{s1} = \left(\dfrac{Q_{s1}}{f_2}\right)_0 \Delta f_2 - \left(\dfrac{Q_{s1}}{2(P_2 - P_a)}\right)_0 \Delta P_2$

Since in our case P_a is constant. $\Delta P_a = 0$.

Therefore $\Delta Q_{s1} = K_1 \Delta f_2 - K_2 \Delta P_2$ ....(1)

Similarly it can be shown that

$$\Delta Q_s = \Delta Q_{s1} + 13 A_2 \frac{d}{dt} \Delta x$$

$$= \Delta Q_{s1} - K_3 p \Delta Q \qquad ....(2)$$

where 13 is a conversion factor and x is displacement of piston.

$\Delta Q_3 = K_4 \Delta(P_1 - P_2)$ ....(3)

$\Delta Q_F = \Delta Q_s + \Delta Q$ ....(4)

$\Delta Q_F = K_5 \Delta P_1$ (assuming $\Delta P_3 = 0$) ....(5)

Consider out-of-balance loads on the pump servo piston.

$$A_1 \Delta P_1 = A_2 \Delta P_2 - R_2 \Delta x - K \Delta P_1$$
i.e. $\quad (A_1 + K) \Delta P_1 = A_2 \Delta P_2 - R_2 \Delta x \qquad \ldots\ldots\ldots(6)$

where

$$K_1 = \left(\frac{Q_{s1}}{f_2} \right)_0$$

$$K_2 = \left(\frac{Q_{s1}}{2(P_2 - P_a)} \right)_0$$

$$K_3 = m.13 A_2$$

$$m = \frac{\Delta x}{\Delta Q}$$

$$p = \frac{d}{dt}$$

$$K_4 = \left(\frac{Q_s}{2(P_1 - P_2)} \right)_0$$

All constants K_1, K_2, etc. are computed from the steady state or datum conditions. The method outlined above is condensed but shows the technique used in arriving at the pump operational equations (1) to (6), all of which have to be satisfied simultaneously when considering the performance of the system.

Combining equations (1) to (6) gives a complete pump transfer function of the form:

$$\frac{Q_F}{f_2} = \frac{-\beta_1}{1 + \tau_1 p}$$

which is a simple first-order lag with respect to the response of fuel flow Q_F to a change in valve flow number, f_2.

β_1 is the frequency invariant gain constant and τ_1 is the time constant, both of which are only constant for a given set of values of pump delivery pressure and flow datum.

(b) *Flow Control*

By following the same procedure we obtain the following equation giving the transfer functions for the flow control in terms of fuel flow and throttle signal

$$\beta_2 \Delta Q_F = (1 + \tau_2 p) \Delta f_2 = B_3 \Delta W \qquad \ldots\ldots\ldots(7)$$

3.1.2. Gas turbine engine

The transfer function of the engine itself is calculated from the known aerodynamic characteristics of the engine components. In our example we will consider the engine

transfer function to consist of two simple time constants and one time delay lag. The time constants represent the effects of engine rotor inertia and the inflation time of the engine air space. The time delay is an item not yet fully understood, but it has been shown by response testing to exist on some engines and it may be connected with the type of combustion chamber or fuel burning system used.

$$\frac{\Delta N}{\Delta Q_F} = \frac{K \exp(-\xi p)}{(1 + \tau_1 p)(1 + \tau_2 p)}$$

Typical values which will be used in the investigation given here representing sea-level static operation of an engine are:—

$\quad K = 2.5$ rev/min. per gal/hr; $\xi = 0.10$ sec;
$\quad \tau_1 = 0.8$ sec; $\tau_2 = 0.05$ sec.

3.2. *Analogue Computer Analysis of System*

Having decided on the characteristics of what might be termed the invariable components of the system, namely the pump and flow control and the engine itself, we are now able to consider the type of system to be used for closing the loop and satisfying the control system operational requirements.

We are free to vary within limits the constants of the fuel system components but not the form of equations. We are given an entirely free hand however to specify the type and behaviour of additional equipment which may be added and we will therefore examine in detail some of these possibilities to show how the choice can be made.

It is necessary to review the way in which a speed governor behaves on an aero engine to appreciate the way in which engine speed may vary. (See Fig. 5.)

If we are to use a pure "scheduling system," it has been stated that we may expect a total speed variation at a fixed throttle position of ± 400 rev/min. Conversely, the fuel flow required for constant speed can vary by ± 160 gal/hr using the engine characteristic quoted above.

In order to provide a governing system to maintain engine speed within ± 20 rev/min, a loop gain of the order of 20 is required. It will be shown, however, that this is impossible with a system using only proportional control because of instability. In practice a lower gain must be employed and means provided of

eliminating the resulting change of speed or "creep" as it is known.

3.2.1. Proportional governor control

An additional valve is now to be added to the flow control so that the pressure difference appearing across the diaphragm (in Fig. 4) in the flow control may be made some variable proportion of that across the main metering orifice f_E.

Hence $(P_1{}' - P_3{}') = k(P_1 - P_3)$

Now the pump and flow control system works so that $(P_1{}' - P_3{}')$ is kept to the value selected by W and hence we can vary $(P_1 - P_3)$ and also the fuel flow, by varying the ratio k.

Fig. 5. Engine fuel requirements and governor rate curve.

This additional means of fuel flow control is provided by putting a fixed restrictor at f_3 and a variable restrictor f_5 as a bleed from the diaphragm chamber as shown in Fig. 6.

The operation of the flow control is now as follows. There are three means of varying the controlled fuel flow: —

(a) The size of the metering orifice f_E is altitude controlled and therefore provides approximately the required proportional control of fuel flow with change of height.

(b) The spring force is varied by the input signal W which would be linked directly to the throttle to provide schedule fuel control. The governor signal could be combined with the throttle linkage to act on the movement W but it is an advantage to separate this by the addition of the third control.

(c), which is the variation of the restrictor f_5 as described above. This avoids the necessity

Fig. 6. Scrap view of flow control showing addition of control orifice f_5.

for the governor signal going through a flow control throttle servo, which necessarily would add a large time constant to the loop.

The equation for the flow control now needs to be modified to include the effect of this governor controlled bleed and hence a relationship is established for the response of the valve f_5 following a change of f_5.

The complete flow control equation is given by

$$\beta_2 \Delta Q_F - \beta_1 \Delta f_5 - \beta_3 \Delta W = (1 - \tau_{2p}) \Delta f_2$$

where β_2, β_3, and β_1 and τ_2 are constants for the flow control.

The pilot's throttle will control both W, which schedules a fuel flow, and the selected governor datum. Hence to obtain the full system analysis and results for a step change in throttle position both inputs ΔW and Δf_5 must be retained in this equation.

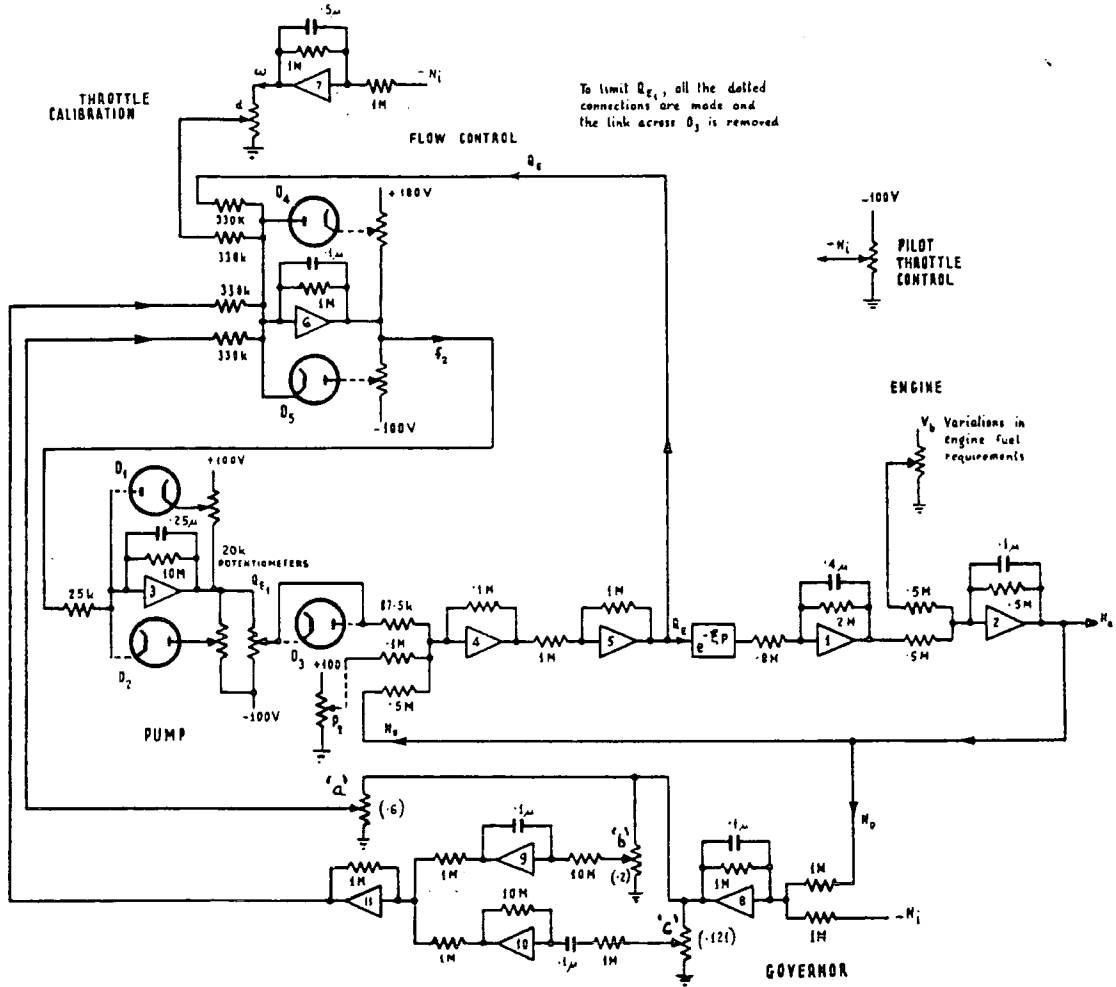**Fig. 7.** Application of governor speed signal to movement of valve f_5.

Fig. 8. Computer set-up for complete system.

Figure 7 now shows the way in which the speed error signal is applied to the valve lift through a normal governor weight and spring device driven directly from the engine. The governor datum is altered by the cam on the spring linked to the pilot's throttle and the system gain is determined by the governor spring rate.

The change in the flow number of the flow control valve f_3 is given directly by the linearized equation $f_3 = Z_1 N_e$ where N_e is the speed error.

The system is fully linearized and can be applied to the analogue computer by standard

methods. Fig. 8 shows the computer set up for the complete system. When simulating a proportional governor, the coefficients "b" and "c" are zero and the limiters are out of circuit. The potentiometer "a" is used to represent the adjustment to loop gain provided by changing the spring rate.

Figure 9 shows the result of a step change in selected engine speed from 8000 to 8600 rev/min when the gain is adjusted to 6. The

results throughout are shown for an engine operating under conditions when maximum positive errors exist. With this gain the band width of possible variation is ±80 rev/min and is not acceptable. In addition overshoot and damping are poor and additional means
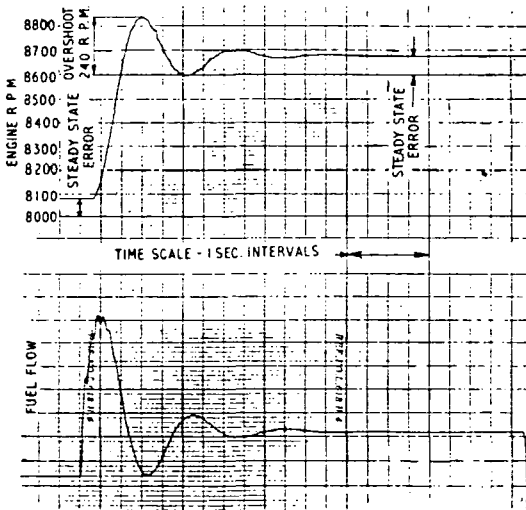

Fig. 9. Response of engine to throttle change from 8000 rev/min—8600 rev/min with proportional system. Loop gain=6.

are required of improving these conditions. It is seen that there is an initial overshoot of 240 rev/min above the selected datum.

3.2.2. Removal of steady state error

A method of improving the accuracy of the governor other than by increasing the gain must now be found. We can accept the error for a short period of time, say 6 seconds during which time some means is needed of trimming out the error. This can be done in several ways and for our purpose here we will consider a direct approach where the error continues to be removed until the governor weights and arm have returned to a unique position. This position will only be reached when the speed error is zero.

The controlling influence of the governor on the fuel flow relies on a change in f_3. Hence some way to modify f_5 must be found in order that the governor arm may be allowed to retain its unique position with zero speed error.

This can be done as shown in Fig. 10 where f_5 has now been replaced by f_5' and f_5''. Here the valve f_5' is in parallel with a long taper needle f_5'', so that the effective flow number f_5 is now the sum of f_5' and f_5''. The position of f_5'' is controlled by a piston having a fixed pressure difference across it. A bleed hole allows fuel through the piston and out of a further variable restrictor valve controlled by the governor arm. It can be seen that the needle valve piston is stationary only when the flow through the piston restrictor f_6 equals that through f_7. With a constant pressure drop across f_5' this condition will exist when the governor arm is in its unique position.

It is noted that the system as described will wander if the supply pressure to the engine P_2 varies. Addition of a constant pressure valve across f_5' is therefore necessary.

The equation for the governor is now modified as follows:

$$\Delta f_5 = \Delta f_5' + \Delta f_5'' = Z_1 N_e + Z_2 \int f_2 \, dt$$

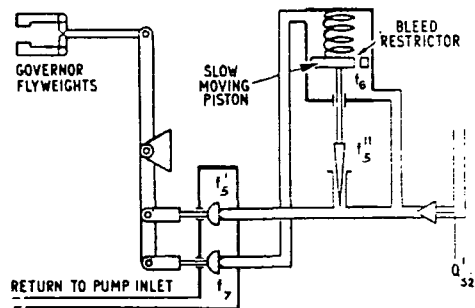$$= Z_1 N_e + Z_2 \frac{N_e}{p} \quad (\text{since } f_2 \propto N_e)$$

Fig. 10. Method of removing steady state error.

The integrating constant Z_2 is adjusted by the dimensions of the system. On the computer set up in Fig. 8 this integration is introduced by adjustment of potentiometer "b" to give the best rate of removal of the error without too great an increase in the value of the overshoot.

Figure 11 shows the results of this computer test when the integrating constant has been chosen so that the possible ± 80 rev/min error can be corrected in a time of 6 seconds. It is seen now that the initial overshoot has been
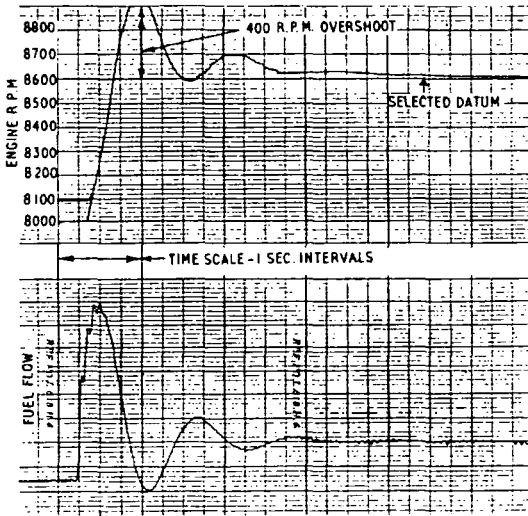
Fig. 11. Response of engine with addition of integrator—removal of steady state error.

increased to about 400 rev/min due to the introduction of the integration.

3.2.3. Limitation of initial overshoot

The initial overshoot which is seen to be of the order of 240 rev/min on Fig. 9 and 400 rev/min on Fig. 11 requires reduction. This overshoot could be reduced by lowering the loop gain but the rate of response would also suffer and the system would become too sluggish. Alternative means must therefore be found to limit the overshoots.

The method to be described is an addition to the governor flyweight system. Use is made of hydraulic pressure for transmitting signals
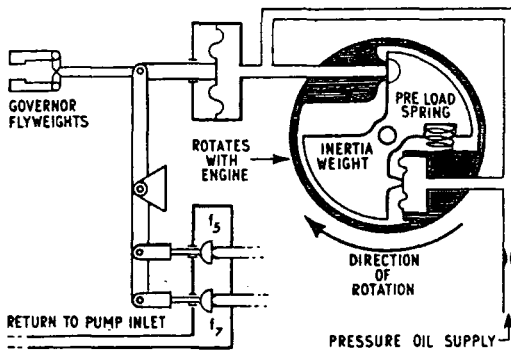
Fig. 12. Method of reducing overshoot of engine speed.

and bellows for changing the pressure into an applied force. The rate of change of engine speed, or derivative signal, is derived by measuring the force needed to accelerate a floating inertia weight at the same rate of acceleration as the engine. Fig. 12 illustrates how this force is measured.

The inertia weight is carried inside a rotating shell running on a direct drive from the engine, normally on an extension from the flyweight governor. Oil is supplied through the drive shaft and a fixed restrictor, to a pressure diaphragm and a variable restrictor. As the engine accelerates the inertia weight lags slightly so closing the variable restrictor.

This builds up pressure in the diaphragm to apply an accelerating force to the inertia weight. When in equilibrium it is seen that the change of oil pressure in the diaphragm is always proportional to the rate of change of engine speed. This pressure is then applied to a second diaphragm on the governor arm to bias the force applied by the governor flyweights.

The signal applied to the governor arm is then proportional to the rate of change of engine speed, but because flow is required to inflate the diaphragm it is subject to a single inflation time constant.

The total effect on f_s is then given by:

$$\Delta f_s = \left[Z_1 \div \frac{Z_3 p}{1 + \tau_{3p}} \right] N_e \div \frac{Z_2}{p} . N_e$$

where the second term in brackets represents the effect of the inertia weight.

On the computer set up in Fig. 8 this effect is introduced by adjustment of the potentiometer "c." Fig. 13 shows the results when the optimum setting of the potentiometer is chosen.

It is seen now that the overshoot has been restored to 240 rev/min with the proportional control of Fig. 9. This would still be too high an overshoot when accelerating to maximum revolutions although would probably be accepted for lower ranges. A non-linear means of reducing this overshoot at maximum revolutions is shown later.

Figure 14 shows the effect of the derivative term only on the proportional governor when it is seen that the overshoot is reduced from 240 to 160 rev/min.
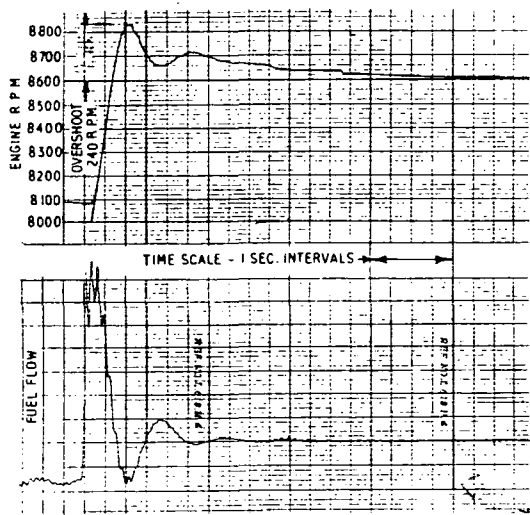
Fig. 13. Response of engine with addition of integrator and derivative term—zero steady state error and reduction of overshoot.
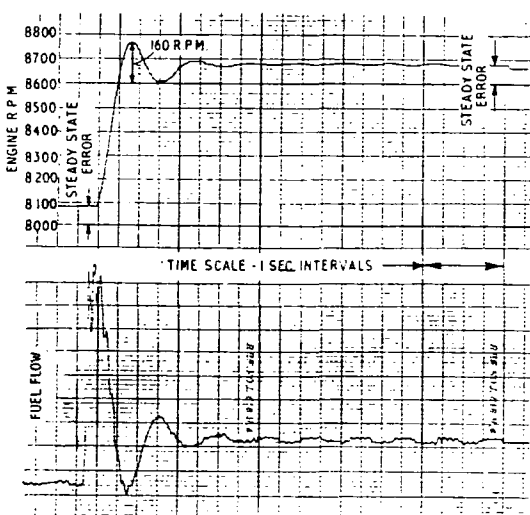

Fig. 14. Response of engine with proportional and derivative terms—reduction of overshoot to 160 rev/min.
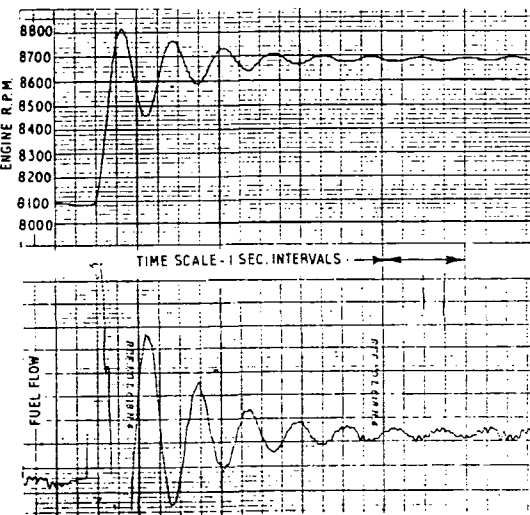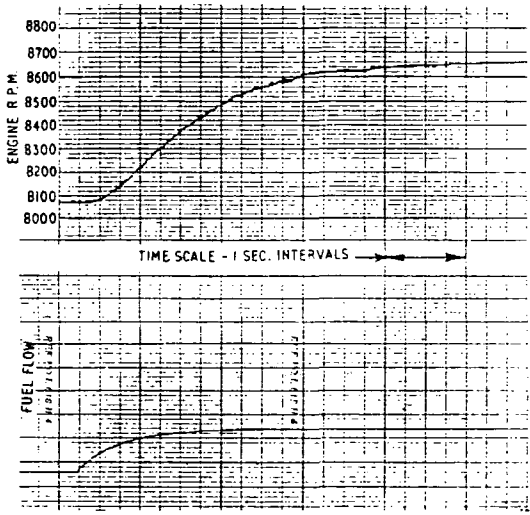

Fig. 15. Effect of increasing derivative term

Fig. 16. Engine response with schedule system only.

Increasing the derivative term produces a destabilizing effect as shown in Fig. 15.

3.3. *Results of Linear Analysis*

Taking a survey of the results so far we can see how the response of the engine to a step change in throttle position (i.e. selected engine speed) has been improved by the addition of the modifying elements in the device closing the loop.

When the optimum values have been chosen from this linear analysis the values of the constants can be specified and the detail design of the system components can commence.

For comparison the response of the engine with a scheduling system only is shown in Fig. 16 for a speed change of 600 rev/min when it can be seen at once how the response to throttle movement has been improved by the governor (see Fig. 13).

We have of course only considered one particular engine operating condition (namely, sea-level static) in our work given here. As stated before, the engine is to operate under many combinations of altitude and forward speed. Governing at different engine settings must be considered, and variation in the engine transfer function allowed for when the engine is used to supply power for aircraft services or compressed air for cabin pressurization, etc. The study must cover all the possible variations before the constants for the various control components can be finally specified.

4. Introduction of Non-Linearities

When the work has progressed so far and the basic operating constants have been specified so that the mechanical design of the components can proceed. it is necessary to make a much deeper exploration of the system. In particular when the components have been given detailed design consideration. the possible sources of additional disturbances must be considered. The flow control and pump for example must be examined to make an assessment of where

(a) friction forces may affect their operation;

(b) limitation of travel of valves and pistons may put restriction on the control;

(c) the types of valves proposed do not have linear characteristics;

(d) their position is to be affected by fuel pressures under the valve seats.

Where it is thought that any of the effects may constitute an important modification to the basic transfer function it is necessary to modify the constants given for the design of the system or recommend changes in the type of design to reduce their effects. In some cases, of course, the effect may be beneficial in which case recommendations can be made so that the effect can be retained as a permanent design feature.

Finally consideration should be given to the possible introduction of deliberate non-linear effects. These may be used in certain cases to make further improvements in the response of a system.

4.1. *Examination of Practical Design Components*

Typical pump and flow control diagrams which illustrate practical designs based on the principles we have been considering are shown
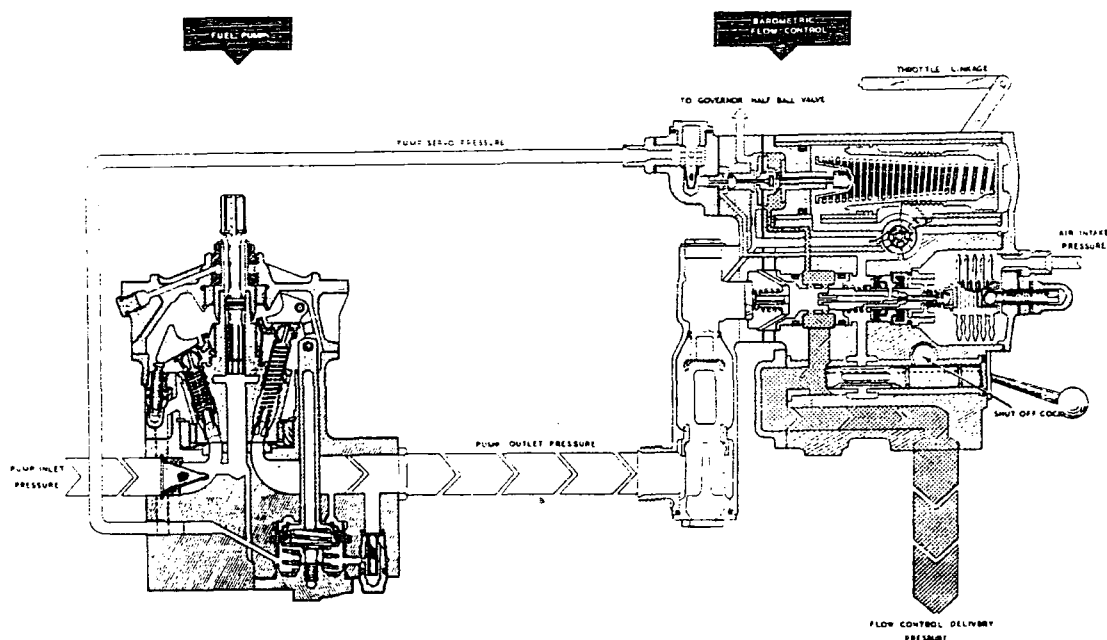

Fig. 17. Schematic diagram of components of hypothetical fuel system.

in Fig. 17, where it can be seen that many additional features have to be added to make the system a reality.

The need for the original simplified diagrams where basic considerations only are used can now be seen.

In considering the cases of the pump and flow controls as shown in Fig. 17 the following are the major non-linearities which should be considered and applied to the computer:

(a) Friction of seal on pump servo piston.

(b) Limitation of travel of pump servo piston. This provides a maximum fuel flow stop which may help to limit overshoots on acceleration to maximum revolutions.

(c) Limitation of travel on valve at the end of the pump servo pressure line. (This is shown as valve f_2 in Fig. 4.) The type of valve chosen is called a "half-ball valve" and the change of flow number is approximately proportional to the valve lift over a limited range.

(d) Friction in push rods between the half-ball valve, the diaphragm and the throttle spring.
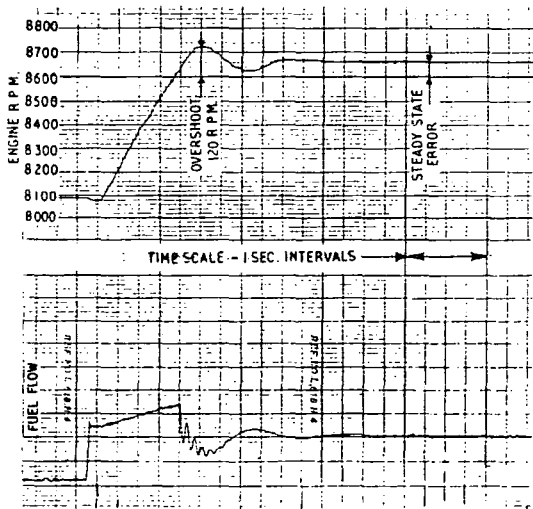

Fig. 18. Response of system with limitation on pump displacement.

A similar survey could be made of the other components in the system such as the governor arm and its associated items previously discussed.

For the purpose of illustration we shall consider the effect of (b) above. Limitation of maximum fuel flow is used on some existing simple governor systems in order to achieve satisfactory handling without the use of derivative devices.

The way in which fuel flow limitation can affect overshoot of engine speed is shown by the computer results given in Fig. 18. This non-linearity has been applied to the computer set-up shown in Fig. 8. The results given are for proportional control only. It can be seen that the maximum overshoot is reduced from 240 rev/min to 120 rev/min. A similar improvement would be shown with the derivative and integral terms added bringing the maximum overshoot to acceptable limits.

Other non-linearities can be treated in a similar way on the computer.

5. The Present Position and Future Trends

The examples given in the preceding sections show in a general way the development of a suitable fuel governor system for an aero engine. The procedure followed illustrates how a system based on an initially conceived idea of a pump and flow control may be developed to give the required handling and stability characteristics. The full work would, of course, include considerations of altitude and high forward speed operation where the engine "gain" may cover the range from 2 to 10 and its main time-constant vary from 0·8 sec to 11 sec.

The system as determined for the sea-level case may require either some compromise in results to satisfy also altitude conditions or additional components may be required, so extending the procedure described.

The control engineer must of course bear in mind the many other requirements of the system in addition to the governing requirements and these must also be developed alongside the governing system.

The development of an aero engine from its initial project stage to bench and flight testing is a process occupying several years of work, and as yet a control system based on this type of investigation has not yet reached a testing state on a new engine. When such a stage is reached, considerable bench and flight testing time will be saved.

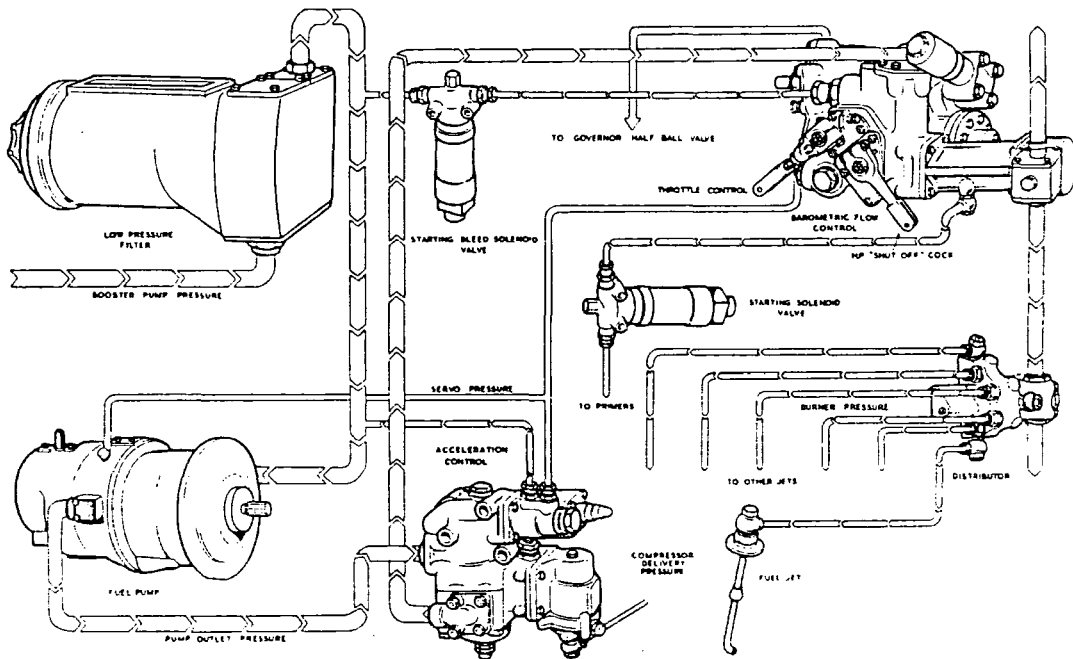ANALOGUE COMPUTER FOR AERO ENGINE CONTROL PROBLEMS

Fig. 19. Complete hypothetical fuel system

On systems which have been analysed by computer techniques equivalent test-bed running has shown results to be quite consistent, bearing in mind that the method still requires further development as mentioned below.

The importance of following up the analysis work with response testing as the manufactured components become available cannot be over emphasized. At its best, the mathematical analysis of the behaviour of each component must simplify the component. Any important deviations from the theoretical design therefore should be found as soon as possible so that their effects may be studied. Where non-linearities are involved, the normal response testing techniques fall down since the output of the component is then sensitive to input amplitude as well as input frequency. It is therefore necessary to carry out response testing with varying amplitude as well as varying frequency.

In conclusion it will be an advantage to discuss briefly the way in which further development of computer techniques will enable more reliable predictions to be made. Accuracy is limited at the moment by incomplete knowledge of the engine behaviour when operating under transient conditions away from its normal steady state working line. The engine transfer function quoted earlier is true only for small disturbances and the values of the constants as well as the assumption of strict linearity must be in doubt for larger disturbances.

With the development of engine simulation over greater operating ranges will come the possibility of incorporating acceleration controls and the determination of the most desirable form of such controls. This is a subject which at the moment occupies a considerable proportion of the available flight testing time. Any assistance that can be given to reduce this testing therefore would be of considerable advantage.

Figure 19 shows a complete fuel system (not including the governor) where other essential items have been included to show that the pump and flow control loop is but one consideration in the system. The other items are essential components which cater for the other running and starting problems on the engine, conditions which require very full consideration but do not come under our present problem of governing.

6. Conclusions and Acknowledgments

A review has been given of the present state of analogue computer application to aero engine control system development together with specific examples taken for the purpose of illustration. It can be seen that whilst the present techniques provide very real assistance in control system design, refinements are necessary, particularly in our ability to understand engine transient conditions.

This paper has shown the benefits to be gained by analogue simulation in the field of engine control system design.

As further non-linear effects are appreciated simulation techniques must be developed by co-operation between the computer designers and the control system engineers. The preparation of this paper has been an example of this co-operation and the authors are indebted to the managements of Elliott Bros. and Armstrong Siddeley Motors for permission to carry out this work.

PAPER 4

Analysis of a Gas Turbine Engine Fuel System

By J. SCHWARZENBACH, M.Sc.,* and K. F. GILL, M.Sc., Ph.D.*

Linearised control theory is applied to the design of a hypothetical fuel control system in order to determine the most suitable combination of terms in a governor three-term controller. The results obtained from frequency response techniques are compared with those obtained from transient performance data, and this information is used to determine the usefulness of root locus plots in the design of the system. It is shown how over-simplification, before qualitative understanding of components becomes quantitative, may lead to completely misleading results. The conclusions are drawn that estimation of system performance is possible from harmonic response data providing experience has been gained in the design and testing of similar systems of known harmonic response characteristics; the Nichols chart is the most convenient method of display for obtaining the harmonic response characteristics of the system; the Root Locus method is superior to the harmonic response method when design information is necessary on the transient response characteristics of the system ; experience with the root locus method gives a more clear picture of the effects on system performance arising from the introduction of additional elements into the system loop than is possible from harmonic response data; and that neglect of apparently small valued time constants without preliminary system investigation could result in incorrect selection of compensating term coefficients during system design.

THE demand for ever increasing engine performance has brought about the need for greatly improved accuracy of speed control. The control systems required for accurate scheduling for installations working on widely and continuously varying load requirements are extremely complex, and difficult to design and calibrate, and most current design applications are based on closed loop control theory. The effect of closing the scheduling loop of any system is to alter both the static and the dynamic response of the system. It may make the system more accurate, faster, or smoother, or it may introduce instabilities which will make the system unstable, depending on the nature of the feedback signal used. To facilitate a clearer understanding of such systems, a hypothetical system has been analysed using the well proven linear control theory, and the results are presented in this report.

* Department of Mechanical Engineering. University of Leeds.

1. THE HYPOTHETICAL SYSTEM

The hypothetical system investigated was based on a previous study[1] indicating the use of an analogue computer for the design of an aero-engine fuel control system. The purpose of the present investigation is to determine the relative usefulness of the different techniques available for analysis of system stability and performance. The transient response of the simulated system to a step input in speed selection is used as a criterion to determine the influence on system performance of the variation in the basic settings of each term (proportional, integral and derivative) in the "three term" governor controller unit used in the system analysed. The optimum combination of these three governor coefficients is also selected from the transient response data, since a step input can be characterised as the most severe disturbance to which any linear control system can be subjected.

The techniques to be discussed in this article, namely root locus plots and Nichols charts, are fully described in many text-books and research papers on control theory, and a useful bibliography is given at the end of the article. The more familiar Nyquist diagrams used in system frequency analysis are included in the report for interest, but the Bode diagrams are not included, since all the relevant information is equally well displayed on a Nichols chart.

It must be understood that system diagrams or engineering drawings of control systems are generally too congested with detail to be immediately usable. It is, therefore, essential to use a clear-cut method of simplification when dealing with systems of a complicated nature, otherwise the study will be burdened with much unnecessary detail. The "block diagram" (such as in Fig. 2) is the usual method of system representation to show in a compact way the inter-relationship between the elements in an otherwise complex system arrangement. The preparation of an equivalent schematic diagram (as in Fig. 1) is the first convenient step towards establishing the principle components and parameters in the system, and thereafter the preparation of the block diagram follows as a logical development. It is generally unwise to oversimplify the schematic representation until it is certain that the diagram truly represents the dynamic problem to be studied.

The dynamic equations used in this analysis have been expressed in the Laplace Transform notation, and this enables the complete mathematical description of the dynamic system behaviour to be specified with the minimum of writing. Further, when the behaviour of the system is described with the aid of transfer relationships, it is often possible by inspection alone to deduce many interesting properties of the system.

2. SYSTEM AND SIMULATOR CIRCUIT

2.1. DESCRIPTION OF FLOW CONTROL SYSTEM

The system used in the investigation is shown schematically in Fig. 1. The units comprising the system are all hypothetical items assumed to be representative of proprietary items commercially available. The three basic elements shown in Fig. 1 are:

(a) *Pump.*—This unit is assumed to be a variable displacement engine-driven pump which is controlled by means of an integral positional hydraulic servo.

(b) *Flow Control Valve.*—This device monitors the pressure drop across a metering orifice f_1 and uses the signal to position the

---

Nomenclature:

$\left.\begin{array}{l} A_1 \\ A_3 \end{array}\right\}$—Pump servo piston areas.

a_1–a_n—Equation coefficients.

$\left.\begin{array}{l} a \\ b \\ c \\ d \end{array}\right\}$—Potentiometer settings (see Fig. 4).

f—Generalised flow number.
f_1—Flow number of altitude controlled metering orifice.
f_2—Flow number of pump servo half-ball valve.
$\left.\begin{array}{l} f_3 \\ f_4 \\ f_6 \end{array}\right\}$—Flow restrictors.
$f_6 = f'_6 + f''_6$
$\left.\begin{array}{l} f'_6 \\ f_7 \end{array}\right\}$—Integrating mechanism flow restrictors.
$\left.\begin{array}{l} f_8 \\ f_9 \end{array}\right\}$—Derivative mechanism flow restrictors.
$\left.\begin{array}{l} f(s) \\ g(s) \end{array}\right\}$—Polynominals in s.
$G(s)$—Transfer function for (Flow Control +Pump+Engine).
$G_1(s)$—Transfer function for governor.
I—Engine rotor inertia.
$\left.\begin{array}{l} K \\ K' \end{array}\right\}$—Gain parameters for characteristic equation.
K_1–K_6—Equation constants.
k—Integration constant.

M_p—Peak resonance amplitude.
m—Fuel pump parameter.
N—Generalised engine speed.
N_c—Engine speed error.
N'—Governor derivative mechanism speed parameter.
N_s—Selected engine speed.
N_a—Actual engine speed.
P—Generalised pressure.
P_c—Compressor delivery pressure.
P_{LP}—L.P fuel pressure.
P_1—Pump delivery pressure.
P_2—Pump servo pressure.
P_3—Turbine inlet pressure.
P_4—Servo pressure (derivative control).
p—Modified Laplace operator.
Q—Generalised fuel flow.
Q_1—Fuel pump delivery flow
Q_T—Engine fuel flow.
$\left.\begin{array}{l} Q_1 \\ Q_{11} \end{array}\right\}$—Pump servo flows.
$\left.\begin{array}{l} Q_{12} \\ Q_{13} \end{array}\right\}$—Flow control servo flows.
Q_{14}–Q_{17}—Governor servo flows.
q—Engine air mass flow.
q_T—Turbine air mass flow.
R—Universal gas constant.
r—Pump servo spring rate.
s—Laplace operator.
t—Time.

T—Engine torque.
T_2—Compressor delivery temperature.
T_3—Turbine inlet temperature.
W—Throttle movement.
V_2—Combustion zone secondary volume.
V_3—Combustion zone primary volume.
x—Pump servo piston displacement.
$\left.\begin{array}{l} y_1 \\ y_2 \end{array}\right\}$—Diaphragm movements.
Z_1—Governor proportional term.
Z_2—Governor integral term.
Z_3—Governor derivative term.
z—Integrating lever arm movement.
α—Angular displacement of inertia disc of derivative mechanism.
$\left.\begin{array}{l} \beta_1 \text{-} \beta_3 \\ \beta_4 \end{array}\right\}$—Frequency invariant gain terms.
Δ—Finite change from steady state datum.
τ_1–τ_6—Time constants for control elements.
τ_r—Engine rotor inertia lag.
τ_c—Combustion zone inflation lag.
μ_1–μ_{10}—Equation constants.
ω_n—System natural frequency.
ω_p—Peak resonance frequency.
ζ—Damping factor.

Subscript o—Datum condition.
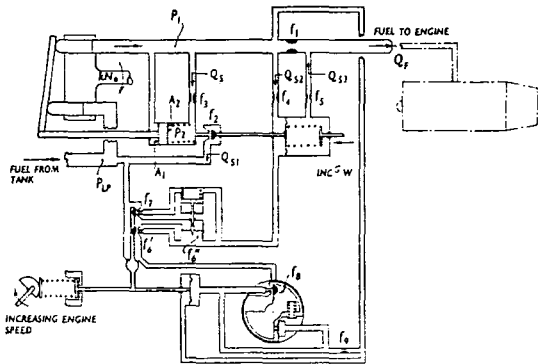
Technical Contributors Section *(Continued)*

Fig. 1—Diagram of engine
fuel control system

half-ball valve f_2 of the pump positional
servo. The hydraulic principle used is well
known commercially.

(c) *Governor.*—Basically this unit is a
hydraulically actuated three term controller.
The hydraulic circuit shown in Fig. 1 is one
possible way of obtaining proportional.
derivative and integral action. The numerical

can be derived separately as outlined in the
Appendix, and these are quoted below.
   (a) *Pump.*—

$$\Delta Q_F = -\frac{\beta_1 \Delta f_2}{1 - \tau_1 s} - \beta_3 \Delta N_0 \quad . \quad . \quad (1)$$

where β_1 and β_3 are frequency invariant gain
constants and τ_1 the time constant due to lag

Fig. 2—Multiloop feed-
back control system

values chosen in the analysis are assumed to
be practically possible with this form of
compensation device.

2.2 DESCRIPTION OF ANALOGUE CIRCUIT

The analysis of the hypothetical system was
carried out on a "PACE" 221R analogue
computer, and the circuit layout used is
shown in Fig. 4 with each control element
and the engine indicated in separate blocks.
Variation in the coefficients of the governor
was achieved by alteration of the potentio-
meter settings *a*, *b* and *c*. Variation
of the engine fuel requirements about any
engine operating datum could be achieved by
variation of the potentiometer setting *d*,
and the associated initial conditions were
introduced in the normal way. The setting
used for each potentiometer in the circuit is
indicated, together with the multiplying
coefficients for each amplifier.

3. THEORY

3.1. DERIVATION OF TRANSFER FUNCTIONS

In order to derive a complete set of transfer
relationships for the hypothetical control
system under consideration it is necessary to
make certain plausible assumptions. The
most important of these is to assume that
perturbations about the datum conditions
are small, and hence that a linearised theory
can be applied. The equations describing
the transfer relationships for the four parts
into which the system has been subdivided

in the controlling servo. The numerical value
for each of these constants for the particular
datum conditions used can be calculated
from the normal flow/speed characteristics
of the pump.

(b) *Flow Control Valve.*—

$$(1 + \tau_2 s)\Delta f_2 = \beta_2 \Delta Q_F - \beta_1 \Delta f_3 - \beta_3 \Delta W \quad . \quad (2)$$

where β_2, β_3 and β_4 are gain constants and τ_2
a time constant. the numerical values for
which are obtained from the characteristics of
the flow control valve.
   (c) *Governor.*—

$$\frac{\Delta f_4}{\Delta N_c} = Z_1 + \frac{Z_2}{s} + \frac{Z_3 s}{1 + \tau_3 s} \quad . \quad . \quad (3)$$

and

$$\Delta N_c = \frac{\Delta N_i - \Delta N_0}{1 + \tau_4 s} \quad . \quad . \quad (4)$$

Z_1, Z_2 and Z_3 are the loop variables for the
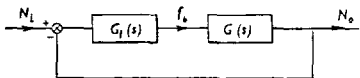proportional. integral, and derivative terms

Fig. 3—Reduction of system in Fig. 2

of the governor respectively, and τ_4 is the
lag in the error sensing unit.
   (d) *Engine.*—

$$\frac{\Delta N_0}{\Delta Q_F} = \frac{\beta_5}{(1 - \tau_5 s)(1 - \tau_6 s)} \quad . \quad . \quad (5)$$

where τ_5 is the rotor inertia lag, τ_6 the com-
bustion zone inflation lag, and β_5 the fre-
quency invariant gain term derived from the
engine performance characteristics.

The system can now be represented most
conveniently by the block diagram. Fig. 2.
and it can be seen that the system contains
two minor feedback loops in addition to the
main feedback loop. It is assumed for this
analysis that the engine is operating with an
all speed governor at constant altitude and
forward speed, and the change in values of
terms p_1 (total intake pressure) and W will be
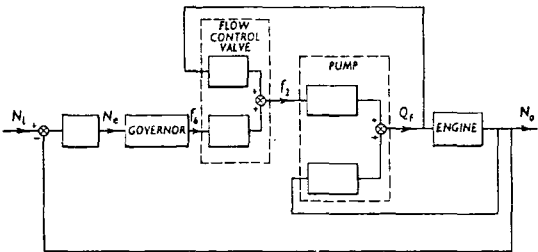zero and hence are not included on the
block diagram.

3.2. DEVELOPMENT OF CHARACTERISTIC EQUATION

3.2.1. *Block Diagram Reduction.*—The
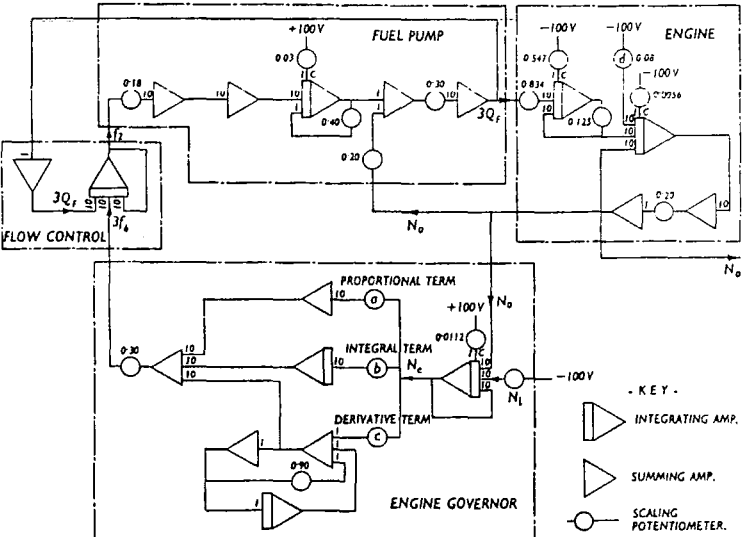block diagram (Fig. 2) may be simplified by

Fig. 4—Computer circuit for engine and control system

combining the transfer relationships for the flow control valve, pump and engine. By manipulation of Equations (1), (2), and (5), and by substitution of the numerical values of the gain and time constants quoted in Appendix I, the following relationship is obtained:

$$G(s) = \frac{\Delta N_0}{\Delta f_s} = \frac{337\,500}{s^4 + 31 \cdot 6s^3 + 5638s^2 + 115\,000s} \\ + 135\,000$$

. . . . (6)

A reduced block diagram can now be drawn, Fig. 3, and this simplified diagram in which minor feedback loops no longer appear can more readily be used for analysis.

3.2.2. *Closed Loop Transfer Function.*— The closed loop transfer function for Fig. 3 is:

$$\frac{G_1(s)\ G(s)}{1 + G_1(s)\ G(s)}$$

Hence the characteristic equation is:

$$1 + G_1(s)\ G(s) = 0$$

For the single-termed proportional governor arrangement (i.e., $Z_2 = Z_3 = 0$) in conjunction with Equations (3), (4) and (6), the characteristic equation becomes numerically equal to:

$$s^5 + 41 \cdot 6s^4 + 5954s^3 + 17\,380s^2 + 1\,285\,000s \\ + (1\,350\,000 + K) = 0$$

where $K = 3 \cdot 375 \times 10^9 Z_1$

In order to reduce the variation in the magnitude of the equation coefficients it is useful to introduce the variable $p = 0 \cdot 1s$, which transforms the characteristic equation to:

$$p^5 - 4 \cdot 16p^4 - 59 \cdot 54p^3 - 17 \cdot 38p^2 - 128 \cdot 5p \\ + (13 \cdot 5 + K') = 0 \quad . \quad . \quad . \quad (7)$$

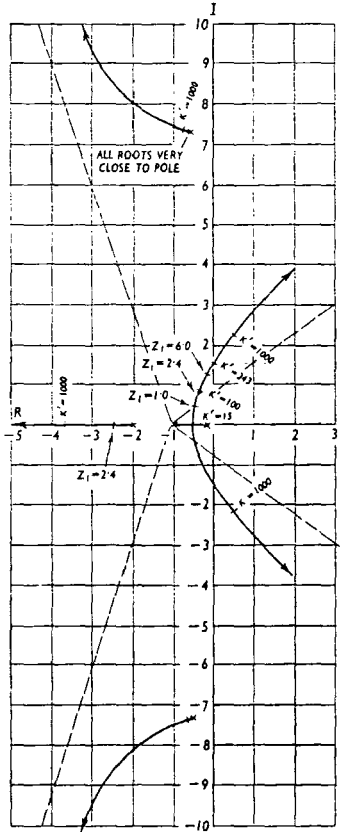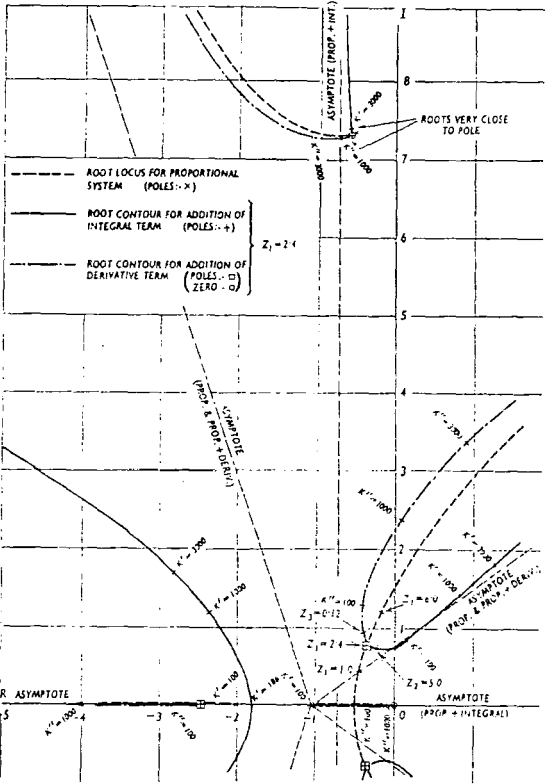where $K' = 33 \cdot 75 Z_1$

Fig. 5—Root locus plot—proportional system

Fig. 6—Root contour plot

3.3. CONSTRUCTION OF ROOT LOCUS

The basic steps in the construction of the root locus plot[2,3] are outlined below for the above characteristic equation, Equation (7).

(a) Starting points: The loci start at the poles of $G_1(s)\ G(s)$ for $K = 0$ i.e. the factors of Equation (7), which are:

$(p - 0 \cdot 125)(p + 1)(p + 2)(p + 0 \cdot 52 \\ - j7 \cdot 32)(p + 0 \cdot 52 - j\,7 \cdot 32)$

(b) Ending points: There are no zeros, hence all loci move ultimately to infinity, approaching asymptotes at 36°, 108°, 180°, 252° and 324°.

(c) Number of loci: Since there are no zeros and five poles there will be five loci.

(d) Intersection of asymptotes: This lies on the real axis at $p = -1 \cdot 04$.

(e) Loci on real axis: There will be loci between $p = -0 \cdot 125$ and $p = -1 \cdot 0$, and to the left of $p = -2 \cdot 0$, since along these sections of real axis the total number of poles and zeros to the right of each section is odd.

(f) Intersection with imaginary axis: By use of the Routh criterion this is found to be at $\pm j1 \cdot 49$.

(g) Breakaway point: A breakaway point exists on the real axis between $p = -0 \cdot 125$ and $p = -1 \cdot 0$, and can be found as a real root of the equation $dK/dp = 0$, and is $p = -0 \cdot 50$.

(h) Using the above information the general shape of the loci can be drawn approximately, and then more accurate curves found by obtaining by trail and error several points on the loci using the angle condition.

(i) Values of K can then be calculated using the magnitude condition, and the position of the required roots found.

The root locus plot for the proportional system obtained with the above information is shown on Fig. 5, and roots for $Z_1 = 1 \cdot 0$, $2 \cdot 4$ and $6 \cdot 0$ are indicated.

3.4. DEVELOPMENT OF ROOT CONTOURS

To study the effects on the closed loop system poles resulting from the addition of integral and/or derivative compensation it is necessary to rearrange the closed loop transfer function in the manner shown below.

Consider the introduction of an integral term into the governor equation. The closed loop transfer function is now:

$$\frac{33 \cdot 75\left(Z_2 - \dfrac{Z_2}{10p}\right)}{p^5 + 4 \cdot 16p^4 - 59 \cdot 54p^3 - 171 \cdot 38p^2 - 128 \cdot 5p \\ + 13 \cdot 5 + 33 \cdot 75\left(Z_1 + \dfrac{Z_2}{10p}\right)}$$

and this can be written as:

$$1 + \frac{\dfrac{33 \cdot 75\left(Z_1 + \dfrac{Z_2}{10p}\right)}{p^5 + 4 \cdot 16p^4 + 59 \cdot 54p^3 - 171 \cdot 38p^2 - 128 \cdot 5p \\ - (13 \cdot 5 - 33 \cdot 75 Z_1)}}{\dfrac{3 \cdot 375 Z_2}{p(p^5 - 4 \cdot 16p^4 - 59 \cdot 54p^3 - 171 \cdot 38p^2 \\ + 128 \cdot 5p + 13 \cdot 5 + 33 \cdot 75 Z_1)}}$$

from which the characteristic equation is:

$$1 + \frac{3 \cdot 375\ Z_2}{p(p^5 + 4 \cdot 16p^4 + 59 \cdot 54p^3 + 171 \cdot 38p^2 \\ + 128 \cdot 5p + 13 \cdot 5 + 33 \cdot 75\ Z_1)} = 0$$

. . . . (8)

It can be seen that the coefficient Z_2 now appears only as a multiplying factor, and hence the conventional root locus technique can be applied. The poles of Equation (8) will include the roots of Equation (7), and for any given value of Z_1 a set of contours can be drawn. In a similar fashion the closed loop transfer function for the addition of a derivative term can be manipulated to yield a characteristic equation amenable to the same process. The two sets of root contours obtained by the addition of an integral term, and a derivative term respectively to the proportional governor are shown in Fig. 6 for the single value of $Z_1 = 2 \cdot 4$.
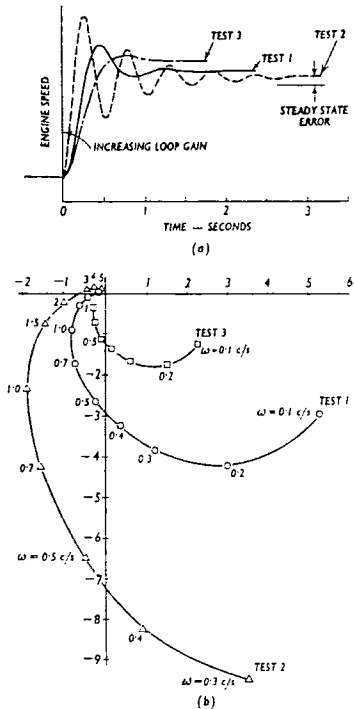
Technical Contributors Section *(Continued)*

(a)

(b)

(a) Transient response.
(b) Nyquist diagram.

Fig. 7—Effect of changes in loop gain of proportional system
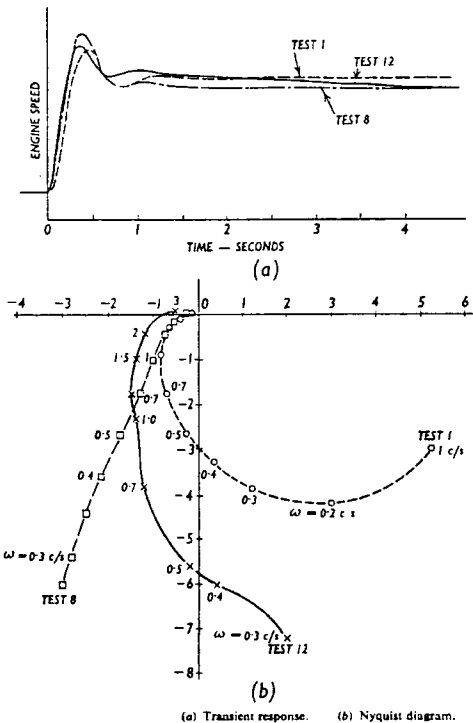
4. PROCEDURE AND RESULTS

To obtain a clear understanding of what effects on the system performance resulted from changes in the value of each term in the governor controller, the simulated system was investigated for both transient and harmonic responses. The harmonic response tests for various combinations of the coefficient settings of the governor terms were carried out, using a commercially available transfer function analyser, and the resulting Nyquist plots are shown in Figs. 7(b), 8(b), 9(b) and 10(b). This information was then transferred to the Nichols chart shown in Fig. 13. The transient response to a step input for the same governor settings is given in Figs. 7(a), 8(a), 9(a) and 10(a). Given in Table I is a summary of the more important data obtainable from all these tests, together with the values of the governor coefficients for each test.

The root locus and root contour plots for the same sets of governor coefficients were constructed in the conventional way as described in Sections 3.2, 3.3 and 3.4. The root locus plot for the proportional system is shown in Fig. 5, and two representative sets of root contour plots are shown on Fig. 6, only one-half of the symmetrical plot being included.

5. DISCUSSION OF RESULTS

5.1. HARMONIC ANALYSIS

True sinusoidal system excitation is seldom encountered in practice, but the technique of frequency response analysis finds justification in its ease of application, and in the practical

usefulness of results obtained from it. This technique enables comparisons between systems to be carried out in an intelligent fashion, and is the basis for system synthesis. It is essential, however, for the design of certain systems to know the transient response characteristics of the system, and methods are available to enable the frequency response data([a,b]) to be translated into transient response data. The classical solution of system equations is generally precluded because of the complex nature of practical systems.

Experience in both linear control theory and engine governing suggests that acceptable engine system performance can be achieved if the harmonic response characteristics of the system lie within the following limits:

M_p ... ...   1·1–1·4
ω_p ... ...   1·1 c/sec. to 1·6 c/sec
Phase margin   ...   40°–50°
Gain margin   ...   6 dB–10 dB
Band width ... ...   1·1 c/sec to 1·5 c/sec

The associated transient performance characteristics considered to be acceptable are:

	Maximum
Rise time	0·3 seconds
Settling time	2 seconds
Initial overshoot	25%
Number of oscillations	1½

and such values should be obtained with the above harmonic response characteristics.

5.2. NYQUIST DIAGRAMS

Fig. 7(a) shows typical transient performance curves for a proportional system in which the loop gain has been changed from 2·5 to 15·1. The effect of increasing

(a)

(b)

(a) Transient response.   (b) Nyquist diagram.

Fig. 8—Effect of addition of integral and derivative terms

(a)

(b)

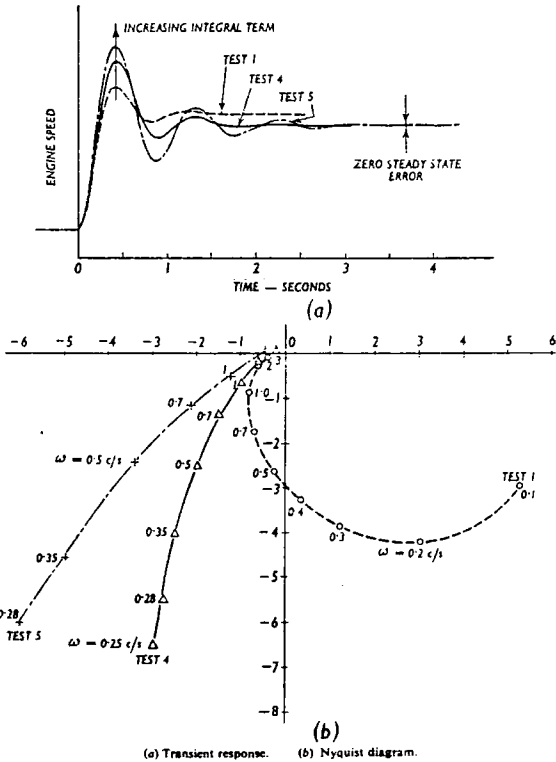(a) Transient response.   (b) Nyquist diagram.

Fig. 9—Effect of addition of integral term

the loop gain can be seen to increase the magnitude of the initial engine speed overshoot and result in a more oscillatory response, i.e. less damping. The Nyquist plots associated with these transient curves are shown in Fig. 7(b): similar frequency points on each Nyquist diagram have the same argument, but a changed loop magnification value. For a loop gain of six the system behaviour is reasonable in so far as it most nearly meets the desired values specified in Section 5.1, but there exists a steady state error which is unacceptable. To achieve isochronous governing, i.e. the elimination

Fig. 10—Effect of addition of derivative term

(a) Transient response.
(b) Nyquist diagram.

of this steady state error, without seriously affecting the system performance it is necessary to introduce "compensation" into the system.

The effect on the transient response of the addition of integral and derivative action to the governor loop can be seen in Fig. 8(a). which shows the elimination of the steady

state error and modification to the form of the transient response curve. The reshaping of the Nyquist plots as a result of introducing this compensation is shown in Fig. 8(b).

The effect of the integral and derivative terms individually can be seen in the transient response curves of Figs. 9(a) and 10(a) respectively. Curves for two values of each term are shown, together with that for the simple proportional system, the values of the terms having been selected as those which give the most acceptable performance. It is evident, particularly from the respective Nyquist diagrams. Figs. 9(b) and 10(b), that

Fig. 11—Speed response to unit step input

the effect of the integral term is the more pronounced. The reason for the introduction of the integral term is to eliminate the steady state error, while the introduction of the derivative term results in a reduction in the amplitude of initial speed overshoot. preferably to a value below that which existed before the introduction of the integral term.

One physical explanation of why derivative action achieves this can be understood from examination of the hypothetical speed response curve, shown in Fig. 11, which

would result from a step change in selected engine speed.

The new selected speed datum during the transient period is effectively changed by the action of the derivative term. and the magnitude and direction of this change is determined by the magnitude and sign of the term dI/dt (N). The engine governor behaves as though the engine has reached the selected speed. and causes a subsequent change in fuel, thus "anticipating" and acting to reduce the engine speed overshoot.

The functioning of the integral term is illustrated in Fig. 12. It will be realised that true isochronous governing can never be achieved in conjunction with stable linear operation, but a technique for achieving the same result can be realised by the introduction of integral action into the governor unit. At first, when the transient response is most violent, the integral action has little effect, and the governor behaves as a proportional device. As the amplitude of the oscillations decreases the integral mechanism becomes more effective and reduces the speed error by "biasing" the proportional governor characteristics to achieve isochronous conditions. The change in the value of this biasing. with engine loading, is determined by the speed error.
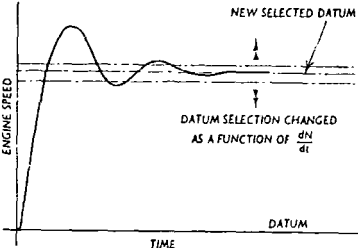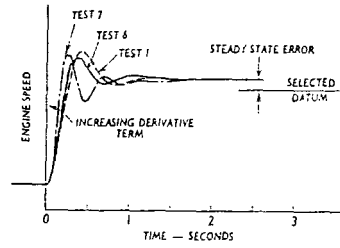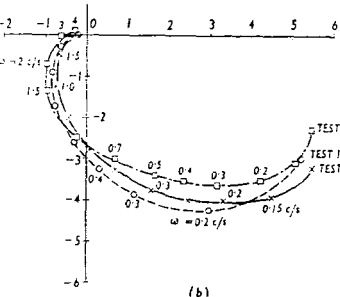
5.3. NICHOLS CHARTS

Nyquist plots having constant M contours superimposed can be used for both the analysis and design of servo systems. but generally it is more convenient to have this information transposed to the form of a Nichols chart. The specifications for the design of servo systems using the frequency domain criterion i.e. bandwidth, resonance peak, resonance frequency, gain margin and
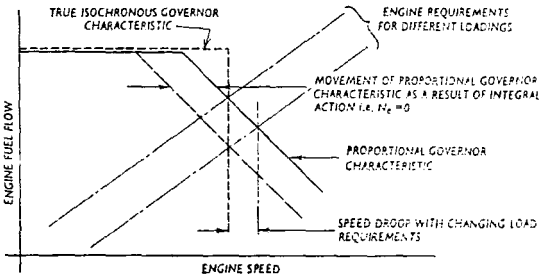

Fig. 12—Governor characteristics

TABLE I

Test Number	System characteristics				Harmonic response characteristics						Transient response characteristics					Steady state
	Governor Characteristics			Loop gain	Gain margin dB	Phase margin, °	Band width, c/s	Resonance peak, M,	Resonance frequency W,	Rise time to selected datum, sec.	Overshoot %	Number of oscillations	Settling time, sec	Speed error N%
	Number Terms	Value Z₁	Value Z₂	Value Z₃												
1	Proportional	2·4	—	—	6·0	10	38	2·1	1·5	1·3	0·26	36	1·5	1·6	9·5
2		6·0	—	—	15·1	2·0	8·0	2·7	>4·0	2·1	0·20	68	5·5	3·1	3·3
3		1·0	—	—	2·5	18·0	80	0·9	0·8	0·7	0·45	26	0·5	1·4	21·5
4	Proportional plus Integral	2·4	5·0	—	6·0	8·6	28	1·9	2·1	1·2	0·32	62	2·5	2·7	0
5		2·4	8·0	—	6·0	5·2	14	2·2	3·9	1·3	0·30	78	4·5	4·5	0
6	Proportional plus Derivative	2·4	—	0·12	6·0	11·6	48	2·3	1·35	1·4	0·31	31	2·0	1·7	9·5
7		2·4	—	0·60	6·0	6·0	28	3·6	2·4	2·6	0·27	35	3·0	1·7	9·5
8	Proportional, integral and derivative	2·4	5·0	0·12	6·0	9·6	34	2·4	1·7	1·4	0·30	52	2	1·8	0
9		2·4	5·0	0·60	6·0	5·4	28	3·6	2·6	2·6	0·21	46·5	2·5	2·4	0
10		1·0	5·0	0·12	2·5	12·8	38	1·5	1·7	0·6	0·30	50	2·0	4·0	0
11		1·0	0·8	0·12	2·5	17·1	85	1·1	—	<0·25	0·31	24	long 0·5	5·3	0
12		2·4	0·8	0·12	6·0	8·2	44	2·5	1·4	1·6	0·21	33	1·5	5·5	0
13		2·4	0·8	0·48	6·0	7·4	30	3·3	2·0	2·2	0·16	34	2·5	5·5	0
14	Proportional	2·4	—	—	6·0	26·5	57	1·9	1·0	1·1	0·26	9·5	1·0	1·2	9·5
15		2·4	—	—	6·0	8·0	32	1·7	2·0	1·2	0·30	33·5	2·5	3·0	9·5
16		2·4	—	—	6·0	2·5	94	—	3·5	11·1	0·70	0	0	0·70	9·5

Technical Contributors Section *(Continued)*

phase margin are more easily studied using the gain-phase plane of this chart. The information obtained from the Nyquist diagrams for the tests conducted has been plotted in Fig. 13, and the salient points of interest taken from these Nichols charts are shown in tabular form in Table I.

For the linear proportional governor system it is apparent from tests 1–3 that for no value of loop gain can all four requirements for the transient response be realised. For a loop gain of 6 the most promising transient values result; for lower loop gains the rise time and speed error becomes too high, and for higher loop gains the initial overshoot is excessive and the response too

oscillatory. The same conclusion would be drawn from examination of the harmonic response characteristics since for the higher and lower gain settings they are in less agreement with the desired values given in Section 5.1. To achieve the desired performance compensation must be introduced to the proportional system of loop gain 6.

Inspection of Table I, for the various combinations of governor terms, shows that the harmonic response characteristics can be best achieved with the governor settings of test 12. The transient performance data do not quite satisfy the suggested values stated in Section 5.1.

The settling time is too high, but it can be seen from Fig. 8(a) that after a time of three seconds the speed error is within tolerable limits for most engine installations. With a band width of 1·5 seconds a greater possibility exists that control could be lost if the noise/signal ratio became too high. Although the harmonic requirements are attained the maximum overshoot is still high and could only be further reduced (with the maintenance of the other required characteristics) by the introduction of some non-linear element in the system.

5.4. ROOT LOCUS AND ROOT CONTOUR PLOTS

The application of harmonic response data to the design of linear control systems is a very useful tool providing the system specifications are known in terms of the gain margin, phase margin, resonance peak M_p, and bandwidth. If, however, it is necessary to have transient response information during system design for systems in which the gain constant is a variable to be chosen, then the graphical methods based on frequency domain studies become very laborious, time consuming and generally a most unrealistic approach.

Knowledge of the position of the roots of the characteristic equation of a servo system plotted in the complex plane makes a complete analysis of the system behaviour possible. A method that enables these roots to be easily located is the Root Locus technique devised by Evans[2].

This technique is a graphical approach for determining the roots of the characteristic equation. It simplifies the problem of finding the Laplace Inverse and hence the solution, in the time domain, of the mathematical equations that represent the dynamic behaviour of the system. The chief advantage of working in the s-plane is that the roots of the characteristic equation not only give information concerning the transient response directly, but also indicate the harmonic response behaviour.

The first introduction to this technique may give the impression that it is not readily applicable to engineering design rules, since at first no clear physical picture of system performance is given from the location of the roots in the s-plane. Experience shows, however, that certain roots are more important than others, which then enables much design data to be computed with greater speed and ease. For instance, any closed-loop poles that lie in the right half-plane will result in unrestrained oscillation; this is so because exponential terms of the form e^{+at} are present in the equation solution. The dominant mode of oscillation is determined by the location of the complex conjugate poles and those nearest the origin will govern
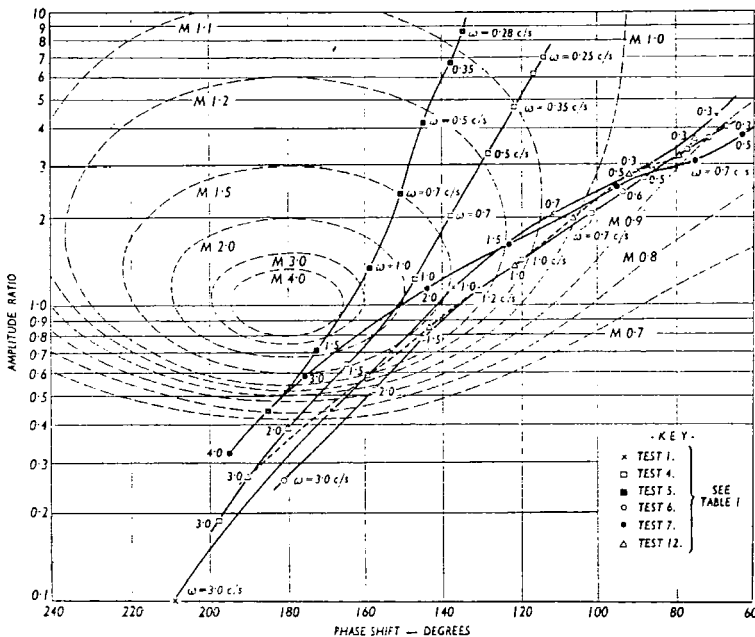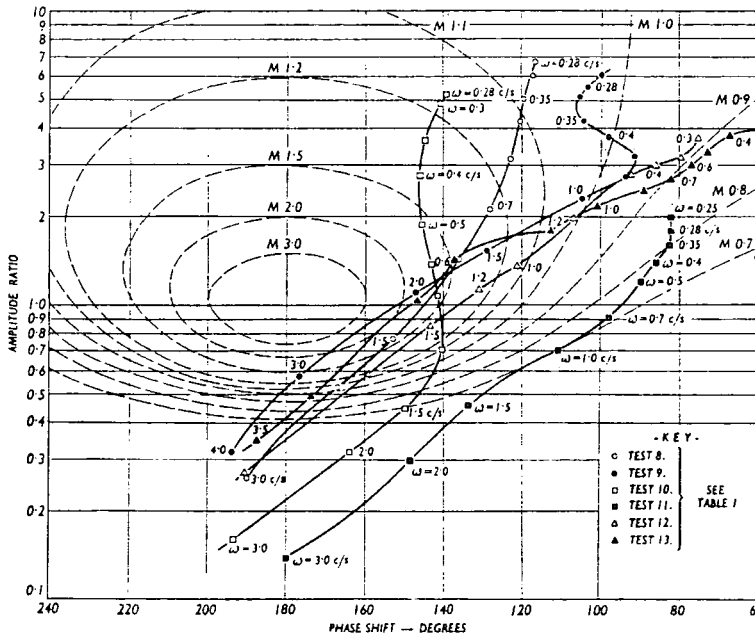

Fig. 13(a)—Nichols chart

Fig. 13(b)—Nichols chart

this mode. Any other pole or zero will have less and less effect the farther it is to the left of the complex conjugate poles.

Further, a system with a real pole nearer the origin than the nearest pair of complex conjugate poles will display a slow, i.e. over damped, response since the response is determined by the pole nearest to the origin. A zero positioned near a pole will reduce the value of the coefficient of the time function whilst the coefficient of the time function will be increased if two poles are located close together.

To illustrate this, consider as an example the transfer function relating engine speed to desired engine speed, i.e. the closed loop transfer relationship, for the proportional governor system. This is obtained, for the desired value of the loop gain, by means of the root locus plot of Fig. 5 and is:

$$\frac{N_0(p)}{N_i(p)} = \frac{8\cdot1}{(p-2\cdot48)(p+0\cdot56-7\cdot32j)(p+0\cdot56-7\cdot32j)(p+0\cdot34+0\cdot79j)(p+0\cdot34-0\cdot79j)}$$

and for a unit step input in selected engine speed the Laplace Transform for $N_a(p)$ is:

$$N_a(p) = \frac{8\cdot1}{p(p-2\cdot48)(p-0\cdot56-7\cdot32j)(p+0\cdot34-0\cdot79j)}$$

It can be shown[6], that if $\bar{y}(s)=f(s)/g(s)$, where $f(s)$ and $g(s)$ are polynomials in s, the degree of $f(s)$ being less than that of $g(s)$, and if

$$g(s) = (s-a_1)(s-a_2)\ldots(s-a_n)$$

where $a_1, a_2, \ldots\ldots a_n$ are constants, which may be real or complex but must be different, the Laplace Inverse is:

$$y(t) = \sum_{r=1}^{n} \frac{f(a_r)\,e^{a_r t}}{(a_r-a_1)\ldots(a_r-a_{r-1})(a_r-a_{r+1})\ldots(a_r-a_n)} \qquad \ldots \ldots (9)$$

Application of this theorem to the proportional governor system will result in an analytical expression from which the engine transient speed response can be plotted. Since the predominant pair of complex poles are $(-0\cdot34 \pm0\cdot79j)$, see Fig. 14, the complex
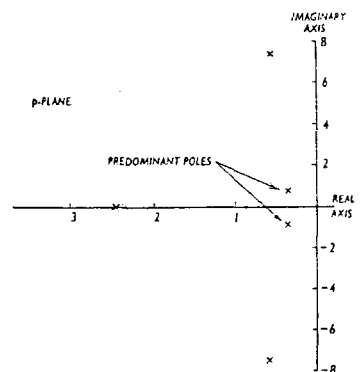

Fig. 14—Pole configuration of proportional system

poles $(-0\cdot56 \pm7\cdot32j)$ can be neglected, thus requiring less mathematical manipulation to obtain the desired expression. Also since the distance of the real pole from the origin is more than five or six times the distance from the origin of the complex conjugate poles this pole could be neglected without detectable error resulting. Including this pole, but neglecting the distant pair of complex conjugate poles, the Laplace Transform now becomes:

$$N_0(p) = \frac{8\cdot1}{p(p+2\cdot48)(p+0\cdot34\pm0\cdot79j)}$$

which yields the solution:

$$N(t) = 4\cdot35\{1 -0\cdot144e^{-2\cdot48t}-1\cdot2e^{-3\cdot4t}\sin(7\cdot9t+0\cdot81)\}.$$

It can be found that this third pole will have negligible effect on the value of $N(t)$ for time values greater than $0\cdot05$ seconds.

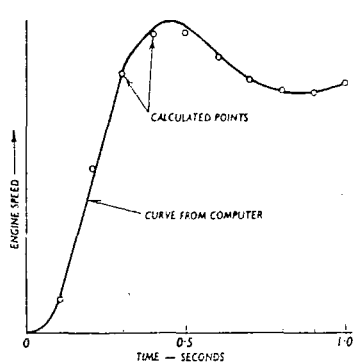This equation was evaluated and plotted in Fig. 15, together with a copy from the

Fig. 15—Transient response of proportional system

computer solution for the proportional system. The results are in excellent agreement and are indicative of the power of the root locus technique for obtaining transient response data.

It can be determined from this "reduced root configuration" that the value of the natural frequency of the system will be $\omega_n=7\cdot9$ rad/sec., and the associated damping factor is $\zeta=0\cdot40$, since the distance from the origin to the governing complex poles gives the value of the natural frequency, and the damping factor is determined from the value of $\cos\phi$, Fig. 16. The plot of Fig. 16
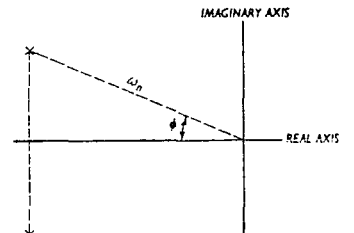

Fig. 16—Method of determining ω_n and ζ from the pole location

is in fact the root configuration of a second order system, which means the resonant frequency can be calculated from the equation $\omega_p=\omega_n\sqrt{1-\zeta^2}$ and Fig. 17 shows the transient response for different values of damping factor.

Plausible approximations of this nature always enable vital information on system behaviour to be computed quickly and easily.

5.5. EFFECTS OF OVERSIMPLIFICATION

It is necessary during system design to produce a simplified system that will truly represent the dynamic behaviour of the physical system. Generally, in order to determine whether any small time lag can be neglected, the minor loop containing the element under examination should be investigated to determine the loop behaviour with and without this lag included. For instance, consideration of the engine alone would suggest that the effects of the inflation lag would be small in comparison with those

of the inertia lag. However, Fig. 18 shows a marked change in system transient response as the inflation lag is varied from 0 in Test 14 to $0\cdot1$ in Test 15.

The harmonic response data (Fig. 19) indicates the effect of the change in inflation lag on loop performance to be a change in cross-over frequency from approximately $1\cdot6$ c/s to $8\cdot5$ c/s, which again clearly indicates that the inflation lag should not be neglected.

The root locus plot for the system with zero inflation lag shows a completely changed
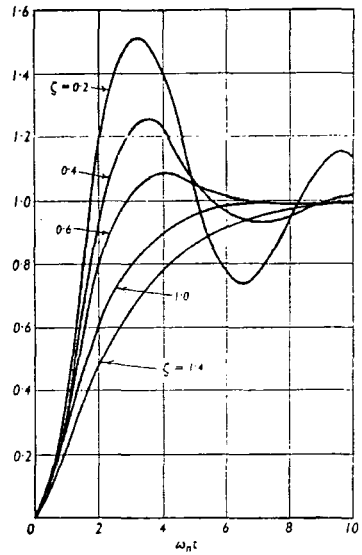

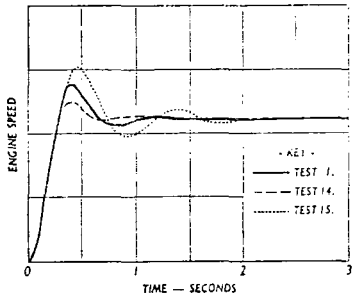Fig. 17—Transient response to unit step input location

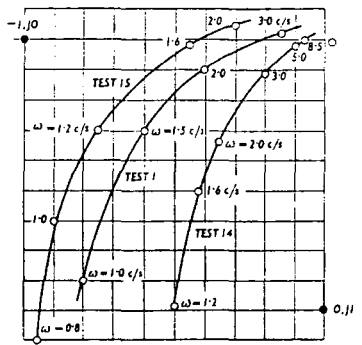Fig. 18—Change in transient response with change in value of engine inflation lag

Fig. 19—Nyquist plot showing change in region —1.J0 with change in inflation lag

Technical Contributors Section *(Continued)*

root configuration (Fig. 21) to that for the system with inflation lag of 0·05 (Fig. 5). The limiting frequency for stability can be seen to be 54 rad/sec. compared to 15 rad/sec. for the latter case.

Considering each unit in association with the system as a whole it might be assumed that time lags of 0·1 seconds were small in comparison with those for the fuel pump and the engine, and could be neglected without detectable error. Neglecting the error lag in addition to the inflation lag would result in the changed system performance shown in Fig. 20. Test 16, the Bode diagram being used as it shows the effect most clearly. This diagram shows a very pronounced resonance peak at approximately 11 c/s giving rise to a very low gain margin. The high phase margin for this test further illustrates the changed system performance to be expected, and the errors resulting from such assumptions.

6. SUMMARY OF CONCLUSIONS

1. Faster engine speed response and a reduced steady state speed error can be obtained by closing the loop of a proportional scheduling system. The speed error, which is the most serious disadvantage, could be further reduced by increasing the loop gain, but this leads to a more violent oscillatory motion. The larger initial overshoots resulting on selection of a higher speed datum could cause mechanical failure; the selection of a lower speed datum for a high performance aircraft could lead to engine "blowout", with possible loss of the aircraft at low altitude due to lack of sufficient time to effect relight procedure.
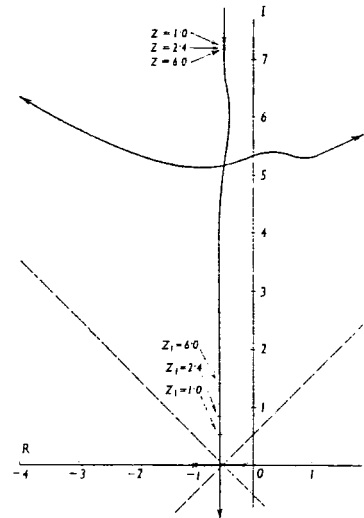

Fig. 21—Root locus plot for proportional system without inflation lag

2. The elimination of the steady state speed error is possible by the introduction of an integral term within the governor loop, but this gives rise to an increase in the value of the initial overshoot. Improvement in the transient response, however, can be achieved by additional compensation in the form of a derivative term.

3. The suggested transient response characteristics listed in the article are acceptable values for most engine systems, and could form the basis for the design of practical engine systems.

4. Design procedure using transient response data is usually lengthy and complex, and harmonic response techniques are more readily applied. Experience has shown that to achieve an acceptable transient response the harmonic response characteristics listed in the article can be used as the basis for design.

Table 1 shows the variations in harmonic data which can be expected for typical transient performance characteristics.

5. At the design stage it is more convenient to plot the harmonic response characteristics on a Nichols chart since the values of peak resonance, phase margin. &c., can be obtained directly from the chart. However, it is at times difficult to appreciate the significance of changes which occur in the harmonic response data as a result of modification to system design. The root locus method is a method by which better understanding is gained.

6. The root locus method for new designs gives a better physical picture of the system performance, since the result of changes in design and in values of design parameters can be more fully understood by the changes that occur in the numbers and position of poles and zeros plotted in the s-plane.

7. During the initial stages of design, when simplification of the system equations is necessary, individual time constants which may be considered of secondary importance can only be neglected when investigation has shown their effect on the loop performance to be small.

APPENDIX

DERIVATION OF TRANSFER RELATIONSHIPS

1. GAS TURBINE ENGINE

(a) Inertia of Rotor System.—The torque relationship for a gas turbine engine can be expressed as a function of engine speed, engine fuel flow and engine air mass flow.

i.e. $T = T(N, Q, q)$

During any period of unsteady running conditions the fluctuation in engine torque will be dT. i.e.

$$dT = \frac{\partial T}{\partial N} \cdot dN - \frac{\partial T}{\partial Q} \cdot dQ - \frac{\partial T}{\partial q} \cdot dq$$

and for an engine running with a choked propelling nozzle the air mass flow will be sensibly constant. i.e. $dq = 0$

$$\therefore dT = \frac{\partial T}{\partial N} \cdot dN + \frac{\partial T}{\partial Q} \cdot dQ$$

For a single rotor engine system, and by the application of Newton's law for a rotating body, the dynamic equation of motion can be written as:

$$I \frac{dN}{dt} = \frac{\partial T}{\partial N} N + \frac{\partial T}{\partial Q} \cdot Q$$

where

I = inertia of the rotor system.
N and Q are the values for engine speed and fuel flow respectively measured from the selected steady state datum condition.
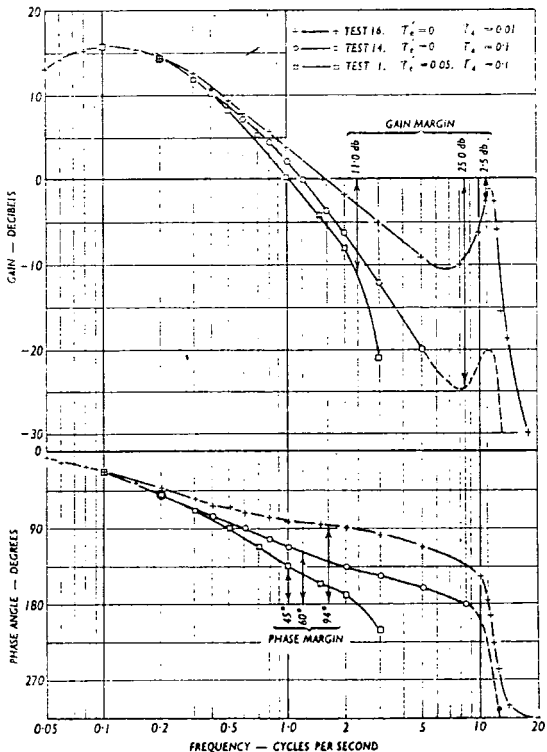

Fig. 20—Bode diagram

The Laplace transform of this is:

$$\left[\frac{I}{\left(-\frac{\partial T}{\partial N}\right)}\, s+1\right]N(s)=\left\{\frac{\frac{\partial T}{\partial Q}}{-\frac{\partial T}{\partial N}}\right\}\,Q(s)$$

where the term I

$$-\frac{\partial T}{\partial N}$$

has the dimensions of time and is the time constant of the rotor system.

For equilibrium conditions $(s\rightarrow 0)$ it follows that

$$\frac{N(s)}{Q(s)}=\left\{\frac{\partial T/\partial Q}{-\partial T/\partial N}\right\}=\beta_e$$

which is the slope of a steady-state operating curve relating engine speed to engine fuel flow.

Hence the engine transfer function is

$$\frac{N(s)}{Q(s)}=\frac{\beta_e}{1+Tes}\quad\text{for the rotor system}\quad.\quad(10)$$

(b) *Combustion Zone Inflation.*—With a step increase in turbine inlet temperature T_3, the turbine mass flow changes from q_0 to

$$\frac{q_0}{\sqrt{1-\frac{\Delta T_3}{T_3}}}$$

since it can be assumed that

$$\frac{q\sqrt{T_3}}{P_c}$$

is a constant value.

Initially, since the inflation lag is very small compared to the rotor inertia lag, it can be assumed that the engine is constrained to run at constant rotor speed, then the turbine mass flow, having suddenly dropped from q_0 to

$$\frac{q_0}{\sqrt{1+\frac{\Delta T_3}{T_3}}}$$

will gradually rise again to q_0.

Let the primary and secondary combustion zone volumes to be inflated be at temperatures T_3 and T_2 respectively.

Then the mass flow to inflate the combustion zone is

$$q_0-q_r=\frac{V_2}{RT_2}\frac{d}{dt}(P)+\frac{V_3}{RT_3}\frac{d}{dt}(P)$$

where

q_0=flow into zone.

q_T=flow to turbine wheel.

Now

$$q_T=\frac{q_0}{\sqrt{1+\frac{\Delta T_3}{T_3}}}\frac{P}{P_c}$$

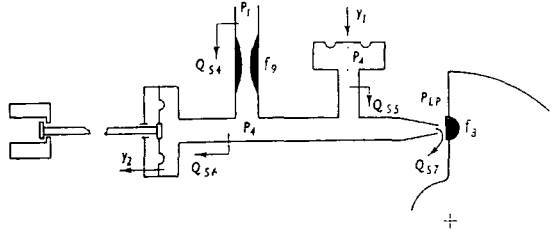$$\therefore q_0-\frac{q_0}{\sqrt{1-\frac{\Delta T_3}{T_3}}}\left\{\frac{P}{P_2}\right\}=\frac{V_2P_2}{RT_2}\frac{d}{dt}\left(\frac{P}{P_2}\right)$$

$$+\frac{V_3P_2}{RT_3}\frac{d}{dt}\left(\frac{P}{P_2}\right)$$

i.e. $q_0\left[1-\dfrac{\left(\dfrac{P}{P_2}\right)}{\sqrt{1+\dfrac{\Delta T_3}{T_3}}}\right]$

$$=\frac{V_2P_2}{RT_2}\left[1+\frac{V_3}{V_2}\frac{T_2}{T_3}\right]\frac{d}{dt}\left(\frac{P}{P_2}\right)$$

For small perturbations about a selected datum engine running speed, $\Delta T_3/T_3\ll1$ hence it can be seen that the inflation time constant can be calculated from

$$T'_e=\left(\frac{V_2P_2}{RT_2}\right)_0\left(1+\frac{V_3}{V_2}\frac{T_3}{T_2}\right)_0\frac{1}{q_0}$$

whence the complete linearised engine transfer relation can be written as

$$\frac{N(s)}{Q(s)}=\frac{\beta_e}{(1-T_es)(1+T_e's)}\quad.\quad.\quad(11)$$

2. FUEL PUMP

The flow equation for an incompressible fluid flowing through a restriction is

$$Q=f\sqrt{\delta P}$$

Logarithmic differentiation results in the linearisation of this equation

i.e. $\dfrac{\Delta Q}{Q_0}=\dfrac{\Delta f}{f_0}-\dfrac{\Delta(P-P_{LP})}{2(P-P_{LP})_0}$

where $\delta P=P-P_{LP}$

Application of this equation to the system shown in Fig. 1, and considering the pump running at fixed speed, results in the following equations:

$$\Delta Q_{s1}=\left(\frac{Q_{s1}}{f_2}\right)_0\Delta f_2-\left(\frac{Q_{s1}}{2(P_2-P_{LP})}\right)_0$$

Since is is assumed P_{LP} is const. $\Delta P_{LP}=0$

$$\therefore\Delta Q_{s1}=K_1\,\Delta f_2+K_2\,\Delta P_2\quad.\quad.\quad.\quad(12)$$

Similarly it can be shown that

$$\Delta Q_1=\Delta Q_{s1}+13\,A_2\frac{d}{dt}(\Delta x)$$

$$=\Delta Q_{s1}+K_3\,s\Delta Q\quad.\quad.\quad.\quad(13)$$

where 13 is a conversion factor and x is the displacement of the piston.
Also

$$\Delta Q_2=K_4\Delta(P_1-P_2)\quad.\quad.\quad.\quad.\quad(14)$$

$$\Delta Q_F=\Delta Q_1-\Delta Q_s\quad.\quad.\quad.\quad.\quad(15)$$

$$\Delta Q_F=K_5\Delta P_1\text{(assuming }\Delta P_2=0)\quad.\quad(16)$$

From consideration of force balance on the pump servo piston:

$$(A_1+K_6)\Delta P_1=rm\Delta Q_1-A_2\Delta P_2\quad.\quad(17)$$

where

$$K_1=\left(\frac{Q_{s1}}{f_2}\right)_0$$

$$K_2=\left(\frac{Q_{s1}}{2(P_2-P_{LP})}\right)_0\quad\begin{array}{l}K_6\Delta P_1=\text{Pump}\\ \text{piston load.}\end{array}$$

$$K_3=m\,.\,13A_2$$

$$m=\frac{\Delta x}{\Delta Q_1}$$

and

$$K_4=\left(\frac{Q_2}{2(P_1-P_2)}\right)_0$$

$$K_5=\left(\frac{Q_F}{2P_1}\right)_0$$

The numerical values of the coefficients K_1, K_2, &c., are evaluated from use of the pump flow characteristics about the selected datum condition.

Combining Equations (12) to (17) gives the complete transfer function: .

$$\frac{\Delta Q_F}{\Delta f_2}=\frac{-\beta_1}{1+\tau_1s}$$

for the pump running at constant speed.

Fig. 22—Governor derivative mechanism

The numerical value chosen for β_1 is 450 gall/hour/in and τ_1 is 2·5 seconds. For the variable speed pump the linearised transfer relation is

$$\Delta Q_F=-\frac{450}{1+2\cdot5s}-0\cdot2\,N_0\quad.\quad(18)$$

3. FLOW CONTROL VALVE

By adopting the same procedure the transfer relationship for the flow control valve in terms of fuel flow and throttle signal can be shown to be

$$(1+\tau_2s)\Delta f_2=\beta_2\Delta Q-\beta_1\Delta f_6-\beta_3\Delta W\quad.\quad(19)$$

It is assumed, however, for this analysis that the governor is working as an all-speed device and, therefore, $\Delta W=0$. From the flow characteristics of the flow control valve, the numerical value of β_2 is 3 g p.h. in, β_3 is 3 g.p.h./in and τ_2 is 0·1 sec.

4. GOVERNOR

(a) *Derivative Action.*—From Figs. 1 and 22 it can be seen that the following are the basic equations for the part of the governor giving derivative control:

Flow equations:

$$\Delta Q_{s5}=\mu_1s\Delta y_1\qquad\text{where }\Delta y_1=-\mu_2\Delta f_9$$

$$\Delta Q_{s6}=\mu_3s\Delta y_2$$

$$\Delta Q_{s4}=-\mu_4P_4$$

$$\Delta Q_{s7}=\mu_5\,\Delta f_9+\mu_6\Delta P_4$$

$$\Delta Q_{s7}=\Delta Q_{s4}+\Delta Q_{s5}-\Delta Q_{s6}$$

Force equations on bellows:

$$\Delta P_4=\mu_7\Delta y_2$$

$$\Delta P_4=\mu_8s\,N_e'$$

Angular displacement of inertia disc:

$$\Delta x=\mu_9\int(Ne-N'e)\,dt.\quad\text{Also }\Delta x=-\mu_{10}\Delta f_9$$

Combining these equations and simplifying gives a result of the form:

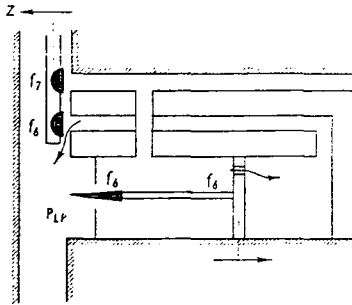$$\Delta y_2=\frac{Z_3(1+\tau_5s)\,s\,N_e}{(1+\tau_6s)}$$

Fig. 23—Governor integrating mechanism

For the system used $\tau_5=0$, $\tau_6=0\cdot1$ sec. and Z_3 is variable.

(b) *Integral Action.*—Applying similar reasoning to Fig. 23 yields the result:

$$\Delta f_6'=\frac{1}{k_3}\Delta z$$

where k is the constant of integration (variable).

The overall transfer function for this three-term governor device is then:

$$f_6(s) = \left\{ Z_1 + \frac{Z_2}{s} + \frac{Z_3 s}{(1 + 0 \cdot 1 s)} \right\} N_c(s)$$

BIBLIOGRAPHY

1. Brown and Campbell, *Principles of Servo Mechanisms*, Wiley and Co., 1948.
2. Chestnut and Mayer, *Servomechanisms and Regulating System Design*, Vols. I and II, Chapman and Hall, 1955.
3. Bruns and Saunders, *Analysis of Feedback Control Systems*, McGraw-Hill, 1955.
4. Raven, *Automatic Control Engineering*, McGraw-Hill, 1961.
5. Stockdale, *Servomechanisms*, Pitman and Sons, 1962.
6. Taylor, *Servomechanisms*, Longmans, 1960.
7. Webb, *Automatic Control*, McGraw-Hill, 1964.
8. Korn and Korn, *Analogue Computers*, McGraw-Hill, 1954.

9. Johnson, *Analogue Computer Techniques*, McGraw-Hill, 1963 (two editions).
10. Blackburn, Reethof and Shearer, *Fluid Power Control*, Technology Press and Wiley, 1960.
11. Lewis and Stern, *Design of Hydraulic Control Systems*, McGraw-Hill, 1961.
12. Lawrence, "Fuel Systems for Gas Turbine Engines", *Journal Royal Aeronautical Society*, November, 1955.
13. Welbourn, Roberts and Fuller, "Governing of Compression-Ignition Oil Engines", *Proc. Inst. Mech. Eng.*, Vol. 173, 1959.

REFERENCES

[1] Saville and Gill, "The Application of Analogue Computer Techniques to the Design of Aero-Engine Control Systems", *Brit. I.R.E. Convention on Electronics in Automation*, June, 1957.
[2] Evans, "Control System Synthesis by Root Locus Methods", *Trans. A.I.E.E.*, Vol. 69, 1950.
[3] Kuo, *Automatic Control Systems*, page 270, Prentice Hall, 1962.
[4] Bruns and Saunders, *Analysis of Feedback Control Systems*, McGraw-Hill, 1955.
[5] Gardner and Barnes, *Transients in Linear Systems*, John Wiley, 1949.
[6] Jaeger, *An Introduction to the Laplace Transformation*, Methuen and Co., 1949.

PAPER 10

Design of an optimum relay-type governor for a gas-turbine engine

by **K. F. GILL**, M.Sc., Ph.D. *and* **J. SCHWARZENBACH**, M.Sc.

A governor based on a relay-type principle,
utilizing a minimum time-response switching criterion,
has been incorporated into a hypothetical aircraft gas-turbine-engine speed-control loop.
The change in performance for different approximations to the theoretical switching criterion
has been investigated. The types of governor arrangement studied, are limited to those
which can be implemented hydraulically, without undue complexity.

ONE IMPORTANT DYNAMIC-PERFORMANCE REQUIREMENT for aircraft-engine speed-control systems, is that the output response to an input step variation approximates, as closely as possible, to a step function. In practice, provided that the rise time is 0·3s maximum, the settling time to the selected speed datum is 2s maximum, initial overshoot is ⩽25%, and there are not more than 1½ oscillations to datum, then the dynamic performance is considered to be acceptable. By changing the emphasis on these requirements, it becomes possible to consider forms of governor arrangement other than the conventional two-term or three-term controller. In particular, by accepting sustained small-amplitude oscillations, an alternative type of governor in the form of a 'bang-bang' regulator becomes worthy of consideration. Reduction of the initial overshoot, towards the amplitude of the constant oscillations, would lessen the rise-time requirement, provided that the 'settling time' is maintained within the 2s maximum. It is assumed that isochronous governing is essential for multi-engine installations and, hence, integral action must be retained in any modified governor arrangement.

It is usually preferable to have hydraulic rather than electronic controllers for aircraft-engine applications, because high ambient temperatures in the engine nacelles would create cooling problems in the latter controller. Also, the available high-pressure fuel provides a convenient source of power for servo-elements' actuation. With this preference in mind, any proposed governor arrangement should be capable of simple realization in a hydraulic system.

To have appropriate data available for comparison, it was decided to use a hypothetical engine system (*1*) in this investigation. The aim of the previous work was to determine the optimum coefficients for a three-term controller meeting the dynamic requirements quoted above. It was not possible to satisfy these requirements completely and, hence, alternative governors, utilizing component non-linearities, were investigated (*2*). This resulted in the possibility of simplifying the governor by replacing the derivative and integral terms with a two-rate integral term. The value of the latter's integrating coefficient was increased for small error-signal values, and provided some improvement in dynamic performance. The present paper is an extension of this work.

Fig. 1 shows two systems used in the present investigation, which was carried out on a Pace 231R analogue computer. The computer circuit configuration (fig. 2) shows the engine, fuel pump, flow-control valve, governor, and optimum switching-curve generator, for system B. The minor circuit changes necessary to obtain system A are not shown.

Optimum switching curve

For a second-order system, an expression can be derived for use as a switching curve, which gives the minimum-time response for this type of relay-governor control unit. The use of such an optimum switching curve theoretically permits the final condition to be reached in two steps with a single switching action,

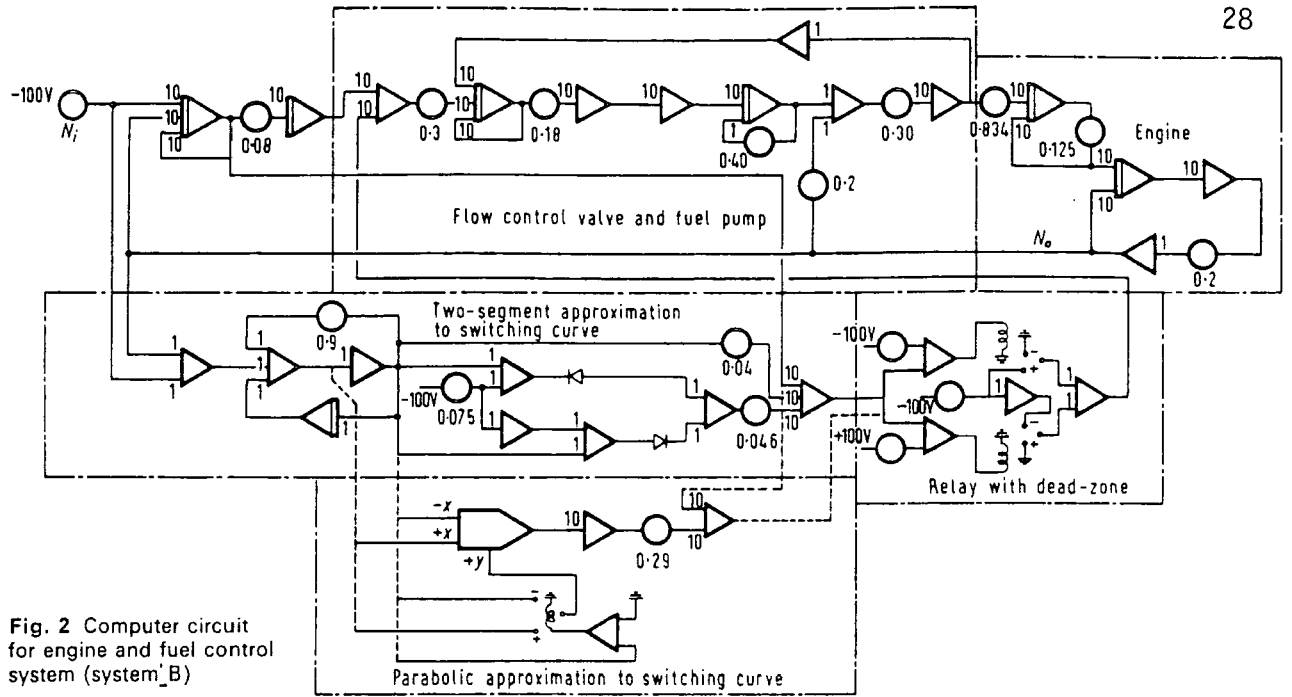**Fig. 1** Block diagram of engine and fuel control system
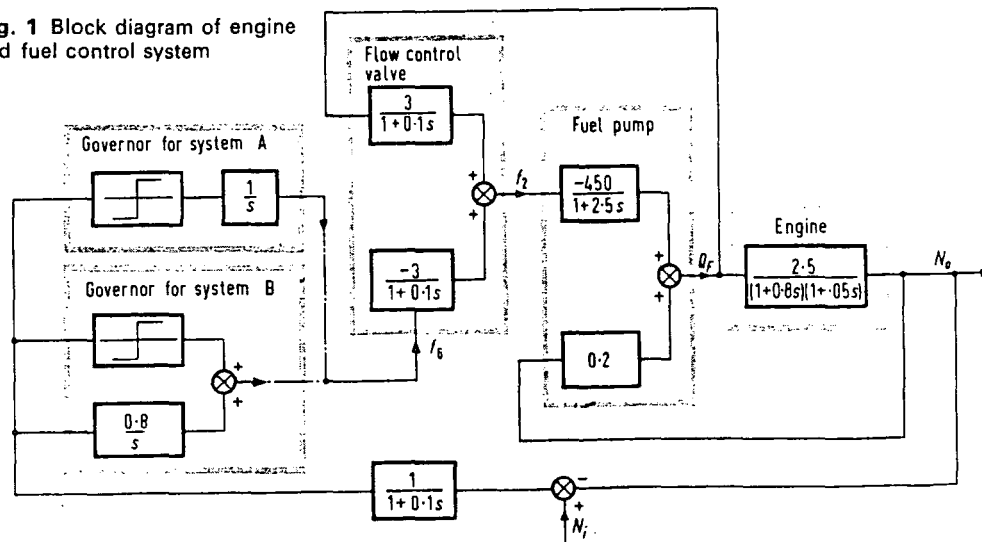
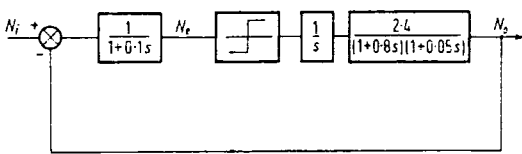**Fig. 2** Computer circuit for engine and fuel control system (system B)

Fig. 3 Reduced block diagram

irrespective of the initial conditions. If the order of the gas-turbine engine system being studied could be reduced to two, without sensibly changing the overall dynamic performance, then the idea of optimum switching can be used.

The composite transfer function for the engine, pump, and flow control valve is—

$$G(s) = \frac{337500}{s^4 + 31 \cdot 6s^3 + 5638s^2 + 115000s + 135000}$$

Two of the characteristic-equation roots are predominant and, hence, this can be simplified to—

$$G^1(s) = \frac{2 \cdot 4}{(1 + 0 \cdot 8s)(1 + 0 \cdot 05s)}$$

To satisfy the requirement for isochronous governing, system A (fig. 1) has been chosen as the simplest arrangement. From the reduced block diagram (fig. 3), when the system is autonomous—

$$Ni = 0$$

$$\therefore \quad Ne(s) = \frac{-2 \cdot 4K}{s^2(1 + 0 \cdot 8s)(1 + 0 \cdot 1s)(1 + 0 \cdot 05s)}$$

$$\simeq \frac{-2 \cdot 4K}{s^2(1 + 0 \cdot 8s)}$$

$$\therefore \quad Ne(t) = -2 \cdot 4K (t - 0 \cdot 8 + 0 \cdot 8e^{-1 \cdot 25t})$$

which, upon differentiation, gives—

$$\dot{Ne}(t) = -2 \cdot 4K(1 - e^{-1 \cdot 25t})$$

These equations describe the phase-plane trajectory (fig. 4) for zero initial conditions. The optimum switching curve and a typical trajectory, for a given initial condition, are also shown in this figure.

The augmentation of this switching curve requires the generation of the derivative signal, $\dot{Ne}(t)$, with which are associated certain practical difficulties. Because of noise susceptibility, the development of a true differentiating device is impracticable and a suitable
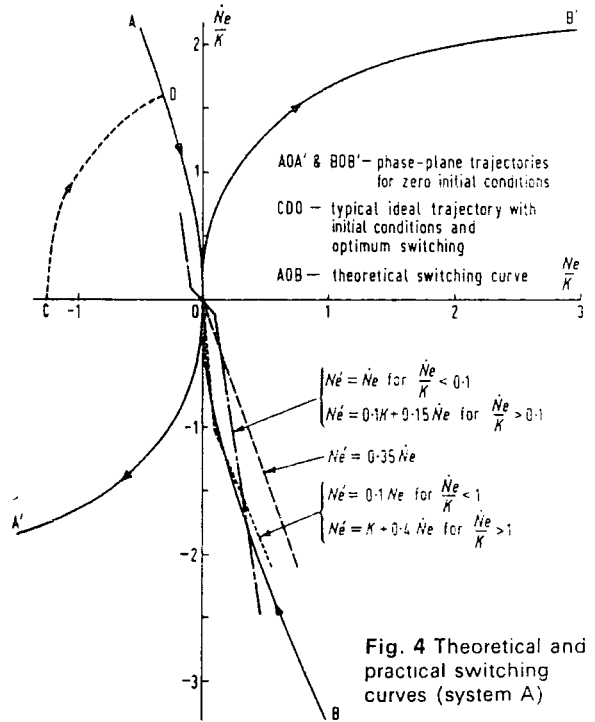
Fig. 4 Theoretical and practical switching curves (system A)

Nomenclature

c	Coefficient for parabolic approximation.
D	Half-width of dead-zone.
E	Peak amplitude of forcing function.
$G(s)$	Transfer function of engine, pump, and flow-control valve.
$G^1(s)$	Approximation to $G(s)$.
$G_1(s)$	Transfer function of linear proportional + integral governor.
K	Gain term in switching device.
Ne	Speed error signal.
Ne^1	Speed error at which switching should occur for minimum time response.
No	Engine speed.
s	Laplace operator.
ω	Angular frequency.

approximation to this function must be used. The approximation generally includes a small time-constant in the derivative mechanism. The value of this time constant is a function of the signal/noise ratio for the differentiator input.

For a governor, including a differentiating device, to be acceptable, the dynamic system performance must show an appreciable improvement over that for the non-linear governor previously investigated (2).

To augment the switching signal, the theoretical error (determined by the switching curve) is compared with the actual error, and switching is arranged to occur when their difference is zero.

Tests conducted

In an attempt to discover the accuracy with which the practical switching curve must match the theoretically predicted one, a number of trigonometric functions were generated and each fitted the curve with varying degrees of accuracy. The functions chosen could be easily generated hydraulically, and are: (a) two straight lines; (b) a parabola; and (c) a single straight line. Transient responses were obtained for step-function inputs of different magnitudes. The more suitable switching curves were then chosen, and further tests carried out in which the dynamic engine coefficients of engine primary time-constant and gain were varied by a factor of three.

The rise time, maximum overshoot, amplitude of persisting oscillations and settling time (for the more significant tests of system A) are given in tables 1 and 2, and typical response curves are shown in figs 5 and 6. For comparison, the dynamic behaviour of the system fitted with a linear proportional and integral governor is also shown.

To eliminate the steady-state oscillations, it is necessary to introduce a dead-zone in the switching relay, which results in the loss of isochronous governing
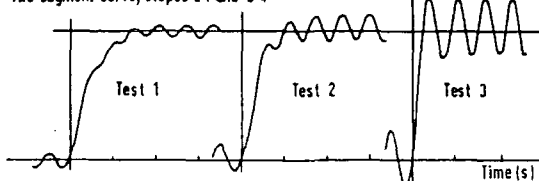
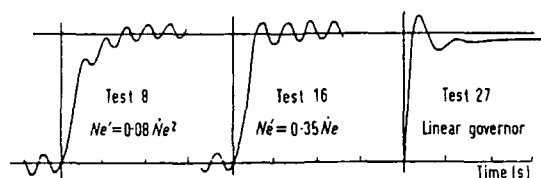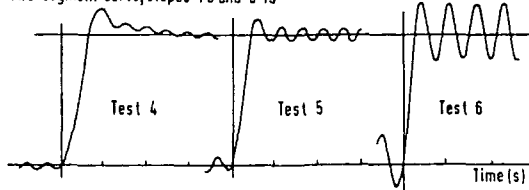**Fig. 5** Transient step responses for variations in the form of switching curve (system A)
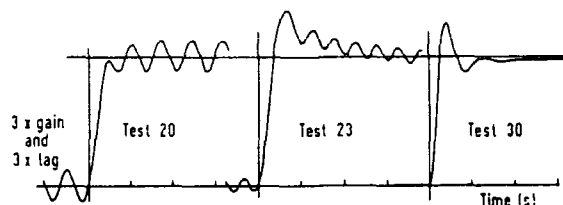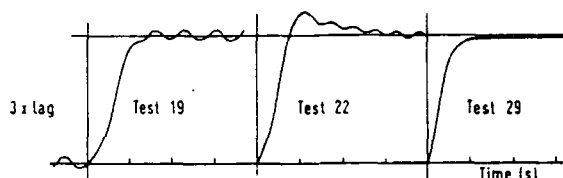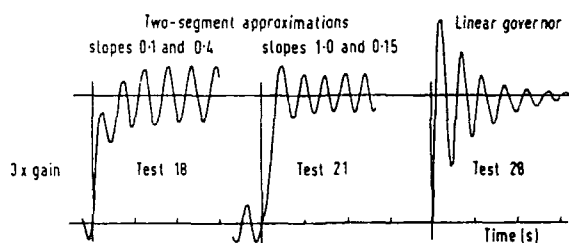

Fig. 6 Transient step responses for variations in engine parameters (system A)

K. F. Gill served an apprenticeship with Richardsons, Westgarth and received his technical education at West Hartlepool Technical College and Durham University. From 1955 to 1957, he was a control engineer with Bristol Siddeley Engines. In 1958, he was awarded an M.Sc. in thermodynamics and related studies at Birmingham University. He then returned to Bristol Siddeley Engines and was later accepted for research at Birmingham University on non-steady gas flow in engine-exhaust systems. A Ph.D. followed in 1961. From 1961 to 1963, Gill was a senior scientific officer at the Admiralty Weapons Establishment, Portland. He is now a lecturer in control in the mechanical engineering department of Leeds University.

J. Schwarzenbach graduated from Glasgow University, in 1955, with first-class honours in mechanical engineering. He was awarded an exchange scholarship which enabled him to spend one year at Cornell University, U.S.A., and to obtain an M.Sc. upon the completion of a course in gas-turbine engineering. After a graduate apprenticeship with Rolls-Royce, he obtained experience as a designer, and later as a section leader, in the accessory design department of Rolls-Royce. In 1964, he became a lecturer at the University of Leeds, teaching various aspects of design, lubrication and control and doing research on the optimizing control of internal-combustion power plants.

conditions. The dead-zone required, in this case, was very large and resulted in unacceptably large steady-state errors.

In an attempt to avoid this difficulty, the alternative governor arrangement of system B was studied. The integrating action which has been introduced, in parallel with the switching action, is slow and has been neglected in the development of the theoretical switching curve (fig. 7). Transient response results, for this alternative arrangement, are listed in tables 3 and 4, with typical responses shown in fig. 8. The effect of dead-zone is shown in fig. 9.

Discussion

A close approximation to the switching curve is possible, over a limited range, by the use of a hyperbola or a parabola, particularly around the origin. The shape of the switching curve makes it impossible to fit either

Table 1 Effect on the transient step response of different approximations to the theoretically optimum switching curve—system A ($K=15$)

Test number	Rise time (s)	Amplitude of steady oscillations	Maximum overshoot (if different to previous columns)	Settling time (s)	Step size	Actual switching curve
1	2	0·10	—	—	2	Two linear segments: Initial slope 0·1
2	1·8	0·20	—	—	1	Final slope 0·4
3	0·3	0·44	—	—	0·5	Break-point 1·0
4	0·6	0·06	0·20	1·5	2	Initial slope 1·0
5	0·4	0·11	0·14	0·8	1	Final slope 0·15
6	3	0·22	—	—	0·5	Break-point 0·1
7	0·5	0·26	0·23	1·8	1	Parabola $Ne^1 = c(Ne)^2$: $c = 0·03$
8	2·2	0·12	—	—	1	$c = 0·08$
9	3·6	0·12	—	—	1	$c = 0·16$
10	5	0·10	—	—	1	$c = 0·32$
11	5	0·10	—	—	1	Straight line: Slope = 1·0
12	2	0·13	—	—	1	Slope = 0·5
13	0·4	0·20	0·28	1·2	1	Slope = 0·25
14	0·3	0·72	0·80	1·5	1	Slope = 0·125
15	0·7	0·07	—	—	2	
16	0·4	0·15	—	—	1	slope = 0·35
17	0·3	0·32	0·31	2	0·5	
27	0·25	1½ osc. only	0·14	1·3		Linear system with P+I governor $G_1(s) = [2·4 + (0·8/s)]$

Table 2 Effect on the transient step response of changes in engine parameters and the addition of dead-zone—system A (step size=1)

Test number	Rise time (s)	Amplitude of steady oscillations	Maximum overshoot (if different to previous columns)	Settling time (s)	Test conditions	
2	1·8	0·20	—	—	Basic engine	Two-segment approximations (coeff.s as test 2, table 1).
18	1·9	0·46	—	—	3 × gain	
19	1·3	0·09	—	—	3 × lag	
20	0·9	0·26	—	—	3 ×(gain & lag)	
5	0·4	0·11	0·14	0·8	Basic engine	Two-segment approximation (coeff.s as test 5, table 1)
21	0·3	0·32	0·25	1·7	3 × gain	
22	0·7	0·04	0·22	4	3 × lag	
23	0·3	0·12	0·36	4	3 ×(gain & lag)	
16	0·4	0·15	—	—	Basic engine	Linear switching curve (slope = 0·35)
24	0·2	0·44	0·50	1·3	3 × gain	
25	0·9	0·07	0·20	1·9	3 × lag	
26	0·4	0·18	0·28	1·2	3 ×(gain & lag)	
27	0·25	1½ osc.	0·14	1·3	Basic engine	Linear governor $G(s) = [2·4 + (0·8/s)]$
28	0·10	>6 osc.	0·64	3·8	3 × gain	
29	1·10	0	0	1·1	3 × lag	
30	0·25	1½ osc.	0·26	1·7	3 ×(gain & lag)	
31	(0·5)	Steady-state error ±0·25		6	Dead-zone width = 2 ×0·25 (minimum value which eliminates oscillation)	
32	(0·5)	Steady-state error ±0·30		4	Dead-zone width = 2 ×0·3	

of these functions over a wide range. A choice has to be made, therefore, between a good fit near the origin only, and a poorer fit over a wider range. Although the hyperbola appears to give a better approximation over a wide range, and there is no significant difference if the only requirement is for a good fit near the origin, the hyperbola provided no noticeable improvement to the dynamic behaviour shown by a parabolic switching curve. Consequently, no results are presented.

Easier approximations to implement are two linear segments or a single straight line, but these suffer the disadvantage that an accurate fit near the origin is impossible.

Two-segment approximation to switching curve

In an attempt to obtain a good approximation to the ideal switching curve, and one which is simple to augment hydraulically, a function comprising two straight lines and a single break-point was investigated. Sample results are shown as tests 1–3 (table 1 and fig. 5) for the approximation, shown in fig. 4, using small, medium and large steps. It can be logically deduced that the slope near the origin primarily governs the amplitude of steady-state oscillations, while the slope remote from the origin dictates the rise time and magnitude of initial overshoot. Adjustment of both

the break-point and the slope of the two straight lines, to give small-amplitude oscillations and a fast rise time with little overshoot for a medium-sized step input, results in a switching curve shown in fig. 4 and the speed responses of tests 4–6. Surprisingly, although the latter switching function is of quite different shape to the theoretical switching curve, the transient responses (for all step sizes) show a marked improvement over those obtained with the better fitting curve. From these results. it would seem unnecessary to use a larger number of segments; moreover, it would be inconsistent with the design philosophy of a simple governor.

Parabolic approximation

The parabolic relationship between Ne^1 and Ne is—

$$Ne^1 = c(Ne)^2$$

where the coefficient, c, dictates the region in which there is close agreement between the parabola and the ideal switching curve. For increasing values of c. the changes in dynamic system behaviour are shown as tests 7–10 for the medium-sized step. Table 1 shows that there are two main changes in transient behaviour of the engine system for increasing values of c. (i.e. increasing rise time and decreasing amplitude of persisting oscillations). This is consistent with the fact that switching occurs earlier than it does in the optimum case, and implies that a practical compromise must be made between a fast rise time and small persisting oscillations.

Straight-line approximation

As a logical extension suggested by the results of the preceding approximations, and because it would be the simplest to implement hydraulically, a single straight-line approximation to the switching curve was investigated. Results for different slope values are given as tests 11–17; the best of these (tests 15–17), with switching curve $Ne^1 = 0·35 Ne$, are marginally poorer than the best obtained from the two-segment approximation (tests 4–6).

Changing engine dynamics

Changing flight conditions experienced by aircraft engines result in large changes in their dynamic characteristics. The most significant are the changes in engine primary time-constant and engine gain constant. To ensure that satisfactory dynamic behaviour is maintained with the chosen type of governor, tests were carried out in which these engine parameters were increased by a factor of three, both separately and simultaneously. Results are shown as tests 18–26 (table 2 and fig. 6) for the two-segment switching curves previously described. For comparison, the transient response has been obtained for the system controlled by a linear governor with the transfer function—

$$G_1(s) = [2·4 + (0·8/s)]$$

The results for the engine operating with this governor. under the same conditions, are given as tests 27–30. The switching curve with large slope near the origin, again gives the best transient behaviour, but this is generally inferior to that of the linear system.

Introduction of dead-zone

In order to reduce the amplitude of the steady-state oscillations, or eliminate them completely, it is necessary to introduce a dead-zone into the switching characteristics. This effect is present inherently, to some degree, in all practical systems. The magnitude necessary to give a particular reduction in the amplitude of the steady-state oscillations, can readily be predicted by
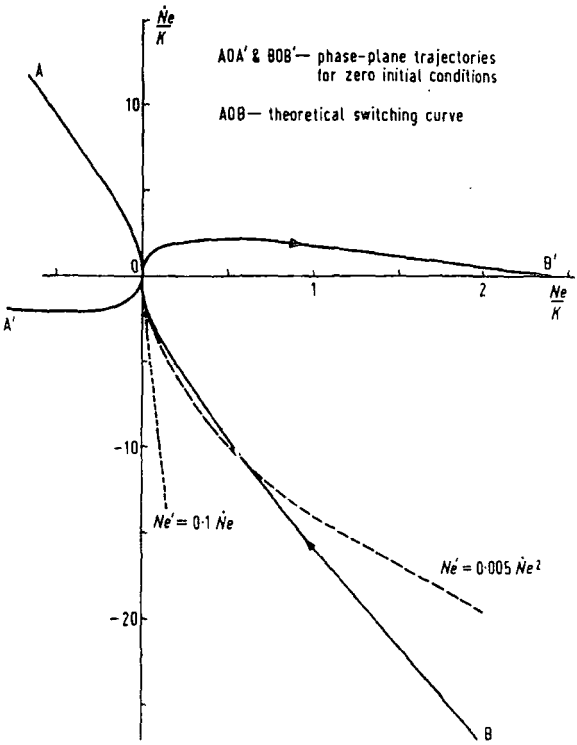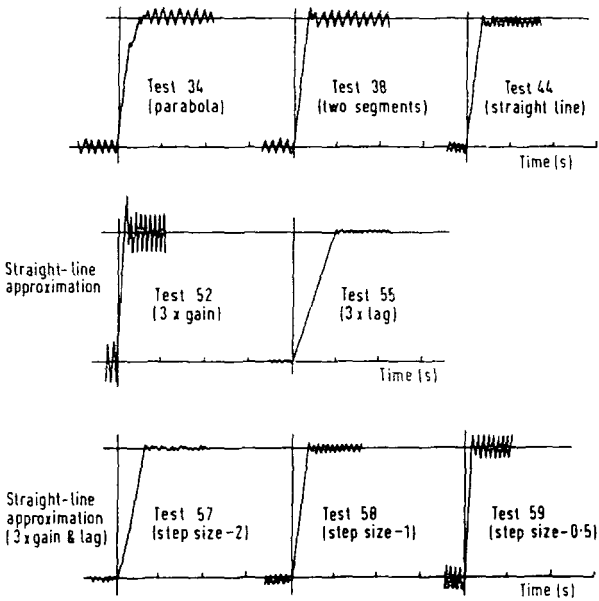
Fig. 7 Switching curves (system B)

AOA' & BOB'— phase-plane trajectories for zero initial conditions

AOB— theoretical switching curve

$\dot Ne' = 0.1 \dot Ne$

$\dot Ne' = 0.005 \dot Ne^2$

Table 3 Effect on the transient step response of different approximations to the theoretically optimum switching curve—system B

Test number	Rise time (s)	Amplitude of steady oscillations	Maximum overshoot	Settling time (s) (if different to previous columns)	Actual switching curve		
33	0.35	0.24	—	—	Parabola $\dot Ne^1 = c(\dot Ne)^3$	c = 0.005	
34	0.8	0.16	—	—		c = 0.02	
35	1.2	0.08	—	—		c = 0.05	
36	1.6	0.08	—	—		c = 0.1	
					Initial slope	Final slope	Break-point
37	0.35	0.16	0.12	0.4	0.040	0.086	0.075
38	0.3	0.16	—	—	0.004	0.086	0.010
39	0.35	0.26	—	—	0.004	0.086	0.030
40	0.35	0.16	—	—	0.040	0.086	0.030
41	2.1	0.12	—	—	0.400	0.086	0.030
42	0.4	0.48	—	—	Slope = 0.004		
43	0.35	0.16	—	—	0.04		
44	0.35	0.10	—	—	0.10		
45	1.80	0.10	—	—	0.40		

(Two linear segments for tests 37–41; Straight line for tests 42–45)

Table 4 Effect on the transient step response of changes in engine parameters and the addition of dead-zone—system B

Test numbers	Rise time (s)	Amplitude of steady oscillations	Maximum overshoot	Settling time (s) (if different to previous columns)	Step size	Test conditions	
38	0.30	0.16	—	—	1	Basic engine	Two-segment approximation (coeff.s as test 38, table 3)
46	0.15	0.32	0.36	0.35	1	3 × gain	
47	0.9	0.04	0.08	1.8	1	3 × lag	
48	0.35	0.10	0.16	0.7	1	3 × (gain & lag)	
49	0.7	0.05	—	—	2		
44	0.35	0.10	—	—	1	Basic engine	
50	0.2	0.20	—	—	0.5		
51	0.2	0.16	0.10	0.4	2		Linear switching curve (slope = 0.10)
52	0.15	0.36	0.30	0.3	1	3 × gain	
53	0.1	0.68	0.40	0.2	0.5		
54	1.5	0.02	—	—	2		
55	0.9	0.02	—	—	1	3 × lag	
56	0.4	0.05	0.05	0.6	0.5		
57	0.6	0.04	—	—	2		
58	0.35	0.08	0.08	0.45	1	3 × (gain & lag)	
59	0.2	0.20	—	—	0.5		
60	0.35	—	0	8.0	1	Dead-zone width = 0.16	
61	(2.0)	—	0	6.0	1	Dead-zone width = 0.32	

Fig. 8 Transient step responses (system B)

inspecting the plot of the characteristic equation—

$$1 + N(\omega,E)G(s) = 0.$$

Complete elimination is achieved, theoretically, by satisfying the expression—

$$(\pi D/2K) > |G(s)/180°|$$

where $2D$ is the width of the dead-zone. Satisfying this requirement, for the switching curve with large slope near the origin, requires $D > 22\%$ of the step size. The associated steady-state speed error is quite unacceptable.

System B

System A has been shown, in general, to give a poorer performance than the engine with a linear proportional plus integral governor. System B was created to satisfy the isochronous-governing requirement. The effect of the integral action was neglected during the development of the theoretical equations which specify the switching function. This arrangement suffered the disadvantage that the switching curve was only operative for limited regions of initial conditions; the system only functioned for other regions because of the slow integrating action. The phase-plane trajectories and theoretical and actual switching curves are shown in fig. 7.

Tests, similar to those for the previous system, were undertaken and the results showed similar trends. Results of the tests are given in tables 3 and 4, and sample transient responses are shown in fig. 8.

Approximations, utilizing a parabolic switching curve, were investigated first (tests 33–36), and the best response (test 34) is shown in fig. 8. The two linear-segment approximation (test 38) gave the best response for the different combinations of slope and break-point investigated, and this was superior to the parabolic approximation with amplitude of steady oscillations reduced by 30% for a 0.35s rise time. A switching curve with high slope near the origin, and low slope beyond this region, gave an inferior response, unlike the results for system A. The single straight-line
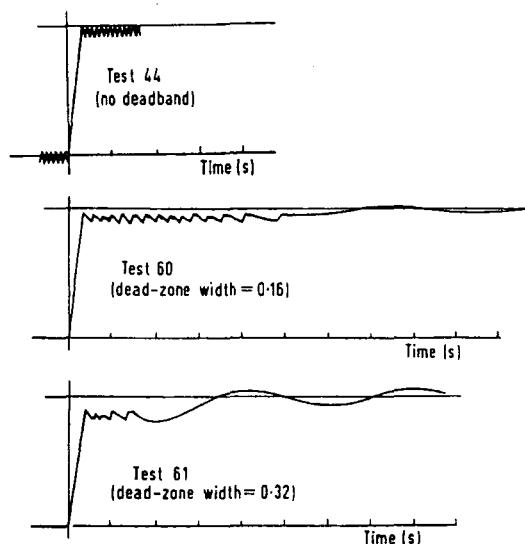
Fig. 9 The effect of dead-zone on transient step response (system B)

approximation (test 44) gave an improvement over both of these. This improvement was maintained with engine-parameter variations, and system B, with this linear switching curve, showed a clear improvement over the linear proportional plus integral governor—provided that small-amplitude persisting oscillations are acceptable. The size of dead-zone required to

eliminate these oscillations, is considerably smaller than with system A, and fig. 9 shows the resulting types of transient response with test 60 being the most suitable.

Conclusions

1. The logical arrangement for a 'bang-bang' type of governor (system A) gives a generally poorer performance than the linear two-term governor. Furthermore, if steady-state oscillations are reduced in this system, by the use of a dead-zone, then the steady-state speed error makes the system even more unacceptable.

2. System B, although not utilizing the true criterion for minimum time response, shows an improvement in system dynamics over that for the linear system.

3. The switching curve which gives the best transient performance, is also the one which could most easily be implemented hydraulically.

4. Controlled size of the dead-zone can be used to eliminate any persistent steady-state oscillations, without the loss of isochronous governor conditions for system B.

5. The performance of system B with changing engine dynamics is superior to that of the linear system.

References
1. Schwarzenbach, J., and Gill, K. F.: 'Analysis of gas turbine engine fuel system', *The Engineer*, 1965, Vol. 219, pp. 209–218.
2. Gill, K. F., and Schwarzenbach, J.: 'A theoretical look at the use of functional non-linearities in a gas-turbine control system,' *Control*, Sept. 1966, Vol. 10, pp. 465–468, and Oct. 1966, pp. 531–535.

PAPER 11

A theoretical look at the use of functional non-linearities in a gas turbine control system

K. F. GILL, M.Sc., Ph.D., and J. SCHWARZENBACH, M.Sc., University of Leeds

□ A three-term governor for a gas turbine engine system is studied with a view to reducing its physical complexity and increasing its reliability without damaging its dynamic behaviour.

◩ The significance of internally generated pressure noise on the performance of different possible hydraulic control systems is assessed.

◪ A root-locus plot is used to predict the approximate transient behaviour of the non-linear system

◩ The correlation between harmonic response criteria for the linear and non-linear systems is examined

It turns out that a simplified governor with improved dynamic performance can be obtained by removing the derivative term of a linear three-term controller and modifying the integral term to give double rate integral action. Pressure noise generated within the pump of a hydraulic system is found to have negligible effect. The authors conclude that general trends in the dynamic behaviour of simple non-linear systems can be predicted from modified root-locus and harmonic response diagrams, but that for more detailed information further experience with non-linear systems must be obtained.

PRESENT PERFORMANCE SPECIFICATIONS of aircraft engines, such as continuously varying load requirements, rapid response, and isochronous governing, have made it necessary to replace the earlier scheduling systems with more complex closed-loop systems. Generally the loop is closed on a three-term linear governor with proportional, integral and derivative terms.

Hydraulic governor units are usually more attractive for this purpose than their electrical counterparts, since high ambient temperatures in the engine nacelles raise problems of cooling. A further strong factor influencing the choice of hydraulic components for engine control systems is that high-pressure fuel is the most convenient source of power for actuation of servo-elements controlling fuel pump stroke,
inlet guide vane position. etc.

The hydraulic governors used are highly complex and hence costly to manufacture. difficult to calibrate and service, and susceptible to failure, and, in our opinion, any scheme that can reduce this complexity would be useful. Our theoretical study here shows that, by selective use of functional non-linearities within an otherwise linear governor, a simpler system with better performance characteristics can be achieved.

The investigation is based on a hypothetical aero-engine fuel system for which we have published the results of a study to determine the most suitable combination of terms in a three-term governor (1). The most difficult of the three terms to generate hydraulically. and possibly the most difficult to design,

Dr Gill served an apprenticeship with Richardson Westgarth and received his technical education at West Hartlepool Technical College and Durham University. From 1955 to 1957 he was a control engineer with Bristol Siddeley Engines. In 1958 he was awarded an M.Sc. in thermodynamics and related studies at Birmingham. He then returned to Bristol Siddeley Engines and was later accepted for research at Birmingham University on non-steady gas flow in engine exhaust systems. A Ph.D. followed in 1961. From 1961 to 1963 Gill was a senior scientific officer at the Admiralty Weapons Establishment, Portland. He is now lecturer in control in the mechanical engineering department of Leeds University.

J. Schwarzenbach graduated from Glasgow University in 1955 with first-class honours in mechanical engineering. He was awarded an exchange scholarship which enabled him to spend one year at Cornell University, U.S.A., and to obtain an M.Sc. after completion of a course in gas turbine engineering. After a graduate apprenticeship with Rolls-Royce he obtained experience as a designer, and later as a section leader, in the accessory design department of Rolls-Royce. In 1964 he became a lecturer at the University of Leeds, teaching various aspects of design, lubrication, and control, and doing research on the optimizing control of internal combustion power plants.

because of its susceptibility to noise, is that of derivative action. The remaining two terms are necessary for stable operation, if isochronous governing is to be achieved, but the best system performance obtainable from proportional and integral governor terms alone is generally not acceptable. The aim of the investigation has been to find the form of non-linear function which, when used in conjunction with proportional and integral terms in a governor, gives the most acceptable system performance, and to compare this with that obtainable from the three-term controller.

SYSTEM AND SIMULATOR CIRCUIT

The engine and its speed control system are shown schematically in fig. 1. The control system comprises three basic elements, assumed to be representative of units which are commercially available.

They are:

■ FUEL PUMP. Assumed to be a variable-displacement engine-driven pump, controlled by means of an integral positional hydraulic servo-mechanism.

■ FLOW CONTROL VALVE. Monitors the pressure drop across the metering orifice, f_1, and uses the signal to position the half-ball valve, f_2, of the pump positional servo-mechanism.

■ GOVERNOR. Shown in two basic forms, indicated by separate blocks in fig. 1. The first is one possible way of obtaining a hydraulically actuated three-term controller with proportional, derivative and integral action. The other is a non-linear device, basically similar to the three-term controller, but with the portion generating the derivative term replaced by a profiled valve, f_3. This second block is a schematic representation of the non-linear controller which gave the most acceptable system performance of the types investigated.

The block diagram for the system under consideration, together with the component transfer-functions, is shown in fig. 2, and in its reduced form in fig. 3. The transfer-functions for the linear system have been derived (1), and that for the non-linear governor is developed in Appendix 1 of the present article.

The hypothetical engine system with the various alternative governor arrangements studied has been analysed on a Pace 221R analogue computer. The circuit layout for the two arrangements of fig. 1 is shown in fig. 4, the engine, fuel pump, flow control valve, and governor being indicated by separate blocks. The circuit was programmed in such a way that the effect on engine performance of variation in governor characteristics, i.e. loop gain, integrating coefficient, and derivative coefficient or parameters of the different non-linear functions, could be easily studied.

NOMENCLATURE

|	
D	Limiting value of rev/min error signal
E	Rev/min error signal
G_1	Transfer relationship of governor
G_2	Transfer relationship of engine and fuel system
M	Closed-loop system gain
M_p	Peak resonance amplitude
$\overline{N}_e$	Describing function
N_e	Engine speed error
N_i	Selected engine speed
N_o	Actual engine speed
p	Modified Laplace operator
s	Laplace operator
ω_p	Peak resonance pulsatance
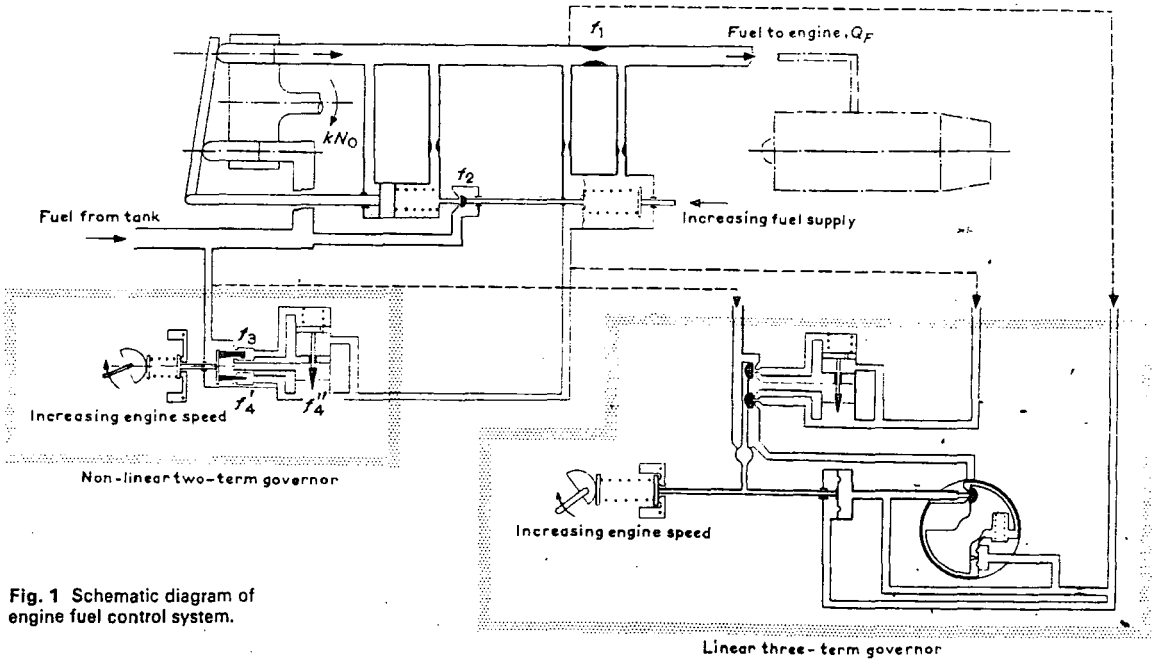
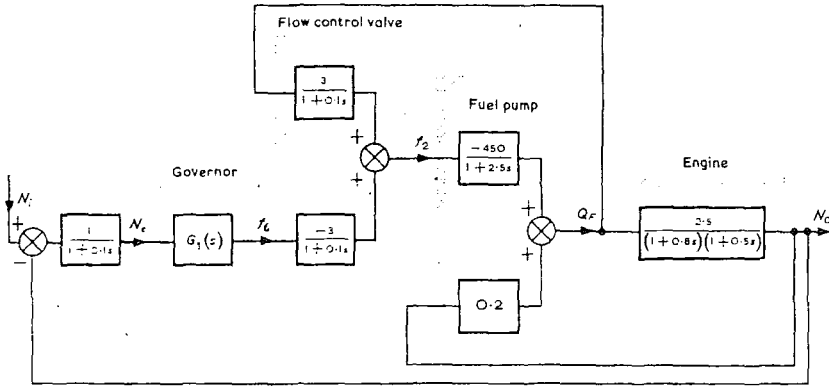**Fig. 1** Schematic diagram of engine fuel control system.
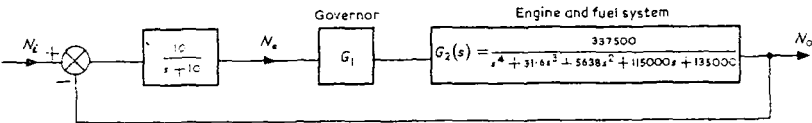
Fig. 2 Block diagram of engine and fuel control system.

Fig. 3 Reduced block diagram. For linear governor $G_1 = f(s) = 2.4 + 0.8/s + 0.12s$.
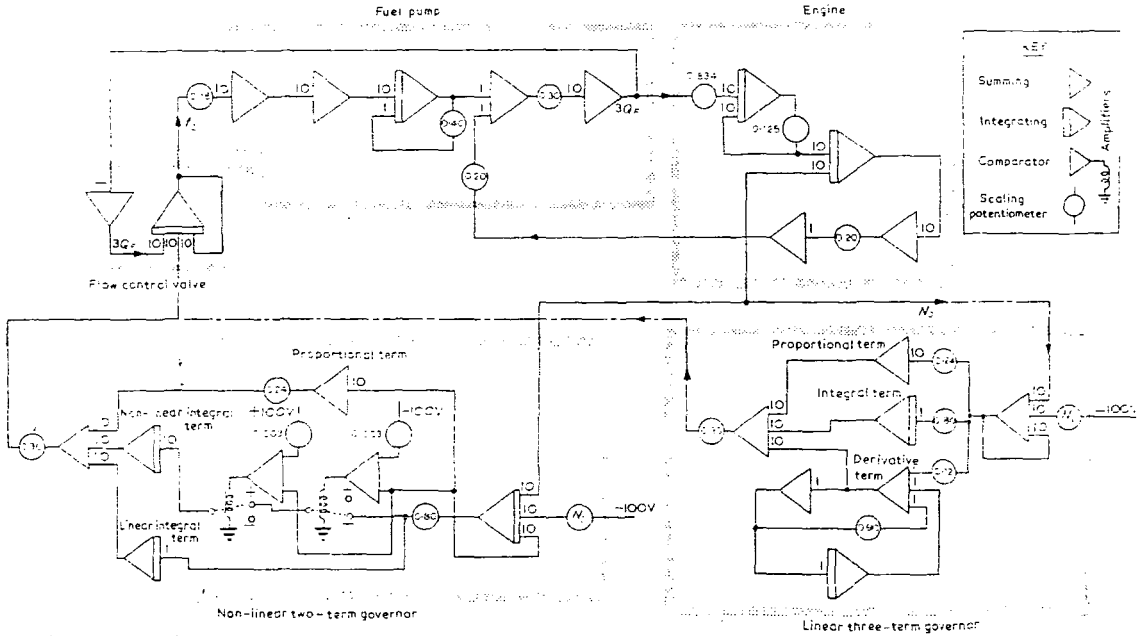For non-linear governor $G_1 = f(s,\bar{N}_c) = 2.4 + 0.8/s - 8\bar{N}_c/s$.

Fig 4 Computer circuit for engine and fuel control system.

PERFORMANCE CRITERION

The investigations have been restricted to 'range speed governing' within an engine speed range of 8000-8600 rev/min, chosen to be representative of many actual engines. Full-range speed governing from ground idling to maximum engine speed is not practically possible: the shape of the compressor characteristics much below engine speeds of this range make it essential to limit engine acceleration to avoid compressor surge and stall. Fortunately full-range speed governing is not generally necessary because of the restricted operating range requirement when in flight.

The criterion chosen to compare system performance for the different governor configurations studied is the transient response of the simulated system to a step change in selected speed, which can be considered as the most severe disturbance to which a system must respond. The following characteristics are considered necessary for acceptable transient performance:

■ rise time to selected speed datum, 0·3 s max.
■ settling time to selected speed datum, 2 s max.
■ initial overshoot, 25% max.
■ number of oscillations, 1½ max.

RESULTS AND DISCUSSION

TABLE 1

| Test number	1	2	3	4	5	6	7	8	9	10	11	12	13	14	15	16
SYSTEM CHARACTERISTICS																
Governor characteristics																
Terms	Proportional ·			Proportional + integral		Proportional + derivative		Proportional, integral and derivative						Proportional		
Value Z_1	2·4	6·0	1·0	2·4	2·4	2·4	2·4	2·4	2·4	1·0	1·0	2·4	2·4	2·4	2·4	2·4
Value Z_2	—	—	—	5·0	8·0	—	—	5·0	5·0	5·0	0·8	0·8	0·8	—	—	—
Value Z_3	—	—	—	—	—	0·12	0·60	0·12	0·60	0·12	0·12	0·12	0·48	—	—	—
Loop gain	6·0	15·1	2·5	6·0	6·0	6·0	6·0	6·0	6·0	2·5	2·5	6·0	6·0	6·0	6·0	6·0
TRANSIENT RESPONSE CHARACTERISTICS																
Rise time to selected datum, s	0·26	0·20	0·45	0·32	0·30	0·31	0·27	0·30	0·21	0·30	0·31	0·21	0·16	0·26	0·30	0·70
Overshoot, %	36	68	26	62	78	31	35	52	46·5	50	24 long	33	34	9·5	33·5	0
Number of oscillations	1·5	5·5	0·5	2·5	4·5	2·0	3·0	2·0	2·5	2·0	0·5	1·5	2·5	1·0	2·5	0
Settling time, s	1·6	3·1	1·4	2·7	4·5	1·7	1·7	1·8	2·4	4·0	5·3	5·5	5·5	1·2	3·0	0·70
STEADY STATE																
Speed error N_e, %	9·5	3·3	21·5	0	0	9·5	9·5	0	0	0	0	0	0	9·5	9·5	9·5
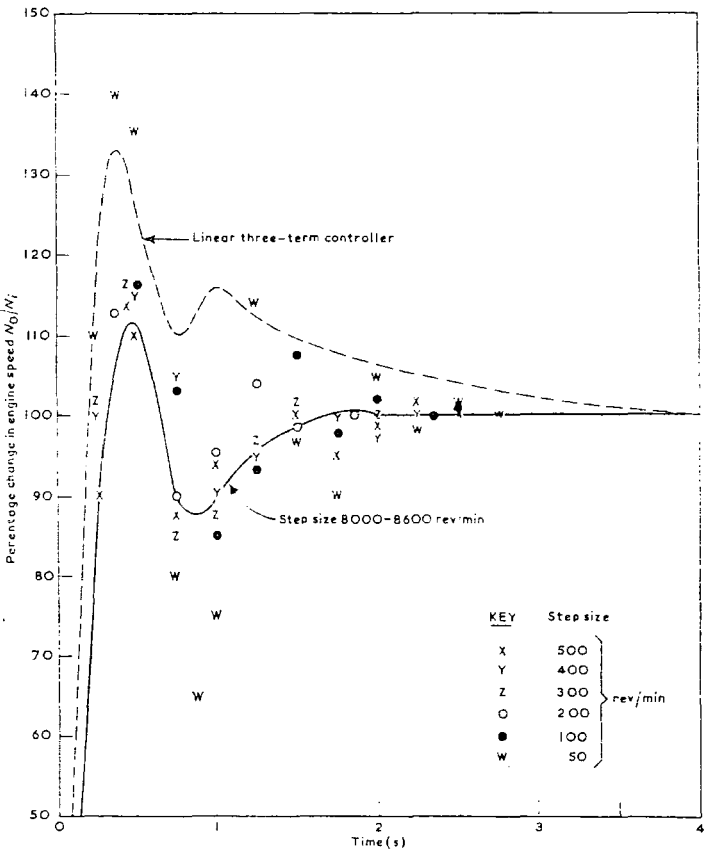
Fig. 5 Transient response.

Linear three-term governor

In an attempt to achieve the required system performance the system response was investigated for various combinations of coefficients of the three terms in the linear controller (1). From table 1 it can be seen that the desired transient response requirements were not fully attained. The best system response results with all three terms in use, and the nearest approach to the performance criteria specified earlier (in the section entitled *Performance criterion*) is Test 12 with a rise time of 0·21 s, overshoot 33%, oscillations 1½, and settling time 5½ s.

The transient response curve for this test is shown in dimensionless form in fig. 5. After a 4 s interval the speed error is sensibly zero, and after a period of 3 s is within acceptable limits for most engine installations. The overshoot is, however, considerably larger than the 25% maximum specified, and could in practice result in mechanical engine failure on selection of a higher speed datum. Conversely, the selection of a lower speed datum for high-performance aircraft would lead to engine 'blow-out',* with possible loss of aircraft at low altitude owing to lack of sufficient time for the relight procedure.

References

1. Schwarzenbach and Gill: 'Analysis of a gas turbine engine fuel system', *The Engineer*, Vol. 219, p.209. Jan. 1965.

Blow-out is the jargon term for flame extinction.

PAPER 12

A theoretical look at the use of functional non-linearities in a gas turbine control system

K. F. GILL, M.Sc., Ph.D., *and* J. SCHWARZENBACH, M.Sc., *University of Leeds*

For the reasons given last month the linear three-term controller does not give an ideal system performance.

Effect of noise

It has generally been thought that the noise generated at the outlet of high-speed plunger-type hydraulic pumps could have considerable effect on the correct functioning of the derivative term with certain types of component layout. Certain commercially available pumps have ripple suppressors to reduce the amplitude of the pressure fluctuations.

A theoretical study of such a unit indicated that the frequency of the pressure fluctuations would be at some frequency exceeding 200 c/s (Hz), the actual magnitude depending on the rotational speed and on the number of plungers in the pump. The amplitude of the pressure oscillations would not exceed $\pm 10\%$ of mean delivery pressure, provided that the length of the delivery pipe and the flow velocity were not excessive.

Noise signals composed of two saw tooth waveforms with suitably displaced frequencies and amplitudes were used to simulate the type of pressure ripple which might occur in practice. This signal was injected into the various points in the simulated governor unit where the effect would be most marked. For both the linear and non-linear systems studied no noticeable change in engine speed response occurred at these frequencies.

To show an effect it was necessary to reduce the signal frequency by a factor of ten, and only when frequencies of the order of 5 c/s (Hz) were used did the effect become serious. At these lower frequencies the amplitude of any noise signal which might

be present would be considerably smaller than the $\pm 10\%$ mentioned above, and could be ignored.

Non-linearities investigated

An essential design criterion for aircraft engines is that governing be isochronous. In single-engined aircraft this relieves the pilot of unnecessary attention to engine control; with multi-engined installations the problems associated with engine synchronization are greatly reduced. Further, isochronous governing allows fuel requirement predictions to be more accurate for any given flight plan.

It will be realized that system operation can never be stable if a linear isochronous governor of integral action alone is used. Introduction of non-linear effects into the pure integrating governor results in a combination of rise time and overshoot which is greatly inferior to that obtainable with a linear proportional + integral controller. In the latter case the desired transient response is still not achievable. Hence in this work the governors investigated have all contained proportional and integral action, and various types of non-linearity have been introduced in turn in an attempt to improve upon the transient characteristics of the linear three-term controller.

The main types of non-linearity investigated, together with the resulting transient performance characteristics, are shown in table 2. A first attempt to improve the transient performance characteristics of the system using a simple linear proportional + integral governor was made by restricting the excess fuel available to accelerate the engine. The coefficients of the terms of the two-term controller were adjusted so that the rise time

TABLE 2

System	Type of non-linearity	Step size, rev/min	Proportional governor gain	Integration coefficient time, s	Rise time, s	Overshoot %	Settling time, s	Number of oscillations	Steady-state oscillations, re/min	Comments
(a)	High loop gain with limit to proportional band at ±20 rev/min +linear integrating coefficient	600 300 150 30	25 25 25 25	0·08 0·08 0·08 0·08	0·7 0·5 0·25	13 21 40	1·1 0·8 0·6 ——— Unstable ———	– – –	87 80 90	Rise time too high, and oscillations in steady state. For small signal size overshoot large + instability.
(b)	High loop gain with limit to proportional band at ±15 rev/min +deadband of ±10 rev/min +linear integrating coefficient	600 300 75	36 36 36	0·08 0·08 0·08	0·8 0·5 0·15	10 31 66	2·4 2·6 1·6	3 – –	0 26 16	System no more satisfactory than system (a). Also, limits too narrow for practical design.
(c)	Two-rate proportional governor with increase in rate at ±175 rev/min +linear integrating coefficient	600 250 125	6 and 15 6 and 15 6 and 15	0·5 0·5 0·5	0·2 0·25 0·25	42 42 47	2·0 2·2 1·8	2 2 1½	0 0 0	Excessive overshoot.
(d)	Medium loop gain +two rate integrating coefficient with decrease in value at ±50 rev/min	600 300 100 50	6 6 6 6	0·88 and 0 08 0·88 and 0 08 0·88 and 0 08 0·88 and 0 08	0·3 0·3 0·25 0·25	11 13 35 68	1·6 2·0 2·1 2·5	1 2 2 2	0 0 0 0	System performance improved over three-term controller. System potentially simpler. Large% overshoots for small step sizes are small in absolute value.
(e)	Linear three-term controller (1)	Not applicable	6	0·8	0·21	33	4	1½	0	Derivative coefficient 0·12.

became acceptable, and, in order to bring the overshoot to within the acceptable limit of 25%, it was necessary to restrict the engine overfuelling to a value within 5% of the required steady-state fuel flow. This limitation unfortunately increased the rise time appreciably, so the possibility of a physical system to achieve this form of fuel flow characteristic was not further investigated.

The introduction of further non-linearities outside the governor unit was not considered since they could not be readily achieved on the physical system. The only realistic way to achieve the desired transient response was to add simple non-linearities, which could easily be physically produced, to the two-term governor unit itself. The non-linearities chosen for investigation were limitation of linear characteristics, dead band, hysteresis and double-rate 'linear' characteristics. Of these hysteresis proved to be of no greater advantage than dead band, and more difficult to produce physically.

Examination of the table shows that:

■ System (a) is completely unacceptable owing to the relatively large steady-state oscillations, which would result in objectionable beat notes in multi-engined installations.

■ In system (b) the limits imposed to obtain a more satisfactory system than (a) were such that would be impossible to achieve in practice.

■ System (c) was an attempt to eliminate the steady-state oscillations of (a) by reduction of the proportional system gain for speed errors less than 100 rev/min. The shortcoming of this otherwise satisfactory system was the high initial overshoot which occurred with all sizes of step rev/min input.

None of the tested systems using non-linearities applied to the proportional term of the governor unit gave a performance which was considered to be sufficiently satisfactory. It was therefore decided to operate on the integral term of the governor, and system (d) is that which produced the most acceptable performance. The high percentage overshoots

associated with small rev/min steps can be tolerated because of the small absolute rev/min errors which they represent. This system satisfies the requirement for physical simplicity and ease of introduction into governor units, and one possible method is illustrated schematically in fig. 1.

Comparison with the performance of the three-term governor controller shows that equally acceptable system performance has been achieved from this two-term controller incorporating a simple functional non-linearity. This arrangement should give a cheaper and more reliable unit.

Root locus

The block diagram, including transfer relationships, for the non-linear system (d), is shown in fig. 3. The transfer relationship for the governor depends on a describing function (2), $\bar{N}_e$, as well as the Laplace operator s. The describing function (see Appendix 1) is—

$$\bar{N}_e = \frac{1}{\pi}\left\{2 \arcsin\left(\frac{D}{E}\right) - 2\left(\frac{D}{E}\right)\sqrt{\left[1 - \left(\frac{D}{E}\right)^2\right]}\right\}$$

where D is the limiting value of the error signal E.

The closed-loop transfer relationship for the non-linear system (fig. 3) is—

$$\frac{G_1.G_2(s)}{1 + G_1.\,G_2(s)}$$

from which is obtained the characteristic equation—

$$p^6 + 4·16p^5 + 59·54p^4 + 171·4p^3 + 128·5p^2 + 94·5p + (0·27 + 3·38\bar{N}_e) = 0$$

where $p = 0·1s$ has been introduced to reduce the variation of the equation coefficients.

The root locus in fig. 6 is constructed in the normal way. Indicated are the positions of the important roots for the two values of integrating coefficient used. As an aid (3) to accuracy in the region of interest, graticules

e constructed on which the contribution of e distant pair of complex conjugate poles the angle and magnitude conditions can e specified. They eliminate necessity for aving the distant poles on the diagram. If e describing function is a function of amplitude only, then roots can be indicated on the ot for various values of the describing nction for the quasi-linear system. The ots for $\bar{N}_e = 1$ are the roots for a linear stem with an integrating coefficient of 8 s, while those for $\bar{N}_e = 0$ are the roots of linear system with an integrating coefficient 0·8 s. Study of the plot will show which ots are dominant, and how the system damping and natural frequency change with variation in the value of the describing function. he value of the real root indicates the amount damping, and the position of the complex njugate pair of roots indicates the frequency oscillation. If the describing function is, in ddition, frequency-dependent, then a separate ot locus plot is necessary for each value of ror amplitude, and the labour involved in nstructing the loci makes the method practicable.

Since the integrating coefficient has only o discrete values, exact solutions for the sponse to different inputs can be obtained. he roots obtained from the root locus plot n be used to calculate the transient response a step change in input, if the appropriate itial conditions are introduced at the ginning of each linear segment. The mputational time, even for a simplified stem such as this, is extremely lengthy, and nce of doubtful practical value. The chnique would be to adopt the final values one linear section as the initial conditions r the next linear section, and in this way a ecewise-linear exact solution for the system sponse to a step change could be computed.

Strictly, the describing function is only applicable to systems with sinusoidal inputs. However, for a step input it does permit broad conclusions to be reached about the system transient behaviour. As the step size decreases from 600 to 100 rev/min. the numerical value of the describing function changes from 0 to 0·06 and this causes little variation in the position of the roots. Hence it would be expected that there would be no marked change in system transient response for error step sizes within this range. For error sizes less than 100 rev/min. no general conclusion of this nature can be reached since the movements of the poles are in opposite directions along the separate loci, and only numerical evaluation will show which is the most prominent component. Inspection of the non-dimensional transient response, fig. 5, shows that if the step size of 50 rev/min is ignored the transient response curves for the other steps are very similar. For the larger step sizes an overshoot of less than 20%, a rise time better than 0·3 s, and a settling time better than 3 s can be expected, results better than achieved with the linear system.

Polar plot

A polar plot can be obtained for the simple non-linear system. The plot is analogous to the Nyquist diagram for the linear system. Shown in fig. 7 is the polar plot for the open-loop system together with the negative inverse describing function, $-1/\bar{N}_e$. The curve shows that the system is stable. If the curves had intersected at some value of D/E, sustained periodic oscillation of amplitude E would have occurred, which would be unsatisfactory.
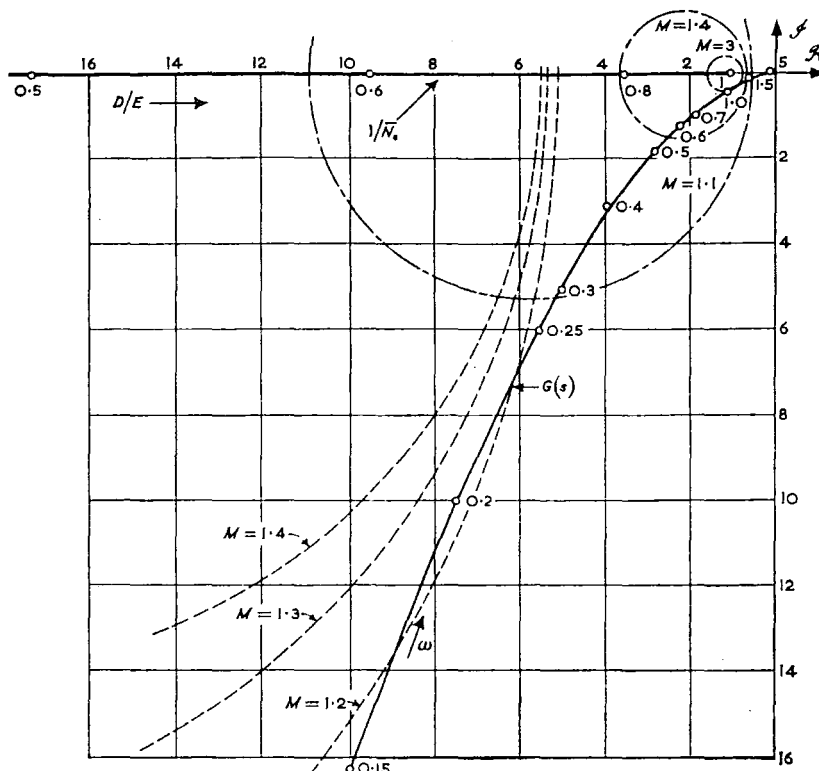
The mathematical explanation for the

g. 6 Root locus.
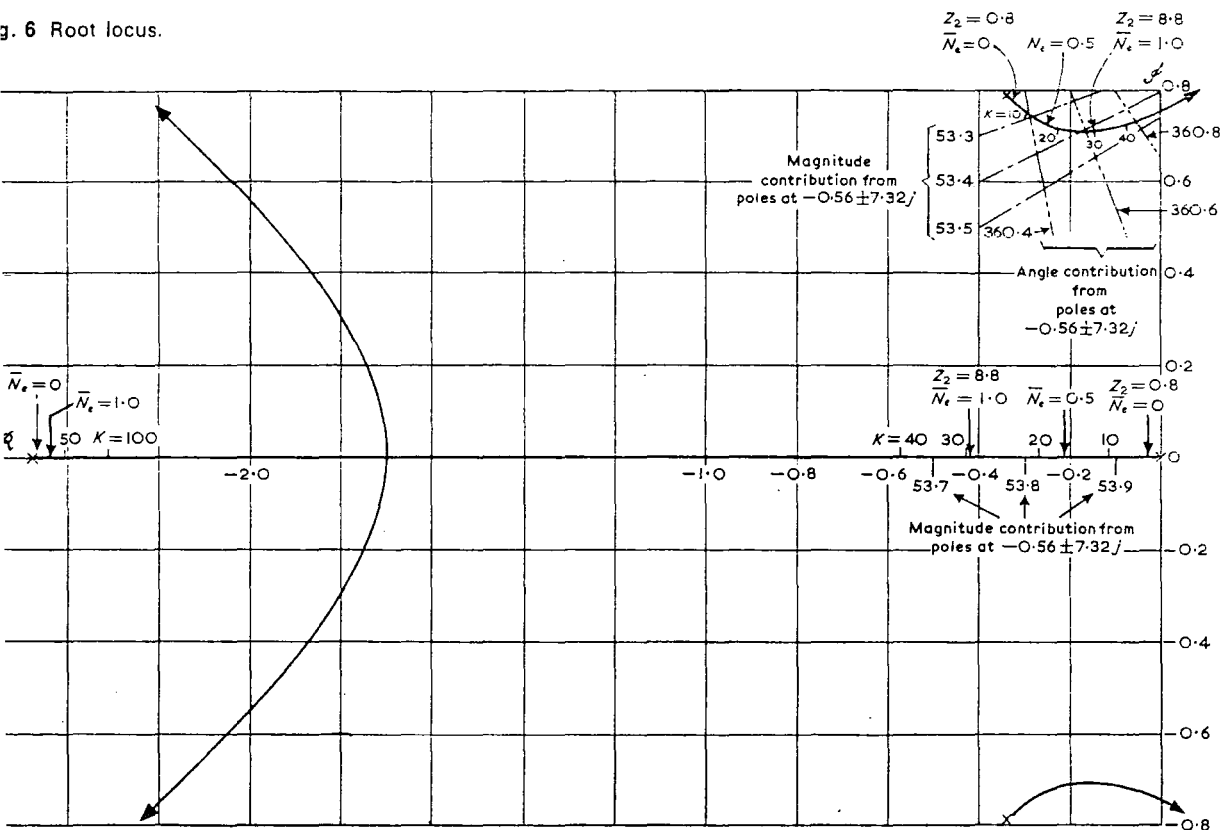
Fig. 7 Polar plot of $G(s)$ and $1/N_e$ with M contours.

construction of the M-circles is given in Appendix 2. The M-contours are moved to the left of the diagram with decreasing values of D/E, and for this system the value of resonance peak, M_p, will decrease as the value of D/E decreases, and the system will become more stable. Fig. 7 shows the M-contours for the range of major interest in linear system harmonic analysis. The value of D/E chosen to reposition the M-contours for the range of M of 1·2 to 1·5 is 0·6.

For the linear system, i.e. $D/E = 1$, the value of the main harmonic performance figures are $M_p = 3$, $\omega_p = 1$ c/s (Hz), phase margin 17°. The introduction of the non-linear element shows a reduction of M_p to 1·2, and an increase in the phase margin to

48°; the value of ω_p becomes 0·24 c/s (Hz).

The value of M_p determined in this way for any fixed value of D/E does not have the same meaning as in the linear system but does give some indication of the relative stability of the system. In terms of transient response, with the larger initial error the small M_p and small ω_p indicate a small overshoot and slow rise time respectively, but as the transient dies out and the signal amplitude decreases the damping decreases (M_p gets larger) and the system gets faster (ω_p increases).

Experience with this type of polar plot may lead to the evolution of fresh criteria which can be used in the harmonic design of systems containing simple functional non-linearities.

CONCLUSIONS

A governor unit with a proportional term and using a simple functional non-linearity in the form of a double rate integral term results in a system performance comparable with that obtainable from a linear three-term governor The complex design for the derivative term could thus be effectively replaced by a relatively simple modification to increase the value of the integrating coefficient for values of error signal within a chosen small rev/min band.

Noise from the pressure ripple of plunger pumps, which can have considerable amplitude, is at a frequency at which it is greatly attenuated by the lags in the system. No effect of noise on the engine speed response could be detected, either with the linear three-term governor or with any of the non-linear governor system investigated. Lower-frequency noise has a greater effect on the

linear three-term governor because of the derivative term than on the corresponding two-term controller with double rate integrating coefficient.

For systems with a simple non-linearity the root locus technique gives a useful indication of the possible change in transient response with changing magnitudes of error signal. The theoretical evaluation of the exact transient response curve using information from the root locus diagram requires a large amount of computational effort.

A modified Nyquist diagram on which a family of M-contours can be plotted for each magnitude of error signal is a useful guide to the type of system harmonic performance to be expected. However, experience with this type of diagram would be necessary before system stability and performance could be predicted with confidence.

See fig. 8. Boundary conditions are—

$Ne'(t) = \sin \omega t \qquad 0 < \omega t < \alpha \qquad \pi - \alpha < \omega t < \pi + \alpha$

$\qquad\qquad\qquad 2\pi - \alpha < \omega t < 2\pi$

$Ne'(t) = 0 \qquad \alpha < \omega t < \pi - \alpha \qquad \pi + \alpha < \omega t < 2\pi - \alpha$

Owing to the symmetry of $Ne'(t)$, the magnitude of its fundamental component can be written as—

$$A = \frac{1}{\pi} \int_0^{2\pi} Ne'(t) \sin \omega t \, d(\omega t)$$

$$= \frac{E}{\pi} \left\{ \int_0^\alpha \sin \omega t \sin \omega t \, d(\omega t) + \right.$$

$$\int_{\pi-\alpha}^{\pi+\alpha} \sin \omega t \sin \omega t \, d(\omega t)$$

$$\left. + \int_{2\pi-\alpha}^{2\pi} \sin \omega t \sin \omega t \, d(\omega t) \right\}$$

$$= \frac{E}{\pi} \left\{ 2\alpha - 2 \sin \alpha \sqrt{(1-\sin^2\alpha)} \right\}$$

Now $\sin \alpha = D/E$. Therefore—

$A = (E/\pi) \{ 2 \arcsin (D/E) - 2 (D/E)\sqrt{[1-(D/E)^2]} \}$

Therefore—

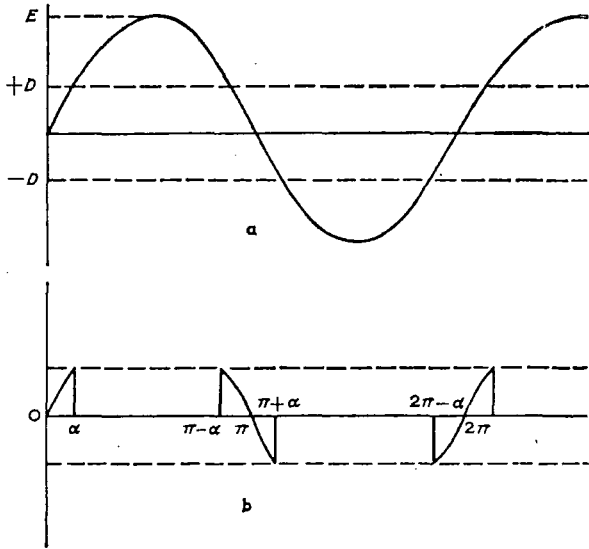$\overline{N_e} = (1/\pi)\{ 2 \arcsin (D/E) - 2(D/E) - 2(D/E)\sqrt{[1-(D/E)^2]} \}$

Fig. 8 (a) Input to non-linear element, $N_e(t)$.
(b) Output from non-linear element $N_e(t)$

Appendix 2. M-contour

Consider a unity feedback control system containing a non-linear element which can be represented by the describing function $\overline{N_e}$, where $\overline{N_e}$ is a complex number and a function of the input signal amplitude and frequency. It follows that the closed-loop system transfer function is—

$$\frac{N_o(s)}{N_i(s)} = \frac{\overline{N_e} (E,\omega) G(s)}{1+\overline{N_e} (E,\omega) G(s)}$$

Let the co-ordinates of the Nyquist plot of $G(s)$ be—

$G = x+jy$

and for the describing function—

$\overline{N_e} = a+jb$

Then $\qquad M = \left| \dfrac{\overline{N_e} (E,\omega) G(s)}{1+\overline{N_e} (E,\omega) G(s)} \right|$

which gives—

$$M = \frac{\sqrt{[(ax - by)^2 + (ay + bx)^2]}}{\sqrt{[(1+ax - by)^2 + (ay + bx^2)]}}$$

which on expansion and rearrangement gives the general equation of a circle with centre at—

$$X_o = - \frac{aM^2}{(a^2+b^2)(M^2-1)} \qquad Y_o = + \frac{bM^2}{(a^2+b^2)(M^2-1)}$$

and radius—

$$R_o = \frac{1}{\sqrt{(a^2+b^2)}} \frac{M}{M^2-1}$$

In fig. 9, for any arbitrary point c in the $-1/\overline{N_e}$ locus with the line oc extended—

$$oc = \frac{1}{\sqrt{(a^2+b^2)}} \qquad od = \frac{a}{a^2+b^2} \qquad dc = \frac{b}{a^2+b^2}$$

For the linear system the centre of the M-contours would be—

$$X'_o = - \frac{M^2}{M^2-1}, \qquad Y'_o = 0. \qquad \text{Radius} = \left| \frac{M}{M^2-1} \right|$$

If these are now constructed on the oc axis—

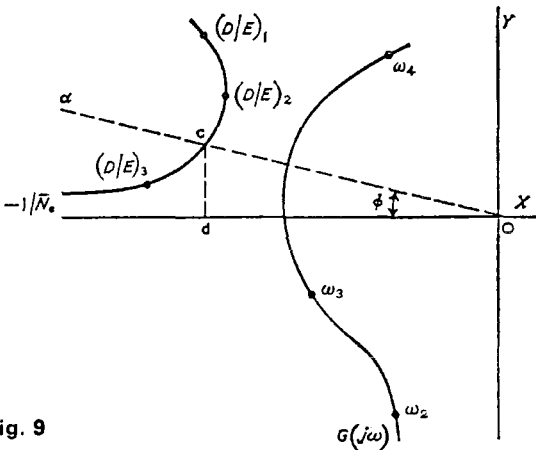$$X_o = \frac{a}{\sqrt{(a^2+b^2)}} \frac{M^2}{M^2-1}; \qquad Y_o = \frac{b}{\sqrt{(a^2+b^2)}} \frac{M^2}{M^2-1}$$

Fig. 9

Taking the point c as the new $-1, j0$ point, the new co-ordinates of the M-contour are—

$$X_o = \frac{a}{a^2+b^2} \frac{M^2}{M^2-1}; \qquad Y_o = \frac{b}{a^2+b^2} \frac{M^2}{M^2-1}$$

and $\qquad r_o = \frac{1}{\sqrt{(a^2+b^2)}} \frac{M}{M^2-1}$

References—continued

2. Chestnut and Mayer: *Servomechanisms and regulating system design*, Vol. II. Ch. 8. John Wiley and Sons.
3. Taylor: *Servomechanisms*. p.334. Longmans.

End

PAPER 13

Design analysis of model reference adaptive control systems applied to a gas-turbine aircraft engine

K. F. Gill, M.Sc., Ph.D., C.Eng., A.M.I.Mech.E., M.I.E.E., J. Schwarzenbach, M.Sc., and G. E. Harland, B.Sc.

Synopsis

A gas-turbine aero-engine speed-control system has been investigated on an analogue computer to determine the possibility of using a model reference adaptive control device to maintain constant dynamic behaviour of engine speed irrespective of altitude and aircraft forward speed. A conventional type of speed-control arrangement has been used in the main loop, and an auxiliary feedback loop has been introduced which biases the flow-control unit by an amount which is proportional to the derivative of engine speed. The constant of proportionality is the parameter which is being changed by the adaptive loop. The adjustment is such that a minimum in the value of integral of error squared is sought, where the error signal used is the instantaneous difference between engine and model speed outputs. The results suggest that it would be physically reasonable to produce such a controller, and that substantially similar dynamic behaviour is obtainable under changing environmental conditions. Such a loop could be added to existing speed-control systems without major modifications in design.

List of principal symbols

a = engine gain
b = engine primary time constant
$G(s)$ = overall transfer function
$G_1(s)$ = governor transfer function
$G_M(s)$ = model transfer function
k = parameter varied by adaptive loop
N_i = desired speed
N_0 = engine actual speed
s = Laplace operator
ϵ = speed error $(N_i - N_0)$
λ = adaptive loop gain
ξ = damping factor
ω_n = undamped natural frequency

1 Introduction

Gas-turbine-engine speed-control systems in use today generally can be considered to comprise three major control devices; namely an acceleration control unit, a flow-scheduling control unit and a governor control unit. Each of these has overriding control within a specified region of the range of operation of the engine.

The most severe requirement for an engine is that it should be capable of accepting a demand for a 'slam' acceleration from ground idling speed to any selected engine speed and giving the fastest possible response rate. The full flow from the flow scheduling unit under these conditions would create a gas pressure in the combustion chamber sufficient to give aerodynamic stall conditions in the compressor, resulting in a severe reduction in engine thrust. The acceleration control unit, which gives a scheduled fuel flow controlled by the compressor delivery pressure, is used to avoid this condition by restricting the fuel flow in such a manner that a predetermined margin from the stall condition is maintained throughout any acceleration.

To achieve satisfactory engine running at speeds between ground idling and a speed somewhat less than that used for engine cruise conditions, the flow scheduling device meters the fuel flow according to throttle position and atmospheric ram pressure. This ram pressure is the total head pressure due to aircraft altitude and forward speed, and is therefore sensitive to these variables of the aircraft flight path. During most of the flight path the engine is under the control of the governor, which takes over control at some engine speed a little below that used for cruise conditions.

Theoretical studies have previously been undertaken by the authors[1] on the analysis of a hypothetical gas-turbine-engine control system. A 3-term hydraulic governor controller with proportional, integral and derivative terms was considered, but it was found that completely acceptable transient per-

formance could not be obtained. This form of governor controller is a highly complex and expensive unit, and in an attempt to reduce the complexity and susceptibility to failure, a simpler form of controller was investigated.[2] This resulted in the derivative term being replaced by a nonlinearity in the integral term to give a system with dynamic characteristics which were sensibly the same as those for the system with the best 3-term controller.

Both of these studies assumed that the engine installation was operating under steady environmental conditions, and no attempt was made to allow for changes in these conditions. Different flight conditions, such as altitude and forward speed, result in changing dynamic characteristics of the engine system. An engine control system must, to give good dynamic performance under all operating conditions, adapt itself to such changes.

The approach used in practice is to determine a series of governor parameters, each attempting to give the desired performance at a particular altitude and forward speed, and to adjust these parameters automatically as predetermined functions of measurable quantities. This form of scheduling of governor gain parameters has been referred to as open-loop adaptation.[3]

The success of such adaptation is dependent on being able to generate sufficiently accurately the governor gain constants for the wide range of possible operating conditions.

While such open-loop adaptation is being used successfully, requirements for engine and aircraft performance are becoming increasingly severe, and this brings attendant difficulties of design, production and maintenance of the controller for scheduling loop adjustment.[4] Attempts have been made, in other fields to produce closed-loop adaptive systems where an ideal performance is specified, and the system attempts automatically to minimise the difference between its actual and ideal performance.

Various approaches to the design of closed-loop adaptive systems have been described,[5-7] and these tend to fall into two classes. In one the dynamic response of the system is continuously forced into correspondence with an ideal response defined by a model, and this is termed a 'model reference adaptive control system'.[8-11] In the other, the system performance is characterised by a single value, a performance index,[12, 13] and the system operates to maximise or mimimise this value.

The hypothetical gas-turbine-engine system previously studied[1, 2] has now been modified to include closed-loop adaptation using a model for reference, and the present paper describes the behaviour of the composite system with a model whose dynamic behaviour can be described by a second-order differential equation, where the damping factor ξ and undamped natural frequency ω_n are chosen to give the ideal response. This is the simplest possible model and is representative to a good approximation of the closed-loop engine system. Inspection of Figs. 5 and 6 of Reference 1

shows that there is just one pair of predominant roots for the engine system chosen, with either proportional governor alone or with a proportional-plus-integral governor. Integral action must be included since isochronous governing is essential.
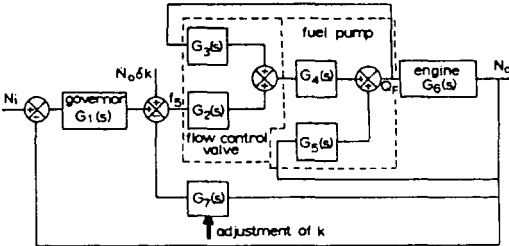

Fig. 1

Block-diagram arrangement of engine system

2 Description of system and simulated circuit

The system considered in this investigation is shown in block-diagram form in Fig. 1. The transfer functions[1] for sea-level conditions are:

$$\text{governor: } G_1(s) = \frac{2\cdot4 + 0\cdot8/s}{1 + 0\cdot1s}$$

$$\text{flow control valve: } G_2(s) = \frac{-3}{1 + 0\cdot1s}, \; G_3(s) = \frac{3}{1 + 0\cdot1s}$$

$$\text{fuel pump: } G_4(s) = \frac{-450}{1 + 2\cdot5s}, \; G_5(s) = 0\cdot2$$

$$\text{engine } \quad G_6(s) = \frac{2\cdot5}{(1 + 0\cdot8s)(1 + 0\cdot05s)}$$

Auxiliary feedback loop: $G_7(s) = ks$

where k is the parameter to be adjusted by the adaptive loop.
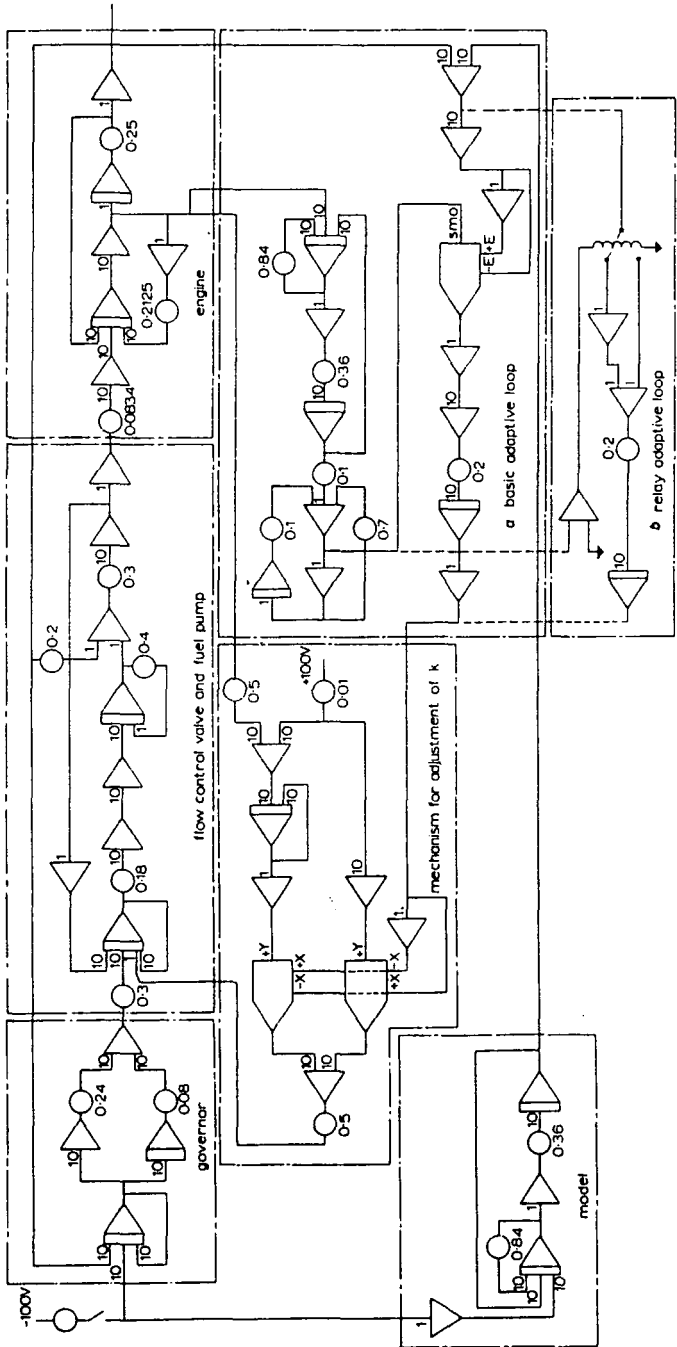

Fig. 2

Computer circuit for engine system and adaptive loop

The values of the engine gain and engine primary time constant are increased by a factor of 3 to represent altitude conditions. The control law for the adaptive controllers is that of steepest descent.

The investigation has been carried out on an analogue computer, and the circuit layout for the system is shown in Fig. 2a. Shown in Fig. 2b is an alternative arrangement for the adaptive loop, where a multiplier has been replaced by a relay, thus giving a somewhat cheaper circuit. To obtain the

system. The most logical parameter for adaptation in a gas-turbine-engine speed-control system is that of the governor proportional gain term. To a first approximation the transfer function of fuel pump, flow control and gas turbine can be represented by the second-order function $\dfrac{a}{(1 + bs)(1 + 0 \cdot 05s)}$, which can be verified by inspection of Figs. 5 and 6 of Reference 1, and then the overall transfer function is

$$\frac{N_0(s)}{N_i(s)} = \frac{aks + 0 \cdot 8a}{0 \cdot 005bs^4 + (0 \cdot 005 + 0 \cdot 15b)s^3 + (0 \cdot 15 + b)s^2 + (1 + ak)s + 0 \cdot 8a} \qquad \ldots \ldots \ldots (1)$$

It can be seen that poor adaptation would result from adjustment of parameter k, since it fails to influence the high-frequency components of the transfer function.

A second possibility would be to use a proportional feedback loop around the engine and fuel system. The form of the transfer function in this case is:

$$\frac{N_0(s)}{N_i(s)} = \frac{2 \cdot 4as + 0 \cdot 8a}{0 \cdot 005bs^4 + (0 \cdot 005 + 0 \cdot 15b)s^3 + (0 \cdot 15 + b + 0 \cdot 1ak)s^2 + (1 + ak + 2 \cdot 4a)s + 0 \cdot 8a} \qquad \ldots \ldots (2)$$

This can be seen to be an improvement over the first system.

A better behaved system results if the derivative of engine speed is fed back across the engine and fuel system as shown in Fig. 1, the transfer function being

$$\frac{N_0(s)}{N_i(s)} = \frac{2 \cdot 4as + 0 \cdot 8a}{0 \cdot 005bs^4 + (0 \cdot 005 + 0 \cdot 15b + 0 \cdot 1ak)s^3 + (0 \cdot 15 + b + ak)s^2 + (1 + 2 \cdot 4a)s + 0 \cdot 8a} \qquad \ldots \ldots (3)$$

required gain setting in the auxiliary feedback loop, a quater-square multipler is used. The operating level is moved away from zero by using a fixed bias in order to avoid malfunctioning of the multiplier at and near zero input voltage, and also to improve accuracy at small voltages. In a practical system this operation would be performed by a positional servo-mechanism.

3 Dynamic performance criteria

The system with adaptive loop is nonlinear, which makes it necessary to clearly specify the types of system forcing function to be considered. If the system dynamic behaviour is studied using repetitive step and impulse input functions at both high and low frequencies, information is obtained about deterministic signals. Random-noise inputs cover the case of stochastic signals. If the system adapts satisfactorily with each of these types of forcing function, one can assume with confidence that the system will be satisfactory for any arbitrary input. The results obtained from repetitive step inputs can be compared with the results in the previous reports.

The adaptive loop must be such that there is good selectivity which yields a sharply defined optimum as a function of the system parameters used. The criterion chosen must also be easy to measure and apply.

The most obvious parameter to use when dealing with transient behaviour is that of an error function, where the error ϵ is the instantaneous difference between engine and model speed outputs. Because of the nature of the relationship between this speed error and most system parameters, it is possible to use gradient methods to minimise speed error functions. The primary advantage of gradient methods is that they give to the controller a well defined course of action, and the gradient method considered in this paper is that of steepest descent.

The performance parameter selected for study is ϵ^2. No results have been presented for the parameter $|\epsilon|$, since the $|\epsilon|$ minimisation has the inherent shortcoming that, as the minimum is approached, the rate of change of dk/dt becomes increasingly small since the first order derivatives of ϵ tend to zero. The ϵ^2 minimisation does not have this distressing characteristic; its gradient is always steeper than $|\epsilon|$ in the neighbourhood of the minimum.

4 Design of adaptive loop

The basic object of the adaptive loop is to maintain constant system dynamic behaviour, which mathematically implies a constant closed-loop transfer function for the

Inspection of this relationship shows that the coefficients associated with the high-frequency terms can be maintained sensibly constant by changing k, better performance resulting from changes in a than b. For successful adaptation the model must have dynamic characteristics of the general form of eqn. 3. It is reasonable to neglect the highest-order term, and, by choosing sea-level conditions $a = 2 \cdot 4$, $b = 0 \cdot 8$ as the design datum and dividing the numerator into the denominator, eqn. 3 reduces to one of second order. For $k = 0 \cdot 2$, which was chosen to give a damping factor $\xi = 0 \cdot 7$, this equation is

$$\frac{N_0(s)}{N_i(s)} = \frac{34}{s^2 + 8 \cdot 0s + 34} \qquad \ldots \ldots \ldots (4)$$
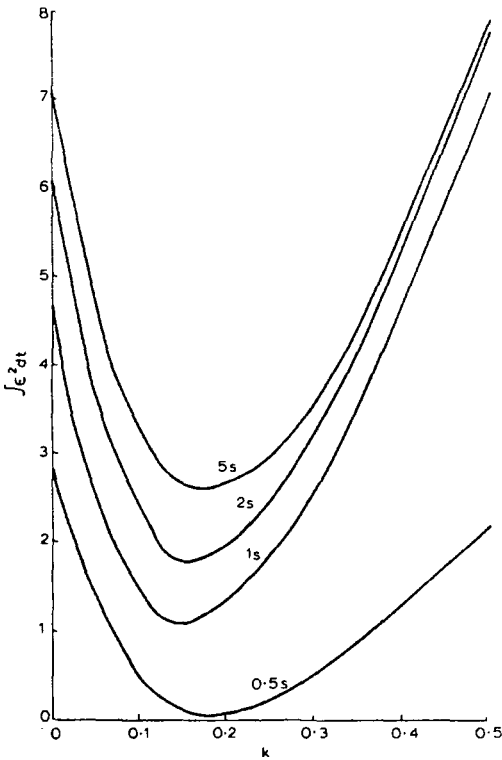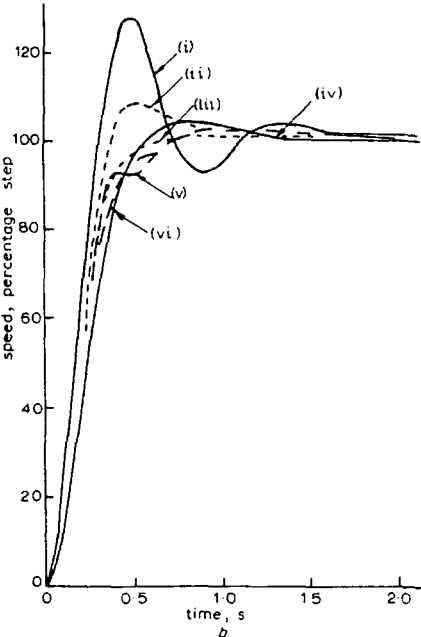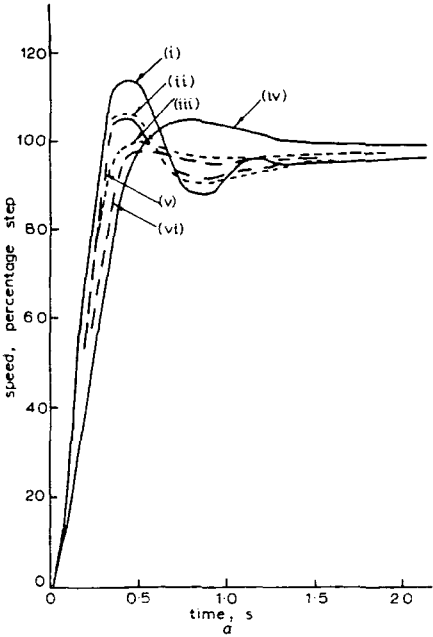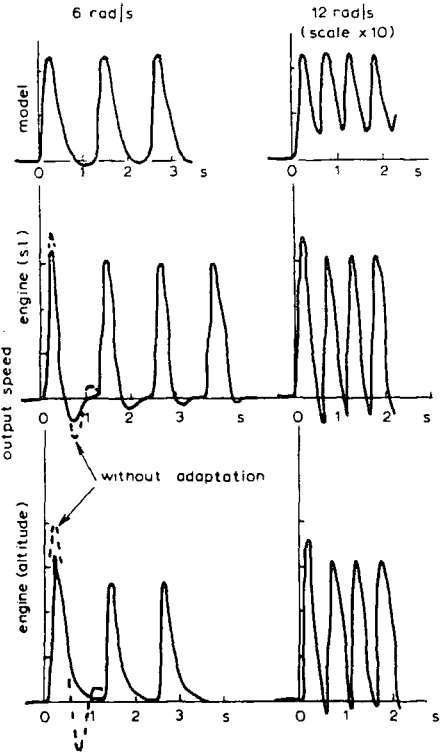
Fig. 3

Dynamic behaviour of $\int \epsilon^2 dt$

For the second-order system with $\xi = 0.7$ and undamped natural frequency $\omega_n = 6$ rad/s, the rise time is 0.5 s, the settling time is 1 s, the maximum overshoot is 5% and there is no undershoot. This is broadly within the generally accepted performance requirements of 0.3 s maximum rise time, 2 s maximum settling time, initial overshoot 25% maximum and number of oscillations $= 1\frac{1}{2}$. Eqn. 4 then specifies the parameters of the model to be used.

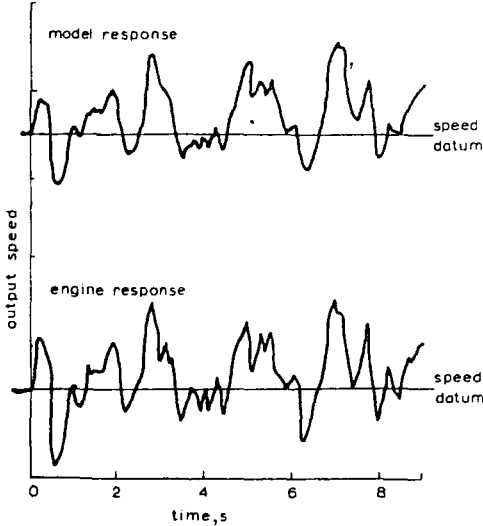The law of steepest descent for the single-variable case is

$$k = -\lambda \frac{\partial}{\partial k} f(\epsilon) \qquad \qquad \qquad (5)$$

In this case a function which yields a well defined optimum is $\int \epsilon^2 dt$. Fig. 3 shows the dynamic behaviour of this function with changes in the gain k of the chosen auxiliary loop, points on these curves being obtained when a step input is

Fig. 4

Typical adaptation to repetitive steps

a Sea level
b Altitude

applied to the engine and model system with auxiliary loop gain fixed. The families of curves represent fixed instants of time within the transient. The implementation of the steepest-descent law in this case, however, leads to severe practical difficulties.

Choosing instead the function $f(\epsilon) = \epsilon^2$, to make the controller more practicable, eqn. 5 becomes

$$k = -2\lambda \int \epsilon \frac{\partial \epsilon}{\partial k} dt \qquad \qquad \qquad (6)$$

Fig. 5

Typical adaptation to repetitive-impulse inputs

Fig. 6

Typical dynamic response with random-signal input

Table 1

RESPONSE TO REPETITIVE STEP INPUTS

	Test number	Test condition		λ	First step				Second step (if different from first)				Number of steps to adapt	Comments
					Overshoot	Rise time	Settling time	Oscillations	Overshoot	Rise time	Settling time	Oscillations		
				s	%	s	s		%	s	s			
Model	1	Model		---	5	0·5	1	½					—	ζ = 0·7, ωₙ = 6 rad/s
Basic adaptive loop	2	Engine only	S.L.	—	14	0·3	2	1½						
	3	Engine with adaptation		2	6	0·3	2	1	—	0·4	1·8	0	2	
	4			8	—	0·2	2	1	—	0·8	1·5	0	2	Deteriorates
	5			0·2	9	0·3	2	1	8	0·3	2	1	>4	Very slow improvement
	6	Engine only	Altitude	—	28	0·3	1·5	1½					—	
	7	Engine with adaptation		2	—	0·6	0·6	—	3	0·7	1·0	½	2	
	8			8	32	0·3	2	½					goes unstable	
	9			0·2	9	0·3	0·8	½	—	0·5	0·5	0	2	
Simplified adaptive loop	10	Engine with adaptation	S.L.	2	8	0·3	1·5	1	—	0·4	1·5	½	2	
	11			8	3	0·3	1·4	1	—	0·9	0·9	0	2	
	12			0·2	10	0·3	1·5	1					1	
	13		Altitude	2	5	0·4	0·8	½	—	0·6	0·6	0	2	
	14			8	—	0·9	0·9	0					1	
	15			0·2	14	0·3	1·2	1	8	0·3	1·0	½	2	

S.L. = Sea level

Table 2

RESPONSE WITH CHANGING ENGINE AND MODEL PARAMETERS (λ = 2s)

Test condition	Test number	Test condition		First step				Second step (if different from first)				Number of steps to adapt	Comments
				Overshoot	Rise time	Settling time	Oscillations	Overshoot %	Rise time	Settling time	Oscillations		
				%	s	s		%	s	s			
Basic adaptive loop	16	Engine only	High gain	68	0·1	4	>6					—	
	17	With adaptation		36	0·15	0·5	1	—	0·6	0·6	0	2	
	18	Engine only	High time constant	---	1	1	0					—	
	19	With adaptation		25	0·6	2	1					1	
	20	High initial conditions		---	2	2	0	—	1·5	1·5	—	>4	
	21	Model only ωₙ = 3 rad/s		5	1·0	2·4	½					—	
	22	With adaptation ωₙ = 3 rad/s		6	0·3	2	1	—	1·0	1·0	0	>4	Very gradual change
	23	Model only ωₙ = 12 rad/s		5	0·3	0·8	½					—	
	24	With adaptation ωₙ = 12 rad/s		22	0·3	1·5	1						No improvement
Simplified adaptive loop	25	Model ωₙ = 3 rad/s		6	0·3	1·0	1	—	1·4	1·4	0	2	
	26	12 rad/s		17	0·25	1·2	1					1	

Table 3

RESPONSE TO SQUARE-WAVE, REPETITIVE-IMPULSE AND RANDOM-NOISE INPUT ($\lambda = 2s$)

Input			Input signal frequency	Amplitude ratio engine/model (peak-to- peak)	Number of cycles to adapt
Square-wave	Basic adaptive loop	S.L.	rad/s 6	0·94	1
			12	1·84	2
	Simplified adaptive loop	S.L.	6	0·96	3
			12	1·78	4
Repetitive-impulse	Basic adaptive loop	S.L.	6	1·27	4
		S.L.	12	1·91	2
		Altitude	6	1·12	1
		Altitude	12	1·74	1
	Without adaptive loop	S.L.	6	1·85	—
		S.L.	12	2·06	—
		Altitude	6	2·02	—
		Altitude	12	2·09	—
	Simplified adaptive loop	Results similar to those for basic adaptive loop			
Random noise (power-density spectrum flat from 0·1 to 10c/s)	For either system, at sea level and altitude, response is very similar to that shown in Fig. 6. Control is good in all cases, with engine response rather more oscillatory than model response				

S.L. = Sea level

The mechanisation of the equation results in the adjustment of k until $\frac{\partial}{\partial k} \int \epsilon^2 dt$ is zero, but at a rate other than that dictated by the law of steepest descent for this integral function.

The value of $\partial\epsilon/\partial k$ is difficult to generate, and can only be obtained in practice on the basis of certain assumptions.[9] The variable k can be represented as a variable sensitivity factor, shown in the block diagram of Fig. 1 as the additional input $N_0\delta k$. It can readily be shown that

$$\frac{\delta N_0}{N_0\delta k} = G(s)\frac{1}{G_1(s)} \qquad . \qquad . \qquad . \qquad . \qquad (7)$$

where $G(s)$ is the overall transfer function of the complete system for $\delta k = 0$. Also, when considering changes in $N_0\delta k$ only,

$$\delta\epsilon = \delta(N_i - N_0) = -\delta N_0 \qquad . \qquad . \qquad . \qquad (8)$$

Around the design condition, where the engine and model response are similar, a reasonable approximation in eqn. 7 would be to make $G(s) = G_M(s)$.

Hence

$$\frac{\partial\epsilon}{\partial k} = -\frac{G_M(s)}{G_1(s)} \dot{N}_0 \simeq -\frac{1\cdot25s}{1+3s}G_M(s)\dot{N}_0 \qquad . \qquad . \qquad (9)$$

and this can be used in the generation of the adaptive law for control.

5 Results and discussion

Typical engine and model speed responses to repetitive-step, repetitive-impulse and random-noise inputs are shown in Figs. 4, 5, and 6, respectively. The salient characteristics of a number of responses for step inputs for tests which show most clearly the effect of changes in altitude condition and adaptive loop gain are given in Table 1. Table 2 shows the effects of various other changes, these being the hypothetical changes of engine gain only and engine primary time constant only, and also the effect of a very large initial value of k instead of the very small value used in other tests and the effect of variation in the natural frequency of the model. Table 3 lists observations made from study of the response curves for square-wave, repetitive-impulse and random-signal inputs.

To determine the quality of the adaptive loop, the initial conditions chosen for k in all tests required large corrective action by the adaptive loop. In spite of this, as can be seen from Table 1, there were few cases in which the optimum value of k was not reached within two step changes. The tests where adaptation occurred more slowly were all for extreme conditions which would not occur in practice. Study

of Fig. 4 and Table 1 gives a clear indication of the improvement in system dynamic behaviour obtainable by the use of an adaptive loop of the form described in this paper.

In an attempt to predict the range of λ for which the adaptive loop is stable a Lyapunov function was sought, but without success. Experience on the computer shows that a suitable maximum value of this parameter can readily be obtained with a reasonable degree of certainty for any given range of conditions. For the system considered in this investigation $\lambda = 2s$ was used, and this was 25% of the value for which the system showed signs of instability at altitude.

Tests not listed in Table 1 confirmed clearly that the system represented by eqn. 3 was far superior to those of either eqn. 1 or eqn. 2, as predicted in Section 3.2. The optimum value of k obtained from the simplified theory and used in the determination of the model characteristics is confirmed by results shown in Fig. 3 obtained from the computer study. The effect predicted in Section 3.2, that adaptation with changes in engine gain alone would be better than that possible for changes in primary engine time constant, is clearly confirmed by tests 16–19 of Table 2.

Tests 1–3 and 21–24 show how critical it is to choose the natural frequency of the model correctly for the system under investigation. It would appear that the estimation of 6 rad/s for the model was a reasonable one, and in practice it could be advisable to be conservative in the choice of this value by choosing a somewhat lower natural frequency.

From the assumptions made in the derivation of $\partial\epsilon/\partial k$, this value will not be obtained very accurately, particularly when large changes of k must be made. It is thus logical to investigate whether the simplification obtainable by using a simple switching circuit generating the function (sgn) $(\partial\epsilon/\partial k)\epsilon$ will give a satisfactory dynamic behaviour. Tests were carried out for a selection of the earlier test conditions, and sample results are included in Tables 1–3. From these it can be seen that the deterioration in the results is slight.

6 General conclusions

With the increasing severity of the specifications required to be met by aircraft-engine control systems, the hydraulic units currently utilised in the speed-control loop are becoming very complex, and hence difficult to service and adjust and more prone to failure. As a result there is a trend towards the use of electronic control units, which makes the consideration of the use of adaptive control feasible. The additional components in the adaptive loop suggested by the authors are themselves well established and developed, and it would be realistic to introduce these in a new design of electronic speed control system.

It has been shown in this paper that useful simplification

can be made by utilising a relay to replace the multiplier required for correct functional operation of the chosen control law, without affecting the dynamic behaviour markedly. It is realistic to use a second-order model for an engine of this type, and $\int \epsilon^2 dt$ is a satisfactory performance criterion to use. Prediction of the optimum values of adjustable parameter k and model natural frequency ω_n are possible theoretically.

Parameter adjustment takes place whenever any normal input signal or disturbance exists, and for all normal parameter changes system adaptation is complete within two transients.

7 References

1 SCHWARZENBACH, J., and GILL, K. F.: 'Analysis of gas turbine engine fuel system'. *Engineer*. 1965, 219, pp. 209–218
2 GILL, K. F., and SCHWARZENBACH, J.: 'A theoretical look at the use of functional non-linearities in a gas turbine control system'. *Control*, 1966, 10, pp. 465–468, pp. 531–535
3 SCHUCK, O. H.: 'Adaptive flight control'. Proceedings of the 1st international congress of the IFAC, Moscow, Vol. 2, 1960, pp. 645–650
4 TYLER, S. R., RUGGLES, R., and WELBOURN, D. B.: 'Theoretical and practical techniques applied to the design of a gas turbine engine governor'. Proceedings of the 1st international congress of the IFAC, Moscow, Vol. 3, 1960, pp. 356–362
5 GIBSON, J. E.: 'Making sense out of the adaptive principle', *Control Engng.*, 1960, pp. 113–119, 109–114, 93–96
6 MISHKIN, E., and BRAUN, L.: 'Adaptive control systems' (McGraw-Hill, 1961)
7 LEONDES, C. T. (Ed.): 'Modern control theory' (McGraw-Hill, 1965), chap. 6
8 DAWSON, D. A.: 'Analysis and computer study of an adaptive control system', National Research Council of Canada, Mechanical Engineering Report Mk–4, Sept. 1959
9 OSBURN, P. V., WHITAKER, H. P., and KEZER, A.: 'New developments in the design of model reference adaptive control systems'. Inst. of Aerospace Sciences, Paper 61–39, 1961
10 HORROCKS, T.: 'Investigation into model reference adaptive control systems', *Proc. IEE*, 1964, 111, (11), pp. 1894–1906
11 DYMOCK, A. J., MEREDITH, J. F., HALL, A., and WHITE, K. M.: 'Analysis of a type of model reference adaptive control system', *ibid.*, 1965, 112, (4), pp. 743–753
12 CARUTHERS, F. P., and LEVENSTEIN, H. (Eds.): 'Adaptive control systems' (Pergamon, 1963), pp. 1–19
13 MILSUM, J. H.: 'Adaptive control of processes by an economic criterion'. Proceedings of the 1st international congress of the IFAC, Moscow, Vol. 4, 1960, pp. 231–240

4. SATELLITE MODELLING AND CONTROL

PAPER 25

PROCEEDINGS

Effects of flexibility on a momentum-stabilised communication-satellite attitude-control system

J. M. Gething, B.Sc., J. A. Holt, M.Sc., C.Eng., F.R.Ae.S., D. Smart, B.Sc., and K. F. Gill, M.Sc., Ph.D., C.Eng., M.I.Mech.E.

ABSTRACT

Transfer functions are derived for the coupled roll-yaw-axes control system of a momentum-stabilised satellite. First-mode approximation to the flexural response of movable solar paddles is included in the dynamic equations. The performance of the control system for varying degrees of flexibility is studied using root-locus techniques. The presence of a single flexural mode in the system transfer functions causes an additional pole-zero pair to appear on, or just to the left of, the imaginary axis in the root-locus diagrams. Instability, recognised by root-loci crossing into the right half s plane does not occur. However, flexible modes could be excited by disturbing forces. and, depending on the amplitude of the ensuing motions, would seriously degrade the attitude performance of the satellite.

LIST OF SYMBOLS

A^i = ith appendage subbody
a = appendage subscript
(a) = appendage axis set
(b) = rigid-body axis set
F = vector of external forces applied to composite vehicle
H = angular-momentum vector for composite vehicle
h = 3 × 1 matrix of wheel angular-momentum components
$-h_w$ = pitch component of wheel angular momentum
I = 3 × 3 diagonal matrix of composite-vehicle principal moments of inertia
K = 6n × 6n structural stiffness matrix for the flexible appendage
K_c = controller gain
K_s = system gain
M = 6n × 6n diagonal matrix whose components are the masses and moments of inertia of the subbodies
m = scalar total mass of the composite vehicle
(n) = inertial axis set
q = 6n × 1 matrix of translational and rotational deformation co-ordinates of the flexible appendage
Q = flexible stiffness coefficient
r^i = 3 × 1 matrix of position co-ordinates of the ith subbody with respect to the vehicle mass centre when undeformed
$\bar{r}$ = 6n × 6n matrix with diagonal entries the 3 × 3 matrices $\bar{r}^1$, 0, $\bar{r}^2$, ..., $\bar{r}^n$, 0, and off-diagonal entries zero
r = rigid subscript
R = flexible inertia coefficient
s = Laplace operator
$\bar{T}$ = vector of external torques applied about the composite-vehicle centre of mass
T = 3 × 1 matrix counterpart of $\bar{T}$
T = superscript denoting matrix transposition
U = 6n × 1 matrix of external forces and torques applied to the subbodies.

$\bar{X}$ = inertial position vector of the centre of mass of composite vehicle
X = 3 × 1 matrix counterpart of $\bar{X}$
α = roll-control-torque yaw-offset angle
β = paddle rotation angle
γ_1 = 1st-mode component of 6n × 3 matrix γ
η = 6n × 1 matrix of modal co-ordinates
$\theta_{1,2,3}$ = roll, pitch and yaw Euler angles
θ = 3 × 3 transformation matrix expressing rotation of body fixed axes (b) relative to inertial axes (n)
θ_e = roll error signal
λ = 6n × 1 matrix of external forces and torques acting on the subbodies
$\bar{p}$ = elemental position vector of the composite vehicle
Σ_{EO}, Σ_{OE} = matrix summation operators defined in terms of the 3 × 3 identity matrix E, and the 3 × 3 null matrix O as follows:

$$\Sigma_{EO} = [EOEO...]^T$$

$$\Sigma_{OE} = [OEOE...]^T$$

τ = controller lead time constant
ϕ = 6n × 6n modal-transformation matrix
ω = 3 × 1 matrix of rigid-body angular rates
ω_0 = orbit angular velocity
ω_N = nutation angular velocity of the rigid-centre body
Ω = 6n × 6n diagonal matrix of mode natural frequencies
Ω_1 = 1st-mode natural frequency

The tilde notation over a matrix is used to denote the matrix counterpart of the vector crossproduct; thus, for example,

$$\tilde{a}b \equiv \underline{a} \times \underline{b}$$

The tilde matrix is formed from the components of the original matrix as in the following example:

$$\tilde{a} = \begin{bmatrix} 0 & -a_3 & a_2 \\ a_3 & 0 & -a_1 \\ -a_2 & a_1 & 0 \end{bmatrix}$$

1 INTRODUCTION

The design of space-vehicle attitude-control systems is usually carried out with the assumption made that the craft is rigid. The next decade will see the use of high-power telecommunication satellites using large extendable solar-array and antenna systems for which the assumption of rigidity is

no longer valid. This study attempts to determine how a control system designed for a rigid vehicle is affected by the presence of flexibility in the vehicle's dynamic equations.

Previous investigations into the effects of flexibility on attitude-control systems[1-3] have dealt with spin-stabilised satellites with comparatively rigid antenna systems. The aim of these investigations has been to determine the feasibility of the proposed system in meeting the desired mission objectives when flexibility is introduced into the system equations. To the authors' knowledge, no published work has attempted to look beyond current projects and make a general appraisal of the effects of flexibility on control-system performance.

By defining flexibility coefficients that can be varied to give a wide range of fundamental frequencies of vehicle flexible motion, this study hopes to fill this gap and provide a better understanding of the effects of flexibility on attitude-control systems.

Hybrid co-ordinate dynamic analysis[1-5] is used to formulate a simple, but representative, dynamic model of a 3-axis-controlled satellite with a flexible solar array. A momentum-stabilised satellite employing a fixed flywheel is used as the basis of the study. The presence of the flywheel causes crosscoupling between two of the control axes, and leads to characteristic nutation in response to control or disturbance torques. Control of the coupled axes is achieved using a pseudorate pulse-modulated control system. [6-8]

Flexibility coefficients in terms of the flexible-solar-array moment of inertia and structural stiffness are defined.

Classical linear control theory is used to derive transfer functions for the controller and vehicle dynamics. A numerical root-locus study is carried out for a range of values of the flexibility coefficients, so that possible régimes of instability can be highlighted.

In this study, the effects of sensor dynamics and signal noise have not been considered. These effects are secondary to the problem of flexibility, and their inclusion would only serve to cloud the fundamental nature of the problem.

2 FLEXIBLE MODEL

The configuration of an idealised flexible vehicle representative of a class of momentum-stabilised satellites is shown in Fig. 1. The satellite is assumed to be in synchronous orbit around the Earth. Reference axes, aligned with the satellite's principal axes, are defined as follows: axis 1, the roll axis, is nominally directed along the line of flight; axis 2, the pitch axis, is directed normal to the orbit plane; axis 3, the yaw axis, is directed along the vector from the satellite centre of mass to the centre of the Earth. The axis set is therefore seen to be rotating at orbit rate about the negative pitch axis.
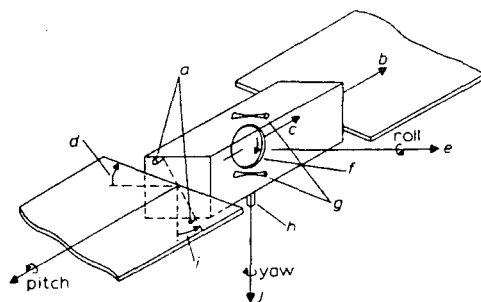

Fig. 1

General configuration of flexible model

a Roll and yaw control jets
b Vehicle orbit rate w_O
c Wheel spin vector h
d Paddle angle β
e Line of flight
f Momentum wheel
g Pitch-control jets
h Horizon sensor
i Jet offset angle
j Towards centre of Earth

Flexibility is introduced into the satellite configuration in the form of solar-array paddles which can rotate with respect to the satellite main body, about the pitch axis. Paddle flexure is considered in a direction normal to the paddle surface, i.e. simple bending of the paddles about the roll and yaw axes. The paddles are assumed to be stiff in all other directions, the corresponding stiffnesses being an order of magnitude greater than the bending stiffnesses. Higher-frequency modes will, in general, fall outside control frequencies, and their effects will be secondary.

A momentum wheel with nominally constant angular momentum is mounted with its momentum vector aligned with the negative pitch axis. The pseudorate control system[6] uses roll-error information provided by a rigidly mounted horizon sensor to determine the pulse frequency of the gas-jet control torques. The presence of the momentum wheel transforms yaw-attitude errors into roll errors which are detected by the roll-horizon sensor. Yaw-restoring torque is provided by the momentum wheel. Damping of the yaw motion is achieved by offsetting the roll-control torque in the orbit plane by the angle α. No yaw sensor is required. Pitch-axis control is by gas jets actuated by a separate control system, and is not considered further.

A block diagram of the coupled roll-yaw-axes control loop is shown in Fig. 3.

3 ANALYSIS

A schematic of the flexible satellite is shown in Fig. 2. The hybrid co-ordinate analysis considers the satellite in two parts: a rigid centre section housing the various vehicle systems and a flexible appendage. Distributed co-ordinates are used to model the flexible appendage motion, while discrete co-ordinates are retained to describe the motion of the composite vehicle and control-system operation.
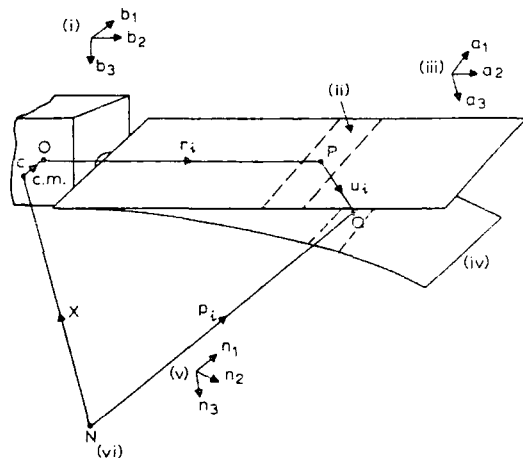
Fig. 2

Lumped-parameter model of flexible solar array

(i)   Body fixed axes (b)
(ii)   ith subbody A_i
(iii) Appendage fixed axes (a)
(iv)   Deformed position
(v)   Inertial axes (n)
(vi)   Inertially fixed point

It is only intended here to give an outline of the analytical method and quote the results. A full derivation of the flexible-appendage equations may be found in Reference 1.

The flexible appendage is idealised as a set of n subbodies $A_i(i = 1, n)$ connected by massless elastic constraints. Newton-Euler equations of motion are written for each subbody.

The resulting 6n 2nd-order total differential equations are then expressed as a single matrix equation of order 6n in terms of the deformation co-ordinate matrix q as

$$U = M\ddot{q} + Kq \tag{1}$$

Classical modal analysis is employed to find a transformation matrix ϕ so that the substitution in eqn. 1 of

$$q = \phi\eta \tag{2}$$

followed by premultiplication by ϕ^T yields the uncoupled set of equations

$$\phi^T U = \ddot{\eta} + \Omega^2\eta \tag{3}$$

Ω^2 is the diagonal matrix of the mode natural frequencies and η is the column matrix of modal co-ordinates

The centre body is considered to be fixed against rotation, yielding the fixed-free bending modes. Mode frequencies are therefore independent of the momentum device housed in the centre body. Eqn. 3 can be reduced in order by deleting the equations for those modes whose contribution to the overall response is small.

The Newton-Euler equations of motion for the composite vehicle are written in vector form as

$$F = m\ddot{\bar{X}} \tag{4}$$

and

$$\bar{T} = \dot{H} \tag{5}$$

In expanding eqn. 5, it is necessary to solve the momentum integral for the composite vehicle

$$H = \int \bar{\rho} \times \dot{\bar{\rho}}\, dm \tag{6}$$

where $\bar{\rho}$ defines the position of the elemental component dm of the composite vehicle with respect to the vehicle mass centre. The total angular momentum of the composite vehicle will comprise the angular momentum of the undeformed composite vehicle (including a contribution due to the presence of the momentum wheel) and the angular momentum due to appendage flexure. In its final form, the matrix torque equation for the class of momentum-stabilised satellite considered may be written as

$$T = I\dot{\omega} + \tilde{h} - \tilde{h}\omega + (\Sigma_{EO}^T M \tilde{r} + \Sigma_{OE}^T M)\phi\ddot{\eta} \tag{7}$$

The full form of eqn. 3 describing the response of the appendage flexible modes is written

$$\ddot{\eta} + \Omega^2\eta = \phi^T\{\lambda - M\Sigma_{EO}\ddot{\bar{X}} - M(\Sigma_{OE} - \tilde{r}\Sigma_{EO})\dot{\omega}\} \tag{8}$$

Eqns. 7 and 8 are used to arrive at a simplified dynamic model of the flexible satellite.

The authors have shown[*] that, for the flexible array configuration considered in this study, the contribution to the dynamic response of the satellite of the lowest-frequency mode is an order of magnitude greater than that due to any higher-frequency modes. In applying eqns. 7 and 8 to the flexible model, therefore, only the lowest-frequency components of the modal equations have been retained.

It is convenient to express the lowest-frequency mode response in the appendage fixed axis set (a) (see Fig. 2). Define η_1 as the lowest-frequency modal co-ordinate in the direction of paddle flexure and Ω_1 as the corresponding mode natural frequency. Eqn. 8 may be written as a scalar equation in η_1 as

$$\ddot{\eta}_1 + \Omega_1^2\eta_1 = -\gamma_1(\dot{\omega}_1 \cos\beta + \dot{\omega}_3 \sin\beta) \tag{9}$$

* SMART, D.R., GILL, K.F., GETHING, J.M., and HOLT, J.A.: 'Deterioration in limit cycle performance of a spacecraft attitude control system in the presence of structural flexibility (to be published)

where γ_1 is the 1st-mode component of the 6n × 3 matrix

$$\gamma = \phi^T M(\Sigma_{OE} - \tilde{r}\Sigma_{EO}) \tag{10}$$

which expresses the relative contribution to the response of each mode of vehicle angular accelerations. In arriving at eqn. 9, the effects of disturbance torques have been ignored, and, to confine the study to attitude rotations, the vehicle centre of mass has been assumed to be nontranslating.

The first mode form of eqn. 7 may be written in terms of the scalar roll and yaw components as

$$T_1 = I_1\dot{\omega}_1 - h_2\omega_3 + \gamma_1^T\ddot{\eta}_1 \cos\beta \tag{11}$$

$$T_3 = I_3\dot{\omega}_3 - h_2\omega_1 + \gamma_1^T\ddot{\eta}_1 \sin\beta \tag{12}$$

where the components of the 3 × 1 matrices T, ω and h are expressed in the body-fixed axis set (b), while η_1 is expressed in appendage axes (a) as before. γ_1^T is the 1st-mode component of the 3 × 6n matrix

$$\gamma^T = (\Sigma_{EO}^T\tilde{r} + \Sigma_{OE}^T)M\phi \tag{13}$$

recognised as the transpose of eqn. 10 and expressing the summation of the contributions of each mode to the composite vehicle motion.

Eqns. 9, 11 and 12 are formulated with respect to the body fixed-axis set (b). The orientation of these axes with respect to the orbit reference axes are given by the standard Euler angles $\theta_1, \theta_2, \theta_3$, denoting roll, pitch and yaw motion, respectively. For small rotations, the body rate ω is related to the Euler angle rate $\dot{\theta}$ by

$$\begin{bmatrix} \omega_1 \\ \omega_2 \\ \omega_3 \end{bmatrix} = \begin{bmatrix} 1 & \theta_3 & -\theta_2 \\ -\theta_3 & 1 & \theta_1 \\ \theta_2 & -\theta_1 & 1 \end{bmatrix}\left(\begin{bmatrix} \dot{\theta}_1 \\ \dot{\theta}_2 \\ \dot{\theta}_3 \end{bmatrix} + \begin{bmatrix} 0 \\ -\omega_0 \\ 0 \end{bmatrix}\right) \tag{14}$$

The last term in eqn. 14 reflects the fact that the orbit reference axes are rotating with orbit angular velocity ω_0 about the negative pitch axis.

Using eqn. 14 and ignoring 2nd-order terms, the satellite equations (eqns. 9-11) become

$$\ddot{\eta}_1 + \Omega^2\eta_1 = -\gamma_1(\ddot{\theta}_1 \cos\beta + \ddot{\theta}_3 \sin\beta) \tag{15}$$

$$T_1 = I_1\ddot{\theta}_1 + h_w\dot{\theta}_3 + h_w\omega_0\theta_1 + \gamma_1^T\ddot{\eta}_1 \cos\beta \tag{16}$$

$$T_3 = I_3\ddot{\theta}_3 - h_w\dot{\theta}_1 + h_w\omega_0\theta_3 + \gamma_1^T\ddot{\eta}_1 \sin\beta \tag{17}$$

and h_2 has been replaced by the value of the pitch component of wheel momentum $-h_w$.

Laplace transformation of these equations is now performed to obtain the roll and yaw transfer functions. Elimination of the modal co-ordinate η_1 from eqns. 16 and 17 yields terms involving the product $\gamma_1\gamma_1^T$. This is the 1st-mode component of the matrix product $\gamma\gamma^T$, which can be shown to be the contribution of the flexible appendage to the satellite total moment of inertia. Thus $\gamma_1\gamma_1^T$ is identified as the moment of inertia of the flexible solar array about the appendage axis a_1:

$$\gamma_1\gamma_1^T = I_{1a} \tag{18}$$

To make use of this relationship, the satellite total moments of inertia about the roll and yaw axes are subdivided into rigid and flexible components:

$$I_1 = I_{1r} + I_{1a} \cos^2\beta + I_{3a} \sin^2\beta \tag{19}$$

$$I_3 = I_{3r} + I_{3a} \cos^2\beta + I_{1a} \sin^2\beta \tag{20}$$

where I_{1R} and I_{3R} are the roll and yaw moments of inertia of the rigid centre body with respect to the (b) axes, and I_{1a} and I_{3a} are the corresponding moments of inertia of the flexible array with respect to the (a) axes. The paddle angle β gives the rotation of axis set (a) relative to (b).

To simplify the resulting equations, moment-of-inertia sym-

metry is assumed for the rigid body and the flexible solar paddle. Thus the following identities follow:

$$I_{1r} = I_{3r} = I_r$$
$$I_{1a} = I_{3a} = I_a \tag{21}$$

The flexible inertia coefficient R is defined as the ratio of flexible to rigid moments of inertia:

$$R = \frac{I_{1a}}{I_{1r}} = \frac{I_{3a}}{I_{1r}} = \frac{I_{1a}}{I_{3r}} = \frac{I_{3a}}{I_{3r}} = \frac{I_a}{I_r} \tag{22}$$

The control-torque offset angle α (see Fig.1) causes a component of the roll-actuated control torque T_C to be applied to the yaw axis. Assuming that external disturbance torques are small compared with control torques, the roll and yaw components of torque are

$$T_1 = T_C \cos \alpha$$
$$T_3 = -T_C \sin \alpha \tag{23}$$

The relationships of eqns.15-23 are used to derive the roll and yaw dynamics transfer functions. After some considerable manipulation, the transfer function for the roll dynamics is written

$$\frac{\theta_1(s)}{T_C} = \frac{\cos \alpha}{I_R(1 + R)} \left\{ \frac{s^4(1 + R\cos^2 \beta - R\cos \beta \sin \beta \tan \alpha) + s^2(1 + R)\Omega_1^2 + (s^2 + \Omega_1^2)(\omega_0 + s \tan \alpha)\omega_N}{s^4\{s^2 + (1 + R)\Omega_1^2\} + \frac{\omega_N}{1 + R}\omega_0 s^2\{(2 + R)s^2 + 2(1 + R)\Omega_1^2\} + \frac{\omega_N^2}{1 + R}(s^2 + \Omega_1^2)(s^2 + \omega_0^2)} \right\} \tag{24}$$

ω_N has been substituted for the term h_ω/I_R, being the satellite-nutation angular velocity for zero appendage moment of inertia. $I_R(1 + R)$ represents the satellite total moment of inertia. The yaw-dynamics transfer function can be found similarly.

Eqn. 24 can now be combined with the transfer function for the pseudorate control system to arrive at the open-loop roll transfer function.

A block diagram of the pseudorate pulse-frequency controller is shown in Fig.3.

This type of control system avoids the need for attitude-rate information by approximate integration of the control-system output signal in the feedback-lag circuit. This provides approximate rate information. Linearisation of the controller yields the following transfer function relating the control torque T_C to the roll error signal θ_e:

$$\frac{T_C}{\theta_e(s)} = K_C(1 + \tau s) \tag{25}$$

where K_C is the controller gain and τ is the controller lead time constant: The controller provides proportional and derivative control action.

Combining eqns. 24 and 25 provides the open-loop roll transfer function

$$G_1(s) = \frac{\theta_1(s)}{\theta_e(s)} = \frac{K_S\left(s + \frac{1}{\tau}\right)[s^4\{1 + R(\cos^2 \beta - \cos \beta \sin \beta \tan \alpha)\} + s^2(1 + R)\Omega_1^2 + (s^2 + \Omega_1^2)(\omega_0 + s \tan \alpha)\omega_N]}{s^4\{s^2 + (1 + R)\Omega_1^2\} + \frac{\omega_N}{1 + R}\omega_0 s^2\{(2 + R)s^2 + 2(1 + R)\Omega_1^2\} + \frac{\omega_N^2}{1 + R}(s^2 + \Omega_1^2)(s^2 + \omega_0^2)} \tag{26}$$

where the system gain

$$K_S = \frac{K_C\tau \cos \alpha}{I_r(1 + R)} \tag{27}$$

is a measure of the velocity imparted to the satellite by the control torque.

The characteristic equation of the closed-loop-roll control system is derived from eqn.26 assuming unity feedback.

1st-mode natural frequency Ω_1 is a function of the append-

age inertia, indicated by the value of R, and also of the structural stiffness of the flexible appendage K_a. To incorporate variations in this parameter in the root-locus study, the flexible stiffness coefficient Q is defined as

$$Q = K_a/I_R \tag{28}$$

To a good approximation, Ω_1 can be expressed in terms of the corresponding appendage moment of inertia and structural stiffness as

$$\Omega_1^2 = K_a/I_a \tag{29}$$

Using the definitions of Q in eqn. 28 and R in eqn. 22, eqn. 29 can be written

$$\Omega_1^2 = Q/R \tag{30}$$

Both Q and R may be varied to achieve different structural representations of the flexible appendage.

4 ROOT-LOCUS STUDY

Root-locus plots for a range of the flexibility coefficients Q and R are presented. The constant system parameters, are listed in Table 1.

The plots have been obtained on an ICL 1906A computer using a root-finding algorithm to compute the roots of the characteristic equation. The time taken for a 6th order characteristic equation with 50 gain increments was about 50 s.

As a basis for evaluating the effects of flexibility, the root locus for the rigid vehicle (R = 0) is shown in Fig.4. The
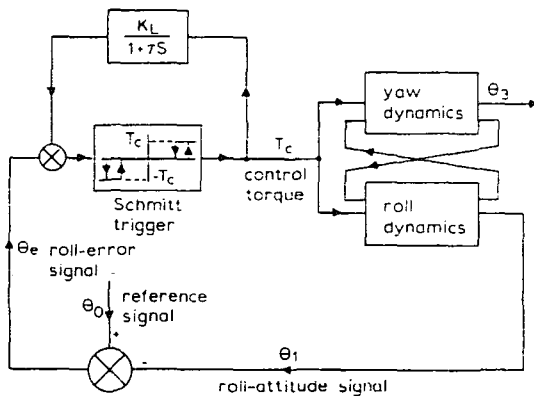
Fig. 3

Block diagram of coupled roll-yaw-axes control system

TABLE 1

PARAMETERS FOR NUMERICAL ROOT-LOCUS STUDY

I_R	$= 100$ kgf m^2
h_ω	$= 50$ kgf m/s^1 (50 Nms)
ω_N	$= 0\cdot5$ s^{-1}
ω_0	$= 0\cdot73 \times 10^{-4}$ s^{-1}
α	$= 5^0$
τ	$= 10$ s

plot consists of two complex pairs of poles and three real zeros. Approximate factorisation of the open-loop transfer function (eqn. 26) for R = 0 reveals that the poles represent the values of the nutation and orbit frequency components of the rigid-body motion. The nutation oscillation is damped by the zero associated with the controller lead time constant, while two further zeros resulting from the roll dynamics damp the orbit-frequency oscillation.

A set of root loci for a typical flexible configuration (R = 1) is presented in Figs. 5-9. The effect of varying the appendage stiffness coefficients Q is illustrated. In Figs. 5 and 6, the paddle angle β = 0°, i.e. paddle flexure is about the roll axis, while, in Figs. 7-9, the paddles are rotated through 90°, causing the paddles to flex about the yaw axis.
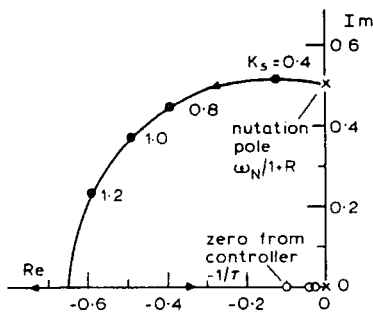
Fig. 4

Root locus for rigid vehicle

Nutation pole 'damped' by controller zero. R = 0
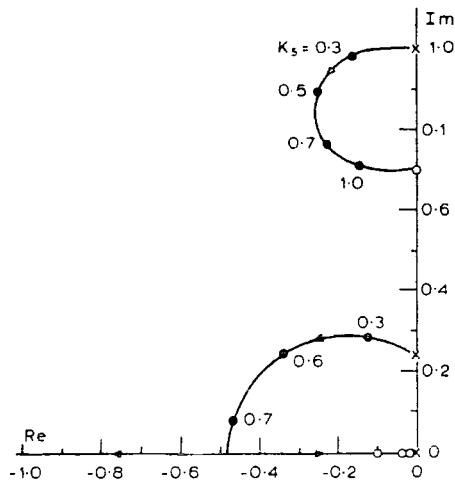
Fig. 5

Root locus for flexible vehicle—flexure about roll axis

1st-mode pole-zero combination on imaginary axis

$R = 1 \cdot 0, Q = 0 \cdot 5, \beta = 0$
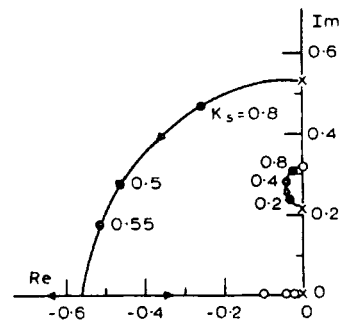
Fig. 6

Root locus for vehicle—flexure about roll axis

Control transfers to upper-valued pole
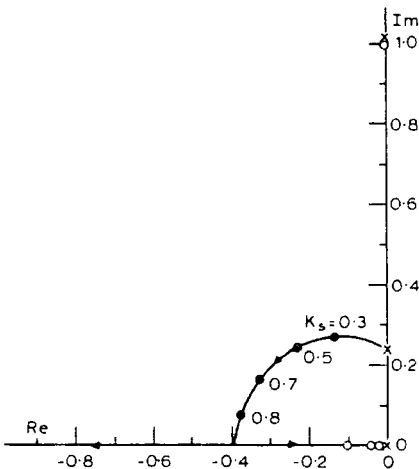
$R = 1 \cdot 0, Q = 0 \cdot 1, \beta = 0$

Fig. 7

Root locus for flexible vehicle—flexure about yaw axis

1st-mode pole-zero pair almost cancelled

$R = 1 \cdot 0, Q = 0 \cdot 5, \beta = 90°$
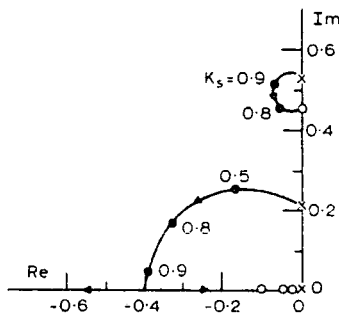
Fig. 8

Root locus for flexible vehicle—flexure about yaw axis

Pole-zero-pole combination approaches real axis

$R = 1 \cdot 0, Q = 0 \cdot 1, \beta = 90°$
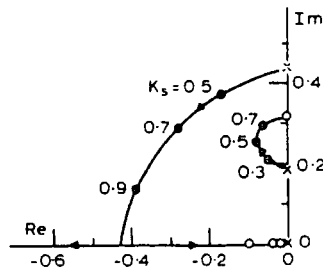
Fig. 9

Root locus for flexible vehicle—flexure about yaw axis

Control transfers to upper-valued pole

$R = 1 \cdot 0, Q = 0 \cdot 05, \beta = 90°$

The presence of the first flexural mode results in an additional pair of complex poles and zeros on the imaginary axis. For values of Q such that the flexural-mode frequency Ω_1 is large compared with the rigid-body nutation frequency ω_N (Figs. 5 and 7), the open-loop roll transfer function (eqn. 26) approximately factorises to give the poles and zeros listed in Table 2.

TABLE 2

POLES AND ZEROS OF THE OPEN-LOOP ROLL TRANSFER FUNCTION FOR $\Omega_1 \gg \omega_N$

Poles	Zeros
$\pm j\omega_0$	$-1/\tau$
$\pm j\sqrt{(1 + R)}\Omega_1$	$-\omega_0/\tan \alpha$
	$-\omega_N \tan \alpha/(1 + R)$
$\pm j\dfrac{\omega_N}{1 + R}$	$\pm j\Omega_1(\beta = 0°) \quad \pm j\sqrt{(1 + R)}\Omega_1(\beta = 90°)$

That this factorisation is only true for $\Omega_1 \gg \omega_N$ can be seen by observing the change in the values of the complex poles and zeros as the appendage stiffness, and hence Ω_1, is reduced (Figs. 6, 8 and 9). The pole-zero pair associated with the flexural mode moves towards the real axis, as would be expected. However, the nutation poles, nominally constant for a given R (see Table 2), also decrease in value. It is difficult to ascribe identifiable algebraic labels to the open-loop poles for Ω_1 close to ω_N.

It will be seen from the Figures that the lead-term zero continues to 'damp' one pair of open-loop poles. The effect of the controller zero is transferred from the lower- to the higher-frequency locus as Q decreases in value (e.g. Figs. 5 and 6).

The value of the complex open-loop zero is affected by the paddle angle β, as shown in Table 2. The effect of this change can be seen by comparing Figs. 6 and 8, where change in the position of the zero causes control to transfer from the lower-valued to the higher-valued pole. For a higher Q

Fig. 10

Constant-gain root contours for varying inertia ratio R and a range of stiffness coefficient Q—flexure about roll axis

System gain $K_s = 2·0$
Paddle angle $\beta = 0$
Axes not to same scale

(Figs. 5 and 7), increasing β causes the zero to approach closely the higher-valued pole and the locus stays close to the imaginary axis. This apparent 'cancellation' of the pole by the zero means that this component of the response is largely unaffected by the control action, but would be excited by external disturbances.

For a gain K_s of 2·0, the loci corresponding to two of the three pairs of complex poles lie on the real axis. The positions of the other loci are largely determined by the value of the complex pair of zeros, and vary depending on Q and R. This effect is demonstrated in Fig. 10, in which constant-gain root contours are presented for varying inertia ratios R and for a range of stiffness coefficients Q. The contours are for a zero-β paddle configuration. Q and R range from 0·1 to 5·0. (Note that the real axis has been exaggerated to demonstrate the effects.)

It will be seen that the contours stay inside the left half-plane. Instability, recognised by the contours crossing into the right halfplane, does not occur. For a given stiffness Q, the contours show that the responses become more damped for initial increases in the appendage moment of inertia. For higher values of R, the contours approach the origin, resulting in a reduction in effective damping.

The corresponding root contours for a paddle angle $\beta = 90°$ are similar in shape, but are very much closer to the imaginary axis. The effect of increasing the paddle angle β is to make the response more oscillatory. This is to be expected, since, at $\beta = 90°$, paddle flexure affects only the yaw response and can only be controlled indirectly by the roll-actuated control system

5   CONCLUSIONS

Hybrid co-ordinate dynamic analysis has been used previously for complex structural systems involving large numbers of flexural modes. As presented in this paper, it has proved to be a useful method for deriving single-mode transfer-function equations for an idealised flexible satellite. The use of separate co-ordinate systems to describe the rigid and flexible motion of the satellite allows the rigid-body configuration to be fixed while the parameters describing the flexible motion are varied to give a range of flexural frequencies and different degrees of interaction between the flexible and rigid sections of the craft. Axis crosscoupling due to the presence of a momentum wheel is handled without difficulty by choosing the reference axes for the flexible motion to be fixed with respect to the rigid centre body containing the momentum device.

For the single-mode model considered in this paper, the addition of a flexible appendage to the rigid satellite control system causes an additional pole-zero pair to appear in the root-locus diagrams on, or just to the left of, the imaginary axis. Instability, recognised by the root loci crossing into the right halfplane, does not occur over the wide range of flexibility parameters investigated. However, excitation of the flexible mode by disturbing forces of sufficient amplitude could seriously degrade the attitude performance of the satellite.

Deformations and angular velocities have been assumed to be small in arriving at the mathematical expressions for the dynamic response of the flexible satellite. The analysis is therefore restricted to small motions of the satellite about its steady operating condition. This paper has been concerned with small transient motion, and the authors would hesitate to extend the results to situations during, for example, the launch and insertion into orbit stage of a satellite mission, where the appendages undergo large deformations and high angular rates are experienced.

For the flexible configuration considered in this paper, the first-mode flexural response provides a close approximation to the flexible motion, the first-mode amplitudes being an order of 10 or more greater than those due to the higher modes. The inclusion of higher-order modes in the analysis causes further pole-zero pairs to appear in the root-locus diagrams, on or to the left of the imaginary axis, at increas-
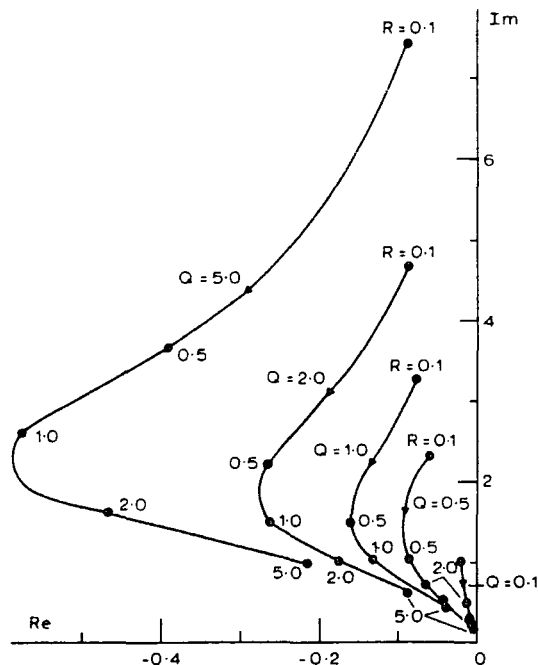
ing distances from the origin. The arguments concerning the effect of the first mode on the rigid system would apply equally to these higher modes, and their presence would not alter the overall conclusions.

The effect of structural damping has not been included in this paper. This term is inherently small in mechanical systems of this type, and is, in any case, difficult to estimate for a vehicle operating in a space environment.

The dynamic characteristics of attitude sensors, control valves and gas jets have not been included in the control-system transfer functions. These could be simple time delays or more complex nonlinear functions, depending on the requirements of the satellite mission. These effects are thought to be secondary in nature, and their inclusion in a study of this kind is inappropriate.

The experience gained from this paper leads the authors to the opinion that severe degradation of the attitude performance of a satellite could arise from excitation of all or some of the flexural modes of the flexible appendages. The magnitude of this problem will certainly increase as solar arrays and antennas increase in size to meet the inevitable demand for more powerful communication satellites. To overcome the problem, some means must be found for the direct control of the flexible motion. This may involve direct measurement of the flexural response using accelerometers, strain gauges or some other form of instrumentation. If this approch is not feasible because of problems of instrumenting lightweight structures and drift of the measuring devices over long periods of service, an alternative line of approach, and one currently being investigated by the authors, is to use Luenberger-observer or Kalman-filter techniques on the available output information to form estimates of the unknown flexible states. These can then be used in an appropriate control law to provide feedback information to a controller.

Finally, it must be stressed that, to arrive at a valid scheme for the design of control systems for flexible craft, detailed information is required concerning mission objectives, external disturbances and the availability of suitable instrumentation.

6   REFERENCES

1   LIKINS, P. W., and GALE, A. H.: 'The analysis of interactions between attitude control systems and flexible appendages', 19th international astronautical congress, New York, NY, USA, 1968, preprint IAFAD29
2   GALE, A. H., and LIKINS, P. W.: 'Influence of flexible appendages on dual spin spacecraft dynamics and control', J. Spacecraft & Rockets, 1970, 7, pp. 1049-1056
3   LIKINS, P. W., and FLEISCHER, G. E.: 'Results of flexible spacecraft attitude control studies utilizing hybrid coordinates'. AIAA paper 70-20, Jan. 1970
4   LIKINS, P. W.: 'Dynamics and control of flexible space vehicles'. Jet Propulsion Laboratory, Pasadena, Calif., USA, technical report 32-1329, 1969
5   LIKINS, P. W., and WIRSCHING, P. H.: 'Use of synthetic modes in hybrid coordinate dynamic analysis', AIAA J., 1968, 6, pp. 1867-1872
6   DOUGHERTY, J. H., SCOTT, E. D., and RODDEN J. J.: 'Analysis and design of WHECON—an attitude control concept'. 2nd AIAA communications satellite systems conference, San Francisco, Calif., USA, 1968, paper 68-461
7   NICKLAS, J. G., and VIVIAN, H. C.: 'Derived-rate increment stabilisation: its application to the attitude control problem', Trans. ASME. [D], 84. 1962. pp. 54-60
8   SCOTT, E. D.: 'Pseudo-rate sawtooth-pulse-reset control system, analysis and design', J. Spacecraft & Rockets, 1967, 4, pp. 781-785

PAPER 28

PROCEEDINGS

Relay control of undamped linear systems using Lyapunov's second method

J. M. Gething, B.Sc., Ph.D., and K. F. Gill, M.Sc., Ph.D., C.Eng., M.I. Mech. E., M.I.E.E.

ABSTRACT

A method is presented for the application of Lyapunov's second method to the synthesis of relay-control systems for plants that have undamped responses. A technique is presented for overcoming the problems associated with the solution of the Lyapunov matrix equation when the plant eigenvalues have zero real part. The method is applied to the attitude control of a flexible space vehicle.

LIST OF SYMBOLS

A	= plant matrix
A_D	= matrix of damping terms
A_M	= modified plant matrix, $A_M = A + A_D$
B	= plant-input matrix
M_i	= maximum value of the control u_i
P	= solution matrix of Lyapunov matrix equation
Q	= right-hand side of Lyapunov matrix equation, $Q = I$
R	= flexible/rigid inertia ratio
$t_{1,3}$	= roll-, yaw-control torques
u	= matrix of controls
$V(x)$	= Lyapunov function
x	= plant state
γ	= flexural-interaction coefficient
ζ	= artificial-damping coefficient in A_D
η_1	= fundamental bending-mode co-ordinate of solar array
$\theta_{1,3}$	= roll-, yaw-attitude angle
λ	= eigenvalue
Ω_1	= fundamental bending-mode frequency of solar array
ω_N	= nutation frequency of rigid satellite
ω_0	= orbit frequency

1 INTRODUCTION

The use of Lyapunov's second method to design state-vector feedback relay-control systems has been widely reported.[1-5] However, the method requires the solution of the Lyapunov matrix equation, which is not known to exist for undamped linear systems that have eigenvalues with zero real part. This paper presents a method for the design of control loops for such systems, which has been applied to the attitude control of a flexible communication satellite.

In an earlier publication,[6] the authors discussed the problems of flexibility of attitude control of a particular class of communication satellite. Eigen analysis of the resulting plant equations revealed that the eigenvalues occurred as complex pairs with zero real part, which can be seen by reference to the root-locus plots given in the earlier paper. This result made the direct application of the Lyapunov method impossible, and led to the method described in this paper.

2 LYAPUNOV'S SECOND METHOD

2.1 Basic theory

A brief account of the basic Lyapunov theory is given to provide the foundation of the modified method described. A fuller treatment may be found in Reference 1.

Consider a dynamic system, described by the matrix equation

$$\frac{dx}{dt} = Ax + Bu \qquad (1)$$

where x is the state vector of the system and u is the control signal to be determined.

If the autonomous system $dx/dt = Ax$ is asymptotically stable, a Lyapunov function for the system will be

$$V(x) = x^T P x \qquad (2)$$

in which P is a positive-definite symmetric matrix.

To ensure asymptotic stability generally, the V-function (eqn. 2) must satisfy the following conditions:

(a) $V(x)$ and all its state derivatives must be continuous

(b) $V(x) > 0$ for $x \neq 0$

$V(x) = 0$ for $x = 0$

(c) $\dfrac{dV(x)}{dn} = \dfrac{dV(x)}{dt} < 0$ for $x \neq 0$

$\dfrac{dV(x)}{dt} = 0$ for $x = 0$

(d) $V(x) \to \infty$ as $\| x \| \to \infty$.

It is seen that the quadratic form (eqn. 2) satisfies conditions a, b and c, and it only remains to show that $(dv/dx)(x)$ is a negative-definite function to satisfy the third condition.

Differentiating eqn. 2 yields $\dot{V}(x)$ as

$$\frac{dV(x)}{dn} = \dot{x}^T P x + x^T P \dot{x} \qquad (3)$$

Substituting from eqn. 1, $\dot{V}(x)$ becomes

$$\frac{dV(x)}{dn} = x^T (A^T P + PA)x + 2u^T B^T P x \qquad (4)$$

The first term on the right-hand side of this equation is made negative-definite by setting

$$A^T P + PA = -Q \qquad (5)$$

where Q is a positive-definite symmetric matrix, normally the unit matrix. Asymptotic stability of the controlled system is guaranteed by choosing u to make the second term negative-definite. It is normal practice to choose u to make the second term as negative as possible. This leads to a control law for a relay element in which the outputs u_i take their maximum permitted value with a sign opposite to the value of the feedback signal B^TPx:

$$u_i = -M_i \text{ sign } (B^TPx)_i \tag{6}$$

where M_i is the maximum value of the control u_i.

A vector block diagram for the system is shown in Fig. 1.
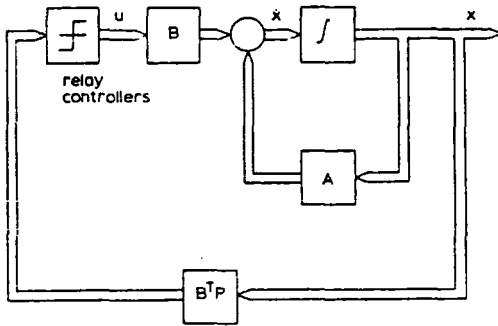
Fig. 1

Vector block diagram of Lyapunov relay control system

2.2 Application to undamped linear systems

When any two of the eigenvalues of the plant matrix A of eqn. 1 are equal in value and opposite in sign, as when they occur as a complex-conjugate pair with zero real part, the Lyapunov equation (eqn. 5) cannot be solved for P. This situation is a characteristic of systems that exhibit undamped free responses.

Mathematically, the condition for the existence of a solution to eqn. 5 may be expressed as follows: if λ_i and λ_j are any two eigenvalues of A, a solution to eqn. 5 exists, only if

$$\lambda_i + \lambda_j = 0 \tag{7}$$

To overcome this problem, a modified plant matrix A_M is formed from the original plant matrix A by the addition of a matrix of artificial-damping terms A_D. This causes the eigenvalues of A_M to have negative real parts, thus guaranteeing a solution to the Lyapunov equation.

2.3 Choice of A_D

The method of modifying A takes the original set of dynamic equations in the characteristic form for undamped 2nd-order

systems,

$$\frac{d^2y_i}{dt^2} + \Omega_i^2 y_i = f(t) \tag{8}$$

and inserts artificial damping in terms of a 'damping' coefficient ζ to achieve the characteristic equations for damped motion

$$\frac{d^2y_i}{dt^2} + 2\zeta\Omega_i \frac{dy_i}{dt} + \Omega_i^2 y_i = f(t) \tag{9}$$

Carrying out the state-vector manipulations of these two sets of equations for the system, the additional damping terms can be isolated into a separate matrix of damping terms A_D, which comprises terms that are either zero or some function of the coefficient ζ. The solution P of the Lyapunov equation for A_M,

$$A_M^T P + PA_M = -Q \tag{10}$$

is found and used in the feedback law of eqn. 6.

3 APPLICATION

This method has been used to design the control loops for a system of three coupled 2nd-order equations describing the motion of a flexible communication satellite.[8] The equations describe the motion of the roll and yaw axes of the satellite, and the fundamental bending mode of flexure of solar-array panels. A 2-input control system applying control torques to the roll and yaw axes of the satellite has been implemented and evaluated using digital simulation. A block diagram of the 2-input control system is given in Fig. 2. The deadband
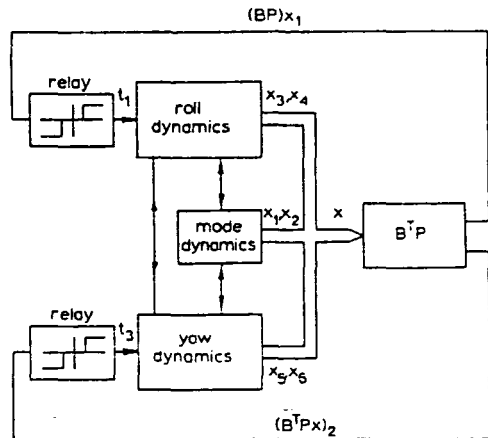
Fig. 2

Block diagram for 2-input control system
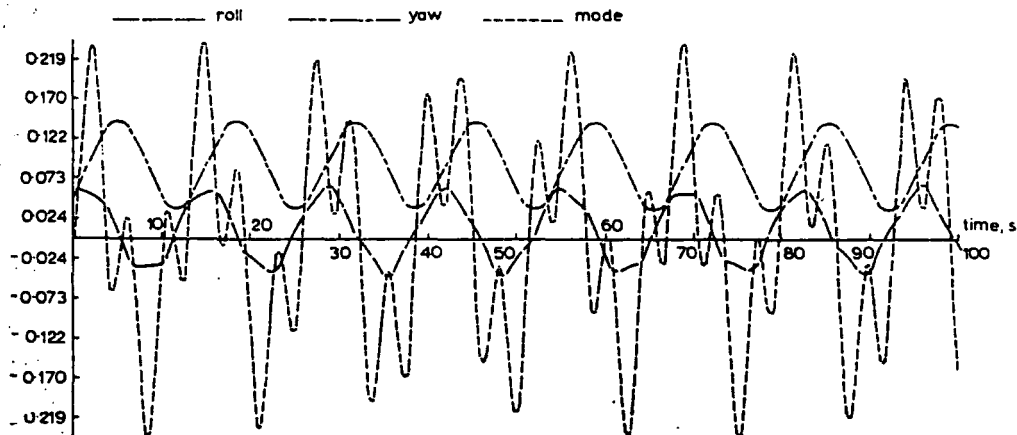
Fig. 3

Free response of flexible satellite showing roll and yaw attitudes and first bending-mode flexure

inherent in a relay switch has been included to prevent un-wanted pulsing of the gas thrusters.

Six state vectors are defined for the system as follows:

$x_1 = \eta_1$ the bending-mode deformation co-ordinate

$x_2 = \dfrac{d\eta_1}{dt}$

$x_3 = \theta_1$, the satellite-roll attitude

$x_4 = \dfrac{d\theta_1}{dt}$

$x_5 = \theta_3$, the satellite-yaw attitude

$x_6 = \dfrac{d\theta_6}{dt}$ (11)

The control vector u then comprises the roll and yaw torques, $u_1 = t_1, u_2 = t_3$. Collecting the 1-order state equations for the system into a single matrix equation in the form of eqn. 1 yields the matrices A and B as follows:

$$A = \begin{bmatrix} 0 & 1 & 0 & 0 & 0 \\ -(1+R)\Omega_1^2 & 0 & \gamma\omega_N\omega_0 & 0 & 0 & \gamma\omega_N \\ 0 & 0 & 0 & 1 & 0 & 0 \\ \gamma\Omega_1^2/I_r & 0 & -\omega_N\omega_0 & 0 & 0 & -\omega_N \\ 0 & 0 & 0 & 0 & 0 & 1 \\ 0 & 0 & 0 & \omega_N/1+R & -\omega_N\omega_0/1+R & 0 \end{bmatrix}$$
    (12)

$$B = \begin{bmatrix} 0 & -\gamma/I_r & 0 & 1/I_r & 0 & 0 \\ 0 & 0 & 0 & 0 & 0 & 1/I_r(1+R) \end{bmatrix}$$
    (13)

The 'damping' matrix A_D is found as

$$A_D = \begin{bmatrix} 0 & 0 & 0 & 0 & 0 \\ 0 & -(1+R)\zeta\Omega_1 & 0 & \gamma\zeta\omega_N & 0 \\ 0 & 0 & 0 & 0 & 0 \\ 0 & \gamma\zeta\Omega_1/I_r & 0 & -\zeta\omega_N & 0 \\ 0 & 0 & 0 & 0 & 0 \\ 0 & 0 & 0 & 0 & -\zeta\omega_N/1+R \end{bmatrix}$$
    (14)

The modified A matrix is found from

$$A_M = A + A_D$$
    (15)

For a particular set of system parameters, the Lyapunov equation (eqn.10) can now be solved for P. A description of the solution method and Fortran subroutine is contained in Appendix 7

4   DIGITAL-SIMULATION RESULTS

The flexible satellite and Lyapunov control scheme have been modelled[8] in Fortran on an ICL1906A computer using Nottingham Algorithm Group (NAG) library subroutines[9] to perform the integrations. Results are presented in computer-plotted form in Figs.3-7 for the set of system parameters given in Table 1, which show the effect of varying the value of the artificial-damping coefficient ζ over a range.

TABLE 1

PARAMETERS FOR DIGITAL SIMULATION

Satellite parameters

Inertia ratio, R	= 1·0
1st-mode frequency, Ω_1	= 1·0 s^{-1}
Nutation frequency, ω_N	= 1·0 s^{-1}
Orbit frequency, ω_0	= 0·73 × 10^{-4} s^{-1}
Roll and yaw rigid inertia, I_r	= 100 kg/m^2
Interaction coefficient, γ	= 10

Initial conditions

Roll attitude	θ_1 = 0·05 rad
Roll rate	$\dot\theta_1$ = 0·02 rad/s
Yaw attitude	θ_3 = 0·05 rad
Yaw rate	$\dot\theta_3$ = 0·02 rad/s

Control-system parameters

Jet-thruster torque	= 1·0 Nm
Relay deadband	= 0·05

Fig.3 shows the free response of the flexible satellite to initial conditions on the roll and yaw attitude and attitude rate, given in Table 1. This is seen to consist of three un-damped interacting 2nd-order motion. Figs.4-7 show the response of the controlled system for values of ζ of 0·01, 0·1, 1·0 and 10·0.
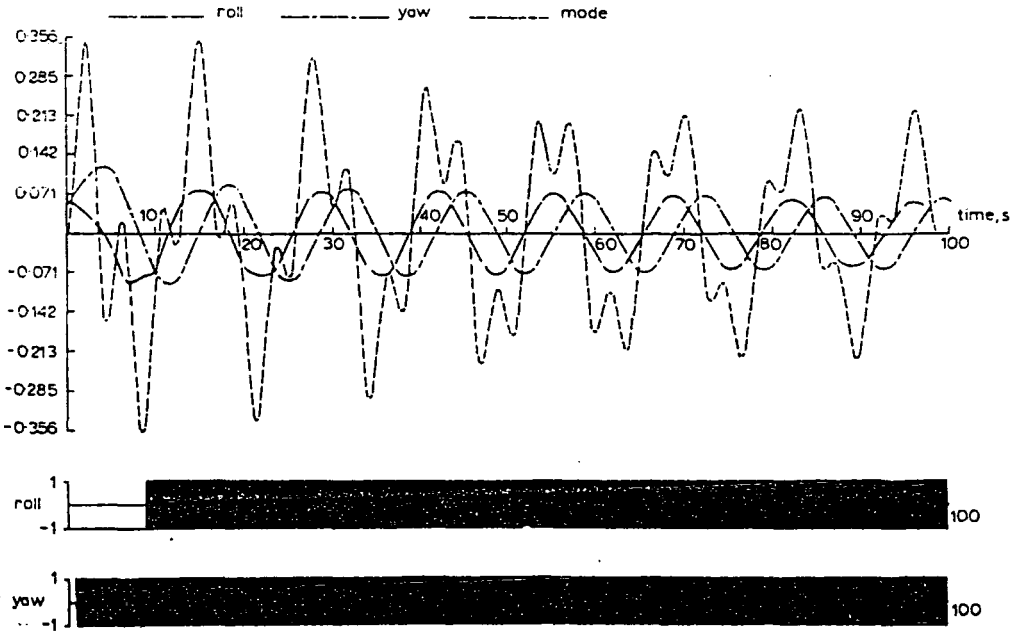
Fig. 4

2-input relay control, artificial damping = 0·01

These plots are obtained in response to the same initial conditions as the free response shown in Fig. 3. As well as the time trajectories of the roll, yaw and flexible solar-array motion, the plots show the operation of the roll and yaw gas thrusters.

From these Figures, it is clear that increasing the value of ζ gives a marked improvement in system performance up to a value of ζ of 1·0. Further increase to a value of 10·0 causes the control action to break down.

Figs. 4-6 suggest that the damping exhibited in the system transient behaviour bears a direct relation to the value of ζ used to modify the A matrix and obtain a solution of the Lyapunov equation. Eigen analysis of the modifed A matrix A_M for these particular parameter values yields a value of artificial damping in the three 2nd-order systems of about

0·7 in the best case Fig. 6. That this is close to the generally accepted optimum value for fast response of 2nd-order systems may be coincidental

The breakdown of the control action shown in Fig. 7 for a value of ζ = 10·0 indicates that there is a limit to the modification procedure. Eigen analysis of the modifed A matrix here shows that two of the three pairs of eigenvalues characterising the system lie on the real axis, and the modified system is far removed from the original undamped plant description.

5   CONCLUSIONS

A novel method for the application of Lyapunov's second method to the synthesis of relay-control systems for plants
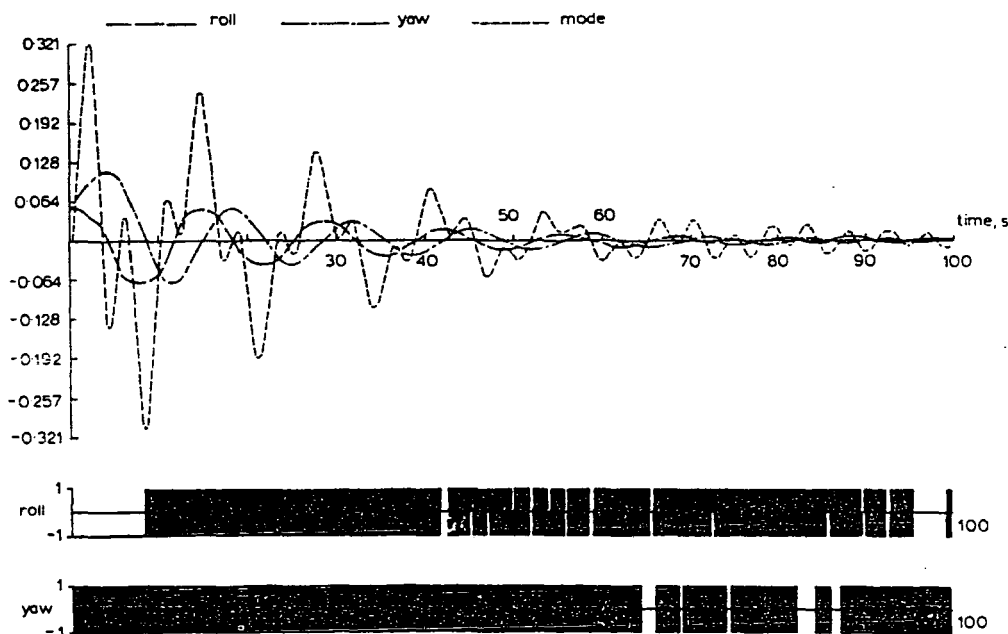
Fig. 5
2-input relay control. artificial damping = 0·1
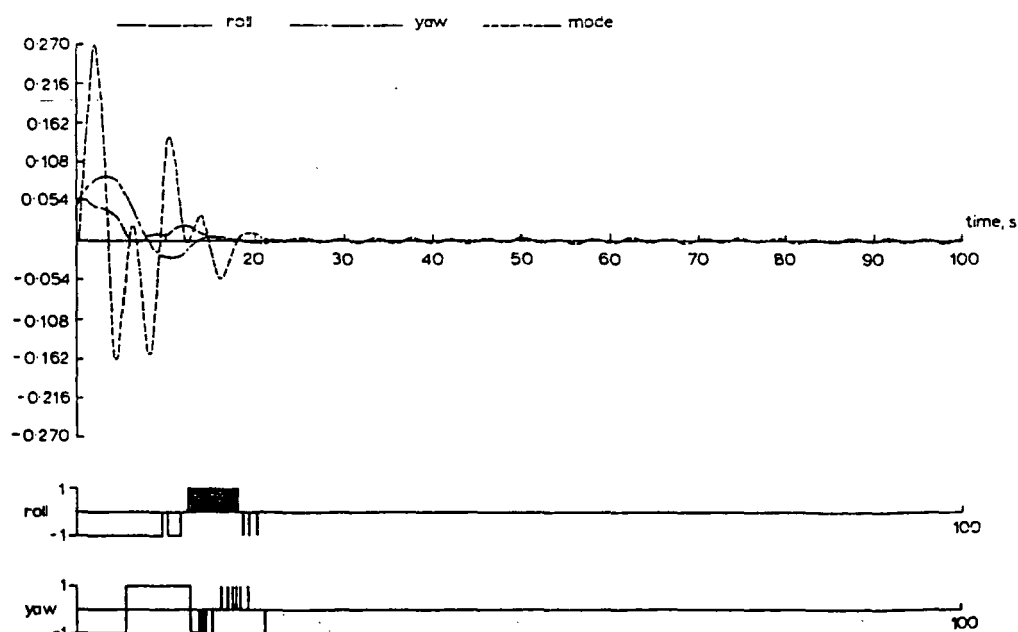
Fig. 6
2-input relay control, artificial damping = 1·0

that have undamped responses is presented. The method is used to derive the control system for a 6th-order plant describing the coupled roll- and yaw-attitude motion of a space satellite with flexible solar arrays.

The method involves modifying the plant A matrix to obtain a solution P to the Lyapunov matrix equation. This is then used in a feedback law to control the original plant. A digital simulation of the control system indicates that best performance is achieved by modifying the A matrix so that 2nd-order components have a damping factor of about 0·7.

Further applications of this method to other systems are necessary to determine if a damping factor of 0·7 in the modified plant matrix will give the most rapid plant control for the minimum control action. If this can be shown to be so, this approach offers a direct solution to the design of control loop for systems having undamped eigenvalues. Extension of the method is clearly possible to systems having low damping.

6   REFERENCES

1   KALMAN, R. E., and BERTRAM, J. E.: 'Control system analysis and design via the second method of Lyapunov'. Pt. I—Continuous-time systems', Trans. ASME, 1960, [D], 82, pp. 371-393

2   GRAYSON, L. P.: 'Design via Lyapunov's second method'. Procedings of the 4th joint automatic-control conference, University of Minnesota, 1963, pp. 589-595

3   GEISEKING, D.: 'An optimum bi-stable controller for increased missile autopilot performance'. Proceedings of the 4th joint automatic-control conference, University of Minnesota, 1963, pp. 553-557

4   JOHNSON, G. W.: 'Synthesis of control systems with stability constraints via the direct method of Lyapunov', IEEE Trans., 1964, AC-2, pp. 270-273

5   BAKKEN, O. A.: 'Some practical considerations in the application of modern control to aerospace vehicles', Proceedings of the 8th joint automatic-control conference, 1967, pp. 158-164

6   GETHING, J. M., HOLT, J. A., SMART, D. R., and GILL, K. F.: 'Effects of flexibility on a momentum-stabilised communication-satellite attitude-control system', Proc. IEE, 1973, 120, (5), pp. 613-619

7   EHNIGK, S. H.: 'Stability theorems for linear motions—with an introduction to Lyapunov's direct method' (Prentice Hall, 1966)

8   GETHING, J. M.: 'Attitude control of a momentum stabilised communication satellite having large flexible appendages'. Ph.D. thesis, University of Leeds, 1973

9   'NAG Library Manual', Mark II ICL1900 series, Nottingham algorithm group, 1972

10   BARNETT, S., and STOREY, C.: 'Matrix methods in stability theory' (Thomas Nelson & Sons, London), 1970

11   MACFARLANE, A. G. J.: 'The calculation of functionals of the time and frequency response of a linear constant coefficient dynamical system', Q. J. Mech. & Appl. Math., 1963, 16, pp. 259-271

7   APPENDIX

7.1   Solving the Lyapunov matrix equation

Having determined a modified plant matrix A_M, a solution matrix P of the matrix equation

$$A_M^T P + PA_M = -Q \tag{16}$$

is required, where P and Q are positive-definite symmetric matrices.

Several methods for the solution of this particular matrix equation have been suggested.[10] The method used solves eqn. 6.23 in this work by direct solution.

Since P and Q are symmetric matrices of order n, the solution of eqn. 16 is reduced to solving for the $\frac{1}{2}n(n+1)$ distinct elements of P. Eqn. 16 can be reformulated into the equivalent set of simultaneous equations for the required elements of P:

$$Dp = -q \tag{17}$$

where the volume matrices p and q are comprised of the upper diagonal elements of the matrices P and Q, ordered as follows:

$$p = [p_{11}, p_{12}, p_{22}, p_{13}, p_{23}, p_{33} \cdots \quad \cdots]^*$$

$$q = [q_{11}, q_{12}, q_{22}, q_{13}, q_{23}, q_{33} \cdots \quad \cdots]^* \tag{18}$$

The matrix D is formed from the elements a_{ij} of A_M as follows:
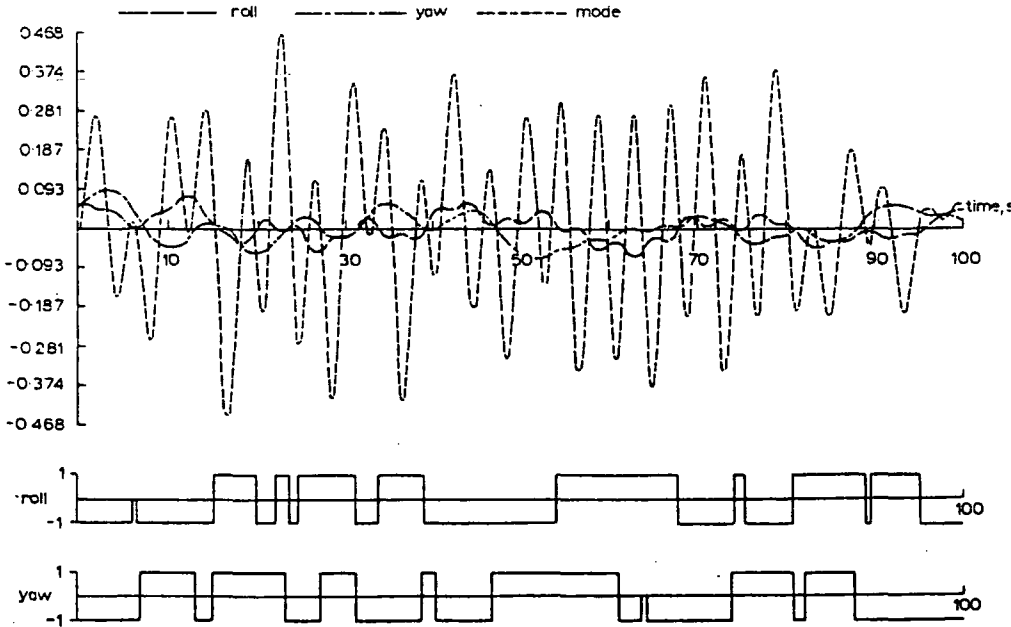
Fig. 7

2-input relay control, artificial damping = 10·0

$$D =$$

$$\begin{bmatrix}
2a_{11} & 2a_{21} & 0 & 2a_{31} & 0 & 0 & \cdots \\
a_{12} & a_{11}+a_{22} & a_{21} & a_{32} & a_{31} & 0 & \cdots \\
0 & 2a_{12} & 2a_{22} & 0 & 2a_{32} & 0 & \cdots \\
a_{13} & a_{23} & 0 & a_{11}+a_{33} & a_{21} & a_{31} & \cdots \\
0 & a_{13} & a_{23} & a_{12} & a_{22}+a_{33} & a_{32} & \cdots \\
0 & 0 & 0 & 2a_{13} & 2a_{23} & 2a_{33} & \cdots \\
\cdot & \cdot & \cdot & \cdot & \cdot & \cdot & \\
\cdot & \cdot & \cdot & \cdot & \cdot & \cdot & \\
\cdot & \cdot & \cdot & \cdot & \cdot & \cdot & \cdots
\end{bmatrix}$$

$$(19)$$

The set of simultaneous equations for the elements of p described by eqn. 17 may be solved digitally for high-order systems. To facilitate this, a systematic method for formulating the D matrix is used.[11] In this method, the elements of D are obtained as the sum of n auxiliary matrices formed from the elements of A* as follows:

(a) Set up the following symmetric integer array J of order $n \times n$:

$$J = \begin{bmatrix}
1 & 2 & 4 & 7 & 11 & \cdots \\
2 & 3 & 5 & 8 & 12 & \cdots \\
4 & 5 & 6 & 9 & 13 & \cdots \\
7 & 8 & 9 & 10 & 14 & \cdots \\
11 & 12 & 13 & 14 & 15 & \cdots \\
\cdot & \cdot & \cdot & \cdot & \cdot & \cdots \\
\cdot & \cdot & \cdot & \cdot & \cdot & \cdots \tfrac{1}{2}n(n+1)
\end{bmatrix}$$

in which, in any row, the terms up to, and including, the diagonal are obtained by adding 1 to the value of the preceding element in the row. The first element in each row or column is found by adding 1 to the diagonal element of the previous row or column, starting with the value of 1 for the first diagonal element.

(b) Formulate the first auxiliary matrix of order $\tfrac{1}{2}n(n+1)$ by considering the first row of the above array. The integer numbers missing from the row correspond to rows and columns of zeros in the auxiliary matrix. The remaining elements of the auxiliary matrix are filled by the elements of A* substituted in their correct order.

(c) Multiply by 2 the row in the auxiliary matrix corresponding to the integer in the diagonal position of the array J, i.e. row 1 for the first auxiliary matrix.

(d) Repeat the procedure for each of the n rows of the array J, the matrix D then being found as the sum of the n matrices so formed.

This process is used in the Fortran subrouting Lyapunov, which uses the Nottingham Algorithm Group (NAG) library subroutine FO4AEF, available on the ICL1906A machine to solve for the elements of the vector p in eqn. 17. The full matrix P is reformulated from the elements of p. A printout of the subroutine is given.

If the subroutine is used in an attempt to solve for P when the condition for its existence is not satisfied, it is found that the matrix D is singular, and hence the numerical routine fails to find a solution.

PAPER 30

Dynamic analysis of flexible space vehicles having uncoupled control axes

D. R. SMART

Electronic and Space Systems Group,
BAC, GW Division, Filton, Bristol

K. F. GILL
Department of Mechanical Engineering,
The University, Leeds

J. M. GETHING
Scientific Services Department,
CEGB, Portishead, Bristol

J. A. HOLT
Electronic and Space Systems Group,
BAC, GW Division, Filton, Bristol

1. INTRODUCTION

Increasingly stringent attitude stabilisation requirements are the current trend in both experimental and commercial satellites as is seen in the current Intelsat, ESRO and UK communication studies. These craft must be lightweight, compact and rugged during the launch phase but after mission capture such requirements no longer apply. The increasingly high power requirements of such craft are met by the use of large flexible solar arrays which are packed away during launch and unfurl when the craft becomes operational. For the three-axis stabilised craft being studied reaction jets are used to achieve the high pointing accuracy required. Such actuators may be hot or cold gas systems or in the future may be electric engines[1]. The broad spectral content of these actuators will inevitably excite modes of vibration in a wide range of frequencies. The influence of these highly resonant modes on the performance of on-board controllers, needing a relatively high bandwidth of 0–10 Hz, to achieve high pointing accuracy of up to a few seconds of arc may lead to design difficulties.

The dynamic analysis of flexible space craft has been considered previously[2-8] and is modified by the authors for use when no rotors, flywheels or sliding masses are present. The advantages of the modifications are simplicity of block diagram representation of the plant, ease of simulation and because the equations for overall motion are not coupled with the modal equation of vibration, the degree of flexibility can be altered without recourse to the complete analysis. In the published work[2] a vector is introduced denoting the translational motion of the mass centre of a structure due to deformations of flexible appendages. This allows the composite body translational equation to be written very simply. A logical extension for the case where no rotating or sliding components are present is to introduce a corresponding rotational vector. This extension is present here and the authors consider it represents an improvement, especially in ease of computation over the previous equations.

The dynamic analysis section describes a completely unconstrained flexible structure having low damping which

MATHEMATICAL ANALYSIS

Nomenclature

Lower case letters are used for vectors or scalars and upper case for matrices where possible.

a, α	rotation of centre of mass due to deformation
c, C	translation of centre of mass due to deformation
D	inertia diadic
E	identity matrix
F	force matrix
g	linear momentum
h, H	angular momentum
i, I, I^T	subscript denoting ith element. Inertia matrix, inertia tensor
K	stiffness matrix
M, m, β	mass representation
O	null matrix
p, P	co-ordinate of mass elements
q, Q	deformation vectors
R, r	modified matrix or r, undeformed geometry definition of structure
T	torques applied
U, u	general matrix, deformation co-ordinates
V, W	general matrices
w, w	rate of rotation, co-ordinate of mass element from mass centre
x, X	co-ordinate of mass centre
	time varying transformation matrix
Θ	angular co-ordinates
ψ	angular velocity of axis set
μ	general vector
Φ	eigenvector matrix
ϕ	rotational deformation of elemental mass
η	transformed deformation co-ordinates
Ω	eigenvalue matrix
λ	external forces and torques
Λ	damping matrix, diagonal

is inherent in mechanical systems of this type, and undergoing unforced vibration. Orbital kinematics are not considered. The vectors denoting translational and rotational motion are derived explicitly in terms of deformation co-ordinates.

The body is modelled on a lumped parameter basis for the above derivation. Using this model, equations are written for the motion of the n-subbodies so defined. An eigen transformation is applied to these equations at which point a symmetric damping matrix may be included. In the present form co-ordinate truncation reduces the order of the mathematical model which means ignoring higher frequency modes of vibration unless such a frequency corresponds to a disturbance or control frequency. To complete the analysis equations are written to incorporate composite body motion in space.

The aim of the investigation is to see what problems might arise when control systems operate in the presence of structural flexibility. The reaction jet system of attitude stabilisation will highlight these problems since it will excite modes in a wide range of frequencies. Very tight specification on pointing error, 0·01 degrees, is employed again, to accentuate any problems that might arise. A control law is selected on the basis of conceptual simplicity and ease of simulation[13]. There is little value in applying a sophisticated control scheme where adverse effects due to flexibility may be shrouded by control scheme complexity. The control law used employs a switching strategy based on attitude error only. The advantage of the system is that no error measurements are required. This information is either noisy or unreliable in practice. If rate gyros are used, there is the weight and reliability penalty to be considered and differentiation of position signals gives noisy data.

The operation and design of the system is fully described in section 5.1. Noise free attitude information is assumed in this preliminary work to avoid involvement with sensor dynamics. Square edged thrust pulses are assumed from the reaction jets and time delays between command and "thrust on-thrust off" are not considered. These assumptions are justified because of the short pulse time of the order of 10 ms in a limit cycle in the region of 10 minutes period.

The paper is presented in two sections, the first deals with the dynamic analysis of a completely unconstrained flexible structure, and introduces the concepts of modal analysis and truncation of the derived equations. The second section gives a detailed description of the vehicle chosen for study and the control system employed. Nomenclature is, as far as possible, consistent with that generally employed in previous publications on similar topics.

2. DYNAMIC ANALYSIS OF A GENERALISED FLEXIBLE STRUCTURE

Consider a general elastic structure with no rotating or sliding components as shown in (Fig. 1). The total structure can be idealised as series of point masses and inertias interconnected by massless elastic constraints. Structural damping, inherently small in mechanical systems of this type, is neglected and all deformations are assumed small. For the body in an undeformed state, a point X is defined as the centre of the mass and is considered fixed within the material of the body at this point. With X at the origin a set of reference axes are defined, for convenience these will be the undeformed structures inertial principal axes. As the body deforms, point X moves and the axes move with it in translation and rotation. Vector c and vector

angle α define this movement about the original position as shown, point X moving from its original position which is denoted as X' in Fig. 1.

2.1. Mathematical derivation of c and α

Consider then, two sets of axes passing through the structures mass centre which, when the structure is undeformed, are coincident. These axes are the principal axes of the structure and as the body moves in space they move with it. Overall motion, translation and rotation, is defined by the motion of these axes with respect to an inertially fixed set, providing the structure does not deform. When the structure deforms the axis set which is fixed within the material of the body at the mass centre move with respect to the second set of axes, which are considered to be unaffected by structural deformation. One set of axes then define the "rigid body" motion, the motion of the other set define motion with respect to the "rigid body" position due to structural deformation. This motion, due to deformation, is defined by vector c and vector angle α.

Under free vibration, axes 1, 2, 3, the "rigid body" axes, are then those about which linear and angular momentum are zero. For the submass A_i define a position vector from X' as w_i then

$$w_i = c + r_i + u_i \qquad . \qquad . \qquad . \qquad (1)$$

where the r_i define the undeformed geometry of the structure and u_i is due to elastic deformation. The u_i and ϕ_i, the equivalent rotational deformation co-ordinate, cause changes in c and α.

For the undeformed body, the centre of mass is at point X and by definition

$$\sum_i m_i r_i = 0 \qquad . \qquad . \qquad . \qquad (2)$$

When the body is deformed with no external forces acting this definition is written as

$$\sum_i m_i w_i = 0 \qquad . \qquad . \qquad . \qquad (3)$$

the centre of mass still being at X', the point X defined previously having moved through vector c.

Equation (3) becomes, when substituting from (1)
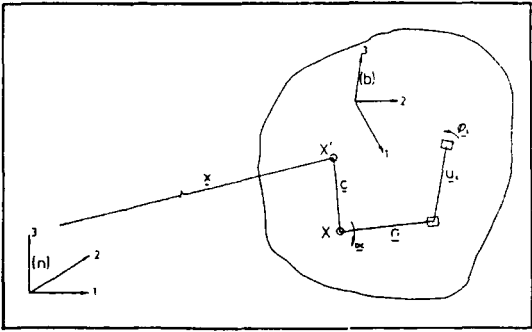
$$\sum_i m_i c + \sum_i m_i r_i + \sum_i m_i u_i = 0.$$

Figure 1.

The second term is zero by (2) and

$$c = -\frac{1}{\beta} \sum_i m_i u_i \qquad \cdots \quad (4)$$

β being the scalar total mass $\sum_i m_i$

If g be the linear momentum of the system, then

$$g = \sum_i m_i \frac{d}{dt}(x + w_i) \qquad \cdots \quad (5)$$

or

$$g = \beta \frac{dx}{dt} + \sum_i m_i \frac{d}{dt} w_i \qquad \cdots \quad (6)$$

Since X' is the centre of mass then the linear momentum must be given by

$$g = \beta \frac{dx}{dt} \qquad \cdots \quad (7)$$

and so

$$\sum_i m_i \frac{d}{dt} w_i = 0. \qquad \cdots \quad (8)$$

If ψ is the angular velocity of the axis set in which $\partial/\partial t \, w_i$ is computed then equation (8) becomes

$$\sum_i m_i \frac{\partial}{\partial t} w_i + \sum_i m_i (\psi \wedge w_i) = 0. \qquad \cdots \quad (9)$$

The second term is zero by equation (3) and so

$$\sum_i m_i \frac{\partial}{\partial t} w_i = 0. \qquad \cdots \quad (10)$$

If h is the angular momentum of the system, then

$$h = \sum_i D^i \cdot \psi^i + \sum_i (x + w_i) \wedge m_i \frac{d}{dt}(x + w_i) \qquad \cdots \quad (11)$$

D^i being the inertia diadic of the ith submass.

Expanding the vector cross product of equation (11) gives

$$h = \sum_i D^i \cdot \psi^i + \sum_i x \wedge m_i \frac{d}{dt} x + \sum_i x \wedge m_i \frac{d}{dt} w_i + \sum_i w_i \wedge m_i \frac{d}{dt} x + \sum_i w_i \wedge m_i \frac{d}{dt} w_i. \qquad \cdots \quad (12)$$

The second term can be ignored as is usual with rotational problems since this is the moment of linear momentum. The third term is zero by equation (8) and the fourth term is zero by equation (3), hence:

$$h = \sum_i D^i \cdot \psi^i + \sum_i w_i \wedge m_i \frac{d}{dt} w_i. \qquad \cdots \quad (13)$$

Substituting from equation (1)

$$h = \sum_i D^i \cdot \psi^i + \sum_i c \wedge m_i \frac{d}{dt} w_i + \sum_i (r_i + u_i) \wedge m_i \frac{d}{dt} w_i \qquad \cdots \quad (14)$$

the second term is zero by equation (8) and expanding the third term gives

$$h = \sum_i D^i \cdot \psi^i + \sum_i r_i \wedge m_i \frac{d}{dt} c + \sum_i r_i \wedge m_i \frac{d}{dt} r_i + \sum_i r_i m_{i\wedge} \frac{d}{dt} u_i + \sum_i u_i \wedge m_i \frac{d}{dt} c + \sum_i u_i \wedge m_i \frac{d}{dt} r_i + \sum_i u_i m_i \frac{d}{dt} u_i. \qquad \cdots \quad (15)$$

The vector ψ^i giving the inertial velocity of each submass and consists of three components. The overall rotational velocity of the body ω, and the term α due to deformations and also the angular velocity of each submass due to deformation ϕ^i. The vectors $c \, u_i$ and r_i are all in a reference frame rotating with angular velocity $\omega + \alpha$. Making these substitutions in (15) and neglecting second terms in small variables $u_i \, c$ and α and their time derivatives (15) reduces to

$$h = \sum_i D^i \cdot (\omega + \alpha + \phi^i) + \sum_i r_i \wedge m_i (\omega \wedge r_i) + \sum_i r_i \wedge m_i (\alpha \, r_i) + \sum_i r_i \wedge m_i (\omega \wedge u_i) + \sum_i r_i \wedge m_i \, u_i + \sum_i u_i \wedge m_i (\omega \wedge r_i). \qquad (16)$$

Making the assumption of small overall rates of rigid body rotation and using that

$$\sum_i D^i \cdot \omega + \sum_i r_i \wedge m_i (\omega \wedge r_i) = I^T \cdot \omega \qquad \cdots \quad (17)$$

I^T being the inertia tensor for the composite body, then (16) reduces to

$$h = I^T \cdot \omega + I^T \cdot \alpha + \sum_i D^i \, \phi^i + \sum_i r_i \wedge m_i \, u_i \qquad \cdots \quad (18)$$

Since momentum is conserved when no external forces act and since there will be some internal structural damping eventually bringing u_i, α and ϕ^i to zero then

$$h = I^T \cdot \omega \qquad \cdots \quad (19)$$

and

$$I^T \cdot \alpha + \sum_i D^i \cdot \phi^i + \sum_i r_i \wedge m_i u_i = 0. \qquad \cdots \quad (20)$$

The time integral of equation (20) is

$$I^T \cdot \alpha + \sum_i D^i \cdot \phi^i + \sum_i r_i \, m_i u_i = \text{const} = 0. \qquad \cdots \quad (21)$$

since, for the undeformed case when the u_i, ϕ_i and α are all zero the constant is zero.

Equations (4) and (21) are now, for convenience, written in matrix notation and this is best achieved by defining the following.

$E = 3 \times 3$ identity matrix.

$O = 3 \times 3$ null matrix.

$\left. \begin{array}{l} \sum EO = |EOEO \ldots O|^T \\ \sum OE = |OEOE \ldots OE|^T \end{array} \right\}$ the order being apparent from the context.

M is the mass-inertia matrix of the n subbodies, null except for the 6×6 block diagonal elements.

$$Q = |u_1^1 \, u_1^2 \, u_1^3 \, \phi_1^1 \, \phi_1^2 \ldots \phi_n^3|^T$$

I is the 3×3 inertia matrix of the total body about axis set 1 2 3.

$$\widetilde{R}_i = \begin{vmatrix} 0 & -r_i^3 & r_i^2 \\ r_i^3 & 0 & -r_i^1 \\ -r_i^2 & r_i^1 & 0 \end{vmatrix} \quad \text{this forms the vector cross product terms.}$$

$\widetilde{R}$ is $6n \times 6n$ subdivided into 3×3 elements and null except for alternate diagonal elements.

$$\begin{vmatrix} \widetilde{R}_1 & & & & & \\ & 0 & & & & \\ & & \widetilde{R}_2 & & & \\ & & & 0 & & \\ & & 0 & & & \\ & 0 & & & & \\ & & & & R_n & \\ & & & & & 0 \end{vmatrix}$$

Using this notation and equations (4) and (21)

$$\underline{c} = -\frac{1}{\beta} \Sigma E O^T M Q \qquad . \qquad . \qquad (22)$$

$$\underline{\alpha} = -I^{-1} (\Sigma E O^T M R + \Sigma O E^T M) Q \qquad . \qquad (23)$$

$\underline{c}$ and $\underline{\alpha}$ being 3×1 column matrices

These vectors, $\underline{c}$ and $\underline{\alpha}$ represent the translational and rotational motion of the body fixed axis set due to elastic deformation of the structure.

2.2. Force and Torque Equations for Lumped Parameter Model

The expression for $\underline{c}$ and $\underline{\alpha}$ are not time dependent, they are merely functions of the deformation co-ordinates and are equally valid when the body deforms under external forces and torques. These external stimuli may be disturbances such as solar radiation pressure, gravity gradient torques, or on a space vehicle, control actuators.

To facilitate investigation of forced motion, an inertial reference frame is required. Define an axis set (n) and an inertially fixed point. If $\underline{x}$ be the vector from the reference point to point X, the mass centre of the body and θ the transform from one axis set (n) to the body axes (b), then

$$\underline{x}(n) = \theta \underline{x}(b) \qquad . \qquad . \qquad (24)$$

where θ is time varying.

The vector position $\underline{p}_i$ of submass A_i is then from Fig. 1

$$\underline{p}_i = \theta \underline{x} + \underline{c} + \underline{p}_i + \underline{u}_i \qquad . \qquad . \qquad (25)$$

The angular position θ_i is

$$\underline{\theta}^i = \underline{\theta} + \underline{\alpha} + \underline{\phi}^i \qquad . \qquad . \qquad (26)$$

To each submass, A_i, apply the Euler equation

$$\underline{F}_i = m_i \ddot{\underline{p}}_i \qquad . \qquad . \qquad (27)$$

$$\underline{T}_i = \dot{\underline{H}}_i \qquad . \qquad . \qquad (28)$$

now

$$\ddot{\underline{p}}_i = \ddot{\theta}\underline{x} + \ddot{\underline{c}} + \ddot{\underline{u}}_i + (\ddot{\theta} + \ddot{\underline{\alpha}})\ (\underline{c} + \underline{r}_i + \underline{u}_i)$$

$$+ 2(\dot{\theta} + \dot{\underline{\alpha}})_\wedge(\dot{\underline{c}} + \dot{\underline{u}}_i) + (\dot{\theta} + \dot{\underline{\alpha}})_\wedge| (\dot{\theta} + \dot{\underline{\alpha}})\wedge (\underline{c} + \underline{r}_i + \underline{u}_i)|. \qquad (29)$$

$$\dot{\underline{H}}_i = \frac{d}{dt}(D^i \cdot \underline{\theta}^i) = D^i \cdot \ddot{\underline{\theta}}_i + \dot{\underline{\theta}}^i {}_\wedge D^i \dot{\underline{\theta}}^i. \qquad . \qquad (30)$$

substituting for $\underline{\theta}^i$

$$\dot{\underline{H}}_i = D^i \cdot (\ddot{\theta} + \ddot{\underline{\alpha}} + \ddot{\underline{\phi}}^i + (\dot{\theta} + \dot{\underline{\alpha}})_\wedge \ \dot{\underline{\phi}}^i$$

$$+ (\dot{\theta} + \dot{\underline{\alpha}} + \dot{\underline{\phi}}^i)_\wedge D^i \cdot (\dot{\theta} + \dot{\underline{\alpha}} + \dot{\underline{\phi}}^i) \qquad . \qquad . \qquad (31)$$

Using equations (22), (23), (27), (28) and (31), assuming small rates of rotation and ignoring second order terms, the following matrix equation results

$$F = M \Sigma E O \ddot{\theta}X - (M\widetilde{R}\Sigma E O - M\Sigma O E)\ddot{\theta} + M \left(E - \Sigma E O \Sigma E O^T \right.$$

$$\left. \frac{M}{\eta} + (\widetilde{R}\Sigma E O - \Sigma O E) I^{-1} (\Sigma E O^T M \widetilde{R} + \Sigma O E^T M) \right) \ddot{Q}$$

$$\qquad . \qquad . \qquad (32)$$

Matrix F comprising the column of forces and torques applied to each submass. This matrix must include external forces and torques as well as those internal to the structure and is written as

$$F = (\lambda - KQ) \qquad . \qquad . \qquad (32)$$

where K is the structural stiffness matrix with respect to X fixed, λ contains all external, non-structural forces and torques.

The $6n$ simultaneous equations in matrix equation (32) must now be supplemented by equations describing the overall motion of the body in space. Because of the definition of vectors $\underline{c}$ and $\underline{\alpha}$ which isolate the actual mass centre from the deformation equations, these can be written as

$$F_c = \beta \ddot{X} \qquad . \qquad . \qquad (34)$$

$$T_c = I\ddot{\theta} \qquad . \qquad . \qquad (35)$$

which are equations describing rigid body motion. A rigorous derivation of equation (35) is given in reference (16).

F_c and T_c denote all possible forces and torques external to the composite body.

For convenience, equations (34) and (35) are written as

$$P_c = M_c \ddot{C} \qquad . \qquad . \qquad (36)$$

P_c being the 6×1 matrix of forces and torques applied to the composite body, M_c is the mass inertia matrix of the undeformed structure and $\ddot{C}$ is the 6×1 matrix of accelerations.

Equations (32) and (36) together describe the motion of the flexible body.

3. MODAL ANALYSIS AND TRUNCATION

Equation (32) is a set of $6n$ coupled second order equations. For even small n this represents an unwieldy set to handle computationally and it is probable that much of the higher frequency information is unnecessary. To ease the computational difficulty, and to facilitate retention of relevant information only, a modal analysis is applied.

The computational technique employed is described in Appendix 1 and an example is given in Appendix 2. A check on the results of Appendix 2 is given in Appendix 3. The example also highlights the differences between the analysis in the previously published work[2] and that presented in this publication.

Equation (32) has the general form

$$U = V\ddot{\mu} + W\mu \qquad . \qquad . \qquad . \qquad (37)$$

the $6n$ equations being coupled. Classical modal analysis is used to uncouple the equations. Using the linear transformation

$$\mu = \Phi\eta \qquad . \qquad . \qquad . \qquad (38)$$

Φ being the matrix of eigen vectors of the homogeneous part of the equation, normalised that

$$\Phi^\tau V\Phi = E$$

and premultiply by Φ^τ then

$$\Phi^1 U = \ddot{\eta} + \Omega^2\eta \qquad . \qquad . \qquad . \qquad (39)$$

Here, Ω is the diagonal matrix of undamped natural frequencies for the flexible structure.

In the uncoupled form, a diagonal matrix representing structural damping may be included and notes dealing with this are included in Appendix 4.

Co-ordinate truncation is possible when the equations are uncoupled and is performed by deleting rows and columns from the matrix equation. It is shown that for the application considered, only the lowest frequency mode of vibration proved to be of significance. It is the lowest frequency mode which has the highest amplitudes in response to a given input. It was found that the smaller amplitude higher frequency modes did not affect the simulated system to any extent comparable with the effects of the fundamental mode.

The equations resulting from the analysis are summarised as

$$P = M_t\ddot{C} \qquad . \qquad . \qquad . \qquad (36)$$

$$\Phi^\tau U = \ddot{\eta} + \Omega^2\eta \qquad . \qquad . \qquad . \qquad (39)$$

$$\underline{c} = -\frac{1}{\beta}\Sigma EO^\tau MQ \qquad . \qquad . \qquad (22)$$

$$\alpha = I^{-1}(\Sigma EO^\tau MR + \Sigma OE^\tau M)Q \qquad . \qquad (23)$$

where U, the matrix of excitations to equation (39) is a function of external forces and of terms $\ddot{C}$ in (36). Remembering that $Q = \Phi_m$ then values c and α of equations (22) and (23) can be calculated and finally the pointing attitude of any mass can be calculated. These equations

are presented in numerical form for the test vehicle in the following section, *see* equations (40)–(42).

4. MODEL OF VEHICLE USED FOR INVESTIGATION

The space vehicle chosen to investigate the control problem associated with craft incorporating large flexible appendages is shown schematically in Fig. 2. The aim is to study the attitude control of a representative vehicle comprising a complex flexible structure.

The body length is 1·4 m and its width 1·0 m. The total mass is 284·0 kg and is assumed to be of uniform density for the purpose of computing moments of inertia. The solar arrays shown in the figure are 3·18 m long and 1 m wide consisting of fibreglass facing sheets on a resin core. The thickness of the facing sheets is $1·02 \times 10^{-4}$ m and of the core $6·45 \times 10^{-3}$ m. Torsional and bending stiffnesses for the core are assumed zero. For the facing sheets the bending stiffness is $2·07 \times 10^{10}$ N/m^2 and the torsional stiffness is $3·10 \times 10^8$ N/m^2. The total mass of the solar arrays is 16 kg.

The lumped parameter model of the vehicle was carried out on the basis of six point masses, as shown together with the centre body. The six masses were considered as points possessing both mass and inertia.

The paddles are divided into three equal lengths, and the submasses considered to be at the centre of mass of each of these sections.
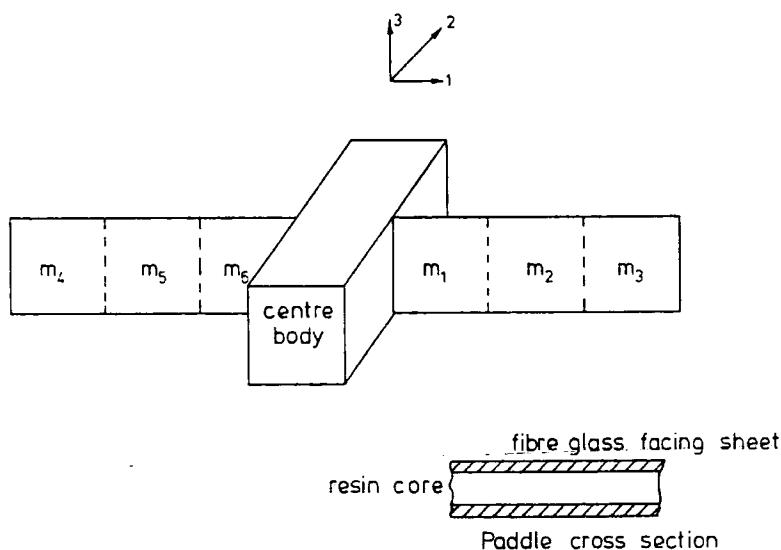
Figure 2.

Since very little Euler coupling of the axes of rotation is present, only one axis attitude control need be considered, the others being similar. Translation equations can be ignored, since only attitude control is of importance and so the mathematical model can be evaluated as:

$$T_3 = 165·7\ \ddot{\theta}_3 \qquad . \qquad . \qquad . \qquad (40)$$

$$\left.\begin{array}{l}\ddot{\eta}_1 + 4·509\ \eta_1 = 12·596\ \ddot{\theta}_3 \\ \ddot{\eta}_2 + 109·1\ \eta_2 = 4·342\ \ddot{\theta}_3 \\ \ddot{\eta}_3 + 1101\ \eta_3 = -3·357\ \ddot{\theta}_3\end{array}\right\} \qquad . \qquad . \qquad . \qquad (41)$$

$$\alpha_3 = 0·076\eta_1 + 0·026\eta_2 - 0·2\eta_3 \qquad . \qquad . \qquad (42)$$

The equations describe rotation about axis 3 since this is the motion most affected by flexibility.

The block diagram representation for these equations is given in Fig. 3. The authors feel this to be an improved representation over those suggested in earlier published work[2-8] from the point of simulation and separation of flexible appendage motion from composite body motion.

In analogue simulation of a plant of the form of the figure, it may be desirable to alter the mode frequencies. This can easily be achieved by resetting one value. For such a change to be made on simulations based on the analysis of references (2–8) a far more complicated procedure will be followed. Indeed this would involve alteration of parameter values in the rigid body block as well as the modal blocks and fairly lengthy calculation of the new values.
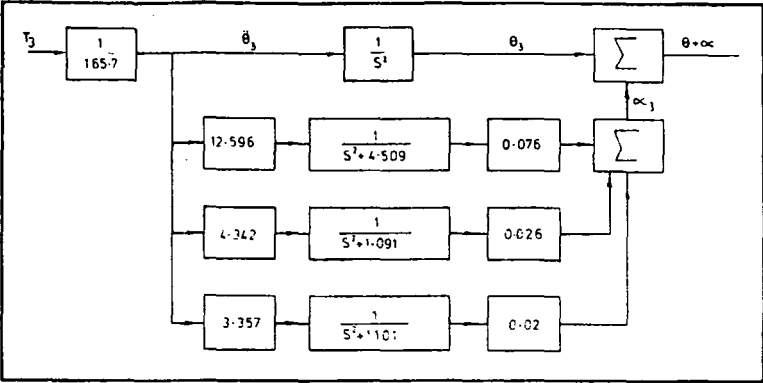
Figure 3.

5. CONTROL SYSTEMS

5.1. Control Studies Applied to Model of Flexible Satellite

In recent years, there have been many control laws[9-13] suggested for application to satellite attitude stabilisation. Very few of these look at the problems associated with flexibility at the outset and the majority have failed to mention such problems in the final stages of simulation. The approach up to the present time seems to have been to design control loops on the basis of a rigid structure and then to adjust the appropriate control parameters to meet the system specification in the presence of non-rigid components. The purpose of this section is to follow such a procedure in an attempt to discover what problems arise, not necessarily to overcome them.

Each of the three axes of rotation is to be controlled separately. This normally means using gas jets and because of the wide spectral content these will excite modes in an extensive frequency range and any control problems should become apparent. The philosophy of the control law[13] chosen for implementation is unsophisticated making for ease of design and simulation. For a rigid vehicle with no external disturbances however, it does force a very efficient limit cycle in terms of gas usage, a very important requirement in most mission specifications.

In the presence of external forces and torques, the control system may not stabilise the attitude of a space craft[14]. The study presented here does not require investigation of behaviour in the presence of such external disturbances and the system is therefore suitable in this application where limit cycle operation only is considered.

5.2. Minimum Impulse Control System for Attitude Stabilisation

The control scheme is described using the error phase plane, Fig. 4. Starting from point i.c the trajectory coasts to switch line SW1 where a fixed pulse is metered from the control actuators. This pulse is set to the minimum impulse capability of the reaction jets. As SW2 is reached, so another pulse is demanded, each time reducing the error rate. The number of switch lines and the size of each pulse each produces is fully described in the published work[13]. A backup switch is also required and its hysteresis is denoted by the different positions of the "on" and "off" lines. The trajectory converges, if certain conditions are met[13] to an unsymmetric limit cycle which is the most efficient possible, using the minimum reliable

impulse possible from practical gas jets. The vertical switch lines are easily generated using comparators or Schmitt triggers for which the hysteresis can be varied. It is not necessary to strive to reduce this hysteresis, in fact the property is most desirable[13]. One obvious attraction of this control strategy is that no rate information is necessary. In practice, this is difficult to achieve when rates are low and any strategy which does not require this very inaccurate information is worthy of consideration. The Schmitt triggers can be used to drive monostable multi-vibrators to meter the correct length of pulse to the reaction jets.

Such a system is designed for the satellite modelled in section 4 (Fig. 2), assuming it to be rigid. The pointing accuracy is one hundredth of a degree with a minimum impulse of 0·05 Nm for 10 ms. For the rigid vehicle with no external torques applied, the limit cycle magnitude is determined by the inner switch lines. In any practical design, consideration of disturbance torques plays a vital part deciding control parameters but for the purpose of this study, the inner switch lines are set at $\pm 1 \times 10^{-2}$ degrees. The backup switches are set at $\pm 2 \times 10^{-2}$ degrees with two intermediate lines.

6. RESULTS OF SYSTEM SIMULATION

The space craft model and control system of section 4 and 5.2 respectively were simulated on a PACE 231 R analogue computer with limited parallel logic facilities.

Figure 4.

Figure 5.

The Figs. 5(a)–5(e) shown are plots of $(\theta + \alpha)$, the attitude of the centre body, against time. All results were obtained by observing the vehicle attitude starting from an initial condition on error just sufficient to enter the backup switch. Every pulse from the react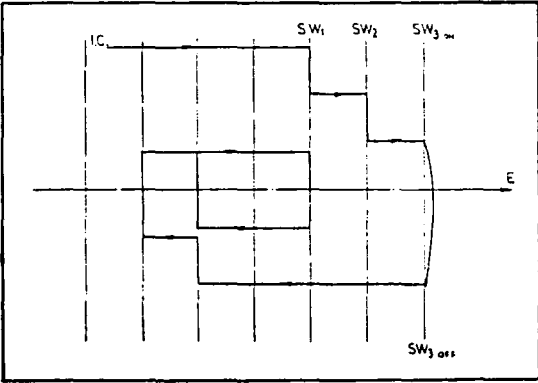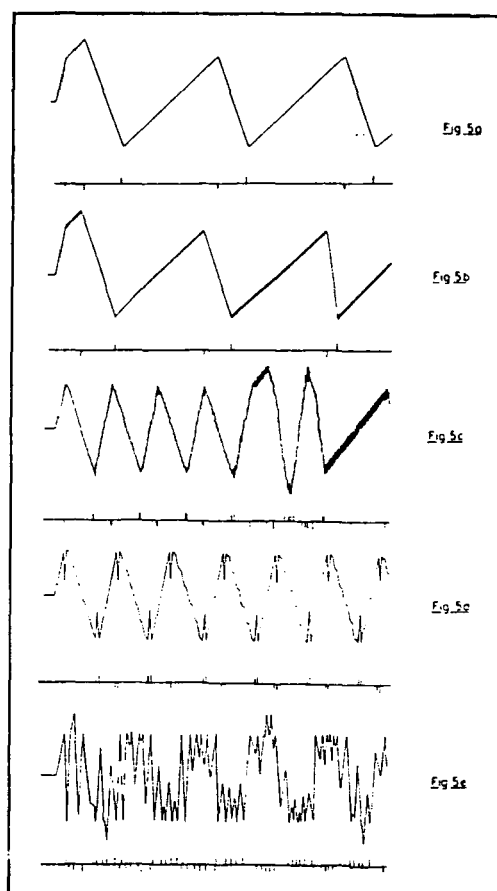ion jet and the associated pulse direction are indicated on the graphs. The first plot, Fig. 5(a), shows the behaviour of the rigid vehicle and is used as a reference criterion for the evaluation of the performance with flexibility present. The limit cycle is unsymmetric, having a single pulse at each of the inner switch lines, never going beyond these switching boundaries. Figure 5(b) shows the behaviour with the lowest frequency mode of equation (41) present. It was found throughout that the higher frequency modes of the appendages had little effect on the centre body attitude and the spacecraft performance degradation resulted from the lower frequency components. This observation is significant in that it allows for extensive truncation of the modal equations. The lumped parameter analysis used is inherently an approximation approach. If greater accuracy in mode frequency is required, the possibility of using a distributed or continuous parameter approach, normally not used because of the computational difficulty in handling the coupled partial differential equations may be employed. The computational difficulties are greatly reduced when only one, the lowest frequency of vibration, is required. Figure 5(b) then shows operation similar to that

in Fig. 5(a) but at one point a double pulse occurs at each switch line. This doubles the frequency of the limit cycle and increases gas usage. For the mode amplitude shown in Fig. 5(b), this problem could be overcome by increasing the hysteresis of the switch line.

The double pulse is caused by the α term resetting the trigger and firing it a second time. There is, however, a limit to the extent of allowable hysteresis which will be dictated by consideration of external disturbance torques. It is this reason that varying hysteresis does not prove an acceptable solution for the general case. Figures 5(c)–5(e) show operation with varying degrees of flexibility. The modal frequency change from one case to the next is the square root of ten, the frequency decreasing each time. This would result from changes in stiffness of the appendage structure and could be achieved by decreasing the core thickness in the sandwich comprising the paddle cross-section. It is shown that increased gas usage and poorer stabilisation result from the increased flexibility. If the mass of the appendages were increased in addition to the mode period, greater deterioration in performance would be inevitable.

7. CONCLUSIONS

For a class of space vehicle which is slowly spinning, having low net angular momentum and no sliding masses or steerable components, the Euler equations for attitude motion reduce to three independent equations, illustrating that no cross coupling exists between axes. Attitude stabilisation can be accomplished by three independent control channels.

For this class of vehicle, the approach to the dynamic analysis presented in this paper has two major advantages over work previously reported. One advantage is the ease of simulation in terms of rigid body equations which are completely divorced from those describing the motion of the flexible components. The other major advantage is the ability to change the parameters within the equations representing the non-rigid elements without recourse to the revision of the complete analysis. As mission requirements change during engineering design of a space vehicle, so will the structure of the craft alter to a greater or lesser extent. These variations in structure should be easily handled by the analysis. The structure of the vehicle chosen for investigation is, in the authors' view, representative of vehicles of the next generation and is based on present day engineering practice. For this vehicle the fundamental mode of flexure of the solar arrays will be altered by decreasing the thickness of the resin core. This will cause a change in the eigen values of the linear transformation used in section 3 but will not alter the eigen vectors. As a result, the only change in the mathematical model will be in the equations describing motion of the flexible components. The rigid body equation is unaltered and only the modal frequencies of the appendages change. Changes in mass of the appendages do affect the rigid body equation but this can be accomplished by simply recalculating the total moment of inertia of the vehicle when in an undeformed state. Modification of the modal equations is also easily carried out.

For this investigation, the flexible solar arrays have been subdivided into three equal length sections, each having the same mass. The authors appreciate that this may not be the best approximation and it may be better for a designer vehicle to segment the arrays by matching the total inertia of the model and craft and also the fundamental frequency of modal vibration.

A method of eigen analysis[15] is employed which avoids the necessity of inverting a cumbersome mass

matrix. From experience in the use of this method, it appears to be insensitive to ill conditioning, giving equal root solutions where they arise. The computational time to give a complete solution to the eigen value problem is less than that required by a procedure necessitating mass matrix inversion.

From the simulation study of the mathematical model and control system, it became apparent that only the fundamental mode of flexure markedly influenced the attitude performance of the vehicle. This was to some extent the result of the reduction in modal amplitude with increased modal frequency. The higher frequency modes of the appendages had little effect on the centre body attitude, the system performance degradation resulting only from the lower frequency component. This observation is significant in that it allows for extensive truncation of the modal equations.

The simulation of the test vehicle (incorporating structural flexibility) and control system demonstrate the deterioration in performance, especially in terms of gas usage and hence operational life. For the problem considered, that of limit cycle in the absence of external disturbance torques, the parameter in the control system which might be varied in an attempt to obtain improved performance is the hysteresis of the switch lines. The level of allowable hysteresis will, however, in any representative environment where disturbances will be present, be governed by the magnitude of these disturbances. Tuning of control parameters will not then, alleviate the difficulties encountered due to structural flexibility. The deterioration in performance observed will be increased if the mass of the flexible appendages is increased, thus causing greater interaction between the plant and its controller.

It can be concluded that present day techniques of design of control systems using rigid body dynamics alone are not adequate and that appreciation of the influence of flexible body dynamics must be present at all stages of design.

Figure 6.

APPENDIX I

Eigen Analysis

The equations for modal deformation take the general form

$$M\ddot{y} + Ky = 0 \quad . \quad . \quad . \quad (43)$$

in the homogeneous case, where K is the structural stiffness matrix and M is a modified mass matrix. We can write this as

$$(M^2 + K)y = 0 \quad . \quad . \quad . \quad (44)$$

or $$(-w^2 M + K)y = 0 \quad . \quad . \quad . \quad (45)$$

putting $$\mu = \frac{1}{w^2} \quad . \quad . \quad . \quad (46)$$

then $$\mu Ky = My. \quad . \quad . \quad . \quad (47)$$

We require the roots of

$$\det(M - \mu K) = 0 \quad . \quad . \quad . \quad (48)$$

Since K is positive definite[15], then there exists a real orthogonal matrix R such that
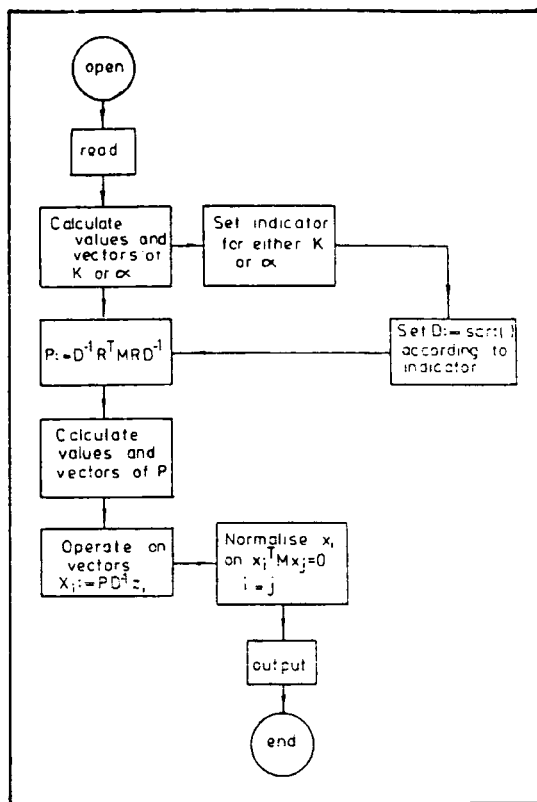
$$R^T KR = \text{diag } (\beta_i)^2 = D^2 \quad . \quad . \quad (49)$$

and conversely

$$K = RD^2 R^T \quad . \quad . \quad . \quad (50)$$

$$\therefore \quad (M - \mu K) = RD (D^{-1}R^T MRD^{-1} - \mu) DR^T. \quad . \quad (51)$$

Put $$P = D^{-1}R^T MRD^{-1}. \quad . \quad . \quad (52)$$

then $\det(M - \mu K) = \det(R)^2 \det(D)^2 \det(P - \mu I).$ (53)

and $$\det(R)^2 = 1 \quad . \quad . \quad . \quad (54)$$

$$\det(D)^2 = \pi\beta_i^2. \quad . \quad . \quad (55)$$

The zeros of $(P - \mu I)$ are then those of $(M - \mu K)$. Now P has a set of normal eigen vectors z_i, with

$$Pz_i = \mu_i z_i \quad . \quad . \quad . \quad (56)$$

$$\therefore \quad D^{-1}R^T MRD^{-1}z_i = \mu_i z_i. \quad . \quad . \quad (57)$$

$$MRD^{-1}z_i = \mu_i RDz_i \quad . \quad . \quad (58)$$

$$MRD^{-1}z_i = \mu_i RD (DR^T RD^{-1}z_i). \quad . \quad (59)$$

$$MRD^{-1}z_i = \mu_i (RD^2 R^T) RD^{-1}z_i. \quad . \quad (60)$$

Let $$RD^{-1}z_i = X_i \quad . \quad . \quad . \quad (61)$$

then
$$MX_i = \mu_i KX_i \quad . \quad . \quad . \quad (62)$$

thus X_i are the vectors of the complete system.

Note
$$z_i^T z_j = 0 \quad . \quad . \quad . \quad (63)$$

$$(DR^T x_i)^T (DR^T x_j) = 0 \quad . \quad . \quad . \quad (64)$$

$$x_i^T K x_j = 0. \quad . \quad . \quad . \quad (65)$$

Hence the x_i are orthogonal with respect to K.

A problem arises in determining the structural stiffness matrix. The most convenient method is to determine the influence coefficients α_i then $K = \alpha^{-1}$. The eigenvalues of K are the reciprocal of those of α and the vectors are the same.

$$Proof \quad R^T K R = \text{diag} (\beta_i)^2 \quad . \quad . \quad (66)$$

$$R^T K^{-1} R = R^T \alpha R = \frac{1}{\text{diag} (\beta_i)^2} \text{q.e.d.} . \quad . \quad (67)$$

A flow chart for the computation is given (Fig. 6).

The value of this approach to the eigen-analysis is that matrix inverses are avoided and the matrices K or α and P are symmetric and positive definite therefore simple Jaccobi methods may be used in computation. The method does not appear sensitive to ill conditioning giving equal root solutions where they occur. All computation was performed on a KDF9 digital computer using standard eigen value routines to find the eigen solutions of the symmetric matrices K or α and also P. Using a Kidsgrove translation of the complete programme EBMDSGJ, the run time for the eighth order case given in Appendix 2 was of the order of 10 seconds.

APPENDIX II

Application of Eigen-Analysis to Simple Test Vehicle

The test vehicle used here is similar to that used in Ref. 2 and is so chosen to highlight the differences in the two methods of analysis. In the reference the analysis constrains the centre of mass against rotation and so the frequencies will be different in instances where such rotation occurs. The test vehicle is depicted in Fig. 7.

The structure consists of four elastic booms attached to centre mass m_0. The booms are massless except for the tip
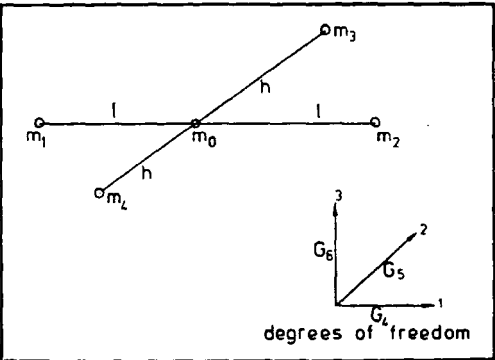
Figure 7.
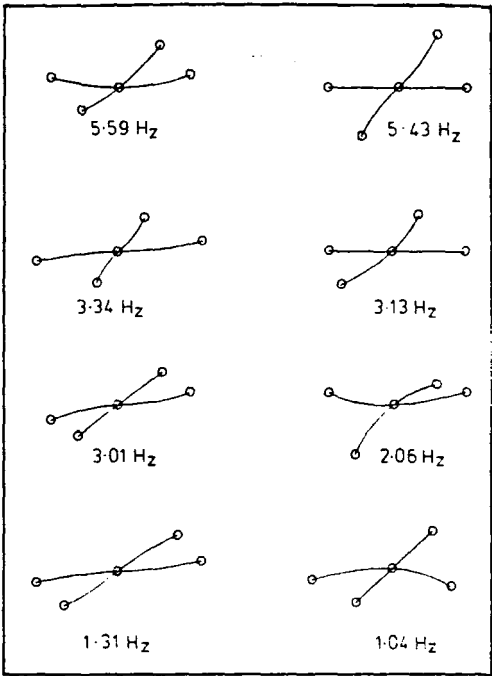
Figure 8. The vectors c and α giving the motion of su: . . $\overline{c}y$ m_0 may be found from equations (22) and (23).

which carries a point mass in each case of 1 lb mass. The centre body m_0 is considered as a point having both mass and inertia, the mass is 4 lb and its inertia is spherical of value 18 lb/ft².

The two longer booms, length l are 4 ft in length whilst for the shorter ones, $h = 2$ ft. Structural stiffnesses are defined as in Ref. 2 on the basis of the cantilever natural frequency. These frequencies are set at 0·90 and 1·81 H_z respectively: in the 1–2 and 1–3 planes of the vehicle when attached to a fixed centre body m_0. The corresponding frequencies for the short beams are 2·71 and 4·52 H_z in the 1–2 and 2–3 planes respectively.

Taking the homogeneous part of equation (32)

$$M \left(E - \Sigma EO \Sigma EO^T \frac{M}{\eta} + (R \Sigma EO - \Sigma OE) l^{-1} \right.$$

$$\left. (\Sigma EO^T M \widetilde{R} + \Sigma EO^T M) \right) \ddot{Q} + KQ = 0. \quad . \quad . \quad (68)$$

the eigen value analysis was applied and the vectors normalised such that

$$\Phi^T N \Phi = E, \quad . \quad . \quad . \quad (69)$$

N being the matrix coefficient of Q. The results are given in Fig. 8. The four modes which do not contain a centre body rotation* are in accord with the results in Ref. 2, but the rotational modes are obviously not. A simple check on these frequencies is made using Lagrange equation techniques and this does verify the values of frequencies obtained. The check on frequencies is to be found in Appendix 3.

*These modes are marked with an asterisk.

APPENDIX III

ENERGY METHODS TO CHECK NATURAL FREQUENCIES OF MODES OF VIBRATION

Consider two of the booms of the test vehicle of Fig. 7 to be reduced to zero length. The tip masses may be combined with the centre mass. The motion will be assumed rotation about the axis of the contracted booms as shown in Fig. 9.

Writing expressions for the kinetic and potential energy

$$K.E. = \tfrac{1}{2}I\dot{\alpha}^2 + \tfrac{1}{2}m_1(\dot{\alpha}r_1 + \dot{u}_1)^2 + \tfrac{1}{2}m_2(\dot{\alpha}r_2 + \dot{u}_2)^2. \quad (70)$$

$$P.E. = \tfrac{1}{2}k_1 u_1^2 + \tfrac{1}{2}k_2 u_2^2 . \qquad (71)$$

but $u_1 = u_2$; $m_1 = m_2 = 1$; $I = 18$; $r_1 = r_2 = r$; $k_1 = k_2$. $\quad (72)$

The Lagrangian function then becomes

$$L = 9\dot{\alpha}^2 + (\dot{\alpha}r + \dot{u})^2 - ku^2. \qquad (73)$$

Taking the partial differentials and writing the two Lagrange equations gives

$$9\ddot{\alpha} + r\ddot{u} + r^2\ddot{\alpha} = 0 \qquad (74)$$

$$\ddot{\alpha}r + \ddot{u} + ku = 0. \qquad (75)$$

Eliminating $\ddot{\alpha}$, yields

$$\ddot{u}\left(1 - \frac{r^2}{9 + r^2}\right) + ku = 0 \qquad (76)$$

from which the natural frequency is

$$\left\{\frac{k}{9}\,(9 + r^2)\right\}^{1/2}\frac{1}{2\pi}\,H_z. \qquad (77)$$

For the case where the longer booms are in flexure $k = 129$ lbf/ft and $r = 4$ ft. Substituting these values the natural frequency is 3.01 H_z which corresponds easily with the results from the eigen-analysis. In the case where the longer booms are contracted, the above equations give 5.44 H_z and the digital analysis gives 5.43 H_z.

APPENDIX IV

Equation (39) of section 3.1 was

$$\Phi^T U = \ddot{\eta} + \Omega^2\eta \qquad (39)$$

This does not include any energy dissipation or damping terms. If some estimate of the damping factor for each mode is available, then a diagonal matrix representing this can be included in (39) to give

$$\Phi^T U = \ddot{\eta} + 2\Delta \cdot \Omega\eta + \Omega^2\eta . \qquad (78)$$

in the standard fashion.

For a space vehicle, an estimate of the inherent structural damping is virtually impossible to obtain. Normal vibration tests are not accurate because of the environment in which they are carried out. Aerodynamic energy losses arise which will not be present in a space environment. In common with all engineering systems of this
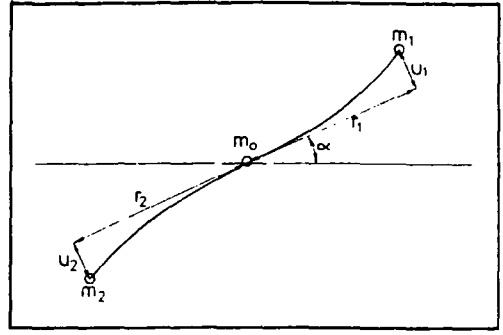
Figure 9.

type, the structural damping coefficient will be low, of the order of 0.1 or less, and this will certainly not cause marked changes in the natural frequencies of vibration. In the simulation carried out for this report, the damping terms have not been included. This omission is not considered to be of great importance and should only serve to highlight the effects of flexibility.

REFERENCES

1. Hughes, W. G. Active stabilisation. AGARD Lecture series No 45 on Attitude stabilisation of satellites in orbit.
2. Likins, P. W. and Fleischer, G. E. Results of flexible spacecraft attitude control studies utilising hybrid coordinates. AIAA paper 70–20.
3. Likins, P. W. Dynamics and control of flexible space vehicles. TR 32–1329, Jet Propulsion Lab. 1970.
4. Likin, P. W. and Gale. A. H. Analysis of interactions between attitude control systems and flexible appendages. Proc of the 15th international Astronautical Congress, (Belgrade. 1968). vol 2. Pergamon Press. 1970. pp 67–90.
5. Gale. A. H. and Likins. P. W. Influence of flexible appendages on dual-spin spacecraft dynamics and control. J of Spacecraft and Rockets, vol 7, pp 1049–1056, 1970.
6. Likins. P. W. Modal method for analysis of free rotation of spacecraft. AIAA Journal, vol 5. No 7. pp 1304–1308.
7. Liking. P. W. and Wirsching, Paul H. Use of synthetic modes in hybrid co-ordinate dynamic analysis. AIAA Journal, vol 6. No 10. October. 1968.
8. Hooker and Margulies. The dynamical attitude equation for an n-Body satellite. Journal of Aeronautical Sciences, vol XII. No 4, pp 123–128.
9. Nicklas. J. C. and Vivian, H. C. Derived-rate increment stabilisation: its application to attitude control problems. ASME Journal of Basic Engineering, 84, 54–60 (1962).
10. MacLaren, A. P. Design of a gas-jet attitude control system for use in satellites. RAE Technical note Space 54 (1964).
11. Melcher, H. J. and Otlen, D. D. Modulating bong-bong attitude controls. Control Engineering, 73–75, November 1965.
12. Scott, E. D. Pseudo-rate sawtooth pulse reset control system analysis and design. AIAA/JACC Guidance and Control Conference Preprint, August 1966.
13. Gaylord, R. S. and Keller, W. N. Attitude control systems using logically controlled pulses. Presented at AS Guidance. Control, and Navigation Conference, Stanford, Calif. Aug 7–9, 1961.
14. Kroy, W. H. Divergence of minimum impulse attitude control system under external torque. Douglas Report No SM–47751, November 1964.
15. Wilkinson, J. H. The Algebraic Eigen value problem. Clarendon Press. Oxford 1965.
16. Smart, D. R. Dynamic Analysis and 3-Axis Attitude Control of a Flexible Space Vehicle. PhD Thesis, Dept of Mechanical Engineering, University of Leeds, June 1973.

PAPER 31

Technical Notes

Attitude control of a flexible space vehicle by means of a linear state observer

D. R. SMART* and K. F. GILL†

1. INTRODUCTION

The two philosophies for the attitude control of flexible space vehicles that appear practicable are: firstly, the complete control of all the plant states, in the sense that all states tend to some bounded value as time tends to infinity; and secondly, to control the rigid body[1] to lie within some bounded region and allow the vibrations within the structure to behave in an uncontrolled manner. If the former strategy is implemented, not only is the attitude of some part of the structure, for example a radio antenna, controlled to lie within some bounded region, but the modes of structural vibration are also explicitly controlled. The second method requires less state information than the first and is the less complex of the two.

The adoption of either approach to the control problem, however, will require more state information than is available from an attitude sensor. No presently available sensors are sufficiently precise to allow accurate, noise free rate information to be obtained directly, especially when this rate is low, as in the case of minimum impulse limit cycle operation. The model reference approach to obtaining this information[2] has been shown inadequate, and the use of such devices as strain gauges on the flexible appendages to measure deformations add additional elements which are liable to failure. To achieve the desired control a method must be found which will provide the required information. Work has been carried out on state observers[3-10] and on Kalman filtering[11,12], and the implementation of these methods should provide possible avenues of approach. The state observer technique is primarily implemented using analogue devices whilst the Kalman filter uses digital equipment. This requirement would be satisfied by the use of a small on-board digital computer which would either be in the form of a special purpose machine constructed for the specific task of state estimation, or it a computer is available on-board for other functions, this could be time shared to achieve the same result.

This paper presents an investigation into the practicability of using a state observer to obtain information necesary for attitude control. The theory of state observers is presented in a brief form and a digital computer program is developed for the solution of the observer equations. This program is used to design a total state observer for the flexible space vehicle, which has been described in reference (1), and it is used in an analogue simulation. Finally, the results of this simulation are presented and discussed.

---

*Electronic and Space Systems Group, British Aircraft Corporation, Filton, Bristol.
†Department of Mechanical Engineering, University of Leeds.

NOTATION

$\underline{b}$ vector formed from elements of B

$\underline{q}$ vector formed from elements of QE

$\underline{t}$ vector formed from elements of T

$\underline{x}$ plant state variables

$\underline{y}$ plant output vector

$\underline{u}$ plant input vector

$\underline{z}$ observer state variables

A plant dynamic matrix

B plant input matrix

H plant output matrix

D observer dynamic matrix

E observer input matrix

G observer onput matrix

T observer transformation matrix or torques applied to vehicle

Im, In identity matrices of order m and n respectively

Q product of E and H

QE matrix Q extend

i, j integers denoting one of a number of matrix or vector elements

t, t_o, t_f time, start time, end time

2. OBSERVABILITY AND CONTROLLABILITY

The conditions of plant observability and controllability[12] are essential if an observer is to be developed and, as a prerequisite, the definitions are given in this section.

(i) A system is said to be completely observable in the interval $t_n \rightarrow t_f$ if the initial states $x(t_o)$ can be determined from the outputs $\underline{y}(t)$ observed over the same interval. For a plant

$$\left. \begin{array}{l} \underline{\dot{x}} = A\underline{x} + B\underline{u} \\ \\ \underline{y} = H\underline{x} \end{array} \right\} \quad \cdots \quad (1)$$

if the matrix

$$| \ H^T \quad A^T H^T \quad A^{2T} H^T \quad A^{n-1T} H^T \ |$$

has rank not less than n, the system is completely observable.

(ii) A system is said to be completely controllable if there exists a finite control u over the interval $t_o \to t_f$, which transfers the system from an initial state $x(t_o)$ to an equilibrium state $x(t_f)$ in this interval.

For the plant described in eqn. (1), if the matrix

$$| B \quad AB \quad A^2 B \quad \ldots \quad A^{n-1} B |$$

has rank not less than n, then the plant is said to be completely controllable.

3. THE LINEAR STATE OBSERVER

It has been shown[4] that a completely observable n'th order system

$$\dot{x} = Ax + Bu \qquad . \qquad . \qquad . \qquad (2)$$

with l independent inputs

$$y = Hx \qquad . \qquad . \qquad . \qquad (3)$$

can be observed with a $(n-l)$th order linear dynamic system. Suppose that the dynamic system comprising the observer has the form

$$z = Dz + Ey + Gu \qquad . \qquad . \qquad . \qquad (4)$$

such that it is driven by the plants outputs y as well as the plants inputs u. The observer must, of course, be controllable with respect to the plant outputs. That is, D and E must form a controllable pair. If an estimate $\hat{x}$ of the plant states is to be achieved from a linear combination of the observer outputs, then an equation of the form

$$z = Tx \qquad . \qquad . \qquad . \qquad (5)$$

must hold. Differentiating this equation with respect to time yields

$$\dot{z} = T\dot{x} \qquad . \qquad . \qquad . \qquad (6)$$

and using eqns. (3) and (4) yields

$$\dot{z} = Dz + EHx + Gu. \qquad . \qquad . \qquad (7)$$

Equating the right hand sides of these two equations gives that

$$T\dot{x} = Dz + EHx + Gu. \qquad . \qquad . \qquad (9)$$

If eqn. (2) is premultiplied by T and used with eqn. (8) then

$$TA - DT = EH \qquad . \qquad . \qquad . \qquad (9)$$

$$TB = G \qquad . \qquad . \qquad . \qquad (10)$$

The solution of eqn. (9) is only possible if the eigenvalues of matrices D and A are different. A further condition on the dynamics of the observer then is that its eigenvalues can be arbitrarily chosen providing they are not the same as those of A.

Using eqn. (7) and subtracting eqn. (2) after premultiplying it by T yields

$$\dot{z} - T\dot{x} = Dz + EHx + Gu - TAx - TBu \qquad . \qquad . \qquad (11)$$

which reduces to

$$\dot{z} - T\dot{x} = D(z - Tx) \qquad . \qquad . \qquad (12)$$

The equation in the variable $(z - Tx)$ has the solution

$$z(t) = Tx(t) + \exp(Dt)(z(0) - Tx(0)) \qquad . \qquad (13)$$

and it can be seen that if the initial conditions are chosen such that

$$z(0) = Tx(0) \qquad . \qquad . \qquad (14)$$

then it is possible to guarantee that x can be exactly reconstructed from y and z.

The observer may be designed by choosing the matrices D and E which must form a controllable pair. The choice of D specifies the dynamics of the observer and eqns. (9) and (10) can be solved to complete the design.

Equation (5) may be augmented by the output equation of the plant to give

$$\left| \begin{array}{c} z \\ \cdots \\ y \end{array} \right| = \left| \begin{array}{c} T \\ \cdots \\ H \end{array} \right| \left| \begin{array}{c} \hat{x} \end{array} \right| \qquad . \qquad . \qquad . \qquad (15)$$

and the state estimates x are given by

$$\hat{x} = \left| \begin{array}{c} T \\ \cdots \\ H \end{array} \right|^{-1} \left| \begin{array}{c} z \\ \cdots \\ y \end{array} \right| \qquad . \qquad . \qquad . \qquad (16)$$

4. SOLUTION OF THE OBSERVER PROBLEM

The solution of eqns. (9) and (10) and the calculation of the inverse of the square matrix of eqn. (16) can most readily be performed on a digital computer. To reconstruct all the unmeasurable plant states, a third order dynamic state observer is required. The only information required for the implementation of the control strategy selected, however, is the "rigid body" position and velocity which would require a first order observer only. It was decided, however, in the light of future work, to develop a total state observer. In conjunction with this, the digital programme for the solution of eqn. (9) was made a general one, capable of accepting and solving an observer problem of any order.

Matrix T of eqn. (9) is of order $m \times n$, matrix A is $n \times n$, D is $m \times n$, H is $l \times n$ and E is $m \times l$. The method of solution developed was to extend the order of the products in the equation by using Kronecker products[13]. This product, sometimes called the direct product, is defined as

$$A \otimes B = (a_{ij}B) \qquad . \qquad . \qquad (17)$$

If A is $m \times n$ and B is $l \times p$, then $A \otimes B$ is $(ml) \times (np)$ partioned into mn blocks. The brackets of eqn. (17) indicate the i, j partition of the product which is composed of the element a_{ij} of matrix A multiplying each element of B. It may be shown[13] that

$$AX = B$$

where X is an $n \times m$ matrix, can be written as

$$(A \otimes I_m)x = b \qquad . \qquad . \qquad (18)$$

where x is the column vector of dimension mn composed

of the rows of X placed in order down the column of $\underline{x}$ and $\underline{b}$ is formed in the same way from B. Also

$$XA = B$$

where X is $m \times n$ can be written as

$$(I_m \otimes A^T)\underline{x} = \underline{b} \quad . \quad . \quad . \quad (19)$$

If the product EH of eqn. (11) is written as Q, it can now be seen that

$$(I_m \otimes A^T)\underline{t} + (D \otimes I_n)\underline{t} = \underline{q} \quad . \quad . \quad (20)$$

or

$$\underline{t} = |(I_m \otimes A^T) + (D \otimes I_n)|^{-1}\underline{q} \quad . \quad . \quad (21)$$

The matrix $(I_m \otimes A^T)$ which will be called AE, for A extended, is composed of $n \times n$ partitions each one containing the matrix A^T. $(D \otimes I_n)$, called DE, is composed of $n \times n$ partitions, the i, j'th partition being the identity matrix multiplied by the i, j'th element of D. Matrix vector q, called QE, is formed from the rows of Q taken in turn. If these extended matrices are formed then the vector $\underline{t}$ can be found from

$$\underline{t} = (AE + DE)^{-1}QE \quad . \quad . \quad . \quad (22)$$

and this can be reduced to T by taking the first n elements as the first row of the $m \times n$ matrix T etc. The Fortran program, developed for the solution of the observer equations, uses the method described and in this way finds the matrix T when D and E are specified. This matrix is then partitioned with H as described in eqn. (14) and its inverse is found using a library subroutine. As a check on the inversion subroutine's accuracy, the ob-server transformation matrix and its inverse are multiplied together and the result is output. Finally the matrix TB is formed. A flow diagram for the program is given in Fig. 1 and the actual program is included in Appendix I.

5. DESIGN OF THE STATE OBSERVER

The dynamics of the flexible space vehicle which has been described in the earlier paper[1] will again be used. Only the fundamental mode of flexure will be included and the dynamic equation describing this vehicle may be written as:

$$T = 165 \cdot 7 \, \ddot{\theta} \quad . \quad . \quad . \quad (23)$$

$$\ddot{\eta} + 4 \cdot 509\eta = 0 \cdot 076T$$

and the output equation is

$$0 \cdot 076\eta + \theta = y \quad . \quad . \quad . \quad (24)$$

y being the attitude of the centre body of the vehicle. Figure 2 shows the vehicle dynamics using the variable x_i as the i'th state variable. From this figure, the eqns. (23) and (24) can be written in state space notation as

$$\begin{vmatrix} \dot{x}_1 \\ \dot{x}_2 \\ \dot{x}_3 \\ \dot{x}_4 \end{vmatrix} = \begin{vmatrix} 0 & -1 & 0 & 0 \\ 0 & 0 & 0 & 0 \\ 0 & 0 & 0 & -1 \\ 0 & 0 & -4 \cdot 509 & 0 \end{vmatrix} \begin{vmatrix} x_1 \\ x_2 \\ x_3 \\ x_4 \end{vmatrix} + \begin{vmatrix} 0 \\ 0 \cdot 00604 \\ 0 \\ 0 \cdot 076 \end{vmatrix} |u| \quad . \quad . \quad (25)$$

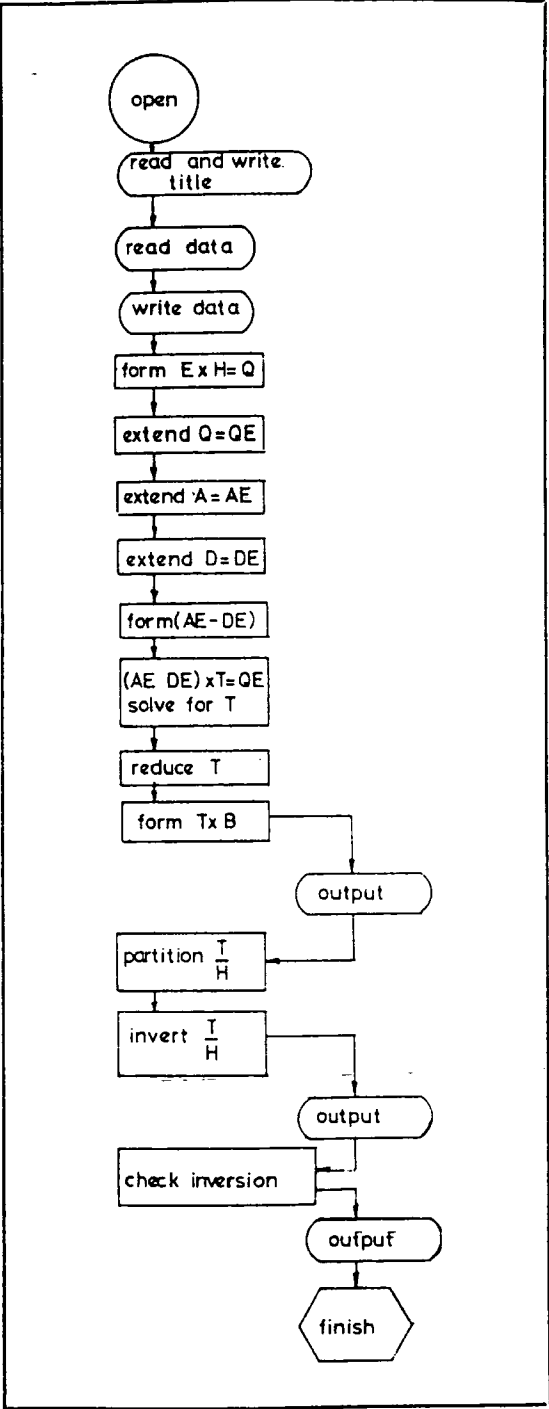*Figure 1.*
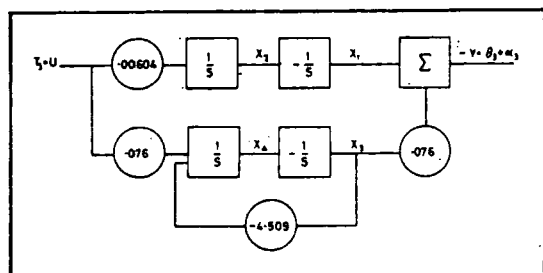
Figure 2.

TOTAL STATE OBSERVER

FLEXIBLE SPACE VEHICLE MODEL
FIRST MODE ONLY, OMEGA SQUARED = 4·509

MATRIX A

```
0·0   -1·0    0·0     0·0
0·0    0·0    0·0     0·0
0·0    0·0    0·0    -1·0
0·0    0·0   -4·509   0·0
```

MATRIX D

```
-0·5    0·0    0·0
 0·0   -0·3    0·0
 0·0    0·0   -0·1
```

MATRIX E

```
0·2
0·2
0·2
```

MATRIX H

```
1·0    0·0    0·076    0·0
```

MATRIX B

```
0·0
0·00604
0·0
0·076
```

MATRIX TB

```
0·004561
0·013160
0·120500
```

OBSERVER TRANSFORMATION MATRIX

```
-5·903     6·615     -0·4909    -0·0510
 0·4423   -0·5513     0·0935     0·0033
77·68    -87·04       6·5640    13·83
881·4    661·4      -38·23      11·89
```

CHECK MATRIX

```
1·000E 00   -2·910E-09   0·000E 00    0·000E 00
0·000E 00    1·000E 00   1·819E-10    0·000E 00
2·910E-09    0·000E 00   1·000E 00    4·547E-11
0·000E 00    0·000E 00  -3·638E 10    1·000E 00
```

Figure 3.

$$\dot{\underline{x}} = A\,\underline{x} + B\,\underline{u}$$

and

$$y = | 1 \quad 0 \quad 0{\cdot}076 \quad 0 | \begin{vmatrix} x_1 \\ x_2 \\ x_3 \\ x_1 \end{vmatrix} \qquad . \qquad . \quad (26)$$

$$y = H\underline{x}$$

The matrices A, B and H must be input to the observer programme and it remans to specify the observer dynamic matrix D and its input matrix E. It has been stated that D will be of order 3×3 and it was decided to make it a series of 3 first order filters. This not only simplifies the simulation of the observer but it also makes clear the value of the time constants of the observer since these will be the reciprocal of the diagonal elements of D, all other elements being zero. E must be chosen to form a controllable pair with D and this can be done by ensuring that no element of E is zero. Considerable difficulty was encountered in the initial attempts to design a suitable observer. It was found that with the diagonal elements of D set to -1, -2 and -3 respectively and all the elements of E set to 1 the observer transformation matrix contained extremely large numbers, of the order of 10^3. Whilst a digital solution of the observer's dynamic equations would have been possible, an analogue solution would have required gains of 10^3 in the simulation to produce a solution. Clearly this would be physically impossible to implement and modification to the observer dynamics was necessary. From trial and observation it was found that, with the diagonal elements of D equal to $-0{\cdot}5$, $-0{\cdot}3$, $-0{\cdot}1$ respectively and the elements of E equal to $0{\cdot}2$, the transformation matrix contained acceptable numbers. The first order filters in the observer have time constants of 2, 3·33 and 10 seconds respectively and the responses of these should be adequate to produce an acceptable estimate of the plant state. The attenuation to signal frequencies of 5 rad/sec is of the order of 20 dbs and the observer should adequately suppress all noise frequencies, although no such investigation is attempted here.

The digital computer solution to the observer problem is given in Fig. 3.

6. SIMULATION

The linear state observer developed is incorporated in a control scheme that employs the yet switching law described earlier[1]. The output from the torquing circuitry is used to drive the dynamics represented by eqns. (25) and (26) and the state observer is represented by the labelled block shown in the complete analogue circuit diagram of Fig. 4.

The simulation was carried out on a PACE 231R$\bar{V}$ analogue computer with limited parallel logic facilities. The logic elements included on the machine do not incorporate monostable devices needed for the generation of the accurately timed pulses supplying command to the torquing mechanisms. It was decided to use a series of integrated circuit monostable multivibrators which are readily available in TTL form to provide this function. The analogue computer diode logic was found to be insufficiently fast to drive the edge triggered monostables and a series of Schmitt triggers were built using solid state components. These triggers together with a buffer stage between them and the integrated circuits were found to work to complete satisfaction, the monostables being capable of driving the diode logic on the machine. Time scaling of the simulation was achieved using the logic facilities of the analogue computer

Assignment Sheet

Principal Amplifier Outputs		Potentiometer Settings			
		P		Q	
00	$-x_2 = -\theta$	06	0·076	00	0·006
01	$x_1 = \theta$	11	0·051	04	0·03
05	$-\dot{x}_1 = -\dot{\alpha}$	12	0·5903	05	0·076
06	$x_3 = \alpha$	13	0·6615	07	0·4509
08	$x_1 + x_3 = \theta + \alpha$	14	0·4989	08	0·2
10	$-Z_1$	15	0·046	10	0·5
11	$-Z_2$	16	0·132	11	0·3
15	$-Z_3$	17	0·1205	13	0·35
12	$-\hat{x}_1$			14	$T/10$ variable
17	$\hat{x}_2$			15	0·1
				16	0·0033
				17	0·4428
				18	0·0551
				19	0·0935

7. RESULTS

Initial checks on the simulation were carried out using the system states x_1 and x_2 as the control variables. In this way the operation of the jet switching logic could be evaluated. Before transferring to control on the observed states, results were taken which show the quality of information produced by the observer. The first trace of Fig. 5 shows the "rigid body" trajectory $x_1 = \theta$ whilst the second trace shows the estimate of this state which has been produced by the observer. The observed "rigid body" attitude rate is shown in the lower trace. The recording facilities available did not allow a record of the actual

attitude rate to be taken. This can be reconstructed by differentiating the position signal and it can be seen that this will produce a trace very similar to the observed attitude rate shown. The slight overshoots which are apparent on the lower trace are a result of the pen recorders response characteristics and they were not present when the signal was displayed on an oscilloscope. The quality of these results indicates that the jet switching logic was working satisfactorily and that the observed states are in very close agreement with those of the plant.

The results given in Fig. 6 show operation when using the observed "rigid body" position and actual attitude rate as inputs to the switching logic circuits. The first trace is the observed rigid body position and the second trace shows the actual position of the centre body of the modelled vehicle, $(\theta + \alpha)$. The oscillatory components of the attitude variations due to structural deformations have been almost completely removed by the state observer. The bottom trace shows the observed velocity of the "rigid body". Comparison of Figs. 5 and 6 shows that negligible deterioration in performance of the attitude stabilisation system results from the use of the observed state. It was found, and this is evidenced in Fig. 7 that when both the observed variables were used for control purposes a slight deterioration in performance occurred. The bottom trace shows the observed velocity and it can be seen that the nominal value of this is increased compared with the two previous cases. An increase in the limit cycle frequency has resulted which will cause increased gas usage and reduced mission life. The top trace showing the "rigid body" attitude and its estimate shown below this appear to be in close agreement and one may be tempted to attribute the deterioration in performance to the slight inaccuracies in the attitude rate estimate. It is more likely, however, that the effect is caused by a combination of errors in both the estimated state variables $\hat{x}_1$ and $\hat{x}_2$. The extra cost of the degraded perfc ,-ance is of the order of 20% in terms of increased gas usage as can be seen from the 20% decrease in limit cycle period. This figure is probably comparable with the
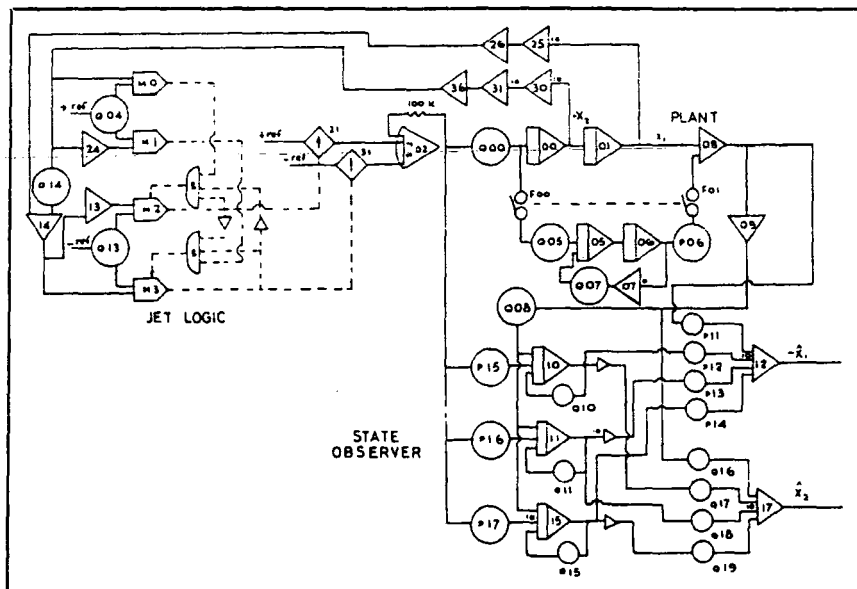
Figure 4
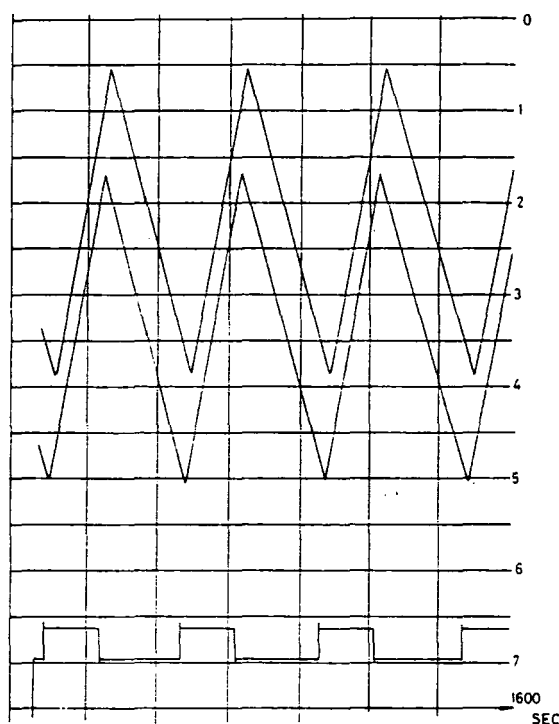
Figure 5.
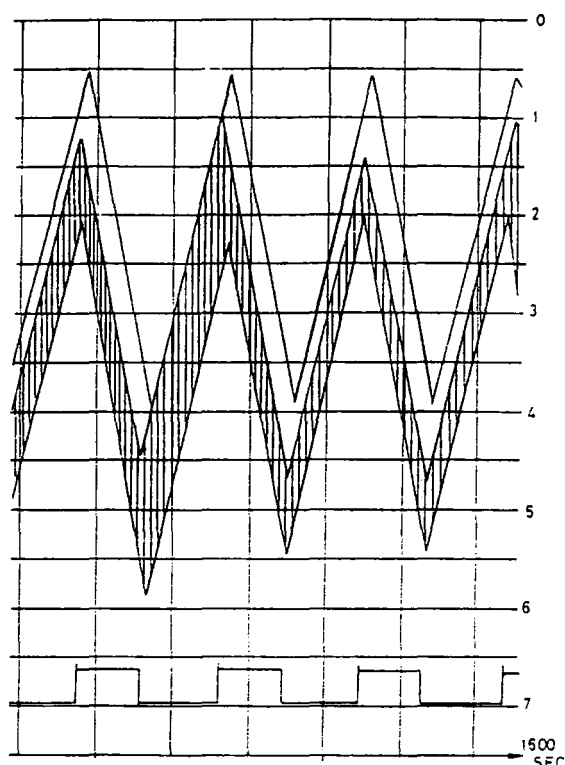
Figure 6.

original gain in performance of a rigid vehicles control by the use of the improved jet switching law. It is suggested that the performance of this system for the attitude control of flexible space vehicles is comparable with the performance of other systems which have been suggested for the control of vehicles which do not incorporate flexible appendages.

In any actual design study, a reasonable estimate of the vehicle's overall moment of inertia is possible. A similar statement cannot be made with regard to modelling of large flexible appendages and errors in the estimated modal frequencies will result. In an attempt to evaluate the effect of such errors, the sensitivity of the overall system to this parameter was investigated. It was found that changes in the mode frequency of ±50%, without adjustment of the observer parameters, caused no detectable change in the performance of the attitude stabilisation system. An error of such magnitude would never arise in the modelling of a physical system and it may be concluded that no real problems due to such errors in modelling should occur.

As was mentioned earlier, a realistic estimate of the appendage damping factor would be less than 0·1. A study was made to determine what effect on vehicle performance the inclusion of structural damping would have.

A value of 0·05 was chosen and comparisons of Figs. 6 and 8 gives this information. The inclusion of this damping factor appears to improve the attitude performance and the results shown in Fig. 8 are very similar to those of Fig. 5, which shows the performance to be expected from a rigid vehicle. No explicit investigation into the effect of noise on attitude sensor output is undertaken although this is not considered to constitute a major problem. Attenuation of noise frequencies of 5 rad/sec (0·8 Hz) is of the order of 20 dBs. This should provide adequate attenuation for any noise occurring at frequencies above this value and ensure the minimum degradation of the quality of estimated state information in the presence of expected noise contamination.

This work indicates that the use of a linear state observer in the attitude control system of a flexible space vehicle is quite feasible. The inclusion of a linear state observer, together with the improved switching law, makes possible craft performance comparable with that to be expected from a totally rigid vehicle. To compensate for the uncontrolled structural deformations, however, it will be necessary to use a smaller dead-band region ensuring that the flexural component of attitude motion does not allow total motion outside the required pointing accuracy.
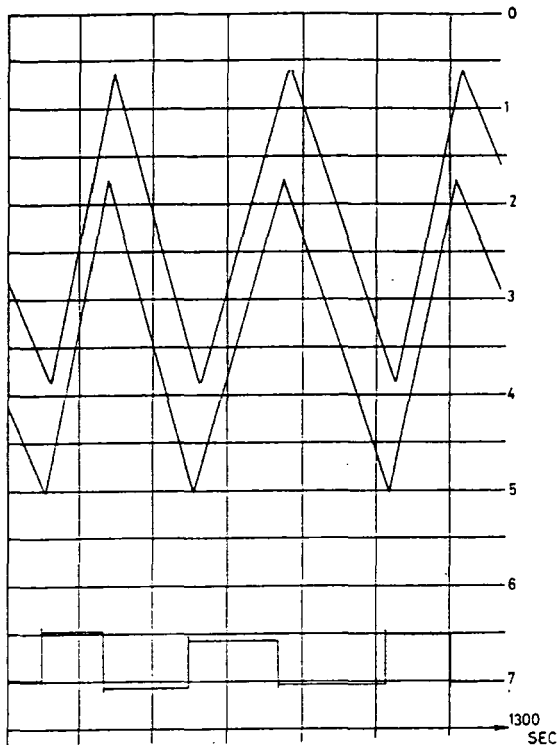
Figure 7.
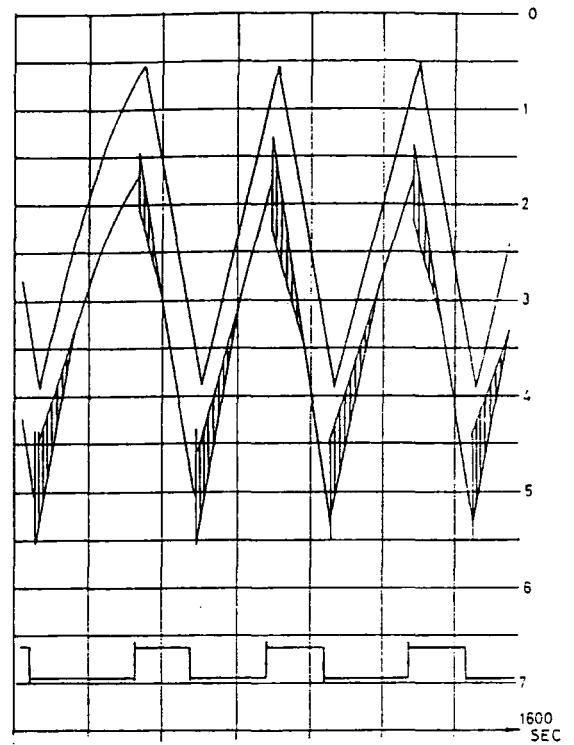
Figure 8.

APPENDIX I
Digital computer program for the solution of linear state observer equation

The computer program given in this appendix was developed for use on the ICL 1906A computer using Fortran IV as the programming language.

A flow diagram for the program is given in Fig. 1 and, together with the explanation given earlier, its operation should be understandable. The program is designed to solve the matrix equation

$$TA - DT = EH$$

for the matrix T given A, D, E and H. The method of solution involves the use of Kronecker or direct products of matrices and these products are formed within the program. The input data are the matrices A, D, E and H together with their respective orders. The output is the required observer transformation matrix.

PROGRAM NOMENCLATURE

Integers

In common with the Fortran convention for integer variables, all integers are designated by the letters i to n inclusively.

- i, j, k general integer variables
- l row dimension of plant output matrix H
- m order of observer dynamic matrix D $m = n - 1$
- n order of plant dynamic matrix
- nb row dimension of plant input matrix B

Arrays

- A (10, 10) plant dynamic matrix, input
- AA (100, 100) working area
- AE (100, 100) Kronecker product of A with Im, A extended
- AG (100, 100) working area for inversion subroutine
- $AINT$ (10) working area
- $AINV$ (10, 10) working area for inversion subroutine
- B (10, 10) plant input matrix, input
- D (10, 10) observer dynamic matrix, input
- DE (100, 100) Kronecker product of D with In, D extended
- E (10, 10) observer input matrix, input
- H (10, 10) plant output matrix, input
- Q (10, 10) product of E and H
- QE (100, 1) Q extended
- T (100, 1) observer transformation matrix
- $WKSP$ (100) working area.

Subroutines

$FO4AEF$. NAG library subroutine to solve general matrix equation

$$AX = B$$

also used for inversion of matrix by putting B to identify matrix before subroutine call.

DOCUMENT OBS05 (/FORT)

```
      LIBRARY (ED, SUBGROUPNAGF)
      PRGRAM (OBSERVER)
      INPUT 1=CRO
      OUTPUT 2=LPO
      END
```

```
      MASTER OBSERVER
C     THE PROGRAM SOLVES THE LUENBERGER OBSERVER
C     PROBLEM PLANT EQUATIONS XDOY=AX+BU AND Y=HX
C     IF A IS N*N AND H HAS ROW DIMENSION L THEN AN
C     OBSERVER OF ORDER N−L IS REQUIRED TO PRODUCE ALL
C     THE PLANT STATES
C     IF N−L=M AND THE OBSERVER EQUATIONS ARE
C     ZDOT=DZ+TBU+EY THEN D IS OF ORDER M*M AND THIS CAN
C     BE CHOSEN TO ACT FASTER THAN THE PLANT
C     I·E· CHOOSE D FOR INPUT TO THE PROGRAM
C     E CAN NOW BE CHOSEN BUT IT MUST FORM A CONTROLLABLE
C     PAIR WITH D.
C     THE PROGRAM INPUT IS N, M, L, NB, A, D, E, H, B AND THE OUTPUT
C     IS IS ALL THE INPUT DATA PLUS THE MATRIX TB
C     AND THE INVERSE OF T/H.
C     THE PLANT STATES ARE GIVEN BYX=INV (T/H) Z/Y
C     WHERE T/H IS T PARTITIONED ABOVE H.
```

```
      DIMENSION A (10, 10), D (10, 10), AE (100, 100), DE (100, 100)
      DIMENSION B (10, 10), E (10, 10), H (10, 10), Q (10, 10), QE (100, 1)
      DIMENSION AG (100, 100), AINV (10, 10), WKSP (100)
      DIMENSION T (100, 1), AA (100, 100), BB (100, 1), AINT (10)
    1 FORMAT (10A8)
    2 FORMAT (1N1/4X, "TOTAL STATE OBSERVER"//7X, 10A8)
    3 FORMAT (4I0)
    6 FORMAT (100E0.0)
    8 FORMAT (//5X, "MATRIX A"/(10X, 4E14.4))
   10 FORMAT (//5X, "MATRIX D"/(10X, 3E14.4))
   12 FORMAT (//5X, "MATRIX E"/(10X, E14.4))
   14 FORMAT (//5X, "MATRIX H"/(10X, 4E14.4))
   16 FORMAT (//5X, "MATRIX B"/(10X, E14.4))
   18 FORMAT (//5X, "MATRIX TB"/(10X, E14.4))
```

```
C     ORDER OF INPUT DATA N, M, L, NB
C     ARRAYS, A BY ROWS TNMB*D, E, H, S ALL BY ROWS
C     AL . IN FREE FORMAT WITH DELIMITER A SPACE
```

```
C     READ AND WRITE TITLE
      READ (1, 1) AINT
      WRITE (2, 2) AINT
```

```
C     READ ARRAY DIMENSIONS
      READ (1, 3) N, M, L, NB
```

```
C     READ IN A, D, E, H, B
C     NOTE A WRITTEN BY ROWS BUT READ INTO COLUMNS
C     I·E· READ AS TRANSPOSE
      READ (1, 6) ((A (J, I), J=1, N), I=1, N)
      READ (1, 6) ((D (I, J), J=1, M), I=1, M)
      READ (1, 6) ((E (I, J), J=1, L), I=1, M)
      READ (1, 6) ((H (I, J), J=1, N), I=1, L)
      READ (1, 6) ((B (I, J), J=1, NB), I=1, N)
```

```
C     WRITE OUT INPUT DATA
      WRITE (2, 8) ((A (J, I), J=1, N), I=1, N)
      WRITE (2, 10) ((D (I, J), J=1, M), I=1, M)
      WRITE (2, 12) ((E (I, J), J=1, L), I=1, M)
      WRITE (2, 14) ((H (I, J), J=1, N), I=1, L)
      WRITE (2, 16) ((B (I, J), I=1, N), J=1 NB)
```

```
C     FORM EXH=Q OF ORDER M*N
      DO 50 I=1, M
      DO 50 J=1, N
      Q (I, J)=0.0
      DO 50 K=1, L
   50 Q (I, J)=Q (I, J)+E (I, K)*H (K, J)
```

```
C     EXTEND Q TO VECTOR OE BY PUTTING ROW ON TOP OF ROW
      DO 55 I=1, M
      DO 55 J=1, N
   55 QE ((I−1)*N+J, 1)=Q (I, J)
```

```
C     EXTEND A BY FORMING KRONECKER PRODUCT WITH IM
C            (IM*A)=AE
C     CALL PRODUCT AE OF ORDER MN*MN
```

```
C       INITIALISE AE
        MN=M*N
        DO 60 I=1, MN
        DO 60 J=1, MN
     60 AE (I, J)=0.0
        DO 65 K=1, N
        DO 65 I=1, N
        DO 65 J=1, N
     65 AE ((K−1)*N+1, (K−1)*N+J)=A (I, J)

C       EXTEND D BY FORMING KRONECKER PRODUCT WITH IN,
C              (D*IN)=DE
C       CALL PRODUCT DE OF ORDER MN*MN

C       INITIALISE DE

        DO 70 I=1, MN
        DO 70 J=1, MN
     70 DE (I, J)=0.0
        DO 75 K=1, M
        DO 75 J=1, N
        DO 75 I=1, N
     75 DE ((K−1)*N+I, (J−1)*N+I)=D (K, J)

C       SUBTRACT (AE−DE) PUT IT IN AE
        DO 80 I=1, MN
        DO 80 J=1, MN
     80 AE (I, J)=AE (I, J)−DE (I, J)

C       CALL SUBROUTINE TO SOLVE (AE−DE) *F=AE*T=QE SOLVE FOR T
        IFAIL=1
C       CALL F04AEF (AE, 100, QE, 100, MN, 1, T, 100, WKSP, AA, 100, BB, 100
        IFAIL)
        IF (IFAIL·EQ·O) GO TO 90
        WRITE (2, 85) IFAIL
     85 FORMAT (//5X, FO4AEF FAILS TO SOLVE EQUS., IFAIL= ,I1)
C       WRITE OUT T
        WRITE (2, 18) (T (I, 1), I=1, 12)

C       REDUCE T AND PARTITION WITH H, ORDER N*N
C       CALL IT MATRIX AA
     90 DO 95 I=1, M
        DO 95 J=1, N
     95 AA (I, J)=T ((I−1) *N+J, 1)

C       PARTITION H INTO LOWER N−M=L ROWS OF AA
        DO 100 I=1, L
        DO 100 J=1, N
    100 AA (I+M, J)=M (I, J)

C       FORM MATRIX TB
        DO 101 I=1, M
        DO 101 J=1, NB
        A (I, J)=0.0
        DO 101 K=1, N
    101 A (I, J)=A (I, J)+AA (I, K) *B (K, J)
        WITE (2, 1S) ((A (I, J), J=1, NB), I=1, M)
C       PUT AG TO IDENTITY MATRIX
        DO 102 I=1, N
        DO 102 J=1, N
    102 AG (I, J)=0
        DO 103 I=1, N
    103 AG (I, I)=1

        IFAIL=1
C       INVERT AA BY SOLVING EQUS WITH UNITY RHS
        CALL F04AEF (AA, 100, AG, 100, N, N, AINV, 10, WKSP, A, 10, D, 10, IL
        IF (IFAIL·EQ·0) GO TO 110
        WRITE (2, 105)
    105 FORMAT (//5X, "FO4AEF FAILS TO INVERT AA")
C       OUTPUT MATRIX AINV
    110 WRITE (2, 115) ((AINV (I, J), J=1, N), I=1, N)
    115 FORMAT (//5X, "OBSERVER TRANSFORMATION MATRIX"/
C       (10X, 4E14.4))

C       CHECK ON INVERSION ROUTINE BY FORMING PRODUCT
        DO 120 I=1, N
        DO 120 J=1, N
        A (I, J)=0.0
        DO 120 K=1, N
    120 A (I, J)=A (I, J)+AA (I, K) *AINV (K, J)
      C WRITE OUT A AS CHECK
        WRITE (2, 125) ((A (I, J), J=1, N), I=1, N)
    125 FORMAT (//5X, CHECK MATRIX /(10X. 4E14.4))
        STOP
        END
        FINISH
```

REFERENCES

1. SMART. D. R., GILL. K. F., GETHING. J. M. and HOLT, J. A. Dynamic analysis of flexible space vehicles having uncoupled control axes. *The Aeronautical Journal of the Royal Aeronautical Society*, Vol 78, pp 560–569. December 1974.

2. HUGHES. W. G. Design for high precision in spacecraft jet attitude control systems. Royal Aircraft Establishment Technical report 71089. April 1971.

3. LUENBERGER. D. G. Observing the state of a linear system. IEEE Transactions on Military Electronics, Vol MIL-8. April 1964. pp 74–80.

4. LUENBERGER. D. G. Observers for multivariable systems. IEEE Transactions on Automatic Control, Volume AC-11, No 2, April 1966. pp 190–197.

5. BONGIORNO. J. J. and YOULA, D. C. On observers in multivariable control systems. *International Journal of Control*. Volume 8, No 3, pp 221–243.

6. SARMA. V. V. S. and DEEKSHATULU, B. L. Optimal control when some of the state variables are not measurable. *International Journal of Control*. Volume 7, No 3, 1968. pp 251–256.

7. NEWMANN, M. M. Design algorithms for minimal-order Luenberger observers, Electronics Letters, 21st August 1969. Volume 5. No 17. pp 390–392.

8. CUMMING. S. D. G. Design of observers of reduced dynamics, Electronics Letters, 15th May 1959. Volume 5, No 10, pp 213–214.

9. CROSSLEY. T. R. and PORTER. B. Modal theory of state observers, Proceedings of the IEE, Volume 118, No 12. December 1971.

10. NEWMANN, M. M. Optimal and sub-optimal control using an observer when some of the state variables are not measurable. *International Journal of Control*. Volume 9. No 3, 1969. pp 231–290.

11. KALMAN. R. E. and BUCY. R. S. New results in linear filtering and prediction theory, Transactions of the ASME. Series D, *Journal of Basic Engineering*. March 1961. pp 95–108.

12. MALMAN. R. E. On the general theory of control systems. Proceedings of the First International Conference on Automatic Control, Moscow, USSR, 1960.

13. BARNETT. S. and STOREY. C. *Matrix methods in stability theory*. Thames Nelson and Sons Ltd. G.B., 1970.

PAPER 32

A digital state observer for the attitude control of a flexible space vehicle

Dr. E. H. SMITH and Dr. K. F. GILL

Department of Mechanical Engineering, The University of Leeds

1. INTRODUCTION

A space vehicle is usually required to maintain a specific orientation with respect to Earth. If flexible appendages (such as panels of solar cells) are associated with the vehicle, the problem of controlling the attitude of the spacecraft becomes more complex[1]. In this paper, attention will be directed towards the control of this class of vehicle when the control law suggested by Hughes[2] is employed. This approach requires that the attitude and its rate of change with time are available in satisfactorily noise-free forms. The measurement of attitude is physically possible, but the measurement of rate is not. Consequently a Luenberger state observer[3] was employed by the authors to reconstruct the rate information. A similar approach was adopted earlier[4] where an analogue model of the observer was employed. It was found that in some situations the design procedure for the observer stipulated that very large amplifier gains should be incorporated into the model, and great care was needed to avoid this problem.

Digital computers are widely used during space missions and thus a discrete model of the observer has its attractions over its analogue counterpart. Such a model would reduce the amount of hardware required, and would not be subject to the design restrictions imposed by an analogue model. This paper describes some work which was performed using a discrete observer for a flexible space vehicle of the type described earlier[1].

2. NOTATION

a_c angular acceleration due to control torque
f_r angular acceleration due to disturbance torque
t time
y attitude of centre-body
x state variable matrix
z observer state variable matrix
A vehicle dynamic matrix
B vehicle input matrix
D observer dynamic matrix
E observer input matrix
G observer input matrix
H vehicle output matrix
T observer transformation matrix
α flexural component of attitude of centre-body
δ minimum burn-time of control jets
θ rigid component of attitude of centre-body
θ_d dead-band of control jets
τ torque applied to vehicle

3. THE DYNAMICS OF THE SPACE VEHICLE

The vehicle consists of two, substantial, flexible solar panels attached to a rigid centre-body—a detailed description is given in Reference 1. It is shown in this paper[1] that only the fundamental mode of flexure of the panels has any significant effect on vehicle performance.

The attitude, y, of the centre-body can be expressed as a function of two independent components, θ and α. The component, θ, is the attitude of the centre-body assuming rigid panels, and α is a measure of the contribution from the flexible panels. Hence, the vehicle dynamics can be described by the following equations:

$$\ddot{\theta} = 0.00604 \, \tau \qquad . \quad . \quad . \quad (1)$$

$$\ddot{\alpha} + 4.509 \, \alpha = 0.076 \qquad . \quad . \quad . \quad (2)$$

$$\text{and,} \quad y = \theta + 0.076 \, \alpha \qquad . \quad . \quad . \quad (3)$$

Integration of eqn. (1) yields,

$$\dot{\theta} = (0.00604 \, \tau) \, t + k_1 \qquad . \quad . \quad . \quad (4)$$

$$\theta = (0.00302 \, \tau) \, t^2 + k_1 t + k_2 \, . \quad . \quad . \quad (5)$$

—where k_1 and k_2 are integration constants. Integration of eqn. (2) gives,

$$\dot{\alpha} = (0.076 \, \tau / 4.509 - k_3) \, \sqrt{4.509} \sin (t \sqrt{4.509})$$
$$+ k_4 \cos (t \sqrt{4.509}) \qquad . \quad . \quad . \quad (6)$$

$$\alpha = (k_3 - 0.076 \, \tau / 4.509) \cos (t \sqrt{4.509})$$
$$+ k_4 \sin (t \sqrt{4.509}) / \sqrt{4.509} + 0.076 \, \tau / 4.509 \qquad . \quad . \quad . \quad (7)$$

—where k_3 and k_4 are the constants of integration. Equations (4) to (7) were used in the digital simulation of the vehicle dynamics. For the design of the observer, it was convenient to rewrite equations (1) to (3) in state-space notation. This can be effected by introducing,

$$x_1 = \theta; \quad x_2 = \dot{\theta}; \quad x_3 = \alpha; \quad x_4 = \dot{\alpha}$$

Thus, in matrix form,

$$
\begin{vmatrix} \dot{x}_1 \\ \dot{x}_2 \\ \dot{x}_3 \\ \dot{x}_4 \end{vmatrix} = \begin{vmatrix} 0 & 1 & 0 & 0 \\ 0 & 0 & 0 & 0 \\ 0 & 0 & 0 & 1 \\ 0 & 0 & -4\cdot509 & 0 \end{vmatrix} \begin{vmatrix} x_1 \\ x_2 \\ x_3 \\ x_4 \end{vmatrix} + \begin{vmatrix} 0 \\ 0\cdot00604 \\ 0 \\ 0\cdot076 \end{vmatrix} \tau
$$

$$
y = \begin{vmatrix} 1 & 0 & 0\cdot076 & 0 \end{vmatrix} \begin{vmatrix} x_1 \\ x_2 \\ x_3 \\ x_4 \end{vmatrix}
$$

or $\dot{x} = A\underline{x} + B\tau$ . . . (8)

$y = H\underline{x}$ . . . (9)

4. THE STATE OBSERVER

Equations (8) and (9) describe a 4th order system with a single output. It has been shown[3] that the state of the system can be reconstructed with a 3rd order linear dynamic observer of the form,

$$
\dot{\underline{z}} = D\underline{z} + Ey + G\tau \quad . \quad . \quad . \quad (10)
$$

(Matrices A and D must form a controllable pair and have different eigenvalues). An estimate of the plant state can be obtained from a linear combination of the observer outputs, if

$$
\underline{z} = T\underline{x}
$$

It has been shown[4] that the plant and observer matrices are related by,

$$
TA - DT = EH \quad . \quad . \quad . \quad (11)
$$

$$
TB = G \quad . \quad . \quad . \quad (12)
$$

Now matrices A, B and H are known from the dynamics of the vehicle, thus equations (11) and (12) contain four unknown matrices D, E, G and T. Clearly, by specifying two of these four matrices, the remaining two can be evaluated. In this work, matrices D and E were specified, leaving G and T to be determined from equations (11) and (12). Matrix T was obtained from equation (11) by the method of Kronecker products thus enabling G to be evaluated from equation (12).

Equation (10) represents three uncoupled, first-order, non-homogenous, differential equations, which were modelled discretely as three, first-order, difference equations. This modelling was effected in the following way:

Consider a first-order, non-homogeneous, differential equation,

$$
\dot{q}(t) + dq(t) = f(t) \quad . \quad . \quad . \quad (13)
$$

If the forcing function, $f(t)$, is considered to be constant over a small time period, Δt, equation (13) can be solved to give,

$$
q(t+\Delta t) = e^{-d\Delta t}q(t) + (1 - e^{-d\Delta t})f(t)/d \quad . \quad . \quad . \quad (14)
$$

Thus equation (14) is a representation, in difference form, of equation (13).

5. THE CONTROL OF THE VEHICLE

No attempt was made to control the deflection of the flexible panels, and it was assumed that no structural damage would occur as a consequence.

As noted earlier, the control law employed was that suggested by Hughes[2]. In addition to attitude information, a knowledge of the rate of change of attitude was required. Simple on-off gas jets were employed on the space vehicle centre-body and these possessed deadbands of $\pm\theta_d$ as shown in Fig. 1. The resultant trajectory in the phase-plane is illustrated in Fig. 2, where a single-pulse limit-cycle can be seen. Starting from point a, the vehicle coasts with power-off under a constant disturbance force which results in a constant acceleration, f_e. At b, the jets fire to retard the vehicle at an acceleration of $(a_c + f_e)$, until point a is again reached. If the minimum burn-time of the jets is δ seconds, it can be shown that the deadband should be set so that,

$$
\theta_d = (a_c\delta)^2/(16f_e).
$$

In addition, a variation of rate within the region $\pm a_c\delta/2$ must be tolerated.
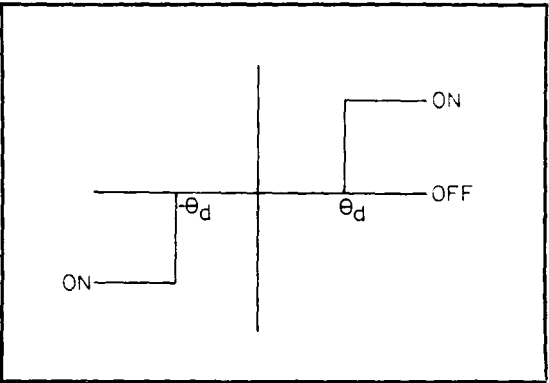
Figure 1.
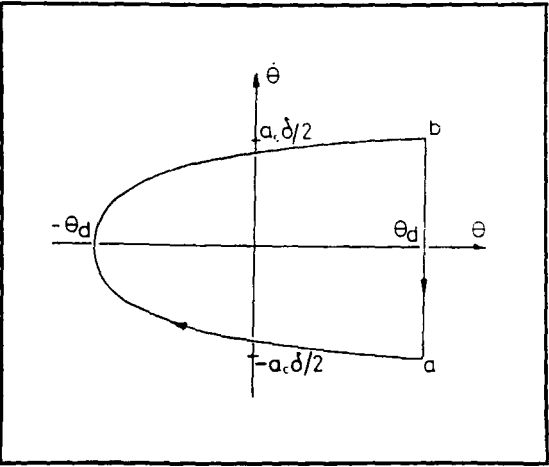
Figure 2.
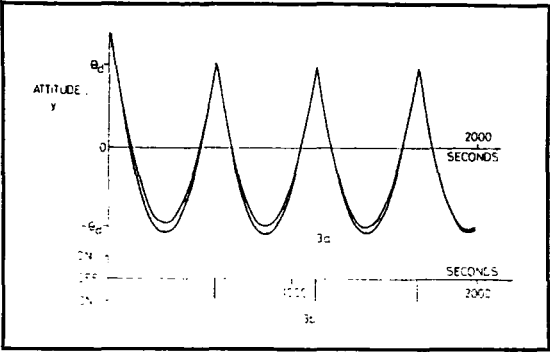
Figure 3a (top), 3b (below).
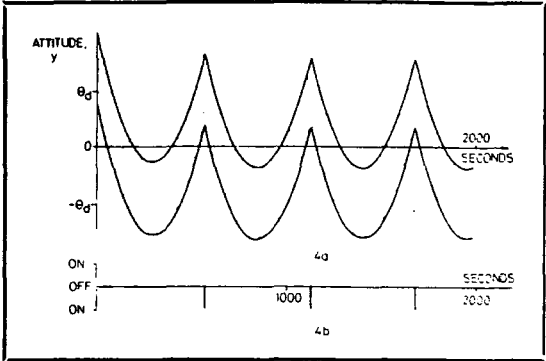
Figure 4a (top), 4b (below).
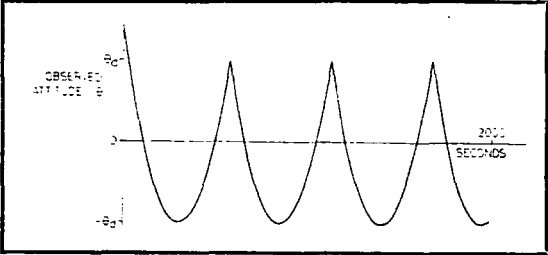
Figure 3c.
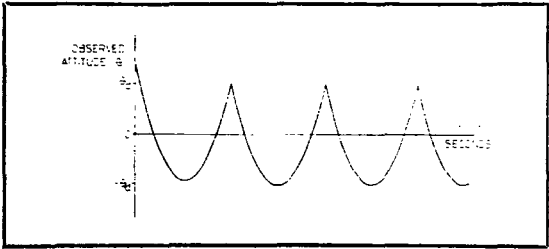
Figure 4c.

Matrix A

0	1	0	0
0	0	0	0
0	0	0	1
0	0	−4·509	0

Matrix B

0
0·00604
0
0·076

Matrix D

−0·05	0	0
0	−0·03	0
0	0	−0·01

Matrix E

1
1
1

Matrix H

1	0	0·076	0

Matrix G

−2·4173
−6·7124
−60·41

Observer Transformation Matrix

−0·1251	0·1350	−0·01	0·0005101
−0·0009380	0·001125	−0·0001875	0·000003327
1·646	−1·777	0·1316	13·15
−185·5	133·5	−7·414	1·184

Figure 5.

6. RESULTS AND DISCUSSION

Illustrated in Figs. 3 and 4 are the results of two separate simulations, the only difference between them being that different initial conditions pertained at time = 0 secs. Both simulations employed the same matrices A, B etc. which are listed in Fig. 5, and also in both cases the observed values of attitude and rate were used for control purposes.

The attitude, y, of the centre-body can be compared, in Fig. 3(a), with the observed value in Fig. 3(c). It can be seen that the deflection, α, due to appendage flexure is virtually eliminated by the observer. Because of the good quality of the reconstructed attitude and rate information, a stable limit-cycle is achieved, the jets firing only once per cycle, as illustrated in Fig. 3(b). Much larger values of α occur in Fig. 4 because of the value of the initial conditions. In this case also, the observer behaves satisfactorily, producing acceptable state information for controlling the vehicle.

The digital state observer, therefore, is seen to provide a practical engineering solution to the problem of obtaining accurate information on the state of a flexible space vehicle. This implies that existing control devices used on rigid spacecraft can also be employed on flexible vehicles, thus reducing development costs.

7. ACKNOWLEDGMENT

REFERENCES

1. SMART. D. R., GILL. K. F., GETHING. J. M. and HOLT. J. A. Dynamic analysis of flexible space vehicles having uncoupled control axes. *The Aeronautical Journal of the Royal Aeronautical Society*, Vol 78. No 768. pp 560–569. Dec. 1974.
2. HUGHES, W. G. Design for high precision in spacecraft jet attitude control systems. Royal Aircraft Establishment Technical Report 71089. April 1971.
3. LUENBERGER. D. G. Observing the state of a linear system. IEEE Trans. on Military Electronics, Vol MIL-8. pp 74–80. April 1974.
4. SMART. D. R. and GILL, K. F. Attitude control of a flexible space vehicle by means of a linear state observer. *The Aeronautical Journal of the Royal Aeronautical Society*. Vol 79, No 770, pp 86–95. Feb. 1975.

PAPER 33

Technical notes

An attitude control system for a flexible satellite providing active damping of flexural motion

J. M. GETHING
Formerly University of Leeds, now CEGB, Portishead

K. F. GILL
Department of Mechanical Engineering, University of Leeds

1. INTRODUCTION

A great deal of interest has been shown in recent years in the problem of flexibility in spacecraft structures. Much published work has been devoted to analysing the dynamic interaction between deformation of flexible appendages and attitude control systems. A limited number of publications have sought to find ways of providing some form of active control of flexible motion. Where this has been attempted idealised systems consisting of flexible coupled pendulums[1] or rotors[2] have been considered.

The problem of flexibility may be tackled in three ways. Where the flexure can be shown to be secondary in nature, careful design of the attitude control system can ensure that interaction is kept to a minimum. To this end surveys of structural flexibility effect in spacecraft are invaluable to the design engineers. Where the flexural motion has a more dominant effect, as will follow from the inevitable increase in power requirements for communications, then a more direct approach will become necessary. Two approaches present themselves. For small but disrupture flexural motion it could be considered as a well defined 'noise' in the attitude sensing system. Removal of this 'noise' by suitable filtering processes would provide clean attitude information to operate control systems and avoid unnecessary control action in response to small interactive motion due to flexure. Where this approach fails to satisfy the demands of fine attitude control then active control (damping) of the flexure motion may become necessary.

In this paper a state-vector feedback relay control system is described which has been applied to the attitude control of the coupled roll-yaw axes of a momentum-stabilised communication satellite. Structural flexibility is introduced into the system equations in the form of the fundamental bending mode of solar array panels. The feedback law to the roll and yaw axis (thrusters) is derived using Lyapunov's Second Method suitably modified for application to undamped systems.

In an earlier paper[4] Gething et al. discussed the effects of flexibility on the attitude control of a particular class of satellite and concluded that some form of direct control of flexural motion would be necessary for satellites having large flexible appendages. This paper extends that work and, to avoid inclusion of unnecessary detail, reference is made to the earlier paper[4] for a description of the satellite and derivation of the system equations.

NOTATION

A plant matrix
B plant-input matrix
h_w pitch component of wheel angular momentum
$I_{1, 3}$ moment of inertia about the roll and yaw axes
I_r moment of inertia of rigid satellite for symmetric roll and yaw configuration
P solution matrix of Lyapunov matrix equation
T or $*$ superscript denoting matrix transposition
$t_{1, 3}$ roll-. yaw-control torques
R flexible inertia coefficient
Q right-hand side of Lyapunov matrix equation
u control vector
x plant state
α roll-control-torque yaw-offset angle
γ flexural-interaction coefficient
β solar array paddle rotation angle
η_1 the solar array fundamental bending-mode co-ordinate
$\theta_{1, 3}$ roll-, yaw-attitude angle
Ω_1 the solar array fundamental bending-mode frequency
ω_o orbit angular velocity
ω_N nutation angular velocity of the rigid-centre body

2. SATELLITE DYNAMICS

The configuration of the satellite considered is shown in Fig. 1. Satellite stabilisation is provided by a fixed momentum wheel which couples the motion at the roll and yaw axes.

The satellite dynamics may be represented by three coupled second order total differential equations describing the roll and yaw attitudes and solar array fundamental bending motion as follows:

$$\begin{aligned}
\text{mode} \quad & \ddot{\eta}_1 + \Omega^2_1\eta_1 = -\gamma\,(\ddot{\theta}_1 \cos \beta + \ddot{\theta}_3 \sin \beta) \\
\text{roll} \quad & t_1 = I_1\ddot{\theta}_1 + h_w\dot{\theta}_3 + h_w\omega_o\theta_1 + \gamma^T\ddot{\eta}_1 \cos \beta \\
\text{yaw} \quad & t_3 = I_3\ddot{\theta}_3 - h_w\dot{\theta}_1 + h_w\omega_o\theta_3 + \gamma^T\ddot{\eta}_1 \sin \beta
\end{aligned} \right\} \quad (1)$$

These equations may be transformed into a sixth order state matrix equation of the form:

$$\dot{x} = Ax + Bu \qquad . \qquad . \qquad (2)$$

by defining the six state variables, $x_1 \ldots x_6$, as follows,
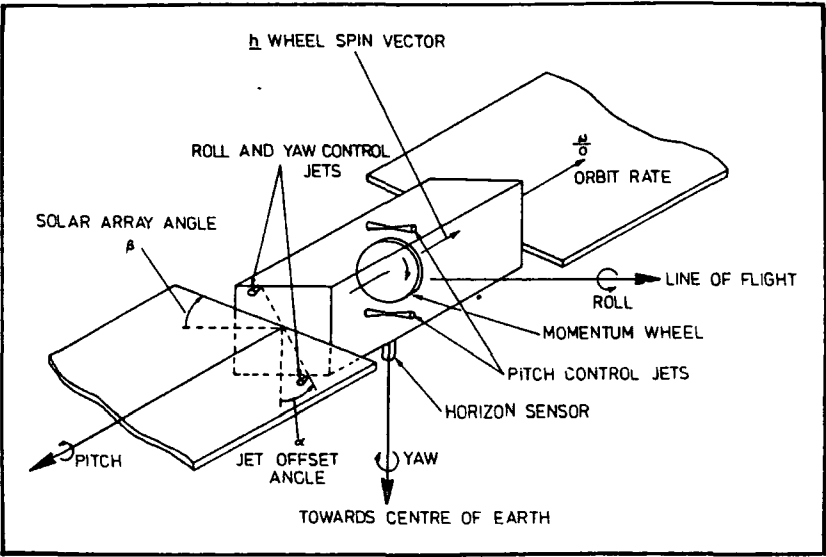
Figure 1. Configuration of the flexible satellite.

$x_1 = \eta_1$, the solar array first bending mode co-ordinate

$x_2 = \dot{\eta}_1$

$x_3 = \theta_1$, the satellite roll attitude   .   .   .   (3)

$x_4 = \dot{\theta}_1$

$x_5 = \theta_3$, the satellite yaw attitude

$x_6 = \dot{\theta}_3$

The control vector, u, comprises the roll and yaw torques, t_1 and t_3.

Substituting these relationships into equations 1 and eliminating first-order terms appearing on the right-hand side of the equations, the matrices A and B of equation 2, for a $\beta = 0$ solar array configuration. (see Fig. 1). may be found as

$$A =$$

$$\begin{bmatrix} 0 & 1 & 0 & 0 & 0 & 0 \\ -(1+R)\Omega_1^2 & 0 & \gamma\omega_N\omega_o & 0 & 0 & Y\omega_N \\ 0 & 0 & 0 & 1 & 0 & 0 \\ Y\Omega_1^2/I_r & 0 & -\omega_N\omega_o & 0 & 0 & -\omega_N \\ 0 & 0 & 0 & 0 & 0 & 1 \\ 0 & 0 & 0 & \omega_N/1+R & -\omega_N\omega_o/1+R & 0 \end{bmatrix}$$

.   .   .   (4)

$$B =$$

$$\begin{bmatrix} 0 & -\gamma/I_r & 0 & 1/I_r & 0 & 0 \\ 0 & 0 & 0 & 0 & 0 & 1/I_r(1+R) \end{bmatrix}^T$$

.   .   .   (5)

A full derivation of these matrices may be found in Ref. 5.

3. CONTROL METHOD

A block diagram of the control scheme is shown in Fig. 2. It will be seen from the figure that a set of feedback gains $B^T P$ are generated which operate on the system states x in order to derive the switching controls u. The key to the method is the evaluation of the matrix P from

the Lyapunov matrix equation,

$$A^T P + P A = -Q \qquad . \qquad . \qquad (6)$$

The controls u_i are then given by

$$u_i = -M_i \, \text{sgn} \, (B^T P x)_i \, . \qquad . \qquad (7)$$

where M_i is the maximum value of the control u_i. Full description of the derivation of these equations and in particular the solution of equation 6 for undamped linear systems are given in Refs. 5 and 6.

As applied to the flexible satellite this control scheme can take two forms as shown in Figs. 3 and 4. Shown in Fig. 3 in the application to a 2-input control system with thrusters acting about both roll and yaw axes. Figure 4 shows a modification where a single thruster offset from both roll and yaw axes is used and a component of the thrust applies about the controlled axes. In this case the control torques are given by

$$\begin{bmatrix} t_1 \\ t_3 \end{bmatrix} = \begin{bmatrix} \cos \alpha \\ -\sin \alpha \end{bmatrix} T_c \qquad . \qquad . \qquad (8)$$
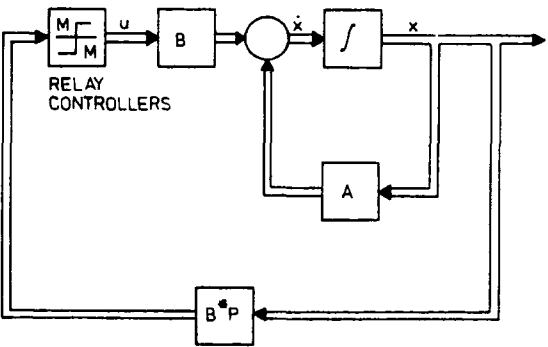
Figure 2. Vector block diagram of Lyapunov relay control system.
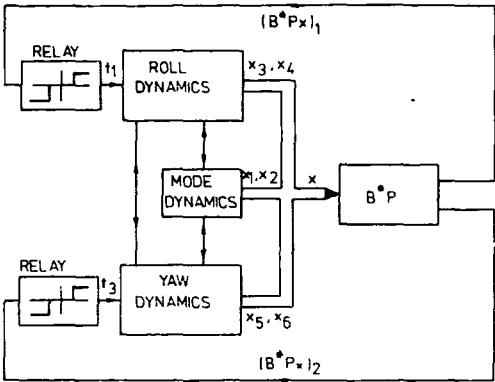
Figure 3. Block diagram for two-input control system.
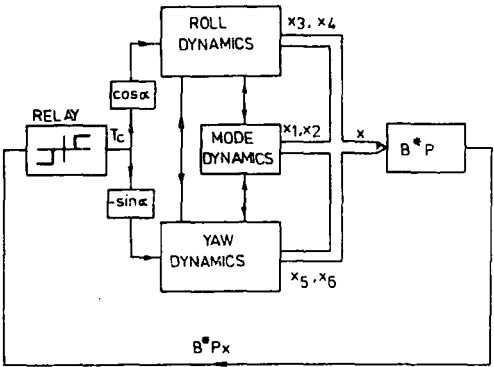
Figure 4. Block diagram for one-input control system.
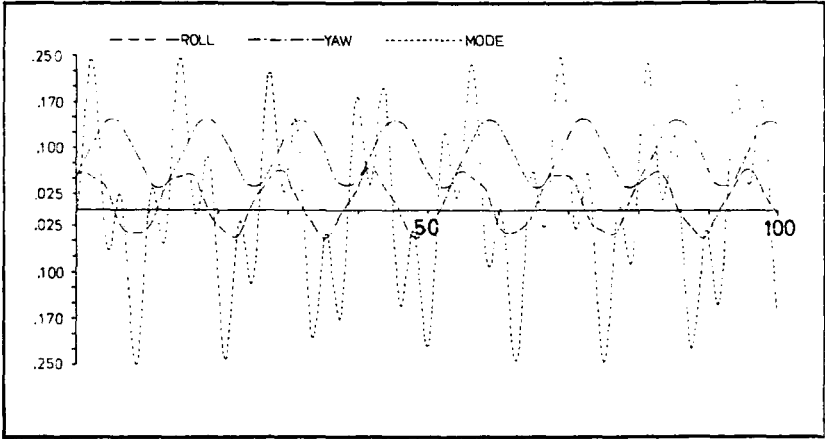
Figure 5. Free response to initial conditions, flexure about roll $\beta=0°$.

the control vector is now a single control torque T_c and the matrix B is of order 6×1. For the array orientations $\beta=0$ the matrix B of equation 5 becomes

$$B = \left[0 \quad \frac{-\gamma\cos 2}{I_r} \quad 0 \quad \frac{\cos\alpha}{I_r} \quad 0 \quad \frac{-\sin\alpha}{I_r(1+R)} \right]^T$$

(9)

In order to prevent limit cycling of the relay control a smal deadband is included in the relay characteristics.

The terms in the feedback matrix P obtained by solving equation 6 will vary depending on the choice of weighting matrix Q. This allows various system states to be differentially weighted to achieve differing control emphasis.

4. DIGITAL SIMULATION

A digital simulation of the transient response of the coupled rolls yaw axes and first mode flexural-response of the satellite under the action of the one-input and two-input control schemes was performed in order to assess the relevance of control system parameters and different satellite configurations. An assessment of the 'cost' of controlling the flexural motion was also carried out in terms of gas usage by the control jets and the effect on the roll and yaw motion.

The simulations were performed on a ICL 1906A computer using the FORTRAN program LYCON. The time responses-of-the satellite-states—were found at discrete time intervals by numerical integration of the first order state equations equation 2. The integrations were performed using the NAG library subroutine D02AEF which uses Gear's method[7]. The time interval between integrations dictates the minimum gas jet on-time.

A full description of the program and listings can be found in Ref. 5.

5. SIMULATION RESULTS

The operation of control system in one-input and two input forms for various system weightings (matrix Q) is illustrated in Figs. 6 to 10. As a basis for comparison the uncontrolled free response of the satellite is shown in Fig. 5. These results were obtained for a particular satellite and controller configuration and initial conditions on the roll and yaw axes. These are listed in Table 1.

The results are presented for flexure about the roll axis only, since similar results were obtained for yaw axis flexure. A complete description of the simulation results can be found in Ref. 5.

In order to aid these comparisons a summary of the pertinent data, the integral error squared (IES) of the

TABLE I
PARAMETERS FOR SIMULATION STUDY

Satellite parameters

Inertia ratio. $R = 1 \cdot 0$
First-mode frequency, $\Omega_1 = 1 \cdot 0 \ s^{-1}$
Nutation frequency, $\omega_N = 1 \cdot 0 \ s^{-1}$
Orbit frequency. $\omega_o = 0 \cdot 73 \times 10^{-4} \ s^{-1}$
Roll and yaw rigid inertia. $I_r = 100 \ Kg \ m^2.$

Initial conditions

Roll attitude. $\theta_1 = 0 \cdot 05 \ rad.$
Yaw attitude. $\theta_3 = 0 \cdot 05 \ rad.$
Roll rate. $\dot\theta_1 = 0 \cdot 02 \ rad/s.$
Yaw rate. $\dot\theta_3 = 0 \cdot 02 \ rad/s.$

Control system parameters

Control Torque $= 1 \cdot 0 \ N.m.$
Relay deadband $= 0 \cdot 05$
'Damping' coefficient ζ $= 1 \cdot 0$
Diagonal elements of Q $= 1 \cdot 0$

time responses over the run length. the average steady state error and the gas jet on-time, is contained in Table II.

Figures 6 and 7 show the response of the one and two input systems with equal weighting on the states. i.e. Q is the unit matrix. For the two input system the roll and yaw attitudes are brought sensibly to zero reference within two nutation cycles. the flexural motion is damped after about five mode oscillations. The control action is seen to be progressive. first reducing the rigid body attitudes. then when these are sufficiently small transferring to the flexural motion. The gas-jets stop pulsing after about 25 seconds. The action of the one input system Fig. 7, is, as would be expected, inferior to this. adequate control being achieved after about 35 seconds compared with 20 seconds for the two input control. However from Table II it can be seen total gas on-time for the 2nd case was 25·1 seconds against 28·8 seconds for the first case.

In order to assess any improvement from weighting

the flexural mode states, simulation results were obtained for weightings of 100, 1000, and 10 000 on x_1 and x_2, the flexural mode states (equation (3)). This was achieved by so modifying the first two diagonal terms of the Q matrix. Figures 8, 9 and 10 show the results of this on the two input control. (cf Fig. 6). Inspection at Table II shows that with $Q_{1,2}$ set at 100 there is a marginal improvement in the flexural response, the IES figure being about 2½% less. The roll and yaw responses are unchanged. The price is a slightly increased roll gas jet on-time. Increasing $Q_{1,2}$ to 1000 (Fig. 9) improves the flexural response significantly. i.e. about 34% less on IES. with only a slight deterioration in the roll yaw response. However the gas usage has been increased by a factor approaching 4 as indicated by the thruster on-time. Further increase in $Q_{1,2}$ to 10 000 results in greatly reduced flexural motion but unacceptable deterioration in the roll and yaw attitude response and continual gas-jet thrusting.

As a final indication of the worth of controlling the flexural motion a simulation run was performed with the mode states removed from the feedback calculations making them effectively uncontrolled with the exception of that through interaction with the rigid body control. Fig. 11 presents the results of this and it can be seen that the roll and yaw responses are little affected but because of the interaction of the flexural motion on the roll axis dynamics the roll thruster is continually activated and the total gas jet on-time is up by a factor of two (Table II).

6. CONCLUSIONS

A control scheme for a flexible spacecraft has been presented which can achieve significant savings in gas-usage and hence payload when flexural interaction with a control axis could cause unwanted gas-jet firing. By increasing the weighting on the flexural states significant reduction in flexural motion can be achieved but only at the expense of increased gas-usage and. in the limit. the rigid body attitude performance of the craft.

In order to apply this scheme. information is required regarding all the state variables comprising the vehicle response. Where direct measurement is not possible. some form of state estimation will be required possibly involving the use of the techniques of Kalman[3] or Luenberger[3].
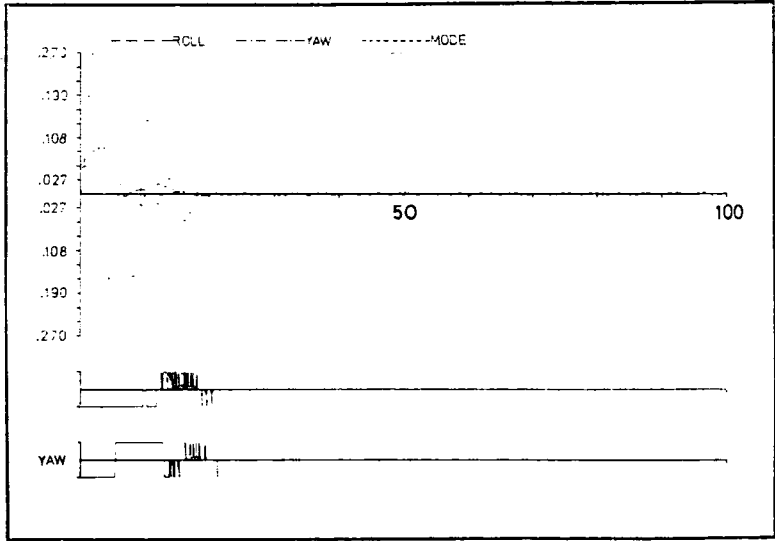
Figure 6. Two-input control flexure about roll $\beta = 0°$.
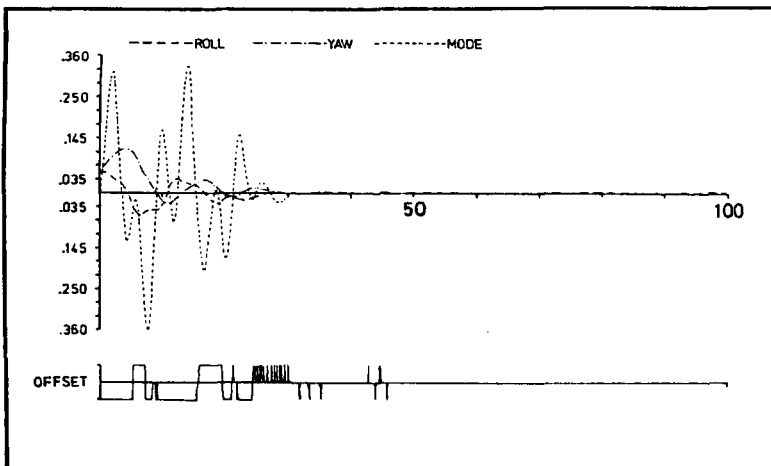
Figure 7. One-input control $\alpha=5°$, flexure about roll $\beta=0°$.

Figure 8. Two-input control mode states weighting $Q_{1,2}=100$.

Figure 9. Two-input control mode states weighting $Q_{1,2}=1000$.
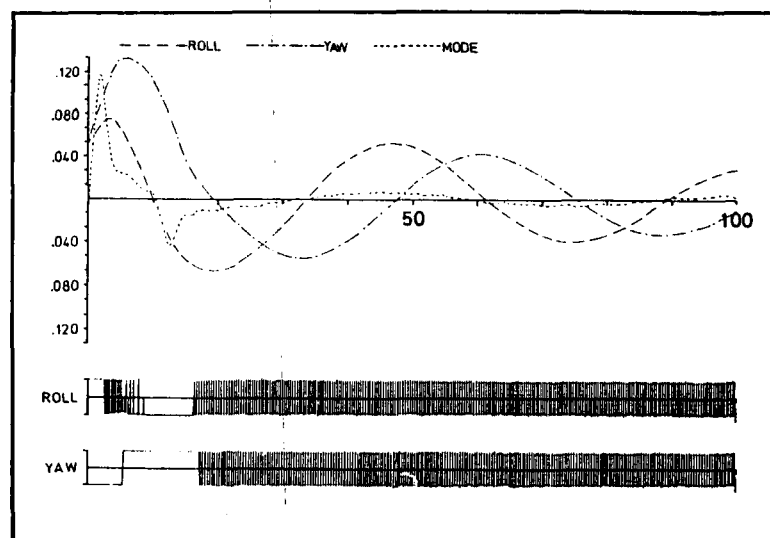
Figure 10. Two-input control mode states weighting $Q_{1,2}=10\,000$.

TABLE II
DIGITAL SIMULATION RESULTS

Figure	Parameter value	Integral-error-squared			Steady-state error (rad).		Gas-jet 'on'-time(s)		
		Roll	Yaw	Mode	Roll	Yaw	Roll	Offset	Yaw
Two-input,					Q=1,				
6	$\beta=0°$	0·012	0·039	0·199	0·0006	0·0003	14·0		14·8
One-input,					Q=1,				
7	$\beta=0°$	0·025	0·072	0·643	0·002	0·003		25·1	
Two-input,					$\beta=0°$				
8	$Q_{1,2}=100$	0·012	0·039	0·194	0·0005	0·0003	14·8		14·6
9	$Q_{1,2}=1000$	0·013	0·043	0·131	0·002	0·001	74·2		33·9
10	$Q_{1,2}=10\,000$	0·154	0·250	0·034	—	—	98·3		92·2
Two-input,					$Q=1$, node states uncontrolled				
		0·013	0·039	0·274	0·0002	0·0001	44·6		14·2
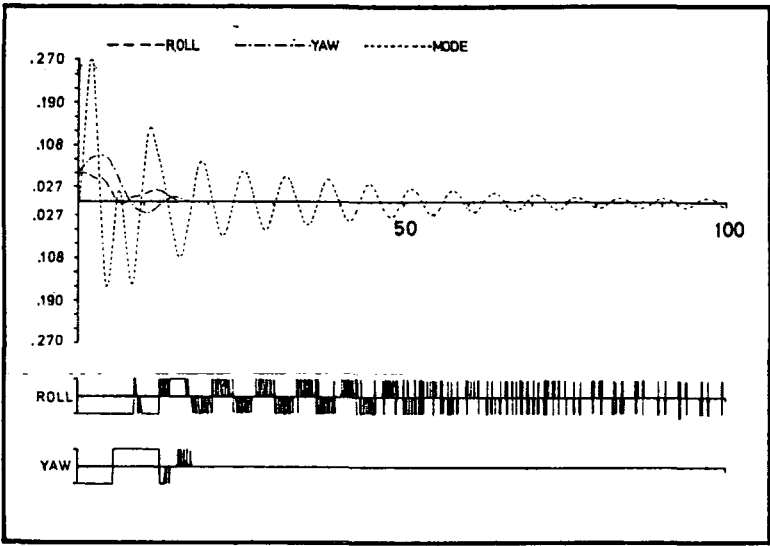
Figure 11. Two-input control mode states uncontrolled.

7. REFERENCES

1. MILLERS, H. F. On the control of flexible structures. PhD dissertation, University of California, Berkely. 1967.
2. PORCELLI, G. Attitude control of flexible space vehicles. *AIAA Journal,* Vol 10, No 6, pp 807–812, June 1972.
3. NOLL, R. B., DEYST, J. J., SPENNY, C. H. A survey of structural flexibility.
4. GETHING, J. M., HOLT, J. A., SMART, D. and GILL, K. F. Effects of flexibility on a momentum-stabilised communi-cation-satellite attitude-control system. *Proceedings IEE,* Vol 120, No 5, pp 613–619, May 1973.
5. GETHING, J. M. Attitude control of a momentum stabil-ised communication satellite having large flexible appen-dages. PhD thesis, University of Leeds, 1973.
6. GETHING, J. M. and GILL, K. F. Relay control of un-damped linear systems using Lyapunov's second method. *Proceedings IEE,* Vol 121, No 4, pp 301–306, April 1974.
7. NAG Library Manual, Mark 11 ICL 1900 Series, Not-tingham Algorithm Group, 1972.
8. KALMAN, R. E. New results in linear filtering and pre-diction theory. Transaction of the ASME, Series D, *Journal of Basic Engineering,* pp 95–108, March 1961.
9. LUENBERGER, D. G. Observing the state of a linear system. *IEEE, Transactions on Military Electronics,* Vol MIL-8, pp 74–80, 1964.

PAPER 34

FLEXIBLE SPACE VEHICLE CONTROL BASED ON STATE OBSERVATION AND LYAPUNOV'S METHOD

Dr. E.H. Smith and Dr. K.F. Gill

Dept. of Mechanical Engineering, The University,
Leeds LS2 9JT, England.

ABSTRACT

A control scheme for a single-mode flexible satellite is described which uses an application of Lyapunov's Second Method to derive the switching law for a relay controller. The method requires complete knowledge of the 'state' of the system. Because such information is not normally available, a Luenberger observer is employed to estimate the states from the output of an attitude sensor. It is shown that flexure can be controlled and a high pointing-accuracy maintained, even i the presence of severe plant and input mismatch, using existing control equipment.

Flexible, Satellite, Control, Attitude, Lyapunov, Observer.

1. NOTATION

k	sample number
t	time
$x(t_k)$	plant state vector at kth sampling instant
$\hat{x}(t_k)$	estimated plant statevector at kth sampling instant
y	attitude of centre-body
$z(t_k)$	observer state vector at kth sampling instant
A	continuous plant matrix
A_1	discrete plant matrix
B	continuous plant-input matrix
B_1	discrete plant input matrix
D,E,G	observer matrices
H	plant output matrix
P	Lyapunov matrix
Δt	sampling interval
T	observer matrix
$V(x(t_k))$	discrete Lyapunov function at kth sampling instant
$\Delta V(x(t_k))$	change in Lyapunov function
a	flexural component of centre-body attitude
δ	deadband
θ	rigid component of centre-body attitude
ω	undamped natural frequency
τ	torque
ζ	damping factor

Subscripts

a	appendage or panel
c	centre-body or control torque
d	disturbance torque
m	modified matrix

Superscripts

T	matrix transpose
-1	matrix inverse

2. INTRODUCTION

On earth-orbiting satellites electrical power is usually generated by panels of solar cells. The panels are often cantilevered from the centre-body (see Fig. 1) and their flexure can cause problems in vehicle control. In particular, the pointing accuracy may be affected by panel vibration and this problem will become more acute as the power requirements - and hence the panel sizes-increase. It is not current practice to actively control panel flexure, but this approach may prove to be unsatisfactory for the next generation of vehicles. In this paper a state-vector feedback control algorithm based on Lyapunov methods[1] is developed for application to a vehicle of the type illustrated in Figure 1. A Luenberger[2] observer is employed for state estimation and it is shown that the panel deflections can be satisfactorily controlled and a high pointing-accuracy maintained.

214

3. VEHICLE DESCRIPTION AND DYNAMICS

The satellite is illustrated in Figure 1, where it can be seen that two large solar panels are attached to a relatively small and rigid centre-body. A small constant disturbance torque, τ_d, acts on the vehicle and a control torque of $\pm\tau_c$ can be applied from thrusters mounted on the centre-body. The attitude, y, of the vehicle in relation to a fixed reference is measured by an instrument mounted on the centre body. It has been shown[3] that only the fundamental flexure-mode of the panels has any significant effect on vehicle behaviour and hence the dynamical equations are:

$$\ddot{\theta} = 0.00604\tau \qquad (1)$$

$$\ddot{\alpha} + \omega_a^2\,\alpha = 0.076\tau \qquad (2)$$

$$\text{and,} \qquad y = \theta + 0.076\alpha \qquad (3)$$

where $\omega_a^2 = 4.509$ $(\text{rads/s})^2$

These are illustrated in block diagram form in Figure 1.

It is convenient to formulate the state-variable equations by choosing:

$$x_1 = \theta; \quad x_2 = \dot{\theta}; \quad x_3 = \alpha; \quad x_4 = \dot{\alpha}$$

Thus, $\underline{x} = A\underline{x} + B\tau \qquad (4)$

$y = H\underline{x} \qquad (5)$

where,

$$\underline{x} = \begin{bmatrix} x_1 \\ x_2 \\ x_3 \\ x_4 \end{bmatrix}$$

$$A = \begin{bmatrix} 0 & 1 & 0 & 0 \\ 0 & 0 & 0 & 0 \\ 0 & 0 & 0 & 1 \\ 0 & 0 & -\omega_a^2 & 0 \end{bmatrix}$$

$$B = \begin{bmatrix} 0 \\ 0.00604 \\ 0 \\ 0.076 \end{bmatrix}$$

$$H = [1 \quad 0 \quad 0.076 \quad 0]$$

4. OBSERVER DESIGN

4.1 Theory

The design of an observer for analogue implementation can be restricted by the maximum potentiometer gains available on the analogue machine[4]. This problem does not arise with digital computers and hence it is more satisfactory to design a discrete observer for implementation on a remote or on-board computer. It is necessary, therefore,

solar panels

centre-body
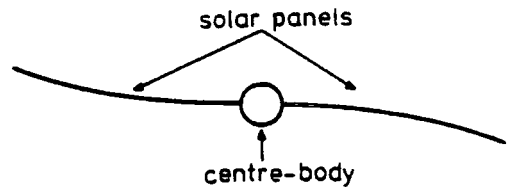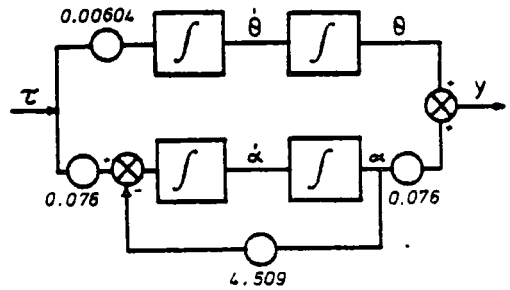
FIGURE 1

FIGURE 2

to formulate the discrete state-variable equations as:

$$\underline{x}(t_{k+1}) = A_1\underline{x}(t_k) + B_1\tau(t_k) \qquad (6)$$

$$y(t_k) = H\underline{x}(t_k) \qquad (7)$$

where,

$$A_1 = \begin{bmatrix} 1 & \Delta t & 0 & 0 \\ 0 & 1 & 0 & 0 \\ 0 & 0 & \cos(\omega_a\Delta t) & \sin(\omega_a\Delta t)/\omega_a \\ 0 & 0 & -\omega_a\sin(\omega_a\Delta t) & \cos(\omega_a\Delta t) \end{bmatrix}$$

$$B_1 = \begin{bmatrix} 0.00604(\Delta t)^2/2 \\ 0.00604\Delta t \\ 0.076(1-\omega_a^2\Delta t)/\omega_a^2 \\ 0.076\,\sin(\omega_a\Delta t)/\omega_a \end{bmatrix}$$

and Δt is the sampling interval.

Equations (6) and (7) describe a fourth-order system with a single output which can, therefore, be observed by a third-order Luenberger observer[2] of the form:

$$\underline{z}(t_{k+1}) = D\underline{z}(t_k) + Ey(t_k) + G\tau(t_k) \qquad (8)$$

Luenberger's approach proposes that the estimated state-vector, $\hat{\underline{x}}(t_k)$, is linearly related to the

observer output, $\underline{z}(t_k)$, by:

$$\underline{z}(t_k) = T\hat{\underline{x}}(t_k) \qquad (9)$$

If a state-error vector, $\underline{\varepsilon}_x(t_k)$ is defined as

$$\underline{\varepsilon}_x(t_k) = \hat{\underline{x}}(t_k) - \underline{x}(t_k) \qquad (10)$$

then Eq. (9) becomes:

$$\underline{z}(t_k) = T\underline{x}(t_k) - T\underline{\varepsilon}_x(t_k) \qquad (11)$$

Substitution of Eqs. (7) and (11) into Eq. (8) yields:

$$T\underline{x}(t_{k+1}) + T\underline{\varepsilon}_x(t_{k+1}) = DT\underline{x}(t_k) + DT\underline{\varepsilon}_x(t_k) +$$

$$EH\underline{x}(t_k) + G\tau(t_k) \qquad (12)$$

And substitution of Eq. (6) into (12) yields:

$$\underline{\varepsilon}_z(t_{k+1}) = D\underline{\varepsilon}_z(t_k) + M\underline{x}(t_k) + N\tau(t_k) \qquad (13)$$

where, $\underline{\varepsilon}_z(t_k) = T\underline{\varepsilon}_x(t_k)$

$$M = DT + EH - TA_1 \qquad (14)$$

$$N = G - TB_1 \qquad (15)$$

By assigning M and N to be null matrices, Eq. (13) becomes,

$$\underline{\varepsilon}_z(t_{k+1}) = D\underline{\varepsilon}_z(t_k) \qquad (16)$$

If the observer is stable, the scalar values of ε_z and ε_x will decay with time, thus ensuring that $\hat{\underline{x}}$ approaches $\underline{x}$.

Since M and N are null matrices, Eqs. (14) and (15) yield:

$$TA_1 - DT = EH \qquad (17)$$

$$G = TB_1 \qquad (18)$$

Following a policy adopted earlier[5], the solution procedure involves the specification of D and E. Eq. (17) will then yield T (the method of Kronecker products being employed[6]) which can be used to calculate G from Eq. (18).

In the solution method adopted here, the elements of E were arbitrarily selected to be unity; that is the plant output was fed directly into the observer. The only restriction which must be applied to D is that the observer must be stable. Within the limits imposed by this restriction, the selection of a matrix D was based upon three criteria:

1) the pattern of convergence with time between the observed and actual states.

2) the low-pass filtering characteristics of the observer.

3) the observer's ability to deal with plant and input mismatch.

4.2 Convergence Pattern

At time t=0, when the observer is activated, the value of z(-Δt) is unknown and hence z(0) cannot be evaluated. It is generally most appropriate, therefore, to assume that the observer output is zero at t=0, and thus the estimation-error vector, $\varepsilon_x(0)$, is non-zero. Examination of the variation with time of scalar value of ε_x revealed that it oscillated about the zero level before becoming sensibly zero. The larger the eigenvalues of D, the more rapid was the decay time but the greater were the initial excursions from the zero level.

4.3 Filtering Characteristics

The plant output, y, will generally be contaminated by noise. Since the observer will act as a low-pass filter, the possible corruption of the estimated states by noise on the plant output will be affected by the observer's filtering characteristics. It was desirable, therefore, to make the observer as slow as possible to attenuate the higher noise frequencies. To enable the filtering performance to be assessed more quickly, D was chosen to be a diagonal matrix possessing eigenvalues within a few per cent of each other.

4.4 Plant and Input Mismatch

It is unlikely that the dynamic characteristics of the actual plant will be identical to the theoretical values assumed for the processes of observer and controller design. That is, there will be a mismatch between the actual and theoretical parameters. Additional mismatch may exist between the actual and assumed plant inputs. The observer and the controller must be able to cope with these mismatches and simulations were undertaken to ensure that no deterioration in performance occurred.

5. CONTROLLER DESIGN

Consider a discrete Lyapunov function, $V(x(t_k))$, of the quadratic form:

$$V(\underline{x}(t_k)) = \underline{x}^T(t_k)P\underline{x}(t_k) \qquad (19)$$

where P is a positive-definite, symmetric matrix. The change in V over a single time period is:

$$\Delta V(\underline{x}(t_k)) = V(\underline{x}(t_{k+1})) - V(\underline{x}(t_k)) \qquad (20)$$

and for asymptotic stability, $\Delta V(t_k)$ should be a negative quantity. Appropriate substitution in Eq. (20) reveals that:

$$\Delta V(\underline{x}(t_k)) = \underline{x}^T(t_k)(A_1^TPA_1-P)\underline{x}(t_k) + \tau^2(t_k)$$

$$B_1^TPB_1 + 2\tau(t_k)B_1^TPA_1\underline{x}(t_k) \qquad (21)$$

The first term on the right-hand side of Equation (21) is negative-definite if,

$$A_1^T P A_1 - P = -Q \qquad (22)$$

where Q is a positive-definite, symmetric matrix. If no restrictions are imposed on $\tau(t_k)$ then $\Delta V(\underline{x}(t_k))$ can be minimised by equating

$$\frac{\partial(\Delta V(t_k))}{\partial \tau(t_k)} \text{ to zero.}[7]$$

This yields,

$$\tau(t_k) = -B_1^T P A_1 \underline{x}(t_k)/(B_1^T P B_1) \qquad (23)$$

In the case studied here the input, $\tau(t_k)$, is limited to three possible torques: the constant disturbance torque, τ_d, acting alone, or the two torques occurring when the jets fire, namely $(\tau_d + \tau_c)$ or $(\tau_d - \tau_c)$. Thus a control law of the following form must be adopted:

$$\tau(t_k) = \tau_d \text{ when } |B_1^T P A_1 \underline{x}(t_k)| \leq \delta \qquad (24)$$

$$\tau(t_k) = \tau_d - \tau_c \text{ sign } (B_1^T P A_1 \underline{x}(t_k)) \text{ when}$$

$$|B_1^T P A_1 \underline{x}(t_k)| > \delta \qquad (25)$$

where $\pm \delta$ is the dead band in the control jet actuator. It is seen, therefore, that the jets are fired in response to a weighted sum of the plant states and the weighting is influenced by the plant matrices, A and B, and the Lyapunov matrix, P. This last matrix can be obtained from Equation (22) by the method of Kronecker products. The process is facilitated by rewriting Eq. (22) as,

$$A_1^T P - P A_1^{-1} = -Q A_1^{-1} \qquad (26)$$

The plant under consideration is composed of two uncoupled, second order systems. The 'rigid-body' component, θ, is obtained from a purely inertial system (Eq. 1)) and the 'flexure' component, α, pertains to an undamped system (Eq. (2)). Thus the free-system is not asymptotically stable and this is reflected in the inability to obtain a unique, positive-definite symmetric matrix, P, from Eq. (26).

In order to use the Lyapunov method, therefore, an approach adopted elsewhere for continuous systems has been employed.[1] This involves the introduction of artificial resistance terms into the equations of motion of the plant in order to yield two systems possessing damped natural frequencies. The resulting modified discrete plant matrix, A_m, and its transpose are then used to replace A_1 and its transpose in Equ. (26), and a positive-definite, symmetric matrix, P_m, is evaluated. The resulting expression for $\Delta V(\underline{x}(t_k))$ is then,

$$\Delta V(\underline{x}(t_k)) = \underline{x}^T(t_k)(A_1^T P_m A_1 - P_m)\underline{x}(t_k) + \tau^2(t_k)$$

$$B_1^T P_m B_1 + \tau(t_k) B_1^T P_m A_1 \underline{x}(t_k) \qquad (27)$$

The similarity in form between Eqs. (21) and (27) is apparent and thus a control law similar to that expressed in Eqs. (24) and (25) is employed, but with P replaced by P_m.

The objectives of the simulations discussed in Section (6) were four fold:

(1) to examine the vehicle performance with different values of P_m and assess fuel usage,

(2) to select a P_m which enabled a high pointing-accuracy to be maintained,

(3) to control panel flexure to be within acceptable engineering limits, so avoiding mechanical failure,

(4) to achieve (1)→(3) in the presence of plant and input mismatch and with existing hardware. The latter would obviate the need for any new monitoring or control equipment and thus associated problems such as "cabling" or "in-built" redundancy" would not require consideration.

6. SIMULATION RESULTS AND DISCUSSION

The simulations are presented in two parts to illustrate:

(1) the influence of P_m on the control system,

(2) the effects of plant and input mismatch.

Common to all the simulations are the list of basic parameters contained in Table 1.

6.1 The Influence of P_m

The elements of P_m are influenced by the magnitudes of the artificial resistance terms introduced into the plant equations, (1) and (2). The effect of these terms is best summarised by quoting the undamped natural frequency, ω, and the damping factor, ζ, of each modified equation.

The control system performance with differing values of appendage and centre-body damping factors, ζ_a and ζ_c respectively, and centre-body undamped natural frequency, ω_c, is illustrated in Figures (3)→(6). The system behaviour with $\omega_c^2 = 0.010(rad/s)^2$, (Figs. (3) and (4)) was unsatisfactory because centre-body and appendage motion was too erratic and fuel consumption was excessive. (Both simulations were terminated after 100 secs). In the two cases when $\omega_c^2 = 0.100 (rad/s)^2$, (Figs. (4) and (5)), the behaviour was excellent: the overall attitude, y, and appendage flexure, α, came quickly under control and remained within close limits. For the case of $\zeta_a = \zeta_c = 0.5$ (Fig. (4)) the jet firetime during the 200 second simulation was 2.88 seconds. The corresponding value for Figure (5) was 2.36 seconds. It is noteworthy that the majority of the firing in

217

TABLE 1
SIMULATION PARAMETERS

SATELLITE

m. of inertia	166 Kg-m^2
nominal array natural frequency	2.12 rads/s

OBSERVER

diagonal elements of matrix D	d_{11}	-2.00
	d_{22}	-2.02
	d_{33}	-2.04

CONTROL SYSTEM

control torque	5×10^3 N-m
relay deadband	10^{-5}
matrix Q	unit matrix

EXTERNAL

nominal disturbance torque	10^{-5} N-m
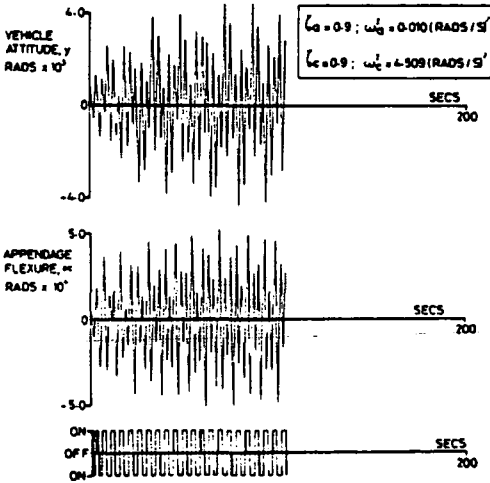
FIGURE 3.

these two simulations occurred during the first 10 seconds during which the effects of the initial transients decayed.

For the purposes of the mismatch investigations, the controller was designed with:

FIGURE 4

FIGURE 5

FIGURE 6

$\zeta_a = 0.9; \quad \omega_a^2 = 0.100$ (rads/s)^2

$\zeta_c = 0.9; \quad \omega_c^2 = 4.509$ (rads/s)^2

The observer was designed on the basis of the unmodified plant equations, as outlined in section 3.

218
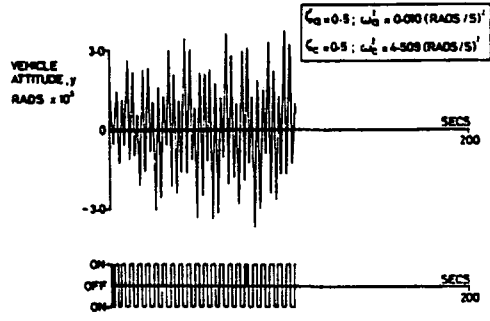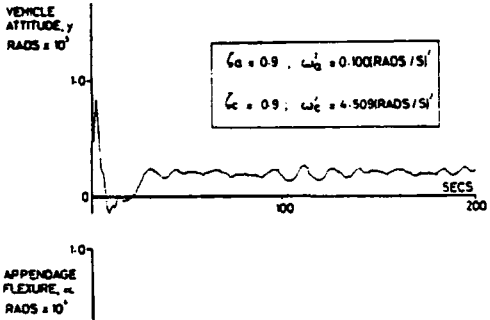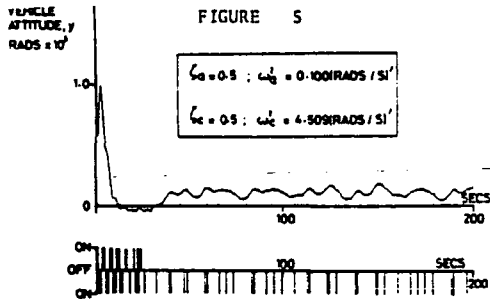
6.2 The effects of plant and input mismatch

Mismatch is best described by the mismatch factors, m_a and m_c, given by:

$$m_a = (\text{actual } \omega_a)/(\text{assumed } \omega_a)$$

$$m_i = (\text{actual } \tau_d)/(\text{assumed } \tau_d)$$

Both factors were varied across the range 0.5→2 and a summary of the results for a set of 200-second simulations is contained in Table 2.   It can be seen that satisfactory performance is achieved over the range $m_a = 0.5$, $m_i = 1$ to $m_a = m_i = 2$ and the simulations corresponding to these two limits are illustrated in Figures (7) and (8).   Unsatisfactory performance occurred when $m_a = m_i = 0.5$ and

TABLE 2

MISMATCH		CONTROL[*]	FIRETIME
m_a	m_i		secs.
	0.5	-	100
0.5	1.0	✦	4.3
	2.0	✦	4.5
	0.5	✦	2.2
1.0	1.0	✦	2.4
	2.0	✦	2.7
	0.5	✦	2.1
2.0	1.0	✦	2.4
	2.0	✦	3.0

✦ good ✦

bad -
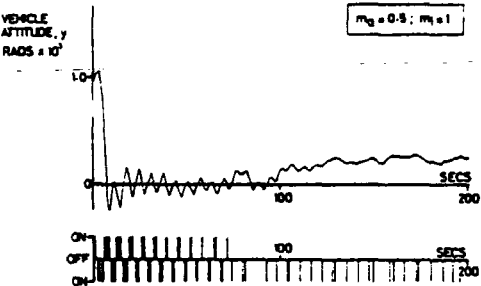
FIGURE   7
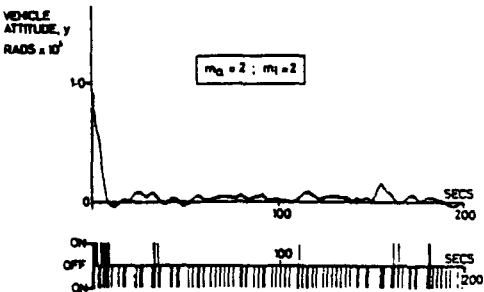
FIGURE   8
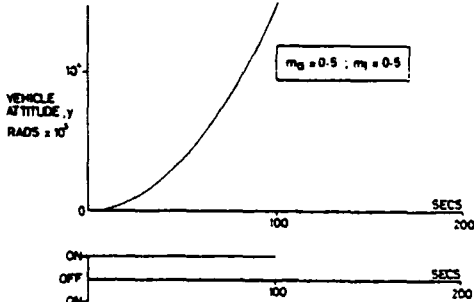
FIGURE   9

this result is represented in Figure (9).

The control jet firetime in the presence of no plant or input mismatch was 2.36 secs.   Table 2 reveals that the only significant departure . from this value occurs when the appendage mismatch factor, m_a, is 0.5.

7.   CONCLUSION

A control scheme for a highly flexible satellite has been presented which controls solar-panel flexure and maintains a high pointing-accuracy, even in the presence of considerable plant and input mismatch.   As in current practice, the scheme is implemented with control jets and a single attitude-sensor mounted on the centre-body.

The controller design is based on a Lyapunov, state-vector-feedback principle which operates on a weighted sum of the plant states.   A Luenberger observer is employed for state estimation.   This removes the need for transducers to sense appendage motion and vehicle rate, thus simplifying the hardware requirements.

The authors have considered the problem of noise on the sensor output.   The major source of low frequency noise is the structural vibration and this is controlled by the control scheme. Any high-frequency noise will be attenuated by the inherent filtering characteristics of the observer.   Hence it is believed that sensor noise can be neglected.

If this control scheme were employed in the next generation of satellites, no costly redevelopment of existing control equipment would be required and the experience gained with current vehicles would be directly applicable.

There is every indication that the design approach presented can be extended for the solution of the 3-axis control problem.

8. ACKNOWLEDGEMENT

9. REFERENCES

1. Gething, J.M. & Gill, K.F. (1974) Relay control of undamped linear systems using Lyapunov's second method, *Proc. I.E.E.*, vol. 121, No. 4, 301-306.

2. Luenberger, D.G. (1974) Observing the state of a linear system, *I.E.E.E. Trans. Mil. Elec.* vol. M.I.L. 8, 74-80.

3. Smart, D.R., Gill, K.F., Gething, J.M. & Holt, J.A. (1974) Dynamic analysis of flexible space vehicles having uncoupled control axes, *Aero. J. Royal Aero. Soc.*, vol. 78, 560-569.

4. Smart, D.R. & Gill, K.F. (1975) Attitude control of a flexible space vehicle by means of a linear state observer, *Aero. J. Royal Aero. Soc.*, vol. 79, 86-95.

5. Smith, E.H. & Gill, K.F. (1975) A digital state observer for the attitude control of a flexible space vehicle, *Aero. J. Royal Aero. Soc.*, vol. 79.

6. Barnett & Storey (1970) *Matrix Methods in Stability Theory*, Thomas Nelson & Sons. Ltd.

7. Kalman, R.E. & Bertram, J.E. (1960) Control system analysis and design via the second method of Lyapunov, Pts. I and II. *Trans. A.S.M.E.*, vol. 82D.

DISCUSSION

A. Baysens (MATRA): 1. How do you observe the torques (disturbing and control)?

2. What is the sensibility of the pointing to the observer errors?

3. Has the transfer function of the sensor been taken into account in the loops, including noise?

4. What are the performances of such a design in terms of total accuracy (with noise), consumption, number of thruster actuations, minimum thruster on-time?

5. What are the results when you assume a null damping of the flexible modes?

Author: Thank you for your questions. To take them in order:

1. Neither torques were observed; their values were assumed and these were input to the observer.

2. The mismatch factors used in the paper measure the uncertainty in disturbing torque and appendage natural frequency. We have not separated the effects due to mismatch caused by the observer from those caused by the controller. However, I think I am correct in saying that the steady-state offset apparent in the results could be a measure of the observer errors, although I am not totally sure of this point.

3. The sensor's transfer function will be considered in a paper in the near future along with the effects of noise. However, we do point out in the paper that the observer is made as slow as possible, thus enhancing its low-pass filtering characteristics.

4. I can give you information regarding fuel usage; this is contained in Table 2 of the paper, where thruster firing-times are presented for 200-second simulations. The thrusters had a minimum burn-time of 0.01 second. The level of pointing accuracy achieved was of the order of 1.50×10^{-4} degrees when the deadband, δ, of the thrusters was 10^{-5}.

5. The control scheme cannot be implemented with zero artificial damping and thus no simulations were performed. I should emphasise that the damping is purely artificial and is introduced in order to obtain a unique, positive-definite symmetric matrix, P_m. Thus the controller thinks that the plant is damped whereas this is not the case in reality.

P. Vo-Han (MATRA): How does your control system compare with a conventional design in terms of gas-jet mass budget and number of firings? How about performance in the case of sensor noise?

Author: The control torque employed in a more conventional design where flexure was uncontrolled (References 4 and 5 of the paper) was different from that employed here and thus any comparison would have no significance. I would refer you to the answer given earlier in relation to the problem of sensor noise.

220

G.T. Tseng (RCA): Your control scheme includes a
Luenberger observer. Could you indicate how you
select the convergence criterion during the pole
allocation process in developing the observer?

Author: In the paper, we derive an estimation-
error vector which can be expressed as a function
of the initial states. The problem is simplified
by ensuring that the diagonal elements of the matrix
D are always very close to each other in magnitude,
and that the elements of E are unity. The procedure
for pole selection then entails the variation of
one parameter (namely one element of D, the other
element being a fixed proportion of this) and obser-
vation of the behaviour of the estimation-error
vector with time. Selection of the elements of D
can then be made at this stage or a full simulation
can be undertaken and pointing accuracy, fuel usage
etc. can be assessed. The chosen structure of D
enables one to quickly assess the filtering
characteristics of the observer and thus determine
the possible corruption of the estimated states by
noise on the sensor output. Some of this will be
contained in a paper which we intend to publish
shortly.

F.R. Vigneron: The method appears to work in some
cases and breaks down in others. Is there any
reason for this?

Author: The method was conceived as a perturbation
approach in which very small levels of damping were
employed. It was found that much higher damping
levels than those first employed resulted in much
more acceptable control. At very high levels of
the damping factor (say around 10) control broke
down. There appears, therefore, to be a region in
which acceptable performance is achieved and
further work is required before a deeper understand-
ing is obtained.

PAPER 37

Technical note

Controlling the attitude and two flexure-modes of a flexible satellite

E. H. SMITH

Formerly with University of Leeds, now with Dept of Mech and Prod Eng, Paisley College of Technology,

and

K. F. GILL

Dept of Mech Eng, University of Leeds

1. INTRODUCTION

Many space satellites consist of a pair of highly-flexible solar panels attached to a relatively rigid centre-body, the recently launched CTS is a good example. The panels supply electrical power to the communications equipment and attitude sensors which are usually mounted on the centre-body. It would appear that in the current generation of vehicles the flexure of the panels does not degrade the quality of the attitude control. This may not be so, however, in the next generation of satellites which will of necessity carry much larger solar panels. If the same high pointing accuracy is to be maintained in these vehicles and problems due to structural damage are to be avoided, then the flexure of the panels will have to be controlled.

In designing control loops for flexible space satellites many workers have considered only a single mode of flexure in the dynamic model of the vehicle (*see*, for example, Refs. 1, 2, 3, 4 and 5). It is likely, however, that additional modes will have a significant effect on vehicle performance and thus the authors present here an extension of their 'single-mode' control scheme[5] to a vehicle exhibiting two, dominant flexure-modes.

A Luenberger observer is employed for state estimation and the controller is designed on the basis of Lyapunov's stability principles.

3. VEHICLE DESCRIPTION AND DYNAMICS

The satellite consists of two large solar panels attached to a relatively small and rigid centre-body. A small, constant disturbance torque, τ_d, acts on the vehicle and a control torque of $\pm \tau_c$ can be applied from thrusters mounted on the centre-body. The attitude, y, of the vehicle in relation to a fixed reference is measured by an instrument mounted on the centre-body.

2. NOTATION

k	sample number
t	time
$\underline{x}$	plant state vector
$\underline{\dot{x}}$	estimated plant state vector
y	attitude of centre-body
$\underline{z}$	observer state vector
A_1	discrete plant matrix
B_1	discrete plant-input matrix
D, E, G	observer matrices
H	plant output matrix
P	Lyapunov matrix
T	observer matrix
V	discrete Lyapunov function
ΔV	change in V
α_1	first flexure-mode component of centre-body attitude
α_2	second flexure-mode component of centre-body attitude
δ	deadband
θ	rigid component of centre-body attitude
ω_1	undamped natural frequency of first mode
ω_2	undamped natural frequency of second mode
τ	torque
ζ_1	damping factor of first mode
ζ_2	damping factor of second mode

Subscripts

c	centre-body or control torque
d	disturbance torque
m	modified matrix

Superscripts

T	matrix transpose
-1	matrix inverse

The dynamical equations are:

$$\ddot{\theta} = 0\cdot00604\tau \qquad . \qquad . \qquad . \qquad (1)$$

$$\ddot{\alpha_1} + \omega_1{}^2\alpha_1 = 0\cdot076\tau \qquad . \qquad . \qquad . \qquad (2)$$

$$\ddot{\alpha_2} + \omega_2{}^2\alpha_2 = 0\cdot038\tau \qquad . \qquad . \qquad . \qquad (3)$$

$$\text{and,} \quad y = \theta + 0\cdot076\alpha_1 + 0\cdot038\alpha_2 \qquad . \qquad (4)$$

where $\omega_1{}^2 = 4\cdot509$ (rads/s)^2 and $\omega_2{}^2 = 9\cdot000$ (rad/s)^2, the two frequencies associated with the dominant flexure modes.

It is convenient to express these equations in discrete. state-variable form as:

$$\underline{x}(t_{k+1}) = A_1\underline{x}(t_k) + B_1\tau(t_k) \qquad . \qquad . \qquad (5)$$

$$y(t_k) = H\underline{x}(t_k) \qquad . \qquad . \qquad . \qquad (6)$$
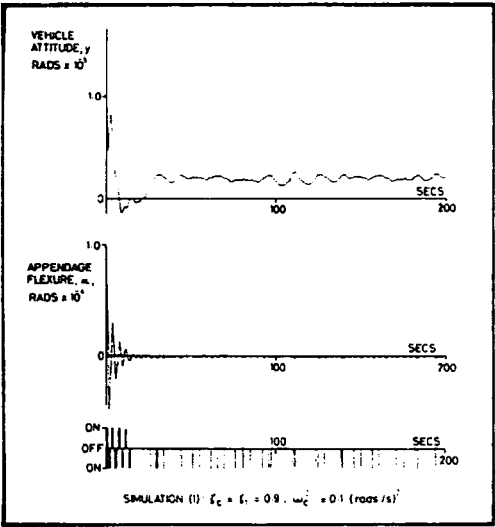
—Figure 1.

$$A_1 = \begin{bmatrix} 1 & \Delta t & 0 & 0 & 0 & 0 \\ 0 & 1 & 0 & 0 & 0 & 0 \\ 0 & 0 & \cos(\omega_1\Delta t) & \sin(\omega_1\Delta t)/\omega_1 & 0 & 0 \\ 0 & 0 & -\omega_1\sin(\omega_1\Delta t) & \cos(\omega_1\Delta t) & 0 & 0 \\ 0 & 0 & 0 & 0 & \cos(\omega_2\Delta t) & \sin(\omega_2\Delta t)/\omega_2 \\ 0 & 0 & 0 & 0 & -\omega_2\sin(\omega_2\Delta t) & \cos(\omega_2\Delta t) \end{bmatrix}$$

$$B_1 = \begin{bmatrix} 0\cdot00604\,(\Delta t^2)/2 \\ 0\cdot00604\Delta t \\ 0\cdot076\,(1-\omega_1{}^2\Delta t)/\omega_1{}^2 \\ 0\cdot076\sin(\omega_1\Delta t)/\omega_1 \\ 0\cdot038\,(1-\omega_2{}^2\Delta t)/\omega_2{}^2 \\ 0\cdot038\sin(\omega_2\Delta t)/\omega_2 \end{bmatrix}$$

and Δt is the sampling interval.

4. OBSERVER DESIGN

Since the plant is sixth-order with a single output, a fifth-order observer is required of the general form:

$$\underline{z}(t_{k+1}) = D\underline{z}(t_k) + Ey(t_k) + G\tau(t_k). \qquad . \qquad (7)$$

The estimated state-vector, $\dot{x}(t_k)$, is linearly related to the observer output by,

$$\underline{z}(t_k) = T\underline{x}(t_k). \qquad . \qquad . \qquad (8)$$

It is shown elsewhere[5] that the estimated state vector will converge onto its real counterpart if the following relations apply:

$$TA_1 - DT = EH \qquad . \qquad . \qquad . \qquad (9)$$

$$G = TB_1. \qquad . \qquad . \qquad (10)$$

By specifying D and E, T can be obtained from equation (9) thus enabling G to be evaluated from equation (10). Details of the design approach are contained in Ref. 5, and only the selected matrices D and E will be listed here:

$$D = \begin{bmatrix} 0\cdot9802 & 0 & 0 & 0 & 0 \\ 0 & 0\cdot9792 & 0 & 0 & 0 \\ 0 & 0 & 0\cdot9782 & 0 & 0 \\ 0 & 0 & 0 & 0\cdot9773 & 0 \\ 0 & 0 & 0 & 0 & 0\cdot9763 \end{bmatrix}$$
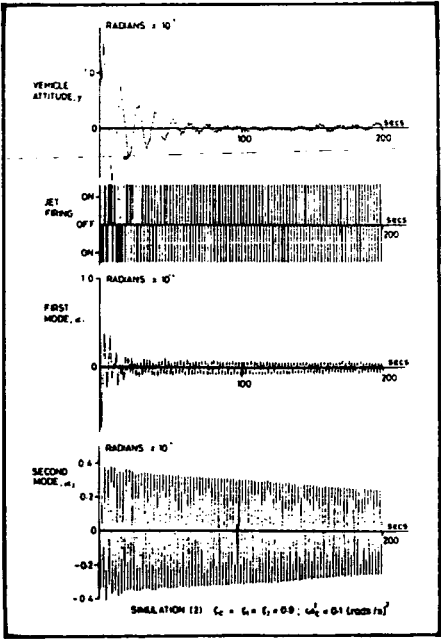
Figure 2.

$$E= \begin{bmatrix} 1 \\ 1 \\ 1 \\ 1 \\ 1 \end{bmatrix}$$

5. CONTROLLER DESIGN

A discrete Lyapunov function, $V(x(t_k))$, is defined by:

$$V(x(t_k)) = x^T(t_k) Px(t_k) \qquad . \qquad . \qquad (11)$$

—where P is a unique, symmetric, positive-definite matrix. The change in V between sampling instants is given by:

$$\Delta V(x(t_k)) = V(x(t_{k+1})) - V(x(t_k)) \qquad . \qquad (12)$$

and, for asymptotic stability, this should be always negative. Now substitution of equations (5) and (11) into (12) yields:

$$\Delta V(x(t_k)) = x^T(t_k)(A_1^{-1}PA_1-P) x(t_k)+\tau^2(t_k) B_1^T PB_1 +$$
$$+ 2\tau(t_k) B_1^T PA_1 x(t_k) \qquad . \qquad . \qquad . \qquad (13)$$

Considering the right-hand side of this expression, the first term will be negative definite if,

$$A_1^{-1}PA_1 - P = -Q \qquad . \qquad . \qquad . \qquad (14)$$

—where Q is a positive-definite, symmetric matrix. The second term in equation (13) is always positive, but the third term will remain negative with the appropriate

selection of the input torque, τ. One method for satisfying equation (14) is to specify Q and then solve for P. Provided that the matrix P thus obtained is symmetric and positive-definite, then equation (11) is satisfied and hence a satisfactory Lyapunov function has been found. Unfortunately, the system under consideration here cannot be asymptotically stable because of the structure of equations (1), (2) and (3), and this is reflected in the inability to obtain a unique, symmetric, positive-definitive matrix, P, from equation (14). In order for the approach to be successful, artificial resistance terms are introduced into equations (1), (2) and (3) in order to furnish them with complex eigenvalues possessing negative real parts. The resulting discrete plant matrix, A_m, of the modified system is then employed in equation (14), i.e.

$$A_m^{-1}P_m A_m - P_m = -Q \qquad . \qquad . \qquad (15)$$

and the unique matrix, P_m, obtained from this equation is then symmetric and positive-definite. Further details of the approach can be found in reference (5), but it is noted here that the degree of modification of equations (1), (2) and (3) is measured by the hypothetical damping factors, ζ_1 and ζ_2, added to equations (2) and (3) and the hypothetical natural frequency, ω_c, and damping factor, ζ_c, introduced to equation (1).

The control law developed from the approach is:

$$\tau(t_k)=\tau_d \text{ when } q \leqslant \delta$$
$$\text{or} \quad \tau(t_k)=\tau_d-\tau_c \text{ sign } (q) \text{ when } |q| > \delta$$

—where $q = B_1 T P_m A_1 x(t_k)$ and $\pm \delta$ is the valve overlap or the deadband in the control-jet actuator.
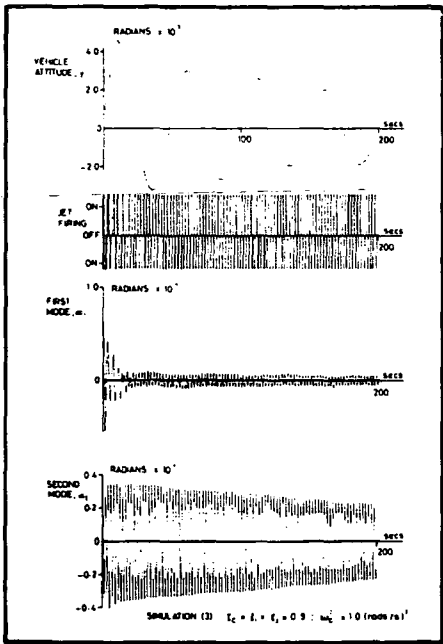
Figure 3.
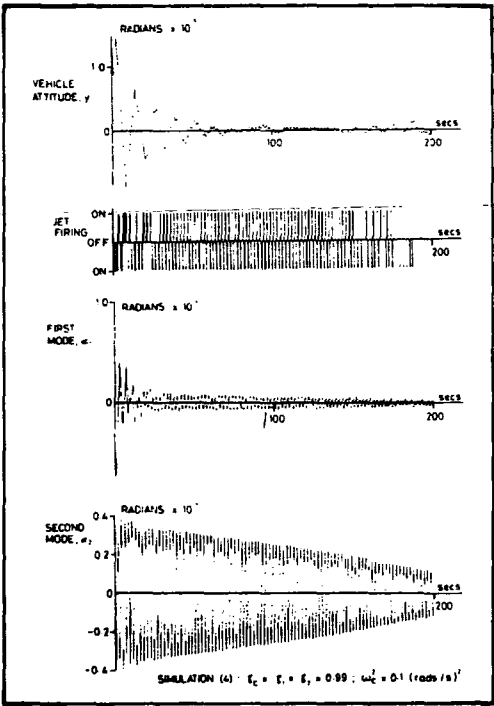
Figure 4.

6. SIMULATION RESULTS AND DISCUSSION

In the 'single-mode' model employed earlier[5] only equations (1) and (2) were applicable. It was found that satisfactory control could be achieved with:

$$\zeta_c = 0.9; \quad \omega_c^2 = 0.1 \text{ (rads/s)}^2$$

and

$$\zeta_1 = 0.9.$$

The results from a 200 second simulation, (1), utilising these parameters are presented in Fig. 1. With the introduction of a second mode, the above parameters remained fixed and an additional damping factor, ζ_2, was introduced and assigned the value 0.9. The results from simulaion (2) run under these conditions are illustrated in Fig. 2. In both simulations, the pointing accuracy is very high after about 100 secs, but an offset in y from the zero value is evident in simulation (1). The first mode in simulation (2) is not controlled as well as in simulation (1) and this is achieved at the expense of a larger total jet firetime—2.4 secs in simulation (1) and 11.5 secs in simulation (2). The amplitude of oscillation of the second mode reduces with time and although the rate of decay is low, the oscillations are, at least, reducing not increasing.

Simulation (3) is illustrated in Fig. 3 and it can be seen that an increase of ω_c^2 to unity does not effect a significant increase in performance. However, improvement in performance was achieved in simulation (4) for which the controller parameters were:

$$\zeta_c = \zeta_1 = \zeta_2 = 0.99; \quad \omega_c^2 = 0.1 \text{ (rads/s)}^2.$$

It can be seen, from Fig. 4, that the amplitude of the second mode is reduced by about one half and the first mode is very quickly reduced. The jets fired for a total of 9.1 seconds during the 200 second simulation, most of the firetime being registered in the first 25 seconds. An extension of the run-time to 800 seconds revealed that α_2 was further reduced to lie within a band of $\pm 3.5 \times 10^{-6}$ radians, α_1 was still small and the high pointing accuracy was maintained (Fig. 5).

7. CONCLUSIONS

A 'two-mode' model of a flexible space vehicle is presented and it is demonstrated that the controller can be designed to control both flexure-modes whilst maintaining a high pointing-accuracy. This is achieved at the expense of an increased fuel usage over simulations with a 'single-mode' vehicle.

The controller is designed on the basis of Lyapunov's stability principles and is implemented as a state-vector-feedback algorithm. The need for transducers to sense flexure is removed by the employment of a Luenberger observer for state estimation.

Thus the control scheme is implemented with a single attitude-sensor and control jets mounted on the centre-
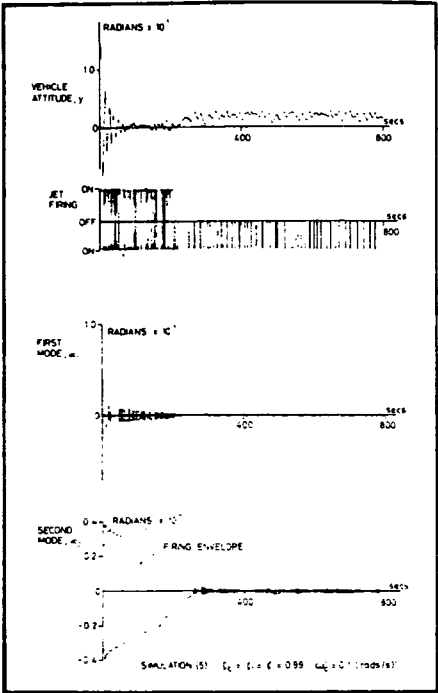
Figure 5.

body. No new equipment is required and hence experience gained with current vehicles is directly applicable.

8. REFERENCES

1. HARRIS, R. S. and TODMAN. D. C. Three axis control of spacecraft with large flexible appendages. ESA Symposium on Dynamics and Control of Non-Rigid Space Vehicles, May 1976.
2. OHKAMI, Y. and LIKINS, P. W. Results of numerical determination of poles and zeros of transfer function for flexible–spacecraft attitude control. ESA Symposium on Dynamics and Control of Non-Rigid Space Vehicles, May 1976.
3. GETHING, J. M. and GILL, K. F. Relay control of undamped linear systems using Lyapunov's second method. Proc IEE, 121, No 4, 1974.
4. SMART, D. R. and GILL, K. F. Attitude control of a flexible space vehicle by means of a linear state observer. The Aeronautical Journal, RAeS, Vol 79, pp 86–95.
5. SMITH, E. H. and GILL, K. F. Flexible space vehicle control based on state observation and Lyapunov's method. ESA Symposium on Dynamics and Control of Non-rigid Space Vehicles, May 1976.

ERRATA

The Editor regrets the following typographical error occurred in the paper *The aero engine and its progress—fifty years after Griffith* by F. W. Armstrong (THE AERO-NAUTICAL JOURNAL, p 499, December 1976):

p 501, lhc, lines 17 and 18: after 'aircraft' read 'which included some discussion on the possibilities of jet propul-'.

PAPER 38

Technical Note

On the design of optimal discrete observers with particular reference to a flexible communications satellite

DR. E. H. SMITH* and DR. K. F. GILL†

*Formerly University of Leeds, now with Department of Mechanical and Production Engineering, Preston Polytechnic.
†Department of Mechanical Engineering, Leeds University

1. INTRODUCTION

The electrical power consumed by an Earth-orbiting satellite is usually generated by panels of solar cells. On a vehicle such as the ESA Orbital Test Satellite the panels are attached, in cantilever fashion, to a relatively rigid centre body upon which are positioned the communication systems, attitude sensors and control equipment. The payload limitations of the launch vehicle imply that the relatively large solar panels must be of a lightweight construction and they are very flexible structures as a consequence. Currently-operating satellites do not appear to be troubled by the flexure of their solar panels. However, it is likely that attitude control problems will arise in the next generation of vehicles which will be equipped with considerably larger panels of solar cells.

Earlier work[1,2] has shown how a flexible vehicle can achieve a good pointing accuracy if the effects of flexure can be removed from the output of the attitude sensor. This was achieved by the employment of a Luenberger[3] state observer. Attitude and rate information were obtained from the observer and these were employed in a control law proposed by Hughes[1]. No attempt was made in this scheme to control the panel flexure, but it has been shown[5] that this can be achieved with a control law based on Lyapunov stability methods.

In this paper attention is directed towards the estimation error incurred by the observer. The influence of the observer dynamics on the estimation error is investigated and an optimum observer is designed that when incorporated within the Lyapunov control scheme[5] will guarantee a high pointing accuracy, minimise fuel consumption and suppress appendage motion in a flexible space vehicle. The ideas presented, however, can be used for control system design in other industrial spheres.

2. VEHICLE DYNAMICS AND CONTROLLER DESIGN

The study relates to a vehicle which consists of a rigid centre body (mass 160 kg) having, attached in cantilever fashion, a pair of highly flexible solar panels (6 metres long by 1 metre wide) capable of generating 1 kW of electrical power. Simple on-off jets are attached to the

NOTATION

k sample number
t time
Δt sampling interval
$\underline{x}, \hat{\underline{x}}$ actual and estimated plant state vectors, respectively $x_1 = \theta$; $x_2 = \dot{\theta}$; $x_3 = \alpha$; $x_4 = \dot{\alpha}$
θ rigid component of centre body attitude
α flexural component of centre body attitude
y centre-body attitude (i.e. plant output)
$\underline{z}$ observer state-vector
A_1, B_1 discrete plant matrices
D, E, G observer matrices
H plant output matrix
T observer matrix

centre body along with an attitude sensor. Only single axis control is considered and it is assumed that the optical sensor gives an error free indication of the attitude of the centre body.

The vehicle model can be described in discrete form by the following state variable equations:

$$\underline{x}(t_{k+1}) = A_1 \underline{x}(t_k) + B_1 \tau(t_k)$$

$$y(t_k) = H \cdot \underline{x}(t_k)$$

and the numerical values of the plant, plant input and plant output matrices are:

$$A_1 = \begin{bmatrix} 1 \cdot 0 & 0 \cdot 01 & 0 & 0 \\ 0 & 1 \cdot 0 & 0 & 0 \\ 0 & 0 & 0 \cdot 999 & 0 \cdot 01 \\ 0 & 0 & -0 \cdot 045 & 0 \cdot 999 \end{bmatrix}$$

$$B_1 = \begin{bmatrix} 0 \cdot 000000302 \\ 0 \cdot 0000604 \\ 0 \cdot 0000038 \\ 0 \cdot 00076 \end{bmatrix}$$

$$H = \begin{bmatrix} 1 \cdot 0 & 0 & 0 \cdot 076 & 0 \end{bmatrix}$$

The control algorithm presented permits the development of discrete state vector feedback control law that

---

have been shown[5] to maintain a high pointing accuracy and suppress appendage motion in a highly flexible satellite. The law is based on the Lyapunov stability method and for completeness is briefly described. A discrete Lyapunov function, $V(x(t_k))$, is defined by:

$$V(\underline{x}(t_k)) = \underline{x}^T(t_k)\, P\underline{x}(t_k)$$

where P is a unique, symmetric, positive definite matrix. The change in the Lyapunov function between sampling intervals, is given by:

$$\Delta V(\underline{x}(t_k)) = V(\underline{x}(t_{k+1})) - V(\underline{x}(t_k)) \quad . \quad . \quad (1)$$

and for asymptotic stability, $\Delta V(x(t_k))$, should be a negative quantity. Appropriate substitution in eqn. 1 reveals that:

$$\Delta V(\underline{x}(t_k)) = \underline{x}^T(t_k)\,(A_1^T P A_1 - P)\,\underline{x}(t_k)$$
$$+ \underline{\tau}^T(t_k)\, B_1^T P B_1 \underline{\tau}(t_k)$$
$$+ 2\underline{\tau}^T(t_k)\, B_1^T P A_1 \underline{x}(t_k).$$

Considering the right-hand side of this equation, the first term will be negative definite if

$$A_1^T P A_1 - P = -W \quad . \quad . \quad . \quad (2)$$

where W is a positive definite, symmetric matrix. The second term is always positive, but the third term will remain negative for the appropriate selection of the input torque, τ. The solution of eqn. 2 for P will ensure that P is positive definite and symmetric, thus satisfying the Lyapunov requirements.

In choosing τ it is assumed that no restrictions are imposed on the values which it may take. In practise, however, the thrusters are relay operated with a finite dead band (δ), hence the control law which is developed from the above approach is:

$$\tau(t_k) = \tau_d \text{ when } |q| \leq \delta$$

$$\tau(t_k) = \tau_d - \tau_I \text{ sign } (q) \text{ when } |q| > \delta$$

where $q = B_1^T P A_1 x(t_k)$ and $\pm \delta$ is the valve overlap, or the dead band in the control jet actuator. The operation
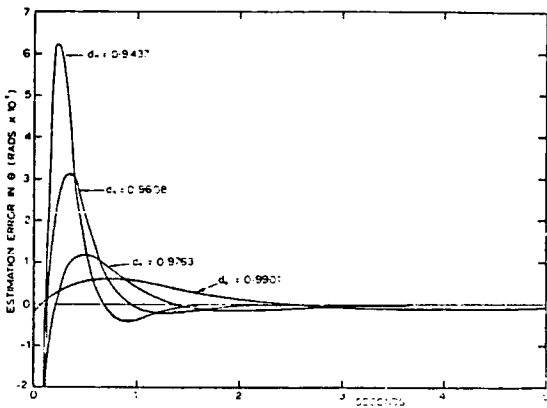
Figure 1.

of the control scheme[5] depends on reconstructed state information from a Luenberger observer. This paper seeks to produce an optimal observer and thus the theory of observers and a technique for assessing estimation error is presented in the following section.

3. THE THEORY OF OBSERVERS

A fourth-order plant[5] with a single output, $y(t_k)$, can be observed by a third-order discrete observer of the form:

$$\underline{z}(t_{k+1}) = D\underline{z}(t_k) + E y(t_k) + G\tau(t_k). \quad . \quad (3)$$

It will be stipulated that the observer output, $\underline{z}(t_k)$, is related to the estimated state vector, $\hat{\underline{x}}(t_k)$, by:

$$\underline{z}(t_k) = T\hat{\underline{x}}(t_k). \quad . \quad . \quad (4)$$

If the estimation-error vector, $\underline{\epsilon}_x(t_k)$, is defined as:

$$\underline{\epsilon}_x(t_k) = \hat{\underline{x}}(t_k) - \underline{x}(t_k) \quad . \quad . \quad (5)$$

then eqn. (4) becomes:

$$\underline{z}(t_k) = T\underline{x}(t_k) - T\underline{\epsilon}_x(t_k). \quad . \quad (6)$$

Substitution of the state variable equations and eqn. 6 into eqn. 3 yields:

$$\underline{\epsilon}_z(t_{k+1}) = D\underline{\epsilon}_z(t_k) + M\underline{x}(t_k) + N\tau(t_k) \quad . \quad (7)$$

where

$$\underline{\epsilon}_z(t_k) = T\underline{\epsilon}_x(t_k) \quad . \quad . \quad (8)$$

$$M = DT + EH - TA_1 . \quad . \quad (9)$$

$$N = G - TB_1. \quad . \quad . \quad (10)$$

If M and N are null matrices, eqn. (7) becomes:

$$\underline{\epsilon}_z(t_{k+1}) = D\underline{\epsilon}_z(t_k) \quad . \quad . \quad (11)$$

and eqns. (9) and (10) yield:

$$TA_1 - DT = EH \quad . \quad . \quad (12)$$

$$G = TB_1. \quad . \quad . \quad (13)$$

Provided that the observer is asymptotically stable, the vector $\underline{\epsilon}_z(t_k)$ will decay with time to a sensibly zero level and hence the estimated state vector, $\hat{\underline{x}}(t_k)$, will converge on to the actual vector, $\underline{x}(t_k)$.

The observer described is of a reduced order because the information contained in the plant output is utilised to formulate the estimated state vector. This technique can be demonstrated by forming the following adjoined equation from eqns. (6) and $y(t_k) = H\underline{x}(t_k)$

$$\begin{bmatrix} \underline{z}(t_k) \\ y(t_k) \end{bmatrix} = \begin{bmatrix} T \\ H \end{bmatrix} \underline{x}(t_k) + \begin{bmatrix} \underline{\epsilon}_z(t_k) \\ 0 \end{bmatrix} \quad . \quad (14)$$

Since $\underline{\epsilon}_z(t_k)$ decays with time, an estimate of the state vector is obtained from:

$$\hat{\underline{x}}(t_k) = \begin{bmatrix} T \\ H \end{bmatrix}^{-1} \begin{bmatrix} \underline{z}(t_k) \\ y(t_k) \end{bmatrix} \quad . \quad . \quad (15)$$

and the estimation-error vector is given by:

$$\underline{\epsilon}_x(t_k) = \left[\frac{T}{H}\right]^{-1}\left[\frac{\underline{\epsilon}_z(t_k)}{0}\right] \quad . \quad . \quad (16)$$

From eqns. (11) and (8) it can be shown that at the kth sampling instant,

$$\underline{\epsilon}_z(t_k) = D^k T \underline{\epsilon}_x(0). \quad . \quad . \quad (17)$$

Now the value of the observer output at time $=0$ cannot readily be evaluated because the observer output at the time instant immediately before is not known. It is most simple, therefore, to assume that $\underline{z}(0)$ is zero, and hence $\hat{x}(0)$ is also zero. Therefore, the error vector at time $=0$ is given by,

$$\underline{\epsilon}_x(0) = -\underline{x}(0). \quad . \quad . \quad (18)$$

Combining eqns. (16), (17), and (18) yields:

$$\underline{\epsilon}_x(t_k) = -\left[\frac{T}{H}\right]^{-1}\left[\frac{D^k T}{0}\right]\underline{x}(0). \quad . \quad (19)$$

Thus, the error vector at any instant can be obtained from a knowledge of the initial states of the plant. It is noteworthy that this information can be obtained at the design stage for any chosen observer before a full scale simulation study is undertaken.

In order to implement the observer, values must be assigned to the matrices D, E, G and T which are related according to eqns. (12) and (13). If T and D are specified, then E can be obtained from eqn. (12). However, in this
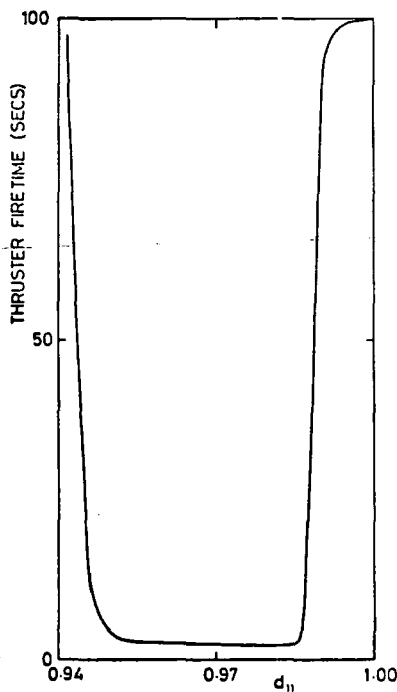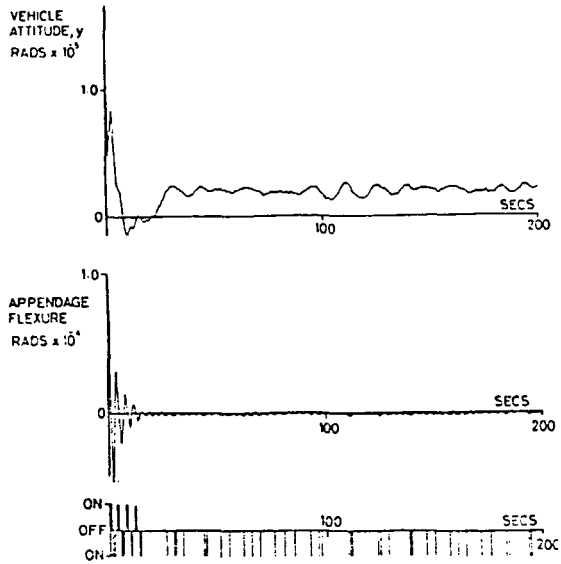
Figure 3.

case, H cannot be inverted because it is not square. The approach adopted here is to specify D and E and solve eqn. (12) for T by the method of Kronecker products[5]. G is then evaluated from eqn. (13).

If the dependence of the estimation errors upon the observer dynamics is to be studied, a number of restrictions must be imposed on matrices D and E in order to reduce the number of independent variables. These restrictions are:

(1) D is a diagonal matrix
(2) the elements of D differ from each other by only a few per cent
(3) the elements of E are made equal to unity.

Restrictions (1) and (2) above permit the observer matrix to be characterised by only one element, d_{ij}, of D. In the work presented here, d_{11} was used for this purpose. The imposition of (1) and (2) also facilitates the assessment of the low-pass filtering characteristics of the observer.

In Fig. 1 the sensitivity of the estimation error of the rigid component of centre body attitude, θ, to the value assigned to d_{11} is illustrated. It can be seen that as the speed of the observer is increased (i.e. as d_{11} decreases) the initial excursions from the zero level increase, but the error settles more quickly to a sensibly zero value. A method for selecting the 'best' value for d_{11} is discussed in the next section.

4. SIMULATION RESULTS AND DISCUSSION

A number of 200-second simulations were undertaken employing different observers. The total thruster on-time was evaluated for each run and these are plotted against the first element, d_{11}, of the observer matrix, D, in Fig. 2. The same controller was employed in all simulations. In the case where the firetime was 100 seconds, the simulation was terminated after 100 seconds of run time.

It can be seen that there is a substantial region in which a very low firetime can be achieved, but it is also

Figure 2.

apparent that inappropriate selection of observer dynamics can produce excessive jet firing times.

The performance of the vehicle when $d_{11} = 0.9803$, a point within the low firetime region in Fig. 2, is illustrated in Fig. 3 and this confirms that the authors have achieved their objectives of minimising fuel consumption while maintaining good attitude control and the suppression of panel flexure. Similar results are achieved with values of d_{11} selected for any point within the low firetime region of Fig. 2. It is interesting to note that with $d_{11} = 0.9803$ the addition of another higher-frequency flexure mode results in vehicle performance of comparable quality to that illustrated in Fig. 3 without any significant increase in fuel consumption[7].

It is recognised that the width of the low firetime region in Fig. 2 leaves considerable room for manoeuvre in selecting all the control loop variables so that the best possible design compromise can be achieved. Based on the experience gained in this work, and as a useful starting point in the iterative process of observer design, the authors recommend the following:

(i) D to be a diagonal matrix possessing eigenvalues within a few per cent of each other (this also facilitates the evaluation of the filtering characteristic of the observer),

(ii) the nominal eigenvalue of the D matrix to be initially about one half of the lowest plant eigenvalue.

The ideas presented for observer design are thus simple and logical in their approach and should recommend themselves to engineers concerned with the design of control systems for many forms of industrial plant.

REFERENCES

1. SMART. D. R. and GILL, K. F. Attitude control of a flexible space vehicle by means of a linear state observer. *The Aeronautical Journal*. RAeS. Vol 79, pp 86–95, 1975.
2. SMITH, E. H. and GILL, K. F. A digital state observer for the attitude control of a flexible space vehicle. *The Aeronautical Journal*, RAeS, Vol 79, No 779, pp 506–509, 1975.
3. LUENBERGER, D. G. Observing the state of a linear system. IEEE Trans Mil Elec, MIL -8, pp 74–80. 1974.
4. HUGHES. W. G. Design for high precision in spacecraft jet attitude control systems. RAE Tech Rep 71089. April 1971.
5. SMITH, E. H. and GILL, K. F. Flexible space vehicle control based on state observation and Lyapunov's method. Proc ESA Symposium on Flexible Space Vehicles. Frascati. Italy. May 1976.
6. SMART. D. R., GILL. K. F.. GETHING. J. M. and HOLT. J. A. Dynamic analysis of flexible space vehicles having uncoupled control axes. *The Aeronautical Journal*. RAeS, Vol 78, No 768. pp 560–569, 1974.
7. SMITH. E. H. and GILL. K. F. Controlling the attitude and two flexure-modes of a flexible space vehicle. *The Aeronautical Journal*. RAeS. Vol 81. No 793. pp 41–44. January 1977.

PAPER 39

DYNAMIC MODELLING AND MULTI-AXIS ATTITUDE CONTROL OF A HIGHLY FLEXIBLE SATELLITE

G. Longbottom**, D. Tate* and K. F. Gill*

Department of Mechanical Engineering, University of Leeds
**Department of Mechanical and Production Engineering, Huddersfield Polytechnic*

Abstract. The paper describes a dynamic modelling procedure and control algorithm design based on state vector feedback. The results presented are most encouraging, and indicate that an optimal control algorithm will reduce fuel usage, whilst maintaining a high pointing accuracy. In addition, appendage flexure is suppressed to within acceptable engineering limits, which will avoid possible mechanical failure.

Keywords. Attitude control, Control-system synthesis, Linear systems, State vector feedback, Discrete systems, Stability.

NOTATION

A	plant matrix	Q,R	cost functional matrices
a_i	modal amplitude	x	state vector
B	input matrix	y	vehicle attitude
H	output matrix	a_i	flexural component
I	centre-body inertia	τ_c	control torque
K	solution matrix	τ_d	disturbance torque
P	Lyapunov matrix	θ_d	centre-body attitude

INTRODUCTION

As spacecraft technology develops, the precise control of vehicle attitude becomes of increasing importance for the aiming of telescopes, cameras and antennae. Many of these craft consist of flexible solar panels attached to a relatively rigid centre-body, the Orbital test Satellite (OTS) is a good example.

It would appear that for the current generation of space vehicles, the flexure of the panels does not degrade the quality of the attitude control. However, this may not be so for the next generation, which will of necessity, carry much larger solar panels. This study relates to a space vehicle which consists of a rigid centre body having attached in a cantilever fashion a pair of highly flexible solar panels capable of generation between 5 to 7 kW of usable power.

Simple on-off jets are attached to the centre body along with an attitude sensor. The performance of the roll and yaw axis control is presented; it has been assumed that the optical sensor gives an error-free indication of the attitude of the centre body.

DYNAMIC MODEL

The first major step in the control system design process, requires the evaluation of

the structural characteristics; these are shown in block diagram form, Fig. 1, to give a clear pictorial representation of the dynamic model. It contains elements whose numerical values are dependent on the physical geometry, elasticity and mass distribution within the structure of the proposed space vehicle.

Before deciding how to formulate the equations of motion for a specific space vehicle, it is convenient to consider four categories of model. These have been named (Williams, 1976) as:

    i) N-body models
   ii) discrete parameter models
  iii) distributed parameter models
and iv) finite element models

These categories overlap as some spacecraft features are common to two or more, but, in a particular application the choice is governed by the physical geometry of the vehicle, and the severity of the specification for the proposed mission. In this presentation finite element (Longbottom, 1973), hybrid co-ordinate (Smart and others, 1974) and transfer matrix (Pestel & Leckie, 1963) approaches, which incorporate the ideas of categories (ii), (iii) and (iv), are adapted.

For the purposes of comparison, three alternative mass matrix representations have been used to demonstrate the subsequent variations in the numerical values of the computed natural
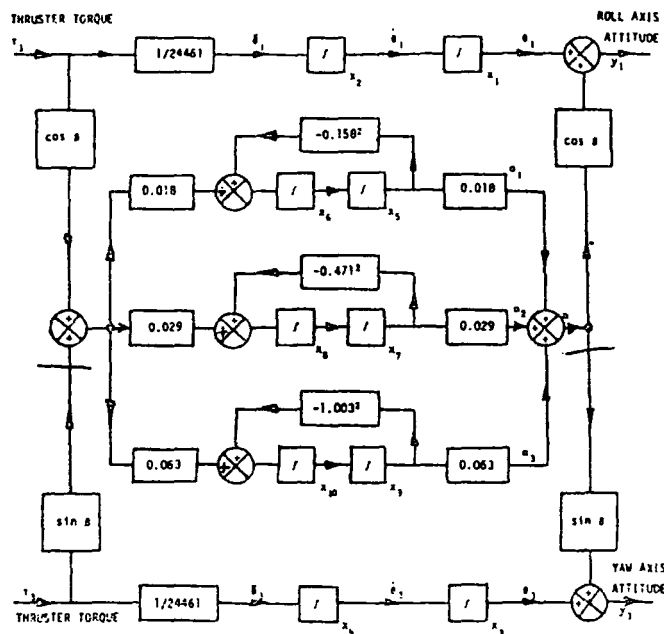
2436　　　　　　　G. Longbottom, D. Tate, and K. F. Gill

Fig. 1　STATE VARIABLE DIAGRAM FOR SATELLITE

frequencies. Mass model A: the simplest possible approach uses a Myklestad type (1944) lumped parameter model for the appendages, and a concentrated mass and moment of inertia, located at the central plane for the vehicle capsule. Mass model B: a modification to 'A' to allow for the mismatch of the actual, and modelled moments of inertia, for the appendage elements. Mass model C: an Archer (1963) type consistent mass matrix.

The three computational procedures are applied to a hypothetical vehicle, which is considered, by the authors, to be representative of the next generation of space vehicles; this comprises of a 2.2m wide, 400 kg, 160 kg m^2 capsule, and two solar panels, each being 18 m long by 2 m wide, having a uniformly distributed mass of 2.5 kg m^{-2}, and a flexural rigidity, for bending calculation purposes of 90 Nm^{-2}. The natural frequencies for the various models considered, are shown in Table 1.

It can be seen that the model 'A' frequencies are in agreement for all six modes, for each of the three methods of calculation considered. Similarly, the model 'B' values found by the finite element and transfer matrix methods, are in agreement with each other, but differ from the corresponding model 'A' values. A similar situation exists for model 'C' as regards the four lower modes, but some variation exists in the fifth and sixth modes. The authors conclude that the calculated natural

frequencies are more dependent on the choice of mass distribution model, than the analytical procedure.

Having written the computer programmes to apply both the finite element, and the hybrid co-ordinate concepts, to the solution of a particular problem, the authors found the finite element method to be the more tractable of the two. The additional axis transformation involved in the use of hybrid co-rdinates, nullifies the doubtful advantage of being able to represent the capsule as a truly rigid body, with the subsequent reduction in the number of degrees of freedom. Also, the distribution of the applied excitation torque between the various uncoupled modes, and the transformation of the responses back to the original co-ordinates, is a more complicated computational procedure for the case of the hybrid co-ordinate method.

The transfer matrix method, as applied here, provides a convenient procedure for the evaluation of the various natural frequencies. The use of low order matrices reduces the magnitude of computation, when compared with the previous two methods. However, difficulties were encountered as a result of differencing two large numbers, and in consequence a modified approach was found to be necessary for the fourth, fifth and sixth mode frequencies; the published literature (Pestel & Leckie, 1963) highlights this inherent problem in the evaluation of higher natural frequencies.

Mode No	Finite Element Method			Hybrid Coordinate Method	Transfer Matrix Method		
	Model A	Model B	Model C	Model A	Model A	Model B	Model C
1	0.0455	0.0511	0.0512	0.0485	0.0484	0.0510	0.0512
2	0.1577	0.1909	0.1742	0.1577	0.1576	0.1909	0.1740
3	0.2568	0.3213	0.3005	0.2569	0.2568	0.3213	0.2996
4	0.4707	0.6105	0.5335	0.4707	0.4707	0.6104	0.5296
5	0.6227	0.6886	0.8283	0.6227	0.6226	0.6887	0.7175
6	1.0034	3.2881	1.0612	1.0040	1.0034	3.2880	0.8303

TABLE 1. Natural frequencies (rad/s) for the spacecraft specified.

To conclude, the authors believe that the numerical values computed for the distributed mass model 'C', should be the most accurate. Table 2 shows the effect of increasing the number of elements in the model from eight to fourteen. The results clearly indicate, in the case of 'C', that, for control system design purposes, a model comprising of eight elements is adequate.

Mode	14 Element Model		8 Element Model	
	Model A	Model C	Model A	Model C
1	0.0497	0.0505	0.0485	0.0512
2	0.1693	0.1738	0.1577	0.1742
3	0.2869	0.2995	0.2568	0.3005
4	0.5097	0.5292	0.4707	0.5335
5	0.7638	0.8203	0.6227	0.8283
6	0.9966	1.0488	1.0034	1.0612

TABLE 2. Structural natural frequencies (rad/s)

CONTROL ALGORITHM DESIGN

The algorithms presented permit the development of discrete state vector feedback control laws; these are shown to maintain a high pointing accuracy, and suppress appendage flexure in a highly flexible space vehicle. The control laws are based on the Lyapunov stability method, and optimal control theory. For completeness, these techniques are described briefly in this section.

Lyapunov Controller

A discrete Lyapunov function, $V(\underline{x}(t_k))$, is defined by:

$$V(\underline{x}(t_k)) = \underline{x}^T(t_k).P.\underline{x}(t_k) \qquad (1)$$

where 'P' is a unique, symmetric, positive definite matrix. The change in the Lyapunov function between sampling intervals is given by:

$$\Delta V(\underline{x}(t_k)) = V(\underline{x}(t_{k+1})) - V(\underline{x}(t_k)) \qquad (2)$$

and for asymptotic stability, $\Delta V(t_k)$, should be a negative quantity. Appropriate substitution in Eq. 2 reveals that:

$$\Delta V(\underline{x}(t_k)) = \underline{x}^T(t_k).(A^T.P.A.-P)\underline{x}(t_k) + \underline{\tau}^T(t_k).$$
$$(B^T.P.B)\underline{\tau}(t_k) + 2\underline{\tau}^T(t_k).(B^T.P.A)$$
$$\underline{x}(t_k) \qquad (3)$$

Considering the right-hand side of this expression, the first term will be negative definite if:

$$A^T.P.A - P = -Q \qquad (4)$$

where 'Q' is a positive definite, symmetric matrix. The second term is always positive, but the third term will remain negative for the appropriate selection of the input torque, τ. The solution of Eq. 4 for 'P' will ensure that 'P' is positive definite and symmetric, thus satisfying the assumption in Eq. 1.

Optimal Controller

The optimal feedback matrix is based on the quadratic cost functional (Nagarth & Gopal, 1975) defined as:

$$J = \Sigma(\underline{x}^T Q\underline{x} + \underline{\tau}^T R\underline{\tau}) \qquad (5)$$

where 'Q' is a positive semidefinite real symmetric matrix, and 'R' is a positive definite real symmetric matrix. The feedback law (Hewer, 1971, 1973), where a steady state exists, is given by:

$$\underline{\tau}(x) = -(B^T.K.B + R)^{-1}.B.K.A\underline{x}(t_k) \qquad (6)$$

where 'K' is the unique positive definite solution of the algebraic discrete Riccati equation:

$$K = A^T.K.A - A^T.K.B.(B^T.K.B+R)^{-1}.B^T.K.A+Q \qquad (7)$$

Of the solution methods available for Eq. 7, the one adopted is due to Hewer (1971), using the recursive algorithm:

$$\phi_j = A - B.L_j \qquad (8)$$

$$V_j = \phi_j V_j \phi_j + L^T_j RL_j + Q \qquad (9)$$

$$L_{j+1} = (B^T.V_j.B+R)^{-1}.B^T.V_j.A \qquad (10)$$

for $j = 1, 2, 3, \ldots$ etc.

This yields $K = \underset{j \to \infty}{\lim} V_j$ which, by substitution in Eq. 5 gives the required feedback matrix for optimum control.

The Kronecker products method of solution for 'V_j' requires the formation and inversion of a matrix of order 'N^2', where 'N' is the order of the plant matrix. To obviate this requirement an iterative solution method was adopted (Smith, 1968).

The initialisation of the algorithm requires a choice of the variable matrix 'L_o' such that all the eigenvalues of 'ϕ_o' are less than unity is absolute value. This is achieved by application of Kleinman's (1974) ideas, using the recursive equations:

$$D_{i+1} = D_i + H_i \cdot D_i \cdot D_i^T \tag{11}$$

and

$$H_{i+1} = H_i^2 \tag{12}$$

for $i = 1, 2, 3, \ldots ,(n-1)$ where the integer 'n' is arbitrarily chosen such that $2^{(n-1)} > N$. For commencement of the recursive procedure, 'D_i' and 'H_i' are given the intial values:

$$D_1 = B^T \cdot R^{-1} \cdot B \tag{13}$$

$$H_2 = A \tag{14}$$

From which the final values 'D_n' and 'H_n' are calculated. Substitution of these values into the equation:

$$L_o = (R + B^T \cdot H_n T \cdot D_n \cdot H_n \cdot B)^{-1} \cdot B^T \cdot H_n T \cdot D_n \cdot H \cdot A. \tag{15}$$

permits the solution of the discrete Riccati equation as presented above. Care must be taken to choose a sufficiently large value of 'n' to permit a machine solution of Eq. 15. If 'n' is too small, then the resultant matrix to be inverted is ill-conditioned.

When choosing τ, for both control methods, it is assumed that there are no restrictions imposed on the values it may take. In practice, the thrusters are relay operated with a finite deadband 'δ', hence the control law becomes:

$$\tau(t_k) = \tau_d \text{ when } |q| \leq \delta$$

$$\tau(t_k) = \tau_d + \tau_c \text{ sign } (q) \text{ when } |q| > \delta$$

where $q = B^T \cdot P \cdot A \cdot x(t_k)$ for the Lyapunov controller

and $q = K \cdot x(t_k)$ for the optimal controller.

Results and Discussion

The results presented are for the plant depicted in Fig. 1, in which the satellite parameters are given together with the control and disturbance torque, and the sample interval.

The response represented by Figures 2, 3 & 4, for a highly flexible vehicle having a single vibrational mode and using the Lyapunov controller, show that both roll and yaw attitude, and appendage flexure, are adequately controlled. A typical roll axis response when using

an optimal controller is shown in Fig. 5, which is seen to be comparable to those for the Lyapunov control. The yaw and appendage responses are not included since these form a similar pattern. The fuel usage does, however, show a marked improvement in the latter case; clearly, optimal control algorithms are worthy of further study for possible inclusion in future space craft designs.

The feedback matrix in both controllers were selected by using a range of "weighting" values for the diagonal elements of the 'Q' matrix; these valves were chosen such that no one state was dominant. The authors' attempts to find an automatic precedure to overcome the trial and observation approach has, as yet, proved unsuccessful. Experience indicates that the displacement terms should, for example, be about three orders in magnitude greater than the velocity terms. In addition, it was also found necessary to separate the centre body and mode terms, in a similar manner, which in essence gives preference to the vehicle attitude, over that of appendage flexure. The values used for the simulations are given in the respective figures.

On extending the above ideas to a three mode model, the response, shown in Figs. 6 & 7, indicated a surprizing change in vehicle performance. The Lyapunov control algorithm was unable to maintain the high pointing accuracy achieved with the single mode dynamics, and variations in the actuator deadband did not improve the response. It should be noted that the fuel consumption appeared to be unaffected by the additional vibrational modes. The optimal control algorithm, however, maintained pointing accuracy, but showed a marked increase in fuel usage. The author's have not been able to find a 'Q' matrix that will reduce the fuel consumption, whilst still maintaining an acceptable degree of pointing accuracy.

The mathematical techniques employed in computing the feedback matrices, required the use of a modified plant matrix, which results due to inserting resistance terms (Smith & Gill, 1976). Further details on the problems in controlling unstable linear systems are given by Smith, Tate & Gill (1978).

The authors have considered the problem of noise on the sensor outputs, the major source of low frequency noise being the appendage vibration, which is suppressed by the control scheme described.

One aim is to eliminate the need to measure flexure, by use of a Luenberger observer to predict the process states (Smith & Gill, 1976). It was found, however, that with the plant description chosen, it was only possible to design an observer for single axis control; with multi-axis control, the observer matrix 'T' is singular, and in consequence state estimation is impossible. The usefulness of these control algorithms depends on finding a solution to this problem.

The effects of a variation in the panel angle
on system performance was found to be negli-
gible for the mismatch conditions taken (±20
degrees), but control algorithm adaptation will
have to be considered seriously in a full
engineering design study.

13. Williams, C.J.H.   (1976) Dynamic modell-
     ing and formulation techniques for non-
     rigid spacecrafts, E.S.A. Symposium on
     the Dynamics and Control of Non-rigid
     Spacecraft, Rome.

REFERENCES

1. Archer, J.S.   1963 "Consistent mass
    matrix for distributed systems",   Proc.
    Americ. Soc. Civ. Eng.

2. Hewer, G.A.   (1971) An iterative techni-
    que for the computation of the steady
    state gains for the discrete optimal
    regulator,   I.E.E.E. Trans. Aut. Con.

3. Hewer, G.A.   (1973) Analysis of a dis-
    crete matrix Riccati equation of linear
    control and Kalman filtering,   Journal
    of Mathematical Analysis and Applications,
    Vol. 42, Pt.1.

4. Kleinman, D.L.   (1974) Stabilizing a dis-
    crete, constant linear system with appli-
    cation to iterative methods for solving
    Riccati equation,   I.E.E.E. Trans. Aut.
    Con., June.

5. Longbottom, G.   (1973) Dynamic modelling
    of structural frames, M.Phil. Thesis,
    Leeds University.

6. Myklestad, N.O.   (1944) A new method of
    calculating natural modes of uncoupled
    bending vibration of airplane wings and
    other types of beams,   Journal of the
    Aeronautical Sciences,   Vol. 11.

7. Nagarth, I.J. and Gopal, M. (1975) Con-
    trol System Engineering, Wiley.

8. Pestel, E.C. and Leckie, F.A.   (1963)
    Matrix Methods in Elastomechanics,
    McGraw-Hill.

9. Smart. D., Gill, K.F., Gething, J.M. and
    Holt, J.A.   (1974) "Dynamic analysis of
    flexible space vehicles having uncoupled
    control axes",   Aeronautical Journal
    (R.Ae.S.), No. 768, Vol.78, pp.560-569.

10. Smith, E.H. and Gill, K.F.   (1976)
    Flexible space vehicle control based on
    state observation and Lyapunov's method,
    E.S.A. Symposium on the Dynamics and
    Control of Non-Rigid Spacecraft, Rome.

11. Smith, R.A.:   (1968) Matrix equation XA
    + BC = C, Siam. Appl. Math., Vol. 16,
    No. 1.

12. Smith, E.H., Tate, D. and Gill, K.F.
    The design of a discrete Lyapunov con-
    troller for an open loop unstable linear
    system, to be published.

G. Longbottom, D. Tate, and K. F. Gill

$$Q = \begin{bmatrix} 10 & & & & & 0 \\ & 0.01 & & & & \\ & & 10 & & & \\ & & & 0.01 & & \\ & & & & 0.001 & \\ 0 & & & & & 1 \times 10^{-6} \end{bmatrix}$$
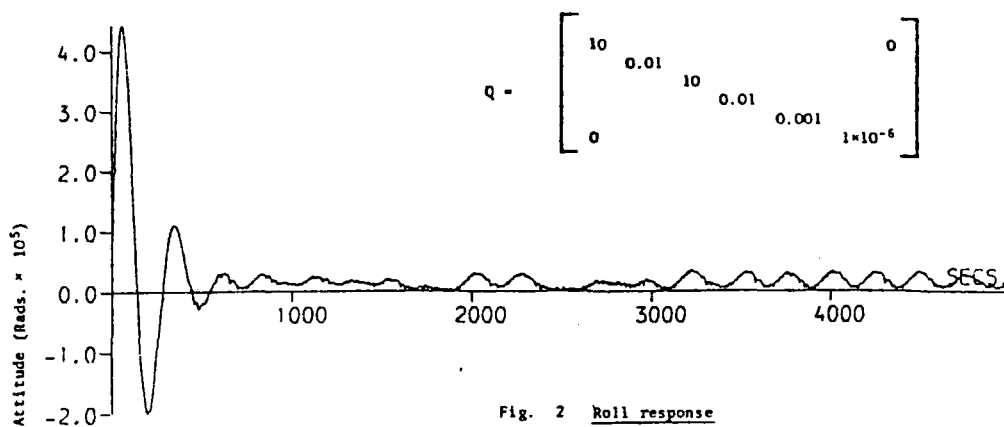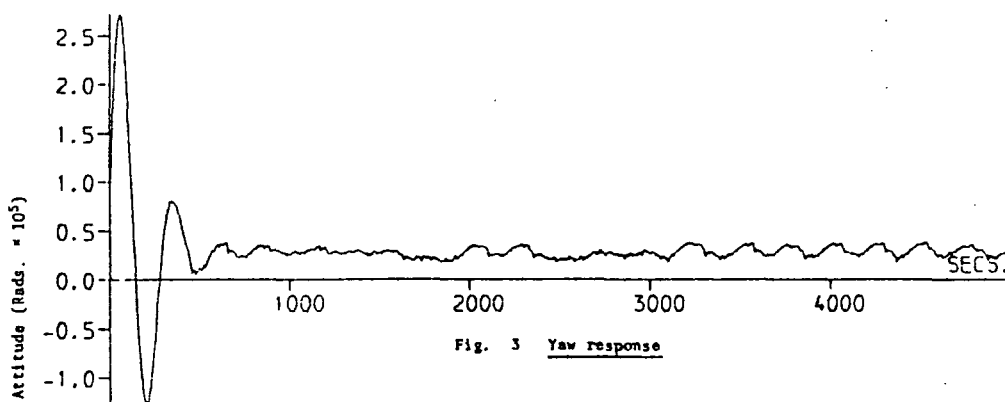
Fig. 2 Roll response

Fig. 3 Yaw response
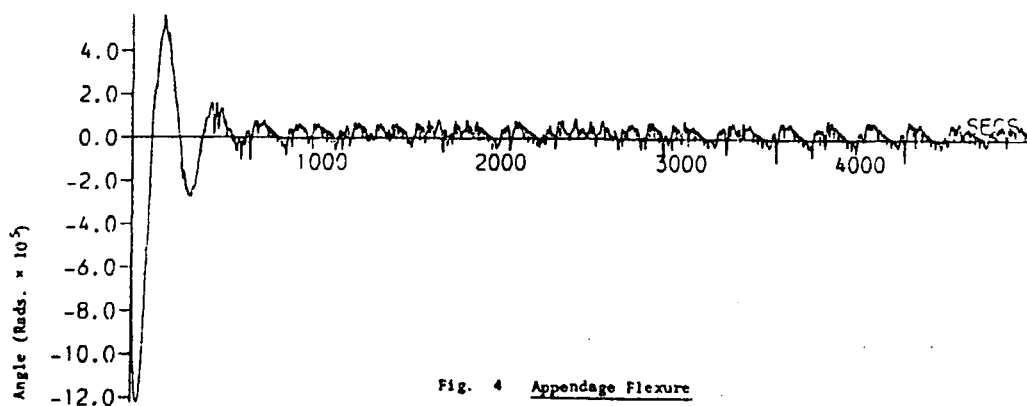
Fig. 4 Appendage Flexure

$$Q = \begin{bmatrix} 10_{0.01}10_{0.01}0.001_{1\times10^{-6}} & 0 \\ 0 & \end{bmatrix} \quad , \quad R = \begin{bmatrix} 1 & 0 \\ 0 & 1 \end{bmatrix}$$
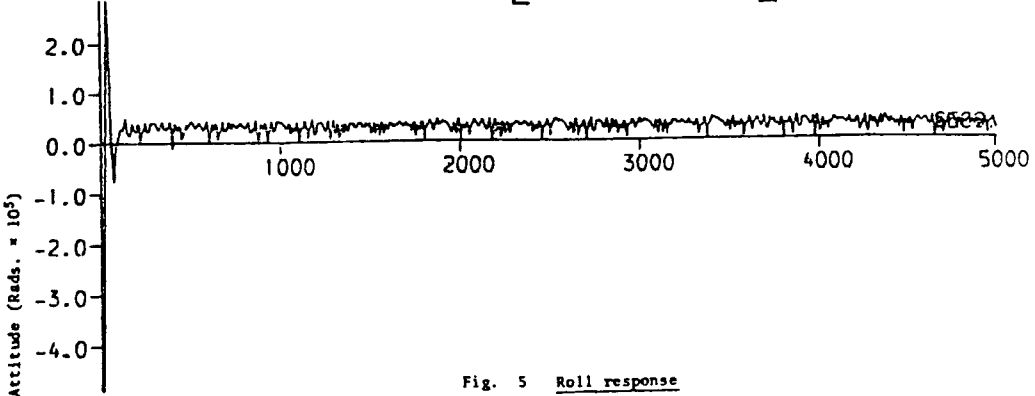
Fig. 5   Roll response

$$Q = \begin{bmatrix} 10_{0.01}10_{0.01}0.001_{1\times10^{-6}}0.001_{1\times10^{-6}} & & 0 \\ 0 & 0.001_{0.001_{1\times10^{-6}}} \end{bmatrix}$$
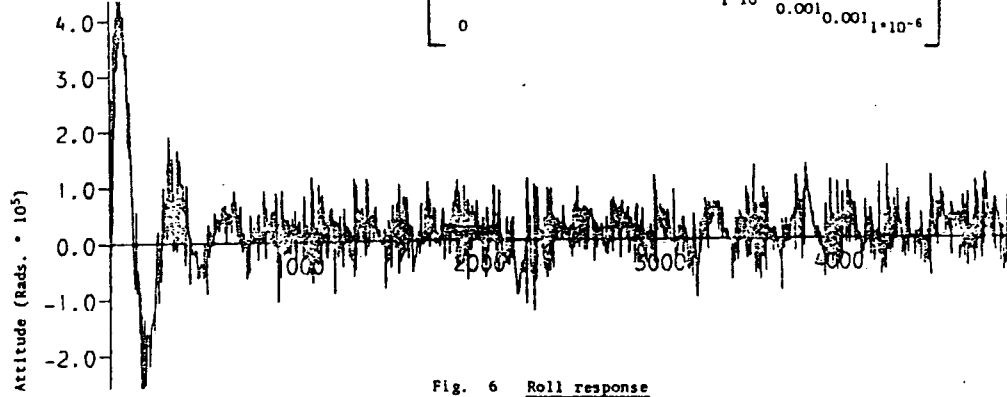
Fig. 6   Roll response

$$Q = \begin{bmatrix} 10_{0.01}10_{0.01}0.001_{1\times10^{-6}} & 0 \\ 0 & 0.001_{1\times10^{-6}} \end{bmatrix}$$

$$R = \begin{bmatrix} 1 & 0 \\ 0 & 1 \end{bmatrix}$$
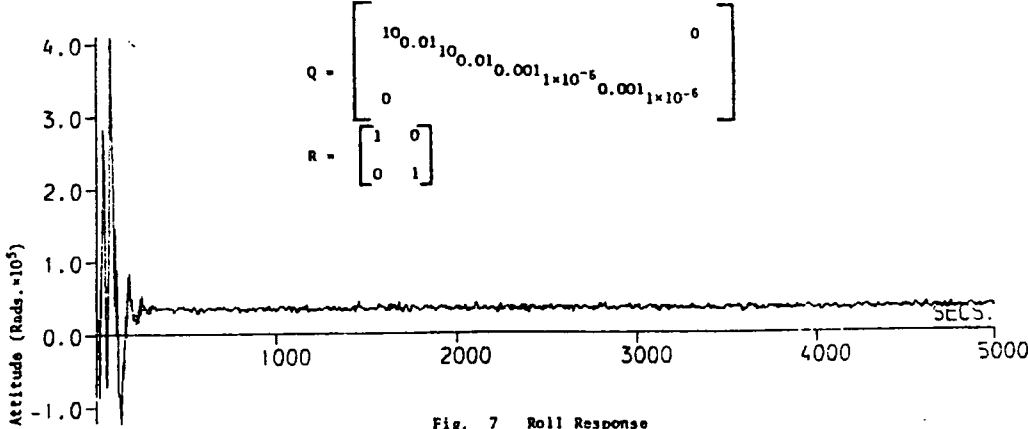
Fig. 7   Roll Response

PAPER 42

Attitude control of a flexible satellite in noisy environment

J. Fenton B.Sc., D.N.L. Horton B.Sc., and K.F. Gill B.Sc., M.Sc., Ph.D., C.Eng., M.I.Mech. E, M.I.E.E.

Indexing terms: Artificial satellites, Attitude control, Control system synthesis, Discrete systems, Lyapunov methods, Stability, State estimation

Abstract

A method is presented for the design of a discrete, state-vector feedback controller operating on an open-loop unstable process. Kalman filtering is used for state estimation and the effectiveness of this technique is evaluated for high levels of noise.

List of symbols

k = sample number
t = time
$x(t_k)$ = plant state vector at kth sampling instant
$\hat{x}(t_k)$ = estimated plant state vector at kth sampling instant
$y(t_k)$ = centre body attitude at kth sampling instant
$r(t_k)$ = process noise signal at kth sampling instant
$w(t_k)$ = measurement noise signal at kth sampling instant
$u(t_k)$ = control signal at kth sampling instant
A_1 = discrete plant matrix
B_1 = discrete plant input matrix
H = plant output matrix
I = unit matrix
$M(t_k)$ = error-covariance matrix at kth sampling instant
P = Lyapunov matrix
Q = state-weighting matrix
$R(t_k)$ = process-noise covariance matrix at kth sampling instant
$V\{x(t_k)\}$ = discrete Lyapunov function at kth sampling instant
$W(t_k)$ = measurement noise covariance matrix at kth sampling instant
T = R/W ratio
α, a_i = sum of panel flexure modes, ith panel flexure mode
β = solar panel angle
δ = Kronecker delta, dead band
θ = rigid component of centre-body attitude
σ_r, σ_w = process- and measurement-noise standard deviations

Subscripts
c denotes control torque
Bold type denotes vector quantity

Superscripts
T denotes matrix transpose
$\hat{}$ denotes estimate of

1 Introduction

With the increasing use of spacecraft in the fields of astronomy, surveillance and communications, evolves the need for precise control of vehicle attitude to aim telescopes, cameras and antennas. A typical configuration of such a vehicle is that of a relatively small rigid centre body, attached to which is a pair of solar panels as shown in Fig. 1. This layout allows simple adaptation to a wide variety of missions, and it is envisaged that these vehicles will be capable of accurate station keeping for up to seven years with a pointing accuracy of better than $\pm 0.2°$ on all three axes.

For the present generation of space vehicle, it is not current practice to actively control the panel flexure as it would appear that this does not significantly affect the attitude. It is envisaged, however, that as vehicle power requirements, and hence the size of their solar panels increase, this problem will become more acute. For this reason, a mathematical model of a hypothetical craft of similar geometrical configuration to the above, but with much larger solar panels than those possessed by present vehicles, has been derived.

The problem to be studied is the attitude control of such a vehicle when subjected to random disturbance torques in association with noisy attitude measurements. The approach adopted is to apply an optimal-filtering technique to estimate attitude information that may be used in conjunction with a state-vector feedback algorithm to control the panel flexure and orientation of the craft. The use of this control scheme removes the need to measure the panel flexure and so avoids the associated instrumentation problems.

Control of the vehicle is effected by simple on/off gas jets attached to the centre body and an attitude sensor. The performance of the roll axis control is presented; that of the yaw behaving in a similar manner.
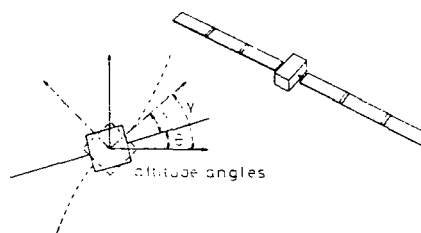
Fig. 1
Schematic diagram of vehicle

2 Dynamic model

The craft considered comprises a 2·2 m wide, 400 kg, 160 kg m² capsule, and two solar panels, each being 18 m long by 2 m wide, having a uniformly distributed mass of 2·5 kg/m² and a flexural rigidity for bending calculation purposes of 90 Nm².

The dynamic model was derived from equations formulated on the basis of the finite-element approach, with three alternative mass-matrix representations: mass model A, the simplest possible approach, uses a Myklestad type[1,2] lumped-parameter model for the appendages and a concentrated mass and moment of inertia, located at the central plane for the vehicle capsule; mass model B, a modification to A allowing for the mismatch of the actual and modelled moments of inertia; mass model C: an Archer[3,4] type consistent mass matrix.

The numerical values given in Table 1 show clearly that model A frequencies are in agreement for all six modes for each of the three methods of calculation employed. Similarly, the model B values found by the finite element[2] and transfer matrix[3] method are in agreement with each other, but they differ from the corresponding model A values. A similar situation exists for model C with the four lower modes, but some variation exists in the fifth and sixth modes. This indicates, as would be expected, that the calculated natural frequencies are more dependent on the choice of mass-distribution model than the analytical procedure adopted.

The effect of increasing the number of elements from 8 to 14 was investigated, but the changes were so small, particularly with model C, that the authors believe a model comprising eight elements is adequate for control-system design purposes.

In the solution of this particular problem it was found that the additional axis transformation involved in the use of the hybrid co-ordinate method[6] nullifies the doubtful advantage of being able to represent the capsule as a truly rigid body, with the subsequent reduction in the number of degree of freedom.

3 Control algorithm design

The algorithm presented permits the development of a discrete state-vector feedback control law. This is shown to maintain a high pointing accuracy in a noisy environment and suppress appendage flexure in a highly flexible space vehicle.

The control law is based on the Lyapunov stability method, and for completeness this technique is briefly described.

The process shown in Fig. 2 can be represented in discrete form as

$$x(t_{k+1}) = A_1 x(t_k) + B_1 u(t_k) + B_1 r(t_k) \qquad (1)$$

$$y(t_k) = Hx(t_k) + w(t_k) \qquad (2)$$

Table 1
NATURAL FREQUENCIES RAD/S) FOR THE SPACECRAFT SPECIFIED

Mode Number	Finite element method			Hybrid co-ordinate method	Transfer matrix method		
	model A	model B	model C	model A	model A	model B	model C
1	0·0455	0·0511	0·0512	0·0485	0·0484	0·0510	0·0512
2	0·1577	0·1909	0·1742	0·1577	0·1576	0·1909	0·1740
3	0·2568	0·3213	0·3005	0·2569	0·2568	0·3213	0·2996
4	0·4707	0·6105	0·5335	0·4707	0·4707	0·6104	0·5296
5	0·6227	0·6886	0·8283	0·6227	0·6226	0·6887	0·7175
6	1·0034	3·2881	1·0612	1·0040	1·0034	3·2880	0·8303

where $u(t_k)$ is the input at the kth sampling instant, and $r(t_k)$ and $w(t_k)$ are noisy process and measurement signals, respectively. It is assumed that $r(t_k)$ and $w(t_k)$ are zero-mean uncorrelated white-noise sequences with covariance matrices

$$R(t_k)\delta_{kj} = E\{r(t_k)r^T(t_j)\} \qquad (3)$$

$$W(t_k)\delta_{kj} = E\{w(t_k)w^T(t_j)\} \qquad (4)$$

where δ_{kj} is the Kronecker delta.

The discrete Lyapunov function $V\{x(t_k)\}$ can be defined as follows (for ease of presentation a single-input case is considered here):

$$V[x(t_k)] = x^T(t_k)Px(t_k) \qquad (5)$$

where P is a positive-definite symmetric matrix. The change in V over a sampling period is

$$\Delta V[x(t_k)] = V[x(t_{k+1})] - V[x(t_k)] \qquad (6)$$

Substitution of eqns. 1 and 5 into eqn. 6 yields

$$\Delta V[x(t_k)] = x^T(t_k)(A_1^T P A_1 - P)x(t_k) + u^2(t_k) B_1^T PB_1$$
$$+ 2u(t_k)B_1^T PA_1 x(t_k) \qquad (7)$$

For a given values of $x(t_k)$, A_1, B_1 and P, ΔV will be a minimum when:

$$\frac{\partial(\Delta V)}{\partial u} = 0 \quad \text{and} \quad \frac{\partial^2(\Delta V)}{\partial u^2} > 0$$

The second condition is satisfied, since

$$2B_1^T PB_1 > 0 \qquad (8)$$

This is always positive because P is positive definite. Thus the minimum value of ΔV occurs when the first derivative is zero, i.e. when

$$u_{min} = -[B_1^T PA_1 x(t_k)](B_1^T PB_1)^{-1} \qquad (9)$$

Substitution of eqn. 9 into eqn. 7 yields

$$\Delta V[x(t_k)]_{min} = x^T(t_k)(A_1^T PA_1 - P)x(t_k)$$
$$- [B_1^T PA_1 x(t_k)]^2 (B_1^T PB_1)^{-1} \qquad (10)$$

The first term is negative definite if

$$A_1^T PA_1 - P = -Q \qquad (11)$$
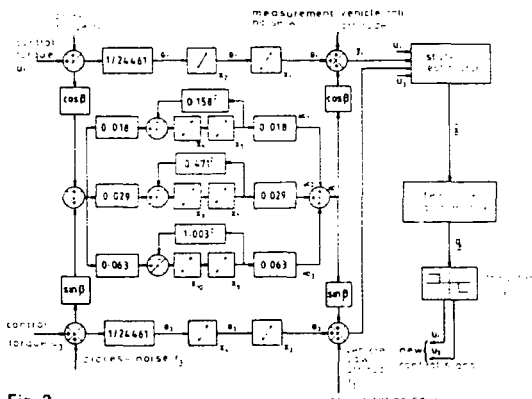
where Q is a positive-definite symmetric matrix. (The solution of eqn. 11 for P will ensure that P is positive definite and symmetric, thus satisfying the assumption in eqn. 5.) The second term in eqn. 10 is positive definite, hence ΔV_{min} is negative definite. Asymptotic stability is therefore guaranteed.

In choosing u according to eqn. 9 it is assumed that no restrictions are imposed on the values which u may take. In this application, however, this is not the case since control is effected by on/off gas jets. Thus the control signal u can be zero or $\pm u_c$ and will be related to u_{min} by

$$u = u_{min} \pm a \qquad (12)$$

where a is a variable quantity. Substitution of eqn. 12 into eqn. 7 yields

$$\Delta V[x(t_k)] = \Delta V[x(t_k)]_{min} + a^2 B_1^T PB_1 \qquad (13)$$

This shows that if a is sufficiently large, ΔV may become positive. Clearly, the aim will be to minimise the relay according to the following control law:

$$u = 0 \quad \text{when} \quad |q| < \delta \qquad (14a)$$

$$u = -u_c \, \text{sign}(q) \quad \text{when} \quad |q| \geq \delta \qquad (14b)$$

where $q = B_1^T PA_1 x(t_k)$ and δ is a dead band in the gas-jet values.

Substitution of eqn. 10 into eqn. 13 reveals that ΔV is negative definite if

$$[B_1^T PA_1 x(t_k)]^2 - a^2 \geq 0 \qquad (15)$$

Eqn. 15 establishes the regions in which ΔV is negative and is shown unshaded in Fig. 3. It is clear from this illustration that if the value of u_c is too great or δ is too small asymptotic stability cannot always be guaranteed. The use of this Figure enables the minimum value of dead band to be found for a given thruster torque.

To summarise, therefore, we must select a positive-definite symmetric matrix Q and solve eqn. 11 for P.[7-10] This matrix is then used to calculate the value of $B_1^T PA_1$, which is then postmultiplied by the state-vector $x(t_k)$ to generate q. The control is then switched on the sign of q, with the inclusion of a correctly chosen dead band $= \delta$. A value of 0·0002 radians (0·015°) was used for each axis, which is in excess of the minimum value obtainable from Fig. 3.

4 State estimation

For the system described by eqns. 1 to 4, the optimal least-squared estimate of the plant states[5] is given by

$$\dot{x}(t_{k+1}) = A_1 \dot{x}(t_k) + B_1 u(t_k) + K(t_k)$$
$$\{y(t_{k+1}) - H[A_1 \dot{x}(t_k) + B_1 u(t_k)]\} \qquad (16)$$

Fig. 2
State-variable diagram of the process using mass model A

β = solar panel angle
Control torque = 0·25 Nm
Sample interval = 0·25 s

Fig. 3
Regions of ΔV negative definite

where $K(t_k)$, the Kalman gain matrix, is derived from

$$M(t_{k+1}) = A_1(I - K(t_k)H)M(t_k)A_1^T + B_1 R(t_k)B_1^T \qquad (17)$$

$$K(t_{k+1}) = M(t_{k+1})H^T[HM(t_{k+1})H^T + W(t_{k+1})]^{-1} \qquad (18)$$

and $M(t_k)$ is defined as the covariance matrix of the error in the best linear estimation, or

$$M(t_k) = E\{[x(t_k) - \hat{x}(t_k)][x(t_k) - \hat{x}(t_k)]^T\} \qquad (19)$$

In order to provide acceptable state estimation and the ability to reject high-frequency noise, the Kalman filter must operate between two limits, which are

(i) the case when the filter gain is so low that it attenuates the measured signals as well as the noise to such a degree that inadequate state estimation results[9]

(ii) the situation where the filter has such a wide bandwidth and high gain that it passes noise as well as the required states.

If accurate noise statistics for the plant exist, then a filter can be obtained from a solution of eqns. 16, 17 and 18 which represent an adaptive optimal filter.

A solution of these equations for the case of a highly flexible satellite could create the need for substantial on-board computing power; and this, coupled with the fact that the noise signals affecting the craft cannot be identified with confidence, poses the following questions:

(a) the effectiveness of a stationary filter in predicting useful plant states for control

(b) the need for an adaptive filter and the frequency with which it would have to be updated to avoid large computational cost.

The steady-state filter gain is affected by the ratio $T(= R/W)$. If T is small, i.e. the measurement noise contamination is high relative to the process noise, then the magnitude of the filter gain is low, placing more reliance on the predicted rather than the measured value.

Therefore the third area of interest is the effect that varying T has on the control of the craft and the amount of fuel used since this represents a condition of mismatch between the actual noise the plant experiences and that assumed in the computation of the filter gain.

5   Simulation results and discussion

A number of simulation runs was undertaken employing both stationary and adaptive Kalman filters for state estimation. The results are presented in two parts to illustrate:

(i) the influence that varying T has on the vehicle performance

(ii) the effectiveness of a stationary filter compared with an adaptive filter under conditions of varying noise statistics.

Table 2
SIMULATION PARAMETERS

$\sigma_r = 0.125 \, \text{Nm}$
$\sigma_w = 0.005 \, \text{rad}$
Dead band $\delta = 0.0002$ rad roll and yaw
Initial conditions = 0.025 rad roll and yaw
Control torque = 0.25 Nm
$\beta = 30°$

$$Q = \begin{bmatrix} 10.0 & & & & & & & & \\ & 0.001 & & & & & & & \\ & & 10.0 & & & & & \text{zeros} & \\ & & & 0.001 & & & & & \\ & & & & 0.001 & & & & \\ & & & & & 0.0000001 & & & \\ & & & & & & 0.001 & & \\ \text{zeros} & & & & & & & 0.0000001 & \\ & & & & & & & & 0.001 \\ & & & & & & & & 0.0000001 \end{bmatrix}$$

Ratio T	Fuel usage, s		Control	Estimation
	roll	yaw		
1.0	2.5	1.25	poor	poor
10.0	31.25	18.25	poor	poor
100.0	101.00	63.50	good	good
500.0	223.00	152.00	good	good
625.0	426.50	193.75	good	good
5000.0	795.50	519.50	good	good
10000.0	1383.25	989.50	good	good

6   Variation of T

The noise statistics were kept constant with $\sigma_r = 0.125 \, \text{Nm}$ and $\sigma_w = 0.005 \, \text{rad}$, which represented a noisy disturbance torque with a standard deviation of half the control torque and an attitude sensor noise with a standard deviation of $0.25°$. These conditions were considered to be a rigorous test for the control system designed. The correct value of T for the optimal filter was therefore

$$\left(\frac{\sigma_r^2}{\sigma_w^2}\right) = 625$$

T was varied in the range of $1-10000$ and a summary of the results for a set of simulations, each of 3000 s, is contained within Table 2 together with a list of basic parameters common to all the simulations. The control performance was considered 'good' if the major transient decayed within 600 s. The estimator was also good if the states reproduced possessed predominantly similar characteristics in phase and amplitude.

It can be seen that acceptable control is achieved for a wide range of T, which shows that the filter still provides good state estimates even with considerable mismatch between the actual and assumed noise statistics. However, as the filter gain is increased, control is achieved only by excessive fuel consumption.

A comparison can be made between the results for values of T of 625 and 10000 from Figs. 4a and b and 5a and b, respectively. From Fig. 4b, it is noteworthy that the majority of the jet firetime occurred within the transient period, and from Fig. 4a, that the jets ceased to fire once the dead band was entered.

This is not the case when $T = 10000$, since the jets are firing almost continuously (Fig. 5b), whereas the transient response (Fig. 5a) is similar to that of Fig. 4a. This clearly shows that noise is being passed by the higher-gain filter to perturb the vehicle and so activate the thrusters.

7   Adaptive-filter performance

In order to compare the adaptive and stationary filters, the simulation run time was increased from 3000 to 6000 s. The noise

Fig. 4
Simulation results without noise mismatch

statistics were initially as for the preceding Section and then the measurement noise was stepped up by a factor of five after 2000 s had elapsed. The starting filter gain was computed using the initial noise statistics and then updated every 500 s as the simulation progressed.

Fig. 6 presents the results of the stationary filter ($T = 625$) and Fig. 7 those of the adaptive filter. The behaviour of the system with the stationary filter was affected considerably by the sudden noise jump, which caused the panels to vibrate continuously as the thrusters were fired to counter the disturbance, resulting in a large fuel consumption.
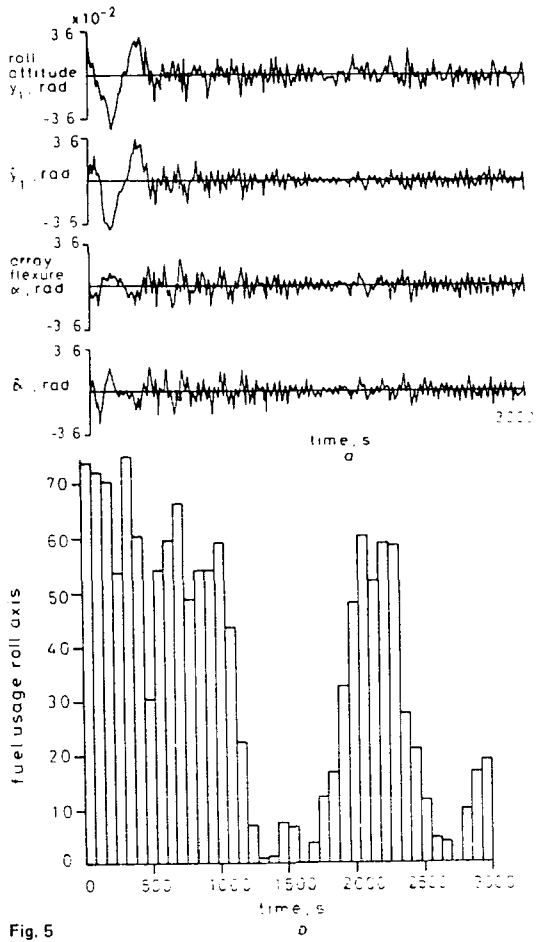

Fig. 5
Simulation results with mismatch

The adaptive filter reacted much better: the fuel usage was halved and the panel vibration was less pronounced, showing the results of enhanced noise rejection properties.

8 Computional cost of adaptive filter

It was found only necessary to recompute the Kalman-filter gain every 500 s and then relatively few iterations were needed before convergence. The c.p.u. time used was evaluated for a set of runs on a PDP 11/70 minicomputer and this was in the region of 10 s, representing a small fraction of the time the vehicle was being observed.

9 Choice of Q matrix

The feedback control matrix was selected by using a range of weighting values for the diagonal elements of the Q matrix and observing the results of the simulation runs. The values were chosen so that the displacement terms were weighted several orders of magnitude higher than the velocity terms. In addition it was found necessary to separate the centre body and mode terms in a similar manner, which in essence gives preference to the vehicle attitude, over the panel flexure. The Q matrix used for the production of the simulation results is contained within Table 2.

10 Sensitivity of control scheme to process variations

Although the control and filter gains were evaluated assuming a constant value of β, which normally varies with time, these

were found to provide acceptable control even when a mismatch in β of 90° was present.

The simulation study indicated that up to ± 30% variation in the flexible frequencies could be tolerated in the presence of noise, and large variations are possible with reduced noise levels. This justifies the use of the simple mass model A in the production of the process model.

11 Conclusions

The control algorithm employed gave good pointing accuracy, 0.12° r.m.s., for the noise statistics given in Table 2. This indicates that good state estimation was achieved even with mismatch between the actual and assumed noise statistics.

The use of Fig. 3 aids the design engineer in his choice of dead band since the minimum possible value to ensure guaranteed stability for a chosen thruster torque is indicated.

A further reduction in fuel usage and panel flexure was obtained with the use of an adaptive filter, necessitating a marginal increase in computation time.
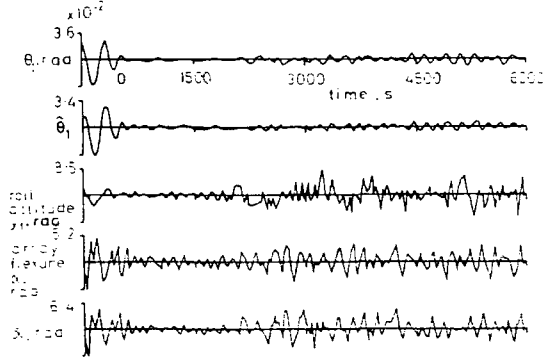

Fig. 6
Simulation results for nonadaptive filter
Roll gas: 2171 s
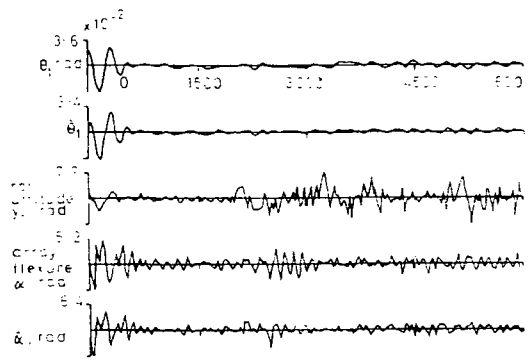Yaw gas: 2317 s
Time scale: 6000 s

Fig. 7
Simulation results for adaptive filter
Roll gas: 1018 s
Yaw gas: 1143 s
Time scale: 6000 s

12 References

1 MYKLESTAD, N.O.: 'A new method of calculating natural modes of uncoupled bending vibration of airplane wings and other types of beams', *J. Aeronaut. Sci.*, 1944, 11, pp. 153–162
2 LONGBOTTOM, G.: 'Dynamic modelling of structural frames'. M.Phil. thesis, University of Leeds, 1973
3 ARCHER, J.S.: 'Consistent mass matrix for distributed systems', *Proc. Am. Soc. Civ. Eng.*, 1963, 89, (2), pp. 161–178
4 LECKIE, F.A., and LINDBERG, G.M.: 'The effect of lumped parameters on beam frequencies', *Aeronaut. Q.*, 1963, 14, (3), pp. 224–240
5 PESTEL, E.C., and LECKIE, F.A.: 'Matrix methods in elastomechanics' (McGraw-Hill, 1963)
6 SMART, D., GILL, K.F., GETHING, J.H., and HOLT, J.A.: 'Dynamic analysis of flexible space vehicles having uncoupled control axes', *Aeronaut. J.*, 1974, 78, pp. 560–569
7 SMITH, R.A.: 'Matrix equation XA + BX = C', *SIAM J. Appl. Math.*, 1968, 16, pp. 198–200
8 KALMAN, R.E. and BUCY, R.S.: 'New results in linear filtering and prediction theory', *Trans. ASME J. Basic Eng.*, 1961, 83, pp. 95–108
9 FITZGERALD, R.J.: 'Divergence of the Kalman filter', *IEEE Trans.*, 1971, AC-16, pp. 736–747
10 GETHING, J.M.: 'Attitude control of a momentum stabilised communication satellite having large flexible appendages', Ph.D. thesis, University of Leeds, 1973

PAPER 43

Flexible spacecraft attitude control using a simple $P + D$ algorithm

J. FENTON AND K. F. GILL
Department of Mechanical Engineering, University of Leeds

1. INTRODUCTION

Two philosophies for the attitude control of space vehicles with flexible appendages have appeared in the literature, these are:

(i) control of the rigid centre body to lie within some bounded region while the flexural vibrations are allowed to behave in an uncontrolled manner[1,2];

(ii) control of all plant states to some finite value as time tends to infinity[3,4].

The former method does not require flexural information and therefore avoids the on-board computational burden associated with state estimation, or the cost of additional instrumentation. However, attitude degradation has been observed and reported[5,6] indicating a clear need to compensate for structural vibrations.

An intermediate approach between these philosophies is to update the computational procedure used to select the coefficients of the proportional plus derivative controller by including the flexural data. The method adopted is based on the design procedure of Paraskevopoulos[7] and is equally applicable in other areas of aeronautical control.

2. DESCRIPTION OF FLEXIBLE SPACE VEHICLE

The configuration of the space vehicle considered in this study is shown in Fig. 1. The satellite is assumed to be operating in a near polar circular orbit around the earth. This orbit is synchronised with the sun and precesses at the same rate as the earth, thus the satellite is required to make no orbital corrections. The craft operates in a fine pointing mode and the orbit reference axes nominally aligned with the satellite body are defined as follows:

Axis 1 — the roll axis is directed along the line of flight;
Axis 2 — the pitch axis is normal to the orbit plane;
Axis 3 — the yaw axis is directed along the vector from the satellite centre of mass to the centre of the earth.

The axis set therefore rotates at orbital frequency about the pitch axis.

The solar array is mounted at the corner of one side of the asymmetric centre body by means of a boom which is orientated parallel to the negative pitch axis. The array can rotate about this axis relative to the centre body in order to maximise exposure to solar energy as the craft traverses the earth.

The vehicle is controlled by three orthogonally positioned reaction wheels, one per axis, which rotate on magnetic bearings to minimise friction. They operate with a linear torque speed characteristic until saturation occurs. A state variable model of the vehicle has been derived using data supplied by British Aerospace Dynamics Group. This data is given, together with a list of state variables, in Appendix I.

3. CONTROLLER DESIGN

The design procedure, detailed elsewhere[7] is included for completeness.
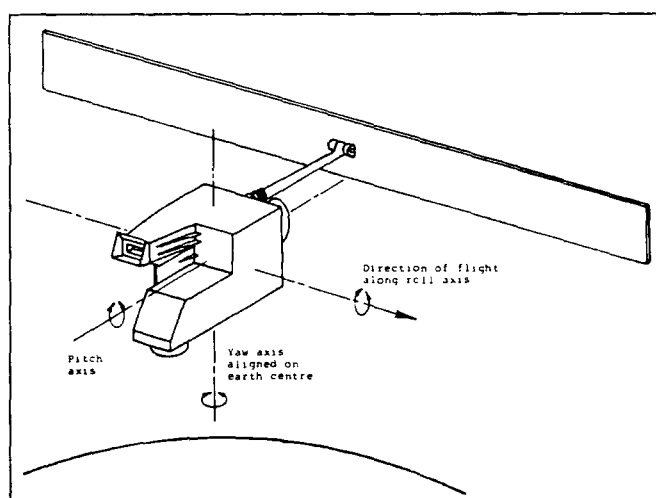
Describing the system in state variable form

Figure. 1 Proposed satellite.

Paper No 890

$$\dot{x} = Ax + Bu$$
$$y = Cx \qquad \qquad \dots \quad (1)$$

where the vectors x, u and y have the dimensions n, m and p, respectively.
A controller is chosen to be of the form

$$u = Py + D\dot{y} \qquad \qquad \dots \quad (2)$$

with P and D constant $m{\times}p$ matrices.
Substitution of eqn. (2) into eqn. (1) yields,

$$\dot{x} = (I - BDC)^{-1}(A + BPC)x \qquad \dots \quad (3)$$

where I is the unit matrix.
To compute P and D such that the system behaves as

$$\dot{x} = Tx \qquad \qquad \dots \quad (4)$$

implies

$$T = (I - BDC)^{-1}(A + BPC) \qquad \dots \quad (5)$$

where the eigenvalues of T are chosen arbitrarily. Thus:

$$T - A = BPC + BDCT \qquad \dots \quad (6)$$

which can be rewritten

$$Z = BME \qquad \qquad \dots \quad (7)$$

where

$$Z = T - A$$

M is the $m{\times}2p$ partitioned matrix.

$$M = [P\,\vert\,D]$$

and E is the $2p \times n$ partitioned matrix

$$E = \left[\frac{C}{CT} \right]$$

In general B and E are non-square matrices thus,

$$M = (B^{T}B)^{-1}\,B^{T}\,Z\,E^{T}(EE^{T})^{-1} \qquad \dots \quad (8)$$

The matrix inverses exist if the columns of B and the rows of C are linearly independent, otherwise the model is not of minimal order and is reducible. The rows of T must be linearly independent of the rows of the unit matrix I.

4. CHOICE OF T MATRIX

For the 14th order system under consideration the problem of positioning a multiplicity of poles is not easily resolved. Therefore, the method adopted to compute the matrices P, D, was to choose T such that

$$T = A - BG \qquad \qquad \dots \quad (9)$$

where G is the state control matrix derived from a solution of the matrix Riccati equation[8].

5. SIMULATION STUDY

The objectives of the simulation study are defined below:

(i) To determine the applicability of the controller to a high order multiaxis multimode system.
(ii) To examine the robustness of the controller when subjected to parameter mismatch.
(iii) To observe the influence of measurement noise on the pointing accuracy and transient behaviour of the vehicle.

To minimise on-board instrumentation, it is assumed that measured rate information is not readily available. To overcome this problem a pseudo differentiator algorithm is employed, with the following transfer function

$$P(s) = \frac{s}{1 + as}$$

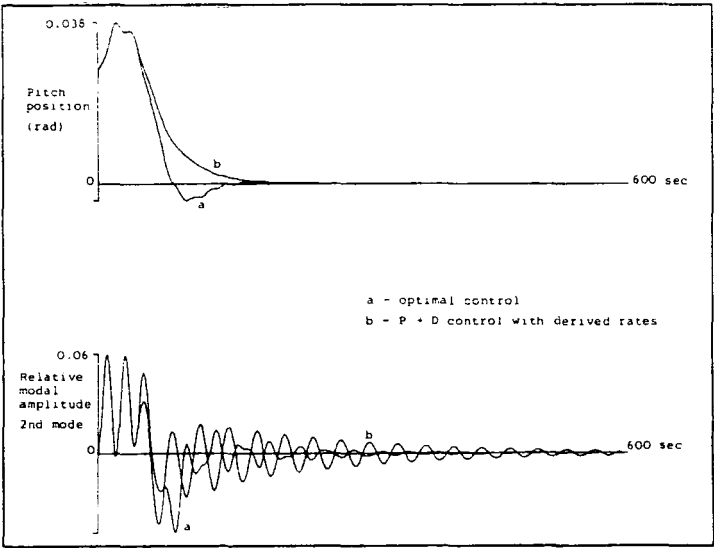where a is adjusted to achieve an acceptable response:

$$a = 0.2$$

Figure 2. Comparison of the pitch and second mode response using optimal and $P + D$ controllers.

a - optimal control

b - P + D control with derived rates

The evidence obtained during the simulation study suggests that no major deterioration in craft performance will result from the replacement of the full state vector feedback control algorithm, by the much simpler proportional plus derivative control law in the absence of measurement noise.

Figure 2 is typical of the behaviour observed for all three axes and flexural mode vibrations. The trend is for the optimal response to decay more quickly than that of the proportional plus derivative.

The introduction of measurement noise, standard deviation 0·03° , does result in degradation of the vehicle behaviour causing the flexural mode responses to be more violent and constantly excited as illustrated in Fig. 3. The vehicle attitude control becomes more oscillatory, (Fig. 4), and requires a significant increase in settling time. Progressively increasing the magnitude of the measurement noise will ultimately lead to instability. Figure 5 indicates clearly the reason for this deterioration in performance since the derivative term acts as a noise amplification process and the derived rate signal becomes noise.

The algorithm is for all practical purposes insensitive to variation in the mode frequencies as demonstrated in Fig. 6, for both an increase and a decrease in frequency. No appreciable difference in system response occurred for positional variations of the solar array.

6. CONCLUSIONS

The results of this work show that a control algorithm utilising attitude positions and derived rates can provide adequate attitude control and regulation of flexural motion, comparable with that obtained from full state vector feedback, if measurement noise can be suppressed.

If measured rates are available for use in the control scheme the measurement noise loses its importance and more stringent control is possible. The control algorithm is robust and will tolerate a high degree of process mismatch.

Preliminary knowledge of the pole positions for acceptable control can be found by means of the Klienman stabilising algorithm[9] to avoid solution of the Riccati equation at the early stages of design.
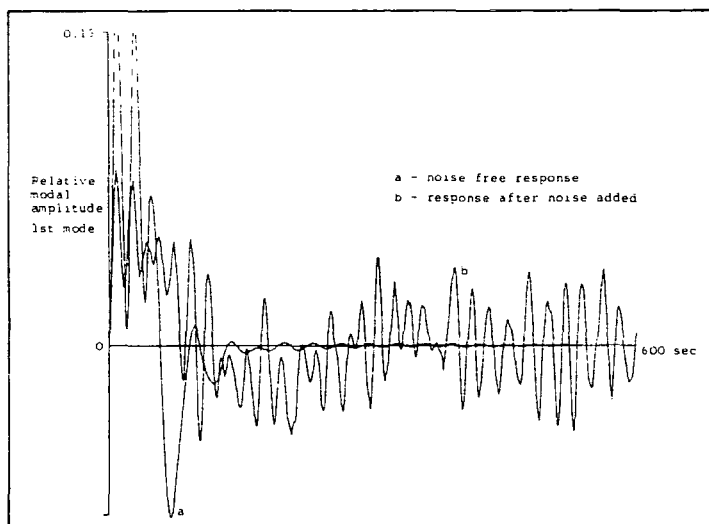
Figure 3. Comparison of the first mode vibration before and after the addition of measurement noise.
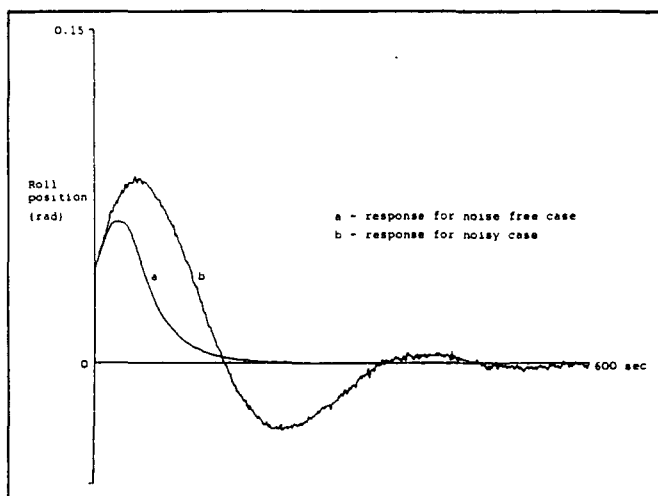

Figure 4. Comparison of roll axis response after addition of measurement noise.
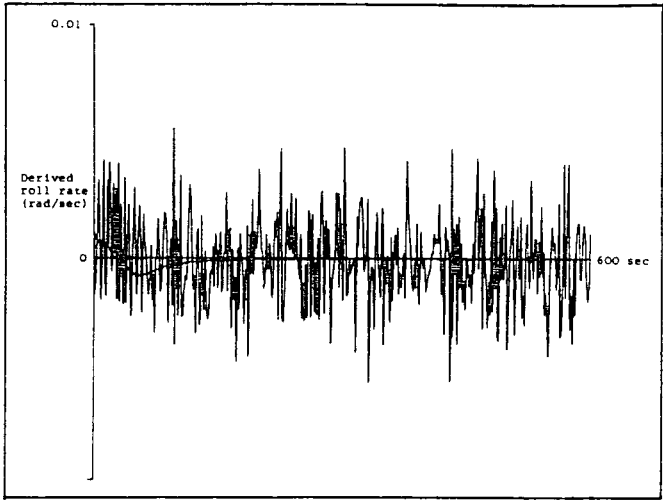
Figure 5. A comparison of the noise free and noisy derived roll rate.

a – response for actual frequencies
b – response for twice actual frequencies

c – response for actual frequencies
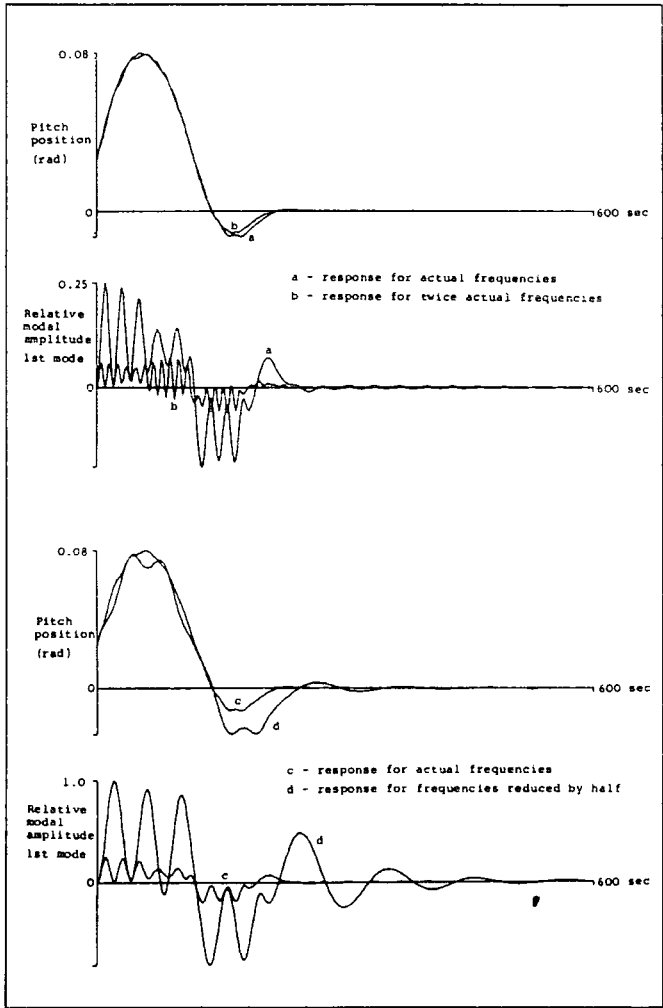d – response for frequencies reduced by half

Figure 6. Showing the effect of frequency mismatch on the system response.

REFERENCES

1. BEYSENS, A. Design of a control loop with flexibility and in-flight identification of the flexible modes. *Dynamics and Control of Non-rigid Spacecraft*, ESA SP-117, pp 273-283, July 1976.
2. HARRIS, R. S., and TODMAN, D. C. Three axis control of spacecraft with large flexible appendages. *Dynamics and Control of Non-rigid Spacecraft*, ESA SP-117, pp 285-296, July 1976.
3. GETHING, J. M. and GILL, K. F. An attitude control system for a flexible satellite providing active damping of flexural motion. *The Aeronautical Journal of the Royal Aeronautical Society*, Vol 80, No 783, pp 134-139, March 1976.
4. LARSON, V., LIKINS, P., and MARSH, E. Optimal estimation and attitude control of a solar electric propulsion spacecraft. *Transactions IEEE*, Vol AES-13, No 1, pp 35-46, January 1977.
5. NOLL, R. B., DEYST, J. J., and SPENNY, C. H. A survey of structural flexibility effects on spacecraft control systems. AIAA Paper No 69-116, presented at the AIAA 7th Aerospace Science Meeting, New York, 20th-22nd January, 1969.
6. LIKINS, P. W. Interactive problems between the dynamics and control system for non-rigid spacecraft. *Dynamics and Control of Non-rigid Spacecraft*, ESA SP-117, pp 265-271, July 1976.
7. PARASKEVOPOULOS, P. N. On pole assignment by proportional plus derivative output feedback. *Electronics Letters*, Vol 14, No 2, pp 34-35, January 1976.
8. ANDERSON, B.D.O., and MOORE, J. B. *Linear Optimal Control*. 1st Edition, Prentice-Hall, 1971.
9. KLIENMAN, D. L. An easy way to stabilise a linear constant system. *IEEE Transactions of Automatic Control*, Vol AC 15, pp 692, December 1970.

APPENDIX I. DATA

The first six states comprise the roll, pitch and yaw positions each followed by the corresponding attitude rate. The remaining eight states are the first, second, third and fourth modes of solar array vibration, each followed by the corresponding rate.

1. Spacecraft

Solar panel angle $0°$
Mass − 1648 kg
Inertia Matrix, E:

$$\begin{bmatrix} 6713.0 & -896.0 & -37.0 \\ -896.0 & 6335.0 & -147.0 \\ -37.0 & -147.0 & 12370.0 \end{bmatrix} \text{kgm}^2$$

2. Control

Control saturation torque, $u_{sat} : 0.2$ Nm
Control cost matrix, $\text{diag}[1, 1, 1,]$
State cost matrix, $\text{diag}[1000, 10, 1000, 10, 1000, 10, 1, 1, 1, 1, 1, 1, 1, 1.]$

Resultant G matrix

$$\begin{bmatrix} 31.2 & 645.6 & -0.008 & -45.48 & -0.042 & -5.325 & 0.0095 \\ -0.007 & -45.0 & 30.94 & 620.4 & -0.0014 & -7.04 & 0.566 \\ 0.417 & -3.773 & 0.003 & -7.04 & 31.3 & 879.2 & 0.0459 \end{bmatrix}$$

$$\begin{bmatrix} 0.436 & 0.165 & 1.235 & 0.0004 & -0.004 & 2.49 & 1.267 \\ 5.377 & 0.117 & 1.456 & 0.0116 & 0.056 & 3.973 & 0.435 \\ 0.0003 & 0.017 & -0.016 & 0.40 & 4.566 & 0.172 & 0.0108 \end{bmatrix}$$

Proportional matrix P

$$\begin{bmatrix} -31.153 & 0.233 & 0.311 \\ 0.03 & -30.534 & -0.46 \\ -0.299 & 0.519 & -31.206 \end{bmatrix}$$

Derivative matrix D

$$\begin{bmatrix} -653.94 & 49.138 & 2.185 \\ 43.935 & -653.31 & -5.778 \\ 5.737 & 17.942 & -879.8 \end{bmatrix}$$

3. Plant matrices

Matrix A:

$$\begin{bmatrix} 0 & 1 & 0 & 0 & 0 & 0 & 0 \\ 0 & 0 & 0 & 0 & 0 & 1.0 \times 10^{-3} & 1.027 \times 10^{-3} \\ 0 & 0 & 0 & 1 & 0 & 0 & 0 \\ 0 & 0 & 0 & 0 & 0 & 0 & 5.294 \times 10^{-3} \\ 0 & 0 & 0 & 0 & 0 & 1 & 0 \\ 0 & -1.0 \times 10^{-3} & 0 & 0 & 0 & 0 & 2.378 \times 10^{-4} \\ 0 & 0 & 0 & 0 & 0 & 0 & 0 \\ 0 & 0 & 0 & 0 & 0 & 0 & -0.4628 \\ 0 & 0 & 0 & 0 & 0 & 0 & 0 \\ 0 & 0 & 0 & 0 & 0 & 0 & -0.0662 \\ 0 & 0 & 0 & 0 & 0 & 0 & 0 \\ 0 & 0 & 0 & 0 & 0 & 0 & -0.0283 \\ 0 & 0 & 0 & 0 & 0 & 0 & 0 \\ 0 & 0 & 0 & 0 & 0 & 0 & -0.0414 \end{bmatrix}$$

$$\begin{bmatrix} 0 & 0 & 0 & 0 & 0 & 0 & 0 \\ 0 & 1.08 \times 10^{-3} & 0 & 2.604 \times 10^{-4} & 0 & 2.738 \times 10^{-2} & 0 \\ 0 & 0 & 0 & 0 & 0 & 0 & 0 \\ 0 & 1.846 \times 10^{-3} & 0 & 1.236 \times 10^{-3} & 0 & 4.436 \times 10^{-2} & 0 \\ 0 & 0 & 0 & 0 & 0 & 0 & 0 \\ 0 & 8.68 \times 10^{-5} & 0 & 3.34 \times 10^{-3} & 0 & 2.096 \times 10^{-3} & 0 \\ 1 & 0 & 0 & 0 & 0 & 0 & 0 \\ 0 & -0.127 & 0 & -0.0849 & 0 & -3.048 & 0 \\ 0 & 0 & 1 & 0 & 0 & 0 & 0 \\ 0 & -0.229 & 0 & -0.0160 & 0 & -0.98 & 0 \\ 0 & 0 & 0 & 0 & 1 & 0 & 0 \\ 0 & -0.010 & 0 & -0.551 & 0 & -0.245 & 0 \\ 0 & 0 & 0 & 0 & 0 & 0 & 1 \\ 0 & -0.0254 & 0 & -0.01 & 0 & -7.912 & 0 \end{bmatrix}$$

Matrix B:

$$\begin{bmatrix} 0 & 0 & 0 \\ 1.97 \times 10^{-4} & 1.51 \times 10^{-4} & 7.7 \times 10^{-6} \\ 0 & 0 & 0 \\ 1.51 \times 10^{-4} & 7.781 \times 10^{-4} & 3.495 \times 10^{-5} \\ 0 & 0 & 0 \\ 7.7 \times 10^{-6} & 3.495 \times 10^{-5} & 1.499 \times 10^{-4} \\ 0 & 0 & 0 \\ -1.037 \times 10^{-2} & -5.346 \times 10^{-2} & -2.4 \times 10^{-3} \\ 0 & 0 & 0 \\ -5.69 \times 10^{-3} & -9.73 \times 10^{-3} & -4.57 \times 10^{-4} \\ 0 & 0 & 0 \\ -8.761 \times 10^{-4} & -4.159 \times 10^{-3} & -1.131 \times 10^{-2} \\ 0 & 0 & 0 \\ -3.762 \times 10^{-3} & -6.097 \times 10^{-3} & -2.879 \times 10^{-4} \end{bmatrix}$$

Matrix C:

$$\begin{bmatrix} 1 & 0 & 0 & 0 & 0 & 0 & 0 \\ 0 & 0 & 1 & 0 & 0 & 0 & 0 \\ 0 & 0 & 0 & 0 & 1 & 0 & 0 \\ & & & & & & \\ 0 & 0 & 0 & 0 & 0 & 0 & 0 \\ 0 & 0 & 0 & 0 & 0 & 0 & 0 \\ 0 & 0 & 0 & 0 & 0 & 0 & 0 \end{bmatrix}$$

4. Orbit

Frequency, $\omega_0 : 0.001$ rad s^{-1}
Period, $2\pi/\omega_0 : 104.7$ minutes
Altitude, 800 km

PAPER 44

Attitude estimation and control of a flexible spacecraft using inertial and optical measurements

D. HORTON, J. FENTON and K. F. GILL
Department of Mechanical Engineering, The University of Leeds

1. INTRODUCTION

It is envisaged that future earth resources satellites will be required to perform frequent attitude manoeuvres and also to maintain a given orientation to within a few seconds of arc. These requirements place a severe demand on the attitude measurement and control systems used, and this demand is increased when the satellite needs to carry large flexible solar arrays[1,2].

By combining inertial and optical measurements using an optimal filter, an attitude estimate can be obtained for which the error components are minimised over a wide frequency band. Jude[3], used intermittent star sensor readings to update the attitude and gyroscope drift estimates from an optimal filter and he noted that it would be useful to study the effect of mismatch between actual sensor models and those assumed in the computation of the optimal filter. Jude's recommendation is investigated in this paper.

2. VEHICLE DYNAMICS

The spacecraft consists of a rigid centre body with a flexible solar array attached asymmetrically as shown in Fig. 1. It is assumed to be operating in fine-pointing mode with the yaw axis directed towards the earth's centre and all three axes dynamically coupled, control being effected by a reaction wheel on each axis. The near-polar circular orbit precesses at a rate of one degree per day, thus maintaining a constant angle between the orbital plane and the earth-sun line. Physical data and orbital characteristics are detailed in the full report.

Attitude is measured by three rate-integrating gyroscopes, one on each axis, together with an infra-red earth sensor (IRES) on each of the roll and pitch axes, and a sun sensor on the yaw axis. The gyroscope and IRES measurements are taken and processed continuously but the sun sensor may only be read intermittently, nominally twice per orbit, owing to the orbital configuration assumed.

The plant dynamics and control are presented in state variable form in Fig. 2 and the theoretical derivations are given in the full report.

3. VEHICLE CONTROLLER

The vehicle control is based on minimisation of the quadratic cost functional defined as:
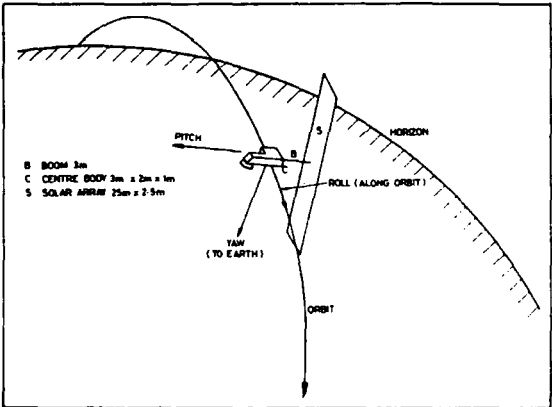
$$J = \Sigma \, (x^T Sx + u^T Ru) \qquad \qquad \text{. . . (9)}$$

Paper No 840.

Figure 1. Spacecraft configuration.

where S is a positive semi-definite real symmetric matrix, and R is a positive definite real symmetric matrix.

The resulting feedback law[4], where a steady state exists, is given by

$$u_k = - \, (Q^T FQ + R)^{-1} \, Q^T FP x_k \qquad \text{. . . (10)}$$

where F is the unique positive solution of the algebraic discrete Riccati equation

$$F = P^T FP - P^T FQ \, (Q^T FQ + R)^{-1} Q^T FP + S \quad \text{. . . (11)}$$

The method of solution used for eqn. (11) is that due to Hewer[4].

4. DIGITAL SIMULATION

Initially a separate filter is used to process the sun sensor measurements. This is due to the different sampling intervals used by the sun sensor, and also facilitates experimentation with various sun sensor reading modes. The simulation proceeds as follows. At each time-step k the three attitude errors ϕ, θ, ψ are passed through the gyroscope model which produces three measurements ϕ^g, θ^g, ψ^g contaminated by drift and pick-off noise. Similarly, the roll and pitch attitude errors are passed through the IRES model to produce measurements ϕ^h, θ^h. These five measurements form the vector y which is used by the Kalman filter to produce a state estimate $\hat{x}$. This is input to the controller to form a control vector u which, together with the disturbance w, drives the dynamic model. A block diagram of this process is shown in Fig. 3.
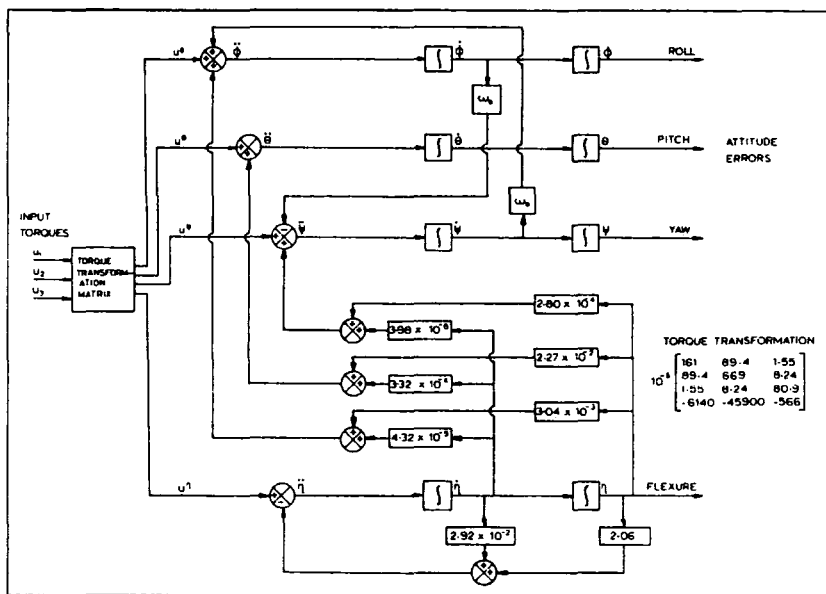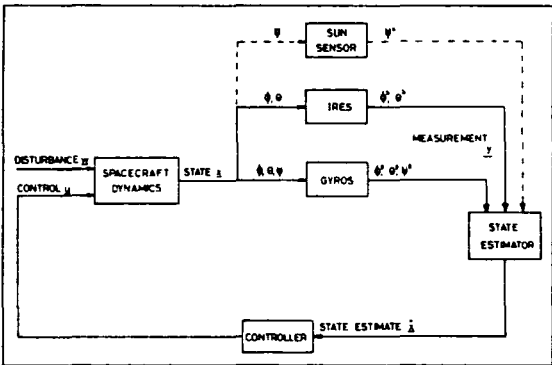
Figure 2. State variable diagram.

Figure 3. Simulation block diagram.

5. SIMULATION RESULTS

To enable yaw control to be effected at each simulation time step it is necessary to estimate yaw and yaw drift between sun sensor readings. Two methods have been investigated:

(a) Exploitation of the coupling between roll and yaw due to the orbital motion.
(b) Linear extrapolation of yaw drift from estimates at the current and previous sun sensor read times.

Comparative simulations over several orbits showed method (a) to be superior in that rms yaw error was lower by a factor of five, and so this method was used exclusively in the work on sensor models. As a consequence of this the yaw estimation could be incorporated in the Kalman filter to give a more unified design procedure.

In order to test the behaviour of the spacecraft during station acquisition a simulation was performed with an initial roll error

of 0·02 rad. Good estimates were produced and both the vehicle attitude and solar array oscillation were brought under control within 0·1 orbit (about ten minutes). Graphs of attitude, attitude estimate and control torque for the roll and pitch axes are shown in Fig. 5. In order to make the controller saturate at 0·2 Nm an initial error of 0·15 rad was required, but control was still effected within 0·1 orbit.

Subsequent simulations assumed all states to be initially zero with results averaged over three ten-orbit runs, each run using a different random number sequence for the generation of noise inputs. The sun sensor was read twice per orbit at equal intervals.

As a basis for comparison, the basic models for the gyroscopes and IRES used in computing K, were also used, together with a linear sun sensor model, in computing gyroscope drift and y during the simulations (see Fig. 4). A typical graph of yaw drift and its estimate is shown in Fig. 6, with the marks on the time axis denoting sun sensor readings. Results of noise mismatch between filter and simulation are summarised in Table 1 with each of the four noise inputs varied in turn, the other three remaining fixed.

A similar experiment was then performed using noise models incorporating extra components not included in the filter computation (Fig. 4). The results were similar to those in Table 1 except that the filter could not cope well with the unobservable biases ϕ^b, θ^b. The yaw bias ψ^b assumed less importance owing to the infrequency of the sun sensor readings. These results suggest that simple sensor models are adequate for attitude control and that good prediction of noise levels used in filter construction is at least as important as choice of these models.

As a final experiment, the mode of sun sensor reading was altered in two ways:

(a) The number of equally spaced readings per orbit was increased.
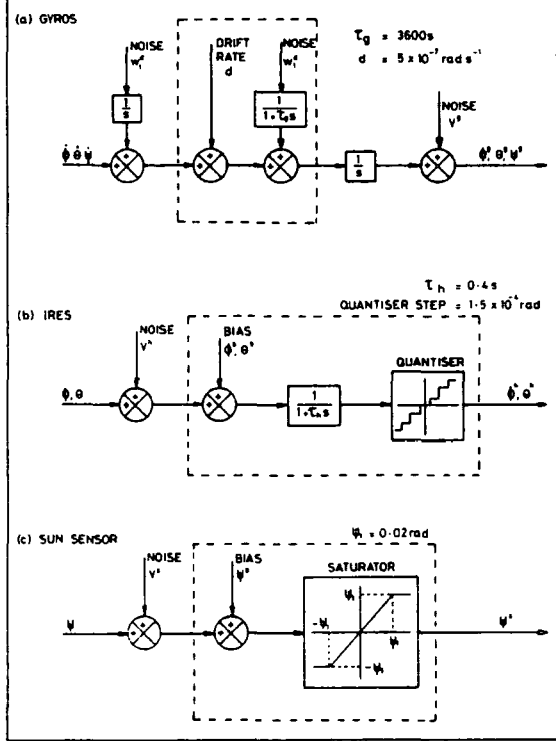(b) Readings were taken continuously during the first half of each orbit and none was taken during the second half.

(a) GYROS

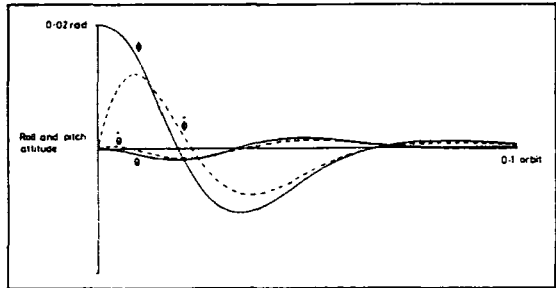NOISE w_i^d DRIFT RATE d   NOISE w_i^d NOISE v^g

τ_g = 3600s
d = 5×10^{-7} rad s^{-1}

$\dot{\phi}, \dot{\theta}, \dot{\psi}$ ϕ^g, θ^g, ψ^g

(b) IRES

NOISE v^h BIAS ϕ^b, θ^b QUANTISER

τ_h = 0·4 s
QUANTISER STEP = 1.5×10^{-4} rad

ϕ, θ ϕ^h, θ^h

(c) SUN SENSOR

NOISE v^s BIAS ψ^b SATURATOR

ψ_s = 0·02 rad

ψ ψ^s

Figure 4.   Sensor models.

0·02 rad

Roll and pitch attitude

0·1 orbit

Figure 5(a).

0·025 N m

Control torque

u_2

u_1

0·1 orbit

Figure 5(b).

0·1 rad

Yaw gyro drift

5·0 orbits
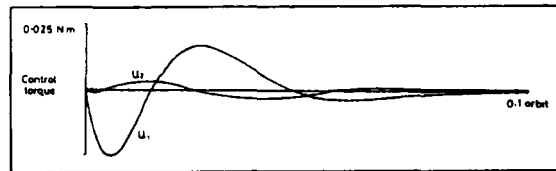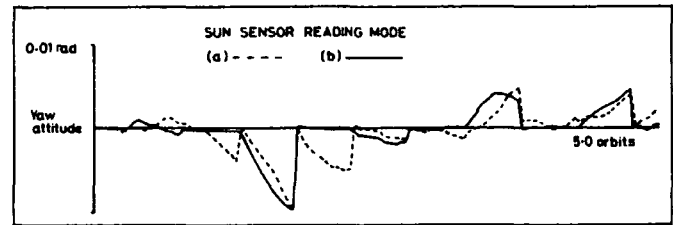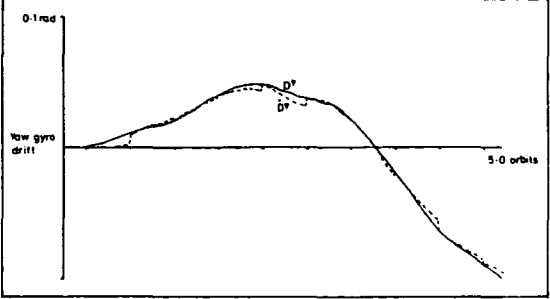
Figure 6.

Table 1   Summary of results for noise mismatch

Values used in computing the filter elements:

σ_1^d 5×10^{-7} rad
σ^g 5×10^{-6} rad
σ^h 3×10^{-4} rad
σ^s 3×10^{-4} rad

			rms ϕ	error θ	10^{-4} rad ψ
σ_1^d	$\leq$	5×10^{-7}	1.1	1.1	38
		5×10^{-6}	1.4	1.5	42
		5×10^{-5}	11.0	11.0	210
σ^g	$\leq$	5×10^{-4}	1.1	1.1	38
		5×10^{-3}	1.3	1.4	39
		5×10^{-2}	4.2	4.3	57
σ^h	$\leq$	3×10^{-5}	1.0	1.0	38
		3×10^{-4}	1.1	1.1	38
		3×10^{-3}	3.9	3.6	39
		3×10^{-2}	3.9	3.6	55
σ^s	$\leq$	3×10^{-4}	1.1	1.1	38
		3×10^{-3}	1.1	1.1	42
		3×10^{-2}	1.4	1.2	190

Table 2   Effect of varying sun sensor readings

	rms yaw error (10^{-4} rad)	Max. yaw error (10^{-4} rad)
(a) N = 2	38	160
4	17	66
8	9	38
16	6	21
(b)	20	110

0·01 rad

SUN SENSOR READING MODE
(a) - - - -   (b) ———

Yaw attitude

5·0 orbits

Figure 7.

In mode (a), measurements ψ were used to update the estimates $\hat{\psi}$ and in mode (b), when no measurement was available, $\hat{\psi}$ was given the current value of $\hat{\psi}$.

The simulations were performed with the basic noise models and standard deviations. Typical yaw profiles for (a), with N=2, and (b) are shown in Fig. 7, with some further results listed in Table 2. These results indicate that for method (a) to be equivalent to method (b), about four readings per orbit are required.

6. CONCLUSION

A method has been detailed for the simulation of the attitude measurement, estimation and control of a flexible, asymmetric spacecraft in earth orbit. For the configuration described, with typical levels of sensor and control noise, the rms attitude errors were of the order of 0·3 arc minutes in roll and pitch, and 6 arc minutes in yaw.

The power of the method, however, lies in the adaptability of the simulation program. This provides a framework in which various types of craft, number of modes of flexure, mixed sensor configurations and methods of control may be combined into a single optimal system.

REFERENCES

1. BRYSON, A. E. and KORTUM, W. Estimation of the local attitude of orbiting spacecraft. *Automatica*, Vol 7, pp 163-180. Pergamon Press, 1971.
2. JORDAN, J. F., MADRID, B. A. and PEASE, G. E. Effects of major error sources on planetary spacecraft navigation accuracies. *Journal of Spacecraft & Rockets*, Vol 9, No 3, pp 196-204, March 1972.
3. JUDE, R. J. System study of an inertial attitude measurement system for earth pointing satellites. Proceedings of the Attitude and Orbit Control Systems Conference, ESA SP-128, pp 131-144, November 1977.
4. HEWER, G. A. An iterative technique for the computation of the steady state gains for the discrete optimal regulator. IEEE Trans. Automatic Control, Vol AC-16, pp 382-383, August 1971.

PAPER 46

FLEXIBLE SPACECRAFT ATTITUDE MEASUREMENT AND CONTROL SCHEME INCORPORATING STATE ESTIMATION

J. FENTON, D. HORTON AND K. F. GILL

Department of Mechanical Engineering, The University of Leeds, Leeds LS2 9JT, U.K.

SUMMARY

The design of an attitude measurement and control scheme for a flexible space vehicle is presented. A proposed spacecraft configuration is used to study the performance of an inertial–optical measurement system incorporating a Kalman filter to obtain the best estimates in the presence of differing noise models. These estimates are used to correct for gyroscope drift and also provide the information necessary to implement optimal attitude control with active damping of the flexural motion.

KEY WORDS   Spacecraft attitude control   Control-system synthesis   Kalman filter design   Inertial-optical attitude measurements

INTRODUCTION

The progressive development of satellite capabilities for fulfilling diverse scientific duties will lead to larger more complex vehicles with associated increased power requirements.

The utilization of large solar arrays will resolve the power problem; however, the necessity for these to be as light as possible in order to remain within rocket payload confines will cause them to be highly flexible. The envisaged need for more accurate attitude stabilization will emphasize the problem of structural interaction with the spacecraft control system and the only solution to this problem may be to actively control the panel flexure.

Examples illustrating the action of anomalous flexible behaviour exist, notably the cases of O.G.O. III[1] and Mariner 10[2], both three-axes-stabilized craft. The former exhibited roll axis oscillations approaching perigee at the end of the first orbit, subsequently found to be caused by boom flexibility. The control system of the latter was excited by bending of the solar arrays and had to be deactivated for a period to conserve fuel and to allow the vehicle behaviour to return to normal.

Porcelli[3] illustrated the advantages of controlling the effects of flexibility with a simple simulation in which multiple single loop controllers were used to control two rigid bodies flexibly connected together. The drawback of the proposed scheme was that sensors and actuators were required to be mounted on each rigid body and this is impractical for the case of a highly flexible solar array.

A root locus study of a flexible spacecraft model was used by Likens[4] to aid in the choice of controller gains. This avoided structural interaction with the control system, but only passively controlled the flexible modes.

A number of control syntheses using observers have been documented. For example, Poelaert[5] used a reduced order observer to generate a function of the state vector to control a simple single-axis model of a space vehicle with flexible appendages. This method of control was found to be sensitive to model mismatch and this led to the suggestions that more complex simulations were needed including sensitivity studies.

Smith and Gill [6, 7] used a Luenburger observer to obtain the state vector of a single-axis model and actively controlled the vehicle attitude and flexure modes using Lyapunov's method.[8, 9] An attempt to extend this technique to the control of a multi-axis vehicle[10] illustrated the difficulties of designing a Luenburger observer for a high order flexible system.

Larson et al.[11] applied modern control theory to a solar electric propulsion spacecraft. Again, a single axis model was used and the effectiveness of Kalman filters designed, using reduced order spacecraft models was investigated, the outcome of this study emphasizing the importance of modelling errors.

The first part of the work presented in this paper is concerned with the design of a control system for a three-axis vehicle, including active control of the flexible modes. A detailed study is made of the robustness of the method when subjected to parameter changes, model mismatch, and noise. A model of a proposed flexible space vehicle is used and results are obtained for two ranges of bending frequencies representing those possessed by the present solar array and those of a hypothetical future array. No additional sensors or actuators are needed to control the panel vibrations.

In order to achieve accurate attitude control, information must be obtained about the rotation of the space vehicle with respect to inertial space. Gyroscopes can be used for this purpose and maintain an accurate attitude reference even when the spacecraft is rotating at high frequency. Unfortunately, it is impossible to predict accurately the spurious torques which act on the gyroscope input axes.[12]

Although normally very small, these torques become significant when accumulated over a long period and give rise to a component in the attitude measurement known as gyroscope drift. On the other hand an optical sensor, although providing an attitude reference which does not deteriorate with time, has a more restricted bandwidth than the gyroscope, and any attempt to increase this bandwidth must be accompanied by a corresponding increase in noise transmission. By combining inertial and optical measurements using an optimal filter,[13] an attitude estimate can be obtained for which the error components are minimized over a wide frequency band.

Jude[14] used intermittent star sensor readings to update the attitude and gyroscope drift estimates from an optimal filter and he noted that it would be useful to study the effect of mismatch between actual sensor models and those assumed in the computation of the optimal filter.

This recommendation by Jude has been fully investigated by the authors of this paper which presents a complete study of vehicle and measurement system performance.

VEHICLE DYNAMICS

The configuration of the satellite considered is shown in Figure 1. The solar array is mounted on a boom affixed to one side of the asymmetric centre body and can be rotated about the negative pitch axis to follow the sun. This changes the craft dynamics and is one of the effects incorporated in this study.

The craft orbits the earth in a sun synchronous near polar circular orbit. It is assumed to be operating in fine-pointing mode with the yaw axis directed towards the earth's centre and the roll axis lying along the line of flight; control of the vehicle is effected by a reaction wheel on each axis.
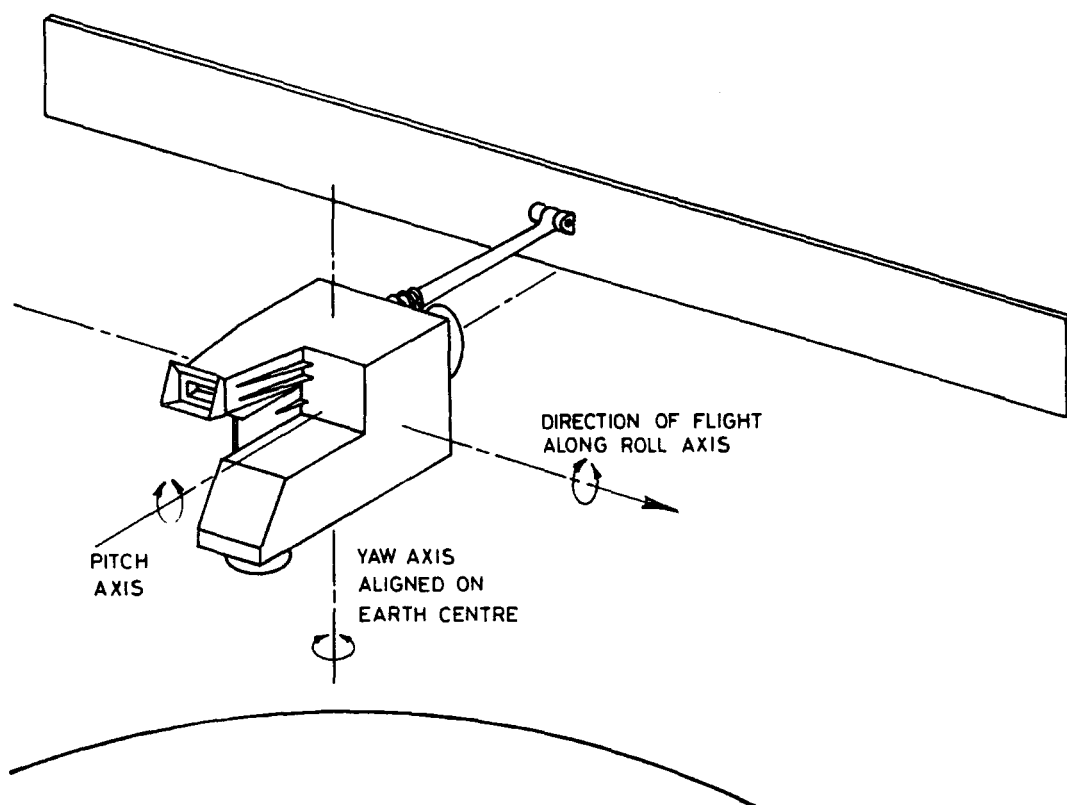
Figure 1

Attitude is measured by three rate-integrating gyroscopes, one on each axis, together with an infra-red earth sensor (IRES) on each of the roll and pitch axes, and a sun sensor on the yaw axis. The gyroscope and IRES measurements are taken and processed continuously, but the sun sensor may only be read intermittently, nominally twice per orbit, due to the orbital configuration assumed.

The hybrid co-ordinate method[15] (data supplied by British Aerospace, Bristol) is used to introduce the effects of flexibility in the vehicle dynamics. Experience has shown that major structural interaction can be attributed to those modes with the lowest vibrational frequencies involving large inertia transfers. Four modes of flexure were included in the model developed using this criterion.

For the conditions of small angle manoeuvres and small attitude rates, the spacecraft dynamics may be represented by differential equations describing roll, pitch, and yaw attitudes, and the solar array bending motion, as follows:

$$T = E\dot{\omega} - \sum_{i=1}^{n} \lambda_i \ddot{\eta}_i \qquad (1)$$

$$\ddot{\eta}_i + 2\xi_i \omega_{0i} \dot{\eta}_i + \omega_{0i}^2 \eta_i = \lambda_i^T \dot{\omega} \quad (i = 1, ..., n) \qquad (2)$$

where n is the number of flexure modes incorporated in the model. The gyroscopic effects of the reaction wheels have been neglected since they are negligible compared to the control torque present.

26   J. FENTON, D. HORTON AND K. F. GILL

Equation (1) represents three coupled equations due to the asymmetry of the craft and the influence of the bending modes of the solar array.

Expressing equations (1) and (2) in the state vector form

$$\dot{\mathbf{x}} = \mathbf{A}\mathbf{x} + \mathbf{B}\mathbf{u} \tag{3}$$

where x is the vector of states and u the vector of inputs, requires the construction of the partitioned matrix equation

$$\left[\begin{array}{c|c} \mathbf{E} & -\mathbf{\Lambda} \\ \hline -\mathbf{\Lambda}^{\mathsf{T}} & \mathbf{I} \end{array}\right] \left[\begin{array}{c} \dot{\boldsymbol{\omega}} \\ \hline \ddot{\boldsymbol{\eta}} \end{array}\right] = \left[\begin{array}{c} \mathbf{T} \\ \hline \mathbf{Q} \end{array}\right] - \left[\begin{array}{c} \mathbf{0} \\ \hline \dot{\boldsymbol{\eta}}_1 \end{array}\right] - \left[\begin{array}{c} \mathbf{0} \\ \hline \boldsymbol{\eta}_2 \end{array}\right] \tag{4}$$

Employing the relationship

$$\dot{\boldsymbol{\Phi}} = \boldsymbol{\Omega}_0 \boldsymbol{\Phi} + \dot{\boldsymbol{\omega}} \tag{5}$$

where

$$\boldsymbol{\Omega}_0 = \left[\begin{array}{ccc} 0 & 0 & \omega_0 \\ 0 & 0 & 0 \\ -\omega_0 & 0 & 0 \end{array}\right] \tag{6}$$

enables equation (4) to be transferred from body to inertial co-ordinates to give

$$\left[\begin{array}{c} \ddot{\boldsymbol{\Phi}} \\ \hline \ddot{\boldsymbol{\eta}} \end{array}\right] = \left[\begin{array}{c|c} \mathbf{E} & -\mathbf{\Lambda} \\ \hline -\mathbf{\Lambda}^{\mathsf{T}} & \mathbf{I} \end{array}\right]^{-1} \left\{ \left[\begin{array}{c} \mathbf{T} \\ \hline \mathbf{0} \end{array}\right] - \left[\begin{array}{c} \mathbf{0} \\ \hline \dot{\boldsymbol{\eta}}_1 \end{array}\right] - \left[\begin{array}{c} \mathbf{0} \\ \hline \boldsymbol{\eta}_2 \end{array}\right] \right\} + \left[\begin{array}{c} \boldsymbol{\Omega}_0 \boldsymbol{\Phi} \\ \hline \mathbf{0} \end{array}\right] \tag{7}$$

which represents a set of second order differential equations with constant coefficients, and thus can be written in state variable form. The state vector is defined in the following manner. The first six states comprise the attitude position and rates, the remaining eight states are the bending model positions and rates.

The matrices describing the craft dynamics are given together with further vehicle data in Appendix I.

The drift components **D** in the three gyroscopes are also modelled[17] in state variable form as

$$\dot{\mathbf{D}} = \mathbf{A}_{\mathrm{D}}\mathbf{D} + \mathbf{B}_{\mathrm{D}}\mathbf{w}_{\mathrm{D}} \tag{8}$$

and are combined with equation (7) to form an augmented state equation

$$\left[\begin{array}{c} \dot{\mathbf{x}} \\ \hline \dot{\mathbf{D}} \end{array}\right] = \left[\begin{array}{c|c} \mathbf{A} & \mathbf{0} \\ \hline \mathbf{0} & \mathbf{A}_{\mathrm{D}} \end{array}\right] \left[\begin{array}{c} \mathbf{x} \\ \hline \mathbf{D} \end{array}\right] + \left[\begin{array}{c|c} \mathbf{B} & \mathbf{0} \\ \hline \mathbf{0} & \mathbf{B}_{\mathrm{D}} \end{array}\right] \left[\begin{array}{c} \mathbf{u} + \mathbf{w} \\ \hline \mathbf{w}_{\mathrm{D}} \end{array}\right] \tag{9}$$

VEHICLE CONTROLLER

The continuous state equations describing the vehicle dynamics can be expressed in discrete form as

$$\mathbf{x}_{k+1} = \mathbf{P}\mathbf{x}_k + \mathbf{Q}\mathbf{u}_k + \mathbf{Q}\mathbf{w}_k \tag{10}$$

$$\mathbf{y}_k = \mathbf{C}\mathbf{x}_k + \mathbf{v}_k \tag{11}$$

$\mathbf{w}_k$ and $\mathbf{v}_k$, the noisy process and measurement signals, respectively, are assumed to be zero-mean uncorrelated white noise sequences with covariance matrices

$$\mathbf{W}_k \delta_{kj} = E\{\mathbf{w}_k \mathbf{w}_j^{\mathsf{T}}\} \tag{12}$$

$$\mathbf{V}_k \delta_{kj} = E\{\mathbf{v}_k \mathbf{v}_j^{\mathsf{T}}\} \tag{13}$$

where δ_{kj} is the Kronecker delta and E denotes the expected value. The vehicle control is based on minimization of the quadratic cost functional defined as

$$J = \sum(x^T S x + u^T R u) \tag{14}$$

where S is a positive semi-definite real symmetric matrix, and R is a positive definite real symmetric matric.

The resulting feedback law,[18] where a steady-state exists, is given by

$$u_k = -(Q^T FQ + R)^{-1} Q^T FP x_k \tag{15}$$

where F is the unique positive solution of the algebraic discrete Riccati equation

$$F = P^T FP - P^T FQ(Q^T FQ + R)^{-1} Q^T FP + S \tag{16}$$

The method of solution used for equation (11) is that due to Hewer.[18] However, this algorithm requires an initial value of F and this is provided by the method of Klienman.[19] Also. the application of Smith's technique[20] to the calculations greatly increases the rate of convergence and reduces the amount of computer storage needed.

When generating u it is assumed that no restrictions are imposed upon the values it may take. In practice the reaction wheels have a maximum torque which they will produce and this is represented in the simulation as a torque saturation, so that

$$u_k = -G x_k \qquad |u| < u_{sat}$$
$$\tag{17}$$
$$u_k = u_{sat} \operatorname{sign}(u) \qquad |u| \geqslant u_{sat}$$

where u_{sat} is the saturation value of u, and

$$G = (Q^T FQ + R)^{-1} Q^T FP \tag{18}$$

The internal torque losses have been neglected.

DIGITAL SIMULATION

For the system described above, equations (10)–(13), the optimal least squared estimate of the plant states[21] is given by

$$\hat{x}_{k+1} = (I - KC)[P\hat{x}_k + Qu_k] + Ky_{k+1} \tag{19}$$

where K, the steady state Kalman gain matrix is computed iteratively from

$$M_{k+1} = P(I - K_k C) M_k P^T + QWQ^T \tag{20}$$

$$K_{k+1} = M_{k+1} C^T (CM_{k+1} C^T + V)^{-1} \tag{21}$$

and M_k is defined as the covariance matrix of the error in the best linear estimate or

$$M_k = E\{[x_k - \hat{x}_k][x_k - \hat{x}_k]^T\} \tag{22}$$

The first part of the simulation is concerned with testing the controller and includes none of the attitude sensor models. Noise is added to the input and output variables and the Kalman filter gain is computed using the spacecraft dynamic model.

With the inclusion of the inertial navigation the simulation proceeds as follows. At each time-step k the three attitude errors of ϕ, θ, ψ are passed through the gyroscope model which produces three measurements ϕ^g, θ^g, ψ^g contaminated by drift and pick-off noise. Similarly the roll and pitch attitude errors are passed through the IRES model to produce measurements ϕ^h, θ^h, and when

required the yaw attitude error is passed through the sun sensor model to produce the measurement ψ^s. When no sun sensor reading is available ψ^s is given the current value of the yaw estimate, namely

$$\psi^s_{k+1} = \hat{\psi}_{k+1}, \quad k \neq k_s \tag{23}$$

These six measurements form the vector y which is used by the Kalman filter to produce a state estimate $\hat{x}$. This is input to the controller to form a control vector u which, together with the disturbance w, drives the dynamic model. A block diagram of the process is shown in Figure 2.
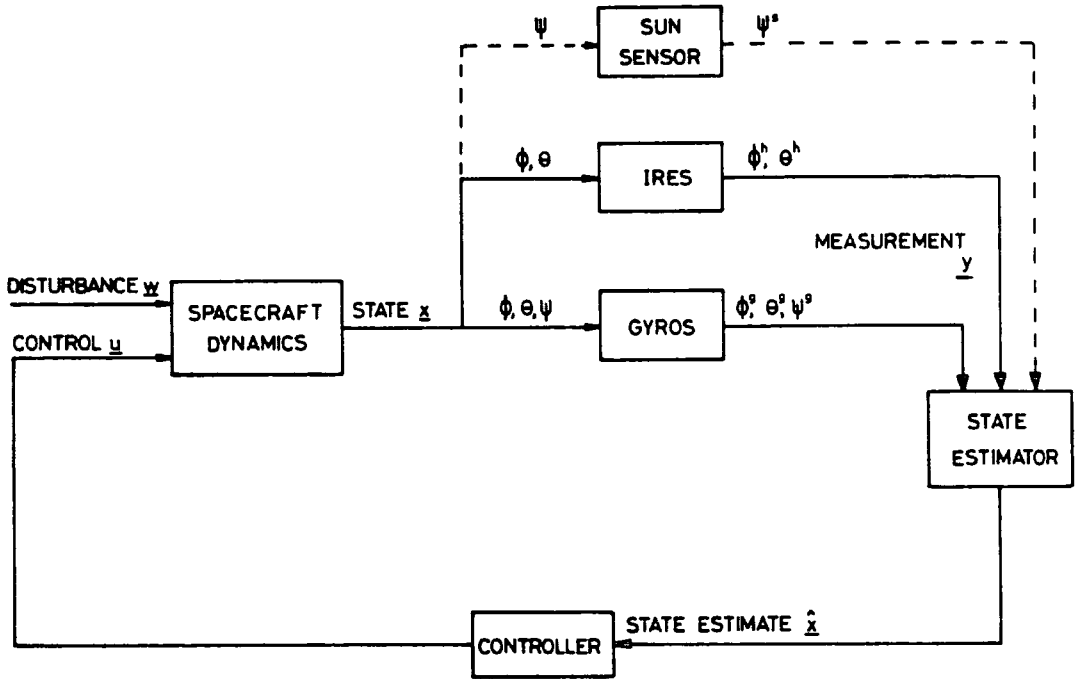
Figure 2. Simulation block diagram

In the calculation of the Kalman gain the **P** and **Q** matrices are now those computed using the augmented state equation, equation (9).

The measurements are modelled linearly in the C matrix as

$$\phi^g = \phi + D^\phi + v^g$$
$$\theta^g = \theta + D^\theta + v^g \tag{24}$$
$$\psi^g = \psi + D^\psi + v^g$$
$$\phi^h = \phi + v^h$$
$$\theta^h = \theta + v^h \tag{25}$$
$$\psi^s = \psi + v^s$$

and in the actual simulation these models are varied, both in form and amount of noise input, to test the behaviour and adaptability of the filter to design mis-match.

Care is required in the processing of sun sensor measurements since these are sampled at a different rate from the gyroscopes and the IRES. Taking the scalar form of equations (20) and (21) with $P = C = 1$ and $Q = h_s$ gives the estimate

$$\hat{\psi}_k^s = (1 - K_s)\hat{\psi}_{k-1}^s + K_s\,\psi^s \tag{26}$$

where, approximately

$$K_s = 1 - 2\left(\frac{\sigma_v^s}{h_s\,\sigma_w^s}\right)^2 \tag{27}$$

Since the standard deviations σ_v^s and σ_w^v are of similar order and h_s is of the order of 10^3, K_s may be taken as unity to give

$$\hat{\psi}^s = \psi^s \tag{28}$$

Thus, when a sun sensor reading is available it is used directly as a yaw estimate, the sampling noise being small compared with that due to the accumulated drift between readings.

SIMULATION RESULTS

Choice of weighting matrices

The design problem studied was the choice of the weighting matrices S and R used in computing the feedback matrix G. Experience suggests that values of both S and R of unity will give adequate dynamic behaviour. If further tuning is necessary then a trial and observation approach to a more suitable selection for S can readily be undertaken; a solution of the Riccati equation being achieved with an average C.P.U. time of 30 s, on a VAX 11-780, using the method described. The larger the elements of S, the larger the controller bandwidth and the larger are the feedback gains.

Figure 3 shows the roll axis response to initial conditions for three different values of S matrix with the corresponding controller actions in Figure 4. The matrix R having the same fixed value of unity in all cases. The weighting of the attitude position and rates were given preference over the modal states, no significant improvement in performance could be achieved by further increased weighting of the modes.

$$S(a) = \text{diag}\,[1,1,1,1,1,1,1,1,1,1,1,1,1]$$
$$S(b) = \text{diag}\,[10,1,10,1,10,1,1,1,1,1,1,1,1,1]$$
$$S(c) = \text{diag}\,[1000,10,1000,10,1000,10,1,1,1,1,1,1,1,1]$$

Figure 3

30   J. FENTON, D. HORTON AND K. F. GILL
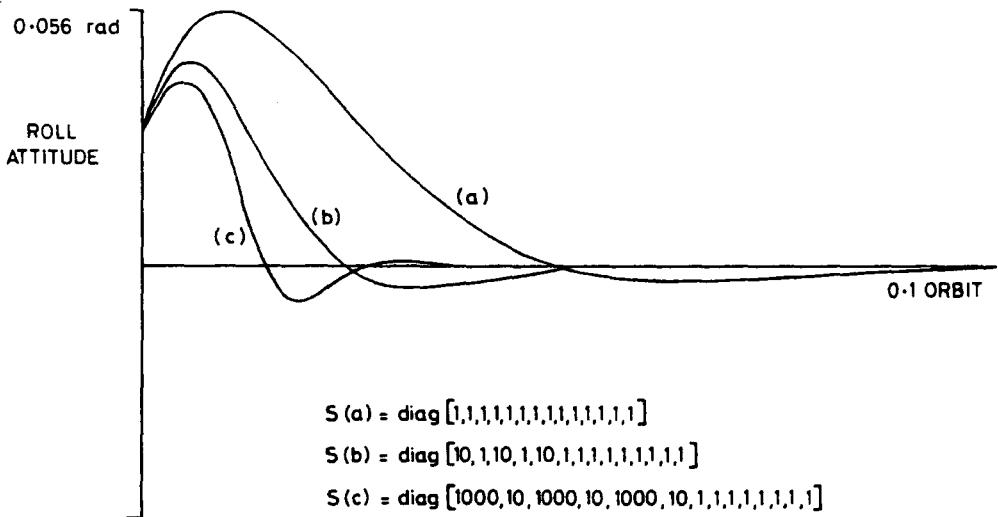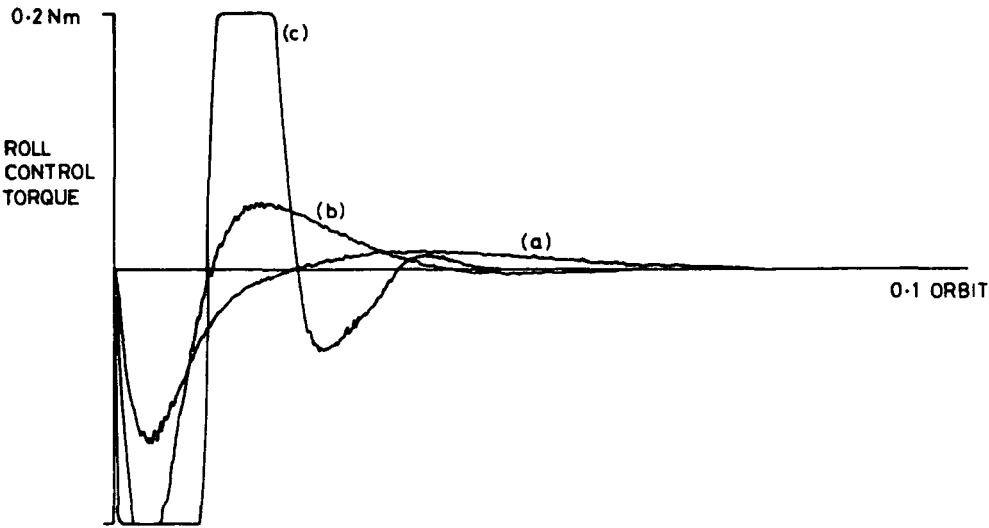
Figure 4

Controller mis-match

Using the value of **G** computed using **S** for case (c) in Figure 3, which resulted in the fastest response with controller saturation, and reducing the panel frequencies by a factor of five, caused no noticeable change in the roll axis response. Only minor response changes can be observed in the controller action, Figure 5, indicating the robustness of this control algorithm given good state estimates.

Variation of solar panel angle

As the solar panel rotates relative to the centre body the craft dynamics changes due to inertia redistribution. The craft was observed for an orbit with the panel angle incremented in steps of 15° to cause maximum system disturbance; the model used in the state estimation was not changed.
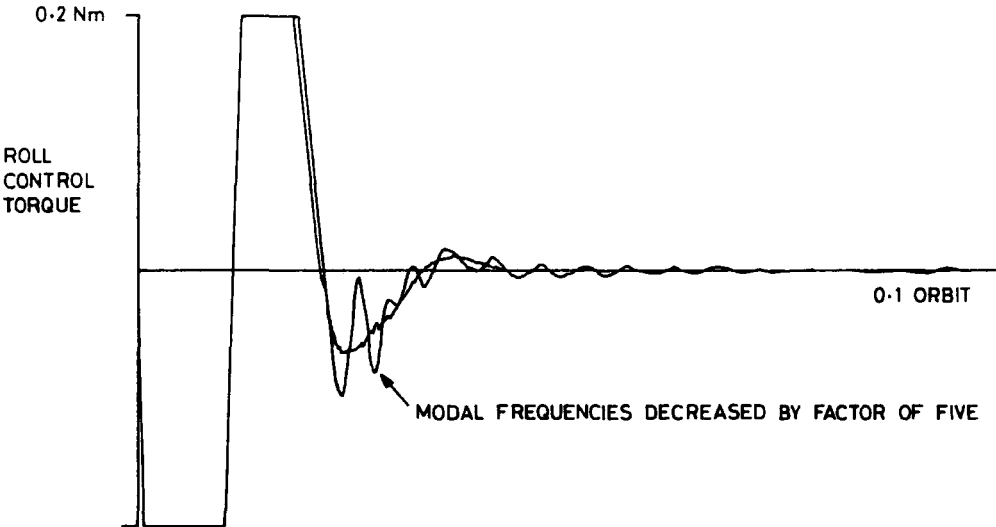
Figure 5

Even with this condition of mis-match, noise, and the low bending frequencies the system remained stable and the state estimator performed satisfactorily.

Estimator mis-match

For the design conditions the quality of the state estimate can be judged from Figure 6, which shows the roll and pitch responses to an initial error in the roll attitude.
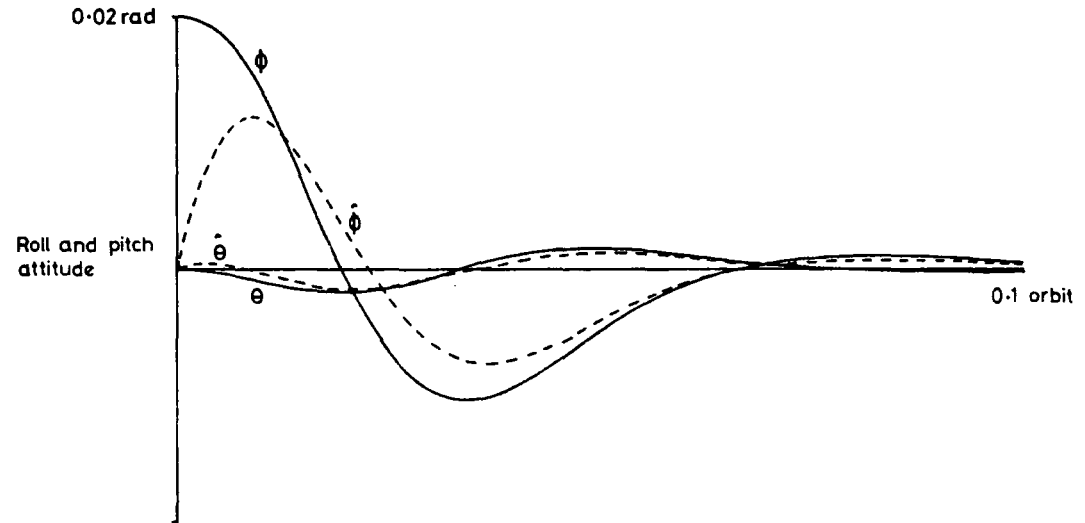
Figure 6

The state estimator was then tested for the condition of frequency mis-match between actual spacecraft and the model used in the filter computation. For the high range of frequencies and the noise conditions given in Appendix I, it was found that mis-match conditions within a range of one half to twice the modal frequencies could be tolerated. This was not the case with the low range of frequencies, mis-match being limited to within a range of ± 20 per cent of the actual frequencies.

This is demonstrated quite dramatically in Figure 7, which shows the amplitude variation of the fundamental mode of the array driven by noise. This increased vibration causes attitude degradation and may lead to structural fatigue.
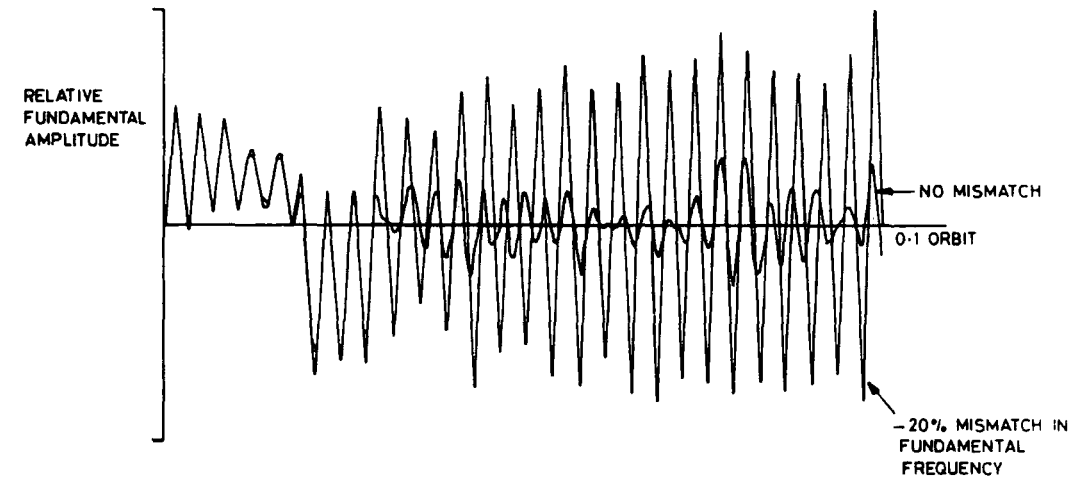
Figure 7

A further mis-match condition tested was that of using the rigid body dynamics for the computation of the Kalman filter. This led to instability indicating clearly the need to include flexibility in a state estimator design. A similar problem did not arise when using the rigid body dynamics to compute the feedback matrix G.

Attitude measurement

The states were set to be initially zero and the results averaged over three ten-orbit runs, each run using a different random number sequence for the generation of noise inputs. A measurement was produced from the sun sensor readings, twice per orbit, at equal intervals.
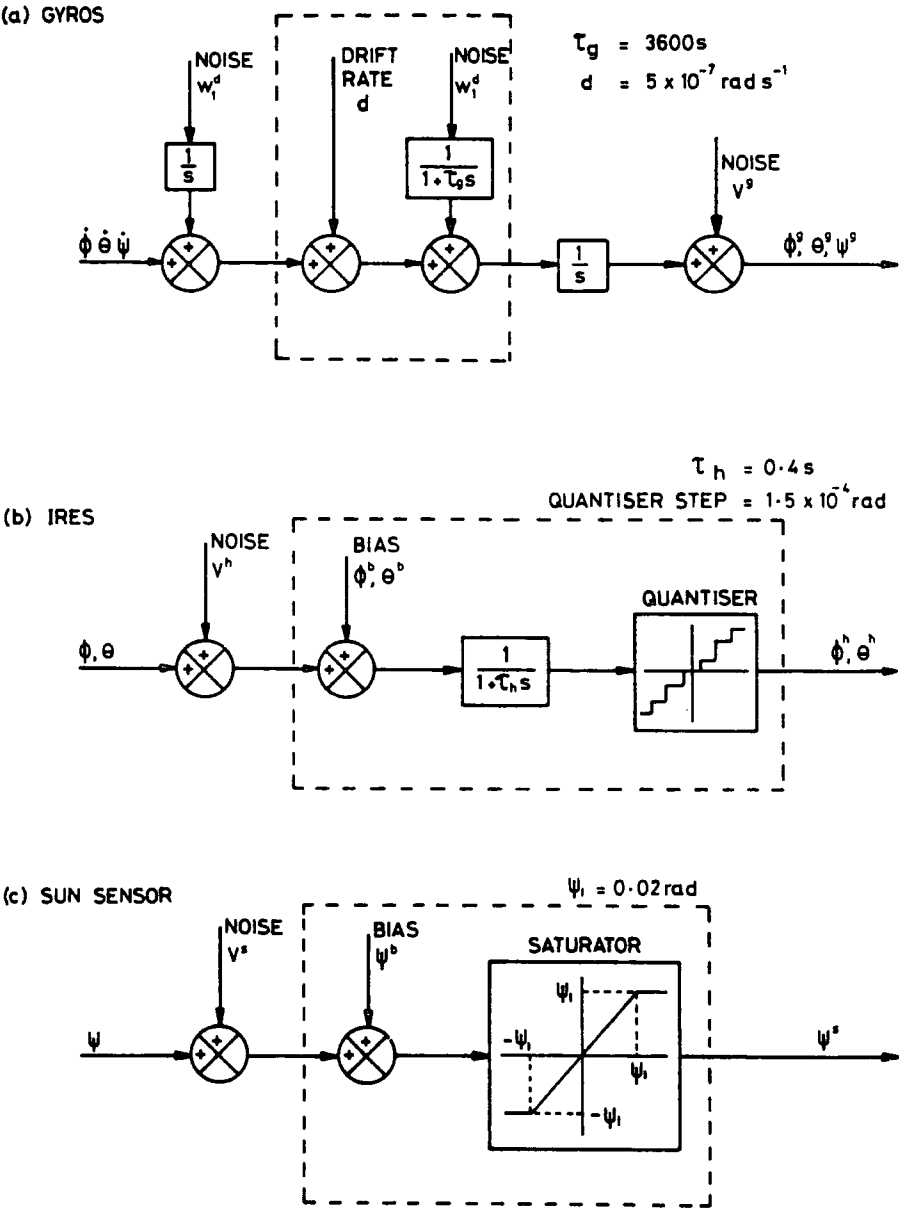
Figure 8. Sensor models. (a) Gyros; (b) IRES; (c) sun sensor

As a basis for comparison, the basic models for the gyroscopes and IRES used in computing the Kalman gain matrix **K** were also used, together with a linear sun sensor model, in computing **D** and y during the simulations, see Figure 8.

A typical graph of yaw drift and its estimate is shown in Figure 9, with the marks on the time axis denoting sun sensor readings. Results of noise mis-match between filter simulation are summarized in Table I with each of the four noise inputs varied in turn, the other three remaining fixed.

A similar experiment was then performed using noise models incorporating extra components not included in the filter computations, Figure 8, inside dotted lines. The results were similar to
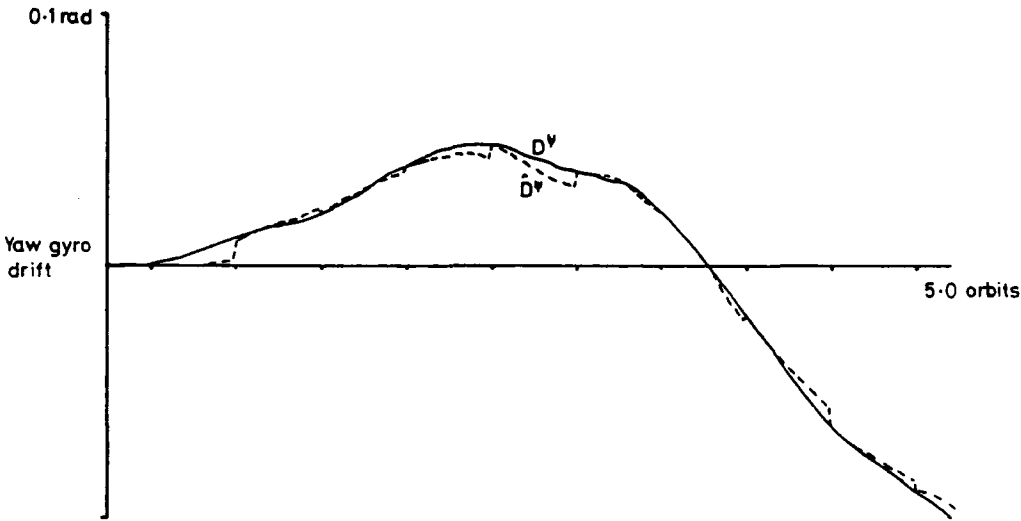
Figure 9

Table I. Summary of results for noise mismatch

	ϕ	θ	ψ
	Rms error (10^{-4} rad)		
$\sigma_1^d \leqslant 5 \times 10^{-7}$	1·1	1·1	38
5×10^{-6}	1·4	1·5	42
5×10^{-5}	11·0	11·0	210
$\sigma^g \leqslant 5 \times 10^{-4}$	1·1	1·1	38
5×10^{-3}	1·3	1·4	39
5×10^{-2}	4·2	4·3	57
$\sigma^h \leqslant 3 \times 10^{-5}$	1·0	1·0	38
3×10^{-4}	1·1	1·1	38
3×10^{-3}	3·9	3·6	39
3×10^{-2}	3·9	3·6	55
$\sigma^s \leqslant 3 \times 10^{-4}$	1·1	1·1	38
3×10^{-3}	1·1	1·1	42
3×10^{-2}	1·4	1·2	190

Values used in computing the filter elements:
$\sigma_1^d = 5 \times 10^{-7}$ rad
$\sigma^g = 5 \times 10^{-6}$ rad
$\sigma^h = 3 \times 10^{-4}$ rad
$\sigma^s = 3 \times 10^{-4}$ rad

those in Table I except that, as expected, the filter could not cope well with the unobservable biases ϕ^b, θ^b. The yaw bias ψ^b assumed less importance owing to the infrequency of the sun sensor readings. These results suggest that simple sensor models are adequate for attitude control and that good prediction of noise levels used in filter construction is at least as important as choice of these models.

As a final experiment, the mode of sun sensor reading was altered in two ways:

(a) The number of equally spaced readings per orbit was increased.

(b) Readings were taken continuously during the first half of each orbit and none were taken during the second half.

In mode (b) the measurement, when available, was processed continuously with the others. Otherwise, it was given the value of the current estimate, see equation (23)

The simulations were performed with the basic noise models and standard deviations. Typical yaw profiles for (a), with $N = 2$, and (b) are shown in Figure 10, with some further results listed in Table II. These results indicate that for method (a) to be equivalent to method (b), about four readings per orbit are required.
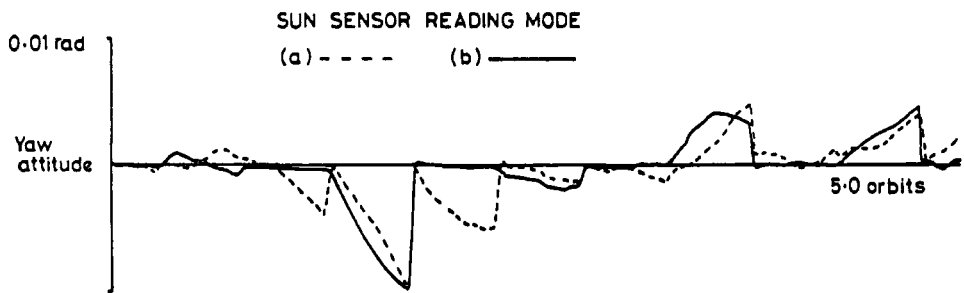
Figure 10

Table II. Effect of varying sun sensor readings

	Rms yaw error $(10^{-4}\,\text{rad})$	Max. yaw error $(10^{-4}\,\text{rad})$
(a) $N = 2$	38	160
4	17	66
8	9	38
16	6	21
(b)	20	110

CONCLUSIONS

Using the optimal control technique presented allows for a simple controller design that will satisfy the stringent pointing requirements of the next generation of spacecraft whilst actively controlling the flexure modes.

The control algorithm is robust and will tolerate a high degree of process mis-match. However, excessive filter model mis-match will lead to system instability.

The attitude measurement system configuration described is easily combined into a single optimal estimation algorithm which allows compensation for gyroscope drift to be made resulting in typical r.m.s attitude errors of 0·3 arc minutes in roll and pitch and 6 arc minutes in yaw.

The inclusion of additional non-linearities to create mis-match in the sensor models was found to have a similar effect to that of noise mis-match. This indicates that good estimates of noise statistics which can be used with confidence when choosing representative sensor models is essential.

APPENDIX I. DATA

Spacecraft

Solar panel angle: 0°

Mass: 1648 kg

$$
\text{Inertia matrix, } \mathbf{E}:
\begin{bmatrix}
6713{\cdot}0 & -896{\cdot}0 & -37{\cdot}0 \\
-896{\cdot}0 & 6335{\cdot}0 & -147{\cdot}0 \\
-37{\cdot}0 & -147{\cdot}0 & 12370{\cdot}0
\end{bmatrix} \text{kg m}^2
$$

Control

Control saturation torque, u_{sat}: 0·2 Nm

Control cost matrix, $\mathbf{R}$: diag [1, 1, 1]

Control cost matrix, $\mathbf{S}$:

diag [1000, 10, 1000, 10, 1000, 10, 1, 1, 1, 1, 1, 1, 1, 1, 1]

Resultant $\mathbf{G}$ matrix

$$
\begin{bmatrix}
31{\cdot}2 & 645{\cdot}6 & -0{\cdot}008 & -45{\cdot}48 & -0{\cdot}042 & -5{\cdot}325 & 0{\cdot}0095 \\
-0{\cdot}007 & -45{\cdot}0 & 30{\cdot}94 & 620{\cdot}4 & -0{\cdot}0014 & -7{\cdot}04 & 0{\cdot}566 \\
0{\cdot}417 & -3{\cdot}773 & 0{\cdot}003 & -7{\cdot}04 & 31{\cdot}3 & 879{\cdot}2 & 0{\cdot}0459
\end{bmatrix}
$$

$$
\begin{bmatrix}
0{\cdot}436 & 0{\cdot}165 & 1{\cdot}235 & 0{\cdot}0004 & -0{\cdot}004 & 2{\cdot}49 & 1{\cdot}267 \\
5{\cdot}377 & 0{\cdot}117 & 1{\cdot}456 & 0{\cdot}0116 & 0{\cdot}056 & 3{\cdot}973 & 0{\cdot}435 \\
0{\cdot}0003 & 0{\cdot}017 & -0{\cdot}016 & 0{\cdot}40 & 4{\cdot}566 & 0{\cdot}172 & 0{\cdot}0108
\end{bmatrix}
$$

Flexure modes

Mode, i	1	2	3	4
Natural frequency, ω_{0i} (rad s^{-1})	0·70371	0·97389	1·21893	6·032
Damping coefficient, ξ_i	0·000	0·000	0·000	0·000
Coupling coefficients, $\lambda_{\phi i}$ (kg$^{\frac{1}{2}}$ m)	0·0	22·68	0	15·38
$\lambda_{\theta i}$	68·7	8·106	1·978	4·852
$\lambda_{\psi i}$	0·0	0·0	75·0	0·0

Note: For case of flexible solar array the above natural frequencies lowered by a factor of five, the coupling coefficients being unchanged.

Plant matrices

Matrix **A**

$$
\begin{bmatrix}
0 & 1 & 0 & 0 & 0 & 0 & 0 & 0 & 0 & 0 & 0 & 0 & 0 & 0 \\
0 & 0 & 0 & 0 & 0 & 1.0\times10^{-3} & 5.136\times10^{-3} & 0 & 5.4\times10^{-3} & 0 & 1.302\times10^{-3} & 0 & 0.1369 & 0 \\
0 & 0 & 0 & 1 & 0 & 0 & 0 & 0 & 0 & 0 & 0 & 0 & 0 & 0 \\
0 & 0 & 0 & 0 & 0 & 1 & 2.647\times10^{-2} & 0 & 9.23\times10^{-3} & 0 & 6.18\times10^{-3} & 0 & 0.2218 & 0 \\
0 & 0 & 0 & 0 & 0 & 0 & 0 & 0 & 0 & 0 & 0 & 0 & 0 & 0 \\
0 & -1.0\times10^{-3} & 0 & 0 & 0 & 0 & 1.189\times10^{-3} & 0 & 4.34\times10^{-4} & 0 & 1.68\times10^{-2} & 0 & 1.048\times10^{-2} & 0 \\
0 & 0 & 0 & 0 & 0 & 0 & 0 & 1 & 0 & 0 & 0 & 0 & 0 & 0 \\
0 & 0 & 0 & 0 & 0 & 0 & -2.314 & 0 & -0.634 & 0 & -0.4246 & 0 & -15.24 & 0 \\
0 & 0 & 0 & 0 & 0 & 0 & 0 & 0 & 0 & 1 & 0 & 0 & 0 & 0 \\
0 & 0 & 0 & 0 & 0 & 0 & -0.3311 & 0 & -1.146 & 0 & -7.96\times10^{-2} & 0 & -4.903 & 0 \\
0 & 0 & 0 & 0 & 0 & 0 & 0 & 0 & 0 & 0 & 0 & 1 & 0 & 0 \\
0 & 0 & 0 & 0 & 0 & 0 & -0.1415 & 0 & -0.050 & 0 & -2.758 & 0 & -1.224 & 0 \\
0 & 0 & 0 & 0 & 0 & 0 & 0 & 0 & 0 & 0 & 0 & 0 & 0 & 1 \\
0 & 0 & 0 & 0 & 0 & 0 & -0.2074 & 0 & -0.127 & 0 & -5.0\times10^{-2} & 0 & -39.56 & 0
\end{bmatrix}
$$

Matrix B

$$
\begin{bmatrix}
0 & 0 & 0 \\
1 \cdot 97 \times 10^{-4} & 1 \cdot 51 \times 10^{-4} & 7 \cdot 7 \times 10^{-6} \\
0 & 0 & 0 \\
1 \cdot 51 \times 10^{-4} & 7 \cdot 781 \times 10^{-4} & 3 \cdot 495 \times 10^{-5} \\
0 & 0 & 0 \\
7 \cdot 7 \times 10^{-6} & 3 \cdot 495 \times 10^{-5} & 1 \cdot 499 \times 10^{-4} \\
0 & 0 & 0 \\
-1 \cdot 037 \times 10^{-2} & -5 \cdot 346 \times 10^{-2} & -2 \cdot 4 \times 10^{-3} \\
0 & 0 & 0 \\
-5 \cdot 69 \times 10^{-3} & -9 \cdot 73 \times 10^{-3} & -4 \cdot 57 \times 10^{-4} \\
0 & 0 & 0 \\
-8 \cdot 761 \times 10^{-4} & -4 \cdot 159 \times 10^{-3} & -1 \cdot 131 \times 10^{-2} \\
0 & 0 & 0 \\
-3 \cdot 762 \times 10^{-3} & -6 \cdot 097 + 10^{-3} & -2.879 \times 10^{-4}
\end{bmatrix}
$$

Matrix C (for control simulation study)

$$
\begin{bmatrix}
1 & 0 & 0 & 0 & 0 & 0 & 0 & 0 & 0 & 0 & 0 & 0 & 0 & 0 \\
0 & 0 & 1 & 0 & 0 & 0 & 0 & 0 & 0 & 0 & 0 & 0 & 0 & 0 \\
0 & 0 & 0 & 0 & 1 & 0 & 0 & 0 & 0 & 0 & 0 & 0 & 0 & 0
\end{bmatrix}
$$

Orbit

Frequency, ω_0: 0·001 rad s^{-1}
Period, $2\pi/\omega_0$: 104·7 min
Altitude, 800 km

Sensor models

d: 5×10^{-7} rad s^{-1}
τ_g: 3600 s
τ_h: 0·4 s
Quantizer step: $1 \cdot 5 \times 10^{-4}$ rad
ψ_1: 0·02 rad

Simulation

Simulation sampling period, h: 0·25 s
Sun sensor sampling period, $2\pi/\omega_0 N$: 3142 s ($N = 2$)
Noise statistics, when noise included in controller study
    process noise covariance matrix, **W**:

$$\mathrm{diag}\,[0 \cdot 125^2, 0 \cdot 125^2, 0 \cdot 125^2]\,(\mathrm{Nm})^2$$

Measurement noise covariance matrix, **V**:

$$\mathrm{diag}\,[0 \cdot 005^2, 0 \cdot 005^2, 0 \cdot 005^2]\,(\mathrm{rad})^2$$

Otherwise noise statistics as given in Table I.

APPENDIX II. NOTATION

Scalars

d	drift rate in gyroscope model
h	simulation sampling period
h_s	sun sensor sampling period
k	simulation time-step counter
k_s	value of k at a sun sensor reading
K_s	gain of yaw drift estimator
n	number of flexure states
N	number of sun sensor readings per orbit
η_i	vibrational coordinate associated with ith flexure mode
ξ_i	damping coefficient for the ith flexure mode
ϕ, θ, ψ	roll, pitch, yaw attitude errors
ϕ^g, θ^g, ψ^g	roll, pitch, yaw gyroscope measurements
ϕ^h, θ^h	roll, pitch IRES measurements
ψ^s	yaw sun sensor measurement
σ^d	standard deviation of drift model input noise
σ^g	standard deviation of gyroscope measurement noise
σ^h	standard deviation of IRES measurement noise
σ^s	standard deviation of sun sensor measurement noise
τ	correlation time
ω_0	orbital frequency
ω_{0i}	natural frequency of ith flexure mode

Vectors

$\mathbf{D}$	gyroscope drift $(D^\phi, D^\theta, D^\psi)^T$
$\mathbf{T}$	external torque acting on spacecraft
$\mathbf{u}$	control $(u_1, u_2, u_3)^T$
$\mathbf{v}$	measurement noise
$\mathbf{w}$	input noise
$\mathbf{w}_D$	input noise (drift model)
$\mathbf{x}$	state
$\hat{\mathbf{x}}$	state estimate
$\mathbf{y}$	measurement
$\boldsymbol{\eta}$	$(\eta_1, ..., \eta_n)^T$
$\dot{\boldsymbol{\eta}}_1$	$(2\xi_1\omega_{01}\dot{\eta}_1, ..., 2\xi_n\omega_{0n}\dot{\eta}_n)^T$
$\boldsymbol{\eta}_2$	$(\omega_{01}^2\eta_1, ..., \omega_{0n}^2\eta_n)^T$
λ_i	quantity measuring the coupling of the ith flexure mode with rotations of the centre body about roll, pitch, and yaw axes
$\boldsymbol{\Phi}$	attitude errors $(\phi, \theta, \psi)^T$
$\boldsymbol{\omega}$	body angular velocity

Matrices

$\mathbf{A}$	state
$\mathbf{A}_D$	state (drift model)
$\mathbf{B}$	input
$\mathbf{B}_D$	input (drift model)

C measurement
E inertia about body axes
F Riccati solution
G control
I unit
K Kalman filter gain
M Kalman filter covariance
P discrete state
0 null
Q discrete input
R control cost
S state cost
V measurement noise covariance
W input noise covariance
Λ $(\lambda_1, ..., \lambda_n)$
Ω_0 transformation from body to inertial coordinates

Superscripts

-1 matrix inverse
T matrix transpose
Λ estimate

Subscripts

k value at sample interval k

REFERENCES

1. Noll, R. B., J. J. Deyst and C. H. Spenny, 'A survey of structural flexibility effects on spacecraft control systems', *AIAA paper no. 69–116*, presented at the AIAA 7th Aerospace Sciences Meeting, New York, 20–22 January, 1969.
2. Likins, P. W. 'Interactive problems between the dynamics and control system for non-rigid spacecraft', *Dynamics and Control of Non-rigid Spacecraft*, ESA SP-117, 265–271 (1976).
3. Porcelli, G., 'Attitude control of flexible space vehicles', *AIAA Journal*, 10, (6), 807–812 (1972).
4. Likins, P. W. and G. E. Fleischer, 'Results of flexible spacecraft attitude control studies utilizing hybrid coordinates', *Journal of Spacecraft and Rockets*, 8, 264–273 (1971).
5. Poelaert, D. H. L., 'A guideline for the analysis and synthesis of a non-rigid spacecraft control system', *ESA/ASE Scientific and Technical Review*, 1, 203–218 (1975).
6. Smith, E. H. and K. F. Gill, 'Flexible space vehicle control based on state observation and Lyapunov's method', *Dynamics and Control of Non-rigid Spacecraft*, ESA SP-117, 213–219 (1976).
7. Smith, E. H. and K. F. Gill, 'Controlling the attitude and two flexure modes of a flexible satellite', *The Aeronautical Journal of the Royal Aeronautical Society*, 81 (793), 41–44 (1977).
8. Gething, J. M. and K. F. Gill, 'Relay control of undamped linear systems using Lyanupov's second method', *Proceedings IEE*, 121 (4), 301–306 (1974).
9. Gething, J. M. and K. F. Gill, 'An attitude control system for a flexible satellite providing active damping of flexural motion', *The Aeronautical Journal of the Royal Aeronautical Society*, 80 (783), 134–139 (1976).
10. Longbottom, G., D. Tate and K. F. Gill, 'Dynamic modelling and multi-axis attitude control of a highly flexible satellite', *Proceedings of the 7th I.F.A.C. World Conference*, Vol. 3, Pergamon Press, Oxford, 1978, pp. 2435–2441.
11. Larson, V., P. Likins and E. Marsh, 'Optimal estimation and attitude control of a solar electric propulsion spacecraft', *Transactions IEEE*, AES-13 (1), 35–46 (1977).
12. Jordan, J. F., B. A. Madrid and G. E. Pease, 'Effects of major error sources on planetary spacecraft navigation accuracies', *Journal of Spacecraft & Rockets*, 9 (3), 196–204 (1972).
13. Bryson, A. E. and W. Kortum, 'Estimation of the local attitude of orbiting spacecraft', *Automatica*, 7, 163–180 (1971).
14. Jude, R. J., 'System study of an inertial attitude measurement system for earth pointing satellites', *Proceedings of the Attitude and Orbit Control Systems Conference*, ESA SP-128, 131–144 (1977).
15. Likins, P. W. and P. H. Wirsching, 'Use of synthetic modes in hybrid co-ordinate dynamic analysis', *AIAA Journal*, 6 (10), 1867–1872 (1968).
16. Gething, J. M. 'Attitude control of a momentum stabilised communication satellite having large flexible appendages', *Ph.D. thesis*, University of Leeds, 1973.

40   J. FENTON, D. HORTON AND K. F. GILL

17. Nash, R. A., J. F. Kasper, B. S. Crawford and S. A. Levine, 'Application of optimal smoothing to the testing and evaluation of intertial navigation systems and components', *IEEE Trans. Automatic Control*, AC-16(6), 806–816(1971).
18. Hewer, G. A. 'An iterative technique for the computation of the steady state gains for the discrete optimal regulator'. *IEEE Trans. Automatic Control*, **AC-16**, 382–383 (1971).
19. Kleinman, D. L. 'Stabilizing a discrete, constant linear system with application to iterative methods for solving the Riccati equation', *IEEE Trans. Automatic Control*, **AC-19**, 252–254 (1974).
20. Smith, R. A. 'Matrix equation $XA + BX = C$', *Siam J. Appl. Math.*, **16**(1), 198–207 (1968).
21. Kalman, R. E. and R. S. Bucy, 'New results in linear filtering and prediction theory'. *Trans. ASME J. Basic Eng.*, **83**, 95–108 (1961).

PAPER 48

A justification for the wider use of fuzzy logic control algorithms

S Daley, BSc, PhD and **K F Gill**, BSc, MSc, PhD, CEng, MIMechE
Department of Mechanical Engineering, University of Leeds

An investigation is described that attempts to demonstrate the benefits that can be gained by wider application of fuzzy logic control. The views presented are based on the control of a flexible communications satellite. Regions are identified in which the fuzzy logic controller's performance is superior to that of a classical design, when process mismatch is significant. Employing an approach incorporating Lyapunov's second method a parameter space is located where controller coefficients can be selected with relative confidence.

1 INTRODUCTION

It has been argued (1) that the main advantage of the fuzzy logic controller is that it can be applied to plants that are difficult to model mathematically. General opinion therefore is that its use should only be considered when conventional techniques have proved inadequate yet a human process controller copes well. As such its range of application will be extremely limited. However, it has been reported in the application studies that the fuzzy logic controller is more robust to plant parameter changes than a classical controller, and has shown some noise rejection capabilities. By the very nature of the fuzzy logic controller design, one would expect it to be robust, which is clearly a desirable characteristic to have and could alone form the justification for using this particular controller. It is therefore an area worthy of investigation that might lead to a more general area of application for the fuzzy logic control strategy.

The paper assumes a basic familiarity with the fuzzy logic controller and the unfamiliar reader is referred to (1, 2) for an introduction to the topic.

2 SCALE FACTOR SELECTION FROM LYAPUNOV'S SECOND METHOD

A major criticism of the fuzzy logic controller is the lack of a sound theoretical procedure for its design. There have been several attempts (2) in the literature to progress towards such a theoretical procedure, however, the techniques presented have been either limited in their range of application or impractical.

It is the opinion of the authors that more general results can be obtained by using a technique developed from Lyapunov's second method. The method provides a means for determining the stability of a system without explicitly finding a solution in the state space.

2.1 Underlying theory

Consider Lyapunov's method as applied to discrete-time systems.

A single input continuous plant of the form:

$$\dot{x} = \mathbf{A}x + \mathbf{B}u \qquad (1)$$

can be represented in discrete form as:

$$x\{(k+1)T\} = \mathbf{A}_1 x\{kT\} + \mathbf{B}_1 u\{kT\} \qquad (2)$$

where x is the state vector, u is the plant input, $\mathbf{A}_1 = e^{AT}$, $\mathbf{B}_1 = \mathbf{A}^{-1}\{e^{AT} - \mathbf{I}\}\mathbf{B}$ and T is the sample time.

Asymptotic stability is guaranteed if a positive definite discrete Lyapunov function, $V\{x(kT)\}$ can be found such that the difference equation $\Delta V\{x(kT)\}/\Delta t$ is negative definite.

$$\frac{\Delta V\{x(kT)\}}{\Delta t} = \frac{V[x\{(k+1)T\}] - V[x\{kT\}]}{T} \qquad (3)$$

As the principal interest is the sign of $\Delta V\{x(kT)\}/\Delta t$ only the numerator of equation (3) need be evaluated.

Consider the quadratic form:

$$V\{x(kT)\} = x^T(kT)\mathbf{P}x(kT) \qquad (4)$$

where $\mathbf{P}$ is a symmetric positive definite matrix (consequently $V\{x(kT)\}$ is a positive definite function).

Substitution of equations (4) and (2) in (3) yields:

$$\Delta V\{x(kT)\} = x^T(kT)(\mathbf{A}_1^T\mathbf{P}\mathbf{A}_1 - \mathbf{P})x(kT) + u^2(kT)\mathbf{B}_1^T\mathbf{P}\mathbf{B}_1 + 2u(kT)\mathbf{B}_1^T\mathbf{P}\mathbf{A}_1 x(kT) \qquad (5)$$

It is apparent that the more negative $\Delta V\{x(kT)\}$, the more rapid the convergence to the equilibrium state. Consequently, it is desirable to obtain the value of u that causes $\Delta V\{x(kT)\}$ to be a minimum.

Thus, equating $\partial(\Delta V)/\partial u$ to zero:

$$u_{\min} = -[\mathbf{B}_1^T\mathbf{P}\mathbf{A}_1 x(kT)][\mathbf{B}_1^T\mathbf{P}\mathbf{B}_1]^{-1} \qquad (6)$$

As $\partial^2(\Delta V)/\partial u^2 = 2\mathbf{B}_1^T\mathbf{P}\mathbf{B}_1$ (i.e. > 0), this is the minimum value.

Substituting equation (6) into (5):

$$\Delta V\{x(kT)\}_{\min} = x^T(kT)(\mathbf{A}_1^T\mathbf{P}\mathbf{A}_1 - \mathbf{P})x(kT) - [\mathbf{B}_1^T\mathbf{P}\mathbf{A}_1 x(kT)]^2(\mathbf{B}_1^T\mathbf{P}\mathbf{B})^{-1} \qquad (7)$$

which can be written as:

$$\Delta V\{x(kT)\}_{\min} = -x^T W x \qquad (8)$$

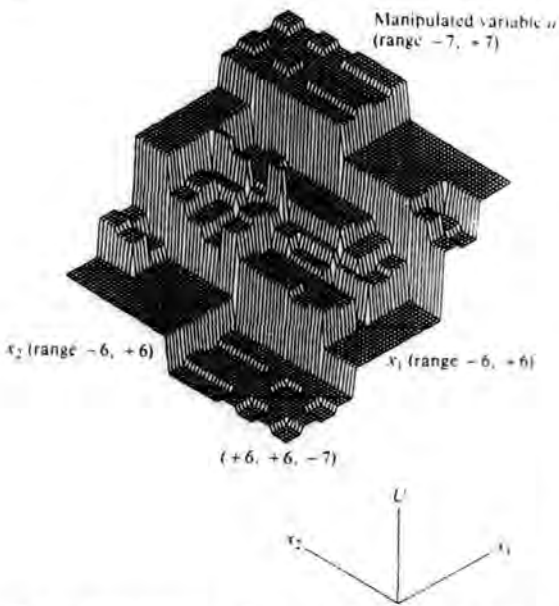44   S DALEY AND K F GILL

Fig. 1   Fuzzy logic controller modelled as a multi-level relay

where

$$W = P - A_1^T P A_1 + A_1^T P B_1 (B_1^T P B_1)^{-1} B_1^T P A_1$$

is the stationary algebraic Riccatti equation.

2.2 Application to fuzzy logic controller

To enable use of the above theory, the fuzzy logic controller must be modelled as a multi-level relay (3). The relay is simply achieved by entering all the input states to the algorithm and observing the subsequent deterministic outputs (obtained from the output fuzzy set by choosing that output value at which the membership function is maximal). The result of this process for the controller structure described in the Appendix is shown in Fig. 1.

By the very nature of the multi-level relay, there are restrictions on the process input, u. In practice, also, there will be a restriction on the upper limit of u, thus the choice of GU is not entirely arbitrary. However, in choosing u in accordance with equation (6), no restriction has been assumed. Thus u_{min} is related to the actual process input, u, by introducing the variable a.

$$u = u_{min} \pm a \tag{9}$$

Substitution of equation (9) into (5):

$$\Delta V\{x(kT)\} = \Delta V\{x(kT)\}_{min} + a^2 B_1^T P B_1 \tag{10}$$

This indicates that it is possible for $\Delta V\{x(kT)\}$ to become positive, so the value of a is critical. Therefore:

$$\Delta V\{x(kT)\}_{min} + a^2 B_1^T P B_1 < 0$$

or

$$|\{(B_1^T P B_1)^{-1} x^T W x\}^{1/2}| > |a| \tag{11}$$

Thus by substituting

$$a = \{(B_1^T P B_1)^{-1} x^T W x\}^{1/2} \tag{12}$$

into equation (9), two critical surfaces, which represent the boundaries between asymptotic stability and possible instability, are obtained for the process input.

$$u_c = -(B_1^T P A_1 x)(B_1^T P B_1)^{-1} \pm \{(B_1^T P B_1)^{-1} x^T W x\}^{1/2} \tag{13}$$

(The upper critical surface is shown in Fig. 3 when the controller described in the Appendix and shown in Fig. 2 is used on the satellite of Section 3.)

Therefore, the multi-level relay must fall within these surfaces. Its position being governed by the value of the scaling factors (assuming GU is fixed by maximum input available) as

$$x = G x^* \tag{14}$$

where $G = \text{diag}(1/G_1, 1/G_2, 1/G_3, \dots 1/G_n)$ and G_n is the scaling factor on controller input x_n, x^* represents the discrete states of the fuzzy base variables discussed in (3).

If equation (14) is substituted into equation (13), it is clear that a parameter space can be identified for the scaling factors for which asymptotic stability is guaranteed. The ease at which this can be done will depend upon the number of inputs to the fuzzy algorithm.

The most stable solution (considering the scaling factors to be the only variables) will occur when $u = u_{min}$ for all states x^*. This, of course, is unlikely to happen in practice, but the closest solution to it can be identified. The method presented below for doing this can be applied generally, but will require increasing amounts of computer time, as the number of inputs to the fuzzy algorithm increases.

Let $u_{min} = U_{mlr}$, where U_{mlr} is the value of the multi-level relay for a particular state x. Rewriting equation (14) as $x = \hat{x} G$ where $\hat{x} = \text{diag}(x^*)$ and $G^T = (1/G_1, 1/G_2, \dots 1/G_n)$. Substituting in equation (6) yields

$$U_{mlr} = -(B_1^T P B_1)^{-1} B_1^T P A_1 \hat{x} G \tag{15}$$

The solution to equation (15) is unlimited for any particular discrete state but if x_k is the matrix constructed from the kth state considered and U_k the corre-
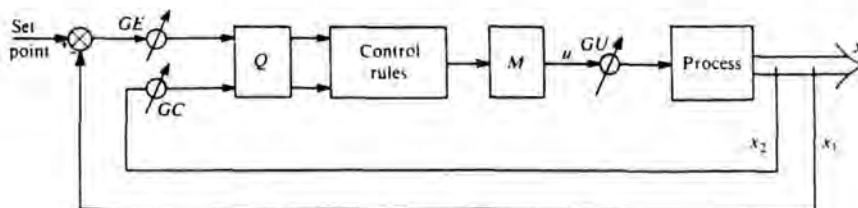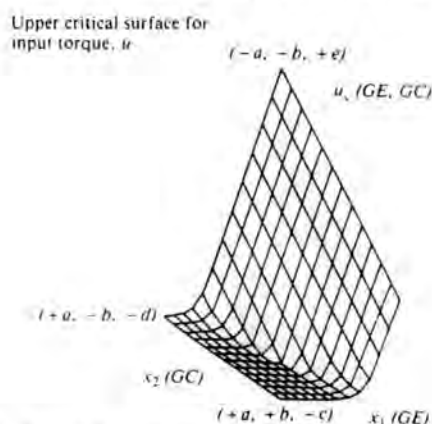

Fig. 2   Structure of the fuzzy logic controller

Fig. 3   Typical form of the critical surface: a and b are functions of GE and GC respectively and c, d and e are functions of both GE and GC

Fig. 4a   Schematic arrangement of satellite

Fig. 4b   Block diagram of satellite

sponding value of U_{min}, then the set of n simultaneous equations can be formed:

$$\begin{bmatrix} U_1 \\ U_2 \\ U_3 \\ \vdots \\ U_n \end{bmatrix} = \begin{bmatrix} -(\mathbf{B}_1^T \mathbf{P}\mathbf{B}_1)^{-1}\mathbf{B}_1^T \mathbf{P}\mathbf{A}_1 \hat{x}_1 \\ -(\mathbf{B}_1^T \mathbf{P}\mathbf{B}_1)^{-1}\mathbf{B}_1^T \mathbf{P}\mathbf{A}_1 \hat{x}_2 \\ -(\mathbf{B}_1^T \mathbf{P}\mathbf{B}_1)^{-1}\mathbf{B}_1^T \mathbf{P}\mathbf{A}_1 \hat{x}_3 \\ \vdots \\ -(\mathbf{B}_1^T \mathbf{P}\mathbf{B}_1)^{-1}\mathbf{B}_1^T \mathbf{P}\mathbf{A}_1 \hat{x}_n \end{bmatrix} \begin{bmatrix} G_1^{-1} \\ G_2^{-1} \\ G_3^{-1} \\ \vdots \\ G_n^{-1} \end{bmatrix}$$

Thus if each possible combination of states is solved simultaneously the average solution vector G will yield the smallest value of a. Consequently the number of intersections of the multi-level relay and the critical surfaces will be minimized.

This procedure can be readily implemented on a digital computer and may also be applied to multi-input systems.

3   PRACTICAL APPLICATION

The investigation is undertaken on a flexible satellite with uncoupled axes as analysed in (4), typically the Hawker Siddeley Dynamics vehicle OTS launched in early 1978. The governing dynamical equations are:

$$\ddot{\theta} = 0.00604\tau$$

$$\ddot{\alpha} + W_a^2 \alpha = 0.076\tau \qquad (16)$$

and

$$y = \theta + 0.076\alpha$$

where $W_a^2 = 4.509$ rad^2/s^2, θ is the centre body rotation due to rigid body motion, α is the centre body rotation due to flexural motion, y is the actual rotation and, τ is the input torque produced by reaction jets.

The satellite type and block diagram is shown in Fig. 4. The system is to be controlled as in Fig. 2 with $\tau = u$.

It is well known that modelling inaccuracies can cause anomalous behaviour in satellite control (5), therefore the main concern of this study is the controller response to parameter changes. To test further the robustness a mismatch condition is introduced by designing the controller based upon a rigid body model.
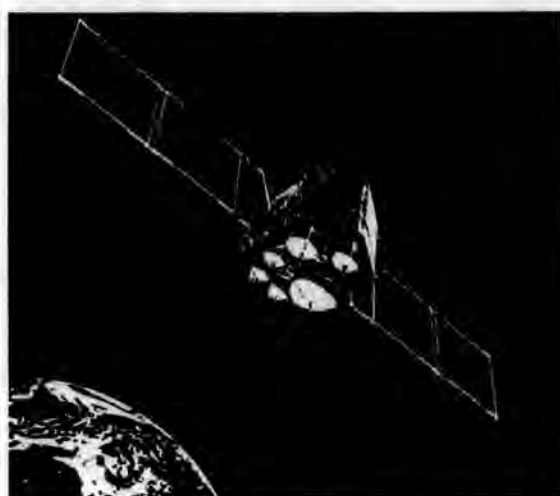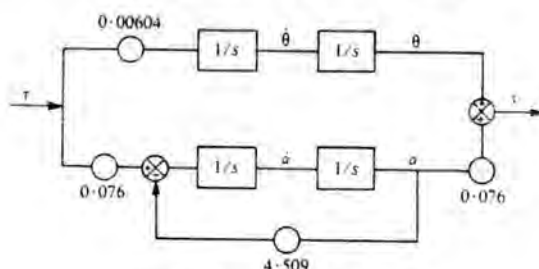
It is assumed that y and $\dot{y}$ are available from on-board instruments. GU is chosen as 0.07 giving a maximum torque input of 0.49 Nm. A selection of 0.01 s for T guarantees good sampled data reconstruction.

3.1   Scaling factors for rigid body motion

Because of the mismatch condition the analysis is carried out on the 'known' information of:

$$\mathbf{x}^T = [\theta, \quad \dot{\theta}]$$

$$\mathbf{A}_1 = \begin{bmatrix} 1 & T \\ 0 & 1 \end{bmatrix} \qquad \mathbf{B}_1 = \begin{bmatrix} 0.00604T^2/2 \\ 0.00604T \end{bmatrix}$$

W is chosen as the unit matrix and the Riccatti equation is solved using the iterative techniques of Hewer (6) and Smith (7), the Hewer algorithm is initialized using the method suggested by Armstrong and Rublein (8).
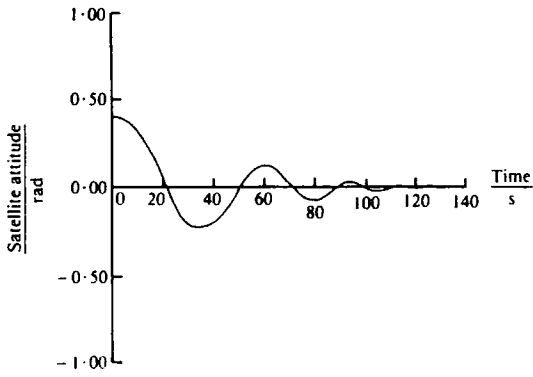
The solution matrix is:

$$\mathbf{P} = \begin{bmatrix} 101 & 0.5 \\ 0.5 & 10 \end{bmatrix}$$
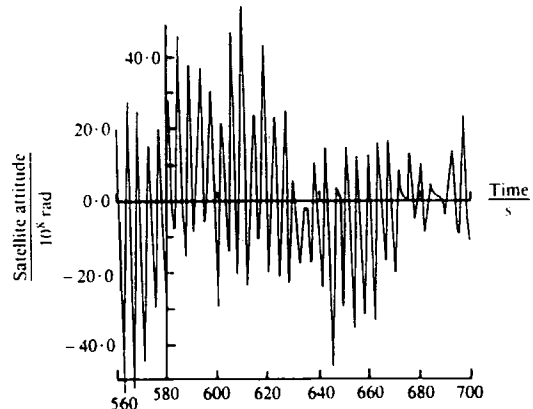
and the technique described in Section 2.1 yields the scaling factors:

$$GE = 9 \times 10^4$$

$$GC = 21 \times 10^4$$

With these values the multi-level relay only intersects the critical surfaces close to the origin for the model

(a)

(b)

Fig. 5 System response with the fuzzy logic controller: nominal configuration

3.2 Comparison with state feedback controller

The system response to the scaling factors $GE = 9 \times 10^4$ and $GC = 21 \times 10^4$ and initial displacement of 0.4 radians is shown in Fig. 5.

To enable performance comparisons to be made the fuzzy logic controller is compared with a controller based upon state feedback and Lyapunov's second method (9). The controller is in the form of a relay with deadband, δ:

$$\tau = \begin{cases} t & q > \delta \\ 0 & |q| < \delta \\ -t & q < -\delta \end{cases}$$

where τ is the controller output torque, $t = 0.49$ Nm and the disturbance is given by $q = -Kx$.

The design procedure described in the above reference requires artificial damping and frequency terms W_c and δ_c respectively to be added to the system equations.

An arbitrary choice of $W_c^2 = 0.1$ and $\delta_c = 0.9$ yields the feedback matrix:

$$K = [302 \quad 1526]$$

The system response to this controller is shown in Fig. 6.

Clearly both controllers cope well with the mismatch condition but the state feedback controller's transient convergence is superior. However, the fuzzy logic controller does converge to a greater pointing accuracy (note the state feedback convergence cannot be reduced by reducing the deadband).

To test further the robustness of the controllers the system parameters are regarded as variables and the governing equations therefore become:

$$\ddot{\theta} = k_1 T$$

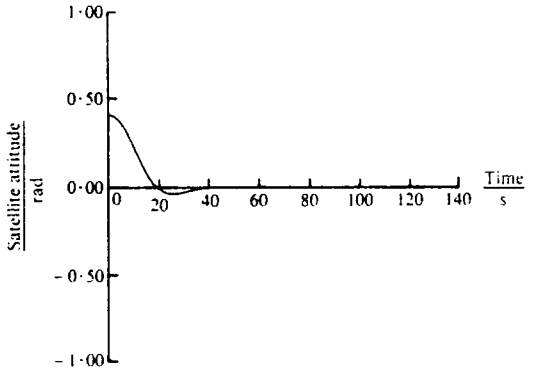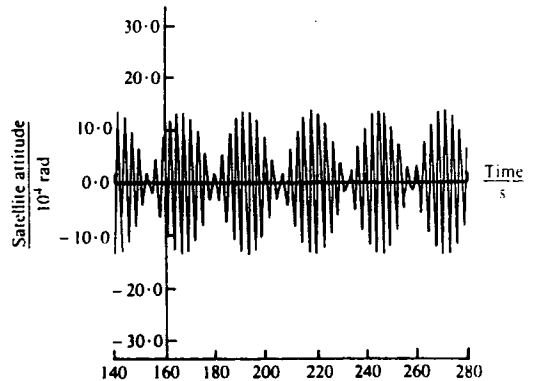$$\ddot{\alpha} + k_2 \alpha = k_3 T$$

and

$$y = \theta + k_3 \alpha$$

First the effect of increasing the magnitude of the solar arrays is investigated. As they are increased the system response to both controllers obviously becomes
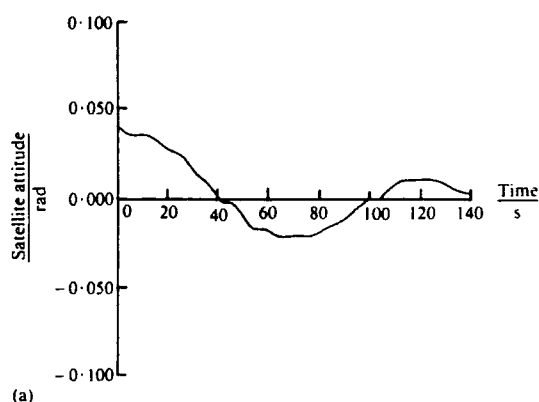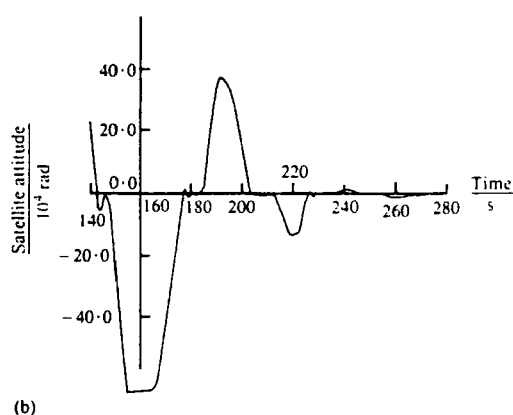

(a)

(b)

Fig. 6 System response with the state feedback controller: nominal configuration

available. This suggests a stable response until the origin is approached.

(a)

10 show the responses to a 100 times reduction and reduction in centre body size $k_1 = 1.764$, $k_2 = 33.15 \times 10^{-4}$ and $k_3 = 4.358$. The fuzzy logic controller is clearly superior but the system is far outside practical design considerations.

When a reduction in array length is considered, which could occur in practice if the arrays were struck by debris, the responses improve similarly. It is interesting to note that for this reduction the steady state error is of the same order for both controllers.

4 DISCUSSION AND CONCLUSION

Present approaches to fuzzy logic controller design are based upon modelling the strategy of a human controller where a reliable mathematical description of the process is difficult to obtain. With this approach there are certain drawbacks:

1. It is implicitly assumed that significant process changes do not occur during operation.
2. There is evidence to suggest that operators do not always report their control strategy reliably (10).

(b)

Fig. 7 System response with the fuzzy logic controller: increased solar array magnitude configuration

more sluggish, however the pointing accuracy decreased more for the state feedback controller. Figures 7 and 8 show the response to a tenfold increase in array surface area for which $k_1 = 15.66 \times 10^{-5}$, $k_2 = 0.268$ and $k_3 = 3.75 \times 10^{-2}$. It is apparent that the state feedback controller may violate the required pointing accuracy.

The greatest difference is observed when the solar array thickness is reduced dramatically. Figures 9 and
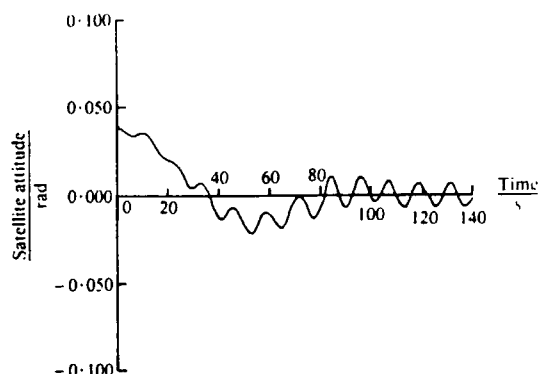

(a)

Fig. 8 System response with the state feedback controller: increased solar array magnitude configuration
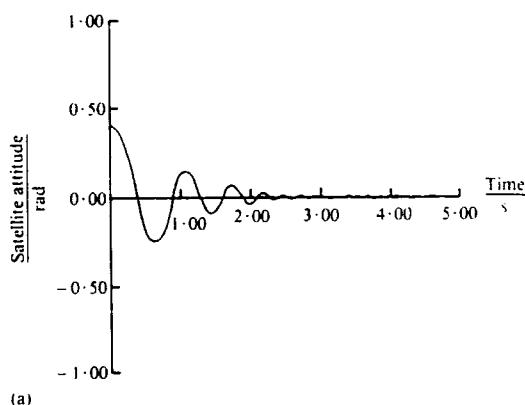

(b)

Fig. 9 System response with the fuzzy logic controller: reduced panel thickness and reduced centre body size configuration

S DALEY AND K F GILL
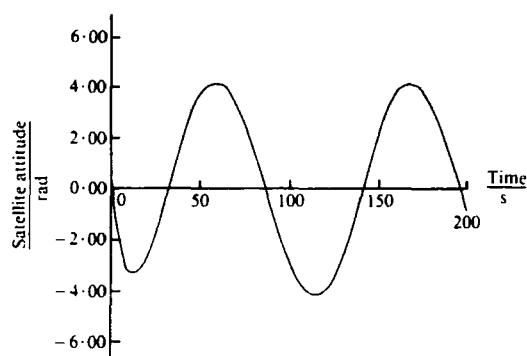
Fig. 10 System response with the state feedback controller: reduced panel thickness and reduced centre body size configuration

3. The subjectivity in choosing certain control parameters and the necessity for their on-line tuning may result in extensive damage to the plant.

A design method has been proposed in this paper that avoids problems 1 and 2. Although in an ideal fuzzy logic control application it could be argued that a process model is not required, the method described does require the best mathematical description available. It has been demonstrated that when the process varies significantly from an assumed mathematical description (problem 1) it performs better than the conventional controller chosen for comparison. Thus areas do exist where a fuzzy logic controller can compete with conventional controller design and its wider application should not be overlooked.

This method for choosing the scaling factors may be further used to aid the selection of other parameters. Typically, if the scaling factors used give undesirable intersections of the multi-level relay with the critical surfaces, the rules that have contributed to an offending state can be identified and the linguistic consequents altered accordingly. For example, if a consequent identified as 'positive big' may have contributed to an intersection with the upper critical surface a change to 'positive medium' is indicated. If the state now intersects with the lower critical surface, then the definition of a new linguistic variable is required to fall between 'positive medium' and 'positive big'. Persistence of the intersection would indicate that the level of discretization of the base variable should be decreased.

Although the method is algebraic in form it does not lose sight of the linguistic structure of the controller. Therefore it could be used to advise linguistic changes to an operator's control strategy, particularly in a hostile environment to minimize trial and observation modifications.

REFERENCES

1 **Mamdani, E. H.** Advances in the linguistic synthesis of fuzzy controllers. *Int. J. Man-Machine Stud.*, 1976, **8**, 669–678.
2 **Tong, R. M.** A control engineering review of fuzzy systems. *Automatica*, 1977, **13** 559–569.
3 **Kickert, W. J. M.** and **Mamdani, E. H.** Analysis of a fuzzy logic controller. *Fuzzy sets and systems*, 1978, **1**, 29–44.
4 **Smart, D. R., Gill, K. F., Gething, J. M.** and **Holt, J. A.** Dynamic analysis of flexible space vehicles having uncoupled control axes. *Aeronaut. J.*, (RAeS) 1974, **78**, 560–569.

5 **Likins, P. W.** Interactive problems between the dynamics and control system for non-rigid spacecraft. In *Dynamics and control of non-rigid spacecraft*, pp. 265–271, Proc. of ESA Symposium, Frascati, Italy, 24–26 May 1976.
6 **Hewer, G. A.** An iterative technique for the computation of the steady gain for the discrete optimal regulator. *IEEE Trans., Automatic Control*, 1971, AC-16, 382–383.
7 **Smith, R. A.** Matrix equation XA + BX = C. SIAM. *J. Appl. Math.*, 1968, **16**, 198–207.
8 **Armstrong, E. S.** and **Rublein, G. T.** A stabilisation algorithm for linear discrete constant systems. *IEEE Trans., Automatic Control*, 1978, AC-21, 629–631.
9 **Smith, E. H.** and **Gill, K. F.** Flexible space vehicle control based on state observation and Lyapunov's method. In *Dynamics and control of non-rigid spacecraft*, pp. 213–220, Proc. of ESA Symposium, Frascati, Italy, 24–26 May 1976.
10 **Bainbridge, L.** The process controller. In *The analysis of practical skills, Vol. 1*, 1975, W. T. Singleton (Ed.) (Academic Press).
11 **Kickert, W. J. M.** and **Van Nauta Lemke, H. R.** Application of a fuzzy controller in a warm water plant. *Automatica*, 1976, **23**, 301–308.

APPENDIX

Design of fuzzy logic controller

The controller is designed to provide single axis control assuming the availability of the attitude y and the attitude rate $\dot{y}$ from on-board instruments.

The fuzzy linguistic algorithm, presented below, is written using a qualitative feel for a general two measurement, one input monotonic undamped process intended to provide fast convergence coupled with the required damping around the equilibrium state to achieve a high pointing accuracy.

		Attitude rate						
		NB	NM	NS	ZO	PS	PM	PB
	NB	PB	PB	PB	PB	PM	PM	PM
	NM	PB	PB	PB	PB	PM	PM	PS
Attitude	NS	PM	PS	PS	PS	PS	NS	NM
	NO	PM	PM	PS	ZO	ZO	NS	NM
	PO	PM	PS	ZO	ZO	NS	NM	NM
	PS	PM	PS	NS	NS	NS	NS	NM
	PM	NS	NM	NM	NB	NB	NB	NB
	PB	NM	NM	NM	PB	PB	PB	PB

For convenience the rules have been written in matrix form and should be interpreted as:

If 'attitude is NM' and 'attitude rate is PS' then 'torque input is PM'

The linguistic elements used are the same as those used in most of the application studies reported; the need for other terms or linguistic hedges is, in the opinion of the authors unnecessary at this stage. These terms have the following meaning:

PB positive big
PM positive medium
PS positive small
PO positive zero
ZO zero
NO negative zero
NS negative small
NM negative medium
NB negative big

The terms PO and NO are introduced to obtain finer control about the equilibrium state, PO being defined

as values slightly above zero and NO terms slightly below zero.

The fuzzy sets are formed upon a discrete support universe of fourteen elements for the attitude, thirteen elements for the attitude rate and fifteen elements for the torque output. Appropriate membership functions are assigned to each element of the support set rather than by functional methods (11). The resulting sets representing the linguistic terms presented above are listed in Table 1.

All the non-fuzzy measurements are represented by fuzzy singletons and the algorithm output is obtained from the output fuzzy set by the mean of maxima procedure; the algorithm output is absolute torque.

Table 1   The fuzzy set definitions

(a) *The attitude, y*

	−6	−5	−4	−3	−2	−1	−0	+0	1	2	3	4	5	6
PB	0	0	0	0	0	0	0	0	0	0	0.1	0.4	0.8	1.0
PM	0	0	0	0	0	0	0	0	0	0.2	0.7	1.0	0.7	0.2
PS	0	0	0	0	0	0	0	0.3	0.8	1.0	0.5	0.1	0	0
PO	0	0	0	0	0	0	0	1.0	0.6	0.1	0	0	0	0
NO	0	0	0	0	0.1	0.6	1.0	0	0	0	0	0	0	0
NS	0	0	0.1	0.5	1.0	0.8	0.3	0	0	0	0	0	0	0
NM	0.2	0.7	1.0	0.7	0.2	0	0	0	0	0	0	0	0	0
NB	1.0	0.8	0.4	0.1	0	0	0	0	0	0	0	0	0	0

(b) *The attitude rate, ẏ*

	−6	−5	−4	−3	−2	−1	0	1	2	3	4	5	6
PB	0	0	0	0	0	0	0	0	0	0.1	0.4	0.8	1.0
PM	0	0	0	0	0	0	0	0	0.2	0.7	1.0	0.7	0.2
PS	0	0	0	0	0	0	0	0.9	1.0	0.7	0.2	0	0
NO	0	0	0	0	0	0.5	1.0	0.5	0	0	0	0	0
NS	0	0	0.2	0.7	1.0	0.9	0	0	0	0	0	0	0
NM	0.2	0.7	1.0	0.7	0.2	0	0	0	0	0	0	0	0
NB	1.0	0.8	0.4	0.1	0	0	0	0	0	0	0	0	0

(c) *The process input, τ*

	−7	−6	−5	−4	−3	−2	−1	0	1	2	3	4	5	6	7
PB	0	0	0	0	0	0	0	0	0	0	0	0.1	0.4	0.8	1.0
PM	0	0	0	0	0	0	0	0	0	0.2	0.7	1.0	0.7	0.2	0
PS	0	0	0	0	0	0	0	0.4	1.0	0.8	0.4	0.1	0	0	0
NO	0	0	0	0	0	0	0.2	1.0	0.2	0	0	0	0	0	0
NS	0	0	0	0.1	0.4	0.8	1.0	0.4	0	0	0	0	0	0	0
NM	0	0.2	0.7	1.0	0.7	0.2	0	0	0	0	0	0	0	0	0
NB	1.0	0.8	0.4	0.1	0	0	0	0	0	0	0	0	0	0	0

PAPER 49

Forum on *Fuzziness*

The Fuzzy Logic Controller: An Alternative Design Scheme?

S. Daley and K.F. Gill
Department of Mechanical Engineering, University of Leeds, Leeds LS2 9JT, U.K.

A method is presented to improve system reliability in *Fuzzy Logic Controller* applications. It is based upon a stability constraint formulated from Lyapunov's second method as applied to discrete systems. As the method requires a mathematical description of the plant, the performance of a *Fuzzy Logic Controller* is compared with a conventional design in the presence of considerable plant mismatch. This investigation is carried out on a flexible communications satellite and regions are identified in which the *Fuzzy Logic Controller's* performance is superior.

Stephen Daley was born in Morecambe, England in 1959. He received the B.Sc. degree in Mechanical Engineering from Preston Polytechnic in 1981. He is currently working on a Ph.D. thesis on fuzzy logic control within the Mechanical Engineering Department of the University of Leeds. His further research interests lie in the field of adaptive control.

K.F. Gill obtained his engineering training with a company manufacturing large steam turbine and alternating equipment for the electrical power supply industry. His academic training was gained at the University of Durham and the University of Birmingham. He was awarded the degrees of B.Sc. in 1955, M.Sc. in 1958 and Ph.D. in 1961. From 1961 Dr Gill was a Senior Scientific Officer at the Admiralty Weapons Establishment, Portland. For the last 21 years he has been a Lecturer, then Senior Lecturer at the University of Leeds, teaching control engineering and engineering dynamics to undergraduate students reading for an honours degree in Mechanical Engineering.

1. Introduction

The basic idea behind the introduction of a Fuzzy Logic Controller was to model the strategy of a human controller for ill-defined systems. In this study its application in more general terms is investigated in an attempt to observe any advantages it may possess over controllers designed in a conventional way. It is the opinion of the authors that any control scheme must be robust to be of practical use and hence must include an attempt at a stability analysis based on the plant knowledge available. Therefore it is an essential requirement that "safe" operating regions be identified for all the parameters used in a controller design. The impact on system performance of parameter variations was implied by Braae and Rutherford [10], illustrating the dominant role of the scaling factors that link the Fuzzy Logic Controller to the "real" world. A method is proposed in Section 4 for selecting these scaling factors based upon a stability constraint.

2. The Fuzzy Logic Controller

The fuzzy control algorithm used (Appendix A) is written in general terms for a monotonic system with two measurements and one input, it is based upon those first suggested by Mamdani [1,2]. The foundation stones for these were laid by Zadeh [3–5], who offered a means of translating linguistically expressed imprecise statements into a clearly defined mathematical representation.

The control algorithm is constructed by a series of fuzzy conditional statements of the form:

If "A OR B is Big" AND "C is Small" then "D is Medium" linked by the connective OR (Else).

nslation is performed by making use of the
g fuzzy set operations:

Union of the fuzzy subsets A and B of the
'erse of discourse E is denoted by $A \cup B$,
, a membership function defined by

$$_B(e) = \max[\mu_A(e); \mu_B(e)] e \in E.$$

: membership function $\mu_A(e) \in [0, 1]$ where
a generic element of E and A is a fuzzy
the value indicates to what extent e is an
ent of A) This corresponds to the connec-
"OR".

Intersection of the fuzzy subsets A and B
enoted $A \cap B$ with a membership function
ned by:

$$_B(e) = \min[\mu_A(e); \mu_B(e)] e \in E.$$

s corresponds to the connective "AND".
: *Complement* of a fuzzy subject A is de-
ed $\lnot A$ with a membership function defined

$$(e) = 1 - \mu_A(e).$$

s corresponds to the negation "NOT".
uzzy *Relation* R from $U = \{x\}$ to $V = \{y\}$
, fuzzy set on the cartesian product $U \times V$
racterised by a function of $\mu_R(x, y)$, by
ch each pair (x, y) is assigned a number in
1] indicating to what extent the relation is
e in (x, y).
the case of binary fuzzy relation, (N.B.
ined on n-ary fuzzy relation in the product
ce $U^1 \times U^2 \times U^3 \dots \times U^n$) the *Composition*
wo fuzzy relations A and B is denoted by
A and is defined as a fuzzy relation in
$\times V$ whose membership function is related
hose of A and B by:

$$_A(x, y) = \max_v \left[\min \mu_A(x, v); \mu_B(v, y)\right].$$

B. A and B are relations from $U = \{x\}$ to
$= \{v\}$ and $Q = \{v\}$ to $V = \{y\}$ respec-
ly.)
s now apparent how the fuzzy conditional
ement can be translated. For example

A then B" is the relation $R = A \times B$ whose
mbership function is defined by:

$$(u, v) = \mu_{A \times B}(u, v)$$

$$= \min[\mu_A(u): \mu_B(v)], u \in U, v \in V.$$

such a relation R is given and the subset

value A' of A is known, then the corre-
sponding value of B' can be obtained by mak-
ing use of the compositional rule of inference

$$B' = A' \circ R = A' \circ (A \times B).$$

3. Theoretical Analysis and Parameter Selection

The most conventional stability analysis was
undertaken by Kickert and Mamdani [6]. The
fuzzy logic algorithm can be considered as a multi-
level relay and consequently non-linear control
analytical techniques can be applied. The method
of analysis chosen was that of the describing func-
tion. However, it is concluded that the procedure
has a limited range of application. A more general
approach, they suggest, will be obtained by inves-
tigations of the underlying logical structure such as
those carried out by Tong [7,8].

Since its introduction, a limited number of
plants have been successfully controlled by a Fuzzy
Logic Controller [9], but there has been little men-
tioned about the criteria used in parameter selec-
tion. As a consequence, Braae and Rutherford
produced a paper discussing parameter selection
and adjustment in detail [10]. The parameters they
considered were:

(1) *The fuzzy language* – One problem is the choice
of terms (e.g. PB-positive Big) to represent the
variation of any linguistic variable (e.g. "Er-
ror"). They suggest that this should be a
compromise between flexibility (high resolu-
tion) and simplicity (low resolution) typically
between two and ten values. Each base varia-
ble has also to be assigned a number of dis-
crete elements (e.g. $-7 \to +7$) to represent the
actual value (the real range of which will be
known based on a prior process knowledge).
This number of elements should be sufficiently
large to accommodate narrow fuzzy sets, but
kept low to reduce storage requirements. In
any practical application, the measurements
used as inputs of the Fuzzy Logic Controller
will be noisy. So fuzzy sets should be selected
to be sufficiently large to avoid undue noise
transmission from the base variable to linguis-
tic variable. The variable domains are chosen
on a trial and observation basis until the closed
loop trajectory fits just inside the domain.

(2) *The set of linguistic rules* – To examine the rules, Braae and Rutherford choose to track the system trajectory through the linguistic elements (e.g. PB) whose membership values are maximal at a sample instant. This is a point on the linguistic phase plane. In this way, the rules used during any run are explicitly defined and may be altered if desired. The major changes are obtained by altering the scale factors, done on a trial and observation basis until the trajectory converges on the equilibrium state. Minor adjustment is made by changing the linguistic elements of the appropriate rules. Thus selection of improved rules at each state relies heavily on an intuitive feel for the behaviour of the closed loop system.

It will be noted that the success of any particular controller structure is heavily dependent upon the value of the scaling factors. It is, therefore, surprising that there has been only one attempt in the literature to identify a suitable parameter space in the choice of scaling factors. Procyk [11] defined two constraints to enable scale factor choice:

(a) Error tolerance is the largest or smallest value in error that can be accommodated without initiating a rule modification in the adaptive controller (rules are modified when they lead to a bad response which is monitored by a performance index).

Error Tol. = $\pm 0.5 \div$ GE

where GE is the scaling factor on the error.

(b) Change in error tolerance is the largest change in the direction of the origin that can be accommodated without initiating a rule modification.

Change in Error Tol. = $\pm 2.5 \div$ GC

where GC is the scaling factor on the change of error.

The values 0.5 and 2.5 are functions of the performance index. Procyk suggests that a suitable value for the error tolerance is 5% of the set-point, and for the change in error tolerance is 1/2 to 1/5 of the error tolerance. It is suggested also that the GU (scale factor on controller output) should be about one-third of the maximum possible process input.

Although the final choice is still subjective, it is restricted, as the tolerances are related to the set point magnitude. These statements have clearly been formulated from empirical data and thus give no indication of the system response or limitations of use.

4. Scale Factor Selection from Lyapunov's Second Method

A more rigorous analytical selection procedure can be developed from use of Lyapunov's second method. This provides a means for determining the stability of a system without explicitly solving the state space, thus lifting the restriction noted by Kickert and Mamdani [6] that the linear parts of the system must be of second order when using a phase plane analysis.

4.1. Underlying Theory

Consider Lyapunov's method as applied to discrete-time systems: A single input continuous plant of the form:

$$\dot{x} = Ax + Bu \tag{1}$$

can be represented in discrete form as:

$$x\{(k+1)T\} = A_1 x\{kT\} + B_1 u\{kT\} \tag{2}$$

where x is the state vector, u is the plant input. $A_1 = e^{AT}$, $B_1 = A^{-1}\{e^{AT} - I\}B$ and T is the sample time. Asymptotic stability is guaranteed if a positive definite discrete Lyapunov function. $V\{x(kT)\}$ can be found such that the difference equation $\Delta V\{x(kT)\}/\Delta t$ is negative definite.

$$\frac{\Delta V\{x(kT)\}}{\Delta t} = \frac{V[x\{(k+1)T\}] - V[x\{kT\}]}{T}.$$
$$\tag{3}$$

nb. of principal interest is only the sign of $\Delta V\{x(kT)\}/\Delta t$

consider the quadratic form:

$$V\{x(kT)\} = x^T(kT)Px(kT) \tag{4}$$

where P is a symmetric positive definite matrix (consequently $V\{x(kT)\}$ is a positive definite function).

Substitution of Eqs. (4) and (2) in Eq. (3) yields:

$$\Delta V\{x(kT)\} = x^T(kT)\left(A_1^T P A_1 - P\right)x(kT)$$
$$+ u^2(kT)B_1^T P B_1$$
$$+ 2u(kT)B_1^T P A_1 x(kT) \tag{5}$$

parent that the more negative $\Delta V\{x(kT)\}$, e rapid the convergence to the equilibrium onsequently, it is desirable to obtain the f u that causes $\Delta V\{x(kT)\}$ to be a mini-

, equating $\partial(\Delta V)/\partial u$ to zero:

$$-\left[B_1^T P A_1 x(kT)\right]\left[B_1^T P B_1\right]^{-1}. \tag{6}$$

$\Delta V)/\partial u^2 = 2B_1^T P B_1$ (i.e. > 0), this is the m value.

tituting Eq. (6) into (5):

$$kT)\}_{\min} = x^T(kT)\left(A_1^T P A_1 - P\right)x(kT)$$
$$- \left[B_1^T P A_1 x(kT)\right]^2\left(B_1^T P B\right)^{-1} \tag{7}$$

an be written as:

$$kT)\}_{\min} = -x^T W x \tag{8}$$

$$- A_1^T P A_1 + A_1^T P B_1\left(B_1^T P B_1\right)^{-1} B_1^T P A_1$$
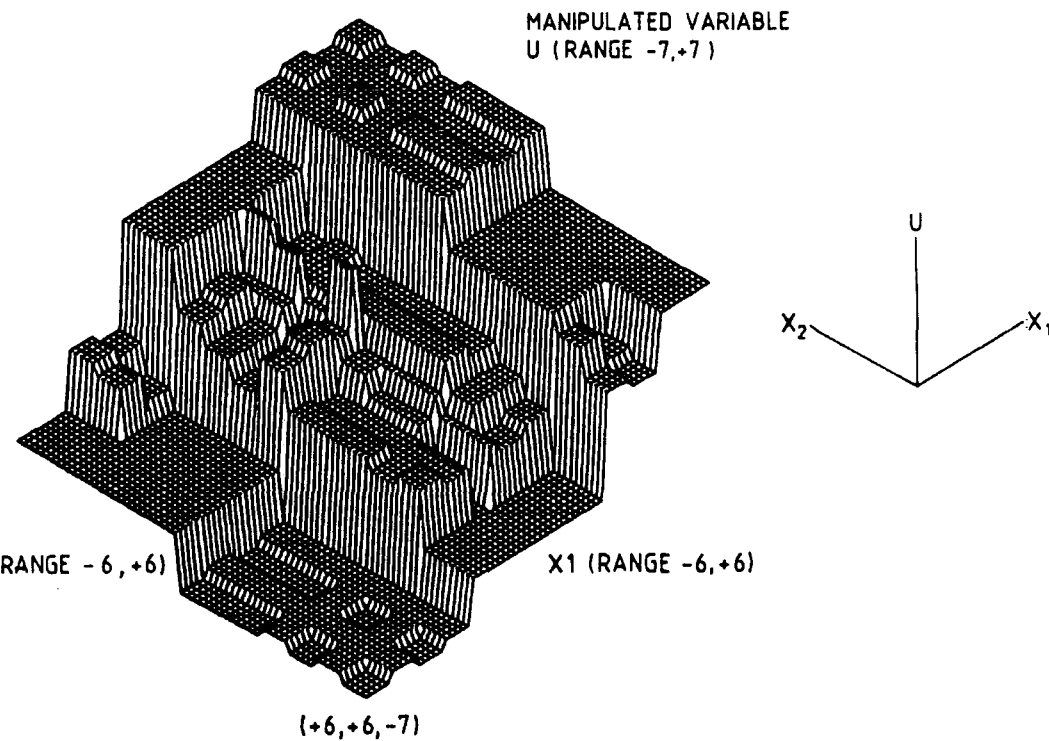
tationary algebraic Riccatti equation.

4.2. Application to a Fuzzy Logic Controller

To enable use of the aforestated theory, a fuzzy logic controller must be modelled as a multilevel relay [6]. The relay is simply achieved by entering all the input states to the algorithm and observing the subsequent deterministic outputs (obtained from the output fuzzy set by choosing that output value at which the membership function is maximal). The result of this process for the controller structure of Appendix A is shown in Fig. 1. By the very nature of the multilevel relay, there are restrictions on the process input, u. In practice, also, there will be a restriction on the upper limit of u, thus the choice of GU is not entirely arbitrary. However, in choosing u in accordance with Eq. (6), no restriction has been assumed. Thus $u_{\min}$ is related to the actual process input 'u' by introducing the variable 'a'.

$$u = u_{\min} \pm a. \tag{9}$$

Substitution of equation (9) into (5):

$$\Delta V\{x(kT)\} = \Delta V\{x(kT)\}_{\min} + a^2 B_1^T P B_1 \tag{10}$$

MANIPULATED VARIABLE
U (RANGE -7,+7)

RANGE - 6 ,+6)   X1 (RANGE -6,+6)

(+6,+6,-7)

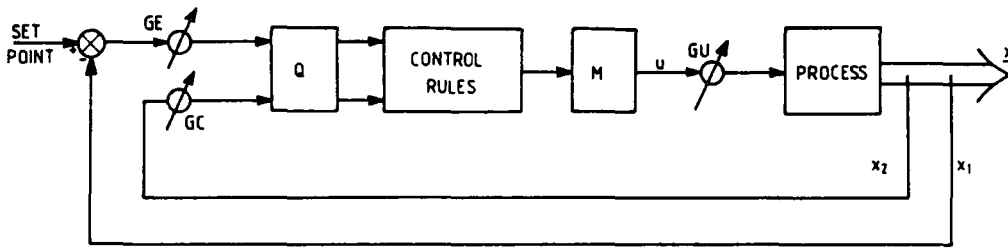he Fuzzy Logic Controller Modelled as a Multilevel Relay.

Fig. 2. The Structure of the Fuzzy Logic Controller.

This indicates that it is possible for $\Delta V\{x(kT)\}$ to become positive, so the value of 'a' is critical.

Therefore:

$$\Delta V\{x(kT)\}_{min} + a^2 B_1^T P B_1 < 0$$

or

$$\left|\{(B_1^T P B_1)^{-1} x^T W x\}^{1/2}\right| > |\forall| \tag{11}$$

Thus by substituting

$$a = \{(B_1^T P B_1)^{-1} x^T W x\}^{1/2} \tag{12}$$

into Eq. (9), two critical surfaces are obtained for process input which represent the boundaries between asymptotic stability and possible instability.

$$u_c = -(B_1^T P A_1 x)(B_1^T P B_1)^{-1}$$

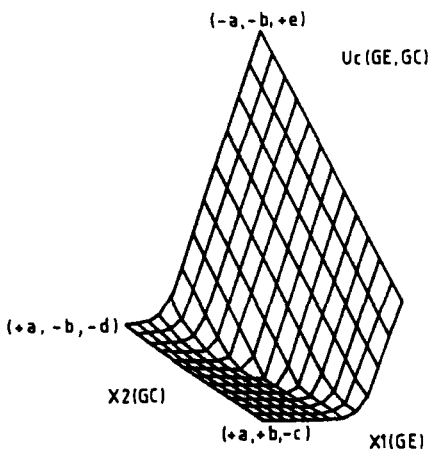$$\pm \{(B_1^T P B_1)^{-1} x^T W x\}^{1/2}. \tag{13}$$

Fig. 3. The Upper Critical Surface for Input Torque U. [The typical form of the critical surface: a and b are functions of GE and GC respectively; c, d, and e are functions of both GE and GC.]

(The upper critical surface is shown in Fig. 3 when the controller of Appendix A and Fig. 2 is used on the satellite of Section 5.)

Therefore, the multilevel relay must fall within these surfaces. Its position being governed by the value of the scaling factors (assuming GU is fixed by maximum input available) as

$$x = Gx^* \tag{14}$$

where $G = \text{diag}(1/G_1, 1/G_2, 1/G_3, \ldots 1/G_n)$ and G_n is the scaling factor on controller input x_n, x^* represents the discrete states of the fuzzy base variables discussed in Section 3.

If eq. (14) is substituted into Eq. (13), it is clear that a parameter space can be identified for the scaling factors for which asymptotic stability is guaranteed. The ease at which this can be done will depend upon the number of inputs to the fuzzy algorithm.

The most stable solution (considering the scaling factors to be the only variables) will occur when $u = u_{min}$ for all states x^*.

This, of course, is unlikely to happen in practice, but the closest to it can be identified. The method presented below for doing this can be applied generally, but will require increasing amounts of computer time, as the number of inputs to the fuzzy algorithm increases.

Let $u_{min} = U_{mlr}$, where U_{mlr} is the value of the multilevel relay for a particular state x.

Rewriting Eq. (14) as:

$$x = \hat{x} G$$

where $\hat{x} = \text{diag}(x^*)$

and $G^T = \left(\frac{1}{G_1}, \frac{1}{G_2}, \ldots \frac{1}{G_n}\right)$

Substituting in Eq. (6) yields

$$U_{mlr} = -(B_1^T P B_1)^{-1} B_1^T P A_1 \hat{x} G \tag{15}$$

The solution to Eq. (15) is unlimited for any particular discrete state but if x_k is the matrix constructed from the kth state considered and U_k the corresponding value of U'_{mlr} then the set of n simultaneous equations can be formed:

$$\begin{bmatrix} U_1 \\ U_2 \\ U_3 \\ \vdots \\ U_n \end{bmatrix} = \begin{bmatrix} -\left(B_1^T P B_1\right)^{-1} B_1^T P A_1 \hat{x}_1 \\ -\left(B_1^T P B_1\right)^{-1} B_1^T P A_1 \hat{x}_2 \\ -\left(B_1^T P B_1\right)^{-1} B_1^T P A_1 \hat{x}_3 \\ \vdots \\ -\left(B_1^T P B_1\right)^{-1} B_1^T P A_1 \hat{x}_n \end{bmatrix} \begin{bmatrix} G_1^{-1} \\ G_2^{-1} \\ G_3^{-1} \\ \vdots \\ G_n^{-1} \end{bmatrix}$$

Thus if each possible combination of states is solved simultaneously the average solution vector G will yield the smallest value of 'a'. Consequently the number of intersections of the multilevel relay and the critical surfaces will be minimised.

This procedure can be readily implemented on a digital computer and may also be applied to multi-input systems.

5. A Practical Application: Satellite Control

The investigation is undertaken on a flexible satellite with uncoupled axes as analysed in [13].
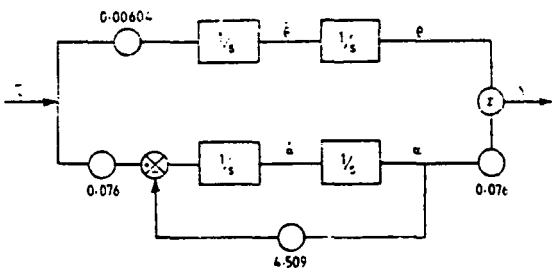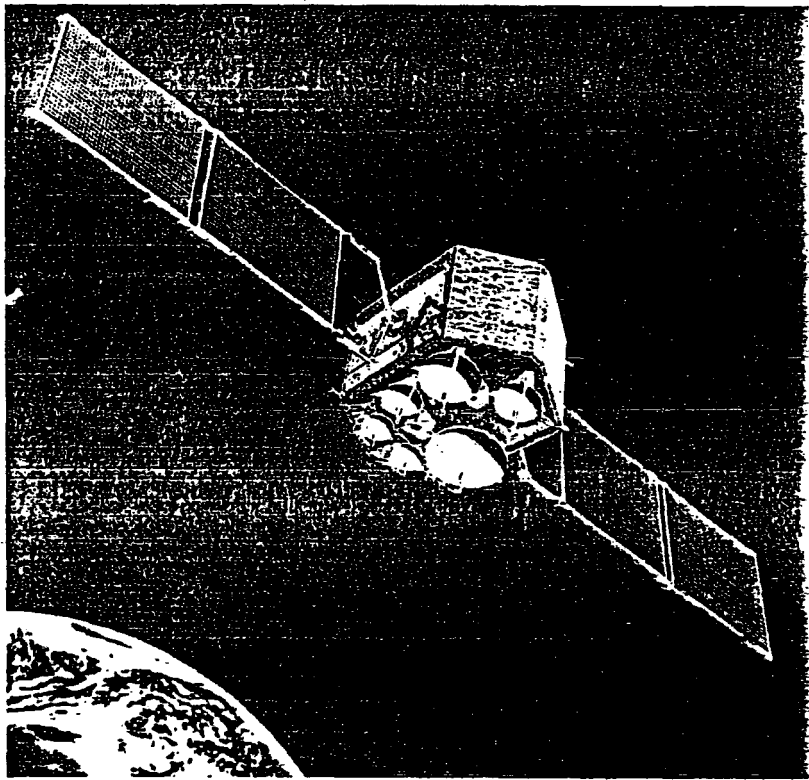

Fig. 4. The Satellite Type (a) and Block Diagram (b).

typically the Hawker Siddeley Dynamics vehicle OTS launched early in 1978. The governing dynamical equations are:

$$\ddot{\theta} = 0.00604\tau$$
$$\ddot{\alpha} + \omega_a^2\alpha = 0.076\tau$$
and
$$y = \theta + 0.076\alpha.$$

(16)

Where $\omega_a^2 = 4.509$ rad^2 s^{-2}, θ is the centre body rotation due to rigid body motion, α is the centre body rotation due to flexural motion and y is the actual rotation. τ is the input torque produced by reaction jets.

The satellite type and block diagram is shown in Fig. 4. The system is to be controlled as in Fig. 2 with $\tau = u$.

It is well known that modelling inaccuracies can cause anomalous behaviour in satellite control [17], therefore the main concern of this study is the controller response to parameter changes. To further test the robustness a mismatch condition is introduced by designing the controller based upon a rigid body model. It is assumed that y and $\dot{y}$ are available from on-board instruments. GU is chosen as 0.07 giving a maximum torque input of 0.49 Nm. A selection of 0.01 s for T guarantees good sampled-data reconstruction.

5.1. Scaling Factors for Rigid Body Motion

Because of the mismatch condition the analysis is carried out on the "known" information of:

$$x^T = [\theta, \dot{\theta}]$$

$$A_1 = \begin{bmatrix} 1 & T \\ 0 & 1 \end{bmatrix} \qquad B_1 = \begin{bmatrix} 0.00604T^2/2 \\ 0.00604\ T \end{bmatrix}.$$

W is chosen as the unit matrix and the Riccatti equation is solved using the iterative techniques of Hewer [14] and Smith [15]. The Hewer algorithm is initialised using the method suggested by Armstrong and Rublein [16].

The solution matrix is:

$$P = \begin{bmatrix} 101.0 & 0.5 \\ 0.5 & 10.0 \end{bmatrix}$$

and the technique described in Section 4.1 yields the scaling factors
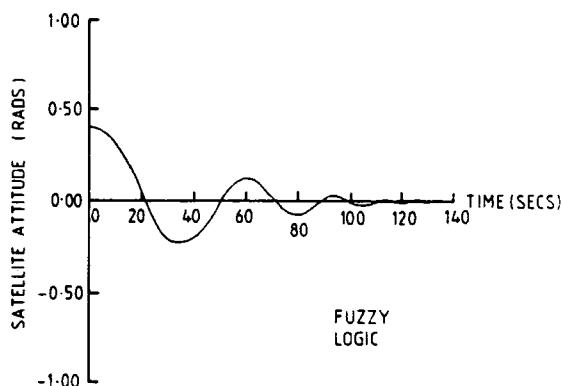
$$GE = 9 \times 10^4$$
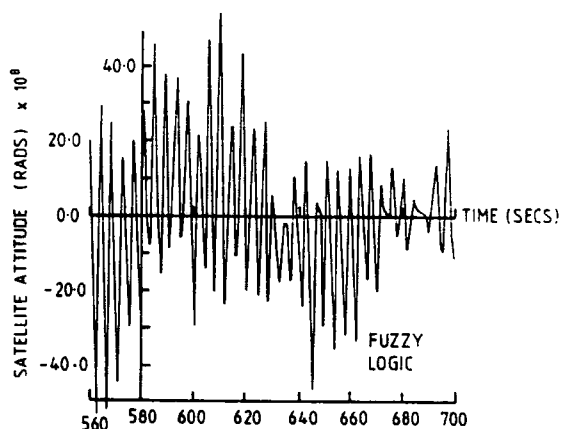
$$GC = 21 \times 10^4.$$

Fig. 5. The System Response with the Fuzzy Logic Controller. [Scaling factors: GE = 9×10^4. GC = 21×10^4. Initial displacement: 0.4 radians].

With these values the multilevel relay only intersects the critical surfaces close to the origin for the model available. This suggests a stable response until the origin is approached.

5.2. Comparison with a State Feedback Controller

The system response to the scaling factors $GE = 9 \times 10^4$ and $GC = 21 \times 10^4$ and initial displacement of 0.4 radians is shown in Fig. 5.

To enable performance comparisons to be made the *fuzzy logic* controller is compared with a controller based upon *state feedback* and Lyapunov's second method [12]. The controller is in the form
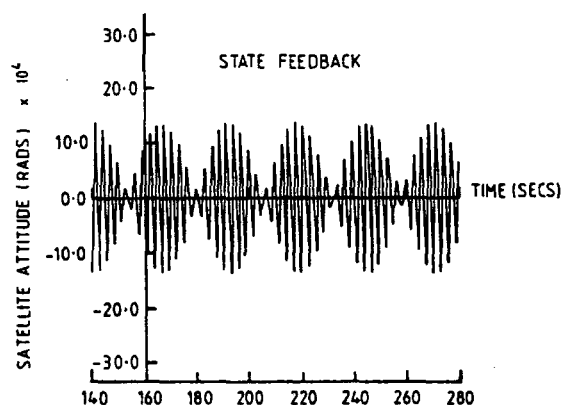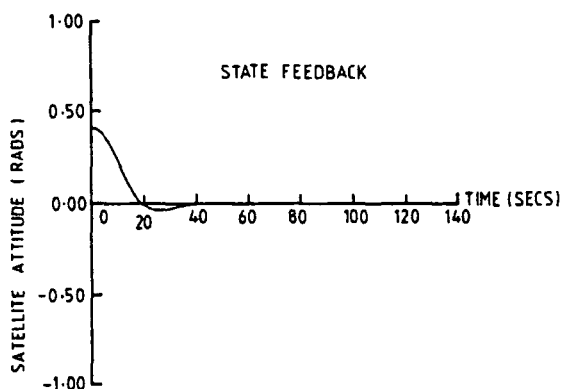
Fig. 6. The System Response with the State Feedback Controller. [Feedback matrix K = [302.0, 1526.0]].

However the *fuzzy logic* controller does converge to a greater pointing accuracy (note the state feedback convergence cannot be reduced by reducing the deadband).

To further test the robustness of the controllers the system parameters are regarded as variables and the governing equations therefore become:

$$\ddot{\theta} = k_1\tau$$

$$\ddot{\alpha} + k_2\alpha = k_3\tau$$

and

$$y = \theta + k_3\alpha.$$

First the effect of increasing the magnitude of the solar arrays is investigated. As they are increased the system response to both controllers obviously becomes more sluggish, however, the pointing accuracy decreased more for the *state feedback* con-

of a relay with deadband, δ:

$$\tau = \begin{array}{ll} t & q > \delta \\ 0 & |q| < \delta \\ -t & q < -\delta \end{array}$$

Where τ is the controller output torque, $t = 0.49$ Nm and the disturbance is given by

$$q = -Kx.$$

Using the approach described in the above reference and the values $\omega c = 0.1$, $\delta c = 0.9$ the feedback matrix is calculated as:

$$K = [302.0 \quad 1526.0].$$

The system response to this controller is shown in Fig. 6.

Clearly both controllers cope well with the mismatch condition but the *state feedback* controller's transient convergence is superior.
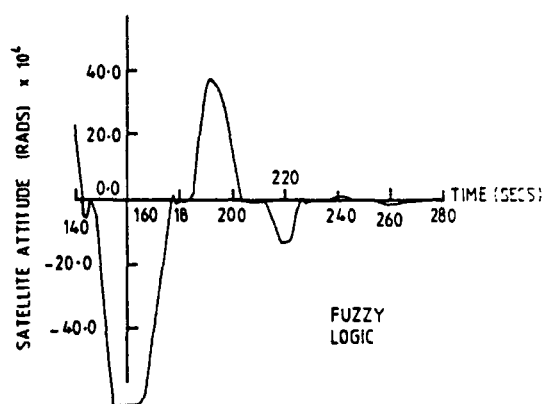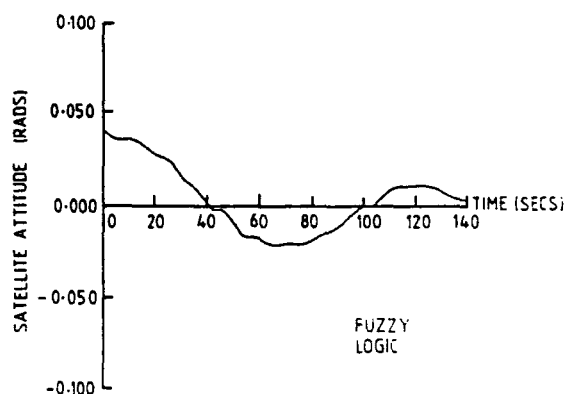

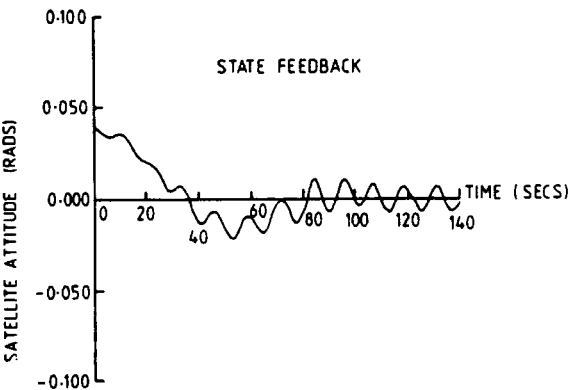Fig. 7. The System Response with the Fuzzy Logic Controller With an Increased Magnitude of Solar Arrays.

Fig. 8. The System Response with the State Feedback Controller With an Increased Magnitude of Solar Arrays.

Fig. 10. The System Response to a 100 Times Panel Thickness Reduction and a Reduction in Centre Body Size with the State Feedback Controller.

troller. Figs. 7 and 8 show the response to a tenfold increase in array surface area for which $K_1 = 15.66 \times 10^{-5}$, $K_2 = 0.268$ and $K_3 = 3.75 \times 10^{-2}$. It is apparent that the *state feedback* controller may violate the required pointing accuracy.

The greatest difference is observed when the solar array thickness is reduced dramatically. Figs. 9 and 10 show the responses to a 100 times panel thickness reduction and reduction in centre body size $K_1 = 1.764$, $K_2 = 33.15 \times 10^{-4}$ and $K_3 = 4.358$. The *fuzzy logic* controller is clearly superior but the system is far outside practical design considerations.

When a reduction in array length is considered, which could occur in practice if the arrays were struck by debris, the responses improve similarly. It is interesting to note for this reduction the steady state error is of the same order for both controllers.

6. Discussion and Conclusion

The contents of this paper were prompted in an effort to improve system reliability in fuzzy logic *controller* applications. Present approaches are based upon modelling the strategy of a human controller where a reliable mathematical description of the process is difficult to obtain. With this approach there are certain drawbacks:

(a) It is implicitly assumed that significant changes do not occur during operation.

(b) There is evidence to suggest that operators do not always report their control strategy reliably [18].

(c) The subjectivity in choosing certain control parameters and the necessity for their on-line tuning may result in extensive damage to the plant.
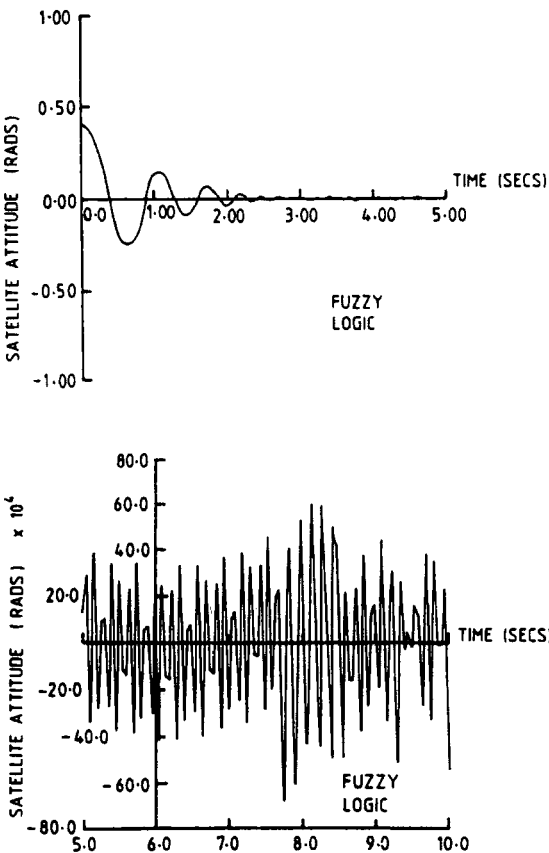
Thus it is felt that some parameter space must be

Fig. 9. The System Response to a 100 Times Panel Thickness Reduction and a Reduction in Centre Body Size with the Fuzzy Logic Controller.
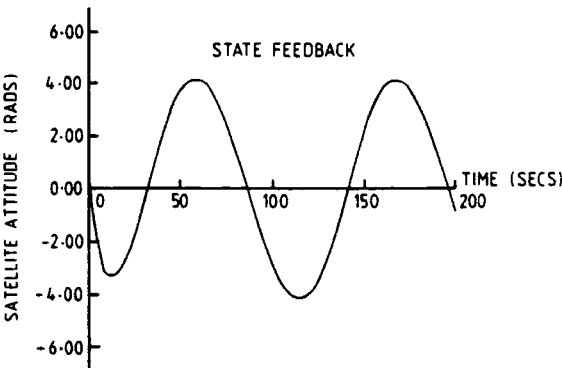
identified whereby the controller can be used with relative confidence. It has been shown how this can be done using Lyapunov's second method to identify a stable choice of scaling factors regardless of the rest of the controller structure. Following this design procedure the performance of the controller is investigated under considerable plant variation and compared to a conventional design. It has been shown that some areas do exist where the Fuzzy Logic Controller performs better, although a more quantitative analysis would give a more complete picture. However for the plant investigated the wide variation in parameter size, required to obtain a significant difference in performance between the two controllers, is perhaps outside practical design considerations.

References

[1] E.H. Mamdani. Application of fuzzy algorithms for control of simple dynamic plant. Proc. I.E.E. 121 (12) (1974) 1585–1588.

[2] E.H. Mamdani and S. Assilian, An experiment in Linguistic synthesis with a fuzzy logic controller. Int. J. Man-Machine Stud. 7 (1975) 1–13.

[3] L.A. Zadeh, Fuzzy sets, Inf. and Control 8 (1965) 338–353.

[4] L.A. Zadeh, Fuzzy Algorithms. Inf. and Control 12 (1968) 94–102.

[5] L.A. Zadeh, Outline of a new approach to the analysis of complex systems and decision processes. I.E.E.E. Trans. Syst. Man. and Cyb. SMC-3 (1973) 28–44.

[6] W.J.M. Kickert and E.H. Mamdani, Analysis of a fuzzy logic controller. Fuzzy Sets and Systems 1 (1978) 29–44.

[7] R.M. Tong, Analysis of fuzzy control algorithms using the relation matrix. Int. J. Man-Machine Stud. 8 (1976) 679–686.

[8] R.M. tong, Analysis and control of fuzzy systems using finite discrete relations. Int. J. Control 27 (1978) 431–440.

[9] E.H. Mamdani, Advances in the linguistic synthesis of fuzzy controllers. Int. J. Man-Machine Stud. 8 (1976) 669–678.

[10] M. Braae and D.A. Rutherford, Selection of parameters for a fuzzy logic controller. Fuzzy Sets and Systems 2 (1979) 185–199.

[11] T.J. Procyk, A self-organizing controller for dynamic processes. Ph.D. thesis, University of London (1977).

[12] E.H. Smith and K.F. Gill, Flexible space vehicle control based on state observation and Lyapunov's method in Dynamics and control of non-rigid spacecraft, Proc. of E.S.A Symposium, Frascati, Italy, 24–26 May, 1976, pp. 213–220.

[13] D.R. Smart, K.F. Gill, J.M. Gething and J.A. Holt, Dynamic analysis of flexible space vehicles having uncoupled control axes. Aero. Journ. Royal Aero. Society 78 (1974) 560–569.

[14] G.A. Hewer, An iterative technique for the computation of the steady state gain for the discrete optimal regulator. I.E.E.E. Trans. Automatic Control, AC-16 (1971) 382–282.

[15] R.A. Smith, Matrix equation $XA + BX = C$. S.I.A.M. J. Appl. Math. 16 (1968) 198–207.

[16] E.S. Armstrong and G.T. Rublein, A stabilization algorithm for linear discrete constant systems. I.E.E.E. Trans. Automatic control, AC-21 (1978) 629–631.

[17] P.V. Likins, Interactive problems between the dynamics and control system for non-rigid spacecraft, in Dynamics and control of non-rigid spacecraft. Proc. of E.S.A. Symposium, Frascati, Italy, 24–26 May, 1976. pp. 265–271.

[18] L. Bainbridge, The process controller, in: W.T. Singleton (Ed.), The Analysis of Practical Skills, Vol. I, (1975).

Appendix A

The Fuzzy Control Algorithm

The input to the controller is the state x_2 and the state x_1, the output from the controller is the input to the process u. x_1 is quantised into 13 points ranging from maximum negative state through zero state to maximum positive state. The zero state is further divided into negative zero state (NO-just below set point) and positive zero state (PO-just above the set point). The fuzzy set for x_1 is shown below:

	−6	−5	−4	−3	−2	−1	−0	+0	1	2	3	4	5	6
PB	0	0	0	0	0	0	0	0	0	0	0.1	0.4	0.8	1.0
PM	0	0	0	0	0	0	0	0	0	0.2	0.7	1.0	0.7	0.2
PS	0	0	0	0	0	0	0	0.3	0.8	1.0	0.5	0.1	0	0
PO	0	0	0	0	0	0	0	1.0	0.6	0.1	0	0	0	0
NO	0	0	0	0	0.1	0.6	1.0	0	0	0	0	0	0	0
NS	0	0	0.1	0.5	1.0	0.8	0.3	0	0	0	0	0	0	0
NM	0.2	0.7	1.0	0.7	0.2	0	0	0	0	0	0	0	0	0
NB	1.0	0.8	0.4	0.1	0	0	0	0	0	0	0	0	0	0

x_2 is similarly quantised but there is no further division of the zero. The fuzzy set for x_2 is shown below:

	−6	−5	−4	−3	−2	−1	0	1	2	3	4	5	6
PB	0	0	0	0	0	0	0	0	0	0.1	0.4	0.8	1.0
PM	0	0	0	0	0	0	0	0	0.2	0.7	1.0	0.7	0.2
PS	0	0	0	0	0	0	0	0.9	1.0	0.7	0.2	0	0
NO	0	0	0	0	0	0.5	1.0	0.5	0	0	0	0	0
NS	0	0	0.2	0.7	1.0	0.9	0	0	0	0	0	0	0
NM	0.2	0.7	1.0	0.7	0.2	0	0	0	0	0	0	0	0
NB	1.0	0.8	0.4	0.1	0	0	0	0	0	0	0	0	0

The process input u is quantised into 15 points. The fuzzy set is shown below:

	−7	−6	−5	−4	−3	−2	−1	0	1	2	3	4	5	6	7
PB	0	0	0	0	0	0	0	0	0	0	0	0.1	0.4	0.8	1.0
PM	0	0	0	0	0	0	0	0	0	0.2	0.7	1.0	0.7	0.2	0
PS	0	0	0	0	0	0	0	0.4	1.0	0.8	0.4	0.1	0	0	0
NO	0	0	0	0	0	0	0.2	1.0	0.2	0	0	0	0	0	0
NS	0	0	0	0.1	0.4	0.8	1.0	0.4	0	0	0	0	0	0	0
NM	0	0.2	0.7	1.0	0.7	0.2	0	0	0	0	0	0	0	0	0
NB	1.0	0.8	0.4	0.1	0	0	0	0	0	0	0	0	0	0	0

The fuzzy sets listed in the preceding are subjective but logic applies constraints on the choice. The same can be said for the set of rules that follow which represent a desired transient trajectory of a lightly damped system.

If x_1 is NB then
If x_2 is NOT (PS OR PM OR PB)
u is PB
ELSE
If x_1 is NB then
if x_2 is PS
u is PM
ELSE
If x_1 is NB then
if x_2 is (PM OR PB)
u is PS
ELSE
If x_1 is NM then
if x_2 is (NB OR NM OR NS)
u is PB
ELSE
If x_1 is NM then
if x_2 is NO
u is PM
ELSE
If x_1 is NM then
if x_2 is PS
u is PS

ELSE
If x_1 is NM then
if x_2 is PM
u is NO
ELSE
If x_1 is NM then
if x_2 is PB
u is NS
ELSE
If x_1 is NS then
if x_2 is (NB OR NM OR NS)
u is PM
ELSE
If x_1 is NS then
if x_2 is NO
u is NO
ELSE
If x_1 is NS then
if x_2 is PS
u is NS
ELSE
If x_1 is NS then
if x_2 is PM
u is NM
ELSE
If x_1 is NS then
if x_2 is PB
u is NB

ELSE
    If x_1 is No then
    if x_2 is ANY
    u is NO
ELSE
    If x_1 is PO then
    if x_2 is ANY
    u is NO
ELSE
    If x_1 is PB then
    if x_2 is NB
    u is NS
ELSE
    If x_1 is PB then
    if x_2 is (NM OR NS)
    u is NM
ELSE
    If x_1 is PB then
    if x_2 is NOT (NM OR NS OR NB)
    u is NB
ELSE
    If x_1 is PM then
    if x_2 is NB
    u is PS
ELSE
    If x_1 is PM then
    if x_2 is NM
    u is NO
ELSE
    If x_1 is PM then
    if x_2 is NS
    u is NS

ELSE
    If x_1 is PM then
    if x_2 is NO
    u is NM
ELSE
    If x_1 is PM then
    if x_2 is (PS OR PM OR PB)
    u is NB
ELSE
    If x_1 is PS then
    if x_2 is NS
    u is NO
ELSE
    If x_1 is PS then
    if x_2 is NB
    u is PB
ELSE
    If x_1 is PS then
    if x_2 is NM
    u is PS
ELSE
    If x_1 is PS then
    if x_2 is (NS OR NO)
    u is NO
ELSE
    If x_1 is PS then
    if x_2 is (PS OR PM)
    u is NM
ELSE
    If x_1 is PS then
    if x_2 is PB
    u is NB

PAPER 51

A design study of a self-organizing fuzzy logic controller

S Daley, BSc. PhD
Control Division, GEC Engineering Research Centre, Whetstone, Leicester

K F Gill, BSc. MSc. PhD, CEng, MIMechE, MIEE
Department of Mechanical Engineering, University of Leeds

A study is described of the application of the self-organizing fuzzy logic controller (SOC), proposed by Procyk and Mamdani, to a complex multi-variable process. The control problem used in the investigation is the attitude control of a flexible satellite that has significant dynamic coupling of the axes. It is found that reasonable control can be obtained for this process, therefore demonstrating the potential of the SOC for complex processes that cannot be reliably modelled.

1 INTRODUCTION

The 'simple' fuzzy logic controller has been successfully implemented in many test cases and in actual industrial applications (1–12). Despite this success there are specific drawbacks in the design approach:

1. A reliable linguistic model of the operator's control strategy will not always be obtainable.
2. It is implicitly assumed that significant process changes do not occur during operations that are outside the operator's experience.

An attractive resolution of these problems is provided by the self-organizing fuzzy logic controller (SOC) (13, 14) which is capable of generating and modifying control rules based upon an evaluation of their performance. Procyk (13) demonstrated the potential of the SOC by simulating the control of several general processes, but realized that its full worth could only be evaluated after many application studies.

This paper describes a design study of the SOC that involves a process of greater complexity and higher mathematical dimension than has previously been investigated. The study highlights specific design problems that can be encountered and in the opinion of the authors represents a valuable extension to the published work in this area.

A basic familiarity with the 'simple' fuzzy logic controller is assumed: the unfamiliar reader is referred to (15, 16).

2 DESCRIPTION OF THE SOC

The SOC is an extension of the 'simple' fuzzy logic controller that incorporates performance feedback (Fig. 1). The performance measure operates locally by assigning a credit or reward value to the individual control action or actions that contributed to the present performance. The credit value is obtained from a fuzzy algorithm which linguistically defines the desired per-

formance and has the same form as the control algorithm of the 'simple' fuzzy logic controller. This information will be available because the control engineer will have a definite idea of the closed loop trajectories that are acceptable.

By implementing the standard techniques of fuzzy calculus the performance index can be written in the form of a 'look-up' table. If the antecedents of the performance rules are *process output a* and *change in process output ca*, then the credit value for a particular process output n at the sample instant kT is given by

$$p_o^n(kT) = f\{a^n(kT), ca^n(kT)\} \tag{1}$$

The vector of credit values for an m output process is

$$P_o(kT)^T = \{p_o^1(kT)p_o^2(kT) \cdots p_o^m(kT)\} \tag{2}$$

These credit values represent required changes of the system output(s) and consequently to enable rule modification they must be translated to changes in the manipulated variable(s) input to the process, $P_i(kT)$. If monotonicity can be assumed, then for the single input–single output system the relationship is simply

$$p_i(kT) = p_o(kT) \tag{3}$$

For the multivariable case, information about the input–output cross-coupling characteristics must be provided. This requirement can be met by including a model of the process in the controller, and due to the SOC's learning capabilities a relatively crude representation is adequate. Procyk and Mamdani (14) propose the use of an incremental model which can be derived as follows.

Consider the general multi-variable process characterized by the state space equation:

$$\dot{x} = f(x, u) \tag{4}$$

For a small change in the input vector u and subsequent change in the state vector x, the change in the first output derivative is given by

$$\delta \dot{x} = \frac{\partial f}{\partial x^T} \delta x + \frac{\partial f}{\partial u^T} \delta u \tag{5}$$

Q Quantization process
M Deterministic output selection
GI Input scaling factors
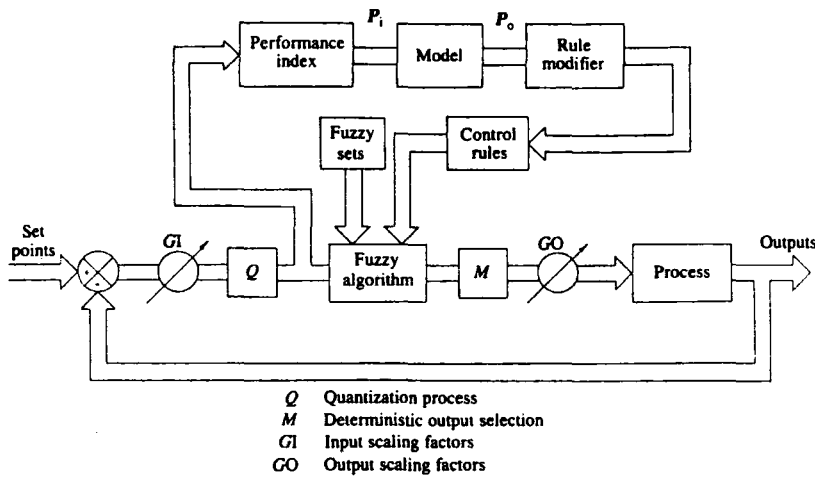GO Output scaling factors

Fig. 1   Form of the SOC

where

$$\frac{\partial f}{\partial x^{\mathsf{T}}} \triangleq \begin{bmatrix} \dfrac{\partial f_1}{\partial x_1} & \dfrac{\partial f_1}{\partial x_2} & \dfrac{\partial f_1}{\partial x_3} & \cdots & \dfrac{\partial f_1}{\partial x_m} \\[2mm] \dfrac{\partial f_2}{\partial x_1} & \dfrac{\partial f_2}{\partial x_2} & \dfrac{\partial f_2}{\partial x_3} & \cdots & \dfrac{\partial f_2}{\partial x_m} \\ \vdots & \vdots & \vdots & & \vdots \\ \dfrac{\partial f_m}{\partial x_1} & \dfrac{\partial f_m}{\partial x_2} & \dfrac{\partial f_m}{\partial x_3} & \cdots & \dfrac{\partial f_m}{\partial x_m} \end{bmatrix} \tag{6}$$

$$\frac{\partial f}{\partial u^{\mathsf{T}}} \triangleq \begin{bmatrix} \dfrac{\partial f_1}{\partial u_1} & \dfrac{\partial f_1}{\partial u_2} & \dfrac{\partial f_1}{\partial u_3} & \cdots & \dfrac{\partial f_1}{\partial u_n} \\[2mm] \dfrac{\partial f_2}{\partial u_1} & \dfrac{\partial f_2}{\partial u_2} & \dfrac{\partial f_2}{\partial u_3} & \cdots & \dfrac{\partial f_2}{\partial u_n} \\ \vdots & \vdots & \vdots & & \vdots \\ \dfrac{\partial f_m}{\partial u_1} & \dfrac{\partial f_m}{\partial u_2} & \dfrac{\partial f_m}{\partial u_3} & \cdots & \dfrac{\partial f_m}{\partial u_n} \end{bmatrix} \tag{7}$$

$$\dot{x}_i = f_i(x, u) \tag{8}$$

and m and n are the state vector dimension and the input vector dimension respectively.

The input changes Δu will give a state vector change Δx after one sample instant T of

$$\Delta x \approx T \,\delta \dot{x} = T \frac{\partial f}{\partial x^{\mathsf{T}}} \Delta x + T \frac{\partial f}{\partial u^{\mathsf{T}}} \Delta u \tag{9}$$

or

$$\Delta x = M \,\Delta u \tag{10}$$

where

$$M = \left(E - T \frac{\partial f}{\partial x^{\mathsf{T}}} \right)^{-1} T \frac{\partial f}{\partial u^{\mathsf{T}}}$$

and E is the unit matrix.

Consequently, if $P_o(kT)$ is a vector of required output changes the vector of input changes can be calculated from

$$P_i(kT) = M^{-1} P_o(kT) \tag{11}$$

Given the input rewards $P_i(kT)$, the rule(s) that most contributed towards the present state, kT. must be selected and modified accordingly. The problem of rule selection is related to the process dynamics and will be discussed in detail in Section 4. The rule modification procedure is as follows and although presented for a single input–single output system, the procedure can be extended to the multi-variable case.

Consider the inputs to the controller to be $a(kT)$ and $ca(kT)$ and the input to the process to be $\tau(kT)$. At some instant kT the process input reward is $p_i(kT)$ and if the process input rT samples earlier contributed most to the present state then the controller output due to the measurements $a(kT - rT)$ and $ca(kT - rT)$ should have been $\tau(kT - rT) + p_i(kT)$. The rule modification can be approached by forming fuzzy sets around the above single values:

$$A(kT - rT) = F_z\{a(kT - rT)\} \tag{12}$$

$$CA(kT - rT) = F_z\{ca(kT - rT)\} \tag{13}$$

$$\Gamma(kT - rT) = F_z\{\tau(kT - rT) + p_i(kT)\} \tag{14}$$

where F_z represents a fuzzification procedure.

Therefore the controller is modified by replacing the rules that most contributed to the process input rT samples earlier with the rule:

$$A(kT - rt) \rightarrow CA(kT - rT)\Gamma(kT - rT) \tag{15}$$

It is apparent how the above procedure can be used to generate rules from an 'empty' controller (that is no initial rules).

3 DESCRIPTION AND MODEL OF PROCESS

The process chosen for the design study is a hypothetical flexible communications satellite similar to the French multi-mission platform SPOT. The configuration of the vehicle is shown in Fig. 2. It is assumed to be travelling in a near polar circular orbit which is synchronized with the Sun and precesses at the same rate as the Earth, therefore no orbital corrections are required. The vehicle is required to function in a fine
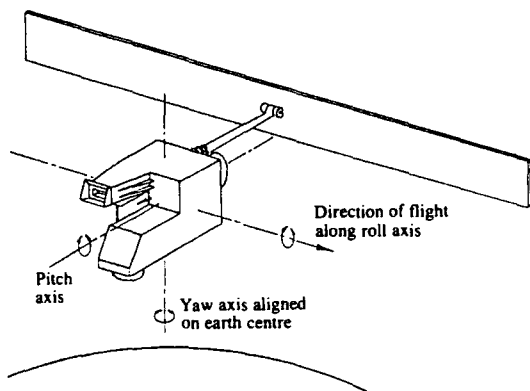
Fig. 2 Spacecraft configuration

pointing mode and the orbit reference axes, aligned with the satellite body are defined as:

(a) the *roll* axis, directed along the line of flight;
(b) the *pitch* axis, normal to the orbital plane;
(c) the *yaw* axis, directed along the vector locating the centre of the Earth relative to the satellite mass centre.

It will be noted that the axis set rotates about the pitch axis at the orbital angular velocity.

The solar array is mounted at the corner of one side of the spacecraft wall by means of a boom which is orientated parallel to the negative pitch axis. The array can rotate about this axis to maximize its exposure to solar energy as the craft traverses the Earth.

The vehicle is controlled by three orthogonally positioned reaction wheels, one per axis, which rotate on magnetic bearings to minimize the friction. The wheels operate with a linear torque–speed characteristic until saturation occurs. The control of all three axes must be considered as there is significant dynamic coupling. This is due to the size of the solar array, the asymmetry of the craft and the coupling effect of the momentum wheels (if small attitude rates are assumed the latter effect is negligible).

A state variable model of this vehicle has been derived (17) using data supplied by the British Aerospace Dynamics Group; a summary of the approach is presented below.

Using hybrid coordinate analysis (18) and assuming small angular rates and small attitude manoeuvres, the spacecraft dynamics may be represented by differential equations describing roll, pitch and yaw attitudes, and the solar array bending motion, as follows:

$$T = I\ddot{\beta} - \hat{\sigma}\ddot{\eta}^2 \tag{16}$$

$$\ddot{\eta} + \Omega^2\eta = \hat{\sigma}^T\ddot{\beta} \tag{17}$$

where T is the error torque acting on the vehicle (difference between external torques and the control torques), I is the 3×3 inertia matrix, β the body angular position, η the vector of modal deformation coordinates of dimension m, $\hat{\sigma}$ a 3×3 matrix whose columns are the moment of the mode shape σ_i, $i = 1$, ..., m and Ω is an $m \times m$ diagonal matrix the elements of which are the modal frequencies.

As the body axis set is rotating with orbital angular velocity ω_o about the pitch axis it must be related to the reference axis set by the transformation (17):

$$\ddot{\Phi} = \tilde{\omega}_o\dot{\Phi} + \ddot{\beta} \tag{18}$$

where

$$\Phi^T = [\phi \ \theta \ \psi] \tag{19}$$

is the vector of attitude angles (roll, pitch and yaw respectively) and

$$\tilde{\omega}_o = \begin{bmatrix} 0 & 0 & \omega_o \\ 0 & 0 & 0 \\ -\omega_o & 0 & 0 \end{bmatrix} \tag{20}$$

Substituting this transformation in equations (16) and (17) yields

$$\ddot{\eta} + \Omega^2\eta = \hat{\sigma}^T(\ddot{\Phi} - \tilde{\omega}_o\dot{\Phi}) \tag{21}$$

and

$$T = I(\ddot{\Phi} - \tilde{\omega}_o\dot{\Phi}) - \hat{\sigma}\ddot{\eta} \tag{22}$$

If equations (21) and (22) are written in the form of the partitioned matrix equation:

$$\begin{bmatrix} I & -\hat{\sigma} \\ -\hat{\sigma}^T & E \end{bmatrix}\begin{bmatrix} \ddot{\Phi} - \tilde{\omega}_o\dot{\Phi} \\ \ddot{\eta} \end{bmatrix} = \begin{bmatrix} T \\ 0 \end{bmatrix} - \begin{bmatrix} 0 \\ \Omega^2\eta \end{bmatrix} \tag{23}$$

then its transformation can be written as a set of second-order differential equations:

$$\begin{bmatrix} \ddot{\Phi} \\ \ddot{\eta} \end{bmatrix} = W^{-1}\left\{\begin{bmatrix} T \\ 0 \end{bmatrix} - \begin{bmatrix} 0 \\ \Omega^2\eta \end{bmatrix}\right\} + \begin{bmatrix} \omega_o\dot{\Phi} \\ 0 \end{bmatrix} \tag{24}$$

which can be written in state variable form.

$$W = \begin{bmatrix} I & -\hat{\sigma} \\ \hat{\sigma}^T & E \end{bmatrix}$$

The state vector of order $(6 + 2m)$ is defined as

$$x^T = [\phi \ \dot{\phi} \ \theta \ \dot{\theta} \ \psi \ \dot{\psi} \ \eta_1 \ \dot{\eta}_1 \cdots \dot{\eta}_m]$$

4 DESIGN OF SELF-ORGANIZING FUZZY LOGIC CONTROLLER

4.1 The performance index

The performance index measures the deviation from the path of the desired trajectory and issues appropriate changes that are required at the output of the controller. The index inputs in the case of the Earth resources satellite are conveniently chosen as attitude and change in attitude. The linguistically expressed desired trajectory will be the same for all three axes, making possible the use of the same performance index for each axis. Although the linguistic trajectory will be the same for each axis, the attainable 'real' trajectory may be different. However, the 'real' value of the performance index is dependent upon the scaling factors and can be different for each axis.

The linguistic performance rules, presented below, are written using a qualitative feel for a general two-measurement, one-input monotonic undamped process, and are intended to provide fast convergence coupled with the required damping around the equilibrium state to achieve a high pointing accuracy.

S DALEY AND K F GILL

Attitude	Change in attitude						
	PB	PM	PS	Z0	NS	NM	NB
PB	NB	NB	NB	NM	NM	NS	Z0
PM	NB	NB	NM	NM	NS	Z0	PS
PS	NB	NB	NS	NS	Z0	PS	PM
P0	NB	NM	NS	Z0	Z0	PM	PB
N0	NB	NM	Z0	Z0	PS	PM	PB
NS	NM	NS	Z0	PS	PS	PB	PB
NM	NS	Z0	PS	PM	PM	PB	PB
NB	Z0	PS	PM	PM	PB	PB	PB

These terms have the following meaning:

PB	positive big
PM	positive medium
PS	positive small
P0	positive zero
Z0	zero
N0	negative zero
NS	negative small
NM	negative medium
NB	negative big

For convenience the rules have been written in matrix form and should be interpreted as:

If 'attitude is NM' and 'change in attitude is PS' then 'credit is PS'.

The 'Z0' elements represent states where the performance is deemed acceptable and it will be noted that there are relatively few of these in the performance rules. This occurs because the rules have been written to generate control rules from an 'empty' controller and are therefore more active than if they were simply to modify existing rules. The more active the performance index the closer the response will be to the time optimal; however, this may result in continual modification of the rules in trying to achieve an unattainable trajectory.

The linguistic elements used are the same as those used in most of the application studies reported: the need for other terms or linguistic hedges such as very, more or less etc. is thought unnecessary for the study.

The terms P0 and N0 are introduced to obtain finer control about the equilibrium state. P0 being defined as values slightly above zero and N0 terms slightly below zero.

The fuzzy sets are formed upon a discrete support universe of 14 elements for the attitude. 13 elements for the attitude rate and 15 elements for the torque output. Appropriate membership functions are assigned to each element of the support set rather than by functional methods (1). The choice of membership functions that form a particular fuzzy set is subjective; however, common sense applies constraints to the values they may take. The resulting sets representing the linguistic terms presented above are listed in Table 1.

If the input states are assumed to be fuzzy singletons (that is fuzzy sets with membership functions equal to zero everywhere except at the measured value where it equals one), the linguistic performance rules can be transformed into a 'look-up' table (Table 2) using the standard techniques of fuzzy calculus (16).

Table 1   The fuzzy set definitions

(a) The attitude y

	−6	−5	−4	−3	−2	−1	−0	+0	1	2	3	4	5	6
PB	0	0	0	0	0	0	0	0	0	0	0.1	0.4	0.8	1.0
PM	0	0	0	0	0	0	0	0	0	0.2	0.7	1.0	0.7	0.2
PS	0	0	0	0	0	0	0	0.3	0.8	1.0	0.5	0.1	0	0
P0	0	0	0	0	0	0	0	1.0	0.6	0.1	0	0	0	0
N0	0	0	0	0	0.1	0.6	1.0	0	0	0	0	0	0	0
NS	0	0	0.1	0.5	1.0	0.8	0.3	0	0	0	0	0	0	0
NM	0.2	0.7	1.0	0.7	0.2	0	0	0	0	0	0	0	0	0
NB	1.0	0.8	0.4	0.1	0	0	0	0	0	0	0	0	0	0

(b) The attitude rate $\dot{y}$

	−6	−5	−4	−3	−2	−1	0	1	2	3	4	5	6
PB	0	0	0	0	0	0	0	0	0	0.1	0.4	0.8	1.0
PM	0	0	0	0	0	0	0	0	0.2	0.7	1.0	0.7	0.2
PS	0	0	0	0	0	0	0	0.9	1.0	0.7	0.2	0	0
Z0	0	0	0	0	0	0.5	1.0	0.5	0	0	0	0	0
NS	0	0	0.2	0.7	1.0	0.9	0	0	0	0	0	0	0
NM	0.2	0.7	1.0	0.7	0.2	0	0	0	0	0	0	0	0
NB	1.0	0.8	0.4	0.1	0	0	0	0	0	0	0	0	0

(c) The credit value p_o

	−7	−6	−5	−4	−3	−2	−1	0	1	2	3	4	5	6	7
PB	0	0	0	0	0	0	0	0	0	0	0	0.1	0.4	0.8	1.0
PM	0	0	0	0	0	0	0	0	0	0.2	0.7	1.0	0.7	0.2	0
PS	0	0	0	0	0	0	0	0.4	1.0	0.8	0.4	0.1	0	0	0
Z0	0	0	0	0	0	0	0.2	1.0	0.2	0	0	0	0	0	0
NS	0	0	0	0.1	0.4	0.8	1.0	0.4	0	0	0	0	0	0	0
NM	0	0.2	0.7	1.0	0.7	0.2	0	0	0	0	0	0	0	0	0
NB	1.0	0.8	0.4	0.1	0	0	0	0	0	0	0	0	0	0	0

Table 2 Performance index 'look-up' table

Attitude	Change in attitude												
	−6	−5	−4	−3	−2	−1	0	1	2	3	4	5	6
−6	7.0	6.5	7.0	6.5	7.0	7.0	4.0	4.0	4.0	3.0	1.0	0.0	0.0
−5	6.5	6.5	6.5	5.0	6.5	6.5	4.0	4.0	4.0	2.5	1.5	0.0	0.0
−4	7.0	6.5	7.0	5.0	4.0	4.0	4.0	1.0	1.0	1.0	0.0	−1.5	−1.0
−3	6.5	6.5	6.5	5.0	4.0	4.0	4.0	1.5	1.5	1.0	0.0	−1.0	−1.5
−2	7.0	6.5	7.0	4.0	1.0	1.0	1.0	0.0	0.0	−1.0	−1.0	−4.0	−4.0
−1	6.5	6.5	6.5	4.0	1.5	1.5	1.5	0.0	0.0	−1.0	−1.5	−4.0	−4.0
−0	7.0	6.5	4.0	3.0	1.0	1.0	0.0	0.0	0.0	−3.0	−4.0	−6.5	−7.0
+0	7.0	6.5	4.0	3.0	0.0	0.0	0.0	−1.0	−1.0	−3.0	−4.0	−6.5	−7.0
1	4.0	4.0	1.5	1.0	0.0	0.0	−1.5	−1.5	−1.5	−4.0	−6.5	−6.5	−6.5
2	4.0	4.0	1.0	1.0	0.0	0.0	−1.0	−1.0	−1.0	−4.0	−7.0	−6.5	−7.0
3	1.5	1.0	0.0	−1.0	−1.5	−1.5	−4.0	−4.0	−4.0	−5.0	−6.5	−6.5	−6.5
4	1.0	1.5	0.0	−1.0	−1.0	−1.0	−4.0	−4.0	−4.0	−5.0	−7.0	−6.5	−7.0
5	0.0	0.0	−1.5	−2.5	−4.0	−4.0	−4.0	−6.5	−6.5	−5.0	−6.5	−6.5	−6.5
6	0.0	0.0	−1.0	−3.0	−4.0	−4.0	−4.0	−7.0	−7.0	−6.5	−7.0	−6.5	−7.0

4.2 Rule modification

For the three-axis control of the earth resources satellite under study a general control rule is the implication:

$$A_\phi \rightarrow CA_\phi \rightarrow A_\theta \rightarrow CA_\theta \rightarrow A_\psi \rightarrow CA_\psi \rightarrow \Gamma_\phi \rightarrow \Gamma_\theta \rightarrow \Gamma_\psi$$

(25)

where A, CA and Γ are fuzzy sets for the attitude, change in attitude and the torque output respectively, the subscript denoting the reference axis. If the controller is 'empty' then an initial rule must be created; further rules will be generated when required by the modification procedure. The initial rule is formed from the fuzzification of the initial conditions a_ϕ^i, ca_ϕ^i, a_θ^i, ca_θ^i, a_ψ^i, ca_ψ^i, $p_{i\phi}^i$, $p_{i\theta}^i$, $p_{i\psi}^i$ (control torques, $\tau_\phi^i = \tau_\theta^i = \tau_\psi^i = 0$). This is done using a fuzzy kernel to provide a spread of values about the single support element, thus creating the following fuzzy sets which are the same for each axis:

$$A = \{(a - x), \mu_K(a - x)\}$$

$$CA = \{(ca - x), \mu_K(ca - x)\}$$

(26)

$$\Gamma = \{(\tau + p_i - x), \mu_K(\tau + p_i - x)\}$$

where

$$\left. \begin{array}{l} \mu_K(a - x) \\ \mu_K(ca - x) \\ \mu_K(\tau + p_i - x) \end{array} \right\} = \begin{cases} 1.0, & x = \pm 0 \\ 0.7, & x = \pm 1 \\ 0.2, & x = \pm 2 \\ 0.0, & 3 \leqslant x \leqslant -3 \end{cases}$$

The single elements at the input and output of the controller at each sample instant are stored for use by the modification procedure. Thus if the present instant is kT and the modification is made to the controller output rT samples earlier, the rule to be included results from the fuzzification of $a_\phi(kT - rT)$, $ca_\phi(kT - rT)$, ... $\tau_\psi(kT - rT) + p_{i\psi}(kT)$. To avoid contradictory rules any rules with similar antecedents to the above must be removed from the rule store. This also removes those rules that most contributed to the control action being rewarded. Procyk (13) forwards an algorithm for achieving the removal when initial rules are present in the controller. The algorithm analyses the membership function as follows.

If $A^R \rightarrow CA^R \rightarrow \Gamma^R$ represents a stored control rule

and A^m and CA^m are the antecedents of the rule to be included, then calculate the fuzzy subsets:

$$DA = \min \{A^R, \text{NOT } (A^m)\}$$

and

$$DCA = \min \{CA^R, \text{NOT } (CA^m)\}$$

If these subsets have all the membership functions less than or equal to 0.5 then the rule should be deleted; if not, it is kept. This is repeated for all stored rules.

In the implementation of the SOC required, the above algorithm would delete only those rules that have identical antecedent fuzzy sets to the rule to be included, as the form of all sets is generated from equation (26). Consequently, the number of operations required for modification can be significantly reduced by checking for coincident support sets. To reduce the number of rules generated, the modification algorithm used deletes rules unless their antecedents have fuzzy sets displaced along the universe of discourse by more than one support value relative to the antecedents of the rule to be added. This operation can be expressed linguistically as:

Delete all rules that are about the same as the one to be added.

4.3 Selection of a 'real world' model

Central to the design of the SOC is the selection of a process model that will reflect the degree of input–output coupling. The models used in this investigation are presented below.

4.3.1 Flexible vehicle model

The mathematical model used for the simulation of the satellite written in state variable form is

$$\dot{x} = Ax + Bu$$

(27)

Implementing equation (10) provides the non-square model M_{ns} where

$$\Delta x = M_{ns} \Delta u$$

(28)

and

$$M_{ns} = (E - TA)^{-1} TB$$

(29)

Clearly this cannot be used in its present form as the requirement is for a model matrix that relates a three-dimensional vector of process output changes P_o to a three-dimensional vector of process input changes P_i and M_{ns} is a 14×3 matrix. This can be achieved by including in the model matrix M only attitude information (ϕ, θ and ψ) formed from the elements of m_{ij} of M_{ns} as follows:

$$M = \begin{bmatrix} m_{11} & m_{12} & m_{13} \\ m_{31} & m_{32} & m_{33} \\ m_{51} & m_{52} & m_{53} \end{bmatrix} \tag{30}$$

Therefore:

$$P_i = \hat{M} P_o \tag{31}$$

where $\hat{M}$ is the M^{-1} matrix after normalization and scaling—a process described later.

4.3.2 Rigid vehicle model

An alternative model is formulated from a satellite description that does not include any flexible information: thus the governing differential matrix equation results from modifying equation (22) to

$$T = I(\ddot{\Phi} - \tilde{\omega}_o \dot{\Phi}) \tag{32}$$

from which the rigid vehicle state equation

$$\dot{x}_R = A_R x_R + B_R u \tag{33}$$

can be formed. The vector x_R is defined as

$$x_R^T = [\phi \ \dot{\phi} \ \theta \ \dot{\theta} \ \psi \ \dot{\psi}]$$

Equation (29) becomes

$$M_{ns} = (E - T A_R)^{-1} T B_R \tag{34}$$

where M_{ns} is a 6×3 matrix and the model matrix M can be obtained by using equation (30)

The matrix M^{-1} relates small 'real world' changes in the process outputs to small 'real world' changes in the process inputs. This must be scaled to the universe of discourse of P_i and P_o by using the scaling factors for each axis:

$$\Delta \tau = M^{-1} \Delta \Phi \tag{35}$$

$$\Delta \tau = \widehat{GT} P_i \tag{36}$$

and

$$P_o = \widehat{GY} \Delta \Phi \tag{37}$$

where

$$\widehat{GT} = \begin{bmatrix} GT_\phi & 0 & 0 \\ 0 & GT_\theta & 0 \\ 0 & 0 & GT_\psi \end{bmatrix}$$

and

$$\widehat{GY} = \begin{bmatrix} GY_\phi & 0 & 0 \\ 0 & GY_\theta & 0 \\ 0 & 0 & GY_\psi \end{bmatrix}$$

Thus

$$P_i = (\widehat{GT})^{-1}(M)^{-1}(\widehat{GY})^{-1} P_o \tag{38}$$

GY, GC and GT are the scaling factors on the attitude, change in attitude and controller output respec-

tively; the subscript denotes the reference axis. $\hat{M}$ is produced from $(\widehat{GT})^{-1}(M)^{-1}(\widehat{GY})^{-1}$ by a normalization process to ensure that P_i cannot exceed the maximum (or minimum) element of its support set (± 7). This condition is satisfied if

$$s_1^{-1} \triangleq \left| \frac{m_{11}}{GY_\phi GT_\phi} \right| + \left| \frac{m_{12}}{GY_\theta GT_\phi} \right| + \left| \frac{m_{13}}{GY_\psi GT_\phi} \right| \leqslant 1$$

$$s_2^{-1} \triangleq \left| \frac{m_{21}}{GY_\phi GT_\theta} \right| + \left| \frac{m_{22}}{GY_\theta GT_\theta} \right| + \left| \frac{m_{23}}{GY_\psi GT_\theta} \right| \leqslant 1 \tag{39}$$

$$s_3^{-1} \triangleq \left| \frac{m_{31}}{GY_\phi GT_\psi} \right| + \left| \frac{m_{32}}{GY_\theta GT_\psi} \right| + \left| \frac{m_{33}}{GY_\psi GT_\psi} \right| \leqslant 1$$

where m_{ij} is an element of M^{-1}. $\hat{M}$ is obtained from

$$\hat{M} = \text{scale} \times (\widehat{GT})^{-1}(M)^{-1}(\widehat{GY})^{-1} \tag{40}$$

where

$$\text{Scale} = \min \{s_1, s_2, s_3\}$$

It will be noted that to ensure the maximum range of use of the universe of discourse for each axis the numerical values of s_1, s_2 and s_3 must be approximately the same.

4.4 Controller parameter selection

The selection of the scaling factors is not wholly subjective (19) since their magnitude is a compromise between sensitivity during rise time and the required steady state accuracy. Procyk (13) attempted to reduce the subjectivity by introducing the terms:

1. *Error tolerance* (ET). This is the largest or smallest value in 'real' error that can be accommodated without initiating a rule modification. From the performance index 'look-up' table (Table 2), it can be seen that this is given by:

$$\text{ET} = \pm \frac{0.5}{GY} \tag{41}$$

2. *Change in error tolerance* (CT). This is the largest change in the direction of the origin during one sample that can be accommodated without initiating a rule modification. From Table 2:

$$\text{CT} = \pm \frac{2.5}{GC} \tag{42}$$

It is suggested by Procyk that suitable values for ET and CT are:

ET $\cong$ 5 per cent of the set point

CT $\cong \frac{1}{2}$ to $\frac{1}{5}$ of ET

These are a subjective selection and as Procyk points out the technique does not yield the best settings since the tolerances could be reduced ad infinitum. Also, since for the multi-variable case the same performance index is used for each axis and the set points are the same, the above procedure would always give the same scaling factors for each axis, which may not be desirable.

However, the procedure provides a starting point for scaling factor selection. Using the initial conditions:

$$\phi = \theta = \psi = 0.025 \text{ rad}$$

$$\dot{\phi} = \dot{\theta} = \dot{\psi} = 0.001 \text{ rad/s}$$

equation (41) is

$$ET = \frac{5 \times 0.025}{100} = \frac{0.5}{GY}$$

or

$$GY = 400$$

and if CT = ET 5, equation (42) gives

$$GC = 10\,000$$

(Note: $GY_\phi = GY_\theta = GY_\psi = GY$ and $GC_\phi = GC_\theta = GC_\psi = GC$)

By making an analogy of the SOC with a conventional PI controller (GY and GC are considered to be the equivalent of the integral and proportional gains respectively) Yamazaki and Mamdani (20) present equations for GY and GC. These equations are functions of the process parameters and are formulated from the characteristic equation method and the Ziegler and Nichols formulae. However, it is demonstrated that the settings obtained from these equations are not the best, thus confirming that the similarity between the SOC and the PI controller is only structural. The authors suggest that qualitative methods only can be used and present a line of reasoning for scaling factor selection similar to Procyk (above) by considering the mapping of 'real' variables to the linguistic term 'zero'.

An alternative qualitative selection can be made as follows. As the initial attitude is 0.025 rad (all axes), then to maximize the sensitivity in the initial transient phase this should be mapped to the maximum discrete support value thus:

$$GY = \frac{6}{0.025} = 240$$

The largest change of attitude (at small attitudes) that is considered acceptable by the authors is 0.025 rad over the 600 s simulation period. For a sample time of 0.5 s, (0.025×0.5) 600 must be mapped to 0.5 (above this value the quantization process registers a support value of one and a value below would register as zero):

$$GC = \frac{600 \times 0.5}{0.025 \times 0.5} = 24\,000$$

The above two sets of input scaling factors represent starting points for scaling factor selection; the optimum parameters will be selected by a logical trial and observation procedure.

The delay in reward parameter DL specifies which input(s) in the past most contributed to the present performance and is therefore related to process lags. Procyk (13) suggests that this can be selected by approximating the process to a pure dead-time process using

$$\frac{e^{-sL}}{s} = \frac{1}{s + s^2 L + s^3 L^2/2! + \cdots}$$

and setting DL to the equivalent dead-time L. For small attitude rates the satellite model is approximately

$$\phi(s) = \frac{b_{21}\tau_\phi + b_{22}\tau_\theta + b_{23}\tau_\psi}{s^2} \tag{43}$$

$$\theta(s) = \frac{b_{41}\tau_\phi + b_{42}\tau_\theta + b_{43}\tau_\psi}{s^2} \tag{44}$$

$$\psi(s) = \frac{b_{61}\tau_\phi + b_{62}\tau_\theta + b_{63}\tau_\psi}{s^2} \tag{45}$$

where b_{ij} is an element of the input matrix B. Clearly for this process the above approach is not suitable.

Yamazaki and Mamdani (20) question whether the Lth previous control action is really the major contribution to the present state and suggest a selection of DL somewhere between L and the time taken to reach a peak in response to an impulse at $t = 0$. From equations (43) to (45) it can be seen that if $\tau = 0$ then $\phi =$ constant, and consequently the impulse response will not peak and the above suggestion cannot be used. However, these methods are only an aid to DL selection and do not necessarily yield the best setting. For more complex processes the only option available is selection by trial and observation. Procyk's experiments indicated that the choice of the parameter was not critical and that better initial performances were obtained if the reward was distributed over several past samples.

4.5 Form of process input and $\widehat{GT}$ selection

If the discrete controller output at sample instant kT is $u^*\{kT\}$ then the process input $u\{kT\}$ is given by

$$u\{kT\} = \widehat{GT}u^*\{kT\} \tag{46}$$

As the maximum available torque is 0.2 N m then $\widehat{GT}$ is formed from

$$GT_\phi = GT_\theta = GT_\psi = \frac{0.2}{7} \cong 0.03$$

5 SIMULATION RESULTS

The figures presented in this section show the satellite response to the various controller parameters and are produced by creating an initial set of rules from an 'empty' controller over a simulation run, then repeating the simulation with the stored rules until the performance converges upon the optimum (for a particular set of controller parameters). Where there is a significant difference between this optimum and the initial response both trajectories are presented upon the same axes sets.

Figure 3a shows the attitude responses to the parameters:

$$GY_\phi = GY_\theta = GY_\psi = 400$$

$$GC_\phi = GC_\theta = GC_\psi = 10\,000$$

$$GT_\phi = GT_\theta = GT_\psi = 0.03$$

and the flexible model. The reward is distributed equally over the last five samples and is used for all results in this section unless otherwise stated. The delay in reward parameter was chosen as such because if only
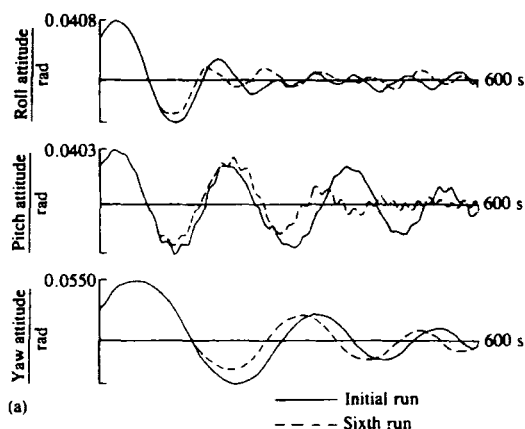
Fig. 3   Responses to SOC
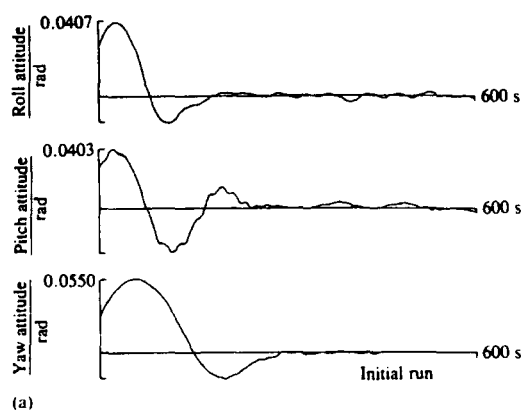
Fig. 4   Responses to SOC
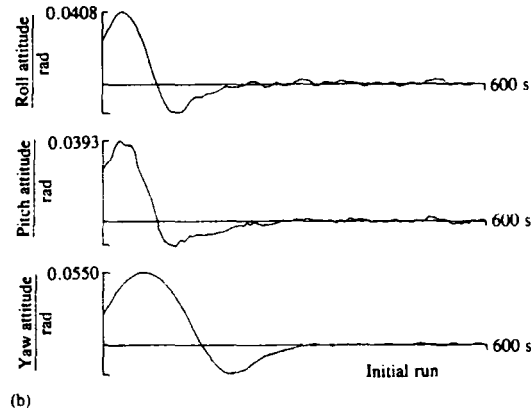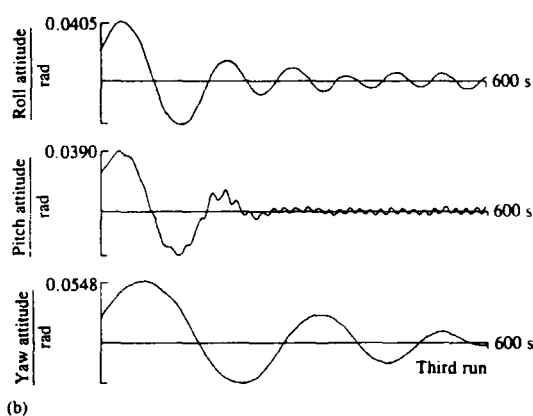
the last sample is rewarded then a very small number of rules is created during each run and system performance is poor. This is due to the rule deletion algorithm employed. To create an acceptable number of rules the delay in reward must be increased, and it was found that the performance was better if the reward was distributed over several samples. Increasing the parameter above five has no significant effect upon the performance and causes an increase in the required computation time. During the initial run 43 rules were created and the best performance occurred on the sixth run, after which 172 rules were stored. It is interesting to note that in achieving this optimum response there was a 'cycling' of performance in that it would improve over a number of simulation runs and then deteriorate before improvement occurred again. This phenomenon is due to the controller trying to achieve a performance that is not attainable and can only be stopped by modifying a combination of the controller parameters, controller model and performance index.

Paradoxically, the above performances, specifically the pitch attitude response, are improved if the rigid model is used in the controller (Fig. 3b). For this case, 84 rules are created on the initial run and the best performance occurs on the third run, after which 110 rules are stored. This performance improvement is not significant since it must be remembered that both models are approximations of the process dynamics.

Figure 4a shows the attitude responses to the parameters:

$$GY_\phi = GY_\theta = GY_\psi = 240$$

$$GC_\phi = GC_\theta = GC_\psi = 24\,000$$

$$GT_\phi = GT_\theta = GT_\psi = 0.03$$

and the flexible model. On the first run, 14 rules are created and the performance is not significantly improved in subsequent runs. Again, the performance is improved by using the rigid model in the controller (Fig. 4b). Clearly these parameter settings are superior to the previous ones.

The transient performance can be improved by decreasing the controller input scaling factors. For example, Fig. 5a shows the attitude response to:

$$GY_\phi = GY_\theta = GY_\psi = 180$$

$$GC_\phi = GC_\theta = GC_\psi = 20\,000$$

$$GT_\phi = GT_\theta = GT_\psi = 0.03$$

and the rigid model. The figure shows the first run, for which seven rules are created. Unfortunately, this improvement in the transient behaviour is accompanied by a slight deterioration in the steady state pointing accuracy.
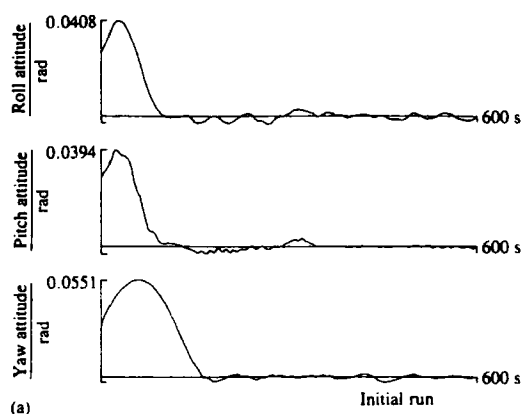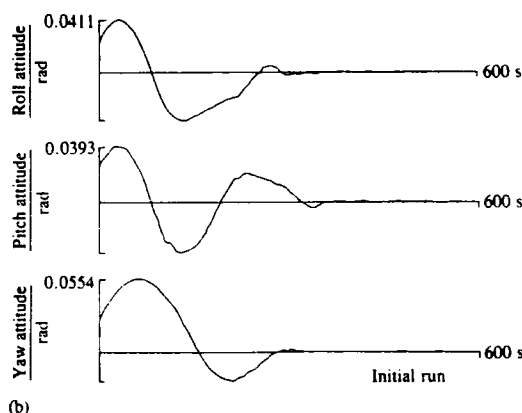
Fig. 5   Responses to SOC

Fig. 6   Responses to SOC

An increase in the scaling factors improves the steady state pointing accuracy but the transient behaviour deteriorates. Figure 5b shows the attitude response to

$$GY_\phi = GY_\theta = GY_\psi = 1600$$

$$GC_\phi = GC_\theta = GC_\psi = 80\,000$$

$$GT_\phi = GT_\theta = GT_\psi = 0.03$$

and the rigid model. This increase in the scaling factors is accompanied by an increase in the number of rules created (for example 79 for the first run illustrated).

It is interesting to note that the steady state performance of Fig. 5a is not significantly worse than that of Fig. 4b. This is due to a combination of the degree of excitation of the flexural modes (that are not actively controlled) and the rule deletion algorithm. The latter problem occurs because close to the origin (specifically within the band attitude $= \pm 0.5/GY$) for a particular sample many of the discrete states of the previous few samples will be 'about the same' (see Section 4.2) as the present state and therefore the rules generated from them will be deleted. Hence there will be fewer rules available for control about the origin. To investigate this, the deletion routine is modified so that a rule is deleted only if its antecedents are identical to the one to be added. Using the controller parameters associated with Fig. 4b and rewarding only the last sample, results in the creation of 310 rules on the first run (Fig. 6a).
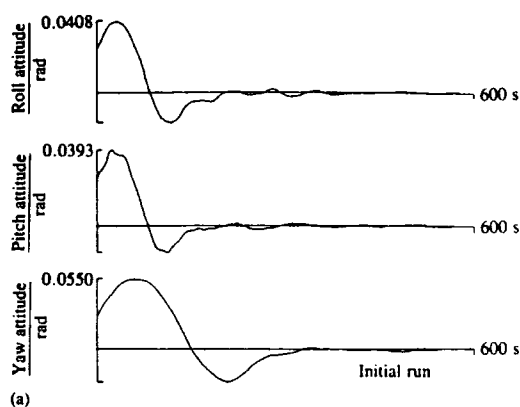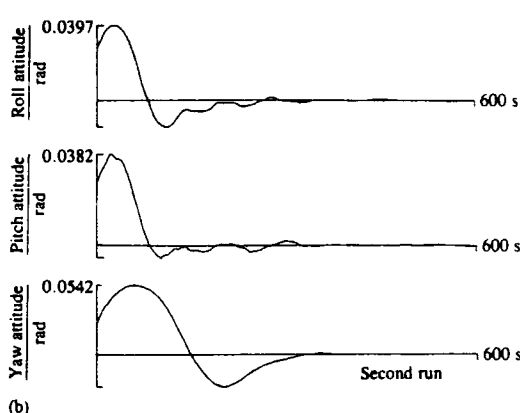
After the second run 490 rules are stored and the response (Fig. 6b) is improved marginally. The number of rules created on the third run exceeded the acceptable limit of 600 set by the authors. Although the responses of Fig. 6b are arguably the best obtained, the number of rules created is too large, requiring long CPU times to calculate the output. For these parameters some control of the modal vibrations is exhibited as they become more dominant (Fig. 7a), whereas for the parameters of Fig. 4b the modes are excited continually throughout the simulation (Fig. 7b). This modal control is also displayed by the parameters used to produce Fig. 5b. The increase in pointing accuracy also results in a decrease in control energy (Fig. 8a) over the control output for the parameters of Fig. 4b (Fig. 8b).

6 CONCLUSIONS

It has been shown that the SOC can perform reasonably well on a complex process with limited process knowledge, therefore encouraging its use in other industrial applications.

In the design of the SOC, the methods proposed by Yamazaki and Mamdani (20) and Procyk (13) to select some of the controller parameters either yielded unsuitable values or were not applicable to the process studied. However, a set of suitable controller param-

S DALEY AND K F GILL
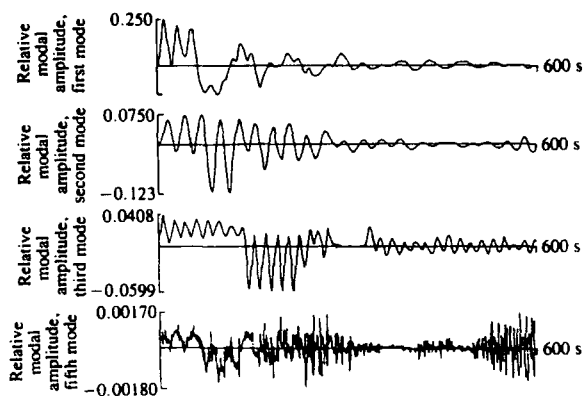
(a)
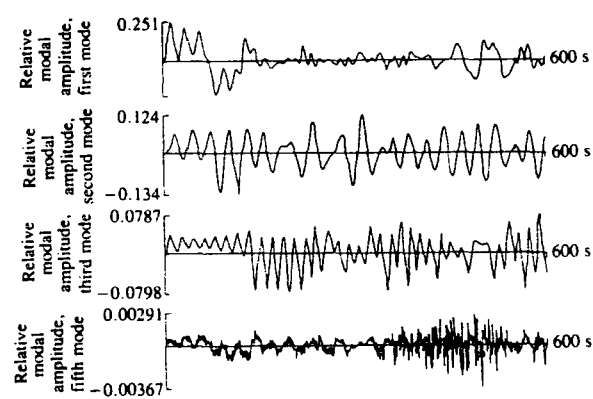
(b)

Fig. 7   Modal responses to SOC
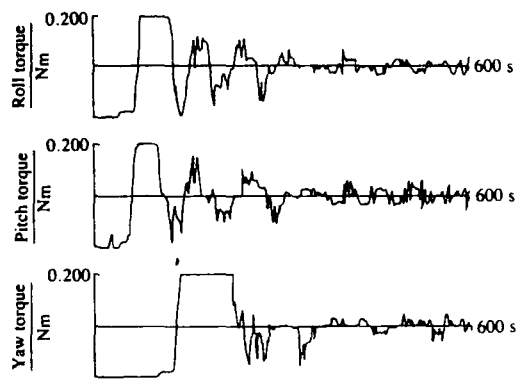
(a)
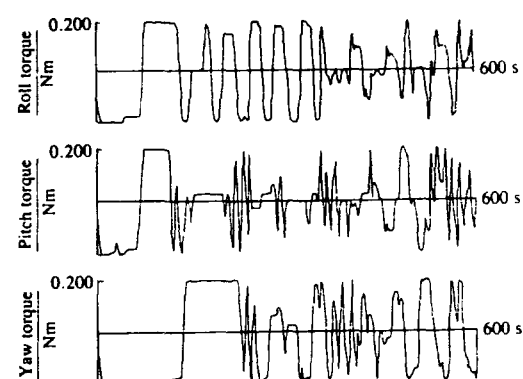
(b)

Fig. 8   Process input

eters were obtained without great difficulty using a trial and observation procedure.

The work of Procyk indicated that the performance of the SOC was relatively insensitive to the accuracy of the process model and the delay in reward parameter, which has been confirmed here. However, the need for a careful selection of the scaling factors has been demonstrated.

The dimension of the process studied made it necessary to employ an alternative to Procyk's rule deletion algorithm to keep the number of rules down to an acceptable level. For processes of higher dimension, further modification to the deletion algorithm may be required that will be a compromise between acceptable control and permissible computation time.

REFERENCES

1 **Kickert, W. J. M.** and **Van Nauta Lemke, H. R.** Application of a fuzzy controller in a warm water plant. *Automatica*, 1976, **23**, 301–208.

2 **Kickert, W. J. M.** Further analysis and application of fuzzy logic control. Internal report F/WK2/75, 1975, Queen Mary College, London.

3 **Østergaard, J. J.** Fuzzy logic control of a heat exchanger process. Internal report 7601, 1976, Electrical Power Engineering Department, Technical University of Denmark.

4 **Rutherford, D. A.** and **Carter, G. A.** A heuristic adaptive controller for a sinter plant. Proceedings of the Second IFAC Symposium on *Automation in mining, mineral and metal processing*, Johannesburg, 1976.

5 **Tong, R. M.** Some problems with the design and implementation of fuzzy controllers. Internal report CUED/F-CAMS/TR 127, 1976, Cambridge University.

6 **Van Amerongen, J., Van Nauta Lemke, H. R.** and **Van der Veen, J. C. T.** An autopilot for ships designed with fuzzy sets. In *Digital computer applications to process control* (Ed. H. R. Van Nauta Lemke), 1977 (IFAC and North-Holland).

7 **Larsen, P. M.** Industrial applications of fuzzy logic control. *Int. J. Man-Mach. Stud.*, 1979, **12**, 3–10.

8 **Tong, R. M., Beck, M. B.** and **Latten, A.** Fuzzy control of the activated sludge wastewater treatment process. *Automatica*, 1980, **16**, 659–701.

9 **Sheridan, S. E.** and **Skjøth, P.** Automatic kiln control at Oregon Portland Cement Company's Durkee plant utilising fuzzy logic. Proceedings of the 25th IEEE Technical Conference on *Cement industry*, San Antonio, Texas, 1983.

10 **Mamdani, E. H.** Application of fuzzy algorithms for control of simple dynamic plant. *Proc. IEE*, 1974, **121**, 1585–1588.

11 **Mamdani, E. H.** and **Assilian, S.** An experiment in linguistic synthesis with a fuzzy logic controller. *Int. J. Man-Mach. Stud.*, 1975, **7**, 1–13.

12 **King, P. J.** and **Mamdani, E. H.** The application of fuzzy control systems to industrial processes. *Automatica*, 1977, **13**, 235–242.

13 **Procyk, T. J.** A self-organising controller for dynamic processes. PhD Thesis, 1977, Queen Mary College, London.

14 **Procyk, T. J.** and **Mamdani, E. H.** A linguistic self-organising process controller. *Automatica*, 1979, **15**, 15–30.

15 **Mamdani, E. H.** Advances in the linguistic synthesis of fuzzy controllers. *Int. J. Man–Mach. Stud.*, 1976, **8**, 669–678.

16 **Tong, R. M.** A control engineering review of fuzzy systems. *Automatica*, 1977, **13**, 559–569.

17 **Fenton, J.** Satellite attitude measurement and control incorporating active damping of flexural motion. PhD Thesis, April 1981, University of Leeds.

18 **Likins, P. W.** Dynamics and control of flexible space vehicles.

Technical Report 32-1329, 1969, Jet Propulsion Laboratory, California.

19 **Brane, M.** and **Rutherford, D. A.** Selection of parameters for a fuzzy logic controller. *Fuzzy Sets and Systems*, 1979, **2**, 185–199.

20 **Yamazaki, T.** and **Mamdani, E. H.** On the performance of a rule-based self-organising controller. IEEE Conference on *Applications of adaptive and multivariable control*, Hull, England, 19–21 July 1982, 50–55.

PAPER 55

Forum on Fuzziness

A Study of Fuzzy Logic Controller Robustness Using the Parameter Plane

S. Daley
Dept. of Electrical Eng. and Electronics, Brunel University, Uxbridge, Middlesex UB8 3PH, U.K.

and

K.F. Gill
Department of Mechanical Engineering, University of Leeds, Leeds LS2 9JT, U.K.

An attempt is made to obtain a quantitative analysis of fuzzy logic controller robustness using parameter plane techniques. The method requires the controller, which is modelled as a multilevel relay, to be represented by a describing function. Therefore, the analysis can only be applied to systems where the input to the non-linearity is sufficiently close to a sinusoid to justify this representation. It is found that, although general quantitative results cannot be obtained, the method does produce a good indication of controller robustness for the plant investigated.

1. Introduction

Since its introduction by Zadeh in 1965 [1] fuzzy logic has been used successfully in a number of control applications [eg. 2–5]. Despite this success, general opinion has been that its use should only be considered when conventional techniques have proved inadequate yet a human process controller has been shown to cope well. If this philosophy is retained, its potential range of application will be extremely limited. However, in many of the application studies the fuzzy logic controller has displayed greater insensitivity to process changes than other, more conventional, controllers. The robust properties of the fuzzy logic controller therefore should not be overlooked and may alone form the justification for its wider use.

In a previous study [6] the authors applied fuzzy logic techniques to the design of an attitude controller for a flexible spacecraft. The robustness of this controller was demonstrated using a digital simulation to study its performance in response to various changes in the process parameters. Although this gave an indication of the robust qualities of the fuzzy logic controller it was concluded that a theoretical analysis was required to give a more complete picture. In this paper the suitability of the parameter plane technique for providing

Stephen Daley was born in Morecambe, England in 1959. He received the degree of B.Sc. in Mechanical Engineering from Preston Polytechnic in 1981 and the degree of Ph.D. for his work on fuzzy logic control algorithms from the University of Leeds in 1984. From 1984 to 1986 Dr Daley worked as a Senior Research Engineer at the Engineering Research Centre of GEC Research Ltd and was involved in the design, development and practical implementation of a self-tuning controller for fast processes. He is currently a lecturer in control engineering at Brunel University and his research interests remain in the areas of fuzzy logic and adaptive control.

Dr. Gill obtained his engineering training with a company manufacturing large steam turbine and alternating equipment for the electrical power supply industry. His academic training was gained at the University of Durham and the University of Birmingham. He was awarded the degrees of B.Sc. in 1955, M.Sc. in 1958 and Ph. D. in 1961. From 1961 Dr. Gill was a Senior Scientific Officer at the admiralty Weapons Establishment, Portland. For the last 21 years he has been a Lecturer, then Senior Lecturer at the University of Leeds, teaching control engineering and engineering dynamics to undergraduate students reading for an honours degree in Mechanical Engineering.

a quantitative measure of fuzzy logic controller robustness is assessed.

2. The Parameter Plane

Parameter plane techniques have long been used in controller design and a historical review of the work carried out by Vishnegradsky, Neimark, Mitrovic and Siljak appears in [7]. The work presented in this paper utilises the methods suggested by Siljak [8-10].

The method involves the mapping of contours in a complex plane to a parameter plane. The result is a partitioning of the parameter plane to give a more compact display of the roots associated with the equivalent complex contour. The parameters that form the axes of the parameter plane appear linearly in the coefficients of the characteristic equation; the coefficients may be real or complex.

2.1. Basic Theory

Consider the polynomial of order m:

$$F(p) = \sum_{k=0}^{m} a_k p^k, \tag{1}$$

where the coefficients a_k are functions of two parameter groups α and β, i.e.

$$a_k = a_k(\alpha, \beta). \tag{2}$$

p represents a point on the complex plane:

$$p = \sigma + j\omega \tag{3}$$

A mapping is required so that a point (α, β) in the parameter plane corresponds to the point (σ, ω) in the complex plane, satisfying $F(p) = 0$.

If the complex variable of Equation 3 is substituted into Equation 1 then the real and imaginary parts of the equation can be written as:

$$\left. \begin{array}{l} R(\sigma, \omega, \alpha, \beta) = 0 \\ I(\sigma, \omega, \alpha, \beta) = 0 \end{array} \right\} \tag{4}$$

This arises from the condition that the summations of the reals and imaginaries must independently be equal to zero.

Since the parameter values of σ and ω are

known, Equation 4 can be solved for α and β provided the Jacobian:

$$J = \det \begin{bmatrix} \dfrac{\partial R}{\partial \alpha} & \dfrac{\partial R}{\partial \beta} \\[2ex] \dfrac{\partial I}{\partial \alpha} & \dfrac{\partial I}{\partial \beta} \end{bmatrix} \tag{5}$$

exists and is non-zero.

It is apparent how, knowing $a_k(\alpha, \beta)$, any contour on the complex plane can be reproduced on the parameter plane. Consequently the extent to which the system parameters can vary and the roots of the characteristics equation still remain within a specified complex plane region can be observed. Robustness is defined in terms of a system property which is invariant under a specified class of perturbations. The system property under investigation in this study is "absolute stability", therefore the contour to be mapped is the imaginary axis of the s-plane (or unit circle of the z-plane).

3. Application to the Fuzzy Logic Controller

The fuzzy logic controller (design details in [6]) can be represented by the multilevel relay shown in Fig. 1, the output (τ) from the controller being defined as:

$$\tau = F(y, \dot{y}). \tag{6}$$

To enable the characteristic equation to be obtained, the relay is linearised using the describing function technique. It must be assumed that harmonics in the loop are of small amplitude and that the input y to the controller can be therefore approximated by a sinusoid of amplitude A and frequency Ω:

$$y = A \sin \Omega t. \tag{7}$$

The output from the controller is approximated by a Fourier series:

$$\tau = F^0 + N_1 y + \frac{N_2}{\Omega} sy + \ldots, \tag{8}$$

where

$$F^0 = \frac{1}{2\pi} \int_0^{2\pi} F(A \sin \Omega t, A\Omega \cos \Omega t) \, d(\Omega t)$$

FUZZY LOGIC CONTROLLER
MODELLED AS A MULTILEVEL
RELAY

MANIPULATED VARIABLE
U (RANGE -7,+7)

X2* (RANGE - 6 , +6)   X1*(RANGE -6, +6)

(+6,+6,-7)
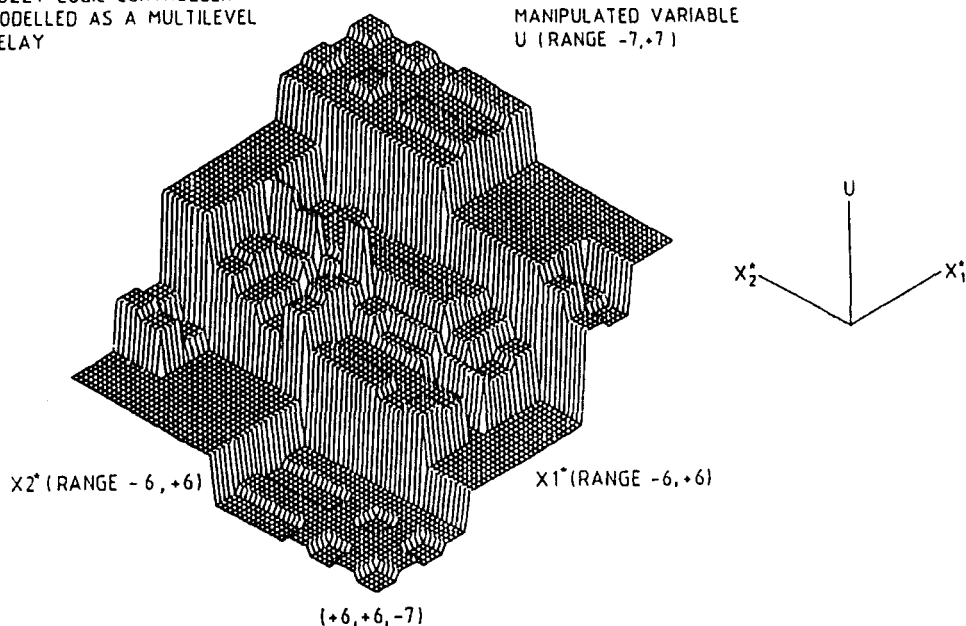
Fig. 1. The fuzzy logic controller modelled as a multilevel relay.

$$N_1 = \frac{1}{\pi A} \int_0^{2\pi} F(A \sin \Omega t, \, A\Omega \cos \Omega t)$$

$$\times \sin \Omega t \, d(\Omega t)$$

$$N_2 = \frac{1}{\pi A} \int_0^{2\pi} F(A \sin \Omega t, \, A\Omega \cos \Omega t)$$

$$\times \cos \Omega t \, d(\Omega t).$$

Higher order terms are neglected and as the relay is symmetrical F^0 is zero, hence Equation 6 is replaced by:

$$\tau = N_1 y + \frac{N_2}{\Omega} \dot{y}. \tag{9}$$

For any particular plant the characteristic equation can be obtained in the form of Equation 1 and the parameter groups can be specified as:

$$\alpha = \alpha(N_1, N_2),$$

$$\beta = \beta(N_1, N_2). \tag{10}$$

A contour representing the describing function

must also be plotted on the parameter plane to represent the operating point. Intersections of this contour with the contour representing the limit of stability, defined as $|z| = 1$, indicate possible system limit cycles. The limit cycle will only occur if the frequency of the $|z| = 1$ contour at the intersection coincides with the frequency of the describing function. Whether the limit cycle is stable or unstable can be determined by observing the change in the describing function contour relative to the intersection for a change in the amplitude. To ensure stability, the describing function contour must be entirely contained by the region representing m stable roots (where m is the order of the characteristic equation).

The algorithm shown in Fig. 2 can be used to calculate a family of describing function contours (the family parameter being Ω) and the result for a range of frequencies and amplitudes is shown in Fig. 3.

Start

Read amplitude range
$A_o \to A_n$
number of points N,
and frequency Ω

Calculate amplitude increment
$A_i = (A_n - A_o)/N$ and
set initial value
$A_j = A_o$

Multiply $\dot{y}$ axis of
multilevel relay by Ω

Calculate position t_k, $k = 0 \to m$
of switches from one output level
U_{k-1} to new output level U_k
at radius A_j
$c = \Omega t$

Evaluate the integrals:
$N_{1j} = \dfrac{1}{\pi A_j} \sum_{k=0}^{m} U_k \left[\cos \right]_{c_k}^{c_{k+1}}$

$N_{2j} = \dfrac{1}{\pi A_j} \sum_{k=0}^{m} U_k \left[\sin \right]_{c_k}^{c_{k+1}}$

$c_o = 0$; $c_{m+1} = 2\pi$

any remaining amplitudes?

Calculate next amplitude
$A_j = A_j + A_i$

Yes

No

Stop

Fig. 2. Flow chart for multilevel relay describing function calculation.

4. Application Study

The method is applied to a system based upon a flexible communications satellite (Fig. 4a) with uncoupled axes, as analysed in [11] and used as an illustrative example in [6].

The governing dynamical equations for the satellite are:

$$\ddot{\theta} = K_1\tau,$$
$$\ddot{\alpha} + K_3\alpha = K_2\tau,$$
and
$$y = \theta + K_2\alpha, \qquad\qquad (11)$$

where θ is the centre body rotation due to rigid body motion, α is the centre body rotation due to flexural motion, and y is the actual rotation.

In any robustness study a class of perturbations must be defined, in this case errors in the model parameters only are considered. Therefore K_1, K_2 and K_3 are considered to be variable parameters and the aim of this study is to define their allowable extremum values.

The sampled data fuzzy logic control system is modelled as shown in Fig. 4b. The characteristic equation is obtained in terms of the z transform and, therefore, the $|z| = 1$ contour results from a mapping of the unit circle from the z-plane.

Equations 1 and 3 become:

$$F(z) = \sum_{k=0}^{m} a_k z^k = 0,$$

and

$$z = \sigma + j\omega.$$

The characteristic equation is obtained in this form, the order m is 5 and:

$$a_k = b_k\alpha + c_k\beta + d_k.$$

where the parameter groups α and β are N_1 and N_2/Ω respectively and the values of b_k, c_k and d_k for $k = 0$ to 5 are listed in Appendix 1.

Equations 4 may be written as:

$$\left.\begin{array}{l} R \equiv B_1\alpha + C_1\beta + D_1 = 0 \\ I \equiv B_2\alpha + C_2\beta + D_2 = 0 \end{array}\right\} \qquad (12)$$

where

$$\left.\begin{array}{l} B_1 = \displaystyle\sum_{k=0}^{m} b_k X_k;\ B_2 = \displaystyle\sum_{k=0}^{m} b_k Y_k \\[2mm] C_1 = \displaystyle\sum_{k=0}^{m} c_k X_k;\ C_2 = \displaystyle\sum_{k=0}^{m} c_k Y_k \\[2mm] D_1 = \displaystyle\sum_{k=0}^{m} d_k X_k;\ D_2 = \displaystyle\sum_{k=0}^{m} d_k Y_k \end{array}\right\} \qquad (13)$$
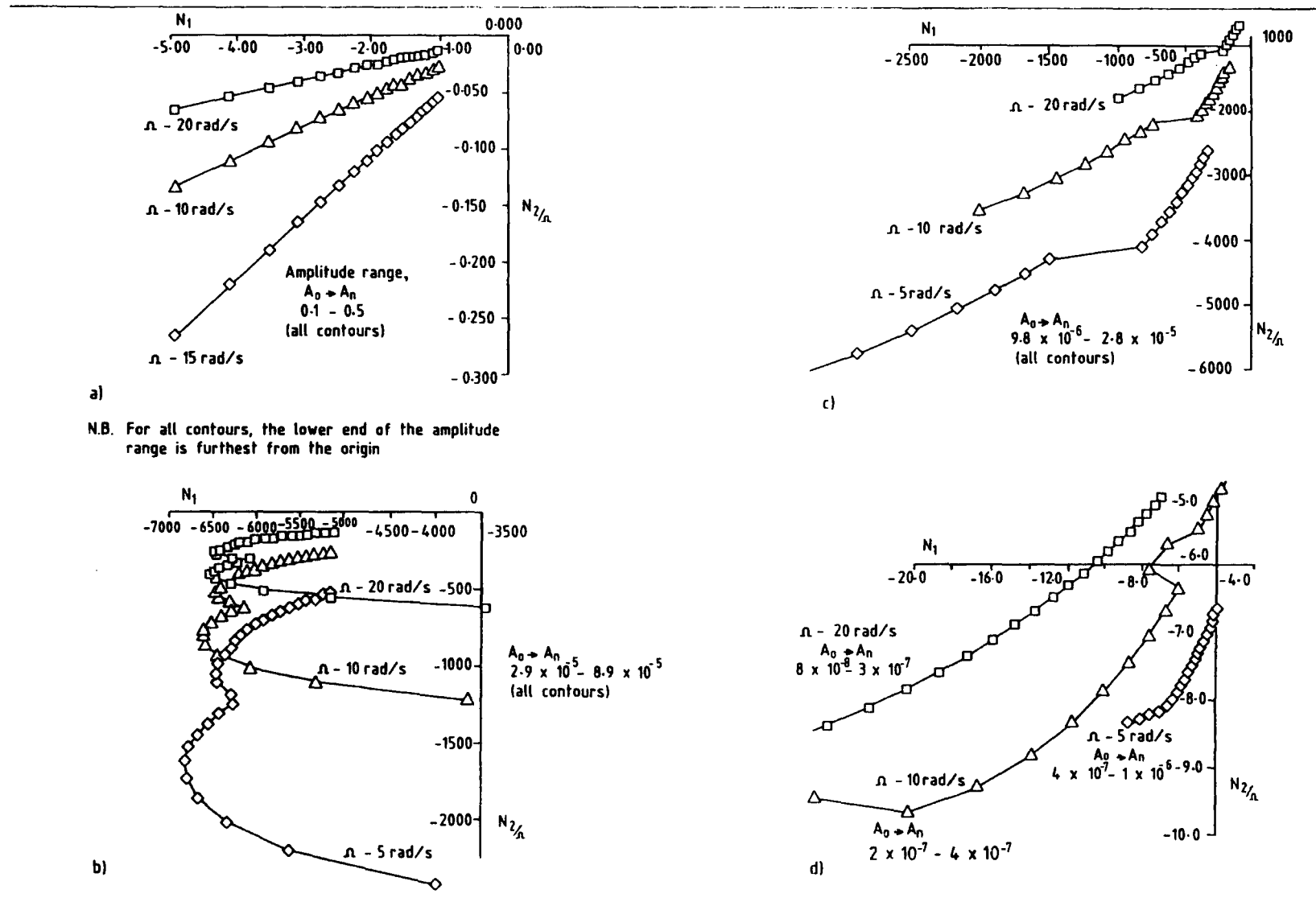
Fig. 3. Describing function contours for the fuzzy logic controller.
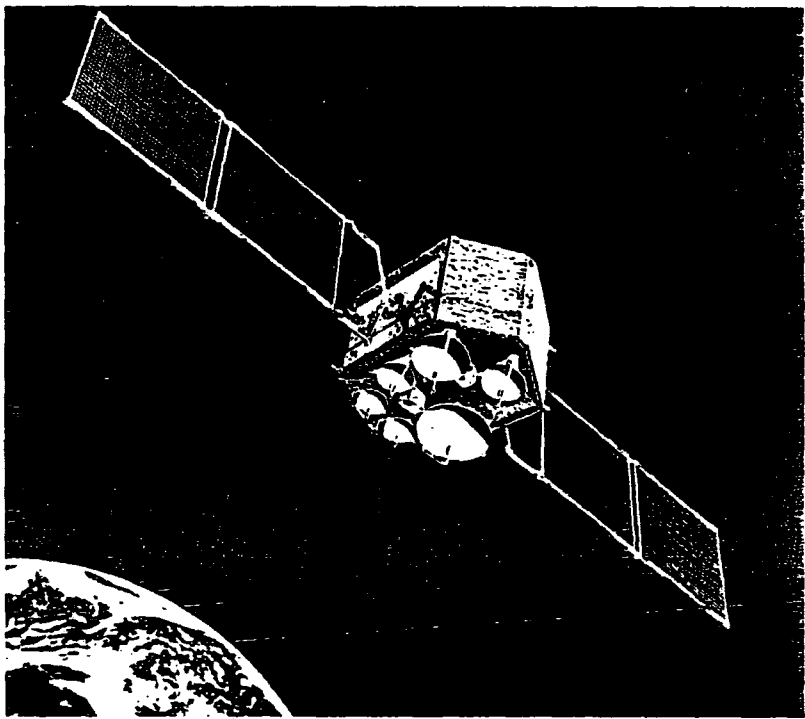
Fig. 4a. The vehicle.

The terms X_k and Y_k are polynomials in σ and ω arising from the expansion of z^{-k} (see Appendix 2) where:

$$z^{-k} = X_k + jY_k$$

and $X_k(\sigma, \omega)$ and $Y_k(\sigma, \omega)$ are obtained from the recurrence formulae:

$$\left.\begin{array}{l} X_{k-1} - 2\sigma X_k + (\sigma^2 + \omega^2) X_{k-1} = 0 \\ Y_{k-1} - 2\sigma Y_k + (\sigma^2 + \omega^2) Y_{k-1} = 0 \end{array}\right\} \qquad (14)$$
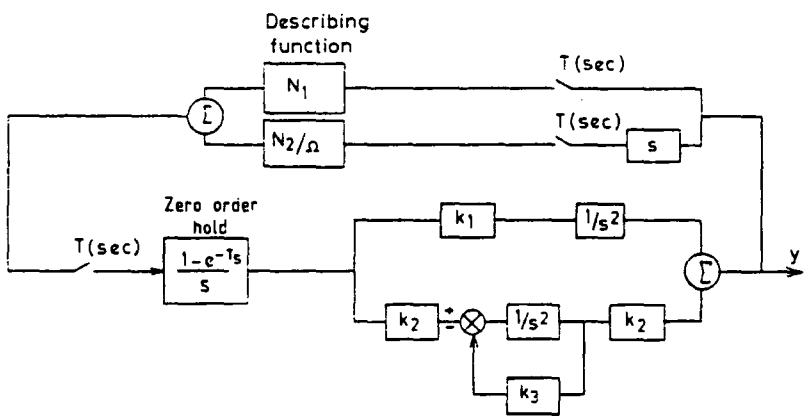
(b)   Block diagram of satellite fuzzy-logic control system

Fig. 4b. Block diagram.

a) Parameter plane for nominal satellite configuration

b) Detail of parameter plane closer to the origin with two fuzzy logic controller describing function contours superimposed
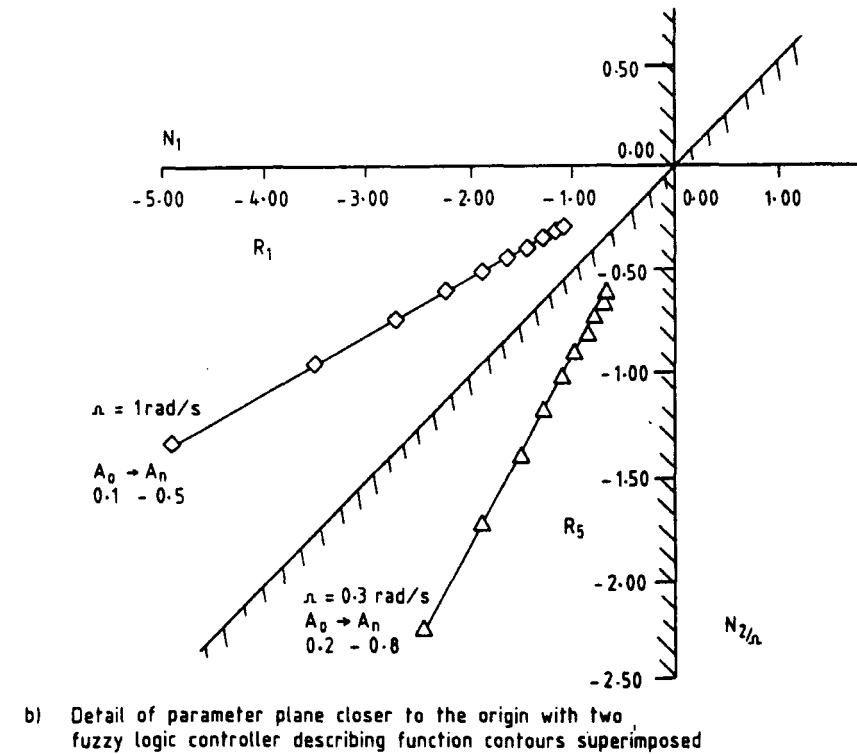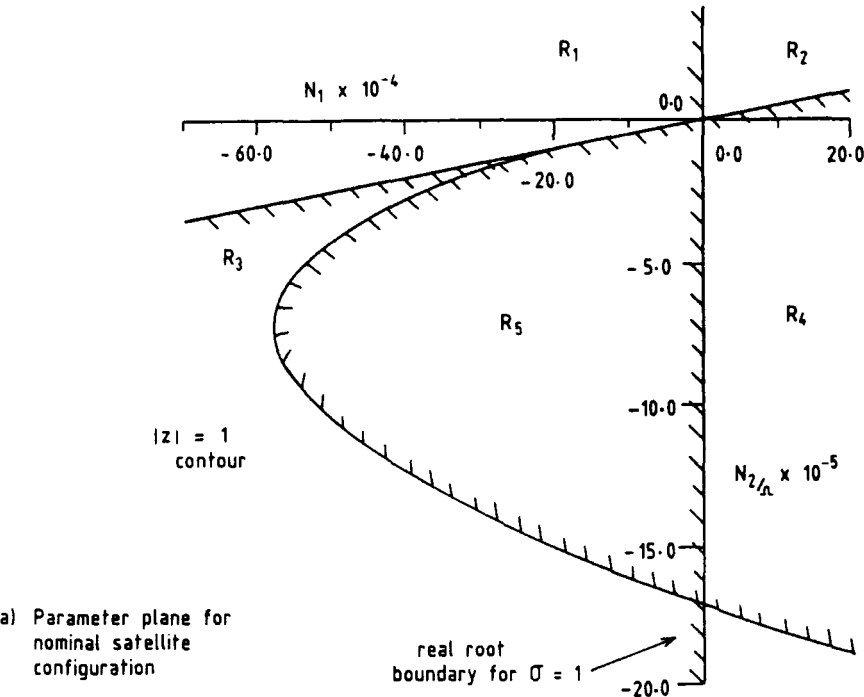
Fig. 5. Parameter plane and detail of parameter plane.

using $X_0 = 1$, $X_1 = \sigma$, $Y_0 = 0$ and $Y_1 = \omega$ solving Equation 12 for α and β yields:

$$\left. \begin{aligned} \alpha &= \frac{C_1 D_2 - C_2 D_1}{B_1 C_2 - B_2 C_1} \\ \beta &= \frac{B_2 D_1 - B_1 D_2}{B_1 C_2 - B_2 C_1} \end{aligned} \right\} \tag{15}$$

The denominator $B_1 C_2 - B_2 C_1$ is the Jacobian J.

Equations 13, 14 and 15 enable a mapping of the unit circle from the z-plane on to the parameter plane of coordinate axes N_1 and N_2/Ω. Because the coefficients a_k are real then the roots of the characteristic equation occur in complex conjugate pairs. Consequently as a root crosses the upper semi-circle of the unit circle, its conjugate crosses the lower semi-circle and only one half of the unit circle has to be mapped. i.e.

$$\alpha(\sigma, \omega) = \alpha(\sigma, -\omega)$$

and

$$\beta(\sigma, \omega) = \beta(\sigma, -\omega).$$

It is apparent from Equations 14 that when

$z = \pm 1$, $Y_k = 0$. As a consequence of this, singularities occur as $J = 0$. These points, therefore, are represented on the parameter plane as straight lines governed by:

$$\left. \begin{aligned} \alpha B_1(\sigma) + \beta C_1(\sigma) + D_1(\sigma) &= 0 \\ \sigma &= \pm 1 \end{aligned} \right\} \tag{16}$$

The resulting contours separate the stable real roots from the unstable ones and are known, therefore, as real root boundaries.

Because of the required form of the parameter groups, an investigation of robustness will not be as explicit as desired. The only procedure for this investigation is to vary the process parameters and observe the movement of the $|z| = 1$ contour relative to the describing function contour.

The parameter plane for the nominal satellite parameters is shown in Fig. 5. The region R_n is that region with n roots within the specified z-plane contour and the shading represents that side of the line enclosed by the contour. If the Jacobian is positive, the enclosed region lies to the left of the parameter plane contour as $\tan^{-1}(\omega/\sigma)$ increases. If the Jacobian is negative the region lies

a) Parameter plane for
$k_1 = 15.66 \times 10^{-2}$
$k_2 = 3.75 \times 10^{-2}$
$k_3 = 0.268$

Fig. 6a. Parameter planes.

b) Parameter plane for
  k_1 = 1.764
  k_2 = 4.358
  k_3 = 0.003315

Fig. 6b. Parameter planes.

a) Parameter plane for
  k_1 = 0.00604
  k_2 = 0.076
  k_3 = 4509.0
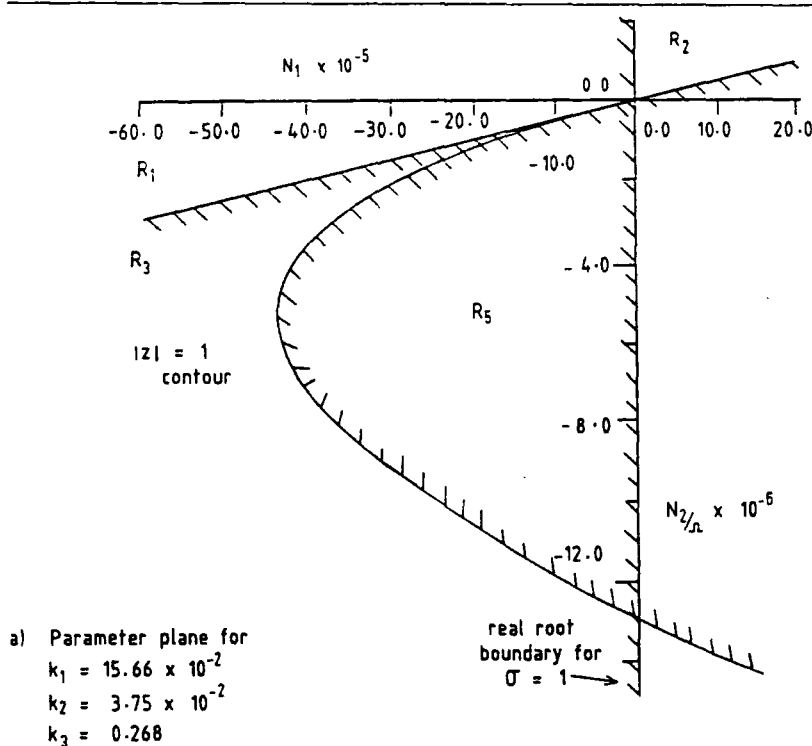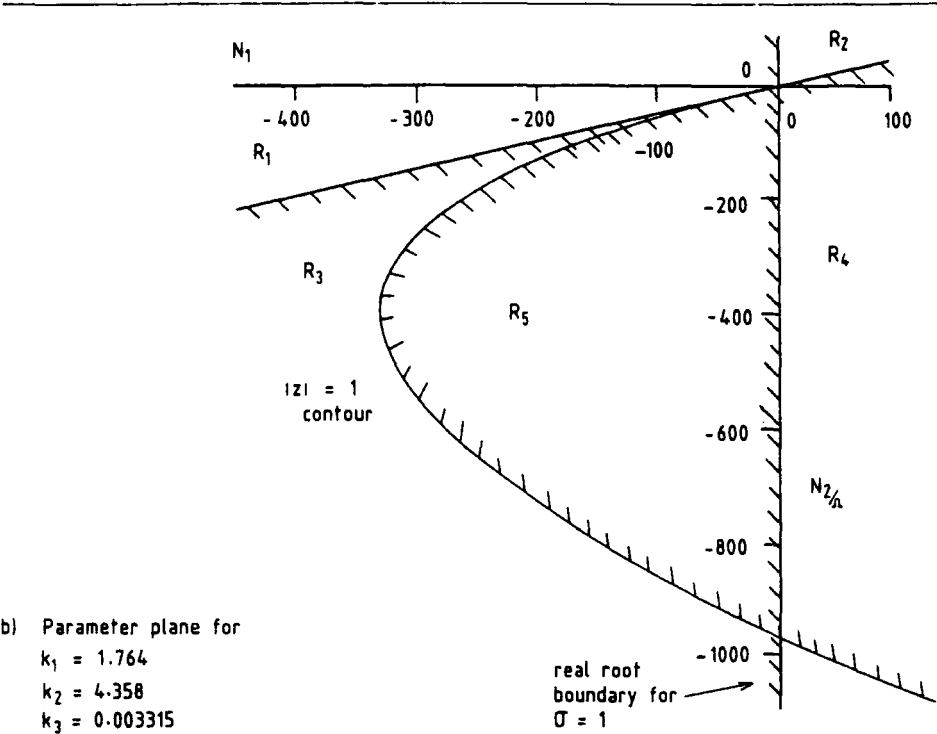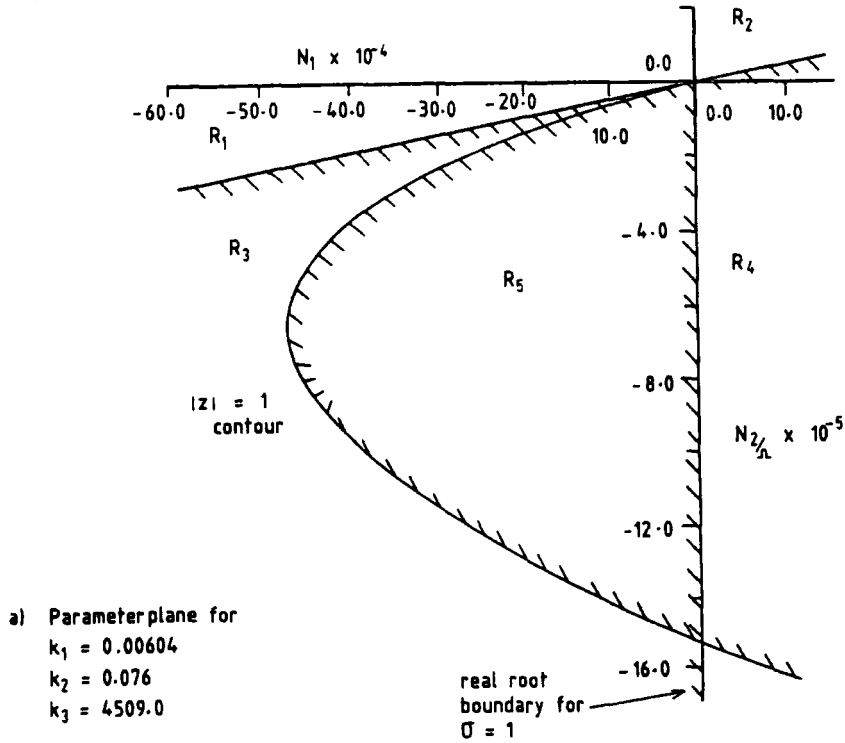
Fig. 7a. Parameter planes.
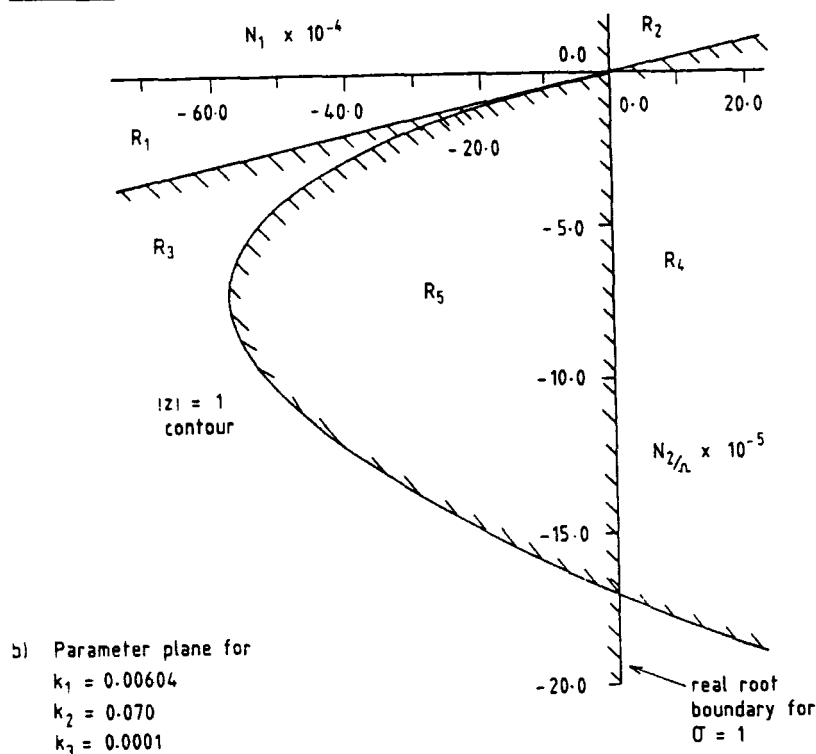
Fig. 7b. Parameter planes.

to the right. Consequently the value of n need only be found for one region. the rest being deduced from it. This value n may be obtained either by Cauchy's principle of the argument or by solving the characteristic equation for a specific point on the parameter plane. The real root boundary $\sigma = -1$ cannot be mapped as B_1 and C_1 of equation 16 are zero.

It can be seen from Figs. 3 and 5 that stability can be expected if the frequency of oscillation is low and the amplitude is not too small. Unfortunately due to the great dependence of the describing function contour on frequency and amplitude, it is difficult to draw less qualitative conclusions.

As the process parameters decrease the stable region increases. see Fig. 6a. thus an increase in pointing accuracy would be expected. However, the frequency of oscillation decreases and therefore the describing function contour moves further from the origin and the pointing accuracy could increase or decrease depending upon the relative movement of the contours. As the process parameters increase the stable region decreases, see Fig.

6b. and consequently a decrease in pointing accuracy is expected. Varying the parameter k_3 independently has very little effect on the $|z| = 1$ contour. see Fig. 7, thus confirming the strong robustness in the presence of modal frequency errors (as indicated in [6]). In all the above cases the gradient of the $|z| = 1$ contour close to the origin is shown in Fig. 5(b).

5. Conclusion

In performing this analysis, it was intended to obtain a quantitative measure of the accuracy required from a plant model controlled by a fuzzy logic controller to obviate the need for a trial and observation simulation study. This aim has not been realised because the non-linear element is represented analytically by a describing function. The parameters N_1 and N_2 must appear in the groups α and β and therefore the only way to observe the effects of modelling inaccuracies is to vary the system parameters and note the change in the position of the $|z| = 1$ contour which dictates

the size of the stable region. The describing function for the multilevel relay is dependent upon both amplitude and frequency which can only be represented by a family of curves on the parameter plane. For the fuzzy logic controller the region embraced by these describing function contours is extensive and hence no unique finite area can be identified in which particular process parameter variations should be constrained.

Despite these problems the approach has been shown to provide some useful qualitative information about system robustness that supports the results presented in [6]. Therefore the use of the parameter plane technique as an analytical tool should not be discouraged, particularly if supported by a trial observation simulation study.

References

[1] Zadeh. L.A.: 'Fuzzy Sets', *Information and Control*. Vol. 8. 1965, pp. 338–353.

[2] Mamdani. E.H.: Application of Fuzzy Algorithm for Control of Simple Dynamic Plant, *Proc. IEE*. Vol. 121. 1974, pp. 1585–1588.

[3] King, P.J. and Mamdani, E.H.: The Application of Fuzzy Control Systems to Industrial Processes, *Automatica*. Vol. 13. 1977, pp. 235–242.

[4] Rutherford, D.A. and Carter, G.A.: A Heuristic Adaptive Controller for a Sinter Plant, Proc. 2nd IFAC Symp. Automation in Mining, Mineral and Metal Processing. Johannesburg, 1976.

[5] Van Amerongen, J., Van Nauta Lemke, H.R. and Van der Veen, J.C.T.: An Autopilot for Ships Designed with Fuzzy Sets, *Digital Computer Applications to Process Control*. H.R. Van Nauta Lemke (Ed.), IFAC and North-Holland. 1977.

[6] Daley, S. and Gill, K.F.: The Fuzzy Logic Controller: an Alternative Design Scheme?, *Computers in Industry*, Vol. 6, No. 1, pp. 3–14, Feb. 1985.

[7] Siljak, D.D.: *Nonlinear Systems; the Parameters Analysis and Design*, John Wiley & Sons, 1969.

[8] Siljak, D.D.: Analysis and Synthesis of Feedback Control Systems in the Parameter Plane, Pt. I – Linear Continuous Systems, *IEEE Trans. Applications and Industry*, Vol. 83, 1964, pp. 449–458.

[9] Siljak, D.D.: Analysis and Synthesis of Feedback Control Systems in the Parameter Plane. Pt. II – Sampled Data Systems, *IEEE Trans. Applications and Industry*, Vol. 83, 1964, pp. 458–466.

[10] Siljak, D.D.: Analysis and Synthesis of Feedback Control Systems in the Parameter Plane. Pt III – Nonlinear Systems. *IEEE Trans. Applications and Industry*. Vol. 83. pp. 466–473.

[11] Smart, D.R., Gill, K.F., Gething, J.M. and Holt, J.A.: Dynamic Analysis of Flexible Space Vehicles Having Uncoupled Control Axes. *Aero. J. Royal Aero. Society*, Vol. 78, pp. 560–569, 1974.

Appendix 1

Characteristic Equation Coefficient Values (See Also Fig. 4)
Idealised Satellite Controlled by Fuzzy Logic Controller

The characteristic equation is of order five with coefficients of the form:

$$a_k = b_k \alpha + c_k \beta + d_k,$$

where

$k = 0$

$b_0 = 0$

$$c_0 = \frac{k_1 T^2}{2} + \frac{k_2^2}{k_3}(1 - C_T)$$

$d_0 = 0$

$k = 1$

$$b_1 = (C_T - 1)\frac{k_2^2}{k_3} - \frac{k_1 T^2}{2}$$

$$c_1 = (2C_T - 2)\frac{k_2^2}{k_3} - k_1 T^2 C_T$$

$d_1 = 1$

$k = 2$

$$b_2 = \frac{k_2^2}{k_3}(1 - C_T) - \frac{k_1 T^2}{2}(1 - 2C_T)$$

$c_2 = 0$

$d_2 = -2(1 + C_T)$

$k = 3$

$$b_3 = \frac{k_2^2}{k_3}(1 - C_T) - \frac{k_1 T^2}{2}(1 - 2C_T)$$

$$c_3 = k_1 T^2 C_T + \frac{k_2^2}{k_3}(2 - 2C_T)$$

$d_3 = 2 + 4C_T$

$k = 4$

$$b_4 = \frac{k_2^2}{k_3}(C_T - 1) - \frac{k_1 T^2}{2}$$

$$c_4 = \frac{k_2^2}{k_3}(C_T - 1) - \frac{k_1 T^2}{2}$$

$d_4 = -2(C_T + 1)$

$k = 5$

$b_5 = 0$

$c_5 = 0$

$d_5 = 1$

$$C_T = \cos(T\sqrt{k_3})$$

Appendix 2

Derivation of the Polynomials X_k and Y_k

The complex point:

$z = \sigma + j\omega$

is written as:

$z = \sigma + \omega e^{j\pi/2}$.

Thus

$z^k = \sigma^k (1 + \sigma^{-1}\omega e^{j\pi/2})^k$.

Expanding this expression binomially:

$$z^k = \sum_{r=0}^{k} K_r \sigma^{k-r}\omega^r e^{jr\pi/2},$$

where

$$K_r = \frac{k(k-1)(k-2)\ldots\ldots(k-r+1)}{1.2.3.\ldots\ldots r}$$

for $r > 0$ and $K_r = 1$ for $r = 0$.
Separating real and imaginary terms:

$z^k = X_k + jY_k,$ (A1)

where

$$X_k = \sum_{\mu=0}^{k} (-1)^{\mu} K_{2\mu}\sigma^{(k-2\mu)}\omega^{2\mu}$$ (A2)

and

$$Y_k = \sum_{\mu=1}^{k} (-1)^{\rho-1} K_{2\rho-1}\sigma^{(k-2\rho+1)}\omega^{(2\rho-1)}.$$ (A3)

The functions X_k and Y_k may also be obtained from recurrence formulae derived as follows:

$z = \sigma + j\omega$

is written as:

$z^2 - 2\sigma z + (\sigma^2 + \omega^2) = 0$.

Multiplying both sides by z^{k-1} yields:

$z^{k+1} - 2\sigma z^k + (\sigma^2 + \omega^2) z^{k-1} = 0$.

Substitution of Equation A1 into this expression yields the two equations (the summation of the real and imaginary terms are independently zero):

$X_{k+1} - 2\sigma X_k + (\sigma^2 + \omega^2) X_{k-1} = 0$

$Y_{k+1} - 2\sigma Y_k + (\sigma^2 + \omega^2) Y_{k-1} = 0$,

and from Equations A2 and A3, $X_0 = 1$, $X_1 = \sigma$, $Y_0 = 1$ and $Y_1 = \omega$.

PAPER 57

Attitude control of a spacecraft using an extended self-organizing fuzzy logic controller

S Daley, BSc, PhD
Department of Electrical Engineering and Electronics, Brunel University

K F Gill, BSc, PhD, CEng, MIMechE, MIEE
Department of Mechanical Engineering, University of Leeds

A simple method for extending the range of sensitivity of the self-organizing fuzzy logic controller (SOC) is proposed. The performance of the resulting controller is studied through its application to the attitude control of a flexible satellite. It is found that the extended SOC can provide excellent control and also possesses a high degree of robustness.

1 INTRODUCTION

Since its introduction by Mamdani and Assilian (1), many successful applications of the 'simple' fuzzy logic controller have been reported (2–9). The performance of the controller, however, is dependent upon the availability of a reliable linguistic control strategy which, in many cases, is not easily formulated (10, 11). This problem can be solved by using the self-organizing fuzzy logic controller (SOC) proposed by Procyk and Mamdani (12, 13) which uses an evaluation of the closed-loop performance to generate and modify the control rules.

In a previous paper (14) the SOC was applied to the attitude control of a flexible satellite. Although this study was successful, in the sense that an acceptable controller was found, the final design was the result of a compromise between the transient behaviour and the steady state accuracy. In this paper a simple extension to the SOC is proposed which obviates the need for this compromise.

2 SUMMARY OF PREVIOUS STUDY

For ease of reference the results of the authors' previous study (14) are summarized below.

2.1 Process model

The process used in the design study was a hypothetical flexible communications satellite similar in configuration to that of the French multi-mission platform SPOT (Fig. 1).

For the conditions of small angle manoeuvres and small angular rates, the spacecraft dynamics may be represented by the following differential equations describing roll, pitch and yaw attitudes, and the solar array bending motion (15):

$$T = E(\ddot{\boldsymbol{\Phi}} - \tilde{\omega}_o \dot{\boldsymbol{\Phi}}) - \hat{\sigma}\ddot{\eta} \qquad (1)$$

$$\ddot{\eta} + \Omega^2\eta = \hat{\sigma}^T(\ddot{\boldsymbol{\Phi}} - \tilde{\omega}_o \dot{\boldsymbol{\Phi}}) \qquad (2)$$
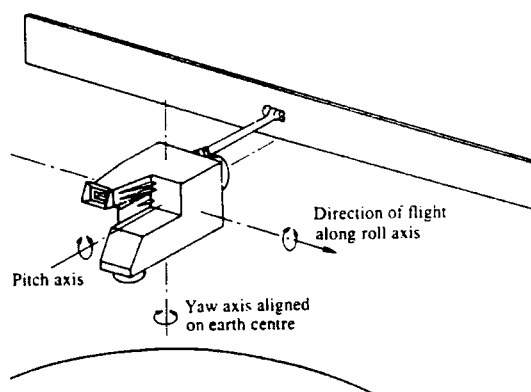
Fig. 1 Spacecraft configuration

where T is the error torque acting on the vehicle (difference between external torques and the control torques), E is the 3×3 inertia matrix, η is the vector of modal deformation coordinates of dimension m, $\hat{\sigma}$ is a $3 \times m$ matrix whose columns are the moment of the mode shape σ_i, $i = 1, \ldots, m$, and Ω is an $m \times m$ diagonal matrix the elements of which are the modal frequencies.

$$\boldsymbol{\Phi}^T = [\phi \; \theta \; \psi] \qquad (3)$$

is the vector of attitude angles (roll, pitch and yaw respectively) and

$$\tilde{\omega}_o = \begin{bmatrix} 0 & 0 & \omega_o \\ 0 & 0 & 0 \\ -\omega_o & 0 & 0 \end{bmatrix} \qquad (4)$$

where ω_o is the orbital angular velocity.

Equations (1) and (2) can be written in the state variable form:

$$\dot{x} = Ax + Bu \qquad (5)$$

by constructing the partitioned matrix equation:

$$\begin{bmatrix} \ddot{\boldsymbol{\Phi}} \\ \ddot{\eta} \end{bmatrix} = \begin{bmatrix} E & -\hat{\sigma} \\ -\hat{\sigma}^T & I \end{bmatrix}^{-1} \begin{bmatrix} T \\ -\Omega^2\eta \end{bmatrix} + \begin{bmatrix} \tilde{\omega}_o & \dot{\boldsymbol{\Phi}} \\ 0 \end{bmatrix} \qquad (6)$$

Q   Quantization process
M   Deterministic output selection
GI   Input scaling factors
GO   Output scaling factors
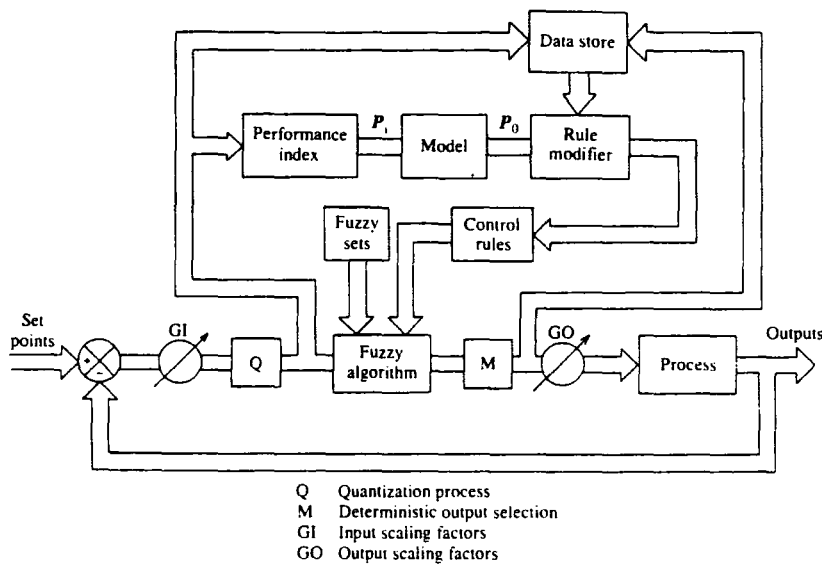
Fig. 2   Form of the SOC

where $\mathbf{I}$ is the $m \times m$ unit matrix. The state vector is defined as

$$\mathbf{x}^{\mathrm{T}} = [\phi \ \dot{\phi} \ \theta \ \dot{\theta} \ \psi \ \dot{\psi} \ \eta_1 \ \dot{\eta}_1 \ \cdots \ \dot{\eta}_m]$$

2.2 Design of the self-organizing fuzzy logic controller

The SOC enables rule modification/creation by adding performance feedback to the 'simple' fuzzy logic controller (Fig. 2). The performance index monitors the closed-loop system trajectories and provides a measure of the changes, P_o, that are required at the process output in order to attain a desired trajectory.

For a multi-variable process a crude system model that reflects the degree of input–output coupling is needed in order to translate the vector P_o to a vector P_i that represents the changes that are required at the process input. The vector $P_i(KT)$ is then used to modify the rules that most contributed to the performance at the sample instant KT. This process of rule modification is continued until the desired trajectory is achieved.

The linguistically expressed performance index used in the previous study is presented below; the same index was used for each satellite axis.

Attitude	Change in attitude						
	PB	PM	PS	Z0	NS	NM	NB
PB	NB	NB	NB	NM	NM	NS	Z0
PM	NB	NB	NM	NM	NS	Z0	PS
PS	NB	NB	NS	NS	Z0	PS	PM
P0	NB	NM	NS	Z0	Z0	PM	PB
N0	NB	NM	Z0	Z0	PS	PM	PB
NS	NM	NS	Z0	PS	PS	PB	PB
NM	NS	Z0	PS	PM	PM	PB	PB
NB	Z0	PS	PM	PM	PB	PB	PB

For convenience the rules have been written in matrix form and should be interpreted as:

If 'attitude is NM' and 'change in attitude is PS' then 'credit is PS'.

The linguistic terms used have the following meaning:

PB	positive big
PM	positive medium
PS	positive small
P0	positive zero
Z0	zero
N0	negative zero
NS	negative small
NM	negative medium
NB	negative big

where P0 is defined as values slightly above zero and N0 as terms slightly below zero.

The fuzzy sets are formed upon a discrete support universe of 14 elements for the attitude, 13 elements for the change in attitude and 15 elements for the torque output. Using the standard techniques of fuzzy calculus (16) and the fuzzy sets detailed in Table 1, the linguistic performance index can be transformed to a 'look-up' table (Table 2).

The requirement for a system model was met by using

$$M = \left[\mathbf{I} - T \, \frac{\partial f}{\partial \mathbf{x}^{\mathrm{T}}} \right]^{-1} T \, \frac{\partial f}{\partial \mathbf{u}^{\mathrm{T}}} \tag{7}$$

where

$$\dot{x}_i = f_i(x, \, u)$$

T is the sampling time and

$$\frac{\partial f}{\partial \mathbf{x}^{\mathrm{T}}} \triangleq \begin{bmatrix} \dfrac{\partial f_1}{\partial x_1} & \dfrac{\partial f_1}{\partial x_2} & \dfrac{\partial f_1}{\partial x_3} & \cdots & \dfrac{\partial f_1}{\partial x_m} \\[2mm] \dfrac{\partial f_2}{\partial x_1} & \dfrac{\partial f_2}{\partial x_2} & \dfrac{\partial f_2}{\partial x_3} & \cdots & \dfrac{\partial f_2}{\partial x_m} \\[2mm] \vdots & \vdots & \vdots & & \vdots \\[2mm] \dfrac{\partial f_m}{\partial x_1} & \dfrac{\partial f_m}{\partial x_2} & \dfrac{\partial f_m}{\partial x_3} & \cdots & \dfrac{\partial f_m}{\partial x_m} \end{bmatrix}$$

Table 1 Fuzzy set definitions

(a) Attitude Y

	−6	−5	−4	−3	−2	−1	−0	+0	1	2	3	4	5	6
PB	0	0	0	0	0	0	0	0	0	0	0.1	0.4	0.8	1.0
PM	0	0	0	0	0	0	0	0	0	0.2	0.7	1.0	0.7	0.2
PS	0	0	0	0	0	0	0	0.3	0.8	1.0	0.5	0.1	0	0
P0	0	0	0	0	0	0	0	1.0	0.6	0.1	0	0	0	0
N0	0	0	0	0	0.1	0.6	1.0	0	0	0	0	0	0	0
NS	0	0	0.1	0.5	1.0	0.8	0.3	0	0	0	0	0	0	0
NM	0.2	0.7	1.0	0.7	0.2	0	0	0	0	0	0	0	0	0
NB	1.0	0.8	0.4	0.1	0	0	0	0	0	0	0	0	0	0

(b) Change in attitude CY

	−6	−5	−4	−3	−2	−1	0	1	2	3	4	5	6
PB	0	0	0	0	0	0	0	0	0	0.1	0.4	0.8	1.0
PM	0	0	0	0	0	0	0	0	0.2	0.7	1.0	0.7	0.2
PS	0	0	0	0	0	0	0	0.9	1.0	0.7	0.2	0	0
N0	0	0	0	0	0	0.5	1.0	0.5	0	0	0	0	0
NS	0	0	0.2	0.7	1.0	0.9	0	0	0	0	0	0	0
NM	0.2	0.7	1.0	0.7	0.2	0	0	0	0	0	0	0	0
NE	1.0	0.8	0.4	0.1	0	0	0	0	0	0	0	0	0

(c) Credit value P_o

	−7	−6	−5	−4	−3	−2	−1	0	1	2	3	4	5	6	7
PB	0	0	0	0	0	0	0	0	0	0	0	0.1	0.4	0.8	1.0
PM	0	0	0	0	0	0	0	0	0	0.2	0.7	1.0	0.7	0.2	0
PS	0	0	0	0	0	0	0	0.4	1.0	0.8	0.4	0.1	0	0	0
N0	0	0	0	0	0	0	0.2	1.0	0.2	0	0	0	0	0	0
NS	0	0	0	0.1	0.4	0.8	1.0	0.4	0	0	0	0	0	0	0
NM	0	0.2	0.7	1.0	0.7	0.2	0	0	0	0	0	0	0	0	0
NE	1.0	0.8	0.4	0.1	0	0	0	0	0	0	0	0	0	0	0

$$\frac{\partial f}{\partial u^T} \triangleq \begin{bmatrix} \dfrac{\partial f_1}{\partial u_1} & \dfrac{\partial f_1}{\partial u_2} & \dfrac{\partial f_1}{\partial u_3} & \cdots & \dfrac{\partial f_1}{\partial u_n} \\[2mm] \dfrac{\partial f_2}{\partial u_1} & \dfrac{\partial f_2}{\partial u_2} & \dfrac{\partial f_2}{\partial u_3} & \cdots & \dfrac{\partial f_2}{\partial u_n} \\[2mm] \vdots & \vdots & \vdots & & \vdots \\[2mm] \dfrac{\partial f_m}{\partial u_1} & \dfrac{\partial f_m}{\partial u_2} & \dfrac{\partial f_m}{\partial u_3} & \cdots & \dfrac{\partial f_m}{\partial u_n} \end{bmatrix}$$

The vector P_i is found from

$$P_i = \hat{M} P_o \tag{8}$$

where $\hat{M}$ is the M^{-1} matrix after a normalization and scaling process (see Section 3). The best model, in terms

of the closed-loop performance, was found to result from the application of equation (7) to be state space description that assumed the governing differential equation to be

$$I = E(\ddot{\Phi} - \tilde{\omega}_o \dot{\Phi}) \tag{9}$$

(that is a description that neglects the effects of structural flexibility).

Central to the design of any fuzzy logic controller is the selection of the scaling factors that relate real world variables to the discrete universe of the fuzzy sets. These were selected by trial and observation, and the best values in terms of an acceptable transient behaviour

Table 2 Performance index 'look-up' table

Attitude	Change in attitude												
	−6	−5	−4	−3	−2	−1	0	1	2	3	4	5	6
−6	7.0	6.5	7.0	6.5	7.0	7.0	4.0	4.0	4.0	3.0	1.0	0.0	0.0
−5	6.5	6.5	6.5	5.0	6.5	6.5	4.0	4.0	4.0	2.5	1.5	0.0	0.0
−4	7.0	6.5	7.0	5.0	4.0	4.0	4.0	1.0	1.0	1.0	0.0	−1.5	−1.0
−3	6.5	6.5	6.5	5.0	4.0	4.0	4.0	1.5	1.5	1.0	0.0	−1.0	−1.5
−2	7.0	6.5	7.0	4.0	1.0	1.0	1.0	0.0	0.0	−1.0	−1.0	−4.0	−4.0
−1	6.5	6.5	6.5	4.0	1.5	1.5	1.5	0.0	0.0	−1.0	−1.5	−4.0	−4.0
−0	7.0	6.5	4.0	3.0	1.0	1.0	0.0	0.0	0.0	−3.0	−4.0	−6.5	−7.0
+0	7.0	6.5	4.0	3.0	0.0	0.0	0.0	−1.0	−1.0	−3.0	−4.0	−6.5	−7.0
1	4.0	4.0	1.5	1.0	0.0	0.0	−1.5	−1.5	−1.5	−4.0	−6.5	−6.5	−6.5
2	4.0	4.0	1.0	1.0	0.0	0.0	−1.0	−1.0	−1.0	−4.0	−7.0	−6.6	−7.0
3	1.5	1.0	0.0	−1.0	−1.5	−1.5	−4.0	−4.0	−4.0	−5.0	−6.5	−6.5	−6.5
4	1.0	1.5	0.0	−1.0	−1.0	−1.0	−4.0	−4.0	−4.0	−5.0	−7.0	−6.5	−7.0
5	0.0	0.0	−1.5	−2.5	−4.0	−4.0	−4.0	−6.5	−6.5	−5.0	−6.5	−6.5	−6.5
6	0.0	0.0	−1.0	−3.0	−4.0	−4.0	−4.0	−7.0	−7.0	−6.5	−7.0	−6.5	−7.0

S DALEY AND K F GILL
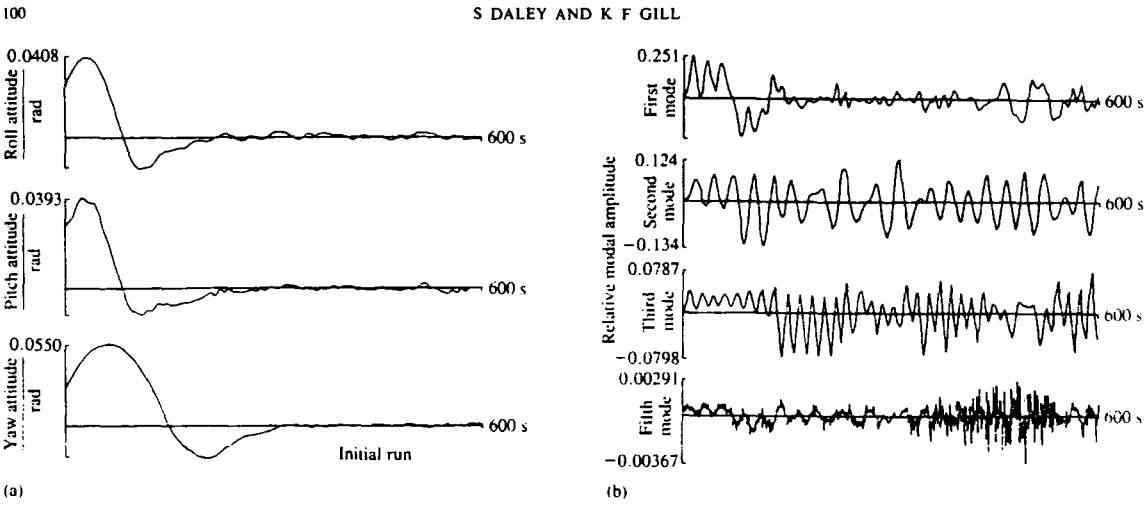
Fig. 3   Response to standard SOC

and acceptable steady state accuracy were found to be

$$GY_\phi = GY_\theta = GY_\psi = 240$$

$$GC_\phi = GC_\theta = GC_\psi = 24\,000$$

$$GT_\phi = GT_\theta = GT_\psi = 0.03$$

where GY is the scaling factor on the measured satellite attitude, GC the scaling factor on the change in attitude over one sample period and GT is the scaling factor on the controller output; the subscript denotes the reference axis.

The satellite response to this controller design and the initial conditions of $\phi = \theta = \psi = 0.025$ rad and $\dot\phi = \dot\theta = \dot\psi = 0.001$ rad/s is shown in Fig. 3. Further details of the design and its implementation can be found in reference (17).

3 EXTENDED SELF-ORGANIZING FUZZY LOGIC CONTROL ALGORITHM

Although the controller design discussed in the previous section was considered to be the most acceptable, the

transient behaviour can be improved (Fig. 4a) by reducing the controller input scaling factors to

$$GY_\phi = GY_\theta = GY_\psi = 180$$

$$GC_\phi = GC_\theta = GC_\psi = 20\,000$$

Unfortunately this leads to a deterioration in the steady state pointing accuracy. Conversely, increasing the controller input scaling factors to

$$GY_\phi = GY_\theta = GY_\psi = 1600$$

$$GC_\phi = GC_\theta = GC_\psi = 80\,000$$

improves upon the steady state pointing accuracy at the expense of the transient response (Fig. 4b).

This problem can be partially resolved by increasing the number of elements in the support set and redefining the fuzzy sets. However, this has the drawback that the time required to compute a controller output would be significantly increased. An alternative to this is to extend the SOC's operation such that the controller input scaling factors are initially relatively small and then when the system trajectory is close to

(a) Decrease in GY and GC

(b) Increase in GY and GC
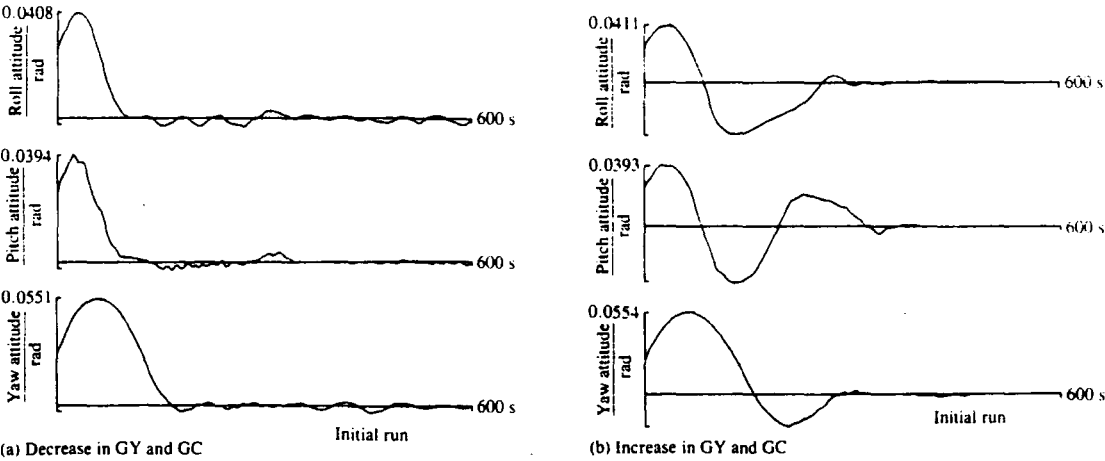
Fig. 4   Response to standard SOC

the origin they are switched to a larger value. With this approach it should be possible to combine the good transient behaviour displayed in Fig. 4a with the steady state accuracy shown in Fig. 4b.

Implementing this extension requires consideration of the following:

1. At what point in the trajectories should the switch occur?

    Ideally this should take place near a turning point close to the origin, or more specifically when

    $$|\text{'real' attitude}| < Y_s/GY_b$$

    $$|\text{'real' change in attitude}| < C_s/GC_b$$

where GY_b and GC_b are the scaling factors before the switch and Y_s and C_s are the scaled values of attitude and change in attitude when the switch occurs. Clearly to utilize the full range of the scaling factors before the switch the values of Y_s and C_s, which will be restricted to being the same for each axis, should lie between 0 and 0.5 (as the quantization process registers a support value of zero in this range). Their final values in this range will be selected by inspection of the attitude response. In the event of a degradation in control it would be desirable to switch back to the original scaling factors, that if:

$$|\text{'real' attitude}| > Y_r/GY_b$$

and

$$|\text{'real' change in attitude}| > C_r/GC_b$$

The limiting conditions for the values of Y_r and C_r are

$$Y_r = Y_s$$

and

$$C_r = C_s$$

Initial tests showed that for this case a poor system performance resulted because the controller constantly switched between the two modes of operation. Consequently, both Y_r and C_r were selected as 1.0 to enable a divergence of the system trajector before the occurrence of a switch back to the original scaling factors.

2. The switch will be made at different times on different axes, hence should there be a separate algorithm for each combination of switches?

    This seems sensible as rules that were created for one combination of switches are not necessarily acceptable for another combination. Therefore eight algorithms could be generated on any simulation run, the regimes being defined as:

Regime	Roll	Pitch	Yaw
1	0	0	0
2	0	0	1
3	0	1	0
4	0	1	1
5	1	0	0
6	1	0	1
7	1	1	0
8	1	1	1

where 0 signifies original scaling factors and 1 signifies switched scaling factors. These separate algorithms can be interpreted as a bracketing of the rules, which has the advantage of reducing the time required to formulate a control output as only the rules in a particular regime need be processed at any one time.

3. Should the controller process model be recomputed at each switch?

The matrix M relates small 'real world' changes in the process inputs to small 'real world' changes in the outputs. Therefore, M^{-1} must be scaled to the universe of discourse of P_i and P_o by using the scaling factors for each axis. Thus:

$$P_i = (\widehat{GT})^{-1}M^{-1}(\widehat{GY})^{-1}P_o \qquad (10)$$

where

$$\widehat{GT} = \begin{bmatrix} GT_\phi & 0 & 0 \\ 0 & GT_\theta & 0 \\ 0 & 0 & GT_\psi \end{bmatrix}$$

and

$$\widehat{GY} = \begin{bmatrix} GY_\phi & 0 & 0 \\ 0 & GY_\theta & 0 \\ 0 & 0 & GY_\psi \end{bmatrix}$$

$\hat{M}$ is produced from $(\widehat{GT})^{-1}M^{-1}(\widehat{GY})$ by a normalization process to ensure that P_i cannot exceed the maximum (or minimum) element of its support set (± 7). This condition is satisfied if

$$\hat{M} = \text{scale} \times (\widehat{GT})^{-1}(M)^{-1}(\widehat{GY})^{-1} \qquad (11)$$

where

$$\text{Scale} = \min\{s_1, s_2, s_3\}$$

and

$$s_1^{-1} \triangleq \left[\frac{m_{11}}{GY_\phi GT_\phi}\right] + \left[\frac{m_{12}}{GY_\theta GT_\phi}\right] + \left[\frac{m_{13}}{GY_\psi GT_\phi}\right] \leqslant 1$$

$$s_2^{-1} \triangleq \left[\frac{m_{21}}{GY_\phi GT_\theta}\right] + \left[\frac{m_{22}}{GY_\theta GT_\theta}\right] + \left[\frac{m_{23}}{GY_\psi GT_\theta}\right] \leqslant 1$$

$$s_3^{-1} \triangleq \left[\frac{m_{31}}{GY_\phi GT_\psi}\right] + \left[\frac{m_{32}}{GY_\theta GT_\psi}\right] + \left[\frac{m_{33}}{GY_\psi GT_\psi}\right] \leqslant 1$$

$$(12)$$

where m_{ij} is an element of M^{-1}.

As a result of this scaling process the suitability of $\hat{M}$ can only be guaranteed when the scaling factors for all the axes have switched.

For example, consider a case where before any switch occurrence the model was such that the element $m'_{33}/GT_\psi GY_\psi$ was the largest, indicating that the yaw input credit value most affects the yaw output credit value. For a switch of the yaw scaling factors only this element would become much smaller and may not remain the largest in the row, which is an undesirable situation. Clearly once all the switches have been made the model should be recomputed; however, if the mag-

nitude of the switch in scaling factors is the same for each axis the model would remain constant as a result of the normalization process and further calculation is unnecessary.

4 PARAMETER SELECTION

Figure 5 shows the satellite response to the parameters:
Before the switch:

$$GY_\phi = GY_\theta = GY_\psi = 180$$

$$GC_\phi = GC_\theta = GC_\psi = 20\,000$$

$$GT_\phi = GT_\theta = GT_\psi = 0.03$$

After the switch:

$$GY_\phi = GY_\theta = GY_\psi = 1600$$

$$GC_\phi = GC_\theta = GC_\psi = 800\,000$$

$$GT_\phi = GT_\theta = GT_\psi = 0.03$$

$$Y_s = C_s = 0.1$$

The value of GC used is ten times larger than the value associated with Fig. 4b because it was found that increasing this parameter, and so increasing the damping at low attitudes, resulted in an improved steady state pointing accuracy. For values of Y_s and C_s much below those given above the second controller mode of operation did not occur for any of the axes. Figure 5 shows the initial simulation run starting from an 'empty' rule set. Repeating the simulation using the stored rules as a starting point does not significantly improve the controller performance. This suggests that all the learning that is required to produce the best response for the selected controller parameters occurs during the first run, and so obviates the need for an on-line (or off-line) series of runs to obtain an acceptable set of rules. This was the case for each controller configuration investigated so it is the response to the initial run that is presented in each figure. The number of rules stored at the end of each simulation is listed in Table 3 and to ease reference the controller parameters used to produce each figure are detailed in Table 4.

The transient behaviour of the pitch attitude, dis-

Table 3 Rules stored after each simulation

Figure	Regime							
	1	2	3	4	5	6	7	8
5	5	0	0	0	16	43	0	31
6	5	0	0	0	15	0	22	12
7	3	0	5	0	0	0	39	86
8	3	0	3	0	0	0	18	7
10	5	0	0	0	8	0	29	81
11	7	0	0	0	17	0	22	91
12	2	0	13	0	0	0	31	123
13(A)	7	10	0	77	0	0	0	0
13(B)	10	42	0	189	0	0	0	183

Table 4 Controller parameters for each simulation

Figure	Before the switch			After the switch			Y_s	C_s
	GY	GC	GT	GY	GC	GT		
5	180	2×10^4	0.03	1600	8×10^5	0.03	0.1	0.1
6	180	2×10^4	0·03	1600	8×10^5	0.003	0.1	0.1
7	180	2×10^4	0.03	1600	8×10^5	0.03	0.5	0.5
8	180	2×10^4	0.03	1600	8×10^5	0.006	0.25	0.25

played in Fig. 5, is not acceptable and is most probably due to the excitation of the flexural modes. In an attempt to suppress this excitation the scaling factors on the torque input vector after the switch were reduced by a factor of 10 to

$$GT_\phi = GT_\theta = GT_\psi = 0.003$$

The improved response is shown in Fig. 6.
Alternatively, the performance shown in Fig. 5 can be improved (Fig. 7) by increasing the switch parameters to

$$Y_s = C_s = 0.5$$

To improve the steady state pointing accuracy of Fig. 7, which is $<0.02°$, the value of GT after the switch for all axes was reduced by a factor of 5. Because of the reduced torque available the switch parameters were also reduced to

$$Y_s = C_s = 0.25$$

to avoid an increase in the transient overshoots. Figure 8 shows the response to these parameters; the steady state pointing accuracy is $<0.002°$.
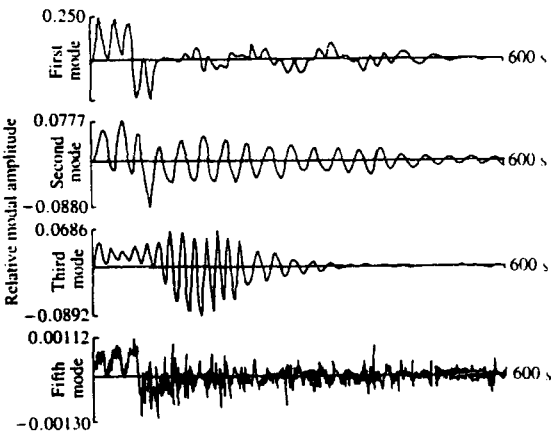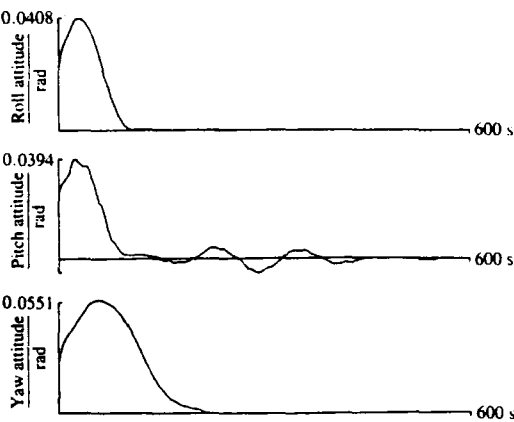
Fig. 5 Response to extended SOC for small values of Y_s and C_s
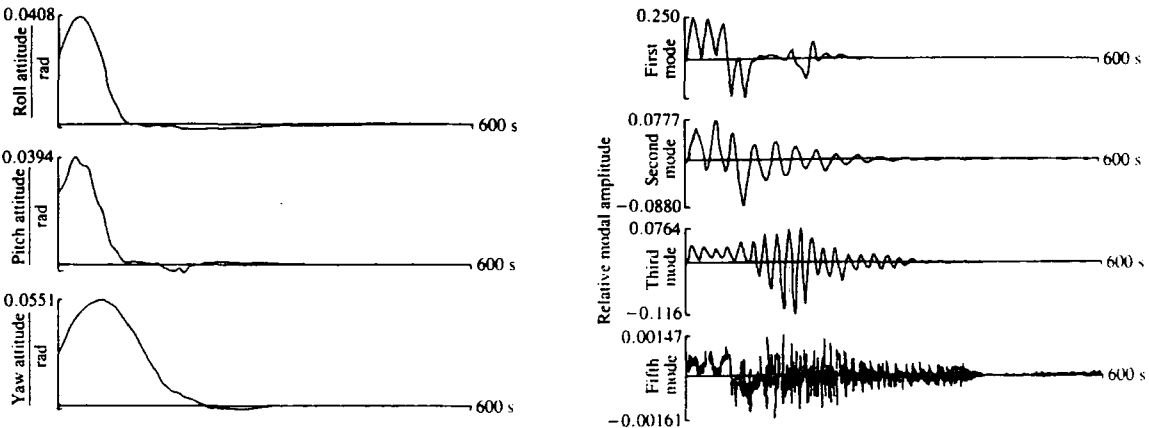
Fig. 6   Response to extended SOC for small values of Y_s and C_s and a reduced value of GT
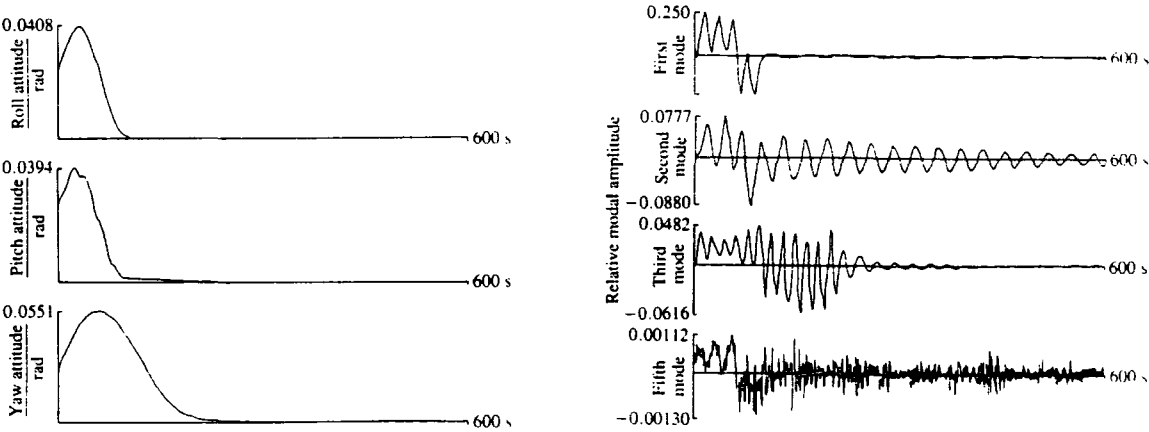
Fig. 7   Response to extended SOC for large values of Y_s and C_s
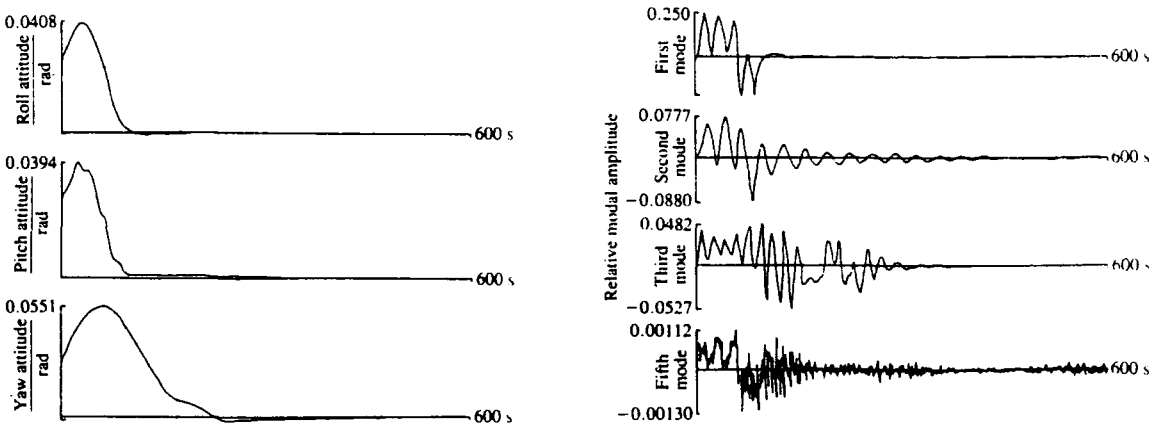
Fig. 8   Response to extended SOC for intermediate values of Y_s and C_s and a reduced value of GT

104   S DALEY AND K F GILL

(a) Unchanged GT   (b) Reduced GT
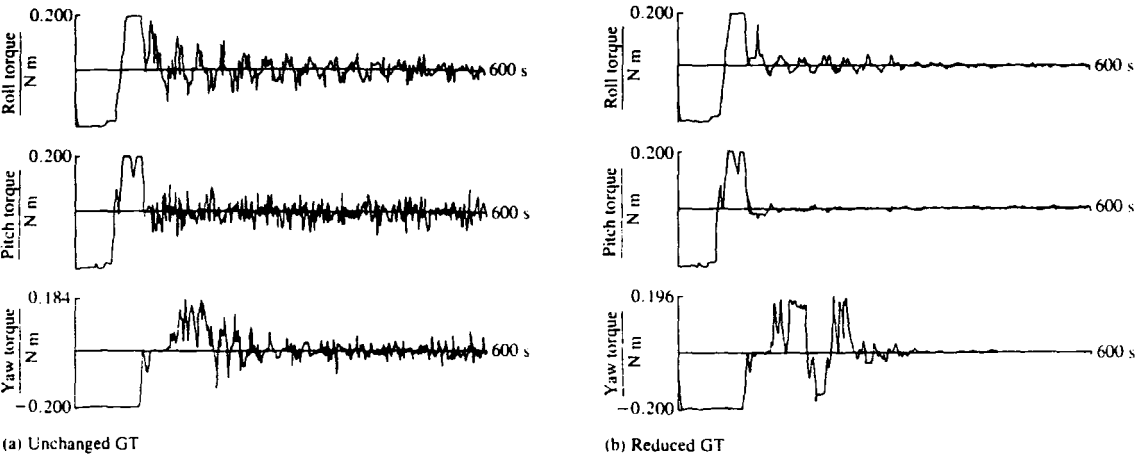
Fig. 9   Process input
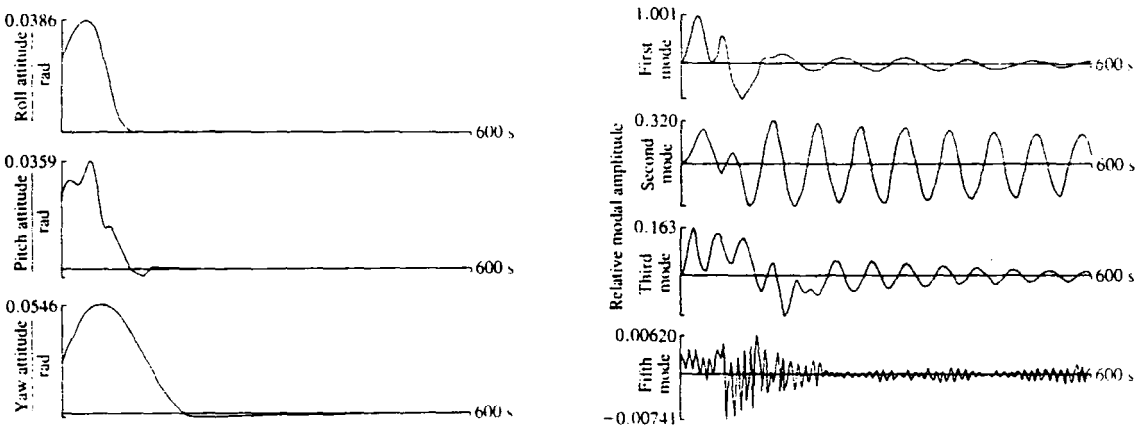
Fig. 10   Response to extended SOC with modal frequencies reduced to 50 per cent of nominal value
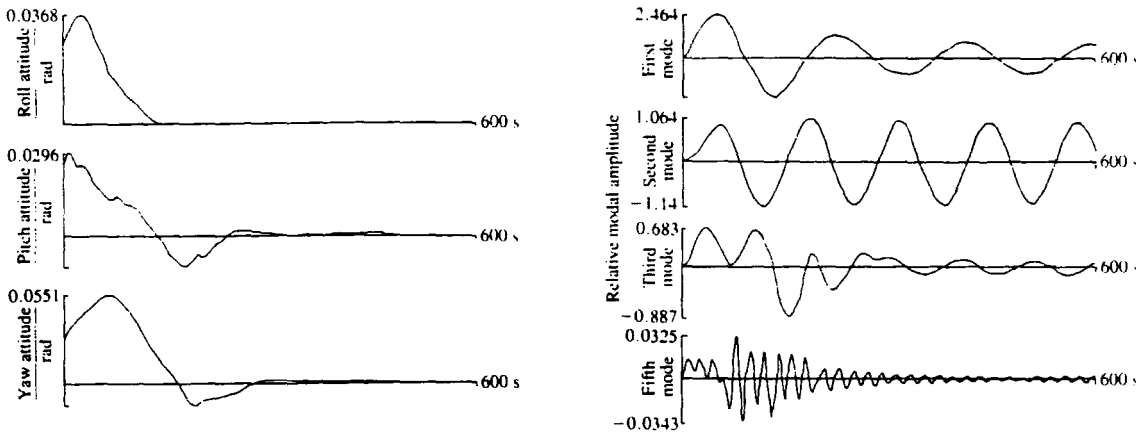
Fig. 11   Response to extended SOC with modal frequencies reduced to 25 per cent of nominal value
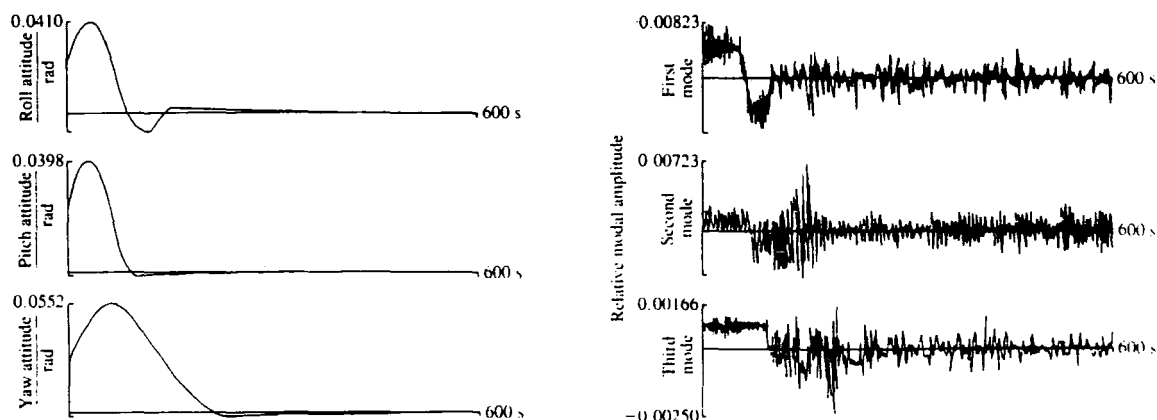
Fig. 12   Response to extended SOC with modal frequencies increased to five times the nominal values

Both the performances shown in Fig. 7 and 8 have their merits. The former has a better transient performance and the latter a better modal, and thus steady state, response accompanied by a much reduced torque requirement (see Fig. 9). The performance shown in Fig. 7 could be improved by incorporating further switches in the controller. thereby improving steady state accuracy and reducing the torque requirement. However. since this performance is considered to be satisfactory by the authors. further modification is unnecessary.

5 ROBUSTNESS STUDY

A study is made in this section of the performance of the SOC in the presence of process mismatch. The controller parameters for the SOC are as associated with Fig. 7. The figures presented show the first simulation run unless otherwise stated and the rules stored at the end of each run are listed in Table 3.

Figure 10 shows the satellite response to the SOC when the modal frequencies [equation (2)] are reduced by a factor of 2. The controller copes well with this mismatch condition and a significant deterioration in performance does not occur until the modal frequencies are reduced to 25 per cent of the nominal values (Fig. 11).
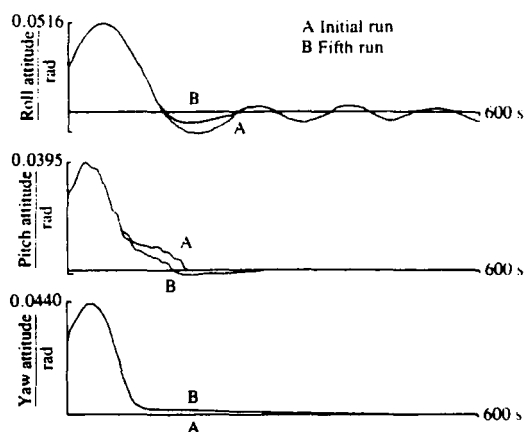
Similarly. increasing the modal frequencies does not degrade the system performance significantly until they are five times the nominal values (Fig. 12).

The solar array (see Fig. 1) is mounted on a boom that is orientated parallel to the negative pitch axis. The array can rotate about this axis to maximize its exposure to solar energy. However, it has been assumed above that the array is fixed parallel to the roll axis. Therefore another possible mismatch condition occurs when the orientation of the solar array is changed. The satellite response to the SOC for a 90° change in orientation. which is the worst possible case. is shown in Fig. 13. The roll attitude response on the initial run is poor but is improved during subsequent runs, with an acceptable performance occurring on the fifth run.

6 CONCLUSIONS

It has been demonstrated that the range of sensitivity of a fuzzy logic controller can be simply and effectively extended by switching the values of the scaling factors. This represents a departure from previous published work where it has been accepted that the sometimes necessary compromise between acceptable transient
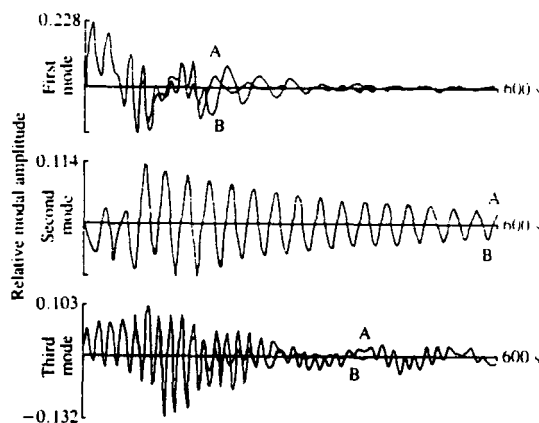
Fig. 13   Response to extended SOC for a 90° change in solar array orientation

behaviour and acceptable steady state accuracy is an inherent weakness of the controller.

The robust qualities of the SOC noted by Procyk and Mamdani (13) have also been shown to hold for the extended SOC. The excellent performance of the SOC was achieved using limited process knowledge, thereby encouraging its use for other complex processes that cannot be reliably modelled.

REFERENCES

1 Mamdani, E. H. and Assilian, S. An experiment in linguistic synthesis with a fuzzy logic controller. *Int. J. Man-Mach. Stud.*, 1975, 7, 1–13.

2 Kickert, W. J. M. and Van Nauta Lemke, H. R. Application of a fuzzy controller in a warm water plant. *Automatica*, 1976, 23, 201–208.

3 Østergaard, J. J. Fuzzy logic control of a heat exchanger process. Internal report 7601, 1976, Electrical Power Engineering Department, Technical University of Denmark.

4 Rutherford, D. A. and Carter, G. A. A heuristic adaptive controller for a sinter plant. Proceedings of Second IFAC Symposium on *Automation in mining, mineral and metal processing*, Johannesburg, 1976.

5 Tong, R. M. Some problems with the design and implementation of fuzzy controllers. Internal report CUED/F-CAMS/TR 127, 1976, Cambridge University.

6 Van Amerongen, J., Van Nauta Lemke, H. R. and Van der Veen, J. C. T. An autopilot for ships designed with fuzzy sets. In *Digital computer applications to process control* (Ed. H. R. Van Naute Lemke, 1977 (IFAC and North-Holland, Amsterdam).

7 Larsen, P. M. Industrial applications of fuzzy logic control. *Int. J. Man-Mach. Stud.*, 1979, 12, 3–10.

8 Tong, R. M., Beck, M. B. and Latten, A. Fuzzy control of the activated sludge wastewater treatment process. *Automatica*, 1980, 16, 659–701.

9 Daley, S. and Gill, K. F. A justification for the wider use of fuzzy logic control algorithms. *Proc. Instn Mech. Engrs*, Part C, 1985, 199(C1), 43–49.

10 Bainbridge, L. The process controller. In *The analysis of practical skills* (Ed. W. T. Singleton), 1975 (Academic Press, London).

11 Umbers, I. G. and King, P. J. An analysis of human decision-making in cement kiln control and the implications of automation. In *Fuzzy reasoning and its applications* (Eds E. H. Mamdani and B. R. Gaines), 1981 (Academic Press, London).

12 Procyk, T. J. A self-organising controller for dynamic processes. PhD thesis, 1977, Queen Mary College, London.

13 Procyk, T. J. and Mamdani, E. H. A linguistic self-organising process controller. *Automatica*, 1979, 15, 15–30.

14 Daley, S. and Gill, K. F. A design study of a self-organizing fuzzy logic controller. *Proc. Instn Mech. Engrs*, Part C, 1986, 200(C1), 59–69.

15 Fenton, J. Satellite attitude measurement and control incorporating active damping of flexural motion. PhD thesis, April 1981, University of Leeds.

16 Tong, R. M. A control engineering review of fuzzy systems. *Automatica*, 1977, 13, 559–569.

17 Daley, S. Analysis of fuzzy logic control algorithms and their application to engineering systems. PhD thesis, September 1984, University of Leeds.

PAPER 63

Comparison of a Fuzzy Logic Controller With a P + D Control Law

S. Daley

Department of Electrical Engineering
and Electronics,
Brunel University,
Middlesex, England

K. F. Gill

Department of Mechanical Engineering,
University of Leeds,
Leeds, England

A study is described that compares the performance of a self-organizing fuzzy logic control law (SOC) with that of the more traditional P + D algorithm. The multivariable problem used for the investigation is the attitude control of a flexible satellite that has significant dynamic coupling of the axes. It is demonstrated that the SOC can provide good control, requires limited process knowledge and compares favorably with the P + D algorithm.

1 Introduction

Since its introduction by Mamdani and Assilian [1], the "simple" fuzzy logic controller has been successfully implemented in many test cases and in actual industrial applications [2-11]. Its performance, however, is dependent upon the availability of a reliable linguistic control strategy which is not always easily formulated [12, 13]. An attractive solution to this problem is provided by the self-organizing fuzzy logic controller (SOC) which can be regarded as a linguistic equivalent to the deterministic approaches of self-tuning and adaptive control. The SOC was proposed by Procyk and Mamdani [14, 15] and uses closed loop performance data to generate and modify the control rules.

This paper describes a design study for the SOC that involves a process of greater complexity and higher mathematical dimension than has previously been investigated. A frame of reference for the performance of the SOC is provided by comparing it with the performance of a P + D algorithm. The study highlights specific design problems that can be encountered and in the opinion of the authors represents a valuable extension to the published work on fuzzy logic control applications.

A basic familiarity with the simple fuzzy logic controller and associated terminology is assumed; the unfamiliar reader is referred to [16-19].

2 Description and Model of Process

The process chosen for the design study is a hypothetical flexible communications satellite similar to the French multimission platform SPOT. The configuration of the vehicle is shown in Fig. 1. It is assumed to be travelling in a near polar circular orbit which is synchronized with the Sun and precesses at the same rate as the Earth, therefore no orbital corrections are needed. The vehicle is required to function in a fine pointing mode and the orbit references axes, aligned with the satellite body are defined as:

(a) the *roll* axis, directed, along the line of flight;
(b) the *pitch* axis, normal to the orbital plane;
(c) the *yaw* axis, directed along the vector locating the center of the Earth relative to the satellite mass center.

It will be noted that the axis set rotates about the pitch axis at the orbital angular velocity.

The solar array is mounted at the corner of one side of the spacecraft wall by means of a boom which is orientated parallel to the negative pitch axis. The array can rotate about this axis to maximize its exposure to solar energy as the craft traverses the Earth.

The vehicle is controlled by three orthogonally positioned reaction wheels, one per axis, which rotate on magnetic bearings to minimize the friction. The wheels operate with a linear torque-speed characteristic until saturation occurs. The control of all three axes must be considered as there is significant dynamic coupling. This is due to the size of the solar array, the asymmetry of the craft and the coupling effect of the momentum wheels; if small attitude rates are assumed the latter is negligible.
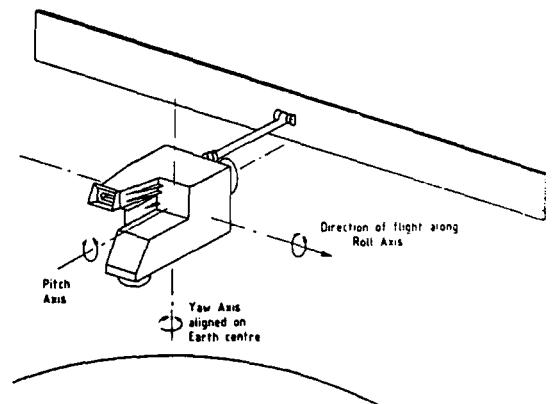
Fig. 1 Spacecraft configuration

A state variable model of this vehicle has been derived [20] using data supplied by the British Aerospace Dynamics Group; a summary of the approach is presented below.

Using hybrid coordinate analysis [21] and assuming small angular rates and small attitude maneuvers, the spacecraft dynamics may be represented by differential equations describing roll, pitch and yaw attitudes, and the solar array bending motion, as follows:

$$T = I\ddot{\beta} - \hat{\sigma}\ddot{\eta}^2 \qquad (1)$$

$$\ddot{\eta} + \Omega^2\eta \neq \hat{\sigma}^T\ddot{\beta} \qquad (2)$$

where T is the error torque acting on the vehicle (difference between external torques and the control torques), I is the 3×3 inertia matrix, β the body angular position, η the vector of modal deformation coordinates of dimension m, $\hat{\sigma}$ a 3×3 matrix whose columns are the moment of the mode shape σ_i, $i = 1, \ldots, m$ and Ω is an $m \times m$ diagonal matrix the elements of which are the modal frequencies.

As the body axis set is rotating with orbital angular velocity ω_0 about the pitch axis must be related to the reference axis set by the transformation [20]:

$$\dot{\Phi} = \bar{\omega}_0\dot{\Phi} + \ddot{\beta}$$

where

$$\Phi^T = [\phi\theta\psi]$$

is the vector of attitude angles (roll, pitch and yaw, respectively) and

$$\bar{\omega}_0 = \begin{bmatrix} 0 & 0 & \omega_0 \\ 0 & 0 & 0 \\ -\omega_0 & 0 & 0 \end{bmatrix}$$

Substituting this transformation in equations (1) and (2) yields

$$\ddot{\eta} + \Omega^2\eta = \hat{\sigma}^T(\ddot{\Phi} - \bar{\omega}_0\dot{\Phi}) \qquad (3)$$

and

$$T = I(\ddot{\Phi} - \bar{\omega}_0\dot{\Phi}) - \hat{\sigma}\ddot{\eta} \qquad (4)$$

If equations (3) and (4) are written in the form of the partitioned matrix equation:

$$\begin{bmatrix} I & \vdots & -\hat{\sigma} \\ \cdots & \cdots & \cdots \\ -\hat{\sigma}^T & \vdots & E \end{bmatrix} \begin{bmatrix} \ddot{\Phi} - \bar{\omega}_0\dot{\Phi} \\ \cdots \\ \ddot{\eta} \end{bmatrix} = \begin{bmatrix} T \\ \cdots \\ 0 \end{bmatrix} - \begin{bmatrix} 0 \\ \cdots \\ \Omega^2\eta \end{bmatrix}$$

then its transformation can be written as a set of second-order differential equations:

$$\begin{bmatrix} \ddot{\Phi} \\ \cdots \\ \ddot{\eta} \end{bmatrix} = W^{-1}\left\{ \begin{bmatrix} T \\ \cdots \\ 0 \end{bmatrix} - \begin{bmatrix} 0 \\ \cdots \\ \Omega^2\eta \end{bmatrix} \right\} + \begin{bmatrix} \omega_0\dot{\Phi} \\ \cdots \\ 0 \end{bmatrix}$$

which can be written in state variable form.

$$W = \begin{bmatrix} I & \vdots & -\hat{\sigma} \\ \cdots & \cdots & \cdots \\ \hat{\sigma}^T & \vdots & E \end{bmatrix}$$

The state vector of order $(6 + 2m)$ is defined as

$$x^T = [\phi \dot{\phi} \theta \dot{\theta} \psi \dot{\psi} \eta_1 \dot{\eta}_1 \ldots \dot{\eta}_m]$$

3 Details of the Proportional Plus Derivative Controller

The formulation of the feedback matrices for the P + D controller using the method detailed in Appendix I requires a feedback matrix formed from the solution of the discrete Riccati equation. This solution may be obtained using the technique of Hewer [22]. The cost function considered is:

$$J = \sum_{k=0}^{\infty} x^T\{kT\} Wx\{kT\} + u^T\{kT\}Ru\{kT\}$$

for which the algebraic Riccati matrix equation is:

$$W = P - A_1^T PA_1 + A_1^T PB_1(B_1^T PB_1 + R)^{-1}B_1^T PA_1$$

where the discrete state equation is:

$$x\{(k+1)T\} = A_1x\{kT\} + B_1u\{kT\}$$

The iterative Hewer algorithm can be written as:

$$\begin{aligned} \phi_j &= A_1 - B_1L_j \\ V_j &= \phi_jV_j\phi_j + L_j^TRL_j + W \\ L_{j+1} &= (B_1^TV_jB_1 + R)^{-1}B_1^TV_jA_1 \end{aligned} \qquad (5)$$

which yields the solution $P = \lim_{j\to\infty} V_j$

K_R of equation (A5) is computed from:

$$K_R = (B_1^T PB_1 + R)^{-1}B_1^T PA_1$$

Equation (5) is solved using the iterative technique of Smith [24] as follows:

$$q_{i+1} = q_i + \phi^{2^i T}q_i\phi^{2^i}$$

for $i = 1, 2, 3 \ldots\ldots$

which yields the solution:

$$V_j = \lim_{i\to\infty} q_i$$

and is initialized by setting:

$$q_0 = L_j^TRL_j + W$$

The initialization of the Hewer algorithm requires L_0 to be chosen such that ϕ_0 is a stabilizing matrix, i.e., $|\lambda^{\phi_0}| < 1$. This is achieved using the recursive method of Kleinman [23] as detailed below:

$$F_{i+1} = F_i + G_iF_iG_i^T$$

$$G_{i+1} = G_i^2$$

for $i = 1, 2, 3, \ldots\ldots, n$

n is arbitrarily chosen such that $2^n > m$, where m is the order of the plant matrix, and must be sufficiently large to avoid an ill-conditioned solution.

The algorithm is initialized by setting

$$F_0 = B_1R^{-1}B_1^T$$

and $G_0 = A_1$

After n iterations the L_0 matrix is calculated from:

$$L_0 = R^{-1}B_1^T(G_n^TF_n^{-1}G_n)A_1$$

Using the above algorithms, the procedure detailed in Appendix I, a computation interval of 0.5 seconds and cost matrices:

$$R = \text{diag } [1, 1, 1]$$

and

$W = \text{diag } [1000, 10, 1000, 10, 1000, 10, 1, 1, 1, 1, 1, 1, 1, 1]$ produces the feedback matrices:

$$P = \begin{bmatrix} -30.540 & -0.485 & 0.422 \\ 0.787 & -29.65 & 0.171 \\ -0.417 & -0.190 & -30.75 \end{bmatrix}$$

and

$$D = \begin{bmatrix} -650.43 & 27.074 & 5.230 \\ 53.009 & -636.540 & 10.732 \\ 3.808 & 1.580 & -870.154 \end{bmatrix}$$

The cost matrices are chosen as such because they were shown to produce the best performance when using an optimal control scheme [20].

Fig. 2 Response to P + D controller

is shown in Fig. 2. The 600 second simulation period represents 1/10th of an orbit and for this nominal configuration the solar array angle $\delta = 0$ is used throughout the simulation.

These simulation parameters are used for all results presented in the paper unless otherwise stated.

4 Design of the Self-Organizing Fuzzy Logic Controller

The SOC enables rule modification/creation by adding performance feedback to the simple fuzzy logic controller (Fig. 3). The performance index monitors the closed loop system trajectories and provides a measure of the changes, P_0 that are required at the process output in order to attain a desired trajectory.

For a multivariable process a crude system model that reflects the degree of input-output coupling is needed in order to translate the vector $\mathbf{P}_0$ to a vector $\mathbf{P}_i$ which represents the changes that are required at the process input. The vector $\mathbf{P}_i(kT)$ is then used to modify the rules that most contributed to the performance at the sample instant kT. This process of rule modification is continued until the desired trajectory is achieved.

The linguistically expressed performance index used is presented below and is the same for each satellite axis.

As the manipulated variable is generated from:

$$\mathbf{u} = P\mathbf{y} + D\dot{\mathbf{y}} \qquad (A3)$$

where

$$\mathbf{y}^T = [\phi \; \theta \; \psi]$$

and rate gyroscopes are not assumed to be mounted on the craft, then $\dot{\mathbf{y}}$ must be approximated. The simplest way of achieving this is to use the difference between successive attitude measurements, however, since the pseudo-differentiator utilized by Harris [25]:

$$\dot{\mathbf{y}}(s) \cong \frac{s}{1 + \tau_D s} \; \mathbf{y}(s)$$

affords a measure of noise suppression it is adopted to synthesize the attitude rates. The value of τ_D is chosen arbitrarily to be as small as the noise level allows.

The satellite response to this controller for $\tau_D = 0.2$ s, momentum wheel saturation torque $u_{sat} = 0.2$ Nm and initial conditions:

$$\phi = \theta = \dot{\psi} = 0.025 \text{ rad}$$

$$\dot{\phi} = \dot{\theta} = \dot{\psi} = 0.001 \text{ rad/s}$$

	Change in attitude						
	PM	PM	PS	Z0	NS	NM	NB
PB	NB	NB	NB	NM	NM	NS	Z0
PM	NB	NB	NM	NM	NS	Z0	PS
PS	NB	NB	NS	NS	Z0	PS	PM
PO	NB	NM	NS	Z0	Z0	PM	PB
NO	NB	NM	Z0	Z0	PS	PM	PB
NS	NM	NS	Z0	PS	PS	PB	PB
NM	NS	Z0	PS	PM	PM	PB	PB
NB	Z0	PS	PM	PM	PB	PB	PB

(row label: Attitude)

The interpretation of this rule matrix is:

If "attitude is NM" and "change in attitude is PS" then "credit is PS"

The terms have the meaning:

PB Positive Big
PM Positive Medium
PS Positive Small
PO Positive Zero
Z0 Zero
NO Negative Zero
NS Negative Small
NM Negative Medium
NB Negative Big

Q   quantisation process
M   deterministic output selection
GI input scaling factors
GO output scaling factors

Fig. 3 Form of the SOC

Table 1 The fuzzy set definition

(a) The attitude

	-6	-5	-4	-3	-2	-1	-0	+0	1	2	3	4	5	6
PB	0	0	0	0	0	0	0	0	0	0	0.1	0.4	0.8	1.0
PM	0	0	0	0	0	0	0	0	0	0.2	0.7	1.0	0.7	0.2
PS	0	0	0	0	0	0	0	0.3	0.8	1.0	0.5	0.1	0	0
PO	0	0	0	0	0	0	0	1.0	0.6	0.1	0	0	0	0
NO	0	0	0	0	0.1	0.6	1.0	0	0	0	0	0	0	0
NS	0	0	0.1	0.5	1.0	0.8	0.3	0	0	0	0	0	0	0
NM	0.2	0.7	1.0	0.7	0.2	0	0	0	0	0	0	0	0	0
NB	1.0	0.8	0.4	0.1	0	0	0	0	0	0	0	0	0	0

(b) The attitude rate

	-6	-5	-4	-3	-2	-1	0	1	2	3	4	5	6
PB	0	0	0	0	0	0	0	0	0	0.1	0.4	0.8	1.0
PM	0	0	0	0	0	0	0	0	0.2	0.7	1.0	0.7	0.2
PS	0	0	0	0	0	0	0	0.9	1.0	0.7	0.2	0	0
ZO	0	0	0	0	0	0.5	1.0	0.5	0	0	0	0	0
NS	0	0	0.2	0.7	1.0	0.9	0	0	0	0	0	0	0
NM	0.2	0.7	1.0	0.7	0.2	0	0	0	0	0	0	0	0
NB	1.0	0.8	0.4	0.1	0	0	0	0	0	0	0	0	0

(c) The credit value p_0

	-7	-6	-5	-4	-3	-2	-1	0	1	2	3	4	5	6	7
PB	0	0	0	0	0	0	0	0	0	0	0	0.1	0.4	0.9	1.0
PM	0	0	0	0	0	0	0	0	0	0.2	0.7	1.0	0.7	0.2	0
PS	0	0	0	0	0	0	0	0.4	1.0	0.8	0.4	0.1	0	0	0
ZO	0	0	0	0	0	0	0.2	1.0	0.2	0	0	0	0	0	0
NS	0	0	0	0.1	0.4	0.8	1.0	0.4	0	0	0	0	0	0	0
NM	0	0.2	0.7	1.0	0.7	0.2	0	0	0	0	0	0	0	0	0
NB	1.0	0.8	0.4	0.1	0	0	0	0	0	0	0	0	0	0	0

Table 2 Performance index "look-up" table

Attitude	Change in attitude												
	-6	-5	-4	-3	-2	-1	0	1	2	3	4	5	6
-6	7.0	6.5	7.0	6.5	7.0	7.0	4.0	4.0	4.0	3.0	1.0	0.0	0.0
-5	6.5	6.5	6.5	5.0	6.5	6.5	4.0	4.0	4.0	2.5	1.5	0.0	0.0
-4	7.0	6.5	7.0	5.0	4.0	4.0	4.0	1.0	1.0	1.0	0.0	-1.5	-1.0
-3	6.5	6.5	6.5	5.0	4.0	4.0	4.0	1.5	1.5	1.0	0.0	-1.0	-1.5
-2	7.0	6.5	7.0	4.0	1.0	1.0	1.0	0.0	0.0	-1.0	-1.0	-4.0	-4.0
-1	6.5	6.5	6.5	4.0	1.5	1.5	1.5	0.0	0.0	-1.0	-1.5	-4.0	-4.0
-0	7.0	6.5	4.0	3.0	1.0	1.0	0.0	0.0	0.0	-3.0	-4.0	-6.5	-7.0
+0	7.0	6.5	4.0	3.0	0.0	0.0	0.0	-1.0	-1.0	-3.0	-4.0	-6.5	-7.0
1	4.0	4.0	1.5	1.0	0.0	0.0	-1.5	-1.5	-1.5	-4.0	-6.5	-6.5	-6.5
2	4.0	4.0	1.0	1.0	0.0	0.0	-1.0	-1.0	-1.0	-4.0	-7.0	-6.5	-7.0
3	1.5	1.0	0.0	-1.0	-1.5	-1.5	-4.0	-4.0	-4.0	-5.0	-6.5	-6.5	-6.5
4	1.0	1.5	0.0	-1.0	-1.0	-1.0	-4.0	-4.0	-4.0	-5.0	-7.0	-6.5	-7.0
5	0.0	0.0	-1.5	-2.5	-4.0	-4.0	-4.0	-6.5	-6.5	-5.0	-6.5	-6.5	-6.5
6	0.0	0.0	-1.0	-3.0	-4.0	-4.0	-4.0	-7.0	-7.0	-6.5	-7.0	-6.5	-7.0

where P0 is defined as values slightly above zero and N0 as terms slightly below zero.

The fuzzy sets are formed upon a discrete support universe of 14 elements for the attitude, 13 elements for the change in attitude and 15 elements for the toruqe output. Using the standard techniques of fuzzy calculus [19] and the fuzzy sets detailed in Table 1, the linguistic performance index can be transformed to a "look-up" table (Table 2).

The requirement for a system model is met using the multivariable process characterized by the state variable expression

$$\dot{x} = f(x,u)$$

and for a small change in the input vector u, the change in state vector x is

$$\delta\dot{x} = \frac{\partial f}{\partial x^T}\delta x + \frac{\partial f}{\partial u^T}\delta u$$

where

$$\frac{\partial f}{\partial \mathbf{x}^T} \triangleq \begin{bmatrix} \dfrac{\partial f_1}{\partial x_1} & \dfrac{\partial f_1}{\partial x_2} & \dfrac{\partial f_1}{\partial x_3} & \dots & \dfrac{\partial f_1}{\partial x_m} \\[2mm] \dfrac{\partial f_2}{\partial x_1} & \dfrac{\partial f_2}{\partial x_2} & \dfrac{\partial f_2}{\partial x_3} & \dots & \dfrac{\partial f_2}{\partial x_m} \\[2mm] \cdot & \cdot & \cdot & & \cdot \\ \cdot & \cdot & \cdot & & \cdot \\ \cdot & \cdot & \cdot & & \cdot \\ \dfrac{\partial f_m}{\partial x_1} & \dfrac{\partial f_m}{\partial x_2} & \dfrac{\partial f_m}{\partial x_3} & \dots & \dfrac{\partial f_m}{\partial x_m} \end{bmatrix}$$

$$\frac{\partial f}{\partial \mathbf{u}^T} \triangleq \begin{bmatrix} \dfrac{\partial f_1}{\partial u_1} & \dfrac{\partial f_1}{\partial u_2} & \dfrac{\partial f_1}{\partial u_3} & \dots & \dfrac{\partial f_1}{\partial u_n} \\[2mm] \dfrac{\partial f_2}{\partial u_1} & \dfrac{\partial f_2}{\partial u_2} & \dfrac{\partial f_2}{\partial u_3} & \dots & \dfrac{\partial f_2}{\partial u_n} \\[2mm] \cdot & \cdot & \cdot & & \cdot \\ \cdot & \cdot & \cdot & & \cdot \\ \cdot & \cdot & \cdot & & \cdot \\ \dfrac{\partial f_m}{\partial u_1} & \dfrac{\partial f_m}{\partial u_2} & \dfrac{\partial f_m}{\partial u_3} & \dots & \dfrac{\partial f_m}{\partial u_n} \end{bmatrix}$$

and m and n are the state vector dimension and the input vector dimension, respectively.

The input changes Δu will give a state vector change Δx after one sample instant T of

$$\Delta x \approx T \delta \dot{x} = T \frac{\partial f}{\partial \mathbf{x}^T} \Delta x + T \frac{\partial f}{\partial \mathbf{u}^T} \Delta u$$

or

$$\Delta x = M \Delta u \qquad (6)$$

where

$$M = \left(E - T \frac{\partial f}{\partial \mathbf{x}^T} \right)^{-1} T \frac{\partial f}{\partial \mathbf{u}^T}$$

and E is the unit matrix.

Consequently, if $\mathbf{P}_0(kT)$ is a vector of required output changes the vector of input changes can be calculated from

$$\mathbf{P}_i(kT) = M^{-1} \mathbf{P}_0(kT)$$

Given the input reward $\mathbf{P}_i(kT)$, the rule(s) that most contributed towards the present state must be selected and modified accordingly.

4.1 Rule Modification. For the three-axis control of the earth resources satellite under study a general control rule is the implication:

$$A_\phi - CA_\phi - A_\theta - CA_\theta - A_\psi - CA_\psi - \Gamma_\phi - \Gamma_\theta - \Gamma_\psi$$

where A, CA, and Γ are fuzzy sets for the attitude, change in attitude and the torque output respectively, the subscript denoting the reference axis. If the controller is "empty" then an initial rule must be created; further rules will be generated when required by the modification procedure. The initial rule is formed from the fuzzification of the initial conditions, a_ϕ^i, ca_ϕ^i, a_θ^i, ca_θ^i, a_ψ^i, ca_ψ^i, $p_{i\phi}^i$, $p_{i\theta}^i$, $p_{i\psi}^i$ (control torques, $\tau_\phi^i = \tau_\theta^i = \tau_\psi^i = 0$). This is done using a fuzzy kernel to provide a spread of values about the single support element, thus creating the following fuzzy sets which are the same for each axis:

$$\begin{aligned} A &= \{ (a-x), \ \mu_K(a-x) \} \\ CA &= \{ (ca-x), \ \mu_K(ca-x) \} \\ \Gamma &= \{ (\tau+p_i-x), \ \mu_K(\tau+p_i-x) \} \end{aligned} \qquad (7)$$

where

$$\left.\begin{aligned} \mu_K(a-x) \\ \mu_K(ca-x) \\ \mu_K(\tau+p_i-x) \end{aligned}\right\} = \begin{cases} 1.0, & x = \pm 0 \\ 0.7, & x = \pm 1 \\ 0.2, & x = \pm 2 \\ 0.0, & 1 \times 1 \geq 3 \end{cases}$$

The single elements at the input and output of the controller at each sample instant are stored for use by the modification procedure. Thus if the present instant is kT and the modification is made to the controller output rT samples earlier, the rule to be included results from the fuzzification of a_o $(kT-rT)$, ca_o $(kT-rT)$, $\ldots$, τ_ψ $(kT-rT) + p_{i\psi}$ (kT). To avoid contradictory rules any rules with similar antecedents to the above must be removed from the rule store. This also removes those rules that most contributed to the control action being rewarded. Procyk [14] forwards an algorithm for achieving the removal when initial rules are present in the controller. The algorithm analyzes the membership function as follows.

If $A^R \to CA^R \to \Gamma^R$ represents the stored control rule and A^m and CA^m are the antecedents of the rule to be included, then calculate the fuzzy subsets:

$$DA = \min\{A^R, \text{NOT } (A^m)\}$$

and

$$DCA = \min\{CA^R, \text{NOT } (CA^m)\}$$

If these subsets have all the membership functions less than or equal to 0.5 then the rule should be deleted; if not, it is kept. This is repeated for all stored rules.

In the implementation of the SOC required, the above algorithm would delete only those rules that have identical antecedent fuzzy sets to the rule to be included, as the form of all sets is generated from equation (7). Consequently, the number of operations required for modification can be significantly reduced by checking for coincident support sets. To reduce the number of rules generated, the modification algorithm used deletes rules unless their antecedent have fuzzy sets displaced along the universe of discourse by more than one support value relative to the antecedent of the rule to be added. This operation can be expressed linguistically as:

Delete all rules that are about the same as the one to be added.

4.2 Selection of a "Real World" Model. Central to the design of the SOC is the selection of a process model that will reflect the degree of input-output coupling. The models used in this investigation are presented below.

4.2.1 Flexible Vehicle Model. The mathematical model used for the simulation of the satellite written in state variable form is

$$\dot{x} = Ax + Bu$$

Implementing equation (6) provides the nonsquare model M_{ns} where

$$\Delta x = M_{ns} \Delta u$$

and

$$M_{ns} = (E - TA)^{-1} TB \qquad (8)$$

Clearly this cannot be used in its present form as the requirement is for a model matrix that relates a three-dimensional vector of process output changes $\mathbf{P}_0$ to a three-dimensional vector of process input changes $\mathbf{P}_i$ and M_{ns} is a 14 $\times$ 3 matrix. This can be achieved by including in the model matrix M only attitude information (ϕ, θ, and ψ) formed from the elements of m_{ij} and M_{ns} as follows:

$$M = \begin{bmatrix} m_{11} & m_{12} & m_{13} \\ m_{31} & m_{32} & m_{33} \\ m_{51} & m_{52} & m_{53} \end{bmatrix} \tag{9}$$

Therefore:

$$\mathbf{P}_i = \hat{M}\mathbf{P}_0$$

where $\hat{M}$ is the M^{-1} matrix after normalization and scaling – a process described later.

4.2.2 Rigid Vehicle Model.

An alternative model is formulated from a satellite description that does not include any flexible information; thus the governing differential matrix equation results from modifying equation (4) to

$$\mathbf{T} = I(\ddot{\Phi} - \bar{\omega}_0 \Phi)$$

from which the rigid vehicle state equation

$$\dot{\mathbf{x}}_R = A_R \mathbf{x}_R + B_R \mathbf{u}$$

can be formed. The vector $\mathbf{x}_R$ is defined as

$$\mathbf{x}_R^T = [\phi \ \dot{\phi} \ \theta \ \dot{\theta} \ \psi \ \dot{\psi}]$$

Equation (8) becomes

$$M_{ns} = (E - TA_R)^{-1} TB_R$$

where M_{ns} is a 6×3 matrix and the model matrix M can be obtained by using equation (9).

The matrix M^{-1} relates small real world changes in the process outputs to small real world changes in the process inputs. This must be scaled to the universe of discourse of $\mathbf{P}_i$ and $\mathbf{P}_0$ by using the scaling factors for each axis:

$$\Delta\tau = M^{-1}\Delta\Phi$$

$$\Delta\tau = \hat{GT}\mathbf{P}_i$$

and

$$\mathbf{P}_0 = \hat{GY}\Delta\Phi$$

where

$$\hat{GT} = \begin{bmatrix} GT_o & 0 & 0 \\ 0 & GT_\theta & 0 \\ 0 & 0 & GT_\psi \end{bmatrix}$$

and

$$\hat{GY} = \begin{bmatrix} GY_o & 0 & 0 \\ 0 & GY_\theta & 0 \\ 0 & 0 & GY_\psi \end{bmatrix}$$

Thus

$$\mathbf{P}_i = (\hat{GT})^{-1}(M)^{-1}(\hat{GY})^{-1}\mathbf{P}_0$$

GY, GC, and GT are the scaling factors on the attitude, change in attitude and controller output, respectively; the subscript denotes the reference axis, $\hat{M}$ is produced from $(\hat{GT})^{-1}(M)^{-1}(\hat{GY})^{-1}$ by a normalization process to ensure that $\mathbf{P}_i$ cannot exceed the maximum (or minimum) element of its support set (± 7). This condition is satisfied if

$$S_1^{-1} \triangleq \left| \frac{m_{11}}{GY_o GT_\phi} \right| + \left| \frac{m_{12}}{GY_\theta GT_\phi} \right| + \left| \frac{m_{13}}{GY_\psi GT_\phi} \right| \leq 1$$

$$S_2^{-1} \triangleq \left| \frac{m_{21}}{GY_o GT_\theta} \right| + \left| \frac{m_{22}}{GY_\theta GT_\theta} \right| + \left| \frac{m_{23}}{GY_\psi GT_\theta} \right| \leq 1$$

$$S_3^{-1} \triangleq \left| \frac{m_{31}}{GY_o GT_\psi} \right| + \left| \frac{m_{32}}{GY_\theta GT_\psi} \right| + \left| \frac{m_{33}}{GY_\psi GT_\psi} \right| \leq 1$$

where m_{ij} is an element of M^{-1}. $\hat{M}$ is obtained from

$$\hat{M} = \text{scale} \times (GT)^{-1}(M)^{-1}(GY)^{-1}$$

where

$$\text{Scale} = \min\{S_1, S_2, S_3\}$$

It will be noted that to ensure the maximum range of use of the universe of discourse for each axis the numerical values of S_1, S_2, and S_3 must be approximately the same.

4.3 Controller Parameter Selection.

The selection of the scaling factors is not wholly subjective (27) since their magnitude is a compromise between sensitivity during rise time and the required steady-state accuracy. A qualitative selection can be made as follows.

As the initial attitude is 0.025 rad (all axes), then to maximize the sensitivity in the initial transient phase this should be mapped to the maximum discrete support value thus:

$$GY = \frac{6}{0.025} = 240$$

The largest change of attitude (at small attitudes) that is considered acceptable by the authors is 0.025 rad over the 600 s simulation period. For a sample time of 0.5 s, $(0.025 \times 0.5)/600$ must be mapped to 0.5 (above this value the quantization process registers a support value of one and a value below would register as zero):

$$GC = \frac{600 \times 0.5}{0.025 \times 0.5} = 24000$$

The above two sets of input scaling factors represent starting points for scaling factor selection; the optimum parameters will be selected by a logical trial and observation procedure.

The delay in reward parameter DL specifies which input(s) in the past most contributed to the present performance and is therefore related to process lags. Aids to the selection of DL have been proposed by Procyk [14], however, for more complex processes the only option available is selection by trial and observation. Procyk's experiments indicated that the choice of the parameter was not critical and that better initial performances were obtained if the reward was distributed over several past samples.

4.4 Form of Process Input and $\hat{GT}$ Selection.

If the discrete controller output at sample instant kT is $\mathbf{u}^*\{kT\}$ then the process input $\mathbf{u}\{kT\}$ is given by

$$\mathbf{u}\{kT\} = \hat{GT}\mathbf{u}^*\{kT\}$$

As the maximum available torque is 0.2 N m then $\hat{GT}$ is formed from

$$GT_o = GT_\theta = GT_\psi = \frac{0.2}{7} \cong 0.03$$

5 Results and Discussion

The responses shown are produced by creating an initial set of rules from an empty controller over a simulation run, then repeating the simulation with the stored rules until the performance converges upon the optimum. Where there is a significant difference between this optimum and the initial response both trajectories are presented upon the same axis sets.

Figure 4(a) shows the attitude responses to the parameters:

$$GY_\phi = GY_\theta = GY_\psi = 400$$

$$GC_\phi = GC_\theta = GC_\psi = 10,000$$

$$GT_\phi = GT_\theta = GT_\psi = 0.03$$

and the flexible model. The controller output is absolute torque and the reward is distributed equally over the last 5

Fig. 4   Response to SOC

Fig. 5   Response to SOC, dual mode operation

number of rules the delay in reward must be increased and it was found that the performance was better if the reward was distributed over several samples. Increasing the parameter above 5 has no significant effect upon the performance and causes an increase in the required computation time. During the initial run 43 rules were created and the best performance occurred on the 6th run after which 172 rules were stored. It is interesting to note that in achieving this optimum response there was a "cycling" of performance in that it would improve over a number of simulation runs and then deteriorate before improvement occurred again. This phenomenon is due to the controller trying to achieve a performance that is not attainable and can only be stopped by modifying a combination of the controller parameters, controller model, and performance index.

Paradoxically the above performances, specifically the pitch attitude response, are improved if the rigid model is used in the controller (Fig. 4(b)). For this case, 84 rules are created on the initial run and the best performance occurs on the 3rd run after which 110 rules are stored. This performance improvement is not significant since it must be remembered that both models are approximations of the process dynamics.

Variations in these parameter values show that transient performance can be improved by decreasing the controller input scaling factors. Unfortunately, this improvement is at the expense of steady-state pointing accuracy. An increase in the scaling factor values improves the steady-state pointing accuracy but the transient behavior deteriorates.

By extending the SOC [28] to operate in a dual mode it is possible to simultaneously improve both the transient and steady state system behavior, without increasing the number of elements in the support set. Thus, the controller input scaling factors will be initially chosen to be relatively small to produce the best transient response and when the trajectory is close to the origin they will be switched to a larger value to enable a high steady-state pointing accuracy to be achieved.

The values chosen are:

$$
\left.\begin{aligned}
GY &= 180 \\
GC &= 20{,}000 \\
GT &= 0.03
\end{aligned}\right\} \text{before the switch}
$$

$$
\left.\begin{aligned}
GY &= 1600 \\
GC &= 800{,}000 \\
GT &= 0.03
\end{aligned}\right\} \text{after the switch}
$$

The result of this change is shown in Fig. 5 for the rigid model.

The choice of a control law is largely dictated by its ability to cope with the off design condition, process and measurement noise disturbance. Figure 6 shows the satellite response when the modal frequencies are reduced by a factor of 2. Both controllers cope well with this mismatch condition, however, the SOC responses are marginally better. If the modal frequencies are reduced further, the SOC responses are significantly better than the P + D controller.

Increasing the modal frequencies by similar factors shows virtually no change in transient response; a slight deterioration in attitude response does occur with the SOC.

The satellite response to the SOC for a 90 deg change in orientation of the solar array, which is the worse possible case, is shown in Fig. 7. The roll atttitude response on the initial run is poor but is improved during subsequent runs, with the best performance occurring on the fifth run. The performance is marginally worse than the performance of the P + D control law.

The noise signals used in this study are Gaussian and White being characterized by the standard deviations:

samples. This distribution in reward is used for all results in this section unless otherwise stated. The delay in reward parameter was chosen as such because if only the last sample is rewarded then a very small number of rules are created during each run and system performance is poor. This is due to the rule deletion algorithm employed. To create an acceptable

a) Response to SOC, dual mode operation

b) Response to P - D controller

Fig. 6 Modal frequencies reduced by 2

Fig. 7 Response of SOC for a 90 deg change in solar array orientation

Process, $\sigma_p = 1 \times 10^{-3}$ Nm

Measurement, $\sigma_m = 2 \times 10^{-4}$ rad

which are the same for each axis.

The introduction of these disturbances seriously degrades the vehicle response to the SOC controller, Fig. 8. The number of rules created is greatly increased with the maximum number of rules allowable, 600, being exceeded on the second run. The presence of noise also results in a deterioration in the response to the P + D controller, although this is not as dramatic as with the SOC. This deterioration in control is due to the amplification of the nominal noise statistics in obtaining rate information. For the P + D controller this problem is not as significant because of the use of the pseudo-differentiator to estimate the angular velocities. The response to the SOC can be improved by calculating the change in attitude using the pseudo-differentiator, however, its performance does still not compare with that of the P + D controller. The high noise sensitivity of the SOC would probably be reduced by using Lukasiewicz logic to interpret the fuzzy linguistic relation [29], this had the effect of making the changes in the control action more progressive. However, the suggestion of Braee and Rutherford [27] that the width of fuzzy sets at the point where the membership function is 0.5 should be 5 times the standard deviation of the noise cannot be used in this case as it would result in an impractically small value of GC.

6 Conclusions

It has been demonstrated that the SOC can provide good attitude control of the earth resources satellite. The controller requires limited process knowledge and its performance compares favorably with that of a complex P + D controller. It should be noted that the SOC has no information about the flexible dynamics of the craft yet it can provide excellent damping of the flexural motion. This demonstrates that the learning capabilities of the controller can compensate for a crude process model.

a) Response to SOC, dual mode operation
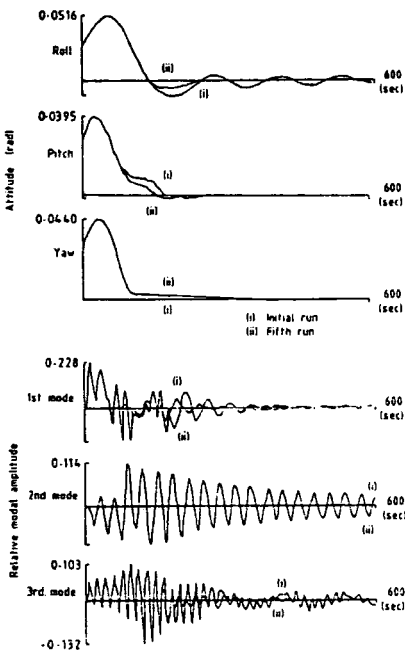
b) Response to P - D controller
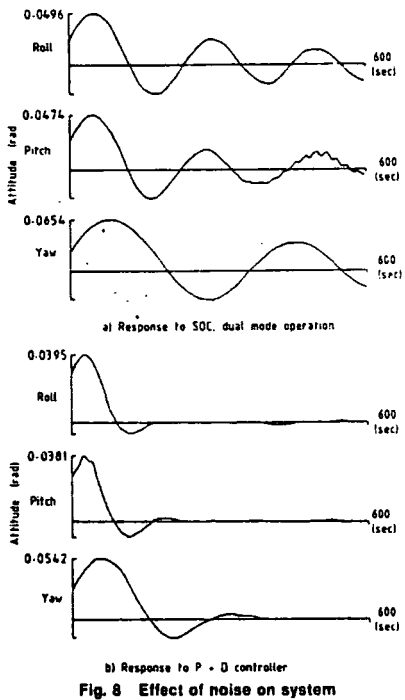
Fig. 8 Effect of noise on system

The parameters that comprise the chosen controllers were selected on a trial and observation basis and do not necessarily represent the best settings. An all embracing testing strategy is difficult to develop because of the many interacting parameters. However, this selection provides good control and was obtained with a minimum of difficulty. This
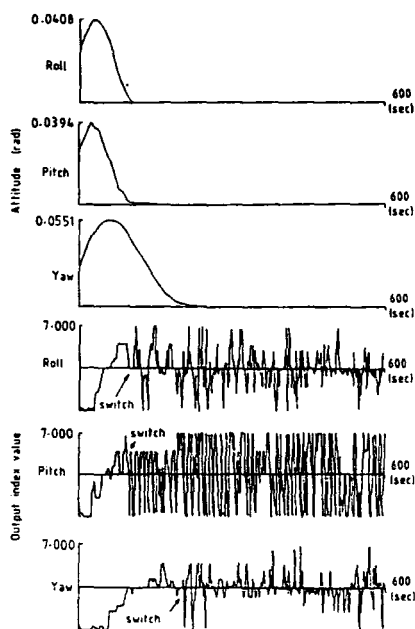
Fig. 9 SOC index values and system response

qualitative approach to the design was undertaken because the available procedures for stability and performance analysis [9, 27, 30, 31] are somewhat limited in scope and are not readily applicable to the SOC due to its complex and time-varying structure.

The cycling of the performance that has been observed is due mainly to the fullness (i.e., few zero states) of the performance index. This is demonstrated by Fig. 9 which shows the SOC's "optimum" performance (the attitude responses of Fig. 5) and the performance index output corrections for that performance. As can be seen the performance index is constantly making changes when the trajectory is considered to be acceptable. This is because the index was written with the aim of creating rules from an initial empty controller. Thus once the best performance for a particular parameter set has been obtained a further run would result in a deterioration in control as the responses cannot be improved upon. After this deterioration the modification procedure would then improve the responses until the best performance was again achieved. This cycling of the response is not a problem as it has been demonstrated that good control is possible and if the rules before the optimum performance are stored (zero rules in the case of the best performance on the initial run), then this response can be reproduced at any time. Convergence of the controller (i.e., no rule modification on sequent runs) could be achieved by making the performance index less active (many zero states) at the expense of the performance.

The study has shown that a specific area does not exist where the performance of the SOC is significantly better than that of a P + D controller. Although this superior performance is not general it does indicate that the fuzzy logic controller can compete with the more conventional techniques of controller design and therefore its wider application should not be neglected.

References

1 Mamdani, E. H., and Assilian, S., "An Experiment in Linguistic Synthesis with a Fuzzy Controller," *Int. J. Man-Machine Stud.*, Vol. 7, 1975, pp. 1-13.

2 Kickert, W. J. M., and Van Nauta Lemke, H. R., "Application of a Fuzzy Controller in a Warm Water Plant," *Automatics*, Vol. 23, 1976, pp. 201-208.

3 Ostergaard, J. J., "Fuzzy Logic Control of a Heat Exchanger Process," Internal Report 7601, Tech. Univ. Denmark, Elec. Power Eng. Dept., 1976.

4 Rutherford, D. A., and Carter, G. A., "A Heuristic Adaptive Controller for a Sinter Plant," Proc. 2nd IFAC Symp. Automation in Mining, Mineral and Metal Processing, Johannesburg, 1976.

5 Tong, R. M., "Some Problems with the Design and Implementation of Fuzzy Controllers," Internal Report CUED/F-CAMS/TR 127, Cambridge University, 1976.

6 Van Amerongen, J., Van Nauta Lemke, H. R., and Van Der Veen, J. C. T., "An Autopilot for Ships Designed with Fuzzy Sets," *Digital Computer Applications to Process Control*, H. R. Van Naute Lemke (ed.), IFAC and North-Holland, 1977.

7 Larsen, P. M., "Industrial Applications of Fuzzy Logic Control," *Int. J. Man-Machine Stud.*, Vol. 12, 1979, pp. 3-10.

8 Tong, R. M., Beck, M. B., and Latten, A., "Fuzzy Control of the Activated Sludge Wastewater Treatment Process," *Automatica*, Vol. 16, 1980, pp. 659-701.

9 Daley, S., and Gill, K. F., "A Justificiation for the Wider Use of Fuzzy Logic Control Algorithms," *Proc. Instn. Mech. Engrs.*, Vol. 199, No. C1, 1985 pp. 43-49.

10 Sugeno, M., ed., *Industrial Applications of Fuzzy Control*, North-Holland, 1985.

11 Gupta, M. M., Kiszka, J. B., and Trojan, G. M., "Multivariable Structure of Fuzzy Control Systems," *IEEE Trans. Syst. Man and Cyb.*, Vol. SMC-16, 1986, pp. 638-656.

12 Bainbridge, L., *The Process Controller, The Analysis of Practical Skills*, W. T. Singleton (ed.), Academic Press, 1975.

13 Umbers, I. G., and King, P. J., "An Analysis of Human Decision-Making in Cement Kiln Control and the Implications of Automation." *Fuzzy Reasoning and Its Applications*, E. H. Mamdani and B. R. Gaines (eds.), Academic Press, 1981.

14 Procyk, T. J., "A Self-Organizing Controller for Dynamic Processes," Ph.D. thesis, Queen Mary College, London, 1977.

15 Procyk, T. J., and Mamdani, E. H., "A Linguistic Self-Organizing Process Controller," *Automatica*, Vol. 15, 1979, pp. 15-30.

16 Mamdani, E. H., "Advances in the Linguistic Synthesis of Fuzzy Controllers," *Int. J. Man-Machine Stud.*, Vol. 8, 1976, pp. 669-679.

17 Tong, R. M., "A Control Engineering Review of Fuzzy Systems," *Automatica*, Vol. 13, 1977, pp. 559-569.

18 Kandel, A., *Fuzzy Mathematical Techniques with Applications*, Addison-Wesley, 1986.

19 Kaufmann, A., and Gupta, M., *Introduction to Fuzzy Arithmetic: Theory and Applications*, Van Nostrand Reinhold, 1985.

20 Fenton, J., "Satellite Attitude Measurement and Control Incorporating Active Damping of Flexural Motion," Ph.D. thesis, Apr. 1981, University of Leeds.

21 Likins, P. W., "Dynamics and Control of Flexible Space Vehicles," Technical Report 32-1329, 1969, Jet Propulsion Laboratory, Calif.

22 Hewer, G. S., "An Iterative Technique for the Computation of the Steady State Gains for the Discrete Optimal Regulator," *IEEE Trans. on Automatic Control*, Vol. 16, 1979, pp. 382-383.

23 Kleinman, D. L., "Stabilising a Discrete Constant Linear System With Application to Iterative Methods for Solving the Reccati Equation," *IEEE Trans. on Automatic Control*, Vol. 19, 1974, pp. 252-254.

24 Smith, R. A., "Matrix Equation AX + BX + C," *SIAM J. Applied Math* Vol. 16, 1968, pp. 198-207.

25 Harris, R. S., and Todman, D. C., "Three Axis Control of Spacecraft with Large Flexible Appendages, Dynamics and Control of Non-Rigid Spacecraft," Proc. of ESA Symposium, Frascati, Italy, 24-26 May 1976, pp 285-296.

26 Paraskevopoulos, P. N., "On Pole Assignment by Proportional Plus Derivative Output Feedback. *Electron Letters*, Vol 14 1976, pp. 34-35.

27 Braae, M., and Rutherford, D. A., "Selection of Parameters for a Fuzzy Logic Controller," *Fuzzy Sets and Systems*, Vol. 2, 1979, pp 185-199.

28 Daley, S., and Gill, K. F., "Attitude Control of a Spacecraft Using an Extended Self-Organising Fuzzy Logic Controller," *Proc. I. Mech. E.*, Vol. 201 No. C2, 1987, pp. 97-106.

29 Baldwin, J. F., and Guild, N. C. F., "Modeling Controller Using Fuzzy Relations," *Kybernetes*, Vol. 9, 1980, pp. 223-239.

30 Kickert, W. J. M., and Mamdani, E. H., "Analysis of a Fuzzy Logic Controller," Fuzzy Sets and Systems, Vol. 1, 1978, pp. 29-44.

31 Daley, S., and Gill, K. F., "A Study of Fuzzy Logic Controller Robustness Using the Parameter Plane," *Computers in Industry*, Vol. 7, 1986 pp. 511-522.

APPENDIX I

Proportional Plus Derivative Controller

The proportional plus derivative controller is designed using a procedure detailed by Parakevopoulos [26].

Describing the satellite by the state equations:

$$\dot{x} = Ax + Bu \tag{A1}$$

$$y = Cx \tag{A2}$$

and the controller by:

$$u = Py + D\dot{y} \tag{A3}$$

where P and D are constant 3×3 matrices that can be evaluated as follows.

Combining equations (A1), (A2), and (A3) yield:

$$\dot{x} = (E - BDC)^{-1}(A + BPC)x$$

where E is the unit matrix.

It is required that the system behaves as:

$$\dot{x} = Fx$$

where the eigenvalues of F have negative real parts and are chosen arbitrarily.

Thus

$$F = (E - BDC)^{-1}(A - BPC) \quad \text{or} \quad F - A = BPC + BDCF$$

which can be written as:

$$Z = BHS \tag{A4}$$

where

$$Z = F - A$$

H is the 3×6 partitioned matrix,

$$H = [P:D]$$

and S is the $6 \times (6 + 2m)$ partitioned matrix,

$$S = \begin{bmatrix} C \\ \cdots \\ CF \end{bmatrix}$$

as B and S are nonsquare then the solution of equation (A4) is obtained from:

$$H = (B^T B)^{-1} B^T Z S^T (S S^T)^{-1}$$

The matrices P and D result from a departitioning of H.

The selection of F such that it has the desired eigenvalues can be done by either:

(i) derivation of a polynomial from the chosen pole locations of the system and construction of F from its coefficients.

(ii) derivation of F from a feedback matrix that will provide the desired dynamic characteristics.

For the system under consideration selection of a multiplicity of poles will not be easy. Thus a feedback matrix K_R calculated from a solution to the algebraic Riccati equation is used to position the poles [20], i.e.,

$$F = A - BK_R \tag{A5}$$

5. NON-STEADY GAS FLOW IN DUCTS

PAPER 2

THE ENGINEER

TECHNICAL CONTRIBUTORS

SECTION

Influence of Exhaust Induction Systems on Air Consumption of a Two-Stroke Oil Engine

By E. H. WRIGHT. B.Sc.. Ph.D.. A.M.I.Mech.E.*
and K. F. GILL, M.Sc.. Ph.D.. A.M.I.Mech.E.*

To determine the validity of published work,[1,2] the scavenging of a naturally aspirated firing two-stroke oil engine using simple exhaust and induction systems was investigated experimentally. For a constant air-fuel ratio of 24 : 1, air consumption trials were performed for the following exhaust and induction system arrangements:

1. Varying length of plain exhaust pipe with a neutral induction system.
2. Varying length of plain pipe—conical diffuser exhaust duct with a neutral induction system.
3. Varying length of induction system with a fixed length plain pipe—diffuser exhaust duct.
4. Asymmetrical exhaust and induction systems.

The general conclusions to be drawn are:
(1) No unique relationship between dimensionless air flow and nL/a exists for a firing engine as obtained from the work done using simulated conditions.
(2) A high air consumption within bands of limited speed range is possible with natural aspiration using symmetrical exhaust and induction systems.
(3) The stable operating speed ranges can be considerably extended without appreciable effect upon air consumption by using an asymmetrical exhaust and a symmetrical induction system arrangement.
(4) The objectionable noise produced by an engine exhaust system is primarily due to shock wave formation within the duct.

THE work presented in this article is the result of an investigation into the scavenging potentialities of wave-action in the induction and exhaust ducts of a firing naturally aspirated opposed piston two-stroke oil engine. incorporating ports designed in accordance with Kadenacy specifications.[4]

The high performance of engines built to Kadenacy specifications cannot be disputed. It is now generally accepted, however, that the performance is due largely to pressure pulsations in the exhaust system. Bannister and Mucklow[4] showed conclusively that the depression in the cylinder following release, the so-called Kadenacy effect, was attributable to wave action. Wallace, Nassif and Boxer [1, 2] extended the work of Bannister and Mucklow using a motored opposed piston two-stroke cycle engine in which the cylinder release pressure was simulated and made comparable with that of a firing engine. This work suggested confirmation of the

* Department of Mechanical Engineering. University of Birmingham.

well-known criterion nL/a. termed the "natural pipe length". as a criterion for air consumption. The simulated results were plotted as dimensionless air consumption against this criterion, and although presentation in this form resulted in considerable scatter. a broad general trend, indicating a systematic variation in air consumption with change in the exhaust criterion, was observed. This scatter was attributed to the effects of speed on certain subsidiary factors and by applying a speed correction factor a unique relationship was obtained.

The engine used by Wallace and others was converted to firing conditions and used to investigate the effect on the air consumption of the exhaust gas and cylinder gas temperatures and the associated flow discontinuities and irreversibilities.

APPARATUS

The engine used in the investigation was an unblown, two-stroke opposed piston oil engine and a cross-sectional arrangement of

the unit is shown in Fig. 1. The original exhaust system incorporated exhaust ejectors designed to Kadenacy specifications. which. for the present research. were rendered inoperative by the insertion of short lengths of pipe. Directly coupled to the engine unit was a swinging field electric dynamometer and the general arrangement is shown in Fig. 2.

Auxiliary shafts. chain driven from the engine crankshaft. provided the drives for the fuel injection pump. the revolution counter and a three-phase a.c. tachometer.

For continuous engine running the fuel injection pump was gravity fed directly from the fuel tank and for accurate fuel measurement the fuel supply was taken from calibrated pipettes. A micrometer attachment

Fig. 1—Sectional arrangement of engine

Technical Contributors Section *(Continued)*

A—Fuel tank.
B—Fuel filter.
C—Pipette.
D—A.C. tachometer.
E—Fuel injection pump.
F—Revolution counter.
G—Contact breaker points.
H—Fuel injector nozzle.
J—Exhaust pipe.
K—Small air box.
L—Metering air box.

M—Orifice plate.
N—Compressed air supply for starting.
P—Pressure gauge (for starting).
Q—Clamp to isolate micromanometer during starting.
R—Micromanometer.
S—Dynamometer.
T—Spring balance.
V—Balance weight.
V—Armature load resistance.
W—Field resistance.
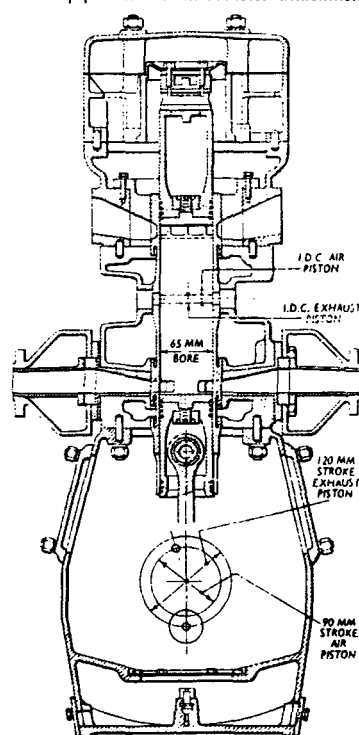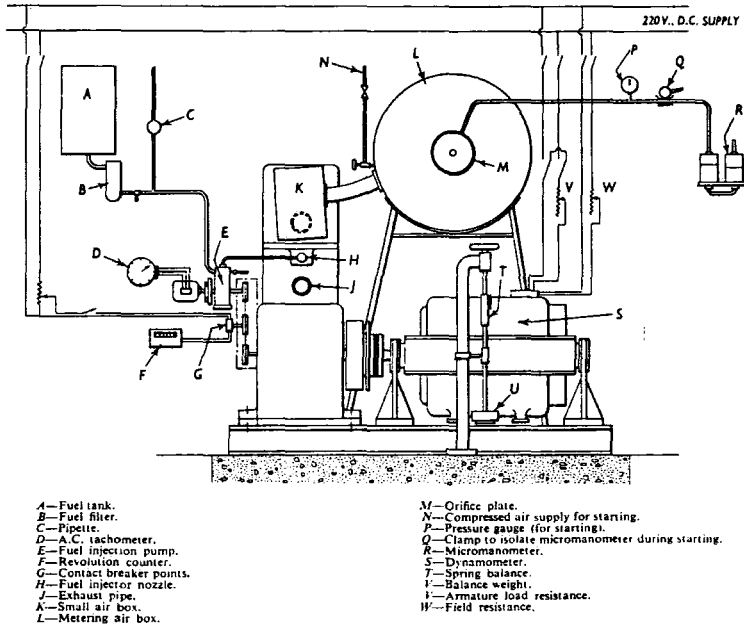
Fig. 2

on the injection pump rack provided control for the pump delivery flow. The exhaust systems discharged into collector tanks which were vented to atmosphere through the laboratory exhaust extraction system. To verify that no scavenging assistance was gained from the extraction system, water manometers were attached to one small air box and one exhaust collector tank to measure the pressure gradient across the engine unit. Bulk exhaust gas temperature was measured by iron-constantan thermocouples positioned at chosen intervals along the duct length.

Both exhaust ducts consisted of a section of solid drawn 1⅛in bore commercially smooth plain pipe to which a conical diffuser assembly could be attached. The construction of each duct was such that the plain pipe could be varied in length by increments of 6in up to a maximum of 11ft. The diffuser assembly, which had a divergence angle of 6°, could also be varied in length by increments of 6in from 1ft to 3ft 6in.

The air circuit can be seen in Fig. 2. Mounted in the frame straddling the dynamometer is a large fabricated steel air box, in one end of which is mounted the metering orifice. A range of orifices designed in accordance with B.S. 1042 were used in the air box and the pressure difference across these recorded with the aid of a micromanometer. Two flexible rubber tubes of 3in bore, connected the large air box with two smaller air boxes. These latter air boxes were either attached directly to the engine ports to give a neutral induction system, or to the upstream end of the induction ducts when these were fitted (Fig. 3). The induction ducts consisted of 2in bore smooth plain pipe, terminating upstream in a diffuser of fixed length, and were variable in length by intervals of 6in in a similar manner to the exhaust system. The rolled steel fabricated

diffusers were 19in in length with a divergence angle of 6°.

PROCEDURE

To reduce the number of engine operating variables and provide a basis for comparison, constant values were used for the air-fuel ratio and the engine cooling water output temperature. The values chosen for all the trials were 24 : 1 and 180°F respectively. The change in the engine air consumption

with the variation in the length of the exhaust and induction ducts, was investigated in five stages, namely:

(1) With a neutral induction system, the plain exhaust pipe length was varied by increments of 6in from a minimum length of 2ft 2in to the maximum length of 10ft 2in, these pipe lengths representing the limiting values beyond which it was not possible to run the engine without the supply of scavenge air.

(2) For a fixed length of diffuser of 3ft 6in and a neutral induction system, a full air consumption trial was carried out in which the exhaust plain pipe length was varied in steps of 6in from a minimum length of 1ft 8in to a chosen maximum length of 5ft 8in.

(3) For a constant plain pipe length of 4ft 8in and a neutral induction system, the effects of diffuser cone length upon engine performance was investigated. This entailed the same procedure as in (2) except that the diffuser length was changed by decrements of 6in from 3ft 6in to a minimum length of 2ft.

(4) The quantitative effect of induction ramming was studied for a fixed exhaust duct length of 8ft 2in. The exhaust duct consisted of a 4ft 8in length of plain pipe terminating in a 3ft 6in length of diffuser cone.

For the same speed range as in the above cases, the induction plain pipe length was varied in 6in intervals between the limits of 7in and 1ft 7in. In all cases the plain pipe terminated in a conical diffuser of length 19in.

(5) Asymmetrical arrangements comprising the following duct lengths were investigated in a similar manner to the above four cases.

The arrangements were:

		Plain pipe		Diffuser	
(i)	Induction ducts ...	7in	...	19in	
		1ft 7in	...	19in	
	Exhaust ducts ...	4ft 8in	...	3ft 6in	
		5ft 8in	...	3ft 6in	
(ii)	Induction ducts ...	7in	...	19in	
	Exhaust ducts ...	3ft 2in	...	3ft 6in	
		5ft 8in	...	3ft 6in	
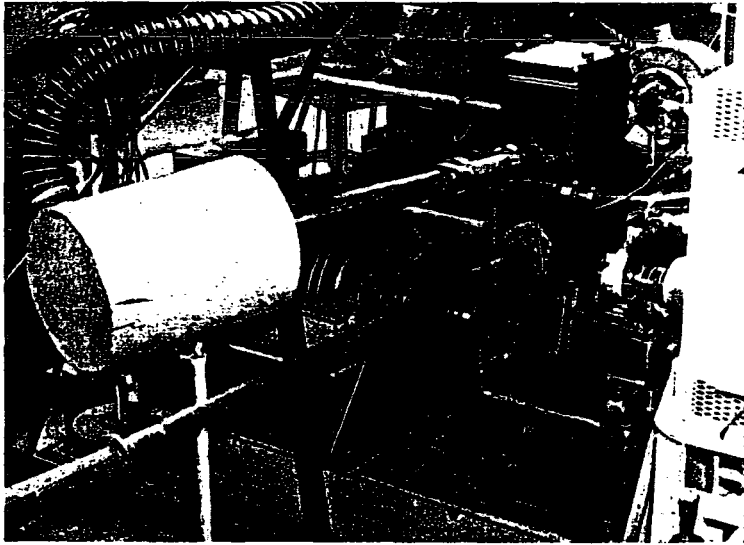
Fig. 3
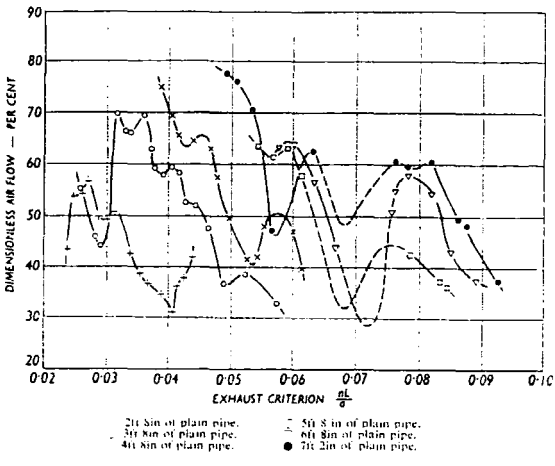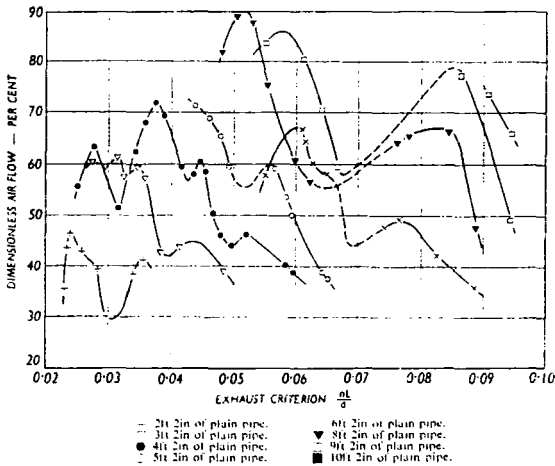
Fig. 4—Variation in air flow with exhaust pipe length. Neutral induction system

Fig. 5—Variation in air flow with exhaust pipe length. Neutral induction system

For each duct length. the readings taken at selected intervals within the stable speed range were: engine torque. micromanometer head. gauge pressures in the small air box. and the exhaust collector tank. and exhaust gas temperature at a number of stations along the duct. The speed range in all five cases was 500 r.p.m. to 1 500 r.p.m. and the results are plotted in Figs. 4. 5, 6. 9. 10 and 11.

DISCUSSION OF RESULTS

(a) *Dynamic Similarity and Air Consumption.*—Scavenging of a naturally aspirated blowerless engine is effected by utilisation of the wave effects in the exhaust system and the criterion for dynamic similarity in this respect has been termed the "natural duct length".[1] This was defined as nL/a where n. L and a denote the engine speed. duct length and mean acoustic velocity in the duct respectively.

For the work presented. the criterion nL/a is used as a basis for comparison with the previous work done using simulated con-

ditions. In the case of the plain pipe system. the above criterion has a definite physical significance if it is assumed that the propagation velocity is a constant. i.e. geometrically similar pressure distributions with respect to crank angle exist in the plane of the exhaust ports. It is difficult to formulate such a criterion with an equally precise meaning in the case of the plain pipe-diffuser arrangement. In addition to the incorrect basic assumption of a constant propagation velocity. the nature of the reflection process is so much more complex in the diffuser. that no single criterion for dynamic similarity can be specified. As a reasonable compromise, Wallace and Boxer[2] suggested $n(L - 0.5L_d)/a$ where L. is the plain duct length and L_d the diffuser length. This equivalent length of diffuser is. however. based on the assumption that the fundamental pulse is of zero amplitude on its arrival at the open end. and this in general is not valid.

The results of the air consumption trials using a neutral induction system. and ob-

tained for both plain pipe and plain pipe-diffuser exhaust systems are shown plotted in Figs. 4. 5. 6 and 7. The ordinate axis in all the figures is the dimensionless ratio V_a/V; where V_a is the volume of air aspirated per cycle at ambient conditions and V; is the effective cylinder trapped volume at the instant of air port closure. From these it can be seen that dimensionless air flows as high as 146% can be achieved with the plain pipe conical diffuser arrangement and thus the prospect of obtaining an improvement in power/weight ratio for the engine unit is good.

Pulse Amplitude.—As a result of the systematic testing of a simulated engine system and the application of a speed correction. it was shown that a unique curve relating V_a/V; and nL/a was possible. In the case of a firing engine. however. the amplitude of the scavenging pulse is attenuated by the flow irreversibilities of wall friction and heat transfer to the surroundings. The effect of friction. due to higher gas velocities and wall soot deposit. has a more marked effect in the

Fig. 6—Variation in air flow with exhaust duct length. Neutral induction system

Fig. 7—Variation in air flow with exhaust duct length. Neutral induction system

Technical Contributors Section *(Continued)*

Fig. 8—The effect of engine speed correction on the air flow curves obtained with a neutral induction system

○ 2ft of plain pipe.
● 3ft of plain pipe.
· 4ft of plain pipe.
□ 4ft 6in of plain pipe.
▼ 5ft of plain pipe.
■ 6ft of plain pipe.
♦ 8ft 6in of plain pipe.
———— Unique curve from simulated work.

firing engine, and the effect of heat transfer is virtually non-existent in the simulated work. Further the pulse amplitude is affected by temperature discontinuities which are established at the interface of the hot gases being discharged from the cylinder and the cooler residual gases from the previous cycle. The volume of the exhaust ducting will, in general, be in excess of the volume of the cylinder gases discharged per cycle and hence several discontinuities will exist in the ducting at any one instant. These discontinuities, in their passage down the exhaust duct, are attenuated by diffusion and mixing, and thus their influence on the pulse amplitude becomes progressively less marked.

The combined effect of the irreversibilities and temperature discontinuities will vary with different duct lengths, and for the same value of nL/a, the air mass flow and thus the cylinder release pressure will vary. The speed

correction, as used for the presentation of the simulated work, was applied to the air consumption results for both the plain pipe and the plain pipe-diffuser exhaust arrangement. These are shown plotted in Figs. 8 and 9 respectively, and the large scatter shows that no unique line relating the dimensionless groups V_a/V_t and nL/a, is obtainable for a firing engine.

Pulse Timing.—Assuming the pulse shape is the same for all operating conditions, the wave configuration in the exhaust duct does not depend exclusively on the three system parameters of duct length, mean acoustic velocity and engine speed. The engine speed, n, is directly proportional to the mean propagation time for a wave, but the latter is not directly proportional to the mean acoustic velocity, a, since the propagation velocity is affected by the gas stream velocity. Further, when using the exhaust

diffuser, the equivalent length used for this cone is based on the assumption that the fundamental pulse is of zero amplitude on its arrival at the open end.

The lower particle velocity associated with a smaller air mass flow causes an earlier return of the scavenging pulse and to maintain a constant scavenge efficiency, i.e. the presentation of the same port configuration to the rarefaction pulse, requires a reduction in engine speed. Hence, for example, the peaks for the differing values of dimensionless air flow obtained with different pipe lengths should lie on a line of positive slope and not on a vertical line. This slope of the peak values can be seen in Figs. 4 and 5, the maxima around $nL/a=0·08$ exhibiting this behaviour clearly.

Most of the results shown in Figs. 6 and 7, and those below a value of $nL/a=0·065$, Figs. 4 and 5, are in the region in which the scavenging action is the result of a complex wave system caused by two or more traverses of the exhaust duct by the fundamental pulse. When such a complex wave action is involved, no marked general trend can be expected and to check the validity of the above argument when operating under these conditions, a test was conducted using a constant length of plain pipe and various lengths of diffuser.

The timing of the complex wave system encountered in all three cases studied is the same, since reflections commence at the diffuser entry section. The scavenging potential, however, is reduced by shortening the diffuser lengths with a consequent reduction in particle velocity. The results are shown in Fig. 10 and these confirm that the argument for the fundamental pulse in the plain pipe case is applicable to a complex wave system and that the term nL/a is not a truly independent dimensionless parameter for the flow encountered in a firing engine.

(b) Effect of Diffuser Length.—For a fixed length of plain exhaust pipe and a neutral induction system, the influence of diffuser length on air consumption is shown in Fig. 10.

The general shape of the air consumption

x 3ft 8in of plain pipe and 3ft 6in of conical diffuser.
▼ 4ft 8in of plain pipe and 3ft 6in of conical diffuser.
○ 5ft 8in of plain pipe and 3ft 6in of conical diffuser.
— — — Unique curve from simulated work.

Fig. 9—The effect of engine speed correction on the air flow curves with a neutral induction system

▼ 3ft 6in of conical diffuser.
○ 2ft 6in of conical diffuser.
x 2ft of conical diffuser.

Fig. 10—Variation in air flow with diffuser cone length. Plain pipe length of 4ft 8in and neutral induction system

Fig. 11—Variation in air flow with induction duct length

Exhaust duct consisted of a length of plain pipe 4ft 8in long terminating in a conical diffuser of length 3ft 6in.

▼ Neutral induction system.
○ 7in of plain pipe and 19in of conical diffuser.
◯ 13in of plain pipe and 19in of conical diffuser.

curves is not affected by the variation of the diffuser length, although improved air consumption results from the use of the longer diffuser. Improved performance is obtained since the amplitude of the fundamental pulse arriving at the open end is smaller and this results in a reduction in the kinetic energy loss during open end reflection. It follows that for the short diffuser, the energy content of the reflected pulse is much less than the fundamental pulse and the duration of the rarefaction pulse will be shorter. Thus as a result of both these effects the scavenging potentiality is curtailed.

(c) *Stable Breathing.*—For stable breathing the curve relating the dimensionless air flow to nL/a. or to speed, requires to be of negative slope. Ideally, therefore, the air breathing curve required for successful operation of a naturally aspirated blowerless two-stroke cycle engine is one which has a constant negative slope for its operating speed range.

With a neutral induction system, the plain pipe-diffuser exhaust systems comprising 4ft 8in, 5ft 2in and 5ft 8in lengths of plain pipe terminating in a 3ft 6in length of diffuser gave the best breathing throughout the operating speed range with the exception of a narrow speed band around 1 300 r.p.m. Operation within the speed range 1 200 to 1 400 r.p.m. was impossible with the system using the 4ft 8in length of plain pipe and represented the worst breathing characteristic of the above optimum exhaust duct lengths. This exhaust arrangement was therefore chosen to investigate the possibility of effecting an improvement by means of induction ramming.

Air consumption trials were performed using induction systems composed of 7in and 13in of plain pipe terminating upstream in a diffuser cone of length 19in. The results of these trials are shown in Fig. 11. Although the air consumption curves were still oscillatory in nature, successful running was achieved with both induction systems over the full speed range. This represented a substantial improvement in the breathing characteristics. An attempt was then made to reduce the oscillatory nature of the air consumption characteristics by selecting from the previous results an asymmetrical arrangement of exhaust and induction systems. The results of this investigation are shown in Fig. 12, together with the comparable results obtained with a neutral induction system. The arrangement with a symmetrical induction system and an asymmetrical exhaust system, curve ●, gave the

most promising characteristic. Although theoretically unstable breathing regions, i.e. characteristics of positive slope, exist, it was found in practice that speed control throughout the full speed range was readily achieved.

(d) *Noise.*—During the course of the experimental programme it was observed that a pronounced "cracking" noise was superimposed on the normal exhaust note when using the plain pipe-diffuser exhaust systems. From a consideration of the wave mechanism involved, it was apparent that the "cracking" sound could not result from the disordered expansion of the fundamental pressure pulse at the open end of the duct. The diffuser provides a controlled expansion, resulting in an appreciable reduction of the pulse amplitude incident at the open end as compared with the plain pipe exhaust system. Examination of the pressure recordings taken at various stations along the exhaust duct showed that a relatively strong shock wave developed behind the main rarefaction pulse within the region of the diffuser entry section. Monitoring of the pressure variations occurring at this section of the duct under different load and speed conditions showed that the "cracking" noise became more pronounced as the shock wave formed in this region became more intense.

SUMMARY OF CONCLUSIONS

(1) No unique relationship exists between the dimensionless air consumption and the dimensionless group nL/a to define the air mass flow in a firing engine, as was suggested by the previous simulated work[1,2]. The results of the simulated work are not applicable to the firing engine due to the presence of temperature discontinuities and flow irreversibilities. Thus, the only method of estimating the air flow which may be expected as a result of wave action in an engine exhaust system, is to perform a theoretical analysis for the system under consideration. Theoretical analyses have been performed, with satisfactory results, for the systems described in this article. The solution of the equations of flow has been effected by the use of a modified form of the "method of characteristics" in which the effects of heat transfer, friction, temperature discontinuities and variation of specific heats have been included. The theoretical treatment is, however, beyond the scope of this article and is in process of preparation for publication as a separate paper.

(2) The experimental results show that efficient scavenge can be achieved by utilisation of the wave effects in the exhaust duct of a two-stroke oil engine without recourse to an external blower, or crank-case compression.

(3) The fitting of a suitable conical diffuser to the plain exhaust duct arrangement, results in a marked improvement in the mass of air breathed and hence the maximum potential power output of the engine.

(4) The poor breathing exhibited over a limited speed range when using a neutral induction system can be improved by induction ramming without material effect on the performance outside this speed range.

(5) A satisfactory practical breathing characteristic can be obtained by using a suitable matched symmetrical induction system and an asymmetrical exhaust system.

(6) The objectionable noise from a reciprocating I.C. engine exhaust system is attributable to the presence of shock waves within the system. This suggests that the theoretical design of effective silencers for reciprocating I.C. engines should be based on the finite wave theory and not on the small wave theory generally adopted.
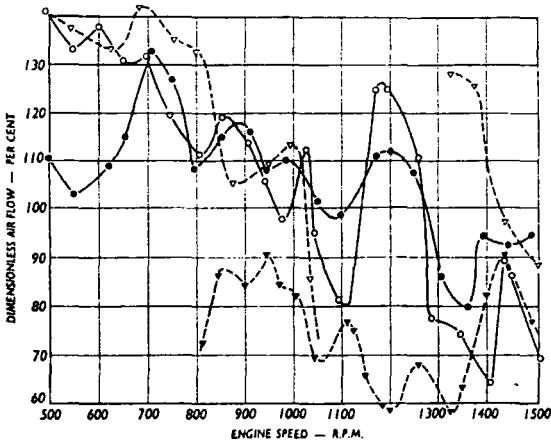
Fig. 12—Air flow curves for asymmetrical duct systems

○ Exhaust duct lengths: 4ft 8in and 5ft 8in of plain pipe terminating in 3ft 6in of conical diffuser. Induction duct lengths: 7in and 1ft 7in of plain pipe terminating in 19in of conical diffuser.
● Exhaust duct lengths: 3ft 2in and 5ft 8in of plain pipe terminating in 3ft 6in of conical diffuser. Induction duct lengths: 7in of plain pipe terminating in 19in of conical diffuser.
▽ 5ft 2in of plain pipe and 3ft 6in of conical diffuser. Neutral induction system.
▼ 3ft 2in of plain pipe and 3ft 6in of conical diffuser. Neutral induction system.

ACKNOWLEDGMENTS

REFERENCES

[1] Wallace, F. J., and Nassif, N. H., "Air Flow in a Naturally Aspirated Two-Stroke Engine", Proc.I.Mech.E., Vol. 168, page 515, 1954.

[2] Wallace, F. J., and Boxer, G., "Wave action in Diffusers for Exhaust-pipe Systems with Special Reference to the Scavenging of Two-Stroke Enginess", Proc. I.Mech.E., Vol. 170, 1956.

[3] Kadenacy, M. E., British Patent Specifications, Nos. 473 684 and 473 686, 1936.

[4] Bannister, F. K., and Mucklow, G. F., "Wave Action Following Sudden Release of Compressed Gas from a Cylinder", Proc. I.Mech.E., Vol. 159, 1948.

PAPER 3

THE ENGINEER

TECHNICAL CONTRIBUTORS

SECTION

Theoretical Analysis of the Exhaust System of an Oil Engine

By E. H. WRIGHT, B.Sc., Ph.D.,* and K. F. GILL, M.Sc., Ph.D.*

The accuracy to which the air consumption and pressure wave profiles in the exhaust duct of a two-stroke oil engine can be predicted theoretically has been examined by the use of the isentropic finite wave flow equations. The isentropic solutions of the gas flow in a plain pipe and a plain pipe-diffuser exhaust arrangements were compared with the actual recorded air mass flow and pressure wave profiles for these systems. The general conclusions to be drawn are:

(1) True application of the theory does not give a good solution of the wave pattern and gas flow in an actual engine system. Caution should therefore be exercised in the use of the simplified theory.

(2) The application of the isentropic finite amplitude wave theory to the exhaust system of a firing engine will only show promise providing high Mach Number flow conditions are not created by the system configuration.

(3) Simulation of an engine system will almost certainly give erroneous solutions to the gas flow in a real engine system. Extreme caution should therefore be exercised in drawing general conclusions regarding the performance of a real engine system from the results of this type of work.

I. Introduction

THE potential advantage of the two-stroke cycle engine over the four-stroke cycle engine of equal swept volume is substantial. The output torque is more uniform and for the same speed of rotation, the power developed is theoretically double giving a much improved power-weight ratio. In addition the number of moving parts is reduced, simplifying maintenance and giving improved reliability. In practice, however, considerable difficulty has been encountered in attempting to realise the potentially high specific output, due primarily to the problem of achieving efficient scavenge.

Success of the two-stroke cycle engine depends upon the efficiency of the air exchange process in the cylinder. In a high-speed engine, the time available for scavenging the cylinder is very small, and hence to gain any measure of success, the scavenge air must be supplied under pressure. This is possible by using either crankcase compression or an air compressor, with the consequent absorption of power, reduction in

Department of mechanical engineering, University of Birmingham.

power-weight ratio, and increased running and capital costs.

The pressure pulsations created in the exhaust system by the cylinder blowdown process contains sufficient energy to effect the scavenge process. One method of utilising this energy is to use an exhaust-gas-driven turbine driving an air compressor to provide the scavenge air and by suitable design this arrangement can increase the b.m.e.p. rating and thus the power-weight ratio. Scavenge can also be achieved by using a suitably designed exhaust system which directly effects scavenge by creating a sub-atmospheric pressure in the engine cylinder and in this case the engine can be termed "naturally aspirated". The most efficient scavenge process, however, would be a combination of these two methods, the scavenging achieved by the latter augmenting the compressor scavenge. Many research workers have published results of investigation into the utilisation of exhaust pressure pulses for scavenging including Jenny Wallace, Nassif and Boxer, but in almost every case, the work has been performed using either a simulated engine system or an actual engine but motored and fed with compressed air to simulate the

actual operating pressures. General conclusions with regard to the scavenging potential of simple exhaust systems have been drawn from the simulated work, but investigations carried out with a firing engine by the authors have shown that certain of these conclusions are not valid.[1] In the author's opinion the only method of estimating the air flow which may be expected as a result of wave action in an engine exhaust system, is to perform a theoretical analysis for the system under consideration.

The simplest analysis to adopt assumes the gas flow to be isentropic and isentropic analyses have been performed in this report for simple exhaust systems and compared with the actual measured values of air mass flow and pressure pulsations produced in the exhaust system.

2. Theory

2.1 INTRODUCTION AND GENERAL EQUATIONS OF FLOW

The flow problem studied is that of the superimposition of two wave trains travelling in opposite directions within the exhaust duct of the engine. These wave trains are created by the discharge of the exhaust

Nomenclature:
A—Cross-sectional area (ft²).
a—Acoustic velocity (ft/sec).
C_r—Coefficient of discharge.
C_r—Specific heat at constant pressure (ft-pdls-ib °C).
C_v—Specific heat at constant volume (ft/pdls.ib °C).
K—Effective area ratio, defined as
  $\dfrac{\text{acoustical port area} \times C_d}{\text{total duct area}}$
k—Ratio of γ values for exhaust gases and air.
l—Distance from projected apex to entrance of diffuser (ft).
m—Mass flow (lb/sec).
$\bar{m}$—Mass (lb).
M—Dimensionless mass flow number.
n—Engine speed (r.p.m.).
P—Pressure (pdls/ft²).
R—Gas constant.
s—Distance from diffuser entrance (ft).
T—Absolute temperature (°C).
t—Time (secs).
U—Dimensionless particle velocity.
u—Particle velocity (ft/sec).
V—Volume (ft³).
$\bar{X}$—Dimensionless pressure ratio, i.e. $\left(\dfrac{P}{P_a}\right)^{\frac{\gamma-1}{2\gamma}}$
x—Dimensionless pressure ratio, i.e. $\dfrac{P}{P_a}$
z—Distance along exhaust duct from engine ports (ft).
a—Engine crank angle (degrees).
γ—Ratio of specific heats $\left(\dfrac{C_p}{C_v}\right)$
Δ—Finite change.
I—Characteristic co-ordinate, rightward wave.
II—Characteristic co-ordinate, leftward wave.
ρ—Density (lb ft³).

Suffixes:
0—Datum state parameter.
1—Cylinder state parameter.
2—Duct state parameter.
os—State parameter referred isentropically to datum isobar.
c—State parameter at cylinder port vena contracta.
a—State parameter of air in the cylinder.
e—State parameter of exhaust gas in the cylinder.

Technical Contributors Section (Continued)

products from the cylinder into the exhaust duct which results in the propagation of a steep fronted pressure wave. The wave, for the plain pipe-diffuser cone arrangement, travels to the junction of the plain pipe with the diffuser cone where it is partially transmitted and partially reflected. The transmitted portion passes along the diffuser and in so doing produces a train of reflected rarefaction pulses which travel towards the cylinder ports in the wake of the initial reflection from the plain pipe-diffuser junction. Final reflection takes place at the open end of the duct and the wave returns along the duct behind the train of reflections preceding it. For the plain pipe exhaust, reflection takes place only at the pipe open end. The arrival of the rarefaction wave at the engine ports produces a depression within the cylinder—kadenacy effect—and thus draws in the fresh charge for the next cycle.

For the solution of the flow problem it is assumed that the flow is one-dimensional and isentropic in nature, enabling the problem to be reduced to that of solving the equations of continuity of mass, momentum and energy for a gas dynamic system. These equations are most conveniently stated in the form:

Mass continuity:

$$u\frac{\partial \rho}{\partial s}+\frac{\partial u}{\partial s}+\frac{\partial \rho}{\partial t}=-\rho\frac{u}{A}\frac{dA}{ds} \quad . \quad . \quad (1)$$

Momentum:

$$u\frac{\partial u}{\partial s}+\frac{\partial u}{\partial t}+\frac{1}{\rho}\frac{\partial P}{\partial s}=0 \quad . \quad . \quad . \quad (2)$$

Energy:

$$u\frac{\partial P}{\partial s}+\frac{\partial P}{\partial t}-\frac{\gamma P}{\rho}u\frac{\partial \rho}{\partial s}-\frac{\gamma P}{\rho}\frac{\partial \rho}{\partial t}=0 \quad . \quad (3)$$

For a constant section duct, the energy equation becomes redundant and is replaced by the isentropic state relation, namely

$$P/\rho^\gamma=\text{constant}$$

The momentum equation then becomes:

$$\rho\frac{\partial u}{\partial t}+\rho u\frac{\partial u}{\partial x}+\frac{\gamma P}{\rho}\frac{\partial \rho}{\partial x}=0 \quad . \quad . \quad . \quad (4)$$

Hence Equation (4) and the mass continuity equation completely define the fluid flow in a constant section duct.

2.2 Solution of Flow Equations

A rigorous solution of the flow equations, which are termed hyperbolic, is possible only by the use of the method of characteristics which has been fully described elsewhere.[2] The equation resulting from the solution of the above partial differential equations, by the theory of characteristics are:

Physical Characteristics.—

$$\left(\frac{dx}{dt}\right)_{I,II}=u\pm a \quad . \quad . \quad (5)$$

This equation signifies that disturbances are propagated on lines which travel either rightward or leftward with the local acoustic velocity of the fluid.

State Characteristic.—Plain pipe-diffuser arrangement

$$(d\bar{U})_{I,II}=\mp\frac{2}{\gamma-1}(d\bar{X})_{I,II}\mp(\Delta\bar{U}_A)_{I,II} \quad . \quad (6)$$

where

$$(\Delta\bar{U}_A)_{I,II}=\frac{2}{\left(1+\frac{s}{l}\right)}\bar{U}\bar{X}\frac{a_0(dt)_{I,II}}{l}$$

Plain pipe arrangement

$$(d\bar{U})_{I,II}=\mp\frac{2}{\gamma-1}(d\bar{X})_{I,II} \quad . \quad . \quad . \quad (7)$$

This is the equation denoting the change in state and particle velocity along a characteristic in the state plane.

If the pressure wave profile is assumed to be of stepped form, the solution of these two Equations (5) and (6), or (5) and (7), can immediately be resolved into the simultaneous construction of two diagrams, known as position and state diagrams. In the position diagram I and II characteristics are drawn, where the I characteristics represents rightward moving waves and the II characteristics leftward moving waves. These characteristics by analogy with two-dimensional steady supersonic flow, are sometimes termed Mach lines and along such lines changes in position with time of a point in a pressure wave takes place. The state diagram is used to correlate values of $\bar{X}$ and $\bar{U}$ for the regions created by the intersection of I and II characteristics in the position diagram. Each point in the state diagram represents a region in the position diagram and along each characteristic drawn in the state diagram the change of state is defined. The equations used for the construction of the characteristic net are Equations (5) and (6), or Equations (6) and (7), depending on the type of exhaust system considered.

2.3. Solution of the Flow Equations with the Formation of a Shock Wave

The propagation of any wave of finite amplitude is accompanied by a change of wave shape since each wave point on a wave profile has a different velocity of propagation to that of its neighbour. In a region in which the gas is undergoing compression, the wave profile tends to develop into a shock front, whilst in a region in which the gas is expanding, the converse is true. Hence steepening of the wave profile occurs on the leading face of a compression wave and the rear face of a rarefaction wave.

The shape of the wave profiles developed in an engine exhaust system are such that only weak shocks occur, and hence for the purpose of calculation these may be treated as continuous waves. The propagation velocity being computed as the arithmetic mean of the absolute wave speeds upstream and downstream of the shock wave. This assumption ignores the entropy increases across the shock wave.

2.4. Solution of Flow Equations with Supersonic Flow

An interesting situation can arise at the junction of a plain pipe with a diffuser cone when a pressure wave is propagated from the plain pipe into the diffuser. Due to the interaction of successive points on the pressure wave with those resulting from the reflections previously initiated within the diffuser, sonic particle velocities can be encountered at the diffuser entry section. The pipe-diffuser junction represents the physical throat of the diffuser and hence the maximum particle velocity attainable at this section is the local acoustic velocity.

With sonic velocity prevailing at the diffuser junction, supersonic velocities will be encountered within the diffuser and all reflected waves generated therein will travel down the diffuser in the same direction as the incident wave. As the reflected waves from the open end of the diffuser attempt to travel back to the pipe-diffuser junction,

superimposition of these waves will occur near the entry section resulting in the formation of a shock wave.

2.5. Boundary Conditions

It has been shown that the construction of a complete net between the physical boundaries of the cylinder ports and the open end of the exhaust duct requires the repeated applications of Equations (5) and (6), or Equations (5) and (7). Additional information is required to effect a solution for the flow equations at the boundaries of the duct, i.e. at the cylinder ports and the pipe open end. An exact analysis of the flow process must account for the unsteady motion in these end regions, which is, however, extremely difficult, and plausible approximations will be made to simplify the analysis without introducing undue error.

(a) *Cylinder Boundary.—*The assumption of quasi-steady flow across the ports enables a theoretical relationship to be established between the pressure on either side of the cylinder ports, the mass flow through the cylinder ports and the associated particle velocity.

*Outflow from Cylinder.—*The flow equations are as follows:

(i) Cylinder to vena-contracta.
Energy equation:

$$u_c^2=\frac{2}{\gamma-1}(a_1^2-a_c^2)$$

Isentropic state equation:

$$P_c/P_1=\left(\frac{a_c}{a_1}\right)^{\frac{2\gamma}{\gamma-1}}$$

Characteristic gas equation:

$$\rho c=\gamma P_c/a_c^2$$

(ii) Vena-contracta to duct entry section.
Energy equation:

$$u_2^2-u_c^2=\frac{2}{\gamma-1}(a_c^2-a_2^2)$$

Continuity equation:

$$u_c\rho_c A_c=u_2\rho_2 A_2$$

or $u_c\rho_c K=\rho_2 u_2$ on putting $K=A_c/A_2$

Characteristic gas equation:

$$\rho_2=\gamma P_2/a_2^2$$

For subsonic flow at the ports, the momentum equation may be applied to the region between the vena contracta and a plane within the duct at pressure P_2, i.e.

$$P_2-P_c=K\rho_c u_2^2-\rho_2 u_2^2$$

Solving this system of equations gives:

$$\left[\frac{P_2}{P_1}\right]^{\frac{\gamma-1}{2\gamma}}\left[\frac{u_2}{a_1}\right]$$

$$=K\sqrt{\frac{2}{\gamma-1}\left[\left(\frac{P_2}{P_1}\right)^{\frac{1-\gamma}{\gamma}}-1\right]\left[1-\frac{\gamma-1}{2}\left(\frac{u_2}{a_1}\right)^2\right]}$$

$$\quad . \quad . \quad . \quad (8)$$

For sonic flow at the port vena contracta,

$$u_c=a_c$$

Hence

$$\frac{P_2}{P_1}=K\left(\frac{2}{\gamma-1}\right)^{\frac{\gamma+1}{2(\gamma+1)}}\left(\frac{a_1}{u_2}\right)\left[1-\frac{\gamma-1}{2}\left(\frac{u_2}{a_1}\right)^2\right]$$

$$\quad . \quad . \quad . \quad (9)$$

*Inflow to the Cylinder.—*The energy mass continuity and the isentropic state equations applied between the duct and the vena contracta at the cylinder ports yields the system

of equations necessary to describe the inflow process. Whence,

$$\left(\frac{u_2}{a_1}\right)^2 = \frac{\frac{2}{\gamma-1}\left[\left(\frac{P_2}{P_1}\right)^{\frac{\gamma-1}{\gamma}}-1\right]}{\frac{1}{K_2}\left(\frac{P_2}{P_1}\right)^{\frac{2}{\gamma}}-1}$$

. . . . (10)

Mass Flow from the Cylinder.—For the evaluation of the pressure changes occurring within the cylinder, it is convenient to introduce a dimensionless mass flow number, M, defined as:

$$M = \frac{A_2 \rho_2 u_2}{A_2 \rho_1 a_1} = \frac{\rho_2 u_2}{\rho_1 a_1}$$

To determine the mass flow relationships, it is sufficient to consider conditions in the cylinder and duct only.

Energy equation

$$\frac{\gamma}{\gamma-1}\frac{P_1}{\rho_1} = \frac{\gamma}{\gamma-1}\frac{P_2}{\rho_2} + \frac{u_2{}^2}{2}$$

Characteristic gas equation

$$\frac{\gamma P}{\rho} = a^2$$

Whence

$$\frac{P_2}{P_1} = M \frac{1 - \frac{\gamma-1}{2}\left(\frac{u_2}{a_1}\right)^2}{\frac{u_2}{a_1}} \quad . . \quad (11)$$

Mass Flow into the Cylinder.—Applying the same definition for mass flow number and using the isentropic state relationship gives

$$\frac{P_2}{P_1} = \left(\frac{M}{\frac{u_2}{a_1}}\right)^{\gamma} \quad . . . . \quad (12)$$

Equations (8), (9), (10), (11) and (12) are plotted in Figs. 1 and 2 for $\gamma=1\cdot4$ and are typical Boundary Diagrams which define the flow conditions met at the engine ports.

(b) *Variation of Pressure in Cylinder*

Fig. 2—Boundary conditions ($\gamma=1\cdot4$). Flow from pipe into cylinder

during Air Exchange Process.—If heat transfer and chemical energy changes in the working fluid are neglected, the rate of change of pressure in the cylinder may be ascribed to:

(i) Mass transfer through the engine ports.
(ii) Changes in cylinder volume with piston movement.

In the analysis that follows, the index marks ′ and ″ will be used to represent the air zone and the residual gas zone within the cylinder respectively since no mixing of the incoming air with the exhaust residuals is assumed to occur within the cylinder. Then the energy equation for the cylinder contents is:

$$\begin{bmatrix}\text{Loss/sec of internal}\\ \text{energy in cylinder}\end{bmatrix} = \begin{bmatrix}\text{Work/sec done}\\ \text{on pistons}\end{bmatrix}$$
$$+ \begin{bmatrix}\text{energy/sec outflow}\\ \text{from exhaust ports}\end{bmatrix}$$
$$- \begin{bmatrix}\text{energy/sec inflow}\\ \text{through inlet ports}\end{bmatrix}$$

Loss/sec of internal energy =

$$\frac{P_1}{\gamma'-1}\left(\frac{dV'}{dt} + k\frac{dV''}{dt}\right) + \frac{1}{\gamma''-1}(V' + kV'')\frac{dP_1}{dt}$$

where

$$K = \frac{\gamma'-1}{\gamma''-1}$$

Work done/sec on pistons

$$= P_1\frac{dV_1}{dt} \quad \text{where} \quad V_1 = V' + V''$$

Energy/sec inflow

$$= \frac{m_a(a^2)'}{\gamma'-1} \quad \text{since} \quad u' \ll a'$$

Energy/sec outflow

$$= \frac{m_e(a^2)''}{\gamma''-1}$$

Therefore the energy equation becomes:

$$P_1\left[(1-k)\frac{dV'}{dt} + \gamma''k\frac{dV_1}{dt}\right] + \left[(1-k)V' + kV_1\right]$$
$$= m_a(a^2)' - km_e(a^2)''$$

If no mixing is assumed to occur then:

$$\frac{dm'}{dt} = m_a$$

and performing logarithmic differentiation

Fig. 1—Boundary conditions ($\gamma=1\cdot4$). Flow from cylinder into pipe

Technical Contributors Section *(Continued)*

(Left) Fig. 3—Position and state diagrams

(Right) Fig. 4—State and position diagrams
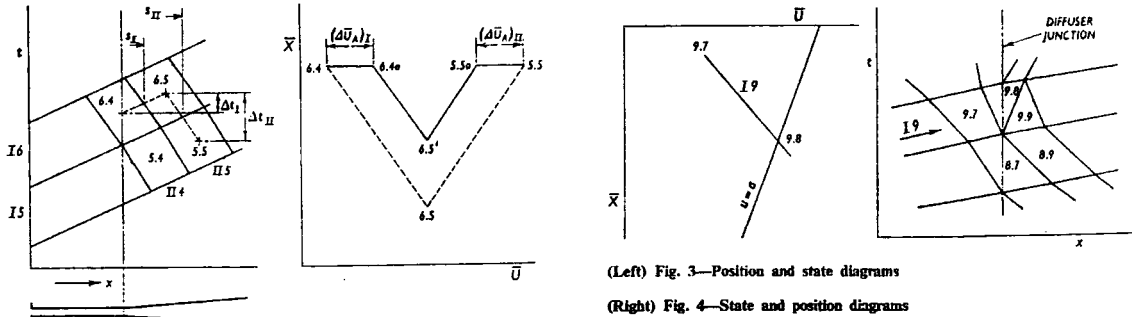
on $PV = \bar{m}RT$ gives:

$$\frac{1}{P_1}\frac{dP_1}{dt} \frac{1}{V'}\frac{dV'}{dt} = \frac{m_a}{\bar{m}'}$$

since T' is assumed constant.

Substituting $d\alpha/dt = 6n$ and $\bar{x} = P_1/P_0$ in the above gives:

$$\frac{dV'}{d\alpha} = \left(\frac{V'}{\bar{m}'}\right)\left(\frac{m_a'}{6_n}\right) - \frac{V'}{\bar{x}}\frac{d\bar{x}}{d\alpha}$$

Substituting this in the energy equation yields on rearrangement:

$$\Delta P_1 = \left(\frac{1}{6ng}\right)\left\{\left[1 - \left(\frac{1-k}{\gamma_a}\right)\right]\frac{m_a}{k} a_a{}^2 - m_e a_e{}^2\right\}\frac{\Delta x}{V_1}$$

$$-\gamma_e P_1\frac{\Delta V_1}{V_1} \quad . \quad . \quad . \quad (13)$$

Applying the principle of logarithmic differentiation to the following equations

$$\left(\frac{P_1}{\rho\gamma}\right)'' = C \text{ and } \frac{P_1}{\rho''} = R''T''$$

gives

$$\left(\frac{\Delta T}{T}\right)'' = \frac{\gamma'' - 1}{\gamma''}\left(\frac{\Delta P}{P}\right)_1 \quad . \quad . \quad (14)$$

$$\left(\frac{\Delta\rho}{\rho}\right)'' = \frac{1}{\gamma''}\left(\frac{\Delta P}{P}\right)_1 \quad . \quad . \quad (15)$$

$$\left(\frac{\Delta a}{a}\right)'' = \frac{\gamma'' - 1}{2\gamma''}\left(\frac{\Delta P}{P}\right)_1 \quad . \quad . \quad (16)$$

Equations (13), (14), (15), and (16) completely define the changes occurring in the state parameters of the cylinder gas contents for a given change of mass inflow and outflow and change in crank angle $\Delta\alpha$.

(c) Boundary Condition at Open End of Duct Outflow.—In the problem considered, only subsonic flow can occur, and neglecting the inertia of the fluid outside the duct exit the state of the gas at the plane of the open end can be assumed to be that of the surroundings. Hence, for subsonic particle velocities in the duct, the instantaneous pressure ratio can be taken as $(P_2/P_0) = 1$, and the state of the gas at this plane can be represented by a horizontal line drawn through the origin of the state diagram.

This means that the boundary conditions at the duct open end can be directly superimposed upon the state diagram, instead of being separately considered on a boundary diagram as is the case at the cylinder ports.

Inflow.—Unlike the case of outflow, the pressure at the plane of the open end is no longer atmospheric but must satisfy the theoretical relationship of the configuration for a Borda mouthpiece. With the assumption of quasi-steady adiabatic flow from the reservoir to the duct inlet plane, the following flow equations hold:

Energy equation

$$\gamma P_2/\rho_2 = a_0{}^2\left[1 - \frac{\gamma - 1}{2}\left(\frac{u_2}{a_0}\right)^2\right]$$

Momentum equation

$$\gamma P_2/\rho_2 = \frac{\gamma u_2{}^2}{(P_0/P_2 - 1)}$$

Solving the above equations and rearranging gives:

$$P_0/P_2 = \frac{\gamma\left(\frac{u_2}{a_0}\right)^2}{1 - \frac{\gamma - 1}{2}\left(\frac{u_2}{a_0}\right)^2} + 1 \quad . \quad . \quad (17)$$

COMPOSITE STATE DIAGRAM.

BOUNDARY DIAGRAM.

POSITION DIAGRAM.

Fig. 5
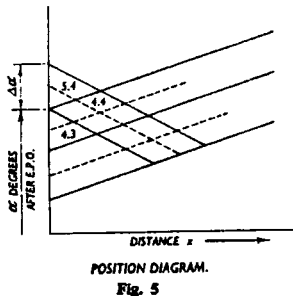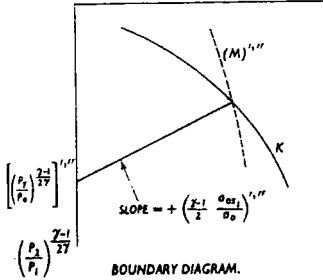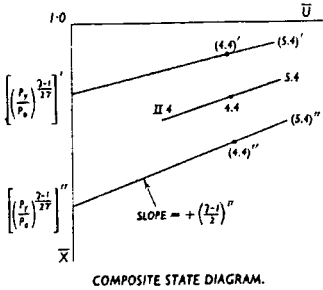
All state points at the duct inlet must lie on the curve defined by Equation (17) which approaches the origin of the diagram as the ratio (P_0/P_2) tends to unity.

Since the flow is not determined by the assumption of subsonic or sonic velocities at the *vena contracta*, then the boundary conditions defined by Equation (17) are valid for both subsonic and sonic flows.

3. Application of Theory
3.1. APPLICATION OF CHARACTERISTICS TO PLAIN PIPE-DIFFUSER ARRANGEMENT

The basic steps in the construction of the nets in both the physical and the state planes are given below.

Given that the state parameters of regions 6.4 and 5.5 (see Fig. 3) are known and that those of region 6.5 are required to be found, the method of solution is as follows:

(i) A first approximation to point 6.5 in
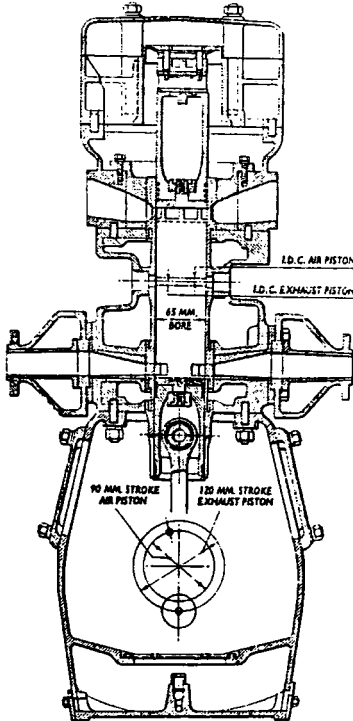
Fig. 6—Sectional arrangement of engine
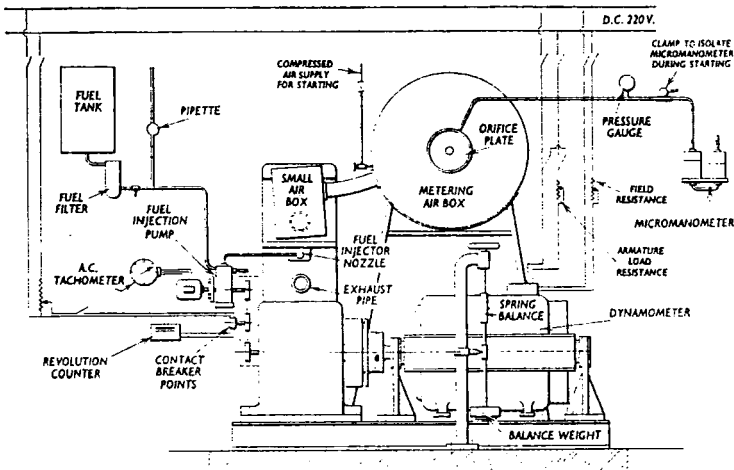
Fig. 7

the state plane is found by ignoring the second term $(\Delta \bar{U}_A)_{I, II}$ in Equation (6). It is then only necessary to find the intersection of the lines passing through the state points 6.4 and 5.5 with the slopes $\mp(\gamma-1/2)_{I, II}$ respectively.

(ii) Using the mean values of u and a in Equation (5) between 6.4 and 6.5, 5.5 and 6.5, and the approximate values of u and a for the field 6.5, the approximate field boundaries to region 6.5 can be drawn in the position diagram. This establishes a first approximation to the field 6.5 in the physical plane and yields tentative values of $(\Delta t)_{I, II}$ and $(s)_{I, II}$.

(iii) The value of $(\Delta \bar{U}_A)_I$ is calculated in which the values of $(\Delta t)_I$ and $(\Delta s)_I$ is taken at the mean conditions between fields 6.4 and 6.5. The numerical value of $(\Delta \bar{U}_A)_I$ is then laid off horizontally from state point 6.4 giving state point 6.4(a). Similarly $(\Delta \bar{U}_A)_{II}$ is calculated and laid off horizontally from state point 5.5, thus yielding state point 5.5(a).

The I, II characteristics with slopes $\mp(\gamma-1/2)_{I, II}$ are then drawn through state points 6.4(a) and 5.5(a) respectively. Their intersection at state point 6.5 gives a second and better approximation to the true state 6.5.

(iv) Using the mean values of u and a between 6.4 and 6.5', and between 5.5 and 6.5', and the values of u and a for 6.5', the field boundaries in the physical plane can be corrected.

(v) The procedure outlined in paragraphs (iii) and (iv) above is repeated until satisfactory convergence of the values $\bar{U}$ and $\bar{X}$ is obtained for the state point 6.5.

3.2 Application of Characteristics For Regions with Sonic Flow

As an example of the application of characteristics for a region with sonic flow, consider a rightward moving wave entering the diffuser junction and encountering sonic flow conditions.

For the rightward moving wave I 9 encountering sonic flow at the diffuser entry section, region 9.8, the state and position diagrams will be as in Fig. 4.

The state point 9.8 must lie on the I 9 characteristic passing through the state point 9.7. Also, since the region 9.8 is situated at the diffuser entry section, the intersection of this I 9 characteristic and the

"sonic line" drawn in the state diagram according to the law $u=a$, fully defines the state 9.8.

The procedure to obtain region 9.9 knowing region 9.8 and 8.9 is identical to that outlined in Section 3.1. The slope of the boundary separating regions 9.8 and 9.9 in the position diagram, see Fig. 4, is evaluated

in the normal manner using Equation (5), i.e.

$$\left(\frac{dx}{dt}\right)_{II} = a - u$$

where u and a are the mean values between region 9.8 and 9.9.

Hence the solution of the flow equations for a region in which the flow is sonic, such as region 9.8, is made possible by the use of one additional law, i.e. the particle velocity equals the local acoustic velocity.

3.3 Application of the Boundary Diagrams

To allow for the variation of the specific heats with temperature, for the residuals of combustion in the cylinder, requires the solution of the boundary equations for the mean value of γ for the cylinder step under consideration. This method is impracticable and the approach adopted is to draw inflow and outflow boundary diagrams for two values of γ ($\gamma=1\cdot3$ and $\gamma=1\cdot4$) and obtain from these, by linear interpolation, the value of mass flow number M, dimensionless pressure ratio $\bar{X}$ and dimensionless particle velocity $\bar{U}$ for the appropriate γ value for the step.

The application of this method makes it necessary to produce two imaginary state diagrams at the exhaust ports, drawn in this case for the values of $\gamma=1\cdot3$ and $\gamma=1\cdot4$, and perform two complete sets of calculations for each cylinder step considered. The

Fig. 8—Position diagram, Isentropic flow
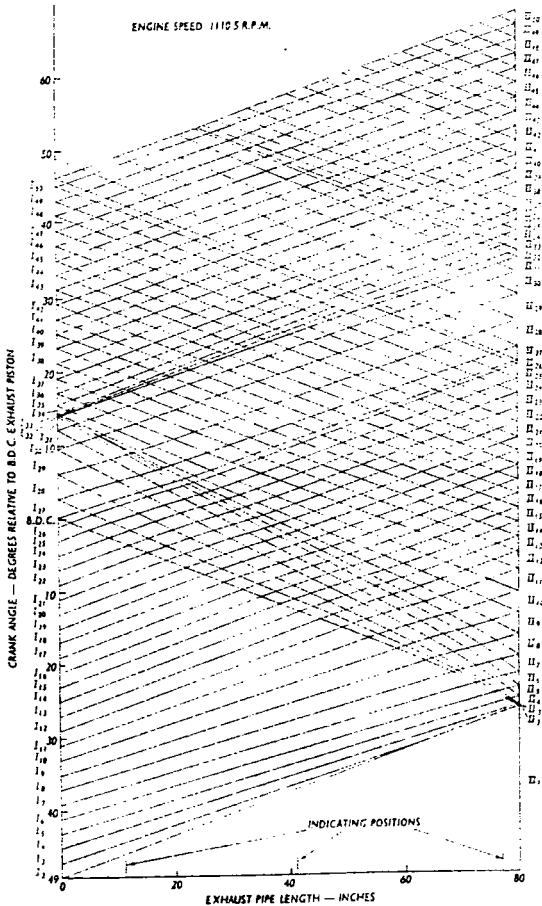
Technical Contributors Section *(Continued)*

actual state change occurring within the exhaust duct for the step is then inferred from these results for the appropriate value of γ existing in the duct.

For inflow at the air ports, however, it is assumed that the entering air is at the ambient condition, γ is constant and equal to $1\cdot4$ and the mass flow number M_a can, without interpolation be determined directly from the boundary diagram plotted for $\gamma = 1\cdot4$.

To illustrate the method of solution, the two boundary diagram values of γ and the associated parameters will be denoted by the index marks ' and " for $\gamma = 1\cdot3$ and $\gamma = 1\cdot4$ respectively. Further, in the explanation that follows, all remarks where applicable, although in the singular, apply to both cases.

As an example, consider the state point 5.4 corresponding to the region commencing at γ degrees after exhaust port opening, see the position diagram Fig. 5. The initial values of the state parameters for this step are given by those at the end of the step immediately preceding it, i.e. state 4.3, and the initial value of C_d found by use of this data. The mean value of the enlargement ratio K can now be determined for the step.

With the approximate value of K found, the approximate state 5.4 can be positioned on the boundary diagram by satisfying the following conditions:

(i) The state point 5.4 must lie on the K line for the step in the outflow diagram.

(ii) The state point 5.4 must lie on the II characteristic drawn through the state point 4.4.

To obtain a first approximation to the value of 5.4 the last known state 4.4 is transferred from the state diagram to the

boundary diagram. This entails the movement of a line between two different sets of co-ordinates, namely

$$\left[\left(\frac{P_2}{P_0}\right)^{\frac{\gamma-1}{2}}\right]^{\prime,\ ''}$$

and

$$(u_2/a_0)^{\prime,\ ''}$$

to

$$\left[\left(\frac{P_2}{P_1}\right)^{\frac{\gamma-1}{2\gamma}}\right]^{\prime,\ ''}$$

and

$$(u_2/a_1)^{\prime,\ ''}$$

and is achieved as follows:

From Equation (7) namely

$$[(\Delta\bar{U})_{II}]^{\prime,\ ''} = \left[-\frac{2}{\gamma-1}(\Delta\bar{X})_{II}\right]^{\prime,\ ''}$$

it can be seen that the slope of the characteristic relating $\bar{X}$ and $\bar{U}$ in the state diagram is:

$$\left[-\frac{\gamma-1}{2}\right]^{\prime,\ ''}$$

Changing the co-ordinate axes from

$$\left(\frac{P_2}{P_0}\right)^{\frac{\gamma-1}{2\gamma}} \text{ and } \left(\frac{u_2}{a_0}\right)$$

to

$$\left(\frac{P_2}{P_1}\right)^{\frac{\gamma-1}{2\gamma}} \text{ and } \left(\frac{u_2}{a_1}\right)$$

in order to transfer the state 4.4 to the boundary diagram, it is a necessary assumption that over the given time interval Δt the cylinder parameters P_1 and a_1 remain constant and equal to the mean value for the region 5.4.

Hence Equation (7) becomes:

$$\left[\left(\frac{P_1}{P_0}\right)^{\frac{\gamma-1}{2\gamma}}\Delta\left(\frac{P_2}{P_1}\right)^{\frac{\gamma-1}{2\gamma}}\right]^{\prime,\ ''} = \left[-\frac{\gamma-1}{2}\frac{a_1}{a_0}\Delta\left(\frac{u_2}{a_1}\right)\right]^{\prime,\ ''}$$

$$\text{. . . (18)}$$

Since isentropic expansion of the cylinder gases is assumed to occur, then:

$$\frac{a_1}{a_{0\,1}} = \left(\frac{P_1}{P_0}\right)^{\frac{\gamma-1}{2\gamma}}$$

Whence Equation (18) reduces to:

$$\left[\Delta\left(\frac{P_2}{P_1}\right)^{\frac{\gamma-1}{2}}\right]^{\prime,\ ''} = \left[-\frac{\gamma-1}{2}\frac{a_{0\,1}}{a_0}\Delta\left(\frac{u_2}{a_1}\right)\right]^{\prime,\ ''}$$

$$\text{. . . . (19)}$$

Therefore, from Equation (19), the slope of the characteristic relating

$$\left[\left(\frac{P_2}{P_1}\right)^{\frac{\gamma-1}{2\gamma}}\right]^{\prime,\ ''} \text{ and } \left(\frac{u_2}{a_1}\right)^{\prime,\ ''}$$

in the boundary diagram is

$$\left[-\frac{\gamma-1}{2}\frac{a_{0\,1}}{a_0}\right]^{\prime,\ ''}$$

The intercept of this characteristic with the ordinate axis in the boundary diagram is given by

$$\left[\left(\frac{P_{\prime}}{P_1}\right)^{\frac{\gamma-1}{2\gamma}}\right]^{\prime,\ ''} = \left[\left(\frac{P_{\prime}}{P_0}\right)^{\frac{\gamma-1}{2\gamma}}\left(\frac{P_0}{P_1}\right)^{\frac{\gamma-1}{2\gamma}}\right]^{\prime,\ ''}$$

$$\text{. . . . (20)}$$

where

$$\left[\left(\frac{P_{\prime}}{P_1}\right)^{\frac{\gamma-1}{2\gamma}}\right]^{\prime,\ ''}$$

denotes the intercept of the characteristic, slope

$$\left[-\frac{\gamma-1}{2}\right]^{\prime,\ ''}$$

Fig. 9—State diagram, isentropic flow

EXHAUST PIPE LENGTH 6'- 8"
ENGINE SPEED 1110.5 R.P.M.
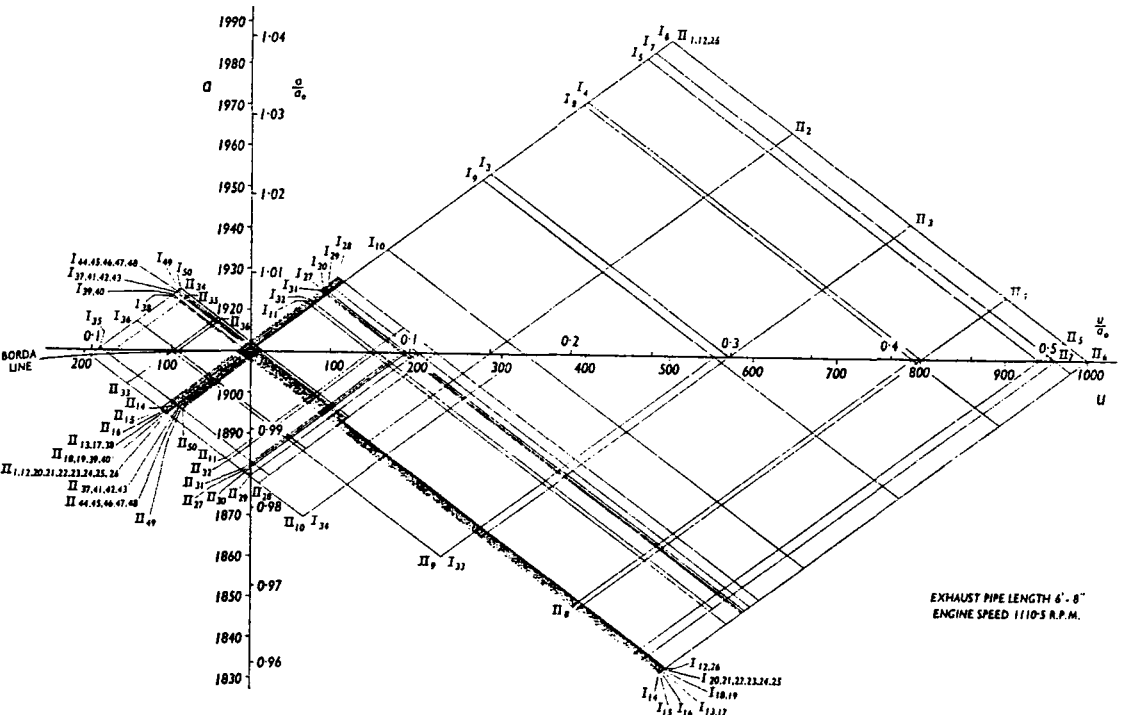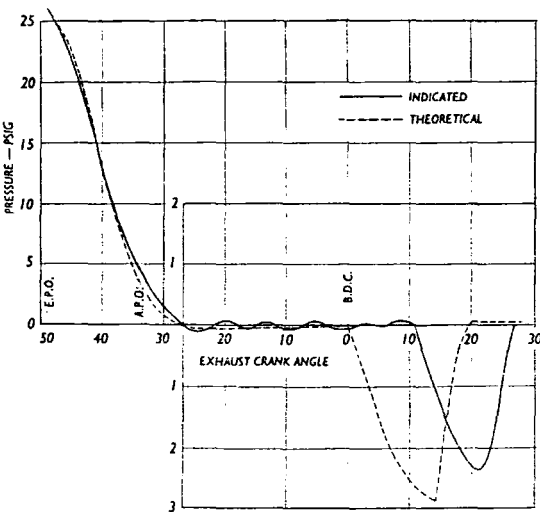
Fig. 10—Cylinder pressure

drawn through the state point (4.4)$'$ $''$ with the ordinate axis in the state diagram. The value of P_1 in Equation (2) for the first approximation must necessarily denote the initial step condition in the cylinder.

Hence the characteristic on which the state point (5.4)$'$ $''$ lies is, to the first approximation, completely defined in the boundary diagram. The intersection of this characteristic with the appropriate K line for the step gives the required values of the cylinder-to-duct pressure ratio

$$\left[\left(\frac{P_2}{P_1}\right)^{\frac{\gamma-1}{2\gamma}}\right]' {}''$$

the exhaust mass flow number $M.'$ $''$, and the dimensionless particle velocity $(u_2/a_1)'$ $''$.

Assuming that region 5.4 falls within the scavenge period, the air mass flow, into or out of the cylinder, must be determined before ΔP_1 can be evaluated. Since the air entering is assumed to be at ambient conditions, γ is constant, and the mass flow number can be determined directly from the boundary chart drawn for $\gamma=1\cdot4$, the value used for air.

The induction duct length is very short and hence the induction system is assumed to be a neutral one, i.e. one in which wave action can be neglected. Thus at the inlet ports the inflow number M_a is found by plotting on the inflow chart the steady flow isentropic ellipse relationship namely:

$$\frac{\left(\frac{u_2}{a_1}\right)^2}{\frac{2}{\gamma-1}\left(\frac{a_a}{a_1}\right)^2}+\frac{\left[\left(\frac{P_2}{P_1}\right)^{\frac{\gamma-1}{2\gamma}}\right]^2}{\left[\left(\frac{P_2}{P_1}\right)^{\frac{\gamma-1}{2\gamma}}\right]^2}=1 \quad . \quad (21)$$

where a_a is the ambient local acoustic velocity. This relationship is derived from the assumption that there is no loss in total head pressure between the surroundings and the boundary of the inlet ports.

The intersection of the characteristic given by Equation (21) with the appropriate K line for the air ports gives the required inflow number M_a for the step.

The incremental change in the cylinder pressure ΔP_1 for the step can now be determined from Equation (13) namely:

$$\Delta P_1=\left(\frac{1}{6nkg}\right)\left\{\left[1-\left(\frac{1-k}{1\cdot4}\right)\right]m_a a_a{}^2-km_e a_e{}^2\right\}\frac{\Delta x}{V_1}$$
$$-\gamma_e P_1\frac{\Delta V_1}{V_1}$$

where V_1 and ΔV_1 are the appropriate mean

values for the step, and Δx is the appropriate change in crank value found by extending the field boundaries of region 4.4 in the position diagram.

The rate of mass flow into and out of the cylinder, the change in cylinder gas acoustic velocity, density and temperature are calculated from the following equations:

$$\frac{\Delta m_a}{\Delta t}=M_a z_a u_a.A_a \qquad \text{(air flow)}$$

$$\frac{\Delta m_e}{\Delta t}=M_e z_e a_e.A_e \qquad \text{(exhaust gas flow)}$$

Fig. 11—Pressure in exhaust pipe

where A_a and A_e are the areas of the air and exhaust ducts respectively

$$\left(\frac{\Delta T}{T}\right)_e=\left(\frac{\gamma-1}{\gamma}\right)_e\left(\frac{\Delta P}{P}\right)_1 \qquad \ldots \quad (14)$$

$$\left(\frac{\Delta\rho}{\rho}\right)_e=\frac{1}{\gamma_e}\left(\frac{\Delta P}{P}\right)_1 \qquad \ldots \quad (15)$$

$$\left(\frac{\Delta a}{a}\right)_e=\left(\frac{\gamma-1}{2\gamma}\right)_e\left(\frac{\Delta P}{P}\right)_1 \qquad \ldots \quad (16)$$

Application of the following identities,

$$\left[\left(\frac{P_2}{P_0}\right)^{\frac{\gamma-1}{2\gamma}}\right]' {}''=\left[\left(\frac{P_2}{P_1}\right)^{\frac{\gamma-1}{2\gamma}}\left(\frac{P_1}{P_0}\right)^{\frac{\gamma-1}{2\gamma}}\right]' {}''$$

and

$$\left(\frac{u_2}{a_0}\right)' {}''=\left[\left(\frac{u_2}{a_1}\right)\left(\frac{a_1}{a_0}\right)\right]' {}''$$

gives the pressure ratio and particle velocity at the port boundary within the duct. From this data the approximate wave paths can be constructed in the position diagram using Equation (5), i.e. $(dx/dt)_I$, $_{II}=u\pm a$.

Having approximately positioned the field boundaries of region 5.4, a nearer approximation to Δx for the step can be measured. Using this nearer approximation to Δx and the calculated approximate mean values of the cylinder parameters for the step, the above procedure is repeated until satisfactory convergence to the value of ΔP_1, is obtained.

4. Determination of Actual System Parameters

4.1 CYLINDRICAL AND DUCT PARAMETERS

A theoretical analysis for the changes occurring within the cylinder gases requires a knowledge of the variation with crank angle of the following physical parameters.

(1) Cylinder volume.
(2) Ratio of port area to duct area for

Technical Contributors Section *(Continued)*

INDICATING STATIONS
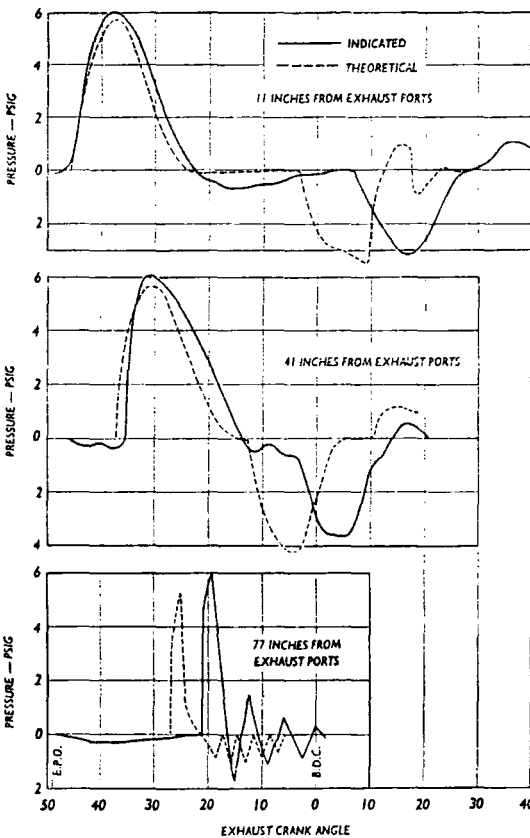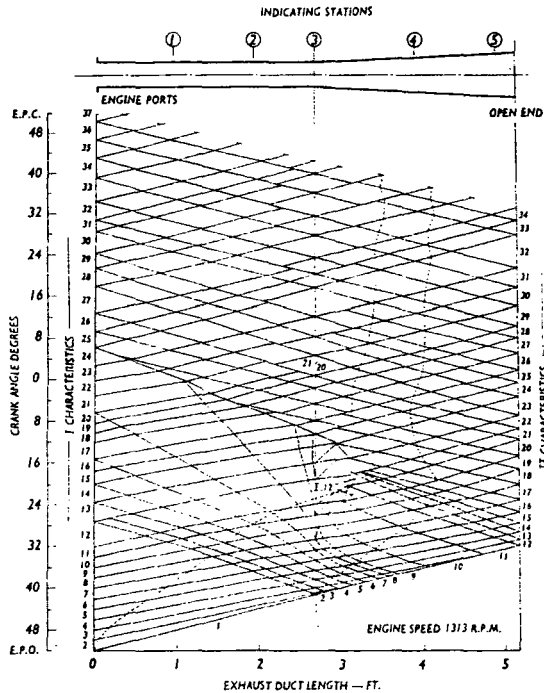
Fig. 12—Position diagram, isentropic flow

both inlet and exhaust ports. This data is calculated from the engine geometry and should be plotted for ease of reference.

In addition to this, it is necessary to know the variation in the coefficient of discharge (C_d) for the cylinder ports. This is normally known as a function of pressure ratio and Reynold's Number, and to determine the latter, the absolute viscosity of the gas flowing through the ports is required.

4.2. EXHAUST GAS PARAMETERS

To evaluate the fluid properties, namely R, C_p and γ for the range of gas temperatures encountered in an actual firing engine, an analysis of the exhaust gases is necessary.

Variation in the Specific Heats.—The values of the specific heats at constant pressure and constant volume for the exhaust gas constituents are taken from gas tables[3] for the required temperature range and the mass mean values for the specific heats are calculated using the mean exhaust gas analysis.

Variation in Absolute Viscosity.—The mass mean value for viscosity is evaluated from the values for the exhaust gas constituents for a range of temperatures. The assumption of mass mean value for viscosity, however, is not strictly correct, but in view of the smallness of the error, a full analysis of the problem is not justified.

5. Procedure and Results
5.1. PROCEDURE

To determine the validity of the theory developed for the solution of the flow problem encountered in a firing engine, the conditions existing in an actual engine system were studied and analysed. The engine used in the investigation is fully described in an earlier report.[1] It operates on a two-stroke

cycle and utilises the energy in the exhaust pressure pulses to effect scavenge. For reference, the cross-sectional arrangement of the engine and general layout of the apparatus

is shown in Figs. 6 and 7 respectively.

The engine was operated with a constant air-fuel ratio and engine cooling water outlet temperature, and a plain pipe and a plain pipe-diffuser exhaust systems were used, together with a neutral induction system.

Indicator diagrams were taken in the engine cylinder and at a number of stations along the exhaust duct, and the air mass flow was measured by means of an air box fitted with an orifice plate.

5.2. RESULTS

The two exhaust arrangements investigated for comparison with the theoretical results were:

(a) A simple plain exhaust pipe of length 6ft 8in. (See Figs. 8, 9, 10 and 11.)

(b) A simple plain exhaust pipe of length 2ft 7in terminating in a conical diffuser of length 2ft 6in and a cone angle of 6°. (See Figs. 12, 13, 14, 15 and 16.)

In each case the engine speed was chosen such that the scavenge was effected by the first reflection of the blowdown pulse to avoid over-complication of the pressure wave pattern in the exhaust duct.

6. Discussion of Results
6.1. THEORETICAL EQUATIONS

In the development of the theoretical equations for the unsteady flow encountered in an engine exhaust system, a number of simplifying assumptions were made. The most important of these is that the flow is geometrically one-dimensional, implying, that all fluid properties are uniform over each cross-section of the exhaust duct. For the plain pipe, the fluctuating nature of the gas movement precludes the establishment of a fully developed velocity profile and hence
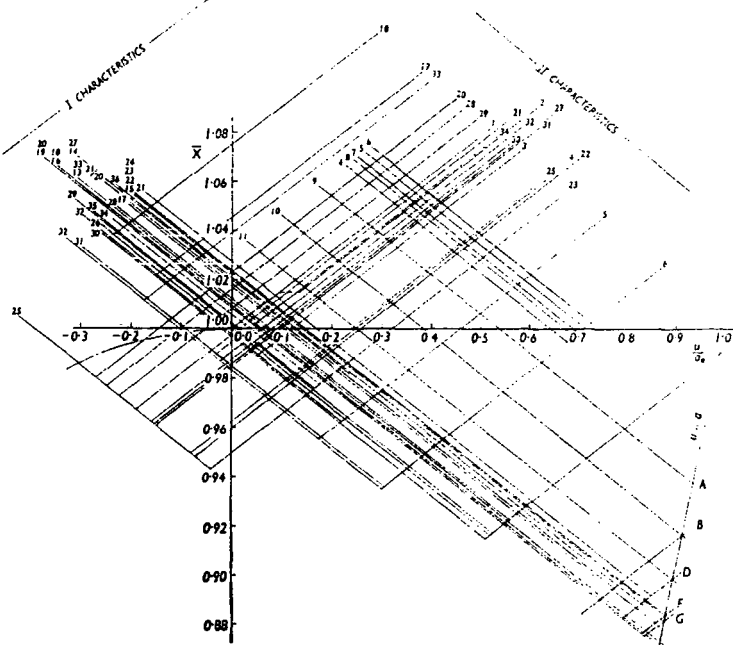
Fig. 13—State diagram, isentropic flow
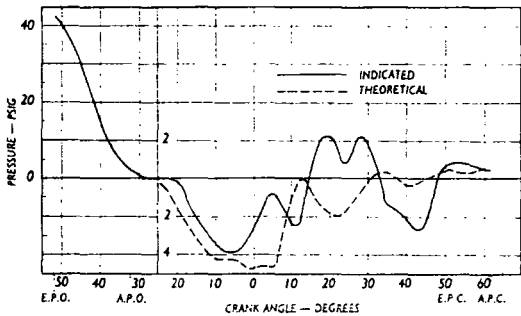
Fig. 14—Cylinder pressure diagram

(Right) Fig. 15—Pressure diagrams
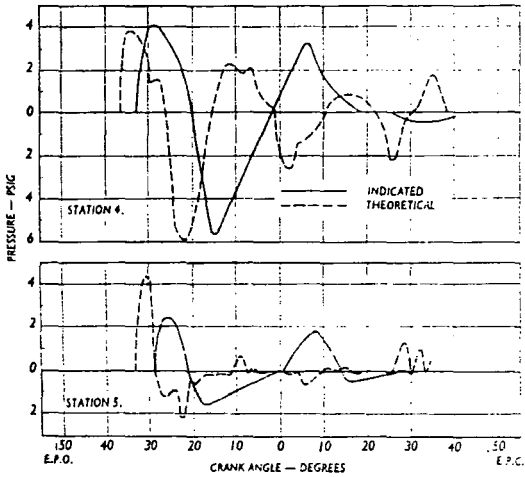
the assumption was considered reasonable. For the diffuser the assumption was also considered reasonable since the rate of change of cross-sectional area with distance is small for a divergence angle of 6°.

6.2. THEORETICAL INDICATOR DIAGRAMS

The cylinder pressure traces for the blowdown period, see Figs. 10 and 14, show very good agreement with the measured trace and this justifies the assumption of quasi-steady flow through the engine ports and isentropic conditions existing in the engine cylinder. The timing and amplitude of the depression produced in the cylinder during the scavenge period show very poor correlation. This considerably affects the scavenge process and results in considerable error in the air mass flow breathed by the engine per cycle, see Table I.

TABLE I

	Volumetric efficiency %	
	Exhaust system (a)	Exhaust system (b)
Theoretical	60·8	186·6
Actual	53·4	76·4

As a result of the assumption of isentropic flow in the exhaust duct, the secondary effects of heat transfer and wall friction are neglected. These effects on the gas flow are additive for pressure and opposing in their effect upon temperature. The former produces wave attenuation, but with regard to the latter, heat transfer is very predominant, the resulting decrease in gas temperature appreciably affecting the propagation velocity and hence wave timing. The error in the timing of the primary pulse created by blowdown resulting from the neglecting of these secondary effects is clearly shown for the longer plain exhaust pipe, whereas for the shorter pipe in the plain pipe-diffuser system, better agreement is obtained, see Figs. 11, 15, and 16.

Examination of the pipe indicator diagrams shows that for the plain pipe system, the actual peak pressure for the primary wave is greater than the theoretical, which contradicts the above statement regarding the effects of heat transfer and friction. In this case, however, a major temperature discontinuity will exist in the pipe at the interface between two successive cylinder discharges. This will give a partial closed end reflection which is superimposed on the primary pulse, resulting in an increase in peak pressure amplitude. This phenomenon is not seen in Fig. 16 for the plain pipe-diffuser arrangement since the reflection from the diffuser throat will be superimposed on the reflections from the temperature discontinuity, the net result being a

decrease in peak pressure amplitude. The shape of the theoretical rarefaction pulse for the plain pipe-diffuser system is markedly different from the actual pulse. This wide departure results from the theoretical establishment of sonic velocity at the diffuser throat which prevents the passage of wave fronts upstream of this region and gives rise to the formation of a shock wave behind the rarefaction wave. In the actual process, the shock will be either extremely weak or completely suppressed as a result of the effects of heat transfer and friction and hence the succeeding exhaust pipe wave pattern is completely distorted. This accounts for the complete lack of correlation after the theoretical establishment of sonic velocities. For the case of the plain pipe exhaust system, the theoretical analysis does not produce a shock condition and hence

Fig. 16—Pressure diagrams

the wave profile correlation is reasonable.

The above argument suggests that this simplified solution of a real system may be used with reasonable confidence providing that insipient shock fronts are not created within the system as the result of duct area change and that the timing can be arbitrarily corrected by introducing an artificial temperature gradient permanently residing at the engine ports. The use of a lower temperature for the gases in the exhaust duct will reduce the propagation velocity and hence the mismatch between the theoretical and actual wave phasing.

7. Conclusions

(1) True application of the theory does not give a good solution of the wave pattern and gas flow in an actual engine system. Caution should, therefore be exercised in the use of the simplified theory.

(2) The application of the isentropic finite amplitude wave theory to the exhaust system of a firing engine will only show promise providing high Mach number flow conditions are not created by the system configuration.

(3) Application of the simplified theory and empirical correction of the propagation velocity should yield a solution which will give a reasonable indication of the actual system performance.

(4) Simulation of an engine system, which of necessity lacks the secondary influences of temperature discontinuities, heat transfer and wall friction, will in most cases give erroneous solutions to the flow in a real engine system. Extreme caution should, therefore, be exercised in drawing general conclusions regarding the performance of a real engine system from the results of this type of work.

(5) The assumption of quasi-steady flow across the cylinder ports, which enables a theoretical relationship to be established between the pressure on either side of the cylinder ports, is justified and permissible.

(6) Greater accuracy in the prediction of the mass flow from the cylinder is possible by making allowance for the specific heat variation within the cylinder, and the boundary chart interpolation technique developed to account for this is adequate.

REFERENCES
[1] Wright, E. H., and Gill, K. F., "Influence of Simple Exhaust and Induction Systems on the Air Consumption of a Firing Naturally Aspirated Two-Stroke Oil Engine. Research Report No. 31, Mech. Eng. Dept., University of Birmingham. 1963.
[2] Bannister, F. K., and Mucklow, G. F., "Wave Action Following Sudden Release of Compressed Gas from a Cylinder", Proc. I. Mech. E. Vol. 159. page 269. 1948.
[3] Keenan, J. H., and Kaye, J., Gas Tables, J. Wiley and Sons Inc., N.Y. 1948.
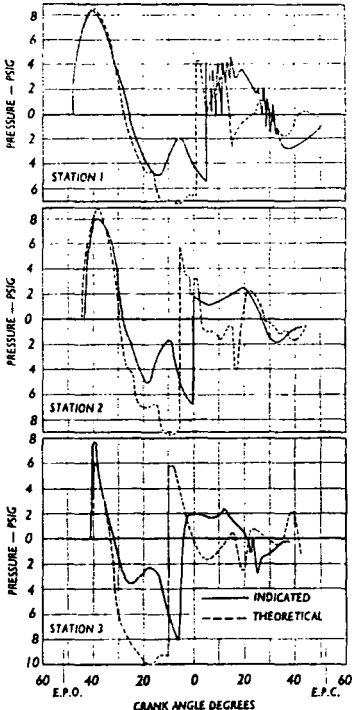
PAPER 6

THEORETICAL ANALYSIS OF THE UNSTEADY GAS FLOW IN THE EXHAUST SYSTEM OF AN ENGINE

By E. H. Wright* and K. F. Gill*

The problem studied is that of unsteady gas motion in ducts of both constant and slowly varying cross-sectional area with the effects of wall friction and heat transfer taken into account. The values of the specific heats used in the analysis are those applicable to the instantaneous gas temperature at the instant under consideration, i.e. thermal lags are ignored.

To solve the unsteady flow equations, a method is developed based on the theory of characteristics and in the application of this method a pure graphical approach is used for convenience. The plotting technique adopted is the 'field method of solution' in which it is assumed that a region of continually varying fluid properties can be broken into a large number of small regions for calculation purposes. The fluid properties are assumed uniform throughout each of these small regions and changes in the fluid properties can only occur across the boundaries or characteristics separating the small regions.

With a firing engine, temperature discontinuities will be established at the interface of the hot gases being discharged from the cylinder and the cooler residuals from the previous cycle. Owing to the interaction of successive points of the fundamental pressure pulse with those resulting from the reflection of previous points of the fundamental pulse, sonic velocities can be encountered at the diffuser entry section. The formation of a steep front at the diffuser entry section as a result of these rarefaction waves can produce a shock wave. A method of solution for the existence in the flow of such discontinuities as temperature and shock is included.

The general conclusions to be drawn are: (1) true application of the irreversible flow theory gives a good solution of the wave patterns occurring in both the cylinder and exhaust pipe of the engine; (2) the air mass flow can be predicted with good accuracy by application of the irreversible flow theory developed; (3) the poor correlation resulting from application of the isentropic flow theory shows caution should be exercised in the use of this simplified theory.

INTRODUCTION

ANY SUPERIORITY of the two-stroke cycle engine over its four-stoke counterpart of equal swept volume depends upon the efficiency of the air exchange process in the cylinder. In a high-speed engine, the time available for scavenging the cylinder is very small and hence to gain any measure of success, the scavenge air must be supplied under pressure. This is possible by using either crankcase compression or an air compressor, with the consequent absorption of power, reduction in power/weight ratio and increased running and capital costs.

The pressure pulsations created in the exhaust system by the cylinder blowdown process contain sufficient energy to effect the scavenge process. One method of utilizing

this energy is to use an exhaust-gas-driven turbine driving an air compressor to provide the scavenge air and by suitable design this arrangement can increase the b.m.e.p. rating and thus the power/weight ratio.

Scavenge can also be achieved by using a suitably designed exhaust system which directly affects scavenge by creating a sub-atmospheric pressure in the engine cylinder. Many researchers have published results of investigations into the utilization of exhaust pressure pulses for scavenging, but in almost every case the work has been performed using either a simulated engine system (1)† or an actual engine motored and fed with compressed air to simulate the actual operating pressures (2). General conclusions with regard to the scavenging potential of simple exhaust systems have been drawn from the simulated work, but investigations carried out with a firing engine by the authors have shown that certain of these

† References are given in Appendix 3.
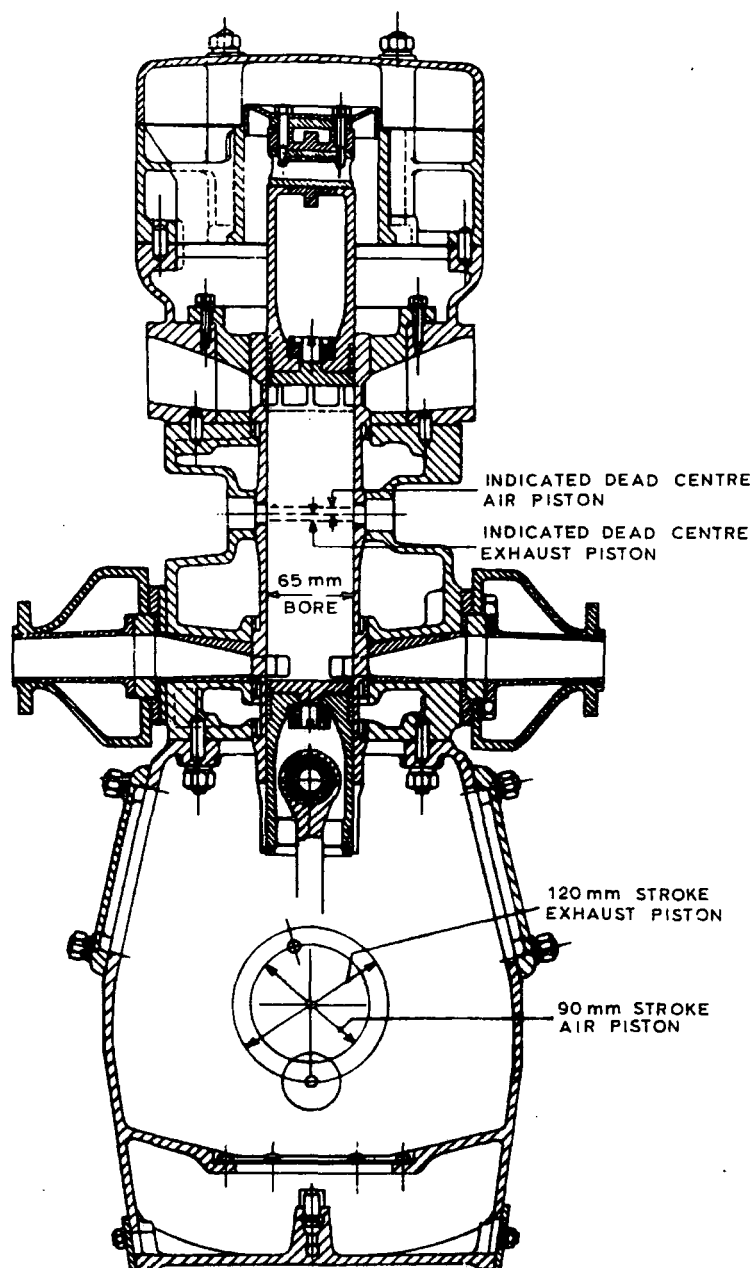
Fig. 1. *Sectional arrangement of engine*

conclusions are not valid (3) (4). In the opinion of the authors the only method of estimating the air flow which may be expected as a result of wave action in an engine exhaust system, is to perform a theoretical analysis for the system under consideration.

The work presented in this paper is the outcome of such a theoretical investigation and the theoretical results are compared with the actual measured values of air mass flow and pressure pulsations produced in a simple exhaust system of a firing oil engine.

In an effort to achieve economic and practical engineering solutions, other workers have developed digital computer programmes to analyse similar and other systems (5) (6).

APPARATUS

The engine used in the investigation was an unblown, two-stroke opposed piston oil engine and a cross-sectional arrangement of the unit is shown in Fig. 1. The original exhaust system incorporated exhaust ejectors designed to Kadenacy specification, which, for the present research, were rendered inoperative by the insertion of short lengths of pipe. Directly coupled to the engine unit was a swinging field electric dynamometer.

Auxiliary shafts, chain-driven from the engine crankshaft, provided the drives for the fuel injection pump, a revolution counter and a three phase a.c. tachometer.

For continuous engine running the fuel injection pump was gravity-fed directly from the fuel tank and for accurate fuel measurement the fuel supply was taken from calibrated pipettes. A micrometer attachment on the injection pump rack provided control for the pump delivery flow.

The exhaust systems discharged into collector tanks which were vented to atmosphere through the laboratory exhaust extraction system.

Bulk exhaust gas temperature was measured by iron-constantan thermocouples positioned at chosen intervals along the duct length.

Both exhaust ducts consisted of a section of solid drawn $1\frac{3}{4}$-in bore commercially smooth plain pipe to which a conical diffuser assembly could be attached. The construction of each duct was such that the plain pipe could be varied in length by increments of 6 in up to a maximum length of 11 ft. The diffuser assembly, which had a divergence angle of 6°, could also be varied in length by increments of 6 in from 1 ft to 3 ft 6 in.

The air circuit consisted of a large fabricated steel air box connected by two flexible rubber tubes of 3-in bore to two smaller air boxes. These latter air boxes could either be attached directly to the engine ports to give a neutral induction system, or to the upstream end of the induction ducts when these were fitted. A metering orifice mounted in one end of the large air box provided the means of determining the rate of air flow.

THEORY

Notation

A Cross-sectional area, ft².
A_w Wall area, ft².
a ˙Acoustic velocity, ft/s.
C_d Coefficient of discharge.
C_p Specific heat at constant pressure, ft/pdl/lb degC.
C_v Specific heat at constant volume, ft/pdl/lb degC.
D Hydraulic diameter, ft.
d Duct diameter, ft.

F Wall friction term, pdl/lb.
f Coefficient of friction.
h Heat transfer coefficient, ft pdl/ft² s degC.
K Effective area ratio, defined as
$$\frac{\text{geometrical port area}}{\text{total duct area}} \times C_d.$$
k Ratio of γ values for exhaust gases and air.
L Total exhaust duct length, ft.
l Distance from projected apex to entrance of diffuser, ft.
M Dimensionless mass flow number.
m Mass flow, lb/s.
$\bar{m}$ Mass, lb.
n Engine speed, rev/min.
P Pressure, pdl/ft².
Q External heat exchange, ft pdl.
q Rate of heat transfer, ft pdl/ft³ s.
R Gas constant.
$\hat{R}$ Recovery factor (7).
Re Reynolds number.
R_m Modified Reynolds number.
r Hydraulic radius, ft.
S Entropy.
s Distance from diffuser entrance, ft.
T Absolute temperature, °C (mean stream).
T_w Wall temperature, °C.
t Time, s.
U Internal energy, ft pdl.
$\bar{U}$ Dimensionless particle velocity.
u Particle velocity, ft/s.
V Volume, ft³.
W Work, ft pdl.
$\hat{W}$ Dimensionless shock speed.
w Velocity of shock front, ft/s.
$\hat{X}$ Dimensionless pressure ratio, i.e. $\left(\frac{P}{P_0}\right)^{(\gamma-1):2\gamma}$.
x Distance along exhaust duct from engine ports, ft.
$\bar{x}$ Dimensionless pressure ratio, i.e. (P/P_0).
I Characteristic co-ordinate, rightward wave.
II Characteristic co-ordinate, leftward wave.
α Engine crank angle, degrees.
γ Ratio of specific heats.
Δ Finite change.
θ Temperature difference, degC.
μ Absolute viscosity, cP.
ρ Density, lb/ft³.
τ_w Wall shear stress, pdl/ft².
ϕ Velocity potential.

Subscripts

a State parameter of air in the cylinder.
e State parameter of exhaust gas in the cylinder.
0 Datum state parameter.
1 Cylinder state parameter.
2 Duct state parameter.
$0s$ State parameter referred isentropically to datum isobar.

Scope of theoretical treatment

The flow problem to be solved is that of one-dimensional unsteady motion in a duct of varying sectional area, with wall friction, heat transfer and temperature discontinuities taken into account. The rate of change of duct cross-sectional area with distance is small and the assumption of one-dimensional flow at each duct section is considered justified. The effects of wall friction and heat transfer, however, are not essentially one-dimensional but to simplify the analysis a one-dimensional model using the appropriate mean quantities is employed.

The equations defining the flow are given in the next section and are derived from consideration of the system's mass continuity, momentum and energy content. To solve the resulting three simultaneous partial differential equations a calculation procedure based on the method of characteristics is used. This method was developed by de Haller (8) and used by Jenny (1) to investigate wave action in a pipe following the discharge of compressed air from a cylinder. Application of this method enables characteristic nets to be constructed, which for given initial conditions give a solution at each physical point x, t, for all the fluid properties, u, a, P, etc. The true curvilinear characteristic net, however, is replaced by a net of straight-line chords. Therefore the characteristic curves which are used for calculation are spaced closely enough so that this linear interpolation is tolerable.

As a result of wall friction and heat transfer effects an entropy gradient must exist along the duct. An allowance for this is made by applying a correction (see a later section) to the local acoustic velocity at each stage region under consideration. By referring the local acoustic velocity at each known state to ambient pressure, the evaluation of the change in fluid properties from one region of state to the next is made possible by following two reversible paths connecting the end states. Using this approach a series of loci producing a net can still be drawn in the state plane.

The passage of a wave point through temperature discontinuities, produced by repetitive cylinder charges remaining in the exhaust duct, can be directly taken into account analytically providing the position of the discontinuity in the duct at any instant of time is known. The method of solution is discussed for various flow conditions in a later section.

The incident and reflected wave profile, to and from the open end of the exhaust duct, is progressively changing during propagation along the duct, and can result in the development of a steep or shock front (9). This phenomenon is discussed later.

The boundary condition, i.e. the conditions at entry and exit from the duct which the flow must satisfy and the varying physical configurations involved therein are discussed in a previous report (4). The theoretical relationships derived in this article are in a form suitable for graphical representation in a framework of dimensionless co-ordinates of pressure and particle velocity. From the energy balance of the cylinder contents, the rate of pressure decay in the cylinder is obtained. Values so found, when inserted in the corresponding boundary curves, yield the instantaneous pressure in the duct.

Unsteady, one-dimensional flow with area change, wall friction and heat transfer

Consideration of the three basic equations of fluid flow, namely continuity of mass, momentum and energy, gives analytical expressions which define the variation in the state parameters for a fluid flowing in a duct. If, since the flow to be examined is of an unsteady nature, it is assumed that a plane velocity profile exists across the duct at any section and hence viscous shearing forces within the fluid can be neglected, these equations can be written as (1):

Mass continuity

$$\rho \frac{\partial u}{\partial s} + u \frac{\partial \rho}{\partial s} + \frac{\partial \rho}{\partial t} = -\frac{\rho u}{A}\frac{dA}{ds} \quad . \quad . \quad (1)$$

Momentum

$$\frac{\partial u}{\partial t} + u \frac{\partial u}{\partial s} + \frac{1}{\rho}\frac{\partial P}{\partial s} = -F \quad . \quad . \quad (2)$$

Energy

$$\frac{\partial P}{\partial t} + u \frac{\partial P}{\partial s} - a^2 \left(\frac{\partial \rho}{\partial t} + u \frac{\partial \rho}{\partial s} \right) = (\gamma-1)(q+u\rho F) \quad (3)$$

where

$$(q+u\rho F) = \frac{4f}{2d}\rho u \left[u^2 \left(\frac{u}{|u|} - \frac{R}{2} \right) + C_p(T_x - T) \right] \quad (4)$$

and

$$F = 4f \frac{u^2}{2D}\frac{u}{|u|} \quad . \quad . \quad . \quad (5)$$

The factor $u/|u|$ is introduced to ensure that the frictional force will always act in a direction opposite to that of motion.

For isentropic flow, both F and q are equal to zero. Further, for a constant section duct, the energy equation (3) becomes redundant and is replaced by the isentropic state relationship. Hence for isentropic flow in a duct of constant cross-sectional area the flow equations become:

Mass continuity

$$\rho \frac{\partial u}{\partial x} + u \frac{\partial \rho}{\partial x} + \frac{\partial \rho}{\partial t} = 0 \quad . \quad . \quad (6)$$

Momentum

$$\rho \frac{\partial u}{\partial t} + \rho u \frac{\partial u}{\partial x} + a^2 \frac{\partial \rho}{\partial x} = 0 \quad . \quad . \quad (7)$$

State

$$\frac{P}{\rho^\gamma} = \text{a constant}$$

Characteristic quantity for the entropy of a gas layer

The irreversible nature of wall friction and heat transfer effects result in an entropy gradient along the duct length.

A most convenient way to evaluate this entropy change between any two states is to follow two reversible paths, one of constant pressure and the other of constant entropy. Then the change in entropy can be taken into account by determining the change in the imaginary acoustic velocity from state 1 to 2, i.e. $_1a_{0s}$ to $_2a_{0s}$.

In the application of the method of characteristics to the solution of the flow equations, all state parameters are related isentropically to the chosen datum reference pressure P_0 and to the acoustic velocity a_{0s} and T_{0s} appropriate to the state under consideration. It can be shown that the required equation denoting the change of entropy along the particle path from state 1 to state 2 is

$$\frac{_2a_{0s}}{_1a_{0s}} = 1 + \frac{\gamma-1}{2\gamma}\left\{\frac{4f}{2d}\frac{u}{RT}\left[u^2\left(\frac{u}{|u|}-\frac{\bar{R}}{2}\right)-C_p(T_w-T)\right]\right\}$$
$$\times \Delta t_{\text{path}} \quad (8)$$

where Δt_{path} is the particle time from state 1 to state 2 and the variables are the mean values between states 1 and 2.

Solution of the flow equations

The effects of heat conduction, diffusion and viscous shearing within the fluid must be neglected to obtain a solution of the fundamental equations governing the unsteady gas flow in a duct. The method of characteristics is only applicable to non-linear equations of the first order. These assumptions were made in an earlier section when developing the three basic equations given in that section.

The operational equations resulting from the solution of these three equations (equations (1)–(3)), by the application of the theory of characteristics are:

Physical characteristics

$$\left(\frac{dx}{dt}\right)_{\text{I, II}} = u \pm a \quad \text{(Mach lines)} \quad . \quad (9)$$

$$\frac{dx}{dt} = u \quad \text{(path line)} . \quad . \quad . \quad (10)$$

Equation (9) signifies that disturbances are propagated on lines which travel either rightward or leftward with the local speed of sound relative to the fluid. Since the heat transfer and friction effects may be varied arbitrarily, the path lines or loci of the fluid particles themselves are characteristic curves given by equation (10) along which the entropy or temperature gradients may have discontinuities.

State characteristics

Plain pipe–diffuser arrangement

$$(dU)_{\text{I, II}} = \mp\frac{2}{\gamma-1}\frac{a_{0s}}{a_0}(dX)_{\text{I, II}} - (\Delta U_{q+F})_{\text{I, II}} \mp (\Delta U_A)_{\text{I, II}}$$
$$. \quad . \quad . \quad (11)$$

where the heat transfer and friction term $(\Delta U_{q+F})_{\text{I, II}}$

$$= \frac{4f}{2D}\frac{u^2}{a_0}\left\{\frac{u}{|u|} \mp (\gamma-1)\frac{u}{a}\left[\left(\frac{u}{|u|}-\frac{\bar{R}}{2}\right)+\frac{C_p}{u^2}(T_w-T)\right]\right\}(dt)$$
$$. \quad . \quad . \quad (11a)$$

and the area change term $(\Delta U_A)_{\text{I, II}}$

$$= \frac{2}{(1+s/l)}UX\left[\frac{a_{0s}(dt)_{\text{I, II}}}{l}\right] . \quad . \quad (11b)$$

Plain pipe arrangement

$$(dU)_{\text{I, II}} = \mp\frac{2}{\gamma-1}\frac{a_{0s}}{a_0}(dX)_{\text{I, II}} + (\Delta U_{q+F})_{\text{I, II}} \quad (12)$$

These are the equations denoting the change in state and particle velocity along a characteristic in the state plane.

If the pressure wave profile is assumed to be of stepped form, the graphical solution for the simple isentropic flow conditions in a parallel-sided duct resolves itself into the simultaneous construction of two diagrams which are known as a position diagram and a state diagram.

The modifications necessary to the state diagram as a result of including the effects of heat transfer, wall friction and area change into the flow problem are:

(1) The variation of a_{0s} which allows for the entropy gradients along the duct and which produces a change in the slope of the characteristics.

(2) The horizontal displacement of the characteristics due to area change, or wall friction, or heat transfer, or any combination of these three effects.

Solution with temperature discontinuity

A temperature discontinuity is said to exist at the interface of two gas regions at different temperatures. When a pressure wave encounters such a fluid discontinuity it undergoes a change of state and is partially transmitted and partially reflected. The transmitted portion of the wave travels in the next gas region at a velocity appropriate to its temperature, and the discontinuity will be swept along in its wake, at a speed equivalent to the local particle velocity. Therefore, the locus described by the movement of the discontinuity is a path line.

In the case of the two-stroke diesel engine used in the tests, temperature discontinuities are established at the interface of the hot gases being discharged from the cylinder and the cooler residual gases in the exhaust duct from the previous cycle. The volume of the exhaust ducting will, in general, be in excess of the volume of cylinder gases discharged per cycle and hence several discontinuities will exist in the ducting at any one instant. A further temperature discontinuity is created when a continuous wave develops a shock front.

To analyse the conditions at a temperature interface, it is a necessary theoretical assumption that no diffusion or heat conduction takes place between the hot and cold gas regions and the discontinuity exists as a definite plane fluid boundary at right angles to the fluid flow. The discontinuity is further assumed to be of negligible thickness

and therefore equal values of fluid pressure and particle velocity will exist on either side and immediately adjacent to it.

The method of solution used in this investigation is fully described in Appendix 1.

Solution of the unsteady flow equations with the formation of a shock wave

The solution of the flow equation with the formation of a shock wave is (10)

$$U_y = \pm \frac{2}{\gamma+1} \frac{a_{0sx}}{a_0} X_x \left[W_x - \frac{1}{W_x} \right] + U_x \quad (13)$$

$$X_y = \left[1 + \frac{2\gamma}{\gamma+1}(W_2{}^2-1) \right]^{(\gamma-1)/2\gamma} X_x \quad . \quad (14)$$

where subscripts y and x indicate conditions upstream and downstream of the shock wave. For this theoretical work, however, a method is developed in Appendix 2 which gives a more rapid numerical solution to these flow equations. The approach is to force the equations (13) and (14) into the form

$$\Delta U \propto \frac{2}{\gamma-1} \frac{a_{0s}}{a_0} \Delta X$$

and by application of this equation replace the shock polar curve given by equations (13) and (14) by a straight line construction. The equation that gives this straight line construction in the state diagram is:

$$\frac{\Delta U}{\Delta X} = \pm \frac{2}{\gamma-1} \frac{a_{0sx}}{a_0} K \quad . \quad . \quad (15)$$

where

$$K = \frac{W_x{}^2+1}{2W_x{}^3 \left[1 + \frac{2\gamma}{\gamma+1}(W_x{}^2-1) \right]^{(\gamma+1)/2\gamma}} \quad (16)$$

The equation to the tangent at any point W_x on the shock polar, given by equation (15), will have the same slope in the state diagram as the I, II characteristic, when the value of W_x approaches unity, i.e.

$$\Delta U \to \pm \frac{2}{\gamma-1} \frac{a_{0sx}}{a_0} \Delta X$$

Hence a weak shock may, for calculation purposes, be treated as a continuous wave and the propagation velocity computed as the arithmetic mean of the absolute wave speeds upstream and downstream of the shock wave. This assumption ignores the entropy increase across the shock wave.

Boundary conditions

It has been shown in an earlier section that the solution of the unsteady one-dimensional flow equations is possible by the construction of characteristic nets in the physical and state plane. The construction of a complete net between the physical boundaries of the cylinder ports and

the open end of the exhaust duct requires the repeated application of equations (9) and (10). The typical steps representing the boundary conditions at both ends of the duct have been fully described in an earlier publication (4).

An exact analysis of the flow process must take account of the unsteady motion in these regions. This is, however, extremely difficult and it is necessary to make plausible approximations which do not introduce undue error to simplify the analysis.

The assumptions made in the development of the flow equations at the boundaries and changes occurring in the cylinder are:

(1) Quasi-steady flow through the inlet and the exhaust ports and at the open end of the exhaust duct. That is, the steady flow adiabatic energy equation applies instantaneously across the cylinder ports and at the open end of the duct. This is equivalent to assuming that the change in flow pattern with respect to time may be neglected in comparison with that due to distance. This assumption is valid for fluid flow through a restriction where the effective flow area is small in comparison with the area of the cylinder, or other reservoir such as a relatively stagnant atmosphere that contains the fluid.

(2) The effect of wave action in the cylinder on the discharge process decreases so rapidly with increase in the ratio of cylinder area to duct area that it may be neglected without detectable error.

(3) The cylinder ports are regarded as a sharp-edged rectangular orifice, the coefficient of discharge depending upon the pressure ratio across them and Reynolds number.

(4) The fluid in the cylinder is regarded as quasi-perfect and the appropriate mean value of γ is used for each step in the process.

(5) The ratio of specific heats γ across the cylinder ports and at the open end of the duct is taken as the upstream value in each case.

(6) There is no mixing of the gases within the cylinder, i.e. two regions exist, one containing air only and the other the residuals of combustion only.

(7) The temperature of the air in the cylinder is assumed to be the same as that of the air upstream of the air ports, i.e. the internal energy of the air remains constant after admission into the cylinder.

(8) The pressure is uniform instantaneously throughout the cylinder.

(9) All changes are adiabatic and not necessarily isentropic with the exception of the cylinder contents for which the process is assumed isentropic.

(10) There is no pressure recovery of the incoming gas into the cylinder after the *vena contracta*, i.e. pressure at the *vena contracta* equals the cylinder pressure.

(11) For fluid flow from the cylinder to the exhaust duct, pressure recovery occurs after the *vena contracta*.

(12) For inflow at the open end of the exhaust duct, the duct mouth behaves as a Borda mouthpiece.

Engine speed 1110·5 rev/min.
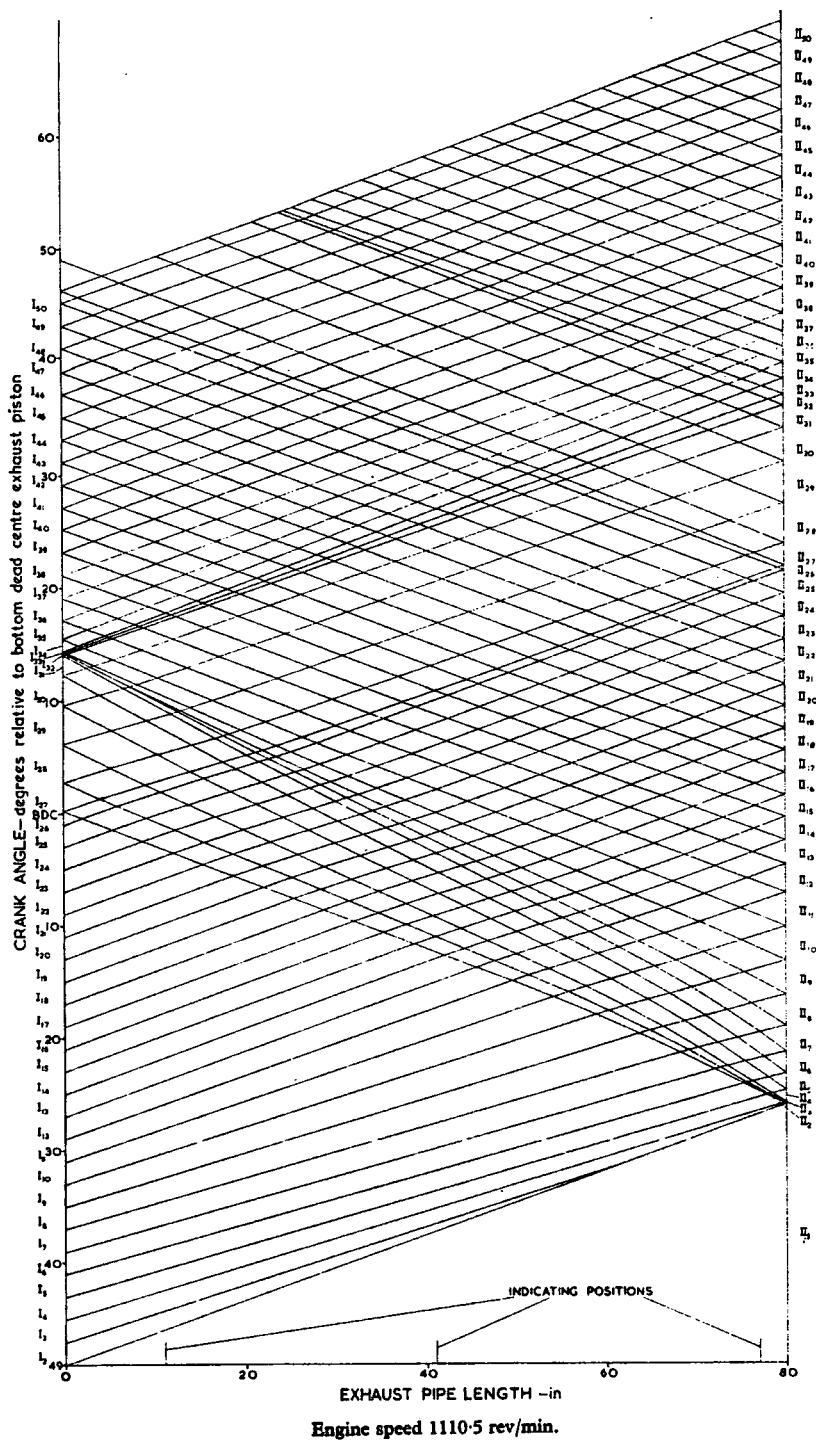
Fig. 2. *Position diagram: isentropic flow*

EXHAUST PIPE LENGTH –in
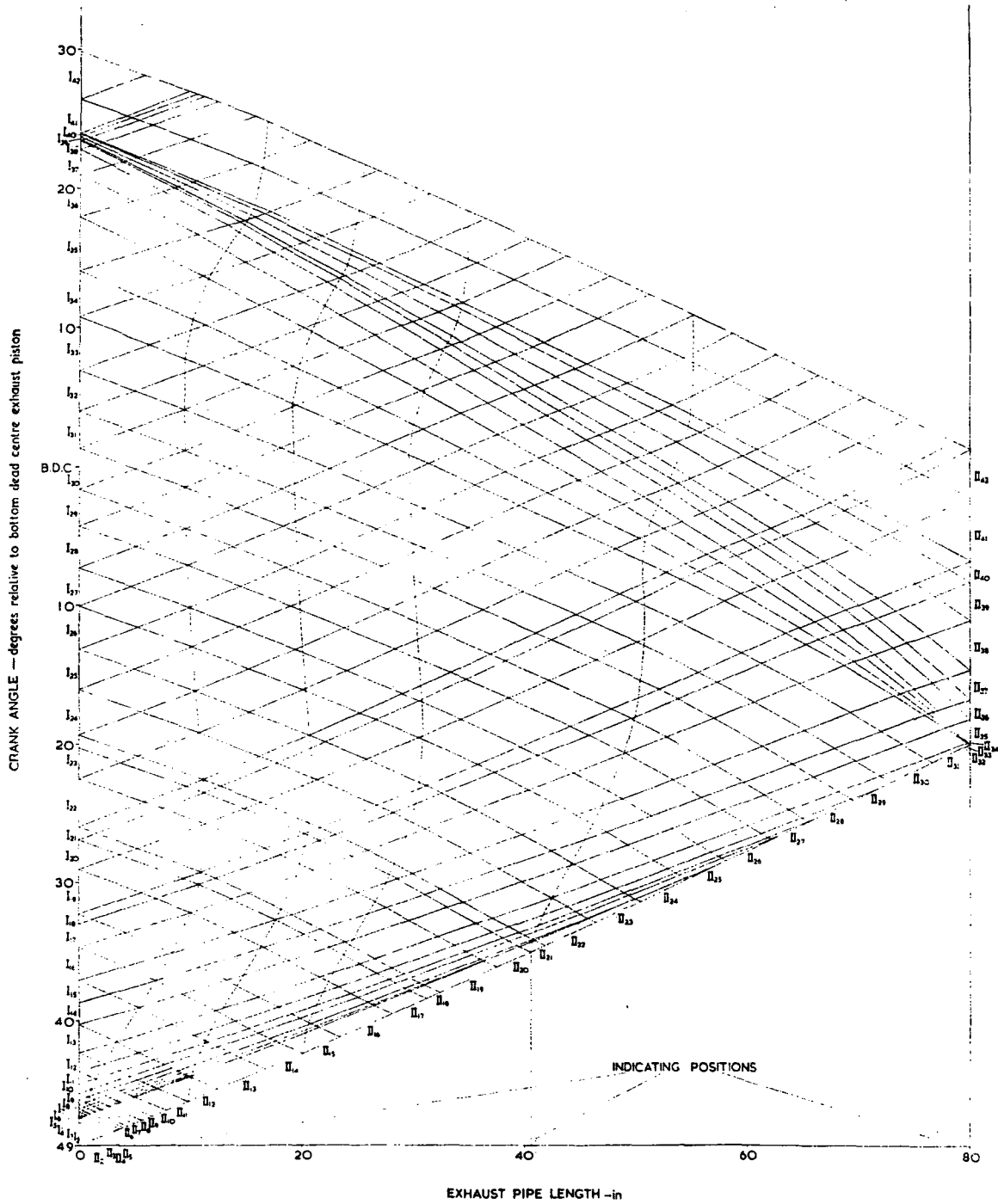
Engine speed 1110·5 rev/min.

Fig. 3. *Position diagram: irreversible flow*
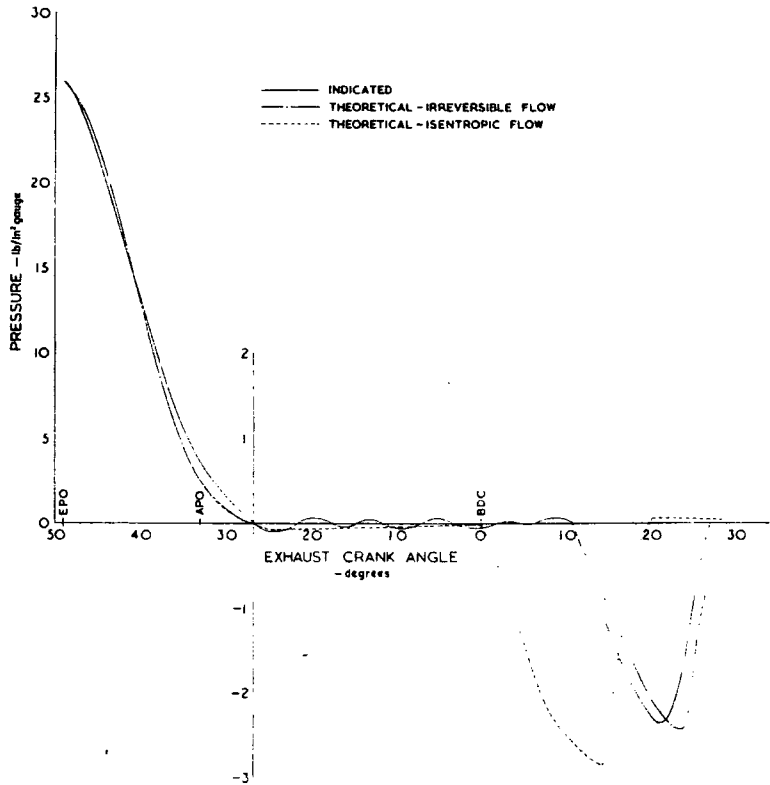
Fig. 4. *Cylinder pressure*

DETERMINATION OF ACTUAL SYSTEM PARAMETERS

Cylinder and duct parameters

A theoretical analysis for the changes occurring within the cylinder gases requires a knowledge of the variation with crank angle of the following physical parameters:

(1) cylinder volume;
(2) ratio of port area to duct area for both inlet and exhaust ports;
(3) hydraulic radius of both the inlet and exhaust ports.

Coefficient of discharge (11) (12)

The variation in the coefficient of discharge (C_d) for the cylinder ports as a function of pressure ratio across the ports and Reynolds number is required. Determination of the Reynolds number requires a knowledge of the value of the absolute viscosity of the gas flowing through the ports at the instant considered.

Friction coefficient for the exhaust duct

The surface roughness within the exhaust duct was determined using a Taylor Hodson model 3 Talysurf on

sections of artificially hardened soot surface in the duct. The variation in friction coefficient (f) with Reynolds number was found by use of the Colebrooke-White (13 function and suggested modification by Moody (14).

Exhaust gas parameters

To evaluate the fluid properties, namely R, C_p and γ, for the range of gas temperature encountered in an actual firing engine, an analysis of the exhaust gases is necessary.

Variation in the specific heats

The values of the specific heats at constant pressure and constant volume for the exhaust gas constituents are taken from gas tables (15) for the required temperature range and the mass mean value for the specific heats are calculated using the mean exhaust gas analysis.

Variation in absolute viscosity

The mass mean value for viscosity is evaluated from the values for the exhaust gas constituents for a range of temperatures. The assumption of mass mean values for viscosity, however, is not strictly correct, but in view of the smallness of the error, a full analysis of the problem is not justified.
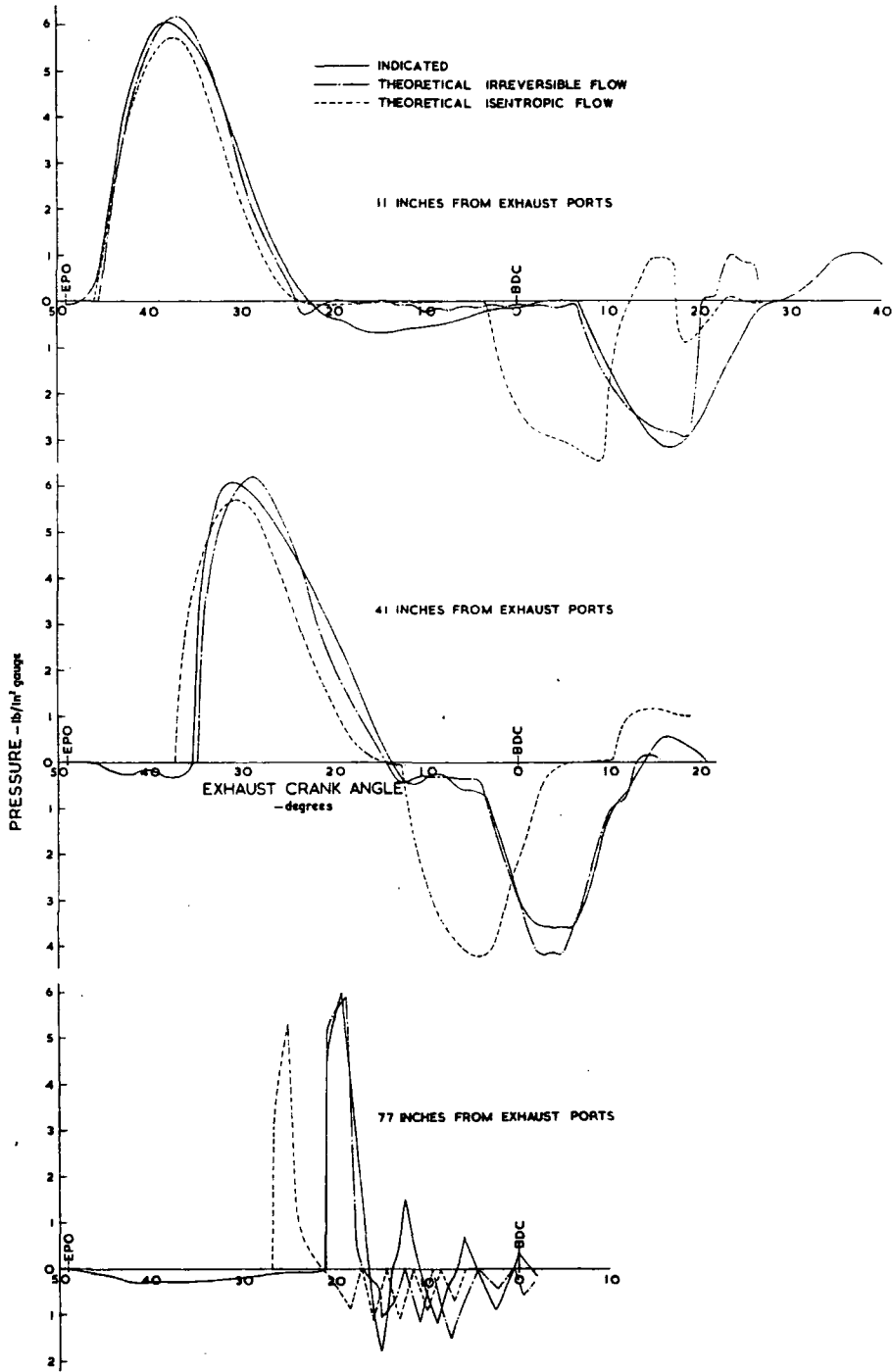
Fig. 5. *Pressure in exhaust pipe*

E. H. WRIGHT AND K. F. GILL
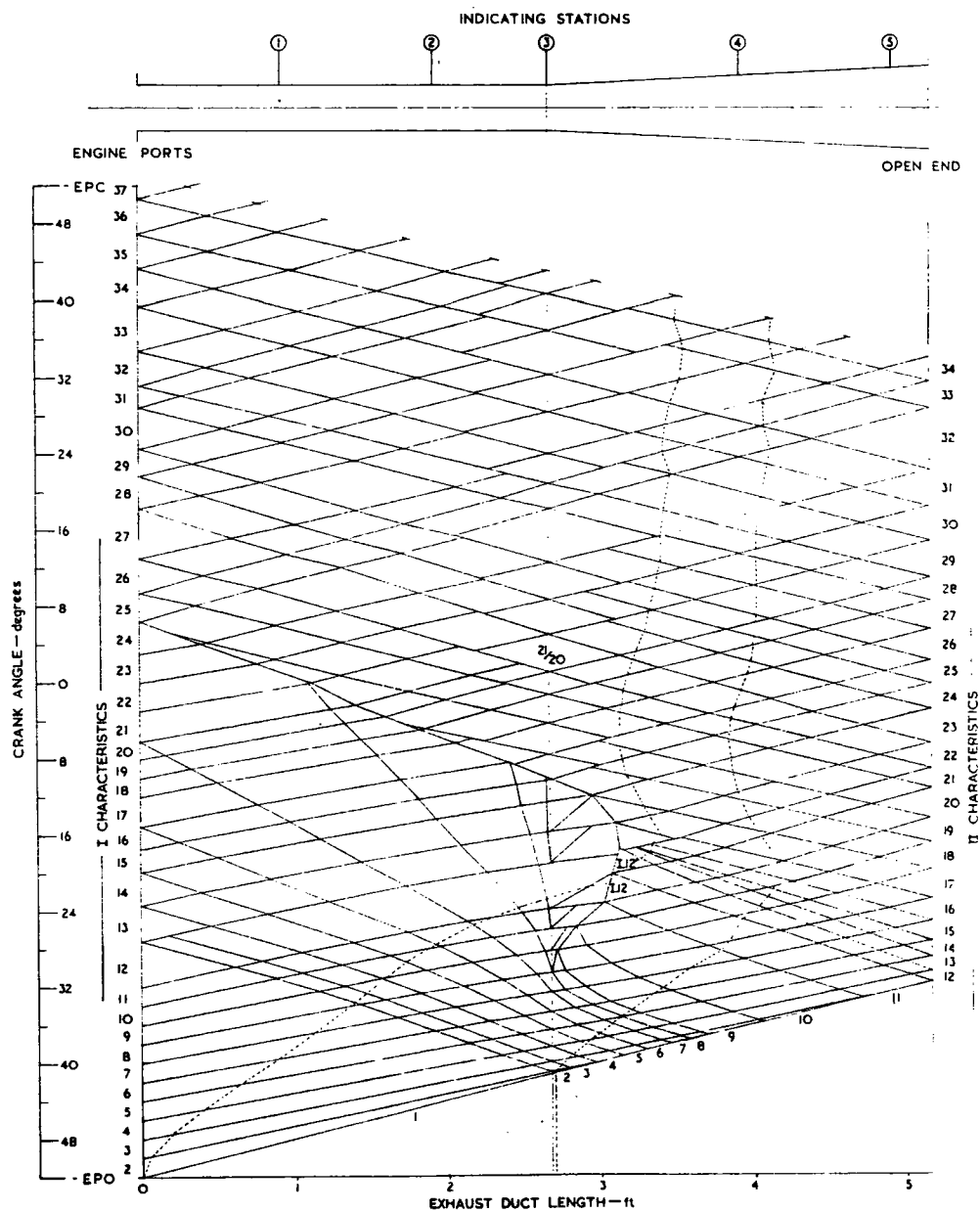
Engine speed 1313 rev/min.

Fig. 6. *Position diagram: isentropic flow*
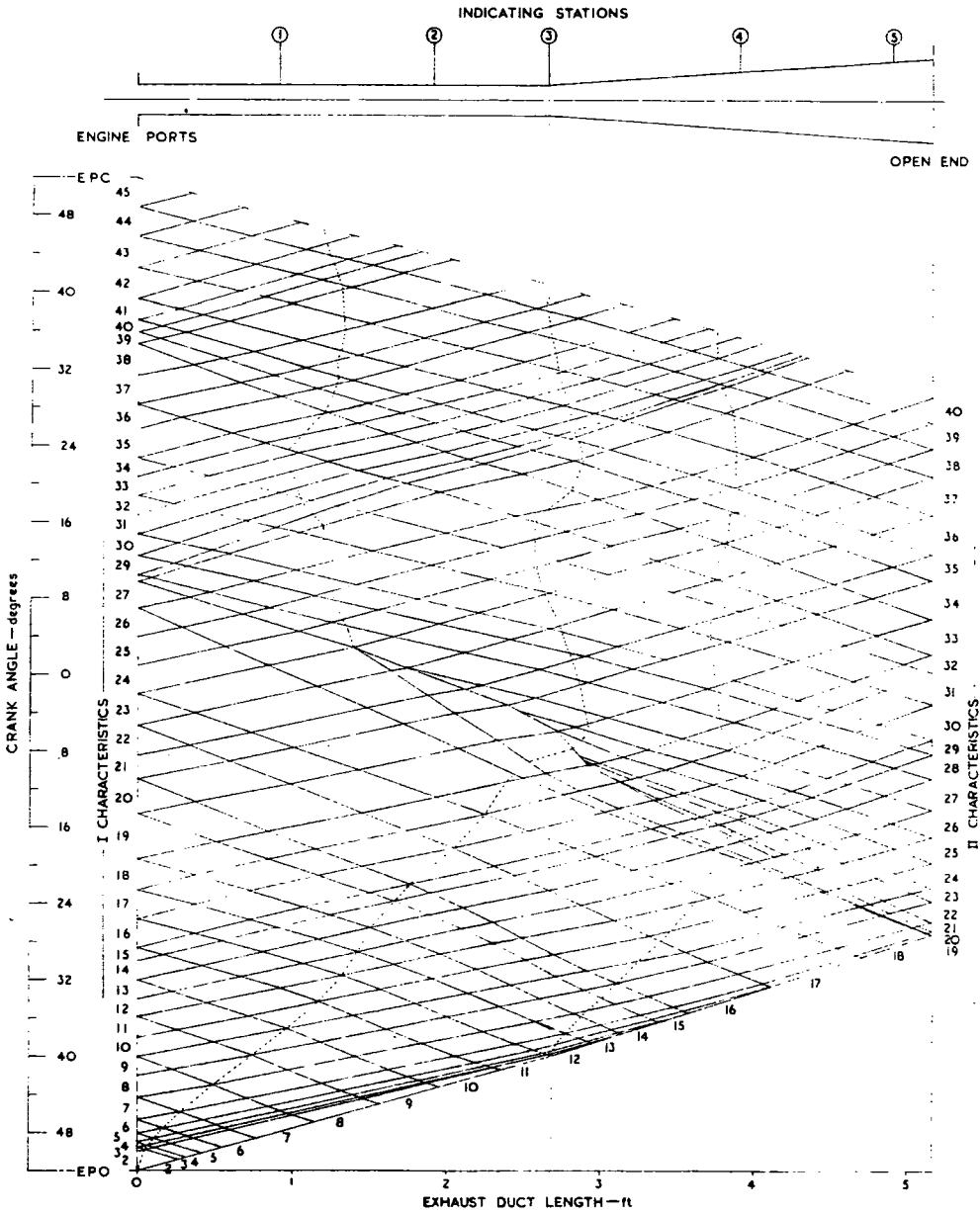
Engine speed 1313 rev/min.

Fig. 7. *Position diagram: irreversible flow*

PROCEDURE AND RESULTS

Procedure

To determine the validity of the theory developed for the solution of the flow problem encountered in a firing engine, the conditions existing in an actual engine system were studied and analysed.

The engine was operated with a constant air/fuel ratio and engine cooling water outlet temperature, and plain pipe and plain pipe–diffuser exhaust systems were used together with a neutral induction system.

Indicator diagrams were taken in the engine cylinder and at a number of stations along the exhaust duct, and the air mass flow was measured by means of an air box fitted with an orifice plate.

Results

The two exhaust arrangements investigated for comparison with the theoretical results were:

(1) a simple plain exhaust pipe of length 6 ft 8 in (Figs 2–5);

(2) a simple plain exhaust pipe of length 2 ft 7 in terminating in a conical diffuser of length 2 ft 6 in and a cone angle of 6° (Figs 6–11).

In each case the engine speed was chosen such that the scavenge was effected by the first reflection of the blow-down pulse to avoid over-complication of the pressure wave pattern in the exhaust duct.

DISCUSSION OF RESULTS

Theoretical equations

In the development of the theoretical equations for the unsteady flow encountered in an engine exhaust system, a number of simplifying assumptions are made. The most important of these is that the flow is geometrically one-dimensional, implying that all fluid properties are uniform over each cross-section of the exhaust duct. For the plain pipe, the fluctuating nature of the gas movement precludes the establishment of a fully developed velocity profile and hence the assumption is considered reasonable. For the diffuser the assumption is also considered reasonable since the ratio of change of cross-sectional area with distance is small for a divergence angle of 6°. Although the wall friction and heat transfer effects are not in essence one-dimensional, a one-dimensional model is used for simplicity.

The identical resultant effect of wall friction and heat transfer together with the tacit assumption that the steady flow equations which define these effects can be applied instantaneously to unsteady flow, permits a further simplification in the derivation of the theoretical equations. Reynolds's analogy, which relates the heat transfer and friction coefficient according to $\frac{1}{2}f = h/\rho u C_p$, is assumed to be valid. Although no information is available regarding the accuracy of the analogy for this problem, its use is considered justified in view of the reduction in computation time it affords.

Experience shows that additional assumptions, which give a more rapid numerical solution, are possible in the theoretical calculations if the step size chosen in the construction of the position diagram is small. Initial values can then be used in the evaluation of the term $(\Delta \bar{U}_{q+F})_{\text{I, II}}$ of equations (11) and (12) without introducing undue error. Further, for values of $s \geqslant 1$ in equation (11), $(\Delta \bar{U}_{q+F})_{\text{I, II}}$ becomes small in comparison with the other terms and can be neglected without detectable error, and a sufficiently correct evaluation to the term $(\Delta \bar{U}_A)_{\text{I, II}}$ of
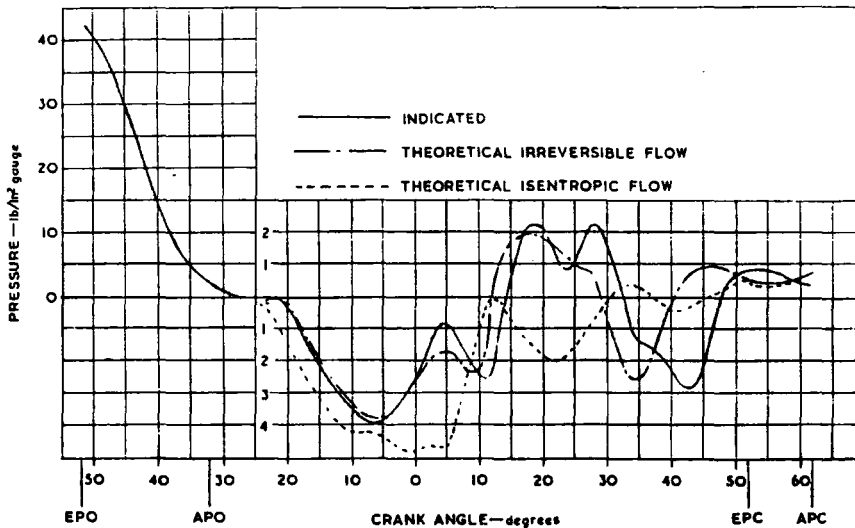
Fig. 8. *Cylinder pressure diagram*

equation (11) is possible by three successive approximations only.

The correction of the boundary state point for irreversibility is found to be primarily dependent on the term $[+2/(\gamma-1)(a_{0s2}/a_{0s1})]$, the value of the term containing $(\Delta \bar{U}_{q+F})$ never exceeding 1·5 per cent of its value. The order of accuracy possible when using the boundary charts is less than a correction of this order and thus the allowance for the heat transfer and friction effects within the duct on mass flow from the cylinder can be discarded. This simplification results in a decrease in computation time at each port boundary state of approximately 30 per cent with no sensible loss of accuracy.

Indicating trials

Indicator diagrams

To confirm the validity of the finite-wave theory, pressure indicator diagrams were taken at a number of stations in the engine system for both exhaust arrangements used and from Figs 8, 9, 11 (plain pipe–diffuser cone exhaust) and Figs 4 and 5 (plain pipe exhaust) it can be seen that good general agreement, both in respect to phasing and amplitude, exists between the observed curves and those obtained by application of the irreversible flow theory.

The poor correlation immediately following the passage of the steep front at station 1, Fig. 9, is primarily the result of lozenge size chosen in the construction of the position diagram, Fig. 7. Although a smooth curve is drawn in Fig. 9, the actual calculated points for this region after the shock are shown in Fig. 10. It is suggested that these points lie on an oscillating pressure trace which could be predicted theoretically by reducing the mesh size in the construction of the position diagram.

It can be seen in Fig. 8 that a 'pressure peak' is suppressed in the theoretical curve at approximately 30° after b.d.c. exhaust piston when compared with the indicated diagram. This is attributed to the lozenge size chosen when plotting Fig. 7 and if further reflections from the plane of the duct open end had been included, better correlation might have resulted.

Fig. 5 shows poor correlation was obtained for the pressure occurring in the region of the pipe open end after the passage of the pressure pulse. The pressure changes are very rapid and oscillatory in nature and again it is suggested that a reduction in the lozenge size in this region would improve the accuracy of the analysis.

The oscillatory nature of the pressure fluctuations in the regions of poor pressure correlation, combined with the effects of the passage length between the duct wall and the pressure transducer diaphragm, and the natural frequency of the latter, will also produce additional local distortion of the recorded trace.

The establishment of a 'plug' of cold air in the exhaust duct just outside the ports as a result of short-circuited air would severely complicate the theoretical evaluation of the flow process. It was considered unlikely that in a uniflow engine running with a volumetric efficiency of the

order of 65 per cent such an effect would be experienced. However, to confirm this a plot of volumetric efficiency against torque was made for a number of air consumption trials. Over 95 per cent of the results, including those of the indicating trials, lay within a straight narrow band, and since a very wide range of operating conditions were covered, it was assumed that, in general, no short-circuiting occurred. The few results which did not come within this linear band were displaced towards the volumetric efficiency axis, indicating that for these isolated cases short-circuiting did occur.

Air flow

Assessment of the mass flow variation can be directly obtained from the theoretical results, but direct experimental confirmation of this was not attempted. In the theoretical analysis, particle velocity and pressure are dependent parameters, and since good agreement is obtained between the theoretical and experimental pressure traces it is considered that the results for mass flow can be used with confidence. The volumetric efficiency, based on ambient conditions, helps to substantiate this, Table 1.

For the plain pipe case, the irreversible flow analysis was not completed, but at the end of the last cylinder step calculated, i.e. 30 per cent after b.d.c. exhaust piston, the mass of air then present represents a volumetric efficiency of 57·5 per cent. It is not possible to estimate the air content of the cylinder at the time of exhaust port closure without completing the analysis, but in the period between this latter event and air port closure, some air is pushed out of the cylinder by the movement of the pistons. Hence the final theoretical result would almost certainly be less than 57·5 per cent and probably less than the measured value due to the early arrival of the theoretical positive pressure pulse following the rarefaction wave (see the theoretical and recorded pressure traces at 11 in from the ports, Fig. 5).

Temperature discontinuity

(1) Plain pipe–diffuser system: Measurements of the bulk gas temperature up to and at a station 3 in upstream of the

Table 1

	Volumetric efficiency, $\left[\dfrac{\text{volume aspirated at intake conditions}}{\text{trapped volume}}\right]$	
	Plain pipe exhaust system	Plain pipe–diffuser exhaust system
Theoretical irreversible flow	Less than 57·5 per cent	93·7 per cent
Theoretical isentropic flow	60·8 per cent	186·6 per cent
Actual flow	53·4 per cent	76·4 per cent
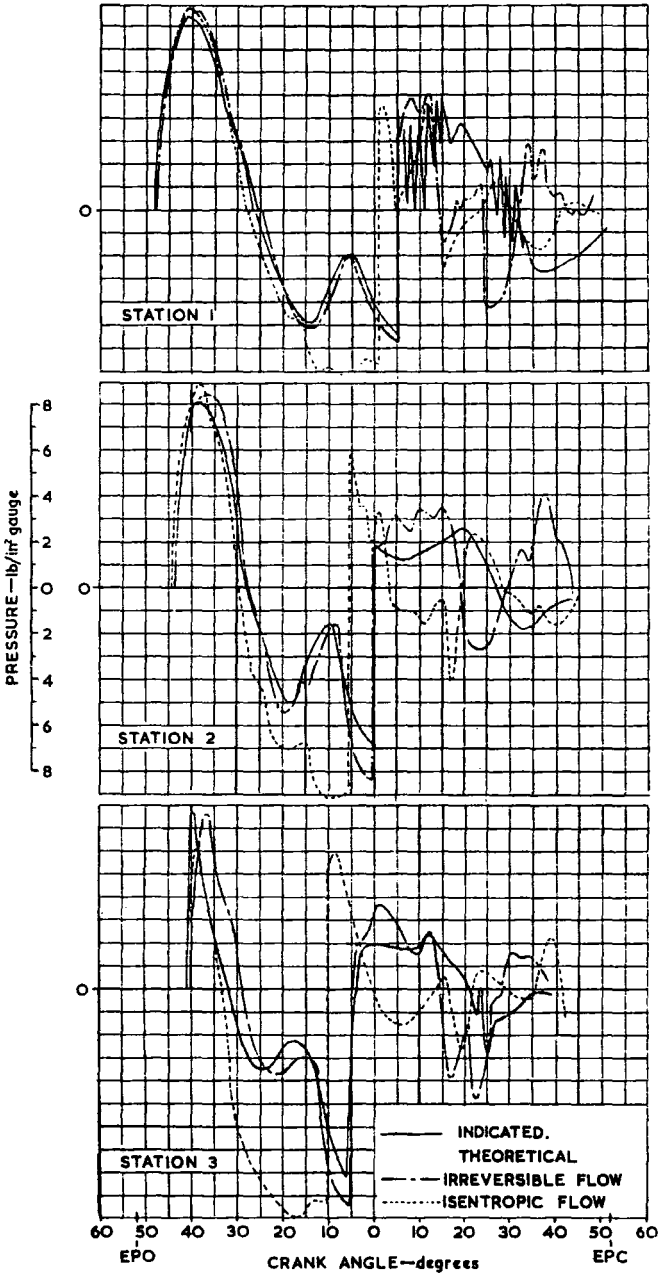
Fig. 9. *Pressure diagrams*

diffuser entry section showed a substantially constant value 190 degC higher than at the diffuser entry section. Downstream of this section a sensibly constant gas temperature was recorded. Therefore, the temperature
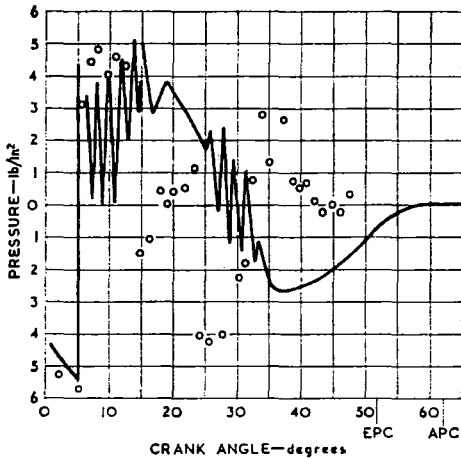
Fig. 10. *Pressure diagram (station 1)*

distribution existing in the duct was taken to be as shown in Fig. 12 and used in the theoretical analysis.

The reflections from the main temperature discontinuity generated at commencement of blowdown were fully accounted for in the construction of the position diagram for the first 37° of crank angle after exhaust port opening. Beyond this point the reflections from the discontinuity were combined with those from the diffuser to simplify computation. A similar technique of combining a number of waves was used at the diffuser entry section, Fig. 7.

The passage of the primary wave through the first temperature discontinuity produces a rise in pressure of 0·02 lb/in² in the calculated value of the initial pulse amplitude as compared with the isentropic analysis. The smallness of the pressure rise through the temperature discontinuity of 190 degC is the result of the superimposition, at this interface, of the reflection promoted by the effects of wall friction and heat transfer from the proceeding wave points.

The propagation along the duct of the main temperature discontinuity, as given by the theoretical irreversible flow analysis, Fig. 7, was such that its final position at e.p.c. was at the diffuser entry section and this result is in excellent agreement with the measured result shown in

Indicated, theoretical.   — – — Irreversible flow.   – – – – – Isentropic flow.
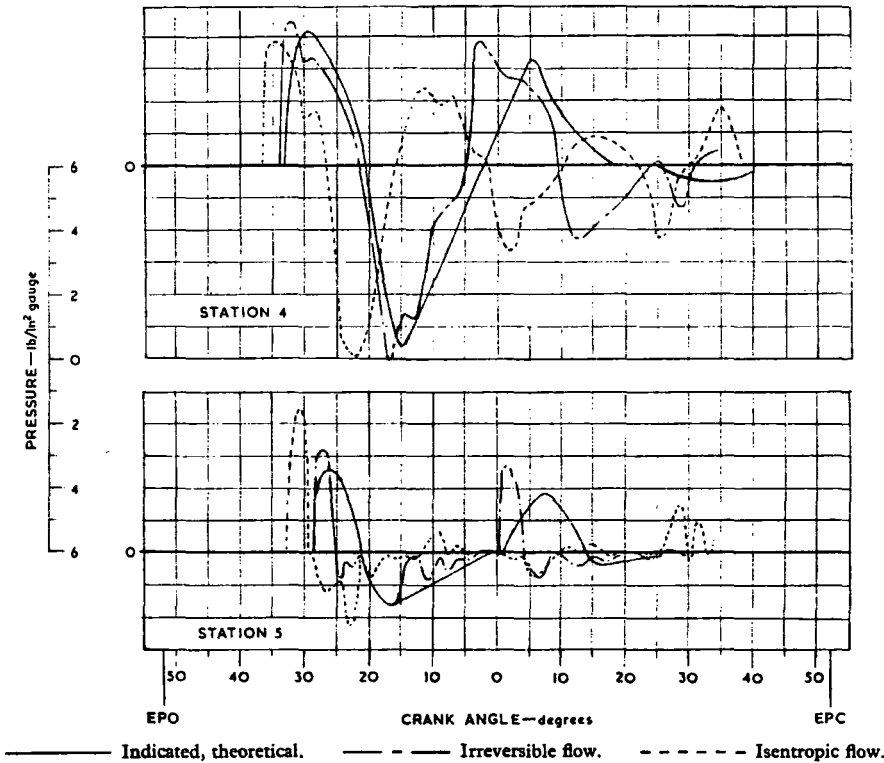
Fig. 11. *Pressure diagrams*

Fig. 12. For the isentropic analysis, the path line which represents the main temperature discontinuity is positioned 10 in downstream of the diffuser entry section at the instant of e.p.c., Fig. 6, and this is indicative of the errors introduced by use of the simpler isentropic analysis.

(2) Plain pipe system: The measured exhaust temperature in the exhaust pipe is shown plotted in Fig. 13. Calculation suggests that two successive temperature discontinuities should exist at approximately 20 in and 37 in from the engine ports. The inflection of the plotted curve at approximately 20 in from the ports indicates that this discontinuity still exists. The next, and successive discontinuities, however, are not at all apparent.

Solution of the exhaust gas flow equations allowing for the measured temperature gradient would involve assuming a small temperature interface to exist in each region used in the construction of the characteristic net along the first wave I_2, Fig. 3. The resulting increase in computation time would be prohibitive, hence a coarse stepped temperature profile was assumed, with the second and third steps approximately coinciding with the position of the decayed temperature discontinuities created by the two previous engine cycles. Consideration of these temperature steps in the theoretical analysis can be regarded as summations of the changes occurring in the regions between them, and the result of this is to alter the timing of the effect of the temperature gradient on the diffusion waves promoted by friction and heat transfer effects back towards the ports.

The predominant effect of the main temperature discontinuity results in an increase in the peak of the blow-

Fig. 12. *Temperature distribution for indicating trial*
(plain pipe–diffuser)

Fig. 13. *Exhaust gas temperature (plain pipe)*

down pressure pulse of 0·54 lb/in² as compared with the isentropic value. The overall decay of this pulse for the 50 in of pipe from the major temperature discontinuity to the point at which it meets the returning rarefaction wave is 0·37 lb/in². The larger amplitude pressure pulse arising in the non-isentropic flow analysis, on arriving at the open end, will give a reflected rarefaction trough which is more intense. This is, however, attenuated by the irreversibilities and the main temperature discontinuity. The net effect is that the irreversible flow theoretical rarefaction wave amplitude is comparable with the isentropic flow value at the 41-in indicating point in the exhaust pipe, but the attenuation at the main temperature discontinuity produces an amplitude comparable with that recorded at the 11-in indicating point.

The steep rise in pressure following the rarefaction wave at the indicating point 11 in from the ports, as given by the irreversible flow theoretical analysis, is exaggerated through not using the full reflection treatment for the temperature discontinuity in this region. From the position diagram, Fig. 3, it can be seen that if all the reflections from the temperature discontinuity had been considered. the time taken for this pressure to rise from the lowest value to the atmospheric value would be increased, with a consequent lessening of the rate of pressure rise.

Shock wave

Owing to the interaction of successive points of the fundamental pressure pulse with those resulting from the reflection of previous points of the fundamental pulse. very high rightward particle velocities are encountered at the diffuser entry section. Although sonic velocities are never quite attained at the diffuser entry section in the irreversible flow analysis, Fig. 7, sonic velocities did occur in the isentropic analysis, Fig. 6. In both cases these high velocities result in the formation of a shock wave at the diffuser entry section. As the shock wave travels leftwards towards the cylinder, its strength is progressively reduced by the rightward moving pressure waves from the exhaust ports. This effect is shown clearly by the curvature of the shock path lines in the position diagram Fig. 7 and Fig. 6. In each region through which the shock front passes a small temperature discontinuity is 'created', but for convenience these are combined and regarded as a single temperature interface emanating from the lozenge I_{2o}, II_{20}. Upstream of this region the shock wave is considered weak and amenable to the approximate treatment described in an earlier section.

The evaluation of a region through which a shock wave is passing was performed using both the exact and approximate theory of that earlier section. The weak shock analysis results in a difference in pressure of 0·21 lb/in² for the region 21·26, which represents something less than 1 per cent error in pressure. Larger errors do result, however, when velocities are compared and if the shock front propagation velocity had been assumed to be represented by term $(u-a)$, then the front would have arrived 2° earlier than shown at Station 1, Fig. 9. This mis-timing is small
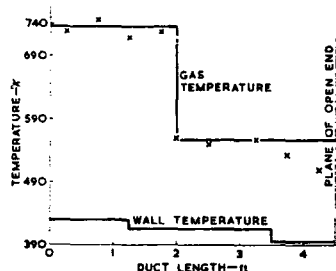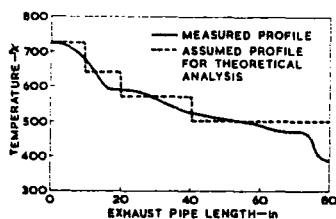
and hence the application of the simplified weak shock analysis is considered sufficient for future analysis in view of the reduction in computation time it affords.

CONCLUSIONS

Summary of conclusions

(1) The good agreement obtained between the irreversible fluid flow analysis and the indicated records for both the cylinder and the exhaust pipe shows the physical premises of the theory to be correct and sufficient. The use of the quasi-steady flow approach, i.e. the use of steady flow data for pipe friction, heat transfer, inflow at the pipe open end and flow through the cylinder ports, is shown to be justified and permissible.

(2) Accurate results are obtainable by the method of characteristics using finite increments of from 1° to 4° of crank angle depending upon the rate of change of pressure and/or velocity at the point under consideration.

(3) In addition to giving good correlation to the form of the pressure changes occurring throughout the cylinder and exhaust pipe system, the composite theory gives an assessment of the mass flow which is significantly more accurate than that given by the earlier and simpler isentropic flow theory.

(4) Greater accuracy in the prediction of the mass flow from the cylinder is expected by making allowance for the variation in the specific heats within the cylinder, and the boundary chart interpolation technique developed to account for this is adequate.

(5) The correction for the flow irreversibilities of heat transfer and wall friction in the exhaust duct adjacent to the exhaust ports, on the gas flow from the cylinder, is small and can be neglected without detectable error.

(6) Effecting the solution by using a position diagram instead of calculated and tabulated ordinates possesses the advantage that a clear picture is presented of the development of the main wave pattern, the origins of secondary waves and reflections, and the history of the motion of gas particles.

(7) In a firing engine, the temperature discontinuities produced within the exhaust pipe are very pronounced and have a marked influence on the wave motion, and the variation of specific heats is significant. The theoretical method developed for the passage of a wave point through a temperature discontinuity is adequate for this type of problem.

(8) The evaluation of air consumption for the indicating trial establishes the validity of the solution using the theory of characteristics applied to the problem of air flow in a naturally aspirated two-stroke oil engine.

APPENDIX 1

SOLUTION WITH TEMPERATURE DISCONTINUITY

To illustrate the method of solution the problem will be considered in three stages, namely:

(1) solution for isentropic flow on either side of the interface with constant specific heats;

(2) solution for isentropic flow with variable specific heats; and

(3) solution for irreversible flow on either side of the interface with variable specific heats.

In all three cases, the parameters referring to the hot and cold regions associated with the discontinuity are identified by the index marks ' and " respectively.

(1) *Solution for isentropic flow on either side of the interface with constant specific heats*

From the characteristic state equation (11)

$$(\Delta u')_{\mathrm{I}} = -\frac{2}{\gamma-1}(\Delta a')_{\mathrm{I}} \left.\vphantom{\frac{2}{\gamma-1}}\right\} \quad . \quad . \quad (17)$$
$$(\Delta u'')_{\mathrm{II}} = +\frac{2}{\gamma-1}(\Delta a'')_{\mathrm{II}}$$

The isentropic state relationship is valid on each side of the temperature discontinuity, thus:

$$a' = a'_{0s}\left(\frac{P'}{P_0}\right)^{(\gamma-1)/2\gamma} \left.\vphantom{\frac{P'}{P_0}}\right\} \quad . \quad . \quad (18)$$
$$a'' = a''_{0s}\left(\frac{P''}{P_0}\right)^{(\gamma-1)/2\gamma}$$

If the region of state associated with the discontinuity is small, then the pressure and particle velocity for the whole region will be the same, whence, $u' = u''$

$$P' = P'' \quad . \quad . \quad . \quad . \quad (19)$$

From equations (17), (18) and (19) it follows that:

$$(\Delta U)_{\mathrm{I}} = -\frac{2}{\gamma-1}\frac{a'_{0s}}{a_0}(\Delta X)_{\mathrm{I}} \left.\vphantom{\frac{a'_{0s}}{a_0}}\right\} \quad . \quad (20)$$
$$(\Delta U)_{\mathrm{II}} = +\frac{2}{\gamma-1}\frac{a'_{0s}}{a_0}(\Delta X)_{\mathrm{I}}$$

where $\Delta U = \Delta U' = \Delta U''$
and $\Delta X = \Delta X' = \Delta X''$

From the above it can be seen that the characteristics in each region have slopes of $[-2/(\gamma-1)(a'_{0s}/a_0)]_{\mathrm{I}}$ and $[+2/(\gamma-1) \times (a''_{0s}/a_0)]_{\mathrm{II}}$ for right and leftward travelling waves respectively.

(2) *Solution for isentropic flow with variable specific heats*

Although the pressure immediately adjacent to and on either side of the temperature interface is the same, the variation in the ratio of the specific heats, i.e. $\gamma' \neq \gamma''$, results in the inequality $X' \neq X''$ for the hot and cold regions on either side of the interface. This requires the problem to be solved algebraically and for completeness the effects of area change are considered.

Consider the superimposition of waves 1 and 2 in region 3, in which a temperature discontinuity exists, Fig. 14.

The characteristic state equation written in finite difference form is:

$$(\Delta U')_{\mathrm{I}} = -\frac{2}{\gamma-1}\left(\Delta\frac{a'}{a_0}\right)_{\mathrm{I}} -(\Delta U'_A)_{\mathrm{I}} \left.\vphantom{\Delta\frac{a'}{a_0}}\right\} \quad . \quad (21)$$
$$(\Delta U'')_{\mathrm{II}} = +\frac{2}{\gamma-1}\left(\Delta\frac{a''}{a_0}\right)_{\mathrm{II}} +(\Delta U''_A)_{\mathrm{II}}$$

If the region of state associated with the temperature discontinuity is small, then:

$$\frac{u'_3}{a_0} = U'_3 = \frac{u''_3}{a_0} = U''_3 \left.\vphantom{\frac{u'_3}{a_0}}\right\}$$
and
$$\frac{P'_3}{P_0} = \frac{P''_3}{P_0} \quad . \quad . \quad . \quad (22)$$

Since the isentropic state relationship is valid on each side of the interface, the pressure ratio of equation (22) may be written as:

$$\left(\frac{a'_3}{a'_{0s}}\right)^{2\gamma'/(\gamma'-1)} = \left(\frac{a''_3}{a''_{0s}}\right)^{2\gamma''/(\gamma''-1)} \quad . \quad . \quad (23)$$

E. H. WRIGHT AND K. F. GILL
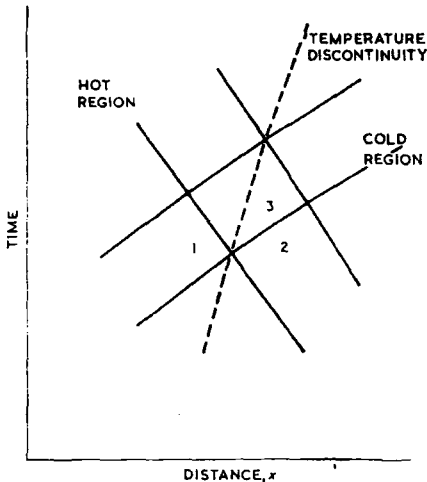
Fig. 14. *Position diagram*
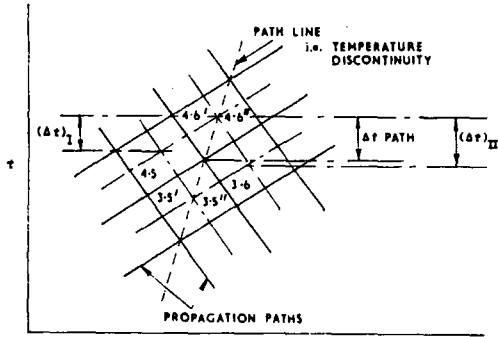
a Position diagram.
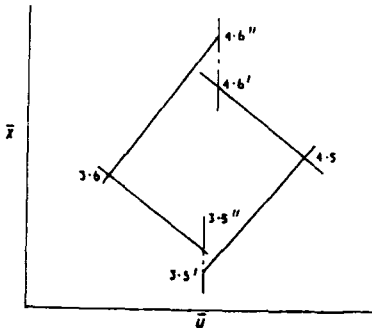
b State diagram.

Fig. 15

From equation (21):

$$U'_3 - U_1 = -\frac{2}{\gamma'-1}\frac{1}{a_0}(a'_3 - a_1) - (\Delta U'_A)_I \quad \left.\right\}$$
$$U^{\cdot}_3 - U_2 = +\frac{2}{\gamma''-1}\frac{1}{a_0}(a^{\cdot}_3 - a_2) + (\Delta U^{\cdot}_A)_{II} \quad \left.\right\} \quad (24)$$

Subtracting these two equations and using the equality given by equation (22) gives:

$$U_2 - U_1 = -\frac{2}{\gamma'-1}\frac{1}{a_0}(a'_3 - a_1) - \frac{2}{\gamma''-1}(a^{\cdot}_3 - a_2)$$
$$-[(\Delta U'_A)_I + (\Delta U^{\cdot}_A)_{II}] \quad (25)$$

From equation (23):

$$a'_3 = a'_{0s}\left(\frac{a^{\cdot}_3}{a^{\cdot}_{0s}}\right)^{[(\gamma'-1)/(\gamma'-1)]\,(\gamma'/\gamma'')}$$

Eliminating a'_3 from equation (25) and rearranging gives:

$$\frac{a^{\cdot}_3}{a^{\cdot}_{0s}} = \left\{\frac{\gamma'-1}{2}\frac{a_0}{a'_{0s}}\left[(U_1 - U_2) - (\Delta U')_I - (\Delta U^{\cdot}_A)_{II}\right.\right.$$
$$\left.\left.+\left(\frac{2}{\gamma'-1}\frac{a_1}{a_0}+\frac{2}{\gamma''-1}\frac{a_2}{a_0}\right)-\frac{2}{\gamma''-1}\frac{a^{\cdot}_3}{a_0}\right]\right\}^{[(\gamma''-1)/(\gamma'-1)]\,(\gamma'/\gamma'')}$$

Let

$$K = (U_1 - U_2) - (\Delta U'_A)_I - (\Delta U^{\cdot}_A)_{II} + \left(\frac{2}{\gamma'-1}\frac{a_1}{a_0}+\frac{2}{\gamma''-1}\frac{a_2}{a_0}\right)$$

$$K_1 = \frac{\gamma'-1}{2}\frac{a_0}{a'_{0s}}$$

$$K_2 = \frac{2}{\gamma''-1}\frac{a^{\cdot}_{0s}}{a_0}\frac{1}{K}$$

and

$$n = \frac{\gamma''-1}{\gamma'-1}\frac{\gamma'}{\gamma''}$$

then

$$\frac{a^{\cdot}_3}{a^{\cdot}_{0s}} = \left[K_1\left(1 - K_2\frac{a^{\cdot}_3}{a^{\cdot}_{0s}}\right)\right]^n \quad . \quad . \quad (26)$$

Expanding equation (26) by the binomial theorem and neglecting second and higher order terms gives to the first approximation the value of $a^{\cdot}_3/a^{\cdot}_{0s}$, i.e.

$$\frac{a^{\cdot}_3}{a^{\cdot}_{0s}} = \frac{K^n}{1 + nK_2K_1^n} \quad . \quad . \quad . \quad (27)$$

To evaluate a region of state such as region 3, Fig. 14, however, an iteration procedure is necessary to solve equation (27) owing to the presence of the terms $(\Delta U_A)_{i, II}$. Once satisfactory convergence to the $a^{\cdot}_3/a^{\cdot}_{0s}$ value is obtained from equation (27), further iteration is necessary to obtain the true state $a^{\cdot}_3/a^{\cdot}_{0s}$ using equation (26). This completed, the value of a'_3/a'_{0s} can be found from equation (23). Use of the characteristic state equation (21) will then yield the value of U_3 and hence the state of region 3 is completely defined.

(3) *Solution for irreversible flow with variable specific heats*

The method of solution for a region containing a temperature discontinuity when the effects of wall friction, heat transfer and area change are present is very similar to that of case (2). The only additional complication involved is determining the change in the value of a_{0s} for both hot and cold parts of the region considered.

The characteristic state equation (11), written in finite difference form, is:

$$(\Delta U')_I = -\frac{2}{\gamma'-1}\left(\Delta\frac{a'}{a_0}\right)_I - (\Delta U'_{q+F})_I - (\Delta U'_A)_I \quad \left.\right\}$$
$$(\Delta U^{\cdot})_{II} = +\frac{2}{\gamma''-1}\left(\Delta\frac{a'}{a_0}\right)_{II} - (\Delta U^{\cdot}_{q+F})_{II} + (\Delta U^{\cdot}_A)_{II} \quad \left.\right\} \quad (28)$$

Hence following the same argument as in case (2), but using equation (28) to replace equation (21), yields the result:

$$\frac{a^{\cdot}_3}{a^{\cdot}_{0s}} = \left[K_1\left(1 - K_2\frac{a^{\cdot}_3}{a^{\cdot}_{0s}}\right)\right]^n \quad . \quad . \quad (29)$$

Expanding equation (29) by the binomial theorem and neglecting second and higher order terms gives to the first approximation the value of a''_3/a''_{0s}, i.e.

$$\frac{a''_3}{a''_{0s}} = \frac{K_1{}^n}{1+nK_2K_1{}^n} \qquad \ldots \quad (30)$$

where

$$K_2 = \frac{2}{\gamma'-1}\frac{a''_{0s}}{a_0}\frac{1}{K}$$

and

$$K = K - [(\varDelta U''_{q+F})_{II} + (\varDelta U'_{q+F})_{I}]$$

As an example, consider the superimposition region 4·6, Fig. 15, of the rightward moving wave from region 4·5 and the leftward moving wave from region 3·6. The method of solution is as follows:

(1) To find the first approximate state ($\sim$ 4·6) construct characteristics in the state and position diagrams neglecting the effects of friction and heat transfer with the aid of the equations developed in case (2).

(2) The approximate mean time ($\varDelta t_{path}$) for particles arriving in region 4·6 from region 3·5 can be obtained by direct measurement from the position diagram. Substitution of this ($\varDelta t_{path}$), together with the mean values for the other variables in equation (8) for both sides of the discontinuity gives the first approximation to the values of a'_{0s} and a''_{0s} for region 4·6. The values of a, γ, f and q will be different for each of these paths.

(3) Using the approximate mean values for the variable parameters between state 4·5 and 4·6' and state 3·6 and 4·6'' and the measured values of $(\varDelta U_{q+F})_{I,\,II}$ the first approximation to the value of the correction terms $(\varDelta t)_{I,\,II}$ can be computed.

(4) A close approximation to the value of $a_{4\cdot6}/a''_{0s}$ can now be evaluated by the solution of equation (30) and the true state 4·6 by solution of equation (29).

(5) The procedure outlined in paragraphs (2), (3) and (4) above is repeated until satisfactory convergence of the values of $u_{4\cdot6}$ and $P_{4\cdot6}$ are obtained.

APPENDIX 2

SOLUTION OF THE UNSTEADY FLOW EQUATIONS WITH THE FORMATION OF A SHOCK WAVE

To evaluate the constant of proportionality in the equation $\varDelta U \propto 2/(\gamma-1)(a_{0s}/a_0)\varDelta X$ it is necessary to find the equation to the tangent of the shock polar, as defined by equations (13) and (14), and is achieved as follows:

Differentiating equations (13) and (14) with respect to W_x gives:

$$\frac{dU}{dW_x} = \pm\frac{2}{\gamma-1}\frac{a_{0sx}}{a_0}X_x\frac{W_x{}^2+1}{W_x{}^2}$$

$$\frac{dX}{dW_x} = 2\frac{\gamma-1}{\gamma+1}\frac{X_xW_x}{\left[1+\frac{2\gamma}{\gamma+1}(W_x{}^2-1)\right]^{(\gamma+1)/2\gamma}}$$

Hence the equation to the tangent of the shock polar at any point W_x is:

$$\varDelta U = \pm\frac{2}{\gamma-1}\frac{a_{0sx}}{a_0}\left[\frac{W_x{}^2+1}{2W_x{}^3\left[1+\frac{2\gamma}{\gamma+1}(W_x{}^2-1)\right]^{(\gamma+1)/2\gamma}}\right]\varDelta X$$

$$\ldots \quad (31)$$

or

$$\frac{\varDelta U}{\varDelta X} = \pm\frac{2}{\gamma-1}\frac{a_{0sx}}{a_0}K \qquad \ldots \quad (32)$$

where

$$K = \frac{W_x{}^2+1}{2W_x{}^3\left[1+\frac{2\gamma}{\gamma+1}(W_x{}^2-1)\right]^{(\gamma+1)/2\gamma}}$$

$$\equiv \left(\frac{1+W_x{}^2}{1+W_x{}^3}\right)\left(\frac{X_x}{X_y}\right)\left(\frac{P_y}{P_x}\right) \qquad \ldots \quad (33)$$

The equation (31) or (32) is of the form $\varDelta U \propto 2/(\gamma-1)(a_{0s}/a_0)\varDelta X$ and the value of the constant of proportionality K can be evaluated on substitution of the appropriate value of W_x for the region under consideration.

The application of equation (31) or (32) enables a straight line construction between states 1 and 3 to be effected and thus eliminates the necessity for repeated solution of equations (13) and (14) for arbitrarily selected values of W_x.

Application of the shock equations to the flow in plain ducts

As a practical example, consider a strong shock wave advancing into a continuous wave train, Fig. 16. Since the change in entropy across the shock from region 2 to region 3 will be much greater than that resulting from the heat transfer and wall friction effects for the same region, the latter effects may be neglected.

Given the data (u, a, x, t) at the two state points 1 and 2, it is necessary to find similar data at the intersection point 3 of the II characteristic passing through the point 1a and the shock polar through 2. The method of applying equation (31) is outlined below.

(1) The II characteristic through the state point 1a is constructed.
(2) From the characteristic equation (11), but neglecting the term representing the secondary effects, the approximate I charac-

a Position diagram.
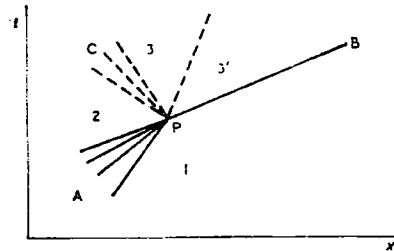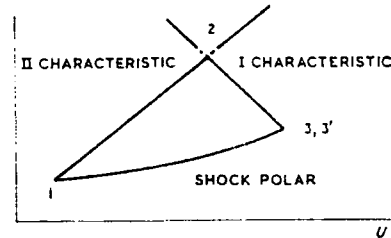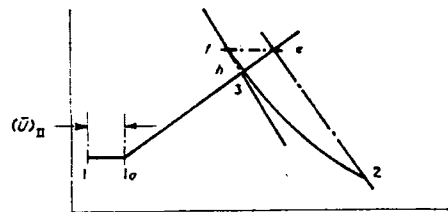
b State diagram.

c State diagram.

Fig. 16

teristic may be drawn through the state point 2 and the state point e determined. The values of γ and a_{0e} used in equation (11) are those appropriate to region 2.

(3) By use of the value of X appropriate to the approximate state e and the known values of state 2, the shock propagation velocity W_2 is calculated from equation (14). The value of U_f for the state f is now obtained from equation (13) on substitution of the known value of U_2 and the above value of W_2.

(4) The tangent to the shock polar at f can be evaluated from equation (31) in which the terms W_x and a_{0sx} are replaced by W_2 and a_{0s2} respectively.

(5) Constructing the tangent through the point f in Fig. 16 determines the position of the point h. This point lies at the intersection of the tangent through f and the II characteristics through the point 1a.

(6) With the value of X_h known, the shock polar value of U appropriate to this pressure is obtained by simultaneous solution of equations (13) and (14) on substitution of the known values for region 2.

(7) The steps 3, 4, 5 and 6 are repeated until satisfactory convergence is obtained for the unknown state 3, i.e. until the calculated shock polar value of U agrees with that at point h in Fig. 16.

APPENDIX 3

REFERENCES

(1) JENNY, E. 'Berechnungen und Modellversuche über Druckwellen grosser Amplituden in Auspuff-Leitungen', Thesis E.T.H. 1949 (see *Brown Boveri Rev.* 1950 **57** (No. 11), 449).

(2) WALLACE, F. J. and NASSIF, M. H. 'Air flow in a naturally aspirated two-stroke engine', *Proc. Instn mech. Engrs* 1954 **168**, 515.

(3) WRIGHT, E. H. and GILL, K. F. 'Influence of exhaust induction systems on air consumption of a two-stroke oil engine', *Engineer, Lond.* 1963 **216** (No. 5618), 501.

(4) WRIGHT, E. H. and GILL, K. F. 'Theoretical analysis of the exhaust system of an oil engine', *Engineer, Lond.* 1964 **218** (No. 5666), 311.

(5) BENSON, R. S., GARG, R. G. and WOOLLATT, D. 'A numerical solution of unsteady flow problems', *Int. J. mech. Sci.* 1964 **6** (No. 1), 117.

(6) BENSON, R. S., GARG, R. G. and WOODS, W. A. 'Unsteady flow in pipes with gradual or sudden area changes'. *Thermodynamics and Fluid Mechanics Convention, Proc. Instn mech. Engrs* 1963–64 **178** (Pt 3I, paper 9).

(7) McADAMS, W. H. *et al.* 'Measurement of recovery factor and coefficient of heat transfer in a tube for subsonic flow of air', *Trans. Am. Inst. chem. Engrs* 1946 **42**.

(8) DE HALLER, D. 'The application of a graphic method of some dynamic problems in gases', *Sulzer Tech. Rev.* 1945 **1**, 6.

(9) BANNISTER, F. K. and MUCKLOW, G. F. 'Wave action following sudden release of compressed gas from a cylinder', *Proc. Instn mech. Engrs* 1948 **159**, 269.

(10) SHAPIRO, A. H. *The dynamics and thermodynamics of compressible fluid flow* 1954 (The Ronald Press Co., New York).

(11) WALLACE, F. J. and MITCHELL, R. W. S. 'Wave action following sudden release of air through an engine port system', *Proc. Instn mech. Engrs* 1952–53 **1B**, 343.

(12) BENSON, R. S. 'Influence of exhaust belt design on discharge process in two-stroke engines', *Proc. Instn mech. Engrs* 1960 **174**, 713.

(13) COLEBROOK, C. and WHITE, C. M. 'Experiments with fluid friction in roughened pipes', *Proc. roy. Soc.* 1937 **161** (Series A), 367.

(14) MOODY, L. 'An approximate formula for pipe friction factors', *Mech. Engng* 1947 **169**, 1005.

(15) KEENAN, J. H. and KAYE, J. *Gas tables* 1948 (J. Wiley and Sons, New York).

6. GAS FLOW MEASUREMENT

PAPER 15

1

Automatic Control of Pulsating Air Flow

by *K. F. Gill, B. W. Imrie
and G. E. Harland

*The time-mean differential pressure associated with the mass flow
of air through a BS square-edged orifice will, for constant mass
flow, be changed by variation in the flow condition from steady
state through a range of pulsation frequencies.*

*The application of feed-back control to maintain a constant
mass flow rate under varying conditions of pulsation is investigated
for a frequency range up to 120 Hz. A two-term controller is used
in an error-actuated system in an attempt to estimate to what
extent it is possible to maintain a desired mass flow rate.*

*An on-line analogue computer is used for data processing and
for the simulation of the hold device and controller used in the
feed-back loop of the system. The method of data processing is
shown to be useful both for eliminating tedious graphical measure-
ment and for widening the scope of the research into the problems
associated with pulsating flow measurements.*

INTRODUCTION

The normal industrial practice for the measurement of pul-
sating mass flow is to use a receiver or expansion volume to
minimise the pressure/velocity variations present and thus
permit flow measurement according to the requirements of BS
1042 : 1964.[1] Situations exist for which this method is not con-
venient due to either the receiver size required or the flow require-
ments of particular processes such as material transport by fluidi-
sation (Roots blower).

For industrial requirements of flow measurement Ramsay[2]
established that the plate orifice, with appropriate pressure and
temperature tappings, was the metering system most frequently
used in the United Kingdom. The plate orifice has many practical
advantages as far as size and installation considerations are
concerned. At present, however, theoretical considerations
applied to conventional pressure measurements at an orifice
are inadequate for estimation of the mass rate of pulsating flow.
Much useful work has been reported by other researchers in this
field.[3-9] To a certain extent, such work has been incorporated
in a draft proposal[10] for an International Standard of flow meas-

Department of Mechanical Engineering, University of Leeds.

urement of pulsating fluid flow.

If an acceptable and repeatable accuracy of pulsating flow
measurement can be established for an orifice plate system, using
the measurement of instantaneous differential pressure only.
then the continuous monitoring and automatic control of a flow
process becomes possible if on-line computer facilities are avail-
able.

The measurement of the time-mean differential pressure as
indicated by the conventional secondary element of the correctly
designed liquid manometers.[11] if used in the standard steady
flow equation[1] for the measurement of pulsating flow. will intro-
duce a 'square-root' error. This square-root error may be re-
moved if the Time Mean Square Root (TMSR) of the time-
dependent differential pressure is used instead of the manometer
mean differential pressure.

The continuous monitoring of this quantity requires the avail-
ability of a suitable on-line computer if it is to be used in the
automatic control of a flow process. Any discrepancy between the
actual mass flow and the mass flow inferred from the TMSR
differential pressure will be due to modifications of the differ-
ential pressure because of inertia effects associated with the choice
of tapping points and due to neglect of the variation of discharge
coefficient (ie vena contracta) with frequency. In an attempt to
minimise the effect of such inaccuracies in the flow measurement,
the differential pressure across the square-edged orifice plate was
measured between tapping points at one diameter D upstream of
the orifice plate and at the downstream corner C position.

The TMSR was evaluated together with other measurements
of the differential pressure wave-form for a range of mass flows
and frequencies and was subsequently used, for control purposes,
as a close approximation to the actual mass flow for any given
condition. The process chosen for control application of the
TMSR of differential pressure is shown in Figure 1A. and
simulates a hypothetical. non-steady flow installation which is
to be controlled automatically to supply any required mass flow.

OBJECTIVES

The initial problem was the calculation, for a range of fre-
quencies, of the value of the instantaneous square-root of a

Fig. 1A. Block Diagram Representation of the Hypothetical Non-Steady Flow Process
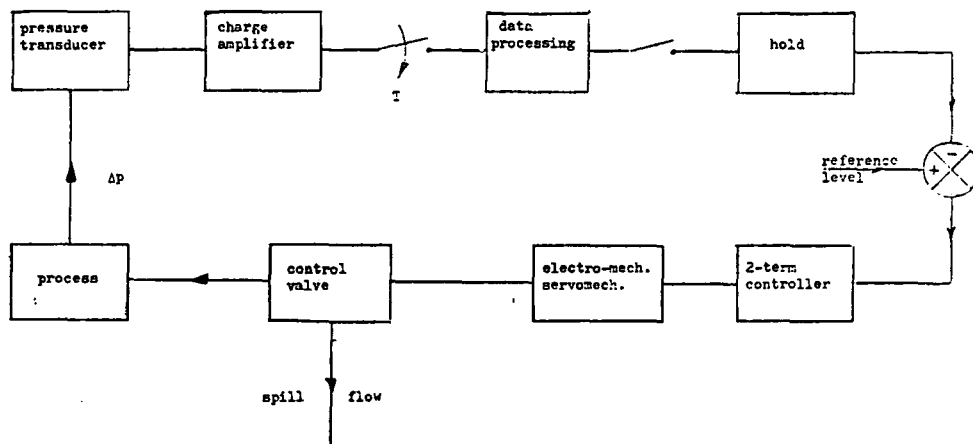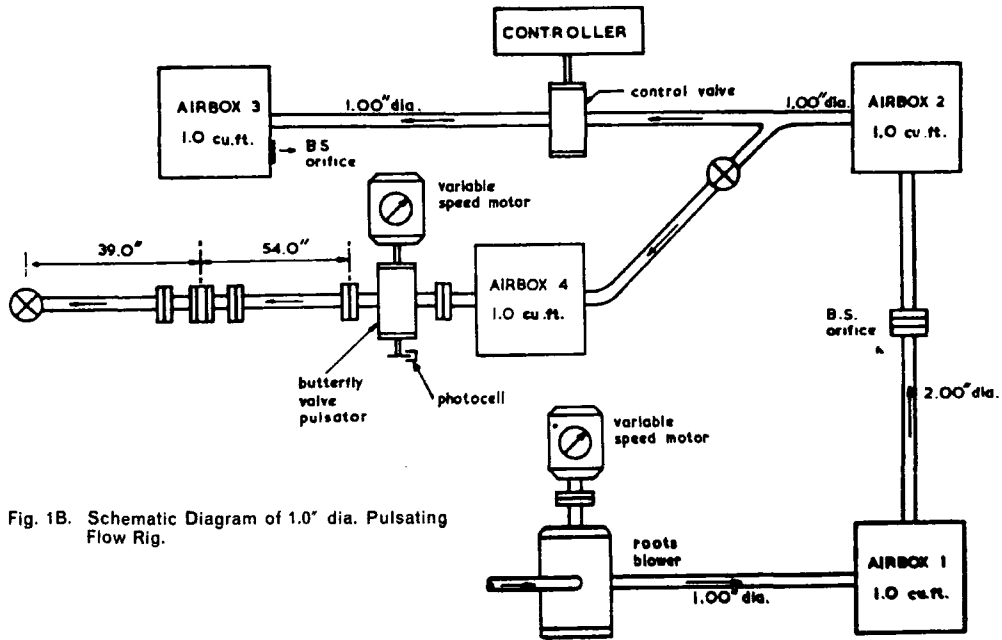
Fig. 1B. Schematic Diagram of 1.0" dia. Pulsating Flow Rig.

differential pressure waveform which had both positive and negative amplitudes with respect to a zero flow datum. The approach adopted was to apply the technique used in the conventional and laborious methods of graphical measurement in which the sign of the recorded trace is ignored. The algebraic characteristic of the recorded waveform is accounted for in the evaluation of the integral of the square-root of the instantaneous pressure measurement. The computer diagram for this calculation is shown in Figure 3A. A similar treatment was adopted for the processing of the pressure waveform measured at the upstream tapping point of the square-edged orifice system used to monitor the pulsating airflow.

Pressure traces were recorded and measurements taken for a range of frequencies and for different mass flow rates so that this part of the investigation would provide an assessment of the monitoring section frequency characteristics and of the validity of using the TMSR differential pressure as an indication of mass flow rate.

With the achievement of the above objective the final problem was that of tracking and storing the TMSR value during each sampling period. Tracking of the TMSR value occurred during the time interval for which this value was held constant and the TMSR value was then stored prior to zero reset of the monitoring circuit. This track and store operation was made possible by use of the computer circuit shown in Figure 3B and will be described in detail later in the paper.

The storing of the TMSR value was necessary for comparison with a preselected reference value to generate an actuating error signal for the control loop. The difference between these two values was used directly as the input to the 2-term controller which repositioned the electro-mechanical servomechanism, until the actuating error signal was zero, in an attempt to maintain constant flow through the monitoring section.

DESCRIPTION OF THE TEST RIG

Figures 1B and 2 show details of the flow system which is basically similar to that described in an earlier paper.[12] The modified system shown schematically in Figure 1B incorporates a 2-in dia pipe section with a 0.7435 in dia BS square-edged orifice plate and corner pressure tappings, which was used for the measurement of mass flow. Downstream of this metering section the flow is divided between two branches one of which contains the monitoring or test section and the other contains the controlled valve. The test section was redesigned to accommodate a square-edged orifice plate, 0.6628 in dia. clamped between O-rings and to provide different tapping point locations.

The variable speed drive of the butterfly pulsator valve included a secondary reduction gear box to provide rotational stability at the low speed end of the motor. The control valve in the second branch is positioned by means of an electro-mechanical servo mechanism and the airflow through this branch is measured by a

Fig. 2. Flow Rig.

Fig. 3A. Data Processing and Reset Circuits

0.6702 in dia BS orifice plate located in AIRBOX 3.

For manometer measurement of pressures under pulsating flow conditions, three different liquids were available: silicone fluid (0.82), carbon tetrachloride (1.58) and mercury (13.6). Care was taken in the design of the manometer system that the bore of the manometer, connections and tappings was uniform at 2 mm which also corresponded to the bore of the transducer connections for measurement of time-dependent pressure. Manometer and transducer measurements were taken at geometrically similar tapping points (asymmetrical pressure variations being negligible). Temperatures were measured by chromel-alumel thermocouples in conjunction with a Comark Electronic Thermometer.

Computer System—Monitoring and Processing Circuits

The monitoring circuit consisted of a proprietary piezo-electric differential pressure transducer connected to a charge amplifier, the output of which was linked to an analogue computer, installed in another laboratory, through 400 yards of low-loss co-axial cable. The cable specification is: impedance 75 Ω, attenuation 0.68 dB at 10 MHz per 100 yard length.

Pressure signals were produced by two different transducers— Kistler 7251 differential pressure transducer and Kistler 412 pressure transducer at the upstream pressure tapping. The output from Kistler 568 charge amplifiers was also observed on a Tektronix 564B storage oscilloscope throughout the tests.

The computer used for processing the instantaneous differential pressure measurements is an EAL Ltd., 231R parallel-logic hybrid analogue computer. The controller for the flow system was also simulated on this machine and the command signals generated were used to drive the electro-mechanical servomechanism which adjusted the opening of the valve in the spill flow line, see Figure 1A.

The co-axial link was connected to the first amplifier of the monitoring stage as shown in Figure 3A. To discriminate between the positive and negative components of the incoming voltage signal it was necessary to provide a two-branch link to the square-root unit (M16). The conducting branch is determined by the polarity of the output of amplifier (A12) by means of the comparator (MO). The comparator closes one or the other D/A switch, (32) or (33). The D/A switch characteristics are: switching time 5 µs, drift 4 mV/3m at $\pm$100 V, and this specification is adequate for the polarity change rates occurring at the output from amplifier (A12). The specifications of the square-root unit (M16) are: full-scale error $\pm$0.01 per cent, bandwidth 30 KHz, again adequate for test requirements.

The output from (M16) is connected to the integrating ampli-

fier (A25) through a similar two-branch link synchronised by the same comparator (MO) through D/A switches, (30) and (31).

The output from amplifier (A25) is the TMSR value of the time-dependent differential pressure $(1/T)$ $\int_0^T \sqrt{\Delta_p}\, dt$ where T is the sampling period.

The control of the monitoring circuit is achieved by means of a triangular waveform, generated separately, of period $2T$ duration controlling the D/A switches (20) and (21) through the comparator (M2). The reset of amplifier A25 is made possible by using a section of the same triangular waveform to close the relays of comparator (M1) thus permitting a short-duration pulse of 45V to be applied to the reset coils of amplifier (A25) as shown in Figure (3A). The switching level of comparator amplifier (M1) is $\pm$ 5 mV.

Control Circuit

The analogue computer circuit for the closed-loop control of the spill flow valve is shown in Figure 3B. The controller used is a simple 2-term controller in which a proportional gain of 1.3 and an integral time of 3.7 seconds was selected in conjunction with a sampling time ($T = 1$ second) to ensure system stability.

The hold device was controlled by the logic output of comparator amplifier (M2) and tracked and stored for the finite time interval in which the TMSR output from amplifier (A25) was held constant. This was made possible by use of the parallel-logic associated with the analogue computer. The circuit for

Fig. 3B. Control and Hold Circuits

the track and store device is shown in Figure (3B).

Electro-Mechanical Servo

Some kind of electro-mechanical transducer was necessary to convert the electrical controlling signal from the analogue computer into rotational movement of the spindle of the butterfly control valve used in the spill flow line. A proprietary electro-mechanical servomechanism was used for this purpose since it was readily available in the laboratory. A block diagram representation of the system is shown in Figure 1B.

TEST PROCEDURE

The investigation was carried out in two parts. The first part of the test programme was to establish basic information on flow characteristics of the test section and to confirm the validity of the monitoring and processing circuits used on the computer for acceptance and processing of the pressure signals produced by the two transducers used to measure differential and upstream pressure.

The calibration factor for each transducer was set accurately, on its respective charge amplifier, by application of a calibrated square-wave voltage signal through a 1000 pF capacitor to the input of the charge amplifier and adjustment of the calibration setting for the calculated output measured by a digital voltmeter. This calibration was separately checked for the complete recording system under steady flow conditions by comparing manometer readings with corresponding oscilloscope trace movements.

The second part of the test programme involved the use of the box orifice plate to measure spill flow past the butterfly control valve when under closed loop control. An intermediate level of flow was selected as an appropriate datum and the control valve was positioned so that the spill flow could be either increased or decreased according to the variation from the reference datum of the TMSR value.

Twelve different frequencies were examined in the range 10–120 Hz. For each constant frequency selected, three different levels of mass flow were investigated for the system operating under closed loop control. Appropriate manometer measurements were taken at the 2 in. dia. pipe orifice and at the box orifice so that the mass flow through the monitoring section under pulsating conditions could be evaluated accurately. The differential pressure oscilloscope trace was photographed for each set of observed results.

As in the first part of the investigation, the calculated characteristics of the differential pressure waveform were obtained from the analogue computer. In the first part of the investigation a sampling time of T = 5 seconds, was chosen to obtain a representative average TMSR value pressure differential over a reasonable number of pressure pulsations at the lower frequencies.

For closed loop control a loop gain was chosen which minimised the effect of deadband and gear backlash of the electro-mechanical positional servomechanism used. With this system gain it was necessary to reduce the sampling time, T, to 1 second to prevent limit cycle oscillations within the closed loop. Any drift in the track and store element used in the loop would be accordingly reduced and the system accuracy improved.

EQUATIONS AND ANALYSIS

The basic standard equation 1, for mass rate of flow or real fluids is:

$$M = \text{constant} \times CZE \ \varepsilon d^2 \ (h\rho)^{\frac{1}{2}} \qquad (1)$$

Where $Cds = CZ\varepsilon$ may be considered as an overall discharge coefficient for compressible fluid flow.

Adapting equation (1) for flow measurement manometer readings under pulsating flow conditions, the indicated time-mean mass flow rate is given by:

$$\bar{M}_i = \text{constant} \times C_{dp} \ (\rho_p \ \bar{\Delta}_p)^{\frac{1}{2}} \qquad (2)$$

and C_{dp} may be obtained if the mass flow is measured separately under steady flow conditions as a reference. Inaccuracies may be due to manometer error whereby the manometers used may
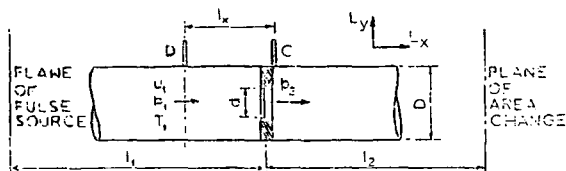
Fig. 4. Schematic of Orifice System.

not give a true time-mean value of the differential pressure Δ_p. This quantity, Δ_p is time-dependent and a square-root error arises from the inequality

$$\frac{1}{T} \int_0^T \left(\Delta_p \right)^{\frac{1}{2}} dt \neq \left(\frac{1}{T} \int_0^T \Delta_p \ dt \right)^{\frac{1}{2}}$$

where the time-mean differential pressure $\bar{\Delta}_p = \frac{1}{T} \int_0^T \Delta_p \ dt$

This can be avoided by consideration[13] of instantaneous mass flow rate

$$\dot{m}_i = [\text{constant} \times CZE \ \varepsilon d^2 \ (\rho_p \Delta_p)^{\frac{1}{2}}]_{\text{inst.}} \qquad (3)$$

and the total mass flow $\dot{M} = \left(\frac{1}{T} \right) \int_0^T \dot{m}_i \ dt \qquad (4)$

If it is assumed that the velocity, $\bar{u}_1$, upstream of the orifice. Figure 4 is dependent on the system geometry as well as on the properties of the time-dependent flow then:

$$\bar{u}_1 = \Phi \ (\bar{\Delta}_p, A_p, \bar{p}_1, \eta, \bar{\rho}_1, f, d, (D-d), l_1, l_2, l_x) \qquad (5)$$

Where $\bar{\Delta}_p$ and A_p are the true mean and the amplitude values respectively of the differential pressure.

It may be shown that:

$$\frac{\bar{\rho}_1 \bar{u}_1^2}{\bar{\Delta}_p} = \Phi \left\{ \frac{\bar{\rho}_1 \bar{u}_1^2}{\bar{\Delta}_p}, \frac{\bar{\rho}_1 \bar{u}_1^2}{\bar{p}_1}, \frac{D-d}{d}, \frac{l_1}{l_x}, \frac{l_2}{l_x}, \frac{\bar{u}_1}{l_x f}, \right.$$

$$\left. \left(\frac{\bar{\rho}_1 \bar{u}_1 (D-d)}{\eta} \times \frac{(D-d)}{l_x} \right) \right\} \qquad (6)$$

or $\bar{\rho}_1 \bar{u}_1 = (\bar{\rho}_1 \bar{\Delta}_p)^{\frac{1}{2}} \ \Phi^1 \left[E_A, E_p, D \frac{-d}{d}, \frac{l_1}{l_x}, \frac{l_2}{l_x}, S, (R_{D-d} \frac{D-d)}{l_x} \right]$

$$\qquad (7)$$

where E_A and E_p are Euler numbers or pressure coefficients, $(D-d)/d$, l_1/l_x, l_2/l_x are geometry characteristics, S is the Strouhal number and $[R_{D-d} (D-d)/l_x]$ is a modified Reynolds number (see later).

If (5) is modified to include total head conditions of pressure P_{01}, and temperature T_{01}, then a non-dimensional mass flow number[14] may be obtained as $(\bar{u}_1 T_{01})/(p_{01} d^2)$ which is of importance for accurate comparison of corresponding flow rates through the same test section under steady flow and pulsating flow conditions.

THEORETICAL CONSIDERATIONS

(1) Choice of tapping points for measurement of the instantaneous differential pressure across a plate orifice.

For steady flow of air through a system as shown in Figure 4, BS 1042:1964 (1) permits different combinations of tapping points by which the differential pressure across the orifice can be measured. Upstream of the orifice plate, pressure tappings are permitted at a distance of one diameter D from the orifice plate and at the corner between the pipe wall and the orifice plate. Downstream of the orifice plate, pressure tappings are specified as corner C, $D/2$ and vena contracta. Different combinations of upstream and downstream tapping points will, in general,

give different measurements of the differential pressure.

For the purposes of this investigation a non-standard combination of tapping points was used for the measurement of the instantaneous differential pressure under steady flow and pulsating flow conditions. The following points were considered:

(2) Upstream Tapping Point

(2.1) The upstream corner tapping, under steady flow conditions, is affected by the impact pressure phenomenon which is described by Engel and Davies[15] who refer to other workers who have studied this problem. The local (corner) increase in pressure has also been referred to as a corner eddy effect, as a momentum defect (related to the concept of impact pressure) or as an effect of streamline curvature.

Under time-dependent flow conditions, work by Rudinger[16] suggests that the different mechanisms of compressive wave reflection from the orifice plate and rarefactive wave reflection from the orifice bore, will produce a non-homogeneous flow condition for an axial distance of approximately one diameter upstream of the orifice. Since the application of the flow equations requires the inference of fluid velocity from pressure measurement, the use of the corner tapping point under pulsating flow conditions will involve error. Hence the D upstream pressure tapping was used to correspond to a position at which the flow velocity and the static pressure would be uniform across the flow passage.

(3) Downstream Tapping Point

(3.1) For $D/2$ and vena contracta tappings, steady flow conditions permit a pressure measurement of a quasistable condition for which streamline curvature will be small. A mean velocity of the 'free' jet may consistently be inferred from the pressure measured at the duct wall and non-isentropic effects should be small.

For pulsating flow conditions the physical concept of a vena contracta has doubtful significance and the Schultz-Grunow hypothesis[17]—as reported by Engel[18] is of interest. It may also be postulated that a non-homogeneous pressure wave region exists immediately downstream of the orifice plate and is similar to that discussed in (2.1) but with a smaller effect. However, it is apparent that the proposition of periodic changes occurring in the cross-section of the free jet will undoubtedly affect the discharge coefficient and the associated concept of a vena contracta.

(3.2) While the downstream corner tapping point C is acceptable for steady flow measurements, pulsating flow conditions still have the problem of a wall pressure tapping remote from the time-dependent velocity of the free jet issuing from the bore of the orifice. Having considered the work of Baird and Bechtold[19] it is felt that the corner tapping provides a pulsating flow pressure measurement which will permit the most accurate interpretation of phase differences between pressure and velocity at the same station and between upstream and downstream pressures under the same conditions. The flow will have experienced negligible free surface shearing and the fluid inertia between the tapping points is minimised for this choice of downstream tapping point.

The disadvantages of using D-upstream and C-downstream tapping points to measure the differential pressure is that the metering system is not symmetrical for flow reversals. As a compromise, it may be that flange taps would give the most reliable measurements for pulsating flow in which flow reversals are significant.

(4) TMSR Value of Differential Pressure

The most sensitive *single* measurement of pulsating air flow through an orifice is that of the differential pressure. Fortier[10] has discussed the usefulness of the mean differential pressure and has rejected it, on theoretical grounds, as a single effective description of the flow rate. Janota[13] has referred to the technique of mass flow measurement by the integration of the instantaneous mass flow. This technique involves the TMSR value of the differential pressure and this *single* quantity has been chosen for the investigation as an accurate indication of mass flow rate.

(5) Choice of Flow Parameters for Description of Pulsating Flow Measurement Characteristics

Dimensional transformation deals with the fundamental equations of fluid flow and is more general than dimensional analysis which is usually applied to a flow situation involving specific geometric and kinematic variations.

Earles and Zarek[6] have used both techniques in the interpretation of the variables involved in mass rate measurement of pulsating flow using an orifice plate system. Engel,[20] has used dimensional transformation together with 'model laws' of dynamic similarity to establish fundamental and complete, ie dimensionally homogeneous parameters which may be applied to time-dependent flow. Engel's work has been discussed[21] by one of the authors and interpretations of the Strouhal number and of the Reynolds number have been established on a common basis of fluid convective inertia and by applying Huntley's[22] vector length concept of linear dimensions having directional significance: Lx, Ly, Lz.

The above considerations were used[12] in applying dimensional analysis to the pulsating flow problem and the following representations of Strouhal and Reynolds number differ only slightly from those previously established.

The Strouhal number is defined[21] as the ratio of convective inertia to temporal inertia and is similarly described by Szebehely[23]. Thus, referring to Figure 4, $S = u_1/l_x f$.

The choice of l_x instead of l_1 or l_2 as equivalent Lx dimensions is also influenced by the contributions to pulsating flow measurement of McCloy[5] and of Benson and El Shafie.[3] Resonance or standing waves are a special frequency/geometry effect and geometry dependence may be allowed for by a modification of the Strouhal number, without loss of completeness, to

$$S = \frac{u_1}{l_x f} \cdot \frac{l_1}{l_2} \quad \text{or} \quad S_r = \frac{a_1}{(l_1 + l_2)f} \quad \Phi(m)$$

where S_r may serve as a simple resonance criterion using the local speed of sound, a_1.

The modification of a dynamically similar parameter by a consistent geometric factor is not without precedent but should not be confused with an arrangement of factors, discussed below, for Reynolds number. In discussing Strouhal number as a parameter, there is also agreement with the views expressed by Engel[18] and by Earles[24] that a distinction should be drawn between the Strouhal number and the Hodgson number on the basis that, while the Hodgson number may be regarded as a modified Strouhal number, it is a criterion only and not a fundamental parameter.

Analysis of a Reynolds number for flow in an axi-symmetrical pipe (D or $d \equiv Ly \equiv Lz$) shows that a Reynolds number may be expressed as $R = u_1 Ly/v \cdot Ly/Lx$.

The ratio (Ly/Lx) is invariably omitted and Ly is usually chosen as D or d to produce R_D and R_d the Reynolds numbers based on pipe and orifice diameters respectively.

R_D represents a description of the pipe flow condition at the upstream tapping while R_D has the disadvantage of an incomplete description of fluid inertia effects at the orifice plate. It is suggested that the use of the dimension $(D - d)$ has greater physical significance and the 'blockage' Reynolds number would be complemented by an orifice blockage description: $(D - d)/D = 1 - \sqrt{m}$.

If Lx is chosen as l_1 the parameter would not be a useful description of the inertia effects at the orifice plate and thus l_x is chosen to produce a modified and complete blockage Reynolds number:

$$R_B = \frac{u_1}{v}(D - d) \cdot \frac{D - d}{l_x}$$

Engel[8] has referred to a similar composite number $R_b = \frac{u_1 D}{v} \cdot \frac{D}{l_1}$ and has separated an 'entry length' effect (D/l_1) but this is contrary to the concept of a 'complete' dimensionless number. The merit of the entry length concept lies in its significance as a
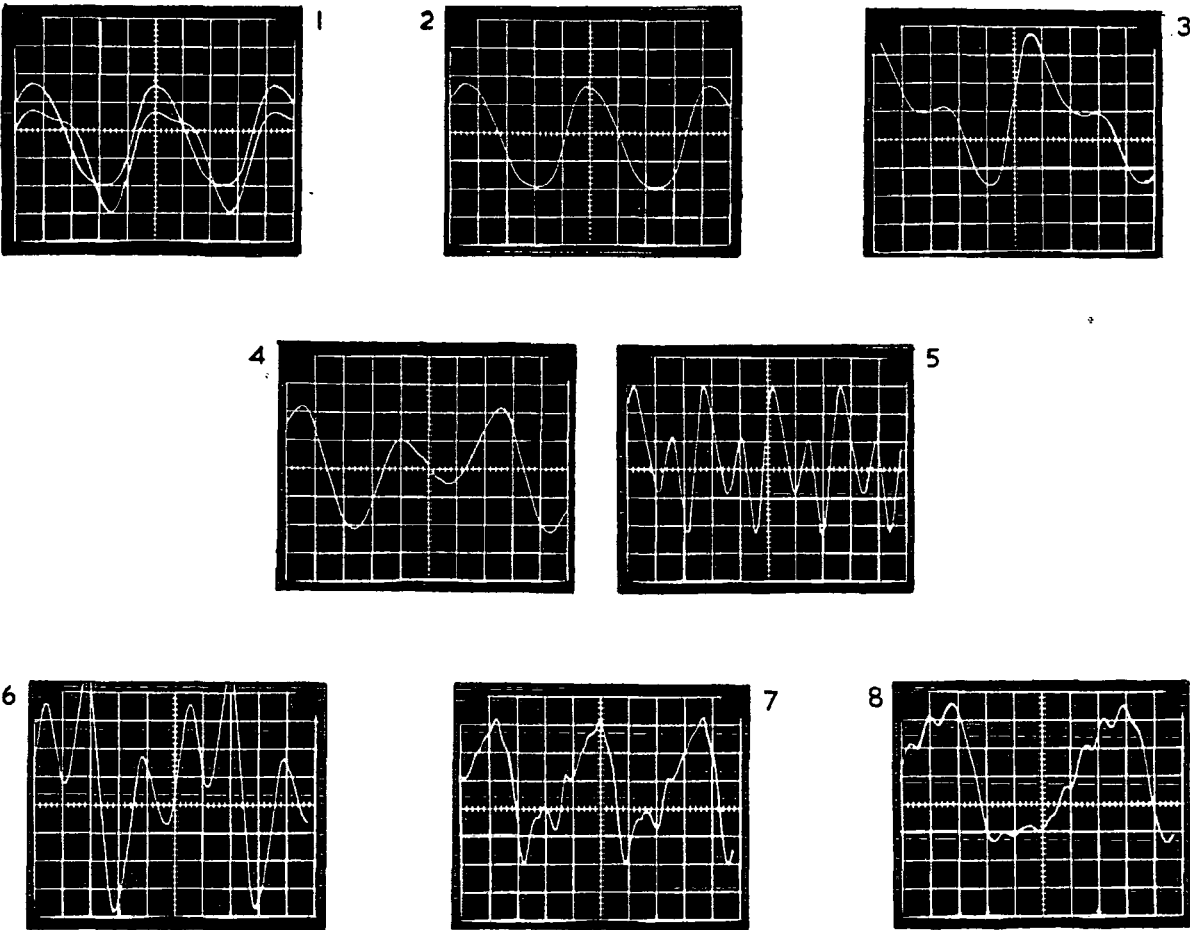
Fig. 5. Details or typical differential traces

Photographs		1	2	3	4	5	6	7	8
Details—(Test Number)		(27)	(27)	(29)	(31)	(54)	(58)	(59)	(60)
time base—ms/div	(o.r.)	2	2	2	2	5	5	10	10
vert. scale—V/div	(o.r.)	*1.0	0.5	0.2	0.1	0.1	0.1	0.1	0.1
frequency—Hz	(o.r.)	107.7	107.7	84.3	66.0	75.7	36.3	25.2	15
Strouhal No. (S)	(d.c.)	—	0.432	0.512	0.701	0.401	0.770	1.123	2.003
Range Factor (RF)	(a.c.)	—	4.59	2.94	3.15	5.33	5.27	3.62	3.71
mass flow—lbm/s	(d.c.)	—	0.0209	0.0193	0.0206	0.0134	0.0124	0.0125	0.0133
TMSR—$\sqrt{}$(in CCl$_4$)	(a.c.)	—	1.249	1.901	1.213	0.772	1.150	1.130	0.851
mass flow number (WMOD)	(d.c.)	—	0.0553	0.0513	0.0549	0.0361	0.0333	0.0336	0.0357
Reynolds No. (R_D)	(d.c.)	—	25 990	23 981	25 638	16 729	15 440	15 608	16 552
Reynolds No. (R_{D-d})	(d.c.)	—	2 679	2 472	2 642	1 724	1 591	1 608	1 706

* Photograph 1 shows the pressure trace indicated at the upstream tapping point (D) with a datum corresponding to atmospheric pressure.
All photographs have the trace datum at + 3 graticules.
(o.r.)—observed result
(d.c.)—digital computation
(a.c.)—analogue computation.
Calibration 0.0632 V/in CCl$_4$
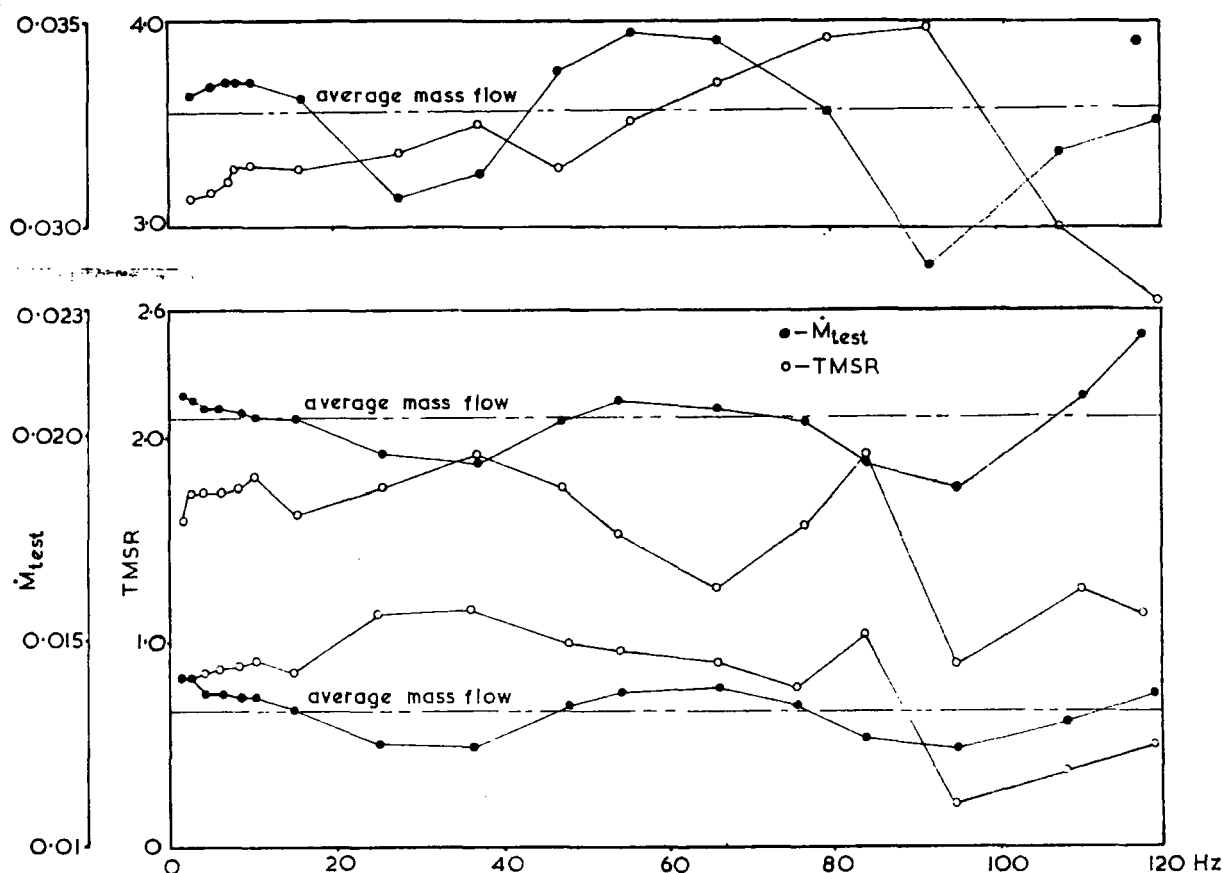
Fig. 6. Graph of M Test and TMSR (Δp) against Frequency

criterion and not as a separated parameter.

The above comments on Strouhal and Reynolds numbers are, of course, pertinent only to comparison of results which are otherwise geometry dependent.

DATA RETRIEVAL

Practical Difficulties

Over a wide range of frequencies, the differential pressure transducer output signal exhibited dc drift which affected the reference datum. Short-time-constant operation of the charge amplifier, which would have minimised drift, was not possible because of the requirement for measuring dc and ac components of the charge amplifier output signal at the analogue computer. Long-time-constant operation, under pulsating conditions, permitted an accumulation of drift over a period of time. This drift, under closed loop control, caused a change of flow rate through the monitoring section and, over long periods, would have given rise to large apparent controlled flow errors.

It was therefore necessary to allow the system to attain equilibrium after each change in test conditions and then to lock the spill-valve to prevent the computer taking further control action due to drift. Before the start of each test the air flow was stopped so that the datum conditions at the charge amplifiers could be re-established. Work is in hand to overcome the drift difficulty by using two, separate, matched pressure transducers and a stable differential amplifier to provide the differential pressure signal.

Another practical problem encountered was the effect on the track and store element of the oven thermostat in the analogue computer. The switching-on of the oven caused arbitrary changes in the value of the track and store output signal which made it necessary to introduce a saturation limit for the control signal to the positional servomechanism. Reducing the sampling time from 5 seconds to 1 second offset the effects of this problem.

Calculated Results

For the second part of the investigation the CONTROL ERROR was calculated as the percentage variation of test section flow from an arithmetic mean value of the tests involved, referred to the total flow supplied to the system. For variations in total flow, three different levels were tested to investigate the quality of the control loop. The variation in total flow was nominally $\pm$ 20 per cent.

DISCUSSION

Pulsating Flow Tests

The first part of the investigation was a preliminary to the application of closed loop control to a system which was to be monitored by a signal related to the mass flow of air through the test section. The tests provided basic information descriptive of the pulsating flow through the orifices. Some typical waveforms are shown in Figure 5, together with representative results obtained for each test condition.

The flow levels used in the tests were intended to be only approximately constant and Figure 6 shows the variation of mass flow and TMSR differential pressure with frequency. The directional changes of the controlling parameter and the quantity to be controlled are at variance with each other, and the assumed direct relationship between M_{test} and TMSR (Δ_p) is frequency dependent. This frequency dependence is probably due to variations in the discharge coefficient which is affected by changes in the time-dependent upstream static pressure and by flow reversal effects.

The effect of resonance condition is clearly seen in Figure 7 in which the non-dimensional flow number is plotted against Strouhal number for the three different mass flow levels. The variation of Strouhal number for this uniform frequency condi-

8
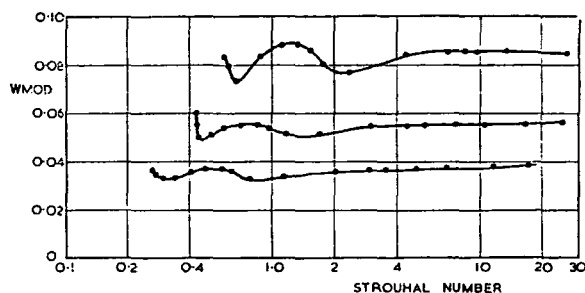
Fig. 7. Variation of WMOD with Strouhal Number

Fig. 8. Variation of Range Factor (RF) with Frequency for different flow levels

tion is, of course, due to the parameters plotted involving variations in u and log u.

The variation of Range Factor (RF) with frequency shown in Figure 8 illustrates the variety of conditions with which a control system might have to cope. This ac/dc ratio of the components of the differential pressure waveform clearly decreases with increase in $\dot{M}_{test}$ and changes markedly with changes in frequency of the pulsating flow.

Control Results

Figure 9 shows the variation of CONTROL ERROR with frequency. The error bandwidth is shown for the mass flow variation investigated at any one frequency. The arithmetic mean value for each frequency is also marked. The maximum CONTROL ERROR, with a mean value of − 14.5 per cent, occurs at a frequency, (88 Hz) for which a resonance condition may be inferred. Figure 8.

The dynamic characteristics of the simple control loop were not intended to accommodate the transient frequencies and amplitudes associated with this resonance condition. The CONTROL ERROR is dependent on frequency and the single parameter value (TMSR), used to indicate flow rates, is shown plotted against frequency in Figure 6.

Any non-linear variation of the mass flow rate through the test section with TMSR, Figure 6 will cause a variation in CONTROL ERROR and such an effect may be attributed to frequency-dependent phase changes in pressure (velocity) measurements across the test section. There will also be some error due to the time-dependent variation of the upstream pressure.

CONCLUSIONS

If the transducer drift problem can be resolved, the simple control loop experiments indicate that effective flow control can be exercised over a wide range of pulsation frequencies. For the range of investigation, if resonance (standing wave) conditions are avoided, the CONTROL ERROR is within practical limits
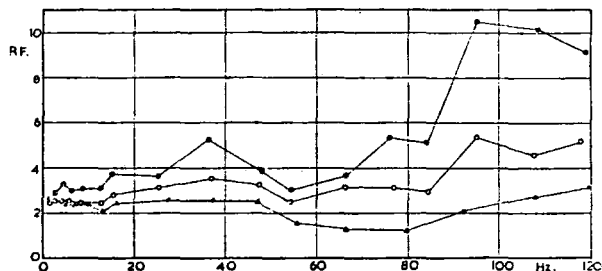
of ± 6 per cent, which can be improved by modifications to the monitoring of the differential pressure. The introduction of adaptive control to give a signal-dependent loop sensitivity may
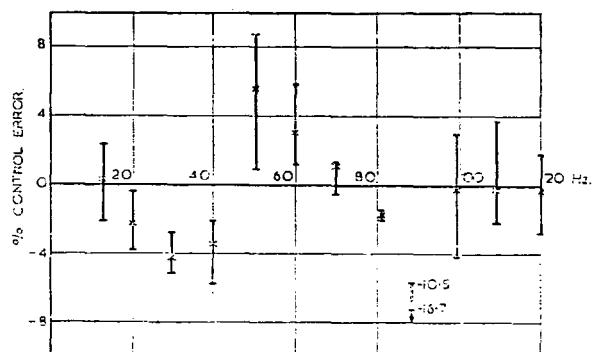
Fig. 9. % Control Error v Frequency.

reduce the overall percentage control error expected in the automatic control of pulsating air flow.

For the first part of the investigation the use of the analogue computer permits rapid and accurate calculation of the parameters and characteristics of pulsating air flow measurement. Square-root error can be investigated, together with the effects of wave shape, by sine-wave simulation of the actual differential pressure waveform and such an investigation is part of a comprehensive programme made possible by use of the analogue computer.

ACKNOWLEDGEMENT

The authors are very grateful for the assistance given in this project by Mr. K. Stables.

NOMENCLATURE

a	local speed of sound		ϵ	compressibility factor
A	amplitude of differential pressure waveform		η	dynamic viscosity
C	basic discharge coefficient		ν	kinematic viscosity
Cdp	overall discharge coefficient (pulsating flow)		ρ	density
Cds	overall discharge coefficient (steady flow)			
d	diameter of orifice		**Suffix**	
D	diameter of pipe		i	instantaneous
E	$1/\sqrt{(1 - m^2)}$		p	pulsating
f	frequency		r	resonance
h	differential pressure (B.S. 1042 : 1964)		s	steady
l	length		spill	spill flow
Lx, Ly, Lz	vector lengths		test	flow through test section
m	area ratio (d^2/D^2)			
$\dot{m}, M$	flow rate		*Non-dimensional numbers*	
p	static pressure		CDMOD	Discharge coefficient modified for total head conditions
p_0	total head pressure		E	Euler number
T	static temperature		R	Reynolds number
T_0	total head temperature		RF	Range factor
TMSR	time-mean square root		S	Strouhal number
u	velocity		WMOD	Mass flow number.
Δ	differential pressure			

84

PAPER 16

THERMODYNAMICS AND FLUID MECHANICS GROUP

A STUDY INTO THE USE OF PSEUDO RANDOM BINARY SEQUENCE PRESSURE DISTURBANCES TO MEASURE SONIC VELOCITY IN A TWO-PHASE FLOW SYSTEM

K. F. Gill, MSc, PhD, CEng, MIMechE*   E. W. Reed, MA, CEng, MIMechE†

A literature survey into gas–solids flow has revealed that most of the existing work is of a theoretical nature. Of fundamental importance to this theoretical work is the concept of sonic velocity. Presented here is a novel method that enables this parameter to be measured experimentally. The technique used is to inject small amplitude pseudo random binary sequence pressure disturbances into a two-phase flow system and compute a cross-correlation function between two measuring locations within the flow system. The time shift of the peak value of this function gives a direct measure of the sonic velocity existing between these two locations. The experimental results demonstrate that by using a pseudo random pressure disturbance on-line evaluation of sonic velocity becomes feasible.

1 INTRODUCTION

IN THE study of gas flow, the sonic velocity and Mach number are of such fundamental importance that attempts have been made to retain these concepts in the understanding of two-phase flow phenomena. The sonic velocity concept makes the gas dynamic equations more compact and indicates the boundary at which the choked flow condition occurs. A mathematical model describing a two-phase flow system would help in the interpretation of this behaviour in many physical processes. To help in the building of this model, experimental work is described which attempts to measure the sonic velocity in a two-phase flow system that to date has only been predicted theoretically. The stream studied is that of air and polystyrene particles.

A literature survey into gas–solids flow at both low and high speeds has revealed that most of the existing work on high speed flows is of a theoretical nature and was stimulated as a result of the presence of solid particles in the exhaust gases of solid-fuelled rocket engines (1)‡. The validity of these theories is such that, provided an estimation of the frictional drag due to the gas skin friction and the solids particle to particle and particle to duct wall interaction can be obtained, the numerical solution gives good results.

Cole et al. (2) have developed a theory and predict that the ratio of the sonic velocity in a gas–solids mixture to the sonic velocity in the gas stream alone will decrease as the

proportion of solids in the mixture increases; the experimental results of the authors support this prediction.

A possible secondary use to which the measuring technique described in this paper may be put is in helping other researchers to develop further measuring techniques which may be more applicable to certain processes. One such technique being investigated is the monitoring of solids flow rate in a gas–solids mixture by measuring the intensity of the sound emission from the flow. At the University of Leeds work is proceeding in this field and knowledge of the speed of sound, within the mixture under various conditions, may help to explain some of the results already obtained.

1.1 Notation

k Ratio of solids velocity to gas velocity.
M Ratio, $\dfrac{v_s}{v_g}$.
n Index of expansion for a two-phase system.
R Specific gas constant.
T Absolute temperature of gas.
t Time variable.
v_g Sonic velocity in pure gas stream.
v_m Mean velocity of stream flow.
v_s Sonic velocity in two-phase stream.
x Ratio of solids mass flow rate to gas mass flow rate.
γ Index of adiabatic expansion for a pure gas.
ζ Damping factor of pressure transducer.
τ Dummy time delay between $x(t)$ and $y(t)$.
τ_{max} Actual time delay between $x(t)$ and $y(t)$.
$\Phi_{xx}(\tau)$ Auto-correlation function of signal $x(t)$.
$\Phi_{xy}(\tau)$ Cross-correlation function of signals $x(t)$ and $y(t)$.

ω Rotational speed of disc in radians per second.

ω_n Undamped natural frequency of pressure transducer.

2 EXPERIMENTAL METHOD

Careful examination of equation (4) indicates the accuracy to which Φ_{xy} may be computed is directly dependent on the independent variable T. Since only finite duration sampling is possible experimentally, the choice of permissible disturbance suitable for use in flow measurement is severely restricted. It is suggested that the most suitable signal would be one periodic in nature, having a well defined maximum value for $\Phi_{xy}(\tau)$, and be readily injected into the flow system under investigation. One such signal that meets these requirements is known as a pseudo random binary sequence.

Pseudo random binary sequences (p.r.b.s.) are fully described in reference (1), and it is sufficient here to limit their description to the needs of this paper. See Appendix 2.

If the injected disturbance, Fig. 1, is a p.r.b.s., then theoretically it is sufficient to integrate equation (4) over one period to obtain an accurate numerical solution. The output from most physical systems, however, will be affected by additive noise and in practice it is necessary to integrate over several cycles and obtain a mean value. The correlogram will be a series of spikes of period $N \Delta t$ and the first peak value will be displaced from the origin by a time $\tau = \tau_{max}$.

One important advantage of using a p.r.b.s. signal is that a small test signal can be easily detected in the presence of extraneous noise and this is of particular relevance to two-phase flow systems since the noise level generated by the solids will far exceed the disturbance being injected.

The simplicity of p.r.b.s. wave shape enables manual calculations of Φ_{xy} to be made quickly and easily and this the authors have found particularly valuable when interpreting the results.

The choice of Δt is a compromise between a sharp spike for the autocorrelation of the p.r.b.s. signal and limiting the bandwidth of the spectral distribution to be approximately 1/10 the natural frequency of the measuring transducers. This is necessary to ensure constant transducer sensitivity within the frequency spectrum of the injected p.r.b.s. signal. For convenience in disc manufacture, the
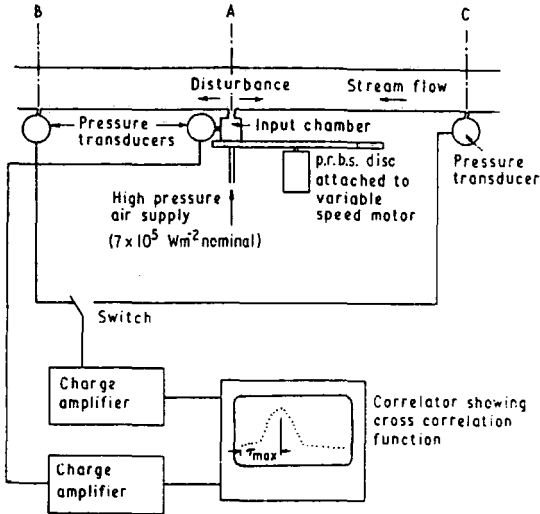
Fig. 1. Schematic diagram of experimental layout

value of N was chosen to be 15. The dynamic characteristics of the transducers and connector tubes were found experimentally to agree with the manufacturer's specifications in that parameter values of ω_n and ζ were 1000 Hz and <0.1 respectively.

3 EXPERIMENTAL ARRANGEMENT AND PROCEDURE

In Fig. 1 the pipe carrying the air–solids mixture had an internal diameter of 22 mm and was 40 m in length. One test station was chosen such that the distance from the inlet of the pipe to A was 5 m with AB = 2.430 m and AC = 2.746 m. A second test station had the distance from the inlet to A as 28 m and AB = AC = 2.746 m.

A p.r.b.s. signal, consisting of small steep fronted pressure disturbances, is introduced into the two-phase stream at A by a jet of high-pressure air which has its flow blocked intermittently by a specially slotted revolving disc. In Fig. 2, it can be seen that if the disc rotates at constant speed, the jet is periodically interrupted, giving the p.r.b.s. output, shown in Fig. 3, of period equal to the time of one revolution of the disc.
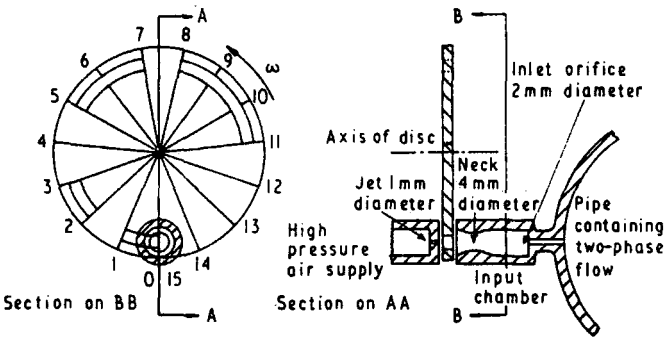
Fig. 2. Disturbance input arrangement
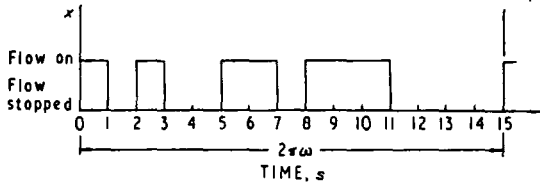
Fig. 3. Pattern of p.r.b.s. air pressure supply

Fig. 4. Auto correlation of p.r.b.s. signal in Fig. 3

In the experiment, the high pressure air was supplied at a nominal pressure of 7×10^5 N m^{-2} and the diameters of the jet and the inlet orifice in the stream flow pipe were 1 mm and 2 mm respectively. It is estimated (Appendix 1) that these values gave an air mass flow rate ratio between stream and disturbance of 1000:1. Preliminary tests using air only in the stream showed no noticeable difference in the results when combinations of larger jet and inlet orifice sizes were used.

Theoretically τ_{max} is independent of the period of the p.r.b.s., and consequently the speed of the disc, it is nevertheless important that the disc is made to rotate at a speed between certain limits. At speeds which are too high the period approaches τ_{max}, or is even less than τ_{max}, and it is not only difficult to determine τ_{max} but, owing to the time constant involved, the pulse shape is destroyed as monitored by the transducers. At slow speeds, the cross correlation takes longer to perform and the base of the spike becomes wider than τ_{max} which makes the reading more difficult to determine. It was found by experience that a period approximately equal to twice the expected τ_{max} was the most convenient. In consequence the disc was driven by an electric motor which could be set within this speed range.

Referring to Fig. 1, the disturbance signal was sensed at A, B and C by piezo-electric transducers. These transducers had specially shortened connectors to ensure that wave action in these connecting pipes was kept to a minimum. At B and C the p.r.b.s. signal was severely contaminated by noise. At A the signal to noise ratio was much better and by saturating the relevant charge amplifier a good clean reference input p.r.b.s. signal could be achieved, and consequently clearly defined values of τ_{max} and τ'_{max} were obtainable. Correlation was done using one of the proprietary correlators which are now available commercially.

Owing to the design of the experimental rig, it was not possible to run for long continuous periods. This made it necessary to devise a procedure that would ensure continuity for a series of results. The only parameter that could be estimated accurately was that of sonic velocity in the air stream alone and this was used to ensure that the monitoring equipment calibration was constant. Delays of up to 24 h between comparable runs were usual, since the solid polystyrene particles had to be returned manually to the upstream storage container.

The method of measuring the polystyrene and air mass flow rates is described fully in reference (4). Briefly, the solids are collected in a drum and weighed continuously; the gradient of the mass flow trajectory is used to estimate a mean mass flow rate for each trial. The air flow rate was measured using a B.S. nozzle in conjunction with a water manometer. It has been estimated that the inaccuracy in
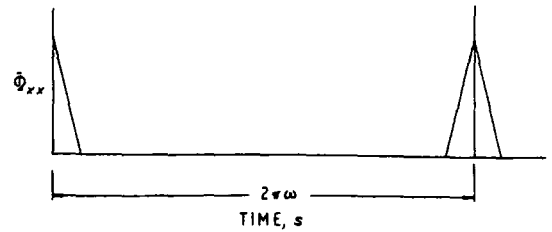
the measurement of the solids flow, especially at low flow rates, could be as much as ± 25 per cent, whilst the air flow measurement would be accurate to within ± 3 per cent.

Owing to the limited amount of solids available for a set of readings, the air flow was kept constant at the relatively low flow rate of 0·0372 kg/s to enable a wide range of solids to gas mass flow ratios to be obtained. To demonstrate that this technique is not restricted to low air flow rates, tests were carried out at much higher flow rates using air alone and sonic velocities were successfully measured. At pressures in the pipe greater than about 4×10^5 N m^{-2}, it was not possible to inject high pressure air and so the disturbance was introduced by using the p.r.b.s. disc to interrupt a jet of air escaping from the pipe.

4 DISCUSSION OF RESULTS

The results of this experiment are plotted on Figs 5 and 6, together with those obtained by the theoretical work (2)–(4). This theoretical work has been chosen as a comparison because the theory has been applied to air and polystyrene flow and it is the most recent work. It can be seen that though M does decrease with increase in air to solids mass flow ratio, there is a marked discrepancy between experimental and theoretical values. The theoretical work (3) and (4), predicts that the value of M will increase along the transporting pipe in the downstream direction, however, the two sets of experimental results are not in agreement with this prediction.

To a first approximation, the theoretical equation (5) (Appendix 2) for sonic velocity in a two-phase flow media is:

$$v_s{}^2 = \frac{n}{1+kx} RT \quad . \quad . \quad . \quad (1)$$

and is of the same form as the established equation relating sonic velocity in a gas, i.e.

$$v_g{}^2 = \gamma . RT \quad . \quad . \quad . \quad (2)$$

From the above two equations, and using γ for air $= 1·4$, it can be seen that:

$$M^2 = \left(\frac{v_s}{v_g}\right)^2 = \frac{n}{1·4(1+kx)} \quad . \quad . \quad (3)$$

Two possibilities for error in the theory suggest themselves, i.e. n and/or k is at fault. Considering Fig. 5b at $x = 10$ and $M = 0·7$, and using $n = 1·14$ equation (3) yields $k = 0·066$.

The few experimental results (4) available, for conditions similar to those of the authors, suggest that k should

— ⊙ — Experimental.
———— Theoretical.
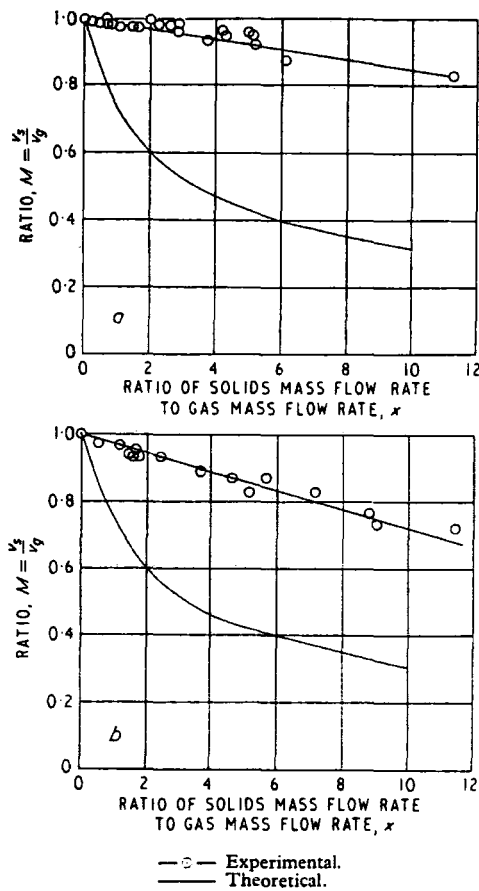
a Results taken at a point 5 m from inlet of 40 m pipe.
b Results taken at a point 28 m from inlet of 40 m pipe.

Fig. 5. Comparisons between experimental and theoretical values of *M*

be of the order of 0·9. This value was obtained experimentally by using a pitot tube to measure gas velocity and a continuously timed photographic technique to measure solid particle velocity. Judging from the description of the experimental procedure used and the difficulties encountered, it seems that little confidence can be attached to these results. The density ratio of polystyrene to air is approximately 1000:1 and if the polystyrene is assumed to occupy 1/10 of the pipe cross-sectional area, then, from the continuity equation, k will be approximately 0·1 which is of the same order as the results presented here. Alternatively, substituting for $k = 0·9$ in equation (3) yields $n = 7·35$ which, from experience, is not realistic since n is normally within the range 1 to 1·4, reference (3).

A range of experimental results are presented in Tables 1 and 2, and typical correlograms are shown in Fig. 6. Since v_d equals $AB.\tau_{max}$ it may be estimated that the total error in v_d and hence v_s is 8 per cent.

To demonstrate the validity of the results presented, various tests were initiated. Firstly, a complete study was made of acoustic behaviour for air alone and all the accepted values were measured to a good degree of accuracy using this experimental technique. Secondly, it was thought that there could be a thin layer of virtually uncontaminated air around the inside of the pipe, through which the disturbance travelled, but a comparison with readings taken with probes at various depths within the pipe showed no evidence of this. A third possibility was that the disturbance could be travelling within the pipe walls; replacing the transporting pipe which was made of brass by one made of polythene gave the same results, as would be expected, since the sonic velocity in a solid is much higher. A fourth possibility was that there was a time lag between the signal as recorded at the input chamber and as it just entered the pipe, but a cross correlation between these two points revealed no detectable time shift.

A last possibility could be, of course, that the mathematical concept of sonic velocity is not applicable as
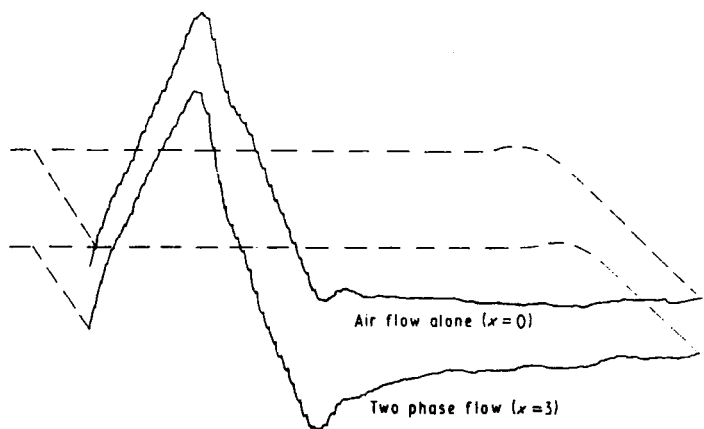
Experimentally, these results were recorded as a series of dots on the correlator screen and values read directly. The results shown are as taken from the correlator by a pen recorder. The time scale is such as to give a full scale base length of 33·3 ms.

Fig. 6. Typical correlograms between a p.r.b.s. disturbance recorded at two stations

13

Table 1

Solids to air mass ratio, x	$\tau_{max}, \div 333$ μs	$v_d = \dfrac{AB}{\tau_{max}}$, m/s	$\tau'_{max}, \div 333$ μs	$v_u = \dfrac{AC}{\tau'_{max}}$, m/s	Sonic velocity $v_s = \dfrac{v_d+v_u}{2}$, m/s	$\dfrac{v_s}{v_g} = M$	Comments
0·00	18·5	394	27·5	300	347 (v_g)	1·000	
5·15	20·0	365	27·6	299	332	0·957	
4·14	19·4	376	28·0	294	335	0·966	
1·66	18·4	396	27·8	297	346	0·998	Results taken at a point 5 m from
2·94	19·0	384	27·2	303	344	0·992	inlet of 40 m pipe.
5·05	19·3	378	28·0	294	339	0·978	
1·23	19·1	382	27·9	296	339	0·978	
0·76	18·6	392	28·0	294	342	0·986	
5·2	20·0	365	29·5	279	322	0·928	
1·04	18·5	394	28·0	294	344	0·992	AB = 2·430 m
1·5	18·9	386	28·0	294	345	0·994	AC = 2·746 m
2·18	18·9	386	27·9	296	341	0·984	
4·32	19·3	378	28·8	286	332	0·957	
0·269	18·7	390	27·7	298	344	0·992	Air flow rate = 0·0372 kg/s
0·455	19·0	384	28·5	290	337	0·971	
0·465	18·6	392	28·5	290	341	0·984	
0·262	18·7	390	28·0	294	342	0·986	
2·96	19·5	375	28·5	290	333	0·960	
2·0	18·5	394	27·5	300	347	1·000	
0·331	19·0	384	27·0	305	345	0·994	
0·7	18·5	394	27·5	300	347	1·000	
2·5	18·5	394	28·5	290	342	0·986	
3·84	19·5	375	29·5	280	327	0·943	
6·1	20·5	356	33·5	246	301	0·868	
1·5	18·5	394	28·5	290	342	0·986	
0·694	18·5	394	28·5	290	342	0·986	
2·31	18·5	394	29·0	284	339	0·978	
11·4	21·5	339	—	—	289 est.	0·833	

Table 2

Solids to air mass ratio, x	$\tau_{max}, \div 333$ μs	$v_d = \dfrac{AB}{\tau_{max}}$, m/s	$\tau'_{max}, \div 333$ μs	$v_u = \dfrac{AC}{\tau'_{max}}$, m/s	Sonic velocity $v_s = \dfrac{v_d+v_u}{2}$, m/s	$\dfrac{v_s}{v_g} = M$	Comments
0·00	21	393	29	285	339 (v_g)	1·000	
2·48	23	359	30	277	318	0·940	
1·15	22	375	29	285	330	0·973	
3·73	25	330	30	277	304	0·897	Results taken at a point 28 m from
8·78	30	277	34	243	260	0·767	inlet of 40 m pipe.
0·00	21	393	29	285	339	1·000	
1·57	23	359	30	277	318	0·940	
1·49	23	359	29	285	322	0·947	
5·73	27	305	30	277	291	0·874	
1·59	23	359	29	285	322	0·967	AB = 2·746 m
1·74	23	359	30	277	318	0·938	AC = 2·746 m
5·10	26	317	30	277	297	0·823	
0·00	21	393	29	285	339	1·000	
7·20	24	344	37	223	284	0·837	Air flow rate = 0·0372 kg/s
0·56	22	375	29	285	330	0·973	
9·00	—	—	40	206	250 est.	0·738	
0·00	21	393	29	285	339	1·000	
4·60	27	305	29	285	295	0·870	
11·50	30	277	40	206	242	0·714	

modelled (2) for the two-phase flow system tested experimentally.

5 CONCLUSION

The outcome of this experiment tends to infer that, to date, assumptions made in the theoretical considerations may be in error for the experimental system studied. The equation developed for sonic velocity may be shown perhaps to be in reasonable agreement with experimental results if the lag between solids and gas velocities can be predicted with certainty. The theory, however, predicts that for a solids to gas mass flow ratio of 10, this ratio will

be about 0·2 and the experimental value was found to be nearer 0·7.

The experimental results demonstrate that the application of p.r.b.s. pressure pulses enable continual measurements to be made within a flow system that to date have not been possible.

6 ACKNOWLEDGEMENT
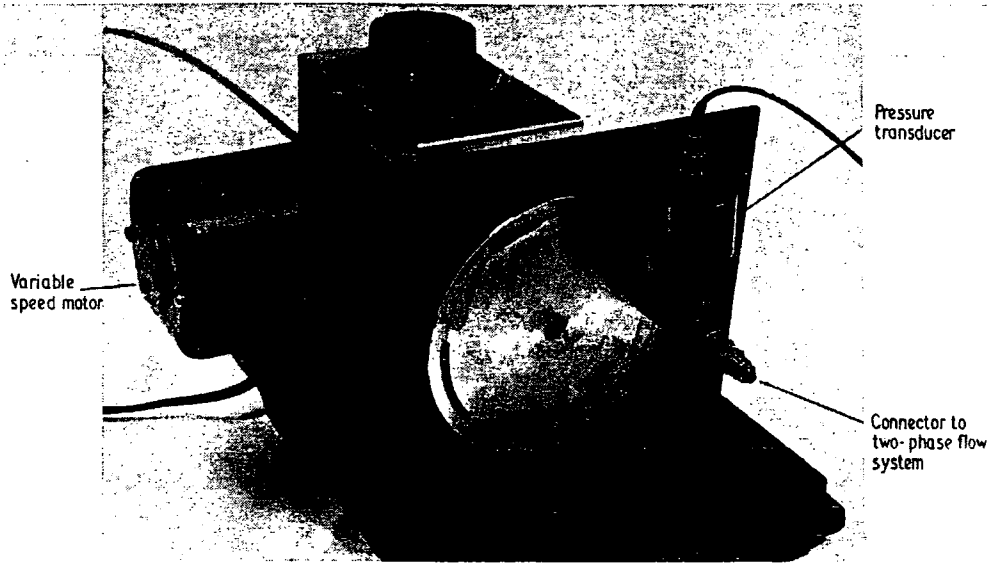
Fig. 7

APPENDIX 1

Correlation theory for velocity measurement

Consider any continuous disturbance travelling along a pipe from A to B as shown in Fig. 1. Assume the signal recorded at A is $x(t)$ and the signal recorded at B is $y(t)$ then the cross-correlation function defined as $\Phi_{xy}(\tau)$ is:

$$\underset{T\to\infty}{\text{Limit}}\frac{1}{2T}\int_{-T}^{+T} y(t)x(t+\tau)\,dt \quad . \quad (4)$$

where τ is a time delay between $x(t)$ and $y(t)$.

For such a function $\Phi_{xy}(\tau)$ a maximum value will occur at some time delay $\tau = \tau_{max}$ which gives a measure of the time necessary for the continuous disturbance to travel from A to B in Fig. 1. This value enables the velocity of the disturbance to be evaluated. If a small steep fronted pressure disturbance is introduced then the value of $\tau = \tau_{max}$ measured will enable the sonic velocity of the fluid system to be found experimentally.

Let the disturbance in Fig. 1 be a series of steep fronted pressure pulses emanating from A in both the upstream and downstream direction. If the mean velocity is v_m and the sonic velocity is v_s, then the wave propagation velocity travelling downstream will be $v_d = v_s + v_m$ and upstream will be $v_u = v_s - v_m$. Hence

$$v_s = \frac{v_d + v_u}{2} \quad \text{and} \quad v_m = \frac{v_d - v_u}{2}$$

where v_d and v_u are evaluated from

$$v_d = \frac{AB}{\tau_{max}} \quad \text{and} \quad v_u = \frac{AC}{\tau'_{max}}$$

and τ_{max} is the time delay of the disturbance travelling from A to B and τ'_{max} from A to C.

Whilst this may prove to be a satisfactory method for measuring the sonic velocity v_s it can be seen to be less reliable for measuring the stream velocity v_m since any small percentage error in measuring v_d and v_u will repre-

sent much larger absolute errors in the calculated value of v_m.

APPENDIX 2

Description of a pseudo random binary sequence

A possible p.r.b.s. is a maximum length sequence of the form $N = 2^n - 1$, where N, the number of bits in a sequence, is determined by n, some positive integer. A bit is a logic 'one' or a logic 'zero' that exists for a time Δt. The sequence is periodic in time, $N\Delta t$, and the exact arrangement of 'ones' and 'zeros' may be obtained from the literature. A 15-bit sequence is shown in Fig. 3. The most important property of a p.r.b.s. signal for this type of work is that its auto-correlation function $\Phi_{xx}(\tau)$ is:

$$\underset{T\to\infty}{\text{Limit}}\frac{1}{2T}\int_{-T}^{+T} x(t)x(t+\tau)\,dt \quad . \quad (5)$$

which is a series of well defined triangular 'spikes' of base width $2\Delta t$ and period $N\Delta t$ (Fig. 4).

APPENDIX 3

Estimation of the air mass flow rate ratio between stream and disturbance

Referring to Fig. 2, it is estimated that since the air expands through the jet from a pressure of 7×10^5 N m^{-2} to a pressure of 1×10^5 N m^{-2}, the flow through the jet will be sonic. The air will be cooled by expansion within the jet to an estimated temperature of 0°C. At the exit of the jet the following may then be estimated:

$$\text{Sonic velocity} = \sqrt{1\cdot4RT} = 330 \text{ m/s}$$

$$\text{Specific volume} = \frac{RT}{\text{pressure}} = 0\cdot78 \text{ m}^3/\text{kg}$$

Hence mass flow rate of air through the jet is $330/0\cdot78\times$ cross-sectional area of jet $= 0\cdot33\times10^{-3}$ kg/s. Due to the flow interruptions by the 15-bit p.r.b.s. disc the mass

entering the input chamber will be $7/15 \times 0.33 \times 10^{-3} =$ 0.15×10^{-3} kg/s.

Once within the input chamber the air will either pass into the two-phase stream or else escape to the atmosphere; the proportion not escaping may be assumed to depend upon the ratio of the cross-sectional areas of the inlet orifice to that of the inlet chamber neck.

Hence the flow rate of the disturbance air finally entering the two-phase flow pipe will be $\frac{1}{4} \times 0.15 \times 10^{-3} \simeq$ 0.04×10^{-3} kg/s. The mass of air flow within the two-phase stream was approximately 0.04 kg/s throughout the experiment. This represents, to a first approximation, the air mass flow rate ratio between stream and disturbance of 1000 : 1.

APPENDIX 4

REFERENCES

(1) BRIGGS, P. A. N., HAMMOND, P. H., HUGHES, M. T. G. and PLUMB, G. O. 'Correlation analysis of process dynamics using pseudo random binary test perturbations', *Proc. Instn mech. Engrs* 1965 **179** (Pt 3H), 37–51.

(2) COLE, B. N., BOWERS, H. M. and MOBBS, F. R. 'A theory for the high-speed flow of gas–solids mixtures under conditions of equilibrium and constant fractional lag', *Proc. Instn mech. Engrs* 1969–70 **184** (Pt 3C), 59–66.

(3) MOBBS, F. R., BOWERS, H. M., RICHES, D. M. and COLE, B. N. 'Influence of particle size distribution on the high-speed flow of gas–solid suspensions in a pipe', *Proc. Instn mech. Engrs* 1969–70 **184** (Pt 3C), 67–76.

(4) BOWERS, H. M. 'A study of gas–solids flows at very high speeds', Ph.D. Thesis 1966 (December), University of Leeds.

PAPER 18

A PRACTICAL INVESTIGATION INTO THE VALIDITY OF THE ELECTRICAL ANALOGY USED TO REPRESENT THE DYNAMIC CHARACTERISTICS OF A PIPE RESTRICTION

by M.A.Ali, B.Sc(Eng); Research Student, Departmentof Mechanical Engineering, The University, Leeds. LS2 9JT.

E.W.Read, M.A., C.Eng., M.I.Mech.E. Lecturer, Departmentof Mechanical and Production Engineering, The Polytechnic, Leeds.

K.F.Gill, M.Sc., Ph.D., C.Eng., M.I.Mech.E., M.I.E.E. Senior Lecturer, Department of Mechanical Engineering, The University of Leeds. Leeds. LS2 9JT.

B.W.Imrie, B.Sc.(Eng), M.Sc., C.Eng.M.I.Mech.E., M.Inst.M.C. Lecturer, Department of Mechanical Engineering, The University of Leeds. Leeds. LS2 9JT.

SYNOPSIS

This paper discusses a flow system which is analogous to a four terminal net-work which can be used to identify the dynamic characteristics of the system. Previously the dynamic characteristics of a flow restriction could not be determined by any other experimental means.

A theoretical model has been developed by using acoustic theory and an electrical analogy. Comparison with experimental results show that this analogy holds.

Correlation techniques linked to a prbs disturbance were used both to isolate the restriction and to obtain the dynamic characterictics of flow through the restriction. The present work may offer a better understanding of problems of metering pulsating flow.

INTRODUCTION

At present the metering of pulsating flow by using a constriction is of doubtful accuracy. A popular line of approach is to use quasi-steady flow theory and accept the errors that result[4,5,6] No allowance is made for the possibility of pressure phase shifts and amplitude changes of the dynamic differential pressure across the metering restriction. The pressure fluctuations at these stations are assumed to be in phase and the authors suggest that a correction may be necessary under certain circumstances.

It is further suggested that a better understanding of this problem may be obtained by knowing the dynamic behaviour of a restriction under pulsating flow conditions. Previously it has been considered impossible to obtain these dynamic characteristics experimentally because of the inability to isolate the restriction from extraneous reflections. This paper describes a correlation method of effectively isolating such a restriction and then obtaining the impulse response of that restriction.

Baird and Bechtold[3] in 1952, suggested a second order linear system as a description of the dynamic characteristics of a restriction under pulsating flow conditions. They postulated an electrical analogy based on acoustic theory describing the behaviour of an Helmholtz resonator. However, their experimental results did not substantiate their model.

The work presented gives an electrical analogy of a restriction and compares it with the experimental results obtained. The analogy would seem to substantiated. The impulse response obtained is a good representation of a second order linear response thus supporting Baird and Bechtoid's prediction.

Isolating the restriction does in fact produce a system analogous to a four terminal electrical network which is necessary for dynamic identification.

ELECTRICAL ANALOGY (AFTER BECHTOLD AND BAIRD)

Nomenclature:

A = resonator opening area

C_0 = the conductivity of the opening = $\dfrac{A}{l_{eq}}$

a = speed of sound

V = volume of the resonator chamber

e_0 = equilibrium density

w = wave frequency

w_n = resonator natural frequency

k   = wave length constant

1   = physical length of the resonator opening

leg   = equivalent length of the resonator opening allowing for end correction

ξ = system damping factor

c   = longitudinal displacement of the wave

x   = volumetric displacement

p   = excess pressure within the wave

p*   = excess pressure wave amplitude

t   = time

Z_a = acoustical impedance

Z_E = electrical impedence

From consideration of Figure 1 it can be shown that the following differential equation governs the flow behaviour in the case of a system that can be approximated to an acoustical Helmholtz resonator.

$$\left| (\frac{e_o}{c_o})\; A\, D^2\; +\; \frac{e_owk}{2\pi}\; A\, D\; +\; \frac{e_oa^2}{V}\; A\; \right|\; \epsilon\; =\; p \tag{1}$$

For $A\epsilon\; =\; x$

$$\left| \frac{e_o}{c_o}\; D^2\; +\; \frac{e_owk}{2\pi}\; D\; +\; \frac{e_oa^2}{V}\; \right|\; x\; =\; p \tag{2}$$

for a harmonic wave

$$p = p*\, e^{jwt}$$

$$x = \frac{p}{\frac{e_owk}{2\pi}\; +\; j(\frac{e_ow}{c_o}\; -\; \frac{e_oa^2}{vw})} \tag{3}$$

giving the acoustical impendance as

$$Z_a\; =\; (\frac{e_owk}{2\pi})\; +\; j\; (\frac{e_ow}{c_o}\; -\; \frac{e_oa^2}{vw}\;) \tag{4}$$

Analogous to the electrical impedance

$$Z_E\; =\; R + j\, (wL\; -\frac{1}{wc}) \tag{5}$$

From equation (4) it can be deduced that the acoustic impedance is the sum of both AC & DC impedances making possible the use of the electrical analogy shown by equation (5) and re-presented graphically in Figure 2.

From this network it can be deduced that the system characteristics are given by

$$w_\eta\; =\; a\; \sqrt{\frac{C_o}{V}} \tag{6}$$

$$\xi\; =\; \frac{wk}{4\pi a}\; \sqrt{VC_o} \tag{7}$$

EXPERIMENTAL PROCEDURE

A schematic representation of the experimental rig used is shown in Figure 3 and is comprised of two sections of 25.4 mm. diameter pipe connected by a long orifice having a bore of diameter 10 mm and a length of 0.98 m. For this arrangement it was estimated that the

natural frequency of the restriction would be of the order of 180 Hz and that it would have a damping factor greater than 0.1. These values were selected to enable the experiment to be done with existing equipment described in the earlier paper. [1]

It has been demonstrated that by using a prbs pressure disturbance it is possible to minimise wave action within a pipe flow system. [2] The approach used in this investigation was to position a pressure transudcer at A and inject prbs pressure pulses at B. By varying the area of the valve at C the reflections within the pipe section were minimised as indicated by the correlogram of the pressure readings taken at A. This procedure was repeated for the other pipe section.

To estimate the dynamic characteristics of the now isolated restriction a prbs pressure disturbance was injected at B using a bit interval Δt of 6 ms and sequence length of 15 bits. These values were arrived at by using empirical rules such that Δt was between one-fifth and one-tenth of

$$\frac{1}{w_n \xi}$$

and the sequence length was longer than four times

$$\frac{1}{w_n \xi}$$

The signals at B and D were cross correlated to give a representation to the system impulse response as shown in Figure 4. Using log decrement approximation the experimental of w_n and ξ were determined.

$$w_n = 166 \text{ Hz} \qquad \xi = 0.15.$$

The dynamic characteristics of the monitoring transducer are given in the earlier paper. [1] It has a natural frequency of 350 Hz and a damping factor of less than 0.1.

To verify these results the system comprising transducers and restriction was simulated on an analog computer as shown in Figure 5 and the results obtained from this simulation are plotted in Figure 6.

DISCUSSION

This work demonstrates the validity of the electrical analogy suggested by Baird and Bechtold. The success of the analogy, however, relies heavily upon the ability to minimise wave action within the ducting adjoining the restriction. The use of correlation is shown to be a very powerful tool in achieving this minimisation. The logical extension is to use a cross correlation function to establish system identification since the same equipment is used for both purposes.

Inspection of Figures 4, 6 shows the close agreement between experimental results and those computed from theoretical consideration.

The polar plot Figure 7 for the tested restrictor is indicative of the errors that migh occur in the measurement of pulsating flow if no allowance is made for the change in wave amplitude and phase shift through a restriction used for the purpose of metering periodic flow.

REFERENCES

1. Reed, E.W., Mobbs, F.R., and Gill, K.F., "Measurement of small amplitude pressure wave propagation in a gas-solids flow". This symposium.

2. Reed, E.W., and Gill, K.F., "An experimental technique for producing a resonance free pipe system". To be published.

3. Baird, R.C. and Bechtold, I.C., "The dynamics of pulsating flow through sharp-edged restrictions (with special reference to origice-metering)". ASME, Nov.1952, 1381.

4. Earles, S.W.E., and Zarek, J.M., "Use of sharp-edged orifices for metering pulsating flow", Proc. I.Mech.E., 1963, 177, 997.

5. Zerek, J.M., "The neglected parameters in pulsating flow measurement" ASME Flow Measurement Symposium, 1966.

6. Sparks, C.R., "Pulsation effects on flow metering of compressible and noncompressible fluids". Proceedings of 17th Annual Symposium on Instrumentation for Process Industries, 1962.
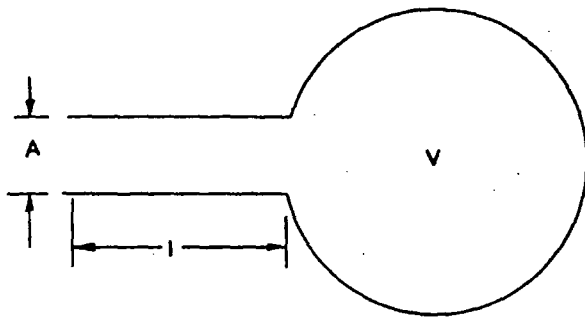
Figure 1
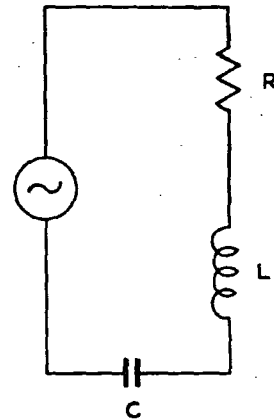
Figure 2
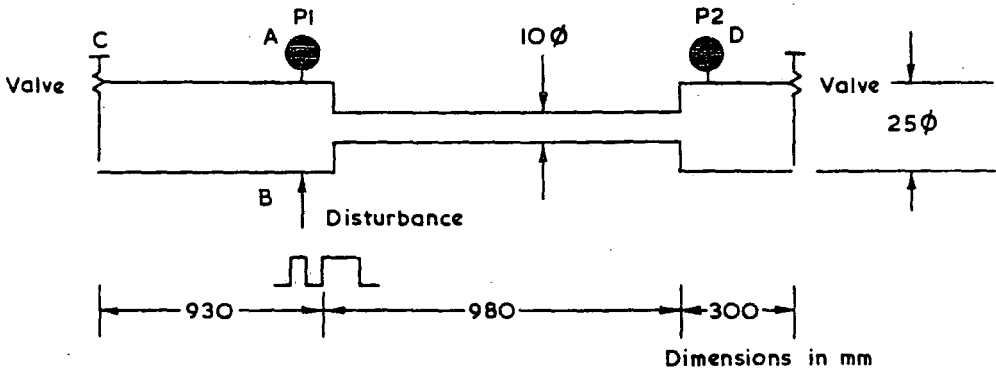
Figure 3
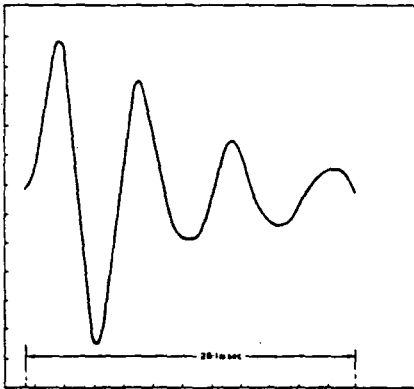
Figure 4
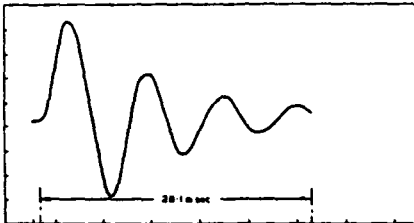
Figure 5
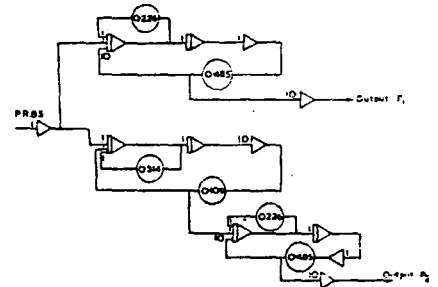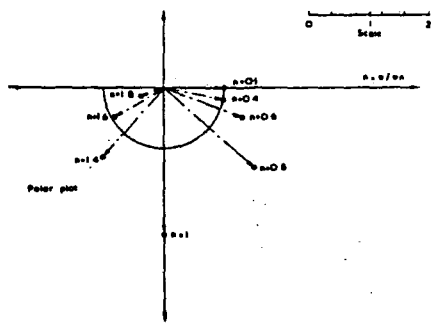
Figure 6

Figure 7

PAPER 19

MEASUREMENT BY CORRELATION OF SMALL AMPLITUDE PRESSURE WAVE PROPAGATION VELOCITY IN A GAS-SOLIDS FLOW

by E.W.Reed, M.A., C.Eng., M.I.Mech.E, Lecturer, Department of Mechanical and Production Engineering, The Polytechnic, Leeds. LS1 3HE.
F.R.Mobbs, M.Sc., D.I.C. Senior Lecturer, Department of Mechanical Engineering, The University, Leeds. LS2 9JT.
K.F.Gill, M.Sc., Ph.D., C.Eng., M.I.Mech.E., M.I.E.E. Lecturer, Department of Mechanical Engineering, The University, Leeds. LS2 9JT.

SYNOPSIS

A novel method has been devised, and is here presented, that enables sonic velocity to be measured in a gas-solids flow system. Correlograms are computed from small amplitude pressure disturbances injected into the system in the form of a pseudo random binary sequence. The role played by the sonic velocity parameter is evidence from the theory presented. The assumptions made in the theoretical derivations should be applicable to the test rig used; however, comparison between theoretical and experimental values suggest that discrepancies exist. The most likely cause of this discrepancy is the assumption that the gas velocity and the solids velocity have the same ratio before and after the passage of the pressure wave.

INTRODUCTION

The concepts of sonic velocity and Mach number are so valuable in the dynamics of a clean gas that it is obviously desirable to establish similar concepts in relation to gas-solids flows. The velocity of sound waves as such through a gas-solid suspension is frequency dependent and it is possible, to distinguish two limiting cases: (a) the "frozen" speed of sound corresponding to the propagation of a high-frequency sound where the solid particles do not respond at all to the disturbance; and (b) the "equilibrium" speed of sound corresponding to the propagation of low-frequency sound where the solid particles remain in equilibrium with the gas.

As far as the dynamics of gas-solids flows is concerned one is not, however, specifically interested in the propagation of sound waves. It is more exact to say that one wishes to know the speed of propagation of pressure discontinuities of small amplitude, although here again the degree of response of the particles to the passage of the wave is of vital importance.

An equation for the critical speed of sound (corresponding to a Mach number of unity) has been developed by Cole, Bowers and Mobbs[1]. This shows the sonic velocity to depend on the ratio of mass rate of flow of solids to mass rate of flow of gas, the ratio of solids velocity to gas velocity, and the ratio of solids temperature to gas temperature. In a gas-solid flow which is accelerating along a pipe, some degree of velocity and temperature lag will always exist between the gas and the solid particles.

The speed of sound was also found to depend on the ratio of the change in solids velocity to the change in gas velocity through the wave and it was assumed that this would be equal to the corresponding ratio of solids velocity to gas velocity ahead of the wave.

A more generalised equation for sonic velocity has now been developed (Appendix 1). This shows that, with the exception of the critical condition, the speed of sound in a gas-solids flow having a solids velocity lag depends on whether the pressure wave is travelling upstream or downstream. However, at the locations in the pipe where the experiments were performed this effect is of small order. It is again assumed that the gas velocity and the solids velocity have the same ratio before and after the passage of the pressure wave.

EXPERIMENTAL METHOD

A well known use of the correlation technique is to measure the time of a transport lag for a signal passing between two measuring stations. This particular university ie Bradford, has done much work in developing techniques and this paper assumes the theory to be well understood.[4] Undoubtedly small pressure (sonic) disturbances were inherent within the gas-solids flow system and the inference is that these could have been detected and used to construct a correlagram from which the sonic velocity can be measured. There was every indication that these inherent disturbances could give satisfactory results when air was flowing alone without the polystyrene but once the air was loaded with polystyrene no consistent set of results were obtainable.

In order to have a definable and easily distinquishable disturbance travelling within the flow system the authors decided to inject a series of small pressure pulses in the form of a

pseudo random binary sequence (prbs). A brief description of a prbs is given, (Appendix 2). It can be seen that providing the prbs is detectable at a measuring station, even though embedded in noise, then a cross correlation of the prbs at input with the signal at that station will result in a series of sharply defined "spikes" in a form similar to a delayed version of Figure 3, (Appendix 2). The time delay of the first "spike" will give the absolute time for the sonic disturbance to travel from its input to the measuring station.

The sonic velocity measured is in fact the absolute velocity and so in order to determine the velocity relative to the transporting media it was necessary to determine the absolute sonic velocities in both an upstream and downstream direction. By taking the difference in these velocities it appeared possible to calculate the absolute velocity of the transporting media; however, the accuracy proved to be poor since the velocity of the sonic disturbance was some 15 times greater than the velocity of the transporting media.

What the individual velocities of the air and polystyrene particles were the authors have not yet been found it possible to determine by a correlation technique, and it is hoped that this symposium will produce some enlightenment.

APPARATUS

The flow system being studied consisted of a pipe some 40m long and 24mm internal diameter through which polystyrene particles were transported by air. The polystyrene was in the form of a coarse powder which had mean diameters ranging from 150-400 microns. Correlation was carried out on a proprietary correlator.

The means employed for injecting the prbs pressure pulses was to use the special generator developed by the authors. Basically this generator consists of a revolving disc, with appropriately cut slots in it, through which a fine jet of air passes. The jet is directed into the flow system and is consequently interrupted in a prbs manner thus producing small prbs pressure pulses into the system.

The method of recording this prbs is to use a sensitive piezoelectric transducer to detect pressure changes within the jet of air flow just downstream of the disc. The output of this transducer is coupled to a charge amplifier, set at a high sensitivity, so that saturation of the amplifier cuts off the top and bottom of the transducer signal; this eliminates the transients and produces a good square edged trace which follows the prbs pattern of the disc as shown in Figure 5.

It was necessary to develop this special generator since initial attempts to inject air flowing through a proprietary solenoid valve, switched by a prbs voltage generator, resulted in serious damage to the valve by polystyrene particles leaking into it. Another disadvantage was that the speed of the prbs was limited by the time constant of the valve which imposed unnecessary restrictions upon the frequency content of any prbs chosen.

The means used to detect the sonic disturbances within the pipe was with a sensitive piezoelectric transducer which had dynamic characteristics approximating to that shown in Figure 6. Care had to be taken in the selection of the revolving disc speed since too fast a prbs would have resulted in the cross correlation appearing band-limited and not giving the familiar "spikey" shape associated with the correlogram of a prbs signal. Considering Figure 4 and Figure 6 it is seen that the speed of the prbs must be such that the bulk of the power in the power density spectrum plot of the prbs is below about 100Hz in order that the prbs is reasonably reproduced by the transducer. Alternatively, if the prbs is too slow then the "spikes" produced will be too wide and the peak of the initial "spike" will not be sharply defined. The problem may be eased if it were possible to increase the resonant frequency of the transducer. This is only possible by using a less sensitive transducer or by enlarging the size of the connecting tube to the transducer. An attempt to do the latter resulted in the blocking up of the transducer by polystyrene particles.

A serious drawback to the air-polystyrene flow rig used was that the polystyrene could only flow for a few minutes. Recharging of the rig was then necessary and this normally took a period of 24 hours. In consequence development of the experimental apparatus and procedure was done using air flow alone. Because of this short experimental time available it was found expedient to tape record readings from the transducers for gas-solids flow and process the results off line.

This approach enabled the maximum number of readings to be obtained per run of the experimental rig since each correlogram needed only a few seconds of running time. In this way the scatter within the experimental results could be observed but this was small compared with the deviation from the theoretical prediction.

Using the thermodynamic equations for gas flow and knowing the dimensions of the jet for injecting the prbs disturbance it is calculated that the mass flow ratio of the gas within the pipe to that of the injected air was of the order of 1000:1. The injected air is therefore considered to have negligible effect upon the gas-solids flow.

RESULTS

The initial results using air flow alone supported the claim that it was the sonic velocity being measured, and further substantiation came from the fact that the inverted correlation "spike" of the reflected prbs disturbance from an open end of the pipe clearly showed itself on the correlogram at the appropriate position of time.

Figure 7 shows graphically theoretical and experimental results for the sonic velocity relating to the transport of polystyrene by air for a range of mass ratios from 0-12. The experimental results suggest a linear relationship between decrease in sonic velocity with increase in mass flow ratio of polystyrene to air.

The discrepancy that occurs between the results taken at two stations separated by 23 m is small compared with the values predicted theoretically. At this stage in the study no attempt was made to explain the difference between the sets of experimental data presented.

CONCLUSIONS

A comparison of the theoretical values of the sonic velocity with the experimental values casts some doubt on the validity of the theoretical assumptions given in the introduction. Since the experimental values lie consistently above the theoretical values and close to the clean gas speed of sound, this results indicate a much lower degree of response of the solid particles to the passage of the wave than that implied by the assumption that the gas velocity and the solids velocity have the same ratio before and after the passage of the pressure wave.

Various attempts were made to explain the wide discrepancies between the experimental results and the theoretical preductions. These included an investigation to determine that the disturbances as measured did infact travel through the two-phase mixture and not through a thin boundary layer relatively free from solid particles or that there was a some undetected time delay at the input. No such effects could be established experimentally. In the experiment the bulk of the power in the density spectrum of the prbs was well below 100Hz which should represent low frequencies to the two phase system. However, it is the authors intention to fully investigate the frequency dependency of the system in this range in order to establish the validity of the experimental findings presented.

To date it may be claimed that this paper presents a method of determining, within a gas-solids flow, the average velocity of a sonic disturbance which has a frequency distribution as shown in Figure 4.

ACKNOWLEDGEMENT

REFERENCES

1.   Cole, B.N., Bowers, H.M. and Mobbs, F.R., "A theory for the high-speed flow of gas-solids mixtures under conditions of equilibrium and constant fractional lag". Proc.I. Mech.E., 1969-70, Vol.184, part 3C.

2.   Mobbs, F.R., Bowers, H.M., Riches, D.M. and Cole, B.N., "Influence of particle size distribution on the high-speed flow of gas-solid suspensions in a pipe" ibid.

3.   Davies, W.D.T., "Random signal testing for evaluating system dynamics". Wireless World pp 407-412, Aug. 1966.

4.   Abeysekera, S.A. and Beck, M.S., "Cross-correlation techniques applied to pulsating flow measurement. Measurement and Control, 3,6, pp. T109-T112, June 1970.

APPENDIX 1

THEORETICAL DERIVATION OF THE GAS-SOLID FLOW SONIC VELOCITY

Notation

a_g	Clean gas speed of sound
a_m	Gas-solids mixture speed of sound
C_p	Specific heat of gas at constant pressure
C_ν	Specific heat of gas at constant volume
C_s	Specific heat of solid particles
j	Ratio of solids temperature to gas temperature using stagnation temperature as a base
k	Ratio of solids velocity to gas velocity
p	Static pressure
u_g	Gas velocity
u_s	Solids velocity
x	Ratio of mass rate of flow of solids to mass rate of flow of gas
β	Ratio C_s to C_ν
τ	Ratio of gas specific heats
ρ_g	Gas density
ρ_s	Distributed solids density

Pressure wave travelling upstream

Consider an infinitesimal amplitude pressure wave propagating at a velocity a_m relative to the gas in an upstream direction in a unit cross-sectional area duct. The initial values of gas and solids velocities are u_g and u_s, respectively. For convenience the wave can be brough to rest by superimposing an additional velocity $(a_m - u_g)$ on the system.
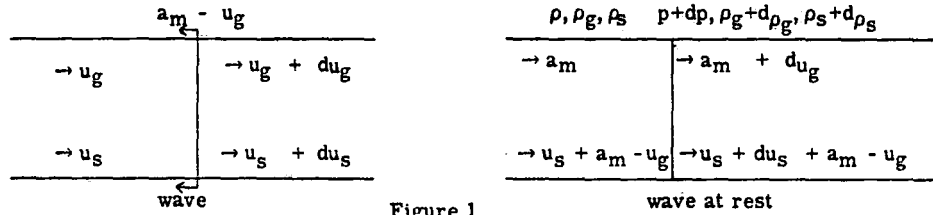
Figure 1

The following equations apply:

Gas continuity: $\rho_g \, a_m = (\rho_g + d_{\rho_g})(a_m + du_g)$

Solids continuity: $\rho_s (u_s + a_m - u_g) = (\rho_s + d_{\rho_s})(u_s + du_s + a_m - u_g)$

Momentum: $dp = \rho_g \, a_m \, du_g - \rho_s (u_s + a_m - u_g) \, du_s$

$\qquad\qquad = \rho_g \, a_m \, du_g - \dfrac{x}{k} \, \rho_g (u_s + a_m - u_g) \, du_s$

From which $\dfrac{dp}{d\rho_g} = a_m{}^2 + \dfrac{x}{k} \, \dfrac{du_s}{du_g} \, a_m [a_m - (1-k) u_g]$

$\qquad\qquad\qquad = \dfrac{n}{\tau} \, a_g{}^2$

Pressure wave travelling downstream

Similar considerations to those above yield

$a_m{}^2 + \dfrac{x}{k} \, \dfrac{du_s}{du_g} \, a_m [a_m + (1-k) u_g] = \dfrac{\eta}{\tau} \, a_g{}^2,$

where η, is the index of expansion of the gas ie $\dfrac{p}{\rho_g{}^\eta}$ = a constant.

η depends on the rate of energy transfer between the gas and the solid particles and has been shown by Cole, Bowers and Mobbs to be given by

$$\eta = \frac{1 + (1 + xj\beta)}{\gamma^{-1}} \bigg/ 1 + \frac{(1 + xj\beta)}{\gamma^{-1}} \qquad - \frac{1 + xk^2}{1 + xk} \, ,$$

making the assumption that $\dfrac{du_s}{du_g} = k$

APPENDIX 2

An understanding of prbs adequate for the needs of this paper may best be obtained by considering Figure 2. Briefly a prbs is a sequence which has only two levels and may switch between levels only at certain fixed intervals of time which are integer multiples of a basic interval of time. Full description and exact forms of prbs may be obtained from the literature[3]. The prbs used in this experiment had the form as shown in Figure 2. One important property of a prbs is that its autocorrelation function is a series of "spikes" as shown in Figure 3. The power spectrum may be obtained from the Fourier Transform of the autocorrelation function and is as shown in Figure 4.
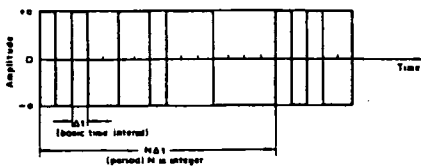
Figure 2   A typical p.r.b.s. signal
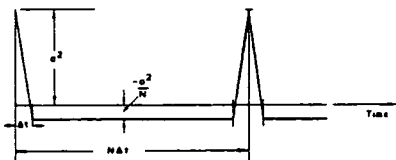
Figure 3   Autocorrelogram of p.r.b.s. in Figure 2
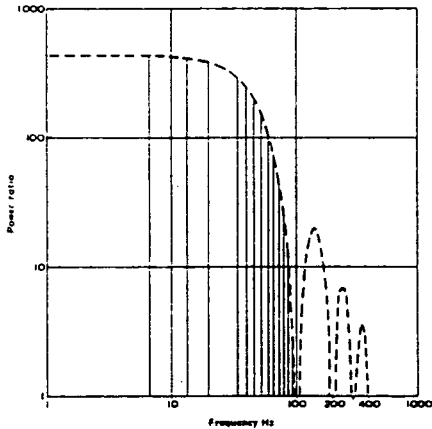
Figure 4   Log log plot of power density spectrum, showing envelope of first four lobes, of p.r.b.s. in Figure 2 where N=15 and Δt=10ms.
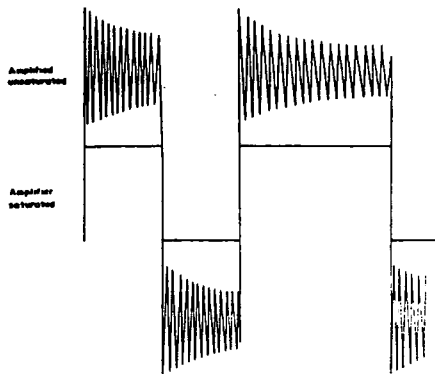
Figure 5   Output from the charge amplifier measuring the input p.r.b.s.
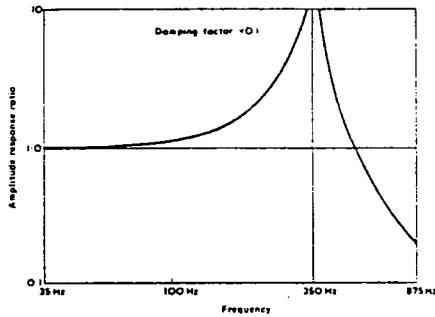
Figure 6   Typical dynamic characteristic plotted on log log axes of a sensitive piezoelectric transducer.
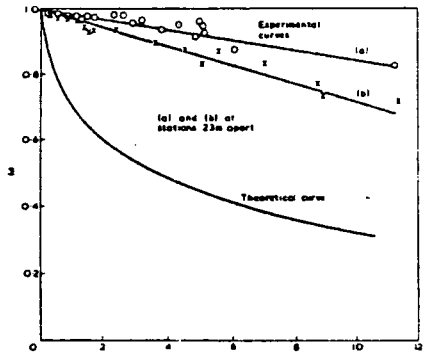
Figure 7   Sonic velocity M, given as a ratio to clean air sonic velocity, plotted against mass flow ratio x of polystyrene to air.

PAPER 22

EXPERIMENTAL TECHNIQUE FOR MINIMIZING RESONANCE WITHIN A DUCTED FLUID

E. W. Reed*   K. F. Gill†

Presented is an experimental method that enables practical pipe systems to be de-tuned so that resonance can be reduced to an absolute minimum. The technique employed is to correlate pseudorandom binary sequence pressure disturbances which are deliberately introduced into the pipe system. It is believed that this is the only method yet available to achieve this minimization of resonance phenomena. The experiment does not require fragile equipment and can be used in two phase flow work. The procedure is unsophisticated and directly applicable to engineering systems requiring this adjustment. The rapid response of the measuring technique makes the approach suitable for automatic control applications. Further extensions of this technique that give a greater insight into the practical behaviour of sonic waves are highlighted in the paper.

1 INTRODUCTION

IN A PREVIOUS PAPER (1)‡ the authors describe a use of correlation to measure the speed of sound in gas–solids flow. They injected small amplitude pressure disturbances in a pattern that could be detected even in the presence of much greater disturbances. The pattern chosen was in the form of a pseudorandom binary sequence (p.r.b.s.) and the authors described the p.r.b.s. pressure pulse generator they have developed for injecting these disturbances.

The object of this paper is to demonstrate to other experimenters that this combination of p.r.b.s. pressure pulses with correlation is a very powerful and useful technique in the de-tuning of a system but could have other important applications.

The behaviour of sonic disturbances is of fundamental importance in the fields of flow or acoustics. The technique is easily applied and the computation relatively straightforward. It is particularly useful in work on gas-solids or other potentially destructive flows since there is no measuring device within the flow to be damaged.

The experiment described here demonstrates a technique that makes possible the detection of reflected sonic waves and hence the de-tuning of pipe systems to completely remove any standing waves. This requirement manifests itself in many forms throughout industry, a typical example being the closing, without damage, of sluice valves in large hydraulic systems. A non-reflecting pipe does, of course, represent the 'infinite' pipe postulated in some reflected wave theories. An immediate application is likely to be at the University of Leeds (2) where research into pulsating flow is in progress and the ability to measure sonic reflections or produce an 'infinite' pipe would be of immense value. Another application is in basic fluid flow problems to confirm accepted electrical analogies, which up to now have been invariably hindered because workers have been unable to establish satisfactory procedures for de-tuning pipe systems. The theory shows clearly that, besides merely detecting reflected waves, one can compute their magnitude, which implies that the

strengths of waves in such engineering installations as waste heat exhaust turbines, fitted to large reciprocating engines, can be computed readily.

It is the aim of the authors to present the technique as it now stands and hence make this useful measuring tool immediately available to other researchers.

1.1 Notation

a	Amplitude of p.r.b.s.
k_A, k_B	Coefficients of reflection.
N	Number of 'bits' in a period of p.r.b.s.
p.r.b.s.	Pseudorandom binary sequence.
t	Time variable.
Δt	Time of one 'bit' of p.r.b.s.
τ	Dummy time delay.
τ_1, τ_2, τ_3	Actual signal time delays.
$\phi_{xx}(\tau)$	Autocorrelation function of signal $x(t)$.
$\phi_{xy}(\tau)$	Cross correlation function of signals $x(t)$ and $y(t)$.

2 DESCRIPTION OF P.R.B.S. AND ASSOCIATED CORRELATION FUNCTIONS

Complete descriptions and exact forms of p.r.b.s. and the normally associated correlation functions are obtainable from the literature (3). To be concise this paper only includes a summary. A p.r.b.s. is a sequence which has only two levels and may switch between levels only at certain fixed intervals of time which are integer multiples of a basic interval of time known as a 'bit'. The sequence is random for a definite period which is continuously repeated in a cyclic manner.

Fig. 1 shows an example with a period length of 15 'bits' and is the p.r.b.s. ideally produced by the authors' generator.

2.1 Autocorrelation

Let the p.r.b.s. signal be represented as $x(t)$, where t is a time variable, then the autocorrelation function of $x(t)$ is by definition (4) (5)

$$\phi_{xx}(\tau) = \underset{T \to \infty}{\text{Limit}} \frac{1}{T} \int_0^T x(t)x(t+\tau)\,dt$$

where τ is a dummy time delay.

$\phi_{xx}(\tau)$ will give the correlogram shown in Fig. 2.
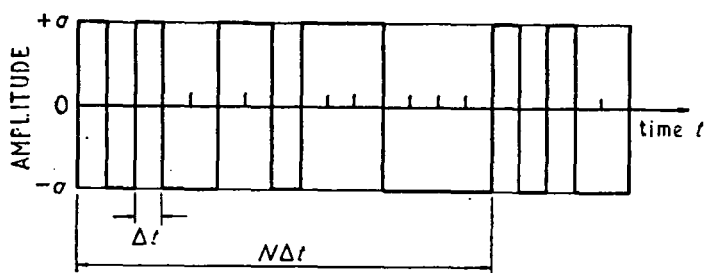
Fig. 1. *15 'bit' period p.r.b.s. signal*
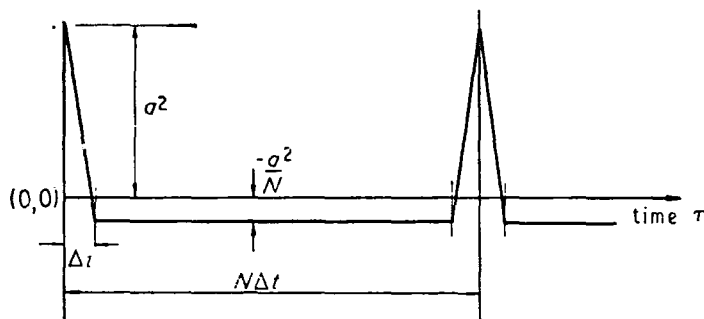
Fig. 2. *Autocorrelogram of p.r.b.s. signal*
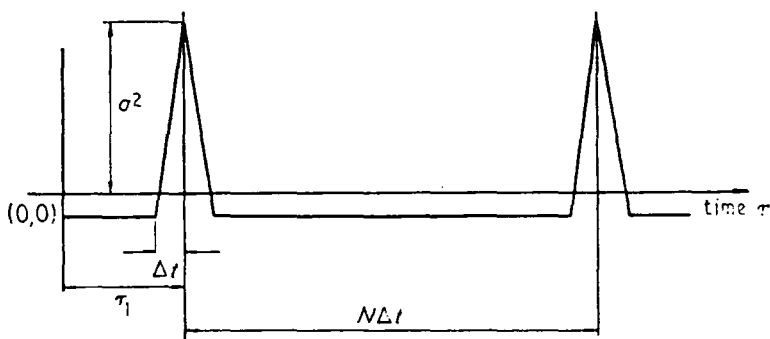
Fig. 3. *Cross correlogram of p.r.b.s. signals*

2.2 Cross correlation

If the p.r.b.s. signal $x(t)$ is now cross correlated with another p.r.b.s. signal $y(t)$ identical to $x(t)$ but delayed by a time τ_1, and given by $y(t) = x(t-\tau_1)$ the cross correlation function is by definition (4) (5)

$$\phi_{xy}(\tau) = \underset{T \to \infty}{\text{Limit}} \frac{1}{T} \int_0^T x(t)x(t-\tau_1+\tau)\,dt$$

$\phi_{xy}(\tau)$ will give the correlogram as shown in Fig. 3.

2.3 Power spectrum of p.r.b.s.

Fig. 4 shows the power spectrum of a 15 'bit' p.r.b.s. The essential point to note is that the bulk of the power in a p.r.b.s. is in frequencies below the frequency equal to $1/\Delta t$.

3 THEORETICAL CONSIDERATIONS

It is well known that sonic waves travelling down a pipe

will be reflected in unlike sense from an open end and in like sense from a closed end (4). Physical argument suggests that a valve at the end of a pipe must have some setting where it is non-reflecting. Below is a generalized analytic model of a pipe system to present the theory of the correlation technique as used to determine this setting.

Consider a continuous small amplitude pressure disturbance, varying with time t, introduced into the pipe at D (see Fig. 5). This disturbance generates two sonic waves travelling in opposite directions from D. Let these waves be reflected from the ends at A and B with assumed coefficients of reflection k_A and k_B respectively. A coefficient of reflection is here defined as the pressure amplitude ratio of the reflected wave to the incident wave. These waves will then continue to be reflected from end to end without influencing each other when passing within the pipe, neglecting all forms of attenuation (6).

Let the times for the sonic wave to travel along the path
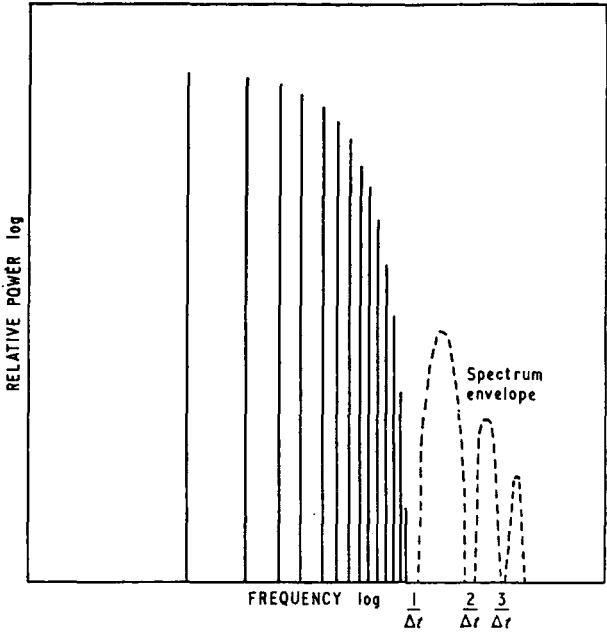
Fig. 4. *Power spectrum of 15 'bit' period p.r.b.s.*
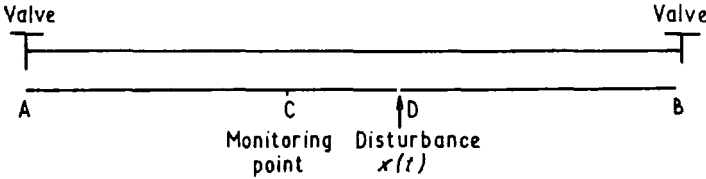
Fig. 5. *Generalized pipe system*
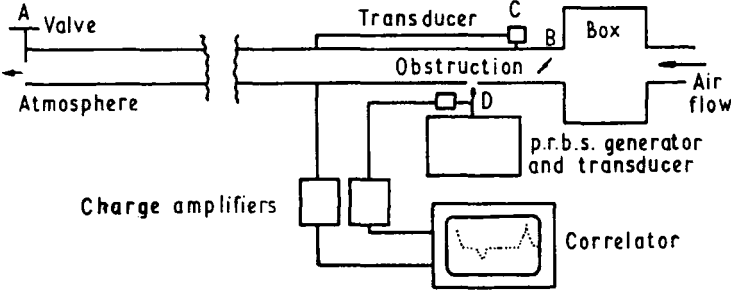
Fig. 6. *Experimental layout*

DAC be τ_1, along the path DBC be τ_2 and along the path DC be τ_3.

If the disturbance at D is $x(t)$ then the signal monitored at C will be

$$c(t) = x(t-\tau_3) + k_A x(t-\tau_1) + k_B k_A x(t-\tau_1-\tau_2-\tau_3)$$
$$+ k_B x(t-\tau_2) + k_A k_B x(t-\tau_2-\tau_1+\tau_3)$$
$$+ k_A k_B^2 x(t-\tau_2-\tau_1+\tau_3-\tau_2-\tau_3)$$

$+$terms involving k_A to powers higher than unity

As the end at A approaches a condition of non-reflection

then k_A approaches zero and terms involving k_A to powers higher than unity may be ignored.

Further simplification of the signal at C is obtained if C and D are located as close to B as is possible so that τ_2 and τ_3 become negligible.

The signal at C then approximates to

$$= (1+k_B)x(t) + k_A(1+k_B)^2 x(t-\tau_1) \quad . \quad (1)$$

This signal may now be processed in either of the following two ways.

Autocorrelating the signal at C

By definition

$$\phi_{cc} = \operatorname*{Limit}_{T \to \infty} (1+k_B)^2 \frac{1}{T} \int_0^T x(t)x(t+\tau)\, dt$$

$$+ \operatorname*{Limit}_{T \to \infty} k_A(1+k_B)^3 \frac{1}{T} \int_0^T x(t)x(t-\tau_1+\tau)\, dt$$

$$+ \operatorname*{Limit}_{T \to \infty} k_A(1+k_B)^3 \frac{1}{T} \int_0^T x(t-\tau_1)x(t+\tau)\, dt \quad (2)$$

If $x(t)$ is a p.r.b.s. then this autocorrelogram will be a trio of spikes repeating with the period of the p.r.b.s. There will be a primary spike with a pair of identical secondary spikes symmetrically displaced by a time τ_1 at either side of it. One of the positions of the primary spike will be at the origin. The autocorrelation function derived is seen to be an even function which is in fact a property of all auto-correlation functions.

Cross correlating the signal at C with the disturbance $x(t)$

By definition

$$\phi_{cx} = \operatorname*{Limit}_{T \to \infty} (1+k_B) \frac{1}{T} \int_0^T x(t)x(t+\tau)\, dt$$

$$+ \operatorname*{Limit}_{T \to \infty} k_A(1+k_B)^2 \frac{1}{T} \int_0^T x(t-\tau_1)x(t+\tau)\, dt \quad (3)$$

If $x(t)$ is a p.r.b.s. then it can be seen that this cross correlo-gram will be a pair of spikes, separated by a time τ_1, and repeating with the period of the p.r.b.s. One of the positions of the primary spike will be at the origin.

Both correlograms show the time delay τ_1 of the reflec-tion from the end A, the secondary spike is directly pro-portional to the coefficient of reflection k_A.

In both cases the ratio of the amplitude of the secondary spike to that of the primary spike is given by $k_A(1+k_B)$ and by extension of this analysis reflection coefficients can be determined. It can be seen that if the end B has been de-

tuned so that $k_B = 0$ then the spike amplitude ratio equals k_A.

4 THE EXPERIMENT

Fig. 6 shows diagrammatically the pipe system to be de-tuned and the necessary measuring equipment. The object of the experiment was to locate the setting of the valve at A so that no sonic pressure waves are reflected.

Since there would be a reflection from the box and ob-struction the distances BD and CB were kept as short as was convenient to the pipe system (see Section 3).

The p.r.b.s. generator used consists basically of a fine jet of air interrupted by a specially slotted disc and directed into the system being tested. A full description of this generator is given in (1) and a photograph is shown in Fig. 7. The result is a train of pressure pulses in a p.r.b.s. pattern similar to that of Fig. 1. This p.r.b.s. pressure signal is detected by a sensitive piezoelectric transducer sufficient to saturate the charge amplifier, a near perfect square edged p.r.b.s. signal results without the transients of the transducer being present.

The pressure transducer at C was a highly sensitive piezoelectric device, and a proprietory correlator, showing correlograms on a screen with X–Y plot out facilities, was available.

Initially the pipe system was de-tuned by cross correla-ting the signals from the transducers at D and C. The p.r.b.s. signal from the generator is near perfect and hence a sharply defined correlogram could be predicted. It was also felt that a cross correlogram would be easier to inter-pret than an autocorrelogram because less spikes would be present (see Section 3).

The experiment, however, was successfully repeated by autocorrelating the signal from the transducer at C show-ing the supposed advantages of cross correlating to be unfounded. This resulted in the saving in equipment of both a transducer and a charge amplifier.

Tuning was a simple procedure and achieved by altering the position of the valve until no reflecting spike appeared
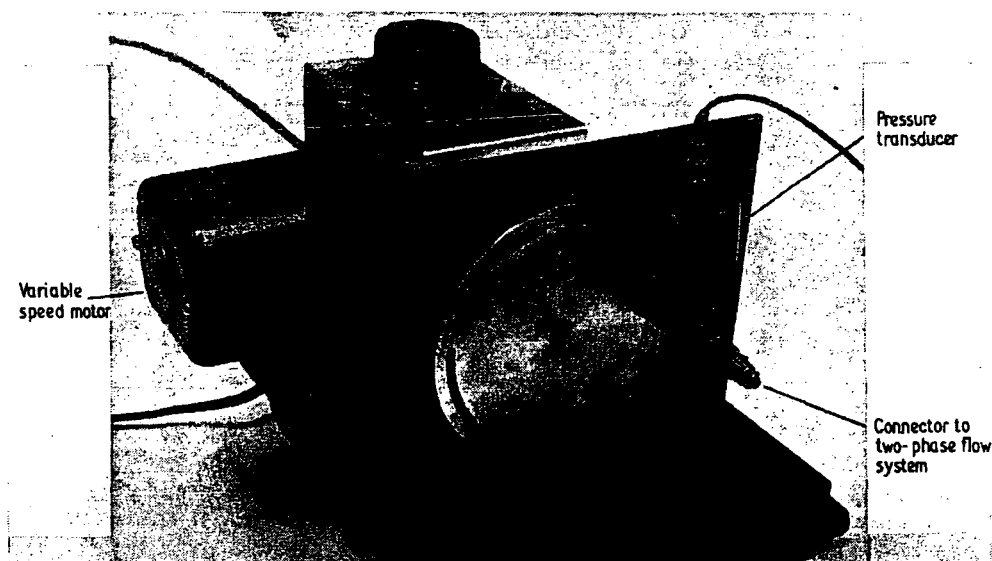
Fig. 7. *P.r.b.s. generator*

30
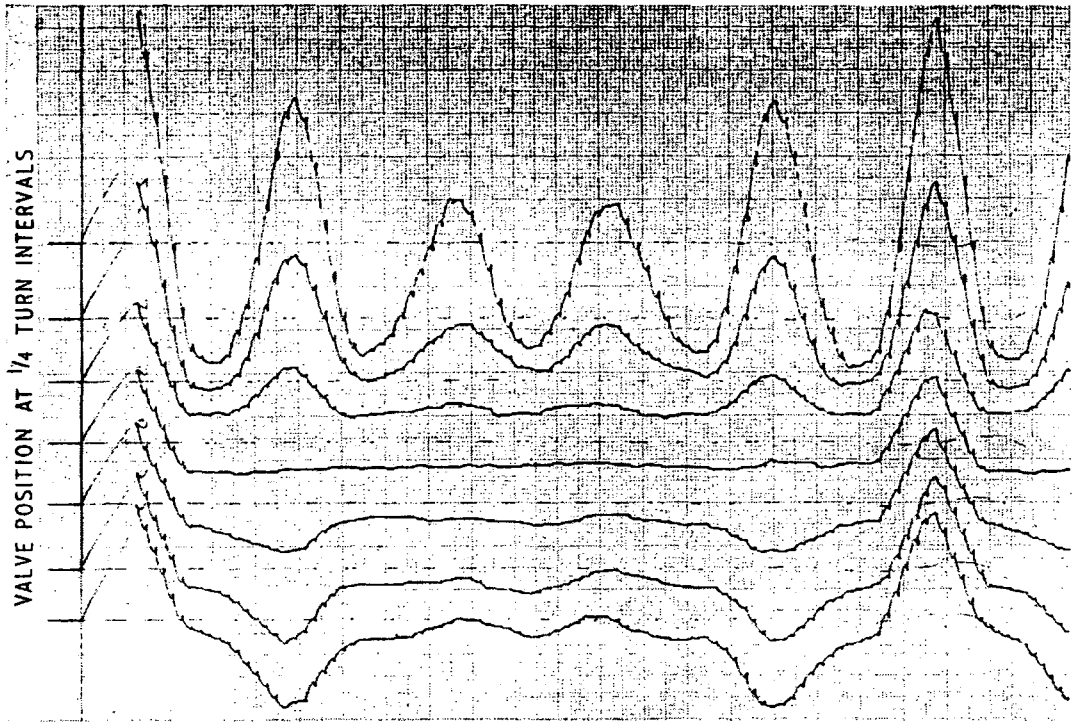
Note increase in complexity of correlogram as valve moves from
de-tuned position.

Fig. 8. *Autocorrelation of signal at* C
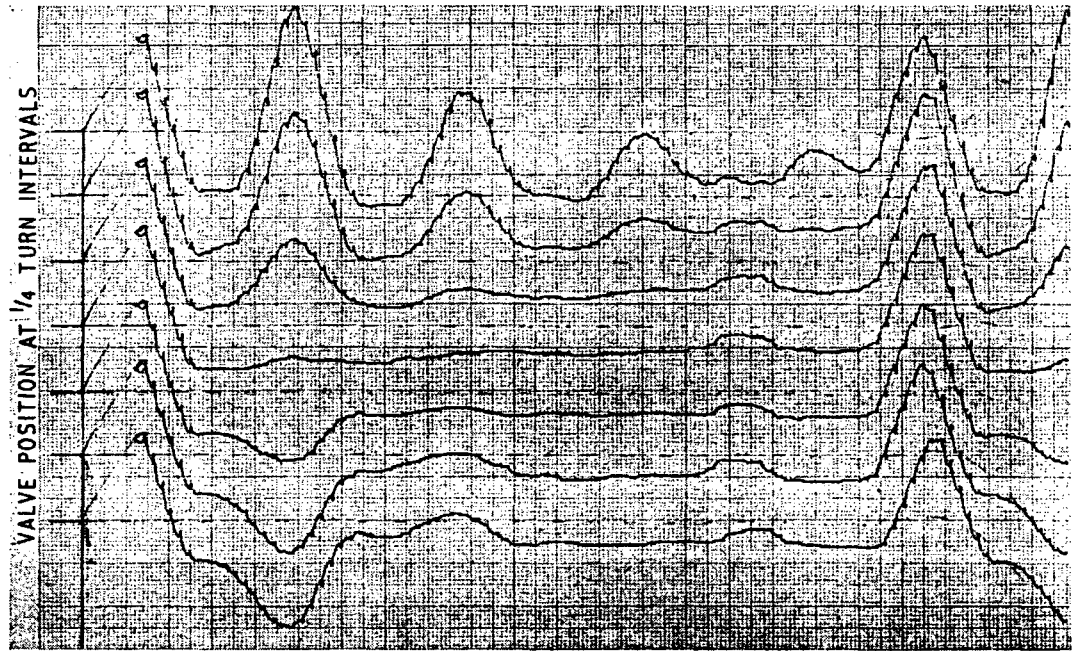
Fig. 9. *Cross correlation of signal at* C *with* x(t)
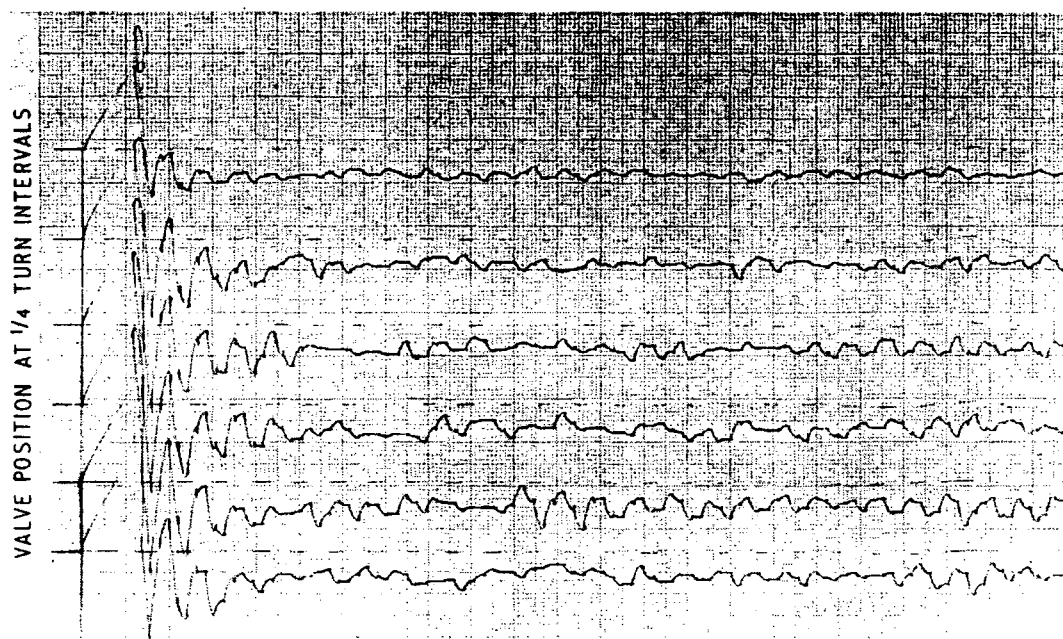
Fig. 10. *Autocorrelation of inherent disturbances at* C

on the correlogram. A positive spike appeared for an over-closed valve position, the reverse for an underclosed position. One second of correlation time was found to be adequate for each reading. A set of autocorrelograms and cross correlograms are shown in Fig. 8 and Fig. 9 respectively.

The speed of the p.r.b.s. generator, whilst not critical, needed consideration and had to lie within a reasonable range having due regard to time of reflection of the pressure wave. It can be seen from Fig. 2 that the breadth of a correlation spike of a p.r.b.s. is directly related to the speed of the p.r.b.s.; the faster the speed so the sharper and better defined the spike will be. Since a p.r.b.s. repeats, the time of reflection could have been greater than a p.r.b.s. period as the reflection spike would still have appeared within the first sequence of a correlogram. The only provision was that the reflection spike must not in any way coincide with the fundamental spike on the correlogram for obvious reasons. The means of calculating p.r.b.s. speeds is indicated in Fig. 2. The time of reflection of the sonic wave can be estimated with sufficient accuracy by measuring the total length of the path and using a local velocity of sound of 347 ms^{-1}.

The upper speed of the p.r.b.s. is limited by the resonant frequency of the piezoelectric transducer which may be considered to have the dynamic characteristics of a second order system with very low damping (damping factor <0·1). The power density spectrum of a p.r.b.s. is shown in Fig. 4. It can be seen that the bulk of the power is below a frequency of $1/\Delta t$ and this frequency must be kept well below the resonant frequency of the transducer if a reasonable p.r.b.s. signal is to be reproduced by that transducer. In the experiment the natural frequency of the transducer and its attachments was 350 Hz and the bulk of the power content of the p.r.b.s. was below 170 Hz.

An attempt to use the sonic pressure disturbances inherently present within the pipe system was unsuccessful as the results show in Fig. 10.

5 DISCUSSION OF RESULTS

The experiment demonstrates an accurate method of monitoring, within a pipe system, the behaviour of small amplitude pressure pulses of which the statistical properties are known. This monitoring is put to good effect here in de-tuning the system from sonic resonances. Using injected p.r.b.s. pressure pulses is shown to be extremely effective and is the only practical way yet known to the authors.

Both Fig. 8 and Fig. 9 show clear and well defined correlograms. It is not necessary to cross correlate at two points since equally as good results are obtained by auto-correlating at one point with consequential saving in equipment. Any discrepancy between Fig. 8 and Fig. 9 is because the exact number of turns of the valve for de-tuning was difficult to record as a precise reference could not be established.

Since de-tuning the system requires determining the null position of a broad based spike it is only necessary to know the position of one time value within that spike. It is therefore possible to de-tune the system equally well by using the simplest form of correlators which determines the correlogram point by point. For practical purposes it is suggested that a point chosen as near to the centre of the spike as possible would be the most desirable. This point can be determined with more than adequate accuracy by calculation, knowing the speed of sound and length of path, though a complicated system could possibly require an initial exploratory correlogram. Using a proprietary correlator, the length of time needed in the experiment to

compute a full correlogram was of the order of 1 s. If it is required merely to show an indication of the direction of growth of the reflection spike then an even shorter time would be necessary. It follows that the technique would allow application to automatic control systems because of this rapid response.

The theory shows that the technique can also be used for measuring reflection coefficients and sonic time delays.

The real value of the experiment is to substantiate the claims of the authors that the application of the technique described here is valuable, straightforward, capable of complete interpretation and may be used with the utmost confidence.

6 ACKNOWLEDGEMENT

APPENDIX

REFERENCES

(1) GILL, K. F. and REED, E. W. 'A study into the use of pseudo random binary sequence pressure disturbances to measure sonic velocity in a two-phase flow system', *Proc. Instn mech. Engrs* 1972 **186** (Pt 1), 449–455.

(2) ALI, M. A., REED, E. W. and GILL, K. F. 'A correlation method for measuring reflection coefficients of sharp edged orifices for small amplitude pressure waves.' (To be published.)

(3) DAVIES, W. D. T. 'Random signal testing for evaluating system dynamics', *Wireless Wld* 1966 407–412.

(4) BRIGGS, P. A. N., HAMMOND, P. H., HUGHES, M. T. G. and PLUMB, G. O. 'Correlation analysis of process dynamics using pseudo random binary test perturbations', *Proc. Instn mech. Engrs* 1965 **179** (Pt 3H), 37–51.

(5) GODFREY, K. R. 'The theory of the correlation method of dynamic analysis and its application to industrial processes and nuclear power plant', *Measmt Control* 1969 **2**, 165.

(6) SHAPIRO, A. H. *The dynamics and thermodynamics of compressible fluid flow* 1954 (Ronald Press Company, New York).

PAPER 23

CORRELATION METHOD FOR MEASURING REFLECTION COEFFICIENTS OF SHARP-EDGED ORIFICES FOR SMALL-AMPLITUDE PRESSURE WAVES

M. A. Ali*   E. W. Reed†   K. F. Gill‡

A correlation technique using pseudo-random binary-sequence pressure-pulse testing is used to measure reflection coefficients of sharp edged orifices at the end of a duct. Within the range of the incident pressure-wave amplitude investigated in this paper it is believed that no other experimental means has yet been devised. A simple formula is derived from one-dimensional flow theory which gives values showing close agreement with the experimental results. End conditions for non-reflection are established to create an analogy to the hypothetical 'infinite pipe'.

1 INTRODUCTION

THE AUTHORS have demonstrated in (1)§ that reflections from an orifice at the end of a duct could be eliminated for sharp fronted flat-topped waves of small amplitude by choosing the correct size of orifice. The technique employed was to correlate pseudo-random binary-sequence pressure disturbances which were deliberately introduced into the pipe system. This paper extends this basic work to provide a reliable means of evaluating reflection coefficients within a pressure range never before attempted. A reflection coefficient is defined as the ratio of the amplitude of the reflected wave to that of the incident wave.

To date no practical solution has been found to the problem of metering the unsteady flow of a fluid by means of a discontinuity in the flow stream (2). This work represents part of a general project aimed towards gaining a deeper understanding of this problem.

The established method for determining the strength of wave reflections, which is only possible for waves of large amplitude, is to use a shock-tube arrangement. The pressure records are analysed on the basis of the non-linear relationship developed theoretically by Bannister and Mucklow (3) and tested experimentally by Mucklow and Wilson (4) for the open and closed end conditions. Their results verified the theoretical formula for the open-end situation but for closed ends gave a 2 per cent discrepancy. A discrepancy was also noticed by Earles and Zarek (5) who quoted a figure of 6–7 per cent; they suggested that the explanation was due to attenuation of the advancing waves by viscosity effects and measuring inaccuracies.

Earles and Zarek compared their experimental work with Nesbitt's theoretical analysis (6) which made the reasonable assumption that the static pressure remained

constant along the axis of the issuing jet from the orifice. In practice, depending upon the orifice pipe diameter ratio, a contraction effect may take place resulting in this static pressure not remaining constant. On comparing their experimental results with the theory, a discrepancy was noted which appeared to be dependent upon the area ratio: they attempted to explain this by introducing the concept of 'the reflection coefficient of contraction' which can only be found experimentally. The indication is that the area responsible for the reflection from an orifice is smaller than the physical area of the orifice. Their results also show that this coefficient depends upon the amplitude of the incident wave.

Trengrouse et al. (7) introduced a similar concept based on the ratio in area between that of an isentropic-convergent nozzle to that of a sharp-edged orifice for measured values of incident and reflected pressure ratios. They used a theory, based on quasi-steady one-dimensional flow conditions in conjunction with finite non-steep wave theory, which showed agreement with experiments for a group of convergent-isentropic nozzles. Their work showed a discrepancy of 7 per cent between the value of the discharge coefficient for sharp-edged orifices measured by a shock-tube technique and the conventional steady-flow technique, both tests being for the same conditions of pressure ratio across the restriction. Prior to this, Rudinger (8) had suggested that the use of the shock-tube technique would be a good alternative to conventional means for obtaining steady-flow data.

A literature survey has not shown any work using pressure amplitudes low enough to be in the range likely to occur in pulsating compressible flows. This paper presents results in the low pressure region for unsteady flow (less than 0·005 bar). This range was limited by the equipment available but the authors suggest that the technique is applicable for higher pressure ranges.

A simple theoretical treatment for the experimental configuration being studied is included in Appendix 1.

1.1 Notation

a Local acoustic speed.
C Reflection coefficient of contraction.
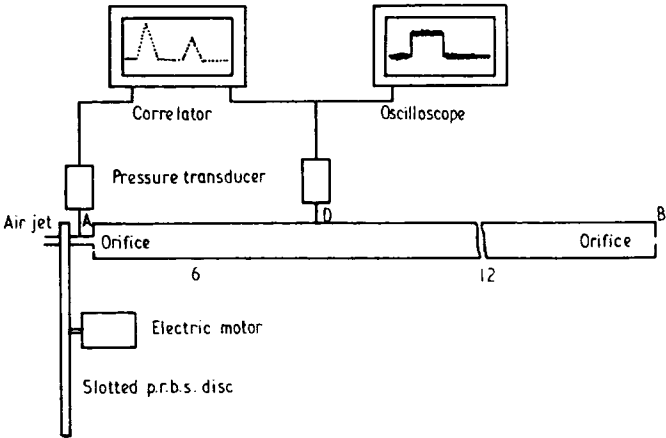
Fig. 1. *Experimental layout*

Fig. 2. *Typical correlogram*

k Reflection coefficient $\left(=\dfrac{\phi_r}{\phi_i}\right)$.

m Orifice to pipe/area ratio.

p Absolute pressure.

T Absolute temperature.

w Induced particle speed.

x $=\left(\dfrac{p}{p_0}\right)^{1.7}$.

y $=\dfrac{w}{a_0}$.

γ Specific heat ratio. For air $\gamma = 1.4$.

ϕ $= x^{\gamma} - 1$.

Subscripts

i   Incident wave.

n   Zone of interaction of incident and reflected waves.

r   Reflected wave.

t   Downstream condition

0   Atmospheric condition.

2 TECHNIQUE

The technique of pseudo-random binary-sequence pressure-pulse testing is fully described (1). Considering Fig. 1, the pulses are injected at A. The pressure signals at A and D are cross correlated so that the correlogram shows a representative spike at each time delay for which the pulses take to reach D either direct or by reflection. The orifice at A is tuned to eliminate reflections from this end so that the third and subsequent spikes on the correlogram are removed. The ratio of the amplitude of the second spike to that of the first will give the appropriate coefficient of

reflection from B. A typical correlogram taken by pen recorder is shown in Fig. 2.

Testing was done for a range of pulse amplitudes with seven different orifice sizes at B.

The amplitude of the incident pulse was measured on an oscilloscope monitoring the transducer at D. A true reading could only be taken when both ends were non-reflecting; once this condition for a particular orifice was attained, the pressure pulses were kept constant and the orifices changed to give a range of values for reflection coefficients. Pressure noise on the oscilloscope trace was partially removed by using a passive filter. A typical trace is shown in Fig. 3.
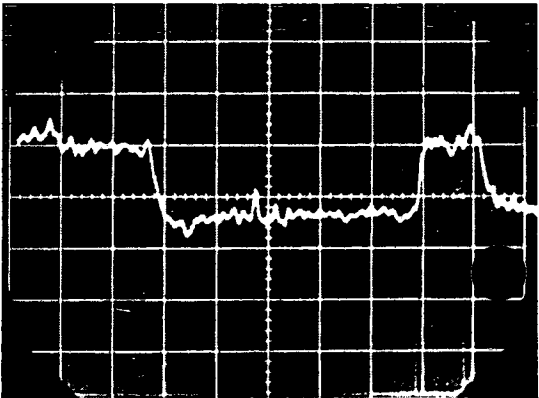
Fig. 3. *Part of a typical pressure pulse trace*

3 RESULTS

Fig. 4a shows a comparison between the experimental and theoretical results for the non-reflecting condition which leads to reflection coefficients of contraction, C, as shown in Figs 4a and b. Using these experimentally obtained values of C in equation (9) a comparison between reflection coefficients obtained theoretically and experimentally for different orifice sizes is given in Figs 5a–d.

4 DISCUSSION OF RESULTS

Fig. 4a shows a definite divergence between theoretically predicted and experimentally obtained results for the non-reflecting conditions of incident wave amplitude for different orifice sizes.

This leads to the reflection coefficients of contraction which vary between 0·67 and 0·63 for the range of pressure amplitudes investigated, as can be seen from Figs 4b and 4c. An explanation of this divergence could be that there is an issuing jet 'boundary effect' resulting in a reduced reflecting area, even though the range of pressure amplitudes is small.

Using the experimentally obtained values of the reflection coefficient of contraction in the theoretically obtained
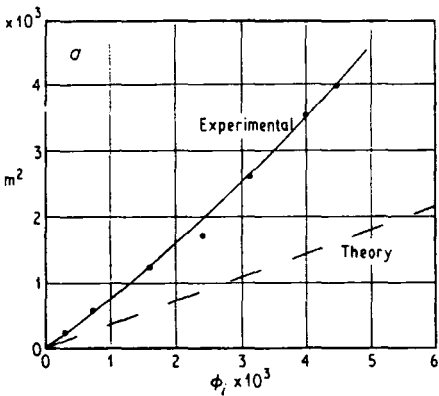
Fig. 5a

Fig. 5b

Fig. 4a
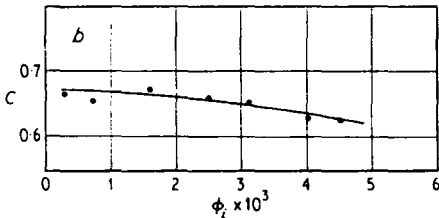
Fig. 4b
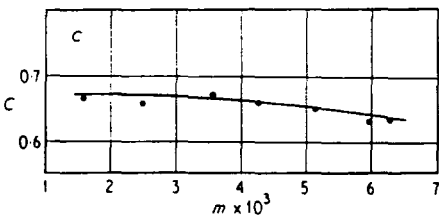
Fig. 4c
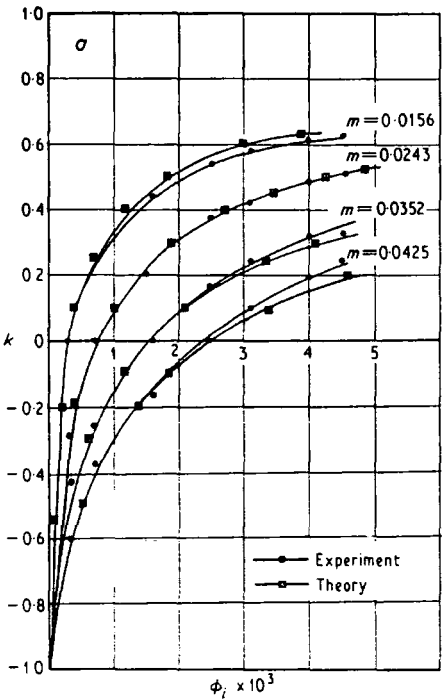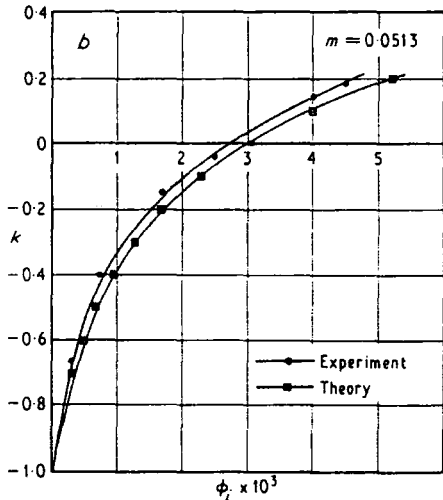
formula (equation (9)) gives agreement within experimental accuracy (Figs 5a–d). These graphs show clearly that for a particular orifice size there is only one value of pressure-pulse amplitude for which the orifice is non-reflecting. The deviation between theoretical and experimental curves seems to increase as the incident-pressure amplitude increases which may be the result of experimental error and truncation error in the binomial approximation used in the theoretical derivation.

The experimental results have all been measured from the screen of the on-line correlator; measuring accuracies

Fig. 5c

Fig. 5d

Fig. 6. *Pressure diagram of wave superposition at the discontinuity*

APPENDIX 1

THEORY

Considering the interaction of a single incident pressure wave of amplitude p_i with that reflected from the discontinuity, the resultant is a wave of amplitude p_n immediately upstream of the plane of discontinuity and a transmitted wave of amplitude p_t (see Fig. 6).

Assuming air to be a perfect gas and applying isentropic conditions

$$\left(\frac{a}{a_0}\right) = \left(\frac{T}{T_0}\right)^{1/2} = \left(\frac{p}{p_0}\right)^{1.7} \quad . \quad . \quad (1)$$

For waves of moderate amplitude

$$w = \frac{2a_0}{\gamma-1}\left|\left(\frac{p}{p_0}\right)^{(\gamma-1)/2\gamma} -1\right| \quad \text{Earnshaw} \ (9) \quad (2)$$

Considering incident wave

$$y_i = 5(x_i-1) \quad . \quad . \quad . \quad . \quad (3)$$

From consideration of the interaction between incident and reflected waves

$$y_n = 5(2x_i-x_n-1) . \quad . \quad . \quad . \quad (4)$$

and

$$x_n = x_i+x_r-1 \quad . \quad . \quad . \quad . \quad (5)$$

Using the continuity and energy equations

$$\frac{y_n}{y_t} = m\left(\frac{x_t}{x_n}\right)^5 \quad . \quad . \quad . \quad . \quad (6)$$

and

$$y^2{}_n+5x^2{}_n = y^2{}_t+5x^2{}_t \quad . \quad . \quad (7)$$

For atmospheric downstream conditions where $p_t = p_0$, using equations (4)–(7) and applying the binomial approximation to them for ϕ_i very small

$$\phi_i = \frac{14}{5}m^2\frac{1+k}{(1-k)^2} \quad \text{(provided } m \text{ is small)} \quad (8)$$

By introducing the reflection coefficient of contraction term equation (8) becomes

$$\phi_i = \frac{14}{5}(mC)^2\frac{1+k}{(1-k)^2} \quad . \quad . \quad (9)$$

For the non-reflecting condition $k = 0$

$$\phi_i = \frac{14}{5}(mC)^2 \quad . \quad . \quad . \quad (10)$$

of the order of 1 mm in 40 mm is the best that can be achieved. However, reflection coefficients of modulus below 0·1 can only be expected to have an accuracy to within ±10 per cent.

5 CONCLUSIONS

The experimental results demonstrate that a unique pressure ratio can be found at which minimum wave reflection from a pipe constriction occurs. The value of the reflection coefficient of contraction measured from the incident wave was found to be between 0·67 and 0·63. This work indicates the effectiveness of pseudo-random binary-sequence pressure-pulse testing as a means of investigating reflection behaviour from pipe constrictions.

6 ACKNOWLEDGEMENT

APPENDIX 2

REFERENCES

(1) REED, E. W. and GILL, K. F. 'Experimental technique for minimizing resonance within a ducted fluid', *J. mech. Engng Sci.* 1973 **15** (No. 2), 95–101.

(2) SHAPIRO, A. H. *The dynamics and thermodynamics of compressible fluid flow* 1954 (Ronald Press Company, New York).

(3) BANNISTER, F. K. and MUCKLOW, G. F. 'Wave action following sudden release of compressed gas from a cylinder', *Proc. Instn mech. Engrs* 1948 **159**, 269.

(4) MUCKLOW, G. F. and WILSON, A. J. 'Wave action in gases: the attenuation and reflection of compression waves propagated in pipes', *Proc. Instn mech. Engrs* 1955 **169**, 69.

(5) EARLES, S. W. E. and ZAREK, J. M. 'Reflection of pressure waves at sharp-edges orifices', *The Engineer* 1965 (February).

(6) NESBITT, M. V. 'The reflection and transmission of pressure disturbances at area changes in infinite ducts', N.G.T.E. Memo. 198 1954 (February).

(7) TRENGROUSE, G. H., IMRIE, B. W. and MALE, D. H. 'Comparison of unsteady flow discharge coefficients for sharp-edged orifices with steady flow values', *J. mech. Engng Sci.* 1966 **8** (No. 3), 322–9.

(8) RUDINGER, G. 'A shock tube technique to determine steady flow losses of orifices and other duct elements', *J. bas. Engng, Trans. Am. Soc. mech. Engrs* 1960 **82**, 195.

(9) EARNSHAW, S. 'On the mathematical theory of sound', *Phil. Trans. R. Soc.* 1960 **150**, 133.

BIBLIOGRAPHY

ALI, M. A., REED, E. W., GILL, K. F. and IMRIE, B. W. 'A practical investigation into the validity of the electrical analogy used to represent the dynamic characteristics of a pipe restriction', *Proc. Int. Symp. Measurement Process Identification by Correlation Spectral Techniques* 1973 (Institute of Measurement and Control, London).

BANNISTER, F. K. *Pressure waves in gases in pipes*, Akroyd Memorial Lectures, University of Nottingham, 1958.

DAVIES, W. D. T. 'Random signal testing for evaluating system dynamics', *Wireless World* 1966.

GILL, K. F. and REED, E. W. 'A study into the use of pseudo random binary sequence pressure disturbances to measure sonic velocity in a two-phase flow system', *Proc. Instn mech. Engrs* 1972 **186**, 449.

REED, E. W. and GILL, K. F. 'Correlation techniques—a guide for the practising engineer.' To be published.

REED, E. W., MOBBS, F. R. and GILL, K. F. 'Measurement by correlation of small amplitude pressure wave propagation velocity in a gas–solids flow'. To be published by Institute of Measurement and Control. *Proc. Symp. Measurement Process Identification by Correlation Spectral Techniques* 1973 (Institute of Measurement and Control, London).

PAPER 24

INVESTIGATION OF NON–REFLECTING END CONDITIONS WITHIN A DUCT BY MEANS OF PSEUDO–RANDOM BINARY PRESSURE PULSES

E. W. Reed

*Department of Mechanical and Production Engineering,
The Polytechnic, Leeds LS1 2HE, England*

AND

M. A. Ali and K. F. Gill

*Department of Mechanical Engineering,
University of Leeds, Leeds LS2 9JT, England*

A newly developed experimental technique is described for detecting in-duct pressure waves reflected from a termination. An application of the technique to making the end of a partially closed pipe non-reflecting is also described. The method is potentially applicable to a wide range of pressure wave action problems. In cases such as in two-phase flow work it may well be the only practical approach. Measuring times are short, less than one second, and readings are easy to take. The technique adopted is to inject small amplitude pressure pulses in the form of a pseudo-random binary sequence which allows on-line and easily interpreted correlograms of incident and reflected waves to be obtained.

1. INTRODUCTION

In an earlier study [1, 2] of two-phase flow systems a generator was developed for injecting small amplitude pseudo-random binary sequence (p.r.b.s.) pressure pulses into a system. Used in conjunction with a correlator, it formed the basic monitoring and test equipment which enabled acoustic velocities within the two-phase system to be measured.

The wider capabilities of this technique are now being realized and an example is presented in this paper. It is hoped that other experimenters will see applications beyond the one demonstrated here.

This paper describes a means of adjusting the partially closed end of a duct containing air, under atmospheric conditions, so that it is non-reflecting to small amplitude pressure pulses of low-frequency content.

2. THEORETICAL CONSIDERATIONS

An understanding of p.r.b.s. may be obtained by considering Figure 1. Briefly, a p.r.b.s. is a sequence which has two levels and may switch between levels only at certain fixed intervals of time which are integer multiples of a basic interval of time known as a "bit". Full description and exact forms of p.r.b.s. may be obtained from the literature [1–3]. The most important property of a p.r.b.s. signal for this type of work is that its auto-correlation function (a list of

(a)

(b)
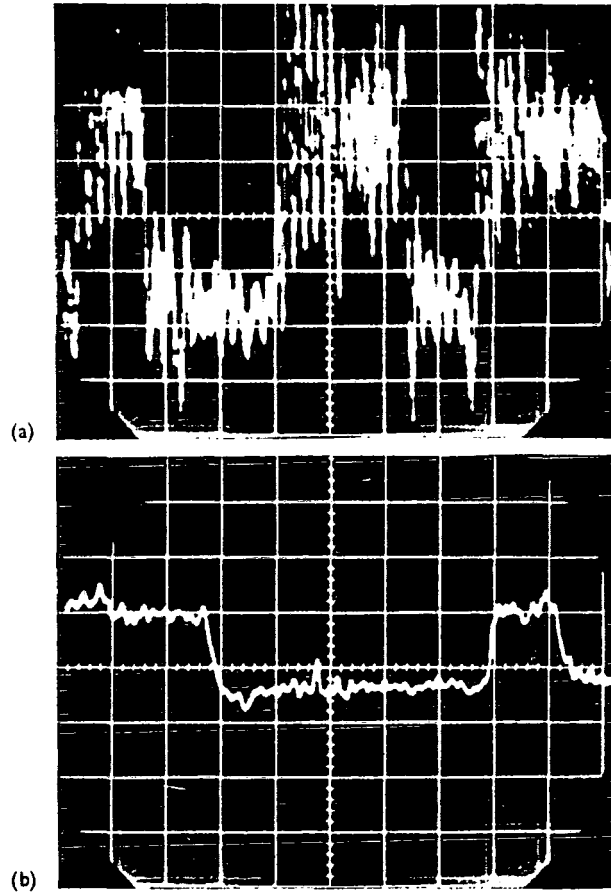
Plate 1. Typical incident pressure pulse at non-reflecting end condition: (a) without filtering; (b) after filtering.
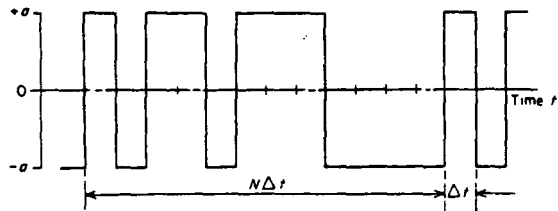
Figure 1. An idealized p.r.b.s. signal.

notation is given in Appendix II),

$$\Phi_{xx}(\tau) = \underset{T \to \infty}{\text{Limit}} \frac{1}{2T} \int_{-T}^{+T} x(t)\,x(t+\tau)\,\mathrm{d}t,$$ (1)

is a series of well-defined triangular "spikes" of base width $2\Delta t$, period $N\Delta t$ and amplitude a^2.

It follows that a p.r.b.s. signal, $x(t)$, cross-correlated with another p.r.b.s. signal, $y(t)$, such that $y(t) = kx(t - \tau_1)$ where k is a constant and τ_1 a time delay, will give the cross-correlation function

$$\phi_{xy}(\tau) = \underset{T \to \infty}{\text{Limit}} \int_{-T}^{+T} kx(t - \tau_1)\,x(t+\tau)\,\mathrm{d}t.$$ (2)

This gives a correlogram identical to that for $\phi_{xx}(\tau)$ but delayed by τ_1 and with "spike" amplitude ka^2 (see Figure 2).

Consider Figure 3. Any small pressure disturbances within the pipe between A and B will be reflected from both the ends with reflection coefficients k_A and k_B, respectively. These reflections will travel to and fro between A and B without any influence on one another [4]. For the purpose of this analysis a reflection coefficient is defined as the ratio of the amplitude of the reflected wave to that of the incident wave. For simplicity, low frequencies are assumed, so that both incident and reflected waves will be essentially plane and the reflected wave will have approximately the same shape as the incident wave, although of course it may differ in either amplitude or phase, or both.

Let the p.r.b.s. pressure pulses injected at A be $x(t)$ and let the time for these pulses to travel the distances AC and CB be τ_1 and τ_2, respectively. The signal $y(t)$ recorded at C will then be

$$y(t) = x(t - \tau_1) + k_B x(t - \tau_1 - 2\tau_2) + k_A k_B x(t - 3\tau_1 - 2\tau_2) + k_A k_B^2 x(t - 3\tau_1 - 4\tau_2). \quad (3)$$
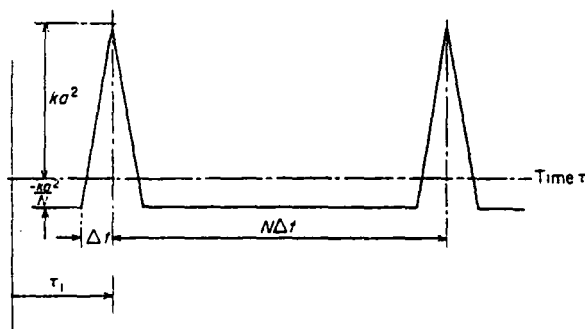
Figure 2. Idealized cross-correlogram given by equation (2).
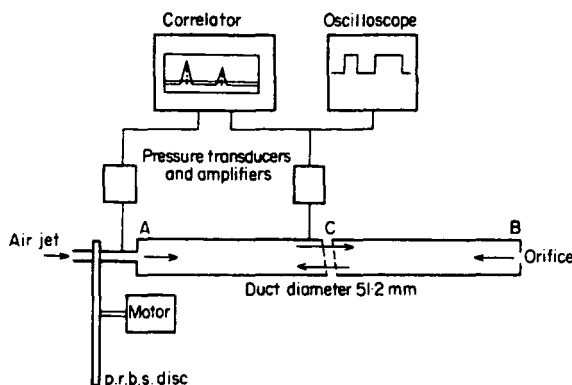
Figure 3. Schematic of experimental arrangement.

As the non-reflecting condition is approached k_B tends to zero and if k_A is made small then clearly only the first two terms are significant. The cross-correlation function, $\phi_{xy}(\tau)$, then approximates to

$$\underset{T \to \infty}{\text{Limit}} \frac{1}{2T} \int_{-T}^{+T} x(t-\tau_1)\, x(t+\tau)\, dt + \underset{T \to \infty}{\text{Limit}} \frac{1}{2T} \int_{-T}^{+T} k_B\, x(t-\tau_1+2\tau_2)\, x(t+\tau)\, dt. \qquad (4)$$

This will give a correlogram showing two sets of periodic spikes. The first will be delayed from the origin by τ_1. The second set will be delayed from the first set by $2\tau_2$ and have a relative amplitude of k_B. The direction and magnitude of this second spike is directly dependent upon k_B. For the non-reflecting condition $k_B = 0$ and the second spike disappears.

3. THE EXPERIMENTAL METHOD

Figure 3 shows diagrammatically the pipe system under investigation and the necessary measuring equipment. The aim of the experiment was to investigate the conditions for the end of the duct at B to be non-reflecting. This condition was obtained for end plates with holes of different sizes; the amplitude of the p.r.b.s. pressure pulses was altered until the second spike, on the cross-correlogram of the signals from the pressure transducers at A and C, just disappeared. Figure 4 shows typical correlograms.

The p.r.b.s. generator basically consisted of a specially slotted disc which rotated to interrupt a fine jet of air. The train of pressure pulses which resulted has a p.r.b.s. pattern similar to that of Figure 1, and was detected by a sensitive piezoelectric pressure transducer. A full description of this generator is given in reference [1].

The pressure transducer at C was a highly sensitive piezoelectric device, and a proprietary correlator, showing correlograms on a screen with X-Y plot-out facilities, was available.

The output from the transducer at C was recorded on a storage oscilloscope from which the amplitude of the p.r.b.s. pressure pulses within the pipe could be obtained. A photograph of a typical oscilloscope record is shown in Plate 1.

Before the termination conditions at B were adjusted the end at A was made as non-reflecting as possible so that an easily interpreted correlogram would be produced. This was done by altering the size of the hole at A until third and subsequent spikes on the correlogram were eliminated.

The speed of the p.r.b.s. generator, whilst not critical, needed consideration and had to lie within a reasonable range having due regard to time of reflection of the pressure pulses.
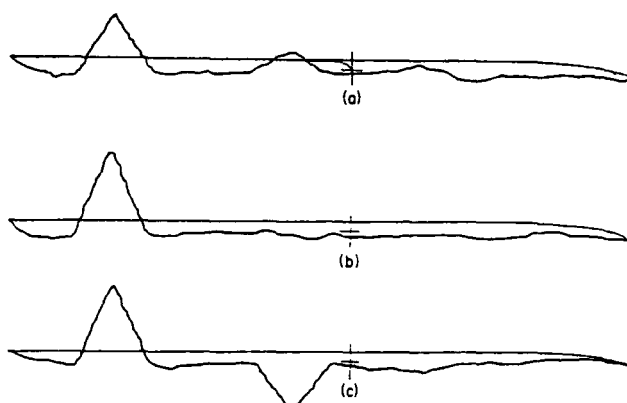
Figure 4. Typical experimental cross-correlograms: (a) showing positive reflection spike; (b) showing reflection spike eliminated; (c) showing negative reflection spike.

It can be seen from Figure 2 that the breadth of the correlation spike of the p.r.b.s. is directly related to the speed of the disc; the faster the speed the sharper and better defined the spike will be. The only provision was that the reflection spike must not in any way coincide with the fundamental spike on the correlogram. The means of calculating p.r.b.s. periods and bit intervals is indicated in Figure 2. The time of reflection could be estimated with sufficient accuracy by measuring the total length of the path and using a local velocity of sound of $347\ \mathrm{ms}^{-1}$.

The upper speed of the p.r.b.s. is limited by the resonant frequency of the piezoelectric transducer which may be considered to have the dynamic characteristics of a second order system with very low damping (damping factor $<0\cdot1$). It is known [2, 3] that the bulk of the power in a p.r.b.s. is below a frequency of $1/\Delta t$ and this frequency must be kept well below the resonant frequency of the transducer if a reasonable p.r.b.s. signal is to be reproduced by that transducer. In the experiment the natural frequency of the transducer and its attachments was 40 kHz and the Nyquist frequency of the p.r.b.s. used was 90 Hz.

4. DISCUSSION OF RESULTS

The experimental results demonstrate the effectiveness of using p.r.b.s. pressure pulses and correlation analysis in the study of small amplitude plane wave reflections (less than 0·005 bar) from an aperture at the end of a duct. The cross-correlograms (Figure 4) are readily interpreted and can be used with confidence. The frequency content of the p.r.b.s. disturbance used had a Nyquist frequency of 90 Hz; it is seen, for this frequency range, by comparing the incident and reflected correlogram spikes, that no sensible band limiting occurred in the reflected pulses.

However, the measurement of pressure amplitude still leaves something to be desired. The high frequency noise can be removed to some extent by the use of passive filters to give a clearer picture on the oscilloscope. An accuracy of $\pm10\%$ is the best the authors can attribute to the pressure measurements made since the mean level fluctuation about a binary level was found to be less than 10% of the binary step. A typical trace is shown in Plate 1.

Figure 5 indicates the divergence between experimental and some theoretically predicted (see equation (A10) of the Appendix) values of area ratio for the non-reflecting condition. This discrepancy may be similar to that reported by Earles and Zarek [5] working in considerably higher pressure ranges; they attempted to explain the difference between theory and experiment by the introduction of a parameter they called the "reflection coefficient of
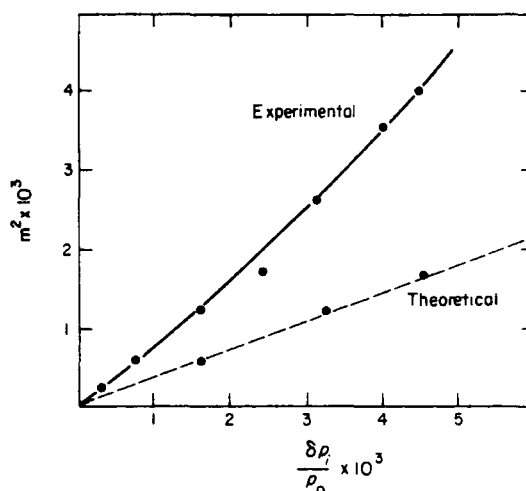
Figure 5. The effect of incident pulse amplitude on area ratio for non-reflecting end condition.

contraction". The numerical value of this coefficient can only be found experimentally and its magnitude is dependent upon the amplitude of the incident pulse. It is believed by the authors that this paper presents the first experimental results indicating the presence of such a coefficient within the low pressure range investigated.

This technique makes possible a straight forward on-line "turning" procedure for making ducts non-reflecting to binary waves with a low Nyquist-frequency and whilst it has only been used here for pulses of small amplitude, due to the limitations of the generator, it is reasonable to suppose that the technique can be extended for use with larger pulses. It thus can be regarded as an alternative, for both small and large pulses, to the traditional single wave testing, which is only possible for large amplitude waves.

ACKNOWLEDGMENT

REFERENCES

1. K. F. Gill and E. W. Reed 1972 *Proceedings of the Institution of Mechanical Engineers* **186**, 39/72 449–455. A study into the use of pseudo random binary sequence pressure disturbances to measure sonic velocity in a two-phase flow system.
2. E. W. Reed, F. R. Mobbs and K. F. Gill 1973 (January). To be published by Institute of Measurement and Control. *International Symposium on Measurement and Process Identification by Correlation and Spectral Techniques, Bradford University.* Measurement by correlation of small amplitude pressure wave propagation velocity in a gas-solids flow.
3. W. D. T. Davies 1966 (August) *Wireless World* **72**, 407–412. Random signal testing for evaluating system dynamics.
4. A. H. Shapiro 1954 *The Dynamics and Thermodynamics of Compressible Fluid Flow.* New York: Ronald Press Company.
5. S. W. E. Earles and J. M. Zarek 1965 (February) *The Engineer* **219**, 383–386. Reflection of pressure waves at sharp-edged orifices.
6. Rev. S. Earnshaw 1860 *Philosophical Transactions of the Royal Society* **150**, 133–136. On the mathematical theory of sound.

E. W. REED, M. A. ALI AND K. F. GILL

APPENDIX I

THEORETICAL ANALYSIS FOR THE NON-REFLECTING END CONDITION

One dimensional isotropic flow conditions are assumed and an equivalent nozzle is postulated to represent the flow through the orifice. When the incident wave reaches the plane of discontinuity XX part of it is reflected and the rest is transmitted (see Figure 6). The reflected
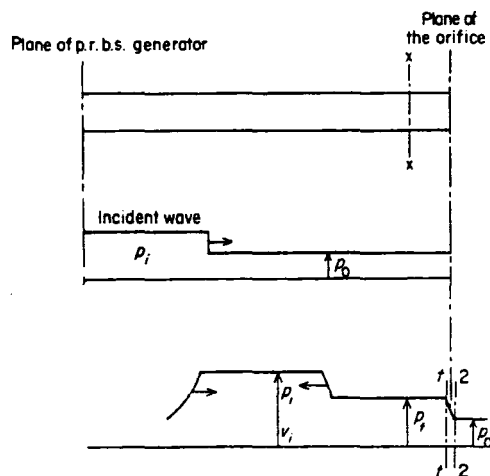
Figure 6. Pressure profile in region of duct construction.

wave is superimposed on the incident wave, which, advancing in the opposite direction, results in a net pressure of amplitude P_t and induced particle velocity v_t.

If the reflection is assumed to be a rarefaction wave, as in Figure 6, then

$$v_{t-1} = v_t - v_t. \tag{A1}$$

After Earnshaw [6],

$$v_t = 5a_0(x_i - 1) + 5a_0(x_t - 1), \tag{A2}$$

$$y_t = 5(x_i + x_t - 2). \tag{A3}$$

For a reflected compression wave

$$y_t = 5(2x_i - x_t - 1). \tag{A4}$$

From wave superposition,

$$x_t = x_i + x_r - 1. \tag{A5}$$

From consideration of the continuity and energy equations,

$$\frac{y_1}{y_2} = m\left(\frac{1}{x_t}\right)^5, \tag{A6}$$

$$5x_t^2 + y_t^2 = 5 + y_2^2. \tag{A7}$$

The condition for a non-reflecting end is

$$x_r = 1. \tag{A8}$$

Hence it can be shown that the nozzle exit area ration necessary for creating a non-reflecting end is

$$m = \left| \frac{5(x_i - 1) x_i^{10}}{(6x_i - 4)} \right|^{1/2}.$$ (A9)

The binomial expansion can be used and equation (A9) squared to give

$$m^2 = \frac{5}{14} \frac{\delta p_i}{p_0}.$$ (A10)

APPENDIX II

NOTATION

p.r.b.s.	pseudo-random binary sequence
t	time variable
Δt	time of one "bit" of p.r.b.s.
N	number of "bits" in a p.r.b.s. after which the sequence repeats
a	amplitude of p.r.b.s.
$\phi_{xx}(\tau)$	Auto-correlation function of signal $x(t)$
$\phi_{xy}(\tau)$	cross-correlation function of signals $x(t)$ and $y(t)$
τ	dummy time delay
τ_1, τ_2	actual signal time delays
k_A, k_B	coefficients of reflection
A_1	cross-sectional area of the duct
A_2	area of the aperture
m	area ratio $= A_2/A_1$
v	induced particle velocity
y	velocity ratio $= v/a_0$
a_0	acoustic velocity
x	pressure ratio $= p/p_0$
p	absolute pressure
p_0	atmospheric pressure
δp	gauge pressure

Suffixes

i	incident wave
r	reflected wave
t	superposition of incident and reflected waves

PAPER 26

Pseudo-random pressure pulses used to determine the shape of reflected waves from an opening

by *E. W. Reed, †M. A. Ali and ‡K. F. Gill

This work forms part of a study into reflection behaviour within a duct directed towards the understanding of the problems associated with metering pulsating gas flows.

A novel application of correlation analysis is used to predict the shape of the reflected wave from an opening of finite thickness. The incident wave is in the form of a pseudo-random binary sequence pressure pulse sequence which enables incident and reflected waves to be distinguished one from the other.

It is shown that for waves of small amplitude, reflections do not occur in like shape to that of the incident wave. These shapes are influenced by both the amplitude of the incident wave and the geometry of the opening. It is believed that this technique makes an original contribution to the study of reflection behaviour and the use of correlation analysis.

1. INTRODUCTION

This paper presents a study of reflection behaviour from a sharp-edged constriction at the end of a duct. It forms part of a general investigation into the problems associated with the metering of pulsating flows by a duct constriction; at present this method does not always give results which can be used with confidence. A novel interpretation procedure is shown, for use with a correlation technique, to obtain the reflection shapes from pipe constrictions.

In the study of pulsating flows it is necessary to be able to measure reflection behaviour within a duct. As an example, Baird and Bechtold[1] supposed that a sharp-edged metering orifice within a pipe possessed dynamic characteristics in the same way as a Helmholtz resonator. Before such ideas could be investigated it was necessary to create the condition in which all reflections from end terminations were suppressed. The hypothesis of Baird and Bechtold has in fact been shown to be unfounded.[2]

The authors have demonstrated, using correlation techniques, how reflections at the end of a duct containing air can be eliminated for the specific set of conditions that the end must terminate in a thin sharp-edged orifice and the incident pressure wave must have an amplitude which is binary in nature.[3,4] Theory suggests[4] that this condition should be obtainable using a short nozzle as the constriction, but the experimental tests leading to the paper presented here failed

* Lecturer, Department of Mechanical and Production Engineering, The Polytechnic, Leeds.
† Research Student, Department of Mechanical Engineering, The University, Leeds.
‡ Senior Lecturer, Department of Mechanical Engineering, The University, Leeds.
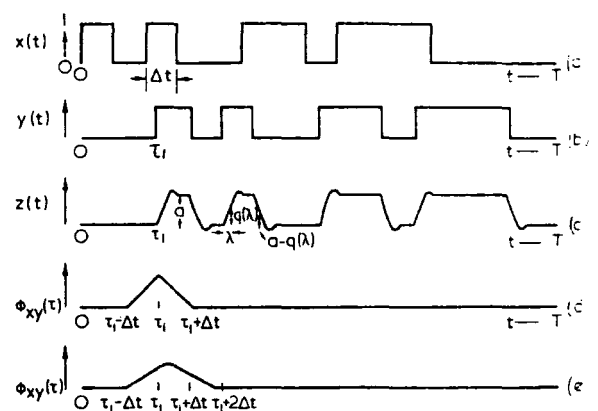
Fig 1   PRBS waveforms.

to support this. The correlograms obtained all follow an unfamiliar but distinctive pattern and consequently a means of interpretation is found so that some explanation can be given for reflections from such constrictions.

The authors suggest that the ideas presented are applicable to the study of reflection behaviour generally. They offer an advance on traditional techniques, are simple to apply and can be used on-line.

For the musically inclined, the reflection shapes occurring at constrictions may give some insight into the behaviour of the sound holes in the bellies of stringed musical instruments.

2. THEORY

An understanding of prbs adequate for the needs of this paper may best be obtained by considering Fig 1. Briefly, a prbs has only two levels and may switch between levels only at certain fixed intervals of time which are integer multiples of a basic interval of time known as a bit. The sequence is random for a definite 'period' which continuously repeats itself in a cyclic manner. Full description and exact forms of prbs may be obtained from the literature.[5] The prbs used in this experiment had a 15-bit sequence of length T and a bit length Δt. It has the form as shown in Fig 1a. One important property of a prbs is that its autocorrelation function is a series of triangular 'spikes', the first 'spike' being at zero time displacement. Similarly, a prbs, Fig 1a, cross-correlated with a delayed version of itself, Fig 1b, the amplitudes not necessarily being the same, will give a cross-correlogram with the first spike delayed as shown in Fig 1a.
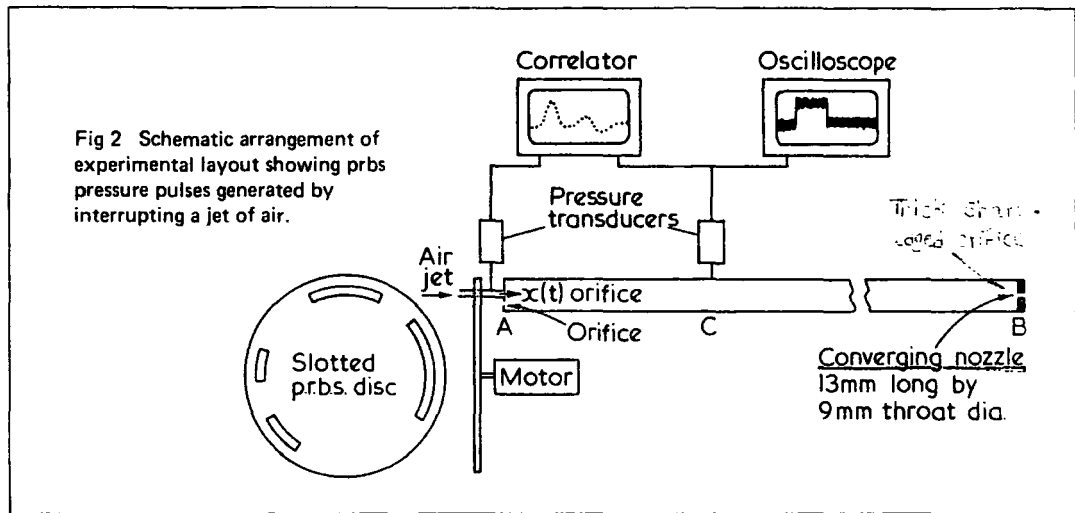
Fig 2 Schematic arrangement of experimental layout showing prbs pressure pulses generated by interrupting a jet of air.

Considering the experimental layout, Fig 2, the injected prbs pressure pulse disturbance at A may be represented by $x(t)$, Fig 1a, where t is a time variable. What the wave at C would be if the prbs were unaltered by the reflection at B is represented by $y(t)$, Fig 1b. The actual reflection, with a shape to be determined, is represented by $z(t)$, Fig 1c. It is assumed that reflections from sharp fronted waves both compressive and rarefactive, behave in the same manner for the same size of amplitude. Considering Fig 1c, λ represents the time, and $q(\lambda)$ the amplitude, at any point on the reflected wave front. Both λ and $q(\lambda)$ are measured from the origin of the wavefront and the time for establishing the wave is such that it is less than Δt.

The cross-correlation function of $x(t)$ and $z(t)$ may be written

$$\phi_{xz}(\tau) = \frac{1}{T} \int_0^T x(t - \tau)\, z(t)\, dt \qquad \ldots (1)$$

where τ represents a time delay in $x(t)$. The limits of integration may be used as shown since both $x(t)$ and $z(t)$ are periodic in time T. Fig 1e represents $\phi_{xz}(\tau)$.

In order to interpret the cross-correlogram, it is necessary to consider the steps required to obtain that cross-correlogram, viz:

1. The signals $x(t)$ and $z(t)$ are sampled and digitized at equally spaced time divisions each of length δt such that $T = n\delta t$.
2. The corresponding values of $x(t)$ and $z(t)$ are multiplied together over a period T and the average value obtained. Since $x(t)$ has only values of 'one' or 'zero', this can be simplified by merely adding together appropriate values of $z(t)$ and dividing by n. This gives one value of the cross-correlation function.
3. The signals are now displaced relative to one another by a series of time delays τ and the process repeated so that a complete cross-correlogram can be plotted.

Hence

$$\phi_{xz}(\tau) = \frac{\sum_{i=0}^{i=n} z(t - \tau_i)}{n} \qquad \ldots (2)$$

for values of $z(t - \tau_i)$ when $x(t) = 1$. From the evaluation of equation (2) it is found that $\phi_{xz}(\tau)$ is constant except for the range where τ lies between $\tau_1 - \Delta t$ and $\tau_1 + 2\Delta t$.

Consider the range $\tau_1 - \Delta t \leqslant \tau \leqslant \tau_1$

$$\phi_{xz}(\tau_1 - \Delta t + \lambda) = \phi_{xz}(\tau_1 - \Delta t + \lambda - \delta t)$$
$$+ \frac{2q(\lambda) - 2|a - q(\lambda)| + 2a}{n} \qquad \ldots (3)$$

Rewriting and using $T = n\delta t$ gives:

$$\frac{\phi_{xz}(\tau_1 - \Delta t + \lambda) - \phi_{xz}(\tau_1 - \Delta t + \lambda - \delta t)}{\delta t} = \frac{4q(\lambda)}{T} \qquad \ldots (4)$$

If δt is small then in the range $\tau_1 - \Delta t \leqslant \tau \leqslant \tau_1$ the slope of

$$\phi_{xz}(\tau) = \frac{4q(\lambda)}{T} \qquad \ldots (5)$$

In practice, correlation is done on a proprietary correlator and so it is more useful to write equation (5) as the slope of

$$\phi_{xz}(\tau) = Cq(\lambda) \qquad \ldots (6)$$

where C is a constant dependent upon the correlator settings.

Similarly it may be shown that, in the range $\tau_1 < \tau \leqslant \tau_1 + \Delta t$, the slope of

$$\phi_{xz}(\tau) = C|a - 2q(\lambda)| \qquad \ldots (7)$$

and that, in the range $\tau_1 + \Delta t < \tau \leqslant \tau_1 + 2\Delta t$, the slope of

$$\phi_{xz}(\tau) = C|q(\lambda) - a| \qquad \ldots (8)$$

It follows that by dividing into three zones, each of length Δt, that part on the cross-correlogram corresponding to the reflected wave and measuring a series of slopes then $q(\lambda)$ may be deduced. The absolute magnitudes of the reflected wave may be obtained by comparison with the amplitude of the incident wave which may be similarly obtained from the cross-correlogram.

3. EXPERIMENTAL METHOD

The technique of prbs pressure pulse testing is fully described in References 6, 7 and 8. Considering Fig 2, the pulses are injected at A. The pressure signals at A and C are cross-correlated and the correlogram shows representative 'spikes' at each time delay for which the pulses take to reach C, either direct or by reflection. The orifice at A is tuned to minimise reflections from this end so that third and subsequent 'spikes' on the correlogram can be neglected.

Correlograms were taken by pen recorder direct from the correlator. Computation from the slope of this correlogram

Fig 3   The values of the reflected wave amplitude are calculated from the formula:

Slope of reflection wave spike

$$\frac{\text{Slope of reflection wave spike}}{\text{Slope of incident wave spike}} \times \text{Amplitude of incident wave}$$
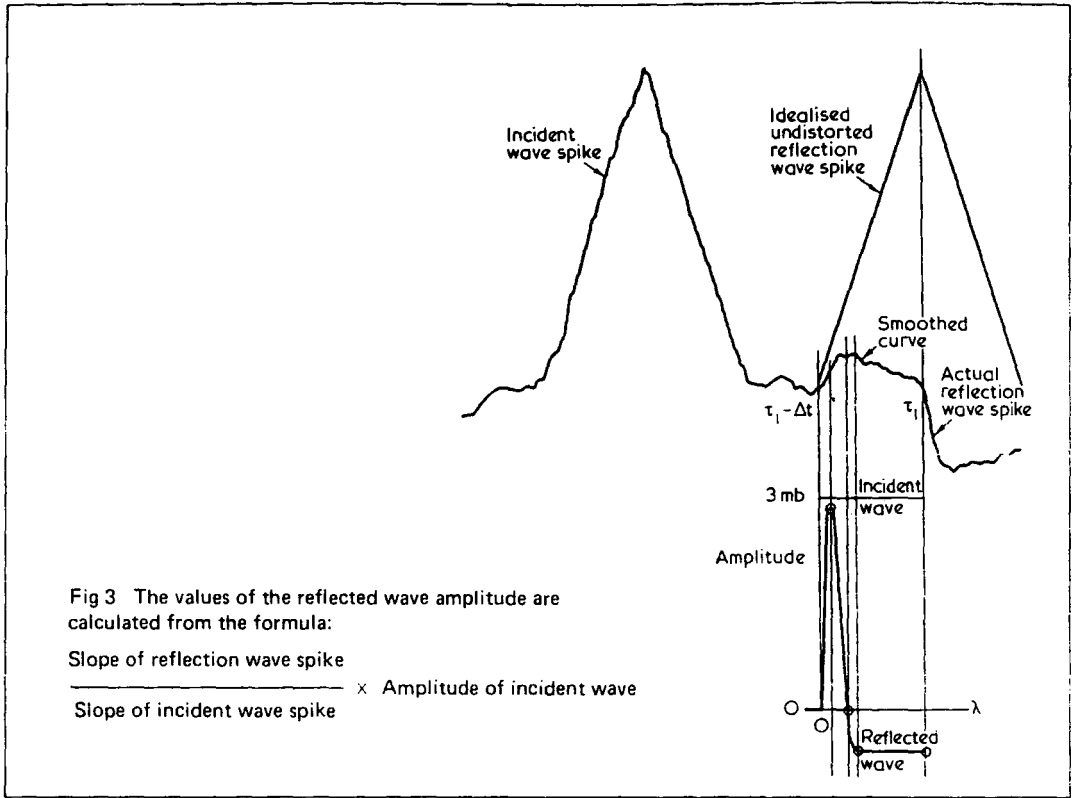
was used to indicate the shape of the reflection wave. The shape was sketched from points of most significance on the correlogram, ie, steady state, maximum value, etc, and the values normalised by comparison with the amplitude of the incident wave obtained from the same correlogram. Fig 3 gives an example using the correlogram of the 3 mb incident wave given in Fig 4.

Nominal absolute values of the incident wave amplitude were obtained from an oscilloscope trace.

4. DISCUSSION OF RESULTS

The experiment demonstrates an approach that enables the shape of the wave, reflected from an opening, to be predicted for a steep fronted flat-topped incident wave of known statistical properties. Using an incident pressure wave in the form of a prbs is shown to be extremely effective and is the only practical way yet known to the authors for waves of small amplitude.

Fig 4 shows clearly the well-defined trend of the reflection spike in the correlograms for the series of tests undertaken. Fig 5 shows the estimated wave shapes as computed from these correlograms. If the shape of the reflected wave had been similar to the incident wave then the respective part of the correlogram would likewise have been similar; this difference is ascribed to the changed shape of the reflection.

The opening chosen was such that if it had been sharp-edged, a non-reflecting condition could have been obtained within the pressure range of testing.[3,4] It is seen that there is always an initial pressure change of the same polarity as the incident wave whatever the final value of the steady pressure state. This indicates that tuning for a non-reflecting state is not possible with end constrictions of finite thickness. It is suggested that for a sharp-edged orifice this initial pressure overshoot becomes undetectable.

Earlier experiments using a sharp-edged orifice[3,4] showed that reflection behaviour was dependent upon incident wave

amplitude. It can be seen that this condition still applies with the introduction of a constriction of finite thickness indicating that reflection behaviour is influenced by both orifice geometry and incident wave amplitude.
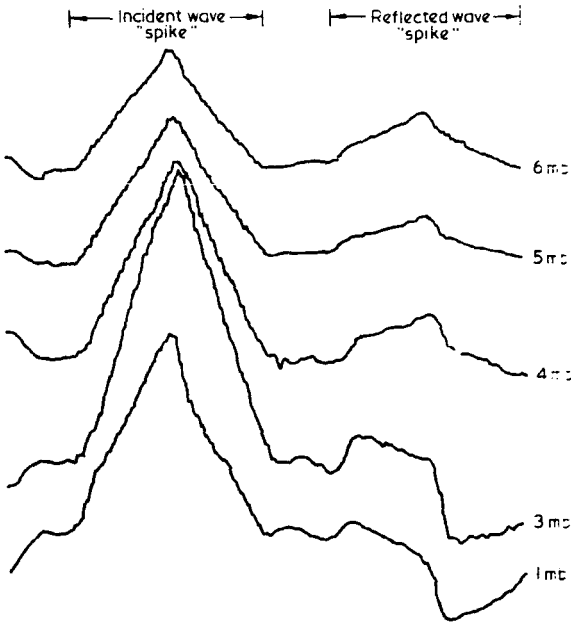
Fig 4   Cross-correlograms (full scale 333 ms)

Fig 5 Estimated wave shapes computed from correlograms in Fig 4.
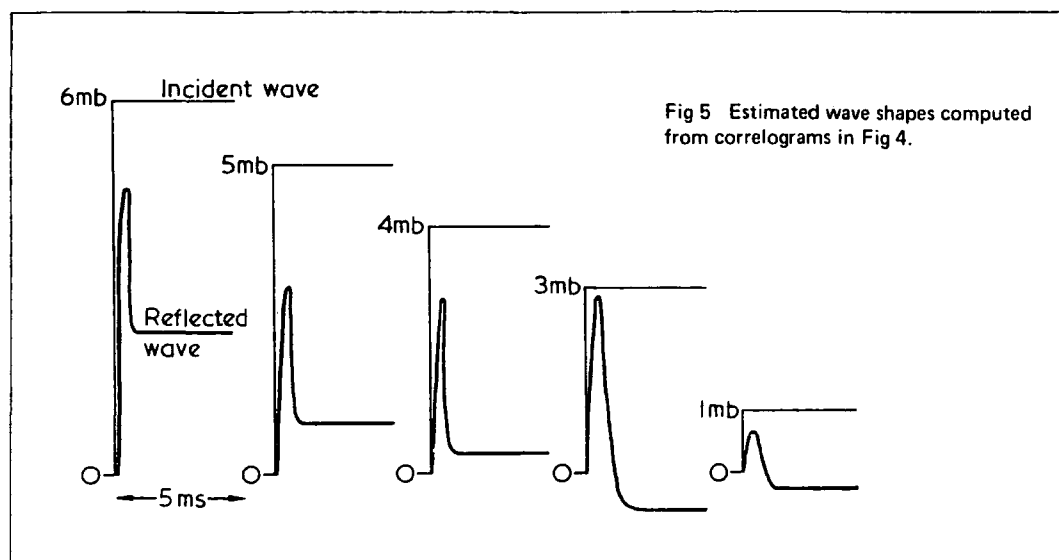
5. REFERENCES

1. **Baird, R C, and Bechtold, I C.** 'The dynamics of pulsating flow through sharp-edged restrictions (with special reference to orifice-metering)', ASME, Nov 1952, 1381.
2. **Ali, M A, Reed, E W, and Gill, K F.** 'A study into the dynamic characteristics of wave action through a duct constriction'. Offered to ASME, Mar 1973.
3. **Reed, E W, Ali, M A, and Gill, K F.** 'An investigation of non-reflecting end conditions within a duct using pseudo-random pressure pulses'. Offered to Institution of Sound and Vibration Research, Nov 1972.
4. **Ali, M A, Reed, E W, and Gill, K F.** 'A correlation method for measuring reflection coefficients of sharp-edged orifices for small amplitude pressure waves'. To be published by I Mech E.
5. **Shapiro, A H.** 'The Dynamics and Thermodynamics of Compressible Fluid Flow', Ronald Press Company. New York, 1954.
6. **Gill, K F, and Reed, E W.** 'A study into the use of pseudo-random binary sequence pressure disturbances to measure sonic velocity in a two-phase flow system', *Proc I Mech E.* 1972, Vol 186, 39/72.
7. **Reed, E W, Mobbs, F R, and Gill, K F.** 'Measurement by correlation of small amplitude pressure wave propagation velocity in a gas–solids flow'. International Symposium on Measurement and Process Identification by Correlation and Spectral Techniques, Bradford Univ. Jan 1973. Published by Institute of Measurement and Control.
8. **Reed, E W, and Gill, K F.** 'An experimental technique for minimizing resonance within a ducted fluid'. *JMES.* Vol 15, No 2, 1973.
9. **Davies, W D T.** 'Random signal testing for evaluating system dynamics', *Wireless World,* Aug 1966.

PAPER 27

1

PSEUDO-RANDOM BINARY-SEQUENCE PRESSURE-PULSE TESTING IN THE
STUDY OF FLOW BEHAVIOUR

E.W. Reed*, K.F. Gill[+] and M.A. Ali[+]

A technique has been developed which is described
by the authors as "pseudo-random binary-sequence
pressure-pulse testing" for the investigation of
difficult flow problems.

The aim of the paper is to demonstrat the
technique, since it is believed that it will be
of use to workers in the field of multi-phase
flows in which traditional measuring techniques
are so difficult to apply. It will be shown in
the paper that the technique is easy to apply and
that it is robust and reliable.

INTRODUCTION

Traditional on-line measuring techniques applied to two phase flow
systems containing gaseous and solid particle streams have limited
value since the presence of solid particles can cause structural
damage or block entry passages to the monitoring devices commonly
used. The technique of pseudo-random binary-sequence (p.r.b.s.)
pressure-pulse testing is a possible general means of making
measurements in such fluid systems. It is easy to apply, it is
robust in structure and it gives results that can be used with
confidence. It enables on-line measurements to be made that
previously have been unobtainable.

The phenomena of gas-solids flow occurs throughout industry
in such applications as the pneumatic transportation of foods,
fertilisers, ceramics, cosmetics, chemicals and so on. Since in
the study of gas flow the sonic velocity and Mach number are of
fundamental importance, attempts have been made to retain these
concepts in the understanding of gas-solids flow phenomena. The
sonic velocity concept makes the gas dynamic equations more
compact and indicates the boundary at which the choked flow
condition occurs. A mathematical model describing a two phase
flow system would help in the interpretation of this behaviour in
many physical processes. To help in the building of this model,
experimental work is described which measures the sonic velocity
in a two-phase flow system that to date has only been predicted
theoretically.

*Department of Mechanical and Production Engineering, The Poly-
 technic, Leeds LS1 3HE.
+Department of Mechanical Engineering, The University, Leeds 2.

Clearly an effective on-line means of measuring this sonic velocity was required if the assumptions made in the derivation of these models were to be substantiated. The p.r.b.s. pressure pulse testing technique was developed initially as a practical method of measuring this sonic velocity parameter in an air and polystyrene particle stream (Gill and Reed (1972)). Because of the inadequacy of the gas-solids flow rig available subsequent work has been limited to clean gas flows. A series of original experiments was conducted in order to gain extra insight. Applying the technique has enabled measurements to be made which had never before been obtained.

The experimental results did demonstrate that the application of p.r.b.s. pressure pulse testing makes possible continuous on-line measurements to be made with minimal interference to the flow system. This is a method that is useful and practical in both an experimental and industrial environment.

METHOD

The method is to inject, into the system under test, small amplitude pressure disturbances of a controlled nature and investigate the subsequent behaviour of these pulses by statistical processing. These pulses are described by a pseudo-random binary-sequence (p. r.b.s.), Fig. 1., which has the special property that its auto-correlation function is a series of well defined triangular spikes of base width $2\Delta t$ and period $N\Delta t$, Fig. 2.

The p.r.b.s. pressure pulse generator used basically consists of a fine jet of air interrupted by a specially slotted disc and directed into the system being tested Fig. 3. The pressure signals are detected by robust piezoelectric transducers which can be mounted in the wall of the duct.

The choice of Δt is a compromise between a sharp spike for the autocorrelogram of the p.r.b.s. signal and limiting the band-width of the spectral distribution to be approximately half of the natural frequency of the measuring transducers. This is necess-ary to ensure constant transducer sensitivity within the spectrum of the injected p.r.b.s. signal. The line spectrum of a p.r.b.s. is shown in Fig. 4.

1.   Sonic Velocity Measurement in Gas-Solids Flow

The p.r.b.s. pressure pulse disturbances was injected at station A and detected at station B, Fig. 5. Cross-correlating these two signals resulted in a correlogram showing a peak shifted from the origin by a time corresponding to the transport delay of the disturbance travelling between stations A and B.

The output from most physical systems will be corrupted by additive noise and in practice it is necessary to correlate over several cycles to obtain a well defined correlogram. To measure sonic disturbances, it is essential to inject very small amplitude pressure pulses which inevitably will be swamped by the noise inherent in a gas-solids system, and the important advantage of using correlation is that these small test signals can still be detected.

3.

Some experimental results are presented, Fig. 6, and compared
with those obtained from theoretical work (Cole et al (1969)). The
marked discrepancy between the experimental and theoretical values
led to a thorough investigation of the validity of the experimen-
tal technique.

Firstly, a complete study was made of acoustic behaviour for
air alone and all the accepted values were measured to a good
degree of accuracy using this experimental technique.

Secondly, it was thought that there could be a thin layer of
virtually uncontaminated air around the inside of the pipe,
through which the disturbance travelled, but a comparison with
readings taken with probes at various depths within the pipe
showed no evidence of this.

A third possibility was that the disturbance could be travel-
ling within the pipe walls; replacing the transporting pipe, which
was made of brass, by one made of polythene gave the same results,
as would be expected, since the sonic velocity in a solid is much
higher.

A fourth possibility was that there was a time lag between
the input signal as recorded and as it just entered the pipe, but
a cross correlation between these two points revealed no detect-
able time shift.

A last possibility could be, of course, that the mathematical
concept of sonic velocity is not applicable as modelled (Cole et al
(1969)) for the two-phase flow system tested experimentally.

2.   Mean Velocity Measurement of Pulsating Gas Flows
(Reed et al (1973 (a)   (b)))

Using both p.r.b.s. pressure pulses and natural disturbances
it has been found possible to obtain accurately mean velocities of
fast flows by differencing the propagation velocity and the sonic
velocity.   This represents a major contribution to a region where
established measuring techniques are extremely cumbersome.   The
results of these tests are shown in Fig. 7.

From the results obtained so far, and considering all the
attempts already made by other workers, leads one to the general
conclusion that the large errors, associated with metering pulsa-
ting flows by a duct constriction, are so complex and far from
being understood that this alternative approach to metering these
flows is the more profitable.   Even if these errors were under-
stood it is likely that the monitoring equipment, necessary to
take these errors into account, would be complex and far removed
from the simple manometry used in steady flow measurements.

3.   Production of a Non-Reflecting Air Duct (Reed et al (1974))

There is a time delay between incident and reflected waves
and hence individual spikes, corresponding to each wave sequence,
appear uniquely on the correlogram.   Consequently, it has been
found possible to monitor reflection behaviour and tune the end of
an air duct so that no reflections occur, Fig. 8.   This creates

the infinite pipe much postulated in the text books.

The main points to note are that for tuning to be at all possible, the following conditions must apply:
(i)   the end of the pipe must terminate in a sharp edged orifice;
(ii) the incident wave must be binary in nature and have a specific value of amplitude for a given pipe-orifice geometry.

The traditional sine wave testing could never have revealed this condition.

4.   Determination of Reflection Coefficients at the End of a Duct (Ali et al (1973 (a)))

The height of the spikes appearing on the correlogram are a measure of the amplitude of the corresponding waves.   It follows that reflection coefficients can be estimated from the height of the appropriate spike, Fig. 8.

It is shown that this method enables reflection coefficients to be measured with considerable ease for waves of small amplitude The established method is to set up a standing wave within the pipe system and infer the reflection coefficient from the standing wave ratio.   It is shown that reflection coefficients are dependent upon constriction size and incident wave amplitude.   As the condition for minimum reflection is approached for smaller orifices the reflection coefficient is particularly sensitive to changes in incident pressure wave amplitude, thus ruling out the possibility of some wave testing within this region.

5.   Other Studies

(i)   The concept of the "reflection coefficient of contraction" has been shown to exist for waves of small amplitude Ali et al (1973 (a))).   This coefficient was found to lie between 0.65 and 0.67.   Previously no such experimental evidence was available since the established experimental techniques were limited to waves of large amplitude (7).
(ii)   The hypothesis of Baird and Bechtold (1952) that a duct constriction possesses second order dynamic characteristics of the same form as a Helmholtz resonator is shown to be without substance (Ali et al (1973 (b))).   These dynamics are shown to exist for a Helmholtz resonator when subjected to p.r.b.s. pressure pulse testing but when applied to a duct constriction no evidence of the existence of acoustic dynamics could be found.   The only suggestion about the phase shift measured by Baird and Bechtold is that their experimental procedure was inadequate.

DISCUSSION

The results of the thorough investigation initiated because of the discrepancy with the theory (Cole et al (1969)), has validated p.r. b.s. pressure pulse testing.   The outcome is to establish that the answers produced by this method were essentially correct and that the theory must therefore have been at fault.   This has led to a revised approach to the theoretical study of gas-solids flows

by the workers at Leeds University (Marquand, Warda). A broad conclusion that was drawn was that the sonic velocity within a gas-solids system was little influenced by the solids loading. This leads one to believe that it may be possible to devise a means of measuring the velocity of the gas flow, within a fast gas-solids flow system, by the principle of differencing sonic velocity measurements as has been demonstrated for the measurement of pulsating clean gas flow.

It was noticed that the amplitude of the peak of the corre-logram diminished as the solids to gas flow rate increased. It is felt that this is a line of research worthy of pursuit as it would seem to offer a ready means of monitoring solids flow rates. This is a region of measurement which at present is very inade-quate. For non-steady flow regions, air box damping is totally unacceptable since the box would be filled with solids and at present no technique for such gas flow measurements is available.

Experiments on end reflection behaviour produced several important results. The most significant, as far as further experiments on acoustic work is concerned, is the discovery of a means of tuning a pipe system so as to eliminate end reflections. This has not only enabled the series of experiments, illustrated in this paper, to be carried out but should help other experimen-ters in this field of study.

In addition to the useful information shown in this paper the tests indicate the potential of p.r.b.s. pressure pulse testing as a general means of obtaining measurements in fluid systems. The technique is seen to be easy to apply, it uses robust equip-ment and gives reliable results. It has enabled measurements to be made which previously were unobtainable.

<div align="center">APPENDIX 1.</div>

Correlation Theory For Velocity Measurement

Consider any continuous disturbance travelling along a pipe from A to B as shown in Fig. 5. Assume the signal recorded at A is x(t) and the signal recorded at B is y(t) then the cross-correlation function defined as $\phi_{xy}(\tau)$ is:

$$\underset{T \to \infty}{\text{Limit}} \quad \frac{1}{2T} \int_{-T}^{+T} y(t)x(t+\tau)dt \tag{1}$$

where τ is a time delay between x(t) and y(t).

For such a function $\phi_{xy}(\tau)$ a maximum value will occur at some time delay $\tau = \tau_{max}$ which gives a measure of the time necessary for the continuous disturbance to travel from A to B in Fig. 5. This value enables the velocity of the disturbance to be evaluated. If a small steep fronted pressure disturbance is introduced then the value of $\tau = \tau_{max}$ measured will enable the sonic velocity of the fluid system to be found experimentally.

6.

SYMBOLS USED

$x(t)$, $y(t)$ = signals as functions of t

t = time s

T = length of time sample s

τ = time delay s

$\phi_{xy}(\tau)$ = cross-correlation between functions $x(t)$ and $y(t)$.

REFERENCES

Gill, K.F. and Reed, E.W., 1972, Proc. I. Mech. E., 186, 39/72.

Cole, N., Bowers, H.M. and Mobbs, F.R., 1969-70, Proc. I. Mech. E., 184, part 3C.

Reed, E.W., Ali, M.A. and Gill, K.F., 1973, offered to I. Mech. E.,

Reed, E.W., Ali, M.A. and Gill, K.F., 1974, Inst. of Meas. and Control, 7 31-34.

Reed, E.W., Ali, M.A. and Gill, K.F., 1974, J. of Sound and Vibr. 33

Ali, M.A., Reed, E.W. and Gill, K.F., 1973, J. Mech. Eng. Sci, 15, 321-325.

Earles, S.W.E. and Zarek, J.M., 1965, The Engineer, Feb.

Baird, R.C. and Bechtold, I.C., 1952, Trans. of A.S.M.E., Nov.

Ali, M.A., Reed, E.W. and Gill, K.F., 1973, offered to A.S.M.E., March 1973.

Marquand, C.J., 1972, Ph.D. Thesis, Leeds. Univ.,

Warda, H.A.H., Ph.D. Thesis, Leeds Univ. Being prepared.
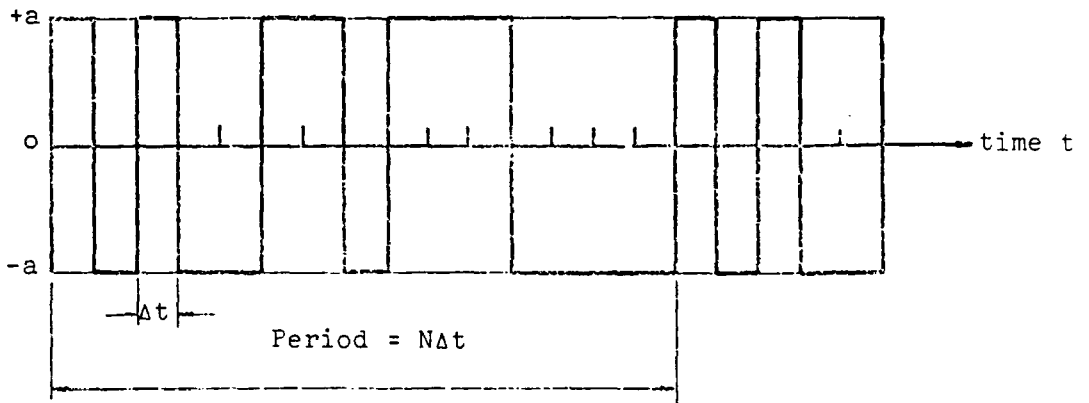
Fig. 1.   A typical pseudo-random binary sequence
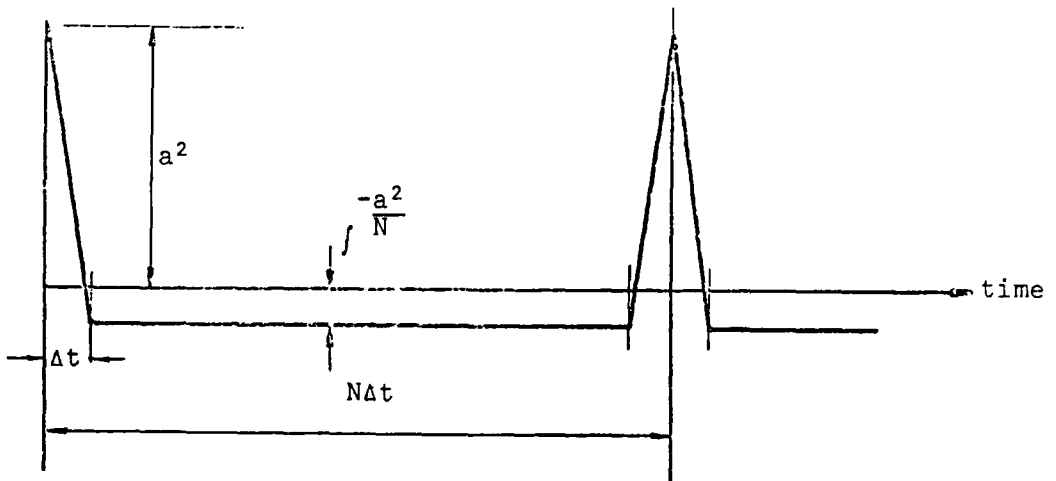
Fig. 2.   Autocorrelogram of sequence shown in Fig. 1.
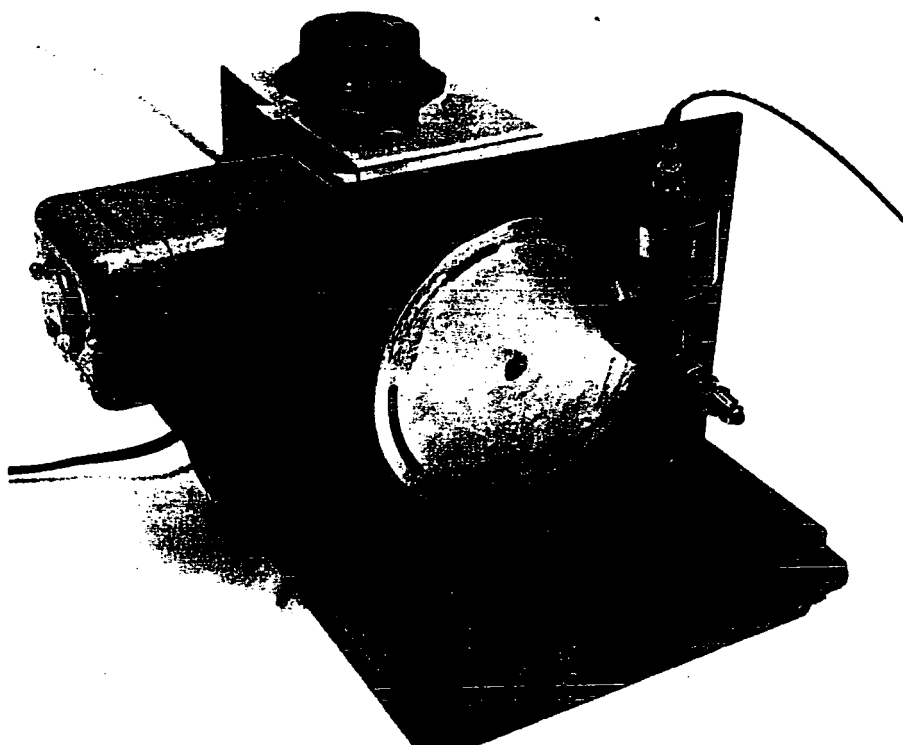
Fig. 3.   Pseudo random binary sequence pressure
         pulse generator.
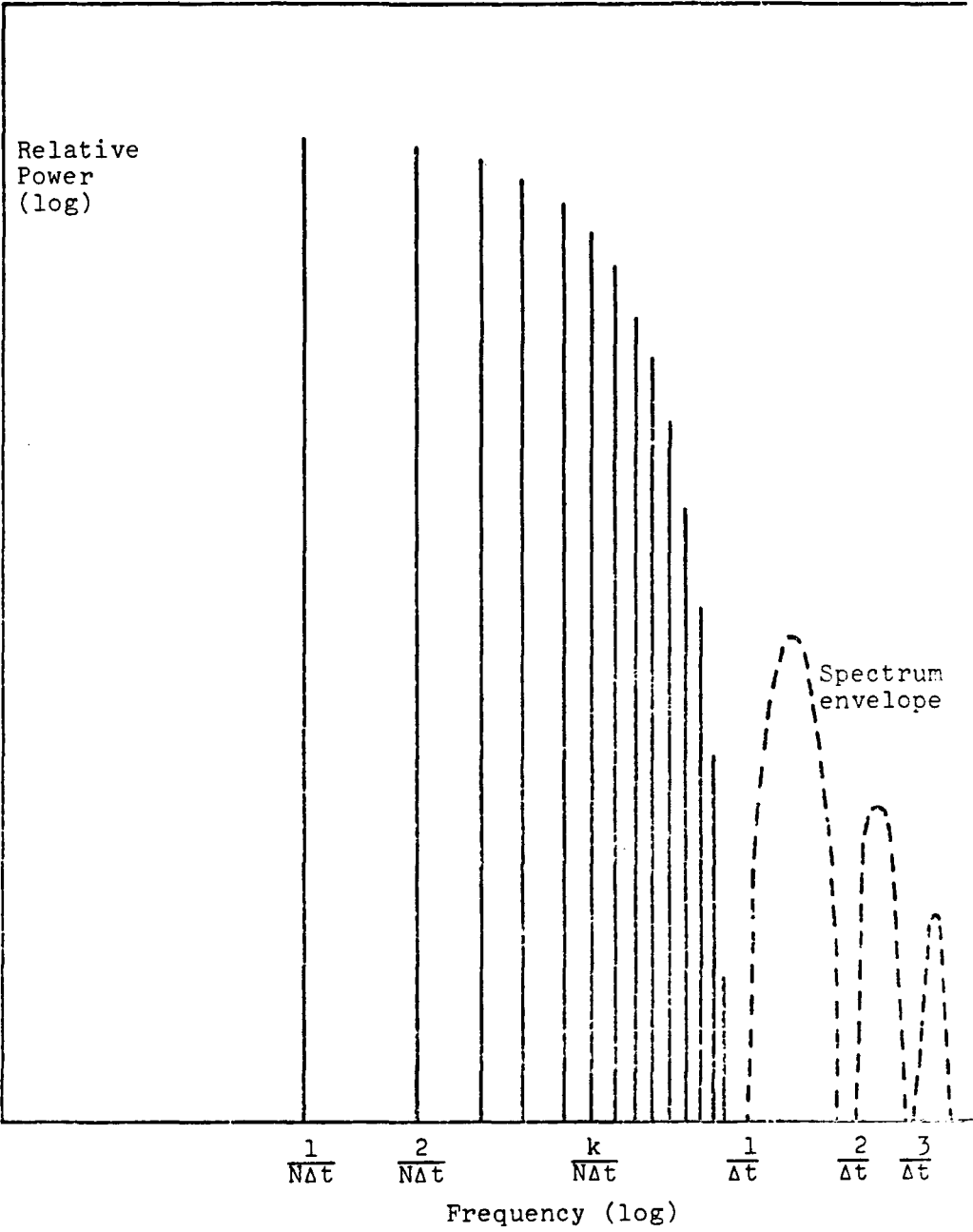
Fig. 4.   Power Spectrum of 15 "bit" period p.r.b.s.
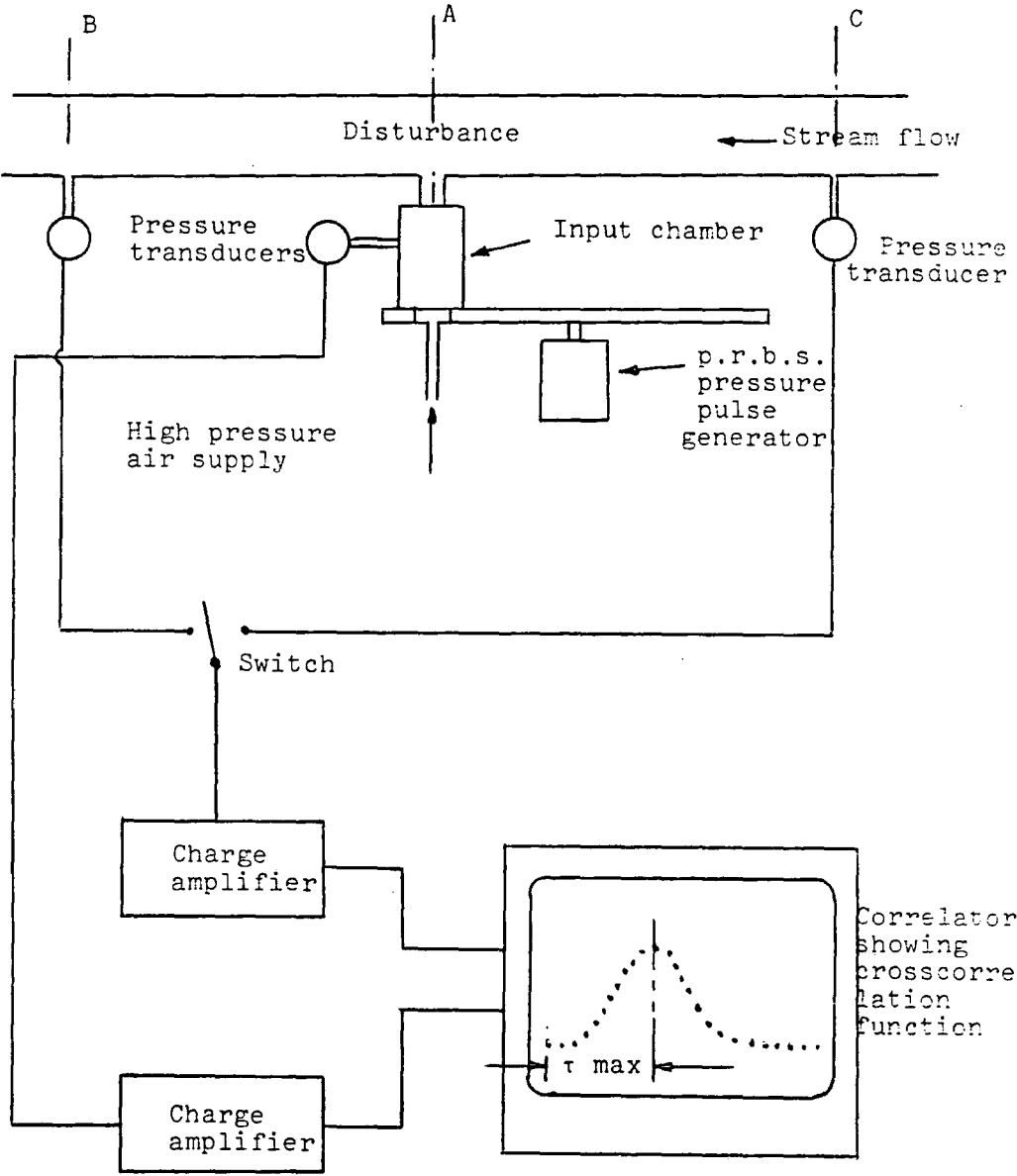
Fig. 5.   Schematic diagram of experimental layout.
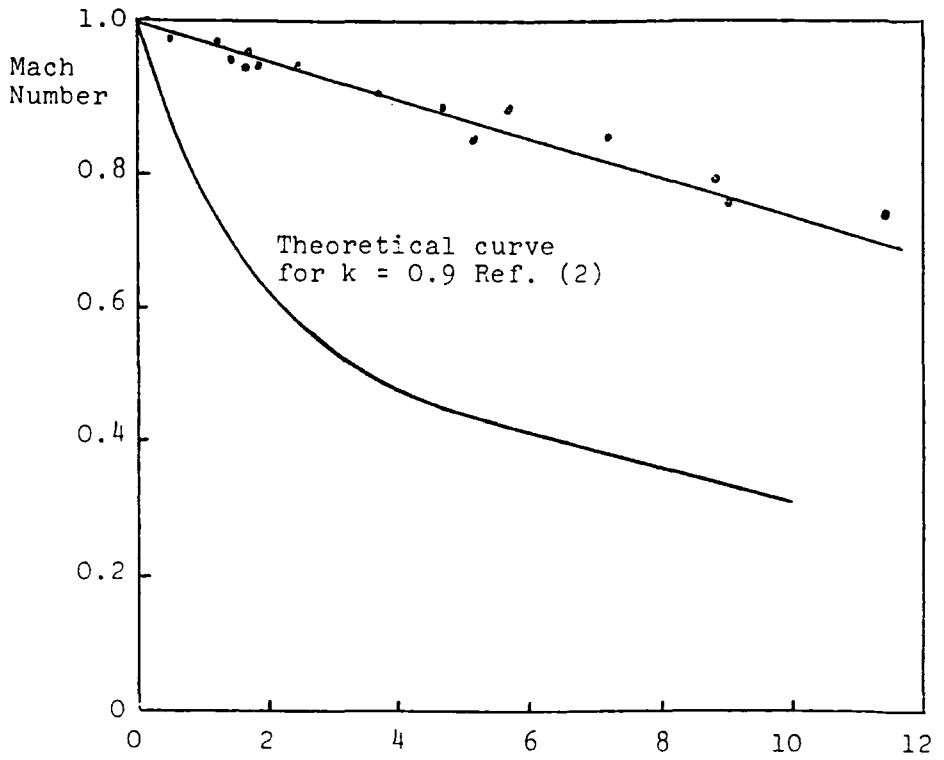
Ratio of solids to gas mass flow rates

Results taken at a point 28m from inlet of 40m pipe.

Fig. 6.   Comparison between experimental and
           theoretical values of M.
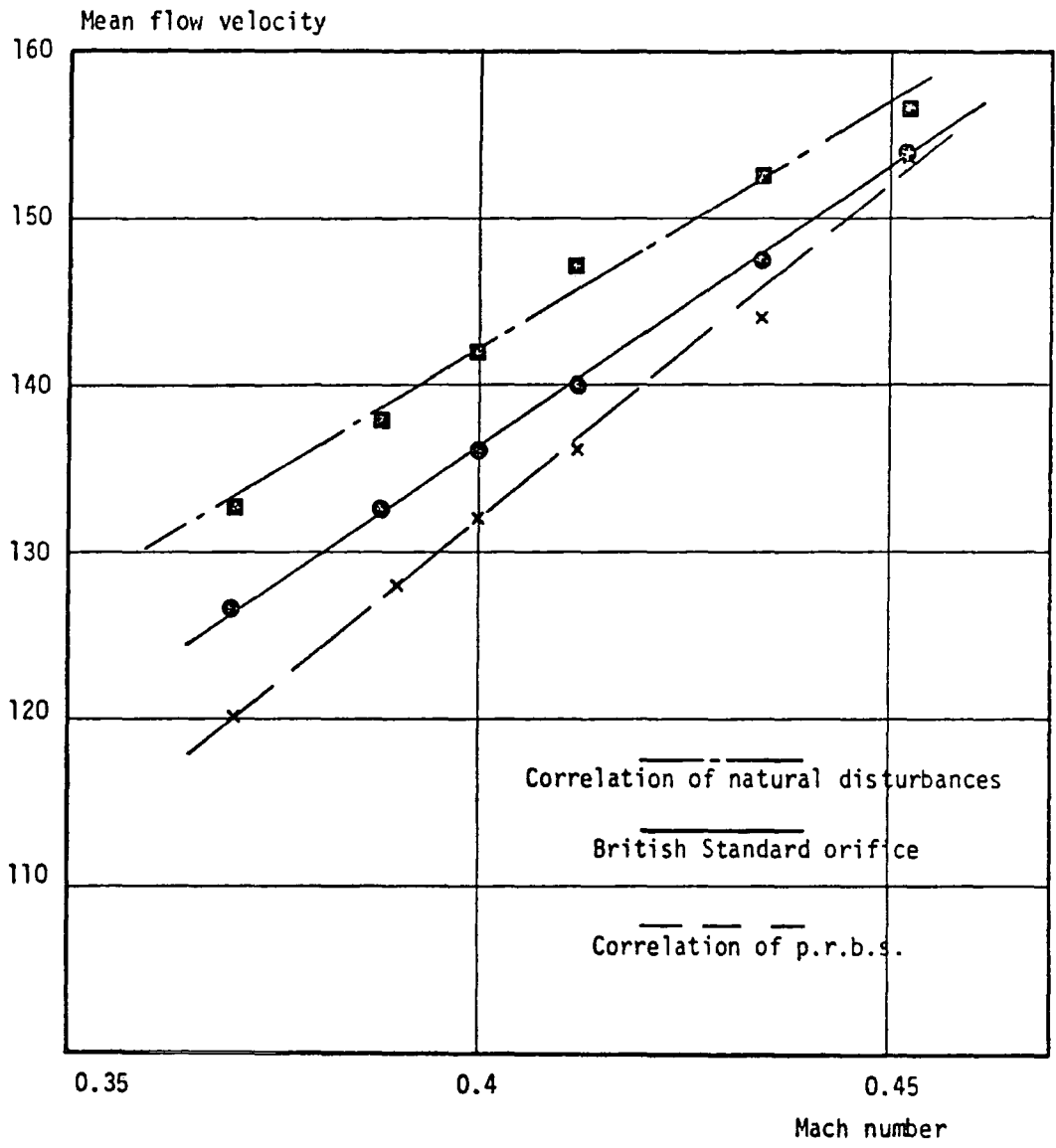
Fig. 7.   Comparison of mean pulsating air velocity as
obtained by different methods.

The figure shows "Mean flow velocity" on the y-axis (110 to 160) and "Mach number" on the x-axis (0.35 to 0.45). Legend:

Correlation of natural disturbances

British Standard orifice

Correlation of p.r.b.s.

Showing positive reflection spike.

Showing reflection spike eliminated.

Showing negative reflection spike.
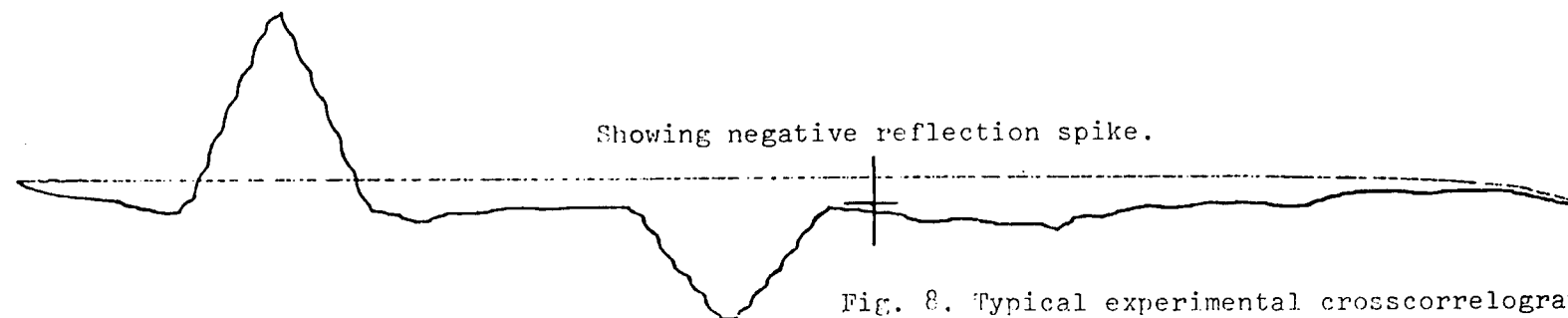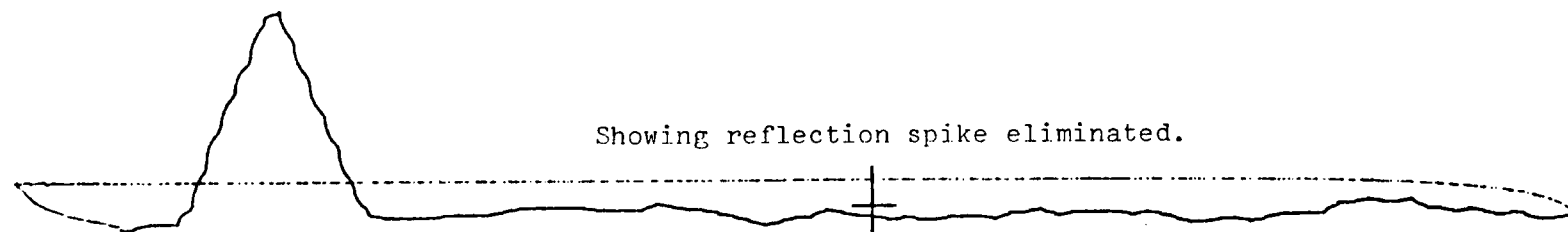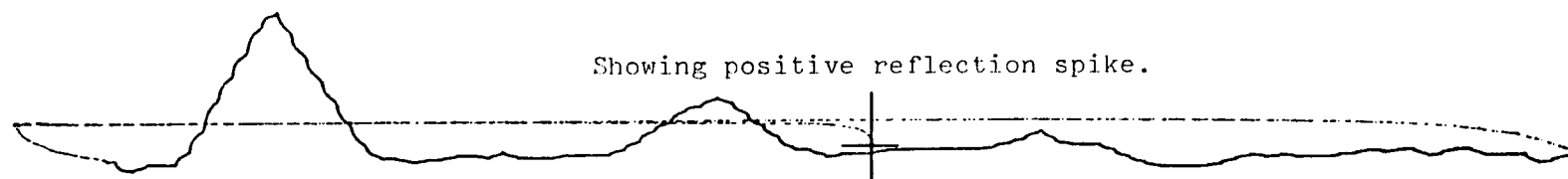
Fig. 8. Typical experimental crosscorrelograms

PAPER 29

The measurement of pulsating gas flow velocities using pseudo-random pressure pulses

by *E. W. Reed, †M. A. Ali and ‡ K. F. Gill

Demonstrated is an experimental means of measuring the mean flow velocity of a pulsating gas flow without the use of pipe constrictions. Small pseudo random binary sequence pressure pulses are injected into the flow. Correlation techniques are used to determine the velocity of propagation of these pulses from which the mean gas flow velocity can be calculated. The method is shown to be especially effective for high-velocity pulsating flows where measuring techniques at the present time are inadequate.

INTRODUCTION

The fluid dynamic behaviour associated with steady gas flow through pipe constrictions is understood and the mathematical descriptions which have been derived for the flow conditions existing are sufficiently detailed for most practical requirements.

Pulsating gas flows are common in practice and invariably occur when there is any rotating or reciprocating machinery within the system. The standard method of metering such flows is to first damp out the fluctuations with one or more air boxes and then use a steady flow measuring device. This method is adequate for low flow rates but as the flow rate increases so, of necessity, do the dimensions of the air boxes until grossly inconvenient sizes are reached.

One method of determining steady flow is from the measured pressure difference across a duct constriction using the well-known Bernoulli equation. Applying this technique to undamped pulsating flow produces answers with errors which are totally unacceptable and many workers have unsuccessfully attempted to make corrections for these errors.[1-10]

One cause suggested is that the constrictions have dynamic properties which will affect the pressure waves passing through the constrictions.[10] The authors have searched for these dynamics by developing special techniques for use with correlation methods.[11-14] The results show that these dynamics cannot be found to exist within the range of their tests which was for pressure waves of amplitudes below 6 m bar and frequencies below 400 Hz; this is in fact a contradiction of results produced by previous workers using less sophisticated techniques.[10] The conclusion is that an alternative approach to constriction metering is necessary for determining the velocities of pulsating gas flows; one possible

method of use to the practising engineer is described in this paper.

THE BASIC TECHNIQUE

The principle involved is that of measuring the absolute propagation velocity of a sonic wave travelling within the pulsating gas flow. This velocity will have a value given by the algebraic sum of the gas velocity and the relative sonic velocity. The relative sonic velocity can be calculated from the gas temperature, so allowing the gas velocity to be determined. It is clear that this method will be the more accurate as the gas velocity increases but it is precisely in this region where the present measuring difficulties lie.

A method of measuring the sonic velocity within fast pulsating gas flows within a pipe is to adopt the method already developed for measuring sonic velocities within relatively slow gas-solids flows.[15,16] This method is to inject artificially produced small pseudo random binary sequence (prbs) pressure pulses into the flow and cross correlate the pressure signal from the input with that from some station along the pipe. The time shift of the first peak from the origin on the crosscorrelogram gives the transit time of the pressure pulses from the input to the measuring station. The main advantages of this technique are that the correlogram is effectively independent of the natural pressure pulsations and incident and reflected waves can be identified since prbs signals correlate to give clearly defined and spaced out, triangular spikes.[11,12]

The pressure signals are monitored by sensitive piezoelectric pressure transducers. The prbs pressure pulses are produced by a specially developed generator consisting of a slotted disc which revolves so that it interrupts a fine jet of high-pressure air directed into the flow (Fig 1). The disc is slotted in such a way that the interruptions cause a series of pressure pulses to be generated in the pattern given ideally by Fig 2. Previous experiments[14] have shown that the amplitude of these pulses is of the order of 3 mbar and that the mass flow rate of air added is less than one part in a thousand.

EXPERIMENTAL METHOD

The rig available was one used at Leeds University for general experiments on pulsating air flow. A schematic layout is shown in Fig 3. As shown, a British Standard orifice was available in order to compare measurements. Because of the non-uniformity of velocity from C to A, the transit time from A to B was calculated from the difference of the transit times between C to B and C to A. A typical crosscorrelogram is shown in Fig 4. Direct correlation between A and B would have produced no useful information since the prbs was of much smaller amplitude than the pulsating pressures occurring

* Lecturer, Department of Mechanical and Production Engineering, The Polytechnic, Leeds LS1 2HE.
† Research Student, Department of Mechanical Engineering, The University, Leeds LS2 9JT.
‡ Senior Lecturer, Department of Mechanical Engineering, The University, Leeds LS2 9JT.
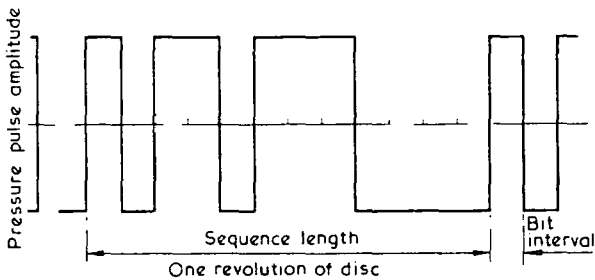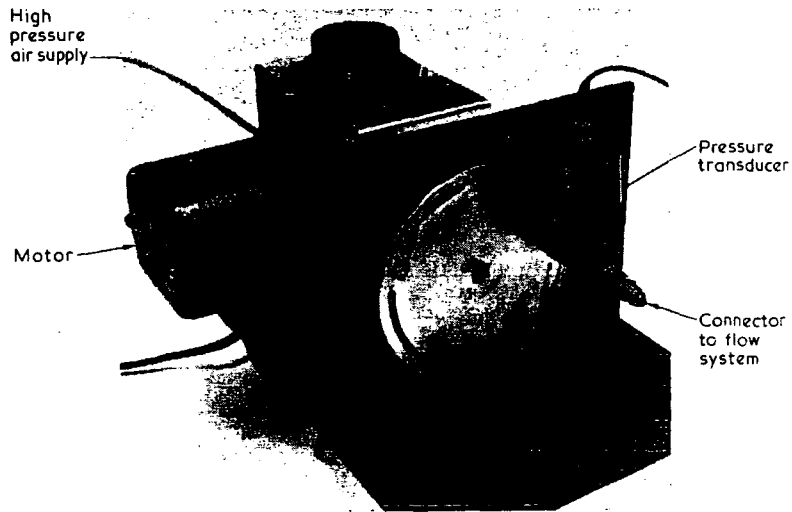
Reed, Ali and Gill

Fig 1   PRBS pressure pulse generator

High
pressure
air supply

Motor

Pressure
transducer

Connector
to flow
system

Fig 2   Output waveform from the prbs pressure pulse generator

Sequence length

Bit interval

One revolution of disc

Pressure pulse amplitude

within the gas stream. The mean flow velocity v is calculated from the formula

$$v = \frac{\text{distance AB}}{\text{transit time between A and B}} - a$$

where $a = 20\sqrt{T}$ m/s is the relative sonic velocity in air and T is the temperature in degrees Kelvin.

The high pressures within the duct prevented the injection of prbs pressure pulses using the available generator. This was overcome by injecting the disturbances over the outlet of a nozzle. Previous work, as yet unpublished, showed that pressure disturbances originating outside a jet were amplified

within the jet. The exact mechanism of this behaviour is not fully understood. Nevertheless, the pulse amplitudes were still sufficiently small to make the use of a high resolution proprietary correlator necessary.

DISCUSSION

The results indicate that the use of small artificial pressure disturbances in the form of a prbs is an acceptable method for estimating fast mean stream velocities in pulsating gas systems. Comparison of measurements with a British Standard orifice metering method shows close agreement, especially with increasing velocities (Fig 5). It is seen that as the velocity of flow decreases so the divergence between the two sets of results increases. It is expected that inaccuracies would increase as the velocity decreases since the difference between absolute and relative sonic velocities will decrease thus making more significant any measurement errors. It is suggested that this method as it stands would be unsuitable for velocities much lower than those recorded. However, it is in the higher mass flow regions where traditional methods are least effective.

The method of injecting the pressure disturbances made it necessary to use the propagation velocity in the direction of flow. Results over shorter duct lengths maintaining the same accuracy would be possible by using the propagation velocity measured against the direction of flow. Measuring with and against the direction of flow makes possible flow measurement without the calculation involving the velocity of sound which could be a cause of considerable error in low velocities.

Burdon-tube
gauge
C
p.r.b.s. input

5·04cm diameter duct

Air from suppy

Pressure-regulator   Valve   Sonic nozzle

2·54cm diameter duct

Station A   Station B

Direction of flow ⟶

Air
box

Plane of the pulsator

B.S orifice
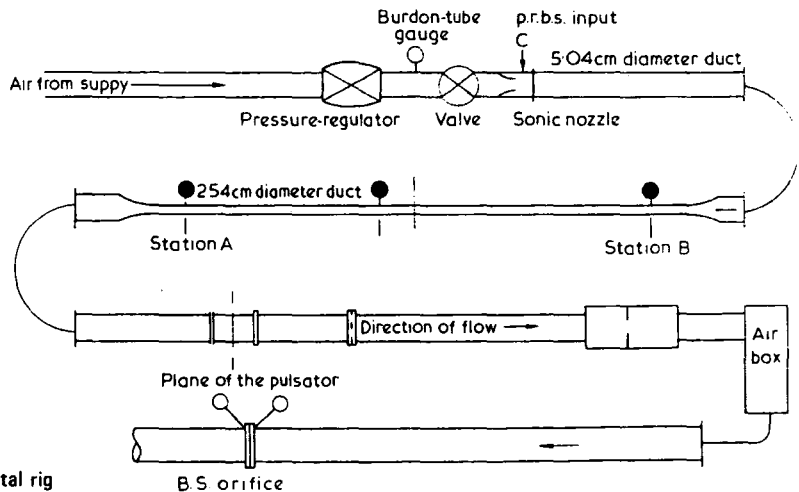
Fig 3   Schematic diagram of the experimental rig

(T71) 347

Reed, Ali and Gill
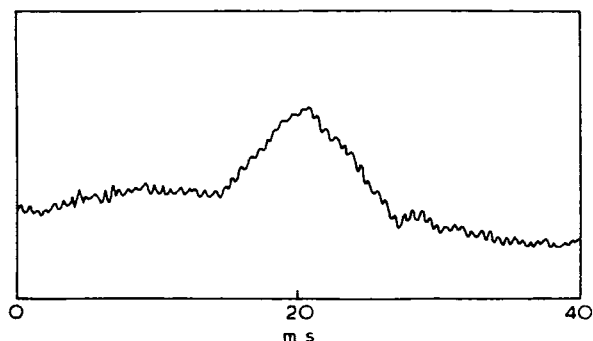
Fig 4   Typical correlogram showing distinctive prbs peak
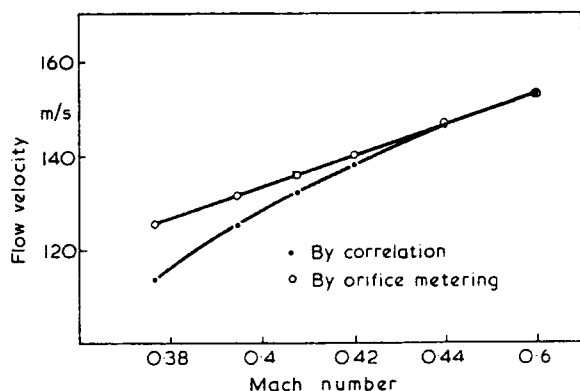
Fig 5   A comparison of velocity measurements

The artificial disturbances used were of small amplitude since the authors wished to utilise the existing generator. If the monitoring equipment had been less sensitive then it is suggested that the use of larger amplitudes of pressure disturbances would have produced results equally as good.

The natural turbulent pressure disturbances, to the best of the author's knowledge, have not been used in flow measurement. This is attributed chiefly to the non-stationary phenomena associated with turbulence. ie. the constant changing pattern of the resulting pressure signals due to the breaking down of the eddies. However, the use of inherent pressure pulsations could possibly be to infer applied mean gas flow velocities provided that wave reflections between the monitoring stations, due to geometrical duct discontinuities, are not pronounced.

Previous experiments[11-16] indicate that the prbs pulses are small enough to allow amplitude effects upon the velocity of sound to be neglected and that the only errors likely in the measurement of this parameter would be due to temperature fluctuations. The thermocouple will give the mean

temperature of the gas stream and, providing the reading remains sensibly constant, the average relative sonic velocity may be deduced. Cross correlation is also a time averaging technique and again it is the average absolute sonic velocity which is determined.

REFERENCES

1. **Zarek, J M.** 'Metering pulsating flow', *Engineering*, Vol 179, 1955, p 117.
2. **Earles, S W E, and Zarek, J M.** 'Use of sharp edged orifices in metering pulsating flow', *Proc I Mech Eng.* Vol 177, 1963, p 997.
3. **Jeffery, B J.** 'Pulsating flow through orifices'. PhD Thesis. University of London, 1965.
4. **Mak, F K W.** 'Measurement of pulsating gas flow', PhD Thesis, University of London, 1972.
5. **Sparks, C R.** 'A study of pulsation effects on orifice metering of compressible flow'. Technical report. Program PAR, NQ-15, The American Gas Association, 1963.
6. **Mosley, D S.** 'Measurement error in orifice meter on pulsating water flow', Technical report, Program PAR. NQ-15, The American Gas Association, 1963.
7. **Waters, T F, Imrie, B W, and Cole, B N.** 'Measurement of pulsating airflow by means of a bi-directional orifice meter', *Proc I Mech Eng*, Vol 182, 1968.
8. **Zarek, J M.** 'Neglected parameters in metering pulsating flow', *Trans. ASME*, 1966.
9. **Mottram, R C.** 'The measurement of pulsating flow using orifice plate meters', ASME Symposium on Flow Measurement, May 1971.
10. **Baird, R C, and Bechtold, I C.** 'The dynamics of pulsative flow through sharp-edged restrictions with special reference to orifice-metering', *Trans. ASME*, Nov 1952.
11. **Reed, E W, and Gill, K F.** 'An experimental technique for minimising resonance within a ducted fluid', *JMES*. Vol 15, No 2, 1973, pp 95–101.
12. **Reed, E W, Ali, M A, and Gill, K F.** 'An investigation of non-reflecting end conditions within a duct using pseudo random pressure pulses'. To be published in *Journal of Sound and Vibrations*. 1974.
13. **Ali, M A, Reed, E W, and Gill, K F.** 'A correlation method for measuring reflection coefficients of sharp edged orifices for small amplitude pressure waves', *JMES*. Vol 15. No 5, 1973, pp 321–325.
14. **Ali, M A, Reed, E W, and Gill, K F.** 'An investigation of flow through a constriction using pseudo random pressure pulses'. Offered to ASME. Mar 1973.
15. **Reed, E W, Mobbs, F R, and Gill, K F.** 'Measurement by correlation of small amplitude pressure wave propagation velocity in a gas-solids flow'. International Symposium on Measurement and Process Identification by Correlation and Spectral Techniques, Bradford Univ, Jan 1973. Published by Institute of Measurement and Control.
16. **Gill, K F, and Reed, E W.** 'A study into the use of pseudo random binary sequence pressure disturbance to measure sonic velocity in a two-phase flow system', *Proc I Mech E.* 1972, Vol 186, 39/72.

PAPER 41

THE EFFECT OF MASS FLOW RATE ON THE REFLECTION BEHAVIOUR OF SMALL-AMPLITUDE PRESSURE WAVES FROM DUCT TERMINATIONS

M. A. Ali†   K. F. Gill‡   B. W. Imrie§

This paper describes an investigation of the reflection characteristics of small-amplitude pressure waves in the presence of steady flow in a duct. A correlation technique employing pseudo-random binary-sequence (p.r.b.s.) pulses is introduced. A theoretical model of the process is presented together with considerations of correlation analysis. The results show agreement between the experimental results and the model; they further indicate that, in the presence of a steady flow component, there is a significant effect on the reflection behaviour of plane pressure waves for a reduction in the area terminating a duct.

The experimental technique is effective at very low flow velocities (Mach number = 0·02, Reynolds number = 30 × 10^3) and establishes a linear relationship between a reflection coefficient and a non-dimensional mass flow number. A reflection coefficient of flow is introduced as an appropriate parameter for such conditions.

The procedure could be applied to a wide range of industrial processes to determine flow coefficients of duct elements *in situ*, to optimize flow processes and to locate leakage flows.

1 INTRODUCTION

Previous methods of analysing the mechanism of wave action at geometrical discontinuities, using the shock-tube technique. have been applied to waves of finite amplitude. The pressure records were analysed on the basis of the nonlinear relationships developed theoretically by Bannister and Mucklow (1)� and tested experimentally by Mucklow and Wilson (2) for the two limiting conditions of open and closed ducts.

Earles and Zarek (3) compared their experimental results for the reflection of pressure waves at sharp-edged orifices with Nesbitt's (4) theoretical predictions. On comparing their experimental results with theory, a discrepancy was noted that appeared to be dependent on the area ratio; they attempted to explain this by introducing the concept of 'the reflection coefficient of contraction', which can be determined only from experiment. The indication is that the actual reflecting area of the constriction is not the physical area of the opening but rather a smaller area characterized by 'the reflection coefficient of contraction'.

Trengrouse, Imrie and Male (5) introduced a concept based on the area ratio of a theoretical isentropic convergent nozzle similar to that of a sharp-edged orifice plate for the same measured values of incident pressure wave amplitudes.

Working in a much smaller range of amplitudes, Ali, Reed and Gill (6) introduced a correlation method for investigating the reflection behaviour of small-amplitude pressure waves.

In all the reported cases, however, the effect of end constrictions on wave reflection has been studied in the absence of steady flow. A more general situation would be the presence of an alternating component of flow

representing a train of pressure pulses superimposed on a steady component representing a mean flow value.

This study is aimed at determining the extent to which the small pressure-wave reflection behaviour is influenced by the presence of a steady component of flow for a fixed differential pressure-wave amplitude of the order of 0·008 bar.

1.1 Notation

a	Local acoustic speed
A	Duct area
C_{ds}	Steady flow discharge coefficient, including compressibility
C_r	Reflection coefficient of flow
d	Diameter of constriction at end of duct
D	Duct diameter
M	Mach number
MN	Mass flow number $\left(= \dfrac{\dot{m}a_0}{Ap_0} \right)$
m	Mass flow
m	Constriction/duct area ratio
K	Reflection coefficient
u	Total particle velocity
RN	Reynolds number
p	Static pressure (absolute)
P	Pressure wave amplitude
x	$(p/p_s)^{1/7}$
Y	u/a_s
ρ	Mean flow density
τ	Time delay
$\psi_{AA}(\tau)$	Auto-correlation function
$\psi_{AB}(\tau)$	Cross-correlation function
ϕ	Pressure wave amplitude ratio ($=P/p_s$)

Subscripts

a	Ambient condition (atmospheric)
i	Incident pressure wave
n	Superposition of incident and reflected waves
o	Total head condition
r	Reflected wave
s	Duct condition

2 THEORETICAL CONSIDERATIONS

In the theoretical model, a static pressure term is introduced to allow for the presence of a steady flow component, so that its effect on wave reflection from a constriction termination of a duct can be established (Fig. 1).

For an incident pressure wave (p_i) propagating in a medium air ($\gamma = 1\cdot4$) of absolute static pressure (p_s), density (ρ_s) and particle velocity (u_s), the particle velocity following the passage of the wave is given by

$$Y_i = 5(x_i - 1) + M_s \tag{1}$$

Immediately upstream of an isentropic nozzle, at the plane of superposition,

$$Y_n = 5(2x_i - x_n - 1) + M_s \tag{2}$$

From superposition of the absolute static pressure following the interaction of the incident wave with the plane of the nozzle,

$$x_n = (x_i + x_i - 1) \tag{3}$$

From consideration of mass continuity across the nozzle,

$$\rho_n A_n u_n = \rho_a A_a u_a$$

that is,

$$Y_a^2 = x_n^{10} \cdot x_a^{-10} (1/m^2) Y_n^2 \tag{4}$$

Assuming quasi-steady flow, from energy considerations,

$$5x_n^2 = Y_n^2 = 5x_a^2 + Y_a^2 \tag{5}$$

Combining (4) and (5), it can be shown that

$$5x_n^2 - x_a^2 = Y_n^2 \left(\frac{x_n^{10} x_a^{-10}}{m^2} - 1 \right) \tag{6}$$

For waves of small amplitude, using the binomial expansion, the following approximation can be made:

$$x_n = \left(\frac{p_n}{p_s} \right)^{\frac{1}{7}} = 1 + \tfrac{1}{7}\Phi_n$$

$$\Phi_n = \Phi_i + \Phi_r = \Phi_i(1 + K)$$

where

$$K = \Phi_r/\Phi_i = P_r/P_i$$

Substituting in equation (2) gives

$$Y_n^2 = [M_s + \tfrac{5}{7}\Phi_i(1 - K)]^2 \tag{7}$$

Combining equations (6) and (7), the following equation is deduced:

$$m^2 = \frac{[M_s + \tfrac{5}{7}\Phi_i(1 - K)]^2[1 + \tfrac{10}{7}\Phi_i(1 + K)]}{\times (1 + \tfrac{10}{7}\Delta_s)}{[M_s + \tfrac{5}{7}\Phi_i(1 - K)]^2 + [\tfrac{10}{7}\Phi_i(1 + K)] + \tfrac{10}{7}\Delta_s} \tag{8}$$

where

$$\Delta_s = \frac{p_s}{p_a}$$

Introducing the 'reflection coefficient of flow', C_i, the equation for orifice plates would be

$$C_f^2 m^2 = \frac{[M_s + \tfrac{5}{7}\Phi_i(1 - K)]^2[1 + \tfrac{10}{7}\Phi_i(1 + K)]}{\times (1 + \tfrac{10}{7}\Delta_s)}{[M_s + \tfrac{5}{7}\Phi_i(1 - K)]^2 + [\tfrac{10}{7}\Phi_i(1 + K)] + \tfrac{10}{7}\Delta_s} \tag{9}$$

The reflection coefficient of flow, C_p, is a measure of effects that modify the theoretical prediction of flow through an orifice. The process of reflection of small-amplitude pressure waves is dependent on flow and state parameters, on the geometry of area change and on the nature of the actual path lines or streamlines (in steady flow). The correlation process of sampling statistically the information of controlled sequences of identifiable pressure waves converts the data into an appropriate coefficient.

3 EXPERIMENTAL METHOD

In Fig. 2, pseudo-random binary-sequence (p.r.b.s.) pressure pulses are injected at the end A of the test duct using a 63-bit sequence p.r.b.s. generator. The pressure signals at A and B are cross-related, using a proprietary correlator, so that the cross-correlogram shows a representative spike at each time delay equivalent to the transport lag for the pressure pulses to reach B either directly or by reflection from the end of constriction. The ratio of the amplitude of the second spike to that of the first spike will give the numerical value of the appropriate reflection coefficient (K) from the duct end termination at D (cf. Fig. 7).

Compressed dry air was supplied from a high-pressure receiver and the rate of mass flow through the apparatus was controlled by a pressure-regulating valve installed at approximately 40 pipe diameters upstream of the metering orifice. The orifice itself is square-edged and made in accordance with BS 1042:1964, with D and $D/2$ pressure-tapping positions. The differential pressure across the orifice was measured using a U-tube vertical manometer. The temperature and the static pressure, upstream of the metering orifice, were measured using a thermocouple and mercury manometer, respectively. This metered flow then entered the test duct immediately upstream of end D.

Experiments were carried out for one pressure-wave amplitude of 0·008 bar approximately and for five different orifice sizes and two quadrant nozzles made in accordance with BS 1042: 1964. The quadrant entrance nozzles were used to simulate 'ideal' flow contraction to
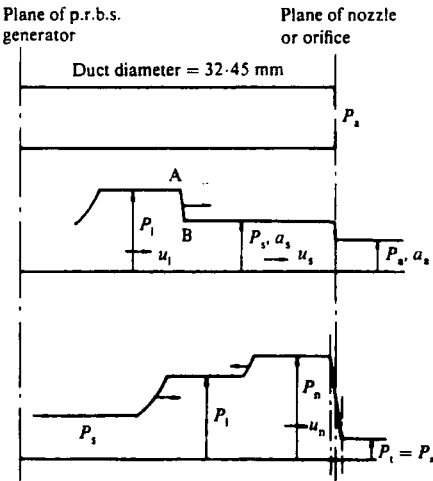
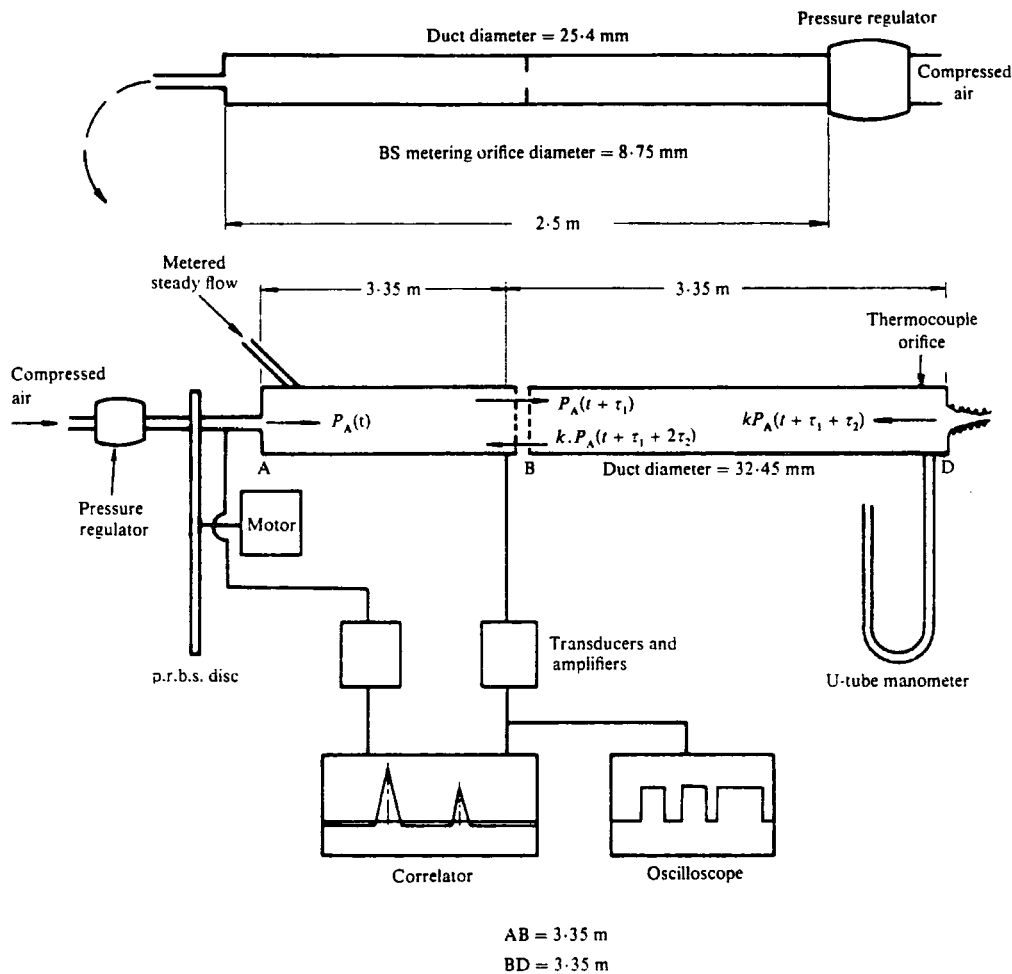Fig. 1. Pressure diagrams of wave propagation and reflection

Fig. 2. Schematic diagram of the experimental rig used in the presence of steady flow component

$$AB = 3 \cdot 35 \text{ m}$$
$$BD = 3 \cdot 35 \text{ m}$$

Table 1. Dimensions of constrictions used in investigating the wave reflection behaviour in the presence of steady flow ($D = 32 \cdot 45$ mm)

Nozzle dimensions	
d (mm)	m (area ratio)
8·38	0·067
9·40	0·084

Orifice dimensions	
d (mm)	m (area ratio)
8·52	0·069
11·51	0·126
12·70	0·153
15·24	0·221
17·78	0·300

provide an exact comparison of the theoretical results with those obtained from experiment. All the duct end constrictions were calibrated under steady flow conditions to determine the steady flow discharge coefficients. Dimensions of the end constrictions are given in Table 1.

The reflection behaviour was investigated using pseudo-random binary-sequence pressure waves of controlled amplitude, which were injected at end A of the test duct. The line pressure upstream of the p.r.b.s. generator was regulated to maintain the pressure pulse amplitude constant over all ranges of rates of mass flow used. This was monitored by using the same settings for the charge amplifiers and the correlator and by adjustment to maintain a constant height (amplitude) for the first spike of the correlogram. A check was made with oscilloscope traces recorded at B for the 'tuned' end condition.

4 RESULTS

To confirm that no wave attenuation occurred within the duct for the range of rates of mass flow used, tests were conducted to estimate the reflection coefficients for the

232   M. A. ALI, K. F. GILL AND B. W. IMRIE
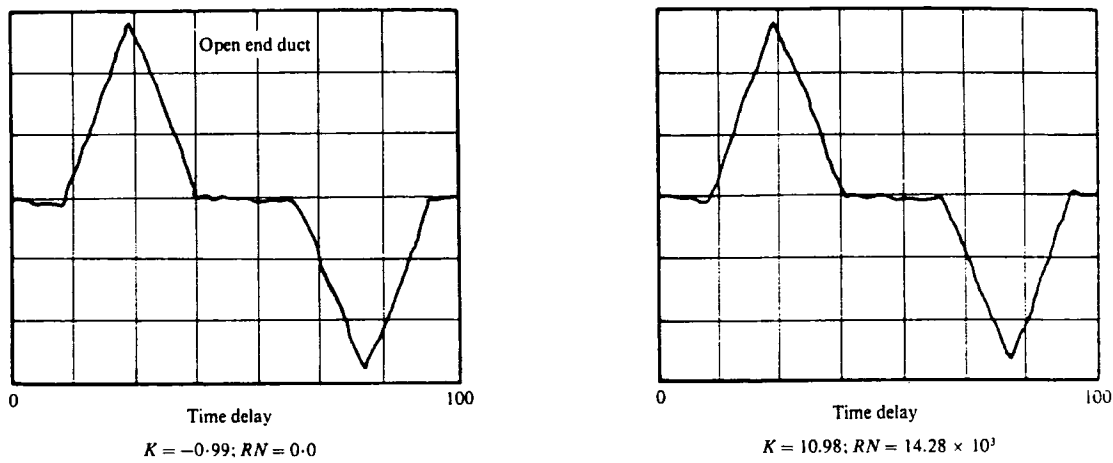
Fig. 3. Cross-correlation function
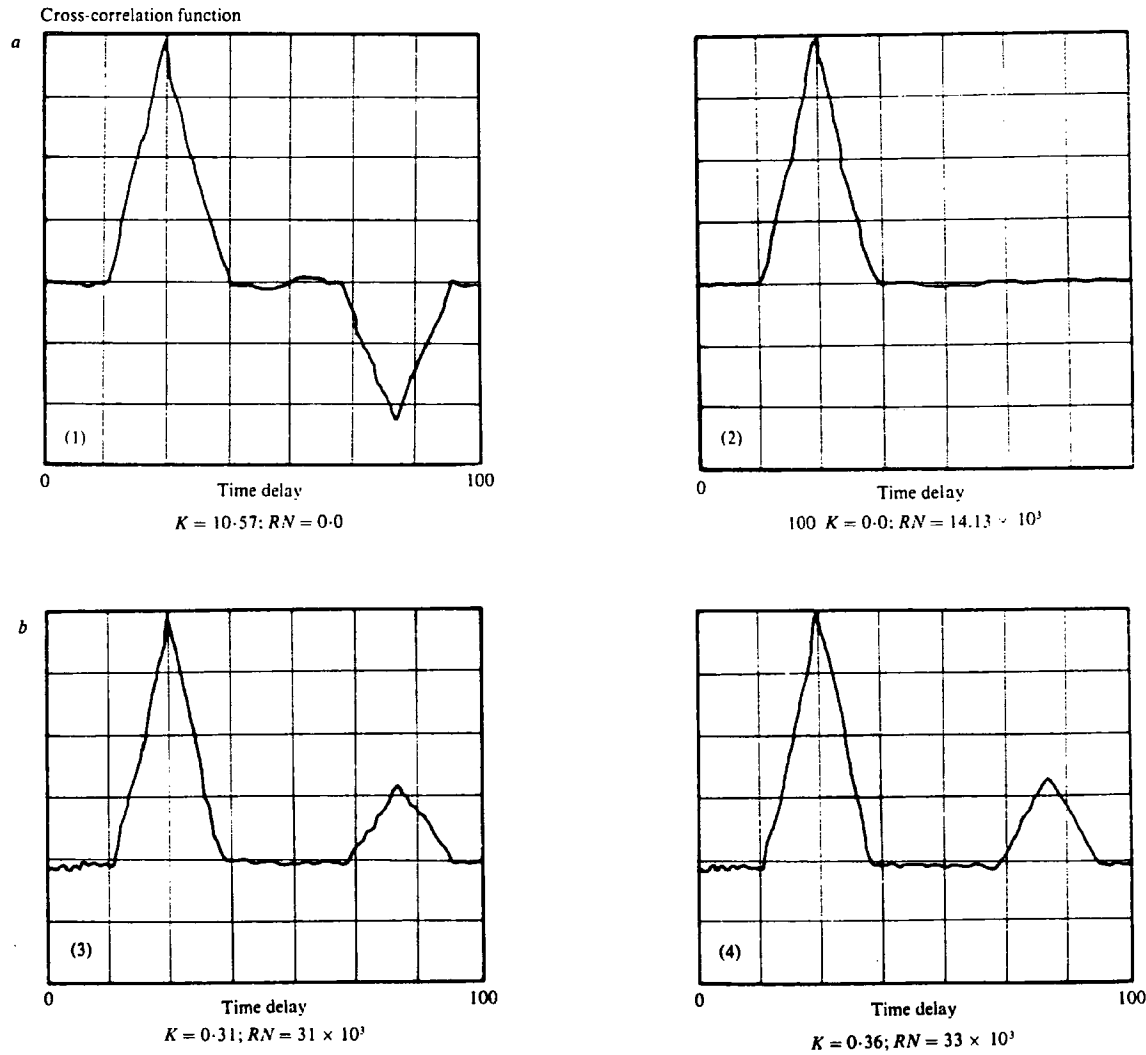
Fig. 4. Effect of steady flow on the reflection from an orifice, $m = 0.223$

THE REFLECTION BEHAVIOUR OF SMALL-AMPLITUDE PRESSURE WAVES   2.3.3
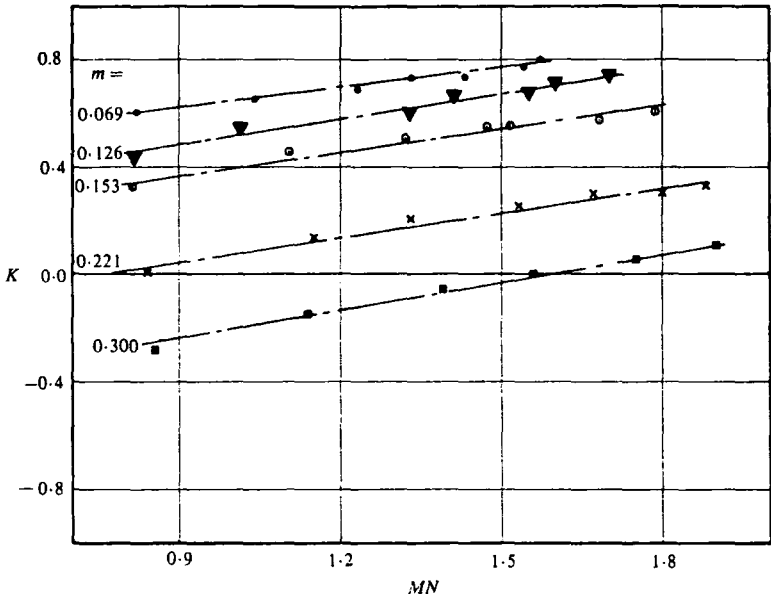
Fig. 5. Variation of the reflection coefficient, K, with the mass flow number $[MN = \dot{m}a_0/P_gA]$ for different orifice area ratios, m
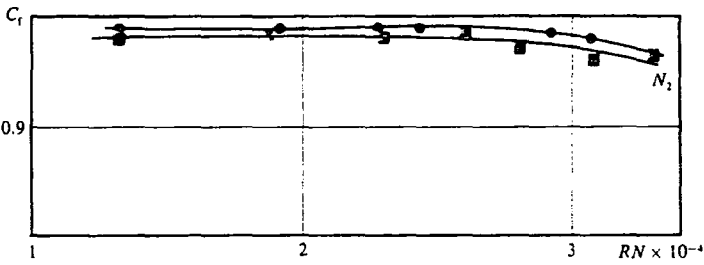
Fig. 6a. Variation of the reflection coefficient of flow with RN (for nozzles)
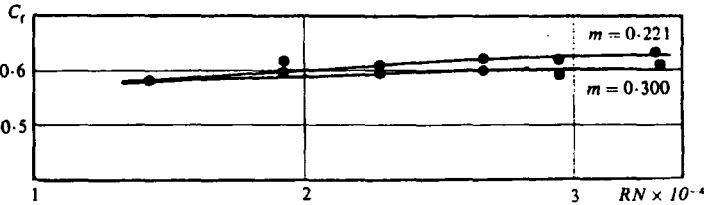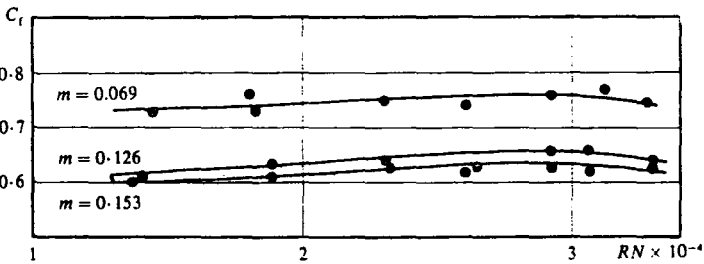
Fig. 6b. Variation of the reflection coefficient of flow with RN (for orifices)

Table 2. Comparison of the variation in the steady-flow discharge coefficient (C_{ds}) and the reflection coefficient of flow (C_r) with Reynolds number for nozzles of area rations $m = 0.084$ and 0.067

Nozzle area ratio = 0.084

$RN \times 10^{-3}$	C_r	C_{ds}
19·2	0·970	0·93
23·2	0·980	0·958
26·3	0·98	0·940
28·2	0·956	0·940
30·8	0·90	0·946
33·0	0·964	0·943

Nozzle area ratio = 0.067

$RN \times 10^{-3}$	C_r	C_{ds}
13·3	0·99	0·95
18·92	0·99	0·978
22·49	0·99	0·98
26·1	0·99	0·978
29·0	0·980	0·96
32·2	0·985	0·98

Table 3a. Variation of the steady-flow discharge coefficient (C_{ds}) and the reflection coefficient of flow (C_r) with Reynolds number for orifices of area ratios $m = 0.069$ and 0.126

Orifice area ratio = 0.069

$RN \times 10^{-3}$	C_r	C_{ds}
14·4	0·73	0·70
19·27	0·73	0·70
23·2	0·77	0·71
26·13	0·74	0·71
29·27	0·77	0·72
31·27	0·77	0·72
32·84	0·752	0·71

Orifice area ratio = 0.126

$RN \times 10^{-3}$	C_r	C_{ds}
14·03	0·61	0·57
19·35	0·64	0·61
23·56	0·64	0·624
25·98	0·61	0·63
29·2	0·66	0·638
30·5	0·66	0·625
33·0	0·64	0·64

Table 3b. Variation of the steady-flow discharge coefficient (C_{ds}) and the reflection coefficient of flow (C_r) with Reynolds number for orifices of area ratios $m = 0.153$ and 0.221

Orifice area ratio = 0.153

$RN \times 10^{-3}$	C_r	C_{ds}
13·85	0·604	0·57
19·13	0·612	0·573
23·2	0·64	0·61
26·27	0·638	0·604
27·27	0·62	0·591
30·9	0·64	0·619

Orifice area ratio = 0.221

$RN \times 10^{-3}$	C_r	C_{ds}
14·13	0·582	0·58
19·3	0·62	0·595
22·8	0·61	0·581
26·3	0·64	0·61
28·9	0·64	0·52
33·0	0·64	0·618

duct open end in the presence of steady flow. Fig. 3 shows typical cross-correlograms for the open-end condition, and it is seen that there is no appreciable wave attentuation. Figs 4a and b show typical experimental cross-correlograms for a sharp-edged orifice plate ($m = 0.221$) over the steady flow range used. It can be seen from these correlograms that, for any particular test, the amplitude of the first spike was kept constant for a constant p.r.b.s. pressure-wave amplitude. The correlograms further indicate that the introduction of steady gas flow into the system has a significant effect on the behavior of reflections from terminating duct constrictions. The range of such variations in magnitude and polarity of the reflection coefficient is demonstrated in Fig. 5. This figure graphically displays the variation of the reflection coefficient with the mass flow number (MN) for different orifice-area ratios.

The variation in the reflection coefficient of flow estimated from equation (9), after substituting for the values of the other parameters with the duct Reynolds number, is shown in Figs 6a and b.

Tables 3a and b compare the steady flow discharge coefficient and the reflection coefficient of flow for different constriction geometry and area ratios over the experimental range of Reynolds number.

5 DISCUSSION AND CONCLUSIONS

The presence of a steady component of flow in a pressure-wave (train) transmitting duct is shown to have a significant effect on the nature of wave reflections from a duct exit reduction in area. The steady flow is accompanied by an increase in static and stagnation pressure in the duct; the increase in the energy of the flow consistently acts to increase the non-flow value of the reflection coefficient at the reduction in area.

For a more generalized interpretation, it is more convenient to use a mass flow number, MN, which incorporates duct dimensions as well as variations in the fluid and flow parameters. Such a mass flow number, MN

$= (\dot{m}a_0)/Ap_0$, can readily be shown to be a function of Mach number for steady flow of a perfect gas in a duct.

Inspection of the curves shown in Fig. 5 indicates that a linear relationship exists between K and MN for the range of orifice sizes tested. As a result, a simple calculation enables the direct prediction of K for any given value of MN and a particular constriction/duct geometry. This suggests that as an alternative, a non-reflecting end condition can be achieved with a high degree of confidence, by variation of the steady flow component, providing that the non-flow value of the reflection

coefficient is negative. The experimental results have all been measured from the screen of the on-line correlator with accuracies of the order of 2·5 per cent.

There are many flow processes in industry that are difficult to monitor or calibrate because of pipework complexity, interaction of duct elements and the nature of the flow or phases of the flow. The procedures described in this paper could be applied in most situations with minimal disruption of the actual flow process.

Flow through valves and other constrictions could be monitored and the flow/geometry optimized by interpretation of the reflection coefficient obtained by cross-correlation. With appropriate development, the reflection coefficient could also be used to determine the location of leakage flows.

APPENDIX 1

REFLECTION OF P.R.B.S. PRESSURE WAVES

From consideration of Fig. 2, the pseudo-random binary-pressure pulses generated at A will travel along the duct with the local speed of sound plus the mean flow speed. When reaching the plane of discontinuity terminating the duct, the pressure pulses are partially reflected and partially transmitted. Two possible means are available for estimating experimentally the reflection coefficient, K:

(a) by auto-correlation of the pressure signal at B;

(b) by cross-correlation of the pressure signal at B with that at A.

Let the p.r.b.s. pulses injected at A be $P_A(t)$ and let the transport lag for these pulses to travel the distances AB and BD be τ_1 and τ_2, respectively. Neglecting secondary reflections, the pressure signal recorded at B is given by

$$p_B(t) = p_A(t + \tau_1) + KP_A(t + \tau_1 + 2\tau_2)$$

The auto-correlogram of a measured pressure signal at B is given by

$$\psi_{BB}(\tau) = \lim_{T \to \infty} (I_1 + I_2 + I_3 + I_4)$$

such that

$$I_1 = \frac{1}{T} \int_0^T p_A(t + \tau_1) \cdot p_A(t + \tau_1 - \tau) \, dt$$

$$I_2 = \frac{1}{T} \int_0^T p_A(t + \tau_1) \cdot KP_A(t + \tau_1 + 2\tau_2 - \tau) \, dt$$

$$I_3 = \frac{1}{T} \int_0^T p_A(t + \tau_1 - 2\tau_2) \, dt$$

$$I_4 = \frac{1}{T} \int_0^T K^2 p_A(t + \tau_1 + 2\tau_2) \cdot p_A(t + \tau_1 + 2\tau_2 - \tau) \, dt$$

Since $P_A(t)$ follows a p.r.b.s. pattern, the auto-correlograms formed consist of a set of spikes repeating themselves after each cycle time of the rotating disc, as shown in Fig. 7. The reflection coefficient (K) is inferred from the amplitude ratio of the first spike to that of the second, occurring at the time delay $\tau = 2\tau_2$. The amplitude ratio predicted from the auto-correlogram is given by

$$\frac{KP_A^2}{(1 + K^2)p_A^2} = \frac{K}{1 + K^2}$$
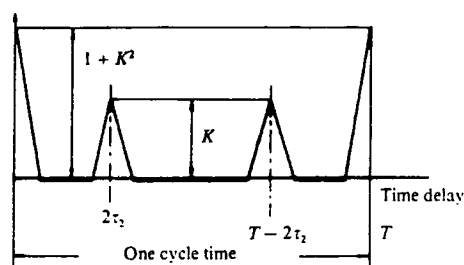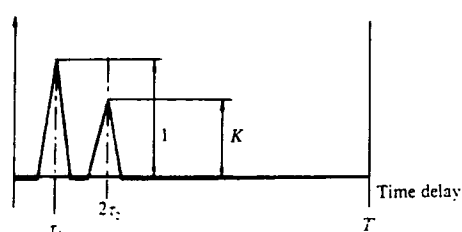
Fig. 7. Auto-correlation and cross-correlation functions for wave reflection

From the cross-correlogram,

$$\psi_{AB}(\tau) = \lim_{T \to \infty} \frac{1}{T} \int_0^T [p_A(t - \tau) P_A(t + \tau_1) \, dt$$

$$+ p_A(t - \tau) KP_A(t + \tau_1 + 2\tau_2) \, dt]$$

The cross-correlogram will be formed with two spikes occurring at time delays $\tau = \tau_1$ and $\tau = 2\tau_2$, respectively. The ratio of their amplitudes gives a direct experimental estimate of K. On both the auto-correlogram and the cross-correlogram, the vertical direction of the reflected spike relative to that of the incident-wave spike determines the reflected-wave polarity.

APPENDIX 2

REFERENCES

(1) BANNISTER, F. K. and MUCKLOW, G. F. 'Wave action following sudden release of compressed gas from a cylinder', *Proc. Instn mech. Engrs* 1948 **159**, 269.

(2) MUCKLOW, G. F. and WILSON, A. J. 'Wave action in gases: the attenuation and reflection of compression waves propagated in pipes', *Proc. Instn mech. Engrs* 1955 **169**, 69.

(3) EARLES, S. W. E. and ZAREK, J. M. 'Reflection of pressure waves at sharp-edged orifices', *The Engineer* 1965 (Feb.).

(4) NESBITT, M. V. 'The reflection and transmission of pressure disturbances at area changes in inifinite dupts', *N.G.T.E. Memo. 198* 1954 (Feb.).

(5) TRENGROUSE, G. H., IMRIE, B. W. and MALE, D. H. 'Comparison of unsteady flow discharge coefficients for sharp-edged orifices with steady flow values', *J. mech. Eng. Sci.* 1966 **8** (No. 3), 322.

(6) ALI, M. A., REED, E. W. and GILL, K. F. 'Correlation method for measuring reflection coefficients of sharp-edged orifices for small amplitude pressure waves', *J. mech. Engng Sci.* 1973 **15** (No. 5), 321.

7. PUBLICATION OF GENERAL NATURE

PAPER 5

Heat Transfer Through a Piston by Electrical Analogy

By J. E. R. CONEY and K. F. GILL

A well established theoretical method for evaluating the heat transfer by conduction within a solid body is used to estimate steady and transient heat transfer through a typical diesel engine piston. The method is that of using an electrical passive network to simulate the mathematical finite difference representation of the temperature variation in a solid body.

MANY important problems in engineering and physics require the solution of partial differential equations of the form $\nabla^2 f = g$ (Poissons Equation) where f is an unknown scalar function of the space co-ordinates x, y, and z. In most practical cases no rigorous solution can be found and either a numerical solution[1] or an experimental analogy[2] must be used. The former is not normally suitable unless computing facilities are available because of the amount of tedious computational work necessary to obtain reasonably accurate results. Of the latter, the most adaptable technique, requiring only a small initial capital outlay to obtain a solution, is the electrical resistance network analogue[3].

An important problem which can be investigated by use of such a network analogue is that of heat transfer within the piston of an internal combustion engine. In the design of pistons for engines, it is essential that adequate allowance be made for thermal stresses, that heat dissipation is adequate to ensure acceptable piston temperatures and that the temperature distribution does not produce undesirable distortion. Hence, it is essential to have a knowledge of how the temperature varies through-out the piston, especially as engine working temperatures are continually increasing due to the perpetual demand for higher power-weight ratios and efficiencies.

From the need to determine these temperature distributions experimentally, the following methods have been used:

(a) Temperature-sensitive paints: this method relies upon the irreversible colour change of these paints on reaching certain known temperatures.

(b) Hardness recovery: it is known that the hardness of certain alloys varies with prolonged temperature subjection. Hence, by determining the change in hardness of the piston material after a prescribed period of running, an estimate of the temperature

Notation:
- a—Mesh size.
- C—Electrical capacitance.
- c—Specific heat (volume basis).
- k—Thermal conductivity.
- Q—Heat transferred.
- R—Electrical resistance.
- t, T—Time.
- V—Voltage.
- x, y, z—Spatial co-ordinates.
- α—Thermal diffusivity.
- ρ—Density.
- θ—Temperature.

Technical Contributors Section *(Continued)*

variation through the piston may be made.

(*c*) Fusible plugs: small plugs of fusible eutectic alloys having a known melting point are inserted into the piston crown, the pattern being chosen to give a useful temperature scan.

(*d*) Thermocouples: these are placed at predetermined points through the piston so as to facilitate the construction of isothermals. However, difficulty is experienced in monitoring the resultant signals.
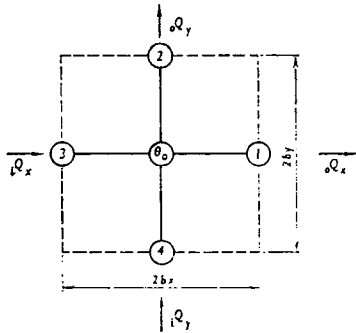
(*e*) Telemetering: this method has been

Fig. 1—Unsteady heat transfer across uniform lattice

used in an attempt to overcome the difficulty experienced in monitoring the thermocouple signals. Small transmitters are mounted on the connecting rod and transmit the signals generated by resistance thermometers.

(*f*) Electrical analogy: the electrical resistance network analogue is a well established device ideally suited for determining theoretically the temperature distribution in the piston of an internal combustion engine. It is the authors' intention to describe the application of this method to the determination of the temperature changes in the piston of a firing engine.

THEORY

For completeness it will be shown that heat transfer through a body may be simulated by an electrical network, heat transfer in two-dimensions only being considered. The following nomenclature will be used.

STEADY STATE HEAT TRANSFER BY CONDUCTION

The general equation for the temperature distribution within a body is given by

$$\frac{\partial^2\theta}{\partial x^2} + \frac{\partial^2\theta}{\partial y^2} + \frac{\partial^2\theta}{\partial z^2} = 0 \quad \dots \quad (1)$$

assuming no heat generation within body.

If q is the heat generated within the body per unit volume and per unit time, then

$$k(\delta x.\delta y.\delta z)\left(\frac{\partial^2\theta}{\partial x^2} + \frac{\partial^2\theta}{\partial y^2} + \frac{\partial^2\theta}{\partial z^2}\right) = -q\,(\delta x.\delta y.\delta z) \quad \dots \quad (2)$$

hence for the two-dimensional case

$$\frac{\partial^2\theta}{\partial x^2} + \frac{\partial^2\theta}{\partial y^2} = -q/k \quad \dots \quad (3)$$

The finite-difference approximation for Equation (3) is (see Appendix I)

$$\frac{\partial^2\theta_0}{\partial x^2} + \frac{\partial^2\theta_0}{\partial y^2} = \frac{\theta_1 + \theta_2 + \theta_3 + \theta_4 - 4\theta_0}{a^2} \quad \dots \quad (4)$$

Equations (3) and (4) gives the relationship

$$R = k/a^2 \quad \dots \quad (5)$$

UNSTEADY STATE HEAT TRANSFER BY CONDUCTION

The heat transfer through a two-dimensional body across a uniform lattice (see Fig. 1) having a nodal temperature θ_0 is given by:

$$_iQ_y = -k2\delta x\frac{\partial}{\partial y}\left[\theta_0 - \frac{\partial\theta_0}{\partial y}\delta y\right]dt$$

$$_0Q_y = -k2\delta x\frac{\partial}{\partial y}\left[\theta_0 + \frac{\partial\theta_0}{\partial y}\delta y\right]dt$$

$$_iQ_x = -k2\delta y\frac{\partial}{\partial x}\left[\theta_0 - \frac{\partial\theta_0}{\partial x}\delta x\right]dt$$

$$_0Q_x = -k2\delta\frac{\partial}{\partial x}\left[\theta_0 + \frac{\partial\theta_0}{\partial x}\delta x\right]dt$$

$$\dots \quad (6)$$

where the prefixes i and 0 are in and out respectively.

Hence the net rate of heat transfer to the body is:

$$4k\delta x\delta y\left(\frac{\partial^2\theta_0}{\partial x^2} + \frac{\partial^2\theta_0}{\partial y^2}\right) = \rho c\,(2\delta x)\,(2\delta y)\frac{\partial\theta_0}{\partial t}$$

i.e.

$$\frac{\partial\theta_0}{\partial t} = \varkappa\left[\frac{\partial^2\theta_0}{\partial x^2} + \frac{\partial^2\theta_0}{\partial y^2}\right] \quad \dots \quad (7)$$

where

$$\varkappa = \frac{k}{\rho c}$$

Equations (4) and (7) give:

$$\frac{1}{\varkappa}\frac{\partial\theta_0}{\partial t} = \frac{\theta_1 + \theta_2 + \theta_3 + \theta_4 - 4\theta_0}{a^2} \quad \dots \quad (8)$$

Similarly it may be shown[2] that for an electrical network

$$C\frac{dV_0}{dT} = \frac{V_1 + V_2 + V_3 + V_4 - 4V_0}{R} \quad \dots \quad (9)$$

For the electrical and thermal systems to be analogous Equations (8) and (9) must be dimensionally comparable: i.e.
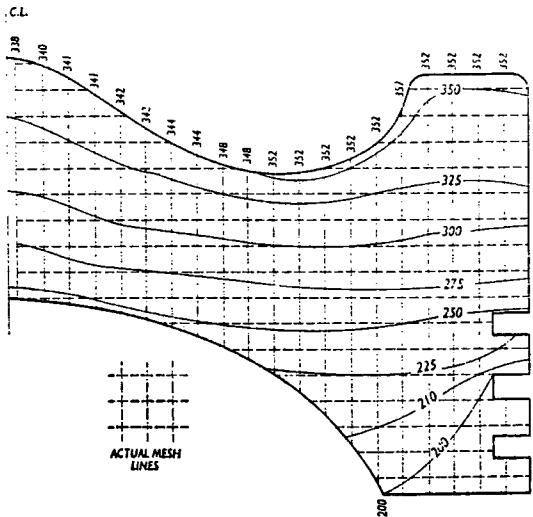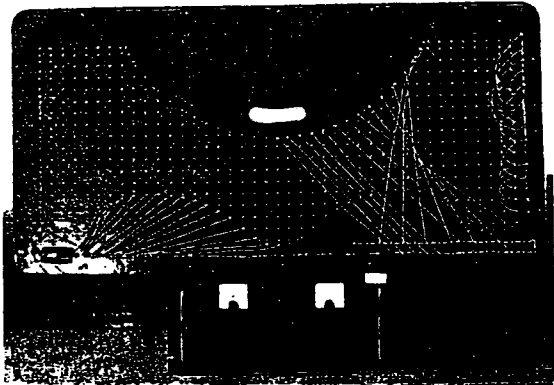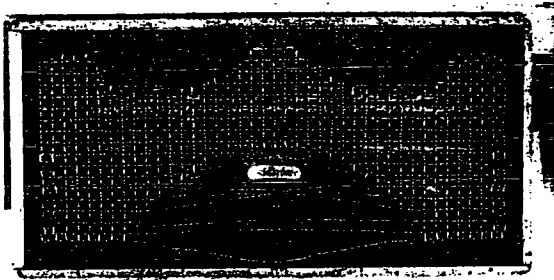

Fig. 2—(Above Left) Four times full scale model of a typical piston laid out for electrical analogy

Fig. 3—(Left) A similar model using a resistance chain to obtain boundary conditions

Fig. 4—(Above Right) Transverse temperature distribution through piston (since the piston temperature distribution about the centre line is assumed to be symmetrical, half of piston only is shown). Temperatures are in °C
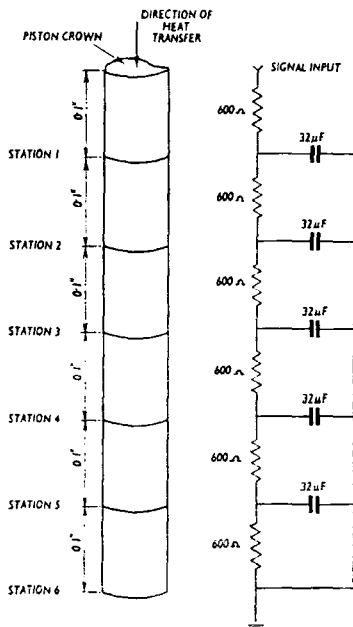
Fig. 5—Simple network for uni-directional transient heat transfer through piston
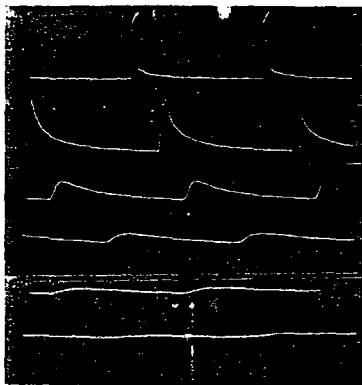

Fig. 6—Transient temperature fluctuations obtained at six stations through the piston at an engine speed of 500 r.p.m.
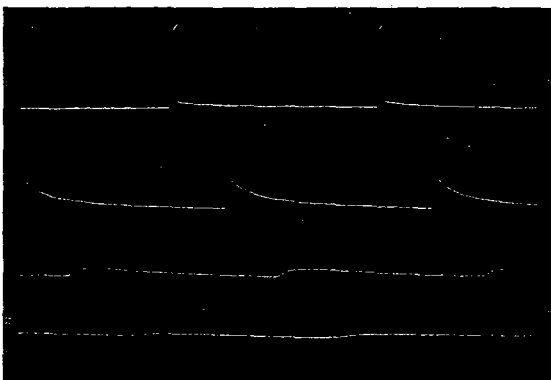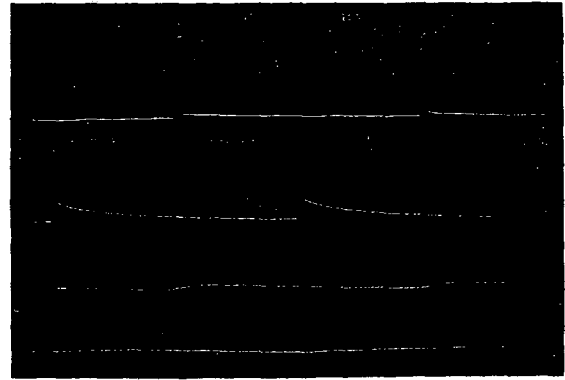
$$\frac{\partial \theta_0}{\partial t} \cdot \frac{\partial T}{\partial V_0} \cdot \frac{1}{C_2} = \frac{R}{a^2} \cdot \frac{f(0)}{f(V)}$$

From which it can be seen the analogy $\partial T/\partial t = RC_x/a^2$ holds.

EXPERIMENTAL DETERMINATION OF PISTON TEMPERATURE DISTRIBUTION

It is well established that, for a homogeneous material subject to known boundary temperatures, application of the Laplace equation facilitates the determination of isothermals in the material to a high degree of accuracy. The experimental methods mentioned earlier yield only approximate results. For instance:

(1) Oil erosion reduces the value of the temperature sensitive paints method.

(2) The hardness recovery method involves a great deal of preliminary work, prolonged tests and ultimate destruction of the piston.

(3) With the fusible plug method, there must be some idea of the temperature distribution in order to successfully make a suitable pattern of plugs of varying melting points. Without this prior knowledge, the method is one of prolonged trial and error. This method has all the attendant inaccuracies of an iterative process.

(4) The restriction on the thermocouple method results from the difficulty in transmitting the e.m.f. generated by the couple to measuring instruments external to the engine. Such is the magnitude of this problem that telemetering has been resorted to, a complicated and expensive system.

Due to the inherent difficulties of these experimental methods, the analytical approach suggests itself since, although the boundary conditions have to be estimated, the results are no less accurate than those obtained experimentally.

TEMPERATURE DISTRIBUTION WITHIN THE PISTON UNDER STEADY STATE CONDITIONS

In order to evaluate the usefulness and economy of this method, the profile of a piston in common use was employed (Fig. 2). The profile was enlarged to four times full size and a 1in square mesh imposed upon it. This mesh size was chosen as a compromise between practicality and accuracy. Since they were both readily available and inexpensive. $1k\Omega \mp 20\%$ tolerance resistors were chosen for the mesh. This was in accordance with the authors' aims of producing an inexpensive net for the solution of this engineering problem. Around the curved boundary of the piston profile where the

distances between the nodes and boundary were less than unity, a linear proportionately rule was used, a gap of 0·75in being represented by a 750-ohms resistor. This is proved rigorously by Liebmann.[2]

The boundary conditions were obtained from a resistance chain the junctions of which were chosen to give the desired boundary value (Fig. 3). It is essential, if continued adjustment of the components comprising the boundary resistance chain is to be avoided, that the impedance of this should be much less than that of the network. Because of the symmetry of the piston longitudinal profile, similar nodal points on either side of the longitudinal centre line were connected (Fig. 2), and hence it was only necessary to impose the boundary voltages on half the piston profile perimeter.

With arbitrarily chosen boundary conditions, a scan of the nodal field was made (Fig. 4), and the results obtained used as the first approximation for a numerical evaluation of the relaxation pattern. From this calculation, it was shown that an accuracy better than 1% was attainable from this network. A formula given by Liebmann[2] for estimating the errors as a result of neglecting the fourth order term in Taylors' expansion was applied to a number of nodes selected at random and these gave an additional error of only 0·1% for the net shown in Fig. 4.

TEMPERATURE DISTRIBUTION WITHIN THE PISTON UNDER TRANSIENT CONDITIONS

Since the unsteady temperature fluctuations did not penetrate to any great depth into the piston, it was not considered worthwhile refining the whole network to inspect phenomena occurring near the boundary only. A simple network (Fig. 5) was constructed therefore, simulating a longitudinal element through the piston. Inspection of the isothermal plot (Fig. 4) shows that over a considerable proportion of the piston profile, the isothermals are sensibly "flat" implying little or no transverse heat transfer. It was therefore considered justifiable to consider this problem using only a small longitudinal element.

The pulse shape used, although not a typical diesel engine combustion temperature profile, nevertheless was adequate for the investigation, since it illustrated clearly how the transient temperature varied near the surface of the piston crown. The results for three engine speeds 500 r.p.m., 1 000 r.p.m. and 1 500 r.p.m. are shown in Figs. 6, 7 and 8. These show that, at the lowest engine speed,

Fig. 7—Similar temperature fluctuations at 1 000 r.p.m.

Fig. 8—Test results at 1 500 r.p.m.

the transient temperature fluctuations almost vanish at a piston depth of 0·2in.

It can be seen from these figures that the distance for temperature transient decay varies with engine speed, until at an engine speed of 1 500 r.p.m. the depth is reduced to 0·1in.

Conclusions

It is difficult to determine theoretically the surface temperature of the piston crown. This does not detract from the value of the method, since much useful information may be obtained by applying a range of surface temperatures in which the operating temperature is likely to fall.

Piston profiles and boundary conditions can readily be changed.

The accuracy necessary in engineering design can be achieved using inexpensive components in the network analogue.

Acknowledgments

The authors are indebted to Messrs. Maughan, Vowles. Walton and Wright for the construction of the networks and the derivation of experimental results. This work represented part of a final year student project in the Department of Mechanical Engineering, University of Leeds.

Appendix

Finite difference representation of $\partial^2\theta/\partial x^2$. Consider the range of solution shown in
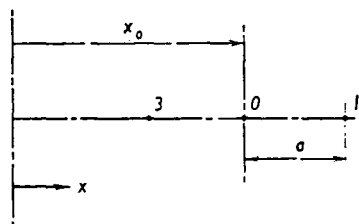
Fig. 9

Fig. 9 and assume in the region of point 0, the function θ can be expanded in a Taylor's series:

$$\theta = \theta_0 + \left(\frac{d\theta}{dx}\right)_0 (x-x_0) + \frac{1}{2!}\left(\frac{d^2\theta}{dx^2}\right)_0 (x-x_0)^2$$
$$+ \frac{1}{3!}\left(\frac{d^3\theta}{dx^3}\right)_0 (x-x_0)^3 + \frac{1}{4!}\left(\frac{d^4\theta}{dx^4}\right)_0 (x-x_0)^4 +$$
$$\qquad \cdots \quad (10)$$

If x is put equal to (x_0+a) Equation (10) gives:

$$\theta_1 = \theta_0 + a\left(\frac{d\theta}{dx}\right)_0 + \frac{a^2}{2}\left(\frac{d^2\theta}{dx^2}\right)_0$$
$$+ \frac{a^3}{6}\left(\frac{d^3\theta}{dx^3}\right)_0 + \frac{a^4}{24}\left(\frac{d^4\theta}{dx^4}\right)_0 + \quad \cdots \quad (11)$$

and if $x=(x_0-a)$ Equation (10) gives:

$$\theta_3 = \theta_0 - a\left(\frac{d\theta}{dx}\right)_0 + \frac{a^2}{2}\left(\frac{dx^2}{d^2\theta}\right)_0$$
$$- \frac{a^3}{6}\left(\frac{d^3\theta}{dx^3}\right)_0 + \frac{a^4}{24}\left(\frac{d^4\theta}{dx^4}\right)_0 + \quad \cdots \quad (12)$$

Adding Equations (11) and (12) gives

$$\theta_1 + \theta_3 = 2\theta_0 + a^2\left(\frac{d^2\theta}{dx^2}\right)_0 + 0\,(a^4) \quad \cdots \quad (13)$$

where all the terms containing fourth or higher powers of a are included together as $0(a^4)$. If a is sufficiently small the quantity $0(a^4)$ can be neglected and the finite difference approximation to $(d^2\theta/dx^2)_0$ is:

$$\left(\frac{d^2\theta}{dx^2}\right) = \frac{1}{a^2}\,[\theta_1 + \theta_3 - 2\theta_0] \quad \cdots \quad (14)$$

References
[1] Southwell, *Relaxation Methods in Engineering Science*, Oxford University Press, 1940.
[2] Liebmann, "Solution of Partial Differential Equations with a Resistance Network Analogue", *British Journal of Applied Physics*. January, 1950.
[3] Soraka, *Analogue Methods of Computation and Simulation*, McGraw-Hill, New York.

PAPER 7

Dynamic Characteristics of a Hydrostatic Thrust Bearing

By J. SCHWARZENBACH, M.Sc.* and K. F. GILL, M.Sc., Ph.D.*

An externally pressurised oil film thrust bearing, which has a theoretically infinite static stiffness resulting from the use of pressure feedback to a flow control valve in the bearing oil supply line, is investigated theoretically to determine the effect on dynamic performance of: (a) recess size; (b) restriction in the feedback line; (c) fluid compressibility in the bearing recess; (d) stiction forces acting on the flow control valve; and (e) pressure noise in the oil supply system. The technique adopted has been to solve the governing equations for the system on an analogue computer to obtain the harmonic response characteristics, from which simple design criteria could with experience be formulated.

THE application of automatic control to machine tools has caused certain characteristics, for which the operator had previously to make allowance based on experience, to assume greater importance. Among these is the non-linear "stick-slip" motion of the machine tool slideway, which introduces complication in the design for automatic positional control systems, where high accuracy of the finished component is of importance. As a result investigations have been carried out into the characteristics of externally pressurised thrust bearings for use in slideway applications[1] to [6].

The positional accuracy of the tool relative to the workpiece, in a direction normal to the plane of the workpiece travel, has been improved for a hydrostatic bearing by closing the loop on a simple hydraulic positional controller[7]. This results in a bearing with infinite static stiffness.

During preparation of lectures for the post-graduate course in "Bearing Design, Lubrication, Friction and Wear" at the University of Leeds the authors found that little information was available about the dynamic performance of such a closed loop system. Of particular interest was the effect of such factors as fluid compressibility, valve stiction forces, and pressure noise in the hydraulic supply.

This report presents the results of a study made of a simulated system for the bearing configuration described in Reference 7. The variation in dynamic performance is obtained for changes in recess size, fluid compressibility, control valve stiction, and pump pressure noise.

Notation:

a₁—Smaller area on differential area control valve.
A—Overall area of bearing pad.
b—Control valve damping coefficient.
C_1, C_2, C_3—Constants.
h—Bearing pad film thickness.
H—Bearing pad film thickness ÷ 1 000.
K_1, K_2—Constants.
m—Mass of control valve.
M—Mass of bearing pad.
n—Ratio of large/small areas of control valve.
P_s—Supply pressure.
P_0, P_1, P_2—System pressures.
q_0, q_1, q_2—System fluid flow rates.
Q_0, Q_1, Q_2—System fluid flow rates × 1 000.
r_i and r_0—Pocket radius, and pad radius.
v—Volume of fluid.
W—Load applied to the bearing pad.
x—Control valve position.
X—control valve position ÷ 1 000.
Z_1, Z_2—Capillary restrictions.
ß—Bulk modulus of fluid.

Subscript
[ ]₀—Datum design conditions.

* Department of Mechanical Engineering, University of Leeds.

DESCRIPTION OF SYSTEM AND SIMULATOR CIRCUIT

System.—A schematic representation of the bearing pad and control valve is shown in Fig. 1. The pad is assumed to be a circular parallel surface thrust bearing with an annular land; oil is supplied through a capillary restrictor Z_1 to the recess of the pad. The recess pressure P_1 is applied to the larger area of a differential area flow control valve, while the smaller area senses the capillary upstream pressure P_0. These pressures control the metering orifice size in such a way that the ratio P_1/P_0 is maintained at a constant value. Assuming that the fluid viscosity is sensibly constant, the land restriction and hence the film thickness h are then maintained constant, irrespective of changes in bearing load W.

Simulator Circuit.—The basic flow continuity and dynamic equations representing the system are given in Appendix I. These equations in linearised form have been solved on a PACE 221R analogue computer. The circuit layout used for the bearing configuration of Fig. 1, incorporating compressibility and the non-linear effect of valve stiction, is shown in Fig. 2, with the bearing
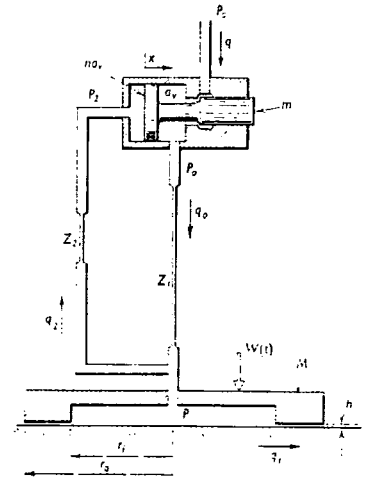

Fig. 1—Schematic diagram of bearing pad and control valve

pad and the control valve shown separately. The computer programme was arranged in such a way that variation in the desired parameters could readily be achieved by adjustment of the appropriate controlling potentiometers.

Design Conditions and Parameters Investigated.—The values chosen for the design point are:

$P_s = 200$ lb/in² gauge
$P_0 = 100$ lb/in² gauge
$P_1 = 50$ lb/in² gauge
$h = 0.001$in and 0.002in

For a given design film thickness the variation in dynamic pad stiffness was studied for changes in:

(a) Recess size r_i/r_0.
(b) Feedback restrictor size Z_2.
(c) Fluid compressibility.
(d) Valve stiction.
(e) Pump pressure noise.

The results are presented in Figs. 3 to 8.

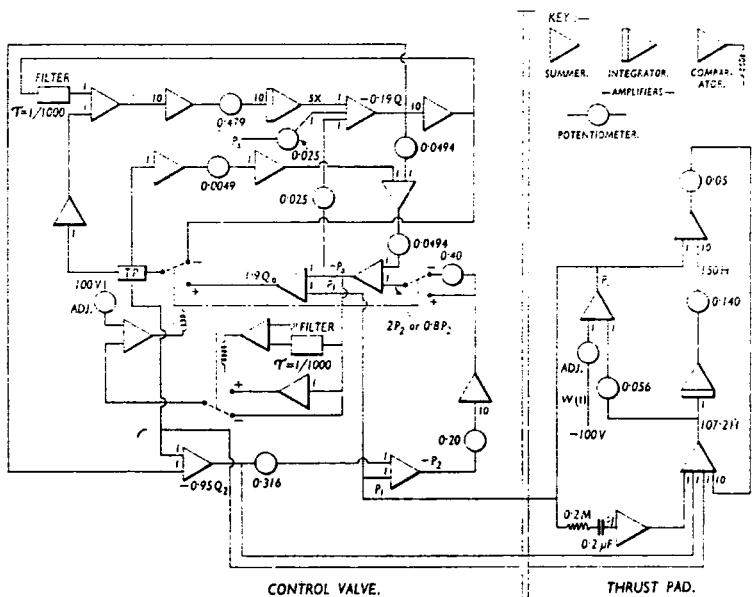CONTROL VALVE.   THRUST PAD.

Fig. 2—Computer circuit diagram

Technical Contributors Section *(Continued)*

DISCUSSION

Harmonic response testing of the simulated system has been used to investigate the bearing configurations chosen for study, including those in which non-linear effects are present. The only design criterion that appears in the literature as a means of determining the suitability of any such arrangement is that of dynamic stiffness. None of the empirical criteria, based on laws of experience, normally used in the harmonic design of linear control systems have been found for the type of system represented by this valve controlled hydrostatic bearing.

To present, in a concise form, the closed loop harmonic information obtained for the system studied a "dynamic response locus" plotted in the s plane and showing lines of constant stiffness and phase angle has been used in this report. The aim has been to obtain a simple analytical approach from which design information can readily be obtained, and thus to avoid the use of random forcing functions and the statistical techniques necessary for accurately analysing any given machining operation.

The results of the computer analysis (Figs. 3 to 8) are plotted in the form of amplitude of bearing movement resulting
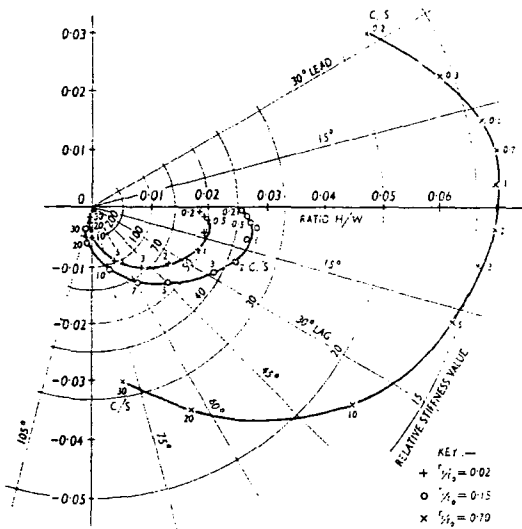
Fig. 3—Linear system $H = 1$
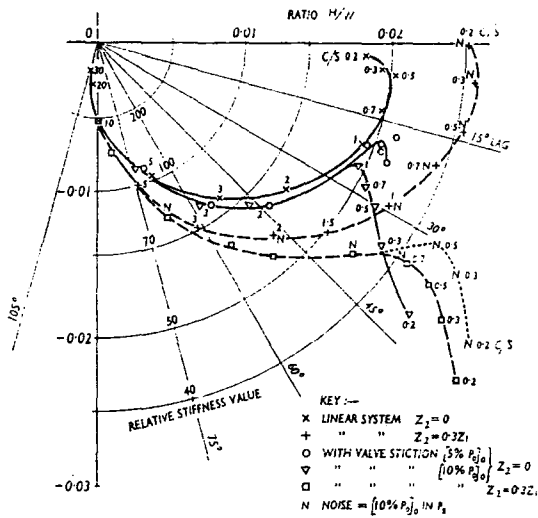
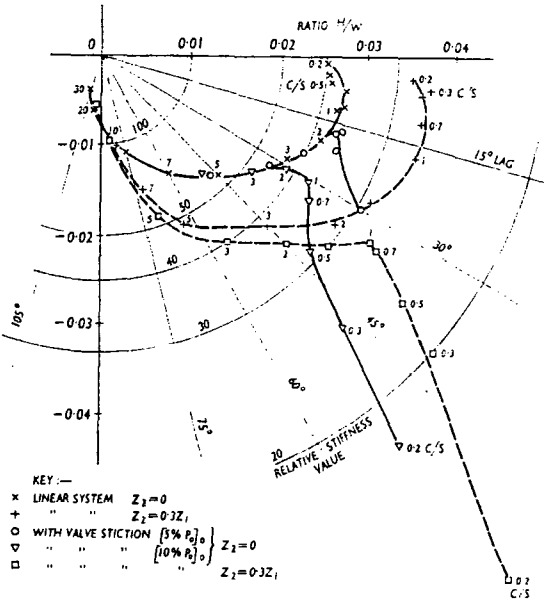Fig. 4—System without recess $(r_i/r_0 = 0.02)$ showing effect of stiction $H = 1$

KEY:—
x LINEAR SYSTEM $Z_2 = 0$
+   "   " $Z_2 = 0.3Z_1$
o WITH VALVE STICTION $[5\% P_s]_0$
▽   "   "   " $[10\% P_s]_0$ } $Z_2 = 0$
□   "   "   " $Z_2 = 0.3Z_1$

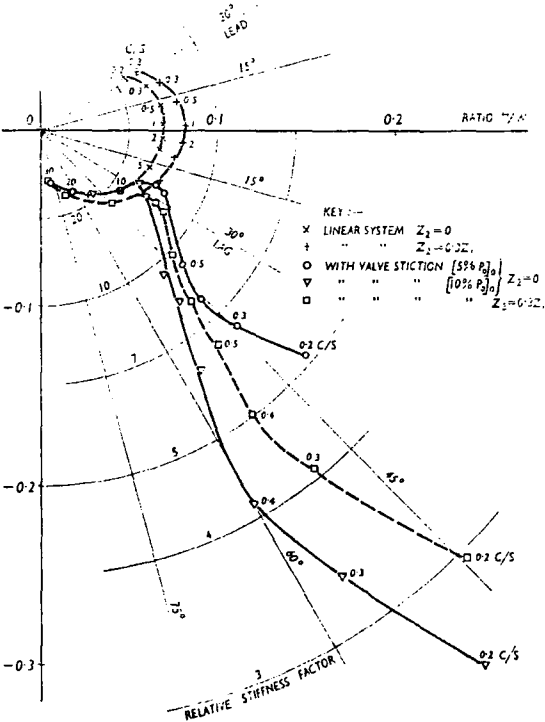Fig. 5—(Above) System with small recess $(r_i/r_0 = 0.15)$ showing effect of stiction $H = 1$

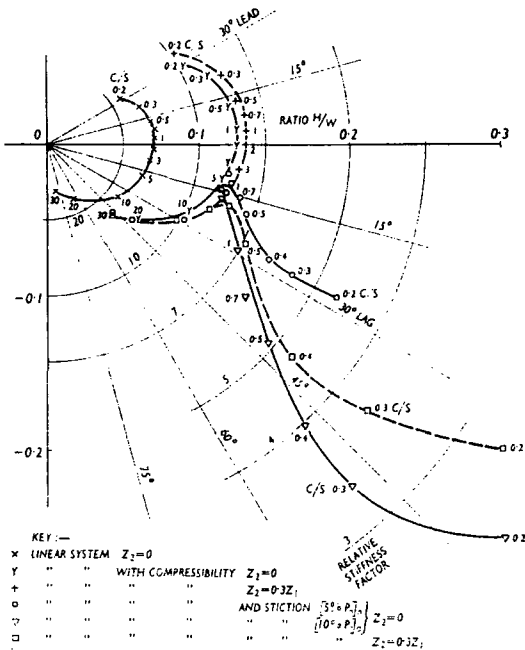Fig. 6—(Right) System with large recess $(r_i/r_0 = 0.7)$ showing effect of stiction $H = 1$

Fig. 7—System with large recess ($r_{ii} r_n - 0.7$) showing effect of compressibility and stiction $H = 1$

ripple suppressors to reduce the amplitude of these pressure fluctuations. A theoretical study of a pump unit has indicated that the frequency of such pressure fluctuations would be of the order of 50 c/s, and the amplitude would not exceed $\pm 10\%$ of the mean delivery pressure.

Noise signals composed of two saw-tooth wave forms with suitably displaced frequencies and amplitudes were used to simulate the worst pressure noise which might occur in practice. With this signal injected at the inlet to the flow control valve no noticeable change in system performance was observed for either the linear or the non-linear system.

CONCLUSIONS

(1) For load changes which are a fixed percentage of the bearing load carrying capacity the dynamic stiffness decreases rapidly with increase in bearing recess area and with increase in design film thickness.

(2) Recess depth should be kept to a minimum to avoid further reduction in dynamic stiffness resulting from the effect of fluid compressibility.

(3) The effect of restriction in the feedback line on bearing stiffness is negligible.

(4) Stiction in the flow control valve reduces the bearing performance both statically and dynamically below about 2 c/s. At frequencies above this there is negligible deterioration.

(5) Pressure noise at pump delivery has no noticeable effect on system performance.

APPENDIX I

EQUATIONS FOR LINEAR SYSTEM

For the system of Fig. 1 the basic flow continuity and dynamic equations. using the symbols of Fig. 1 and Appendix I. are:
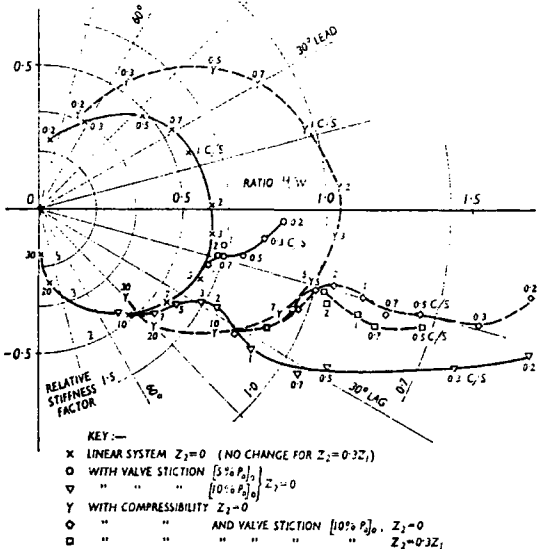For valve:

$$(P_s n - P_o)\, a_r = m\,\ddot{x} - b\,\dot{x} \qquad \ldots \quad (1)$$

$$q = K_1 x \sqrt{P_s - P_a} \qquad \ldots \quad (2)$$

$$q_o - q = \dot{x}\, a_r \qquad \ldots \quad (3)$$

$$q_2 - \dot{x}\, n\, a_r \qquad \ldots \quad (4)$$

$$q_o = \frac{P_a - P_1}{Z_1} \qquad \ldots \quad (5)$$

from a sinusoidal load variation whose amplitude is a fixed proportion of the bearing steady state load carrying capacity. No units are indicated as the results are intended to show the relative changes occurring as a result of changes in system configuration. The range of frequencies covered is 0.2 c/s to 30 c/s. which the authors consider to be the range of engineering interest for such a bearing. At 30 c/s the stiffness of the bearing is relatively large. and at higher frequencies the stiffness increases rapidly. With this restriction on frequency it is justifiable to use within the computer circuit filter networks (Fig. 2) to eliminate parasitic oscillations occurring within the circuitry of the computer.

For the size of bearing and control valve arbitrarily chosen for study it was found that the magnitude of the inertia coefficients were sensibly zero in comparison to the coefficients of the viscous terms (Appendix I). No attempt has therefore been made to include elements in the computer circuit to simulate these effects.

For the simple linear system, Figs. 3 and 8 show the reduction in dynamic stiffness with increasing pocket size and film thickness. the latter showing a larger reduction in relative dynamic stiffness. The effect of restriction in the feedback line on the harmonic response for an increase of Z_2 from zero to 30% Z_1 is a decrease in stiffness which is considerable for small recesses but small for large recesses.

It has been assumed that the control valve is bolted to the bearing pad and that interconnecting drillings are kept as short as possible, and also the enclosed volumes of fluid within the valve are assumed to be small. thus making valid the assumption that compressibility within these elements can reasonably be ignored. The only remaining volume of fluid in which compressibility is likely to have an effect is that within the bearing recess. Characteristic changes in dynamic stiffness for a recess depth as small as 0.003in are shown in Figs. 7 and 8 for the bearing with the largest diameter recess. Increasing the depth to 0.030in decreases

the stiffness by a factor of 5. The effect of changes in Z_2 with valve recess compressibility present is still small.

As was suspected at the start of the investigation stiction forces operating on the control valve can have a significant effect on system performance. From Figs. 4, 5, 6 and 8 it can be seen that this takes the form of a large departure from the linear locus at frequencies below the order of 2 c/s, giving an undesirable decrease in bearing stiffness. Further, positional errors would also result under steady state conditions. and hence a general overall deterioration in bearing performance occurs.

It is thought that pressure noise at the outlet of hydraulic pumps can affect the functioning of flow control valves. Certain commercially available pumps are fitted with

Fig. 8—System with large recess ($r_{ii} r_n - 0.7$) showing effect of compressibility and stiction $H = 2$

8

Technical Contributors Section (Continued)

For restrictor in feedback line:

$$q_2 = \frac{P_1 - P_2}{Z_2} \qquad \ldots \quad (6)$$

For bearing pad:

$$C_1 P_1 - W = M\ddot{h} + \frac{C_2}{h^2}\dot{h} \qquad \ldots \quad (7)$$

$$q_1 = K_2 P_1 h^3 \qquad \ldots \quad (8)$$

$$q_1 = q_0 - q_2 - A\dot{h} \qquad \ldots \quad (9)$$

For small load disturbances Equations (2), (7) and (8) can be written in the linearised form:

$$\frac{q}{[q]_0} = \frac{x}{[x]_0} + \frac{P_s - P_0}{2[(P_s - P_0)]_0} \qquad . \quad (2(a))$$

$$C_1 P_1 - W = M\ddot{h} + C_3 \dot{h} \qquad \ldots \quad (7(a))$$

$$\frac{q_1}{[q_1]_0} = \frac{P_1}{[P_1]_0} + \frac{3h}{[h]_0} \qquad \ldots \quad (8(a))$$

Physical dimensions have been arbitrarily selected for the components, from which the constants are calculated to be:

$$a_r = 0.055 \text{in}^2$$
$$n = 2$$
$$m = 0.00036 \text{ lb}_m$$
$$b = 0.0014 \text{ lb/sec/in}$$
$$[x]_0 = 0.001 \text{in}$$
$$A = 113 \text{in}^2$$

Datum design pressures have been kept constant throughout the investigation, the values being $P_s = 200$ lb/in^2 gauge, $P_0 = 100$ lb/in^2 gauge, and $P_1 = 50$ lb/in^2 gauge. Using these values the values of the remaining constants can be calculated, and these are tabulated below:

The values of the inertia terms in Equations (1) and (7(a)) are small compared to the damping terms, and during the analysis were shown to have negligible effect. They have therefore been deleted and the equations assume the form:

$$2P_2 - P_0 = 0.0255\dot{x} \qquad \ldots \quad (10)$$

$$\frac{q}{[q]_0} = \frac{x}{0.001} + \frac{P_s - P_0}{200} \qquad \ldots \quad (11)$$

$$q_0 - q = 0.055\dot{x} \qquad \ldots \quad (12)$$

$$q_2 = 0.11\dot{x} \qquad \ldots \quad (13)$$

$$q_0 = \frac{P_0 - P_1}{Z_1} \qquad \ldots \quad (14)$$

$$q_2 = \frac{P_1 - P_2}{Z_2} \qquad \ldots \quad (15)$$

$$C_1 P_1 - W = C_3 \dot{h} \qquad \ldots \quad (16)$$

$$\frac{q_1}{[q]_0} = \frac{P_1}{50} + \frac{3h}{[h]_0} \qquad \ldots \quad (17)$$

$$q_1 = q_0 - q_2 - 113\dot{h} \qquad \ldots \quad (18)$$

APPENDIX II

MODIFICATIONS TO LINEAR SYSTEM REPRESENTATION TO INTRODUCE FLUID COMPRESSIBILITY AND VALVE STICTION

(*a*) *Fluid Compressibility.*—To introduce the effect of fluid compressibility and expansion of supply lines under transient pressure variations it is necessary to include terms of the form $\dot{P}_r/\beta$ in Equations (12), (13), (17) and (18).

The only compressibility effect introduced

into the analysis was that of the fluid in the bearing recess. The effect of compressibility under the bearing land is very small and it was assumed that the geometry of the valve and supply lines was such that compressibility in these components could be assumed to be small. Equation (18) then becomes:

$$q_1 = q_0 - q_2 - 113\dot{h} - \frac{v_r \dot{P}_1}{200\,000} \qquad . \quad (19)$$

(*b*) *Valve Stiction.*—When the control valve is stationary, as a result of valve stiction, Equations (10) to (15) for the control valve and restrictor Z_1 are replaced by

$$\frac{q}{[q]_0} = \frac{P_s - P_0}{200} = -\frac{P_0}{200} \text{ since } P_s = \text{const.}$$

and

$$\frac{q_0}{[q_0]_0} = \frac{P_0 - P_1}{[P_0 - P_1]_0} = \frac{P_0 - P_1}{50}$$

Since $q = q_0$ with the valve stationary these equations reduce to

$$P_1 = 1.25 \, P_0 \qquad \ldots \quad (20)$$

Equation (20) applies for a region $2P_2 - P_0 \lessgtr \pm K$, i.e.

$$1.5 \, P_0 \lessgtr \pm K \qquad \ldots \quad (21)$$

where K represents the magnitude of the valve stiction force.

REFERENCES

[1] Tilsley, R., "Developments in the Control of Machine Tools", THE ENGINEER, Vol. 218, page 1111, 1964.
[2] Galloway, D. F., "Machine Tool Research, Design and Utilisation", *Proc. I.Mech.E.*, Vol. 175, page 85, 1961.
[3] Frost-Smith, E. H., "Research on Machine Tools and Automation", *Int. J.Mach. Tool. Drs. Res.*, Vol. 1, page 173, 1961.
[4] Wunsch, H. L., "The Design of Air Bearings and Their Application to Measuring Instruments and Machine Tools", *Int. J.Mach. Tool Des. Res.*, Vol. 1, page 198, 1961.
[5] Wunsch, H. L. and Scoles, C. A., "Automatic Load Compensation Device for Air Bearings", N.E.L. Report No. 86, June, 1963.
[6] Loxham, J. and Hemp, J., "The Application of Hydrostatic Bearings to High Precision Machine Tools", College of Aeronautics, Cranfield, Report J.L. 1306.
[7] Royle, J. K., Howarth, R. B. and Caseley-Hayford, A. L., "Applications of Automatic Control to Pressurised Oil Film Bearings", *Proc. I.Mech.E.*, Vol. 176, page 532, 1962.

r_1/r_0	C_1	M	$h = 0.001$			$h = 0.002$		
			$[q]_0$	Z_1	C_3	$[q]_0$	Z_1	C_3
0.7	80.6	125.0	0.0263	1 900	0.486×10^5	0.210	237	0.061×10^6
0.15	29.2	45.4	0.00497	10 100	7.95×10^5	0.0398	1 267	0.995×10^6
0.02	14.5	22.4	0.00241	20 800	12.95×10^5	0.0193	2 600	1.62×10^6

PAPER 8

Determination of Root Loci

By K. F. GILL. M.Sc., Ph.D., C.Eng., A.M.I.Mech.E., A.M.I.E.E. and
P. H. WALKER. B.Sc., Ph.D., C.Eng., A.M.I.E.E.

A computational technique is developed for the automatic determination of the roots of an nth order polynomial equation using only simple linear computing elements. The programme developed is such that with the minimum amount of operational skill the roots can be rapidly located without ambiguity. As an illustration a root locus plot is constructed for a fourth order characteristic equation.

MANY of the mathematical problems that occur in physics and engineering need for a solution the determination of the roots of a polynomial equation of the nth degree. The root locus technique used in the analysis and design of linear control systems is one important application. In recent years the root locus approach[1, 2], has been used increasingly in control system engineering to obtain information about the stability of servo systems since links between frequency response and the corresponding transient response are somewhat tedious. In practice the harmonic response criterion is based on satisfactory transient response behaviour.

The graphical technique commonly used for the construction of root loci is straightforward but wasteful of time particularly in high order systems. For the solution of polynomials of the fourth and higher orders the use of computing machines, especially digital computers, have found favour, and numerous methods for the machine solution of polynomials have been developed. In addition, proprietary equipment[7] has been manufactured which enables the roots of the characteristic equation of a closed loop transfer function to be more speedily determined for all values of the system's gain constant K.

Analogue programmes have been used for the solution of polynomial equations[3, 4] but have the disadvantage of calling for a considerable amount of skill on the part of the computer operator by requiring a systematic search for roots in the complex domain. An improved technique[5] using the "method of steepest descent" enables a more rapid solution to be obtained but involves the use of a large number of multipliers and multiturn resolvers; equipment normally only available in large analogue computing installations.

The authors' aim has been to investigate and develop a programme for the solution of nth order polynomials which would require the minimum amount of operational skill and utilises the smallest and simplest form of analogue computing equipment, the type of analogue installation frequently available in most engineering establishments. A major disadvantage of the digital computer tech-

nique is the time period normally needed to get the information back to the engineer interested in this type of problem solution. It is an advantage, if only as an alternative, to employ the more readily available inexpensive analogue machine for this purpose.

The technique employed has been developed from that originally suggested by Johnson[6] and satisfies the authors' basic requirements of needing the minimum amount of analogue equipment and operational skill.

THEORY

The Nyquist criterion is based on the theory of complex variables and a theorem which can be put to use in the analogue computer solution of a polynomial equation is as follows: If a closed contour in the complex variable s-plane enclose P poles of

the function $W(s)$ and Z zeros of $W(s)$ then a contour in the $W(s)$ plane will encircle the origin in the $W(s)$ plane N times, where $N=Z-P$. A pole P occurs when for some value of s, $W(s)$ is infinite, therefore for a polynomial equation the statement reduces to that. The number of net encirclements of the origin in the $W(s)$ plane by a contour drawn in this plane equals the number of roots enclosed by a contour drawn in the s-plane.

Consider a polynomial of the nth degree

$$W(s) = a_n s^n - a_{n-1} s^{n-1} + \ldots \ldots a_1 s - a_0 = u - jv \qquad (1)$$

where the complex variable can be written as

$$s = x - jv = r(\cos \theta - j \sin \theta) \qquad (2)$$

The roots s_m of the polynomial satisfy the equation

$$W(s_m) = 0 \text{ for } m = 1, 2, 3, \ldots \ldots n \qquad (3)$$

since it is known from the fundamental theory of algebra that there are exactly n values of s which will satisfy equation (3). Substituting equation (2) into equation (1) and equating real and imaginary terms gives:

$$u = a_0 - a_1 r \cos \theta - a_2 r^2 \cos 2\theta - \ldots \ldots \\ - a_n r^n \cos n\theta \qquad \ldots \ldots$$
$$v = a_1 r \sin \theta - a_2 r^2 \sin 2\theta \qquad \ldots \ldots \\ - a_n r^n \sin n\theta \qquad (4)$$

By plotting u against v as θ varies from 0 to 2π radian it will be clearly shown for which values of θ both u and v have zero value simultaneously.

ANALOGUE COMPUTER PROGRAMME (PACE 221R COMPUTER)

The computer programme shown in Fig. 1 is that used for the solution of the characteristic equation

$$0.7s^4 + s^3 - s^2 - 0.7s - K = 0 \qquad (5)$$

The two dependent variables u and v of equation (4) are obtained by the summation of the outputs from the four harmonic generators (amplifiers 2-13) multiplied by the desired constant coefficients $(a_0 \ldots \ldots a_4)$. This summation together with the introduction of the equation coefficients takes place in amplifiers 14 and 15.

The initial conditions for the four harmonic generator circuits are provided from the servo-multiplier system shown in Fig. 1
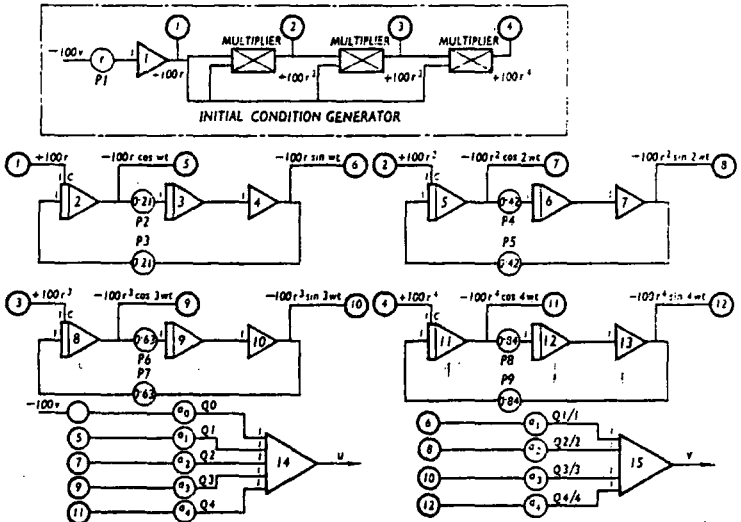

Fig. 1—Computer circuit to find roots of fourth order polynomial equation

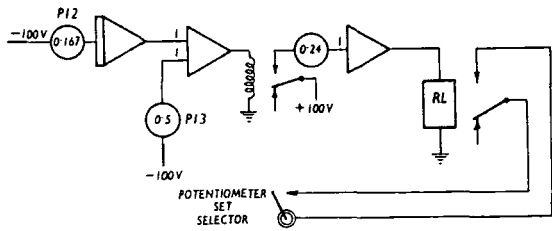## Technical Contributors Section *(Continued)*

Fig. 2—Trigger circuit for cycling sequence

(insert). This enables any desired value of r^n to be automatically available as an initial condition as r is varied from 0 to 1, and has the practical advantage of not requiring any external computation and adjustment.

Automatic computer mode control is provided by the amplifier-relay system shown in Fig. 2. Potentiometers $P12$ and $P13$ control the slope and height of the trigger waveform used to give the circuit cycling time duration. For the values of $P12$ and $P13$ shown the cycling time is of thirty seconds duration.

CONSTRUCTION OF THE ROOT LOCUS

The procedure used and the basic steps in the construction of the root locus plot[1, 5] are outlined below for the characteristic equation:

$$0.7s^4 + s^3 - s^2 - 0.7s - K = 0 \quad . \quad . \quad (5)$$

(*a*) Starting points: the loci start at the poles of $G(s)$ for $K=0$ i.e. the factors of equation (5), which are:

$$s(s+1)(s-0.215= jo.965)$$

(*b*) Ending points: there are no zeros of $G(s)$, hence all loci move ultimately to infinity, approaching asymptotes at angles given by $(2k+1)\pi/P-Z$ where $k=0, 1, 2$ &c. i.e. at angles of $45°$, $135°$, $225°$ and $315°$.

(*c*) Number of loci: since there are no zeros and four poles there will be four loci.

(*d*) Intersection of asymptotes: this lies on the real axis at

$$\delta = \frac{\Sigma \text{ Poles of } G(s) - \Sigma \text{ Zeros of } G(s)}{P-Z}$$

i.e. at

$$\delta = -0.354$$

(*e*) Loci on real axis: there will be loci between $s=0$ and $s=-1$, since along this section of the real axis the total number of poles and zeros to the right of this section is odd.

(*f*) Breakaway point: a breakaway point exists on the real axis between $s=0$ and $s=-1$ and can be found as a real root of the equation $dK/ds=0$ and is $s=-0.65$.

(*h*) Using the above information the general shape of the loci can be drawn approximately, and then the more accurate curves found in the following way from the computer.

(i) With the pen zeroed to some target such as A, Fig. 3, and "r" made equal to unit by adjustment of potentiometer $P1$, the computer was allowed to operate for a time period of 0 to 2π radians, the number of net encirclements of this target point A being equal to the number of roots in the range $r=0$ to 1.

(ii) The value of r was reduced until the trace indicated both u and v were simultaneously zero, i.e. trace passed through target point A. At this instant the computer "hold" was actuated. The voltage output from amplifier 2 gave $|x|$ and the output

from amplifier 4 gave $|y|$ and in this way the x-y co-ordinates of one root were found for some particular value of K.

(iii) For roots in excess of unity a simple substitution is necessary to enable the computer to search for these larger roots. A new polynomial is developed by replacing s by $s=1/p$ and determining the roots of the new polynomial $W(p)$. The new polynomial $W(p)$ has the same coefficients as $W(s)$ except that
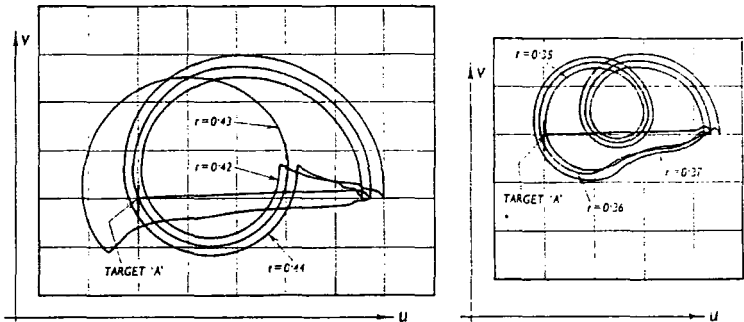

Fig. 3—Computer plots of U and V for $k=32$

the coefficients are in reverse order, as illustrated below. Making the substitution $s=1/p$ in equation (5) gives

$$W(p)=Kp^4-0.7s^3-s^2-s-0.7=0$$

(iv) The co-ordinates for any root of $W(s)$ for $r>1$ can be found as in (i) and (ii), the outputs from amplifiers 2 and 4 being used to evaluate these; i.e.

$$|x|=\frac{\text{output of amplifier 2}}{r^2}$$

$$|y|=\frac{\text{output voltage amplifier 4}}{r^2}$$

where r is the potentiometer value $P1$.

DISCUSSION

Choice of Cycling Time.—To avoid the complication of providing auxiliary equipment necessary for the automatic actuation of the computer "hold" mode at the instant when $u=v=0$ a cycling time of thirty seconds was chosen, i.e. potentiometers $P2$ and $P3$ were set to a value 0.21. This cycling time was governed by the necessary condition that at the instant $u=v=0$ it was physically possible to actuate the hold control and obtain values for u and v that were sensibly zero. The thirty seconds time period chosen as the cycling period proved to be acceptable since it does not result in excessive problem solution time and enables the satisfactory manual actuation of the hold facility.

Initial Conditions.—The initial conditions for each of the integrating amplifiers are generated by a servo-multiplier, a reference and three linear cups being required for the solution of a fourth order polynomial. A standard servo multiplier consists of a reference and five linear cups and is therefore capable of generating the required initial conditions for the solution of a sixth order polynomial. Accuracies of the order of $\pm 0.2\%$ should be achievable by this method as the servo multiplier is operating under steady-state conditions.

It must be emphasised that this facility of automatically generating the initial conditions. r, r^2, ... r^n, for a chosen value of r is essential as otherwise the time required to calculate these values and adjust corresponding coefficient setting potentiometers would make this type of solution impracticable.
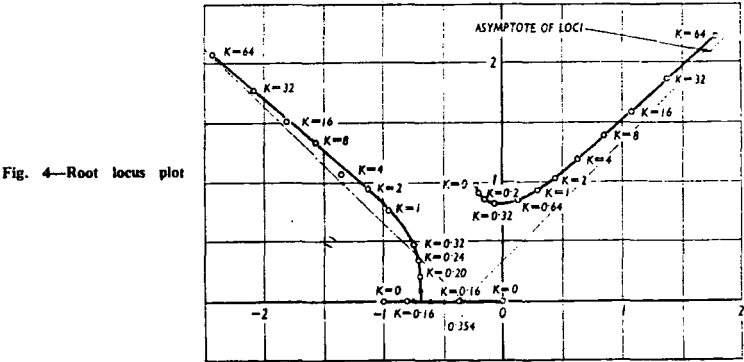

Fig. 4—Root locus plot

The Root Search.—Fig. 3 shows typical search paths as produced by the x and y co-ordinate plotter. The quality and clarity of these traces are indicative of the high order of discrimination achievable by this method. It can be seen that a variation in the value of the modulus of the roots of as little as $\mp 2\%$ results in separate and distinct contours. At the target point the theoretical voltage output from amplifiers 14 and 15 should be zero. In practice, however, it was always found to be of the order of a few millivolts which is within the limits of accuracy of the machine.

Although the cycling time is thirty seconds a decision as to whether the value of r chosen is a root can normally be made in half this time period. A decision, however, on the remaining number of roots in any range $r = 0 - r_i$ will always require the full cyclic plot of $u \approx v$ since the number of net encirclements of the origin of the co-ordinate system used, equals the number of roots still to be found for a complete solution.

The Root Locus Plot.—Shown in Fig. 4 is the location of the roots and hence their loci for the characteristic equation

$$0 \cdot 7s^4 - s^3 - s^2 - 0 \cdot 7s + K = 0$$

as K is varied within the range 0–64. For convenience only half of the diagram is shown.

In the determination of the roots the search was carried out in two stages: (*a*) for roots < 1 the characteristic equation given above was used, the gain constant setting K being provided by the adjustment of one potentiometer $Q0$; (*b*) for roots > 1 the modified equation

$$Kp^4 + 0 \cdot 7p^3 + p^2 + p + 0 \cdot 7 = 0$$

was used. In this case it was necessary to adjust two potentiometers $Q4$ and $Q4/4$ for each value of K selected. This simple adjustment is all that is necessary at each stage in the construction of the full root locus.

CONCLUSIONS

(1) This approach to the solution requires a minimum amount of computing equipment in that it is possible to solve polynomials of the sixth order with as little equipment as eighteen operational amplifiers, three per order, and one six-gang servo-multiplier. This is less than the complement of the smallest computers available commercially.

(2) By choosing a cycling time of thirty seconds it is possible to use manual computer mode control throughout the problem solution.

(3) The minimum amount of operational skill on the part of the operator is required and for a given value of K in the fourth order equation used the roots can be determined in a time period of less than four minutes.

(4) With careful interpretation of the search traces (Fig. 3) the magnitude of the roots can be found to an accuracy better than $\mp 2\%$.

REFERENCES

[1] Evans, "Control System Synthesis by Root Locus Methods", *Trans. A.I.E.E.*, Vol. 69, 1950.

[2] Blackman, "The Pole Zero Approach to System Analysis". Control Monograph 2.

[3] Bubb, "A Circuit for Generating Polynomials and Finding Their Zeros", *Proc. I.R.E.*, Vol. 39, pages 1556–61, 1951.

[4] Bauer and Fifer, "The Solution of Polynomial Equations on the R.E.A.C.", Project Cyclone Symposium 1, Reeves Instrument Corporation, pages 31–36, New York, March, 1951.

[5] Levine and Messinger, "An Automatic Analogue Computer Method of Solving Polynomials and Find Root Loci", *I.R.E. Conv. Record*, Part IV, pages 164–172, 1957.

[6] Johnson, "Analogue Computer Techniques", McGraw-Hill, Chapter 9, Section 7.

[7] Levinge and Thewlis, *An Electronic Root Solver*, *Electronic Engineering*, Vol. 35, No. 419, pages 16–20, January, 1963.

[8] Taylor, *Servomechanisms*, Longman, Chapter 18, 1960.

PAPER 9

THE ENGINEER

TECHNICAL CONTRIBUTORS

SECTION

Stability Analysis for the Practical Engineer

By K. F. GILL*, M.Sc.. Ph.D.. J. SCHWARZENBACH*, M.Sc..
and G. E. HARLAND*. B.Sc.

Reviewed in this report are a number of the most strongly established analytical techniques used in the dynamic analysis of physical control systems. To provide a comparison of their applicability, and the information obtainable, these methods are applied to two typical practical systems—an engine governor system, with a linear and a non-linear proportional governor. The methods considered are: the Routh-Hurwitz criterion, harmonic response criteria utilizing Nyquist, Bode, and Nichols diagrams, the root locus method, and Lyapunov's direct method. It is shown that for general linear system analysis stability can be established by application of the Routh-Hurwitz criterion, and that details of the dynamic performance can be obtained by use of a root locus plot. If system compensation is necessary then the coefficients for the compensating elements can be more readily determined by use of the Bode diagram for the system being analysed. The Bode diagram is also useful for obtaining approximations to system time constants from experimental results. Lyapunov's direct method is the only general approach applicable to systems of any kind, and thus has great potential. It is, however, time consuming for linear systems, and hence at present finds its greatest use in the analysis of non-linear systems.

1. INTRODUCTION

EARLY governing systems, starting with the Watt governor, were developed by trial-and-error design and adjustment, and only very limited, if any, consideration was given to theoretical analysis. The variations possible in the lines of approach when seeking satisfactory systems resulted in many failures, and intuitive knowledge gained by people with years of practical experience was an important factor in the development of successful systems. With the advent of more complex control systems, such as those required for the gas turbine aircraft engines of the 1950s, this method rapidly became totally inadequate.

Since that time there has been a rapid increase in the amount of theoretical work in the field of automatic control, which has led to the situation at the present date where theoretical and analytical techniques available for system investigation are considerably ahead of practical application. Many excellent textbooks on control theory, of which a selection are listed in the Appendix([3, 4, 9, 12, 13]), are available, and in these the more common techniques are described. The practising

* Mechanical Engineering Department. The University, Leeds, 2.

engineer has, in general, difficulty in knowing which of the many methods of stability analysis to use, and tends to avoid the newer and apparently more difficult techniques. The aim of this article is to give guidance in the use of the practically significant methods of stability analysis. The methods are briefly described, and their limitations pointed out. For illustration and comparison they are applied to two examples typical of practical systems.

2. SYSTEM REPRESENTATION

It must be understood that system diagrams or engineering drawings of control systems are generally too congested with detail to be immediately usable. It is, therefore, essential to use a clearcut method of simplification
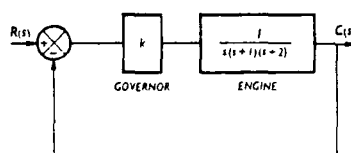

Fig. 1—Linear system

when dealing with systems of a complicated nature, otherwise the study will be burdened with much unnecessary detail.

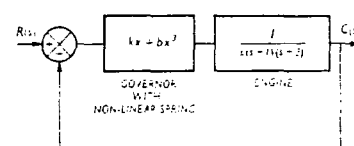The block diagram (such as Figs. 1 and 2)

Fig. 2—Non-linear system

is the usual method of system representation used to show in a compact way the inter-relationship between the elements in an otherwise complex system arrangement. The preparation of a schematic diagram is the first convenient step towards establishing the principal components and parameters in the system, and thereafter the preparation of the equivalent block diagram follows as a logical development. It is generally unwise to oversimplify the schematic representation until it is certain that the diagram truly represents the dynamic problem to be studied.

The dynamic equations used in this paper have been expressed in the Laplace transform notation, and this enables the complete mathematical description of the dynamic system behaviour to be specified with the minimum of writing. Further. when the behaviour of a system is described with the aid of transfer functions, i.e. the ratio of the Laplace transform of the system output to that of the system input, it is often possible by inspection alone to deduce many interesting properties of the system.

3. DEFINITION OF STABILITY

A stable system is generally considered to be one in which all transients decay completely in the steady state, whilst an unstable system is one whose output increases without bound for a bounded input signal. There are. however, several types of stability which can apply to a general system, and these are defined in this section([1]).

If a system is disturbed from an equilibrium state X_e and all subsequent motion remains within a small region around the equilibrium state then the system is described as stable. To formalize the concept of stability the following definitions will be used:

Definition 1.—An equilibrium state X_e of a free dynamic system is "stable" if for every real number $\varepsilon > 0$ there exists a real number $\delta > 0$ such that $|X_{t_0} - X_e| < \delta$ implies that $|X_t - X_e| < \varepsilon$ for all $t > t_0$.

Definition 2.—An equilibrium state X_e of

Technical Contributors Section *(Continued)*

a free dynamic system is "asymptotically stable" if (*a*) it is stable and (*b*) every motion starting sufficiently near X_e converges to X_e as $t \to \infty$, i.e. there is some real constant $\delta > 0$ such that to every real number $\mu > 0$ there corresponds a real number T for which $|X_{t_0} - X_e| < \delta$ implies that $|X_t - X_e| < \mu$ for all $t \geq t_0 + T$.
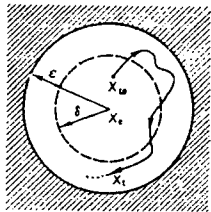
These definitions are illustrated diagrammatically in Figs. 3 and 4 respectively.

Fig. 3—Definition of stability
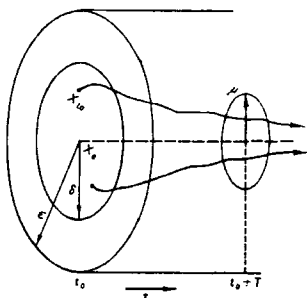
Fig. 4—Definition of asymptotic stability

For linear systems definition 2 for asymptotic stability matches the usual definition of stability. The following example further illustrates the definitions.

Example.—(a) Consider first a harmonic oscillator described by the linear differential equation:

$$\ddot{x}_1 + x_1 = 0,$$

or in equivalent form:

$$\dot{x}_1 = x_2$$
$$\dot{x}_2 = -x_1$$

Nomenclature:
$a_1, \ldots a_n$—Constant coefficient.
$C_1, \ldots C_n$—Constant coefficient.
 C—System controlled output.
 E—Input signal magnitude.
 G—Feedforward transfer function.
 H—Feedback transfer function.
 K—System gain constant.
 M—Closed loop magnification ratio.
 M_p—Peak closed loop magnification ratio.
 N—Closed loop phase angle.
 N—Describing function.
$p_1, \ldots p_n$—Open loop poles.
$P_1, \ldots P_n$—Roots of closed loop system.
 R—Reference signal input.
 s—Laplace transform operator.
 V—Lyapunov function.
 W—dV/dt.
 x_t—State variable.
 X_e—Equilibrium state.
X_t, X_{t_0}—State at time t, t_0.
$z_1, \ldots z_n$—Zeros of closed loop system.
 δ—Constant value.
 ϵ—Constant value.
$\xi = \cos \phi$—Damping factor.
 ω—Frequency.
 ω_n—Natural frequency.
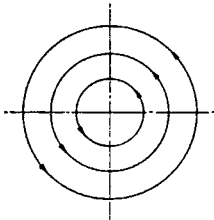 ω_r—Resonance frequency.

Fig. 5—Stable system

The solutions, or trajectories, in the state-plane are concentric circles about the origin (Fig. 5) i.e. the paths are:

$$x_1^2 + x_2^2 = \epsilon$$

If one takes $\delta = \epsilon$ then any circle through a point in the region δ_r remains in δ_r, and hence in the region ϵ_r, and so stability exists. However, since the paths do not tend toward the origin the system is not asymptotically stable.

(*b*) Consider now a system:

$$\dot{x}_1 = -x_1; \quad \dot{x}_2 = -x_2$$

The solution is $x_1 = Ae^{-t}$, $x_2 = Be^{-t}$. The paths are $x_2/x_1 = B/A =$ constant, or rays through the origin (Fig. 6). If one takes $\delta = \epsilon$, any path from a point in the region ϵ_r
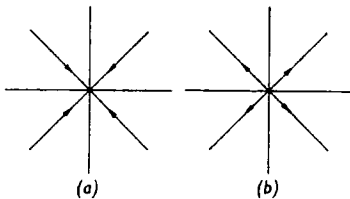

Fig. 6—*(a)* Asymptotically stable system. *(b)* Unstable system

remains in the region, and tends toward the origin. Hence there is asymptotic stability. In fact asymptotic stability exists "globally"— every solution tends toward the origin.

(*c*) Finally consider the system:

$$\dot{x}_1 = x_1; \quad \dot{x}_2 = x_2$$

The solution is $x_1 = Ae^t$, $x_2 = Be^t$. The paths are again $x_2/x_1 =$ constant, rays through the origin, but the path direction is reversed (Fig. 5). Given ϵ, no matter how small a value of δ is chosen the path from any point in the region δ_r crosses the spherical boundary at ϵ, and so instability exists.

Additional terminology exists[1, 2] and the concepts which are in most general use are defined below:

(1) If a control system response satisfies stability definition 1 in the entire state space, it is said to be "globally stable".

(2) If the stability conditions are satisfied in some limited region of the state space, the system is said to be "locally stable".

(3) If asymptotic stability conditions are satisfied in the entire state space the system is "globally asymptotically stable".

(4) If asymptotic stability exists in some limited region about the equilibrium point the system is "locally asymptotically stable".

(5) If the system exhibits stability under every bounded continuously acting disturbing function it is referred to as "totally stable".

These definitions define stability as a property of the system which does not depend upon the type of system excitation, and they

are applicable to all continuous time-invariant linear and non-linear systems.

4. METHODS OF STABILITY ANALYSIS FOR LINEAR SYSTEMS

4.1 SOLUTION OF DIFFERENTIAL EQUATIONS

When a block diagram has been produced for a given physical system, the transfer function obtained for each block, the overall transfer function can be calculated. This is the differential equation governing the operation of the system written in Laplace transform notation. The overall transfer function for the general feedback system shown in Fig. 11 is

$$\frac{C(s)}{R(s)} = \frac{G(s)}{1 + G(s)H(s)}$$

The characteristic equation of the system is the equation obtained by setting the denominator of the transfer function equal to zero, and in this case is

$$1 + G(s)H(s) = 0$$

This is the equation which determines the system stability and most methods of stability analysis investigate this equation.

The time response of the system to any given input change or disturbance can be obtained by solution of the system differential equation, i.e. by obtaining the Laplace inverse of the output signal, or by resolving into the sum of a set of 1st order differential equations. The solution generally consists of two parts:

(1) The transient solution (complementary function).

(2) The steady state solution (particular integral).

In a servomechanism, for example, the steady state response when compared with the reference input signal gives an indication of the system accuracy i.e. the steady state error. Also, because of inertia and friction there will be transient errors. The transient solution gives information about the magnitude, duration, &c., of these transient errors.

In general the complementary function has the form

$$\sum_1^n C_n e^{P_n t}$$

where $P_1, P_2 \ldots P_n$ are the roots of the characteristic equation. For each of the transient terms $C_n e^{P_n t}$ to vanish with increasing time the real part of all the roots must be negative. This is a necessary mathematical condition for stability.

Solution of the differential equation by the classical methods, if possible at all, is long and tedious for all but the simplest systems. A more serious disadvantage is that the effect on system performance of additions to the system cannot readily be studied. Hence the usefulness of complete solution of differential equations for system analysis is rather limited, and various techniques have been developed to indicate the form of the solution.

4.2 ROUTH–HURWITZ CRITERION

A technique which gives information on system stability in the binary sense (i.e. stable or unstable) has resulted from work by Routh and Hurwitz. For any system with linear or linearized differential equations the characteristic equation can be obtained in the form:

$$A_n s^n + A_{n-1} s^{n-1} + A_{n-2} s^{n-2}$$
$$+ \ldots + A_2 s^2 + A_1 s + A_0 = 0$$

Routh showed that if any of the coefficients of this equation other than A_n is equal to

zero, or if all are not of the same sign then the system is unstable. The requirement that all terms of this polynominal should be present and of the same sign is a necessary but not sufficient condition of stability. A development by Hurwitz showed a sufficient condition which must be satisfied by the coefficients of the characteristic equation to ensure system stability. This method entails arranging the coefficients of the characteristic equation in the following array:

$$
\begin{array}{cccc}
s^n & A_n & A_{n-2} & A_{n-4} \\
s^{n-1} & A_{n-1} & A_{n-3} & A_{n-5} \\
s^{n-2} & b_1 & b_2 & b_3 \\
s^{n-3} & c_1 & c_2 & c_3 \\
-- & -- & -- & -- \\
-- & -- & -- & -- \\
s^1 & g_1 & g_2 & 0 \\
s^0 & h & 0 &
\end{array}
$$

Where additional terms are calculated thus:

$$b_1 = \frac{A_{n-2} A_{n-1} - A_n A_{n-3}}{A_{n-1}}$$

$$b_2 = \frac{A_{n-4} A_{n-1} - A_n A_{n-5}}{A_{n-1}}$$

$$c_1 = \frac{A_{n-3} b_1 - A_{n-1} b_2}{b_1}$$

&c., and the process is continued until only zeros exist in all successive rows. Having constructed the array the characteristic equation and hence the system can be seen to be stable or unstable from inspection of the first column of coefficients. Each change in sign of an element in the first column indicates the existence of a root in the right-hand half of the s-plane, and hence system total instability.

The appearance of a zero in the first column, or a row of zeros, each of which prevents the completion of the array, necessitates the use of additional mathematical manipulations, and these are described in References 3 and 4.

4.3 FREQUENCY RESPONSE TECHNIQUES

Frequency response methods of analysis have been very widely used, chiefly because of their ease of application in the practical testing of systems, and of their essentially graphical nature. These methods of harmonic analysis study the response of a system, with the feedback loop opened, to an input signal of sinusoidal form. For a linear or linearized system after the initial transients have died out the output will be sinusoidal, and of the same frequency as the input. There will, however, be a phase difference and a change in amplitude between the two signals, and these will be functions of the forcing frequency.

The results obtained either experimentally or analytically for these parameters can be plotted in a variety of ways. The main and most useful ones are:

(a) *Nyquist Diagram.*—This is a polar plot in the complex plane of the opened loop transfer function $G(j\omega)$ $H(j\omega)$ for values of frequency from zero to infinity. The proximity of this locus to the $-1+j0$ point gives an indication of the relative stability of the system.

(b) *Bode Diagram.*—This consists of the same information plotted on two separate graphs, of magnitude (in decibels) and phase angle respectively plotted against the logarithm to base 10 of the frequency. A big advantage of this diagram is the ease by which the magnitude curve can be plotted by the use of a straight line construction. The effects of the addition of system elements can be readily evaluated by adding the contribution of the magnitude and phase curves of the additional units to those of the original system.

(c) *Nichols Chart.*—If magnitude is plotted

against phase the two curves of Bode reduce to a single plot known as a Nichols chart. Superimposed on this diagram are lines of constant closed loop magnification (M contours) and constant closed loop phase angle (N contours) which enable the closed loop parameters to be readily obtained.

4.3.1 *Harmonic Design Criteria.*—The harmonic parameters of importance in the design of control systems are phase margin, gain margin, resonance frequency ω_p, maximum amplitude ratio M_p, and bandwidth. These are illustrated diagrammatically in Fig. 7. For any given system the values are
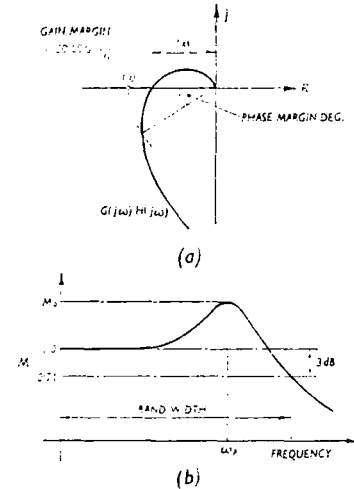

(a)

(b)

Fig. 7—Harmonic design criteria

obtained from one or more of the above plots. The range of acceptable values for these parameters is based on experience gained from similar systems used previously. Typical values, say for an engine governor system[5], are:

M_p	$1 \cdot 1 - 1 \cdot 4$
ω_p	$1 \cdot 1 - 1 \cdot 6$ c/s
Phase margin	$40° - 50°$
Gain margin	$6 - 10$ dB
Bandwidth	$1 \cdot 1 - 1 \cdot 5$ c/s

and these would result in a system with the following transient response characteristics:

Rise time	$0 \cdot 3$ s maximum
Settling time	$2 \cdot 0$ s maximum
Initial overshoot	$25 °_0$ maximum
Number of oscillations	$1\frac{1}{2}$ maximum

4.4 ROOT LOCUS METHOD

The transient response of any system to a disturbance or to a change in input was shown in section 4.1 to consist of the sum of a series of terms of the form $C_n e^{P_n t}$.
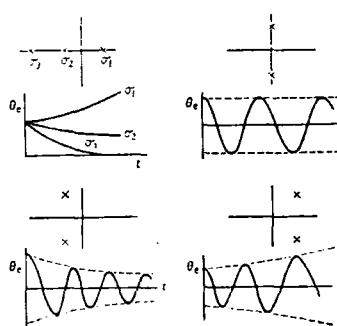

Fig. 8—Effect of root position

The contribution from each term depends on the position in the complex plane of the root P_n of the characteristic equation. For stability all roots must lie in the left half of the complex plane plot, and the farther from the imaginary axis that the roots lie the quicker the transient components decay. Conversely, if any real root is positive its corresponding exponential term will increase, and if any pair of complex conjugate roots has positive real parts a sinusoidal oscillation with increasing amplitude will result; in each case the system would be unstable. The form of the response for roots in these different areas is shown in Fig. 8.

In addition to the requirement of total stability it is generally essential that transients die out fairly quickly, hence certain portions of the left half plane should be avoided. Roots located in region A, Fig. 9,
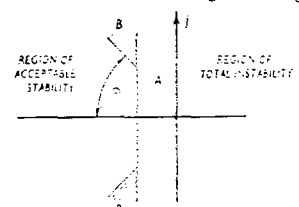

Fig. 9—Region of acceptable stability

are very close to the imaginary axis and would have an exponential decay which is too slow. Roots in region B, lying outside an included angle of 2ϕ would have a response which is too oscillatory due to the low value of damping factor $\xi = \cos \phi$. The angle enclosing the region of acceptable stability can be somewhat wider when dealing with systems where step changes are not physically possible, and the resulting overshoots would still be reasonable.

The root locus method, devised by W. R. Evans[6,7,8], is a graphical technique for determining the position of the roots of the characteristic equation of a linear system as a function of system gain. It can be used to obtain a complete and accurate solution for the response of the system to any given input change or disturbance, but it is more useful for obtaining quickly the form of the solution, as this entails less computational effort, and often suffices. It also affords greater understanding of system behaviour, and enables the effect of system changes to be seen readily, and hence is a useful aid in system design. The root locus method appears to be employed to an ever increasing extent, and is felt to be a powerful and useful tool for system analysis and synthesis.

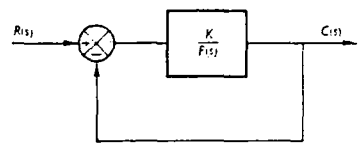Consider the simple unity feedback system shown in Fig. 10, where $P(s)$ is a polynominal

Fig. 10—Generalized block diagram

in s and K is the system gain constant. The characteristic equation is $P(s) + K = 0$, and the values of the roots depend on the value of K. A plot of the roots as K varies from 0 to ∞ is the root locus plot, and it is easy to select the value of K required to give the roots with the most suitable location.

The transfer functions of the elements in a block diagram are generally known in factored form and hence the open loop poles

Technical Contributors Section (Continued)

and zeros are directly obtainable. Each locus starts, $K=0$, at an open loop pole and terminates, $K=\infty$, at an open loop zero or moves to infinity along an asymptote. The number of loci is the same as the order of the characteristic equation, and the loci are always symmetrical with respect to the real axis because complex roots always occur in conjugate pairs for linear rational functions.
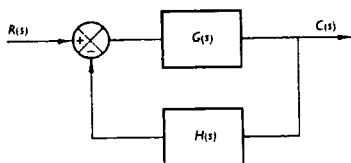

Fig. 11—Generalized block diagram with feedback

Consider now the system with elements in the feedback loop, shown in Fig. 11. The characteristic equation is:

$$1 + G(s)H(s) = 0$$

or

$$G(s)H(s) = -1 = 1/\pm N\pi \qquad . \quad (1)$$

where $G(s)$ $H(s)$ has the form

$$\frac{K(s+z_1)(s+z_2)\ldots(s+z_m)}{(s+p_1)(s+p_2)\ldots(s+p_n)}$$

and

$$N = 1, 3, 5, \ldots$$

To satisfy equation (1) two conditions are necessary: the "magnitude condition"

$$|G(s)H(s)| = 1 \qquad . \quad . \quad (2)$$

and the "angle condition"

$$\underline{/G(s)H(s)} = \pm N\pi$$

$$= \pi \pm 2k\pi \qquad . \quad . \quad (3)$$

where

$$k = 0, 1, 2, 3, \ldots$$

The angle condition is used to obtain points on the loci, and then the magnitude condition determines the values of K along the loci. There are many rules which simplify the plotting of the loci and which considerably narrow the search for points which satisfy the angle condition and hence lie on the loci.

4.4.1 Rules to Aid Construction of Root Loci.

(1) Number of separate loci: equals order of characteristic equation.

(2) Origin: the root loci start at the n poles of $G(s)$ $H(s)$.

(3) Terminus: the root loci end at the m zeros of $G(s)$ $H(s)$. When the order n of the denominator is greater than that m of the numerator (as is usually the case in practice) the remaining $n-m$ loci end at infinity.

(4) Symmetry: the root loci are symmetrical with respect to the real axis.

(5) Loci on real axis: portions of the real axis are sections of root locus if the number of poles and zeros to the right is odd.

(6) Angles of asymptotes: for large values of K the root loci are asymptotic to straight lines with angles given by

$$\frac{(2k+1)\pi}{n-m},$$

where

$$k = 0, 1, 2 \ldots.$$

(7) Intersection of asymptotes on real axis: this is at the point given by

$$\frac{\Sigma \text{ poles} - \Sigma \text{ zeros}}{n-m}$$

(8) Breakaway from real axis or break in point: (a) consider a point a very small distance from the real axis, obtain an algebraic equation by the angle condition, and solve to obtain the required point; or (b) solve for $dk/ds=0$.

(9) Intersection with imaginary axis: this is obtained by use of the Routh–Hurwitz criterion.

(10) Angle of departure from complex pole: this is obtained by applying the angle condition to a point very close to the pole (this also applies to arrival at complex zeros).

After the root loci have been sketched with the aid of the above rules the exact locations of certain intermediate points can be determined by the angle condition, equation (3), and the loci drawn to the desired graphical accuracy. This stage of the construction can be shortened by the use of a "Spirule"[3], which amongst other functions serves as an angle summer. Finally, values of K can be put on the loci by use of the magnitude condition, equation (2), and here again the Spirule can provide some useful assistance.

4.4.2 Use of the Root Locus Plot.—For any given system the roots can be found from the locus plot by finding the points with the appropriate value of K. The pair of complex conjugate roots nearest to the origin, provided all others are considerably farther away, are the dominant roots and will determine the damping factor ξ and natural frequency ω_n of the equivalent second order system. If there is a real root near to the origin this will give rise to a sluggish system.

For small values of K the closed loop response is nearly the same as that of the open loop system. As the loop gain increases certain of the natural modes become less important, but if the rank $(n-m)$ of the system is three or more at least two loci cross the imaginary axis. Study of the plot will show whether a change in K alone could provide an improvement in performance, and what value would be suitable. If no suitable K can be found then compensation must be provided. This consists of adding poles and zeros representing added components in an attempt to pull the locus to the left, so that the dominant poles do not reach the imaginary axis until very much higher values of K are reached. Zeros have the desired effect, but cannot be introduced without the addition of at least the same number of poles. Since these tend to decrease stability they must be placed where they do the least harm.

If required, the values of the roots found above can be used to find the Laplace inverse, and hence the time response of the system to any given input. Roots located more than, say, five times the distance of the predominant poles can safely be neglected as their contribution is very small—and this eases calculation considerably. Transient response curves can be obtained directly by simulating the system on an analogue computer, and an approximately constructed root locus plot is then a great aid to understanding of the system.

4.4.3 Root Contour Plots[4].—If it is desired to study the effect of more than one variable this can be done by constructing a set of root contours. Root loci are drawn for one variable, and for any given value of this variable the roots will be the poles of

further sets of root loci for the second variable.

4.5 LYAPUNOV METHOD

4.5.1 Introduction to the Lyapunov Method.—The "direct method" or "second method" of Lyapunov is a general method which can be used to determine the stability of sets of ordinary autonomous differential equations without actually solving the differential equations. The technique is more accurately described as a point of view, or philosophy of approach, rather than a systematic method. The physical reasoning is that if the rate of change of the energy of an isolated system is negative for every possible state, except for a single equilibrium state, then the energy will continually decrease until it finally assumes its minimum value. It is generally not possible to specify the energy content of a system when the equations of motion are given in purely mathematical terms.

For this case a very important role is played by a scalar function $V(x)$ said to be positive-definite with the following properties:

(a) $V(x)$ is continuous and has continuous first partial derivatives;

(b) $V(x) > 0$ for $x \neq x_e$ i.e. is positive-definite;

(c) $V(x) < 0$ for $x \neq x_e$ i.e. is negative-definite; and

(d) $V(x) = \dot{V}(x) = 0$ when $x = x_e$.

Such a function is called a "Lyapunov function" and a dynamic system is stable if and only if such a function exists. Failure to discover a function to satisfy these conditions yields no information about the system stability or instability. The finding of a suitable Lyapunov function is usually the most difficult part of the analysis.

Although in the above V was specified to be positive-definite and $\dot{V}$ was required to be negative-definite, V can be specified to be negative in which case $\dot{V}$ must be positive-definite. The only restriction is that V and $\dot{V}$ must be of opposite signs, although it has become conventional in the literature to specify V as a positive-definite function.

4.5.2 Application of the Lyapunov Method.—In the absence of input excitation any time-invariant physical system can be described mathematically by a set of simultaneous first-order differential equations, written symbolically as:

$$\frac{dx_1}{dt} = X_i(x_1, x_2, \ldots, x_n) \quad i = 1, 2 \ldots, n \quad (4)$$

It is assumed that the right-hand sides X_i of these equations reduce to zero for $x_1 = x_2 = \ldots = x_n = 0$, and are continuously differentiable functions of the variables $x_1, x_2 \ldots x_n$ within a certain region Ω containing the origin. This can be the whole space $-\infty < x_i < +\infty$, $i = 1, 2, \ldots n$. If the totalities $(x_1, x_2 \ldots x_n)$ and $(X_1, X_2 \ldots X_n)$ are denoted by x and X respectively, each being a row matrix, then the system of Equations (4) takes the vectorial form

$$\dot{x} = X(x) \qquad \ldots \quad (5)$$

This is a considerable assumption, but assumptions must be made in order to bring the system within the range of reasonable mathematics.

One of the simplest functions $V(x)$ that may serve as a Lyapunov function for an autonomous system, and which is

mathematically understood is the generalized quadratic form

$$V(x_1, x_2, \ldots, x_n) = \sum_{i=1}^{n} \sum_{j=1}^{n} a_{ij} X_i X_j, \ (a_{ij} = a_{ji}) \quad (6)$$

Its positive-definiteness is tested using Sylvester's theorem:

Theorem of Sylvester.—A set of necessary and sufficient conditions for the quadratic form (equation (6)) to be positive definite is that all the principal minors of the matrix

$$\begin{pmatrix} a_{11} & \cdots & a_{1n} \\ \cdot & & \\ \cdot & & \\ a_{n1} & \cdots & a_{nn} \end{pmatrix}$$

should be positive; i.e.

$$a_{11} > 0, \quad \begin{vmatrix} a_{11} & a_{12} \\ a_{21} & a_{22} \end{vmatrix} > 0, \quad \begin{vmatrix} a_{11} & a_{12} & a_{13} \\ a_{21} & a_{22} & a_{23} \\ a_{31} & a_{32} & a_{33} \end{vmatrix} > 0 \ \&c.$$

4.5.3 *Existence of Quadratic Form for the Lyapunov Function.*—The quadratic form for the Lyapunov function is mathematically the most convenient to use. If (*a*) a system can be represented by a set of differential equations of the form

$$\dot{x} = AX + F(t, x)$$

in which *A* is a $(n \times n)$ matrix whose coefficients are continuous bounded functions of *t*, and where *F* is some vector function of *t* and *x*, and (*b*) there exists a positive definite function $V(x)$ such that $W = \dot{V}(x)$ is negative definite, then there also exists a $V(x)$ function with the same properties which is a quadratic form in the state variables $x_1, x_2, \ldots, x_n$.

5. NON-LINEAR SYSTEMS

The analysis and design techniques in section 4 have been described for linear systems. All practical systems, however, are non-linear to some extent. Most physical systems can be linearized for a limited range of operation, and linear analysis can then be used to determine approximately the system behaviour.

Where non-linearities are severe, such as when considerable hysteresis is present or when components are driven into regions of non-linear characteristics, a completely erroneous prediction of system performance can result from indescriminate use of linear theory. In such cases it becomes necessary to use modified techniques of analysis. There is no general method of solution for a non-linear differential equation.

5.1 THE DESCRIBING FUNCTION

When a system containing a non-linear element is subjected to a sinusoidal input forcing function the output in general will be a periodic function, and can therefore be represented by a Fourier series. The output will contain the fundamental and harmonic frequencies, but the harmonic components in the output of most practical systems are of smaller amplitude than that of the fundamental. The physical system acts as a low-pass filter and attenuates the higher harmonics. The describing function technique is based on the assumption that the harmonic response of a non-linear element can be adequately described by the fundamental component for systems of any order.

A non-linear element can then be represented by an equivalent transfer function, defined as the ratio of the amplitude of the fundamental component of the output from Fourier analysis to the amplitude of the sinusoidal input signal. This is called the describing function.

The stability of the characteristic equation including the describing function can then be determined by application of the Routh-Hurwitz criterion.

5.2 HARMONIC ANALYSIS METHODS

The application of Nyquist and hence Nichols plots to the design of non-linear systems is possible by introducing the describing function into the mathematical system. The stability of the closed loop non-linear system is dependent on the roots of the characteristic equation which now has the form:

$$1 - \bar{N}(E, \omega) G(s) = 0 \quad \ldots \quad (7)$$

where $G(s)$ is the transfer function for the linear part of the system and $\bar{N}(E, \omega)$ is the describing function which is a function of input amplitude *E* and frequency ω.

Using a Nyquist diagram the system stability can be investigated by plotting the $G(s)$ locus and the $-1/\bar{N}$ locus in the same plane. The $-1/\bar{N}$ plot can be considered to be the locus of the critical point, which in linear theory is the $(-1 + j0)$ point of the complex *G* plane. When $\bar{N}$ is a function of both *E* and ω a family of loci, each for a constant value of ω must be constructed with *E* as the variable parameter.

When the critical points of $-1/\bar{N}$ lie to the left of the $G(s)$ locus then the closed loop system will be asympototically stable, whereas if they are enclosed by the locus totally unstable operation will result. Intersection of the $G(s)$ and $-1/\bar{N}$ loci corresponds to the possibility of periodic oscillations (i.e. a system which is mathematically stable, but not asymptotically stable) characterized by the value of *E* on the $-1/\bar{N}$ locus and the value of ω on the $G(s)$ locus (Fig. 12).

The values of M_p, ω_p &c. determined from the Nyquist or Nichols diagrams for fixed values of *N* do not have the same meaning as in the linear case. M_p for the non-linear system is the maximum value of the closed loop frequency response, but for varying system input amplitudes a range of values of M_p, ω_p &c. will result. The values obtained do, however, still give some indication of the relative stability of the system[10].

5.3 ROOT LOCUS PLOT

Using the above characteristic equation (equation (7)) a root locus plot can be constructed in the normal way. If the describing function is a function of amplitude only then roots can be indicated on this plot for various values of the describing function for the quasi-linear system. A study of the plot will show which roots are dominant, and how the equivalent system damping and natural frequency change with variation in the value of the describing function. If the describing function is, in addition, frequency dependent then a separate root locus plot is necessary for each value of amplitude. The labour involved in constructing these loci makes the method very lengthy. The more common types of non-linearity encountered in practice are primarily amplitude dependent, so a single plot generally suffices.

5.4 LYAPUNOV DIRECT METHOD

Lyapunov's direct method is directly applicable to non-linear systems. The major difficulty of the method again lies in the selection or generation of a scalar function which satisfies the necessary conditions. A number of fairly procedurized analytical techniques are now available for finding Lyapunov functions[11], but each applies only for certain applications.

6. APPLICATION OF STABILITY CRITERIA TO PRACTICAL SYSTEMS

To illustrate the procedures described briefly in sections 4 and 5, and to provide a

basis for comparison, the main methods are applied in this section to a practical linear system, and then to the same system when a non-linearity is present.

The system considered is a hypothetical simplified governed engine system with (*a*) a linear proportional governor and (*b*) a governor with variable spring rate. It is assumed that the system can be represented by the block diagrams of Figs. 1 and 2. It is required to find the range of governor characteristics which will give asymptotic stability.

6.1 LINEAR SYSTEM (Fig. 1)

(*a*) *Routh–Hurwitz Criterion.*—The characteristic equation is

$$s^3 + 3s^2 + 2s - K = 0 \quad \ldots \quad (8)$$

The necessary condition for stability that all coefficients are present and of the same sign is satisfied, provided $K > 0$. The sufficient condition can now be obtained from the Hurwitz array:

$$\begin{array}{cc} s^3 & 1 & 2 \\ s^2 & 3 & K \\ s^1 & 2 - K/3 & 0 \\ s^0 & K \end{array}$$

Hence $0 < K < 6$ for asymptotic stability. Solution of the auxiliary equation will yield the natural frequency of oscillation for $K = 6$.

i.e. $3s^2 + 6 = 0$

∴ $3(j\omega)^2 + 6 = 0$

i.e. $\omega = \sqrt{2}$ rad/sec.

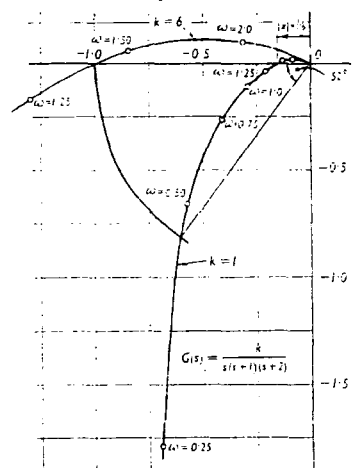For $K = 1$ the system is asymptotically stable, but the criterion gives no indication of how stable the system is.

Fig. 12—Nyquist diagram

(*b*) *Nyquist Diagram (Fig. 12)*—The opened loop system transfer function is

$$\frac{C(s)}{R(s)} = \frac{K}{s(s+1)(s+2)} = \frac{K}{s(s^2 + 3s + 2)} \quad (9)$$

The modulus of this is

$$M = \frac{C(j\omega)}{R(j\omega)} = \frac{K}{\omega\sqrt{(2 - \omega^2)^2 + 9\omega^2}}$$

and the phase lag is

$$\phi = -90° - \tan^{-1}\left(\frac{3\omega}{2 - \omega^2}\right)$$

The polar plot of *M* and ϕ for a value of $K = 1$ is shown in Fig. 12. For asymptotic stability the gain margin $20 \log_{10} 1/|x|$ must be greater than zero. Hence $|x| < 1$, and scaling the diagram, or calculating $|x|$ gives $K < 6$. Also, for $K = 1$ measuring the diagram the phase margin is found to be 52°,

and the gain margin is $20 \log_{10} 6 = 15 \cdot 6$ dB.

(*c*) *Bode and Nichols Diagrams (Figs.* 13 *and* 14).— (i) Modulus curve: for the straight line construction it can be seen that corner frequencies are $\omega = 1$ and $\omega = 2$ rad/sec. The slopes of the lines are

    20 dB/decade for $\omega < 1$

    40 dB/decade for $1 < \omega < 2$

and

    60 dB/decade for $\omega > 2$

For

$$\omega = 0 \cdot 1$$

$$M = \frac{1}{\cdot 1 \sqrt{1 \cdot 99^2 + \cdot 09}} = 4 \cdot 97.$$

i.e. straight line passes through $20 \log_{10} 4 \cdot 97 = 14$ dB point. By summation of the correction for each corner the true curve is obtained as shown in Fig. 13. This curve can also be obtained from points taken from the Nyquist diagram.

(ii) Phase curve: This is obtained by summation of the phase curves for all three components, and is also shown in Fig. 13.

(iii) From the Bode curves the phase margin can be seen to be 52° and the gain margin 15·5 dB. Hence the gain can be increased to 6 before instability will occur.

(iv) When the curve is plotted on the Nichols chart (Fig. 14) the following information can be read off:

    $M_p = 1$ dB or $1 \cdot 12$

    $\omega_p = 0 \cdot 5$ rad/sec

    band width $= 0 \cdot 8$ rad/sec

These characteristics indicate that the response of the system is sluggish compared to the response expected from a high performance engine system.

(*d*) *Root Locus Diagram (Fig.* 15).— (i) There are three loci. starting at the poles $s = 0$, $s = -1$, $s = -2$ and all ending at ∞.

(ii) Loci on real axis lie between origin and $s = -1$, and to the left of $s = -2$.

(iii) Slope of asymptotes is

$$\frac{(2k+1) \pi}{3 - 0}$$

for $k = 0$, 1, 2. i.e. 60°, 180°, 300°.
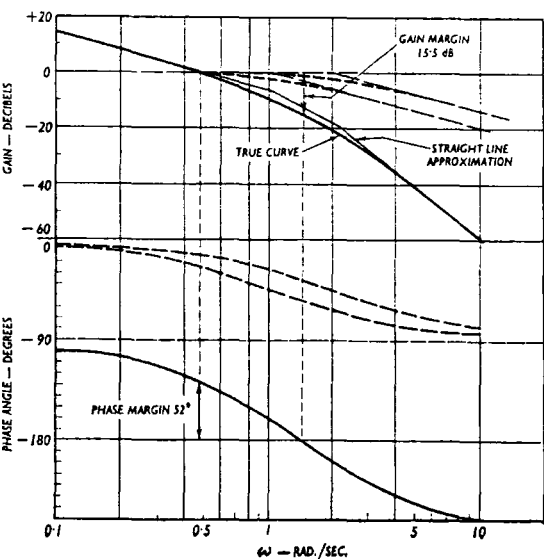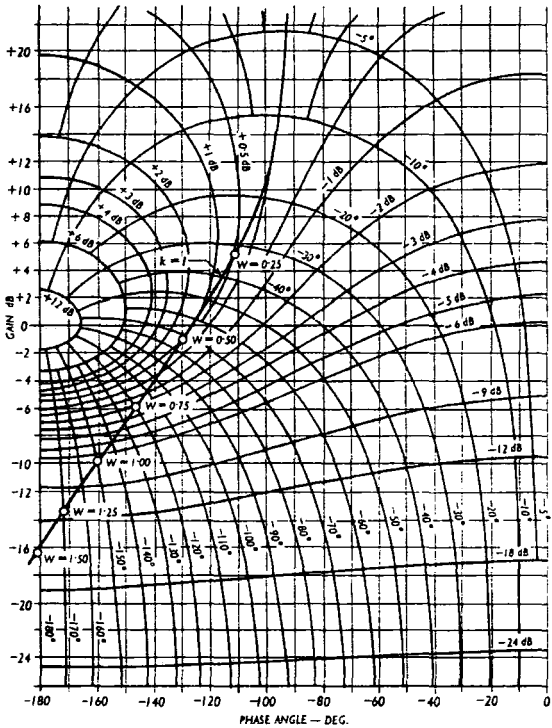
Fig. 14—Nichols chart

(iv) Asymptotes intersect real axis at

$$\frac{(0 - 1 - 2)}{3} = -1$$

(v) Loci cross imaginary axis, section 6.1 (*a*) at $K = 6$, $s = \pm \sqrt{2} j$.

(vi) Breakaway point

$$\frac{dK}{ds} = -3s^2 - 6s - 2 = 0$$

i.e.

$$s = 1 \cdot 58 \text{ or } -0 \cdot 42$$

By inspection. only the latter is relevant.

(vii) Root loci can now be drawn and values of K added.

From the root locus plot it can be seen that for $K = 1$ roots occur close to $-0 \cdot 36 \pm 0 \cdot 57j$, $-0 \cdot 36 - 0 \cdot 57j$. and $-2 \cdot 32$. Hence the system will exhibit characteristics similar to
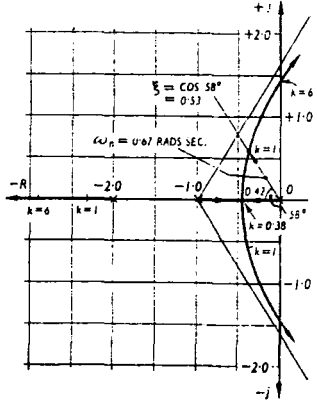
Fig. 13—Bode diagram

Fig. 15—Root locus diagram

a second order system with $\xi = 0 \cdot 53$ and $\omega_n = 0 \cdot 67$ rad/sec., but modified to a minor extent by the real root at $-2 \cdot 32$.

When the values of these roots are calculated accurately the transient response curve for a step input can be determined by obtaining the Laplace inverse of the output. The curve obtained is shown in Fig. 16, and it can be seen that the contribution of the root

at $-2\cdot32$ is very small, which would justify considering only the effect of the dominant roots.

(e) *Lyapunov's Method.*—The characteristic equation (equation (8)) i.e.

$$s^3 + 3s^2 + 2s + K = 0$$

can be written as the following set of 1st order linear differential equations:

$$\frac{dx_1}{dt} = x_2$$

$$\frac{dx_2}{dt} = x_3 - 3x_2$$

$$\frac{dx_3}{dt} = -Kx_1 - 2x_2$$

Let us assume a Lyapunov function as follows:

$$2V = a_{11}(x_1 + a_{12}x_2)^2 + a_{22}x_2^2 + a_{33}x_3^2 \quad . \quad (10)$$

where a_{11}, a_{12}, a_{22} and a_{33} are constants. This is a form of function which contains fewer terms than the generalized quadratic form, and is applicable to a large number of equations of the above type.

Then

$$W = \frac{dV}{dt} = a_{11}\,(x_1x_2 - a_{12}x_1x_3 - 3a_{12}x_1x_2$$
$$+ a_{12}x_2^2 + a_{12}^2x_2x_3 + 3a_{12}^2x_2^2) + a_{22}x_2x_3$$
$$- a_{22}3x_2^2 - a_{33}Kx_1x_3 - 2a_{33}x_2x_3$$

Collecting together the coefficients then coefficients of

x_1^2	are	0
x_2^2	are	$a_{11}a_{12} - a_{11}3a_{12}^2 - 3a_{22}$
x_3^2	are	0
x_1x_2	are	$a_{11} - 3a_{11}a_{12}$
x_1x_3	are	$a_{11}a_{12} - a_{33}K$
x_2x_3	are	$a_{11}a_{12}^2 + a_{22} - 2a_{33}$

To make the V function as simple as possible put the coefficients of x_1x_2, x_1x_3 and x_2x_3 equal to zero. Hence

$$a_{12} = 1/3$$

$$a_{11} = 3a_{33}K$$

$$a_{22} = 2a_{33} - \frac{a_{11}}{9}$$

Let $a_{33} = 1$ arbitrarily, then $a_{11} = 3K$ and $a_{22} = 2 - K/3$. Substituting these values in equation (10):

$$2V = 3K\left(x_1 + \frac{x_2}{3}\right)^2 + (2 - K/3)x_2^2 + x_3^2$$

If this is to be positive definite then

$$3K > 0 \text{ i.e. } K > 0$$

and

$$\left(2 - \frac{K}{3}\right) > 0 \text{ i.e. } K < 6$$

Also

$$W = x_2^2\,(a_{11}a_{12} - 3a_{11}a_{12}^2 - 3a_{22})$$
$$= x_2^2\,(K - K - 6 + K)$$
$$= -x_2^2\,(6 - K)$$
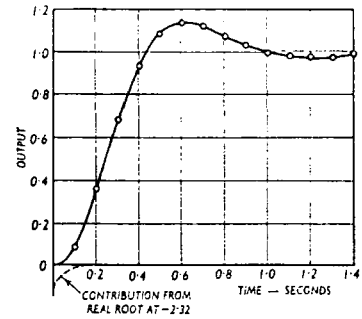
which is negative definite if $K < 6$.

Fig. 16—Transient response to unity step input

6.2 NON-LINEAR SYSTEM (Fig. 2)

Consider the case where the governor spring is no longer of constant rate but has a characteristic of the form $kx + bx^3$.

(a) *Describing Function.*—If the input to the governor is assumed to be sinusoidal, i.e. $E \sin \omega t$, then the governor output will be

$$f(x) = Ek \sin \omega t + E^3 b \sin^3 \omega t$$

$$= Ek \sin \omega t + \tfrac{3}{4} E^3 b \sin \omega t - \tfrac{1}{4} E^3 b \sin 3\omega t$$

The fundamental component is:

$$f(x) = (k + \tfrac{3}{4} E^2 b) E \sin \omega t$$

and hence the describing function is

$$\bar{N}(E) = k + \tfrac{3}{4} E^2 b \quad . \quad . \quad . \quad (11)$$

The stability of the closed loop non-linear system depends on the roots of the characteristic equation.

$$1 + \bar{N}(E)\,G(s) = 0$$

i.e.

$$1 + \frac{k + \tfrac{3}{4} E^2 b}{s(s-1)(s-2)} = 0$$

$$\therefore \quad s^3 + 3s^2 + 2s + (k + \tfrac{3}{4} E^2 b) = 0$$

From the Hurwitz array the condition for stability is found to be

$$k + \tfrac{3}{4} E^2 b < 6 \quad . \quad . \quad . \quad (12)$$
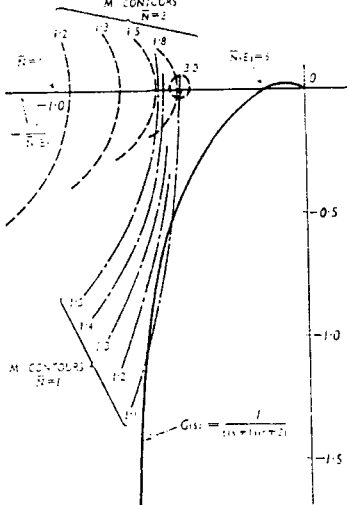
Shown in Fig. 17 is the polar plot of the

Fig. 17—Polar plot, non-linear system

open loop system, together with the negative inverse describing function. The curves can be seen to intersect for a value of $\bar{N}(E) = 6$. For very small values of b or E the describing function approximates to k as in the linear system. As error amplitude E increases, however, the describing function increases, and the M contours move([10]) to the left of the diagram. The value of the resonance peak therefore decreases and the system becomes more stable. The value of M_p determined in this way for any fixed value of E does not have the same meaning as in a linear system but does give some indication of relative system stability.

(b) *Lyapunov's Direct Method.*—The non-linear system shown in Fig. 2 can be represented by the following differential equations:

$$\left.\begin{array}{l}\dot{x}_1 = x_2 \\ \dot{x}_2 = x_3 - 3x_2 \\ \dot{x}_3 = -kx_1 - bx_1^3 - 2x_2\end{array}\right\} \quad . \quad . \quad (13)$$

Using a quadratic V function of the form

$$V(x) = a_{11}x_1^2 + a_{12}x_1x_2 + a_{22}x_2^2$$
$$+ a_{22}x_2x_3 + a_{33}x_3^2 + a_{13}x_1x_3 \quad . \quad . \quad (14)$$

differentiating with respect to time, and substituting from equation (13) gives:

$$W(x) = -ka_{13}x_1^2 - x_2^2\,(2a_{22} + 6a_{33} - a_{12}) + a_{23}x_3^2$$
$$- a_{13}bx_1^4 + x_1x_3\,(a_{12} - 2ka_{33} - 2ba_{33}x_1^2)$$
$$+ x_1x_2(2a_{11} - 3a_{12} - ka_{22} - ba_{23}x_1^2 - 2a_{13})$$
$$+ x_2x_3\,(2a_{22} - 4a_{33} - 3a_{23} + a_{13})$$

Constrain the W function to be negative definite of the form

$$W = -ka_{13}x_1^2 - ba_{13}x_1^4 \quad . \quad . \quad (15)$$

by setting the coefficients of the remaining terms to zero. Hence

$$\left.\begin{array}{l}a_{12} = 2a_{22} + 6a_{33} \\ a_{23} = 0 \\ a_{12} = 2ka_{33} - 2ba_{33}x_1^2 \\ 2a_{11} = 3a_{12} + ka_{22} + ba_{23}x_1^2 - 2a_{13} \\ 2a_{22} = 4a_{33} + 3a_{23} - a_{13}\end{array}\right\} \quad (16)$$

Solving equations (16) in terms of a_{13} gives:

$$a_{11} = \frac{12 + 7k + 7bx_1^2}{12 - 2k - 2bx_1^2}a_{13}$$

$$a_{22} = \frac{k + bx_1^2}{12 - 2k - 2bx_1^2}a_{13}$$

$$a_{33} = \frac{3}{12 - 2k - 2bx_1^2}a_{13}$$

$$a_{12} = \frac{6(k + bx_1^2)}{12 - 2k - 2bx_1^2}a_{13}$$

Application of Sylvester's theorem to the V function to establish the conditions for positive definiteness gives:

$$a_{11} > 0, \quad a_{22} > 0, \quad a_{33} > 0$$

i.e.

$$k + bx_1^2 < 6 \quad . \quad . \quad . \quad (17)$$

The remaining conditions found from Sylvester's theorem are not applicable to this problem.

7. DISCUSSION AND CONCLUSIONS

The control engineer is required to analyse and design a very wide range of physical systems, and there is no single specific procedure which will lead to a definite solution for all physical problems. The analysis of most systems can be undertaken by means of a generalized procedure which incorporates some or all of the above methods of analysis. The system must first be represented mathematically, the most suitable techniques then applied, and finally the results must be correctly analysed.

Analysis is usually carried out either in the time domain or in the frequency domain. Analysis in the time domain produces the transient and steady-state response of the system to any selected forcing function. The most common is a step function input, since this represents the most severe practical disturbance. The system should approach the steady state in the most rapid but least oscillatory way.

From frequency domain analysis harmonic response characteristics such as phase margin, gain margin, M_p &c., can be obtained, and these enable system performance to be predicted. Both analytically and experimentally harmonic techniques produce useful results more easily than time domain techniques.

7.1 *Routh–Hurwitz Criterion.*—For linear systems this technique provides a rapid means for determination of system stability, and for calculation of the resonance frequency, and hence it is useful in the preliminary design stages. Prediction of the complete dynamic system performance is however only possible by applicable of other techniques. For non-linear systems it is only possible to apply this technique where perturbations are sufficiently small to allow the non-linear elements to be linearized, or where the describing function concept has been used to reduce the non-linear element to an equivalent linear element.

Technical Contributors Section *(Continued)*

7.2 *Frequency Response Techniques.*—The popularity of frequency response techniques lies in the ease of their application. Empirical values have been established for phase margin, gain margin, M_p &c., which have been shown by experience to give satisfactory system performance. For experimental determination of system transfer functions harmonic response testing provides the most satisfactory data, but obtaining harmonic generators with suitable frequency range can prove to be an extremely difficult problem.

Of the three basic methods of plotting, Nichols charts present the information in a more generally usable form than Nyquist or Bode diagrams. Presented on this single diagram are the "opened" and "closed" loop harmonic data. The opened loop information is obtained from the co-ordinates of the plot, while the closed loop information is found from the M and N contours of the chart.

Nyquist diagrams are useful for presenting experimental results, from which Bode diagrams can be constructed. Application of the "straight line construction" to this diagram is a useful and generally easy way of estimating the time constants of a system. The design of any compensation networks which may be required to obtain improved dynamic performance is most usefully carried out by use of the Bode diagram.

It is possible to obtain a polar plot for a simple non-linear system which is analogous to the Nyquist diagram of the linear system, and to construct on it families of M contours

for different error signal magnitudes. This can give a useful guide to the type of system harmonic performance to be expected. However experience with this type of diagram would be necessary before system dynamic performance could be predicted with confidence.

7.3 *Root Locus Method.*—The main value of this graphical technique is that the roots of the characteristic equation for any value of system gain constant can be easily obtained, and hence the equation solutions for any given forcing function can be calculated.

The computational effort in obtaining the Laplace inverse can be reduced by inspection of the root locus diagram to determine which roots have the predominant effect. A further virtue is that approximate loci can be sketched very quickly, from which system damping and resonance frequency can be predicted. The technique is of limited value for system compensation since there is little guidance in the selection of the necessary additional roots to give a desired transient response.

7.4 *Lyapunov's Direct Method.*—At present the limitation of this method is the difficulty in finding a suitable Lyapunov function, and no generalized synthesis procedures have been developed which are suitable for all systems. For linear systems of the 4th order and above the solution of the equation matrices becomes lengthy and requires computer solution.

Inspection of section 6.1(e) shows that even for a simple system the computational effort required to obtain a limited amount of

information is considerable. No more information can be obtained for a linear system than by application of the Routh–Hurwitz criterion. Hence for linear systems unless a generalized computer programme becomes available to calculate performance indices and transient behaviour by the Lyapunov method there is little virtue in applying this method.

For non-linear systems Lyapunov's direct method enables regions of asymptotic stability to be predicted accurately, thus avoiding the approximations of the more well known methods. It is the only method applicable to all systems, and considerable effort is being directed towards the development of its application to the analysis of physical systems. It is thus becoming essential for the control engineer to have some knowledge of this method.

REFERENCES
[1] Kalman, R. E. and Bertram, J. E., "Control System Analysis and Design via the 'Second Method' of Lyapunov".
[2] Langill. A. W., *Automatic Control Systems Engineering*, Vol. II, Prentice Hall, 1965.
[3] Taylor, P. L., *Servomechanisms*, Longmans, 1960.
[4] Kuo. B. C., *Automatic Control Systems*, Prentice Hall, 1962
[5] Schwarzenbach, J. and Gill, K. F., "Analysis of a Gas Turbine Engine Fuel System", THE ENGINEER, Vol. 219, page 209, 1965.
[6] Evans. W. R., "Graphical Analysis of Control System" *Trans. A.I.E.E.*, Vol. 67, Part I, page 547, 1948.
[7] Evans. W. R., "Control System Synthesis by Root Locus Method", *Trans. A.I.E.E.*, Vol. 67, Part I, page 66, 1948.
[8] Evans. W. R., *Control System Dynamics*, McGraw Hill, 1954.
[9] Shinners, S. M., *Control System Design*, John Wiley & Sons, 1964.
[10] Gill, K. F. and Schwarzenbach, J., "A Theoretical Look at the Use of Functional Non-Linearities in a Gas Turbine Control System", *Control*. page 465, September 1966, page 531, October 1966.
[11] Leondes. C. T., *Modern Control Systems Theory*, McGraw Hill, 1965.
[12] Raven. F. H., *Automatic Control Engineering*, McGraw Hill, 1961.
[13] Chestnut. H. and Mayer. R. W., *Servomechanisms and Regulating System Design*, two vols, John Wiley & Sons.

PAPER 14

Pseudo-random signal testing applied to a Diesel engine

by **G. E. HARLAND,** B.Sc., **M. A. PAN'KO,** C.T.S., **K. F. GILL,** M.Sc., Ph.D. and **J. SCHWARZENBACH,** M.Sc.

A p.r.b.s. input has been applied to a proprietary laboratory Diesel engine to study the usefulness of the technique in determining the dynamic characteristics of the engine. Analogue evaluation of the values of the correlation function was unsuccessful because of apparent fluctuation of engine conditions while it was nominally at constant speed and load. Better results were obtained by off-line digital computation using experimental results of speed variation during one period of a p.r.b.s. signal. Scatter in the results masked any trend which might exist with changing bit interval or number of bits in the sequence. The results suggest that, in this case, there is no advantage in using sequences of more than 31-bit length, and that any test should be carried out at least three times

THE CLASSICAL TECHNIQUES of dynamic testing of systems using steps, impulses, and sinusoidal-input functions are usually unsatisfactory for on-line systems. In order to obtain usable signal-to-noise ratios, it is normally necessary to inject large-amplitude disturbing signals, although this is unacceptable for efficient plant operation and also makes the assumption of linear plant operation of doubtful validity. An alternative approach is to use stochastic forcing functions in conjunction with correlation techniques, a popular and easily injected disturbance signal being a pseudo-random binary sequence (p.r.b.s.).

It has been shown (e.g., _1, 2_) that the auto-correlation function of such a p.r.b.s. signal is a good approximation to a periodic impulse—if a sufficient number of bit intervals is contained within one period of the sequence. Using this sequence as a system forcing function, and correlating it with the system output, the complete impulsive response of the system is obtained provided that the periodic length of the sequence is arranged to be longer than the system settling time.

Several papers (e.g., _3, 4_) describing the use of p.r.b.s. disturbance signals applied to laboratory equipment have been published and these demonstrate that this technique has potential. The colloquium organized by the I.Mech.E. and the I.E.E. _(5)_ in January 1967, indicated that there was much interest in this type of testing, but that relatively few industrial applications had been reported. This paper presents the results of our investigation of the usefulness of this technique for measuring the dynamic characteristics of a proprietary 35 bhp 4-stroke Diesel engine.

Experimental methods

Generation of p.r.b.s. and delayed sequences

The settling time of the engine being about 2 s, it was necessary to introduce the binary sequence automatically. The sequence was obtained from a shift register, with the appropriate feedback loops _(6)_ constructed from a proprietary electronic teaching logic kit. The number, _n_, of binary elements in the shift register determines the maximum sequence length, which is $(2^n - 1)$ binary states. The clock pulse used for actuating the shift register was generated by a bistable oscillator, the period of which determined the bit interval of the sequence. Delayed versions of the sequence, when required, were generated by modulo-two addition of the outputs from the appropriate shift register elements _(6)_.

Engine system

The characteristic of interest was that of speed response to change in throttle position. Movement of the throttle changed the inlet-manifold pressure, this actuating a pneumatic piston directly coupled to the rack of the fuel-injection pump. Injection of the binary sequence was achieved by moving the throttle between fixed stops by a relay-controlled solenoid. The shift register was protected from overloading by an emitter-follower which, in turn, was protected by diode leaks across the relay points. Engine power was absorbed by a water dynamometer.

To achieve a good signal/noise ratio (4: 1) for a small throttle-movement (10% of throttle range), tests were carried out at a speed of 950 $\pm$ 50 rev/min and at a fixed load. To determine how the signal/noise ratio affects the quality of the results, the same throttle movement was applied to the engine at 1700 rev/min (almost maximum speed) for a further series of tests.

K. F. Gill served an apprenticeship with Richardsons, Westgarth, and received his technical education at West Hartlepool Technical College and Durham University. From 1955 to 1957, he was a control engineer with Bristol Siddeley Engines. In 1958, he was awarded M.Sc. in thermodynamics and related studies at Birmingham University. He then returned to Bristol Siddeley Engines and was later accepted for research at Birmingham University on non-steady gas flow in engine-exhaust systems. A Ph.D. followed in 1961. From 1961 to 1963, Gill was a senior scientific officer at the Admiralty Weapons Establishment, Portland. He is now a lecturer in control in the mechanical engineering department of Leeds University.

J. Schwarzenbach graduated from Glasgow University, in 1955, with first-class honours in mechanical engineering. He was awarded an exchange scholarship which enabled him to spend one year at Cornell University, U.S.A., and to obtain an M.Sc. upon the completion of a course in gas-turbine engineering. After a graduate apprenticeship with Rolls-Royce, he obtained experience as a designer, and later as a section leader, in the accessory design department of Rolls-Royce. In 1964, he became a lecturer at the University of Leeds, teaching various aspects of design, lubrication and control, and doing research on the optimizing control of internal-combustion power plants.

The signal/noise ratio at this speed is of the order of 1:1.

Correlation methods

To determine the impulse response, it is necessary to evaluate the cross-correlation function $\varphi_{oi} = \int_0^T \theta_o(t)$

$\theta_i(t - \tau)\ dt$. The mechanization of the solution to this equation can be simplified since the term $\theta_i(t)$ is a binary number; therefore the product term $\theta_o(t)$ $\theta_i(t - \tau)$ can be simplified to [sgn $\theta_i(t - \tau)$] $\theta_o(t)$. This enables a simple switch to be used in place of the complex operation of multiplication.

The parallel method of computation in which all values of $\varphi_{oi}(\tau)$ are calculated simultaneously on an analogue computer, is generally impracticable because of the large amount of analogue and logic equipment necessary. The serial approach in which each value of

Fig. 1 (a) Auto-correlation function of a p.r.b.s.

Fig. 1 (b) Effect of bit interval on impulse response

$\varphi_{oi}(\tau)$ is calculated separately, and requires a separate run of the sequence through the engine, requires long engine-running periods. A combination of these two methods, in which three values of $\varphi_{oi}(\tau)$ were calculated simultaneously, was used initially, thus reducing somewhat the number of test runs necessary to obtain the complete impulse-response curve.

The main series of tests was carried out by subjecting the engine to two input sequences, recording the changes in engine speed caused by the second sequence, and computing the cross-correlation function off-line on a digital computer.

Choice of p.r.b.s. parameters

The auto-correlation function of a p.r.b.s. signal is strictly a periodic triangular pulse, the base width of which is two bit-intervals, as shown in fig. 1. In an attempt to obtain some knowledge of the quantitative effect of bit interval on system response, a second-order simulated system was subjected to triangular shaped input signals of varying base length. The second-order system used had an undamped natural frequency of 3 rad/s and a damping factor of 0·5, which gives a time constant of 1·5 s for the envelope of the decaying sine wave, and this can be considered to be the major time-constant of the system.

Fig. 1 shows the theoretical impulse-response, together with system responses for triangular shaped input signals of different base lengths. For this second-order system a ratio of $\dfrac{\text{bit length}}{\text{major time-constant}} < \dfrac{1}{30}$ can be seen to give a close approximation to the true impulse response. For engine systems, the order of the characteristic equation is generally higher, but usually a pair of complex roots is dominant, and it would seem logical to assume that the above relationship remains valid. Hence sequences with bit lengths not greater than that defined by this ratio should give results which can be assumed to be the impulsive response of the system. Taking the settling time as 4 T this implies that a 127-bit sequence is required for a complete impulsive response.

Generation of impulsive response curve

Analogue approach

In an attempt to obtain the impulse response directly, during actual engine testing, within the capacity of
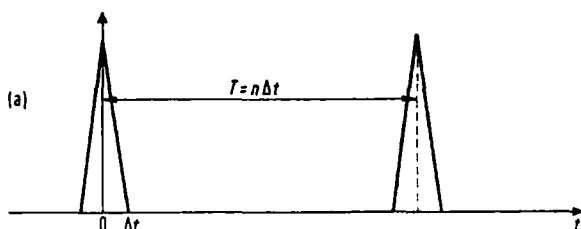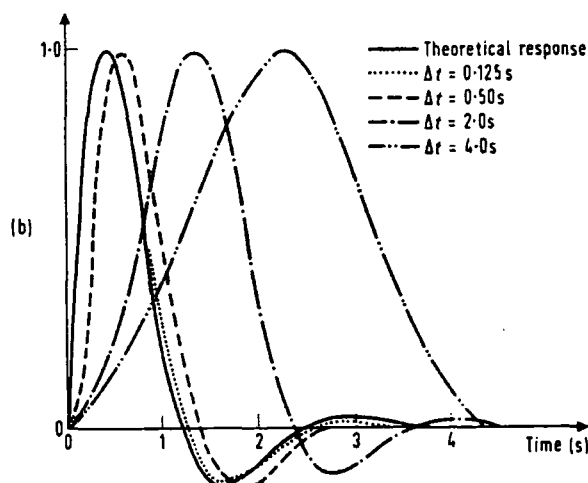
G. E. Harland is a lecturer in control engineering at the University of Leeds. He is engaged on research directed towards the design of an adaptive control system for a Diesel engine using model reference techniques. Prior to this he obtained a B.Sc. with honours in mechanical engineering at the University of Leeds.

M. A. Pan'ko was educated at the Moscow Power Institute and graduated in 1955, later pursuing a postgraduate course there, for which he received an award of Candidate of Technical Science in 1963. He is now a lecturer in the department of thermal measurement and control of the Moscow Power Institute, and in this capacity, spent a year as an Exchange Scholar in the mechanical engineering department of the University of Leeds.
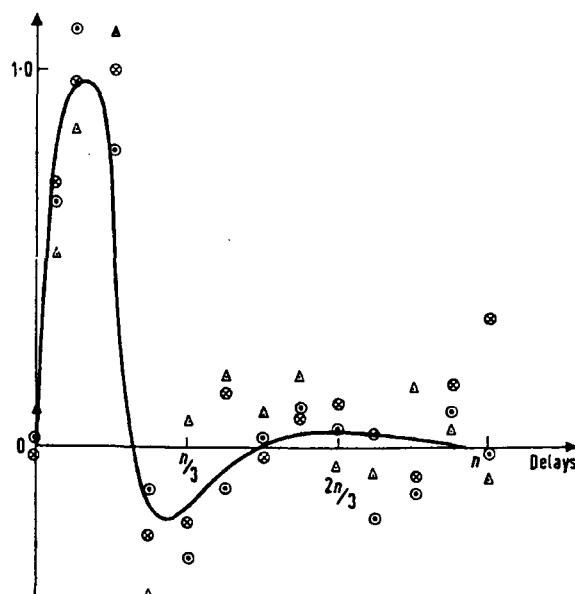
Fig. 2 Scatter at three nominally identical conditions— analogue approach
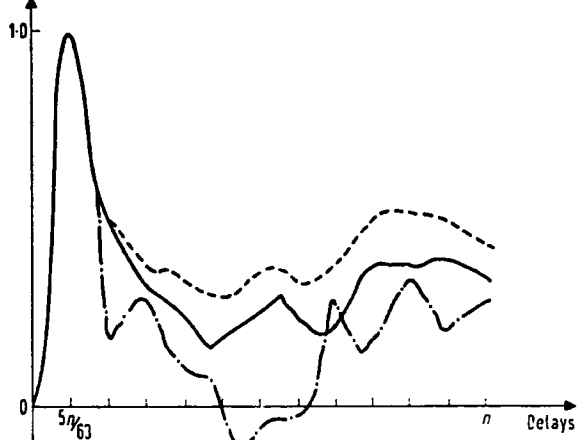
Fig. 3 Scatter at three nominally identical conditions—digital approach

equipment available, three points on the response graph were obtained for each pair of sequences injected. The first sequence gave the initial conditions necessary for the generation of the correlation function during the interval in which the second sequence is injected.

Occasional irregularity in the input sequence was noticed during the running and, to ensure consistency of results, each input sequence was recorded and checked against the true sequence. The logic elements were inspected carefully but no faults were found, and the malfunctioning of the sequence generator was eventually traced to a disturbance caused by switching of the thermostat controlling the computer oven temperature.

The scatter in readings for nominally identical conditions was quite unacceptable, as can be seen from fig. 2 which gives the results for constant engine conditions and a sequence of 63-bit length. The changing thermodynamic conditions occurring within the engine during the long periods of running necessary, were partially responsible for this scatter. It thus seemed unreasonable to accept an average curve from these points in order to derive the dynamic characteristics of the engine.

Digital approach

To eliminate the long-term variations in engine condition, analogue traces were taken for single sequences. The values measured from these traces were then used to compute the cross-correlation function for each test. The use of a digital computer makes this approach a realistic one where many tests are carried out, particularly where curve-fitting techniques are used to evaluate dynamic characteristics.

The amount of scatter was less—as can be seen from fig. 3 which shows three typical traces obtained under nominally identical conditions. There is close agreement for the first 1·25 s, but thereafter there is wide variation in the computed curves. This makes it unreasonable to attempt to fit more than a third-order transfer function to these, and it is known that one time-constant of 0·1 s is that of the filter used in the speed-monitoring circuit. It also suggests that as much useful information can be obtained from a 31-bit sequence as from the longer 63- or 127-bit sequences of the same bit interval.

Tables 1 to 3 show the range of tests carried out. Sequence lengths of 31, 63, and 127 bits, with bit-intervals ranging from 0·1 to 0·6 s, were applied to the engine while running at the two basic conditions described above.

Evaluation of dynamic characteristics from impulse-response curves

To provide a basis for comparison with theoretical impulse responses, all curves were scaled in magnitude

to make the peak values unity in all cases. During initial stages in curve-fitting all points on the impulse responses were used; the latter portion, where the value should be constant, showed a considerable amount of scatter. The values of the parameters calculated showed no change when this latter portion of the curve was neglected and, in order to save computer time, this procedure was adopted for the longer sequences.

A minimum error-squared criterion was used to achieve the best fit to each experimental curve. The computer procedure used initially was a standard library program called FLEPOMIN. This, however, generally failed to complete a search because of the effects of the compound exponential terms in the analytic equation, and all efforts to overcome this problem were unsuccessful. Instead a 'carpet' search procedure was used. The analytical equation chosen as the curve to be fitted, contained three unknown parameters only and, with so few parameters, the carpet-search technique was not too lengthy in computer time.

The tests of Table 1 were directed towards determining the effect of bit interval on the impulse response. All tests were carried out with a sequence of 31 bits and a selection of the resulting impulse curves is given in fig. 4. There is a marked deterioration in the quality of these as bit interval is decreased. This is probably due to the deterioration of the input signal caused by the inertia of the relay-throttle mechanism.

For any group of tests under nominally identical conditions, as can be seen in Table 1, there is a considerable variation in the results for the value of damping factor. This variation masks any trend that might exist with change in bit interval. The consistency of the results between the test groups is surprising, because of the apparent variation in the impulse curves shown in fig. 4.

Table 2 shows the effect of 31-, 63-, and 127-bit sequence lengths for 0·2 and 0·4 s bit intervals. Again no general trend is evident with change in the number of bits per sequence. Table 3, for the engine condition
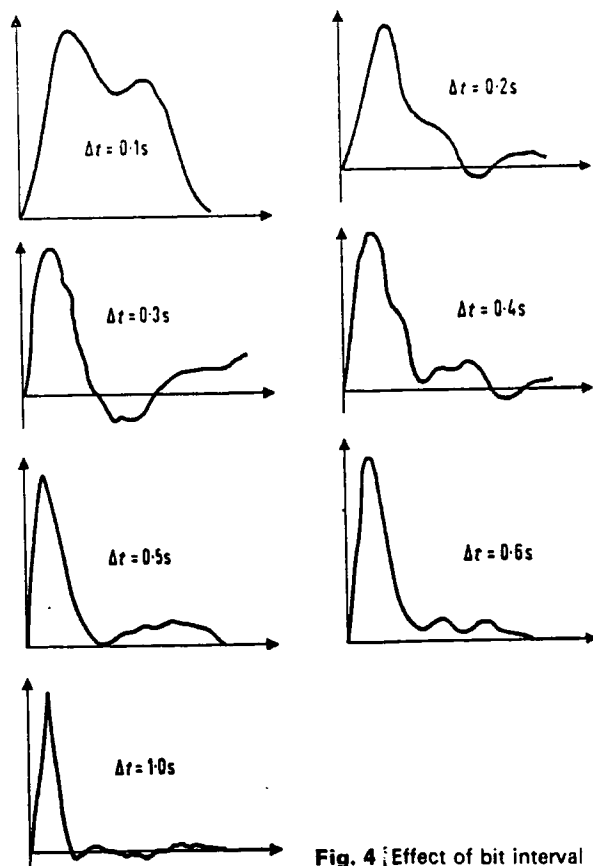

Fig. 4 Effect of bit interval

Test number	Number of bits	Bit interval (s)	Speed	Load at 14in(356mm) radius	Throttle position	Time constant (s)	Damping factor	Frequency (rads/s)
1	31	0·1				0·1	0·725	1·575
2	31	0·1				0·1	0·725	1·575
3	31	0·1				0·1	0·515	1·475
4	31	0·2				0·1	0·865	1·350
5	31	0·2				0·1	0·945	1·525
6	31	0·2				0·1	0·715	1·575
7	31	0·3				0·1	0·615	1·475
8	31	0·3				0·1	0·795	1·475
9	31	0·3	950 ± 50 rev/min	50 ± 5 pounds	2·5 ± 0·5	0·1	0·735	1·475
10	31	0·4				0·1	0·845	1·150
11	31	0·4				0·1	0·945	1·475
12	31	0·4				0·1	0·945	1·475
13	31	0·5				0·1	0·945	1·475
14	31	0·5				0·1	0·725	1·475
15	31	0·5				0·1	0·645	1·525
16	31	0·6				0·1	0·725	1·575
17	31	0·6				0·1	0·475	1·475
18	31	0·6				0·1	0·775	1·575
19	31	1·0				0·1	0·915	1·575
20	31	1·0				0·1	0·945	1·525
21	31	1·0				0·1	0·945	1·525
Average values						0·1	0·793	1·491

Table 1 Effect of bit interval

where the signal-to-noise ratio has reduced to about unity, shows a scatter in the results similar to that obtained at the previous engine condition. This is surprising since the impulse-response traces have deteriorated markedly, as typified by fig. 5. With these results, manual curve-fitting would be quite impracticable.

The average values found were damping factor of 0·79 and natural frequency of 1·49 rad/s for one engine condition, and 0·63 and 0·98 rad/s, respectively, for the second engine condition.

Conclusions

For the engine system considered, which has a relatively fast response, it proved impossible to obtain good and consistent results. The serial type of approach in which points on the impulse-response curve were calculated in groups of three, necessitated many test-runs and this accentuated the scatter in the results. The best approach proved to be calculation of the impulse-response curve off-line on a digital computer.

It proved impossible to predict the most suitable values of bit-length and bit-interval because of the
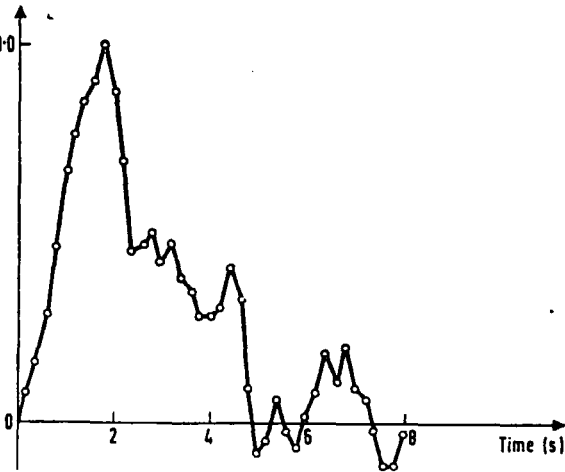
Test number	Number of bits	Bit interval (s)	Speed	Load at 14in(356mm) radius	Throttle position	Time constant (s)	Damping factor	Frequency (rads/s)
4	31	0·2				0·1	0·865	1·350
5	31	0·2				0·1	0·945	1·525
6	31	0·2				0·1	0·715	1·575
10	31	0·4				0·1	0·845	1·150
11	31	0·4				0·1	0·945	1·475
12	31	0·4				0·1	0·945	1·475
22	63	0·2				0·1	0·945	1·100
23	63	0·2				0·1	0·945	1·250
24	63	0·2	950 ± 50 rev/min	50 ± 5 pounds	2·5 ± 0·5	0·1	0·885	1·575
25	63	0·4				0·1	0·665	1·450
26	63	0·4				0·1	0·545	1·450
27	63	0·4				0·1	0·465	1·525
28	127	0·2				0·1	0·515	1·575
29	127	0·2				0·1	0·675	1·575
30	127	0·2				0·1	0·945	1·475
31	127	0·4				0·1	0·945	1·475
32	127	0·4				0·1	0·935	1·475
33	127	0·4				0·1	0·585	1·575
Average values						0·1	0·806	1·448

Table 2 Effect of sequence length

Test number	Number of bits	Bit interval (s)	Speed	Load at 14in(356mm) radius	Throttle position	Time constant (s)	Damping factor	Frequency (rads/s)
34	31	0·2				0·1	0·845	1·025
35	31	0·2				0·1	0·545	1·025
36	31	0·2				0·1	0·915	0·975
37	31	0·4				0·1	0·705	1·075
38	31	0·4				0·1	0·795	0·975
39	31	0·4				0·1	0·545	1·075
40	63	0·2				0·1	0·945	1·075
41	63	0·2	1730 ± 10 rev/min	55·5 pounds	8·0 ± 1·0	0·1	0·895	1·025
42	63	0·2				0·1	0·515	1·075
43	63	0·4				0·1	0·525	1·075
44	63	0·4				0·1	0·615	1·025
45	63	0·4				0·1	0·795	0·975
46	127	0·2				0·1	0·725	0·975
47	127	0·4				0·1	0·285	1·575
48	127	0·4				0·1	0·245	0·575
Average values						0·1	0·626	0·975

Table 3 Effect of large noise-to-signal ratio

general scatter in the results masking any trend which might exist with variation in these two parameters. The computer programme for fitting a third-order equation to the computed impulse-responses produced reasonably consistent results in spite of the poor quality of some of the impulse-response curves.

The results of this investigation suggest that, provided reasonable sequence-lengths and bit-intervals are chosen, exact values of these are not critical. A large number of tests should be carried out with the sequence chosen—say, 31 bits and 0·5 s bit-interval for the type of engine considered—and the results averaged.

Fig. 5 Typical response for large signal-to-noise ratio

References

1. Benes, J.: *Statistical dynamics of automatic control systems*. Iliffe, 1967
2. Davies, W. D. T.: 'Random signal testing for evaluating system dynamics'. *Wireless World*. Aug. 1966.
3. Hughes, M. T. G., and Noton, A. R. M.: 'The measurement of control system characteristics by means of a cross correlator'. *Proc. I.E.E.*, Jan. 1962, p. 77-78.
4. Briggs, P. A. N. *et alia*: 'Correlation analysis of process dynamics using pseudo-random binary test perturbations'. *Proc. I.Mech.E.* 1964–65. Vol. 179, p. 37.
5. Colloquium on 'Pseudo-random sequences applied to control systems'. *I.E.E.* and *I.Mech.E.* Jan. 1967.
6. Davies, W. D. T.: 'Generation and properties of maximum-length sequences'. *Control*, June and July, 1966, Vol. 10, p. 302 and p. 364.

PAPER 17

THEORETICAL DESIGN OF AN ADAPTIVE CONTROLLER FOR AN I.C. ENGINE

by K. F. Gill, G. E. Harland and J. Schwarzenbach

An I.C. engine-speed control system has been investigated theoretically on an analogue computer to determine the degree of improvement in existing speed-control systems that can be obtained by using adaptive techniques.

As electronic devices become cheaper and more reliable, it becomes worth considering their use for controllers which, traditionally, have been hydraulic or mechanical. Current hydromechanical control units are of highly complex design and, in addition to being expensive, require a high degree of skill in their manufacture, assembly and maintenance to achieve the required performance and reliability. There are applications for reciprocating internal-combustion engines and gas-turbine engines, where it is advantageous to have as rapid as possible a response of engine speed to throttle movement under a wide range of engine load and environmental conditions. Here, the main results are reported of a theoretical investigation into the possibility of adding to such an engine system, which incorporates a proportional and integral controller, an auxiliary loop that allows the advantages of adaptive control to be attained.

The design study was based on dynamic-performance information obtained from a laboratory diesel engine. These characteristics are assumed to be typical for this type of prime mover, and variations in prime mover can be accounted for by changes in the coefficients in the characteristic equations. The controller chosen for investigation was a model reference adaptive type which adjusted a parameter in the auxiliary loop to minimise a chosen performance index, and controller and engine were simulated on a PACE 231 R analogue computer incorporating parallel logic elements (fig. 1).

To obtain the engine dynamic characteristics, the throttle was actuated by an electromechanical servomechanism, closely described by a second-order transfer function, in which the values of damping factor and natural frequency could be varied as desired within a limited range.

Engine dynamics

It was decided to attempt to represent the engine dynamically by a linear transfer function. Theoretical evaluation of the transfer function required more detailed engine information than was available and, therefore, the dynamic characteristics were determined experimentally. The information was obtained using two distinct types of forcing function, namely a harmonic input and a statistical p.r.b.s. signal input

To obtain harmonic information for the engine system studied, it was necessary to cover frequencies ranging from approximately 0·01Hz to 4Hz. The phase and magnitude information was obtained using a proprietary transfer-function analyser. The mode of operation of the analyser necessitated long periods of running at the low-frequency end of the spectrum, which proved to be time-consuming. It is important that the engine datum running condition does not change during such lengthy periods of testing, and great care was required to ensure that the results obtained were representative.

The statistical binary input was obtained from a shift register, with appropriate feedback loops, constructed from a proprietary electronic logic teaching kit. The clock pulse used for actuating the shift register was generated by a bistable oscillator, the period of which determined the bit-interval of the sequence. To eliminate the long-term variation in engine condition, analogue traces were taken for single sequences, and values measured from these traces were then used to compute digitally the cross-correlation function for each test. It was found[1] that as much useful infor-

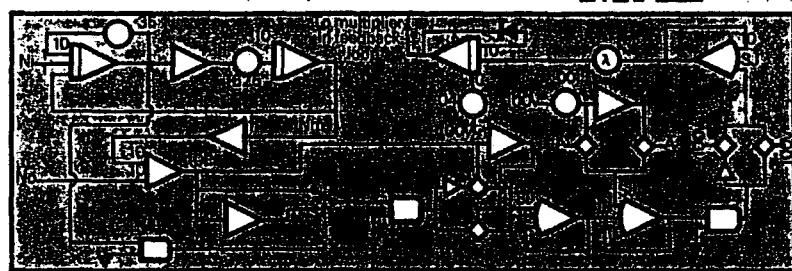1 Block diagram of arrangement of engine system
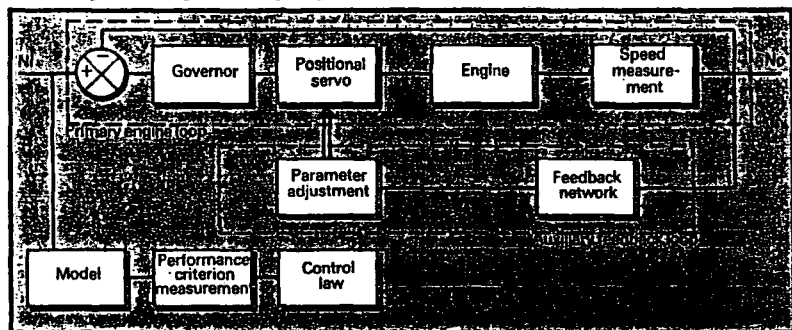
2 Block diagram of primary engine loop

3 Block diagram of primary + auxiliary loop
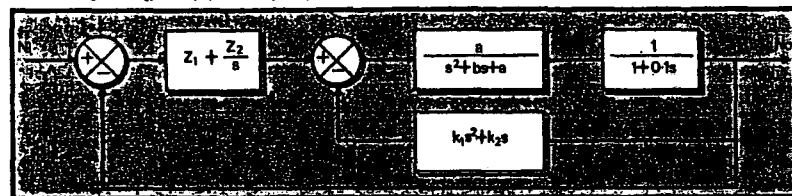
4 Circuit for mechanisation of adaptive loop

mation could be obtained for a 31-bit sequence as for longer sequence lengths of the same bit interval and hence testing was carried out using this sequence length.

The dynamic information was obtained by curve fitting to the polar plot and the cross-correlation function, respectively, and it was found that the best fit resulted from the assumption that the engine and tachogenerator together constituted a third-order system. The tachogenerator was known to be represented to a good approximation by a single time constant of 0·1s arising from the filter network associated with the speed-measuring transducer. The remaining two poles, for the engine transfer function, are complex, from which the natural frequency and damping factor can be evaluated. Variation of the datum engine operating point results in a change in these parameters.

Table I Steepest descent adaptation

Test number	λ	Step size	Step W	Rise-time	% over shoot	Settling time	φ°	M
1	0·4	50	0·1	1·0	31	6·0		
2	0·4	50	0·1	1·0	26	4·0		
3	0·4	50	0·1	1·0	24	4·0		
4	0·4	50	0·2	1·0	31			
5	0·4	50	0·2	1·0	24			
6	0·4	50	0·2	1·0	22			
7	0·4	50	0·4				12	1·75
8	0·4	50	0·4				5	1·95
9	0·4	50	0·4				1	1·98
10	0·4	100	0·1	1·0	26	5·0		
11	0·4	100	0·1	1·0	21	4·0		
12	0·4	100	0·1	1·1	17	4·0		
13	0·4	100	0·2	0·8	27			
14	0·4	100	0·2	1·0	21			
15	0·4	100	0·2	1·1	19			
16	0·4	100	0·4				12	2·16
17	0·4	100	0·4				12	1·50
18	0·4	100	0·4				12	1·24
19	0·4	200	0·1	0·8	21	5·9		
20	0·4	200	0·1	1·0	14	4·0		
21	0·4	200	0·1	1·0	19	4·0		
22	0·4	200	0·2	0·8	29			
23	0·4	200	0·2	1·2	14			
24	0·4	200	0·2	1·2	14			
25	0·4	200	0·4				25	1·55
26	0·4	200	0·4				17	1·18
27	0·4	200	0·4				17	1·18
28	0·8	200	0·1	1·3	10	4·9		
29	0·8	200	0·2	1·2	14			
30	0·8	200	0·4				4·9	1·15
31	0·8	100	0·1	1·0	15	4·0		
32	0·8	100	0·2	1·1	16			
33	0·8	100	0·4				9·8	1·20
34	0·8	50	0·1	0·9	21	5·1		
35	0·8	50	0·2	1·1	21			
36	0·8	50	0·4				0	1·45
37	0·2	50	0·1	0·9	22	5·8		
38	0·2	50	0·2	1·0	26			
39	0·2	50	0·4				27	1·95
40	0·2	100	0·1	1·0	25	4·5		
41	0·2	100	0·2	1·1	22			
42	0·2	100	0·4				7·3	1·63
43	0·2	200	0·1	1·1	15	4·1		
44	0·2	200	0·2	1·1	17			
45	0·2	200	0·4				17	1·17
46	0·2	200	0·1	1·3	8	4·7		
47	0·4	200	0·1	1·2	10	5·0		
48	0·8	200	0·1	1·1	15	3·9		
49	0·2	100	0·1	1·2	10	4·5		
50	0·4	100	0·1	1·3	10	4·5		
51	0·8	100	0·1	1·3	13	5·0		
52	0·2	50	0·1	1·1	16	4·9		
53	0·4	50	0·1	1·2	15	5·0		
54	0·8	50	0·1	1·3	12	5·2		
55	0·4	100	0·2	1·4	17			
56	0·4	100	0·4				14	1·10
57	0·4	100	0·1	1·1	7	3·7		
58	0·4	200	0·1	1·1	9	4·0		
59	0·4	50	0·1	1·0	14	4·0		
60	0·4	100	0·2	1·1	13			
61	0·4	100	0·4				20	1·00
62	0·4	200	0·1	1·0	24	4·5		
63	0·4	200	0·2	1·4	21			
64	0·4	200	0·4				42	0·93
65	0·4	100	0·1	1·1	32	4·5		
66	0·4	100	0·2	1·4	26			
67	0·4	100	0·4				39	0·90
68	0·4	50	0·1	1·1	32	4·5		
69	0·4	50	0·2	1·3	27			
70	0·4	50	0·4				42	1·06
71	0·4	50	0·1	1·1	17	6·0		
72	0·4	50	0·2	1·5	30			
73	0·4	50	0·4				13	1·09
74	0·4	100	0·1	1·0	28	7·0		
75	0·4	100	0·2	1·4	24			
76	0·4	100	0·4				16	1·14
77	0·4	200	0·1	1·2	20	7·0		
78	0·4	200	0·2	1·4	24			
79	0·4	200	0·4				11	1·16
Wnm = 5·0				ζm = 0·7				
80	0·4	200	0·1	1·2	22	5·0		
81	0·4	100	0·1	1·0	24	4·5		
82	0·4	50	0·1	1·1	19	5·2		
Wnm = 1·25				ζm = 0·7				
83	0·4	50	0·1	4·8		4·8		
84	0·4	100	0·1	4·0		4·0		
85	0·4	200	0·1	3·5	1·5	3·7		
86	0·4	200	0·1	5·1		5·1		
87	0·4	100	0·1	5·0		5·0		
88	0·4	50	0·1	4·2		4·2		
Wnm = 5·0				ζm = 0·7				
89	0·4	50	0·1	1·1	16	4·7		
90	0·4	100	0·1	1·0	20	4·0		
91	0·4	200	0·1	1·1	21	4·1		

Design of adaptive loop

A block diagram of the primary engine loop with the associated transfer functions included is shown in fig. 2. If the natural frequency of the positional servo is chosen to be ten times that of the engine, then inspection of a root locus diagram would show clearly that the roots of the engine and speed-measuring transducer are dominant and hence that the influence of the dynamic characteristics of the throttle actuating servomechanism can be ignored. The closed-loop transfer function then reduces to

$$\frac{N_o(s)}{N_i(s)} = \frac{a(Z_1s + Z_2)}{0·1s^4 + s^3(1+0·1b) + s^2(0·1a+b) + s(a+aZ_1) + aZ_2} \quad ... (1)$$

Adaptation must be such that variations occurring within the closed-loop system resulting from changes in environment and power output demand can be corrected for, to give substantially unchanged dynamic behaviour. This can be achieved by the introduction of an auxiliary feedback loop designed to compensate for variations in the parameters a and b, thus ensuring that the system characteristic equation remains sensibly constant.

By trial and observation it was found that a suitable loop, which gave adequate control over the high-frequency coefficients, was that shown in fig. 3. The overall transfer function for the system is then

$$\frac{N_o(s)}{N_i(s)} = \frac{a(Z_1s + Z_2)}{0·1s^4 + s^3(1+0·1b+ak_1) + s^2(0·1a+b+ak_2) + s(a+aZ_1) + aZ_2} ... (2)$$

In practical systems the generation of an $\ddot{N}_o$ term would be impossible because of the inherent noise generation associated with such a double time differentiation. In an attempt to assess the importance of this term it was, however, included for part of the simulation study. To avoid duplication and interaction resulting from two separate adaptation loops, the limitation $k_2/k_1 =$ constant was introduced and a single parameter was adjusted.

In an earlier study[2] a technique used to determine a suitable model transfer function was to divide the numerator of the system transfer function into its denominator. This gave a second-order equation which was used as the mathematical representation for the model. Without knowledge of the value of this ratio k_2/k_1, it is not feasible to utilise this method to arrive at a suitable model relationship.
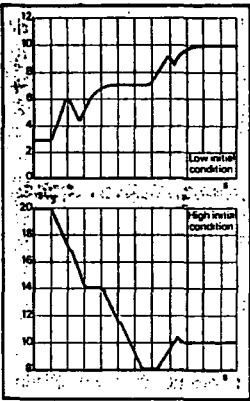
An alternative approach is to accept that,
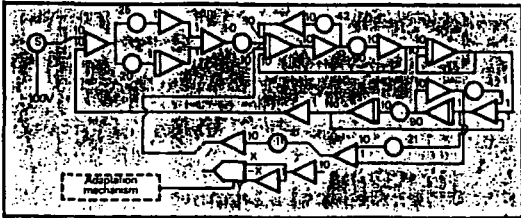
5 Circuit for the simulated engine governor system
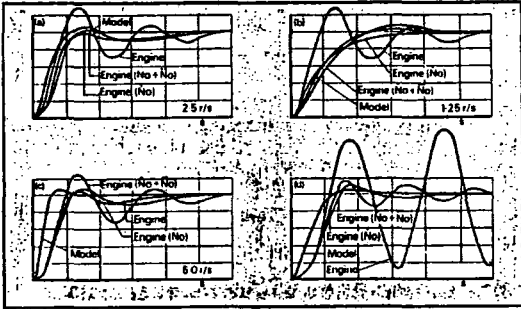
6 (a) Effect of variation in ω_{nm} **7 (c)** Effect of variation in ω_{nm} **8 (b)** Effect of variation in ω_{nm}

9 (d, left) Effect when the positional servomechanism has parameters similar to engine

10 (above) Adaptive behaviour of the variable parameter k.(No + No). S = 100%. F = 0.1. $\lambda = 0.04$

with a correct choice of this ratio, a second-order model is obtainable. The natural frequency of such a model should be close to that of the primary engine loop which,

from experimental results, was estimated to be 2·15rad/s. The damping factor was chosen to be 0·7. If the model equations are not representative, then the model

reference adaptive technique cannot be expected to give very satisfactory results, since the engine will only operate within a limited dynamic range dictated by its own internal characteristics.

Inserting $a=9$, $b=4\cdot2$ for the engine system operating at the chosen datum point, and $Z_1=0\cdot25$, $Z_2=0\cdot2$ for suitable governor coefficients at this datum condition, eqn (2) becomes

$$\frac{N_o(s)}{N_i(s)} = \frac{2\cdot25s + 1\cdot8}{0\cdot1s^4+(1\cdot42+9k_1)\,s^3+(5\cdot1+9k_2)\,s^2+11\cdot25s+1\cdot8} \quad \ldots (3)$$

Neglecting the term in s^4 and equating to the model transfer function

$$\frac{N_M(s)}{N_i(s)} = \frac{4\cdot6}{s^2+3\cdot0s+4\cdot6} \quad \ldots (4)$$

the resulting requirement is

$$(6\cdot5+41\cdot5k_1)\,s^3+(23\cdot5+41\cdot5k_2)\,s^2+52\cdot0s+8\cdot3=7\cdot4s^3+28\cdot0s^2+52\cdot0s+27\cdot2 \quad \ldots (5)$$

Equating coefficients gives values of $k_1=0\cdot022$, $k_2=0\cdot11$ and hence a ratio $k_1/k_2=0\cdot2$. The difference in the value of the constant term in the polynomials results in

Table II Approximate method of adaptation

Test number	λ	Step size (%)	W	Engine ζ	Engine Wn	Was	Wnmm	Rise-time	% over shoot	Settling time	φ°	M	Adaptive parameters
1	0·04	100	0·1	0·7	3·0	3·0	2·5	1·2	5·8	3·3			Ṅo Ṅo
2	0·04	100	0·2	0·7	3·0	3·0	2·5	1·1	5·7				Ṅo Ṅo
3	0·04	100	0·4	0·7	3·0	3·0	2·5				6·5	1·77	Ṅo Ṅo
4	0·04	50	0·1	0·7	3·0	3·0	2·5	0·7	1·3	3·0			Ṅo Ṅo
5	0·04	200	0·1	0·7	3·0	3·0	2·5	1·1	6·0	3·2			Ṅo Ṅo
6	0·02	100	0·1	0·7	3·0	3·0	2·5	0·9	7·7	3·5			Ṅo Ṅo
7	0·08	100	0·1	0·7	3·0	3·0	2·5	1·1	6·6	3·5			Ṅo Ṅo
8	0·04	100	0·1	0·7	3·0	3·0	2·5	2·7		2·7			Ṅo
9	0·04	100	0·2	0·7	3·0	3·0	2·5	0·6	1·8				Ṅo
10	0·04	100	0·4	0·7	3·0	3·0	2·5					1·10	Ṅo
11	0·04	50	0·1	0·7	3·0	3·0	2·5	0·6	1·7	3·4			Ṅo
12	0·04	200	0·1	0·7	3·0	3·0	2·5	3·6		3·6			Ṅo
13	0·08	200	0·1	0·7	3·0	3·0	2·5	1·9	6·0	3·5			Ṅo
14	0·08	100	0·1	0·7	3·0	3·0	2·5	2·4		2·4			Ṅo
15	0·08	50	0·1	0·7	3·0	3·0	2·5	0·5	3·0				Ṅo
16	0·04	100	0·1	0·7	3·0	3·0	2·5	0·6	4·0				Ṅo
17	0·04	100	0·2	0·7	3·0	3·0	2·5						Ṅo
18	0·04	100	0·1	0·7	3·0	3·0	2·5	1·1	6·1	3·0			Ṅo Ṅo
19	0·04	100	0·1	0·7	3·0	3·0	2·5	1·2	6·1	3·5			Ṅo Ṅo
20	0·04	100	0·1	0·7	3·0	3·0	2·5	1·1	6·1	3·0			Ṅo Ṅo
21	0·04	100	0·1	0·7	3·0	3·0	2·5	1·2	7·1	3·8			Ṅo Ṅo
22	0·04	100	0·1	0·7	3·0	3·0	2·5	2·4		2·4			Ṅo
23	0·04	100	0·1	0·7	3·0	3·0	2·5	2·2		2·2			Ṅo
24	0·04	100	0·1	0·7	3·0	3·0	2·5	0·6	3·2	3·0			Ṅo
25	0·04	100	0·1	0·7	3·0	3·0	2·5	0·6	2·1	3·0			Ṅo
26	0·04	100	0·1	0·7	3·0	3·0	2·5	2·1		2·1			Ṅo
27	0·04	50	0·1	0·7	3·0	3·0	2·5	1·9	1·9	4·0			Ṅo
28	0·04	200	0·1	0·7	3·0	3·0	2·5	2·2		2·2			Ṅo
29	0·04	100	0·2	0·7	3·0	3·0	2·5	2·0		2·0			Ṅo
30	0·04	100	0·4	0·7	3·0	3·0	2·5					0·87	Ṅo
31	0·04	100	0·1	0·7	3·0	3·0	2·0	2·5		2·5			Ṅo
32	0·04	50	0·1	0·7	3·0	3·0	2·0	2·0		2·0			Ṅo
33	0·04	200	0·1	0·7	3·0	3·0	2·0	2·4		2·4			Ṅo
34	0·04	200	0·1	0·7	3·0	3·0	3·0	1·7	2·1	3·5			Ṅo
35	0·04	100	0·1	0·7	3·0	3·0	3·0	1·9	2·1	3·8			Ṅo
36	0·04	50	0·1	0·7	3·0	3·0	3·0	1·7	3·0	3·4			Ṅo
37	0·04	100	0·1	0·7	3·0	6·0	2·5	2·1		2·1			Ṅo
38	0·04	50	0·1	0·7	3·0	6·0	2·5	2·1		2·1			Ṅo
39	0·04	200	0·2	0·5	3·0	6·0	2·5	2·1		2·1			Ṅo
40	0·04	100	0·2	0·5	3·0	6·0	2·5	2·0		2·0			Ṅo
41	0·04	100	0·4	0·5	3·0	6·0	2·5						Ṅo
42	0·04	100	0·1	0·5	3·0	3·0	2·5	2·1		2·1			Ṅo
43	0·04	100	0·2	0·5	3·0	3·0	2·5	0·6	2·2	1·4			Ṅo
44	0·04	100	0·4	0·5	3·0	3·0	2·5					0·90	Ṅo
45	0·04	50	0·1	0·5	3·0	3·0	2·5	1·7	8·0	4·1			Ṅo
46	0·04	200	0·1	0·5	3·0	3·0	2·5	2·0		2·0			Ṅo
47	0·04	100	0·1	0·9	3·0	3·0	2·5	2·1		2·1			Ṅo
48	0·04	100	0·2	0·9	3·0	3·0	2·5	1·8		1·8			Ṅo
49	0·04	100	0·4	0·9	3·0	3·0	2·5					0·90	Ṅo
50	0·04	50		0·9	3·0	3·0	2·5	1·6	6·4	4·2			Ṅo
51	0·04	200		0·9	3·0	3·0	2·5	2·0		2·0			Ṅo
52	0·04	100		0·7	5·0	3·0	2·5	1·9		1·9			Ṅo
53	0·04	100	0·2	0·7	5·0	3·0	2·5	0·4	1·4	1·0			Ṅo
54	0·04	100	0·4	0·7	5·0	3·0	2·5					1·05	Ṅo
55	0·04	50	0·1	0·7	5·0	3·0	2·5	1·0		1·0			Ṅo
56	0·04	200	0·1	0·7	5·0	3·0	2·5	2·0		2·0			Ṅo
57*	0·04	100	0·1	0·7	3·0	3·0	2·5	1·2	8·2	3·0			Ṅo Ṅo

a change in the rate of the exponential decay on which the damped sinusoid is superimposed.

Three separate circuits for parameter adjustment have been investigated. Two are based on the law of steepest descent and are identical to those described in an earlier paper[2], and the third approach is to minimise the instantaneous error signal by varying the adaptive parameter at constant rate.

The difficulty in the minimisation of performance indices by the method of steepest descent is that of the generation of the partial derivative $\frac{\partial}{\partial k} f(\varepsilon)$. In practice, it is necessary to make certain basic assumptions[3] which lead to the approximate expression $\frac{\partial \varepsilon}{\partial k} = -\frac{G_M(s)}{G_1(s)} \dot{N}_o$ when a performance index of ε^2 is used. In view of the assumptions made in the derivation of $\frac{\partial \varepsilon}{\partial k}$, this value will not be obtained very accurately, particularly when large changes of k must be made. Thus, it is logical to use the simplification obtainable by using a simple switching circuit to generate the control law $\left(sgn \right. \left. \frac{\partial \varepsilon}{\partial k} \right) \varepsilon$. Tables I and II list the relevant dynamic information for a series of tests utilising the methods of steepest descent.

An alternative approach (not giving steepest descent) which avoids the need to generate this derivative term is to adjust the adaptive term at a constant rate, the direction of adjustment being determined by the relationship $sgn \frac{\partial k_2}{\partial t} = (sgn \ \varepsilon) \left(sgn \ \frac{dN_M}{dt} \right)$.

The magnitude of these terms is not significant and it is only the polarity that determines the direction in which the adaptive parameter is adjusted. Since the rate of the adaptation is uninfluenced by the characteristics of the error signal, the system with this adaptive loop should maintain the value of the adaptive parameter closer to its optimum than do the previous systems. The circuit diagram for this arrangement is shown in fig. 4 and that for the engine primary and auxiliary loops is shown in fig. 5. The results are listed in table II.

Since k_2 is being adjusted at a constant rate, it is necessary to hold the value of k_2 constant once the optimum has been reached. Since the magnitude of ε is unimportant, one possible way to achieve this condition is by the introduction of a dead-zone. This has the advantage of allowing for the small differences between steady-state engine and model speeds which necessarily occur in practice.

Discussion

Typical speed responses of the simulated engine system, including the auxiliary feedback loop, are shown in fig. 6. The characteristics of this loop were as determined above, and the curves were obtained by manual selection of the adaptive parameter k_2. These traces were obtained with the optimum value of k_2 (0·11), and give a measure of the quality of the improvement attainable. The engine response with both terms N_o and $\dot{N}_o$ included in the auxiliary loop shows some improvement over that with the $\dot{N}_o$ term alone. The improvement obtained with the $\dot{N}_o$ term alone is, however, substantial.

The order and the theoretically correct characteristic parameters of the model have been evaluated above. In an attempt to improve the system risetime, the natural frequency of the model was increased, but this resulted in little improvement in system response, as can be seen from comparison of figs 6 and 7, the model natural frequency in the latter having been increased by a factor of 2. Decreasing the natural frequency of the model will result in an increase in system risetime, and in so doing the engine and model response become closer (fig. 8, for halved natural frequency). As before, the $\dot{N}_o$ term gives a secondary improvement. The frequency-dependent terms in the transient response are still controlled by the system inertia, and the auxiliary loop can only influence the damping characteristics of the system.

To demonstrate the effectiveness of the auxiliary loop, the natural frequency of the throttle-actuating servo was reduced to the same order as that of the engine system. The primary loop alone was then on the limit of absolute stability, and a marked improvement in the transient behaviour resulted with the introduction of the auxiliary loop (fig. 9). Under these severe conditions, inclusion of the $\dot{N}_o$ term is seen to bring the transient significantly closer to that of the model than it is when the $\dot{N}_o$ term alone is active.

Test results

To present a comprehensive coverage for the results of a series of tests using a repetitive step input, table I shows the effect of changes in step size, frequency of step, model frequency, and rate of adjustment of k_2. The adjustment of k_2 towards its best value is progressive, and to get some indication of the form of the resulting change, transient responses were recorded for the 1st, 5th and 11th steps. By the 5th step, the transient trace has become very close to the final form. Fig. 10 shows the progressive change occurring in the parameter k_2. From a low initial value, the equilibrium point is reached after two consecutive steps, and from the high initial value it requires three steps. A system with a low value of k_2 would be oscillatory and, as a result, a large overshoot would occur initially, giving the changes in direction of

k_2 seen to occur when k_2 first becomes 0·06 and 0·09.

To achieve a measure of the quality of the response, the values of risetime, percentage overshoot, and settling time in each transient response are listed for comparison. The ideal values are those of the model: risetime 1·3s, overshoot 6%, settling time 3·5s. From table I the overshoot is seen to be significantly higher (on average 15–20%) and as a result the risetime is marginally smaller (of the order of 1s), and the settling time is of the same order. This performance is within the recognised limits for acceptability.

The simplified system with relay included in the adaptive loop shows no real deterioration in system performance and, if anything, shows an improvement.

In most practical situations the adaptive parameter remains close to its optimum value, and in this region, where the approximate equations more nearly represent the laws of steepest descent, minimum benefit is gained from utilisation of this law. For cases in which large changes in k_2 are required, the equations are only very approximate. The application of the relay to the system utilises the sign of $\frac{\partial \varepsilon}{\partial k_2}$, and the rate at which k_2 is adjusted is a function of ε. It would appear sensible to investigate system performance in which a constant rate of adaptation for k_2 was used and the sign of ε used to determine the direction of change of k_2. This reduces the complexity of the parameter-adjustment circuit and increases the sensitivity of the parameter-adjustment loop in the region of the optimum value of k_2. Table II substantiates this view in showing a small value of overshoot, generally of the order of 6%, together with a risetime somewhat shorter and a settling time of the same order as the model. The effect of excluding the $\dot{N}_o$ term is, in most cases, insignificant. A reduction in the value of the throttle servo's natural frequency with an active parameter adjustment loop can result in system instability. Changes in system behaviour for changes in engine damping constant and natural frequency are again small.

In conclusion, it appears that the simplest system gives acceptable transient behaviour which is rather better than that obtainable from either of the steepest-descent approximations, and further is more attractive practically. ■

References

1 Harland, G. E., *et al* : 'Pseudo-random signal testing applied to a diesel engine'. *Control*, Feb. 1969, pp. 137–140
2 Gill, K. F., Schwarzenbach, J., and Harland, G. E.: 'Design analysis of model reference adaptive control systems applied to a gas-turbine aircraft engine'. *Proc I.E.E.*, 115 (1968), pp. 460–466
3 Osburn, P. V., Whitaker, H. P., and Kezer, A.: 'New developments in the design of model reference adaptive control systems'. *Inst. of Aerospace Sciences*, Paper 61–39, 1961

K. F. Gill and J. Schwarzenbach are at the department of mechanical engineering, The University, Leeds, and G. E. Harland is now at The Open University.

PAPER 20

Design of a model-reference adaptive control for an internal combustion engine

by *G. E. Harland and †K. F. Gill

An internal combustion engine speed control system has been investigated to determine the possibility of using a model-reference adaptive control device to maintain constant dynamic behaviour of engine speed irrespective of engine load and environmental conditions. A conventional type of speed control arrangement has been used in the primary loop and an auxiliary loop has been introduced which biases the engine throttle mechanism by an amount which is proportional to the derivative of engine speed. The constant of proportionality is the parameter which is being changed by the adaptive loop.

The results of the engine tests showed good correlation with those obtained in a simulation study and clearly showed that for certain installations the incorporation of a model-reference loop into a conventional speed control system would result in improved engine dynamic behaviour.

1. INTRODUCTION

Early IC engine speed control systems, starting with the Watt governor. 1788, were designed and developed by trial and observation. and only very limited consideration was given to theoretical analysis. With the entry of the gas turbine into military service use and the demand for improved engine dynamic performance for this type of installation, the intuitive approach to system design became unacceptable.

In the late 1940's and early 1950's, attempts were made to achieve the required aircraft engine dynamic performance by the utilisation of fuel scheduling speed control systems. This approach required a thorough knowledge of the full working range of the system and for aircraft of several years ago this information was available. As speed ranges have increased, fuel scheduling inaccuracies have widened until it tends to be impractical to use this form of open loop control for certain engine applications.

This demand has made it necessary to replace the earlier fuel scheduling systems by a more complex closed loop speed control.

As electronic devices become cheaper and more reliable it is worth while considering their use for controllers which traditionally have been hydraulic or mechanical. Current hydro-mechanical speed control units are of highly sophisticated design and in addition to being expensive they require a high degree of skill in manufacture, assembly and maintenance to achieve the required performance and reliability. To replace these hydro-mechanical systems with their electronic counterparts is an unsound engineering solution and it would be more sensible to review the system as a whole. The existing units require considerable *a priori* operational knowledge during the design stages, since changing engine dynamics resulting from different flight conditions are still

pre-programmed in the present range of hydro-mechanical systems.

The pre-programming approach used on aircraft installations is to determine a series of governor parameters, each attempting to give the desired performance at a particular altitude and forward speed, and to adjust these parameters automatically as predetermined functions of measurable quantities. This form of scheduling of governor gain parameters has been referred to as open loop adaptation.[1]

The success of such adaptation is dependent upon being able to generate sufficiently accurately the governor gain constants for the wide range of possible operating conditions.

While such open loop adaptation is being used successfully, requirements for engine and aircraft performance are becoming increasingly more severe. and this brings attendant difficulties of design. production and maintenance of the controller for scheduling loop adjustment.[2] Attempts have been made in other fields to produce closed loop adaptive systems. and various approaches to the design of closed loop adaptive systems have been described.[3,4] These tend to fall into two classes. In one. the dynamic response of the system is continuously forced into correspondence with an ideal response defined by a model. and this is termed a model reference adaptive system.[5-8] In the other. the system performance is characterised by a single value, a performance index[9,10] and the system operates to maximise or minimise this value. The former is the class of adaptive controller chosen for study in this report since it is more readily applicable to an engine installation.

A preliminary study[11] was carried out on a simulated aircraft engine-governor system and the results of this work suggested that satisfactory engine dynamic performance could be maintained with changing environmental conditions. To further substantiate these findings the work has been extended to study the usefulness of these ideas when applied to a laboratory diesel engine, since in general most internal combustion engines tend to have similar dynamic characteristics.

1.1. Basic ideas

There are various methods available by which an adaptive control system can be designed. In the present study. the dynamic response of the system is continuously forced into correspondence with a chosen ideal response as defined by a mathematical model. This class of adaptive control was chosen primarily because a design study[11] indicated that with this form of control the minimum amount of system modification was necessary. Low cost solid state electronic circuit elements are available as proprietary items, so making physically possible the introduction of an adaptive loop into an established engineering system.

In an attempt to keep in line with engineering practice, the adaptive loop was designed in the following way:
An auxiliary loop was first added which contained the appropriate feedback network and adaptive parameters adjustment mechanism. This enables the effectiveness of the auxiliary loop to be demonstrated simply, for a fixed value

* Staff Tutor in Technology (Yorkshire Region), The Open University. Formerly Lecturer in the Department of Mechanical Engineering, The University of Leeds.
† Senior Lecturer, Department of Mechanical Engineering, The University of Leeds.
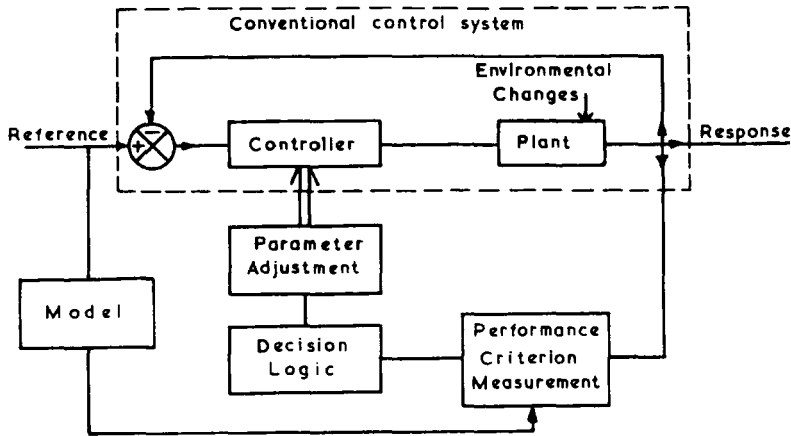
Harland and Gill

Fig 1 Model reference adaptive control system.

of the adaptive parameter. A third loop is necessary in which the performance criterion can be measured and the logic decision made to arrive at the adjustment required in the adaptive parameter. Closing of the third loop gives automatic control over the adaptive parameter and by doing so optimum performance can be realised in accordance with the established strategy. A block diagram representation showing all three loops is given in Fig 1.

No unified approach to the theoretical analysis and design of such systems has been generally accepted by workers in the field, and the authors' theoretical work rests heavily on classical linear theory and elementary laws of physics. Attempts to predict analytically the stability boundary for the rate of adjustment of the adaptive parameter by application of Lyapunov's Direct Method failed, and so it was necessary to use a simulator study to arrive at an estimation for the limiting value.

NOMENCLATURE

a	= Equivalent to $(\omega_n{}^2)_e$
A	= Area of restrictor in pneumatic governor
A_1	= Area of diaphragm in pneumatic governor
b	= Equivalent to $2\zeta_e(\omega_n)_e$
C_d	= Coefficient of discharge, taken as 0·65
D	= Datum speed, rev/min
f	= Fuel flow from fuel pump, in^3
F	= Frequency of step input, Hz
g	= Gravitational constant, taken as 32·2 ft/s^2
$G(s)$	= Transfer function of engine
$G_1(s)$	= Transfer function of governor
$G_M(s)$	= Transfer function of model
I	= Inertia of rotating parts, lbf/in^2
k	= Adaptive parameter
k_1	= Adaptive parameter associated with N_o
k_2	= Adaptive parameter associated with N_o
k'	= Rate of spring in pneumatic governor, lbf/in
M	= Amplitude ratio
N	= Speed, rev/min
P_1	= Manifold pressure, lb/in^2
P_2	= Pressure in pneumatic governor, lb/in^2
Q	= Flow of air through restrictor, lbm/s
s	= Laplace operator
S	= Speed perturbation, rev/min
S_r	= Sampling rate, ms
T	= Torque, lbf/in
x	= Rack displacement, in
Z_1	= Proportional governor parameter
ϵ	= Error, $N_m - N_o$
θ	= Throttle position, radians
λ	= Rate of change of adaptive parameter
μ	= Viscous friction coefficient, lbf/s
ζ	= Damping factor
ρ	= Density of air, lbm/in^3
τ	= Fixed time delay, s
ϕ	= Phase angle, degrees

ω	= Frequency, Hz
ω_n	= Undamped natural frequency, rads/s
Δt	= Bit interval. s

Suffixes

e	= Engine
i	= Input
L	= Load
m	= Model
o	= Output
s	= Positional servomechanism

2. THEORY

To be able to derive theoretically any transfer relationships, it is necessary to make certain plausible assumptions. The most important of these is to assume that perturbations about the datum condition are small. making the use of linear theory possible.

2.1. Derivation of engine system transfer function

The 50 hp David Brown engine was a laboratory unit complete with water brake dynamometer and housed in the soundproof thermodynamics laboratory of the department. Complete water. fuel and exhaust systems were provided in the laboratory. Fig 2.

The fuel was gravity fed from a tank to the C.A.V. fuel injection pump. A metered fuel supply system was fitted to enable the fuel consumption of the engine to be measured. The engine speed was monitored by an electrical tacho-generator and fed directly to the analogue computer for processing. The analogue computer facility, a PACE 221R and a PACE 231R, was housed in another laboratory in the Department of Electrical and Electronic Engineering.

The transfer relationship required is that relating engine speed to throttle movement. One possible way of obtaining this is to consider the complete system to be composed of several parts, Fig 3. Movement of the throttle causes a change in depression in the inlet manifold and this change is detected by the venturi control unit which adjusts the position of the rack of the injector unit. The additional fuel that has entered the engine is used to accelerate it to a new datum speed.

Each transfer relationship shown in Fig 3 can be developed for the data normally found in engineering drawings. This was carried out for the diesel engine used and the relevant equations together with the numerical values computed, are:

$$\frac{\Delta x(s)}{\Delta \theta(s)} = \frac{2·7}{1 + 0·47s} \qquad (1)$$

$$\Delta f(s) = 7·35 \times 10^{-5} \Delta N(s) + 5·6 \Delta x(s) \qquad (2)$$

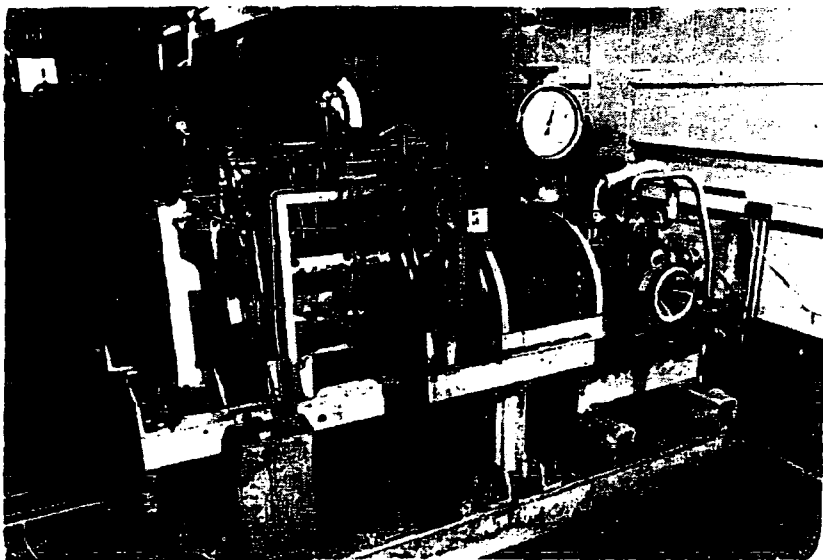$$\frac{\Delta T_E(s)}{\Delta f(s)} = \frac{1}{1 + 0·025s} \qquad (3)$$

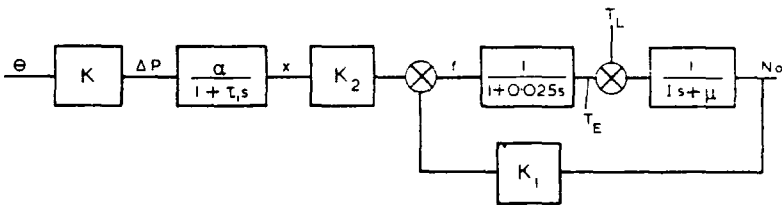Fig 2 50 hp laboratory test engine and dynamometer.

Fig 3 Block diagram of engine.

$$\frac{\Delta N(s)}{\Delta T_E(s)} = \frac{0 \cdot 0397}{1 + 0 \cdot 445s} \qquad (4)$$

Eliminating $\Delta x(s)$, $\Delta f(s)$, $\Delta T_E(s)$:

$$\Delta N(1 + 0 \cdot 445s) = \frac{0 \cdot 0397}{(1 + 0 \cdot 025s)} \ 7 \cdot 35 \times 10^{-5} \Delta N$$

$$+ \frac{5 \cdot 6 \times 2 \cdot 7 \Delta \theta}{(1 + 0 \cdot 47s)}$$

ie,

$$\Delta N(1 + 0 \cdot 94s + 0 \cdot 232s^2 + 0 \cdot 0052s^3 - 2 \cdot 92 \times 10^{-6}$$

$$- 1 \cdot 37 \times 10^{-6}s) = 0 \cdot 6 \Delta \theta(s) \qquad (5)$$

Three of the terms in the above equation are small and can be ignored without much loss in accuracy, the equation then reducing to one of second order:

$$\frac{\Delta N(s)}{\Delta \theta(s)} = \frac{2 \cdot 6}{s^2 + 4 \cdot 05s + 4 \cdot 3} \qquad (6)$$

This gives an undamped natural frequency of 2·07 rads/sec and a damping factor of 0·98.

It is evident that the above analysis can only be a guide to the order of magnitude of the parameters in the engine transfer function. A series of harmonic analysis tests were carried out on the engine system to determine the values of the parameters for a second-order system. Fig 4 shows typical traces obtained at various engine conditions and Fig 5 shows the separate harmonic loci for the filter, servomechanism and the complete engine system.

The averaged values found were a damping factor of 0·81 and an undamped natural frequency of 3·4 rad/s at the low

engine condition, 0·55 and 3·1 rad/s at the higher conditions. These results were then compared with those obtained from statistical response tests[12] and found to be in good agreement.

2.2. Transfer function of closed-loop engine-governor system

A block diagram of the primary engine loop with the associated transfer functions included is shown in Fig 6. A conventional proportional plus integral type governor unit was used in the primary loop to ensure isochronous speed control. The positional servo-mechanism which was used to vary the throttle position had characteristics which could be represented by a second-order equation. If the natural frequency of this servomechanism is chosen to be ten times that of the engine then inspection of a root locus diagram would show clearly that the roots of the engine and speed measuring transducer are dominant and hence the dynamic characteristics of the throttle actuating servomechanism can be neglected. The closed loop transfer function reduces to:

$$\frac{N_o(s)}{N_i(s)} = \frac{a(Z_1 s + Z_2)}{0 \cdot 1s^4 + s^3(1 + 0 \cdot 1b) + s^2(0 \cdot 1a + b)} \qquad (7)$$
$$+ s(a + aZ_1) + aZ_2$$

2.3. Design of adaptive loop

The basic object of the adaptive loop is to maintain constant dynamic behaviour of the system irrespective of changes in system parameters, which mathematically implies that the coefficients in the transfer function are maintained at a constant value. One possible way to achieve this is by the introduction of an auxiliary loop designed to compensate for variations in the engine parameters a and b, and so ensuring constant dynamic performance (Fig 7).

$$\frac{N_o(s)}{N_i(s)} = \frac{a(Z_1 s + Z_2)}{0 \cdot 1s^4 + s^3(1 + 0 \cdot 1b + ak_1) + s^2(0 \cdot 1a + b + ak_2)} \qquad (8)$$
$$+ s(a + aZ_2) + aZ_2$$

Harland and Gill
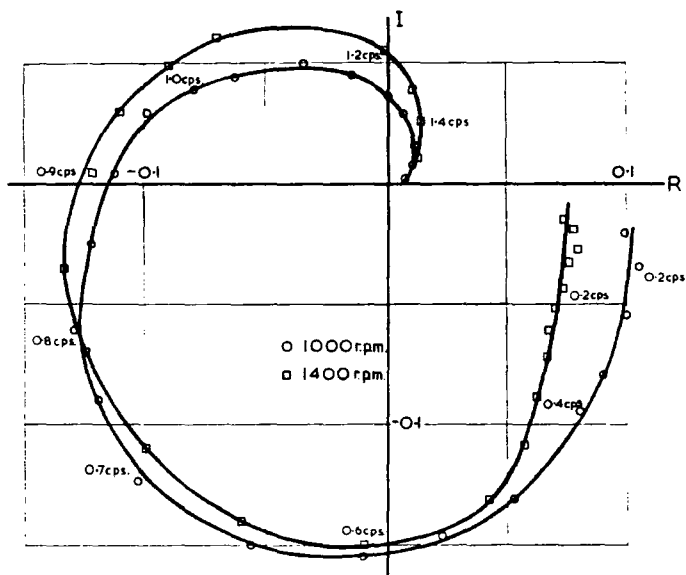
Fig 4 Harmonic response locus for engine system.

O 1000 r.p.m.
$\square$ 1400 r.p.m.
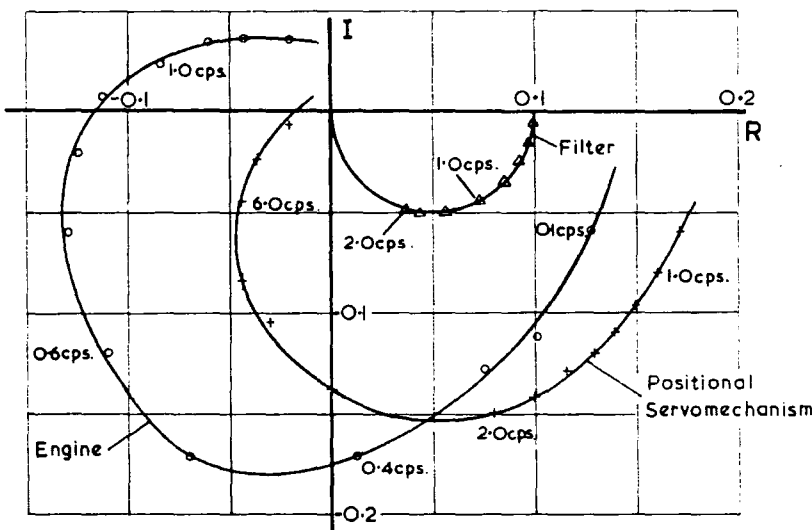
Fig 5 Harmonic response loci for items of engine system.
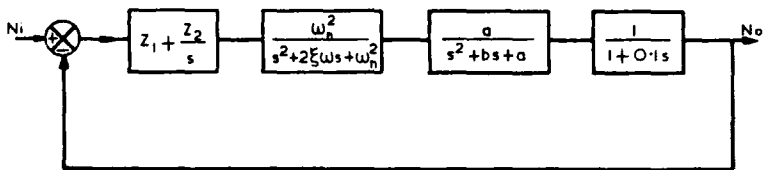
Fig 6 Block diagram of primary engine loop.
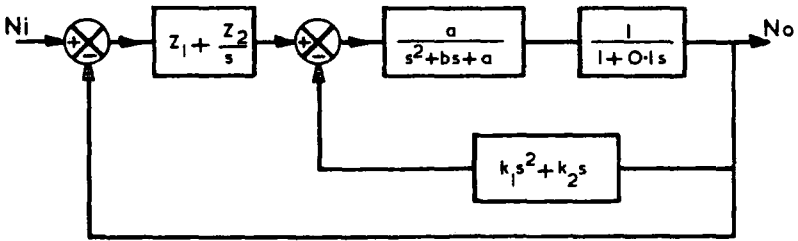
Fig 7 Block diagram of primary + auxiliary loop.

In practical systems, the generation of an $\dot{N}_o$ term would be impossible because of the inherent noise present in the signal at the tachometer output. In an attempt to assess the importance of this term, tests were carried out to compare performance with and without this term. To avoid duplication and interaction resulting from two separate loops, the limitation k_2/k_1 = constant was introduced, and this made possible single parameter adjustment.

2.4. Choice of model

There is no general mathematical procedure known to the authors that is available to enable the best choice of the model in the adaptive loop to be made. In the earlier study,[11] it was realised that one possible approach to the optimum choice of the model was to make use of the system's closed-loop transfer function. An approximation to this function was obtained by dividing the numerator into the denominator which provided a second-order equation which was used as the mathematical representation of the model. Without the knowledge of the value of the ratio k_2/k_1, it is not possible to utilise this method to arrive at a suitable model relationship.

Examination of equation (8) suggests that if a correct choice of k_2/k_1 is made, the equation (8) could be reduced to second order and the model characteristics would then be known. One approach to achieve this end is to accept that the natural frequency of the primary engine loop should be that for the model. From experimental results, Fig 8, it was estimated that the natural frequency was 2·15 rads/sec. For the minimisation of the ITAE criterion for the model, a damping factor of 0·7 is necessary. Taking a representative value for the engine natural frequency as 3 rad/s and a damping factor of 0·7, the values of a and b are 9 and 4·2 respectively. To achieve acceptable governing, it was found experimentally that the most suitable values for the coefficients Z_1 and Z_2 should be 0·25 and 0·2 respectively.

Equation (8) becomes:

$$\frac{N_o(s)}{N_i(s)} = \frac{2 \cdot 25s + 1 \cdot 8}{0 \cdot 1s^4 + s^3(1 \cdot 42 + 9k_1) + s^2(5 \cdot 1 + 9k_2) + 1 \cdot 25s + 1 \cdot 8} \quad (9)$$

Considering that there is an order of magnitude difference

high speed

low speed
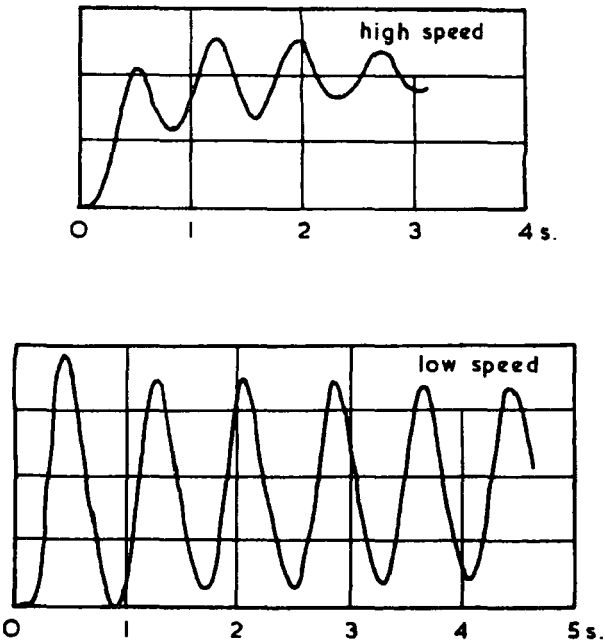
Fig 8 Transient response of primary loop.

2·5 r/s
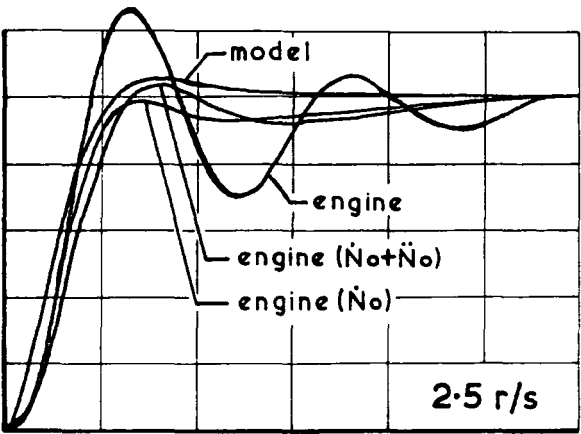
Fig 9 Effect of variation in ω_{nm}.

5·0 r/s
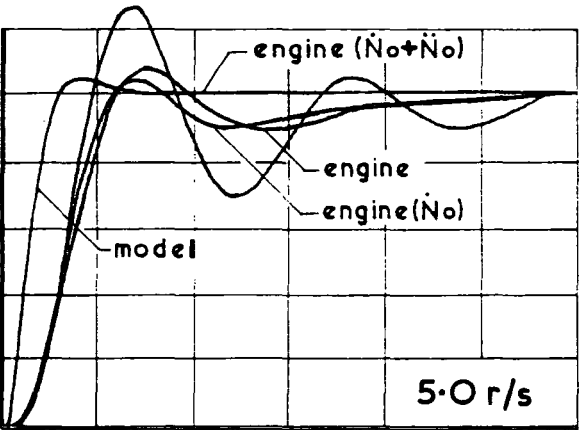
Fig 10 Effect of variation in ω_{nm}.

between the coefficient of s^4 and the other coefficients, it seems reasonable to neglect this term particularly since the engine will not respond to frequencies in excess of 1·5 Hz. If in equation (9) we divide the numerator into the denominator and equate the resulting equation to the model transfer function:

$$\frac{N_m(s)}{N_i(s)} = \frac{4 \cdot 6}{s^2 + 3 \cdot 0s + 4 \cdot 6} \quad (10)$$

the resulting requirements are:

$$(6 \cdot 5 + 41 \cdot 5k_1) \equiv 7 \cdot 4$$

and

$$(23 \cdot 5 + 41 \cdot 5k_2) \equiv 28 \cdot 0$$

From these two equations the values of k_1 = 0·022 and k_2 = 0·11 can be found. Hence using these, a ratio of k_1/k_2 = 0·2 can be established as the optimum value.

3. DISCUSSION

3.1. Design of the adaptive loop

The design procedure in selecting the feedback network associated with the auxiliary loop and the point at which it was closed within the system is given in Section 2.3.

To avoid duplication of equipment within the adaptive loop, a constant value for the ratio k_2/k_1 was chosen. For fixed values of the variable parameter k in the auxiliary loop it is easy by simulation to demonstrate the effectiveness of this loop, Figs 9, 10, 11. In an attempt to improve the system's

Harland and Gill
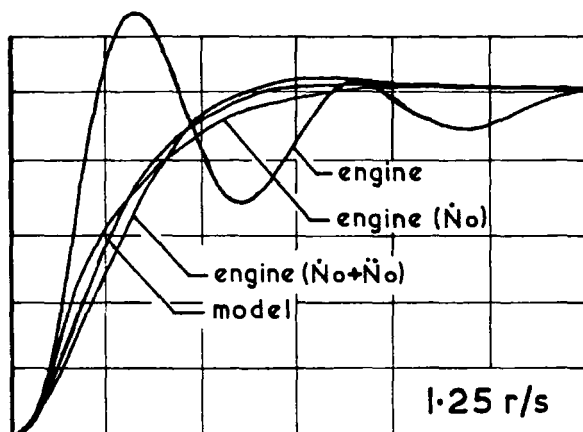
Fig 11 Effect of variation in ω_{nm}.

rise time, the value of the adaptive parameter k was varied but this resulted in little improvement in system initial response as can be seen from Figs 9 and 10. From these it is evident that the damped natural frequency of the engine cannot be altered by changes in the adaptive parameter since this is a function of the system's inertia. The magnitude of the system's inherent damping has been made directly dependent upon the adaptive parameter k. Therefore it is necessary to choose the characteristics of the model as illustrated in Section 2.4 based on a knowledge of the system to which the adaptive loop is to be added in order to achieve optimum system performance.

3.2. Simulation study

The analogue computer circuits used in this study are similar to those shown in Reference 11. To obtain the required gain setting in the auxiliary loop, a quarter square multiplier is used. In a practical system this operation would be provided by a positional servomechanism.

Typical speed response curves for the simulated system including the auxiliary loop are shown in Fig 9 for a value of $k = 0.11$. These curves give an indication of the 'best' possible response achievable and can be used as a measure of the quality of the auxiliary loop. As is expected from inspection of equation (8), the response with both N_o and N_O terms present shows an improvement over the response with only $\dot{N}_o$.
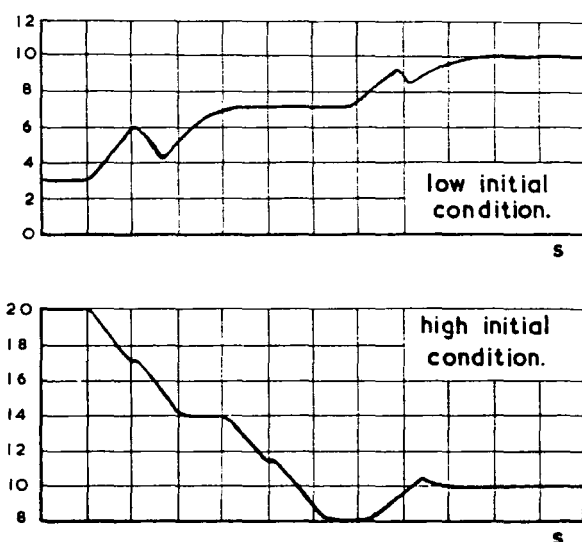
Fig 12 Adaptive behaviour of the variable parameter $k(\dot{N}_O + N_O)$. $S = 100\%$. $F = 0.1$. $\lambda = 0.04$.

For all tests the initial value of the parameter k was chosen so that large changes in its value were necessary and this gave some indication of the quality of the searching technique. Fig 12 shows the progressive change occurring in the parameter k which is representative for both the simulated and actual engine tests.

To achieve a measure of the quality of the response, the values of rise time, percentage first overshoot and settling time in each transient response are listed in the tables for comparison. The ideal values are those of the model: rise time 1.3 sec, percentage first overshoot 6%, settling time 3.5 sec. From Table 1, it is clear that the overshoot is significantly higher (on average 15%–20%) and as a result the rise time is

TABLE 1

Test number	λ	Step Size (%)	ω	Rise time	% Over-shoot	Settling time
1	0.4	50	0.1	1.0	26	4.0
2	0.4	50	0.2	1.0	24	–
3	0.4	100	0.1	1.0	21	4.0
4	0.4	100	0.2	1.0	2?	–
5	0.4	200	0.1	1.0	14	4.0
6	0.4	200	0.2	1.2	14	–
7	0.8	200	0.1	1.3	10	4.9
8	0.8	100	0.1	1.0	15	4.0
9	0.8	50	0.1	0.9	21	5.1
10	0.2	50	0.1	0.9	22	5.8
11	0.2	100	0.1	1.0	25	4.5
12	0.2	200	0.1	1.1	15	4.1

Relay adaption

Test number	λ	Step Size (%)	ω	Rise time	% Over-shoot	Settling time
13	0.2	200	0.1	1.3	8	4.7
14	0.4	200	0.1	1.2	10	5.0
15	0.8	200	0.1	1.1	15	5.9
16	0.2	100	0.1	1.2	10	4.5
17	0.4	100	0.1	1.3	10	4.5
18	0.8	100	0.1	1.3	13	5.0
19	0.2	50	0.1	1.1	16	4.9
20	0.4	50	0.1	1.2	15	5.0
21	0.8	50	0.1	1.3	12	5.2
22		100	0.2	1.4	17	–
23		100	0.1	1.1	7	3.7
24		200	0.1	1.1	9	4.0
25		50	0.1	1.0	14	4.0
26		100	0.2	1.1	1?	–
27		200	0.1	1.0	24	4.5
28		200	0.2	1.4	21	–
29	0.4	100	0.1	1.1	32	4.5
30		100	–	–	–	–
31		50	0.1	1.1	32	4.5
32		50	0.2	1.3	27	–
33		50	0.1	1.1	17	6.0
34		50	0.2	1.5	30	–
35		100	0.1	1.0	28	7.0
36		100	0.2	1.4	24	–
37		200	0.1	1.2	20	7.0
38		200	0.2	1.4	24	–

$\omega_{nm} = 5.0$ $\xi_m = 0.7$

Test number	λ	Step Size (%)	ω	Rise time	% Over-shoot	Settling time
39		200	1.0	1.2	22	5.0
40	0.4	100	1.0	1.0	24	4.5
41		50	1.0	1.1	19	5.2

$\omega_{nm} = 1.25$ $\xi_m = 0.7$

Test number	λ	Step Size (%)	ω	Rise time	% Over-shoot	Settling time
42		50	1.0	4.8	–	4.8
43		100	1.0	4.0	–	4.0
44	0.4	200	1.0	3.5	1.5	5.7
45		200	1.0	5.1	–	5.1
46		100	1.0	5.0	–	5.0
47		50	1.0	4.2	–	4.2

$\omega_{nm} = 5.0$ $\xi_m = 0.7$

Test number	λ	Step Size (%)	ω	Rise time	% Over-shoot	Settling time
48		50	1.0	1.1	16	4.7
49	0.4	100	1.0	1.0	20	4.0
50		200	1.0	1.1	21	4.1

marginally smaller (of the order of 1·0 sec) and the settling time is of the same order. The percentage overshoot, however, is within the recognised limits for acceptability which is normally taken as 25%.

4. CONCLUSION

The simulated study demonstrated that the introduction of an auxiliary loop into the basic speed control system could be used to maintain sensibly constant dynamic system performance. Therefore it seems reasonable to introduce this loop into a practical engine system.

The weakness of this study is the linear modelling of the engine and in future work it would be necessary to upgrade this model to achieve a more accurate representation. The design technique postulated is in line with industrial thinking giving a simple physical arrangement that can be adopted to existing systems with the minimum of system modification.

5. REFERENCES

1. **Shuck, O H.** 'Adaptive Flight Control', Proc 1st IFAC Congress Moscow, 1960, Vol 2, pp 645–650.
2. **Tyler, S R, Ruggles, R, and Welbourn, D B.** 'Theoretical and practical techniques applied to the design of a gas turbine engine governor', Proc 1st IFAC Congress Moscow, 1960, Vol 3, pp 356–362.
3. **Gibson, J E.** 'Making sense out of the adaptive principle', *Control Engng.* 1960, pp 113–119, 109–144, 93–96.
4. **Leondes, C T.** *Modern Control of Theory.* McGraw-Hill, Ch 6, 1965.
5. **Dawson, D A.** 'Analysis and computer study of an adaptive control system', NRCC Mk-4, Sept 1959. Mech Eng Report National Research Council of Canada Mk-4.
6. **Osburn, P V, Whitaker, H P, and Kezer, A.** 'New developments in the design of model reference adaptive control systems', Inst Aerospace Sciences, Paper 61–39, 1961.
7. **Horrocks, T.** 'Investigations into model-reference adaptive control systems', *Proc IEE,* Vol 111, No 11, p 1894, Nov 1964.
8. **Dymock, A J, Meredith, J R, Hall, A, and White, K M.** 'Analysis of a type of model reference adaptive control system'. *IEE,* Vol 112, No 4, 1965, pp 743–753.
9. **Caruthers, F P, and Levenstein, H.** *Adaptive Control Systems,* Pergamon. 1963, pp 1–18.
10. **Milsum, J H.** 'Adaptive control of processes by an economic criterion', Proc 1st IFAC Congress Moscow. 1960, Vol 4, pp 231–240.
11. **Gill, K F, Schwarzenbach, J, and Harland, G E.** 'Design analysis adaptive control systems applied to a gas-turbine aircraft engine'. *Proc. IEE,* Vol 115, No 3, March, 1968.
12. **Harland, G E, Panko, M A, Gill, K F, and Schwarzenbach, J.** 'Pseudo-random signal testing of a diesel engine'. *Control,* Vol 13, No 128, Feb 1969.

PAPER 21

21

Using Correlation Techniques—A Guide for the Practising Engineer

By Captain E. W. Reed (Retd), M.A., C.Eng., M.I.Mech.E., and
Dr. K. F. Gill, B.Sc., M.Sc., Ph.D., C.Eng., M.I.Mech.E., M.I.E.E.

INTRODUCTION

A new technique, making available information that it was once considered impossible to obtain is now, thanks to recent developments in appropriate equipment, being extensively used. The technique is called *correlation analysis*. This short paper attempts to explain correlation analysis in simple terms so that the reader will, at least, understand its capabilities and not be put off by the mystique that invariably surrounds the application of new techniques. The authors predict that within five years correlation analysis will be a standard part of the engineer's art.

Basically, the method allows information to be obtained statistically in the presence of other large extraneous disturbances which normally would completely swamp that which it is hoped to measure. Correlation may be applied to any system; engineering, economic, social or what you will. The authors have used it to measure the sonic velocity of a train of small pressure pulses in a noisy two phase flow system, despite the much larger pressure disturbances present. In this application it enabled valuable information to be obtained that can be used in the study of rocket propulsion systems.[1] As will be evident from the adjoining picture the apparatus is not at all extensive even in a laboratory layout. The authors are seen using the technique they have developed to

The authors (Dr. Gill on the left) using the technique developed by them.

detect, and hence eliminate, resonance effects from a pipe system. Dr. Gill (left) is handling the correlator. The slotted disc (right) revolves to generate a p.r.b.s. (pseudo random binary sequence) disturbance by the appropriate interruption of a fine jet of air directed at the slots.

It is suggested that a recent claim that a bulge in the New York birth rate was directly related to a previous prolonged electricity cut, may in fact have little substance and that a correlation technique properly applied might have revealed this. World wide publicity is more likely to have resulted from the inherent implications associated with such a story rather than from any valid scientific deduction!

MECHANICS OF CORRELATION

The word *correlation* is used to cover both cross-correlation and auto-correlation. Rather than define correlation, which is difficult, a simple example demonstrating the mechanics involved in cross-correlating two signals representing sets of data is given in the first two Figures. If it was desired to auto-correlate, say, the signal given in Figure 1, it would require a duplicate of that signal to be substituted for that in Figure 2 and then for it to be processed as for cross-correlation.

In the context of this paper a *set of data* means any continuously recorded information. This could come from as wide a range of data as blood flow patterns within the human body to vibration and noise problems associated with an armoured fighting vehicle.

Figures 1 and 2 represent parts of wave forms which both have a sequence of what is known as a pseudo random binary sequence, or p.r.b.s. This type of sequence can be particularly useful in correlation work since one of its properties is its simplicity in use and this the example demonstrates. The waveform may have two values which it maintains for a definite interval of time. This interval of time is an exact multiple of an elemental interval of time known as a *bit*. The waveform pattern repeats itself in a periodic manner. Figure 1 shows a p.r.b.s. with levels of 2 or 0 and Figure 2 shows an identical p.r.b.s. but with levels of 1 or 0 and advanced by 5 bits compared with Figure 1. The repeatability period is 15 bits. The aim of the example is to show that by cross-correlating the two waveforms the 5 bit advancement can be clearly determined.

Fig. 1. *A p.b.r.s. with levels of 2 or 0.*   Fig. 2. *A p.b.r.s. with levels of 1 or 0.*

A practical solution, in the form of a *correlogram*, may easily be evolved by following these four simple steps:

1. Cut Figure 2 from the page or, depending on your regard for your copy of the *REME Journal*, copy it onto a separate piece of paper.
2. Place Figure 2 directly under Figure 1. Multiply together a reading on Figure 1 with the corresponding reading on Figure 2. Do this at each bit interval from 1 to 15 inclusive. Add together all the multiplication values so obtained. Because Figure 2 consists only of ones and zeroes the procedure in this particular example is simple and the answer is 6. Plot this value as in Figure 3, which is a correlogram.
3. Shift Figure 2 one bit to the left so that point 1 on Figure 2 corresponds to point 0 on Figure 1. Repeat the calculation, as in 2, again plotting the answer on Figure 3.
4. Repeat this procedure shifting Figure 2 two bits, three bits, and so on.

It is seen that all shifts give an answer of 6, except for a shift of 5 bits when a peak value of 14 appears.

This process of multiplying, adding, and shifting, is the physical interpretation of correlation. This example is a particularly simple one, chosen to demonstrate the mechanics of correlation.

If Figure 1 had represented a totally random set of data and Figure 2 had represented the same basic data,

Fig. 3. *A correlation, developed from Figures 1 and 2.*

but shifted in time, then this time shift could have been detected by cross-correlation.

The amplitude of the correlogram would have been constant except for the case in which the two sets of data exactly coincide, where a large peak would have appeared. To have produced such a correlogram practically, i.e. where the values are random, would have needed at least a thousand pairs of readings. This would have involved two thousand measurements followed by

one thousand multiplications and one thousand numbers all added together to give only one point on the correlogram. A complete correlogram needs about one hundred such points. Fortunately, a first generation of correlators is now being manufactured and these should soon become standard pieces of test equipment. Present prices vary from £600 to £3,600.

CHARACTERISTICS OF CORRELATION

There are certain characteristics of correlation and these may be listed briefly as follows:

1. Two signals *will* cross-correlate (and will only do so) where there is some resemblance one to the other. This is of the utmost significance for it means that information of very small magnitude, which may be swamped in, say, noise or some other large corrupting effect, can be extracted for identification.

2. The time lag of a disturbance travelling between two points can be determined, even if the pattern of the disturbance is distorted in transit.

3. The auto-correlation of a set of data will reveal any periodic behaviour of that data.

4. It may be stated (though this paper does not demonstrate the fact) that a small noise disturbance can be introduced into a system, whilst in full operation, and a cross-correlation between the small noise input and the system output enables the dynamic behaviour of the system to be estimated. This is invaluable information, and necessary for system design. A similar result may be obtained if the noise input is replaced by a small amplitude p.r.b.s. disturbance. This has many advantages in application, the primary one being ease of generation. As with 'correlation' the reader should learn to recognize the term 'p.r.b.s.' for future use.

APPLICATIONS OF THE TECHNIQUE

To date the technique has been used for a wide variety of measurements. It is currently under development as a velocity and flow measuring device since many systems, such as pneumatic transportation of cement or powdered coal, as well as traffic flow systems, present problems which can be effectively tackled in this way.

Professor Towill[2] in this *Journal* last year described a use of the technique in the automatic testing of equipment. He emphasised that testing can be done accurately in the presence of noise and also pointed out the value of using a repetitive pseudo random sequence.

Correlation has been used to predict the stability of a nuclear reactor, though an attempt to predict the next eruption of a volcano, by correlating within its crater, failed because of an untimely eruption prior to the tests being completed. The technique is of course being applied to identify a range of everyday engineering systems such as engines, chemical processes, and machine tool wear.

An obvious application is in security work, where information from a signal can only be obtained if something about the signal is first known. A good example of such an application is in the detection of submarines by sonar located noise. Although ordinary sea noises amount to the 'large extraneous disturbances' referred to in our Introduction, the signal from the submarine would be readily distinguishable, using this technique.

These are but a few of the many practical uses of correlation. Over the next few years the instances of its application are likely to rise rapidly and significantly.

References:

1. Gill, K. F., and Reed, E. W., *A Study into the Use of p.r.b.s. Pressure Disturbances to Measure Sonic Velocity in a Two Phase Flow System.* Proceedings of The Institution of Mechanical Engineers 1972, Vol. 186 39/72.
2. Towill, D. R., *Dynamic Test Techniques Utilized in Automatic Test Equipment.* REME Journal 1972.

PAPER 35

Data collection for plant control studies

D. S. Fenna B.Sc.
Formerly Department of Mechanical Engineering, University of Leeds, Leeds (now Head Wrightson and Co., Ltd., Stockton-on-Tees, Cleveland)

K. F. Gill B.Sc., M.Sc., Ph.D.
Department of Mechanical Engineering, University of Leeds, Leeds

A. Jowett B.Sc., Ph.D., F.I.M.M.
Formerly Department of Mining and Mineral Sciences, University of Leeds, Leeds (now CSIRO Division of Chemical Engineering, Melbourne, Australia)

Synopsis

Over the past few years considerable effort has been made to improve the operation of industrial processes, both existing plant and proposed new designs, by the use of better control devices. This has led to an increasing interest in the measurement of system dynamics — to produce a transfer function model or some equivalent representation. This process, known as system dynamic identification, is a necessary preliminary to the mathematical design of a control scheme.

Among the problems of identifying the dynamics of a plant is that of obtaining valid experimental data. To use the results of such an identification with confidence requires that the data used satisfy certain mathematical criteria. These are highlighted and some guidelines for data collection are given.

No processing plant can be fed and run so consistently as to produce satisfactory products over long periods without some form of control. Even minor variations in quality and quantity of feed can have significant effects, particularly in processes that involve recirculating loads, where the effect of very small variations can be considerable. Control is, therefore, always needed; it can be manual or automatic. On the many plants that operate predominantly on manual control, an operator makes adjustments intuitively, based on tradition and personal experience, and he very rarely knows why.

One often presumes that automatic control, being less subjective, is better than manual control. This presumption is justified only if the automatic control is correctly designed and tailored to the process requirements. There are at least three basic methods used in the development of automatic control systems.

(1) One can make predominantly empirical assumptions about the response characteristics of a unit operation in a plant (as a manual controller does) and install appropriate instrumentation and control loops. This is the type of automatic control that is most likely to fail — generally because the assumptions made about response characteristics are incorrect.

(2) On the basis of a mass of experimental work aimed at elucidation of the fundamentals of a unit operation, one can build a theoretical model of the operation and use this model for the design of the control system. This approach is very long-term, and it has, so far, had some success in only a few instances in the mineral processing industry in predicting changes in steady-state operation. There is very little published work on the dynamics of mineral processing plant.

(3) One can regard the unit operation as a 'black box' and collect input—output data to establish the response characteristics. This, unfortunately, is difficult in the mineral processing field, because there is a lack of measuring instruments capable of successful on-stream operation. In those cases, however, where suitable instruments do exist, data can be collected and analysed by statistical methods to yield equations that represent the response characteristics of the plant. These equations are neither assumed nor theoretical; they are proved empirical relationships, which, when coupled with some basic understanding of the process, can be used with confidence in control system design. This paper is only concerned with the third procedure.

Practical experience of many mineral processing operations indicates that plant response time is short, relative to the times associated with significant changes in quality and quantity of feed (which, generally, is the factor that initiates a need for control). In these circumstances operations are observed to move from one steady state to another, and control measures can be relatively simple, assuming that it is known what new steady-state condition is wanted and how it may be achieved. Roughing operations in froth flotation are a good example of this type of situation. The kinetic response of a mineral to flotation is typically such that recovery will be some 80% complete in 2 or 3 min, whereas even with poorly organized feed arrangements one expects time-periods of some 20 or 30 min for significant feed changes — on account of the smoothing action of bunkering and grinding systems. In consequence, so far as is known, plant test work associated with the development of flotation control systems (as distinct from computer simulation) has been based on the use of step changes in input to establish response characteristics. The errors involved in such testing, which arise from uncontrolled variations and also frequently from sampling errors, necessitate the use of some kind of regression model to express response characteristics; but, within the limits of accuracy of the regression equation, simple control measures will take the plant smoothly from one steady state to another.

At present, very few control systems are working successfully in the mineral processing field.[1,2,3] There are many different reasons for this, among which can be listed (a) the difficulty and/or expense of most on-line measurements; (b) process complexity (e.g. selective flotation of Cu—Pb—Zn—Fe), necessitating many control measures and subsequent unexpected interactions;

Table 1 Data sources

Type of plant	Type of data	Sample interval, record length and type	Comments
Pb—Zn concentrator	Off-line assays, special test	5 min, 8 h, manual	Complex recirculations; sampling points unsuitable for finding simple input—output relationships; sample interval too long, record too short
Cu concentrator, sulphide—oxide	On-line XRF and mass flow rate	5 min, 8 h, pen recorder	Total copper measured; responses confused by different minerals; new installation with teething troubles, hence record too short
Cu—Zn concentrator	On-line XRF and mass flow rate	5 min, 14 h, digital printout	Sampling points located to provide no input—output relationships; figures truncated, sample interval too long
Cu—Zn concentrator	On-line XRF and mass flow rate	5 min, 40 h, digital printout	Complex plant with sampling points unsuitable for finding simple input—output relationships; sample interval too long
Cu—Zn concentrator	On-line XRF and mass flow rate	5 min, 25 h, pen recorder	Complex plant with many interactions; good data except sample interval too long
Sn concentrator	On-line XRF of feed, concentrates and tails	5 min, 16 h, digital printout	Figures truncated; sample interval too long
Sand drier	Input moisture, output temperature	4.5 h, pen recorder	Most data offered do not represent input and output at same time
Cu concentrator	On-line XRF and mass flow rate	5 min, 24 h, digital printout	Some figures truncated; several simple input—output relationships; sample interval too long; some data are computed from different points on the plant
Cu—Ni concentrator	On-line XRF	10 min, 4 days, digital printout	Some figures truncated, sample interval too long; length ideal
Sinter strand feeder	Weigh-feeder demand signal and hopper level	1 sec, 2 h, digital datalogger	Data entirely adequate for dynamic analysis

(c) the extensive use of feedback circuits for repeat processing, which frequently leads to cyclic and surging operation; (d) time-lags, as in bunkering or flow through a large flotation plant;[4,5,6] (e) operator idiosyncracies and interference, especially at the data collection stage; and (f) response time and disturbance time of similar duration.

In general, few systems would not incorporate one or more of these complicating factors.

Obviously, control is impossible if the basic measurements cannot be made. For example, scientific control of plants processing minerals of the low atomic number elements is precluded by the lack of on-line methods of chemical analysis for these elements in the solid state. Even if instruments are available, it is not possible to investigate and implement control measures unless there is full understanding and cooperation on the part of management and staff. Naturally, it is rarely possible to persuade operators to let a plant 'float' so that its response can be measured, especially if the test procedures that involve pulse, step or similar deliberate perturbations are causing detrimental effects.

The other factors mentioned are characteristics inherent in plant design and operation that can easily lead to undesirable behaviour, such as overshoot and 'hunting', unless the dynamic features of a disturbance and its effects are fully understood. Such conditions frequently occur in a multi-stage cleaning section of a froth flotation plant (e.g. acid-grade fluorspar). Such units are often observed to surge (hunt), and the surging is difficult to correct — except when a very experienced operator uses all his expertise to make intuitive adjustments. It is much more difficult to conduct the test work and analyse the data to predict an effective control procedure in such circumstances, where the dynamic characteristics of the plant are of overriding importance. Steady-state testing is not appropriate, as the rate of transition from one steady state to another is of primary importance. Some form of dynamic testing procedure must be used, and this also creates problems in sampling to obtain useful data, and in the analyses of that data.

The 'black-box' approach

On a single input—single output plant, where the natural variations in feed, and consequent product variation, are of sufficient magnitude and suitable form, one can detect from input—output records that a measurable plant response relationship exists (Fig. 1). The problem then reduces to that of analysing such data to identify the dynamic relationship.

In instances where the response to feed variations is not so obvious, usually because the significant feed variations are obscured by miscellaneous unidentified variations (noise), it is necessary to apply analytical techniques[7] to determine the frequency content of these natural variations. The aim is to produce a magnitude—phase—frequency plot from which the dynamic response of the process can be deduced. To do this with confidence each data stream must contain

significant components over a sufficiently wide frequency range: it is usually necessary to perturb the plant feed deliberately to ensure this. Exactly what constitutes a 'significant' component depends
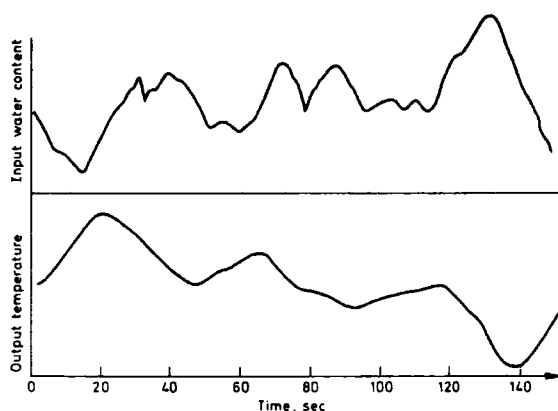
Fig. 1   Typical plant operating record

on the method of data analysis being used; in this context statistical methods are very important, because they facilitate process dynamic analysis by use of very small, deliberately introduced, variations in feed. Research is continuing[8] on the application of statistical methods that can identify the process without any extra disturbance, but it appears that these are unlikely to be applicable to a wide range of plant.

Traditional test procedures that involve deliberately introduced feed variations are based on step, ramp, sinusoidal and pulse signals, followed by relatively simple analysis of output response curves (in steady-state testing the time response is ignored). The variations used for this technique, in most cases, need to be much larger than normal operating variations, so the results may not be representative of normal conditions. In many cases they would need to be larger than management, or even plant, can tolerate, and so these methods cannot be used. An alternative procedure, which at this stage still remains to be proved on processes with a long residence time, is based on statistical analysis of input—output data. A pseudo-random binary sequence (prbs) is a mathematically defined signal,[9] with a wide frequency range, which is used as the deliberate disturbance (Fig. 2).

The magnitude of the prbs need only be small, and normally becomes indistinguishable from the natural variations on chart records. The disturbance pattern, however, imposes itself on the output, but this is also obscured in normal operating records by the inherent natural noise. Nevertheless, when the correct statistical procedure is used to analyse the data, the effect of the unwanted noise is largely eliminated and the response characteristics can be established. The technique involves the analysis of time series by correlation methods.[10,11] The penalty for using a small disturbance is that *it must be applied for a long time*, of the order of 10—100 times the longest holding time of material in the plant, but because the artificial disturbances are not normally detectable in the output, normal operation of the plant is not interrupted.

It is essential to have uninterrupted records over this long period of the variation in a significant feed

attribute, and, simultaneously, to determine the consequent variation in a significant output attribute: for example, X-ray fluorescence (XRF) records of total copper in the feed and tailings of a flotation plant; moisture measurements on feed to a sand drier, and temperature of dry product; and measurements of a metal ion concentration in feed solution and in loaded solvent, in a solvent extraction process. Recordings made while the plant is not operating normally are of no use; nor are data where the 'output' quantity does not depend on the 'input' quantity.

Data collection problems

Mathematical analysis of suitable input—output data records for the evaluation of dynamic characteristics involves, essentially, cross-correlation of the data to arrive at a response curve, followed, if necessary, by Fourier analysis of the response curve to break it down into a family of sinusoidal responses of specified frequency and amplitude.

A normal sampling scheme at a mineral processing plant aims to obtain representative samples from which metallurgical balances can be calculated. Generally, the frequency of sampling is not a critical factor, the aim being to guarantee reasonable representation by collecting an adequate number of increments over, say, one shift. Collection of increments by automatic sampler at perhaps half-hourly intervals to provide a multi-increment average shift sample would be fairly typical.
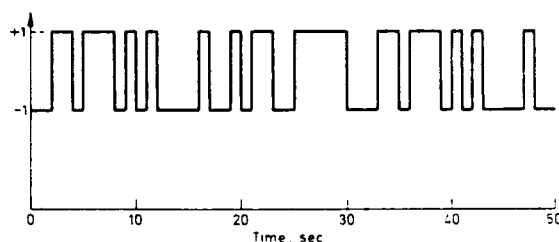
Fig. 2   Example of pseudo-random binary sequence (prbs)

As plant instrumentation has progressed, however, this pattern is changing. Electromagnetic flowmeters, γ-gauge pulp density meters and pH meters (and possibly other electrode meters) supply continuous records, and modern XRF analysers can supply chemical analyses of many pulp streams on about a 5-min cycle time. Figures flow abundantly from a modern well instrumented plant, so either the plant metallurgist can observe change and take immediate (intuitive, manual) corrective action, or they provide the data for computer control, usually via steady-state regression models of the process. So far as is known, little use[4,5,6] has been made of the vast amount of data now being produced on well instrumented plants to investigate in detail dynamic response and to develop dynamic control models. This may be because the data are not suitable, and it will be instructive to look, first, at the problems of data collection for dynamic analysis.

Statistical techniques can only be used in practice on a digital computer because of the computational effort involved. Inevitably, this means working with sampled data, since digital

computers cannot handle continuously varying signals. Any sampling technique will, of necessity, lose some of the information from the continuous signal, and it is therefore essential that care be taken in choosing the sampling rate. (It is assumed that sampling will take place in such a locality and in such a manner that the sample is truly representative of material in that locality at that time.)
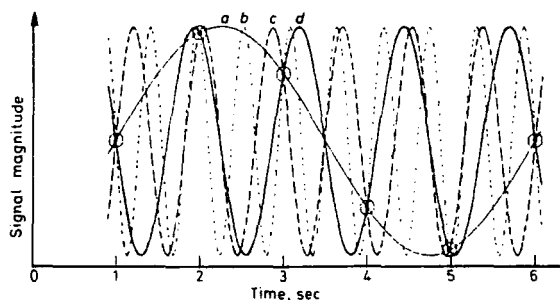

Fig. 3   Four different signals giving same samples

Problems arise because a given series of instantaneous samples can be derived from an infinite number of different continuous signals. Fig. 3 shows how four different sine waves (a, b, c, d) can give the same sampled value if monitored at 1-sec intervals. It is interesting to contemplate that a fortuitously inappropriate sampling frequency on a plant subject to a regular surge (which may not always be easily detected) would give rise to gross errors in a multi-increment sample and a very bad metallurgical balance. This possibility was expected in some recent test work, directed by one of the authors, which aimed to establish steady-state response on a copper concentrator. Under nominal steady-state conditions multi-increment samples were collected manually over a period of several hours from 18 points, the increment collection sequence on each sampling cycle being randomized by computer; some remarkably good metallurgical balances were obtained.[12]
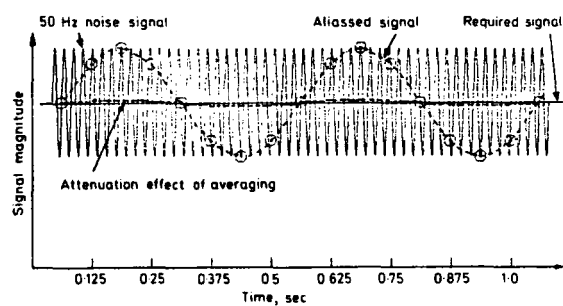
Fig. 4   Examples of aliassing

For the samples to be truly representative of the original signal it must be possible to deduce the original signal from the samples. As is well known in communication theory,[13] this is possible when the sampling frequency is higher than twice the highest frequency component in the signal — this is known as Shannon's rule. In Fig. 3, where the highest frequency wave is 1.8 Hz, sampling faster than 3.6 samples/sec would produce a

different series of samples for each of the four sine waves, and, furthermore, would produce a different series again for any other sine wave up to 1.8 Hz, or any linear combination of such sine waves. The choice of sampling rate is related to the frequency content of the wanted data and the frequency content of the actual signal before sampling.

To study the plant dynamics it is necessary that the recorded data contain components at a large number of frequencies up to several times the reciprocal of the shortest significant holding time of the plant. This gives the value for the wanted data band width; for example, on a flotation bank of average residence time 15 min, the flow frequency could be represented as $1/(15 \times 60)$ Hz(≈ 0.001 Hz); a sampling frequency of 0.005 Hz might suffice: that is, a sample measurement every 3 min (the present limit of a Courier on-line XRF analyser is about a 5-min cycle). Thus, the sampled data would contain all frequencies between 0.005 Hz and zero, but any higher frequencies that may have been present in the original signal would be lost, and would reduce the validity of the reconstructed signal.

In practice, the signal from the plant almost
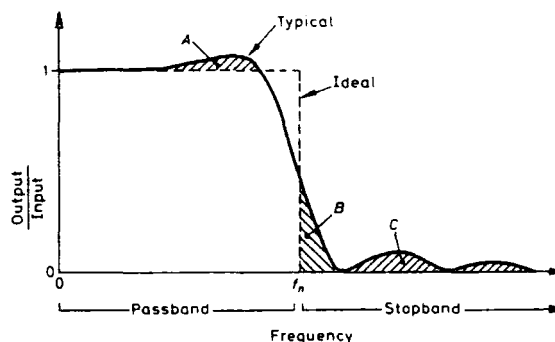
Fig. 5   Low-pass filter characteristics

always contains components that extend to much higher frequencies than the wanted data because of noise pick-up, and this noise must be considered. Where the noise frequency is much greater than the wanted frequencies, it would be a waste of effort to sample at a rate high enough to record the noise accurately, but mere reduction of the sampling rate may give misleading results. Fig. 4 shows how a signal that represents an unvarying quantity, but contaminated with 50-Hz noise, would appear to have a 2-Hz oscillation if sampled at 16 samples/sec. This phenomenon of frequency changing, known as 'aliassing', can only be avoided by removal of the unwanted high-frequency components from the signal by filtering *before* sampling so that Shannon's rule is satisfied. The sampling rate can then be reduced to suit the frequency content of the wanted data. It is not possible to remove the aliassed components after filtering because the filter needs information between samples, as is apparent from Fig. 4.

FILTERING
The purpose of the filter is to remove all signal components that would otherwise be aliassed (i.e. all components with a frequency greater than

$f_n = \frac{1}{2}\Delta t$, where Δt is the time between samples), so its frequency response should approximate to the ideal low-pass characteristic (Fig. 5). Any practical filter will deviate from this; the effects of such deviations depend on the frequencies at which they occur.

Deviations from the ideal in the passband (A) will have a direct effect on the output of the sampler; but, if necessary, it can be compensated for at a later stage. Any deviations in the stopband, however, will admit signal components that will be aliassed to the sampler, e.g. in Fig. 4 the amount of the reduction in amplitude of the apparent 2-Hz component in the sampled signal will be the same as the reduction of the 50-Hz component in the filter. Components in the filter output at frequencies just greater than f_n (region B) will be aliassed into frequencies just less than f_n. Any signal components at substantially higher frequencies that pass through the filter (region C) will cause aliassed components to be added to the results desired; filters with significant lobes in the stopband are therefore particularly unsuitable.

The most straightforward way of achieving this filtering when the signal is available in electrical, continuous form is to use an electronic filter:[14] in its simplest form this consists of a resistance—capacitance network. Analogous arrangements are possible for fluid signals. If the sampler, instead of measuring the instantaneous value of the signal, works by integrating or averaging the signal over a period of time, then this performs a low-pass filter function. Examples of such integrating samplers are pulse counters, some digital voltmeters, γ-gauge pulp density meters and XRF analysers. The low-pass characteristics of integrators are poor, however, in that the attenuation changes only slowly with increasing frequency: it should not be thought that they eliminate the need for a purpose-built unit to filter the instrument input signal. Fig. 4 indicates the result of averaging over each $\frac{1}{16}$-sec sampling period and the 2-Hz variation is still detectable.

A mineral processing circuit exhibits low-pass filter characteristics inherently through the smoothing action of the many large-volume, mixing items of equipment in a typical plant (mills, mixers, flotation banks, thickeners, etc.). Any high-frequency variation in mill feed delivered from a bunker, for example, can be expected to have been eliminated after grinding and classification. Thus, data that originate from measurements on flotation feed (flow rate, pulp density and chemical composition) might be expected to be devoid of high-frequency components other than instrument 'noise', which should be suppressed when the data are recorded.

If the signal already exists in digital form, it may be convenient to use a digital filter.[15,16] Except for very simple cases, it is easier to implement a digital filter to a given specification than the analogue form; in addition, digital filters can be formed for which there is no analogue counterpart.

RECORDING MEDIA
In the simpler installations, the data are usually recorded on strip charts and manually digitized later. It is important to realize that this digitization is a form of sampling, and Shannon's rule must be

satisfied. The samples must be sufficiently close that f_n is greater than the wanted data band width. Any noise on the signal must either be removed by filtering before recording or by taking samples so close that f_n is greater than the noise band width.

Where digital data logging is used, the printout must contain sufficient significant figures to represent the expected smallest significant variations between samples. A specific example of this type of error has been encountered by one of the authors in connexion with output of results from an XRF analyser on a flotation tailings stream. Modern analysers can measure reliably to three significant figures, but on this particular installation a computer printout truncated results to two significant figures. A relative change in tailings grade of about 10% was necessary to register a different computer printout figure — a very substantial change. From the point of view of providing data for dynamic analysis, the truncated printout would lose most of the wanted information, especially when advanced dynamic testing techniques were used, such as pseudo-random statistical perturbations, where very much smaller changes would be significant.

Data analysis
To identify the plant dynamics it is necessary to calculate the frequency spectra of the input—output data to find how the composition of each signal is distributed among the various frequency components and how the plant modifies each component in amplitude and phase. This is done
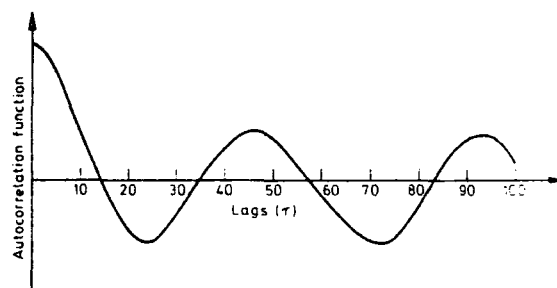
Fig. 6   Auto-correlellogram derived from Fig. 1

by taking the Fourier transform, either directly or via the covariance (correlation) functions (see Appendix 1). There is some redundant information in this process, and this can be used as a check on the reliability of the results, presented as a confidence interval.

The auto-correlellogram (acg) can show up any very strong periodicity directly, without proceeding to the Fourier analysis;[17] Fig. 6 gives the acg of the input data of Fig. 1 and clearly shows an oscillation with a period of 47 sample intervals. The cross-correlellogram (ccg) may also be used directly in some cases. If it is known that the plant dynamics can be adequately represented by a combination of transport lag (flow-through time) and exponential lag (mixing effect), the input acg should be examined to see if it falls to near zero in a time much less than the expected values of total plant lag. If this is so, the plant lag values can be deduced from the ccg (Appendix 2). The prbs is

useful in this technique because it has the required form of acg.

EXAMPLES

The data in Fig. 1 (which originate from a sand drier) were recorded every minute for 2½ h, and the smoothed spectrum (Fig. 7) stems from these
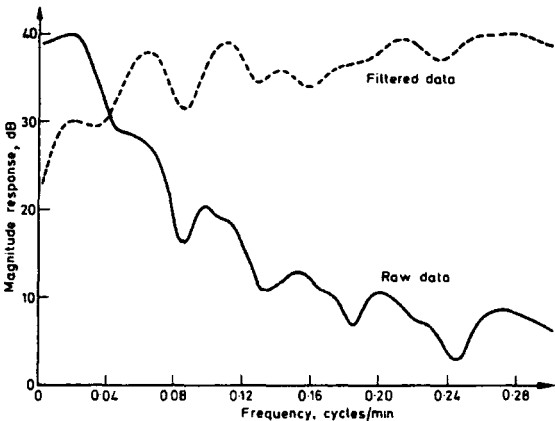

Fig. 7   Comparison of spectra derived from data given in Fig. 1

input data. It is dominated by a component at 0.02 cycle/min, as expected from the acg, and a lesser one at 0.06 cycle/min. If these data were used for dynamic identification, the results would be based almost entirely on the response at these two frequencies, since the other components, which are more than 20 dB lower, contain less than 0.001 of the total response power. For a good spectral estimate some ten components of similar power are required.
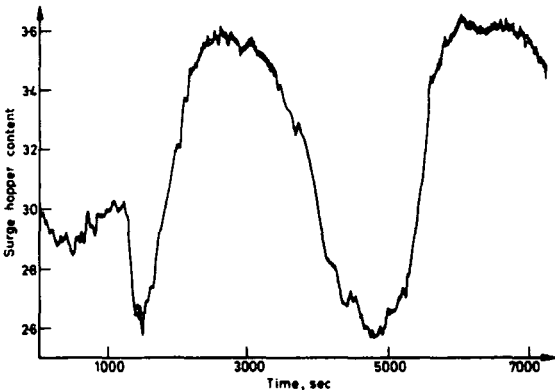
Fig. 8   Plant record: sinter mix in surge hopper

If the response were needed only for low frequencies, say, up to 0.1 cycle/min, spectrum information would be needed at a frequency spacing of about 0.01 cycle/min. With a data record length of only 150 min, however, the maximum resolution obtainable with reasonable confidence[18] is 0.03 cycle/min, and so the data record length is inadequate.

If the whole range of frequencies shown in Fig. 7 is of interest, this resolution is just adequate and it is reasonable to proceed with the frequency response study; but it is still necessary to reduce the relative

contributions of the dominant components. This can be done by digital filtering. If the same filter is applied to both input and output data, no correction of the results because of this filtering is necessary. Fig. 7 shows also the spectrum of the data after a simple filtering operation,[15] and now there are many components of comparable amplitude so a good estimate of plant dynamics up to 0.3 cycle/min would be possible from these data.

Fig. 8 shows a 45-min record at 1-sec intervals of the level of material in a hopper, and Fig. 9 its spectrum after filtration to remove the dominant very low-frequency variations. In this case there is a strong oscillation at about 0.1 Hz in the middle of the required range of frequencies and overshadowing neighbouring frequencies. There was an oscillating feeder operating at this frequency. It may be possible to overcome this overshadowing by digital filtering. Alternatively, if these data
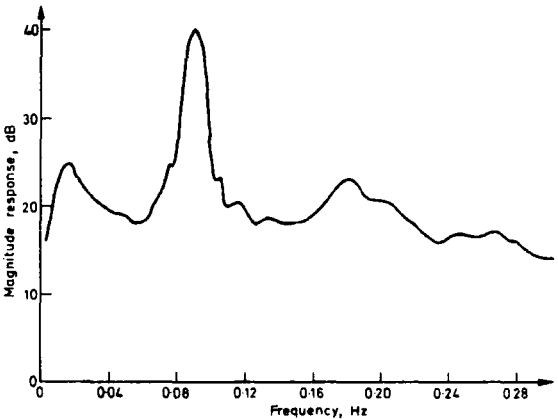
Fig. 9   Spectrum from surge hopper content data

represented the input to a plant, i.e. the natural feed variations, a disturbance such as a prbs could be added to increase the power at all frequencies and thereby reduce the relative contribution of the dominant oscillation.

Conclusion

By reference to various examples that relate to mineral processing it has been shown that several factors need to be considered in the planning of a dynamic identification experiment so that the data collected may be used with confidence to give the required information about plant response characteristics.

The first step is to make an order-of-magnitude estimate of all of the plant's significant time constants and transport lags; in some cases these include characteristics of the data collection system. The reciprocals of these time constants dictate the range of frequencies that needs to be covered by the data recordings, which must extend by a considerable margin above and below the estimated frequency values. In particular, the record length must be at least ten times longer than the longest expected lag in the plant. The maximum frequency leads to the minimum sampling rate. With this information a pilot experiment may be made to assess whether the natural variations have a suitable form, either in the acg, where a dynamically simple plant is being examined, or in

the spectrum for a deeper study. If it is not suitable, digital filtering may be able to make it so; otherwise, it will be necessary to introduce artificial disturbances into the plant and a further pilot study must be made. The pilot experiments may also suggest a change in sampling rate or record length.

Acknowledgement

The observations made in this paper arose from analysis of data from many sources (listed in Table 1). The authors gratefully acknowledge the help of the companies concerned, without which this research would have lost much of its generality.

References

1. Paakkinen V. Kreula S. and Heikkilä S. Computer control of Outokumpu Oy concentrators. In *Tenth Int. Miner. Process. Congr., 1973* Jones M. J. ed. (London: IMM, 1974), 969—82.
2. King R. P. Computer-controlled flotation plants in Canada and Finland. *Rep. natn. Inst. Metall.* no. 1517, 1973, 13 p.
3. Feurings J. H. Control of a grinding circuit using a digital computer. In *Symposium on automatic control systems in mineral processing plants* (Brisbane: Australasian IMM, 1971), 333—57.
4. Jowett A. Use of on-stream analytical data for development of flotation models: a report on a preliminary examination of data from the Chingola concentrator. Internal Report, Dept. of Mining and Mineral Sciences, Leeds Univ., 1971.
5. Jozsa R. O. Lawrence B. R. and Harris R. A. Feasibility of Fluctuating Analysis for Flotation Plant Dynamics Identification AMIRA Symposium on Optimisation and Control of Mineral Processing Plants, Brisbane, 9th July 1974.
6. Mączka W. Sztaba K. and Tumidajski T. Regressive model of actual process of ore beneficiation and its application for building sampling scheme and control algorithm. Paper presented at 11th International Mineral Processing Congress, Cagliari, 1975, no. 37, 10 p.
7. Gustavsson I. Comparison of different methods for identification of linear models for industrial processes. In *IFAC symp. on identification and process parameter estimation* (Prague: Academia, 1970), paper 11.4, 10 p.
8. Gustavsson I. Survey of applications of identification in chemical and physical processes. In *Identification and system parameter estimation, part 1* Eykhoff P. ed. (Amsterdam: North-Holland, 1973), 67—85. *(Proc. 3rd IFAC Symp.)*
9. Roe G. M. Pseudo-random sequences for the determination of system response characteristics: sampled-data systems. *Rep. Res. Lab. General Electric Co.* 63-RL-334-E, 1963.
10. Godfrey K. R. The theory of the correlation method of dynamic analysis and its application to industrial processes and nuclear power plants. *Measurement Control,* 2, 1969, T65—72.
11. Briggs P. A. N. Correlation analysis of process dynamics using pseudo-random binary test perturbations. In *Advances in automatic control* (London: Institution of Mechanical Engineers, 1965), 37—51. *(Proc. Instn. mech. Engrs, 179, 1964—65, pt 3H)*
12. Casson G. Mathematical models of flotation processes. Ph.D. thesis, Leeds University, 1973.
13. Sakrison D. J. *Communication theory* (New York: Wiley, 1968), p. 59.
14. Hilburn J. L. and Johnson D. E. *Manual of active filter design* (New York: McGraw-Hill, 1973), 192 p.
15. Gold B. and Rader C. M. *Digital processing of signals* (New York: McGraw-Hill, 1969), 269 p.
16. Special issue on digital filters: the promise of LSI applied to signal processing. *IEEE Trans., audio electro-acoustics,* AU16, 1968, 301—436.
17. Lee Y. W. *Statistical theory of communication* (New York: Wiley, 1960), chapter 12.

Appendix 1

COVARIANCE FUNCTIONS

A covariance function is a function of time (τ), and is the mean value of the instantaneous product of two time series, of which one is displaced in time ('lagged') by τ. If the two series are the same series, the result is the autocovariance function (acf) of that series; otherwise, it is the cross-covariance function (ccf). The time series are adjusted to zero-mean before the mean lagged product is calculated, in every case. Thus, the ccf of two series $x(t)$, $y(t)$ of length N and means $\bar{x}$, $\bar{y}$ is given by

$$\phi xy(\tau) = \frac{1}{N-\tau} \sum_{t=1}^{N-\tau} \left\{ x(t) - \bar{x} \right\} \cdot \left\{ y(t+\tau) - \bar{y} \right\}$$

The acf has the property that all sinusoidal components in the original series are transformed into cosine terms — hence, its Fourier transform is wholly real and equal to the modulus of the Fourier transform of the original series, i.e. its spectrum. Normally, the acf is calculated to only about one-tenth the length of the original series, and can be modified to yield a smoothed spectrum more easily than by taking the transform of the original series. The smoothed spectrum is more useful for frequency response work. The ccf is similar in that it easily yields a smoothed spectrum, but in this case the relative phase information is preserved (for full text and algorithms see Jenkins and Watts*). It should be noted that to keep computation time within reasonable bounds the routine to calculate covariances must be designed to take maximum advantage of the machine's storage arrangements, and should be written in machine code for maximum efficiency in execution.

The covariance functions are also known as correlation functions, and a correlellogram is a plot of covariance against lag.

Appendix 2

Input data suitable for dynamic analysis have an acg that dies away to near zero at a value of lag small in comparison with the significant plant time constants. For a plant that is adequately represented by a transport lag with an exponential lag, the corresponding ccg will have the form shown in Fig. 1.

Mathematical analysis of the response of such a system when the input has an acg of triangular or similar form, as shown, has revealed that the transport lag value is given by the lag value at which there is greatest slope in the rising part of the ccg (A in Fig. 1), which corresponds to a magnitude of 50—60% of the peak.

The value of the time constant is found by fitting an exponential to the falling part of the ccg, starting at a lag of $C = A + B$, where B is the lag beyond which the acg is approximately zero. A simple estimate may be found by measuring the time taken for the magnitude to fall to 37% of its value at C, but a more accurate method has been described by Simoyu† by use of a logarithmic-magnitude plot. For either of these methods is it important that there is no low-frequency drift on the ccg. It is usually necessary to evaluate sufficient of the ccg to have the exponential

---

*Jenkins G. M. and Watts D. G. *Spectral analysis and its applications* (Holden-Day, Inc., 1968)

†Simoyu M. P. Determination of transfer functions from the time response of linear systems. *Automatica,* 18, pt 1, 1969, 15—23.

part (after C) available for at least four times the plant time
constant, and to draw a revised zero line to which this tail
is asymptotic, as shown at D. As can be seen from the
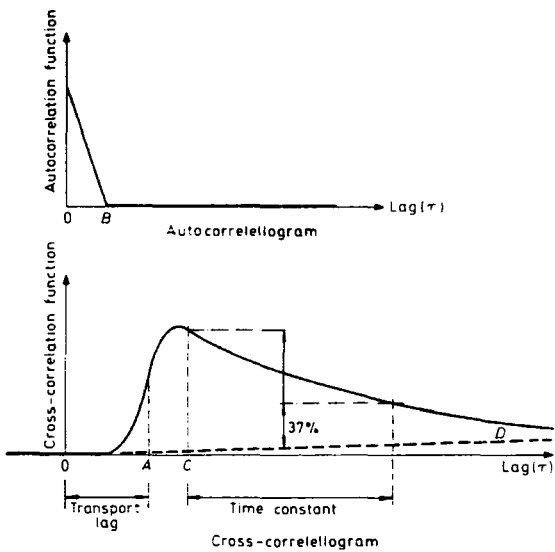mathematical definition of ccf in Appendix 1, the reliability

Fig. 1   Interpretation of correlellograms

of the ccg decreases as lag increases because less data values
are included in the sum, and this is why the data record
needs to be so long.

When the value of exponential lag has been determined,
it should be confirmed that the acg falls to near zero in a
time less than this — otherwise, the results are not reliable.

PAPER 36

The estimation of natural frequencies by use of sturm sequences

G Longbottom * *and K F Gill*†

*Senior Lecturer, Department of Mechanical and Production Engineering, The Polytechnic, Huddersfield
†Senior Lecturer, Department of Mechanical Engineering, University of Leeds

A method is presented which allows the evaluation of natural frequencies and modal shapes from data which is presented in matrix form. The mathematics is understandable by engineers who have only a rudimentary knowledge of matrices. The properties of a Sturm Sequence are used to isolate particular natural frequencies, which are then evaluated to any required numerical accuracy using a bisection technique. The modal shapes are readily evaluated from the computed frequencies. Detailed calculations are included in the appendices to extend the explanation. For those recently introduced to computer programming, a Fortran program is included for reference purposes.

During an investigation [1] into the dynamic behaviour of an engineering structure it was necessary to evaluate the structural undamped natural frequencies from data presented in matrix form. The problem to be solved was described by the set of dynamic equations $M.\ddot{q} + K.q = 0$. The classical assumption of simple harmonic motion was retained and these equations were reduced to $[K - \omega^2 M] \cdot \{q\} = 0$ where K and M are square matrices describing the structural stiffness and mass respectively and q is a normal mode vector corresponding to a natural frequency ω.

Of the solution methods available, that involving the use of a Sturm sequence [2, 3] most adequately satisfied the normal engineering requirements. The published material, however, would be unfamiliar to most practising engineers and hence it is the aim of this paper to present it in a form which will permit the ideas to be readily understood and applied with confidence.

The computational procedure outlined satisfies the following criteria:

1. it permits the evaluation of any or all of the natural frequency values;
2. it allows the evaluation of a particular natural frequency value without recourse to the frequency values previously evaluated and thus eliminates the effect of accumulated errors;
3. the numerical accuracy attained promotes confidence in the subsequently evaluated relative amplitudes of vibration;
4. it is ideally suited for use with small electronic digital computers.

The authors demonstrate in a simple way, the application of the Sturm sequence method in the evaluation of structural natural frequencies, which will give the engineer a physical insight into the solution method. The approach comprises three solution stages:

1. the use of the Sturm sequence property locates a solution region which isolates a particular natural frequency from its immediate neighbours;

2. the subsequent evaluation of the natural frequency to the desired numerical accuracy and

3. the determination of the relative amplitudes of motion. This is repeated for each natural frequency of interest.

Isolation of a natural frequency

The location of the ith natural frequency and its subsequent isolation from the $(i - 1)$th and the $(i + 1)$th natural frequencies is facilitated by the use of the properties of a Sturm sequence [4].

Sturm sequence
The Sturm sequence associated with a particular matrix is a sequence of numbers which comprises the leading principal minors [5] of the matrix. The sequence of leading principal minors of a matrix $[A] = [a_{i, j}]$ is defined by the determinants

$$p_0 = 1, p_1 = a_{1,1}, p_2 = \begin{vmatrix} a_{1,1} a_{1,2} \\ a_{2,1} a_{2,2} \end{vmatrix}, p_3 = \begin{vmatrix} a_{1,1} a_{1,2} a_{1,3} \\ a_{2,1} a_{2,2} a_{2,3} \\ a_{3,1} a_{3,2} a_{3,3} \end{vmatrix}$$

$$\ldots \ldots p_n = |A|$$

In the present context the matrix is $[A] = [K - \omega^2 M]$ where ω is an arbitrarily chosen test value for the natural frequency. The properties of the Sturm sequence formed from this matrix are such that the number of agreements in polarity of consecutive elements of the sequence is equal to the number of natural frequencies greater than the chosen test value. By repeated use using different test values for ω, the solution region may be monitored and part of that region containing only the frequency of immediate interest may be located. The procedure is demonstrated numerically in Appendix 1.

Practical application of the Sturm sequence
Two factors emerge from the calculation given in Appendix 1:

1. for matrices of order n, the number of determinants calculated is $(n - 1)$, their orders increasing from 2 X 2 to n X n and

2. the numerical values of the elements of the sequence are unimportant, the polarity only being required to indicate the number of agreements in sign.

Diagonalization [5] of the $[K - \omega^2 M]$ matrix initially, using a Gaussian type reduction procedure, permits the evaluation of the number of sign agreements without the necessity of numerically evaluating the determinants. For numerical stability, it is desirable that a pivoting arrangement be introduced.

The suggested procedure consists of $(n - 1)$ major steps as follows: In the first major step, the leading diagonal element having the largest numerical value is determined by inspection. If this is term $a_{r, r}$, then rows 1 and r are interchanged followed by the interchange of columns 1 and r. Gaussian reduction then reduces each of the coefficients of the off-diagonal elements in the first column to zero by subtracting multiples of the new row 1 from each row in turn. A counting procedure commencing at zero is now introduced, if $a_{1,1}$ is positive the running total count becomes 1, otherwise it remains at zero. This completes the first major step.

The second major step is a repetition of the first except that the first row and column is excluded from the operation. If, after any interchanges of rows and columns, the value of $a_{2,2}$ is positive, the running total count is increased by one.

This procedure is repeated to complete the $(n - 1)$ steps, a further row and column being

excluded from the operation at each stage. At the conclusion of the reduction process, the value of the running count is equal to the number of natural frequencies numerically greater than the chosen test value. This is so since the consecutive elements in the Sturm sequence are now

$$p_0 = 1, p_1 = a_{1,1}, p_2 = a_{1,1} \cdot a_{2,2}, p_{3,3} = a_{1,1} \cdot a_{2,2} \cdot a_{3,3}, \ldots,$$

$$p_{r,\,r} = a_{1,1} \cdot a_{2,2} \cdot \ldots a_{r,\,r}, \ldots, p_{n,\,n} = a_{1,1} \cdot a_{2,2} \cdot \ldots a_{n,\,n}$$

and the polarity of any element relative to the preceding element is dependent on the polarity of the last term in its expression. The numerical values of the various elements of the Sturm sequence are not required in this context. In general, at the commencement of the evaluation of the natural frequencies for a particular structure the order of magnitude of the numerical values of ω is not necessary since repeated application of the Sturm sequence routine will isolate the region or regions in which the natural frequencies lie without recourse to engineering intuition. Initially, a wide band of trial frequency values will be used. In subsequent runs this will be reduced until an individual value is isolated from its neighbours. Appendix 5 lists a Fortran sub-program written to apply the above whilst Appendix 2 gives a numerical application.

Evaluation of a natural frequency

The bisection technique used by the authors was adopted to permit the evaluation of a natural frequency to a desired degree of numerical accuracy within the arithmetic range of the computation equipment.

Bisection procedure

A solution space bounded by the selected upper and lower values ω_1 and ω_2 containing a single natural frequency will result from the application of the Sturm sequence procedure outlined earlier.

The determinants $|K - \omega_1^2 . M|$ and $|K - \omega_2^2 . M|$ will be of opposite polarity.

One of the determinants will be of opposite polarity to a third determinant $|K - \omega_3^2 . M|$ where $\omega_3 = 0.5 (\omega_1 + \omega_2)$. In this way, the frequency bandwidth enclosing the required natural frequency may be repeatedly halved until its width is such that adequate numerical accuracy is achieved.

Using this technique, the number of bisections can be predicted knowing the initial and final bandwidths.

Practical application

The polarity of a determinant $|K - \omega . M|$ is most easily determined by inspection of the polarities of the leading diagonal elements of the matrix after diagonalization, an odd number of negative elements correspond to a negative determinant whilst an even number of negative elements correspond to a positive determinant. Where a digital computer is to be programmed to apply the Sturm sequence property and the subsequent bisection routine, it is convenient to incorporate both within the one program, the bisection routine being triggered by the detection of a pair of frequency values which enclose a single frequency value. The diagonalization would apply equally to the Sturm sequence and the bisection procedures, the difference being in the interpretation of the polarities of the leading diagonal elements.

Appendix 3 illustrates the above with a numerical calculation.

Relative amplitudes of vibration

The column vector is evaluated, depending on the accuracy of the natural frequency value, either by direct calculation or by the use of an iteration technique.

Direct calculation method

The evaluation of a normal mode shape corresponding to a known exact natural frequency requires the solution of the set of equations

$$[K - \omega^2 . M] . \{q\} = 0$$

This is readily achieved by first reducing the dynamic matrix to upper triangular form using Gaussian elimination with pivoting procedures. The pivoting reorders the elements of the vector. To monitor these changes, a dummy column coefficient matrix having elements whose values are $1, 2, 3, 4 \ldots, n$ is used. Elements of the matrix are interchanged during the Gaussian reduction process.

The vector in its reordered form is evaluated element by element. To demonstrate this procedure simply, a 4 × 4 reduced matrix example is given as follows

$$\begin{bmatrix} a_{1,1} & a_{1,2} & a_{1,3} & a_{1,4} \\ 0 & a_{2,2} & a_{2,3} & a_{2,4} \\ 0 & 0 & a_{3,3} & a_{3,4} \\ 0 & 0 & 0 & a_{4,4} \end{bmatrix} . \begin{Bmatrix} q_1 \\ q_2 \\ q_3 \\ 1 \end{Bmatrix} = 0$$

Note that the final term q_4 has been assigned the arbitrary value of unity is $q_4 = 1$.

For an exact value of natural frequency, the term $a_{4,4}$ will be zero. For an inexact value of ω, the term $a_{4,4}$ will have a small numerical value compared with the other non-zero terms in the matrix.

The vector terms are evaluated in turn commencing with q_3 as follows

$$q_3 = - \frac{a_{3,4} . 1}{a_{3,3}}$$

$$q_2 = - \frac{(a_{2,3} . q_3 + a_{2,4} . 1)}{a_{2,2}}$$

$$q_1 = - \frac{(a_{1,2} . q_2 + a_{1,3} . q_3 + a_{1,4} . 1)}{a_{1,1}}$$

The elements of the column vector may now be repositioned to the original order by reference to the dummy column matrix elements. They may also be normalized as required.

Effect of an approximate natural frequency value

It has been shown [6] that with some inexactness in the value of ω, considerable errors can be introduced into the vector $\{q\}$ using the procedure outlined above.

However, it has been shown [6] that this can be overcome by using an iteration scheme which can be written in the form

$$[K - \omega^2 . M] . \{_{r+1} q\} = [K] . \{_r q\}$$

where $\{_r q\}$ is a trial vector and $\{_{r+1} q\}$ is a more exact vector. If it is decided that this refinement is to be adopted on a particular occasion, it is suggested that the vector $\{_1 q\}$ be evaluated as indicated above.

Again it is recommended that the dynamic matrix $[K - \omega^2 . M]$ should be reduced to upper triangular form to facilitate the operation.

It should be noted that as the value of ω approaches the exact value of the natural frequency the value of $a_{n,n}$ also approaches zero with the pivoting scheme which has been adopted. This precludes the evaluation of the vector element q_n. In these circumstances, the value of $a_{n,n}$ may be replaced by an arbitrarily chosen small value of say $10^{-15} \cdot a_{(n-1),(n-1)}$.

It can be further noted that when this occurs, the errors introduced by the inexactness of the ω value will necessarily be small. This will reduce the necessity to use the iteration scheme.

Not more than two iterations should be necessary to correct even a very approximate initial vector.

Appendix 4 gives a numerical illustration of the above.

Conclusions

The authors have outlined a procedure for the evaluation of natural frequencies and normal modes which they have found to be both useful and convenient to operate. The elementary mathematical ideas permit practising engineers to monitor the various stages in a problem solution. In practice, with the accuracies of numerical evaluation used by the authors (of the order of 0.1 per cent) they have found the iteration scheme outlined above to be unnecessary. However, if the interest is in the mode shape rather than the natural frequency, this can be obtained accurately without recourse to an accurate value for the natural frequency.

References

[1] LONGBOTTOM G, Dynamic modelling of structural frames, MPhil thesis, Leeds University, 1973.

[2] GUPTA K K, Free vibrations of single branch structural frames, *JInst Maths Applics*, 5, p 351, 1969.

[3] GUPTA K K, Solution of Eigenvalue Problems by Sturm Sequence Method, *Int Journal for Num Methods in Eng*, 4, p 379–404, 1972.

[4] WILKINSON J H, *The Algebraic Eigenvalue Problem*, Oxford University Press, p 300, 1965.

[5] AYRES F, *Matrices*, Schaum Pub Co, 1962.

[6] WILKINSON J H, *The Algebraic Eigenvalue Problem*, Oxford University Press, p 315, 1965.

Appendix 1

Consider a cantilever beam carrying three concentrated masses represented by the matrices.

$$[K] = \begin{bmatrix} 800 & 600 & 0 \\ 600 & 800 & 300 \\ 0 & 300 & 600 \end{bmatrix} \text{ and } [M] = \begin{bmatrix} 2 & 0 & 0 \\ 0 & 1 & 0 \\ 0 & 0 & 1 \end{bmatrix}$$

An arbitrarily chosen value of $\omega^2 = 0$ gives

$$[K - \omega^2 . M] = \begin{bmatrix} 800 & 600 & 0 \\ 600 & 800 & 300 \\ 0 & 300 & 600 \end{bmatrix}$$

for which the Sturm sequence is

$$p_0 = 1, p_1 = 800, p_2 = 280\,000, p_3 = 52\,800\,000$$

Since each of three pairs of consecutive terms in the sequence is of the same polarity, there are three natural frequencies greater than the chosen value of $\omega^2 = 0$
Similarly, for a value $\omega^2 = 100$

$$[K - \omega^2 .M] = \begin{bmatrix} 600 & 600 & 0 \\ 600 & 700 & 300 \\ 0 & 300 & 600 \end{bmatrix}$$

and the Sturm sequence is

$$p_0 = 1, p_1 = 600, p_2 = 60\,000, p_3 = -24\,000\,000$$

There are two agreements in sign of pairs of members of the sequence (p_0, p_1) and (p_1, p_2) indicating that there are two natural frequencies numerically larger than $\omega^2 = 100$.
Again for $\omega^2 = 1000$, the dynamic matrix is

$$[K - \omega^2 .M] = \begin{bmatrix} -1200 & 600 & 0 \\ 600 & -200 & 300 \\ 0 & 300 & -400 \end{bmatrix}$$

and the Sturm sequence is

$$p_0 = 1, p_1 = -1200, p_2 = -120\,000, p_3 = 1\,320\,000$$

Only one pair of terms (p_1, p_2) have polarity agreement. Therefore only one natural frequency is numerically greater than $\omega^2 = 1000$. Summarizing, the fundamental natural frequency lies in the solution space $\omega^2 = 0$ to $\omega^2 = 100$, the first harmonic lies between $\omega^2 = 100$ and $\omega^2 = 1000$ and the second harmonic lies above $\omega^2 = 1000$.

Appendix 2
Consider again the situation detailed in Appendix 1 and use a trial value $\omega^2 = 100$. Then

$$[K - \omega^2 .M] = \begin{bmatrix} 600 & 600 & 0 \\ 600 & 700 & 300 \\ 0 & 300 & 500 \end{bmatrix}$$

Operation 1. Inspect the elements on the leading diagonal to determine the largest numerical value ie $a_{2,2} = 700$.

Operation 2. Interchange rows 1 and 2 to give

$$[K - \omega^2 .M] = \begin{bmatrix} 600 & 700 & 300 \\ 600 & 600 & 0 \\ 0 & 300 & 500 \end{bmatrix}$$

Operation 3. Interchange columns 1 and 2 to give

$$[K - \omega^2.M] = \begin{bmatrix} 700 & 600 & 300 \\ 600 & 600 & 0 \\ 300 & 0 & 500 \end{bmatrix}$$

Operation 4. Reduce the off-diagonal elements in column 1 to zero using Gaussian reduction

$$[K - \omega^2.M] = \begin{bmatrix} 700 & 600 & 300 \\ 0 & 85.7 & -257 \\ 0 & -257 & 371.4 \end{bmatrix}$$

The procedure is now repeated with row 1 and column 1 excluded:

Operation 1. Maximum numerical value on leading diagonal is $a_{3,3} = 371.4$

Operation 2. Interchange rows 2 and 3

$$[K - \omega^2.M] = \begin{bmatrix} 700 & 600 & 300 \\ 0 & -257 & 371.4 \\ 0 & 85.7 & -257 \end{bmatrix}$$

Operation 3. Interchange columns 2 and 3

$$[K - \omega^2.M] = \begin{bmatrix} 700 & 300 & 600 \\ 0 & 371.4 & -257 \\ 0 & -257 & 85.7 \end{bmatrix}$$

Operation 4. Gaussian elimination of $a_{2,3}$ gives

$$[K - \omega^2.M] = \begin{bmatrix} 700 & 300 & 600 \\ 0 & 371.4 & -257 \\ 0 & 0 & -92.2 \end{bmatrix}$$

The triangularization is now complete. Inspection of the leading diagonal indicates two positive terms which give two agreements in sign of adjacent terms in the Sturm sequence and hence there are two natural frequencies numerically greater than (and one natural frequency less than) the chosen value of $\omega^2 = 100$.

The Sturm sequence is

$$p_0 = 1, p_1 = 700, p_2 = 700 \times 371.4, p_3 = -700 \times 371.4 \times 92.2$$

Appendix 3

In Appendix 1 it was shown that the first harmonic frequency lay in the space between $\omega^2 = 100$ and $\omega^2 = 1000$.

For $\omega^2 = 100$

$$[K - 100.M] = \begin{bmatrix} 600 & 600 & 0 \\ 600 & 700 & 300 \\ 0 & 300 & 500 \end{bmatrix} = \begin{bmatrix} 700 & 300 & 600 \\ 0 & 371.4 & -257 \\ 0 & 0 & -92.2 \end{bmatrix}$$

One negative term on the leading diagonal indicates that $|K - 100M|$ is negative.
For $\omega^2 = 1000$

$$[K - 1000M] = \begin{bmatrix} -1200 & 600 & 0 \\ 600 & -200 & 300 \\ 0 & 300 & -400 \end{bmatrix} = \begin{bmatrix} -1200 & 0 & 600 \\ 0 & -400 & 300 \\ 0 & 0 & 335 \end{bmatrix}$$

Two negative terms on the leading diagonal indicates that $|K - 1000M|$ is positive.
Using the bisection procedure, a trial value of $\omega^2 = 0.5 \, (100 + 1000)$ is introduced to give

$$[K - 550M] = \begin{bmatrix} -300 & 600 & 0 \\ 600 & 250 & 300 \\ 0 & 300 & 50 \end{bmatrix} = \begin{bmatrix} -300 & 600 & 0 \\ 0 & 1450 & 300 \\ 0 & 0 & -121 \end{bmatrix}$$

Two negative terms on the leading diagonal shows that the determinant is positive and therefore the required natural frequency lies between $\omega^2 = 100$ and $\omega^2 = 550$.
Subsequent trial values of ω^2 and the corresponding determinant polarities are listed below

Frequency	325	438	494	522	543	540	542	541
Polarity	−	−	−	−	+	−	+	−

Therefore $541 < \omega^2 < 542$ and $23.26 < \omega < 23.28$

Appendix 4

For a value $\omega^2 = 541$, the equations to be solved (according to the direct calculation method) are

$$[K - 541M] \cdot \{q\} = \begin{bmatrix} -282 & 600 & 0 \\ 600 & 259 & 300 \\ 0 & 300 & 59 \end{bmatrix} \cdot \begin{Bmatrix} q_1 \\ q_2 \\ q_3 \end{Bmatrix} = 0$$

During the triangularization, no reordering of the rows and columns is necessary. The equations become as follows

$$\begin{bmatrix} -282 & 600 & 0 \\ 0 & 1535.6 & 300 \\ 0 & 0 & 0.39 \end{bmatrix} \cdot \begin{Bmatrix} q_1 \\ q_2 \\ 1 \end{Bmatrix} = 0$$

when q_3 is assigned unity value. Then

$$q_2 = -\frac{300 \times 1}{1535.6} = -0.195$$

$$q_1 = -\frac{600 \times 0.195}{282} = -0.4157$$

The vector is $\begin{Bmatrix} q_1 \\ q_2 \\ q_3 \end{Bmatrix} = \begin{Bmatrix} -0.4157 \\ -0.1954 \\ 1.0 \end{Bmatrix}$

To indicate the effect of the iterative procedure outlined above using $\omega^2 = 541$, evaluate $\{_2q\}$ from the equations

$$[K - 541.M] \cdot \{_2q\} = [K] \cdot \{_1q\}$$

$$\begin{bmatrix} -282 & 600 & 0 \\ 600 & 259 & 300 \\ 0 & 300 & 59 \end{bmatrix} \cdot \begin{Bmatrix} q_1 \\ q_2 \\ q_3 \end{Bmatrix} = \begin{bmatrix} 800 & 600 & 0 \\ 600 & 800 & 300 \\ 0 & 300 & 600 \end{bmatrix} \cdot \begin{Bmatrix} -0.4157 \\ -0.1954 \\ 1.0 \end{Bmatrix}$$

Triangularization gives

$$\begin{bmatrix} -282 & 600 & 0 \\ 0 & 1535.6 & 300 \\ 0 & 0 & 0.3908 \end{bmatrix} \cdot \begin{Bmatrix} q_1 \\ q_2 \\ q_3 \end{Bmatrix} = \begin{bmatrix} 800 & 600 & 0 \\ 2302.1 & 2076.6 & 300 \\ -449.7 & -105.7 & 541.4 \end{bmatrix} \cdot \begin{Bmatrix} -0.4157 \\ -0.1954 \\ 1.0 \end{Bmatrix} = \begin{bmatrix} -449.7 \\ -1062.6 \\ 749.0 \end{bmatrix}$$

whence $q_3 = 1916, q_2 = -374.4, q_1 = 796.6$

giving a vector $\{q\} = \begin{Bmatrix} -0.4157 \\ -0.1954 \\ 1.0 \end{Bmatrix}$

No change in the coefficient values is apparent. In fact, the values only change in the seventh significant figure.

However, if a natural frequency value of $\omega^2 = 500$ be used ie a value having an error of approximately 8 per cent we may evaluate the vector as follows. The initial vector is obtained from

$$\begin{bmatrix} -200 & 600 & 0 \\ 600 & 300 & 300 \\ 0 & 300 & 100 \end{bmatrix} \cdot \begin{Bmatrix} q_1 \\ q_2 \\ 1 \end{Bmatrix} = 0$$

After triangularization we may evaluate

$q_2 = -0.142$ (compare with -0.195 previously calculated)

$q_1 = -0.423$ (compare with -0.415 previously calculated)

The iteration scheme based on

$$\begin{bmatrix} -200 & 600 & 0 \\ 600 & 300 & 300 \\ 0 & 300 & 100 \end{bmatrix} \cdot \begin{Bmatrix} q_1 \\ q_2 \\ q_3 \end{Bmatrix} = \begin{bmatrix} 800 & 600 & 0 \\ 600 & 800 & 300 \\ 0 & 300 & 600 \end{bmatrix} \cdot \begin{Bmatrix} -0.428 \\ -0.142 \\ 1.0 \end{Bmatrix}$$

gives after reduction and evaluation a vector

$$q = \left\{ \begin{array}{c} -0.413 \\ -0.192 \\ 1.0 \end{array} \right\}$$

The coefficient values for q_1 and q_2 are, after one iteration, accurate to 0.63 per cent and 1.7 per cent respectively using a ω^2 value which is in error by 8.2 per cent.

Appendix 5

A computer subprogram written for use with an IBM 1130 machine to use the Sturm Sequence property in the location of natural frequency values is listed below.

```
      SUBROUTINE STURM (C, N, X)
C     THIS PROGRAMME APPLIES THE STURM SEQUENCE PROPERTY TO A
C     DYNAMIC MATRIX C OF ORDER N FORMED USING A NATURAL FREQUENCY
      TRIAL VALUE X.
      DIMENSION C (20, 20)
      RES=0.0000001
      JCOUN=0
      JZERO=0
      N1=N-1
      DO 1 I=1,N1
      AM=0.0
      DO 3 J=I, N
      IF (ABS(C(J,J)-AM) 3, 3, 2
2     AM=ABS(C(J,J))
      K=J
3     CONTINUE
      IF (K-I) 4, 5, 4
4     DO 6 J=I,N
      AM=C(J,K)
      C(J,K)=C(J,I)
6     C(J,I)=AM
      DO 7 J=I,N
      AM=C(K,J)
      C(K,J)=C(I,J)
7     C(I,J)=AM
5     IF (ABS(C(I,I))-RES) 8, 10, 10
8     JZERO=1
      GOTO 9
10    IF (C(I,I)) 12, 12, 11
11    JCOUN=JCOUN+1
12    I1=I+1
      DO 1 J=I1,N
      AM=C(J,I)/C(I,I)
      DO 1 K=I1,N
1     C(J,K)=C(J,K)-C(I,K)XAM
      IF (ABS(C(N,N)-RES) 13, 14, 14
13    JZERO=2
      GOTO 9
14    IF (C(N,N)-RES) 9, 15, 15
15    JCOUN=JCOUN+1
9     CONTINUE
      IF (JZERO-1) 23, 24, 23
```

```
23   WRITE (5, 103) X,JCOUN
103  FORMAT ('THE NUMBER OF NATURAL FREQUENCIES GREATER THAN', F12.6,
     1 'IS', I4)
     GOTO 21
24   IF (JZERO-2) 26, 25, 26
25   WRITE (5, 104) X
104  FORMAT (F12.6, 'IS A NATURAL FREQUENCY')
     GOTO 21
26   IF (JZERO-1) 21, 27, 21
27   WRITE (5, 105) X,JCOUN
105  FORMAT ('THE NUMBER OF NATURAL FREQUENCIES GREATER THAN',F12.6,
     1 'IS AT LEAST', I4)
21   CONTINUE
     RETURN
     END
```

PAPER 45

Controlling systems with long time delays using pole-positioning technique and optimal-linear-regulator theory

by S. M. M. Badrah* and K. F. Gill†

A method is described for control of plants with long transportation lags. This is achieved by making use of the design advantages offered by optimal-linear-regulator theory and the pole-positioning technique. The system states required by the state-vector feedback algorithm are obtained from a Luenberger observer, thus eliminating the need for specific plant instrumentation to implement the scheme. To demonstrate the proposed ideas, a sinter plant model is used in the case study presented.

1. Introduction

Many industrial processes contain significant amounts of dead time, owing to the transportation of materials from one point in a process to another, without any change occurring in the properties or characteristics of the material. The additional design problems to be overcome resulting from the presence of dead time are a reduction in the size of the stability region (Abou El-Nasr, 1980) and an inherent deterioration in transient behaviour.

The characteristic equation is no longer algebraic but a transcendental equation containing the exponential term representing the transportation lag, hence most of the well known control-algorithm design methods normally employed in industry are not applicable. In order to avoid a trial and observation design procedure and to minimise dependency on simulation studies, a method is presented based on positioning the roots of the characteristic equation. The computational techniques used in the evaluation of the weighting matrices associated with the proposed control algorithm are well documented and readily available (Anderson & Moore, 1971; Kalman, 1964; Kuo, 1975; and Wonham, 1967).

The advantage of this method is that it gives a systematic design approach and choosing the position of the roots of the characteristic equation does guarantee system stability within the bounds of the physical constraints which are made.

The procedure for the design of the control algorithm is fully detailed by Badrah (1981) and this paper simply outlines the general approach behind the method. The computer programs necessary to apply these ideas directly are also fully documented by Badrah (1981). Typical system responses for a 3-term controller and a Smith's predictor algorithm are included to indicate the improvement in response which can be achieved.

A brief description of the plant is given so that the reader not familiar with the process employed in the case

study can gain some physical understanding of the control problems to be overcome.

2. Sintering process

The sintering process is illustrated schematically in Fig 1. It consists mainly of mixing iron-ore fines and other appropriately sized materials (limestone and/or dolomite) with coke breeze as a solid fuel. Water is added to moisten the fines in order to help with the agglomeration process and to impart permeability to the mix. A further increase in the permeability is gained by rolling the mix in revolving drums, known as nodulising drums, prior to the actual sintering process, which involves igniting the mix layer by layer. Air is drawn through the mix, and the hot gases leaving the combustion zone will dry and preheat the successive layers before ignition. In the combustion zone itself, bonding takes place between the grains and a strong agglomerate is formed.

When the combustion reaches the base of the mix, the process is complete, and the sinter is broken up, cooled and screened. The undersize sinter (that return fines) is recycled to be used as a component of the raw-materials feed to increase the initial permeability of the mix; the remaining sinter, or product, is ready to be used in the blast furnace.

In a sinter plant, the adjustment of the material flow rate must be synchronised with the sinter strand speed. The transportation time of the material on its way from the storage bins to the sinter strand amounts to several minutes. If it were physically possible, and economically sound, to increase the hopper size significantly to neutralise the dead-time effect, the increased compression at the lower levels in in the bin would reduce the raw feed permeability severely at discharge to the strand. This alone would lead to an appreciable reduction in the commercially viable product yield from the plant; hence the demand for improved bin level control in high production sinter plants.

3. Control-algorithm design

In order to obtain a state-vector representation of the sinter plant, which is essential for the design procedure presented, the transfer function must be expressed as a rational polynomial in the Laplace operator 's'. To achieve this, an approximation for the transportation lag has to be adopted. A second-order Padé approximation was chosen, after inspection of a series of transient responses, typically Fig 2, which the authors believe is an adequate representation for the design approach adopted. Several methods are discussed by Badrah (1981) for the evaluation of a reduced-order transfer function for this exponential term.

* Lecturer in Mechanical Engineering Department Helwan University, Cairo, Egypt. † Senior Lecturer in Mechanical Engineering Department, University of Leeds, Leeds LS2 9JT, UK.
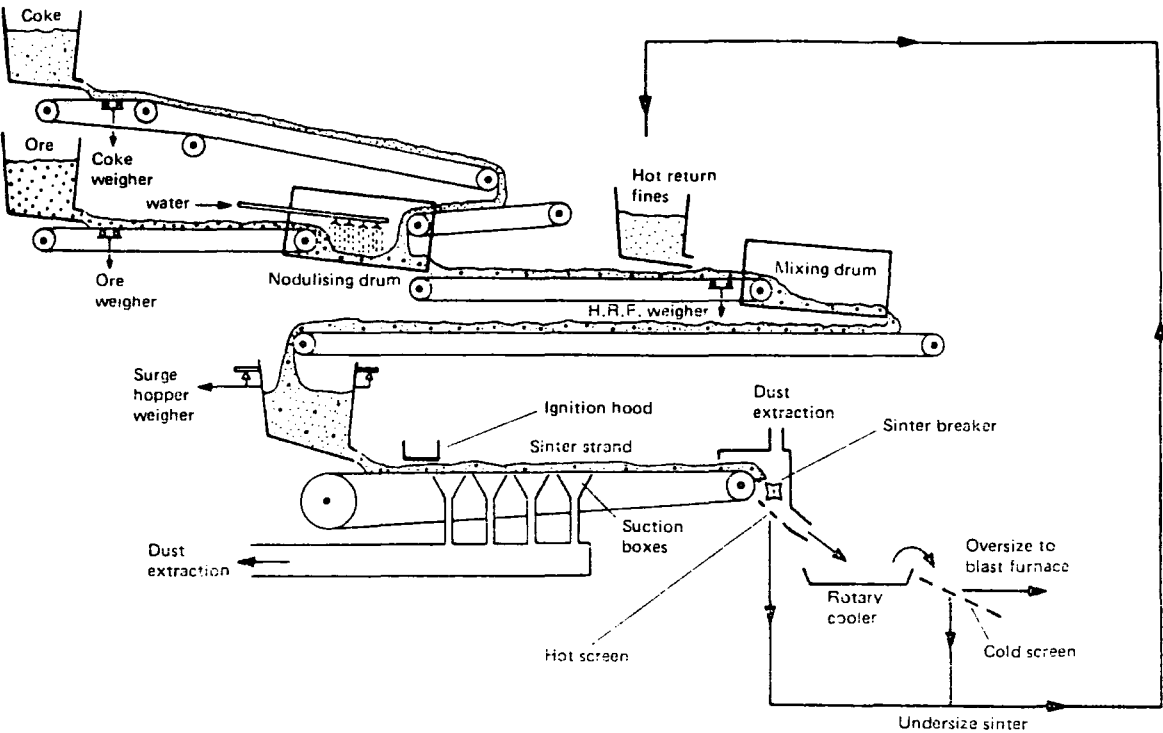
Badrah and Gill

Fig 1 Schematic flow diagram of the raw-mix feed system to sinter strand

Whence

$$\exp(-Ls) = \frac{6 - 2Ls}{6 + Ls + L^2 s^2} \qquad \ldots(1)$$

as detailed by Badrah (1981).

Control of a process described by the state equations

$$\dot{x} = Ax + Bu \qquad \ldots(2)$$

$$y = Hx \qquad \ldots(3)$$

can be achieved by minimising the quadratic index of performance

$$IP = \int_{t_0}^{\infty} [X'QX + u'Ru]\,dt \qquad \ldots(4)$$

This was shown by Kalman (1964), Anderson & Moore (1971), and Kuo (1975) to yield the control law

$$u = R^{-1}B'Px \qquad \ldots(5)$$

where Q and R are symmetric positive semidefinite and positive-definite matrices respectively. P is a symmetric positive-definite matrix that can be obtained by solving the algebraic Riccati equation

$$A'P + PA - PB\,R^{-1}B'P = -Q \qquad \ldots(6)$$

The infinite-time linear-regulator problem requires that the pairs $[A, B]$ must be completely controllable and $[A, D_1]$ must be completely observable, where D_1 is a matrix with suitable dimension such that

$$D_1'D_1 = Q \qquad \ldots(7)$$

a — Exact representation for exp $(-Ls)$
b — Using Padé approximation for exp $(-Ls)$
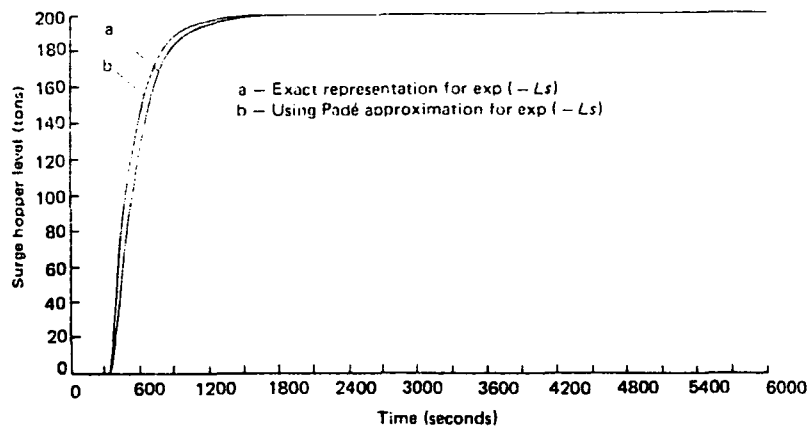
Fig 2 Responses to a unit step in sinter-plant model

A derivation for Eqn (7) is given by Badrah (1981) which is obtained by comparing the conditions for optimality of Eqn (5) given by Kalman (1964) with those given by Anderson and Moore (1971).

Elements of D_1 are calculated by equating the co-efficients of the like powers of the following equation:

$$N(j\omega)N(-j\omega) - q(j\omega)q(-j\omega) = d(j\omega)d(-j\omega) \quad \ldots(8)$$

where $N(s)$ and $q(s)$ are the closed-loop and open-loop system characteristic equations.

$$d(s) = d_1 + d_2 s + \ldots + d_n s^{n-1} \quad \ldots(9)$$

in which $d_1, d_2, \ldots d_n$ are the unknown elements of D_1 and can be evaluated to achieve preassigned characteristic root values for Eqn (8). The corresponding weighting matrix Q can be computed by direct substitution in Eqn (7) leading to the required symmetric positive-definitive matrix P as the unique solution of Eqn (6).

4. Luenberger observer design

If the system under consideration is completely observable a reduced-order observer can be used (Luenberger, 1964 and 1971) of the form

$$\dot{z} = Dz + Ey + TBu \quad \ldots(10)$$

in which the observer output z is related to the estimated vector $\dot{x}$ by

$$z = T\dot{x}$$

A number of restrictions must be imposed on matrices D and E in order to reduce the number of independent variables. These restrictions are:

(1) D is selected to be diagonal matrix;
(2) the elements of D differ from each other by only a few per cent;
(3) the characteristic roots of matrices D are made different to the plant matrix A; and
(4) matrix E is selected to form a controllable pair with D by ensuring that no element of E is zero. Normally, the elements of E are made equal to unity.

Restrictions (1) and (2) above permit the observer matrix to be characterised by only one element of D. In the study presented here, d_{11} is used for this purpose. The imposition of (1) and (2) also facilitates the assessment of the lowpass-filtering characteristics of the observer. Condition (3) must be satisfied in order to find a solution for the observer matrix equation.

The matrices introduced in Eqn (10) are all clearly labelled in Fig. 3, and the computer programs used in the design are given by Badrah (1981).

5. Illustrative examples

The effectiveness of the proposed control algorithm is judged from simulation results. To conserve computer time, it is sensible to represent the plant in its simplest form while still maintaining its fundamental dynamic and static characteristics. Similar restrictions on the plant model
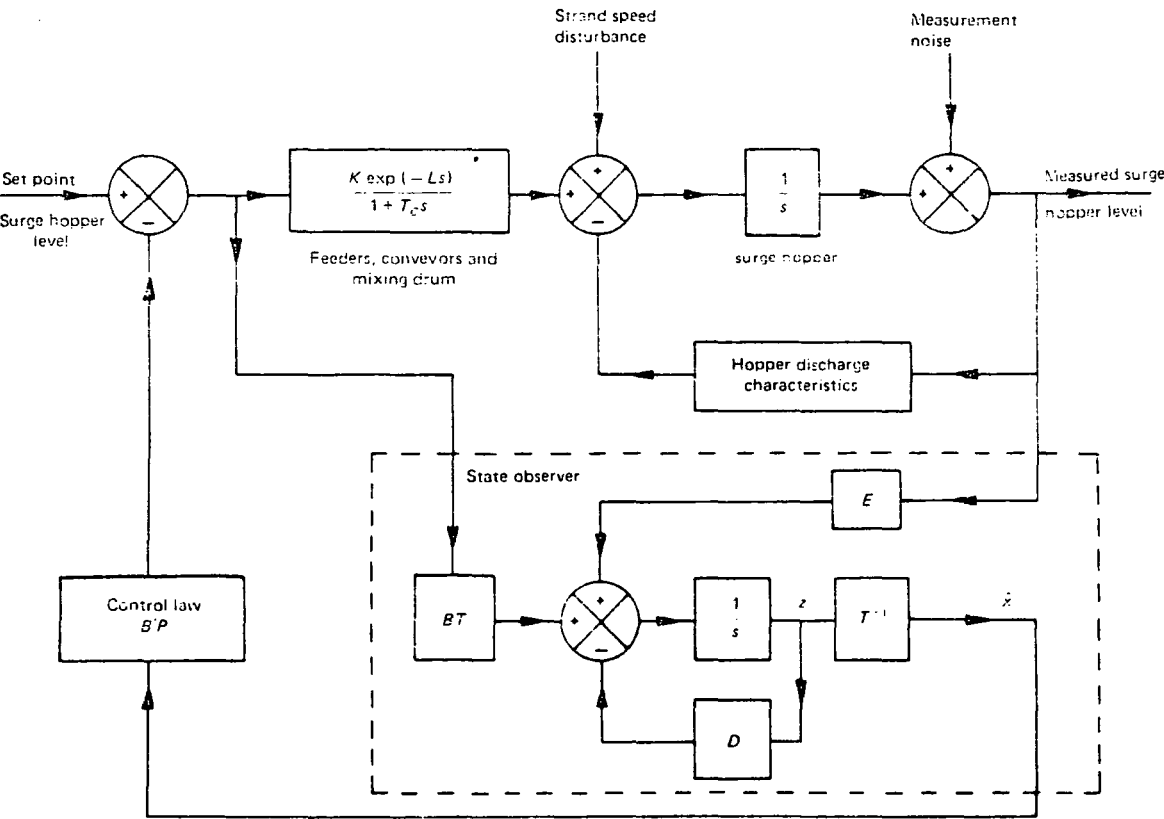
Fig 3 Block diagram for the process with state estimator

6*

Badrah and Gill

characteristics used in the observer and control-algorithm design are also desirable.

These requirements are achieved by representing the process, except for the surge hopper, by a first-order transfer function that describes to a good approximation the transient behaviour of the actual system being modelled. The total dead time is measured as the time it takes for the ore to be transported from the first ore bin to the surge hopper; the surge hopper is represented, as any reservoir, by a simple integrator. The block diagram for this simplified plant is shown in Fig 3.

Confirmation of the mathematical model predicted from engineering drawings and data sheets was not possible, because no test data for the subsystems of an operating plant were available.

Using the approximation of Eqn (1), the plant matrix can be evaluated as:

$$A = \begin{bmatrix} -0.005 & 1.0 & -120.0 & 0 \\ 0 & 0 & 1.0 & 0 \\ 0 & -0.0000463 & 0.0111111 & 0.0000463 \\ 0 & 0 & 0 & -0.025 \end{bmatrix}$$

The driving vector B will be:

$$B' = \begin{bmatrix} 0.0 & 0.0 & 0.0 & 0.025 \end{bmatrix}$$

and the output vector H is:

$$H = \begin{bmatrix} 1.0 & 0.0 & 0.0 & 0.0 \end{bmatrix}$$

The suitable values of the observer matrices are found in Badrah (1981) to be:

$$D = \begin{bmatrix} -0.0026 & 0 & 0 \\ 0 & -0.0025 & 0 \\ 0 & 0 & -0.0024 \end{bmatrix}$$

$$E' = \begin{bmatrix} 1.0 & 1.0 & 1.0 \end{bmatrix}, \text{ and}$$

$$T = \begin{bmatrix} -416.67 & -242521.22 & -22619990.15 & -46750.98 \\ -400.00 & -228784.98 & -20994387.03 & -43198.33 \\ -384.62 & -216118.86 & -19511292.54 & -39969.06 \end{bmatrix}$$

The computation details are given in Badrah (1981).

6. Design procedure

The significant steps to be taken by the practising engineer in the application of this design approach are:

(1) identify the dominant characteristic roots of each subsystem in the process. From a limited simulation study establish the lowest-order mathematical model consistent with engineering and plant experience that represents the process dynamics;

(2) approximate the dead time exponential term by direct substitution in Eqn (1);

(3) select the location of the modelled system's characteristic roots and input these to the computer program, filename TEST.FOR (Badrah, 1981), to estimate the weighting matrix Q and hence matrix P as the unique solution of the Riccati equation;

(4) choose the elements of the observer matrix E to be unity and D as a diagonal matrix, such that the first element is equal to one-half of the smallest characteristic root, while the remaining elements are made progressively a few percent less than this value;

(5) the observer matrix T is evaluated from the computer program given in Badrah (1981), filename RIC.FOR, which also checks dynamically the suitability of the chosen parameters. Trial and observation data obtained from RIC.FOR can also be used to 'fine tune' the control algorithm if necessary.

7. Simulation results and discussion

It is believed by the authors that the most serious single disturbance to which the sinter plant can be subjected under normal operation is one of 10% in either setpoint value or strand speed; hence the value used in the simulation trials presented.

Since the control algorithm is based on the location of the characteristic roots, responses to variation in the position of these are shown in Figs 4 and 5. From these figures it can be seen that a compromise has to be drawn between the 'best' dynamic response to surge-hopper level for a change in setpoint value (curve *d*) and the response in hopper level to strand speed (curve *c*) if steady-state errors are to be minimised when production rates are changed. However, the number of simulation runs needed to achieve this end is minimal.

The + signs on these figures indicate typical response that could be achieved if a correctly tuned 3-term control

a — (-0.025, -0.005, -0.0059 ± j0.0042)
b — (-0.025, -0.006, -0.0065 ± j0.0046)
c — (-0.025, -0.006, -0.0070 ± j0.0049)
d — (-0.025, -0.008, -0.0085 ± j0.0060)
e — (-0.025, -0.010, -0.0150 ± j0.0106)
f — (-0.025, -0.015, -0.0200 ± j0.0141)
+ — 3-term controller

Fig 4 Responses to an increase of 10% in set points

a — (−0.025, −0.005, −0.0059 ± j0.0042)
b — (−0.025, −0.006, −0.0065 ± j0.0046)
c — (−0.025, −0.006, −0.0070 ± j0.0049)
d — (−0.025, −0.008, −0.0085 ± j0.0060)
e — (−0.025, −0.010, −0.0150 ± j0.0106)
f — (−0.025, −0.015, −0.0200 ± j0.0141)
+ — 3-term controller
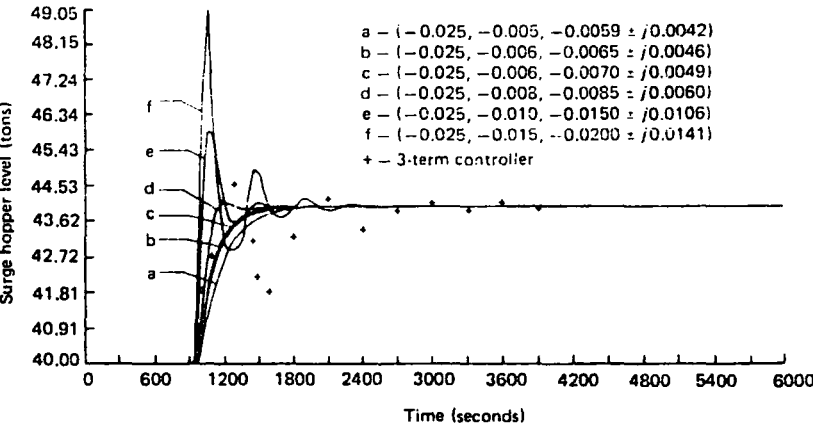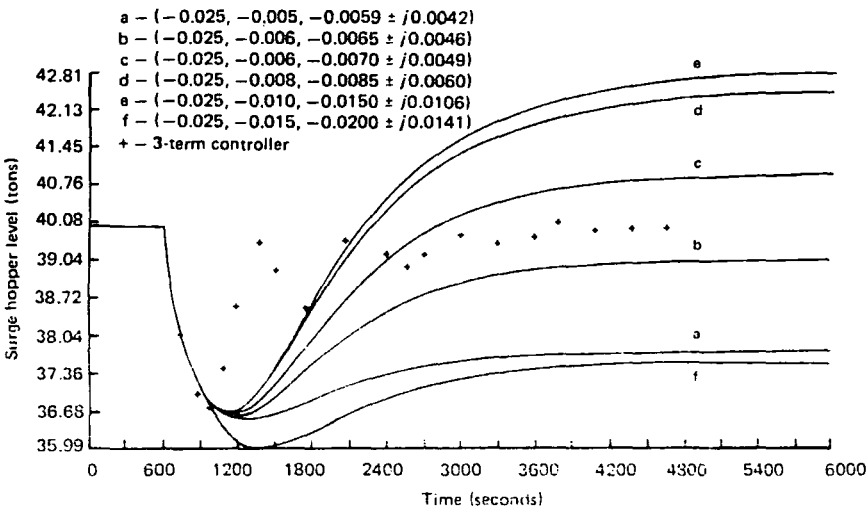
Fig 5   Responses to an increase of 10% in strand speed

were used. The weakness of this controller is that the responses are sensitive to small changes in the tuned values used for the controller, and any increase in these values as a means of improving the transient performance will quickly lead to system instability.

In all operational plant extraneous disturbances (noise) are present and the nature of the impact of these on the plant performance, when using the proposed control algorithm, is shown in Figs 6 and 7. To give some indication of the power of this algorithm, hopper-level responses to

a — Using Smith predictor.
b — Applying pole positioning technique.
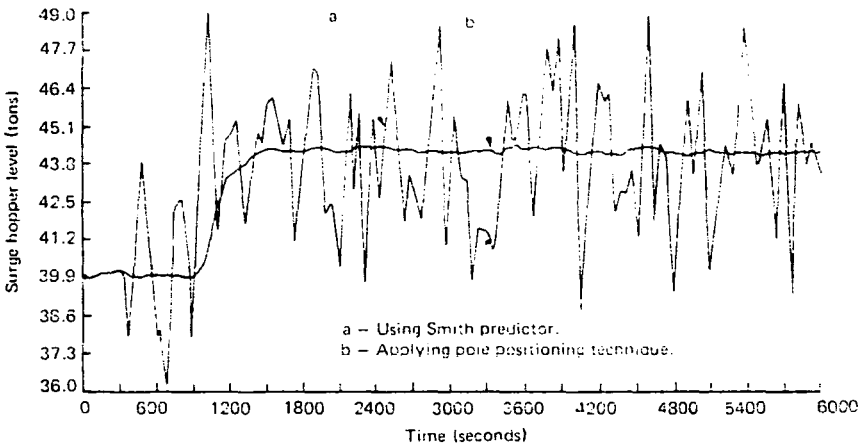
Fig 6   Responses to an increase of 10% in set point, measurement noise included

a — Using Smith predictor.
b — Applying pole positioning technique.
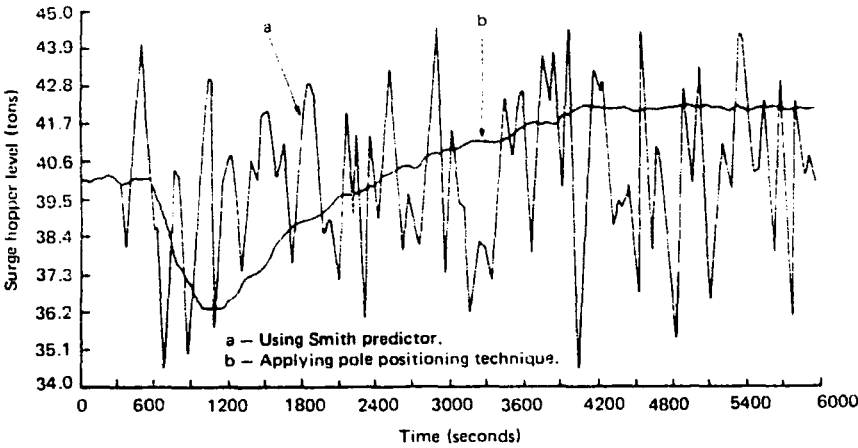
Fig 7   Responses to an increase of 10% in strand speed, measurement noise included

identical disturbances (Badrah, 1981) are superimposed on these figures for the process when controlled by a Smith's predictor algorithm

These results show that the Luenberger observer gives adequate state information for control purposes, minimises the effects of measurement noise, and eliminates the need for additional instrumentation. This control concept employing state estimations will not be acceptable to all plant engineers; however, these ideas can be incorporated into any standby system that is used to maintain controlled plant operation in the event of instrument failure or at times of instrument servicing.

The process dynamics can be effectively controlled using this design procedure and a direct method for computing the weighting matrix, Q, has been established. Using this matrix, a simple and effective procedure for solving the Riccati equation has been presented which minimises the dependency on simulation results for selecting the parameters in the control algorithm adopted. The time-delay approximation leads to a direct engineering solution and avoids unnecessary mathematical analysis.

The availability of fully documented computer programs (Badrah, 1981) should make this an attractive industrial procedure that has the potential to make savings possible in control-algorithm design costs.

References

Abou El-Nasr, A. 1980. 'Control strategy to minimize the effect of dead time in a sinter plant', *PhD Thesis*, Department of Mechanical Engineering, University of Leeds.

Anderson, B. D. O. and Moore, J. B. 1971. *Linear optimal control*, Prentice Hall Inc., Englewood Cliffs, New Jersey.

Badrah, S. M. M. 1981. 'Control-algorithm design for sinter plants containing significant transportation lag', *PhD Thesis*, Department of Mechanical Engineering, University of Leeds.

Hitz, K. L. and Anderson, B. D. O. 1972. 'Iterative method of computing the limiting solution of the matrix Riccati differential equation', *Proc. IEEE* 119 (9), 1402–1406.

Kalman, R. E. 1964. 'When is a linear control system optimal?', *Trans ASME, J Basic Eng*, Ser. D, 86, 51 –60.

Kleinmann, D. L. 1968. 'On iterative technique for Riccati equation computation', *Trans IEEE* AC-13 (1), 114 – 115.

Kuo, B. C. 1975. *Automatic control systems*, Prentice-Hall Inc., Englewood Cliffs, New Jersey.

Levin, J. J. 1959. 'On the matrix Riccati equation', *Proc Am Math Soc*, 10, 519–524.

Luenberger, D. G. 1964. 'Observing the State of Linear Systems', *Trans IEEE* MIL-8 (2), 74–80.

Luenberger, D. G. 1971. 'An introduction to observers', *Trans IEEE* AC-16 (6), 596–602.

O'Donnel, J. J. 1966. 'Asymptotic solution of the matrix Riccati equation of optimal control', *Proc 4th Am Allerton Confr Circuit System Theory*, 577–586.

Reid, W. T. 1964. 'A matrix differential equation of the Riccati type', *Am J Math*, 68, 237–146.

Vaughan, D. R. 1969. 'A negative exponential solution to the matrix Riccati equation', *Trans IEEE* AC-14 (1), 72–75.

Wonham, W. M. 1967. 'On pole assignment in multi-input controllable linear systems', *Trans IEEE* AC-12 (6), 660–665.

Wonham, W. M. 1968. 'On a matrix Riccati equation of stochastic control', *SIAM J Control*, 6 (4), 681–698.

PAPER 52

Performance of a telescopic dual-tube automotive damper and the implications for vehicle ride prediction

B B Hall, BSc(Eng), PhD, CEng, MIMechE
Department of Mechanical and Production Engineering, Huddersfield Polytechnic

K F Gill, BSc. MSc. PhD, CEng, MIMechE
Department of Mechanical Engineering, University of Leeds

This paper outlines a theoretical model of a dual-tube damper, presents the results of a digital simulation and compares them with previous experimental results. The damper characteristics are confirmed as being highly non-linear and exhibiting hysteresis effects. A prediction of the ride performance of a vehicle fitted with these dampers is made and shows that the typical linear and bilinear models of the damper are inappropriate and lead to over-optimistic estimates of ride performance.

NOTATION

Listed are the symbols not adequately described in the text.

Damper simulation

A_c, A_r	cross-sectional areas of compression and rebound chambers (m^2)
A_0	area of orifice (m^2)
A_v	area of compression control valve plate (m^2)
C_d	coefficient of discharge
C_f	momentum force coefficient
C_v	valve damping coefficient (Ns/m)
d_{in}, d_{or}	inlet and orifice diameters for valves (m)
d_v	diameter of valve plate (m)
f	frequency (Hz)
h	height of slot in compression control valve spool (m)
k, k_c	valve spring and valve seat stiffness (N/m)
m	mass of valve plate (kg)
Q_{vc}, Q_{vr}	'vapour' flowrates in compression and rebound chambers (m^3/s)
V_c, V_r	volume of 'vapour' in compression and rebound chambers (m^3)
β	compressibility of fluid (Pa^{-1})
Δp, Δp_3	pressure drop between compression and rebound chambers and between compression and reserve chambers (Pa)
μ	coefficient of friction
ρ	density of fluid (kg/m^3)

Derived constants

$$a_0 = \sqrt{2C_d} A_0 / \sqrt{\rho} \qquad a_v = \sqrt{2C_d} d_v / \sqrt{\rho}$$

$$b_v = 4C_f \rho / \pi d_{in. or}^2 \qquad e_v = \mu C_f C_d^2 d_0$$

$$f_a = \mu d_0 \qquad f_b = (\pi d_0)^2 / 2\rho$$

1 INTRODUCTION

The need for the introduction of non-linear damping characteristics into passive vehicle suspensions is

necessary to satisfy the conflicting requirements of ride and handling (1). However, the dynamic behaviour of practical dampers has been shown (2) to differ from the ideal because of the complex fluid/valve interactions occurring within such devices. Indeed, the force developed by a damper is not only velocity dependent but a function of the disturbing frequency. At frequencies greater than about 1 Hz, it is possible for hysteresis loops to develop in the force–velocity diagram. These are caused by the compressibility of the damper fluid and the expansion of entrapped gases. Preliminary comparisons made between ride predictions using linear and bilinear dampers (3) with those based on a more detailed damper description indicate that predictions based on these linear and bilinear models are over-optimistic.

2 DAMPER DESCRIPTION

A typical arrangement for such a unit is shown in Fig. 1. The double cylinder is normally connected to the axle or wheel suspension and the piston rod to the body of the vehicle.

The volumes above and below the piston are filled with a hydraulic fluid and are called respectively the rebound and compression chambers. The main connection between these is by orifices and one-way valves. The single-ended piston rod makes it necessary to have a reserve chamber to accommodate the difference in swept fluid volumes on either side of the piston. The reserve chamber is created by the outer cylinder and this is connected to the compression chamber directly by orifices and one-way valves. These form the valve assembly at the bottom of the inner cylinder.

The reserve chamber also contains a gas phase, normally an air or gas-filled sack, in addition to the displaced hydraulic fluid, the gas volume being sufficient to accommodate the difference in volume produced by movement of the piston rod with only a small change in reserve chamber pressure. In practice, this pressure is essentially atmospheric and has been found to vary by no more than 22 kPa, for a 75 mm rod movement.
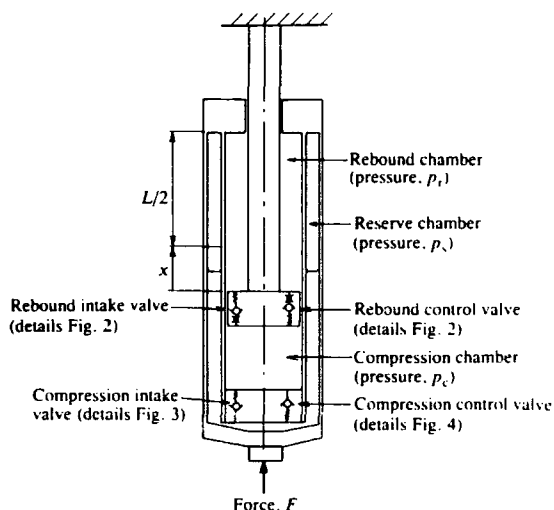
Fig. 1 Diagrammatic representation of damper

When the upward velocity of the dual-cylinder exceeds that of the piston, the fluid in the compression chamber is compressed and the pressure differential across the piston and between the compression chamber and reserve chamber causes flow into both the rebound and reserve chambers. If the relative velocity between piston and cylinder is reversed, the flows are reversed, resulting in flow from the reserve and rebound chambers into the compression chamber.

2.1 Intake and control valves

The intake valves offer little resistance to flow in one direction but prevent flow completely in the opposite direction when the pressure difference is reversed. Control valves are spring preloaded valves which do not open until a predetermined pressure difference is exceeded. Since these valves are closed when the pressure differential is reversed, they too are single-acting valves.

The damper investigated has coil-type valve springs. The other forms of spring, however, typically disc and leaf, can readily have their characteristics incorporated into the analysis.

The piston is fitted with two valves, a rebound control valve, which controls the flow of the fluid from the rebound chamber into the compression chamber, and a rebound intake valve, which controls the flow in the reverse direction. Two further valves are fitted between the compression chamber and the reserve chamber, one to control the flow from the compression chamber to the reserve chamber (compression control valve), the other (compression intake valve) to control the flow in the reverse direction.

2.2 Flow constriction orifices

Initial orifices or 'notches' are used to provide a highly restricted flow path between the chambers when the valves are closed and a pre-orifice is placed in series with a valve to provide additional flow constriction when a valve is open.

3 DYNAMIC ANALYSIS OF DAMPER

The damper chosen for the study was an AC Delco 'take-apart' design; the pertinent details are given in Table 1. The digital simulation work was based on a continuous system modelling program (CSMP) (4) software package requiring careful formulation of the process equations. These will be presented to highlight the assumptions made in modelling this damper.

Figures 2 to 4 illustrate the principle of operation of the damper valves together with corresponding valve equations. Note that whereas the rebound intake and control valves were fitted with pre-orifices, the compression control and intake valves were not. Also the design of the compression control valve is different from that of the other valves.

The damper studied was not fitted with initial notches and leakage flows were neglected. The additional assumption made are:

(a) the reserve chamber pressure remains constant:
(b) valve plate damping is viscous:
(c) valve seat stiffness is included:
(d) the momentum force is proportional to the theoretical momentum force (2):
(e) inertia forces are included for compression control and intake valve plates:
(f) for the compression control valve.
   (i) the pressure under the valve plate is approximately equal to the reserve chamber pressure since $d_v \gg d_0$.
   (ii) the transverse exit of fluid from the spool spindle results in transverse pressure and momentum forces, both of which affect the coulomb friction force:
(g) the compressibility of the fluid and cylinder walls is represented by a combined coefficient:
(h) effects due to temperature changes are negligible.

3.1 Expansion and contraction of entrapped gases

Lang (2) found experimentally that lower pressure limits were reached in the rebound and compression chambers

Table 1   Damper data

$A_c = 5.066 \times 10^{-4}$ m^2	$P_s = 100$ kPa
$A_r = 3.84 \times 10^{-4}$ m^2	$\beta = 0.6525$ Pa^{-1}
$L = 0.254$ m	$\rho = 751.5$ kg.m^3

Valve parameter	Compression control	Compression intake	Rebound control	Rebound intake
$A_v \times 10^4$	1.387	—	—	—
$d_{in} \times 10^3$	—	7.254	—	—
$d_{or} \times 10^3$	—	—	3.175	3.708
$d_v \times 10^3$	—	16.08	10.45	13.77
$d_i \times 10^3$	1.626	—	—	—
$d_0 \times 10^3$	3.06	—	—	—
C_d	0.7	0.7	0.7	0.7
C_f	0.3	0.3	0.3	0.3
C_v	6.73	4.978	8.239	2.731
F_{sp}	44.5	1.914	178	8.9
$h \times 10^3$	2.54	—	—	—
$k \times 10^{-3}$	23.14	3.637	89.75	15.25
$k_c \times 10^{-6}$	1.753	17.5	17.5	17.5
$m \times 10^3$	1.963	6.854	2.75	0.489
μ	0.1	—	—	—
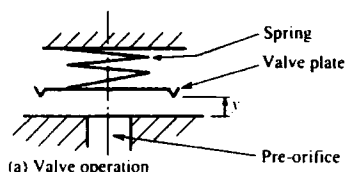
(a) Valve operation
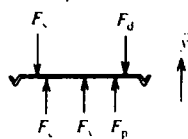
(b) Free-body diagram of valve plate

Valve equations

$$Q = \pm a_0 a_v z_y \{z_1/[(a_v y)^2 + a_0^2]\}^{1/2} = \text{flowrate}$$

where

+ sign for $\Delta p > 0$
− sign for $\Delta p < 0$

$z_y = y$ for $y > 0$

$\quad = 0$ for $y \leqslant 0$

$z_1 = |p_c - p_r| = |\Delta p|$

$\Delta p_1 = (Q/a_0)^2 = \text{pressure drop across orifice}$
$\Delta p_2 = \Delta p - \Delta p_1 = \text{pressure drop across valve plate}$
$F_c = -k_c y = \text{valve seat force } (F_c = 0 \text{ for } y > 0)$
$F_p = a_v \Delta p_2 = \text{pressure force}$
$F_v = b_v Q^2 = \text{momentum force}$
$F_d = c_v \dot{y} = \text{damping force}$
$F_s = ky + F_{sp} = \text{spring force}$

Equation of motion

$$m\ddot{y} = F_c + F_p + F_v - F_d - F_s$$

Fig. 2 Principle of operation of rebound intake and control valves with associated equations
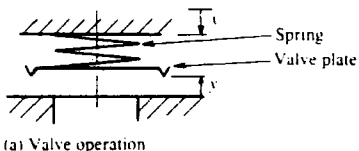
(a) Valve operation
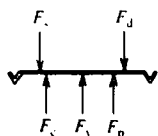
(b) Free-body diagram

Valve equations

$$Q = -a_v z_y \sqrt{z_2} = \text{flowrate}$$

where

$z_y = y$ for $y > 0$

$\quad = 0$ for $y \leqslant 0$

$z_2 = |p_c - p_r| = \Delta p_3$

$F_c = -k_c y = \text{value seat force. } (F_c = 0 \text{ for } y > 0)$
$F_v = b_v Q^2 = \text{momentum force}$
$F_p = -A_v \Delta p_3$
$F_i = m\ddot{x}$
$F_d = c_v \dot{y}$
$F_s = ky + F_{sp}$

Equation of motion

$$m\ddot{y} = F_c + F_v + F_p + F_i - F_s - F_d$$

Fig. 3 Operation of compression intake valve with associated equations

(approximately 3 kPa in the rebound chamber and 65 kPa in the compression chamber) and concluded that since these were in excess of the vapour pressure of the oil (typically as low as 0.003 Pa) they were due to expansion and contraction of entrapped gases. An equivalent vaporization model was postulated to account for these effects. It is proposed that an equivalent vapour pressure of 41 kPa (an average lower limit) be used, being equivalent to 1.8 per cent of gas in the compression chamber at normal atmospheric temperature and pressure. It follows that when the pressure attempts to fall below this limit, there is an increase in

(a) Valve structure

Section q–q
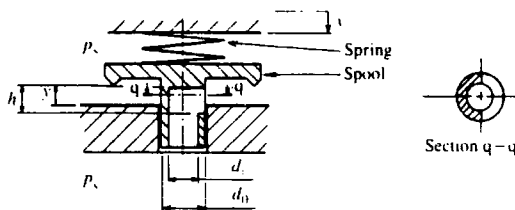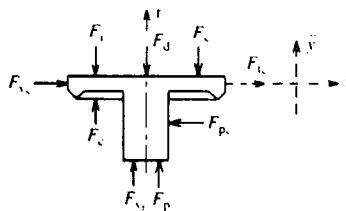
(b) Free-body diagram of valve spool

Valve equations

$$Q = a_v z_y \sqrt{z_1/2} = \text{flowrate}$$

where

$z_y = y$ for $y > 0$

$\quad = 0$ for $y \leqslant 0$

$z_2 = |p_c - p_r| = |\Delta p_3|$

$F_c = -k_c y = \text{valve seat force } (F_c = 0 \text{ for } y > 0)$
$F_{vr} = b_v Q^2 = \text{momentum force in r-direction}$
$F_p = A_v \Delta p_3$
$F_f = F_{f_1} + F_{f_2} + F_{f_3} = \text{friction force}$

where

$F_{f_1} = 2e_v z_y \Delta p_3 \dot{y}/|\dot{y}|$
$F_{f_2} = 0$ when $y \geqslant h$
$\quad = f_a(h - y)p_c \dot{y}/|\dot{y}|$ when $0 < y < h$
$\quad = f_a hp_c \dot{y}/|\dot{y}|$ when $y < 0$
$F_{f_3} = 0$, when $y \leqslant 0$
$\quad = -f_a(h - y)u_v^2 \Delta p_3 \dot{y}/4f_b|\dot{y}|$, when $0 < y < h$
$\quad = 0$ when $y \geqslant h$

$F_d = c_v \dot{y}$
$F_s = ky + F_{sp}$
$F_i = m\ddot{x}$

Equation of motion

$$m\ddot{y} = F_c + F_{vr} + F_p - F_f - F_d - F_s - F_i$$

Fig. 4 Principle of operation of compression control valve with associated equations

the volume of the gas at constant pressure. This model of the gas behaviour is emulated by generating an equivalent 'vapour' flowrate Q_v whenever the pressure drops to a notional vapour pressure p_v of the fluid–gas combination. This results in a vapour volume $V_v = \int Q_v \, dt$ being formed. This volume of vapour is dissipated as the pressure attempts to increase above p_v. The pressure in a chamber, however, does not begin to increase until $V_v = 0$.

3.2 Balance of flowrates

Using a double-suffix notation for the flowrates through the valves as follows:

cc   compression control
ci   compression intake
rc   rebound control
ri   rebound intake

and taking the flowrates into the rebound and reserve chambers as positive, it can be shown that the rates of change of pressure in the compression and rebound chambers are given by

$$\dot{p}_c = \frac{A_c \dot{x} - Q_{ri} - Q_{rc} - Q_{ci} - Q_{cc}}{\beta A_c[(L/2) - x]} \tag{1}$$

and

$$\dot{p}_r = \frac{Q_{ri} + Q_{rc} - A_r \dot{x}}{\beta A_r[(L/2) + x]} \tag{2}$$

In these equations, x is the displacement of the cylinder relative to the piston, measured from the mid-stroke position (x is taken to be positive during the compression stroke).

Furthermore, when $p_c = p_v$ and $V_c > 0$, the rate of vapour formation in the compression chamber is

$$Q_c = Q_{ri} + Q_{rc} + Q_{ci} + Q_{cc} - A_c \dot{x} \tag{3}$$

Similarly, when $p_r = p_v$ and $V_r > 0$, the corresponding equation for the rebound chamber is

$$Q_r = A_r \dot{x} - Q_{ri} - Q_{rc} \tag{4}$$

4 DIGITAL SIMULATION

To permit ease of comparison with existing published results (2), it is necessary to subject the damper to a quadratic form of periodic excitation applied to the body of the damper, while holding the piston stationary. The comparison of results is made for a displacement amplitude of 38.1 mm and a frequency of 5 Hz.

4.1 Mathematical description of the excitation

The quadratic displacement and velocity variation shown in Fig. 5 are described by the equations

$$x = -8x_m(2t_r^2 - 3t_r + 1) \tag{5}$$

$$\dot{x} = -\frac{8x_m}{T}(4t_r - 3) \tag{6}$$
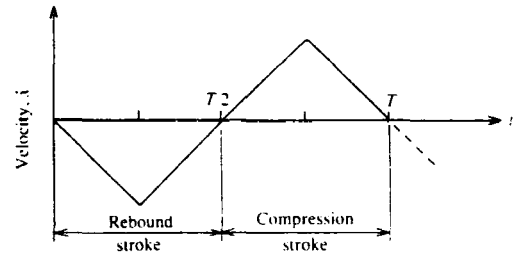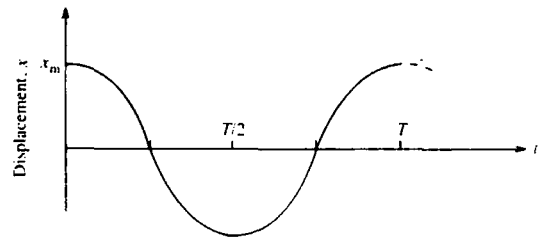
Fig. 5   One cycle of quadratic excitation

for $0 < t \leqslant T/4$ and $3T/4 < t < T$, and

$$x = 8x_m(2t_r^2 - t_r) \tag{7}$$

$$\dot{x} = \frac{8x_m}{T}(4t_r - 1) \tag{8}$$

for $T/4 < t \leqslant 3T/4$, where $t_r = T^{-1}(t + 0.75T)$.

For $t > T$, equations (5) and (8) still apply provided that t_r is replaced by $t_r = t_r - \text{aint}(t_r)$. The term $\text{aint}(t_r)$ is the next smallest integer less than t_r.

4.2 Program structure and operation

Figure 6 shows the structure of the CSMP simulation program. Valve data and initial conditions are entered into the 'initial' segment of the program, where calculations of fixed parameters are made.

It was found by experience that an integration step size greater than 10^{-5} s produced errors which halted the execution of the program. Such a step size required 837 s of central processing unit (CPU) time for two cycles of excitation.

At the beginning of each computation time step, the flowrates through each valve are determined from the current inputs x and $\dot{x}$ together with the valve displacements from the previous step. A test is carried out for the presence of vapour and the appropriate revised pressures are calculated. This allows new valve displacements to be computed for each valve. The algorithm then loops back to calculate revised flowrates and continues to cycle round the loop until the change in pressure difference Δp falls below a specified error.

4.3 Results

Shown in Fig. 7 are the results of the simulation for $x_m = 38$ mm and $f = 5$ Hz plotted on force–velocity
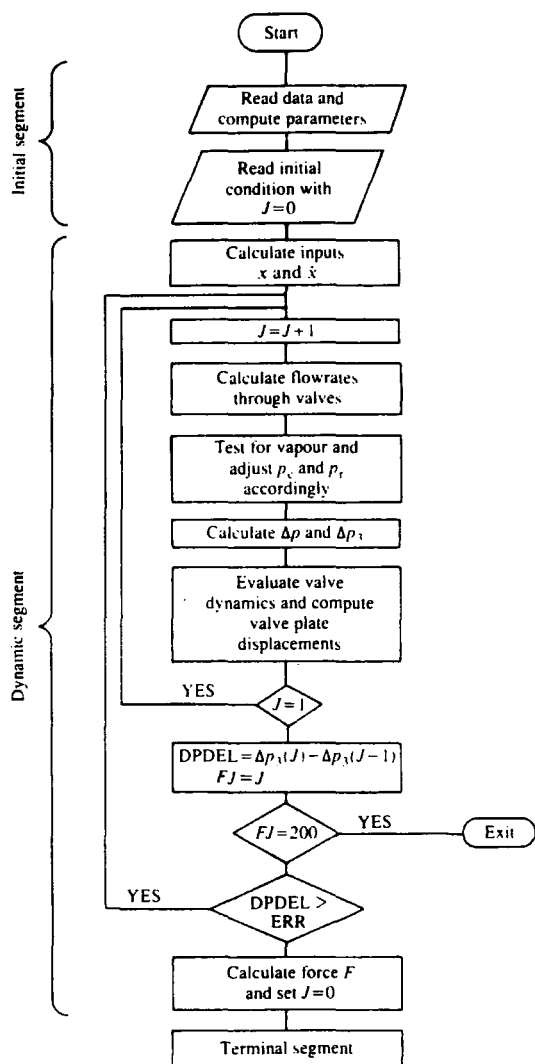
Fig. 6 General structure of program

axes together with the experimental data (2) superimposed. It is seen that the simulation results for $p_v = 85.4$ kPa are generally in good agreement with the experimental results. The former, however, tend to be more oscillatory, apparently due to fluctuations in pressure produced by vibration of the control valves. These differences in the results are possibly due to:

(a) inaccurate damping coefficients for the valves, or
(b) limitations of the frequency response of the instrumentation and/or transducers used to obtain the experimental data.

Experimental results for $x < -1.0$ m/s are not available.

Effects of frequency on the characteristics of the damper are shown in Fig. 8 for $p_v = 41.3$ kPa (that is a reduced amount of entrained gas compared with the previous case).

© IMechE 1986

These results generally support previous findings (2) that:

(a) an increased amount of entrained gas increases the size of the hysteresis loop, and
(b) increasing the excitation frequency produces the same result.

5 THE PREDICTION OF RIDE PERFORMANCE

Confidence in any vehicle ride prediction data depends on the adequacy of:

(a) the road profile description;
(b) the vehicle model;
(c) the interpretation of vehicle response related to human response to vibration.

Typically a road profile induces random distrubances into a moving vehicle and hence the occupants are subjected to a modified form of this random excitation. The human response to this disturbance can be predicted quantitatively (ride performance) by the introduction of appropriate frequency weighting.

The quarter vehicle model shown in Fig. 9 has been widely used (3, 5, 6) to assess ride and also the performance of vehicle suspensions in the bounce mode. By subjecting this model to a weighted white noise input, the effect of road surface irregularities can be predicted. Weighting the response of the 'sprung-mass', m_s, enables an estimate of ride performance to be obtained.
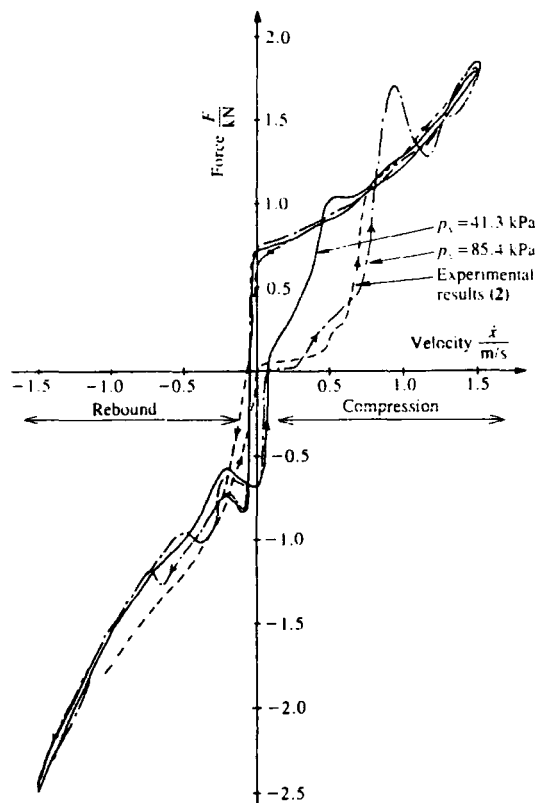
Fig. 7 Comparison of results of damper simulation ($x_m = 38$ mm, $f = 5$ Hz)

B B HALL AND K F GILL
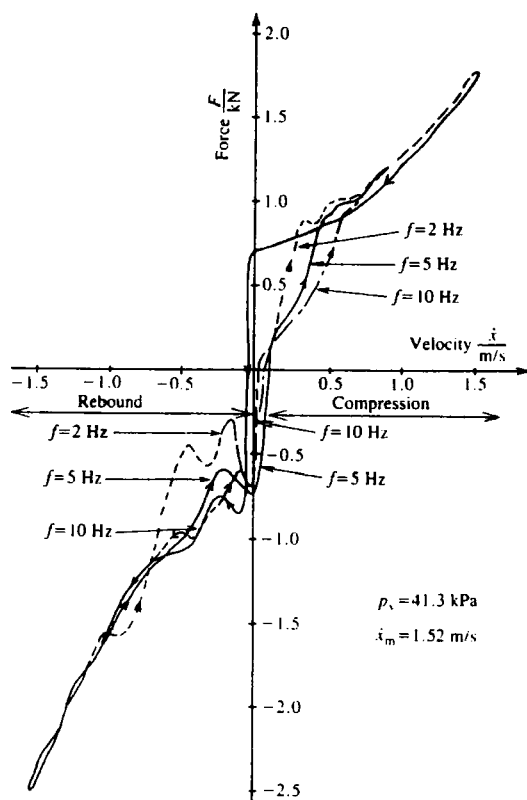
Fig. 8 Effect of frequency on F-x characteristics

5.1 Road profile description

The characteristics of a particular type of road profile can be represented by the mean square spectral density S of the height variations as a function of the spatial frequency (or wave number, n) along the length of road. Several mathematical descriptions have been fitted to measured road profile data (7, 8), one of the simplest and most convenient of these for a single track description* being

$$S(n) = S(n_0) \left(\frac{n_0}{n}\right)^2 \qquad (9)$$

where reference wave number $n_0 = 1/2\pi$ cycles/m and $S(n_0)$ is the reference spectral density (m³/cycle), which characterizes the road type. Typically $S(n_0)$ is 20 for a good motorway, 80 for an average principal road and 320 for a poor minor road.

It may be shown (9) that the single-sided mean square spectral density S_v of the random (time-varying) input to a vehicle travelling with a constant velocity V along a road described by spectral density S is

$$S_v(f) = \frac{1}{V} S\left(n = \frac{f}{v}\right)$$

where the units of $S_v(f)$ are typically m²/Hz when V is expressed in m/s.

* $S(n) \to \infty$ as n becomes small (long wavelengths), hence it is necessary to place a lower limit on n.

An appropriate random input to a vehicle model may be generated by passing a white noise signal through a first order filter. Schaefer (10) devised a digital random signal having a Gaussian distribution, zero mean and a constant spectral density $S_1(f)$ (up to a cut-off frequency w_{co}) using standard functions available in CSMP software. Passing this signal through a first-order filter having a gain A and cut-off frequency $f_c = 0.5$ Hz, it is easily shown that the relationship between A and road speed V is

$$A = \sqrt{\left\{\frac{S(n_0)[1 + (V/\pi)^2]}{S_1 V}\right\}} \qquad (11)$$

5.2 Vehicle model

With reference to Fig. 9, the equations of motion are:

$$m_u \ddot{y}_1 + (k_t + k_s)y_1 - k_s y_2 + f_d = k_t y_0$$

$$m_s \ddot{y}_2 - k_s y_1 + k_s y_2 - f_d = 0$$

where $f_d =$ damping force.

The following numerical data typical of conventional automobile front suspensions were adopted in the emulations:

$m_u = 37$ kg	$m_s = 259$ kg
$k_t = 130$ kN/m	$k_s = 13$ kN/m

Four possible descriptions of a dual-tube damper were examined in a study into their effects on ride predictions:

(a) linear (viscous) approximation;
(b) bilinear approximation;
(c) non-linear approximation (excluding hysteresis);
(d) detailed description.

Using the results of the earlier analysis (Figs 7 and 8):

(a) for the linear approximation

$$f_d = 1375(\dot{y}_1 - \dot{y}_2), \text{ Newtons}$$

(b) for the bilinear approximation

$$f_d = 1133(\dot{y}_1 - \dot{y}_2), \text{ Newtons, for } \dot{y}_1 > \dot{y}_2$$

$$= 1667(\dot{y}_1 - \dot{y}_2), \text{ Newtons, for } \dot{y}_1 < \dot{y}_2$$
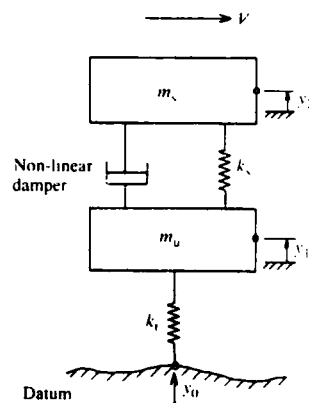
Fig. 9 Quarter vehicle model

5.3 Human response weighting

When the human body is subjected to broad-band excitation, a number of resonances are excited. For the seated occupant of a vehicle, the most important of these lie in the range between 4 and 8 Hz for vertical vibration.

International Standard ISO 2631 (11) recognizes this and presents fatigue-decreased proficiency curves plotted on axes of r.m.s. acceleration and frequency for durations between 1 and 24 h. While there is as yet no accepted standard to assess ride quality specifically, the profile of the fatigue-decreased proficiency standard can be used to devise a ride-meter filter. By processing the sprung-mass acceleration through such a filter, the mean-squared output can be treated as a measure of ride performance. Indeed, this process forms the basis of operation of at least one commercially available ride-meter. The transfer function of a suitable ride-meter filter can be synthesized from a transfer function of the form

$$T(s) = \frac{a_1 s + a_0}{s^3 + b_2 s^2 + b_1 s + b_0}$$

Using the values:

$$a_0 = 5.924 \times 10^4$$

$$a_1 = 1.126 \times 10^4$$

$$b_0 = 1.782 \times 10^5$$

$$b_1 = 1.145 \times 10^4$$

$$b_2 = 1.95 \times 10^2$$

results in the practical filter weightings shown in Fig. 10. It is seen that:

(a) there is good agreement between the ideal and practical filter gains;
(b) the filter weights most heavily those frequencies in the 4 to 8 Hz range.
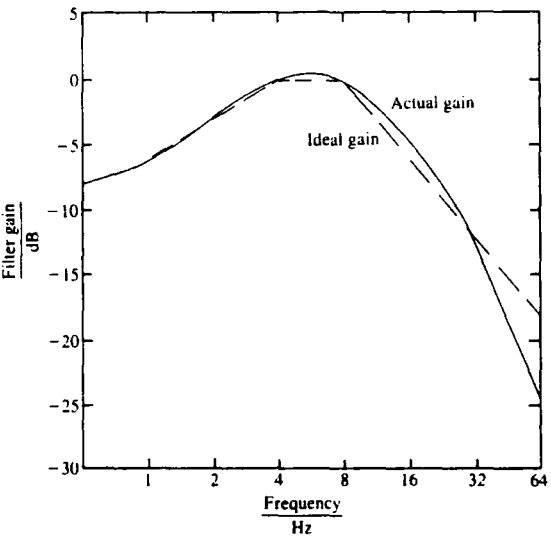
Fig. 10 Comparison of ideal and practical ride-meter filter gains
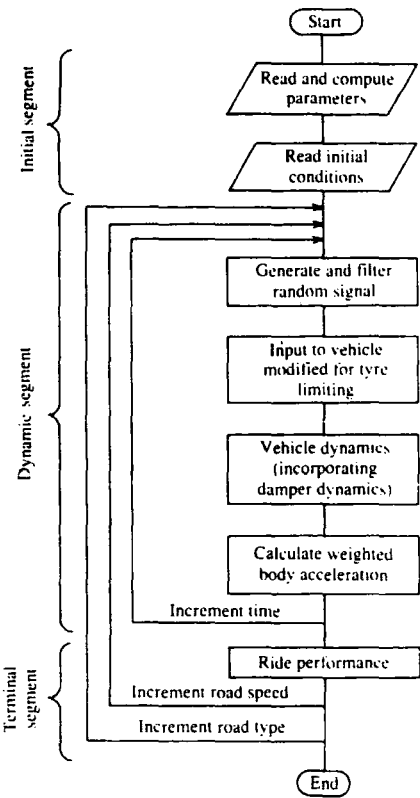
Fig. 11 General structure of program

5.4 Vehicle simulation

The general structure of the program is shown in Fig. 11. Similar comments to those in Section 4.2 apply regarding the entering of data and the use of a 'Nosort' declaration for the 'dynamic' segment. A fixed step Runge–Kutta integration algorithm was used for the reasons previously discussed.

The random disturbance input was generated by using the CSMP functions GAUSS, IMPULS and ZHOLD, together with a fourth-order smoothing filter, the cut-off frequency of spectral density being $w_{co} = 275.25$ rad/s and $S_1(f) = 5.868 \times 10^{-7}$ m²/Hz respectively. When used in conjunction with a road profile filter having a cut-off at 0.5 Hz, the road filter gain can be found from equation (11).

The simulations included the effect of 'tyre-limiting', to take account of those occasions when the tyre breaks contact with the road. Road speeds from 5 to 40 m s were used for each of the three road types identified in Section 5.1.

For the simpler linear model, the system resonances lie between 1 and 10 Hz and it was found that an integration step size of 0.002 s gave a good compromise between accuracy and computation time. This gives approximately 50 integration steps/period at the highest resonant frequency and can be expected (4) to give an average absolute error of the order of 10^{-5}. Because of the complexity of the full damper model, it is very difficult to estimate the highest system resonance and hence
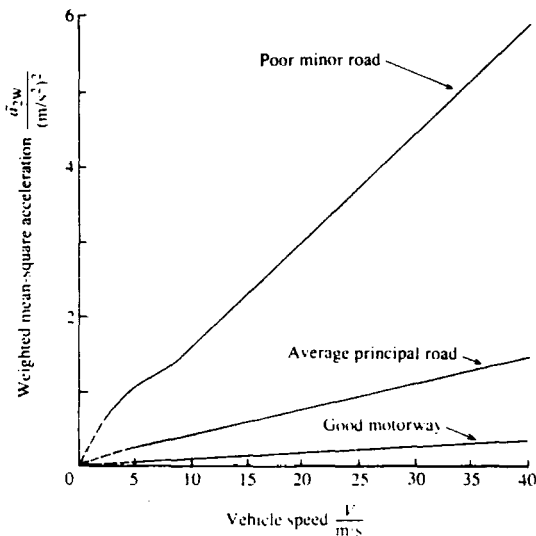
Fig. 12   Effect of road type on ride (bilinear damping)

ride predictions than are likely to occur in practice, if this quarter vehicle model is a faithful representation of the real situation.

6 CONCLUSIONS

A detailed simulation of the dynamics of the damper has produced characteristics which adequately match those obtained experimentally. It has, however, been necessary to use a vapour collapse concept to account for the expansion and collapse of entrained gases. This tends to give rise to transient effects at the transition between 'vapour' and 'non-vapour' phases, which are not present in the experimental results. The quality of the damper model may, therefore, be improved if a better model for the expansion and contraction of entrained gases can be found. Such a model would have to take account of the mechanism of gas transfer and quantify the amounts of gas present in rebound and compression chambers at a given instant.

It is apparent from the analyses that the entrained gases have a deleterious effect on the damper performance since they lead to an increase in size of the hysteresis loop. Design improvements which prevent the transport of gas from the reserve chamber are obviously very desirable.

The investigation into ride prediction indicates that for a given road speed and type, the best ride is given by a damper having a bilinear characteristic. In practice, however, satisfactory ride and handling have to be

deduce an optimum integration step size. However, the resonant frequencies of the valve plate sub-systems range up to more than 900 Hz, thus a step length of 10^{-5} s was found to be necessary for numerical stability.

The accuracy of the weighted mean-square sprung-mass acceleration, $\bar{a}_{2w}$, is dependent on the averaging time T_{AV}. It was found that 13.4 s of simulation time was required to ensure an accuracy of $\bar{a}_{2w}$ of 2.5 per cent. This duration results in excessive CPU time on the computer and had to be reduced to 5 s for runs incorporating the detailed damper, resulting in reduced accuracy estimated at 10 per cent for $\bar{a}_{2w}$. For the simplified damper, total CPU time (eight road speeds at each of three road types) was found to be 1470 s. The CPU time for the model, with the detailed damper, required in excess of three hours for each estimate of $\bar{a}_{2w}$.

5.5 Results

Figure 12 shows predictions of $\bar{a}_{2w}$ as a function of road speed for three road types, based on the bilinear approximation. Noting that increasing values of $\bar{a}_{2w}$ indicates a deterioration in ride, it is seen that:

1. Ride performance deteriorates linearly for increasing road speed greater than 10 m/s. This is in accord with the deductions of Thompson (12) for a random road surface described by equation (9) and a linear suspension system.
2. Over the whole speed range, the ride on a poor minor road and on an average principal road are significantly worse than on a good motorway.

Figure 13 shows, for a poor minor road, the comparison between the predictions of $\bar{a}_{2w}$ and hence ride for the four models of damping. The most significant feature is the major difference in ride prediction with a detailed damper model and those based on the other three damper approximations. The implication of this is that the latter indicate significantly more favourable

Fig. 13   Effect of damper model on ride prediction (poor minor road)

achieved simultaneously. The former calls for low vehicle body accelerations, while the latter requires tyre force fluctuations to be minimized. These conflicting requirements call for a compromise in the performance of the suspension damper, exemplified by the characteristics shown in Fig. 8 (but without the hysteresis effects). The results shown in Fig. 13 for the non-linear damper, excluding hysteresis, show that the compromise in the damper requirements leads to a moderate deterioration in ride performance.

The presence of hysteresis, however, in the damper characteristic has a noticeably detrimental effect on ride, represented in Fig. 13 by a significantly increased level of acceleration at the vehicle body. It follows that in the modelling of suspensions in which damper hysteresis is significant, it is essential that a detailed representation of the damper is used to ensure reliable predictions of ride and handling. This does require (a) a complete set of data for the dampers and (b) a significant amount of extra computing time. These penalties must be paid if the results are to be used with confidence.

REFERENCES

1 Bastow, D. *Car suspension and handling*. 1980 (Pentech Press, London: Plymouth).

2 Lang, H. H. A study of the characteristics of automotive dampers at high stroking frequencies. PhD thesis, Department of Mechanical Engineering, University of Michigan, 1977.

3 Mitschke, M. Comparison of different mathematical models of oscillations of passenger cars. Dynamics of vehicles on roads and on tracks. *Proc. IAVSD Eighth Symp.*, Cambridge, Mass., Aug. 1983, pp 362–376 (Swets and Zeitlinger, Lisse, Netherlands, 1984).

4 Speckhart, F. H. and Green, W. L. *A guide to using CSMP—the continuous system modelling program*. 1976 (Prentice-Hall, Inc., Englewood Cliffs, New Jersey).

5 Morman, K. N. and Giannopoulos, F. Recent advances in the computational aspects of modelling active and passive vehicle suspensions. Applied Mechanics Symposia, AMD Vol. 50, *Computational methods in ground transportation vehicles*, M. M. Kamal and J. A. Wolf (Eds) Nov. 1982 (ASME, New York).

6 Thompson, A. G. Optimal and sub-optimal linear active suspensions for road vehicles. *Vehicle System Dynamics*, 1984, 13, 61–72.

7 Dodds, C. J. and Robson, J. D. The description of road surface roughness. *J. Sound Vib.*, 1973, 31(2), 175–183.

8 *Proposals for generalized terrain—dynamic inputs to vehicles*, 1972. ISO/TC, 108/WG9 (BSI Panel MEE/158/3/1).

9 Newland, D. E. *An introduction to random vibration and spectral analysis*, second edition, 1984, pp 196–200 (Longmans, London).

10 Schaffer, W. S. Applied digital simulation of random signals and step response of a heat exchanger optimised for random signals. MSc thesis, Department of Mechanical Engineering, Ohio State University, Columbus, 1972.

11 *Guide to the evaluation of human exposure to whole-body vibration*, ISO 2631-1978(E) and Amendment 1, ISO 2631-1978 A1-1982 (E) (International Standards Organization).

12 Thompson, A. G. An active suspension with optimal linear state feedback. *Vehicle System Dynamics*, 1976, 5, 187–203.

PAPER 58

Performance evaluation of motor vehicle active suspension systems

B B Hall, BSc(Eng), PhD, CEng, MIMechE
Department of Mechanical and Production Engineering, Huddersfield Polytechnic

K F Gill, BSc, MSc, PhD, CEng, MIMechE
Department of Mechanical Engineering, University of Leeds

The essential features and potential of active suspensions are presented and selected systems are examined to relate the effects of closed-loop pole location to system performance. Results are compared with those for well-designed passive systems.

NOTATION

d ratio c_1/c_2 for sky-hook damper
F_t tyre force (N)
R_d ride discomfort value (m/s^2)
S_c clearance space (m)
z damping ratio of suspension sub-system
ω_1 natural frequency of unsprung mass sub-system (rad/s)
ω_2 natural frequency of sprung mass sub-system (rad/s)
Ω ratio $(\omega_1/\omega_2)^2$

1 INTRODUCTION

Active suspension systems are being employed as a means of overcoming many of the performance limitations inherent with the use of a passive suspension system. In essence they are of the form shown in Fig. 1 for the case of a quarter vehicle model. This model can be justified for bounce motions for vehicles with inertia coupling ratios close to unity—typified by a conventional automobile. They differ fundamentally from passive systems in that energy is supplied to the active system from an external agency (typically a hydraulic actuator); a passive system consists only of energy storage (spring) and dissipation (damper) devices. The active system is a closed-loop control system incorpo-

Fig. 1 Quarter vehicle model of an active suspension

rating a controller and controlled actuator with feedback signals from transducers sensing the required input variables within the complete system. As such, the dynamic performance of the system is potentially capable of being maintained in a near-optimal state with changes in road and speed conditions. The advantages of active suspensions are cited in reference (1) as

(a) low natural frequencies, with resulting improved ride, while still maintaining small static deflections,
(b) low dynamic deflections under transient excitation,
(c) suspension characteristics maintained irrespective of loadings,
(d) flexibility in the choice of desired dynamic characteristics, particularly between different modes of vehicle body oscillation, that is bounce, pitch and roll.

Constraints do exist, however, being typically

(a) a trade-off between ride and handling (2) and
(b) power requirements to operate them, which are appreciable (typically several kilowatts).

Finding a universally acceptable design has been taxing the ingenuity of engineers for many years. It has led to the evolution of a wide range of design proposals and practical implementations, including semi-active and adaptive systems. The developments have been comprehensively reviewed by Mormon and Giannopoulos (3) and Goodall and Kortum (4).

Although many different forms of active suspension have been proposed, attention will be confined in this paper to investigating a fully active system with displacement and velocity feedback.

The performance of the active system will be compared with that of an optimally designed passive linear system (see the Appendix). The results from this are used as a basis for assessing the performance of the active system.

While optimal control theory can be used to predict the feedback coefficient values for the active system (5), an alternative approach has been adopted based on pole placement (6). This essentially relates the position of the closed-loop poles in the s plane to the performance of the system. An attempt was made to relate the pole locations for a well-designed 'sky-hook' system (2) to those required for a well-designed active system.
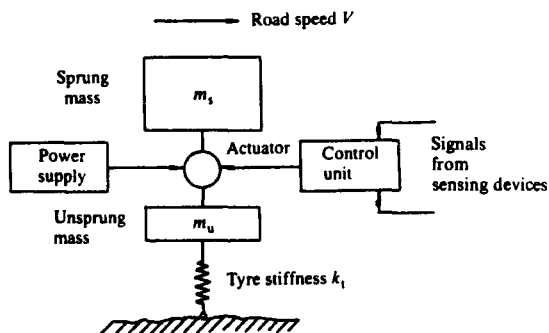
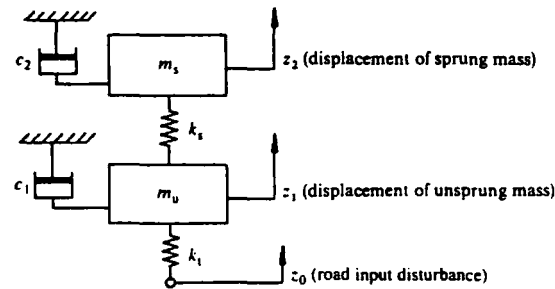136   B B HALL AND K F GILL

Fig. 2 The sky-hook model of a vehicle suspension

This is shown to be unsatisfactory and thus it was necessary to resort to scanning the s plane to find the most appropriate pole locations. The results of this are compared with those in reference (5) and the performance of the active systems are compared with those for an optimal linear passive system.

2 THE SKY-HOOK MODEL

The 'sky-hook' concept of damping, shown in Fig. 2, has been used by Margolis (2) as the basis for the evaluation of active and semi-active suspensions. The idea was considered worth extending to investigate the possibility of using the pole locations for a well-designed sky-hook system to predict the best pole locations of an active system. It must, of course, be recognized that the sky-hook model is physically unrealizable for a practical suspension system. The transfer functions relating the velocities of the masses to that at the base of the tyre are derived from the standard equations of motion developed using Newton's second law. These transfer functions (2) are

$$T_1(s) = \frac{\dot{z}_1}{\dot{z}_0}(s) = \frac{\omega_1/\omega_2\{(s/\omega_2)^2 + 2\zeta_2(s/\omega_2) + 1\}}{\Delta(s)} \quad (1)$$

and

$$T_2(s) = \frac{\dot{z}_2}{\dot{z}_0}(s) = \frac{(\omega_1/\omega_2)^2}{\Delta(s)} \quad (2)$$

where the dots denote differentiation with respect to time and

$$\Delta(s) = s^4 + \omega_2\{2z(1 + \mu d)\}s^3$$
$$+ \omega_2^2\{1 + \mu + \Omega + (2z)^2\mu d\}s^2$$
$$+ \omega_2^3\{2z\mu(1 + d) + 2z\Omega\}s + \omega_2^4\Omega \quad (3)$$

From Fig. 2,

$$\omega_1^2 = \frac{k_1}{m_u}$$

$$\omega_2^2 = \frac{k_s}{m_s}$$

$$\zeta_1 = \frac{c_1}{2m_u\omega_1}$$

$$\zeta_2 = \frac{c_2}{2m_s\omega_2}$$

$$z = \zeta_2$$

$$d = \frac{c_1}{c_2}$$

$$\mu = \frac{m_s}{m_u}$$

$$\Omega = \left(\frac{\omega_1}{\omega_2}\right)^2$$

The characteristic equation is obtained by setting

$$\Delta(s) = 0 \quad (4)$$

The roots (poles) of equation (4) give the values of s which cause the system to become unstable (6). If the roots of the characteristic equation are $-p_x \pm p_y$i and $-q_x \pm q_y$i, the corresponding characteristic equation is

$$s^4 + 2(p_x + q_x)s^3 + (p_x^2 + q_x^2 + 4p_x q_x + p_y^2 + q_y^2)s^2$$
$$+ 2(p_x q_x^2 + p_x^2 q_x + p_x q_y^2 + q_x p_y^2)s$$
$$+ (p_x^2 + p_y^2)(q_x^2 + q_y^2) = 0 \quad (5)$$

For the poles of equations (4) and (5) to be identical, the coefficients must be equal, that is

$$\omega_2 z(1 + \mu d) = A_r$$
$$\omega_2^2\{(1 + \mu + \Omega) + (2z)^2\mu d\} = B_r$$
$$\omega_2^3\{z\mu(1 + d) + z\Omega\} = C_r \quad (6)$$
$$\omega_2^4\Omega = D_r$$

where

$$A_r = p_x + p_y$$
$$B_r = p_x^2 + q_x^2 + 4p_x q_x + p_y^2 + q_y^2$$
$$C_r = p_x q_x^2 + p_x^2 q_x + p_x q_y^2 + q_x p_y^2 \quad (7)$$
$$D_r = (p_x^2 + p_y^2)(q_x^2 + q_x^2)$$

For prescribed pole locations, equation (6) can be solved for z, d, Ω and ω_2.

For harmonic excitation, the transmissibilities corresponding to equations (1) and (2) are obtained by replacing s with $i\omega$ to give

$$T_{r1} = \frac{V_1}{V_0}(\omega)$$

$$= \frac{(\omega_1/\omega_2)^2[\{1 - (\omega/\omega_2)^2\}^2 + (2\zeta_2\omega/\omega_2)^2]^{1/2}}{|\Delta(i\omega)|} \quad (8)$$

(a) Handling   (b) Ride
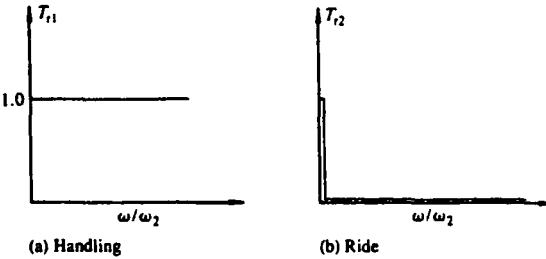
Fig. 3 Ideal transmissibilities for a sky-hook damper model

$$T_{r2} = \frac{V_2}{V_0}(\omega) = \frac{(\omega_1/\omega_2)^2}{|\Delta(i\omega)|} \qquad (9)$$

where V_0, V_1 and V_2 are velocity amplitudes corresponding to $\dot{z}_0$, $\dot{z}_1$, $\dot{z}_2$ and

$$|\Delta(i\omega)| = \left[\left\{g_0 - g_2\left(\frac{\omega}{\omega_2}\right)^2 + \left(\frac{\omega}{\omega_2}\right)^4\right\}^2 \right.$$
$$\left. + \left\{g_1\left(\frac{\omega}{\omega_2}\right) - g_3\left(\frac{\omega}{\omega_2}\right)^3\right\}^2\right]^{1/2} \qquad (10)$$

where

$$g_0 = \left(\frac{\omega_1}{\omega_2}\right)^2$$

$$g_1 = 2\zeta_2\frac{m_s}{m_u}\left(1 + \frac{c_1}{c_2}\right) + 2\zeta_2\left(\frac{\omega_1}{\omega_2}\right)^2$$

$$g_2 = 1 + \frac{m_s}{m_u} + \left(\frac{\omega_1}{\omega_2}\right)^2 + (2\zeta_2)^2\frac{m_s}{m_u}\frac{c_1}{c_2}$$

$$g_3 = 2\zeta_2\left(1 + \frac{c_1}{c_2}\frac{m_s}{m_u}\right)$$
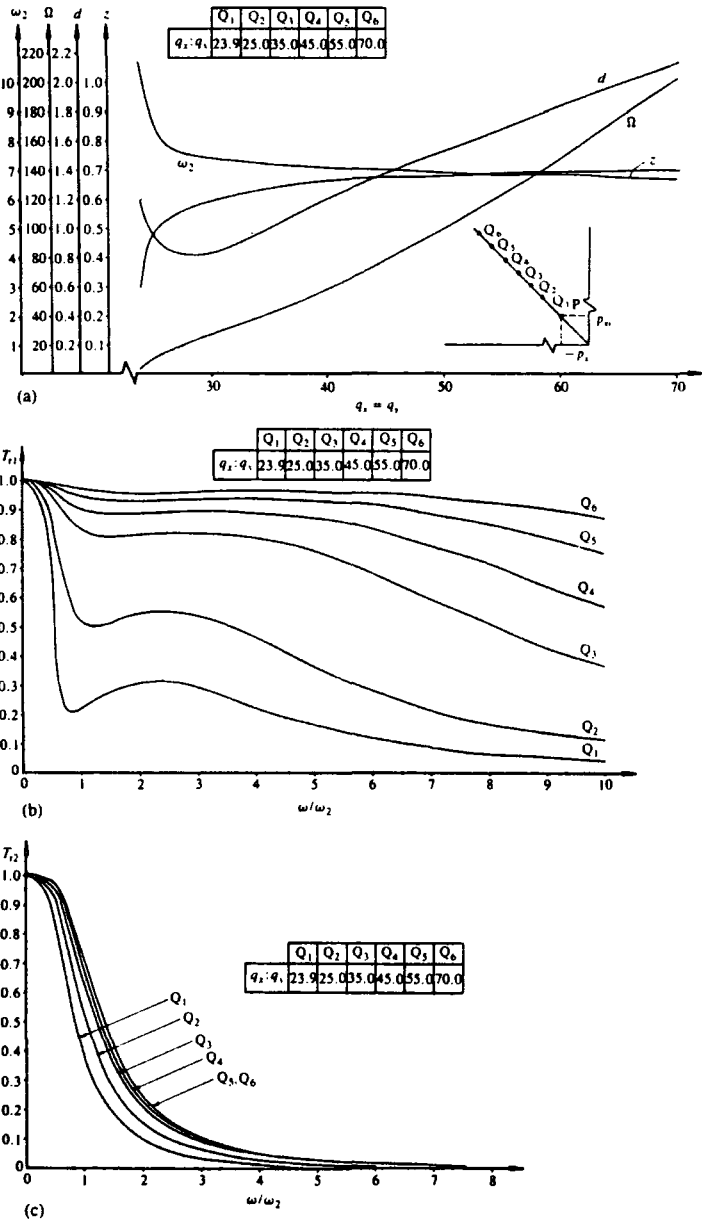
Fig. 4 Variation of (a) z, d, Ω, ω_2, (b) T_{r1} and (c) T_{r2} with pole location Q
($p_x = p_y = 4.7 =$ constant)

B B HALL AND K F GILL
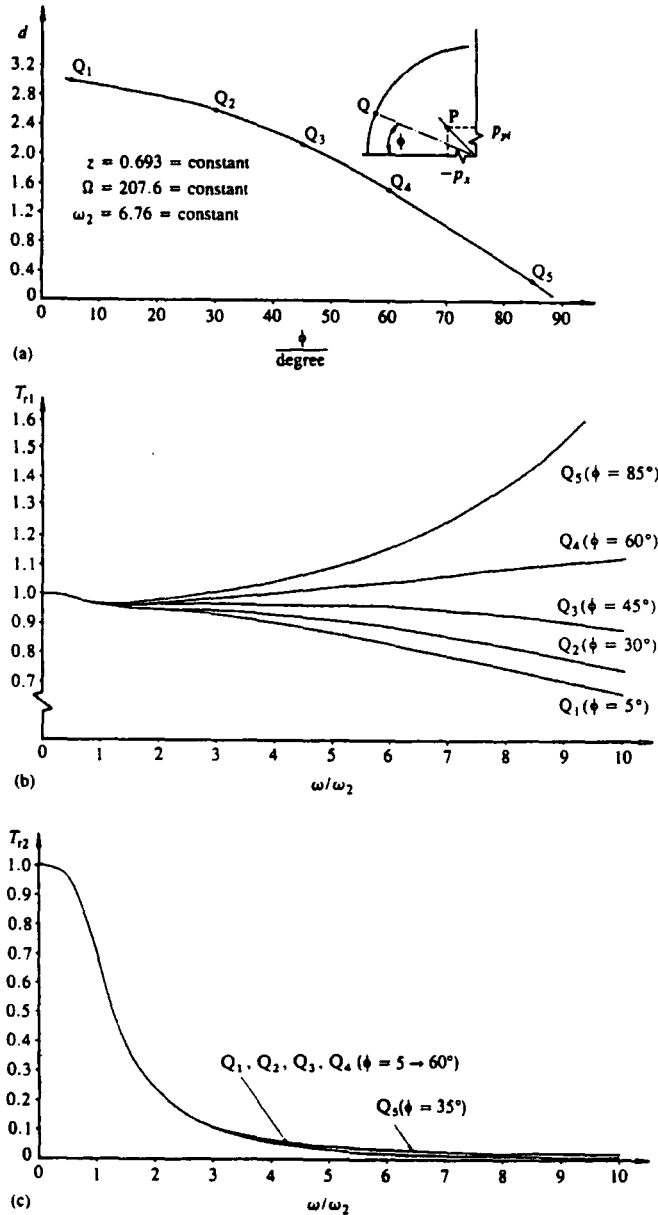
Fig. 5 Variation of (a) d, (b) T_{r1} and (c) T_{r2} with pole location Q on arc of radius 99 ($p_x = p_y = 4.7 =$ constant)

For ideal handling the displacement of the unsprung mass must follow the road contour and for ideal ride the sprung mass must remain stationary. To ensure this, the transmissibilities are of the form shown in Fig. 3.

A systematic search of the s plane (6) was carried out to locate the pole positions which would result in transmissibilities similar to those in Fig. 3. The procedure was to keep one of the pole locations fixed and move the second pole either radially outwards from the origin or along an arc centred on the origin. For the locations of each pole pair

(a) the non-linear set of simultaneous equations (6) was solved and

(b) the transmissibilities were determined from equations (8) to (10) for ω/ω_2 in the range from zero to 10.

The steps in the investigation, together with the results were as follows:

1. Pole P fixed ($p_x = p_y = 4.7$), pole Q moved radially outwards, with $q_x = p_y = 23.9$, 25.0, 35.0 45.0, 55.0, 70.0. The corresponding variations of z, d, Ω and ω_2 with location Q are shown in Fig. 4a while the corresponding transmissibilities T_{r1} and T_{r2} are shown in Fig. 4b and c respectively. In general as Q moves radially outwards T_{r1} improves considerably, while there is a slight deterioration in T_{r2}.
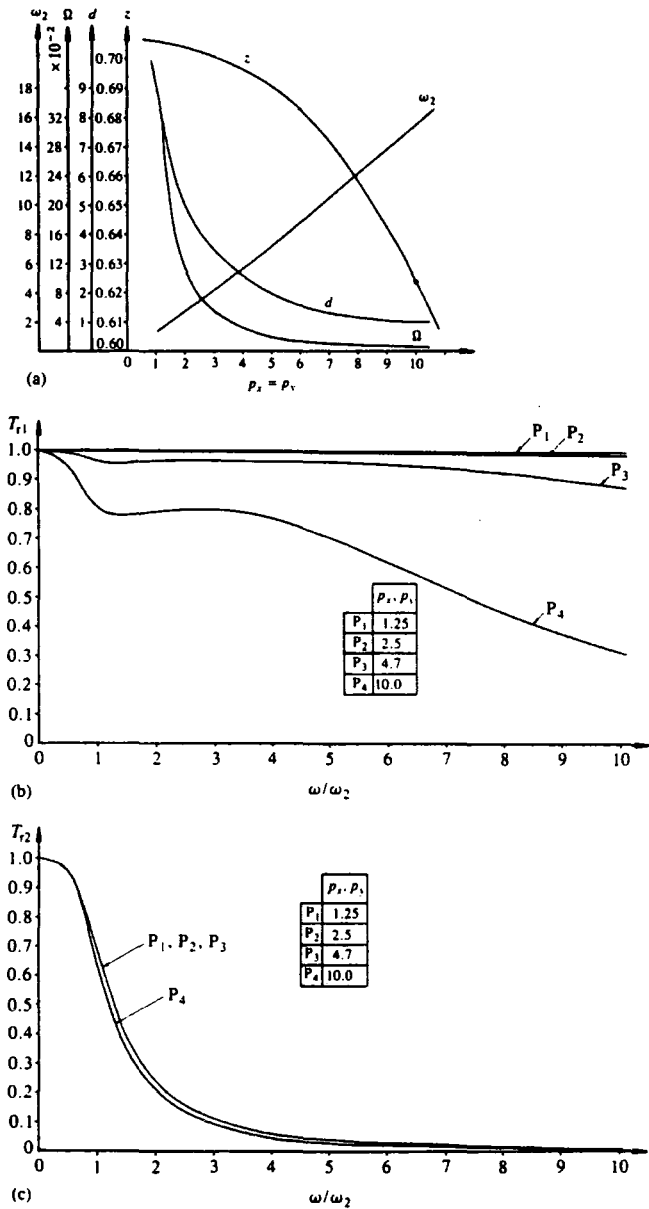
Fig. 6 Variation of (a) z, d, Ω, ω_2, (b) T_{r1} and (c) T_{r2} with pole location P
$(q_x = q_y = 70 = \text{constant})$

2. Pole P fixed $(p_x = p_y = 4.7)$, pole Q moved along an arc of radius 99 (corresponding to the maximum radius in step 1). The angular locations of pole Q were measured in terms of angle ϕ measured from the negative real axis of the s plane. The variation of d with pole location is shown in Fig. 5a (z, Ω and ω_2 were all constant), while the corresponding effects on T_{r1} and T_{r2} are shown in Fig. 5b and c respectively. It is seen that the location of Q has negligible effect on T_{r2}, while the optimum value in terms of T_{r1} is $\phi \simeq 45°$.

3. Pole Q fixed $(q_x = q_y = 70)$, pole P moved radially outwards, $p_x = p_y = 1.25$, 2.5, 4.7, 10.0. The varia-

tions of z, d, Ω and ω_2 with the location of P are shown in Fig. 6a, while the corresponding transmissibilities are shown in Fig. 6b and c. The radial location of P has very little effect on T_{r2} while its best position in terms of T_{r1} is nearest the origin ($p_x = p_y = 1.25$ at a radius of 1.77).

4. Pole Q fixed $(q_x = q_y = 70)$, pole P moved along an arc of radius 1.77, the angular locations of P being $\phi = 5°$, 20°, 45°, 70°, 85°. The variation of z and c with pole location P is shown in Fig. 7a (Ω and ω_2 were both constant), while the corresponding effect on T_{r1} and T_{r2} is shown in Fig. 7b and c respectively. Comparing these curves with the ideal (Fig. 3), it was

140
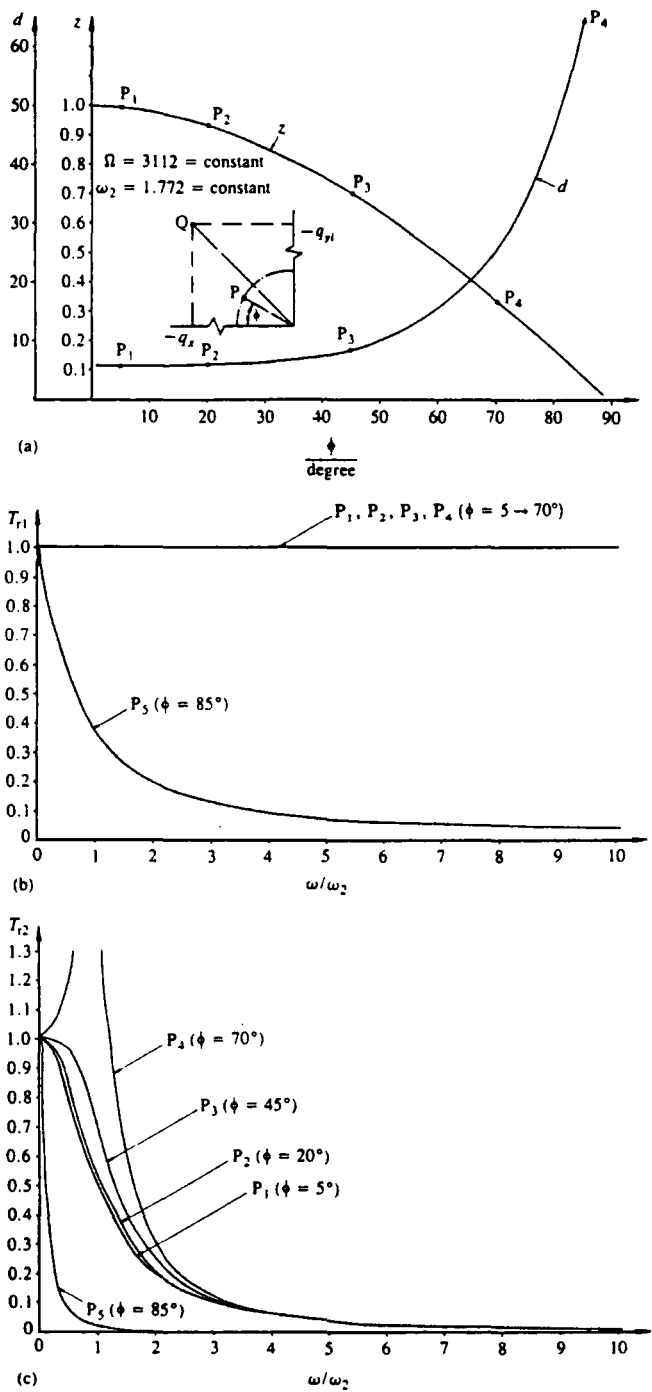
Fig. 7 Variation of (a) z, d, (b) T_{r1} and (c) T_{r2} with pole location P on arc of radius 1.77 ($q_x = q_y = 70$ = constant)

concluded that the best angular location for P was at $\phi = 5°$.

Hence it was deduced that the best pole locations to produce a well-designed sky-hook system were $p_x = 1.763$, $p_y = 0.154$, $q_x = q_y = 70$.

3 EVALUATION OF CONTROL LAWS AND PERFORMANCE OF SOME ACTIVE SUSPENSIONS

Three active configurations were examined with the aim of determining the effect of closed-loop pole locations on the ride, handling and clearance space. Performance
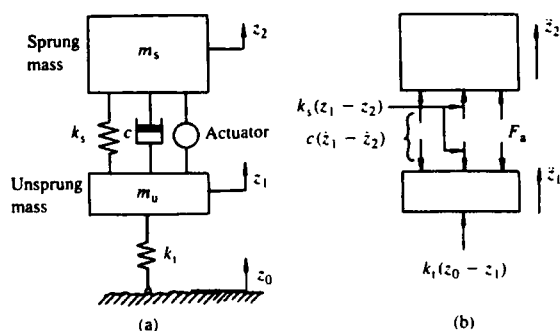
Fig. 8 Quarter vehicle model of active suspension and free-body diagram

was assessed for the reference conditions comprising road speed $V = 20$ m/s and road roughness parameter $S(n_0) = 320 \times 10^{-6}$ m^3/cycle.

3.1 The addition of an actuator to an otherwise conventional passive suspension

The configuration for the quarter vehicle model is shown in Fig. 8. Such an arrangement may be justified because the conventional suspension system would act as a back-up in the event of the active part failing.

Selecting a control law of the form

$$F_a = h_1 z_1 + h_2 z_2 + h_3 \dot{z}_1 + h_4 \dot{z}_2 \qquad (11)$$

where F_a is the force exerted by the actuator and h_1, h_2 etc. are the feedback coefficients, the transfer functions (ratio of input disturbance to output response with zero initial conditions) are found to be

$$\frac{z_1}{z_0}(s) = \frac{k_t(s^2 + q_4 s + q_3)}{m_u \Delta(s)} \qquad (12)$$

$$\frac{z_2}{z_0}(s) = \frac{k_t(q_2 s + q_1)}{m_u \Delta(s)} \qquad (13)$$

where

$$\Delta(s) = s^4 + (p_2 + q_4)s^3 + (p_2 q_4 - p_2 q_4 + p_1 + q_3)s^2$$
$$+ (q_3 p_2 - p_3 q_2 + p_1 q_4 - q_1 p_4)s + q_3 p_1 - p_3 q_1 \qquad (14)$$

In these equations

$$p_1 = \frac{k_t + k_s + h_1}{m_u}, \qquad q_1 = -\frac{k_s + h_1}{m_s}$$

$$p_2 = \frac{c + h_3}{m_u}, \qquad q_2 = -\frac{c + h_3}{m_s}$$

$$p_3 = -\frac{k_s - h_2}{m_u}, \qquad q_3 = \frac{k_s - h_2}{m_s}$$

$$p_4 = -\frac{c - h_4}{m_u}, \qquad q_4 = \frac{c - h_4}{m_s}$$

The transmissibilities corresponding to equations (12) and (13) are

$$T_{r1} = \frac{V_1}{V_0}$$

$$= \frac{k_t}{m_u} \sqrt{\left\{ \frac{(q_3 - \omega^2)^2 + (q_4 \omega)^2}{(\alpha_4 - \alpha_2 \omega^2 + \omega^4)^2 + \omega^2(\alpha_3 - \alpha_1 \omega^2)^2} \right\}} \qquad (15)$$

and

$$T_{r2} = \frac{V_2}{V_0}$$

$$= \frac{k_t}{m_1} \sqrt{\left\{ \frac{q_1^2 + (q_2 \omega)^2}{(\alpha_4 - \alpha_2 \omega^2 + \omega^4)^2 + \omega^2(\alpha_3 - \alpha_1 \omega^2)^2} \right\}} \qquad (16)$$

where

$$\alpha_1 = p_2 + q_4$$

$$\alpha_2 = p_2 q_4 - q_2 p_4 + p_1 + q_3$$

$$\alpha_3 = q_3 p_2 - p_3 q_2 + p_1 q_4 - q_1 p_4 \qquad (17)$$

$$\alpha_4 = q_3 p_1 - p_3 q_1$$

Assuming the closed-loop poles are $-p_x \pm p_y \mathrm{i}$ and $-q_x \pm q_y \mathrm{i}$ and noting that the characteristic equation is

$$s^4 + \alpha_1 s^3 + \alpha_2 s^2 + \alpha_3 s + \alpha_4 = 0$$

It follows that $\alpha_1 = 2A_r$, $\alpha_2 = B_r$, $\alpha_3 = 2C_r$ and $\alpha_4 = D_r$ where A_r, B_r, C_r and D_r are given by equations (7). Thus if the closed-loop poles are specified or are to be the same as those for a well-designed sky-hook model, α_1 to α_4 can be evaluated. Substituting for p_1 to p_4 and q_1 to q_4 into equations (17) results in the following equations for the feedback coefficients:

$$h_2 = k_s - \frac{\alpha_4 m_u m_s}{k_t} \qquad (18)$$

$$h_4 = c - \frac{\alpha_3 m_u m_s}{k_t} \qquad (19)$$

$$h_3 = \frac{1}{m_s} \{\alpha_1 m_u m_s - c(m_u + m_s) + m_u h_4\} \qquad (20)$$

$$h_1 = \frac{1}{m_s} \{\alpha_2 m_u m_s - m_u(k_s - h_2) - m_s(k_t + k_s)\} \qquad (21)$$

Equations (18) to (21) can be solved for h_1 to h_4 provided that m_u, m_s, k_t, k_s and c are specified. Using the data given in reference (7) (that is $m_u = 37$ kg, $m_s = 259$ kg, $k_t = 1.3 \times 10^5$ N/m and $k_s = 1.3 \times 10^4$ N/m), with $c = 1364$ N s/m together with the optimum pole locations for the sky-hook model ($p_x = 1.763$, $p_y = 0.154$, $q_x = q_y = 70.0$), produced the following feedback coefficients: $h_1 = 0.2377 \times 10^6$, $h_2 = 0.1075 \times 10^5$, $h_3 = 0.3578 \times 10^4$ and $h_4 = -0.1216 \times 10^4$.

These values were used in equations (15) and (16) to determine the transmissibilities T_{r1} and T_{r2}. The results were totally unacceptable, as seen in Fig. 9. The general shape of the graph for T_{r1} is not acceptable while the zero frequency value was 110.9 instead of unity. Examination of equations (15) and (16) and comparison with

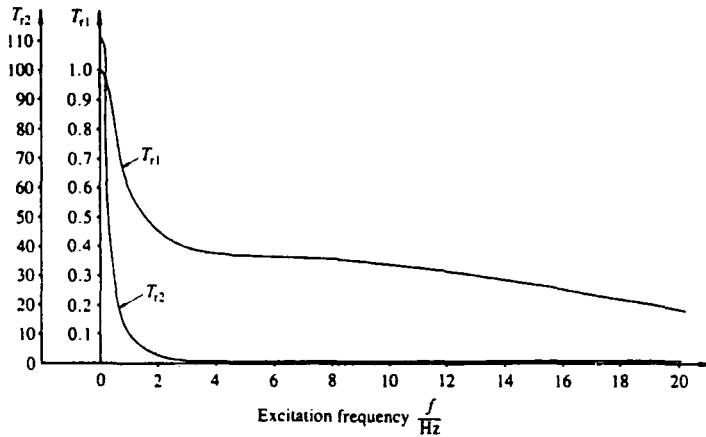142   B B HALL AND K F GILL

Fig. 9   Transmissibilities of an active suspension based on pole locations for
a well-designed sky-hook system

equations (8) and (9) respectively shows that even though the denominators of the equations will be equal when the characteristic equations are the same, the numerators are different. Clearly, this is responsible for the differences in the two sets of transmissibilities curves. It follows that, in general, the use of the optimum pole locations for the sky-hook system is not valid for predicting the best pole locations for an active system.

Indeed, if we examine equations (15) and (16) it may be shown that as ω approaches zero

$$T_{r2} \rightarrow \frac{k_s + h_1}{k_s - h_2}$$

and hence for $T_{r2} \rightarrow 1$, $h_1 = h_2 = 0$, that is displacement feedback must be zero, resulting in only two coefficients, h_3 and h_4, to be evaluated. The best combination of the coefficients to produce transmissibilities variations approximating those of Fig. 3 were $h_3 = 500$ and $h_4 = 0.5$. Defining ride discomfort R_d as the weighted r.m.s. sprung mass acceleration, r.m.s. tyre force F_t and clearance space between sprung and unsprung mass S_c, values corresponding to these feedback coefficients are

$$R_d = 2.064 \text{ m/s}^2, \qquad F_t = 859 \text{ N}, \qquad S_c = 0.0787 \text{ m}$$

It was noticed that other (very different) combinations of h_3 and h_4 gave approximately similar T_{r1} and T_{r2} results, but widely differing results for R_d, F_t and S_c. Hence the credibility of using T_{r1} and T_{r2} as a necessary and sufficient indicator of suspension performance was called into question.

Since in none of the cases was the ride discomfort value less than that for the passive suspension ($h_1 = h_2 = h_3 = h_4 = 0$), it was decided to examine an alternative form of control law.

3.2 An active suspension of the form proposed by Thompson (5, 8)

Consider the more general active system in Fig. 1 and let the force u exerted by the actuator be of the form

$$u = h_1 z_1 + h_2 z_2 + h_3 \dot{z}_1 + h_4 \dot{z}_2 - (h_1 + h_2)z_0 \qquad (22)$$

Then equation (22) can be arranged to give

$$u = h_1(z_1 - z_2) + h_3(\dot{z}_1 - \dot{z}_2)$$
$$\qquad + (h_1 + h_2)(z_2 - z_0) + (h_3 + h_4)\dot{z}_2 \qquad (23)$$

where the first and second terms on the right-hand side represent spring and damping forces (with $k_s = h_1$ and $c = h_3$).

The suspension then resolves itself into the form shown in Fig. 8a, but with a modified actuator force given by

$$F_a = (h_1 + h_2)(z_2 - z_0) + (h_3 + h_4)\dot{z}_2 \qquad (24)$$

that is the last two terms in equation (23). Equation (22) will subsequently be referred to as Thompson's control law.

It may be shown that the transfer functions for the system are

$$\frac{z_1}{z_0}(s) = \frac{m_s(k_t + h_1 + h_2)s^2 - k_t h_4 s - k_t h_2}{m_u m_s \Delta(s)} \qquad (25)$$

and

$$\frac{z_2}{z_0}(s) = -\frac{m_u(h_1 + h_2)s^2 + k_t h_3 s - k_t h_2}{m_u m_s \Delta(s)} \qquad (26)$$

where

$$\Delta(s) = s^4 + \left(\frac{m_t h_3 - m_u h_4}{m_u m_s}\right)s^3$$
$$\qquad + \left\{\frac{m_s(k_t + h_1) - m_u h_2}{m_u m_s}\right\}s^2$$
$$\qquad - \frac{k_t h_4}{m_u m_s}s - \frac{k_t h_2}{m_u m_s}$$
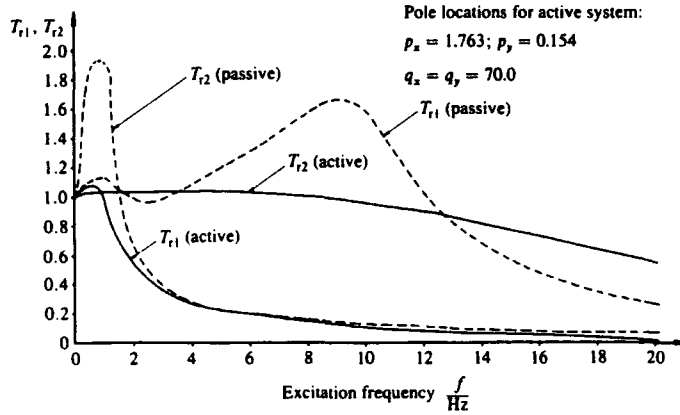$$\qquad = s^4 + v_1 s^3 + v_2 s^2 + v_3 s + v_4 \qquad (27)$$

Fig. 10 Comparison of transmissibilities for a passive system and an active system based on Thompson's control law

and

$$v_1 = \frac{m_s h_3 - m_u h_4}{m_u m_s}$$

$$v_2 = \frac{m_s(k_t + h_1) - m_u h_2}{m_u m_s}$$

$$v_3 = \frac{-k_t h_4}{m_u m_s} \tag{28}$$

$$v_4 = \frac{-k_t h_2}{m_u m_s}$$

Replacing s by $i\omega$, the transmissibilities corresponding to equations (25) and (26) are

$$T_{r1} = \frac{V_1}{V_0} = \frac{1}{m_u m_s}$$

$$\times \left[\frac{\{-k_t h_2 - (k_t + h_1 + h_2)m_s \omega^2\}^2 + (k_t h_4 \omega)^2}{(v_4 - v_2 \omega^2 + \omega^4)^2 + \omega^2(v_3 - v_1\omega^2)^2} \right]^{1/2} \tag{29}$$

$$T_{r2} = \frac{V_2}{V_0} = \frac{1}{m_u m_s}$$

$$\times \left[\frac{\{-k_t h_2 + m_u(h_1 + h_2)\omega^2\}^2 + (k_t h_3 \omega)^2}{(v_4 - v_2 \omega^2 + \omega^4)^2 + \omega^2(v_3 - v_1\omega^2)^2} \right]^{1/2} \tag{30}$$

Assuming that the closed-loop poles are $-p_x \pm p_y i$ and $-q_x \pm q_y i$, it follows that $v_1 = 2A_r$, $v_2 = B_r$, $v_3 = 2C_r$ and $v_4 = D_r$, where A_r to D_r are given by equations (7). Thus if the closed-loop poles are specified, v_1 to v_4 can be evaluated. The feedback coefficients can then be determined from equations (28) as follows:

$$h_2 = \frac{-m_u m_s v_4}{k_t} \tag{31}$$

$$h_4 = \frac{-m_u m_s v_3}{k_t} \tag{32}$$

$$h_3 = \frac{m_u m_s v_1 + m_u h_4}{m_s} \tag{33}$$

$$h_1 = \frac{m_u m_s v_2 + m_u h_2}{m_s} - k_t \tag{34}$$

Table 1 Comparison of active and passive suspension performances for reference road and speed conditions

	$\dfrac{R_d}{\text{m/s}^2}$	$\dfrac{F_t}{\text{N}}$	$\dfrac{S_c}{\text{m}}$
Passive system	1.8	877	0.078
Active system (Thompson's control law, optimum sky-hook pole locations)	2.17	650	0.105
Active system (Thompson's control law, poles on Thompson's optimum root locus)	2.46	644	0.065

If the optimum pole locations for the sky-hook system are used ($p_x = 1.763$, $p_y = 0.154$, $q_x = q_y = 70.0$) the feedback coefficients are found to be $h_1 = 2.507 \times 10^6$, $h_2 = -2.63 \times 10^3$, $h_3 = 4.942 \times 10^3$ and $h_4 = -2.58 \times 10^3$. The corresponding transmissibilities T_{r1} and T_{r2} are compared in Fig. 10 with those for a passive system.

The performance parameters R_d, F_t and S_c were evaluated for:

(a) the above coefficients,
(b) the passive system,
(c) a pair of closed-loop poles lying on Thompson's optimum root loci ($\rho = 10^{-10}$, $q_1 = 10$, $q_2 = 1$, ρ, q_1 and q_2 being weighting factors) (5),

and the results are given in Table 1. The general conclusions from this are:

1. There are no significant improvements in performance of either active system when compared with the passive system.
2. Despite having apparently much better transmissibility characteristics (Fig. 10), the active control based on the optimum sky-hook pole locations does not lead to an improved performance in terms of R_d, F_t and S_c.

It is concluded that transmissibilities T_{r1} and T_{r2} are necessary, but not sufficient, indicators of suspension performance. The other factors, which must apparently be taken into account as well, are the desirable phase
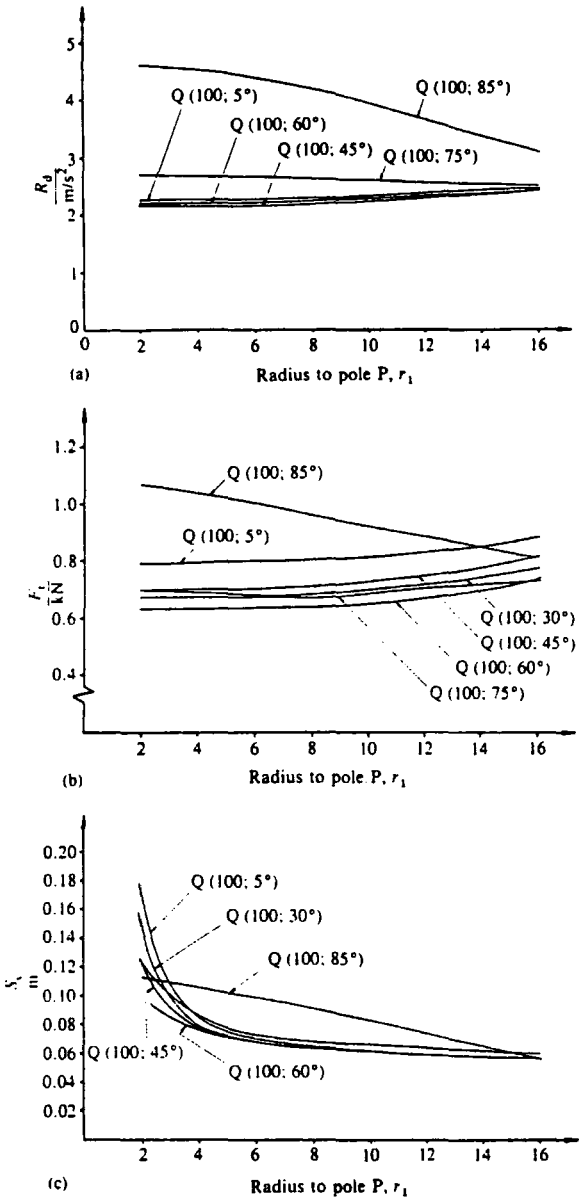
Fig. 11   Effect of pole locations on (a) R_d (b) F_t and (c) S_c
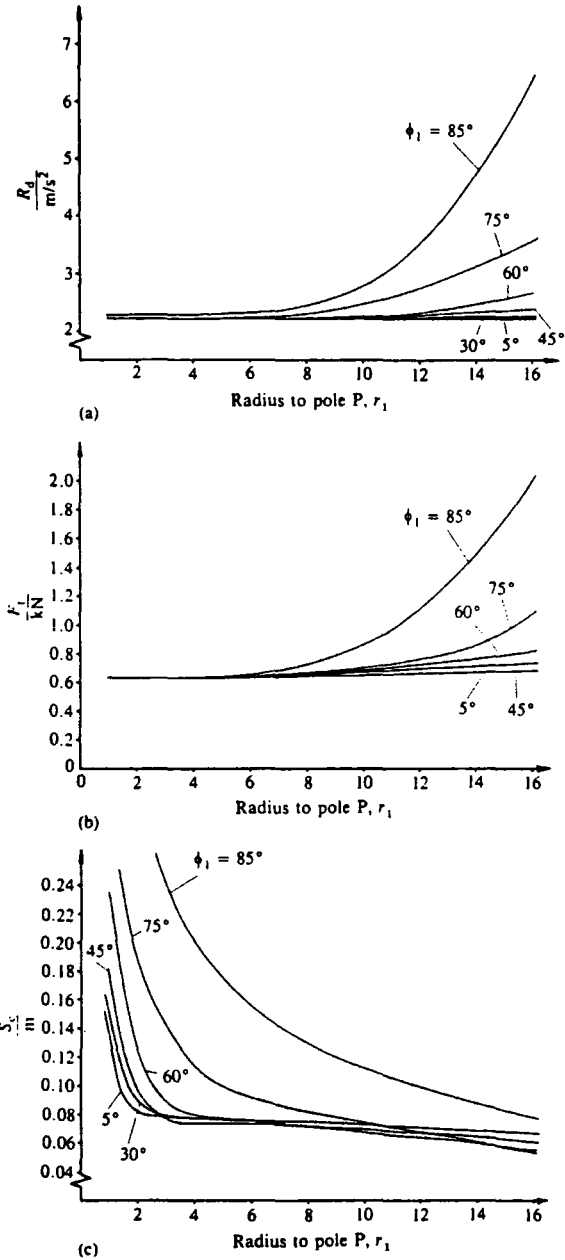($\phi_1 = 45°$, $r_2 = 100$, both constant)

relationships that must also exist, for example z_0 and z_1 must be in phase for good road holding.

The use of T_{r1} and T_{r2} as sole predictors of performance [proposed by some authors, for example Margolis (2)] was subsequently abandoned and trial and observation scanning of the s plane was resorted to.

3.3 Pole locations by scanning the s plane (Thompson's control law)

Assume two pairs of complex poles and denote those in the upper left-hand quadrant of the s plane as P and Q. Their locations can be defined by their respective radii

Fig. 12   Effect of pole locations on (a) R_d, (b) F_t and (c) S_c
[Q (100, 60°) is constant]

r_1 and r_2 and angular locations ϕ_1 and ϕ_2, where the ϕ's are measured from the negative real axis. The steps in the investigation together with the results were as follows:

1. Pole P located on radial line $\phi_1 = 45°$, r_1 varied from 2 to 16, pole Q on an arc of radius 100, ϕ_2 varied from 5° to 85°. The corresponding variations of R_d, F_t and S_c are shown in Fig. 11. In general:

(a) The lowest ride discomfort is given by Q (100, 45°) and for this pole location R_d is quite insensitive to r_1.

(b) The lowest dynamic tyre force is obtained for Q (100, 60°) and tends to become smaller as r_1 increases.

Overall the best compromise between R_d, F_t and S_c is for pole locations P (8, 45°), Q (100, 60°).

2. Pole Q located at Q (100, 60°), r_1 varied from 2 to 16 and ϕ varied from 5° to 85°. The corresponding variations of R_d, F_t and S_c are shown in Fig. 12; this shows:

(a) R_d and F_t are independent of r_1 and ϕ provided $1 < r_1 < 8$.

(b) As r_1 becomes greater than 8, both R_d and F_t increase. This increase is quite pronounced for $45 < \phi_1 < 85°$.

(c) Clearance space decreases with r_1 for all ϕ_1, a limiting value of approximately 0.07 m being reached for $r_1 > 2$ and $5° < \phi_1 < 45°$.

The optimum location for the dominant pole P would appear to be at $r_1 = 8$, $\phi_1 = 5°$. This gives a good balance between ride, handling and clearance space. Indeed it is seen from Fig. 12c that movement of pole P along the radial line $\phi_1 = 5°$ towards the origin will give control over the clearance space without affecting ride and handle.

3.4 An active suspension with displacement and velocity feedback

Assuming the general form of active system shown in Fig. 1 together with an actuator force u, given by the control law

$$u = h_1 z_1 + h_2 z_2 + h_3 \dot{z}_1 + h_4 \dot{z}_2 \qquad (35)$$

it follows that the characteristic equation is still given by equation (27). It is now assumed that the closed-loop poles consist of a pair of real poles and a pair of complex poles. Denoting the real poles as P and Q (at $-p$ and $-q$ respectively) and the complex pole R (at $-r_x + r_y i$) in the upper left-hand quadrant of the s plane, the characteristic equation becomes

$$s^4 + (p + q + 2r_x)s^3 + \{pq + r_x^2 + r_y^2 + 2r_x(p + q)\}s^2$$
$$+ \{(p + q)(r_x^2 + r_y^2) + 2pqr_x\}s + pq(r_x^2 + r_y^2) = 0 \quad (36)$$

The feedback coefficients are still given by equations (31) and (34) except that now

$$v_1 = p + q + 2r_x$$

$$v_2 = pq + r_x^2 + r_y^2 + 2r_x(p + q)$$

$$v_3 = (p + q)(r_x^2 + r_y^2) + 2pqr_x$$

$$v_4 = pq(r_x^2 + r_y^2)$$

The effects of varying the locations of P, Q and R on R_d, F_t and S_c were investigated and it was found that significant improvements in ride could be obtained by placing the poles in the vicinity of -1, -0.5, $-2 \pm 59.2i$. Some of the effects of pole locations on R_d, F_t and S_c are shown in Fig. 13. It is seen that
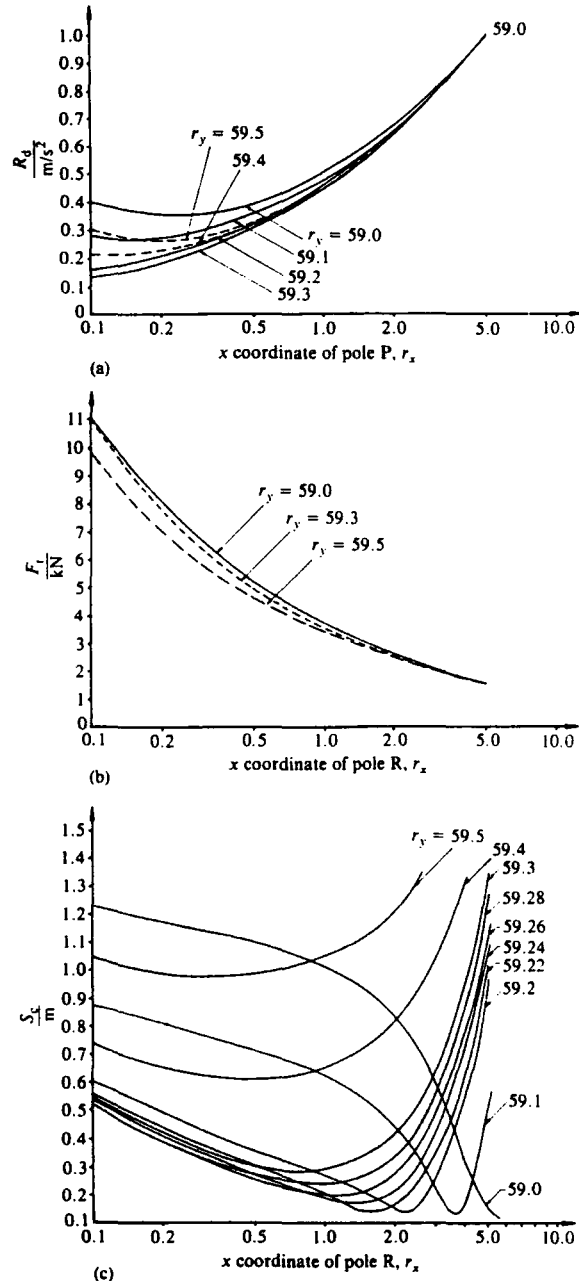

(a)

(b)

(c)

Fig. 13 Effect of pole location R on (a) R_d, (b) F_t and (c) S_c ($p = 1.0$, $q = 0.5$, both constant)

1. Ride deteriorates as r_x increases.
2. Dynamic tyre force decreases as r_x increases.
3. Minimum clearance space is dependent on r_x and r_y. $(S_c)_{min} = 0.13$ and may be obtained with R pole locations $-1.5 + 59.22i$, $-2.3 + 59.2i$ or $-3.7 + 59.1i$.

Clearly the improvements in ride performance (typically $R_d = 0.65$ m/s^2) is obtained at the expense of handling $(F_t = 2.6$ kN) and clearance space $(S_c = 0.15$ m). If the suspension designer wishes to exercise discretion over the weighting between the three design criteria, then a
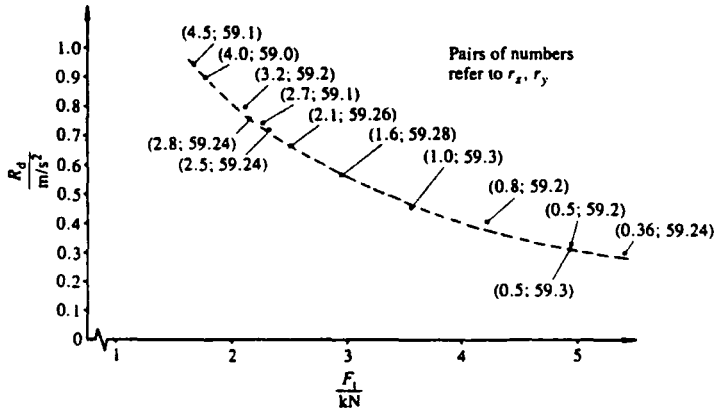
Fig. 14 Relationship between R_d and F_t for $S_c = 0.3$ m ($p = 1.0$, $q = 0.5$ and pairs of numbers refer to r_x, r_y)

diagram of the type shown in Fig. 14 can be constructed. This indicates the pole locations required for a particular choice of R_d and F_t for a typical clearance space (in this case 0.3 m).

4 CONCLUSION

The closed-loop poles which result in ideal transmissibilities do not necessarily result in optimum suspension performance under normal operating conditions because phase information is neglected. Ideal transmissibilities are necessary but not sufficient conditions for optimum performance. The concept of using ideal transmissibilities of a hypothetical model with sky-hook dampers as a means of determining the best pole locations is also invalid because the zeros of the transfer function for the hypothetical model are different from those of a physically realizable system.

A trade-off between ride, handling and clearance space is possible by control of the feedback coefficient values. Poles can be located to satisfy prescribed design criteria.

REFERENCES

1 Sutton, H. B. The potential for active suspension systems. *Automot. Engr (Lond.)*, 1979, 4(4), 21–24.
2 Margolis, D. L. Semi-active control of wheel hop in ground vehicles. *Vehicle System Dynamics*, 1983, 12, 317–330.
3 Mormon, K. N. and Giannopoulos, F. Recent advances in the analytical and computional aspects of modelling active and passive vehicle suspensions. ASME Applied Mechanics Symposia. In *Computational methods in ground transportation vehicles* (Eds M. M. Kamal and J. A. Wolf), AMD Vol. 50, November 1982.
4 Goodall, R. M. and Kortum, W. Active controls in ground transportation—a review of the state-of-the-art and future potential. *Vehicle System Dynamics*, 1983, 12, 225–257.
5 Thompson, A. G. Optimal and sub-optimal linear active suspensions for road vehicles. *Vehicle System Dynamics*, 1984, 13, 61–72.
6 Schwarzenbach, J. and Gill, K. F. *System modelling and control*, 2nd edition, 1984 (Edward Arnold, London).
7 Hall, B. B. and Gill, K. F. Performance of a telescopic dual tube automotive damper and the implications for vehicle ride prediction. *Proc. Instn Mech. Engrs*, Part D, 200 (D2), 115–123.
8 Thompson, A. G. An active suspension with optimal linear state feedback. *Vehicle System Dynamics*, 1976, 5, 187–203.

APPENDIX

Passive suspension

For the quarter vehicle model the natural frequency and damping ratio of a passive suspension system is

$$\omega_2 = \sqrt{\frac{k_s}{m_s}} \tag{37}$$

and

$$\zeta = \frac{c}{\sqrt{(2m_s k_s)}} \tag{38}$$

the symbols having their normal meaning. Typical values for tyre stiffness, sprung and unsprung mass are

$$k_t = 1.3 \times 10^5 \text{ N/m}$$

$$m_s = 259 \text{ kg}$$

$$m_u = 37 \text{ kg}$$

Selecting a road speed $V = 20$ m/s and road roughness parameter $S(n_0) = 320 \times 10^{-6}$ m³/cycle, R_d, F_t and S_c were evaluated for $\zeta = 0.2(0.1)0.8$ and $\omega_2 = 2(2)14$ rad/s, which are displayed graphically in Figs 15 to 18.

Suspension optimization

For prescribed clearance spaces, typically 0.07, 0.08, 0.09 and 0.1 m, the corresponding natural frequencies ω_2 for each of the damping ratios can be found from Fig. 15. The corresponding ride discomfort and dynamic tyre force values can be found from Figs 16

Table 2 Optimum R_d, F_t, k_s and c for a range of S_c

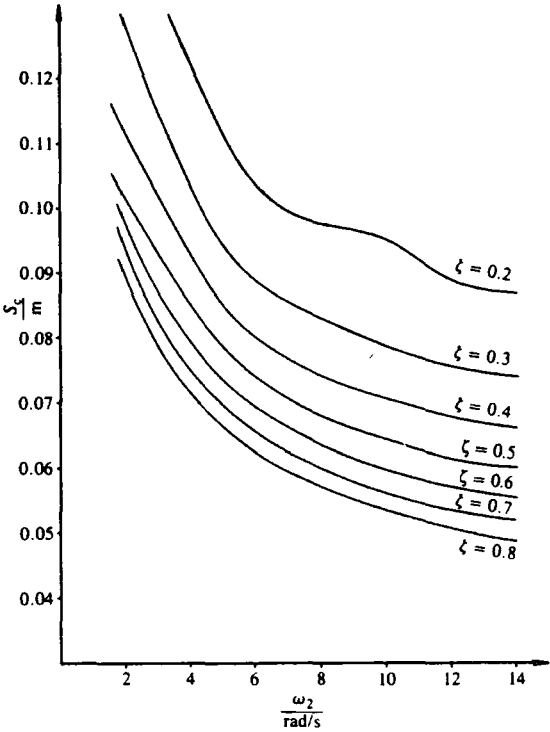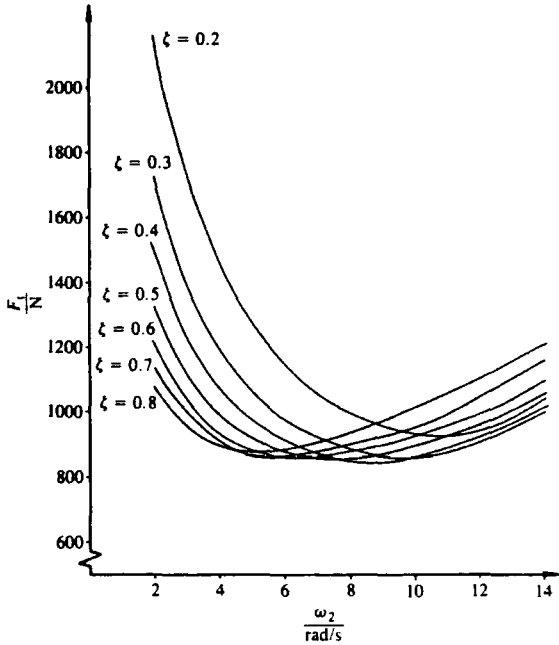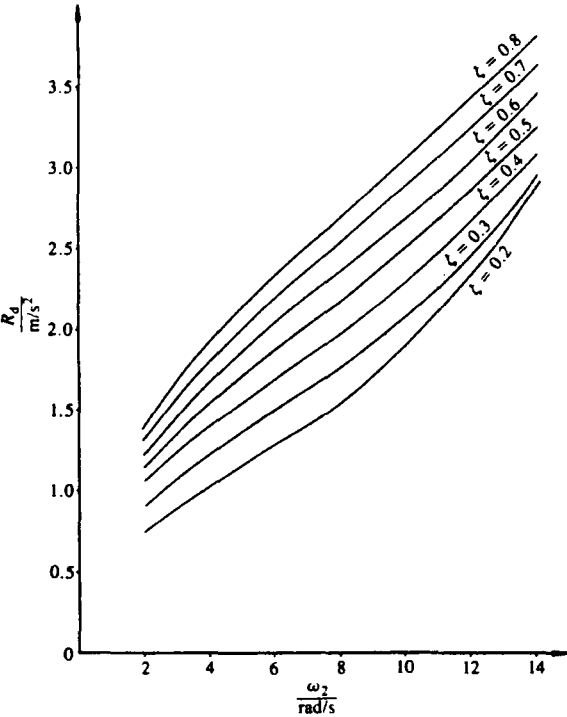| $\frac{S_c}{m}$	$\frac{R_d}{m/s^2}$	$\frac{F_t}{N}$	Optimum suspension parameters	
			$\frac{k_s}{N/m}$	$\frac{c}{Ns/m}$
0.07	1.98	860	8415	1772
0.08	1.68	880	9014	1222
0.09	1.48	990	8713	901
0.10	1.28	1130	5014	684

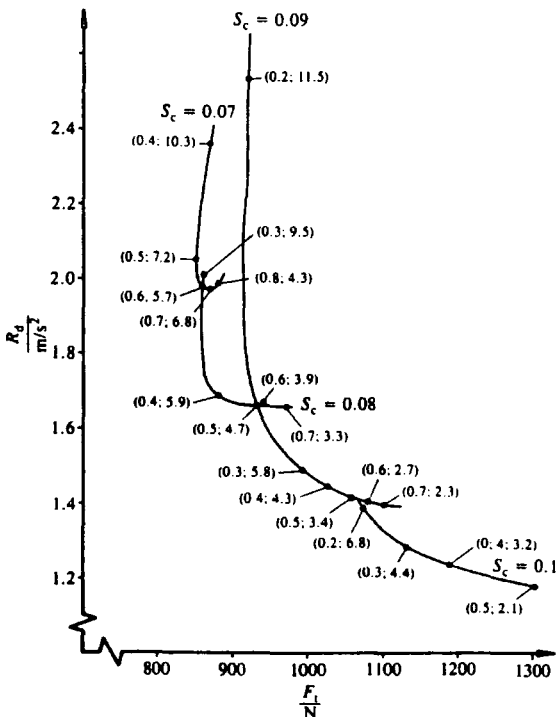**Fig. 15**

Fig. 17

Fig. 16

Fig. 18

and 17 respectively. These values enable graphs of R_d versus F_t to be plotted for each prescribed S_c. The results are shown in Fig. 18.

Even though these curves do not have clearly defined minima, they can still be used (with a little judgement) to obtain a good compromise for R_d and F_t. Clearly these values must be selected to be collectively as small as possible. Having selected the appropriate point on a particular S_c curve, ω_2 and ζ can be estimated and

hence k_s and c found from equations (37) and (38) respectively. Typical results are given in Table 2.

This approach to suspension design is quite simple, but it must always be remembered that the system will only be optimal for one road type and vehicle speed combination. This clearly is a major limitation of a passive system.

The values of R_d and F_t given in Table 2 may be used as a basis for comparison of active suspension systems.

PAPER 59

The Drying and Curing of Latex-backed Carpets

R.M. Baul, K. Gill and I. Holme   University of Leeds, UK

INTRODUCTION

The drying and curing of foamed latex applied to a latex pre-coated tufted carpet are processes that must be carefully controlled during carpet backing to ensure that high levels of quality and performance are attained at minimum operating costs. Quality and performance depend not only upon the control of material specifications, but upon factors such as foam gauge (thickness), the foam density when wet, the degree of "blowing up" on curing (i.e. expansion of the foam), and the degree of cure.

One of the most difficult production problems in carpet backing is ensuring under all production running conditions that a satisfactory degree of cure for the latex foam has been achieved. If this is not achieved, inferior physical and mechanical performance can lead to substandard carpet quality, irrespective of the quality of tufting.

The work described in this paper summarizes much consolidated effort on the part of all those associated with the Teaching Company Scheme established in 1980 between the Departments of Mechanical Engineering and of Textile Industries in the University of Leeds with Carpets International (UK) Limited. One of the principal objectives was to improve manufacturing performance in the foam backing.

The results of this study are concerned with the measurement and control of drying and curing processes in foam backing to ensure a more efficient use of raw materials and energy, and to enable a more closely controlled range of carpet qualities to be achieved.

EXPERIMENTAL WORK

Latex Foam

Domestic-quality foam was generated using proprietary products to give a no-gel carboxylated SBR latex foam containing a resin and catalyst to effect curing together with fillers, pH stablizers, etc.

Carpet

Conventional tufted carpet was first pre-coated with a synthetic latex anchor-coat, which was dried prior to the application of the foamed latex.

Foam generation and application

Small-scale experiments were conducted using a Cowie and Riding CR Twin foam generator and applied to carpet samples using a Werner Mathis laboratory coater. Production trials were conducted using a manually controlled Cowie

and Riding foam generator that applied foam to a foam bank. Foam was applied to the moving pre-coated carpet using a foam-application roller held at a fixed height above a fixed horizontal bedplate.

Drying and curing

Laboratory-scale drying and curing trials were conducted on a Werner Mathis Laboratory Drying and Curing Oven. Production-scale trials were conducted on the carpet backing plant of Carpets International (UK) Ltd. at Brighouse.

Measurement of temperature/time profiles

Laboratory-scale trials were conducted using a Coomark electronic thermometer using chromel/alumel sheathed thermocouples.

for production-scale trials, a self-contained monitoring probe was designed and built at Leeds University. This device recorded the temperatures along the length of the dryer, both of the air and of the foam/carpet interface. The device was interrogated (after recovery at the end of the carpet drying and curing oven) by a micromputer that reconstructed the temperatures from the recorded data. These could be presented in graphic or tabular form, and also recorded for playback and subsequent analysis.

The unit was designed to operate in dryer temperatures to 180°C for as long as 15 minutes. The construction of the dryer imposed a height limit of 5 cm and weight had to be minimized to prevent carpet sagging in the dryer. Power was supplied by using rechargeable batteries that lasted from 50 to 100 hours between charges.

Eight thermocouple sensors can be attached to the unit and their temperature can be measured every 4 seconds. CMOS logic and ADC integrated circuitry are used together with high-density CMOS memories, which can store more than 4000 readings.

RESULTS AND DISCUSSION

FOAM-TEMPERATURE MEASUREMENT IN LABORATORY TRIALS

It was realized early in this project that it would be necessary to obtain a full understanding of all the aspects of the foaming, drying, and curing processes. Laboratory trials were therefore conducted in the University, to obtain information on the drying and curing process for latex-backed carpets.

The method used in each of these trials was to foam over a thin wire thermocouple probe to guarantee that the temperature was always taken at the carpet/foam interface. Temperatures were taken every 10 s and the results are shown in Figs. 1 to 6. The results of these trials are summarized below.

Weight of foam applied

The rate of heat transfer from oven air temperature to carpet surface was measured with and without steam present in the oven. The temperature rise at the carpet surface to the oven air temperature of 150°C was rapid and took less than 100 s.

R.M. Baul, K. Gill and I. Holme

The foam weights tested were 3.7, 6.8, 7.8, and 8.5 g/100 cm^3 respectively. This was achieved by varying the foam thickness and maintaining the foam density constant.

In each case the foam backed carpet was placed in the oven at room temperature. The carpet/foam interface temperature initially increased to approximately 70°C in 120 to 150 s and remained constant for a finite period. The length of the constant-temperature plateau was proportional to the foam thickness, i.e. to the amount of water present in the foam. At the end of this period, the temperature rose rapidly to the nominal oven temperature (Fig. 1 and Fig. 2).

The constant-temperature plateau is a significant percentage of the time required for the interface conditions to reach the cure temperature, which then has to be maintained for a period of 1.5 minutes.
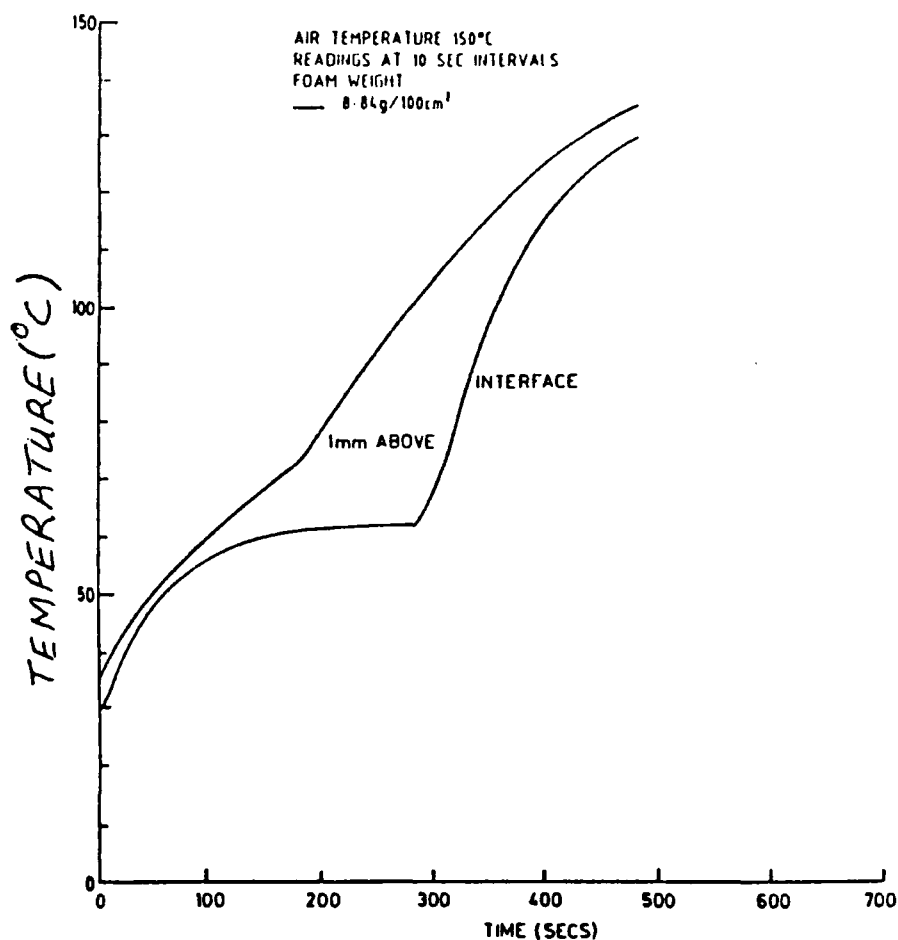
Fig. 1. Temperature profiles at differant heights within the foam.

Effect of introducing steam into the oven

As indicated above, the length of the temperature plateau is principally governed by the foam moisture content; an attempt was made to reduce this by increasing the heat-transfer rate to the foam. Wet steam was introduced into

Carpets: Back to Front

the oven to increase the heat transfer coefficient at the start of the drying cycle and, although the wet-bulk temperature increased to 80°C and the plateau temperature increased by 28°C, the length of the plateau remained sensibly constant (Fig. 3).
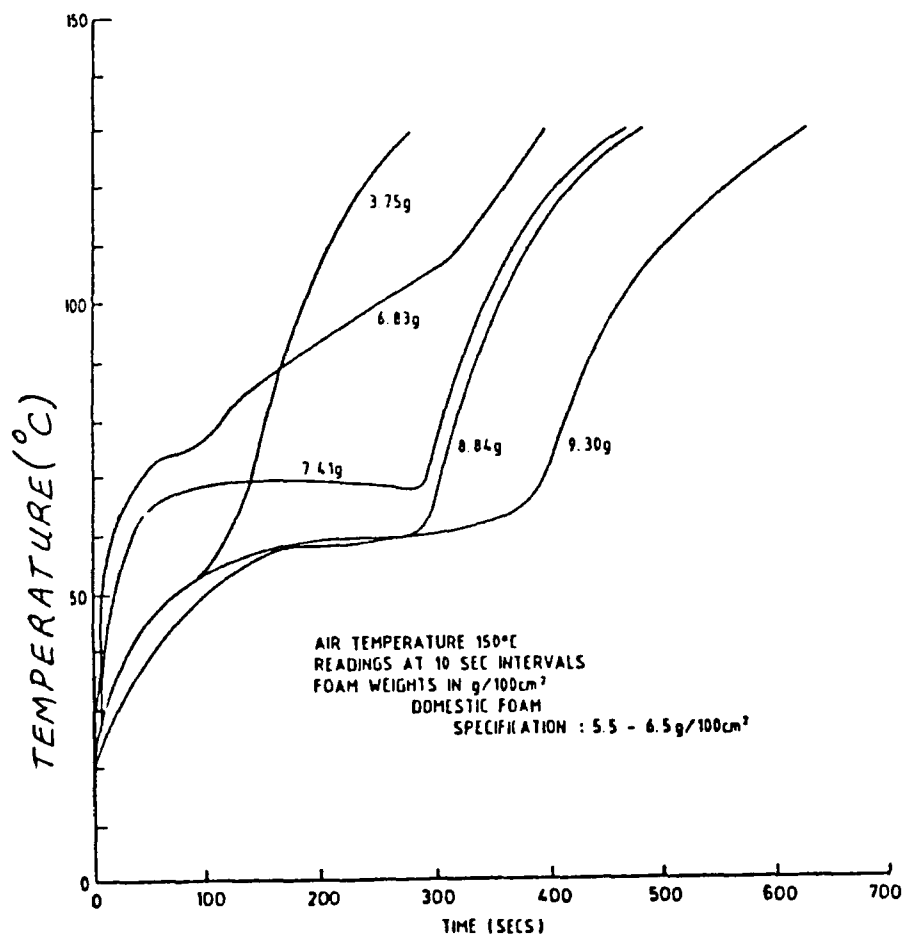

Fig. 2. Effect of varying foam weight on temperature profiles.

Effect of pre-gelling

If the backing foam on a carpet is heated too quickly or subjected to too high a temperature, severe cracking will occur. This is eliminated by passing the weft foam under an infrared heater to pre-gel the surface. Trials were conducted to discover whether this operation had any influence on the interface temperature/time profile. As expected "cracking" occurred on the non-gelled surface, but the temperature profile remained the same in both cases. Samples were prepared with varying degrees of gelling:

(1) 45 s IR - cooled - cured (normal plant practice)
(2) 30 s IR - cooled - cured
(3) 45 s IR - no cooling - cured
(4) 90 s IR - no cooling - cured

Condition (4) gave an initial temperature boost, but within 2 minutes the
temperature returned to that observed in the other trials. Condition (2)
required the longest drying and curing cycle. Increasing the gelling time
reduced the oven time needed because the infrared heating did reduce the
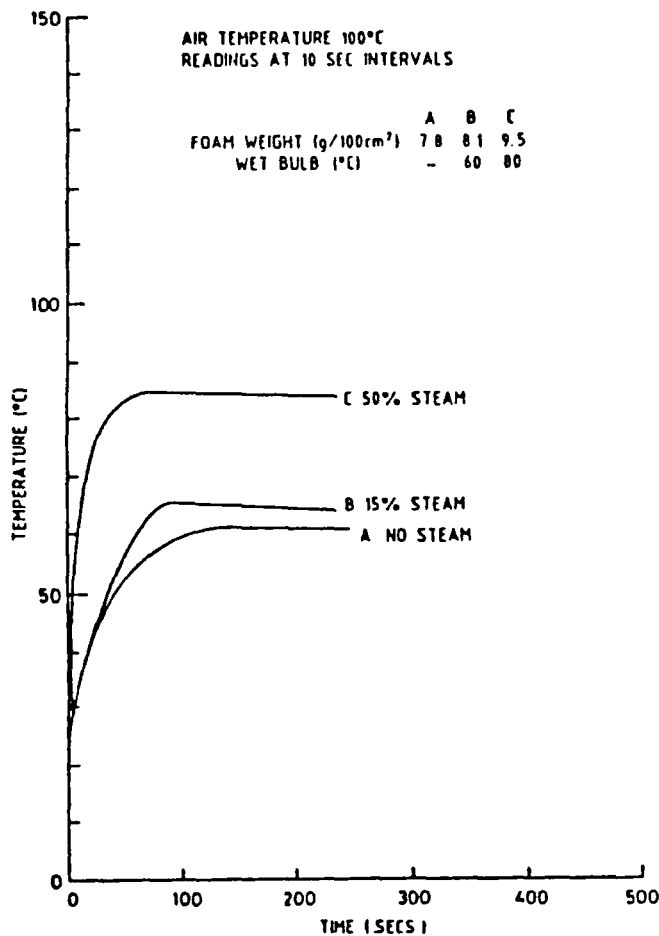moisture content in a sample.

Fig. 3. Effect of steam on initial stages of temperature profiles.

Effect of reducing tuft-side temperature

Oven gas temperatures on the plant are set to give 160°C on the foam side of
the carpet and 120°C on the tuft side. It was noticed in earlier work that
the carpet was a very good heat insulator, suggesting that the heat flow
through the carpet might be changed only marginally by variations in the tuft-
side gas temperature (Fig. 4). To emulate plant conditions "Sindanyo" heat-
resistant board was used to insulate the tuft face. The results of the trial
supported the view that major changes to the tuft-side temperature might be
possible without significantly changing the interface temperature/time profile
(Fig. 5). It is normally considered that this heat is necessary to "burst"
the carpet pile, but no evidence of this was seen in the trial. This
reduction in extra heat generation would make a saving in energy cost.
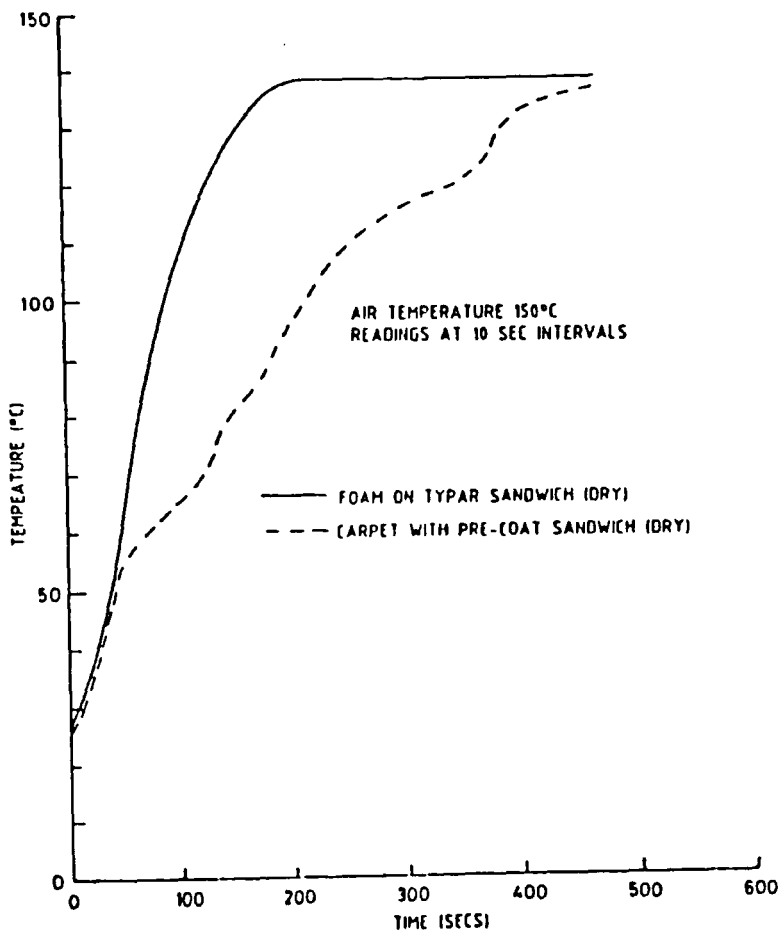
Carpets: Back to Front

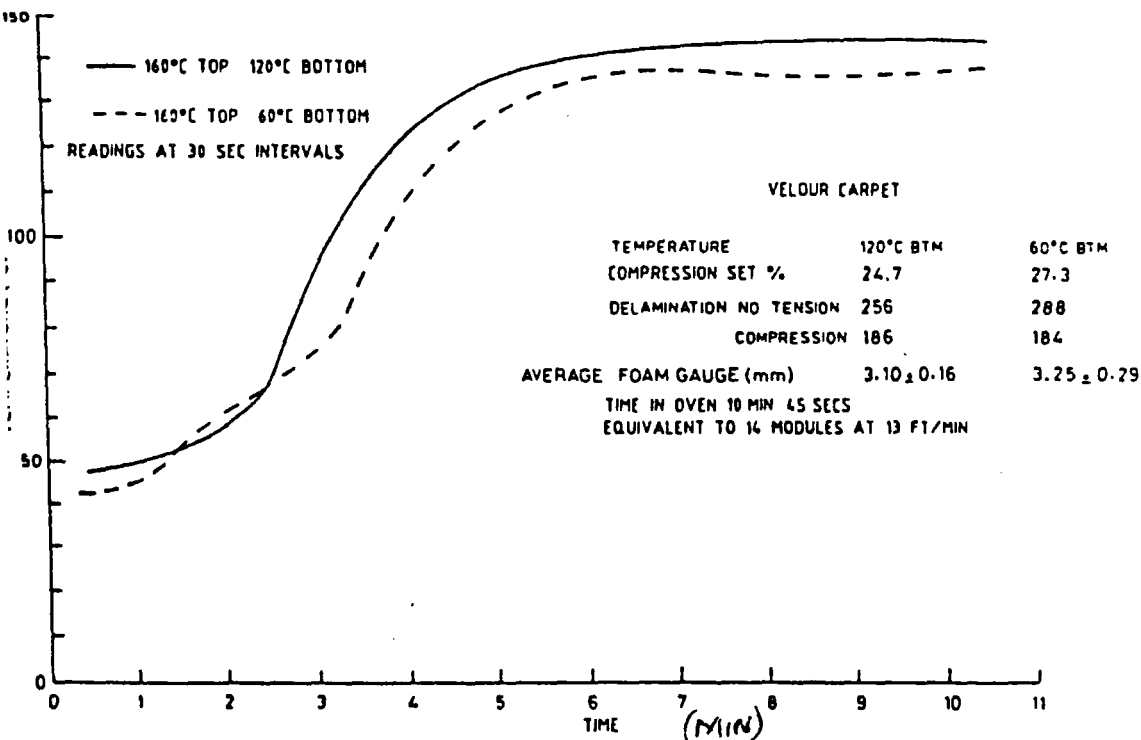Fig. 4. Temperature profiles showing the insulation properties of carpet an foam.

Fig. 5. Effect of reduced bottom temperature on interface temperature durin drying and curing.

Effect of reducing oven temperature

All measured interface temperature/time profiles showed that there is a stage at which the temperature remains relatively constant before rising rapidly to the curing temperature of $130^{0}C$. This indicates that it is unnecessary to heat at the higher temperature of $160^{0}C$ throughout the drying and curing cycle, because the foam temperature will not exceed 50 to $60^{0}C$. To confirm this in the laboratory trials, the temperature was reduced to $110^{0}C$ (Fig. 6). This demonstrated that the time to reach the curing phase was the same at both temperature settings. These findings and those of the previous section were confirmed by plant trials.

READINGS AT 10 SEC INTERVALS
FOAM WEIGHT 11.9 g/100cm²

AIR TEMPERATURE

150°C

110°C
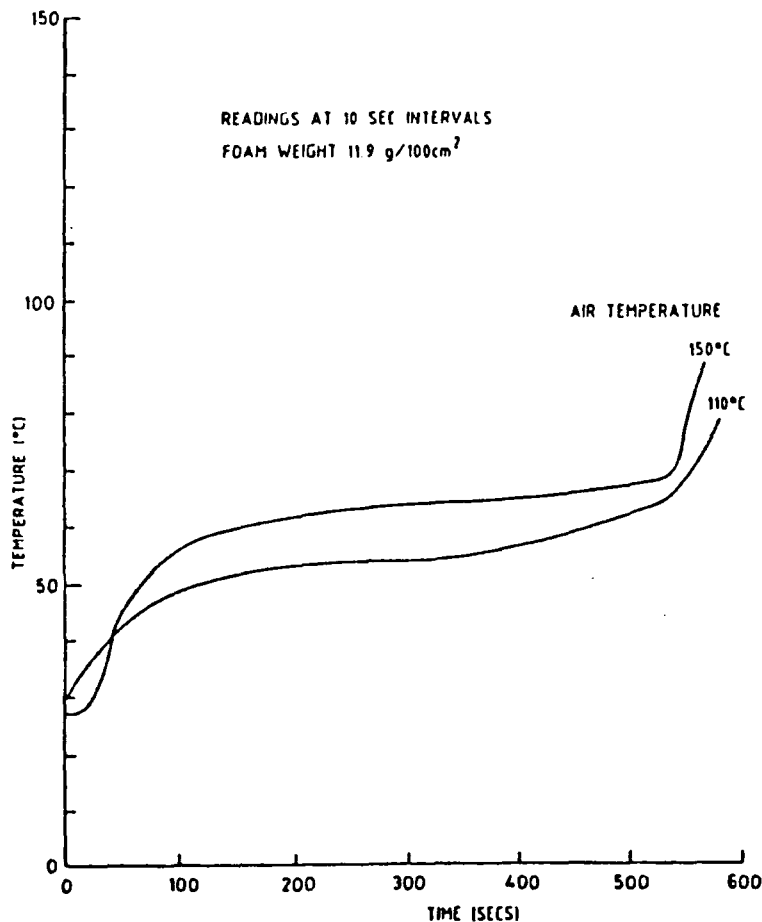
Fig. 6. Effect of air temperature on time to leave constant drying rate period.

Temperature gradient through foam thickness

Before cure can occur, the foam must reach a temperature of at least $130^{0}C$. To confirm that the interface was at the lowest temperature, measurements were taken at different depths in the foam. The results showed that it took an appreciably longer time for the interface to reach the optimum curing temperature than at other foam depths, indicating that the moisture moves upwards as the foam dries. It is therefore essential to ensure that any temperature measurement used to indicate foam cure must be taken at the interface of the foam and tufted substrate.

Comparison of domestic and contract foam

The majority of the work done in this project was undertaken on domestic-quality foam for convenience. A limited series of trials was conducted on contract-quality foam to determine the change in interface temperature/time profile for this higher-density foam. The results supported the earlier findings and illustrate that the temperature plateau of $65^{\circ}C$ to $70^{\circ}C$ is longer because of the higher moisture content of the foam.

FOAM-TEMPERATURE MEASUREMENT ON PLANT

A series of plant trials was conducted to supplement the knowledge gained from the laboratory trials. The object was to demonstrate that a reduction in energy usage was possible with the same carpet throughput and without major structural changes to the drying and curing oven modules.

Preliminary trials were conducted using untufted "Typar" (a non-woven polypropylene fabric) to remove the variable effects of the carpet pile on foam-thickness control.

These trials indicated that foam-temperature profiles could be successfully obtained using the mobile temperature probe designed and developed by the Teaching Company. Further exploratory trials were conducted using "velour" carpet and these confirmed that the probe would be satisfactory for all future plant work. To minimize foam-thickness variations the roller-to-bed gap was set and adjusted during running using the dial-gauge readings available at either end of the roller for best control.

Trails were conducted to establish that during manufacture similar temperature/time profiles occured to those measured in the laboratory. To demonstrate this phenomenon, the bulk gas temperature was progressively raised in the first eight modules of the oven, representing the anticipated period for the temperature plateau for the plant conditions to exist. The results, however, initially failed to confirm the laboratory results. A variety of plant measurements were made before it was appreciated that the manner in which the probe entered the foam dictated the temperature profile recorded. Random variations in foam thickness also created some difficulties.

It was eventually concluded that introducing the thermocouple probe perpendicular to the carpet/foam interface produced misleading temperature profiles. This may be due to heat being conducted along the probe sheath towards the thermocouple junction. Almost all of the sheath is exposed to the high oven gas temperature. Laying 5 cm of the probe along the carpet/foam interface showed the constant-temperature plateau.

Successful trials were conducted and typical temperature profiles are shown in Figs. 7 and 8. The results displayed in Fig. 7 are those with normal working conditions, while in Fig. 8 the first seven modules were set to a top gas temperature of $110^{\circ}C$, the drying phase for the foam conditions in use. All bottom burners were switched off and recirculation was used. With the recirculation air "make up" vents closed, the drop in gas temperature from the top section of a module to the bottom section was approximately $25^{\circ}C$. Oven flue-gas analysis showed that ducting gas between modules before exhausting to atmosphere did not significantly increase the risk of explosion if partial or complete closure of exhaust vents on certain oven modules took place.
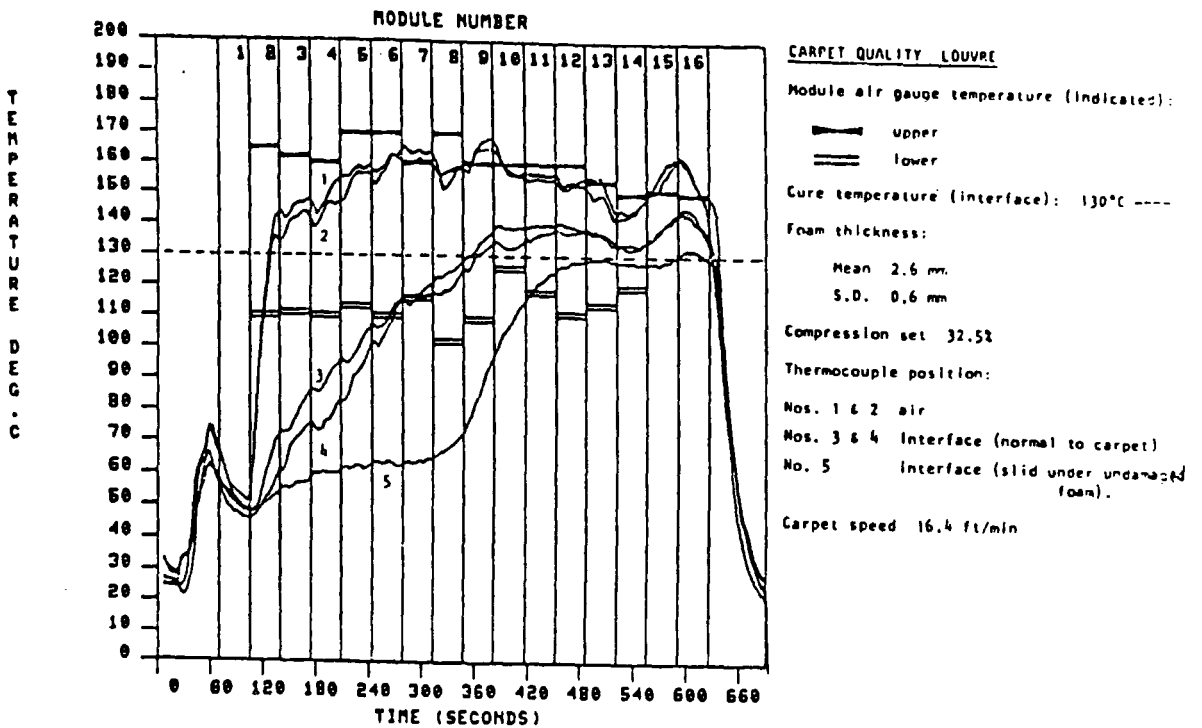
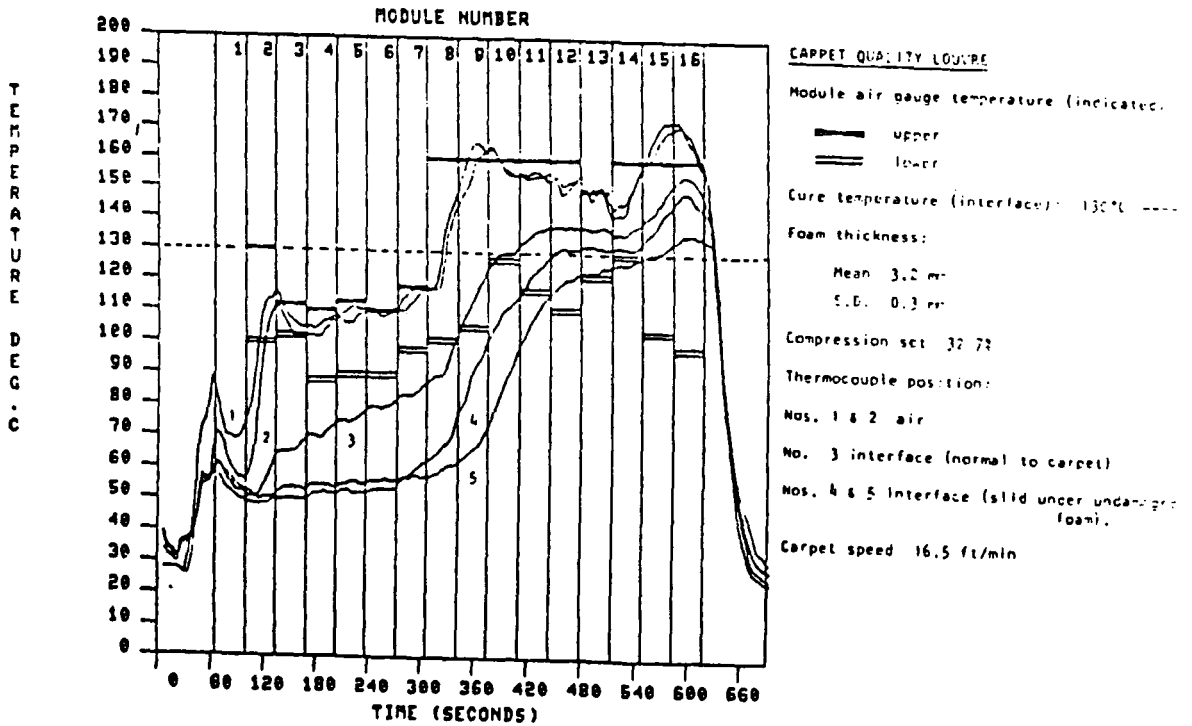*Fig. 7. Interface and air temperature profile measurements.*

Fig. 8. Interface and air temperature profile measurements.

Carpets: Back to Front

Review of plant trials

(1) The trials confirmed that the requirements for a satisfactory cure of the latex foam as applied to a carpet in the production plant are to maintain carpet substrate to latex interface at a temperature of 130°C for a period of 1.5 minutes. These values are within the temperature/time range suggested by the latex manufacturer.

(2) Both laboratory results and plant trial results confirmed that the carpet/foam interface temperature remains sensibly constant at a temperature of 50 to 60°C during the drying phase. Variations in measured interface temperatures were observed. These were found to be dependent upon how the thermocouple probe was introduced to the interface of the moving carpet. Subsequent trials revealed that to obtain results that could be used with confidence, the thermocouple must be slid under undamaged foam.

(3) The high oven module temperature of 160°C used on plant does not significantly influence the drying phase and is therefore wasteful of heat energy. The upper temperature setting for the first seven modules could be reduced to 110°C.

(4) The hot gas exhausted from the top section of a module could safely be recirculated to other sections. Oven modifications can be made so that the hot gas generated in one module can be ducted to a number of modules connected in the series.

(5) Tight control must be exercised over foam thickness to minimize variations, both in materials usage and in degree of cure.